N.N. Kovalev

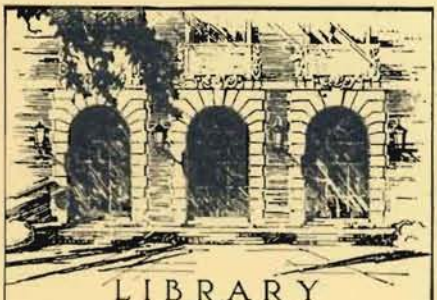
HYDROTURBINES

DESIGN AND CONSTRUCTION

TRANSLATED FROM RUSSIAN

Published for the U.S. Department of the Interior
and the National Science Foundation, Washington D.C.
by the Israel Program for Scientific Translations

OAK ST. HDSF



LIBRARY
OF THE
UNIVERSITY
OF ILLINOIS
621.24
K84gEs
cop. 2

TT 64-11087

Published Pursuant to an Agreement with
THE U.S. DEPARTMENT OF THE INTERIOR
and
THE NATIONAL SCIENCE FOUNDATION, WASHINGTON, D.C.

Copyright © 1965
Israel Program for Scientific Translations Ltd.

IPST Cat. 1192

Translated by M. Segal, Mech. Eng.

Printed in Jerusalem by S. Monson

Binding: K. Wiener

Available from the Office of Technical Services
U.S. Department of Commerce, Washington 25, D.C.

N. N. KOVALEV

HYDROTURBINES

DESIGN AND CONSTRUCTION

(Gidroturbiny. Konstruktsii i voprosy proektirovaniya)

Mashgiz
Gosudarstvennoe Nauchno-Tekhnicheskoe Izdatel'stvo
Mashinostroitel'noi Literatury
Moskva-Leningrad
1961

Translated from Russian

Israel Program for Scientific Translations
Jerusalem 1965

TABLE OF CONTENTS

LIST OF ABBREVIATIONS vi
PREFACE 1

Chapter I. GENERAL DATA ON HYDRAULIC TURBINES 3
1. Types of hydroelectric plants 3
2. Power output of hydraulic turbines 4
3. Classification of hydraulic turbines 7
4. Designs of hydraulic turbines 10
5. Design features of hydro generators 15
6. Development of turbine construction in the U.S.S.R. . . 17

Chapter II. FUNDAMENTALS OF THE THEORY OF TURBINES . . 21
7. Basic equations in turbine design 21
8. Similarity laws and dimensionless numbers 24
9. Specific speed 28
10. Power losses and efficiency of homologous turbines . . . 30
11. Cavitation coefficient and draft head 37

Chapter III. TURBINE PARAMETERS AND DESIGNS 43
12. Model tests and turbine characteristics 43
13. Classification of hydraulic turbines 49
14. Selection of turbine parameters from the universal chart . 63
15. Runaway speed 67
16. Experimental stress analysis on turbine components 76

Chapter IV. DESIGN AND SELECTION OF THE WATER PASSAGES OF THE TURBINE 88
17. Types of turbine casings 88
18. Hydromechanical computation of the scroll casing 99
19. Design of steel scrolls for strength 104
20. The speed ring 117
21. Parameters of reaction-turbine runners 126
22. Throat rings in Kaplan turbines 130
23. Draft tubes 135

Chapter V. TURBINE DESIGNS 150
24. Layout of turbine units 150
25. Design of Francis turbines 156

26. Kaplan turbine designs 164
27. The turbines of the Volga HEP imeni V. I. Lenin 174
28. Designs of horizontal-shaft turbines 178
29. Special turbines 192

Chapter VI. THE DISTRIBUTOR 198
30. Types and designs of distributors 198
31. Guide-vane operating mechanism 207
32. Guide-vane assembly 215
33. Hydraulic forces acting on the guide vanes 219
34. Determination of servomotor parameters 227
35. Graphical layout of the distributor 238
36. The guide vanes 244
37. Components of the guide-actuating mechanism 259
38. The gate ring 267
39. Distributor servomotor 280
40. Distributor upper ring and turbine cover-plate 295
41. Remarks on strength calculation for guide vanes of conical distributors 317

Chapter VII. FRANCIS TURBINE RUNNERS 319
42. Runner designs 319
43. Axial water pressure 335
44. Approximate strength calculation of the runner 341
45. Exact strength calculation of medium-head runners 347
46. Strength calculation of a high-head runner 380
47. Runner-band seals 388

Chapter VIII. KAPLAN RUNNERS 399
48. Runner designs 399
49. Forces acting upon the runner 423
50. Determination of the required runner servomotor force 432
51. Design and calculation of the blade-actuating mechanism parts 453
52. Runner blades 474
53. Runner-hub body 503
54. Servomotor cylinder and cover 517

Chapter IX. TURBINE BEARINGS 523
55. General 523
56. Journal bearings — a brief summary 523
57. Thrust bearings for vertical hydro units — a brief summary 529
58. Oil-lubricated turbine guide bearings 533
59. Guide-bearing seals 538
60. Water-lubricated guide bearings 540

Chapter X. TURBINE SHAFTS 557
61. General notes 557
62. Shaft designs 558
63. Design of vertical turbine shafts 567
64. Shaft vibrations 574
65. Calculation of the flange-joint bolts 584

Chapter XI. AUXILIARY EQUIPMENT 588
66. Oil supply head and rods 588
67. Transmissions and piping 597
68. Pressure regulator 597
69. Gates and valves 602

Chapter XII. TURBINE REGULATION 615
70. Hydromechanical governors 615
71. Basic principles of automatic control 627
72. Interaction of governor elements in the Kaplan turbine . 631
73. Electrohydraulic governors 634
74. Selection of basic parameters for turbine regulating systems 642

Chapter XIII. HYDRAULIC-TURBINE DESIGN AND MANUFACTURE 650
75. Design procedure 650
76. Runaway protection in hydro units 653
77. Manufacturing technique 655
78. Selection of turbine size 659
79. Means to reduce the turbine weight 664
80. Materials used in turbine construction 671

BIBLIOGRAPHY 676

After a brief survey of the theory of hydraulic turbines, the book presents a detailed description of various designs of Francis and Kaplan turbines as well as of their main components and auxiliary equipment, such as scroll casings, guide vanes, runners, shafts, bearings, governors, guide-vane and blade-actuating mechanisms, etc.

The problem of selecting constructional parameters and designs of hydraulic turbines is given due consideration. Information is given on turbine governors, and control problems are discussed.

This book is intended for both designers and students of hydraulic engineering.

EXPLANATORY LIST OF ABBREVIATED NAMES OF U.S.S.R. INSTITUTIONS, ORGANIZATIONS, ETC. APPEARING IN THIS TEXT

Abbreviation	Full name (transliterated)	Translation
DNTP	Dom Nauchno-Tekhnicheskoi Propagandy	Center for the Dissemination of Scientific and Technical Information
Gidroproekt	Vsesoyuznyi Proektno-Izyskatel'nyi Institut imeni S. Ya. Zhuka	All-Union Design and Research Institute imeni S. Ya. Zhuk
GOELRO	Gosudarstvennaya Komissiya po Elektrifikatsii Rossii	State Commission for the Electrification of Russia
GOST	Gosudarstvennyi Obshchesoyuznyi Standart	All-Union Government Standard
IMASh	Institut Mashinovedeniya	Institute of Science of Machines
KhTZ	Khar'kovskii Turbinnyi Zavod	Khar'kov Turbine Plant
KPSS	Kommunisticheskaya Partiya Sovetskogo Soyuza	Communist Party of the Soviet Union
LGU	Leningradskii Gosudarstvennyi Universitet	The Leningrad State University
LMZ	Leningradskii Metallicheskii Zavod	Leningrad Metallurgical and Machine-building Works
LPI	Leningradskii Politekhnicheskii Institut	Leningrad Polytechnic Institute
NKMZ	Novo-Kramatorskii Metallurgicheskii Zavod	The New Metallurgical Works of Kramatorsk
TsAGI	Tsentral'nyi Aerodinamicheskii Institut imeni N. E. Zhukovskogo	Central Aerodynamic Institute imeni N. E. Zhukovskii
TsKTI	Tsentral'nyi Kotloturbinnyi Institut imeni I. I. Polzunova	Central Research and Design Institute for Boilers and Turbines, imeni I. I. Polzunov
TsNIITMASh	Tsentral'nyi Nauchno-Issledovatel'skii Institut Mashinostroeniya	Central Research Institute for Machine Building
VNIIG	Vsesoyuzni Nauchno-Issledovatel'skii Institut Gidrotekhniki	All-Union Scientific Research Institute of Hydraulic Engineering
VNITOE	Vsesoyuznoe Nauchnoe Inzhenerno-Tekhnicheskoe Obshchestvo Energetikov	All-Union Scientific Technical Society of Power Engineers

PREFACE

The Soviet hydraulic-turbine industry has considerable achievements to its credit, and units manufactured in the U.S.S.R. - with a total capacity of over 10,000,000 kw - are rendering commendable service in many parts of the world.

The production of the most powerful Kaplan (adjustable-blade)-type turbines in existence for the hydroelectric plants [HEP] on the Volga River, imeni Lenin and imeni XXII Party Congress, is an outstanding achievement. These turbines have been in operation for a considerable period and have given satisfactory results.

The most powerful Francis (radial-axial)-type turbines yet built, with a capacity of 226,000 kw, are now being manufactured for the Bratsk HEP. Detailed drawings and preparations for construction are now in progress for even bigger turbines, with a capacity of 500,000 kw, for the Krasnoyarsk HEP. The design of the high-head turbines for the Nureksk HEP has begun. New turbine designs, such as the diagonal Deriaz, submersible (tubular) and reversible types are now being developed too.

The future development of power engineering in the U.S.S.R. demands a rapid increase in the production of various types of turbines, and an improvement both in design and in power and cavitation characteristics.

The reduction of construction costs for hydroelectric plants is an important problem. Although the cost of turbines themselves is not a major element in the total cost of the plant, the over-all sizes of their water passages, especially in low-head turbines, play a significant part in determining total construction costs, particularly of that part below water level. Turbine design, therefore, has a considerable bearing on the reduction in cost, and the length of construction time, for the hydroelectric plant as a whole.

Most hydraulic turbines are manufactured at the LMZ*, which has always been the leading plant in this field, and remains so today.

The author has been working in the design department of this plant for 30 years. The present study is an attempt to generalize the experience gained by turbine builders, and analyze the positive and negative features of the various models produced.

The experience amassed at LMZ in calculation, design and manufacture of hydraulic turbines has already been set out in monographs and technical articles published over the past years.

Turbines are described in monographs /24/, /95/, and /46/. Monograph /53/ reviews modern methods for the design and calculation of turbine water passages.

Technological problems in the construction of large turbines are presented in /15/ and /89/.

Regulation of hydraulic turbines and problems in the design of LMZ governors are dealt with in monographs /16/, /4/, /31/, and /32/.

[* See list of abbreviations on page 683.]

[Monograph /64/, edited by A. A. Morozov, discusses problems connected with the selection of hydraulic-turbine characteristics. Most of the contributors to this work belong to the LMZ staff.]

Editions I, III, IV, and VIII of LMZ technical and scientific papers, and the jubilee edition published on the occasion of the plant's centenary, cover problems of design, calculation, research, construction, and production technology of hydraulic turbines.

In his monograph, /78/, I. N. Smirnov deals with general problems of hydraulic turbines, and gives a partial summary of the LMZ practice in this field.

The present study covers the construction of hydraulic turbines, their evolution,and the design of their components. Among other problems dealt with are the procedure of design and all related questions which arise in the course of design and production of modern turbines.

In order to afford an over-all picture, the present book opens with a general statement of the theory and structure of hydraulic turbines. Some information on auxiliary equipment and regulation is included at the end.

The study is based on the experience of the LMZ in the construction of hydraulic machinery which has already been reviewed to some extent in the papers mentioned above, and therefore some repetition is unavoidable. Although the design of a large turbine is the result of team work, this book also singles out the contribution of various individuals to technical progress in this field.

The monograph is divided into 13 chapters.

Chapters I and II contain general information on hydraulic turbines and basic theory; Chapter III deals with selection of the characteristics of hydraulic turbines; Chapter IV deals with the water passages of the turbine; Chapter V with various types of hydraulic turbines; Chapters VI, VII, VIII, IX and X are concerned with the design of the main components of the turbine; Chapter XI, with auxiliary equipment; Chapter XII gives concise details on regulation; and finally, Chapter XIII gives the order of steps in the design of hydraulic turbines and their components.

The author wishes to express his indebtedness to G. S. Shchegolov for his review of the manuscript, to A. Ya. Aronson, B. A. Berkman, V.S. Postoev and I. E. Etinberg for their remarks on separate chapters of the manuscript, to Yu. U. Edel' for his aid in editing this book, and to O. N. Debrinskaya for her assistance in the preparation of the manuscript.

The author

Chapter I

GENERAL DATA ON HYDRAULIC TURBINES

1. TYPES OF HYDROELECTRIC PLANTS

Hydraulic turbines convert the potential energy of water into kinetic energy by utilizing the difference in elevation between two water levels which is called head (H). To utilize the energy of water apart from turbines proper, special hydro structures are also required.

The difference between water levels (head) is usually obtained by building a dam, whose height will depend upon conditions at the site.

On lowland rivers the dam is usually located near the powerhouse. On mountain rivers, dams may be built at a distance from the powerhouse; the water reaches the turbines through a tunnel or channel, called a diversion channel, and a penstock. Hydroelectric plants are accordingly termed run-of-river plants or diversion plants.

Hydroelectric plants for heads ranging from 2 to 2,000 m have been built, depending on the natural conditions and the hydraulic layout adopted.

The head represents the energy of a unit weight of water. The power developed by the water depends on the head and the discharge, i.e. the quantity of water passing per second. When comparing turbines of approximately equal power, it is obvious that those working under a higher head will have a smaller discharge, and hence smaller dimensions. In modern low-head turbines, the discharge Q reaches ≈ 700 m^3/sec. The most important turbine dimension is the runner diameter, and the largest turbine ever built has a runner diameter $D_1 = 9300$ mm.

The type of turbine depends on the head-to-discharge ratio.

Figure I. 1 shows a cross section through a low-head (H = 10 to 20 m) hydroelectric plant with the powerhouse adjacent to the dam.

The vertical shaft turbine (1) is coupled to the generator (2). From the storage reservoir created by the dam where the water is at a certain elevation ∇HW, called headwater, the water stream is directed to the turbine and then discharged to the lower reservoir [if a river cascade scheme is planned] where the elevation is denoted by ∇TW (tailwater).

Figure I. 2 shows a sectional view through the powerhouse of a high-head HEP (H = 300 m). The water reaches the turbine (1) through a long steel penstock, part of which (3) is visible in the figure. The gate (2) is located on the penstock, upstream from the turbine. The water is discharged directly into the tailrace. The turbine is coupled to the generator (4).

Sometimes, in run-of-river hydro plants, the equipment may be located right inside the dam. Considerable savings may be obtained by eliminating the powerhouse building. Such a plant, operating under a relatively low head, may be seen in Figure I. 3. Figure I. 4 shows a medium-head hydroelectric

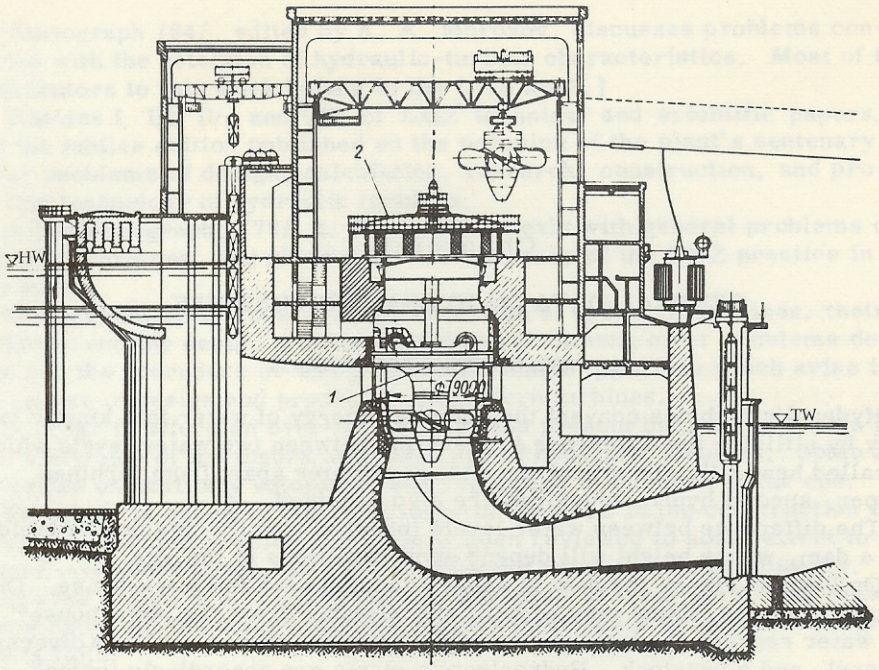


FIGURE I.1. Sectional view of a low-head hydro-plant powerhouse adjacent to the dam

plant (*H* 80 to 100 m), where the generating unit (1, 2) is located inside the dam. The water reaches the turbine through the steel penstock (3).

It is more convenient to house horizontal turbines inside the dam. During recent years, a great deal of attention has been paid to improved designs for horizontal-shaft turbines.

It sometimes proves economical to pump water from the tailwater to the headwater side for certain periods of time, for use later on in the turbine. Such plants are termed pumped-storage plants. The operation may be effected by specially installed pumps; a better method still is to use the turbine itself for pumping. The generator then works as a motor, drawing current from the network, and the unit is called a pump-turbine unit.

The turbines used in tidal hydroelectric-power plants which harness the energy of marine tides are of special construction. Their characteristic feature is the periodic interchange of headwater and tailwater sides.

2. POWER OUTPUT OF HYDRAULIC TURBINES

The hydraulic turbine utilizes the energy of the water, which develops a torque on the generating-unit shaft.

The power developed by the water depends both on discharge and on head; it may be determined according to the general laws of mechanics.

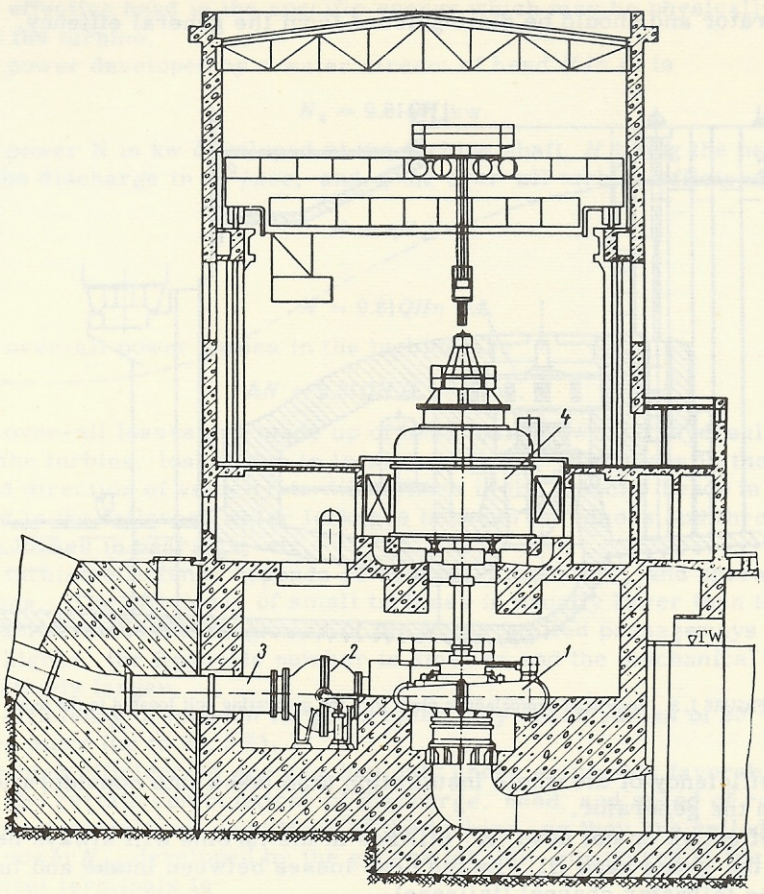


FIGURE I.2. Sectional view of a high-head hydro-plant powerhouse

The water power developed

$$N_n = \frac{\gamma Q H_{gr}}{102} = 9.81 Q H_{gr} \text{ kw}, \qquad \text{(I. 1)}$$

where $\gamma = 1000 \text{ kg/m}^3$ = specific weight of water;
Q = water discharge, m^3/sec;
H_{gr} = gross head, m.

Water power is not completely utilized in the turbine, and unavoidable losses always occur.

If N is the power as measured on the turbine shaft, the following relation will always be valid

$$N < N_n \quad \text{or} \quad N = \eta_y N_n,$$

where η_y is the turbine efficiency. This does not include the power losses of

the generator and should be distinguished from the general effiency.

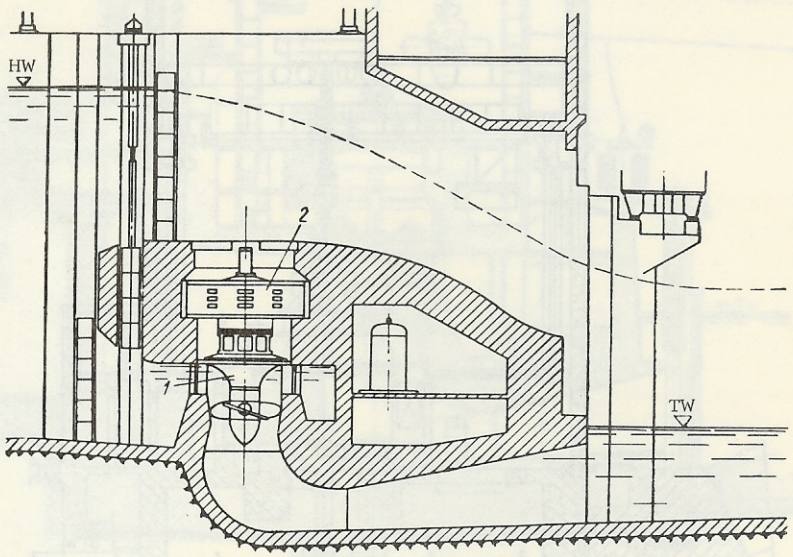


FIGURE I.3. Low-head hydroelectric plant with the generating unit located in the dam

The efficiency of the whole installation also takes into consideration the losses in the generator.

The effective or net head, H, utilized in the turbine will always be smaller than the gross head H_g by the head losses between intake and turbine, and in the tailwater channel (tailrace).

$$H = H_g - (\Delta h_f + \Delta h_\kappa),$$

where Δh_f = head losses from intake to turbine;
Δh_κ = head losses in the tailrace.

The effective (net) head may be defined as the difference between the energy of 1 kg of water at the entrance to the turbine, and at the beginning of the tailrace [less all losses].

$$H = \left(\frac{p_e}{\gamma} + z_e + \alpha_e \frac{v_e^2}{2g}\right) - \left(\frac{p_\kappa}{\gamma} + z_\kappa + \alpha_\kappa \frac{v_\kappa^2}{2g}\right), \qquad \text{(I. 2)}$$

where p_e and p_κ = average pressures, kg/cm^2;
z_e and z_κ = elevations, m;
v_e and v_κ = average water velocities, m/sec;
g = acceleration of gravity, m/sec;
α_e and α_κ = coefficients introduced to allow for the uneven velocity distribution in a cross section.

In these formulas the subscript e refers to the entrance cross section of the turbine casing, and the index κ to the beginning of the tailrace.

The effective head is the specific energy which may be physically utilized by the turbine.

The power developed by a water stream of head H in m is

$$N_0 = 9.81QH \text{ kw.}$$

The power N in kw developed at the turbine shaft, H being the head in m, Q the discharge in m^3/sec, and η the over-all turbine efficiency, is

$$N = \eta N_0$$

or

$$N = 9.81QH\eta \text{ kw.}$$

The over-all power losses in the turbine are

$$\Delta N = 9.81QH\,(1 - \eta) \text{ kw.}$$

The over-all losses are made up of head losses owing to hydraulic friction in the turbine, losses due to local turbulence, to changes in the magnitude and direction of velocity, to differences in the velocity heads in the draft tube and in the tailrace, water leakages between the blades and throat ring, friction losses in bearings, etc.

The turbine efficiency depends on design, dimensions, and operating conditions. The efficiency of small turbines is usually lower than that of larger units, since the roughness of the water-spilled passageways is relatively higher, the Reynolds number is smaller, and the mechanical losses are relatively larger.

The efficiency of modern large turbines may reach values of 90 — 93% and even more (up to 94.5%).

Very high efficiencies are reached only under extremely favorable conditions, by certain combinations of discharge, head, and speed of rotation, or optimum operational conditions of the turbine, as they are called.

The power N_{unit} developed by the generating unit, measured at the generator output terminals is

$$N_{unit} = 9.81QH\eta\eta_g \text{ kw}$$

where η_g is the generator efficiency.

The efficiency of a generator coupled with a turbine varies from 95 to 98%. Thus the over-all turbine-plus-generator efficiency varies from 90 to 91%.

The power developed by a turbine may vary within very large limits, depending on discharge, head, and the combination of the two. At present, there are turbines in existence with a maximum capacity of more than 200,000 kw. A turbine of given capacity may have a runner with a large or a small diameter, depending on the head.

3. CLASSIFICATION OF HYDRAULIC TURBINES

The wide variety of head and discharge combinations in hydroelectric plants requires a large number of types and a considerable range of dimensions for turbines. The classification of modern turbines is given in Table I.1.

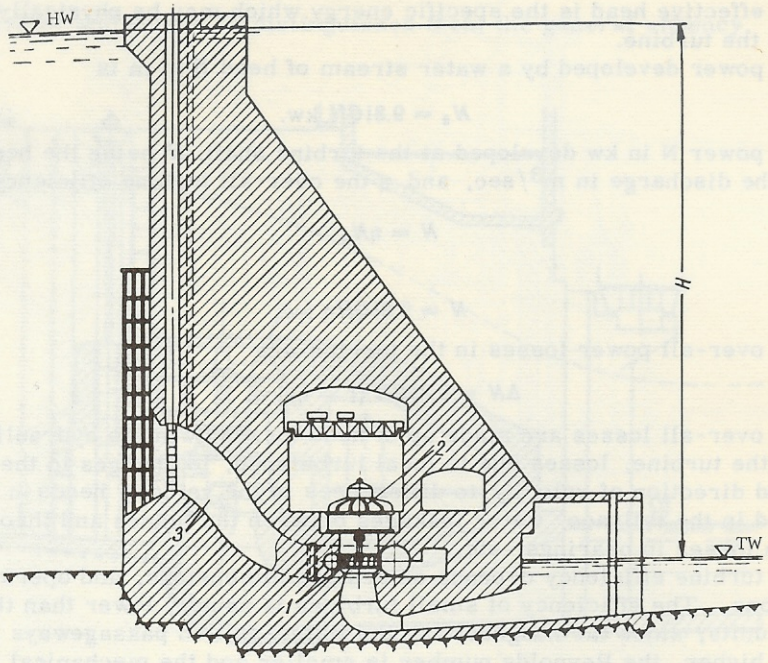


FIGURE I.4. Medium-head hydroelectric plant, with the generating unit and steel penstock located in the dam

As may been seen from the table, hydraulic turbines fall into two general classes, reaction and impulse turbines.

These terms are, to a certain extent, arbitrary. It would be more correct to call the reaction type, velocity-pressure turbines, and the impulse type, free-jet turbines, thus indicating the true nature of the phenomena involved more precisely.

According to the Bernoulli theorem, which expresses the law of energy conservation in hydromechanics,

$$\frac{v^2}{2g} + \frac{p}{\gamma} + z = E = \text{const}, \qquad \text{(I. 3)}$$

the energy of unit weight of water flow is the sum of three different kinds of energy, corresponding to the three terms of this equation (kinetic energy $\frac{v^2}{2g}$, and two kinds of potential energy, the pressure $\frac{p}{\gamma}$ and the elevation z). Turbines are grouped into various classes according to the type of energy converted by the runner.

The water energy delivered to the runner will evidently equal the difference in the stream energies before and after the runner. Denoting the entrance to the runner by subscript 1 and the exit by subscript 2, we may write

$$\frac{v_1^2 - v_2^2}{2g} + \frac{p_1 - p_2}{\gamma} + z_1 - z_2 = A. \qquad \text{(I. 4)}$$

TABLE I. 1

Classification of hydraulic turbines

Classes	Reaction			Impulse		
Systems	Axial (propeller)		Francis (axial-radial)	Pelton	Inclined jet	Double jet
	Kaplan (adjustable blades)	Fixed blades				
Limits of applicability	H = 2—70 m D_1 = 1.0—10.0 m N up to 250,000 kw	H = 2—70 m D_1 = 0.35—9.0 m N up to 150,000 kw	H = 30—450 (large sizes) H = 2—200 (small sizes) D_1 = 0.35—7.5 m N up to 500,000 kw	H = 300—1700 (large sizes) H = 40—250 m (small sizes) D_1 = 0.36—5.2 m N up to 110,000 kw	H = 30—400 m N = 10—4000 kw	H = 10—60 m N = 10—150 kw

With reaction turbines,

$$\frac{p_1 - p_2}{\gamma} + z_1 - z_2 > 0.$$

The larger the difference

$$\left(\frac{p_1}{\gamma} + z_1\right) - \left(\frac{p_2}{\gamma} + z_2\right),$$

the larger the quantity of energy A received by the runner at the expense of potential energy, and vice versa.

Reaction turbines are the type most widely used and cover the range of heads (1.5 - 300 m) most often encountered in hydroelectric plants.

With free-jet or impulse turbines, the pressures at the runner entrance and exit are equal, i.e., $p_1 = p_2$.

Only kinetic energy of the jet discharging into the atmosphere is used up in the runner. The impulse turbine is operated under atmospheric pressure by the free jet, which does not fill the passages. The available head is converted into velocity head $v = K_v\sqrt{2gH}$, where K_v is a coefficient depending on the losses due to jet formation. Usually K_v = 0.97 to 0.985.

The two classes of hydraulic turbines (reaction and impulse) in turn are divided into various sub-types. In modern practice the most important types of reaction turbines are the following: adjustable blade [Kaplan], fixed-blade, and radial-axial [Francis]; the impulse turbines are: fixed bucket [Pelton], inclined jet, and double-jet types.

The turbine types most widely used are the Kaplan, Francis, and Pelton types.

The hydraulic turbine generally consists of the following basic elements: the casing, the distributor, the runner (water wheel), the throat ring, the draft tube, the shaft, and the bearings.

In reaction turbines, the casing is usually a scroll (spiral) casing whose function is to guide the water fully and uniformly all around the circumference toward the distributor. In impulse turbines, the water does not bear against the entire circumference of the runner, but strikes it in jets. Hence the casing of the impulse turbine, especially that of the Pelton type, is the penstock itself (with "Y" pieces provided for multiple-jet turbines, with a corresponding number of branches).

The purpose of the distributor is to direct the water flow entering the runner, and to regulate the discharge through the turbine. In reaction turbines, the distributor consists of guide vanes which are angularly adjustable by means of a special mechanism. The vane axes may be parallel to the turbine center line (radial guide vanes), perpendicular to it (axial guide vanes) or inclined (diagonal guide vanes). The distributor of the Pelton turbine is a contracting nozzle, inside which a pear-shaped needle moves in an axial direction. The movement of the needle alters the free section of the nozzle, thus regulating the discharge.

The main direction of the flow near the Kaplan turbine runner is parallel to the turbine center line. The runner blades may turn about their axes, which are perpendicular to the turbine center line. Blade angles may thus be adjusted, obtaining a high efficiency under all operating conditions. The diagonal Deriaz-type turbine is a variety of the Kaplan (adjustable-blade) turbine; the blades are inclined at a sharp angle with respect to the turbine axis.

The direction of flow in the Francis-type runner changes gradually from radial to axial. The blades are fixed, and fastened by a band (called the shroud). The Pelton runner buckets are bowl-shaped.

The draft tube, of the diverging type, reduces the velocity at the turbine exit, and is intended primarily for the regain of head. For constructional reasons most plants have elbow-type draft tubes. In Pelton turbines, as already indicated, pressure at the runner exit equals atmospheric pressure and a draft tube is not required.

Each turbine class is subdivided into a number of series. The turbines in each series have geometrically similar water passages.

In turbine construction the turbines belonging to a certain series are characterized by their specific speed, which is determined from the formula

$$n_s = 1.167 \frac{n\sqrt{N\ (\text{kw})}}{H\sqrt[4]{H}}. \qquad (1.5)$$

Depending on the specific speed, the turbines are divided into low-, medium-, and high-speed types.

TABLE I. 2

Turbine types	Specific speed		
	Low-speed	Medium-speed	High-speed
Kaplan	300-450	500-700	800-1100
Francis	60-150	150-250	250-400
Pelton	4-10	14-25	30-60

4. DESIGNS OF HYDRAULIC TURBINES

Since large and medium hydro plants are usually equipped with Kaplan, Francis, and Pelton turbines, only the various parts and operating principles of these turbines require detailed consideration.

The schematic diagram of a Kaplan turbine is shown in Figure I. 5.

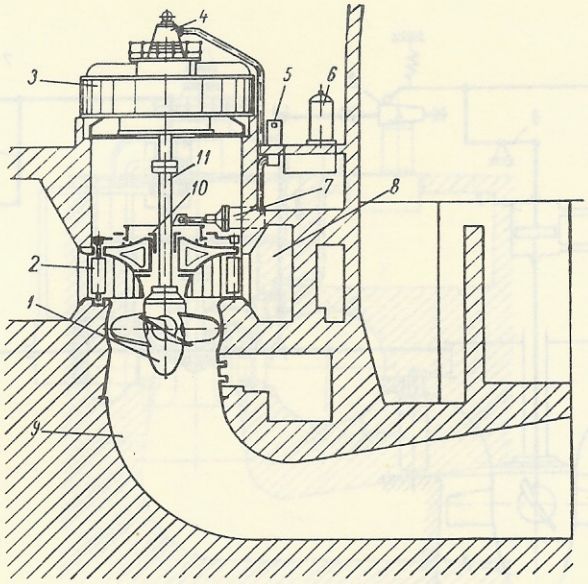


FIGURE I.5. Kaplan turbine

From the storage reservoir created by the dam, water is fed to the spiral casing (8). The guide vanes (2) are located inside the spiral casing.

With the guide vanes adjusted, the distributor directs the flow toward the runner (1), controls the amount of water supplied to it, and also makes it possible to interrupt the water supply to the runner completely.

The turbine output may be regulated by varying the water discharge with the aid of the distributor.

The distributor is a mechanism consisting of a large number of hydrodynamically-shaped guide vanes, disposed around the circumference. The vanes can be turned simultaneously at a certain angle, thus creating channels for the passage of water; the width of these channels changes, depending on the turning angle of the guide vanes. When the distributor is closed, the guide vanes touch each other, and the water flow through the turbine is shut off. The distributor leads the water uniformly toward the entire circumference of the runner. The guide vanes are kinematically linked to the oil-pressure operated piston-type servomotor (7).

The servomotor consists of cylinder and piston. When oil is admitted under pressure into the cylinder the piston moves, thus pulling the sliding ring which turns the guide vanes. From the distributor, the water passes through the runner.

The Kaplan-turbine runner (1) usually has only a few blades (4 to 7), fastened to the runner hub by the blade stems. Within the hub are the crankshaft mechanism for blade pivoting and an oil-pressure piston-operated servomotor, for its actuation.

The oil is supplied to the servomotor through hollow rods located within the shaft (11). These rods are connected to the oil-supply head (4) installed on the generator. The oil-supply head is connected to the oil pumping system (6).

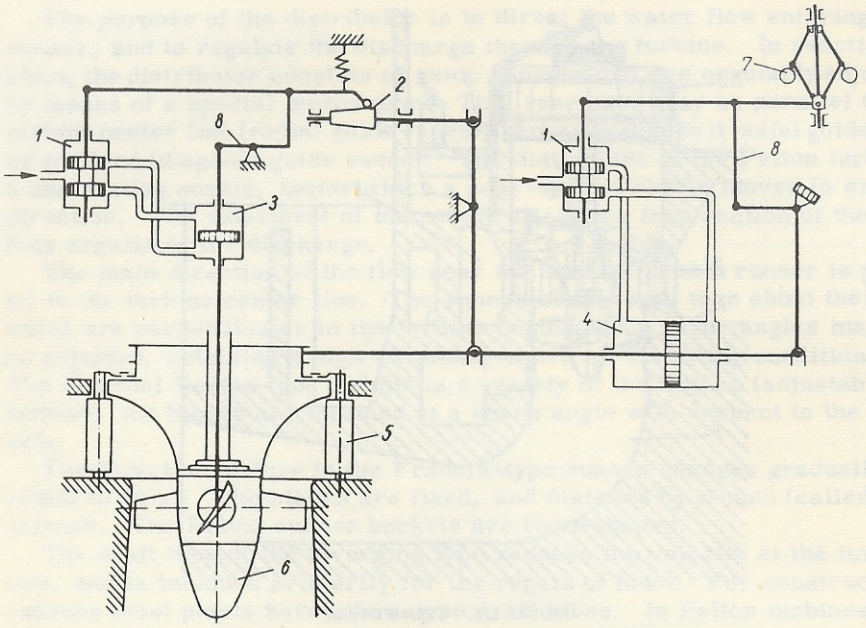


FIGURE I. 6. Schematic diagram of a Kaplan-turbine regulation system

The runner blade angle may be adjusted to a certain water discharge, in accordance with the distributor opening.

From the runner the water enters the draft tube (9) whence it is discharged into the tailrace.

The runner is mounted on the vertical shaft (11) which is guided in the bearing (10). The turbine shaft is coupled to the generator shaft. The governor (5) regulates the operating conditions of the turbine according to changes in power demands (load).

The layout of the Kaplan-turbine regulation system is shown in Figure I. 6.

The governor has a highly sensitive speed-responsive flyballs system (7). Receiving small impulses from the flyballs - measurable in grams - the governor amplifies them considerably, sometimes up to hundreds of tons, by means of hydraulic amplifiers (pilot valve (1) and servomotors (3 and 4)), in order to turn the movable guide vanes (5) of the distributor and the adjustable runner blades (6).

The blade-control valve [in Russian terminology - kombinator], which ensures the required interdependence between the guide-vane position and runner blades position, is denoted by (2), and the restoring mechanism by (8).

The arrangement of a Francis turbine, shown in Figure I. 7, is similar to that of a Kaplan turbine (Figure I. 5). The difference is that the Francis runner has fixed blades (14-20) which are surrounded by a shroud. Hence, the Francis turbine attains high efficiency under certain operating conditions only. If these conditions alter, the efficiency markedly decreases.

The regulating system of these turbines is much simpler, since no special mechanism for runner-blade adjustment is required.

The arrangement of a horizontal Pelton turbine for high-head plants is shown in Figure I. 8.

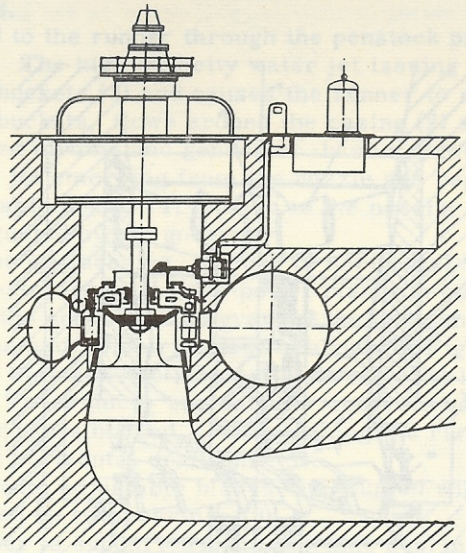


FIGURE I. 7. Schematic diagram of a Francis turbine

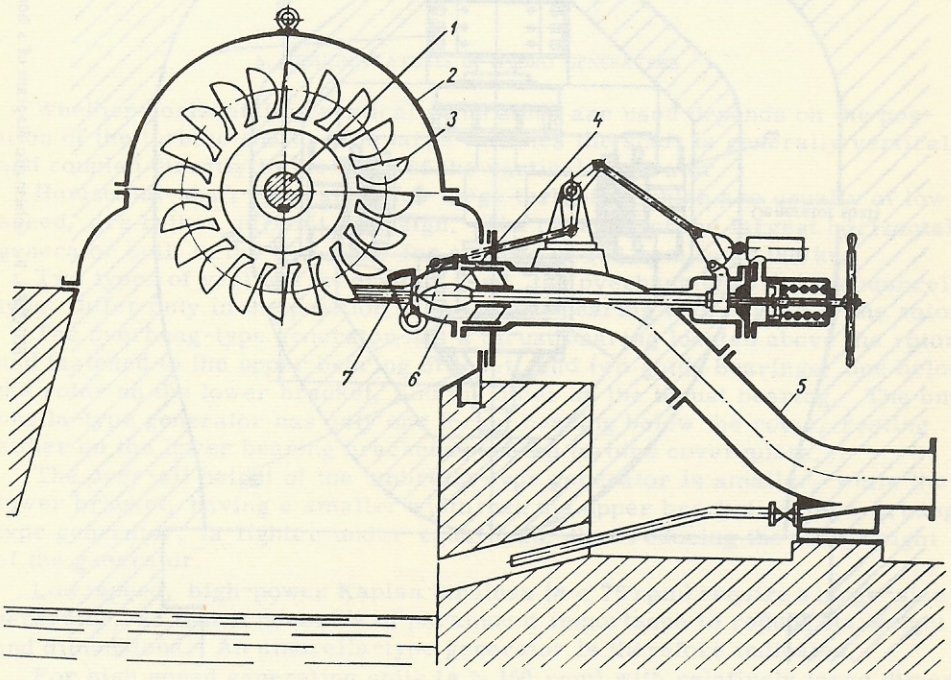


FIGURE 1.8. Schematic diagram of a Pelton turbine

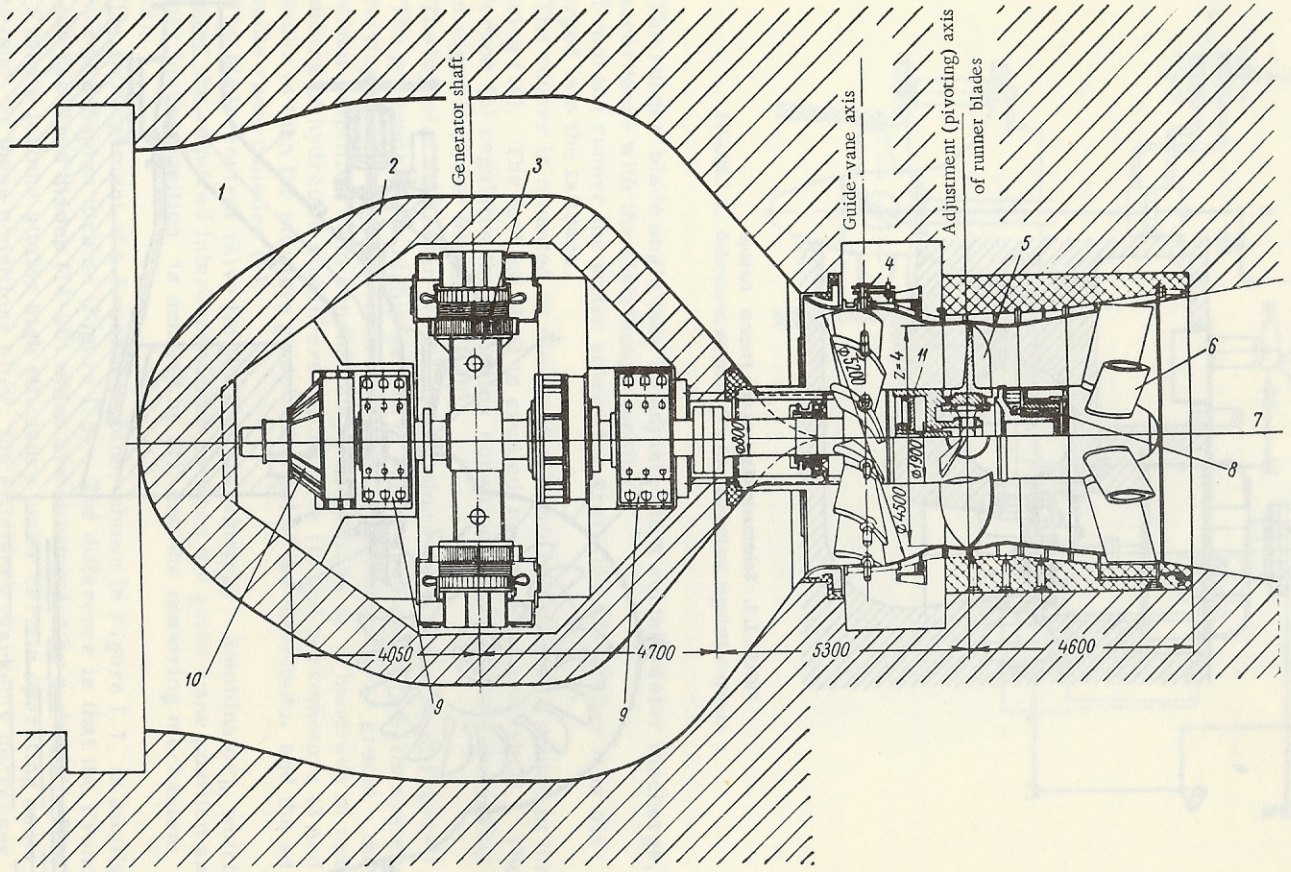


FIGURE I. 9. Schematic diagram of a horizontal-shaft (tubular) turbine

The arrangement of a horizontal Pelton turbine for high-head plants is shown in Figure 1.8.

The water is fed to the runner through the penstock provided at its end with the nozzle (6). The high-velocity water jet issuing from the nozzle strikes the runner buckets (3) and causes the runner to rotate. The water, leaving the runner buckets, flows around the casing (2) and passes into the tailrace. Quite often turbine and generator have a common shaft (1). Regulation of the water jet emerging from the nozzle and reaching the runner is effected by the movable needle (4) located in the nozzle, and by the jet deflector (7), both actuated by the governor.

In modern turbine engineering, the use of horizontal Kaplan turbines for spill-type, pumped-storage, and tidal-power plants is continually spreading.

As an example, the schematic diagram of the horizontal-shaft Kaplan turbine for the Kama hydroelectric plant is shown in Figure I. 9.

Water is fed into the axial distributor (4) through two lateral rectangular-shaped ducts (1). These ducts enclose the concrete casing (bulb) (2) where the generator (3) is housed. When leaving the runner, the water flows through the straight horizontal draft tube (7).

The runner (5), with adjustable blades, is coupled with the generator shaft which is located on two bearings (9).

The turbine runner is supported by the turbine bearing (8), located in the outlet stator (6).

The servomotor (11) and the blade-adjustment mechanism are located inside the runner. The oil is supplied to the servomotor (11), through rods connected to the supply head (10) mounted on the generator-shaft end.

5. DESIGN FEATURES OF HYDRO GENERATORS

Whether horizontal or vertical generators are used depends on the position of the turbine shaft. For large turbines the shaft is generally vertical, and coupled directly to the shaft of the vertical generator.

Horizontal-shaft generators for large turbines, which are usually of low speed, are rather difficult to design. The capacity of the largest horizontal generator built in the U. S. S. R. for a speed of 125 rpm is 23,000 kw.

Two types of vertical generators used, the overhung type and the umbrella type, differ only in the position of the thrust bearing with regard to the rotor.

The overhung-type generator has a thrust bearing located above the rotor and fastened to the upper bearing bracket, and two guide bearings, one below the rotor on the lower bracket, and the other on the thrust bearing. The umbrella-type generator has only one thrust bearing below the rotor, resting either on the lower bearing bracket or on the turbine cover-plate.

The over-all height of the umbrella-type generator is smaller, while the lower bracket, having a smaller width than the upper bracket of the overhung-type generator, is lighter under equal load, thus reducing the total weight of the generator.

Low-speed, high-power Kaplan turbines ($n < 75$ rpm) require a large-size generator, so that it becomes of paramount importance to reduce its weight and dimensions. An umbrella-type generator is therefore indicated.

For high speed generating units ($n > 150$ rpm) with relatively large dimensions (stator diameter < 10 m), the overhung-type generator is commonly used.

A sectional view of an overhung-type generator is shown in Figure I. 10.

The stator (5) consists of the frame, the laminated core, and the stator windings (6). The stator frame usually rests on the foundation.

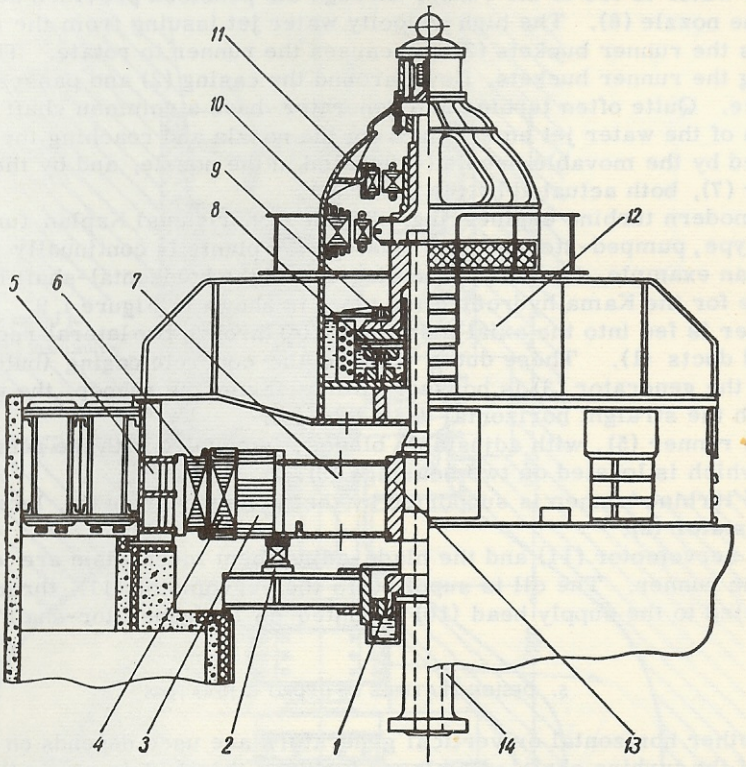


FIGURE I.10. Sectional view of an overhung-type generator

The rotor (3) consists of the rim, mounted on the spider (7), with the hub (13) shrunk on the generator shaft (14). The excitation current from the exciter (10) enters the pole windings (4), producing a magnetic flux in the rotor poles and the stator core. The relative motion between the rotor and the stator causes the magnetic flux lines to intersect the stator winding, thus inducing a current which is delivered to the electrical network. In large generators an additional pilot (booster) exciter (11) is provided to excite the main exciter.

The stationary thrust collar (8) on the upper bracket (12), carries the whole axial load of the runner. The generator shaft (14) transmits the torque from the turbine shaft to the rotor, being guided by two bearings (1) and (9).

Hydraulic brakes are provided below the rotor to stop it when the load is disconnected; otherwise, continued rotation due to inertia would upset lubrication conditions between the sliding surfaces of the thrust bearing and the thrust-bearing collar might heat up and suffer damages.

An umbrella-type generator is shown in Figure I. 11. It is similar in design to the overhung type, except for the stationary thrust collar (1), which is located below the rotor on the lower bearing bracket (2).

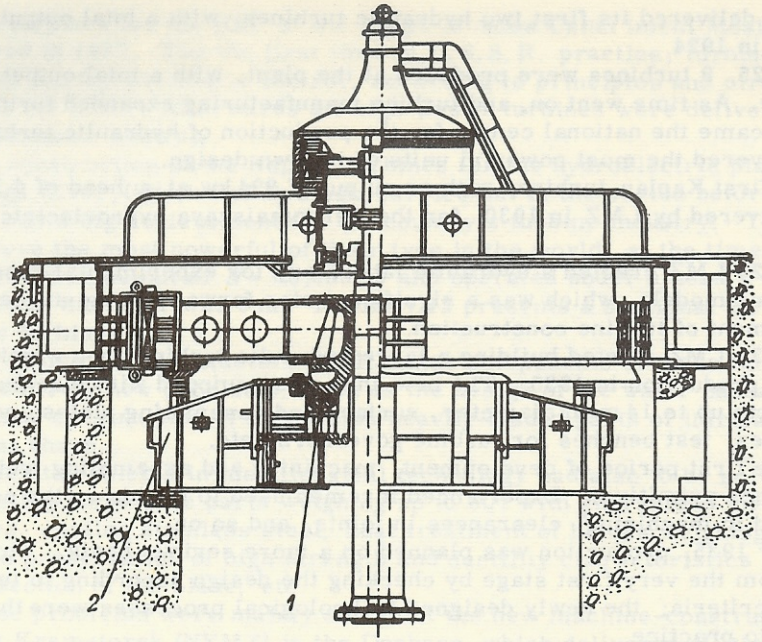


FIGURE I.11. Sectional view of an umbrella-type generator

As a rule the generators are of the a.c. three-phase type [alternators]. When selecting the turbine speed, and hence the generator speed, it should be remembered that in the U.S.S.R. the a.c. frequency f=50 cycles.

The number of pole pairs, p, depending upon the speed n (rpm), may be computed from the formula

$$p = \frac{60f}{n} = \frac{3000}{n}.$$

6. DEVELOPMENT OF TURBINE CONSTRUCTION IN THE U.S.S.R.

The manufacture of hydraulic turbines started in the U.S.S.R. only after the revolution.

In 1920, the VIII All-Union Session of the Soviets approved the first plan for the economic development of the country — GOELRO. This plan envisaged the erection of 30 power plants (including 9 hydro plants) totalling 1,750,000 kw over a 10-15 year period.

The hydraulic power equipment for the first hydroelectric plants built under the GOELRO was purchased abroad.

The manufacture of hydraulic turbines started simultaneously at the plant imeni Kalinin in Moscow, and at the plant imeni XXII Congress of the KPSS in Leningrad. Before World War II the plant imeni Kalinin supplied only small-size turbines. After the war, the production of small turbines was begun in the Urals too.

LMZ delivered its first two hydraulic turbines, with a total output of 425 kw, in 1924.

In 1925, 9 turbines were produced at the plant, with a total output of 4,560 kw. As time went on, and turbine manufacturing expanded further, LMZ became the national center for the production of hydraulic turbines, and delivered the most powerful units of its own design.

The first Kaplan turbine, with an output of 294 kw at a head of 4.25 m, was delivered by LMZ in 1930, for the Pervomaiskaya hydroelectric power plant.

In 1928 LMZ erected a hydraulic laboratory for experimental research on turbine models, which was a significant step forward in the successful development of turbine construction.

In 1931 LMZ started building a large hydraulic-turbine shop which commenced production in 1935. The new shop was equipped with machines to take parts up to 14 m in diameter, surface and assembling plates, powerful cranes, test benches for turbine governors, etc.

In the first period of development, machining and assembling technology was rather primitive. Experienced foremen used to decide on the accuracy required in machining, clearances in joints, and so on.

After 1935, production was planned on a more serious basis. This was done from the very first stage by checking the design according to technological criteria; the newly designed technological processes were then translated into practice.

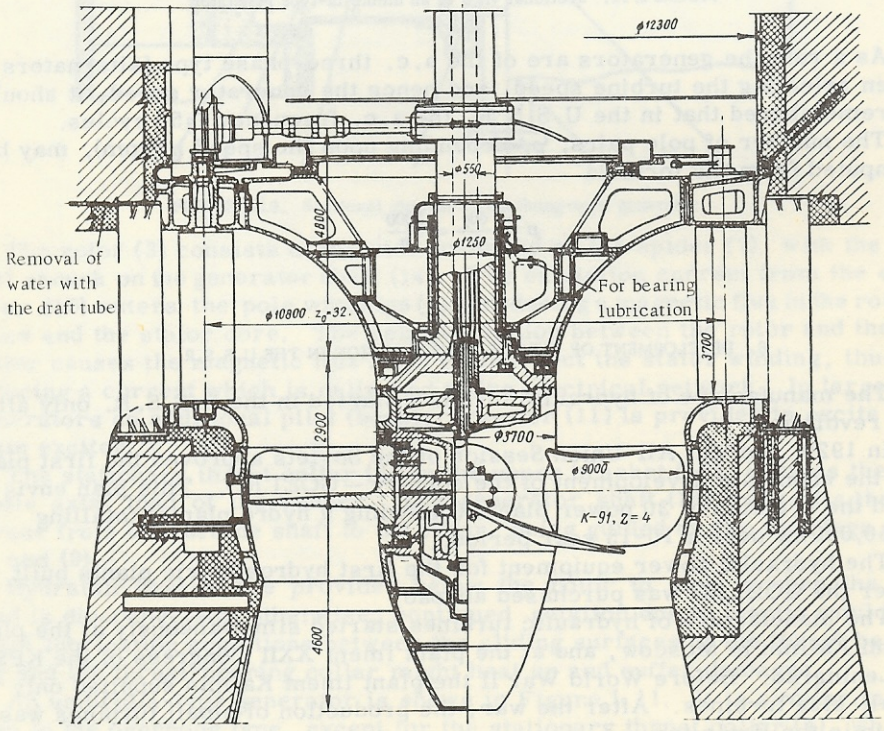


FIGURE I. 12. Turbine for the Rybinsk hydroelectric plant (N = 65,000 kw; H = 17.5 m; D = 9 m)

The turbines for the HEP of the Volga-Moscow Canal imeni Moskva were delivered in 1937. For the first time in U. S. S. R. practice, turbines were designed for full automatic control, according to principles and circuits devised at the LMZ. Afterwards all high-power turbines were delivered with fully automatic control.

The construction of the Kaplan turbines for the hydroelectric plants on the Volga River, Uglich and Rybinsk, carried out in the period before World War II was a big achievement for the country's turbine industry. These units were the most powerful of their type in the world, at the time.

They had an output of $N = 65{,}000$ kw and operated under a head $H = 15.5$ m. The runner diameter was 9 m. Figure I.12 presents a sectional view of one of these turbines.

The design and manufacture of all major components of these turbines raised entirely new problems, such as the design of the water passages, and design and construction of large-size heavily-loaded parts of intricate geometrical shape.

Difficult problems in metallurgical technology had also to be solved, such as: casting large-size parts weighing up to 60 t with guaranteed mechanical qualities, casting stainless steel, heat treatment of blades weighing up to 20 t with preservation of high strength and ductility characteristics in each cross section of the blade, etc.

These problems were mainly solved at the new machine-construction plant at Kramatorsk (NKMZ) in the Donbass, which delivered all the large steel castings and forgings for these turbines.

Special instruments and devices had to be provided and new advanced methods of machining established, such as: simultaneous machining of components on several machine tools, more efficient machining conditions, machining of large-size parts with cutters of larger cross section, machining of parts on vertical mills with a more efficient use of lathe capacity. Meanwhile research was carried out into the technology of rubber bearing-liner manufacture, pressing-in of bronze-bushing without subsequent machining, methods for detecting shaft defects and for precise static balancing of assembled runners weighing up to 300 t, etc.

Before World War II, the plant manufactured and installed several large turbines, proof of the success of the U. S. S. R. turbine industry.

The efficiency of these turbines, as measured during actual operation, attained 92 — 93.5 %.

During World War II, turbine production in the U. S. S. R. was interrupted until 1944, when work started simultaneously at the LMZ on reconstructing the plant itself, and on repairing and restoring turbine equipment for the destroyed hydroelectric plants.

A considerable amount of work was required to restore the Dnieper HEP. The turbines for this plant had been delivered in the thirties by the Newport-News Company in the U. S. A.

The first three units (turbines and generators) for the reconstructed plant were purchased in the United States, and the other six units were delivered by the U. S. S. R. plants LMZ and Elektrosila.

Without increasing the over-all sizes of the former designs, the new turbines installed were more powerful (80,000 kw instead of 67,000 kw), with an efficiency of 93 % instead of 90.2 %.

For the first time U. S. S. R. engineers succeeded in manufacturing and transporting an all-cast runner with a diameter of 6.1 m, a height of 3.1 m,

and a weight of 92 t. American companies have manufactured similar runners, but in sections. The manufacture of all-cast runners saved 12 t of steel and shortened manufacture and erection time by three months for each turbine.

After World War II, much was done to improve the design of Kaplan turbines. Improvements in regulation systems led to smaller servomotors and distribution valves, and oil-pumping units of reduced over-all dimensions. A novelty in turbine design was arranging the thrust bearing on the turbine cover-plate. This made it possible to eliminate the bearing bracket, thus reducing the weight and the total height of the turbine unit, which is even more important.

In 1952, the production of hydraulic turbines was begun at the Harkov Turbine Plant which has manufactured many large Kaplan turbines in recent years.

After the war, standard turbine parts were largely used in the U. S. S. R. turbine industry, thus eliminating many of the shortcomings of the custom-made products.

LMZ and VIGM jointly developed a specification for hydraulic turbines, which established the types and dimensions of runners covering the whole field of application of hydraulic turbines, for heads ranging from 3 to 300 m and outputs from 500 to 150,000 kw.

The design and manufacture of turbines for the most powerful hydroelectric plants in the world, imeni Lenin and imeni XXII Congress of KPSS (D_1=9.3 m) on the Volga River, was an important step in the development of turbine construction.

These units — among the largest and most powerful Kaplan turbines in the world — have a capacity of N=108,500 kw under a rated head of H=19 m, and 126,000 kw under a maximum head of H=22.5 m. A large series of 41 turbines was produced.

All the turbines at the Volga HEPs have given satisfactory service, and demonstrate high technical characteristics.

Complicated technical problems had to be solved in the construction of the powerful Francis turbines for the Bratsk and Krasnoyarsk hydroelectric plants.

LMZ is at present manufacturing turbines with an output of 225,000 kw under a head H=100 m for the Bratsk HEP. The turbines manufactured for Krasnoyarsk have an output of 500,000 kw.

The increase in specific power in the generating unit leads to higher stresses in the turbine parts. Hence these must be built on the basis of careful calculation and research.

Since the cost of the hydro structures largely depends on the size of the turbine water passages, it is very important to look for ways and means of reducing their dimensions.

Chapter II.

FUNDAMENTALS OF THE THEORY OF TURBINES

7. BASIC EQUATIONS IN TURBINE DESIGN

When the water passes through the runner blades, a reciprocal action takes place between them. The stream deviates from its initial direction, and its pressure on the blades causes their rotation, thereby creating a torque upon the turbine shaft.

The runner reaction on the stream at steady operational conditions of the turbine may be determined thus:

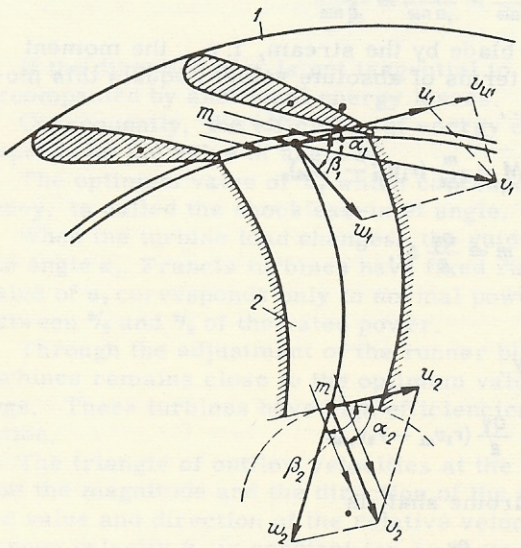


FIGURE II.1. Diagram of the water flow through the distributor (1) and the channels between the runner blades (2)

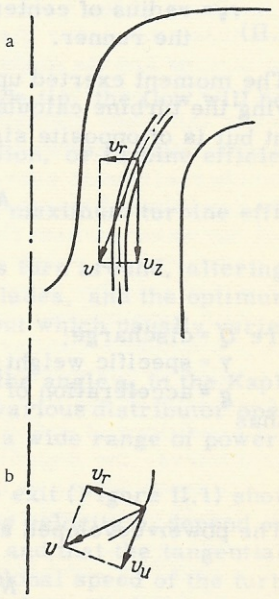


FIGURE II.2. Velocity of a water particle in the runner area (a) in meridian and (b) horizontal planes

After a time interval Δt, a quantity of water having the mass m reaches the runner blades (Figure II. 1). According to the law of mass conservation, the same quantity is discharged from the runner.

By v_1 we denote the mean velocity of a water particle before entering the blade, and by v_2 the mean velocity after its exit.

At the entrance to the blade the mass m, having the velocity v_1 carries the momentum mv_1 and after leaving the runner it carries the momentum mv_2 away into the draft tube.

It is known that a variation in the momentum of a mass in a unit of time is proportional to the force exerted on it.

This force is the runner reaction.

Let the velocity have radial, axial, and tangential components (Figure II. 2) v_r, v_z, and v_u respectively

$$v = \sqrt{v_r^2 + v_z^2 + v_u^2}.$$

As can be seen from the figure, the moment of the components v_r and v_z with respect to the turbine axis is zero. Hence, the moment of the velocity v is determined only by the component v_u. The variation in the moment of momentum of the mass m during time Δt equals the product of the moment of the driving forces (M) and their action time Δt

$$M\Delta t = mr_2v_{u2} - mr_1v_{u1} \text{ or } M = \frac{m}{\Delta t}(r_2v_{u2} - r_1v_{u1}),$$

where r_1 = radius of center of gravity of the water mass at the entrance to the runner;

r_2 = radius of center of gravity of the water mass at the exit from the runner.

The moment exerted upon the blade by the stream, i. e., the moment driving the turbine calculated in terms of absolute values, equals this moment but is of opposite sign, i. e.,

$$M_T = -M = \frac{m}{\Delta t}(r_1v_{u1} - r_2v_{u2}),$$

but

$$m = \frac{Q\gamma}{g}\Delta t,$$

where Q = discharge;

γ = specific weight;

g = acceleration of gravity;

thus

$$M_T = \frac{Q\gamma}{g}(r_1v_{u1} - r_2v_{u2}).$$

The power developed at the turbine shaft is

$$N_T = M_T\omega = \frac{Q\gamma}{g}(r_1v_{u1} - r_2v_{u2})\omega,$$

where ω = the angular velocity.

Since the peripheral velocities at the entrance and exit are $r_1\omega = u_1$ and $r_2\omega = u_2$, respectively, then

$$N_T = \frac{Q\gamma}{g}(v_{u1}u_1 - v_{u2}u_2).$$

The turbine power is also

$$N_T = \gamma QH\eta.$$

By inserting N_T into the foregoing equation, we obtain

$$\eta g H = v_{u1} u_1 - v_{u2} u_2. \qquad \text{(II. 1)}$$

This equation may also be written as:

$$\eta g H = \frac{\Gamma_1 - \Gamma_2}{2\pi} \omega,$$

where $\Gamma_1 = 2\pi v_{u1} r_1$ - circulation before the runner;
$\Gamma_2 = 2\pi v_{u2} r_1$ - circulation after the runner.

These equations show that the moment transmitted to the runner equals the difference between the moments of momentum, at the inlet and the outlet of the runner, of a mass of water Q flowing through the turbine during unit time.

This relationship was found by Euler (in 1754), who was also the first to prove the necessity of a distributor (guide vanes) in the hydraulic turbine.

The absolute water velocity v_1 created by the distributor at the entrance to the runner, together with the relative velocity w_1 and the tangential runner velocity u_1 form a closed triangle (Figure II. 1). A primary condition is that w_1 must be tangential to the entrance tip of the runner blade. When this is so

$$\frac{v_1}{\sin \beta_1} = \frac{w_1}{\sin \alpha_1} = \frac{u_1}{\sin (\beta_1 - \alpha_1)}. \qquad \text{(II.2)}$$

If the direction of w_1 is not tangential to the blade tip, the flow will be accompanied by additional energy losses.

Consequently, the efficiency of energy conversion, or turbine efficiency, depends on the value of angle α_1.

The optimum value of α_1 which corresponds to maximum turbine efficiency, is called the shockless-inlet angle.

When the turbine load changes, the guide vanes turn around, altering the angle α_1. Francis turbines have fixed runner blades, and the optimum value of α_1 corresponds only to normal power output which usually varies between $^3/_4$ and $^7/_8$ of the rated power.

Through the adjustment of the runner blades, the angle α_1 in the Kaplan turbines remains close to the optimum value for various distributor openings. These turbines have high efficiencies over a wide range of power variation.

The triangle of outflow velocities at the runner exit (Figure II.1) shows that the magnitude and the direction of the absolute velocity v_2 depend on the value and direction of the relative velocity w_2 and that the tangential runner velocity u_2 is constant for a constant rotational speed of the turbine.

When designing a runner, normal practice is to have the lowest possible value for v_2. This value cannot equal zero, since then the water discharge would be nil.

For this purpose, the runner blades are shaped in such a manner that the tangential projection of the velocity v_2 becomes $v_{u2}=0$, i. e., the velocity v_2 becomes perpendicular to u_2.

In effect, the vanishing of v_{u2} means that the vector v_2 lies in the same plane as the turbine axis, and, consequently, that the water passes from the runner to the draft tube without whirling (rotation).

Laboratory research carried out in recent years in the U. S. S. R. shows that for certain types of turbines a small positive whirl in the direction of rotation has a favorable influence on turbine efficiency.

If the water flow at the exit is axial and $v_{u2} = 0$, the fundamental formula becomes

$$\eta g H = v_{u1} u_1. \qquad \text{(II.3)}$$

Analysis of the fundamental formula shows that energy conversion in the runner depends (neglecting losses) on blade design.

8. SIMILARITY LAWS AND DIMENSIONLESS NUMBERS

In turbine construction it is common practice to design the water passages of the turbine first, and then test them on a laboratory model. These results are finally applied in the construction of the full-scale turbine.

In laboratory model tests, the similarity laws must be observed, and in particular, the requirements of geometrical, kinematic, and dynamic similarity.

The basic conditions of geometrical similarity require that the streamlined surfaces of the water passages should be similar in configuration. In other words, the linear dimensions of the streamlined surfaces of the prototype turbine and its model have to be proportional.

Quite often, however, only the runner undergoes tests, whereas the influence of the other elements of the water passages, which are not modeled (scroll case, distributor, draft tube, etc.), are allowed for by modifying the characteristic curves obtained by testing.

The condition of kinematic similarity refers to the similarity of the pattern of the water stream flowing through the water passages of the turbines being compared, in which case, as in geometrically similar turbines, the absolute and relative velocities and their components have the same directions, with proportional values at corresponding flow points. The condition of kinematic similarity thus equates with the similarity of the velocity triangles at corresponding points of the flow. This condition is called the isogonality of the flow pattern.

The conditions of dynamic similarity are defined by the equality of several parameters: the Reynolds number (Re), which expresses the ratio of inertia to viscous forces at corresponding points of geometrically similar turbines; the Froude number, which expresses the ratio of inertia to gravity forces, etc.

All similarity conditions cannot be simultaneously fulfilled. The equality of Reynolds numbers for model and prototype, for instance, is practically impossible to obtain. On the other hand, numerous tests have shown that for $\mathrm{Re} > 10^6$, which is usually the case for full-scale and model turbines alike, any changes in the Re number do not markedly affect the flow pattern.

The influence of the Re number on the turbine efficiency, as well as of the difference in the roughness between prototype and model, are allowed for by empirical approximate formulas.

Relationship (II.2) is determined from the triangle of inflow velocities

$$\frac{v_1}{\sin \beta_1} = \frac{w_1}{\sin \alpha_1} = \frac{u_1}{\sin (\beta_1 - \alpha_1)}.$$

Similarly, from the triangle of outflow velocities, we obtain

$$\frac{v_2}{\sin \beta_2} = \frac{w_2}{\sin \alpha_2} = \frac{u_2}{\sin (\beta_2 - \alpha_2)}.$$

Hence

$$\left.\begin{aligned} v_1 &= \frac{u_1 \sin \beta_1}{\sin (\beta_1 - \alpha_1)}; \\ w_1 &= \frac{u_1 \sin \alpha_1}{\sin (\beta_1 - \alpha_1)}; \\ v_2 &= \frac{u_2 \sin \beta_2}{\sin (\beta_2 - \alpha_2)}; \\ w_2 &= \frac{u_2 \sin \alpha_2}{\sin (\beta_2 - \alpha_2)}; \\ v_{u1} &= v_1 \cos \alpha_1 = \frac{u_1 \sin \beta_1 \cos \alpha_1}{\sin (\beta_1 - \alpha_1)}; \\ v_{u2} &= \frac{u_2 \sin \beta_2 \cos \alpha_2}{\sin (\beta_2 - \alpha_2)}. \end{aligned}\right\} \qquad \text{(II.4)}$$

By using the expressions (II.4), we rewrite the fundamental formula (II.1), with due allowance for the fact that

$$u_2 = K u_1,$$

where $K = \frac{D_2}{D_1}$.

We then obtain

$$\eta g H = \frac{u_1^2 \sin \beta_1 \cos \alpha_1}{\sin (\beta_1 - \alpha_1)} - \frac{u_1^2 K^2 \sin \beta_2 \cos \alpha_2}{\sin (\beta_2 - \alpha_2)},$$

whence

$$u_1 = \sqrt{\frac{\sin (\beta_1 - \alpha_1) \sin (\beta_2 - \alpha_2)}{\cos \alpha_1 \sin \beta_1 \sin (\beta_2 - \alpha_2) - K^2 \sin \beta_2 \cos \alpha_2 \sin (\beta_1 - \alpha_1)}} \cdot \sqrt{\eta g H},$$

or, denoting the expression under the radical sign by K_u, we obtain

$$u_1 = K_u \sqrt{\eta g H} \qquad \text{(II.5)}$$

and similarly

$$v_1 = K_v \sqrt{\eta g H}; \qquad \text{(II.6)}$$

$$w_1 = K_w \sqrt{\eta g H}. \qquad \text{(II. 7)}$$

The coefficients K_u, K_v and K_w, which are direct factors of the angles α_1, β_1, α_2, and β_2, are identical for turbines of the same type operating under isogonal conditions.

Consequently, the flow velocity of the water in homologous turbines is proportional to $\sqrt{\eta g H}$.

The relationship between the speed (rpm), discharge, and power of two homologous turbines may be determined from the expressions (II.5), (II.6), and (II.7).

The peripheral velocity at the entrance to the runner is

$$u_1 = K_u \sqrt{\eta g H} = \frac{\pi D_1 n}{60}.$$

Consequently, for two homologous turbines a and b, if we disregard the differences in their efficiencies, we obtain

$$\frac{n_a}{n_b} = \frac{D_{1b}\sqrt{H_a}}{D_{1a}\sqrt{H_b}}. \qquad \text{(II.8)}$$

The water discharge through the turbine runner

$$Q = Fwz = zFK_w \sqrt{\eta g H},$$

where F = the cross-sectional area of the channel between two runner blades, perpendicular to the velocity w;

z = the number of runner blades.

For two homologous turbines a and b we have

$$\frac{Q_a}{Q_b} = \frac{D_{1a}^2\sqrt{H_a}}{D_{1b}^2\sqrt{H_b}}, \qquad \text{(II.9)}$$

since

$$\frac{F_a}{F_b} = \frac{D_{1a}^2}{D_{1b}^2}.$$

The power of the turbine

$$N = \frac{\gamma Q H \eta}{102} \text{ kw}.$$

For turbines a and b we have

$$\frac{N_a}{N_b} = \frac{Q_a H_a}{Q_b H_b}.$$

By combining with expression (II.9) we obtain

$$\frac{N_a}{N_b} = \frac{D_a^2 H_a \sqrt{H_a}}{D_b^2 H_b \sqrt{H_b}}. \qquad \text{(II.10)}$$

Formulas (II.8), (II.9) and (II.10) are called the similarity equations.

It can be seen from these expressions that, for identical turbines, the speed and discharge vary directly as the ratio of the square roots of the heads, and the turbine power is proportional to $(H_a/H_b)^{3/2}$.

Knowing the results of model tests, we may calculate from the equations the diameter for a turbine which develops the required power, when operated with a given head, speed, and discharge.

It is common practice in turbine design to use so-called unit quantities: unit speed n_1', unit discharge Q_1', and unit power N_1'.

The unit values are defined respectively as the speed, discharge, and power of a turbine having a runner diameter of 1 m, for a head of 1 m.

If we assume $D_a=1$ and $H_a = 1$ m in the formulas (II. 8), (II. 9), and (II. 10), then n_a, Q_a, and N_a will become respectively n_1', Q_1', and N_1'. Then by dropping the subscript b we obtain the following values for the unit quantities

$$\left.\begin{aligned} n_1' &= \frac{nD_1}{\sqrt{H}}; \\ Q_1' &= \frac{Q}{D_1^2\sqrt{H}}; \\ N_1' &= \frac{N}{D_1^2 H\sqrt{H}}. \end{aligned}\right\} \qquad \text{(II. 11)}$$

The unit quantities are usually determined by model tests, and apply to all homologous turbines of a given series.

The expressions (II. 11), written in the form

$$\left.\begin{aligned} n &= \frac{n_1'\sqrt{H}}{D_1} && \text{for speed} \\ Q &= Q_1' D_1^2\sqrt{H} && \text{for discharge} \\ N &= N_1' D_1^2 H\sqrt{H} = 9.81\, Q_1'\eta H\sqrt{H} D_1^2 \text{ kw} && \text{for power} \end{aligned}\right\} \qquad \text{(II. 12)}$$

may conveniently be used in the selection and computation of the basic turbine parameters.

The difference between turbine efficiencies was disregarded in the determination of the unit quantities.

It is, however, impossible to fulfill all the requirements of the similarity laws in practice. Hence, the efficiencies of geometrically similar turbines are not strictly identical, and consequently the unit quantities also differ.

In calculating the unit quantities of a prototype according to model test results, with allowance for efficiency differences, the following relationships are used:

$$\left.\begin{aligned} n_{1T}' &= n_{1m}'\left(\frac{\eta_T}{\eta_m}\right)^{\frac{1}{2}}; \\ Q_{1T}' &= Q_{1m}'\left(\frac{\eta_T}{\eta_m}\right)^{\frac{1}{2}}; \\ N_{1T}' &= N_{1m}'\left(\frac{\eta_T}{\eta_m}\right)^{\frac{3}{2}}. \end{aligned}\right\} \qquad \text{(II. 13)}$$

For the characterization of hydraulic turbines, A. A. Sabaneev and A. M. Chistyakov / 93/ suggested the so-called serial unit speed $n_1'^*$ and discharge $Q_1'^*$ which allow for the volumetric and hydraulic efficiencies η_g and η_h respectively. These unit values are computed from the formula

$$n_1'^* = \frac{nD_1}{\sqrt{\eta_h H}};$$

$$Q_1'^* = \frac{\eta_g Q}{D_1^2 \sqrt{\eta_h H}}.$$

These values are not used in practice, because of the difficulties encountered in the determination of efficiencies.

9. SPECIFIC SPEED

The term "specific speed" was introduced into turbine construction to characterize the hydraulic properties of a turbine in terms of speed and discharge capacity, as well as to compare various types of turbines and runners.

The specific speed is numerically equal to the rotational speed of a turbine of a given series which develops the power of N = 1 h.p. with a head of H = 1 m.

From expression (II. 8) we have

$$n_a = \frac{D_{1b}}{D_{1a}} n_b \frac{\sqrt{H_a}}{\sqrt{H_b}}.$$

Putting $n_b = n_s$; H_b = 1 m and n and H instead of n_a and H_a, we obtain

$$n_s = \frac{D_a}{D_b} \cdot \frac{n}{\sqrt{H}}. \qquad \text{(II. 14)}$$

From the expression (II. 10) we have

$$N_a = N_b \frac{D_a^2}{D_b^2} \cdot \frac{\sqrt{H_a}}{\sqrt{H_b}} \cdot \frac{H_a}{H_b}.$$

By inserting in the above relation N_b = 1 h.p. and H_b = 1 m, and, substituting N for N_a, H for H_a, we obtain

$$N = \frac{D_a^2}{D_b^2} \cdot H\sqrt{H}. \qquad \text{(II. 15)}$$

Consequently

$$\frac{D_a}{D_b} = \sqrt{\frac{N}{H\sqrt{H}}}. \qquad \text{(II. 16)}$$

By inserting (II. 16) in (II. 14), we obtain

$$n_s = \frac{n\sqrt{N}}{H\sqrt[4]{H}}, \qquad \text{(II.17)}$$

where N = turbine power, in hp;
n = speed (rpm).

By expressing the specific speed in terms of unit quantities, (II. 17) becomes

$$n_s = 3.65\, n_1' \sqrt{Q_1' \eta}, \qquad \text{(II.18)}$$

where Q_1' is expressed in m^3/sec.

The specific speed changes with changes in the operating conditions of the turbine (i. e., power or speed at given head). Hence different types of turbines may be compared in terms of specific speed only if they are designed for predetermined operating conditions.

Usually the specific speed is computed for rated power output of a turbine under computed head and normal speed. Sometimes the specific speed is computed for the operating conditions corresponding to maximum efficiency.

The basic trend in hydraulic turbine development is to increase the specific speed.

For a given power and head, an increase in specific speed permits smaller turbine dimensions and higher speed, i. e., lower weight.

As seen from equation (II.18), the specific speed may be increased by increasing the speed n_1' and the discharge Q_1'.

It is more convenient to increase the specific speed by increasing the unit discharge Q_1' since in this manner the runner diameter is reduced proportionally to the square root of the unit discharge and the rotational speed is increased proportionally to the specific speed.

From the formula which expresses the relationship between power, torque, and angular velocity

$$N = M\omega = M\frac{\pi n}{30},$$

we find that a given power may be obtained with a smaller torque, if the speed is correspondingly greater.

Consequently, smaller turbine weight and dimensions may be obtained by reducing the runner diameter D_1 and increasing the unit discharge Q_1', thus diminishing the forces acting by increasing the speed.

In order to illustrate this, Figure II.3 represents the classified [unit] runner diameters, designed to develop the power $N = 1$ h. p. under the head $H = 1$ m, for various specific speeds.

It will be seen from Figure II.3 that the specific speed of a turbine depends on the shape of its water passages. It also depends on the number and shape of the blades. When the specific speed rises, the runner dimensions decrease, and vice-versa.

Specific-speed selection is very important from the design angle. It permits a general comparison of all classes and series of turbines, and their classification according to rotational speed and discharge capacity. In common practice, however, turbines are selected by means of univer-

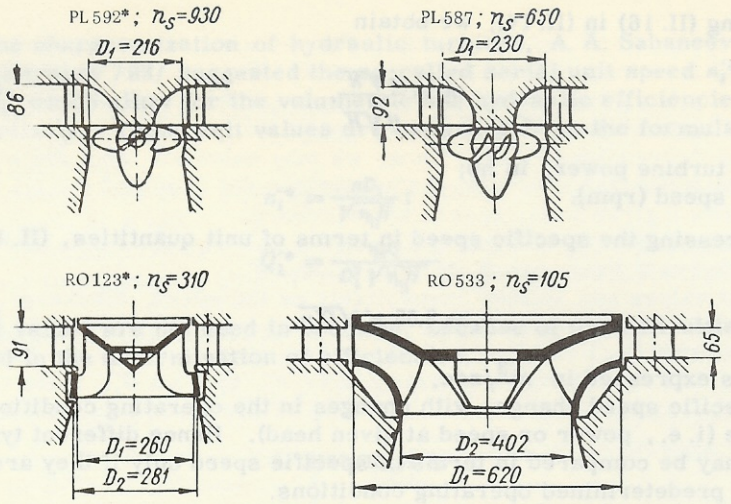


FIGURE II. 3. Dimensions of [unit] runners developing
* PL stands for Kaplan turbines; RO stands for Francis turbines.
= 1 h.p. under = 1 m for various specific speeds.

sal characteristic curves, which permit a thorough quantitative analysis of turbine parameters under any operating conditions.

10. POWER LOSSES AND EFFICIENCY OF HOMOLOGOUS TURBINES

The efficiency of a certain turbine type operating under isogonal conditions increases, as a rule, with the runner diameters, i. e., the relative power losses are smaller in the full-scale turbine than in the model.

Many investigators have paid attention to these losses and proposed a series of approximate formulas for their determination. These formulas contain correction coefficients for the efficiency when passing from the model to the full-scale turbine.

The efficiency losses of a turbine may be divided into several groups. The hydraulic losses in the water passages include losses in the scroll case, distributor, runner, and draft tube.

The (skin) friction at the runner rim (beyond the water passages) creates the so-called disk-friction losses.

The water leakages through various gaps in the water passages are called volumetric losses.

The mechanical losses caused by friction in the bearings and stuffing boxes depend on turbine parameters and construction.

We may analyze these losses in detail as follows:

1. The hydraulic losses in the water passages of the turbine are governed by the general laws of hydraulic friction in conduits. At a uniform turbulent flow, the head losses due to friction against relatively smooth walls may be expressed by the formula

$$h_T = a\frac{Lv^n}{R^m}, \qquad \text{(II.19)}$$

where R = the hydraulic radius of the flow;
a = coefficient allowing for the wall roughness;
v = the flow velocity of water;
L = the length of the water passage.

In the water passages of the turbine, the stream area changes continuously along the flow line. Formula (II. 19) is therefore valid only for a small length ΔL, for average values of R and v.

The friction losses over a certain length ΔL may be expressed

$$\Delta h_T = a \frac{\Delta L}{D_1} \cdot \frac{v^n}{D_1^{m-1}}. \qquad \text{(II. 20)}$$

In this formula, diameter D_1 instead of hydraulic radius R, is used. For geometrically similar turbines operating under isogonal conditions, $\frac{\Delta L}{D_1}$ is obviously a constant, and the velocity v varies proportionally to $\sqrt{H}$, therefore,

$$\Delta h_T = k \frac{H^{\frac{n}{2}}}{D_1^{m-1}}, \qquad \text{(II. 21)}$$

where k is a constant coefficient for similar turbines. By summarizing the friction losses for the whole stream flow, we obtain

$$h_T = \Sigma \Delta h_T = \frac{H^{\frac{n}{2}}}{D_1^{m-1}} \Sigma k,$$

or denoting $\Sigma k = K = \text{const}$, we obtain

$$h_T = K \frac{H^{\frac{n}{2}}}{D_1^{m-1}}. \qquad \text{(II. 22)}$$

The efficiency of a full-scale turbine, taking into account the losses, is

$$\eta_T = \frac{H_T - h_T}{H_T} = 1 - \frac{K}{D_{1T}^{m-1} H_T^{1-0.5n}}. \qquad \text{(II. 23)}$$

Similarly, the efficiency of the turbine model,

$$\eta_m = 1 - \frac{K}{D_{1m}^{m-1} H_m^{1-0.5n}}. \qquad \text{(II. 24)}$$

After substituting in (II. 23) the value of K from (II. 24), we obtain

$$\eta_T = 1 - (1 - \eta_m) \left(\frac{D_{1m}}{D_{1T}}\right)^{m-1} \left(\frac{H_m}{H_T}\right)^{1-0.5n}. \qquad \text{(II. 25)}$$

Replacing $m - 1$ by $\frac{1}{\alpha}$, and $1 - 0.5n$ by $\frac{1}{\beta}$, we obtain the relationship between prototype and model efficiencies.

$$\eta_T = 1 - (1 - \eta_m) \sqrt[\alpha]{\frac{D_{1m}}{D_{1T}}} \cdot \sqrt[\beta]{\frac{H_m}{H_T}}. \qquad \text{(II. 26)}$$

According to various authorities, the values of the root exponents α and β range for α from 3 to 10 and for β from 8 to ∞.

It will be seen from expression (II.26) that the over-all efficiency increases with runner diameter and effective head even if such an increase involves higher hydraulic losses.

2. The so-called "eddy-losses", caused by variations in magnitude and direction of velocity, are identical with local losses in conduits. This group also includes the kinetic-energy losses at the exit from the draft tube.

According to the conventional formulas of hydraulics, this head loss may be expressed as

$$h_v = \sum \zeta_i \frac{v_i^2}{2g},$$

where v_i and ζ_i are the velocity and the loss coefficient at the i-th flow section, respectively.

Allowing for the fact that $v = \frac{Q}{F} = \frac{Q_1' D_1^2 \sqrt{H}}{D_{1e}^2}$, we obtain

$$h_v = \sum \zeta_i \frac{Q_1'^2 H}{2g e^2}.$$

The efficiency, with allowance for these losses, equals

$$\eta_v = \frac{H - h_v}{H} = 1 - \frac{h_v}{H} = 1 - \sum \zeta_i \frac{Q_1'^2}{2g e^2} = 1 - K_v Q_1'^2,$$

where

$$K_v = \sum \zeta_i \frac{1}{2g e^2}.$$

K_v has the same value for all geometrically similar turbines operating under isogonal conditions [at large Reynolds numbers].

Consequently,

$$\eta_{vT} = \eta_{v_m} = 1 - K_v Q_1'^2. \qquad \text{(II. 27)}$$

It results from this expression that for turbines with larger unit discharge Q_1', i.e., higher specific speeds, the losses caused by velocity variations will be larger, and the efficiency smaller. This must be kept in mind.

3. The volumetric losses are due to the fact that only part of the water reaching the runner flows through it. Part of the water bypasses the runner; in Francis turbines through the shaft sealings along the rim, in Kaplan turbines through the clearances between the runner case and the throat ring.

The leakages through the clearances are computed by the formula

$$\Delta Q = \mu F \sqrt{2gH},$$

where F = cross-sectional area of the clearance space;
μ = discharge coefficient.

Since $F = eD_1^2$, then

$$\Delta Q = \mu e D_1^2 \sqrt{2gH} = K_q D_1^2 \sqrt{H},$$

where $K_q = \mu e \sqrt{2g}$.

The numerical value of coefficient Kq may be determined by computing the leakage through the labyrinth seals, or by experiments.

The volumetric efficiency, with allowance for water leakages through clearances, is

$$\eta_q = \frac{Q - \Delta Q}{Q} = 1 - \frac{\Delta Q}{Q} = 1 - K_q \frac{1}{Q_1'}. \qquad \text{(II. 28)}$$

Hence the volumetric efficiency will be smaller when Q_1' decreases, i. e., the volumetric losses for the same diameters and heads will be greater in turbines having low specific speeds.

By analyzing the experimental results of various researches, I. M. Shchapov /94/, established that the ratio of the volumetric losses of two turbines having similar water passages and seals may be determined approximately from the formula

$$\frac{\frac{\Delta Q_T}{Q_T}}{\frac{\Delta Q_m}{Q_m}} = \sqrt[6]{\frac{D_{1m}}{D_{1T}}} \cdot \sqrt[8]{\frac{H_T}{H_m}}.$$

The volumetric losses of a given turbine at a given head vary with $\frac{\sqrt[4]{n_1'}}{Q_1'}$.

However, when applying the results of model tests to actual turbines allowance must be made for the fact that the latter have more complicated seals, and the gaps are usually narrower and longer. Therefore the volumetric losses of the full-scale turbine may be smaller.

4. Mechanical losses in bearings are due to the friction of the revolving parts of the turbine.

For vertical turbines, these losses occur mainly in the thrust bearing, and their value depends on the axial load.

The power losses caused by friction in bearings are

$$\Delta N_f = M_f \omega = M_f \frac{\pi n}{30}, \qquad \text{(II.29)}$$

where M_f is the friction moment in the bearings.

The efficiency, with allowance for these losses, is

$$\eta_f = \frac{N - \Delta N_f}{N} = 1 - \frac{M_f \pi n}{30 \gamma Q H}. \qquad \text{(II.30)}$$

By writing the unit values Q_1' and n_1', instead of Q and n we obtain

$$\eta_f = 1 - \frac{M_f \pi n_1'}{30 \gamma D_1^3 H Q_1'}. \qquad \text{(II.31)}$$

In laboratory research on the model, H and D_1 usually have constant

values, and therefore we may write

$$K_{f.m} = \frac{\pi}{30\gamma D_1^3 H}$$

and the formula (II.31) becomes

$$\eta_{f.m} = 1 - K_{f.m} M_{f.m} \frac{n_I'}{Q_I'}. \qquad \text{(II. 32)}$$

For a prototype (full-scale) turbine, the head is usually variable, while the speed is constant.

By substituting in formula (II.31) $H = \left(\frac{nD_1}{n_I'}\right)^2$, we obtain

$$\eta_{f.T} = 1 - \frac{M_{fr.T}\pi n_I'^3}{30\gamma Q_I' n^2 D_1^5}.$$

Denoting

$$K_{f.T} = \frac{\pi}{30\gamma n^2 D_1^5},$$

we obtain

$$\eta_{f.T} = 1 - K_{fr.T} \frac{M_{f.T} n_I'^3}{Q_I'}. \qquad \text{(II. 33)}$$

5. Losses caused by disk friction, i. e. power losses caused by friction between the revolving surfaces of the turbine and water outside the water passages, will be greater in Francis turbines because they have larger rotating surfaces at the inner and outer bands and at their seals.

The power losses from disk friction are given by the formula

$$\Delta N_d = A D_1^5 n^3,$$

where A is a coefficient depending on the viscosity, fluidity, dimensions, and on the shape of the friction surfaces.

The efficiency, with allowance for these losses, is

$$\eta_d = 1 - \frac{\Delta N_d}{N} = 1 - \frac{A D_1^5 n^3}{\gamma Q H}. \qquad \text{(II.34)}$$

Expressing Q by Q_I' and n by n_I', we have

$$\eta_d = 1 - \frac{A n_I'^3}{\gamma Q_I'}. \qquad \text{(II.35)}$$

It follows from expression (II.35) that, for geometrically similar turbines operating under isogonal conditions, η_d will be a constant.

When the specific speed decreases, Q_I' varies more rapidly than n_I' and, disregarding the fact that n_I' in the numerator is of the third power, the power losses due to disk friction will be greater for small turbines; furthermore, with low specific speeds, turbines have longer labyrinth seals.

It appears that of all losses due to hydraulic friction, eddies, leakages, mechanical friction in bearings, and disk friction, only the mechanical losses cannot be tested on models; the hydraulic friction losses are a function of the turbine diameter and the head. As far as other losses are concerned, one may consider with satisfactory accuracy that, for geometrically similar turbines of similar design, operating under isogonal conditions, the relative value of the losses is constant.

Hence, when determining the efficiency of a prototype by model tests, one assumes that the basic losses in a turbine are governed by the law of hydraulic friction on the surfaces of the water passages, and one computes the efficiency of the prototype from the efficiency of the model, by the formula (II.26).

$$\eta_T = 1 - (1 - \eta_m) \sqrt[\alpha]{\frac{D_{1m}}{D_{1T}}} \sqrt[\beta]{\frac{H_m}{H_T}}.$$

The correction, allowing for the influence of the magnitude of head, is usually not applied for small and medium heads; the efficiency for $H < 100$m is computed from the formula

$$\eta_T = 1 - (1 - \eta_m) \sqrt[4]{\frac{D_{1m}}{D_{1T}}}. \qquad \text{(II. 36)}$$

when one assumes that $\alpha = 4$.

However, some investigators recommend $\alpha = 5$, which apparently is more in conformity with actual practice.

Formula (II.36) then becomes

$$\eta_T = 1 - (1 - \eta_m) \sqrt[5]{\frac{D_{1m}}{D_1}}. \qquad \text{(II.37)}$$

Others, by putting $\alpha = 4$, suggest that 25% of the losses $1 - \eta_m$ do not depend on the turbine diameter, and introduce the correction to the remaining 75% $(1 - \eta_m)$.

The efficiency formula takes the form

$$\eta_T = 1 - 0.25 (1 - \eta_m) - 0.75 (1 - \eta_m) \sqrt[4]{\frac{D_{1m}}{D_1}}. \qquad \text{(II. 38)}$$

For heads $H > 100$ m the following formula is usually applied

$$\eta_T = 1 - (1 - \eta_m) \sqrt[4]{\frac{D_{1m}}{D_1}} \cdot \sqrt[10]{\frac{H_m}{H_T}}. \qquad \text{(II.39)}$$

LMZ designers use formula (II.36) for heads $H < 100$m; the efficiency calculated from formula (II.36) is reduced by Δ according to the table given below

Runner diameter D_1, m	Δ, %
1.2—1.8	1.0
2.0—2.75	0.9
3.0—4.1	0.8
4.5—6.0	0.7
6.6—9.0	0.5

LMZ designers disregard the correction for the magnitude of head. The corrections determined according to LMZ practice, yield values close to those computed by formula (II.37) with the index $\alpha = 5$.

The computed correction for efficiency becomes more accurate as operating conditions approach the optimum.

For loads below optimum efficiency, the relative value of other than friction losses increases. The eddy losses increase even more rapidly, as a consequence of the deviation of the flow conditions from the conditions of shockless inlet and normal outlet from the runner.

The absolute value of the mechanical losses remains constant, but their relative value increases for low-power turbines. Hence efficiency correction according to the foregoing formulas leads too high values for small loads.

For geometrically similar turbines, LMZ designers introduce the correction in the following way:

1. For Francis and axial fixed-blade turbines, the correction $\Delta\eta = \eta_T - \eta_m$ applies equally at any point on the universal characteristic for efficiencies greater than 75%, and is computed for maximum efficiency, i. e., for a certain point on the curve we have

$$\eta_T = \eta_m + \Delta\eta = \eta_m + (\eta_{T\,opt} - \eta_{m.opt}). \qquad (II.40)$$

2. For Kaplan turbines, the $\Delta\eta$ correction is determined from the maximum efficiency on the runner characteristic for each given runner blade angle, φ_1 its value being kept constant along the lines $\varphi_1 = \text{const}$ of the universal characteristic. Very often complete geometric similarity is not achieved; for instance, the draft tube and throat ring differ in shape and proportions. It is thus necessary to introduce a correction to the efficiency which allows for the influence of those parts not to scale.

At present, both in the U. S. S. R. and abroad, research is being carried out to find new efficiency formulas, more adequate to the present development of the theory of hydraulic turbines.

The basic idea of these new methods is to split up the turbine losses into components according to their point of occurrence, and to find the relationship between hydraulic losses and turbine size and head, according to the most recent hydrodynamical data. In model tests, mechanical losses are either determined separately, or completely eliminated, and the conversion calculations are carried out for hydraulic losses only.

At the TsKTI, attempts are being made under I. E. Etinberg's guidance, to establish a calculation method for converting the efficiency of Kaplan turbine models to full-scale sizes.

Basically, this method is as follows. The main hydraulic losses in the Kaplan turbine are regarded as those in the runner and draft tube. According to their origin, these losses are divided into profile and exit losses in the runner, and internal and outlet losses in the draft tube. The profile losses in the runner blades are taken to be similar to the losses in a blade cascade immersed in a viscous liquid. The exit losses may be computed similar to the induced resistance of a finite-span wing. Finally, the internal and outlet losses in the draft tube may be calculated by means of experimental flow measurements on models. By summing up the losses in various areas we obtain the balance of losses in turbines of various specific speeds. The

calculations of the balance of losses showed that the fraction of each kind of loss in the total losses for turbines of different specific speeds is almost the same, and may therefore be assumed to be equal.

Since the profile losses in the runner and the internal losses in the draft tube are caused by the viscosity of the liquid, they may be computed by means of the Reynolds number. Therefore, these losses have to be calculated afresh when passing from the model to the full-scale turbine. The exit losses in the runners, which in character are actually eddy losses, as well as the outlet losses in the draft tube, obviously do not depend on the Reynolds number Re ; therefore, they may be considered identical both in model and full-scale turbine.

On the basis of the foregoing considerations, a formula has been suggested below for converting hydraulic efficiency from model to full-scale:

$$\frac{1-\eta_T}{1-\eta_m} = \varepsilon + (1-\varepsilon)\left(\frac{Re_m}{Re_T}\right)^{\frac{1}{n}},$$

where ε = coefficient depending on the operating conditions of the turbine, and n = 5 to 7.

The ratio of Reynold numbers is

$$\frac{Re_m}{Re_T} = \frac{D_m}{D_T}\sqrt{\frac{H_m}{H_T}}.$$

The computation of the balance of losses shows that for optimum operating conditions $\varepsilon = 0.5$.

By putting $n = 5$, the formula becomes

$$\frac{1-\eta_T}{1-\eta_m} = 0.5\left[1 + \left(\frac{Re_m}{Re_T}\right)^{\frac{1}{5}}\right],$$

the well known Ackeret formula.

At present, research is under way to determine the relationship between ε and the operating conditions of the turbine more accurately, as well as the value of the index n.

11. CAVITATION COEFFICIENT AND DRAFT HEAD

In reaction turbines, the water is discharged from the runner into the tailwater through the draft tube.

The purpose of the draft tube is:

1) to recover part of the velocity head of the flow at the runner exit;

2) to permit the runner to be set below the tailwater level without loss of head, thus simplifying the building of the powerhouse substructure.

However, this is possible up to certain limits determined by the occurrence of cavitation, which is related to the hydrodynamics of the water particles in the runner and at the entrance to the draft tube.

Cavitation is a complicated physical phenomenon, which appears in hydraulic turbines in two stages.

In the first stage, the so called "cold boiling" [formation of water-vapor bubbles] occurs, accompanied by slight damage to the blades. Cavitation becomes more extensive during the second stage, which is characterized by a loss of efficiency, severe vibration and a sudden drop in power output.

Research has shown that when the water has a high velocity, or when a solid body moves rapidly within it (e. g., the propeller blades), the continuity of the flow is disturbed, and vapor-filled pockets appear in the areas of high velocity.

The possibility of cavities forming in the stream results from the equation of conservation of energy.

For $z = 0$ the Bernoulli formula becomes

$$\frac{p}{\gamma} + \frac{v^2}{2g} = \text{const.}$$

At points where the velocity v increases, the component $\frac{v^2}{2g}$ also has a higher value and the pressure decreases. As a result, at the reduction of pressure to the vapor pressure of the water for a given temperature, the water begins to boil and vapor-filled pockets are formed within the stream. These pockets (cavities) are carried away by the stream into areas of lower velocity and increased pressure. Here, the vapor will condense instantaneously.

If the pockets form between the stream and a metallic surface, this surface begins to deteriorate [pitting] since, as experiments have shown, high pressures and temperatures occur when the bubble is compressed.

The compression of the cavitational bubble also sets up electrical phenomena, which create bubble luminescence.

Observations showed that the cavitation bubbles oscillate continuously, and resonance occurs under certain flow conditions. The pressure around the bubble may reach extremely high values of the order of 15,000 atm.

If the cavitation bubbles oscillate near the surface of a turbine, they act like sharp cutting tools, and destroy the metal surface.

Chemical reactions add to the mechanical action, since cavitation is associated with evolution of oxygen-rich gases, which enhance oxidation, intensively corroding the metal.

Usually the zones on the back of the blades near the exit of the stream flow, the outer band of the Francis runner, and the throat ring of the Kaplan turbine, are zones of high velocity, and it is here that cavitation is liable to occur.

As stated above, cavitation may appear only if the absolute pressure is smaller than the vapor pressure, i. e.,

$$\frac{p}{\gamma} \leqslant \frac{p_v}{\gamma}. \qquad \text{(II.41)}$$

The temperature of vaporization $t°$ decreases with the reduction in pressure. Figure II. 4 represents the vapor pressure plotted against the water temperature. From this curve, one may determine the pressure drop and temperature at which cavitation pockets are liable to appear.

The pressure in the stream close to the runner outlet, in the area where the highest water velocities appear, may be determined by means of the Bernoulli formula. The Bernoulli formula for the relative motion between the point κ of minimum pressure on the blade, and the point *2* after the runner belonging to the same flow line, may be written

$$z_\kappa + \frac{p_\kappa}{\gamma} + \frac{w_\kappa^2}{2g} - \frac{u_\kappa^2}{2g} = z_2 + \frac{p_2}{\gamma} + \frac{w_2^2}{2g} - \frac{u_2^2}{2g} + \Delta h_{\kappa-2}. \qquad \text{(II.42)}$$

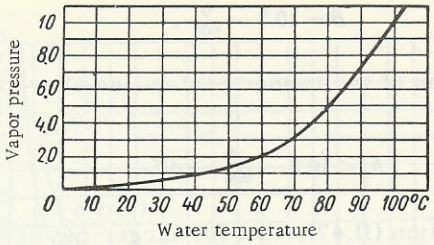


FIGURE II.4. Vapor pressure as a function of water temperature

The Bernoulli formula for the flow between point 2 and point 5 in the tailwater of the HEP may also be written

$$z_2 + \frac{p_2}{\gamma} + \frac{v_2^2}{2g} = B + \Delta h_{2-5}. \qquad \text{(II.43)}$$

By combining equations (II.42) and II.43) we obtain the pressure at point κ

$$\frac{p_\kappa}{\gamma} = B - z_\kappa - \left(\frac{v_2^2 + w_\kappa^2 - w_2^2 + u_2^2 - u_\kappa^2}{2g} - \Delta h_{\kappa-5} \right), \qquad \text{(II.44)}$$

where B = atmospheric pressure in m W. G.

$z_k = h_s$ = elevation above tailwater level of point κ (called the theoretical static draft head).

The magnitude shown in parentheses is basically a dynamic pressure developed by the flow. The ratio of this value to the total head is called the cavitation coefficient (number) of the runner or turbine.

$$\sigma = \frac{\frac{v_2^2 + w_\kappa^2 - w_2^2 + u_2^2 - u_\kappa^2}{2g} - \Delta h_{2-5}}{H}. \qquad \text{(II.45)}$$

By inserting this coefficient into the equation (II.41) we obtain

$$B - h_s - \sigma H \geqslant \frac{p_v}{\gamma},$$

whence the permissible draft head is

$$h_s \leqslant B - \sigma H - \frac{p_v}{\gamma}.$$

The ratio $\frac{p_v}{\gamma}$ may be neglected due to the small value of the vapor pressure at normal temperatures. Then

$$h_s < B - \sigma H.$$

The atmospheric pressure B depends on the elevation of the power plant above sea level.

B is usually determined from the formula

$$B = 10.3 - \frac{\nabla}{900}. \qquad \text{(II. 46)}$$

where ∇ is the elevation of the runner center line above sea level.

Finally, we obtain

$$h_s \leqslant 10.3 - \frac{\nabla}{900} - \sigma H. \qquad \text{(II. 47)}$$

It follows from relation (II.47), that for larger cavitation coefficients, a smaller draft head must be chosen.

The permissible value of the cavitation coefficient may be computed from the relation (II.47)

$$\sigma_s = \frac{-h_s + 10.3 - \frac{\nabla}{900}}{H}. \qquad \text{(II. 48)}$$

σ_s is usually termed the cavitation coefficient of the power station, because it depends only upon H, elevation (∇), and h_s, i.e., the three main parameters of the plant.

Relationship (II.45) characterizes the cavitation coefficient as a function of the runner parameters. σ_T is therefore called the turbine cavitation coefficient.

Modern turbine construction aims at increased runner discharges and hence increased runner speed and reduced head losses in the draft tube, which in turn favors the occurence of cavitation phenomena.

The turbine cavitation coefficient σ_T is usually determined by laboratory tests on models. It has a definite value for each runner and every set of operating conditions, and is plotted on the universal characteristic of the turbine in the form of special curves.

It is obvious that in order to eliminate cavitation, the turbine cavitation coefficient should be smaller than the plant cavitation coefficient $\sigma_T < \sigma_s$.

This can be achieved either by selecting turbines with small σ_T, or by increasing σ_s. To increase σ_s it becomes necessary to lower the draft head.

This, however, involves a greater amount of constructional work on the erection of the substructure. Hence the tendency is to use turbines with a smaller σ_T, i. e., with improved cavitation characteristics.

From the above it follows that the improvement of the cavitational properties of the turbine is of great importance as it permits the construction cost of the hydroelectric plant to be reduced.

It is difficult to determine the theoretical value of the draft head h_s, for the exact position of point κ is sometimes unknown. It is therefore common practice in the U. S. S. R. to calculate the relative (unit) value of H_s for a given type of turbine from a certain plane in the runner region.

For vertical Francis turbines, H_s is considered as the difference in elevation between the surface of the lower ring of the distributor and the tailwater level.

For Kaplan turbines the draft head is considered as the difference in elevation between the blade-adjustment axis and the tailwater level.

For horizontal-shaft turbines, the draft head is considered as the difference in elevation between the highest point of the runner blades and the tailwater level. This is due to the fact that in these turbines the most unfavorable cavitation conditions occur on the periphery of the blades at their highest point.

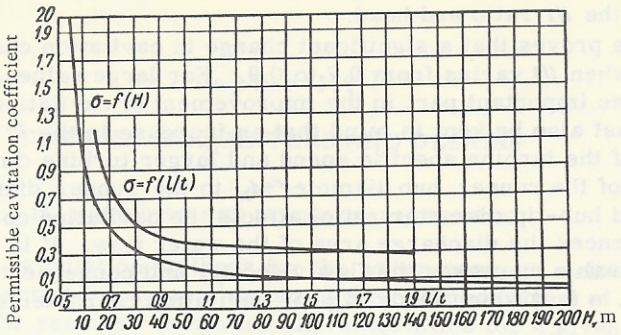


FIGURE II.5. The cavitation coefficient, as a function of head H and the ratio l/t

The draft head for vertical turbines is sometimes taken as the distance between the middle of the distributor height and the tailwater level. Denoting this head by H'_s, we obtain

a) for the Francis turbine

$$H'_s = H_s + \frac{b_0}{2};$$

b) for the Kaplan turbine

$$H'_s = H_s - \varepsilon D_1,$$

where b_0 = height of the distributor;

ε = coefficient allowing for the distance between the blade-adjustment axis and the middle of the distributor height.

The draft head is considered positive if the tailwater level is below the relative elevations mentioned above; conversely, the head is negative if the runner setting is below the tailwater level.

When designing a turbine and selecting the draft head, the general aim is to achieve cavitation-free operating conditions. It is, however, impractical to try to avoid cavitation completely, because the reduction of the turbine elevation with respect to the tailwater level usually involves a considerable increase in the amount of excavation for the substructure. Therefore, the turbine manufacturer, in his technical conditions, usually stipulates the permissible amount of damage due to cavitation in the metallic parts of the water passages.

Only such damage is permitted as may be repaired on the spot without dismantling the turbine.

When designing new turbine runners, the cavitation characteristics may be improved by increasing either the number of blades, or the ratio of blade

length to blade pitch l/t (pitch ratio), i. e., by increasing total blade area. Thus, as a consequence of the reduced specific load on the blade, the depression on its convex side is reduced.

However, a considerable increase in the l/t ratio without changing the number of blades leads to large-size blades, thus rendering their fastening to the hub more difficult. Figure II. 5 shows the approximate dependence of σ on the l/t ratio and head.

This curve proves that a significant change in cavitation characteristics occurs only when l/t varies from 0.7 to 0.9. For large values, the ratio l/t plays a less important part in the improvement of cavitation characteristics. It must also be kept in mind that an increase in the l/t ratio means a reduction of the turbine specific speed and larger turbine dimensions.

The ratio of the runner hub diameter d_h to the runner diameter D_1 (the so-called hub-tip diameter ratio) affects the cavitation coefficient, since it influences the discharge area of the water flow. It is obvious that a greater l/t value increases the flow velocity, and consequently reduces the pressure, a fact which leads to poor cavitation characteristics.

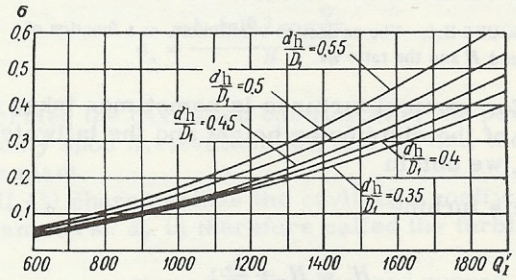


FIGURE II. 6. Dependence of the cavitation coefficient on the hub-tip diameter ratio

Figure II.6 shows (according to LMZ data) the relationship between the value and the unit discharge Q_1' for various hub-tip diameter ratios. Thus, for instance, for Q_1' = 1500 and a hub-tip diameter ratio $\frac{d_h}{D_1}$ = 0.35, the cavitation coefficient σ = 0.25, and for $\frac{d_h}{D_1}$ = 0.55, we have σ = 0.38, i.e., an increase of 50%. Consequently, in order to improve Kaplan turbine cavitation characteristics, the hub-tip diameter ratio should be lowered.

Chapter III

TURBINE PARAMETERS AND DESIGNS

12. MODEL TESTS AND TURBINE CHARACTERISTICS

Present-day calculation methods for the water-passage elements of a turbine do not permit the determination of the optimum shape of the water passages with the required cavitation characteristics for a given head and discharge.

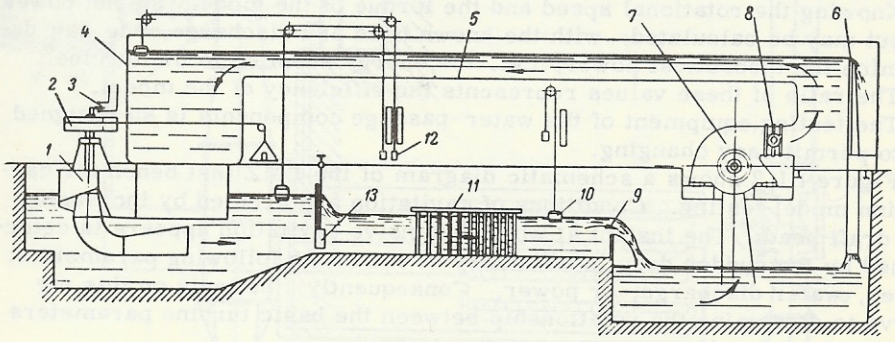


FIGURE III. 1. Schematic diagram of a power test stand for turbine models

It is more difficult still to determine the turbine power and cavitation parameters for operating conditions which differ from those rated. Hence when designing a modern turbine, several alternatives for its water passages are calculated. The most favorable shapes for the water passages are then determined by laboratory tests on models of each design variant.

The tests are carried out under a wide range of operating conditions, and their results are used to plot the turbine-characteristic curves. These curves provide an over-all picture of the power and cavitation characteristics of the turbine.

According to the problems to be investigated, laboratory installations for turbine model testing fall into two groups: for power tests and for cavitation tests.

The equipment for power tests makes it possible to investigate the relationship between the efficiency of a turbine of given design and its operating conditions.

The equipment for cavitation tests is used to investigate the relationship between the turbine cavitation coefficient and the operating conditions.

Figure III.1 gives the schematic diagram of the LMZ laboratory stand for power tests. The centrifugal pump (7), driven by an electric motor, discharges

the water through the gate valve (8) into the stilling chamber. The water enters the inflow flume (5). One of the flume walls is a sharp-crested weir, which allows the discharge of the excess water flow, in order to maintain a constant water level in the stilling chamber. From the inflow flume the water enters the pit, passing from there to the scroll case (1) of the turbine model.

The water, leaving the model draft tube, enters the inferior channel, and after passing adjustable valve (13) which regulates the tailwater level, it reaches the downstream channel of the weir. One of the channel walls (9) is built as a weir for measuring the water discharge. The stilling racks (11) (screens) are installed in front of the weir in the downstream channel.

The headwater and tailwater levels are measured by means of floats and are recorded on scale (12). Float (10) measures the level before the weir.

The rotational speed of the model shaft is measured by a revolution counter (3), automatically set for a one-minute period by means of a special electrical clock-mechanism.

The torque developed at the model shaft is balanced by means of rope brake (2). The frictional moment is balanced by the moment of the counterweight which pulls at the cable end.

Knowing the rotational speed and the torque of the model, the net power output may be calculated; with the known head and discharge, one can determine the theoretical power, i.e., the energy supplied to the turbine.

The ratio of these values represents the efficiency of the model.

The testing equipment of the water-passage components is so designed as to permit easy changing.

Figure III. 2 shows a schematic diagram of the LMZ test bench for cavitation model-testing. Conditions of cavitation are created by increasing the draft head. The instant at which extensive cavitation appears is determined by the sudden drop in efficiency of one of the following parameters: speed, water discharge, or power. Consequently, the tests on this rig serve to determine the relationship between the basic turbine parameters and the draft head.

The equipment operates on the closed-circuit principle.. The water fed by the centrifugal pump (7) circulates through the unit and does not come into direct contact with the atmosphere at any point. The negative pressure under the runner, corresponding to a given draft head, is created by means of the vacuum pump (6), which draws the air out of the pressure tank (5).

The pressure (head) in the system may be regulated by changing the rotational speed of the electric motor.

The pressure before the runner, and the vacuum in the tank, are measured during the tests by mercury pressure-gages (8).

The rate of discharge is measured by flowmeter (1), installed in front of the pressure tank.

The torque on turbine shaft (2) and the rotational speed are measured by means of brake (3) and speedometer (4).

The cavitation coefficients σ, for various discharges Q_1' and speeds n_1', are determined during the tests. Other rig layouts for power and cavitation tests are also common.

The diameters of the model runner range from 180 to 800 mm, but those most widely used in power tests have a diameter of 250 to 460 mm, and in cavitation tests, of 250 mm.

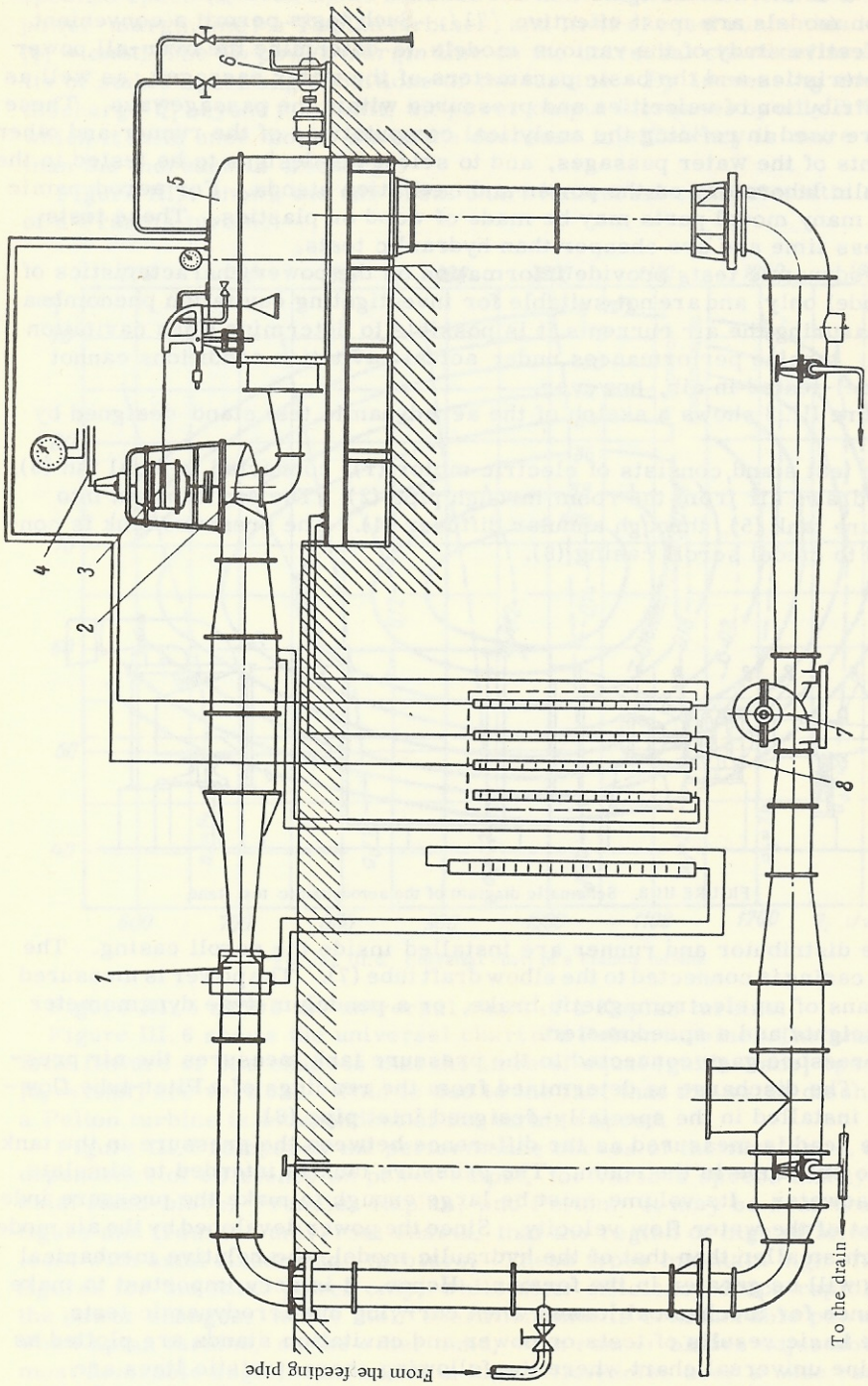


FIGURE III.2. Schematic diagram of a cavitation test stand for turbine models

For a detailed investigation of the turbine water passages, aerodynamic tests on models are most effective /71/. Such tests permit a convenient and effective study of the various models to determine the over-all power characteristics and the basic parameters of the water passages, as well as the distribution of velocities and pressures within the passageways. These data are used in refining the analytical computations of the runner and other elements of the water passages, and to select the designs to be tested in the hydraulic laboratory on the power and cavitation stands. For aerodynamic tests, many model parts may be made of wood or plastics. These tests take less time and are cheaper than hydraulic tests.

Aerodynamic tests provide information on the power characteristics of the model only, and are not suitable for investigating cavitation phenomena. By measuring the air currents it is possible to determine when cavitation begins; turbine performances under actual cavitation conditions cannot be model-tested in air, however.

Figure III. 3 shows a sketch of the aerodynamic test stand designed by TsKTI.

The test stand consists of electric motor (1), connected to axial fan (3), which draws air from the room through pipe (2). The air is blown into pressure tank (5), through annular diffuser (4). The pressure tank is connected to model scroll casing (6).

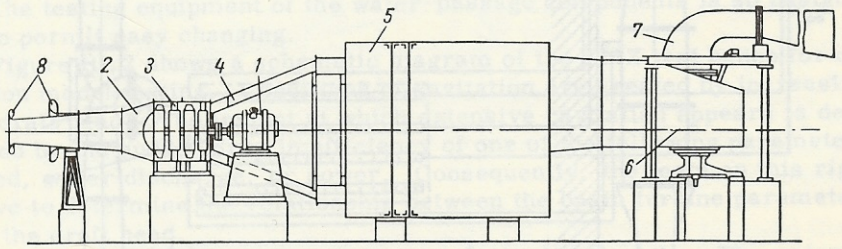


FIGURE III.3. Schematic diagram of the aerodynamic test stand

The distributor and runner are installed inside the scroll casing. The scroll casing is connected to the elbow draft tube (7). The power is measured by means of an electromagnetic brake, or a pendulum-type dynamometer with weights and a speedometer.

A pressure gage connected to the pressure tank measures the air pressure. The discharge is determined from the readings of a Pitot-tube flowmeter installed in the specially-designed inlet pipe (8).

The head is measured as the difference between the pressure in the tank and the pressure in the room. The pressure tank is intended to simulate the headwater. Its volume must be large enough to make the pressure independent of the water flow velocity. Since the power developed by the air model is much smaller than that of the hydraulic model, the relative mechanical losses will be greater in the former. Hence, it is very important to make allowance for mechanical losses when carrying out aerodynamic tests.

The basic results of tests on power and cavitation stands are plotted as a turbine universal chart where the following characteristic lines are plotted in coordinates of unit speed n_1' and unit discharge Q_1': of equal efficiency ($\eta = \text{const}$), of equal opening of the distributor ($a_0 = \text{const}$), of equal

specific speed (n_s = const), of equal cavitation coefficients (σ = const), the 5 % power-margin line for Kaplan turbines, and lines of equal runner blade angles (φ_1 = const). The 5% power-margin line on the universal chart defines the limits of stable operating conditions of the turbine. By increasing the unit discharge Q_1' beyond this limit, the power output increases by only 5 %, after which it falls once more, since the decrease in efficiency is more rapid than the increase in discharge.

Figure III.4 shows the universal chart (universal characteristic curves) of a Francis turbine.

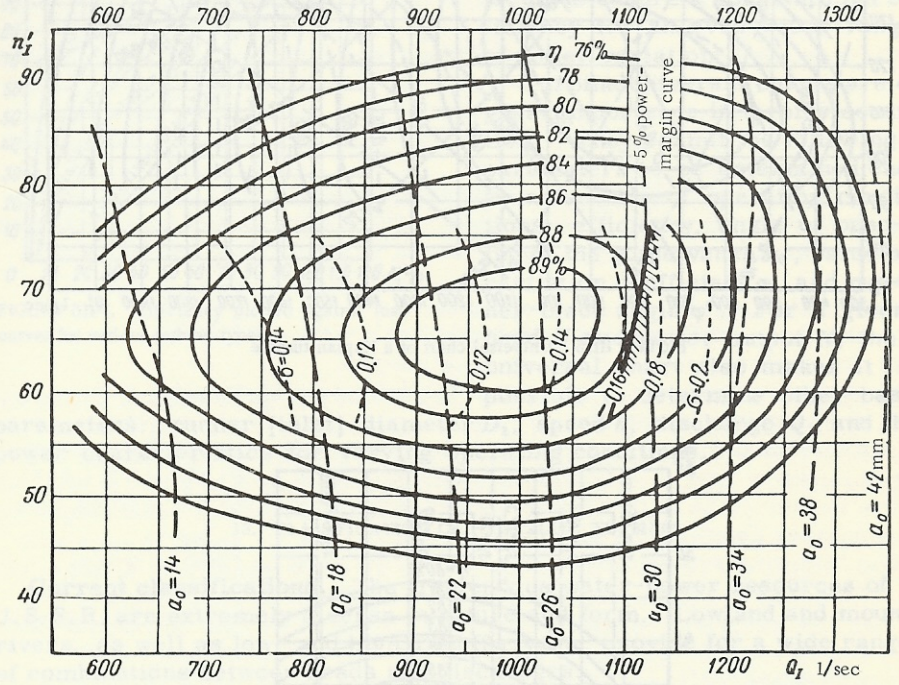


FIGURE III.4. Universal chart of a Francis turbine

Figure III. 5 shows the universal chart of a Kaplan turbine.

Figure III. 6 shows the universal chart of a Pelton turbine. The characteristic feature of this chart is that the lines of equal [guide-vane] opening [a_0 = const] are vertical. This is due to the fact that the water discharge in a Pelton turbine is independent of the turbine speed.

Figure III.7 compares the performance curves of the turbine, i. e., the dependence of efficiency on power output, for various speeds and types: axial fixed-blade, Francis, Kaplan, and Pelton. It may be seen from this figure and from the universal charts, that the region of high efficiencies is least with axial fixed-blade turbines. These types maintain high efficiency figures for the rated power only, while their efficiency drops rapidly when the power changes; hence their operation entails considerable power losses. The Kaplan turbine, on the other hand, with runner blades adjustable to the most favorable angle, can maintain high efficiencies over a wide range of power output, and its efficiency does not drop so rapidly when the head changes, as does the efficiency of axial fixed-blade turbines.

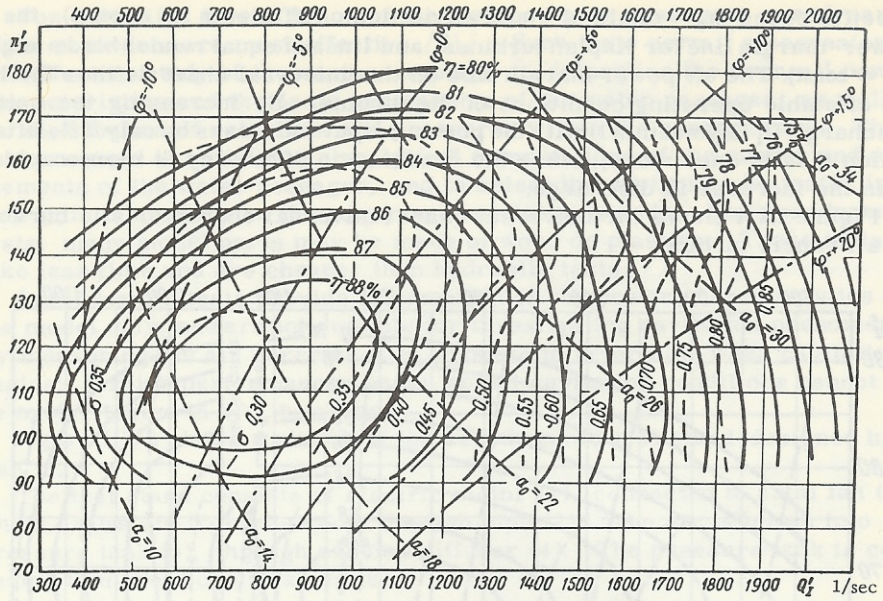


FIGURE III.5. Universal chart of a Kaplan turbine

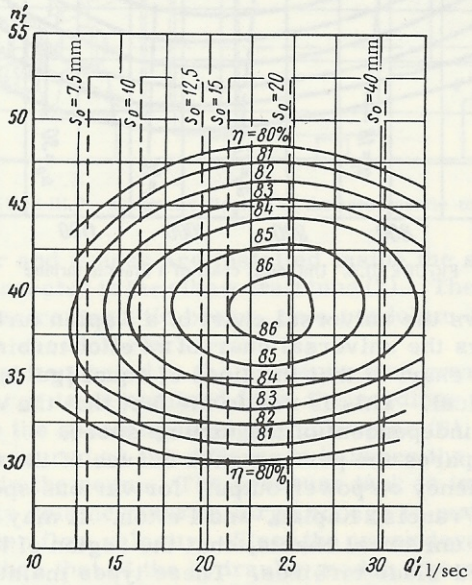


FIGURE III.6. Universal chart of a Pelton turbine

Thus, under variable operating conditions, the Kaplan turbine has a higher average efficiency and generates more power than the propeller turbine.

Both types of axial turbines are characterized by large cavitation coefficients σ and are therefore used at low heads.

As can be seen, the efficiency curves of the Francis turbine have intermediate values between those of the axial fixed-blade and Kaplan turbines.

Francis turbines have very high efficiency values, but their zone of maximum efficiency is much narrower than that of Kaplan turbines; they have a lower specific speed and larger runner diameters under the same operating conditions.

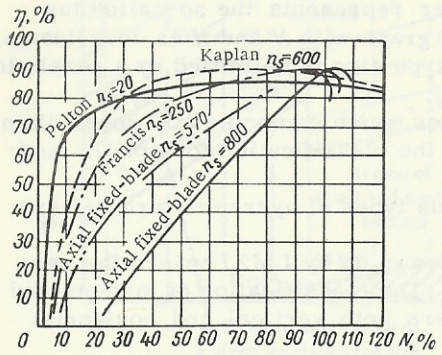


FIGURE III. 7. Efficiency plotted against load curves for various turbine types

The characteristics of the Pelton turbines ensure a constant high efficiency for an even wider range of power variation.

Turbine universal charts are of great importance in turbine construction. They permit the following parameters to be determined easily as a function of operating conditions: efficiency, angle of opening of the guide vanes a_0, value of cavitation coefficient σ, and runner-blade angle $\varphi°$. For a given head H and power output N, the universal chart also makes it possible to determine other basic parameters: runner [inlet] diameter D_1, speed n, discharge Q, and the power characteristics for varying operating conditions.

13. CLASSIFICATION OF HYDRAULIC TURBINES

Current classifications. The tremendous water-power resources of the U. S. S. R. are extremely diverse in nature and form. Lowland and mountain rivers, as well as low- and high-runoff rivers, provide for a wide range of combinations between heads and discharges.

This unique feature of water-power engineering has led to a great diversity in hydraulic turbines, as regards power output, type, dimensions, and construction.

Depending on the available head, a given power may require a turbine with a smaller or a larger runner diameter.

In the U. S. S. R., for purposes of standardization, turbines are divided into small, medium, and large-size types, depending on the power output, dimensions, and weight of their components.

In small turbines, runner diameters may attain 1.2 m for a low head and 0.5 m for a high head, with power outputs up to 1,000 kw.

Medium turbines have runner diameters up to 2.5 m for low heads and 1.6 m for high heads, with power outputs up to 15,000 kw.

Large turbines nowadays have runner diameters up to 10 m (Kaplan turbines) and 7.5 m (Francis turbines). Their power output may attain 500,000 kw.

A great deal of progress has been made toward unifying and standardizing hydraulic turbines, as a result of which turbine construction could be, to a certain degree, switched over to series production.

A classification was drawn up for the most widely-used types of large, medium, and small-size reaction turbines.

This classification divides the entire field of application of large, medium, and small reaction turbines for heads ranging from 2 to 300 m, into sections covered by the smallest possible number of standardized runner types (series).

Each series comprises several runners of the same diameter, whose number covers the whole range of required power outputs.

The combination of series and diameter represents the so-called turbine standard-type size. When plotting a graph with N and H as coordinates, the zone of application of each standard-type size is delimited by a parallelogram.

The sum total of all standard-type sizes which comprise all runner diameters and series considered, constitutes the classification for small, medium, and large-size reaction turbines.

The fields of application for the various types of hydraulic turbines are shown in Figure III. 8.

The classification of large turbines (drawn up by LMZ) covers the vertical-shaft Francis and Kaplan turbines. The classification of medium and small turbines (drawn up by VIGM) covers both vertical and horizontal turbines.

The turbine classification establishes:

1) the runner type according to head;
2) the shaft position and casing construction;
3) the basic dimensions of the turbine (runner diameters);
4) the turbine designation.

The turbine designation consists of three symbols separated by dashes: type of runner – type of installation – dimensions (e.g. PL587 – VB – 600).

The runner class is designated by two letters denoting the turbine type, and a number denoting the runner type.

The following symbols were adopted for the various turbine types: PR – axial fixed-blade; PL – Kaplan; RO – Francis; K – Pelton.

The type of installation is shown by two capital letters: the first specifies the shaft position, and the second, design of the casing.

V – vertical shaft; G – horizontal shaft; O – open flume; B – concrete scroll casing; M – steel scroll casing.

The turbine dimension is designated by the nominal runner diameter D_1 (cm).

The nominal runner diameter D_1 is (Figure III. 9):

1) in Kaplan and axial fixed-blade turbines, type (a) — the largest diameter of the throat ring;
2) in Francis turbines, (b and c), — the largest runner diameter as measured at the inlet;
3) for Pelton turbines, (d) — the diameter of the runner circle tangential to the axis of the water jet issuing from the nozzle.

The standardized rotational direction in turbines is clockwise when looking at the turbine from the generator side.

The turbine classification comprises the smallest possible number of runner types, which covers almost the entire field of application of Kaplan and Francis turbines.

Figure III. 10 gives, in logarithmic coordinates, a graphical representation of the classification for large turbines, for heads ranging from 3 to 250 m

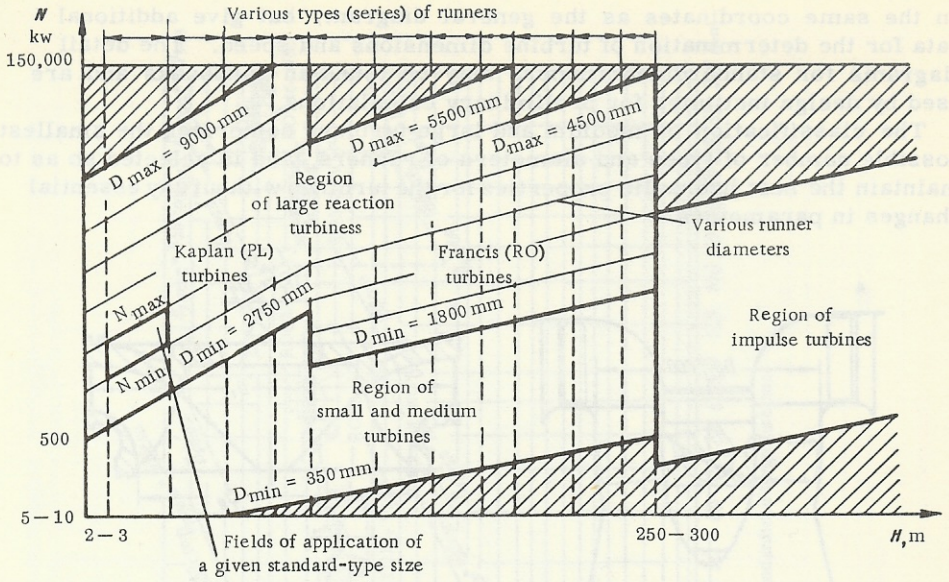


FIGURE III.8. Fields of application of various hydraulic turbines

and power outputs of up to 150,000 kw; ten turbine series (four Kaplan and six Francis) with runner diameters from 1,800 to 9,000 mm were selected.

The zones of power output for each field of application are delimited by the largest and smallest runner diameters $D_{1\,max}$ and $D_{1\,min}$. The diameters are represented by inclined parallel lines.

The zone of heads for each field is established on the basis of economically suitable draft head H_s and the mechanical strength of the runner blades.

The various types of turbines, covering the entire field of heads and power outputs of the classification for large turbines, are given in Table III. 1. This table contains also data on specific speeds, number of guide vanes, standardized runner diameters, and guide-vane circle diameters.

Figure III. 11 gives a graphical representation of small and medium-size reaction turbines /35/. On the graph, the field of application of medium turbines borders at the upper edge on the field of large turbines, and at the lower edge on the field of small turbines.

The ranges of heads from 2 to 200 m and of power output from 60 to 20,000 kw, are covered by nine types of runners - three of the Kaplan and axial fixed-blade types, and six of the Francis type.

The runner diameters vary - according to their type - between 350 and 2500 mm. The classification of medium turbines comprises only twelve runner diameters [see Table III. 2].

The basic dimensions of the standardized Kaplan runners are given in Figure III. 12, and those of the Francis runners in Figure III. 13.

These tables show that with decreasing specific speed, i.e. at high heads, the dimensions of the water passages of Kaplan and Francis turbines become less.

The turbine classification also comprises detail diagrams for the field of application of each type of turbine runner. These diagrams are plotted

on the same coordinates as the general diagram, but give additional data for the determination of turbine dimensions and speed. The detail diagrams for standardized runners may be found in handbooks and are used by design institutes for preliminary calculations.

The classification of medium and large turbines comprises the smallest possible number of types and diameters of runners, and is selected so as to maintain the best hydraulic properties for the turbines without any essential changes in parameters.

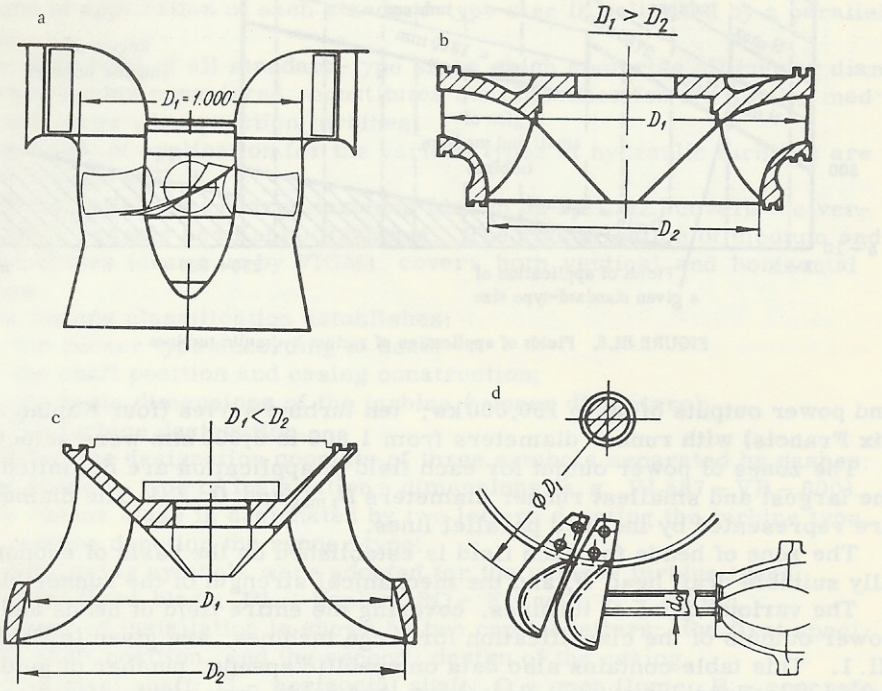


FIGURE III. 9. Nominal diameters for various types of runner

This is achieved by using the system of nominal runner diameters. Each nominal runner diameter included in the classification also defines the diameters of the turbine speed-ring elements.

The basic nominal dimension of the turbine speed-ring is the guide-vane (pitch) circle diameter D_0; the actual runner diameter D_1 may differ, under special circumstances, from the nominal value.

By expressing the discharge in the formula of the turbine power output $N = 9.81QH\eta$, in terms of the unit discharge N_1', we obtain

$$N = 9.81 Q_1' D_1^2 H^{\frac{3}{2}} \eta .$$

Thus, to achieve the required range of power outputs $N_{max} - N_{min}$ at constant head and with the smallest number of diameters in any standard series of turbines, Q_1' and D_1 should be varied.

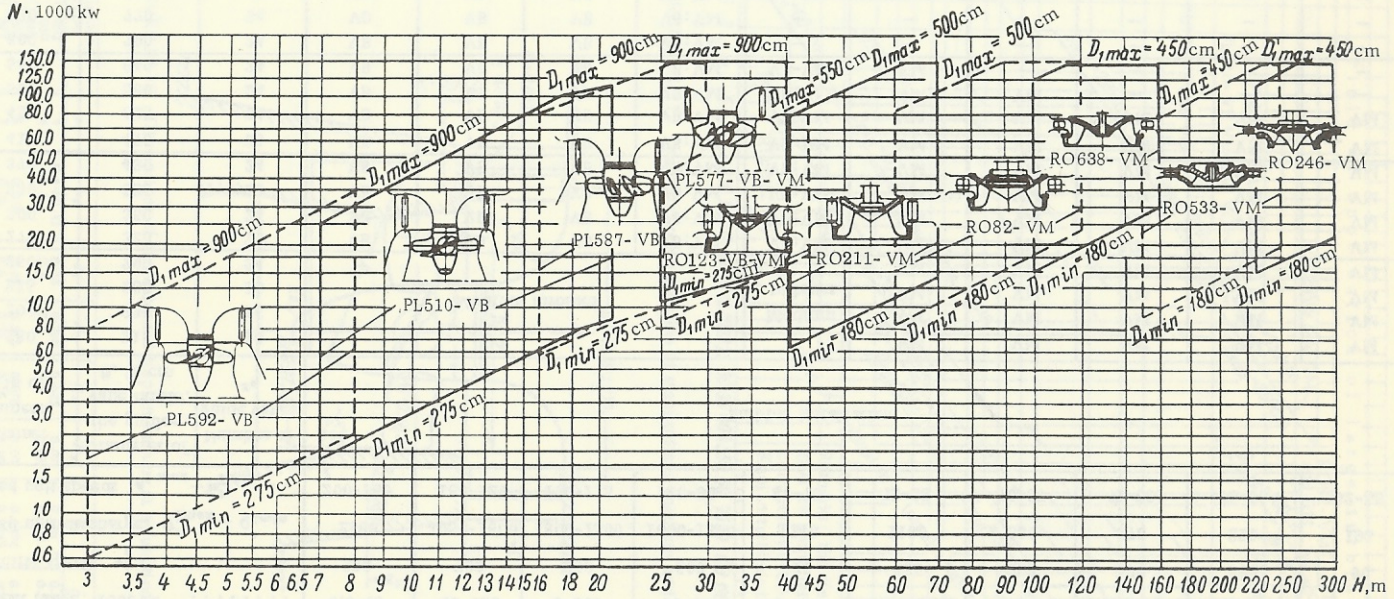


FIGURE III.10. Graphical representation of standardized large turbines

TABLE III. 1

Classes and dimensions of large turbine runners and types of installation

Parameters			Turbine system									
			Kaplan				Francis					
Runner type			PL 529	PL 510	PL 587	PL 577	RO 123	RO 211	RO 82	RO 638	RO 533	RO 246
Head range, m			3-8	7-21	16-30	25-40	25-45	40-70	60-120	100-160	150-250	130-300
Output range, 1000 kw			0.6-48	22-125	6-162	10-225	9-103	6-175	8-235	15-250	9-160	15-180
Specific speed, n_s^1			930	700	650	500	280	235	200	190	100	90
Rated unit discharges $Q'_{1max} - Q'_{1min}$			2200	1950-1600	1800-1500	1600-1300	1240	1100	800	670	220	196
Rated unit speeds $n'_{1\,max} - n'_{1\,min}$			200-160	160-120	150-115	120-90	80-70	72-58	70-57	71-65	65-55	62-55
Runner diameter, D_1 in cm	Diameter of the guide-vane circle, D_0 in cm	Number of guide vanes, z_0	Turbine installation									
180	215	16	Medium turbines				Medium turbines	VM	VM	VM	VM	VM
200	235	16						VM	VM	VM	VM	VM
225	265	16						VM	VM	VM	VM	VM
250	290	24						VM	VM	VM	VM	VM
275	320	24	VB	VB	VB	VB:VM	VB:VM	VM	VM	VM	VM	VM
300	350	24	VB	VB	VB	VB:VM	VB:VM	VM	VM	VM	VM	VM
330	385	24	VB	VB	VB	VB:VM	VB:VM	VM	VM	VM	VM	VM
370	430	24	VB	VB	VB	VB:VM	VB:VM	VM	VM	VM	VM	VM
410	475	24	VB	VB	VB	VB:VM	VB:VM	VM	VM	VM	VM	VM
450	525	24	VB	VB	VB	VB:VM	VB:VM	VM	VM	VM	VM	VM
500	580	24	VB	VB	VB	VB:VM	VB:VM	VM	VM	–	–	–
550	640	24	VB	VB	VB	VB:VM	VB-VM	VM	–	–	–	–
600	700	24	VB	VB	VB	VB:VM	–	–	–	–	–	–
660	770	24	VB	VB	VB	VB:VM	–	–	–	–	–	–
720	840	32	VB	VB	VB	VB:VM	–	–	–	–	–	–
800	930	32	VB	VB	VB	VB:VM	–	–	–	–	–	–
900	1050	32	VB	VB	VB	VB:VM	–	–	–	–	–	–

For Kaplan turbines the specific speed n_s corresponds to the point of $Q'_{1\,max}$ and $n'_{1\,max}$ on the main characteristic, and for Francis turbines to the point of optimum n'_1. on the curve of 5% power margin.

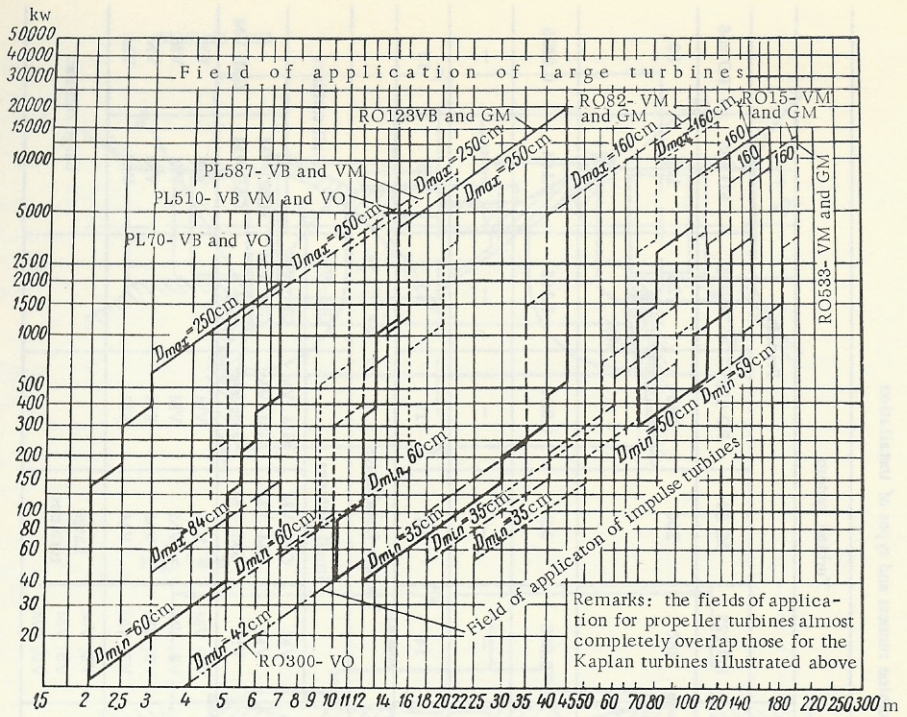


FIGURE III.11. Graphical representation of standardized medium and small turbines

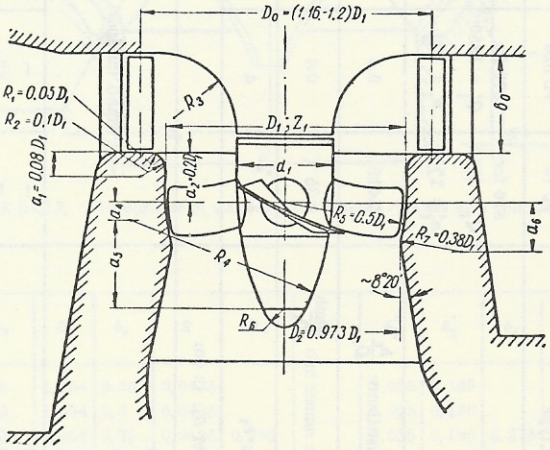


FIGURE III.12. Dimensions of standardized Kaplan runners as a function of D_1

Runner type	z_1	b_0	d_1	R_3	R_4	R_6	a_4	a_5	a_6
PL 592	4	0·4÷0·45	0.35	0·325	0·525	0·07	0·09/	0.291	0.1543
PL 510	4	0.4	0.4	0·3	0.6	0·08	0.103	0·332	0·1543
PL 661									
PL 587	6	0.376	0.45	0.275	0.675	0.09	0.1094	0.374	0.1543
PL 577	7	0·35	0.5	0·25	0·75	0.10	0.1145	0.415	0·2089
PL 642	8								

Note. The geometrical dimensions of the turbine are given in relation to the nominal runner diameter D_1.

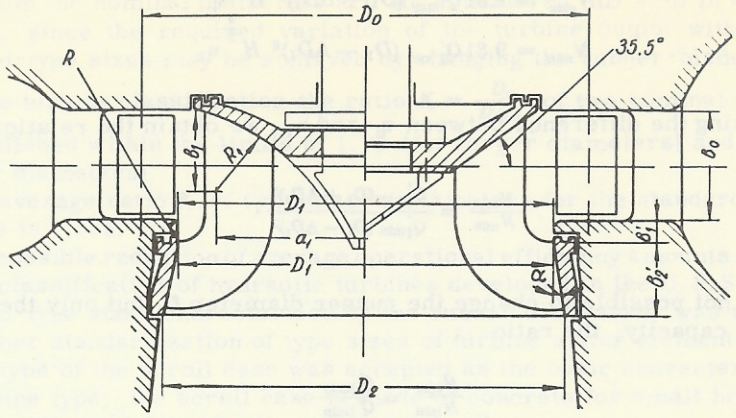
TABLE III. 2

Classes and dimensions of medium and small turbine runners and types of installation

Parameters	Turbine system								
	Kaplan			Francis					
Runner type	PL 70	PL 510	PL 587	RO 123	RO 82	RO 638	RO 15	RO 533	RO 246
Specific speed n_s^1	810 for $Q_1' = 2150$ $n_1' = 170$	670 for $Q_1' = 1850$ $n_1' = 150$	600 for $Q_1' = 1750$ $n_1' = 140$	280	200	190	120	100	90
Relative height of the distributor $\frac{b_0}{D_1}$	0.415	0.4	0.4	0.365	0.2	0.224	0.105	0.104	0.0825
Relative diameter of the runner hub $\frac{d_{hub}}{D_1}$	0.35	0.4	0.45	—	—	—	—	—	—
Number of runner blades z_1	4	4	6	14	15	17	19	15	17
Runner diameter D_1, in cm	Turbine installation								
50	Small turbines			Small turbines			GM; VM	Small turbines	
60				VM	GM; VM	GM; VM	GM; VM		
71				VM	GM; VM	GM; VM	GM; VM	GM; VM	
84				VM	GM; VM	GM; VM		GM; VM	GM; VM
100	—	—	—	VB; VM	VM	VM		VM	VM
120	—	VB	VB	VB; VM	VM	VM		VM	VM
140	VB	VB	VB	VB; VM	VM	VM		VM	VM
160	VB	VB	VB	VB; VM	VM	VM		VM	VM
180	VB	VB	VB	VB; VM	Large turbines			Large turbines	
225	VB	VB	VB	VB; VM					
250	VB	VB	VB	VB; VM					

The values of n_s for Francis turbines are given for operational conditions corresponding to the curve of 5% power margin.

Medium head



High head

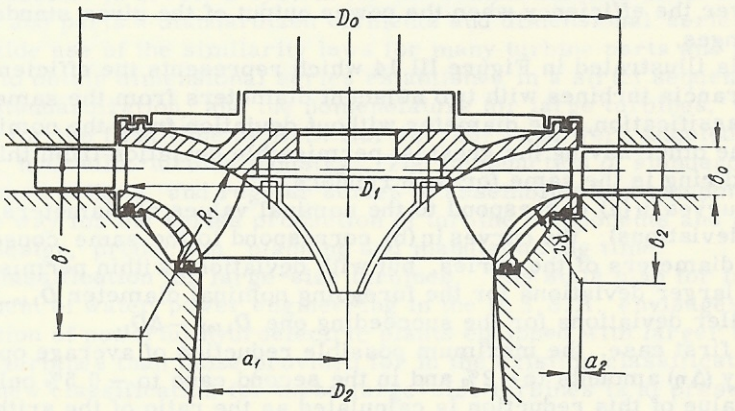


FIGURE III.13. Dimensions of standardized Francis runners as a function of D_1

Runner type	D_0	D_2	D_1'	b_0	R	R_1	R_2	b_1'	b_2'	b_1	b_2	a_1	a_2
RO 123	1.16-1.2	1.08	1.004	0.35	0.0435			0.055	0.165		0.02		
RO 211	1.16-1.2	1.09	1.004	0.3	0.0435			0.055	0.190		0.03		
RO 697	1.16-1.2	1.13	1.004	0.25	0.0435	0.275		0.055	0.190	0.275		0.765	
RO 82	1.16-1.2	1.025	1.004	0.2	0.0435			0.055	0.190		0.152		
RO 638	1.16-1.2	1.0343	1.004	0.224		0.4389		0.055	0.148	0.439		0.505	
RO 533	1.2	0.6426		0.104		0.4746	0.198				0.198		0.0129
RO 683	1.2	0.684		0.10		0.338	0.158					0.47	0.005
RO 246	1.2	0.705		0.08		0.375	0.1125				0.1065		0.0462

* Note: The dimensions of the turbine are given in relation to runner diameter.

$$N_{max} = 9.81\, Q'_{1max}\,(D_1 + \Delta D_1)^2\, H^{\frac{3}{2}}\,\eta_1;$$

$$N_{min} = 9.81\, Q'_{1\,min}\,(D_1 - \Delta D_1)^2\, H^{\frac{3}{2}}\,\eta_2$$

or, neglecting the difference between η_1 and η_2, we obtain the relation

$$\frac{N_{max}}{N_{min}} = \frac{Q'_{1max}\,(D_1 + \Delta D_1)^2}{Q'_{1min}\,(D_1 - \Delta D_1)^2}.$$

If it is not possible to change the runner diameter D_1 but only the runner discharge capacity, the ratio

$$\frac{N_{max}}{N_{min}} = \frac{Q'_{1max}}{Q'_{1min}}$$

will be smaller, and consequently, to obtain the same efficiency, it is necessary to increase the number of standardized diameters in the series, or to lower the efficiency when the power output of the given standardized size changes.

This is illustrated in Figure III.14 which represents the efficiency curves of two Francis turbines with two adjacent diameters from the same series of the classification, one diameter without deviation from the nominal value and the other having the greatest permissible deviation from this value; the speed ring is the same for both runners.

The curves in (a) correspond to the nominal values of diameters (without any deviations); the curves in (b) correspond to the same consecutive nominal diameters of the series, but with deviations within permissible limits - larger deviations for the foregoing nominal diameter $D_{1\,(n-1)} + \Delta D_1$ and smaller deviations for the succeeding one $D_{1\,(n)} - \Delta D_1$.

In the first case, the maximum possible reduction of average operational efficiency ($\Delta\eta$) amounts to ~2% and in the second case to ~ 0.5% only.

The value of this reduction is calculated as the ratio of the arithmetical means of the efficiencies corresponding to loads N, $0.9N$, $0.8N$, $0.7N$, and $0.6N$.

The above method of calculating the deviations from the nominal runner diameters D_1, maintaining the speed-ring diameter D_0 unchanged, may be applied only to Francis turbines, as these permit variation in relatively narrow limits of discharge capacity Q'_1.

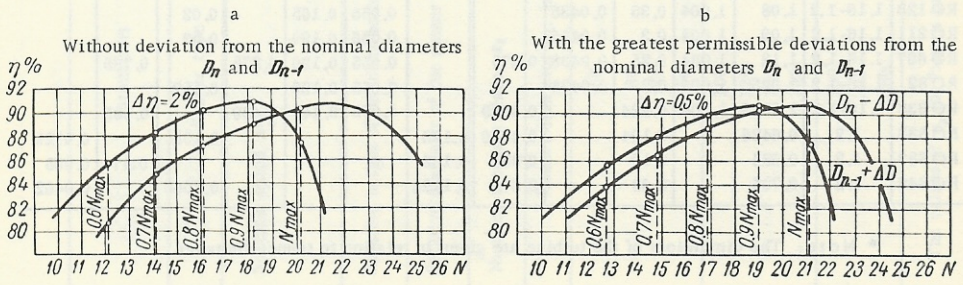


FIGURE III. 14. Efficiency curves of a turbine for two adjacent diameters

The efficiency curve $\eta = f(N)$ for Kaplan turbines slopes gently; deviations from the nominal diameters are not considered ($\Delta D = 0$) in the classification, since the required variation of the turbine output within the standard-type sizes may be achieved by changing the runner-blade angle.

In the turbine classification the ratio $K = \frac{D_n}{D_{n-1}}$ of two nominal diameters is established within the limits of 1.10 (for larger diameters) and 1.13 (for smaller diameters).

The average ratio K of two adjacent diameters for the standardized diameters is 1.115.

The possible reduction of average operational efficiency amounts to $\sim 0.5\%$.

The classification of hydraulic turbines developed in the U. S. S. R., with standard-type sizes characterized by the runner diameters, was the basis for further standardization of type sizes of turbine stator elements.

The type of the scroll case was accepted as the basic characteristic of the turbine type; the scroll case is made of concrete for small heads or of cast or welded steel for medium and high heads.

Precise fields of applicability (in terms of available head H) of standardized runners and types of speed rings, and the existence of diameter series, made it possible to create a system for the standardization of turbine assemblies and parts. Standardized elements and dimensional series permit the wide use of the similarity laws for many turbine parts and make it possible to obtain dimensional series established in a strict sequence.

This standardization, and the nomenclature for large turbines, were drawn up for the first time by B. E. Gol'din /23/, and were adopted by the U. S. S. R. hydraulic-turbine industry. The introduction of standard-type sizes, constructions, and regular series of assemblies and components paved the way for the series production of turbine components and helped shorten design, production, planning and manufacturing time.

New classification for large-size turbines. The state plan for further development of water-power engineering in the U. S. S. R. envisages the construction of powerful hydroelectric plants equipped with larger and more powerful turbines than those provided for in the existing classification. Hence a new classification for these large-size turbines is at present in preparation.

A characteristic feature of the new classification is that it proceeds not only from the existing types of runners, but also from types not yet devised, but having technically feasible parameters. These improved parameters are the result of theoretical computations and of the analysis of existing experience, both in the U. S. S. R. and abroad.

As will be seen, the new classification not only specifies present standards, but also indicates development trends in the design of new runners.

The new classification allows for the characteristic geometrical parameters of runners which to a large extent determine their hydraulic characteristics. Such parameters are the hub-tip diameter ratio $\bar{d}_{hub} = \frac{d_{hub}}{D_1}$ and the number of blades (Figure III. 15) for Kaplan turbines, and the relative height of the distributor $\bar{b}_0 = \frac{b_0}{D_1}$ for Francis turbines.

The designation of runners in the new classification shows a certain departure from previous designations. As in the previous one, the runner type is designated by two letters (PL or RO), followed by the maximum head under which the runner may be installed, and its serial number.

Accordingly, the turbine designation consists of symbols separated by dashes: the runner type – the installation (vertical or horizontal shaft) — the runner diameter, in mm.

PL 40/07 — V — 500 or RO 80/01 — V — 300

In the new classification the runner diameters have been changed. The ratio of two adjacent diameters is increased up to 1.12 (as against the former 1.11) for smaller diameters, and lowered to 1.073 (as against 1.12) for larger diameters. The average ratio of two adjacent diameters is reduced to 1.12 (as against 1.15).

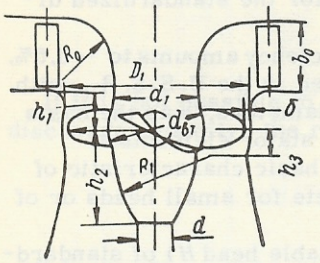


FIGURE III. 15. Dimensions of water passages of Kaplan turbines, according to the new nomenclature

Eight standardized runners were selected for Kaplan turbines, for heads up to 80 m. Eight standardized runners were selected for Francis turbines for maximum heads H up to 500 m. The limits of diameter series are somewhat widened: for Kaplan runners to D_1 = 1,000 cm, and for Francis runners to D_1 = 850 cm. The numerical values of diameters of the new series are in accordance with GOST 8032-56 (preferential numbers and series of preferential numbers).

In the light of experience gained in the design of hydraulic turbines, the guide-vane circle diameter D_0 (characteristic speed-ring diameter) and the number of guide vanes were also revised. The values of D_1, D_0, and z_0 are given in Table III. 3.

TABLE III. 3, a

Dimensions of the water passages of Kaplan runners, according to the new nomenclature

Runner type / Runner parameters	PL 10	PL 15	PL 20	PL 30		PL 40		PL 50		PL 60	PL 80
z_1	4	4	4	5	6	6	7	7	8	8	8
$\frac{b_0}{D_1}$	0.45	0.45	0.4	0.4	0.375	0.375	0.375	0.375	0.35	0.35	0.35
$\frac{d_{hub}}{D_1}$	0.33	0.35	0.37	0.41	0.43	0.45	0.47	0.49	0.51	0.54	0.6
$\frac{d_1}{D_1}$	0.28	0.3	0.32	0.36	0.38	0.40	0.42	0.44	0.46	0.49	0.55
$\frac{R_0}{D_1}$	0.36	0.35	0.34	0.32	0.31	0.3	0.29	0.28	0.27	0.25	0.22
$\frac{h_2}{D_1}$	0.31	0.33	0.35	0.4	0.42	0.44	0.46	0.48	0.5	0.54	0.6
$\frac{h_2}{D_1}$	0.087	0.09	0.093	0.098	0.10	0.103	0.105	0.108	0.11	0.113	0.12
$\frac{R_1}{D_1}$	0.315	0.338	0.360	0.406	0.430	0.453	0.477	0.500	0.520	0.560	0.635

$h_1 = 0.2085 D_1 \quad d = 0.1 D_1 \quad \delta = 0.001 D_1$

Tables III. 4 and III. 5 show the basic design and hydraulic parameters of the runners, according to the new classification.

In both tables, the lower limits $Q'_{I\,max}$ and σ_{cr} correspond to the upper limits of heads for each range, and vice-versa. The value of σ_{cr} corresponds to the value of σ for the model runner. In order to calculate it for the full-scale turbine a correction coefficient allowing for the scale effect should be introduced.

TABLE III.3

Runner and speed-ring diameters D_1 and D_0 respectively, in cm and the number of guide vanes z_0

D_1	Kaplan		Francis		D_1	Kaplan		Francis	
	D_0	z_0	D_0	z_0		D_0	z_0	D_0	z_0
180	-	-	220	16	500	580	24	580	24
200	-	-	240	16	550	640	24	640	24
225	-	-	275	16	600	700	24	700	24
250	220	24	300	24	650	750	24	750	24
280	325	24	335	24	700	810	32	810	24
320	375	24	385	24	750	875	32	875	24
360	420	24	430	24	800	930	32	930	24
400	465	24	480	24	850	985	32	985	24
450	525	24	525	24	900	1050	32	-	-
					950	1100	32	-	-
					1000	1150	32	-	-

TABLE III. 4

Basic design and hydraulic parameters of Kaplan runners according to the new classification

Runner type	PL 10	PL 15	PL 20	PL 30	PL 40	PL 50	PL 60	PL 80
Head limits H_{min}—H_{max} m	3—10	5—15	10—20	15—30	20—40	30—50	40—60	50—80
Number z_1 of runner blade	4	4	4	5	6	7	8	8
Hub-tip diameter ratio $\bar{d}_{hub} = \frac{d_{hub}}{D_1}$	0.33	0.35	0.37	0.41	0.43—0.45	0.47—0.49	0.51—0.54	0.54—0.60
Relative height of the distributor $\bar{b}_0 = \frac{b_0}{D_1}$	0.45	0.45	0.40	0.40	0.375	0.375	0.35	0.35
Ratio l/t (average)	0.62	0.75	0.87	1.10	1.30	1.50	1.75	1.75
Blade coverage (enveloping) angle θ	—	—	78—79°	78—79°	78—79°	78—79°	78—79°	79—79°
Unit speed n'_{Iopt}	165	150	138	125	115	108	100	100
n'_{Irat}	200	180	160	140	130	120	110	110
$Q'_{I\,max}$ without output drop, with allowance for 5% power margin	2250	2130	2040	1940	1840	1705	1580	1480
Q'_I for cavitation-free operating conditions	2250—2130	2130—1870	2040—1700	1940—1410	1655—1190	1355—1150	1190—970	1020—750
$\sigma_{cr.max.}$	1.4—1.275	1.0—0.84	0.832—0.68	0.775—0.505	0.68—0.4	0.505—0.325	0.4—0.27	0.325—0.205

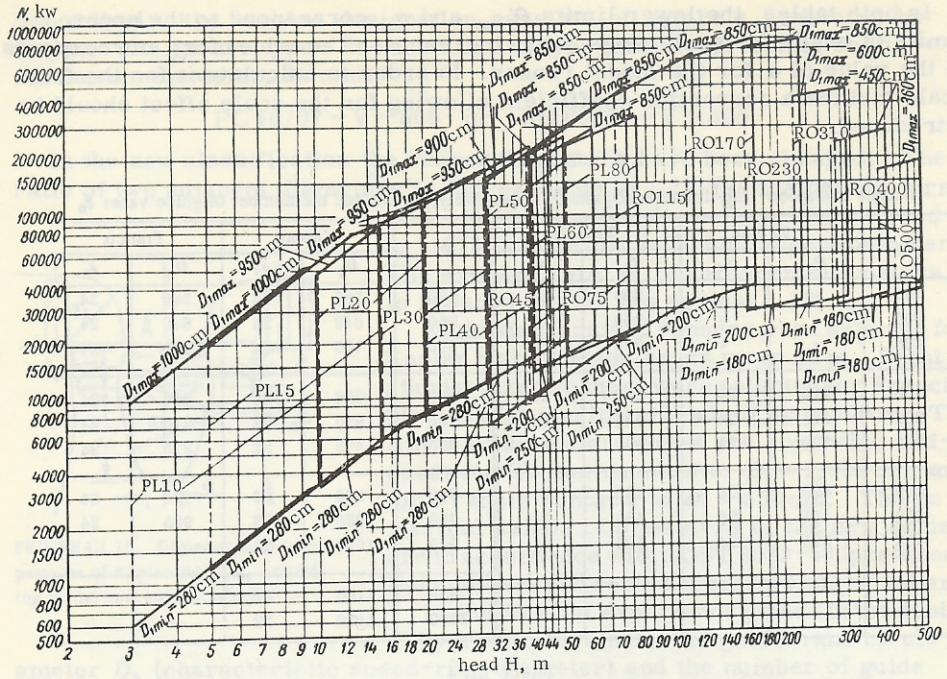


FIGURE III.16. Fields of application of large turbines, according to the new classification

Figure III. 16 presents a summary diagram of the fields of application for large turbines. The new classification was drawn up at the LMZ and the TsKTI by I. E. Etinberg, A. Yu. Kolton and I. N. Umikov.

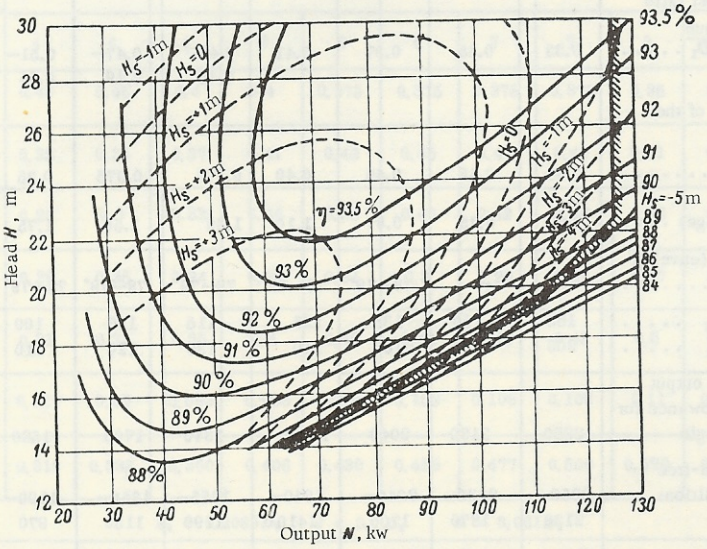


FIGURE III. 17. Universal performance chart of a Kaplan turbine

Fuller information about this problem may be found in /64/. The steps taken to select the turbine parameters are briefly outlined below.

The basic turbine parameters are chosen for given power, head, and headwater and tailwater levels.

Where head fluctuations occur, the turbine parameters are selected according to the rated head.

The values of N, $H_{rat} H_{max}$ and H_{min} are given by the designer of the hydroelectric plant. The turbine parameters are chosen from the universal chart plotted from the test results of the standardized runner models.

The turbine and runner types are chosen according to the rated head H_{rat}

The runner diameter is found from formula

$$D_1 = \sqrt{\frac{N}{9.81 \eta Q_1' H_{rat} \sqrt{H_{rat}}}}.$$

where N is given in kw and H in m,

In determining the runner diameter the efficiency range is taken from the table below:

for Francis turbines	η = 0.88 - 0.90
for Kaplan turbines	η = 0.84 - 0.86.

The unit discharge Q_1' (m^3/sec) for Francis turbines is usually selected on the curve for 5% power margin; with Kaplan turbines, one must allow for cavitation in order to obtain feasible draft heads.

The runner diameter, calculated from this formula, is rounded off to the nearest nominal diameter. Owing to the considerable head fluctuations under which Kaplan turbines operate, it is convenient to select the runner diameter for the lowest head which would ensure the rated power. The permissible draft head H_s, is calculated in relation to this head.

The turbine speed is given by the formula

$$n = \frac{n_1' \sqrt{H_{rat}}}{D_1}.$$

The value of n_1' is selected from the chart, on the curve which passes through the point of optimum efficiency or a little above it.

The correction $\Delta n_1'$ is usually assumed to be constant for all points of the chart. It is computed for the optimum point of the chart from the formula

$$\Delta n_1' = n_1' \left(\sqrt{\frac{\eta}{\eta_m}} - 1 \right).$$

The speed n is computed from the corrected value of n_1' and adjusted to the nearest larger synchronous speed.

The draft head may be calculated from the formula

$$H_s = 10.0 - \frac{\nabla}{900} - k\sigma H,$$

where k = 1.05 to 1.1 = safety factor used at LMZ;

∇ = elevation of the hydroelectric plant.

The coefficient σ is taken from the universal chart.

The magnitudes of Q_1' and n_1' and σ vary with power output and head. The permissible draft head H_s thus depends on the effective head and power. The plant head depends in turn on the variations in the headwater and tailwater levels. The draft head has therefore to be matched with the different combinations in head between headwater and tailwater levels.

Adding the draft head H_s to the lowest tailwater level, one obtains the highest permissible runner elevation for each case. Of the elevations obtained, the lowest has to be selected, in order to obtain cavitation-free operation under all conditions.

The values selected for the nominal diameter and the synchronous speed must be checked on the chart by plotting a tetragon with sides

$$n_1' = \text{const. at } H_{min};$$
$$n_1' = \text{const. at } H_{max}$$

having vertices with the ordinates Q_1', corresponding to the maximum and minimum power outputs at these head limits. If this tetragon adequately covers the central area of the chart within the region of high efficiencies, the parameters have been selected correctly; if the central area of the chart has markedly shifted with respect to the center of the tetragon, the runner diameter D_1 or the speed n, or both of them, have to be changed.

It is sometimes more convenient to select a smaller value of Q_1' for high-head Kaplan turbines than those determined from the chart and allowed by the degree of opening of the distributor. In this manner it is possible to reduce σ and to increase the permissible draft head H_s.

Since turbines are usually operated under variable head H and output [load] N_1, the discharge Q, the efficiency η, and the cavitation coefficient σ change as well. As a rule, turbine speed does not change. For proper turbine operation, it is therefore important to know the relationship between the basic turbine parameters. For this purpose, after turbine diameter D_1 and speed n have been properly selected, the universal efficiency and performance charts are plotted.

The efficiency characteristic $\eta = f(N)$ shows efficiency as a function of load N under constant head H and speed n. Since hydroelectric plants operating at constant head are rather infrequent, an over-all picture of turbine performance is best obtained by plotting the turbine performance chart from data on the individual efficiency characteristics.

The universal performance characteristics show the dependence of efficiency η on power output N and head H, at speed n = const. These characteristics consist of a family of lines of equal efficiency η, plotted with N and H as coordinates (Figure III. 17). On this characteristic are plotted: the line of upper output limit, the lines of constant efficiency, and the lines of constant draft head.

The turbine efficiency and performance characteristics are plotted on the basis of the universal chart of the selected runner model for the given diameter D_1, speed n, and heads H_{rat}, H_{min} and H_{max}.

In order to plot the efficiency curve the following steps are taken:

1) from data given in Section 10, Chapter II, the maximum efficiency of the turbine η_{max} is plotted as a function of the turbine head, with due allowance for the scale effect;

2) the correction for unit speed is calculated, allowing for the difference between the turbine and model efficiencies

$$\Delta n_1' = n_{1\,opt}' \left(\sqrt{\frac{\eta_{max}}{\eta_{M\,max}}} - 1 \right)$$

and the corrected unit speed n_{1c}' corresponding to the unit speed n_1' on the characteristic curve of the model

$$n_{1c}' = \frac{nD_1}{\sqrt{H}} - \Delta n_1' \ ;$$

TABLE III. 5

Principal design and hydraulic parameters of Francis runners, according to the new classification

Runner types	RO 45	RO 175	RO 115	RO 170	RO 230	RO 310	RO 400	RO 500
Relative height of distributor $\overline{b}_0 = \frac{b_0}{D_1}$	0.35	0.30	0.25	0.20	0.16	0.12	0.10	0.08
Head limits H_{min}—H_{max}, m	30-45	40-75	70—115	110—170	160—230	220—310	290—400	380—500
Unit discharge Q_1', l/sec	1440—1380	1380—1210	1210—970	970—650	650—420	420—280	280—200	200—150
Unit speed n'_{1opt}, rpm .	78	73	70	68	65	60	58	58
σ cr. max	0.27—0.23	0.243—0.16	0.168—0.097	0.1—0.06	0.065—0.047	0.048—0.04	0.042—0.035	0.036—0.03

3) the relationship $\eta_m = f(Q_1')$ for n_{1c}', is obtained from the universal chart in the following way: the values of the unit discharges are selected on the lines of equal efficiencies η_m for Francis and axial fixed-blade, and on the lines of equal angle φ for Kaplan turbines; this relationship is then written in tabulated form;

4) the scale-factor correction for the conversion from model to prototype efficiency is calculated, and the turbine efficiency is determined for each point;

5) the turbine power output is calculated for each point, from formula

$$N = 9.81 \eta Q_1' D_1^2 H \sqrt{H};$$

6) the efficiency characteristic is then plotted.

In order to plot the performance chart, the range of variation of n_1', corresponding to the given amplitude of head fluctuations (from H_{min} to H_{max}) is divided into 4-5 intervals and the efficiency characteristics are plotted for the heads obtained.

The points of equal efficiency η for various heads are represented with N and H as coordinates and linked up by a family of smooth curves — the performance chart.

To obtain the minimum head for each curve $\eta = \text{const}$ of the performance chart, an auxiliary curve $\eta_{max} = f(H)$ must be plotted. The minimum values of H, corresponding to each curve $\eta = \text{const}$, may be found on this curve. The lines of equal H_s are plotted on the basis of the lines of equal σ from the universal chart.

To plot the lines of equal H_s on the performance chart the following steps should be taken:

1) the auxiliary function $N = f(Q_1')$, being selected on the universal chart of the model, is determined for each of the heads used in plotting the efficiency characteristics;

2) the following relationships are written in tabulated form for each head:

$$Q_1' = f(\sigma);\ N = f(Q_1');\ H_s = f(N),$$

where Q_1' corresponds to the values of σ from the universal chart; N is computed from $N = f(Q_1')$, and the draft head is calculated from formula

$$H_s = 10.0 - \frac{\nabla}{900} - k\sigma H;$$

3) the curves $H_s = f(N)$, are drawn for each head and the points of equal H_s from these curves are transferred onto the turbine performance chart and linked up by smooth curves.

The output curve on the performance charts for Francis and axial fixed-blade turbines is determined either from the curve of 5% power margin of the universal chart, or directly from the efficiency characteristics.

The power output of Kaplan turbines is limited for the maximum rated head H_{rat} by the largest blade angle $\varphi°_{max} = \text{const}$, and for the minimum rated head, by the largest opening of the guide vanes $a_{0\,max} = \text{const}$.

The values of $\varphi°_{max}$ and a_{0max} on the turbine universal chart may be determined from the position of the operating point corresponding to the rated power N and rated head H_{rat}.

The plotting of the performance chart is based upon full geometrical similarity between model and prototype. However, this similarity does not always obtain. In practice, selection is often made according to the universal chart of a model whose water passages differ from that of the turbine. When this is the case, the effect of differences between water passage elements of model and prototype upon the turbine characteristics must also be found.

The water passages of a reaction turbine consist of the casing, the speed ring, the distributor, the throat ring, and the draft tube.

If the profile of the guide vanes and the ratio of guide-vane circle diameter to runner diameter remain unchanged, variations in other constructional dimensions of the distributor and stator speed-ring do not markedly affect the turbine parameters. The shape of the casing has a certain influence on the turbine parameters: the replacing of open-flume casings by spiral casings causes additional head losses due to friction; these losses increase with the specific speed and with the reduction in the cross-sectional area of the spiral casing.

Experimental data show that replacement of open-flume casings by spiral casings reduces the maximum efficiency by about 0.5% and that for large openings [of the distributor] even a drop in power output of 2—5% is recorded.

These figures, which are considered as correction values, are very important for turbines with small and medium diameters (range of D_1 from 2.5 - 3 m). When the diameter increases, these values decrease, and for D_1 = 8 - 9 m they may be neglected, since the relative head losses in the spiral casing diminish as the dimensions increase.

The shape of the draft tube affects head losses to a much larger extent: local losses are greater in the elbow of the bent draft tube than in the straight draft tube, due to the changes in the value and direction of flow velocity in the elbow.

The drop in efficiency and power depends on the geometrical shape and depth of the elbow draft tube, as well as on the turbine type.

With Francis turbines, the efficiency of an elbow draft tube compared with that of a straight conical draft tube of identical exit area is less by approximately 0.5 - 1%, depending on the turbine power output. The efficiency reduction is greater at full load, and smaller at part load.

For Kaplan turbines, especially high-speed ones, the shape of the draft tube affects efficiency and discharge capacity in particular. Therefore, when selecting their parameters, it is imperative to use the characteristic curves obtained from model tests in which the draft tube has been modelled for all its elements, i.e., for vertical turbines with an elbow draft tube and for horizontal-shaft turbines with a straight draft tube.

From the unit discharge of the model, the unit discharge of the horizontal turbine, with the shaft passing through the elbow of the draft tube, may be determined from the formula

$$Q_1' = Q_{1m}' \psi,$$

where ψ = coefficient allowing for the restriction in the cross-sectional area by the shaft

$$\psi = \frac{D_{ex}^2 - d_s^2}{D_{ex}^2},$$

where D_{ex} = the exit diameter of the runner
d_s = the shaft diameter.

For the case considered, the efficiency reduction due to eddy losses in the draft-tube elbow equals $\Delta\eta$ = 1-2%.

For turbines with cylindrical casing, the influence of the latter on η and Q_1' is allowed for by the following correction factors:

$$\Delta\eta = 0.5 \text{ to } 1.0\%$$
$$\psi = 0.98 \text{ to } 0.95.$$

The larger values for $\Delta\eta$ and the smaller for ψ should be selected for turbines with high specific speed.

15. RUNAWAY SPEED

The basic equation of turbine dynamics is:

$$J\frac{d\omega}{dt} = M_d - M_r,$$

where J = the moment of inertia of the rotating parts;
ω = the angular velocity;
t = the time;
M_d = the driving moment;
M_r = the moment of resistance forces.

In the operation of an hydraulic turbine, three situations may occur:

1. $M_d = M_r$.

In this case the turbine power output N_t equals the load demand of the generator N_g.

Thus $\frac{d\omega}{dt} = 0$, i.e., $\omega = \text{const}$, which corresponds to a constant speed, i.e., to steady operation of the unit.

2. $M_d < M_r$.

In this case, the turbine power output is smaller than the load demand of the generator:

$$N_t < N_g, \quad \text{so that} \quad \frac{d\omega}{dt} < 0,$$

i.e., the turbine speed decreases when the load on the generator increases.

3. $M_d > M_r$.

In this case the power output of the turbine is greater than the load delivered by the generator into the network:

$$N_t > N_g, \quad \text{so that} \quad \frac{d\omega}{dt} > 0,$$

i.e. the turbine speed increases when the generator load is reduced.

In the second and third cases, the operation of the turbine unit is unsteady. Under normal operating conditions, the regulating system of the turbine assures a balance between the moments of the driving and the resistance forces. When a change in load and a rise or fall in speed occurs, the governor operates immediately, narrowing or widening the distributor opening accordingly: the turbine output is then altered owing to the change in discharge. The turbine speed increases or decreases slightly, in accordance with the generator output, and is brought back to normal by the regulating system.

If during operation a sudden load drop occurs and the guide vanes remain open due to a failure in the turbine-regulating system, then the speed rises sharply and, after some time, reaches the maximum value — called runaway speed.

The runaway speed may be determined from the corresponding unit speed n'_{1r} from formula

$$n_r = n'_{1r} \frac{\sqrt{H_{max}}}{D_1}.$$

In turbine tests the model is brought to the runaway speed and the characteristic curve of unit runaway speed n'_{1r} is plotted; this curve represents the relationship between the unit runaway speed n'_{1r} and the guide-vane opening a_0.

The runaway speed of Francis turbines depends on the distributor opening and the head; for Kaplan turbines it depends on the runner-blade angle as well.

The highest runaway speed occurs when the distributor is fully open, or nearly so.

With Kaplan turbines the highest runaway speed is reached if the distributor-blade angle connection fails to operate, the distributor remaining fully open and the runner blades being set at a small angle.

The runaway speed may be characterized by the coefficient $K_r = \frac{n_r}{n}$ i.e., the ratio of runaway to normal speed.

For Francis and Pelton turbines	$k_r = 1.7 - 1.9$
For Kaplan turbines with the distributor-runner blade connection operating	$k_r = 2.0 - 2.2$
For Kaplan turbines with failure in the distributor-runner blade connection control-valve	$k_r = 2.4 - 2.6$

Figure III.18 represents the runaway-speed characteristic curves for a number of Francis runners of the RO 123, RO 211, RO 638, RO 82 and RO 246 types, as a function of the distributor opening. From this figure it will be seen that as a rule the runaway speed increases with the specific speed.

Figure III.19 represents the runaway-speed characteristic curves of the PL 587 Kaplan runner, for different blade angles $\varphi°$ as a function of the distributor opening.

These curves show that the highest runaway speed corresponds to small angles $\varphi°$ and large distributor openings.

Such a combination can occur only when the distributor-runner blade connection fails to operate.

Normally, a large distributor opening a_0 corresponds to a large runner-blade angle $\varphi°$. Consequently the runaway speed depends on the unit speed n_1' corresponding to the normal operating conditions of the turbine. The runaway speed increases with the unit speed n_1'. This is illustrated by the family of n_1' curves on the universal chart, corresponding to various unit speeds under normal operating conditions.

The high runaway speed for small runner-blade angles may be explained as follows:

Figure III.20 shows the velocity triangles at the inlet and exit of the Kaplan runner blades under both normal and runaway conditions. At runaway speed, the peripheral velocities u_{1r} and u_{2r} increase, owing to the appreciable increase in the relative velocities w_{1r} and w_{2r}, and deviate from the direction tangential to the blade entrance and exit tips, thus increasing the eddy losses caused by the water flowing around the blade.

At steady runaway speed, all the energy is dissipated.

If the runner blades are then turned to a greater angle $\varphi°$ (Figure III.20), the conditions of flow around the blade deteriorate, due to the increase in the angles between the relative velocities w_{1r} w_{2r} and the corresponding tangents to the blade entrance and exit tips. The hydraulic losses increase so that equilibrium between the driving and resisting moments obtains at low runaway speeds. On the contrary, if we close the blade opening by reducing the angles $\varphi°$, the conditions of flow around the blade improve, due to the decrease in the angle between the relative velocity and the tangent to the blade profile. The equilibrium condition then obtains at a higher runaway speed. This characteristic feature of the Kaplan turbine — different runaway speeds corresponding to different blade angles — must be carefully considered when designing a turbine and selecting the runaway speed.

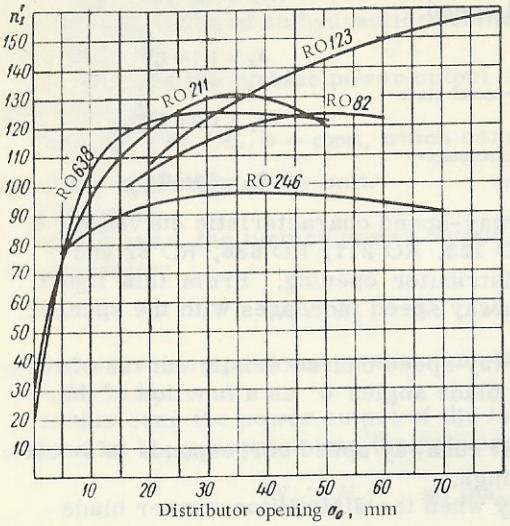


FIGURE III.18. Runaway-speed characteristic curves of some Francis runners

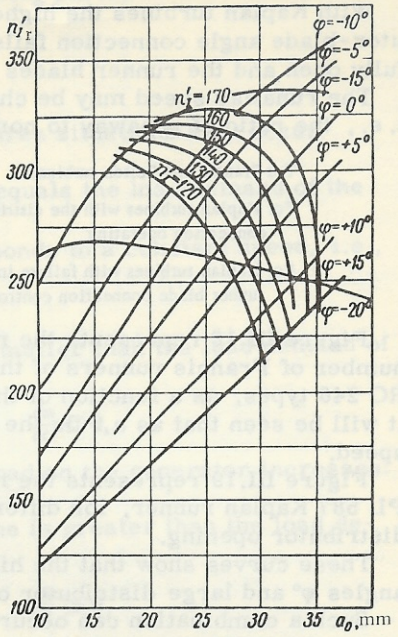


FIGURE III.19. Runaway-speed characteristic curve of a Kaplan turbine, for various runner-blade angles with distributor-runner blade connections operative

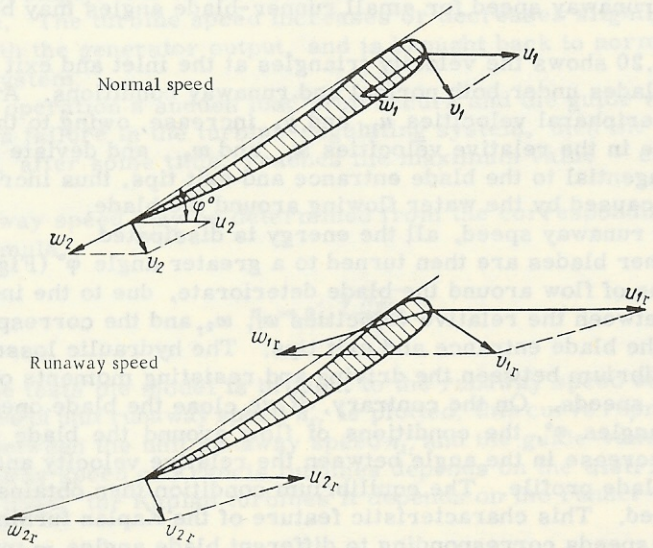


FIGURE III.20. Inlet- and exit-velocity triangles at the blade of a Kaplan runner, for normal and runaway speed conditions

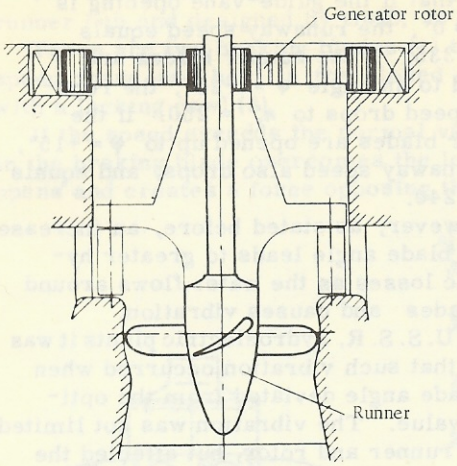


FIGURE III. 21. Schematic diagram of a turbine unit (turbine runner and rotor of generator)

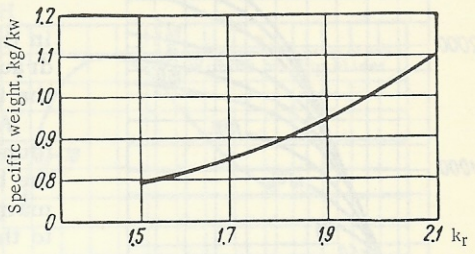


FIGURE III. 22. Specific weight of generator as a function of runaway-speed coefficient

The increase in runaway speed causes an increase in the centrifugal forces, a fact which should be considered when calculating the strength of the turbine rotating-parts. Due to the considerable energy losses at runaway speed, dangerous vibrations of the runner may occur as well. The centrifugal forces are computed from the formula

$$C = mr\omega^2,$$

where m = the mass of the rotating parts;
r = the radius of center of gravity;
ω = the angular velocity.

The main part of the rotor mass is concentrated at its rim. Since the rim has a large diameter, the centrifugal forces developing in the generator at runaway speed are greater than in the turbine, where the main part of the runner mass is concentrated close to the axis of rotation. This can be seen in Figure III. 21. Therefore, the selection of the rated runaway speed, with due allowance for operation or failure of the distributor-runner blade connection, or for the existence of a runaway-protection device (which reduces the runaway speed) is an important economic consideration, since at low runaway speed, the turbine runner and especially the rotor of the generator have smaller over-all sizes and weight, and are less expensive to construct.

The dependence of the specific weight of the generator on the runaway coefficient, plotted according to data from Gidroproekt, is shown in Figure III. 22. If the runaway coefficient is reduced from $k_r = 2.0$ to $k_r = 1.5$, the weight of the generator may be reduced by about 30%.

This characteristic feature of the Kaplan turbine—different runaway speeds corresponding to different blade angles—is used in practice as a means to prevent excessive increase of speed.

Thus, if the unit reaches the runaway speed, two methods may be used to restore normal conditions: the closing of the runner blades, and the adjustment of the runner blade angle to a greater value /61/.

As an example, Figure III. 19 shows that if the guide-vane opening is a_0 = 35 mm and the runner-blade angle $\varphi = 0°$, the runaway speed equals $n'_{1r} = 335$. If the runner blades are closed to an angle $\varphi = -20°$, the runaway speed drops to $n'_{1r} = 250$. If the runner blades are opened up to $\varphi = +15°$, the runaway speed also drops, and equals $n'_{1r} = 240$.

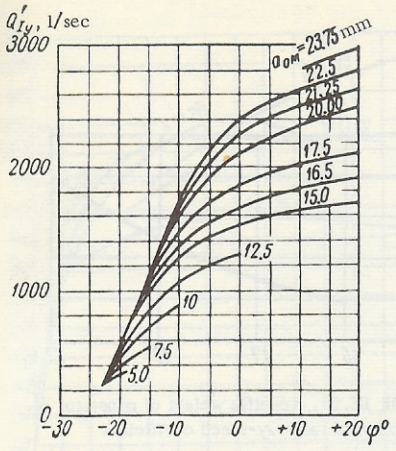


FIGURE III. 23. Dependence of discharge at no-load Q'_{1y} on the runner-blade angle $\varphi°$ for various guide-vane openings a_0 of the PL-91 distributor

However, as stated before, an increase in the blade angle leads to greater hydraulic losses as the water flows around the blades and causes vibration.

At U. S. S. R. hydroelectric plants it was found that such vibration occurred when the blade angle deviated from the optimum value. The vibration was not limited to the runner and rotor, but affected the whole unit, and even the building. The larger the unit, the stronger the vibration.

Another drawback of this method is the large amount of water flowing through the turbine when the guide vanes are open.

When the runaway speed is lowered by reducing the runner-blade angle $\varphi°$ (see Figure III. 23), the blades must be adjusted until complete closing is obtained, or, if the l/t ratio permits, they can be opened in the opposite direction. The water passages of the runner may be completely closed, and runner rotation stopped.

The curves in Figure III. 23 show, that if the blades have a large coverage angle $\varphi°$ and an l/t ratio which permits their adjustment to complete stoppage, the water discharge at no-load through the closed blades will be small, even if the distributor is fully-open.

At a certain rate of increase in the normal speed and blade-closing time, the connection between the distributor opening and runner-blade adjustment mechanism may be disturbed to such a degree as to cause the runaway speed to attain its maximum value (see curves in Figure III. 19).

Consequently, the unit may reach the runaway speed, even if only for a short time, a fact which has to be considered in the turbine design. This is the disadvantage of the second method.

Turbine builders outside U. S. S. R. do, however, use this technique in order to prevent prolonged operation at runaway speed. Thus, oil under high pressure is supplied to the servomotor controlling the adjustment of the runner blades.

In order to reduce the runaway speed of Kaplan turbines, it is possible to use special braking blades located below the runner or above it.

At normal speed, for instance, these blades are located in the runner hub. When the runner speed increases, the centrifugal forces drive these blades outward from their seats into the water stream, where they create a braking moment which reduces the runaway speed.

The schematic diagram of braking blades of this type, located in the runner hub and designed by LMZ, is given in Figure III. 24.

There are two braking blades (1) turning around shaft (2); at normal speed these are held in the closed position by means of a stopping device with a locking pawl (3).

If the speed exceeds the normal value, the increased centrifugal force in the braking blade overcomes the locking force of the device; the blade opens and creates a force opposing the runner rotation.

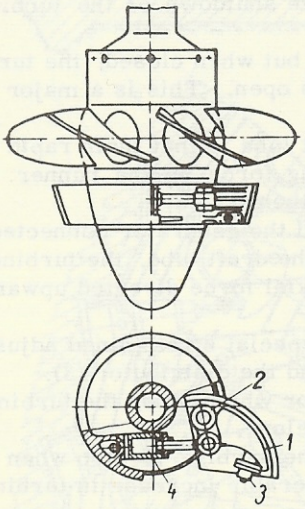


FIGURE III. 24. Kaplan runner fitted with braking blades

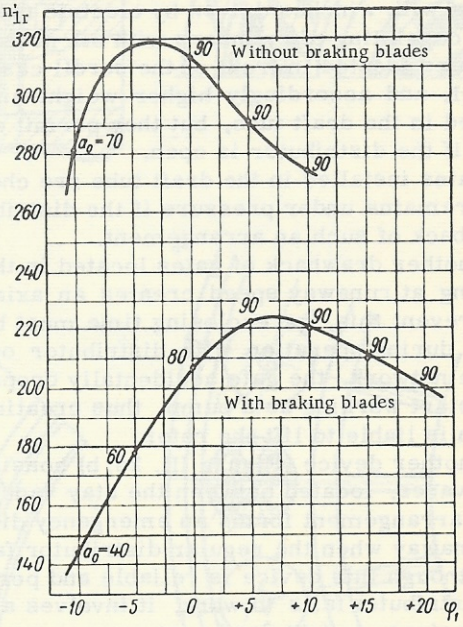


FIGURE III. 25. Values of unit runaway speeds of the PL 201 runner, with and without braking blades

The oil-pressure servomotors (4) bring the braking blades back into their initial position, after the turbine is halted; these servomotors serve also as shock absorbers for the braking blades.

The oil is supplied to, and removed from, the servomotors through a pipe located in the hollow shaft of the turbine. Model tests carried out by LMZ on the PL 201 runner provided with such a device have shown that the braking blades reduce the maximum runaway speed by about 35%. This is illustrated by the curves in Figure III. 25.

The maximum unit runaway speed of the PL 201 runner provided with braking blades drops from $n'_{1r} = 318$ to $n'_{1r} = 223$.

LMZ developed a turbine design provided with braking blades (see Figure III. 24), but this model was never manufactured because, under normal conditions, the moving mechanisms of the braking blades operate only seldom and remain constantly under water, making it impossible to count on their reliable operation.

Moreover, the presence of braking blades is liable to increase the vibrations.

The prospectuses of the "English Electric Company" list a Kaplan runner with braking blades located above the runner blades. In this design the braking blades also open under the action of the centrifugal forces, and create a hydraulic moment opposing that acting upon the runner blades.

Other devices are more frequently used to counter high runaway speed. Figure III. 26 shows schematically several antirunaway devices.

Plain sliding gates (Figure III. 26, a), installed in special grooves in front of the scroll casing (1) or in the draft tube (2), are still the most widely used. The quick-acting gates are lifted and lowered by hoists provided either with winches driven by electric motors or with hydraulic servomotors consisting of cylinders with oil-pressure-operated pistons.

Gates located in front of the scroll casing have greater dimensions and travel, and accordingly higher weight and cost, compared with gates installed in the draft tube, but they permit complete shutdown of the turbine, even if the distributor is open.

Gates installed in the draft tube are cheaper, but when closed, the turbine remains under pressure if the distributor is open. This is a major drawback of such an arrangement.

Another drawback of gates located in the draft tube is that their rapid closing at runaway speed creates an axial lifting force on the runner. To prevent this, gate-closing time must be lengthened.

If, during operation with distributor open and the generator connected to the network, the gate accidentally drops into the draft tube, the turbine will start working as a pump, thus creating an axial force directed upwards, which is liable to lift the rotor.

Another device (Figure III. 26, b) consists of special streamlined adjustable vanes, located between the stay vanes (1) and the distributor (3). This arrangement forms an emergency distributor which stops the turbine at runaway when the regular distributor fails to close.

Although this device is reliable and permits the turbine to stop when the distributor fails to work, it involves a considerable increase in turbine dimensions, weight, and cost.

It is an accepted fact that the weight of a conventional distributor in a low-head turbine with bearing ring and distributor-actuating mechanism may attain 40% of the total weight of the turbine.

Separate servomotors, installed on each guide vane, may also be used as an antirunaway device. The servomotors may be located on the turbine cover-plate, or in the turbine pit (Figure III. 26,c). Servomotors installed in the pit are more reliable.

These servomotors may replace the main servomotors in an emergency, not only for the distributor-actuating mechanism, but also for the governor system, since they are supplied with oil-pressure from a special emergency distribution-valve.

At present, antirunaway devices with separate servomotors are undergoing practical trials.

The operation of separate servomotors is rendered more difficult by the presence of special breaking elements on the distributor-actuating mechanism: the vanes must be separated from the ring should the gate ring jam. If this should be effected by breaking the special elements provided for this purpose, either the separate servomotors must be made very powerful or a special device for disconnecting the vanes from the jammed gate ring has to be fitted.

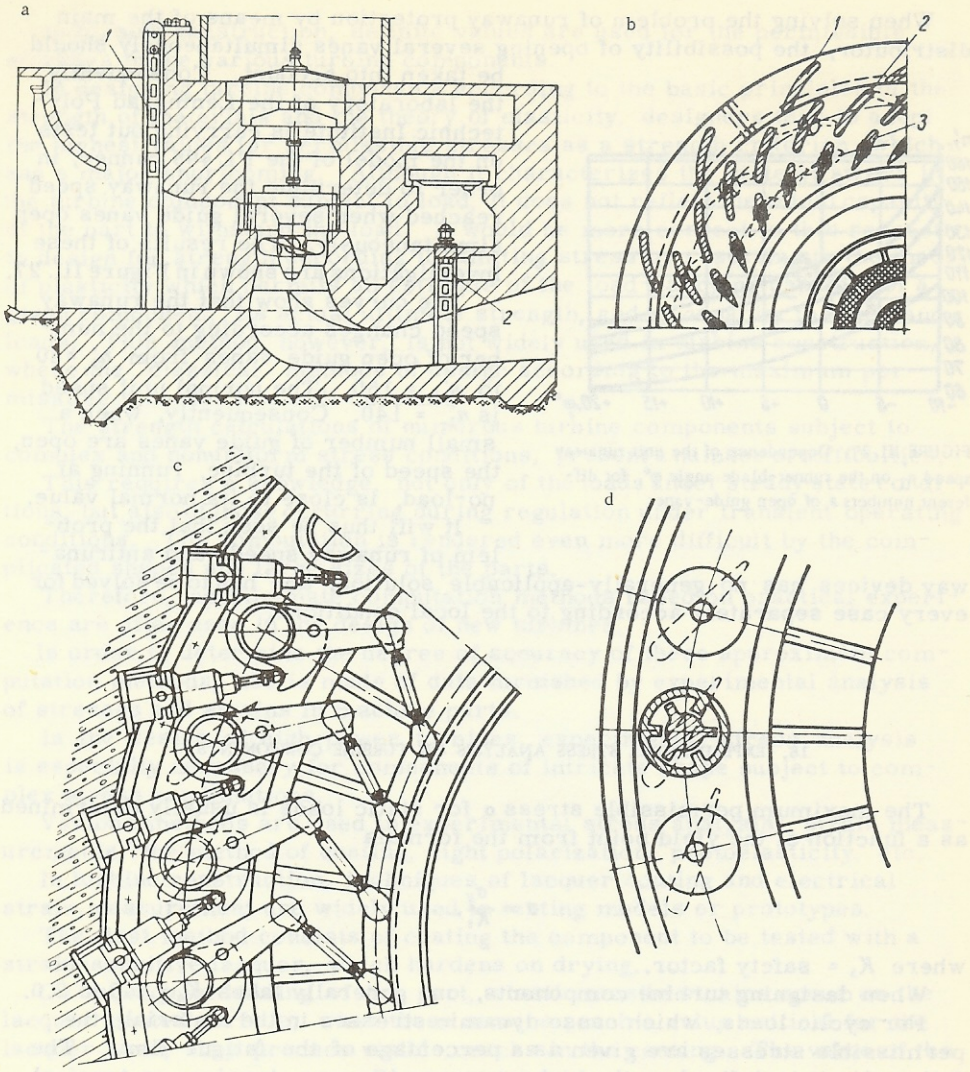


FIGURE III. 26. Schematic diagrams of various antirunaway devices

It is also possible to use propeller-type servomotors to adjust the guide vanes (Figure III. 26, d), but these are difficult to synchronize. Such servomotors may be used as an antirunaway device if the oil is supplied from an emergency distribution valve.

At present, the possibility is being investigated of using a self-closing distributor as an antirunaway device, with vanes whose profile is designed so as to develop a hydraulic closing moment at any degree of vane opening.

In this case, however, the danger arises of sudden, spontaneous closing of the guide vanes, and appearance of water hammer in the water passages. Difficulties also stem from the fact that the hydraulic moment exerted on the guide vanes depends upon their position with respect to the scroll casing.

When solving the problem of runaway protection by means of the main distributor, the possibility of opening several vanes simultaneously should be taken into account. Consequently, the laboratory of the Leningrad Polytechnic Institute is carrying out tests on the model of the PL 495 runner, in order to determine the runaway speed reached when several guide vanes open simultaneously. The results of these investigations are shown in Figure III. 27.

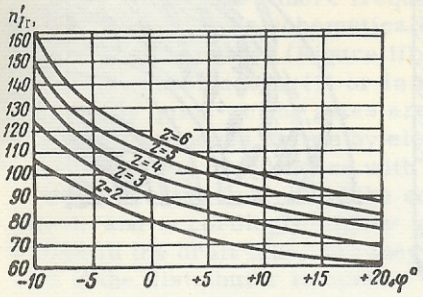


FIGURE III.27. Dependence of the unit runaway speed n'_1 on the runner-blade angle φ°, for different numbers z of open guide-vanes

The curves show that the runaway speed changes according to the number of open guide vanes from $n'_{1r} = 60$ to $n'_{1r} = 160$. The normal unit speed is $n'_{1r} = 140$. Consequently, when a small number of guide vanes are open, the speed of the turbine, running at no-load, is close to its normal value.

It will thus be seen that the problem of runaway speeds and antirunaway devices has no generally-applicable solution, and has to be solved for every case separately according to the local conditions.

16. EXPERIMENTAL STRESS ANALYSIS ON TURBINE COMPONENTS

The maximum permissible stress σ for static loads is usually determined as a function of the yield point from the formula

$$\sigma = \frac{\sigma_y}{K_s},$$

where K_s = safety factor.

When designing turbine components, one generally takes $K_n = 1.5$ to 2.0.

For cyclic loads, which cause dynamic stresses in the material, the permissible stresses are given as a percentage of the fatigue limit. The fatigue limit is defined as the highest stress (flexure, tension, or torsion) at symmetrical load cycles that a test specimen may withstand for a practically infinte number of loadings (more than 10^7 for ferrous metals, and more than 10^8 for nonferrous metals).

Materials are usually subjected to static and dynamic stresses simultaneously. Besides the stresses due to external loads, residual stresses often occur, especially in pieces of intricate shape, as a consequence of nonuniform heat treatment or temperatures in various parts of the component. In such cases, even for symmetrical external loads, alternating stresses with an asymmetrical cycle occur. Smaller values are accepted for permissible stresses when the alternating loads have an asymmetrical cycle, than for those with a symmetrical one. These values also depend on the static stress; the larger the static stresses, the smaller the permissible alternating stresses.

In turbine construction, definite values are used for the permissible stresses in the various turbine components.

In designing turbine components according to the basic principles of the strength of materials and the theory of elasticity, designers tend to adopt the highest values for permissible stresses as a strength criterion, which has a major shortcoming. Although it characterizes the state of stress in the turbine component subject to load, it does not reflect the actual capacity of the part to withstand the load. It would be more correct in this respect to design for strength according to limiting stress by resorting to the theory of plasticity which permits an estimate of the load-carrying capacity of a given component, its actual ultimate strength, and its capacity to withstand loads. This method, however, is not widely used in turbine construction, where the "classical" methods of design according to the maximum permissible stresses are still current.

The strength calculations of numerous turbine components subject to complex and nonuniform stress conditions, present a number of difficulties.

This requires a knowledge, not only of the loads under steady-state conditions, but also of those occurring during regulation under transient operating conditions. The computation is rendered even more difficult by the complicated shapes and large sizes of the parts.

Therefore, approximate computation methods based on practical experience are often used in the design of new turbines.

In order to determine the degree of accuracy of these approximate computation methods, use is made of data furnished by experimental analysis of stresses and strains in machine parts.

In the design of high-power turbines, experimental stress analysis is especially necessary for components of intricate shape subject to complex stress combinations.

Various methods are used in experimental stress analysis: strain measurements, the method of coating, light polarization, photoelasticity, etc.

In turbine construction, techniques of lacquer coating and electrical strain measurement are widely used in testing models or prototypes.

The first method consists of coating the component to be tested with a strain-sensitive lacquer, which hardens on drying.

On subsequent loading of the part, elastic tensile strains occur on the lacquer-coated surface; when these strains reach a value critical for the lacquer used, they produce visible cracks in the coating. The value of the rupture strain $\varepsilon_r = \frac{\sigma_r}{E}$ for the given lacquer is called the coating "constant". It is essential that the lacquer coating constant be smaller than the strains to be expected in the component being tested. The lacquer-coating method provides an overall stress picture and gives the principal stress directions. Its results are accurate to within 10 to 20%.

If greater accuracy is required, further measurements are made by means of wire-type strain gages cemented to the part along the principal stress directions (normal and tangential to the crack lines in the coating).

The method of direct strain measurement consists of cementing a strain-sensitive device, called a resistance-wire gage, to the surface of the component. This so-called active gage, together with an identical one for thermal compensation, and two adjustable resistances (mounted on the measuring device) constitute a measuring bridge. The thermal compensation

element is set for the same temperature conditions as the active strain gage, but is not connected to the component to be tested, thus eliminating errors due to temperature fluctuation.

Upon deformation, the gage length and the cross-sectional area of the active strain gage change, and with them its electrical resistance. The change in the resistance of the active gage which is connected to one of the bridge arms disturbs the bridge balance. The strain in the part being tested is determined by means of this electrical imbalance.

The gage consists of a long, thin wire looped back and forth, bonded to a paper backing. Usually, constantan or nichrome wires are used with a diameter of 10 to 60μ. The gage length is 5 to 20 mm, sometimes attaining 50 mm. The ohmic resistance of the gage usually varies between 70 and 200 ohm.

For short-time measurements, the gage is bonded to the component by means of a special cement consisting of a solution of 5 – 8% celluloid in acetone. For more extended measurements, other types are used, e.g., silicone glycerol-phtalate (No. 192T), BF4, and methanol-base cements, because celluloid-base cement is not heat-resistant and starts to flow. The strain gage is sensitive to both tension and compression of the metal, and to static as well as dynamic strains.

Beside strains, water pressure and vibration occurring under normal conditions should also be measured. Special pressure and vibration gages, installed at various points of the stationary or rotating parts, are used for this purpose.

The sensing element of the pressure gage is a membrane. Water pressure deforms the membrane which has a strain gage fastened to its inner surface. The pressure gages are installed in special seats provided in the part, so that the membrane is flush with the surface of the component. The leads from the gages are laid in a brass tube.

For measurement of vibrations in the frequency range 30 – 1,200 c, piezoceramic gages are used. The vibration transducer is fastened to the component to be tested. Inside the transducer body, an inertia mass is supported by piezoelectric plates made of quartz or other materials. When the component vibrates, the pressure exerted on the plates by the mass is proportional to the acceleration, the result being an electromotive force proportional to the pressure.

Protection of transducers and cables against the high velocity of the water stream around the turbine parts is essential. For this purpose, metal plates and clamps, resin coatings, and special cements are used.

Usually, a large number of transducers are installed simultaneously.

Multiple-point strain measurements are carried out by successively connecting the transducers to the measuring instrument through plug-in switches (for 20 – 30 gages) or remote-control switches (for 100 – 150 gages). The remote-control commutating-switch consists of contacts and a control board interconnected by cables.

For strength tests on models, plastics such as the cast phenol plastics and plexiglass are suitable.

Blocks of cast phenol plastics and plexiglass are used to manufacture models of thick-walled parts.

Plexiglass sheets, machined and cemented, are used for models of the welded and thin-walled parts.

The characteristics of these materials are given in Table III. 6.

TABLE III. 6

Approximate characteristics of the materials used for elastic models in strain measurements and tests

Material	Thickness, mm	Modulus of elasticity E at 20 – 25°C, kg/cm^2	Proportional limit σ_{pr}, kg/cm^2	Max. stress at which creep is less than 0.005%, kg/cm^2	Poisson's ratio μ
Plexiglass sheets	up to 5-10	$2.7 \cdot 10^4$	300	120	0.35
Plexiglass blocks	up to 400	$2.6 \cdot 10^4$	300	100	0.34
Phenol plastics in shaped blocks	up to 400-600	$3.2 \cdot 10^4$	400	150	0.35

The total load on the model is determined from the ratio of the load acting on the prototype P_{pr} to the limiting stresses in both the model and prototype materials σ_{mod} and σ_{pr} and from the scale ratio α of the geometrical similarity, by the formula

$$P_{mod} = \frac{1}{\alpha^2}\left(\frac{\sigma_{mod}}{\sigma_{pr}}\right) P_{pr} .$$

When studying a new design, either the maximum stress must be computed approximately, or trial tests must be made.

Model tests are carried out in the following manner. The regions of highest tensile and compressive stresses, and the principal strain directions, are revealed by means of brittle lacquer coatings.

The value of the highest stresses is estimated by using calibrated coatings. The wire-type strain gages permit the relative strains ε to be measured at various points. The displacements are measured by means of dial gages.

Once the principal strains ε_1 and ε_2 are found, the principal stresses σ_1 and σ_2 can be determined.

$$\sigma_1 = \frac{E}{1-\mu^2}(\varepsilon_1 + \mu\varepsilon_2);$$

$$\sigma_2 = \frac{E}{1-\mu^2}(\varepsilon_2 + \mu\varepsilon_1),$$

where E = modulus of longitudinal elasticity;

μ = Poisson's ratio for the material of the model.

Model tests are also important for measurements on prototypes, since they make it possible to find the most highly stressed regions where measurements have to be carried out on the prototype turbine, and to reduce the number of transducers in places where their installation is difficult.

The methods of stress analysis on models made of materials with a low modulus of elasticity were devised, verified, and applied for the first time at the strain and stress laboratory of the Institute of Machines of the Academy of Sciences of the U. S. S. R. [/76/, /77/].

The same institute also developed methods and test equipment for multiple-point strain, pressure, and vibration measurements under normal operating conditions. The work was carried out by N. I. Prigorovskii, G. E. Rudashevskii, M. L. Daichik, and others, in cooperation with LMZ specialists V. A. Nemm and M. S. Kustanovich, in connection with the design of large turbines.

Several stationary and rotational turbine parts, such as runner blades, shaft, cover plate, throat ring, etc., were investigated on full-size turbines, under various operating conditions and during regulation. Many complicated problems connected with the specific conditions of turbine operation had to be solved in the course of this research. Some of these problems were: the fastening and protection of the transducers and the connecting cables against water flow and mechanical damage without affecting the streamlined shape of the turbine parts; the length of the cables required to connect the gages to the recording equipment; the difficulty in carrying out measurements on turbines operating according to the schedule of the connected power grid.

In strain, pressure, and vibration measurements of rotating turbine parts, e.g., runrer blades, certain difficulties may arise in the fixing and removal of the cables connecting the transducers to the recording equipment, located a considerable distance away (up to 50m) in the turbine room. The connection between the rotating and stationary parts is effected by means of a current collector, located on the turbine shaft either above the exciter or above the oil-supply head.

The danger of damaging the transducers and the cables is aggravated by the possibility of cavitation. Hence, the pressure, strain, and vibration transducers must be sealed as tightly as possible, securely attached, and well protected against mechanical damage. The best way to fix the transducers to the surface of the turbine part is by means of methanol-base cement, or by electrical welding. It is convenient to cover the gages with sheets about 1 mm thick and 10 mm wide, electrically welded to the turbine part. The brass tubes containing the leads from the strain gages have to be grouped together and fastened to the surface of the turbine part, (e.g., the blade) by means of clamps made of a thin nichrome strips. The tube bundles must be covered with welded steel plates. The projecting ends of the tubes should be coated with methanol-base cement containing 30 – 50% dry river-sand.

The pressure and vibration gages for the distributor are fitted into threaded holes prepared beforehand, and fixed in the manner previously described.

In the turbines of the Volga hydroelectric plant imeni Lenin, the brass tubes containing the cables were fastened along the blade and led out to the bolt heads, where contacts for connection with the cables passing through the runner hub were provided. The space around the bolt heads was filled with a special putty, hermetically sealing the cable inlet to the hub.

All cables passing through the hub should be properly insulated to ensure prolonged operation in oil. In Francis turbines, it is easy to lay the cables from the runner blades through the hollow shaft. In Kaplan turbines /49/, where the shaft bore is used for the piston rods of the runner-blade adjustment system, it is more convenient to lay the cables through the flange connections between the turbine shaft and the runner, as was

done in the turbines for the Tsimlyansk and Narva hydroelectric plants (Figure III. 28). The current collector is located beside the turbine bearing.

In the design of the turbines for the Volga hydroelectric plant imeni Lenin, provision was made for laying the cables inside the shaft, thus simplifying cable installation. The cables ran along the shaft axis toward the current collector located above the oil-supply head. Their layout is shown in Figure III. 29. Current collectors located above the generator require smaller dimensions than those located around the shaft which has a large diameter, and their construction is simpler and less expensive.

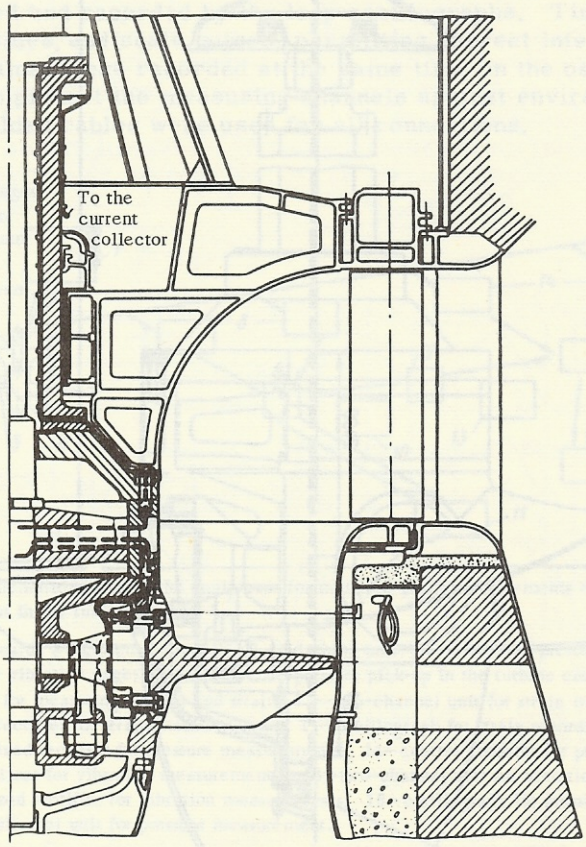


FIGURE III. 28. Cable layout in turbines of the Tsimlyansk and Narva hydroelectric plants

LMZ carried out the most complete multiple-point measurements in its history when testing the turbines for the Volga hydroelectric plant imeni Lenin, using equipment designed by G. E. Rudashevskii. The basic elements of the new measuring systems are:

1) strain, pressure, and vibration transducers, located on the runner blades;

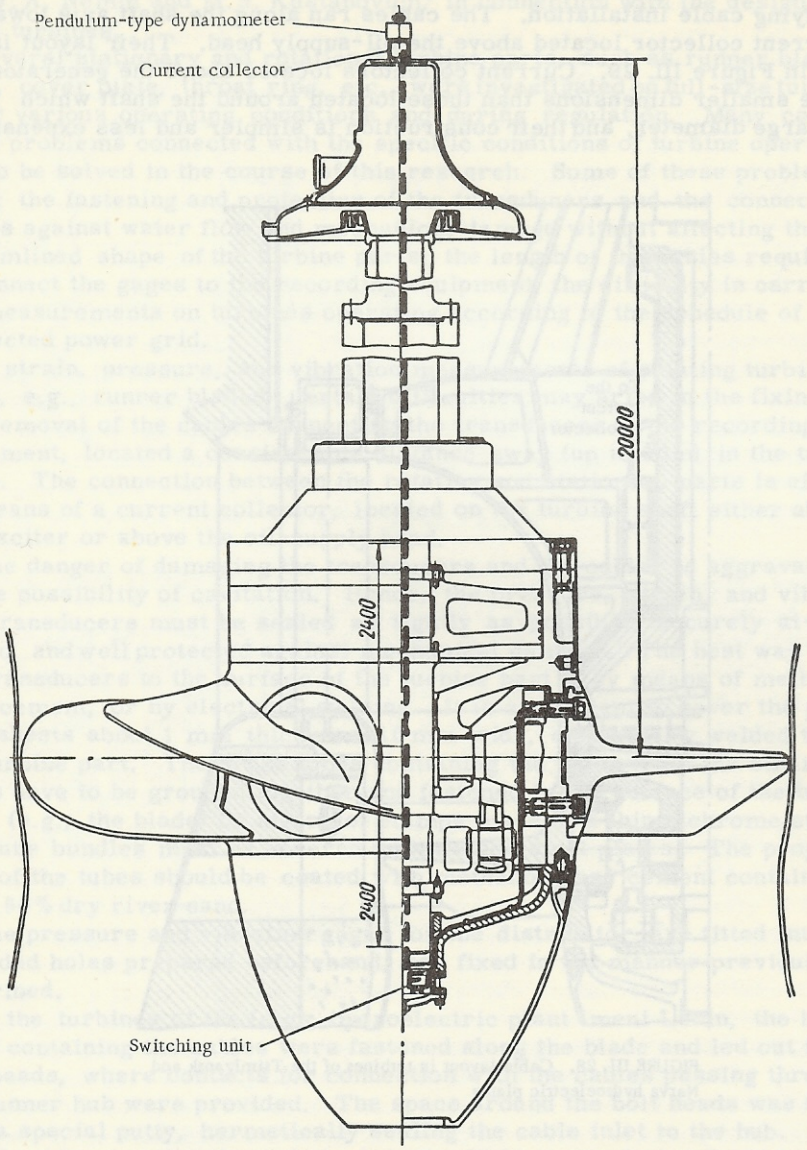


FIGURE III. 29. Cable layout in the turbines of the Volga hydroelectric plant imeni Lenin

2) switching units located inside the runner hub;

3) current collector, located on the generator shaft above the oil-supply head;

4) control switchboard, strain and pressure compensating elements included in the switchboard, loop oscillographs, and other devices located in the turbine room. The schematic layout of the equipment is shown in Figure III. 30.

The new measuring equipment made it possible to obtain cyclic recordings by merely pushing the starting button on the control switchboard. The gages were connected to the measuring channels according to a predetermined program by means of special switches. The signals from the gages were amplified and recorded by the loop oscillographs. Time marks, turbine-speed values, and scale pulses, permitting correct interpretation of the oscillograms, were recorded at the same time on the oscillograph tapes.

In order to protect the measuring channels against environmental interference, shielded cables were used for all connections.

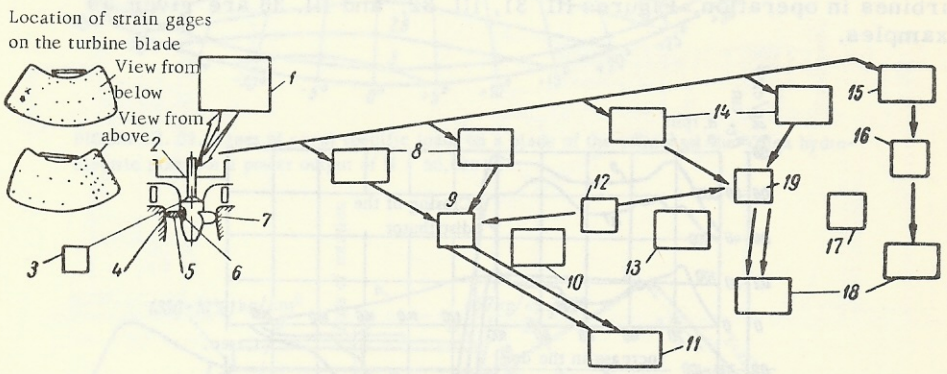


FIGURE III. 30. Schematic layout of the equipment for multiple-point measurements of strains, pressures, and vibrations in the turbine:

1— control switch board; 2— current collector; 3— switching unit; 4— inductive pressure gage; 5— strain gage; 6— vibration gage; 7—tensiometric pressure pick-up in the turbine casing; 8—control consoles for measuring stresses and strains; 9—two-channel unit for strain measurements; 10—voltage-stabilized rectifier for strain measurements; 11—oscillograph for strain recording; 12—generator; 13— voltage-stabilized rectifier for pressure measurements; 14—control consoles for pressure measurements; 15—frequency stabilizer for vibration measurements; 16—two-channel unit for vibration measurements; 17—voltage-stabilized rectifier for vibration measurements; 18—oscillograph for pressure and vibration recording; 19—two-channel unit for pressure measurement.

With the aid of this equipment, specialists at the Volga hydroelectric plant imeni Lenin investigated the forces acting on the runner blades and on the throat-ring shell and determined the strains and stresses occurring in the blades and shafts under the following operating conditions:

1) starting and stopping of the turbines;

2) no-load conditions and synchronization;

3) turbine operation at various power outputs: 25, 50, 75, 100, and 114 Mw;

4) transient conditions during speed regulation;

5) load drops, 125, 90, 60, and 30 Mw.

Sixty pressure gages, 80 strain gages, and 10 vibration gages were mounted on the blades.

The pressure transducers were placed on three cylindrical sections of the blade: at the base, in the middle, and on the periphery.

The strain and vibration transducers were located at points subject to the strongest strains and vibrations.

As a result of investigations made at the above plant, some 400 oscillograms and a few thousand measured values for strain, pressure, and vibration under widely differing operating conditions were collected.

Similar, but less extensive, investigations were carried out at the Tsimlyansk, Narva, Dnieper, and Niva hydroelectric plants. All these not only furnished valuable reference data on the stresses acting on the turbine-unit components, but were also of great importance for general research on turbine operating conditions.

In order to illustrate the data obtained by measurements on full-size turbines in operation, Figures III. 31, III. 32, and III. 33 are given as examples.

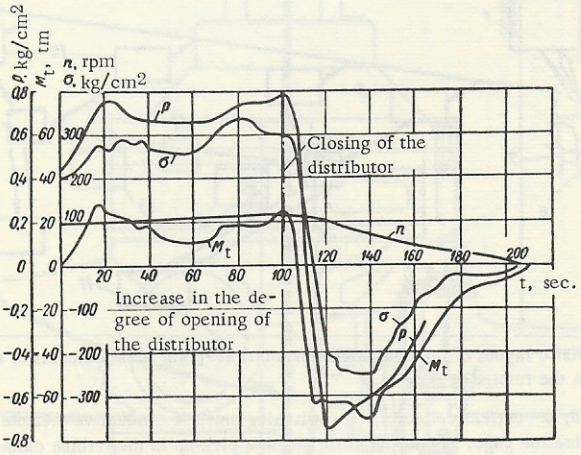


FIGURE III.31. The values of M_t, n, P and δ during load increase and turbine shutdown

Figure III. 31 shows the curves (for the Kaplan turbine at the Narva HEP) of the dependence of torque M_t, speed n, blade pressure P, and stresses σ at a certain point of the blade, on time t during the load increase, and when the turbine is brought to rest.

Figure III. 32 shows the lines of equal specific loads on the turbine blade at the turbines of the Volga hydroelectric plant, for a power output of N = 50,000 kw.

Figure III. 33 shows the lines of equal principal stresses on the upper side of a blade of the turbine at the Volga hydroelectric plant at an output 25,000 kw. Location of gages is also shown.

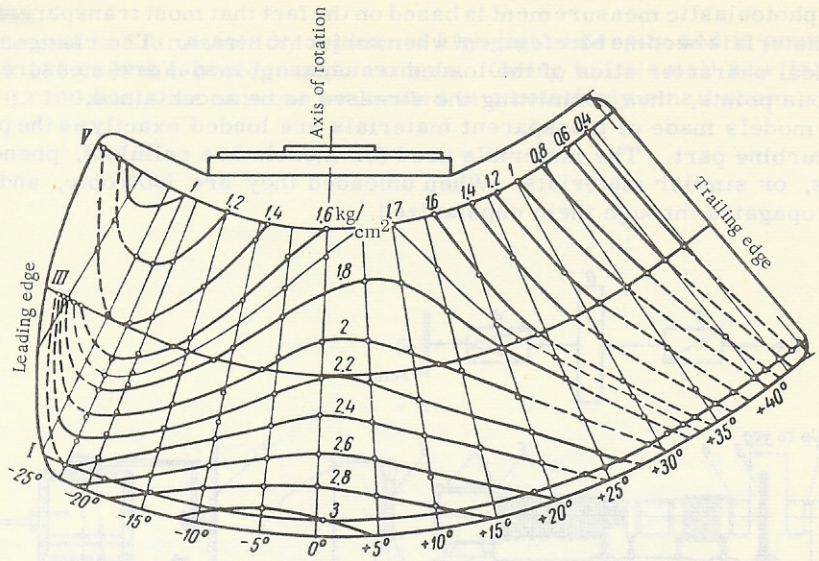


FIGURE III. 32. Lines of equal specific loads on a blade of the turbine at the Volga hydroelectric plant for a power output of N = 50,000 kw

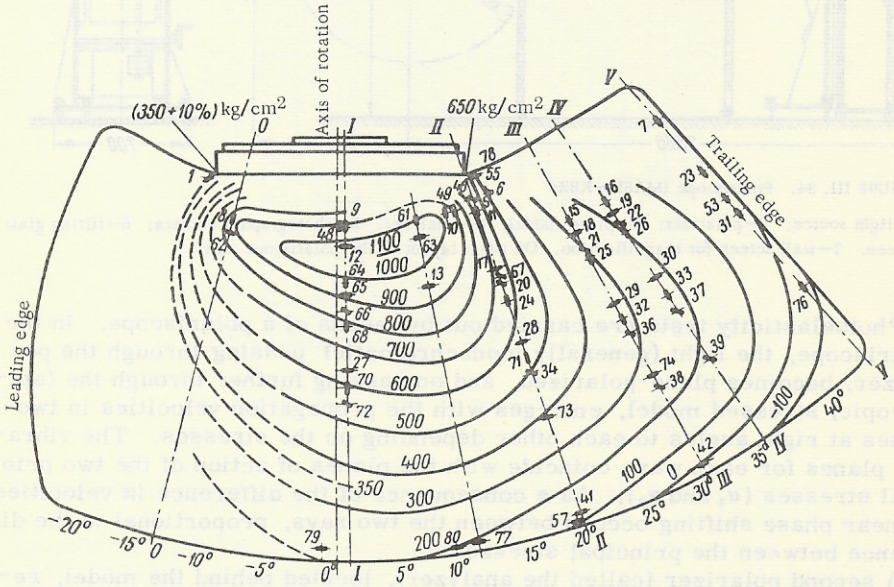


FIGURE III. 33. Lines of equal principal stresses σ_1 on the upper side of a blade of the turbine at the Volga hydroelectric plant, output = 25,000 kw

In turbine construction, photoelastic strain measurements are less frequently used in model testing than direct strain measurements. The principle of photoelastic measurement is based on the fact that most transparent isotropic materials become birefringent when subject to strain. The changes in the optical characteristics of the loaded transparent model are measured at various points, thus permitting the stresses to be ascertained.

The models made of transparent materials are loaded exactly as the prototype turbine part. The materials used for models are celluloid, phenol plastics, or similar materials. When unloaded they are isotropic, and light propagates through them unpolarized.

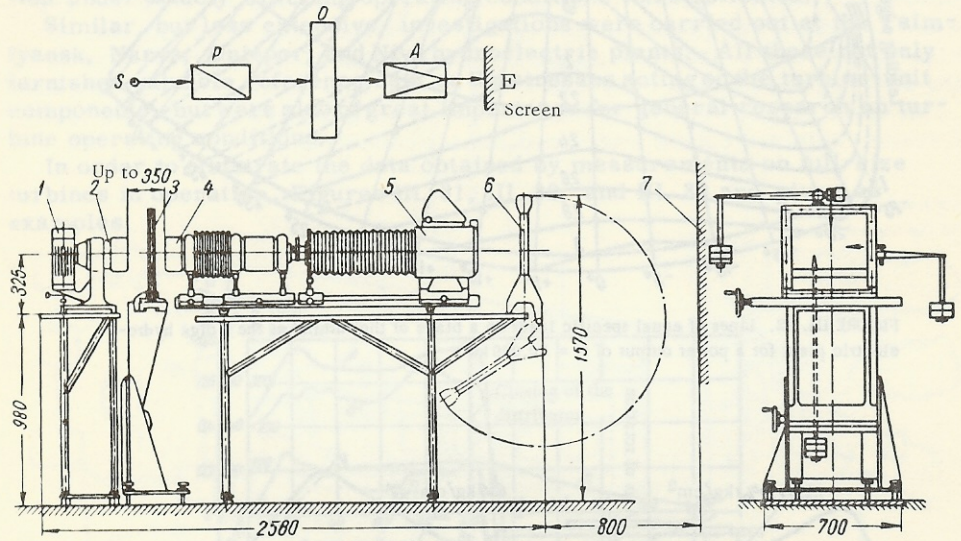


FIGURE III. 34. Polariscope IMASh–KB2:

1—light source; 2—polarizer; 3—plane model; 4—analyzer; 5—photographic camera; 6—tilting glass screen; 7—wall screen for magnification. On top: layout of the polariscope unit.

Photoelasticity tests are carried out by means of a polariscope. In the polariscope, the light (generally monochromatic) passing through the polarizer, becomes plane-polarized, and on passing further through the (anisotropic) stressed model, emerges with the propagation velocities in two planes at right angles to each other depending on the stresses. The vibration planes for each wave coincide with the planes of action of the two principal stresses (σ_1 and σ_2). As a consequence of the difference in velocities, a linear phase shifting occurs between the two rays, proportional to the difference between the principal stresses.

A second polarizer (called the analyzer), located behind the model, recombines the two waves and throws onto the screen an image of the model with dark and light fringe patterns of different widths, corresponding to the distribution of the stresses in the model.

The schematic layout of the polariscope unit is shown in Figure III. 34, with the following notations: *S* —light source, *P* —polarizer, *O* —model,

A—analyzer, E—viewing screen. Underneath is a view of the polariscope built by IMASh (IMASh-KB2 type) with an active-field diameter of 130 mm.

The unit is illuminated by a lamp of high light-intensity and is provided with a 130×180 mm photographic camera. Owing to its small size (3360×××1570×700 mm), the unit can be located in a relatively small room.

Chapter IV

DESIGN AND SELECTION OF THE WATER PASSAGES OF THE TURBINE

17. TYPES OF TURBINE CASINGS

In reaction turbines, the water enters through casings or flumes, extremely diverse both in shape and design. These may be open flumes, cylindrical, or scroll casings (made of concrete or metal).

The type of casing depends on the size of the turbine and on the water head (pressure).

Figure IV. 1 shows the fields of application of various types of casings, depending upon the turbine output and head.

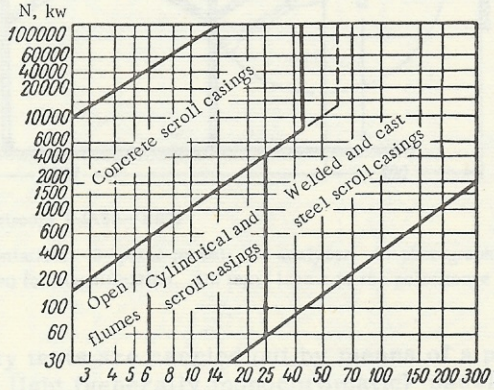


FIGURE IV. 1. Fields of application of various types of casings

Open flumes are used only for small turbines with runner diameters of up to 1.2 m and heads up to 5 or 6 m.

To obtain favorable hydraulic characteristics, relatively large casings are required to prevent the water velocity from exceeding 1 m/sec. The width (B) of the casing (in a plane normal to the turbine center line) should be no less than $3 D_1$. For higher heads, the over-all sizes of open flumes become so large that cylindrical or scroll casings become preferable.

Cylindrical steel casings with frontal water inlet are used for horizontal-shaft turbines with runner diameters of 0.5 to 1.0 m in the range of heads from 5.5 to 25 m.

The most common type of casing is the scroll type (Figure IV. 2). The radial cross-sectional area of the scroll decreases uniformly from the entrance toward the tip (nose). The speed ring, which carries the turbine, is located inside the casing, with the distributor inside it. The speed ring consists either of separate well-streamlined columns (stay vanes) or of a circular piece consisting of an upper and a lower ring and the stay vanes. In concrete scroll casings the speed ring transmits the load from the scroll ceiling to the foundation of the casing. The speed ring in metal casings is the framework which holds together the entire casing.

The scroll casing ensures satisfactory water inflow with the smallest over-all casing size. In well designed casings, the losses are very small. Unlike open flumes and cylindrical casings, the scroll casings permit many components of hydraulic turbines to be located outside the water flow.

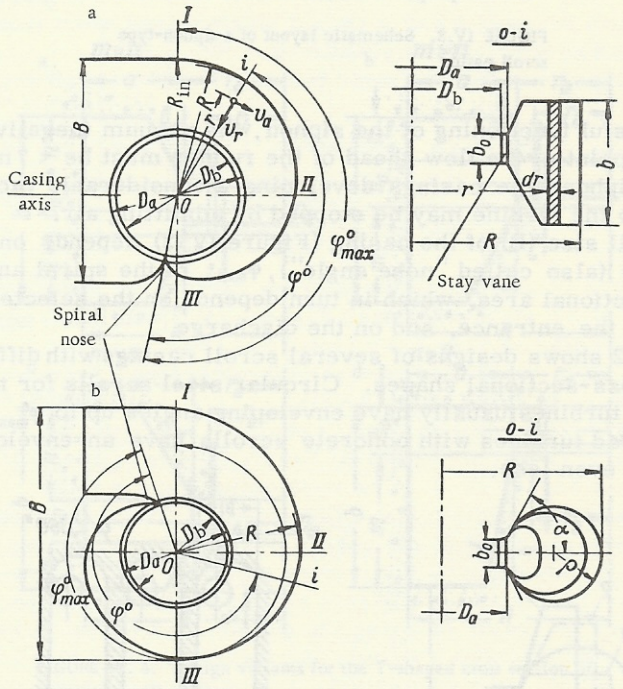


FIGURE IV. 2. Scroll casings:

a — with T-shaped cross section; b — with circular cross section.

Scroll casings are made of concrete or steel, depending on the available head. Concrete casings with T-shaped cross section are used for heads up to 40 m. For heads above 30 m, round, welded or cast casings are used.

Siphon-type scroll casings are used only for very low heads. This type of casing permits installing even large turbines below the headwater level without large-scale excavation work.

The ceiling of the siphon casing is located above the headwater level; the siphon is filled with water by means of an ejector or a vacuum pump. Figure IV. 3 shows schematically a siphon-type scroll casing.

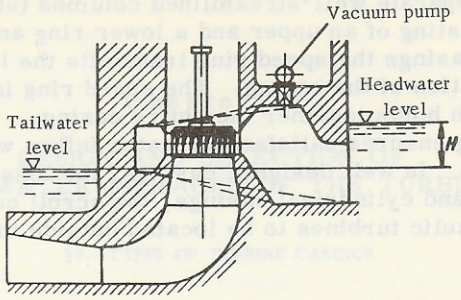


FIGURE IV.3. Schematic layout of a siphon-type scroll casing

For successful functioning of the siphon, the vacuum (negative pressure) at the highest point of the flow ahead of the runner must be < 7 m W.G.

In certain siphon-type casings developing a considerable vacuum, the water flow into the turbine may be stopped by admitting air.

The over-all size (B) of the casing (Figure IV. 2) depends on the enveloping angle (also called "nose angle"), φ_{max}, of the spiral and on the inlet cross-sectional area, which in turn depends on the selected water velocity V_c at the entrance, and on the discharge.

Figure IV. 2 shows designs of several scroll casings with different nose angles and cross-sectional shapes. Circular steel scrolls for medium-head and high-head turbines usually have enveloping angles up to φ^0_{max} = 345 to 360°. Low-head turbines with concrete scrolls have an enveloping angle $\varphi_{max} \cong 180°$ or even less.

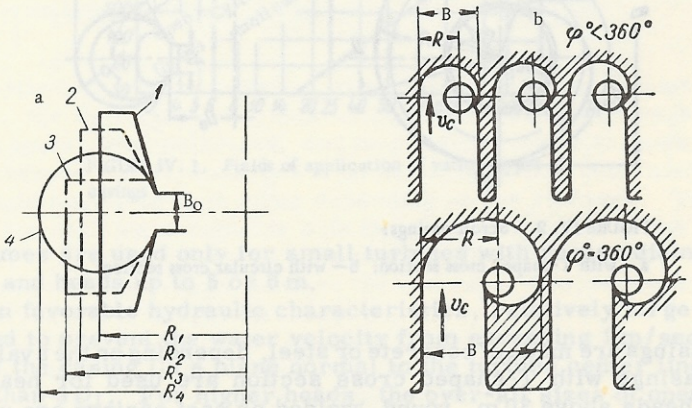


FIGURE IV. 4. Comparison between the over-all sizes of scroll casings:

a— for different cross sections (circular or T-shaped); b— for different nose angles.

A large nose angle of the spiral requires increased casing-width B.

The width (B) is the sum of the speed-ring diameter D_a and the dimensions in the horizontal plane of the cross sections I and III. It is obvious that the discharges through the cross sections I and III, and consequently, their dimensions, diminish with the angle.

The cross-sectional shape of the scroll also affects the magnitude of B. The magnitudes of B for circular and T-shaped casings are shown in Figure IV. 4.

The circular cross section has the largest entrance radius (R), since the T-shaped cross section is narrower and elongated in the vertical plane both in the upward and the downward direction.

Alternative designs of the T-shaped cross section of scroll casings in common use are shown in Figure IV. 5. With respect to the distributor center line, the cross sections are symmetrical (a) and asymmetrical (b, c, d). The ratio between dimensions m and n depends on the design of the powerhouse substructure and the location of the turbine equipment.

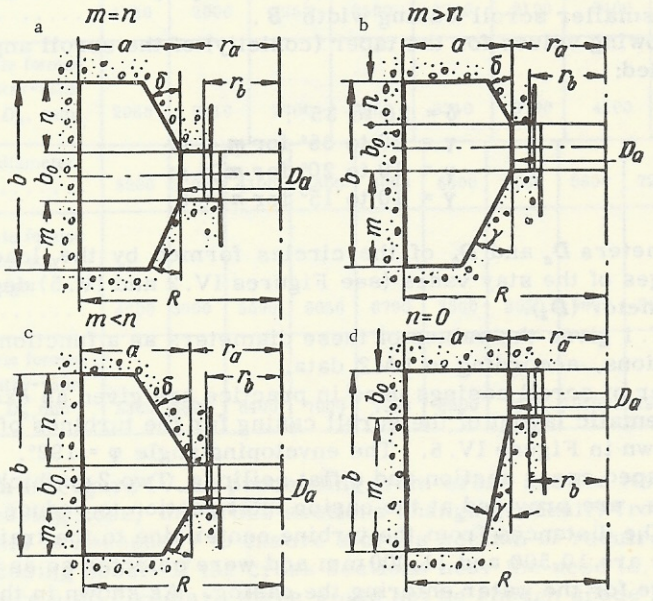


FIGURE IV. 5. Design variants for the T-shaped cross section of concrete scroll casings

All these cross sections are almost equivalent hydraulically. The cross section with a flat ceiling is more convenient for the layout of the turbine-unit equipment. With this particular cross section it is easier to locate the passageways to the turbine pit, and to install the auxiliary equipment and the pipes.

However, as this type of casing is at a considerably lower elevation, the distance between the bottom of the scroll casing and the ceiling of the horizontal diffuser (enlarged section) of the draft tube might prove insufficient.

Although the upward-elongated asymmetrical shape makes the layout of the turbine equipment inside the pit more difficult, it leaves more free space between the scroll and the draft tube; this may be used to accomodate galleries for the discharge of floodwater through the powerhouse.

In selecting the dimensions of the scroll-casing entrance section, especially for $m = 0$ or $n = 0$, care should be exercised to prevent the cross section from becoming too narrow. The following proportions between a and b, resulting from practical experience, are often used (Figure IV. 5):

for $n = 0$ or $m = 0$

$$\frac{b}{a} = 1.5 - 1.8;$$

for $n > 0$ or $m > 0$

$$\frac{b}{a} = \frac{m + n + b_0}{a} = 1.5 - 2.0.$$

A larger ratio between b and a should be employed when it is imperative to obtain a smaller scroll-casing width B.

The following values for the taper (conicity) of the scroll angles are recommended:

δ = 20 to 35°;
γ = 20 to 35° for $m \leqslant n$;
γ = 10 to 20° for $m > n$;
γ = 10 to 15° for $n = 0$.

The diameters D_a and D_b of the circles formed by the leading and trailing edges of the stay vanes (see Figures IV. 2 and IV. 5) depend on the runner diameter (D_1).

Table IV. 1 gives the values of these diameters as a function of the runner dimensions, according to LMZ data.

A number of scroll casings used in practice are given as examples.

The schematic layout of the scroll casing for the turbines of the Uglich HEP is shown in Figure IV. 6. The enveloping angle φ = 192°. The casing has a T-shaped cross section and a flat ceiling. Two 2 m-thick columns, called piers, are provided at the casing inlet section to reduce its internal opening. The distances from the turbine center line to the trailing edges of the piers are 10,500 and 11,000 mm and were selected so as to leave sufficient space for the water entering the casing. As shown in the figure, one of the piers has an inclined trailing edge (see projection (a) in Figure IV. 6) parallel to the scroll cone generatrix, for the same purpose.

Figure IV. 7 shows the design of a turbine scroll casing at the Volga HEP.

To suit construction conditions, the turbine design had to provide for a symmetrical layout of the turbine unit, with the center line passing through the middle of the turbine bay. A scroll casing with an enveloping angle φ = 180° would not meet this requirement. A scroll casing with an enveloping angle φ = 135°, with the bottom of the floor sloping gradually, was therefore used. One dividing pier was provided at the casing entrance.

The scroll shape determines both location and shape of the stay vanes, as well as the load on them. Hence, the design of the speed ring has to be

coordinated with the design of the casing. Speed-ring design will be considered in a separate chapter of this book.

Steel scroll casings with circular cross section, for medium heads, are made of steel plates welded to the speed ring. Formerly, the plates were riveted. The schematic layout of this casing is shown in Figure IV. 8; a plan and a cross section of the welded casing are shown in Figure IV. 9.

This casing is intended for a turbine operating at H = 100 m.

TABLE IV. 1

Diameters D_a and D_b, as a function of D_1 for standard-type sizes of turbines

Nominal runner diameter D_1, mm	1200	1400	1600	1800	2000	2250	2500	2750	3000
Diameter of circle formed by the speed-ring stay-vane leading edges, D_b, mm	1750	2000	2250	2500	2750	3100	3400	3750	4100
Diameter of circle formed by speed-ring stay-vane trailing edges D_a, mm	2060	2410	2700	3000	3340	3700	4100	4400	4800

Nominal runner diameter D_1, mm	3300	3700	4100	4500	5000	5500	6000	6600	7200	8000	9000
Diameter of circle formed by the speed-ring stay-vane leading edges D_b, mm	4500	5000	5500	6050	6700	7350	8050	8800	9600	10700	12000
Diameter of circle formed by speed-ring stay-vane trailing edges D_a, mm	5300	5800	6400	7000	7900	8600	9450	10400	12000	12500	14000

As shown in Figure IV. 8, proceeding from cross section No. 7 toward the scroll-casing nose, the cross sections change gradually from circular to oval. This is necessary to ensure a cross section of required area at the scroll-casing nose. If the cross sections near the nose (e. g., sections 23 or 24) were also circular, there would not be enough space left for them between the circular entrance section and the speed ring. The spiral contour is represented on the plan view by a broken line from sections 1 to 23 instead of being shown by the theoretical curve. The scroll casing may easily be constructed from conically rolled plates.

If the spiral casing sections were not made of flat plates, but, as demanded by theory, of curved ones, they would have to be stamped instead of rolled, which would require a large quantity of expensive stamping dies.

The replacement of the curvilinear contour of the spiral by a polygonal contour scarcely affects conditions of water flow. The number of sections is selected so as to make the contour sufficiently smooth.

Each cross section requires plates of different thickness. The plates at the entrance section are 30 mm thick, becoming thinner as the cross-sectional area decreases, until they reach S = 16 mm at the spiral nose. In spirals with a full opening angle ($\varphi°$) all the speed-ring stay-vanes have the same profile.

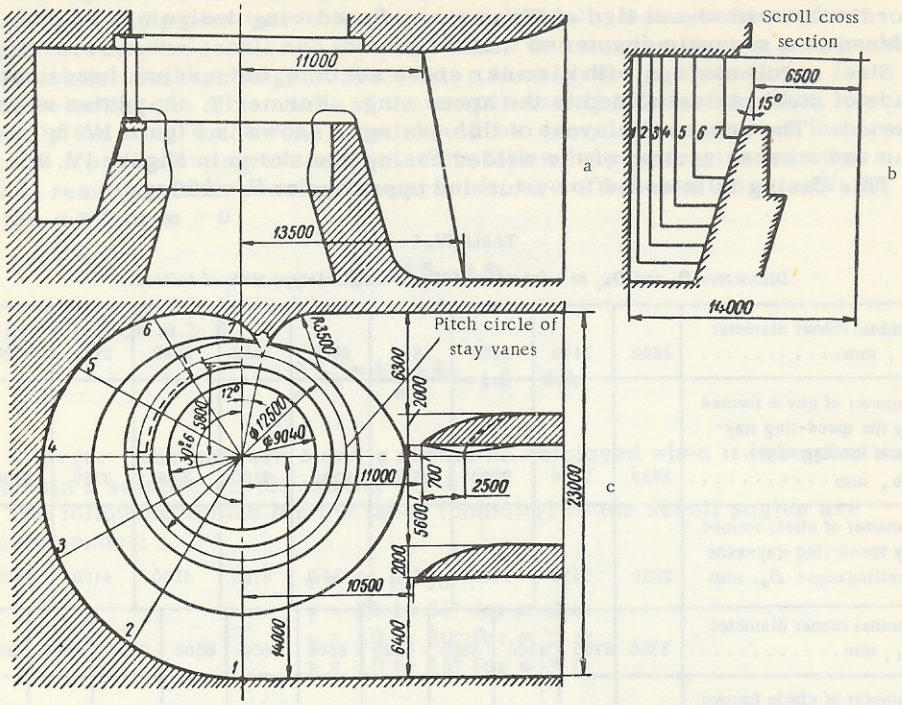


FIGURE IV.6. Scroll casing for the turbines of the Uglich HEP

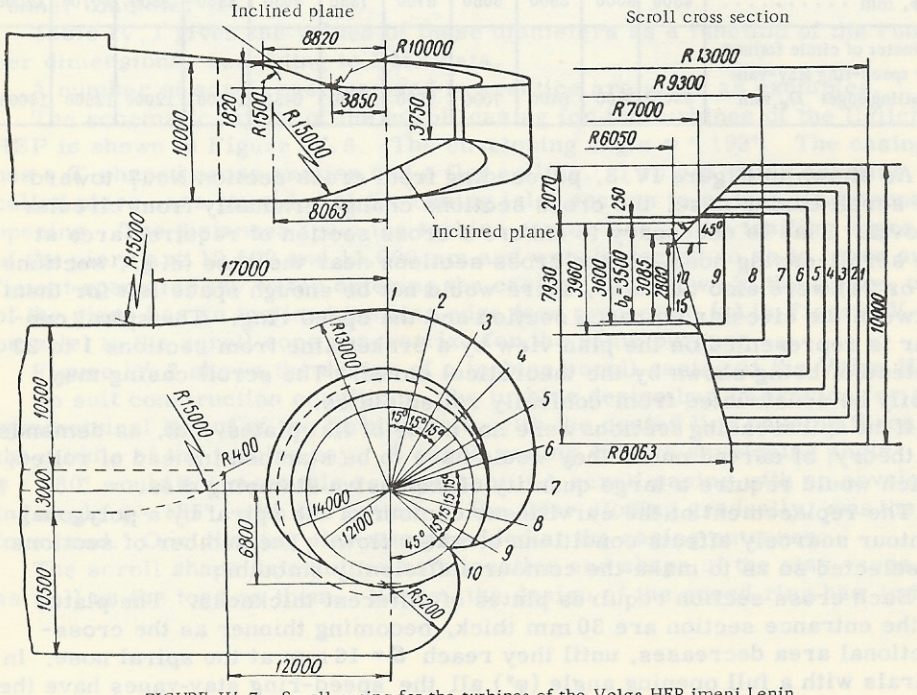


FIGURE IV.7. Scroll casing for the turbines of the Volga HEP imeni Lenin

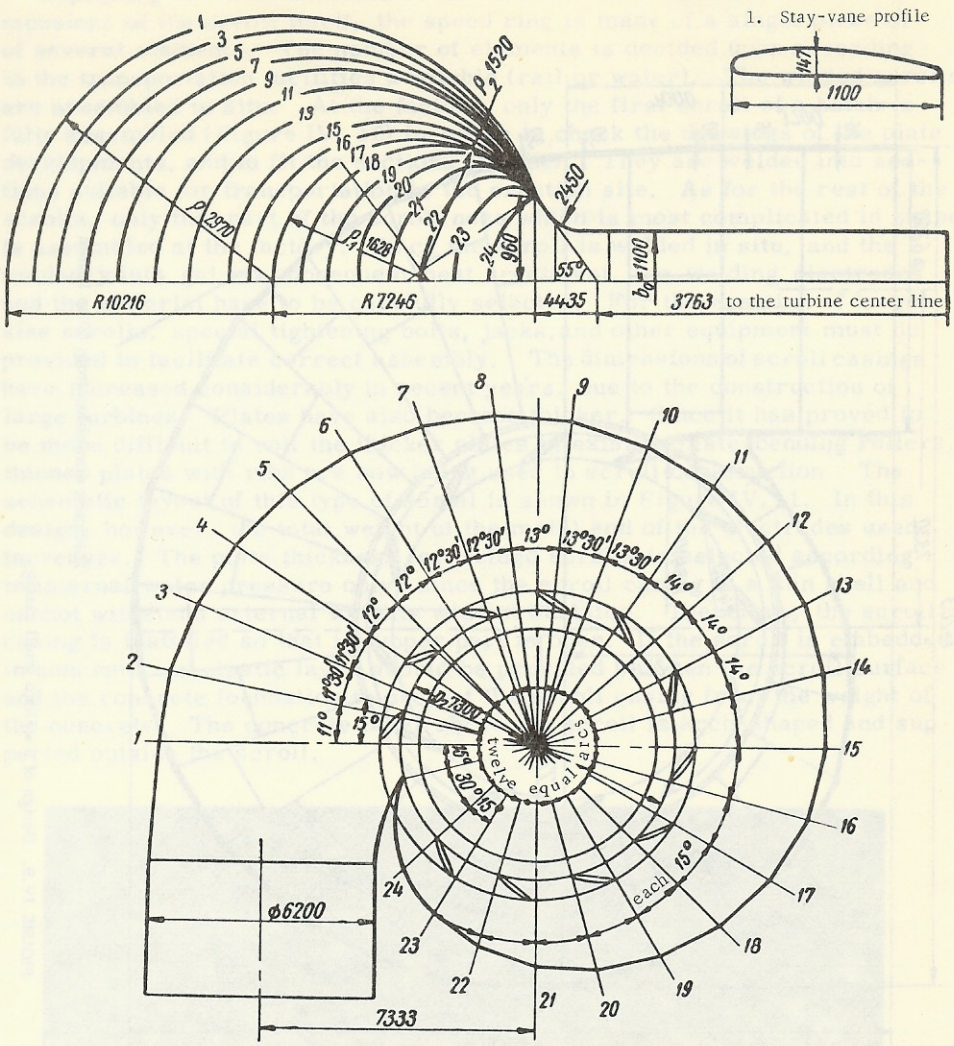


FIGURE IV. 8. Design of a steel scroll casing

Table of scroll-casing cross-sectional dimensions

Designation	Number of the scroll section											
	1	2	3	4	5	6	7	8	9	10	11	12
R	10 216	10 071	9927	9772	9627	9472	9295	9150	8972	8762	8583	8382
Q	2970	2900	2830	2755	2685	2610	2525	2455	2370	2270	2185	2090
Q_1												
Q_2												
Designation	Number of the scroll section											
	13	14	15	16	17	18	19	20	21	22	23	24
R	8190	7975	7758	7516	7246	6957	6660	6349	6022	5680	5310	4935
Q	2000	1900	1800	1690								1172
Q_1					1628	1571	1512	1451	1386	1319	1246	
Q_2					1520	1380	1135	930	715	490	247	

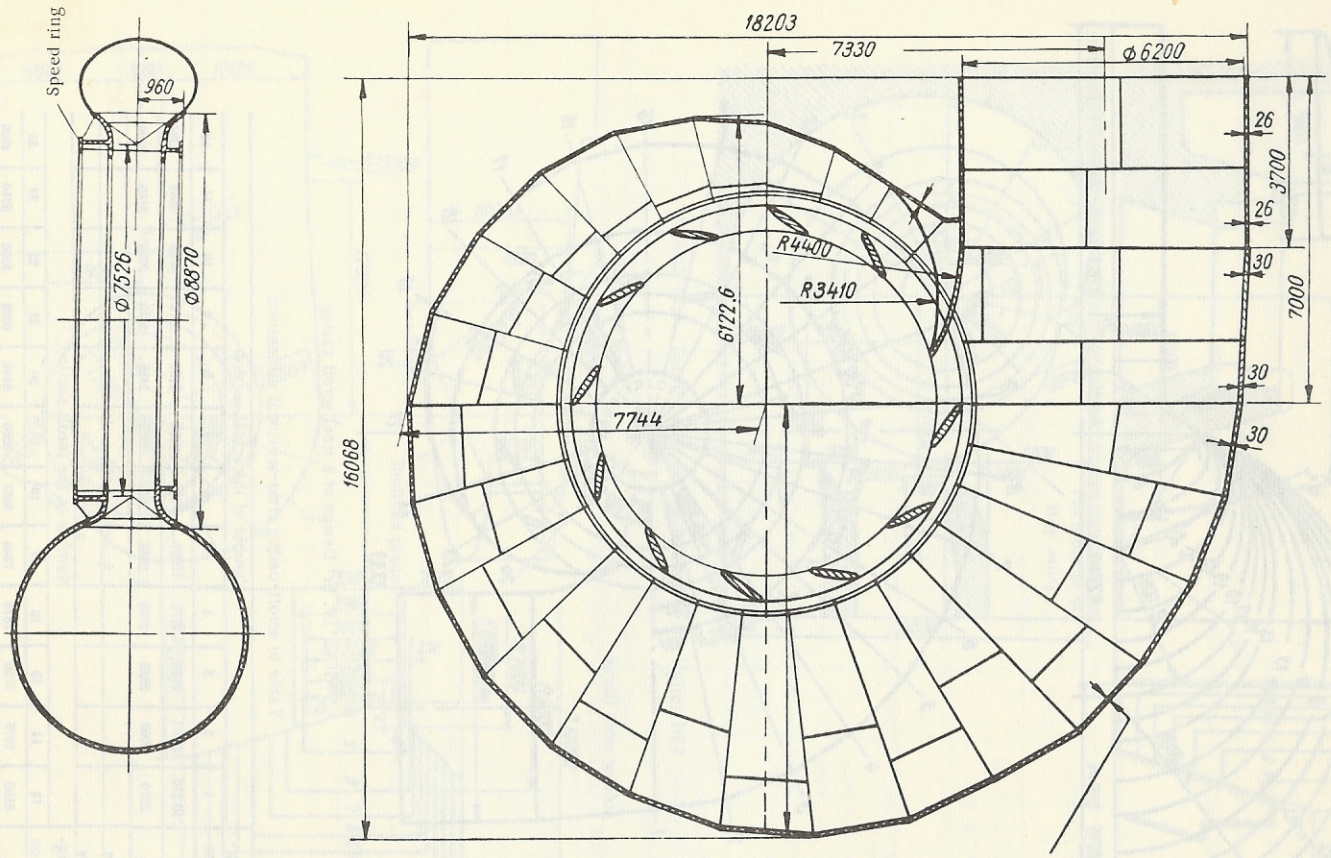


FIGURE IV.9. Design of a welded scroll casing

Depending on the dimensions of the entrance cross section and the dimensions of the scroll itself, the speed ring is made of a single piece or of several elements. The number of elements is decided upon according to the transportation facilities available (rail or water). The welded scrolls are assembled in situ. At the factory, only the first scroll of a batch is fully assembled (Figure IV. 10) in order to check the drawings of the plate developments, and to fit the sections together. They are welded into sections suitable for transportation to the erection site. As for the rest of the scrolls, only that part of the scroll nose which is most complicated in shape is assembled at the factory. Since the scroll is welded in situ, and the welded joints get no subsequent heat treatment, the welding electrodes and the material have to be carefully selected. For the erection of large-size scrolls, special tightening bolts, jacks, and other equipment must be provided to facilitate correct assembly. The dimensions of scroll casings have increased considerably in recent years, due to the construction of large turbines. Plates have also become thicker. Since it has proved to be more difficult to roll the thicker plates in existing plate-bending rollers, thinner plates with ribs are now being used in scroll construction. The schematic layout of this type of scroll is shown in Figure IV. 11. In this design, however, the total weight of the metal and of the electrodes used increases. The plate thickness for welded scrolls is selected according to internal water pressure only, since the scroll casing is a thin shell and cannot withstand external weights without buckling. Therefore, the scroll casing is installed so that its upper part is open. If the scroll is embedded in concrete, an elastic layer should be provided between the scroll surface and the concrete foundation to protect the scroll casing from the weight of the concrete. The concrete layer above the scroll is arch-shaped and supported outside the scroll.

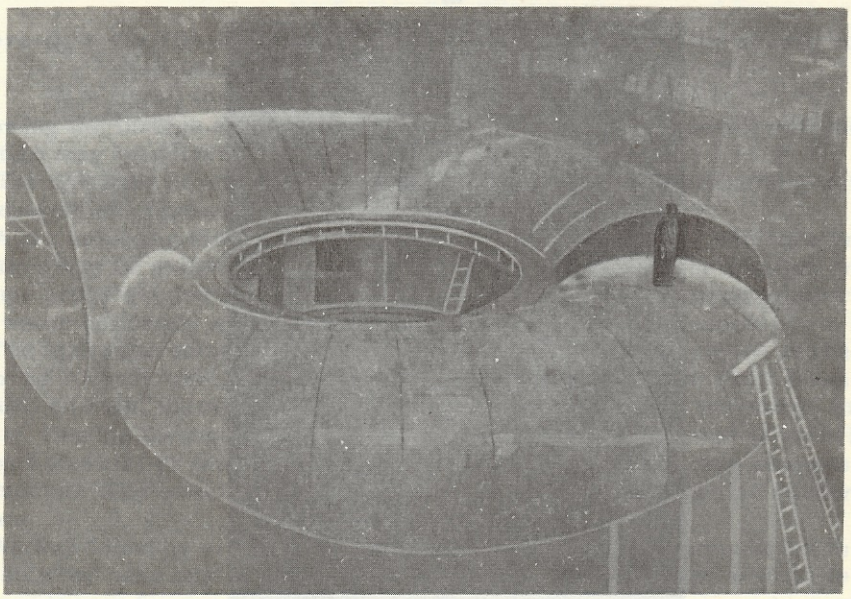


FIGURE IV. 10. Assembly of a welded scroll casing

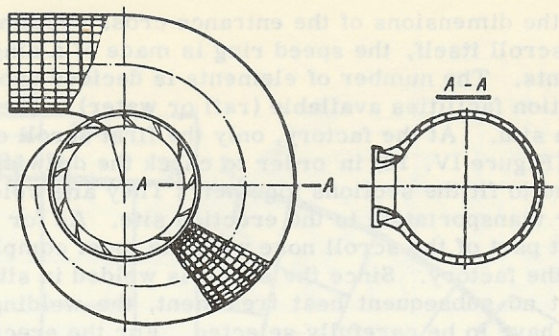


FIGURE IV.11. Design of a welded scroll casing with ribs

Cast-steel scroll casings are used for high-head turbines (Figure IV.12). A high-head turbine is usually characterized by a small water discharge, the entrance cross section of the scroll thus becoming rather small. Because of the high head, the scroll walls have to be very thick. To facilitate railroad transportation of cast-steel scrolls, they are usually made of several sections divided along radial planes and bolted together at the flanges.

Figure IV. 12 shows a scroll casing of a turbine for a head of 300 m.

Cast scroll casing usually serves as support for the turbine and accommodates the distributor, servomotors, guide bearings, and other components. Therefore, bosses and projections for locating the servomotors and connections for the pressure regulator and other parts should be provided on the scroll. Cast scroll casings are usually completely machined at the factory, where the temporary assembly for inspection purposes, and hydraulic tests according to the standards in force, are also carried out.

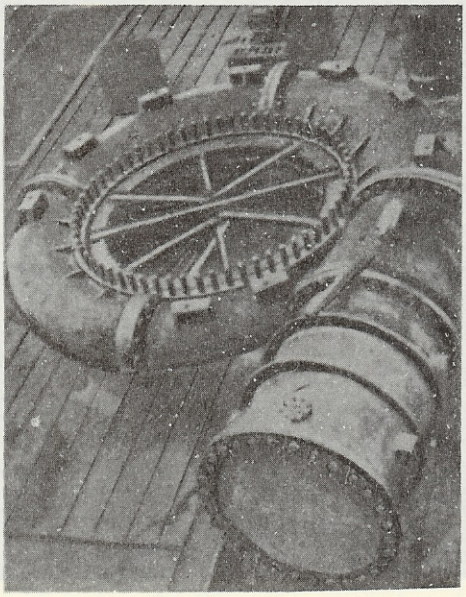


FIGURE IV. 12. Shop assembly of a cast steel scroll casing

When designing a cast scroll casing for high heads, consideration must be given not only to the strength of the walls, but also to the rigidity of the flange connections. If the latter are too thin and insufficiently rigid, they might not ensure sufficient tightness of the whole assembly.

Usually, cast scroll casings are not completely embedded in concrete, but are either laid on a ring-shaped concrete foundation or partially embedded in it.

18. HYDROMECHANICAL COMPUTATION OF THE SCROLL CASING

In designing a scroll casing the first parameter to be established is the water discharge. Usually, the scroll is designed for a discharge which corresponds to the maximum power output under the rated head. The scroll may also be designed for a discharge corresponding to the maximum efficiency. In this case the dimensions will be less. It is sometimes necessary to design the scroll for the maximum discharge corresponding to the rated power under the minimum head, in which case the dimensions will increase. For the design of casings, the discharge should be selected according to steady operating conditions.

The water flow in the scroll casing should be axisymmetrical and form a potential vortex.

The meridian section of the scroll is selected so that the water flows uniformly around the circumference of the distributor. In other words, the following condition should be satisfied:

$$Q_\varphi = \frac{Q\varphi}{2\pi}, \qquad \text{(IV. 1)}$$

where Q_φ = the discharge through the meridian section of the scroll, corresponding to the nose angle φ;

Q = (total) discharge through the turbine.

Knowing the turbine discharge, the discharge through the scroll entrance section may be determined according to the nose angle φ.

The entrance cross-sectional area (F_{en}) is determined according to the predetermined (given) mean velocity at the entrance section.

After selecting the shape of the scroll cross section, the entrance cross section may be calculated from the known value of F_{en}. The adopted entrance cross section determines the adjacent sections required to distribute the water uniformly around the whole distributor circumference.

The hydraulic computation of the scroll casing according to the relationship $v_u r$ = const, proceeds from the assumption that when a fluid flows around an axis, the moment of momentum of each particle is constant: the liquid, flowing through the spiral, performs no work at all, but is merely caused to whirl by the scroll and distributor; the whirling flow changes its momentum only on entering the runner, thus causing the turbine runner to rotate.

As was found by practical experience, this method of computation is suitable for nose angles $\varphi \geqslant 180°$, and ensures a scroll shape with little energy losses for properly selected velocities, thus imparting a high efficiency to the turbine.

The mean velocity at the entrance cross section of the scroll is selected according to the head: $v_m = k\sqrt{H}$.

For concrete scroll casings k = 0.9 to 1.1; for metal scrolls k = 0.8 to 1.0.

At each point of the flow in the scroll casing, the water velocity may be divided into two components: the radial velocity v_r directed along the radius toward the turbine center line, and the peripheral velocity v_u, normal to the radius (Figure IV. 2).

The radial velocity is

$$v_r = \frac{Q}{\pi D_e b_0}, \qquad \text{(IV. 2)}$$

where Q = discharge through the turbine;
D_e = diameter of circle formed by trailing edges of stay vanes;
b_0 = distributor height.

The radial velocity component should be constant, to ensure a uniform water flow around the whole circumference of the distributor.

At each point, the peripheral velocity should obey the law of constant areas

$$v_u r = \text{const} = K,$$

where r = distance from the turbine center line to the point considered;
K = a constant of the spiral casing.

Consequently, the discharge through any section i having an outer radius R equals:

$$q_i = \frac{Q\varphi_i^\circ}{360} = \int_{r_e}^{R} v_u \, dF,$$

but

$$v_u = \frac{K}{r}, \text{ and } dF = b\,dr,$$

consequently,

$$q_i = K \int_{r_e}^{R} \frac{b}{r}\, dr. \qquad \text{(IV. 3)}$$

The central angle corresponding to the i-th section is

$$\varphi_i^\circ = \frac{360 q_i}{Q} = \frac{360K}{Q} \int_{r_e}^{R} \frac{b}{r}\, dr. \qquad \text{(IV. 4)}$$

The discharge through the entrance section of the scroll, corresponding to the largest nose angle φ_{max}° is

$$Q_{en} = \frac{Q\varphi_{max}^\circ}{360} = K \int_{r_e}^{R_{en}} \frac{b}{r}\, dr. \qquad \text{(IV. 5)}$$

With known discharge through the entrance section Q_{en}, and given entrance velocity and section shape, the entrance cross-sectional area F_{en} and the scroll constant K can easily be determined.

The position in the horizontal plane of other similar scroll sections is then calculated.

Calculations for scroll casings of T-shaped cross section. It is easier to calculate concrete scroll casings of T-shaped cross section by the graphic-analytical method, as follows.

One draws the entrance section ABCHDE (Figure IV. 13) so that the discharge Q_{en} may pass through it with velocity v_m; afterwards, one determines the position on the horizontal plane of the other scroll cross sections.

Changes in the section dimensions are calculated according to a given law. For instance, the location of the exterior angles should be on the lines AC and EH or on curves, such as parabolas.

Assuming preliminarily the constant $K = 1$ in the formula (IV. 5), we obtain

$$q'_{max} = \int_{r_B}^{R_{en}} \frac{b}{r}\, dr.$$

This integral is calculated by a graphical method. The values $\frac{b}{r}$ as a function of radius R, for the entrance section and for the intermediate sections 1, 2, 3, and 4, are laid off on the vertical to an arbitrary scale.

The areas bounded by the curves $mnab$, m_1n_1ab, m_2n_2ab, m_3n_3ab, m_4n_4ab and by the axis of abscissas, will represent the discharges q'_{max}, q'_1, q'_2, q'_3, and q'_4 for $K = 1$ through the above-mentioned sections.

After determining the area $mnab$ with due regard for the selected scale, the value of the constant K may be caluclated from $K = \frac{q_{max}}{q'_{max}}$.

Knowing the value of K, one may also determine the true values of $q_1 = Kq'_1$, $q_2 = Kq'_2$, $q_3 = Kq'_3$ and $q_4 = Kq'_4$.

The curve $Q = f_1(R)$ may be plotted (see Figure IV. 13) from the calculated values q_{max}, q_1, q_2, q_3, q_4 and the corresponding radii R_{en}, R_1, R_2, R_3, R_4.

The curve $\varphi = f(R)$, calculated by the formula $\varphi = \frac{360q}{Q}$, is plotted on the same diagram. It is obvious that for $\varphi = 0$ the discharge $q = 0$, and that the radius R_{en} corresponds to the angle φ_{max}.

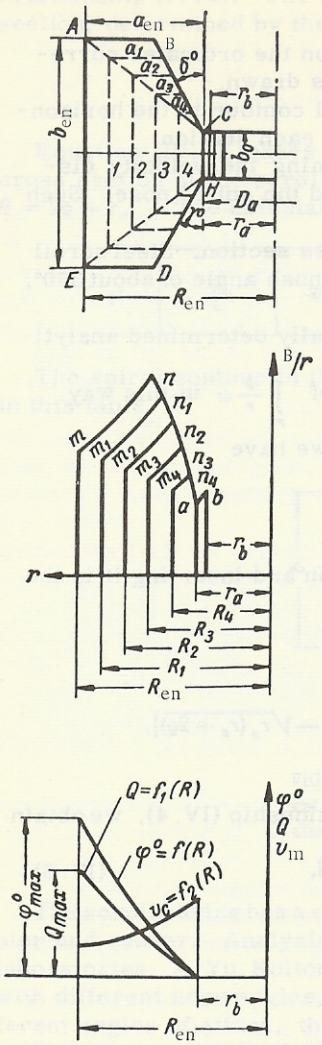


FIGURE IV. 13. Graphic-analytical computation of concrete scroll casings for $v_u r = \text{const}$.

The curve $\varphi = f(R)$, calculated by the formula $\varphi = \frac{360q}{Q}$, is plotted on the same diagram. It is obvious that for $\varphi = 0$ the discharge $q = 0$, and that the radius R_{en} corresponds to the angle φ_{max}.

The mean velocity through each section is calculated from the relationship $v_m = \frac{q_i}{F_i}$, where F_i is determined by the geometrical dimensions of the section i.

The velocity v_m is plotted to an arbitrary scale on the ordinates corresponding to each section, and then curve $v_m = f_2(R)$ is drawn.

Using the curve $\varphi = f(R)$, we may plot the spiral contour in the horizontal plane, as well as its dimensions determined for each section.

Sometimes, scroll casings are computed assuming the velocity distribution to be uniform, or falling constantly toward the spiral nose. Such methods are not common in Soviet practice.

Computation of scroll casings with circular cross section. Steel scroll casings with circular cross section usually have a nose angle of about 360°, and are computed assuming $v_u r$ = const.

The dimensions of the circular sections are usually determined analytically, since it is quite easy to calculate the value of $\int_r^b \frac{b}{r}\,dr$ in this way.

According to the designations in Figure IV. 14, we have

$$\left(\frac{b}{2}\right)^2 + (r-a)^2 = \varrho^2.$$

By determining the value of b from this relation and inserting it in the integral $\int \frac{b}{2}\,dr$, we obtain

$$2\int_{r_a}^{r_a+2\varrho} \frac{b}{2}\,\frac{dr}{r} = 2\int_{r_a}^{R} \sqrt{\varrho^2-(r-a)^2}\cdot\frac{dr}{r} = 2\pi\left[r_a+\varrho-\sqrt{r_a(r_a+2\varrho)}\right].$$

By inserting the value of the integral in the relationship (IV. 4), we obtain

$$\varphi_i^\circ = C\left[r_a+\varrho-\sqrt{r_a(r_a+2\varrho)}\right], \qquad \text{(IV. 6)}$$

where

$$C = \frac{720K\pi}{Q}.$$

The discharge through the entrance cross section of the scroll $Q_{max} = Q\frac{\varphi^\circ_{max}}{360}$. For the permissible mean value of velocity v_m, the sectional area is

$$F = \pi\varrho^2_{max} = \frac{Q\varphi^\circ_{max}}{v_m 360},$$

whence

$$\varrho_{max} = \sqrt{\frac{Q\varphi^\circ_{max}}{360 v_m \pi}}.$$

The constant C may be calculated by inserting the values for the enveloping angle and the radius of the entrance cross section ϱ_{max}, into the relationship (IV. 6). The relationship (IV. 6) gives the value of ϱ for any section, determined by the angle $\varphi°$

$$\varrho = \frac{\varphi°}{C} + \sqrt{2r_a \frac{\varphi°}{C}} \qquad \text{(IV. 7)}$$

Equation (IV. 7) makes it possible to calculate the radius of the circular cross section of the scroll case for the angles $\varphi°$, and to determine $R = 2\varrho + r_a$. The calculation is usually tabulated:

$\varphi°$	$\frac{\varphi°}{C}$	$2r_a \frac{\varphi°}{C}$	$\sqrt{2r_a \frac{\varphi°}{C}}$	ϱ	2ϱ	$R = 2\varrho + r_a$

The spiral contour in the horizontal plane may be drawn from the data in this table.

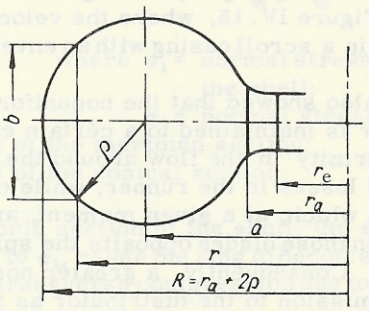


FIGURE IV.14. Diagram for the analytical computation of the scroll casing with circular cross section

The scroll casing has a considerable influence on the losses in the distributor and runner. Analyzing the experimental data obtained in the LMZ laboratories, A. Yu. Kolton points out that scroll casings of different shape, with different nose angles, guide the flow toward the distributor under different angles of attack, thus causing different losses in the distributor.

Inasmuch as the angle of attack changes with the variation in the degree of the distributor opening, an optimum opening of the distributor for a certain given shape of the guide vanes exists for each scroll casing.

There is an optimum range of discharges for each shape of scroll casing, within which higher turbine efficiencies may be obtained than for any other shape and dimensions.

It is thus possible — within certain limits, of course — to adapt the region of optimum efficiencies to corresponding discharges by choosing a suitable scroll casing.

It was also found experimentally that the discharge capacity of a turbine does not depend upon the scroll casing, since the discharge through the runner is determined solely by the direction of the flow prior to entry; this direction depends entirely on the distributor, which acts like a relatively dense radial blade cascade.

Investigations were carried out at the LMZ laboratories into the effect of the scroll-casing nose angle on velocity fluctuations. It is an established fact that in the scroll casing the radial and peripheral velocity components v_r and v_u are almost uniformly distributed along the distributor circumference, and coincide with the rated values.

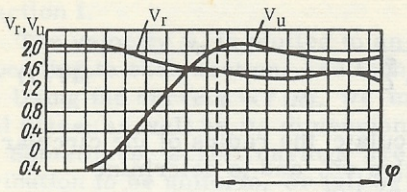


FIGURE IV. 15. Velocity distribution in the scroll casing ($\varphi < 360°$)

The distribution of the velocities v_u and v_r is nonuniform in that part of the distributor periphery not enveloped by the scroll. At the casing axis, the peripheral velocities v_u are almost equal to zero, increasing toward the entrance cross section, and even becoming negative in the vicinity of the spiral nose. The radial velocities v_r have maximum values at the casing axis, and diminish toward the spiral nose (see Figure IV. 2).

The smaller the enveloping angle φ, the greater the velocity fluctuations. This is illustrated in Figure IV. 15, where the velocity distribution of the components v_u and v_r in a scroll casing with an enveloping angle $\varphi < 360°$ is given.

The investigations also showed that the nonuniformity of the flow before entering the distributor is maintained to a certain extent behind the distributor, causing nonuniformity in the flow around the runner blades. This fact leads to increased losses in the runner, while cavitation appears earlier on those runner blades which, at a given moment, are opposite to the casing entrance, whereas on those blades opposite the spiral part of the casing cavitation is delayed. Consequently, a greater nose angle improves the conditions of water admission to the distributor as it ensures a more uniform velocity distribution.

However, an increase in the nose angle, with the width of the scroll and consequently of the turbine bay kept unchanged, leads to higher velocities in the scroll and, hence, to greater losses.

The experimental data from LMZ show that the optimum enveloping angle for medium-head Kaplan turbines varies from φ = 180 to 195°. The recommended value of the external-wall radius of the entrance cross section is R_{en} = (1.5 to 1.6) D_1.

An increase in the enveloping angle up to φ = 240 to 270° for the same radius R_{en} leads to a drop in turbine efficiency of 2 to 2.5%.

Comparative tests on scroll casings of the same width and for the same mean velocity, but with different enveloping angles, φ = 180° and φ = 135°, showed that the efficiency of the turbine model with φ = 180° exceeds the efficiency of the turbine model with φ = 135° by 1 to 2%.

19. DESIGN OF STEEL SCROLLS FOR STRENGTH

The steel scroll casing is designed to withstand the internal water pressure, and the thickness of the shell is determined as a function of this pressure.

The internal water pressure in the scroll casing changes according to the operating conditions. It is constant during the steady operation of the turbine, and varies during the transient regulation process.

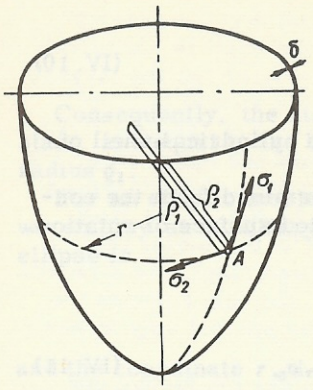


FIGURE IV.16. Stresses in a shell-like body of revolution, caused by uniform pressure

Until recently, the design of the scroll casing for strength was carried out by the method proposed by A. E. Zhmud' /21/. According to him, computation is based on the assumption that each radial section through the scroll casing is a shell, obtained by rotating the given section about the turbine center line, i.e., variations in the casing cross sections are neglected. For the shell represented in Figure IV. 16, the relationship between the stress at point A and the pressure p, is expressed (according to Timoshenko) by

$$\frac{\sigma_1}{\varrho_1} + \frac{\sigma_2}{\varrho_2} = \frac{p}{\delta}, \qquad \text{(IV. 8)}$$

where σ_1 = normal stress at a horizontal section of the shell;
σ_2 = normal stress at a meridian section;
ϱ_1 = radius of curvature of the meridian section;
ϱ_2 = radius of curvature of the conical section;
δ = shell thickness.

In any ring-shaped conic section of the shell, the stresses σ_1 acting in the shell, and σ_2 normal to σ_1, cause the ring to become elongated; the relative elongation, allowing for transverse compression due to σ_1, is given by

$$\frac{2\pi(r+\Delta r)-2\pi r}{2\pi r} = \frac{1}{E}(\sigma_2 - \nu\sigma_1),$$

where r = radius of the ring;
E = modulus of elasticity;
ν = Poisson's ratio (ν = 0.3 for steel).

Consequently, the changes in the radius of the ring-shaped section are

$$\Delta r = \frac{r}{E}(\sigma_2 - \nu\sigma_1). \qquad \text{(IV. 9)}$$

Besides the stresses due to the internal pressure, additional stresses occur in the shell at the joints between the scroll and the speed ring and at the joints between scroll elements of different thickness at the meridian section. These three types of stresses are added, and the resulting stress calculated.

Stresses in the shell due to internal pressure (tensile shell stresses). In the circular meridian section, through the scroll element, the scroll shell represents a torus (Figure IV. 17). If the radius of the meridian section of the torus is ϱ_1, the other principal radius ϱ_2 at any point A at radius r is

$$\varrho_2 = \frac{r}{\sin\alpha} = \frac{r\varrho_1}{(r-r_0)}.$$

Then, according to formula (IV. 8),

$$\frac{\sigma_1}{\varrho_1} + \frac{\sigma_2 (r - r_0)}{r \varrho_1} = \frac{p}{\delta}$$

or

$$\sigma_1 + \frac{(r - r_0)}{r} \sigma_2 = \frac{p \varrho_1}{\delta} = \sigma_0, \qquad \text{(IV. 10)}$$

where σ_0 = the transversal stress in the thin-walled cylindrical shell of radius ϱ_1.

The stress σ_1 in the meridian section can be determined from the condition of equilibrium of the forces acting on the shaded surface of rotation.

$$2\pi r \delta \sigma_1 \sin \alpha = p\pi (r^2 - r_0^2),$$

whence

$$\sigma_1 = \frac{p (r^2 - r_0^2)}{2r\delta \sin \alpha} = \frac{p (r^2 - r_0^2) \varrho_1}{2r\delta (r - r_0)} = \frac{(r + r_0)}{2r} \sigma_0. \qquad \text{(IV. 11)}$$

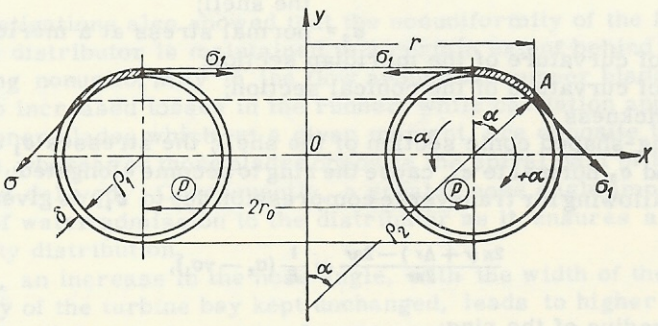


FIGURE IV.17. Stresses in a torus of circular cross section

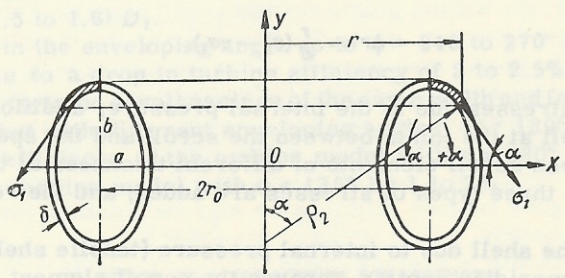


FIGURE IV.18. Stresses in a torus of elliptical cross section

It results from the expression (IV. 11) that stress σ_1 increases inversely with r, becoming largest at the point where the scroll element is connected to the speed ring, where $r = r_s$. For $r = r_0$; $\sigma_1 = \sigma_0$. It follows from the relationships (IV. 10) and (IV. 11)

$$\sigma_2 = \frac{r}{r - r_0}(\sigma_0 - \sigma_1) = \frac{\sigma_0}{2}. \qquad \text{(IV. 12)}$$

Consequently, the stresses in a meridian section of the torus are constant, and equal to the corresponding stresses in a cylindrical pipe of radius ϱ_1.

For an elliptic meridian section near the spiral nose (Figure IV. 18), we employ an auxiliary system of coordinates x, y. The equation of the ellipse is

$$\frac{x^2}{a^2} + \frac{y^2}{b^2} = 1,$$

and the coordinate r, i.e., the radius, is related to the coordinate x by expression

$$r = r_0 + x.$$

For constructional reasons, b is always greater than a. The angle α is determined from the relationship,

$$\tan \alpha = -\frac{dy}{dx} = \frac{bx}{a\sqrt{a^2 - x^2}},$$

hence,

$$\sin \alpha = \frac{b(r - r_0)}{\sqrt{a^4 + (r - r_0)^2 (b^2 - a^2)}}. \qquad \text{(IV. 13)}$$

The radius of curvature ϱ_1 of the meridian section, i.e., the radius of curvature of the ellipse is, according to the formulas of differential geometry,

$$\varrho_1 = \frac{1}{a^4 b}\left[a^4 + (r - r_0)^2 (b^2 - a^2)\right]^{\frac{3}{2}}. \qquad \text{(IV. 14)}$$

According to Meunier's theorem, the radius of curvature ϱ_2 of a conic section is

$$\varrho_2 = \frac{r}{\sin \alpha} = \frac{r\sqrt{a^4 + (r - r_0)^2 (b^2 - a^2)}}{b(r - r_0)}. \qquad \text{(IV. 15)}$$

The stress σ_1, in the meridian section, is analogous to the stress in a circular section

$$\sigma_1 = \frac{p(r^2 - r_0^2)}{2r\delta \sin \alpha} = \frac{p(r + r_0)\sqrt{a^4 + (r - r_0)^2 (b^2 - a^2)}}{2rb\delta}. \qquad \text{(IV. 16)}$$

From the expressions (IV. 16) and (IV. 8) we find

$$\sigma_2 = \varrho_2\left(\frac{p}{\delta} - \frac{\sigma_1}{\varrho_1}\right) = \frac{p\left[a^4 + 2r(r - r_0)(b^2 - a^2)\right]}{2b\delta\sqrt{a^4 + (r - r_0)^2 (b^2 - a^2)}}; \qquad \text{(IV. 17)}$$

and obtain for $r = r_0$

$$\sigma_1 = \frac{pa^2}{b\delta}; \quad \sigma_2 = \frac{pa^2}{2b\delta}.$$

From expression (IV. 16) the conclusion can be drawn that the greatest possible stress σ_1 occurs either at the point where the shell is connected to the speed ring, where r has the smallest value $r = r_s$, or for the largest value of $r = r_0 + a$.

For $a = b$, the cross section becomes circular.

Stresses in the joints between the scroll elements and the speed ring. Since the speed-ring edges are very rigid and do not deform easily, the scroll elements are assumed to be rigidly fastened to the speed ring. As a consequence, additional local stresses will arise in the scroll shell.

To compute local stresses in the joints (with the speed ring), the stresses in the edge of the scroll element must be determined; for this purpose the shell is considered to be free, not rigidly attached, and subject only to shell stresses.

On the basis of the calculated stresses, one determines the forces and moments acting at the joints, and the value of the bending stress, from the formula given in A. E. Zhmud's manual mentioned above.

$$\sigma_b = \pm \frac{1}{2} \sqrt{\frac{3}{1-\nu^2}} \left[(1-\nu) - \nu \frac{r_0}{r_s} \right] \sigma_0, \qquad \text{(IV. 18)}$$

for $\nu = 0.3$

$$\sigma_b = \pm \left(0.635 - 0.272 \frac{r_0}{r_s} \right) \sigma_0. \qquad \text{(IV. 19)}$$

The total tensile stresses in a circular meridian section, in the joint between the scroll element and the speed ring ($r = r_s$), equal the sum of the shell stresses σ_1, according to relationship (IV. 11) and the positive bending stresses according to relationship (IV. 18):

$$\sigma_j = \sigma_1(r_s) + \sigma_b = \left\{ \left(1 + \frac{r_0}{r_s} \right) + \sqrt{\frac{3}{1-\nu^2}} \left[(1-\nu) - \nu \frac{r_0}{r_s} \right] \right\} \frac{\sigma_0}{2}. \qquad \text{(IV. 20)}$$

For a steel scroll casing

$$\sigma_j = \left(1.135 + 0.228 \frac{r_0}{r_s} \right) \sigma_0 = \left(1.135 + 0.228 \frac{r_0}{r_s} \right) \frac{pQ_1}{\delta}.$$

Since the ratio $\frac{r_0}{r_s}$ has its maximum value in the scroll elements nearest the entrance cross section of the casing and is there approximately equal to 1.8, the maximum value of σ_j is

$$\sigma_{j\,max} \approx 1.55 \frac{pQ_1}{\delta}.$$

The relative increase of the total stress at the joint between scroll element and speed ring, due to bending, namely

$$\frac{\sigma_j - \sigma_1(r_s)}{\sigma_1(r_s)},$$

varies between 10 and 30%, increasing with the reduction of the ratio $\frac{r_0}{r_s}$.

For an elliptical meridian section, the bending stresses are

$$\sigma_b = \pm \frac{1}{2}\sqrt{\frac{3}{1-\nu^2}}\left\{\frac{[a^4+2r_s(r_s-r_0)(b^2-a^2)]}{\sqrt{a^4+(r_s-r_0)^2(b^2-a^2)}} - \right.$$
$$\left. - \frac{\nu(r_s+r_0)}{r_s}\sqrt{a^4+(r_s-r_0)^2(b^2-a^2)}\right\}\frac{p}{b\delta}. \qquad \text{(IV. 21)}$$

The total tensile stresses occurring in the joint between the elliptical scroll element and the speed ring ($r = r_s$) equal the sum of the bending stresses σ_b and the meridian shell stresses determined from the relationship (IV. 16)

$$\sigma_j = \left\{\frac{1}{2}\sqrt{\frac{3}{1-\nu^2}}\left|\frac{[a^4+2r_s(r_s-r_0)(b^2-a^2)]}{\sqrt{a^4+(r_s-r_0)^2(b^2-a^2)}} - \right.\right.$$
$$\left. - \frac{\nu(r_s+r_0)}{r_s}\sqrt{a^4+(r_s-r_0)^2(b^2-a^2)}\right| +$$
$$\left. + \frac{r_s+r_0}{2r_s}\sqrt{a^4+(r_s-r_0)^2(b^2-a^2)}\right\}\frac{p}{b\delta}. \qquad \text{(IV. 22)}$$

For a steel scroll case, Poisson's ratio is $\nu = 0.3$, so that

$$\sigma_j = \left\{0.908\left|\frac{[a^4+2r_s(r_s-r_0)(b^2-a^2)]}{\sqrt{a^4+(r_s-r_0)^2(b^2-a^2)}} - \right.\right.$$
$$\left. - \frac{0.3(r_s-r_0)}{r_s}\sqrt{a^4+(r_s-r_0)^2(b^2-a^2)}\right| +$$
$$\left. + 0.5\left(\frac{r_s-r_0}{r_s}\right)\sqrt{a^4+(r_s-r_0)^2(b^2-a^2)}\right\}\frac{p}{b\delta}. \qquad \text{(IV. 23)}$$

For $a = b$, the formulas (IV. 22) and (IV. 23) become the formulas (IV. 20) and (IV. 21).

Stresses in the joints between plates of varying thickness in a meridian section. The stresses are determined in the same way as the stresses in the joints between the scroll and the speed ring.

The maximum bending stress in the thinnest plate is determined from the formula

$$\sigma_{b\max} = \pm 1.4\sqrt{\frac{3}{1-\nu^2}}\,\frac{\delta_1^2(\delta_1+\delta_2)}{(\delta_1^2+\delta_2^2)(\delta_1+\delta_2)+2(\delta_1\delta_2)^{\frac{3}{2}}} \times$$
$$\times \frac{E(\Delta r_I - \Delta r_{II})}{r}. \qquad \text{(IV. 24)}$$

For steel plates ($\nu = 0.3$), the formula becomes

$$\sigma_{b\max} = \pm 2.55\,\frac{\delta_1^2(\delta_1+\delta_2)}{(\delta_1^2+\delta_2^2)(\delta_1+\delta_2)+2(\delta_1\delta_2)^{\frac{3}{2}}} \cdot \frac{E(\Delta r_I - \Delta r_{II})}{r}, \qquad \text{(IV. 25)}$$

where Δr_I = changes in radius of the circular section, due to deformation of the thin plate section;

Δr_{II} = changes in radius of the circular section, due to deformation of the thick plate.

Deformations Δr are calculated according to expression (IV. 9).

In order to determine the total tensile stress, the bending stress should be added to the corresponding shell stress σ.

The stresses, calculated in this way, agree closely with the stresses actually measured on scroll models by means of strain gages.

The plates, whose thickness has been determined by calculation, should be chosen from the existing specifications for rolled sections and plates.

A thickness 2 mm greater than the calculated value is usually selected, since allowance must be made for prolonged operation of the scroll case, as well as corrosion and erosion caused by suspended matter in the water stream.

Material for the steel plates and the welds must be given particular attention and, for this purpose, material of high plasticity is usually chosen. This is important since the casing plates, apart from preliminary roll bending and stamping, undergo bending operations during assembly and erection. Furthermore, a material of high ductility ensures an easy smoothening-out of stress peaks should the scroll elements deviate from their calculated shape.

Since brief pressure fluctuations in the scroll occur only during the regulation process, the permissible stress is usually selected according to the static head with the distributor closed, allowing for higher stresses during the regulation process.

Welded scroll casings are usually made of sheet steel, having the following mechanical characteristics:

yield point	$\sigma_y = 24\,kg/mm^2$
ultimate strength	$\sigma_u = 44$ to $47\,kg/mm^2$
percentage elongation	$\delta = 25\%$.

The permissible stresses, with allowance for the increase in dynamic pressure, are $\sigma_a = 1{,}300\,kg/cm^2$. With allowance for the local stresses, according to formulas (IV. 21 and (IV. 23), the permissible stresses are $\sigma_a = 1{,}550\,kg/cm^2$.

The same formulas are used to determine the casing-wall thickness.

The wall thickness of the casing is selected, bearing in mind the availability of all-cast casings or casings made up of separate segments.

The transportation facilities should also be considered.

Cast scroll casings are usually made of steel having the following characteristics:

yield point	$\sigma_y = 23\,kg/mm^2$
ultimate strength	$\sigma_u = 45\,kg/mm^2$
percentage elongation	$\delta = 16\%$

The permissible stresses are 10 to 20% smaller than for welded casings, since, owing to the complicated shape of the cast pieces, the cast metal is liable to display nonuniform characteristics.

Scrolls for high-head turbines, in which the water stream carries suspended matter, are cast of corrosion-resistant steel.

The assumption made in the foregoing method of computation, that the speed ring to which the spiral casing is connected is absolutely rigid, does not agree with the actual conditions. The elastic displacement of the upper part of the speed ring is liable to be so great that additional bending stresses arise in the casing.

In this connection, V.S. Postoev and V.I. Mikheev /72/ refined the method for calculation of scroll casings; their method considers the effect of deformations in the upper part of the speed ring on the state of stress in the joints of the scroll.

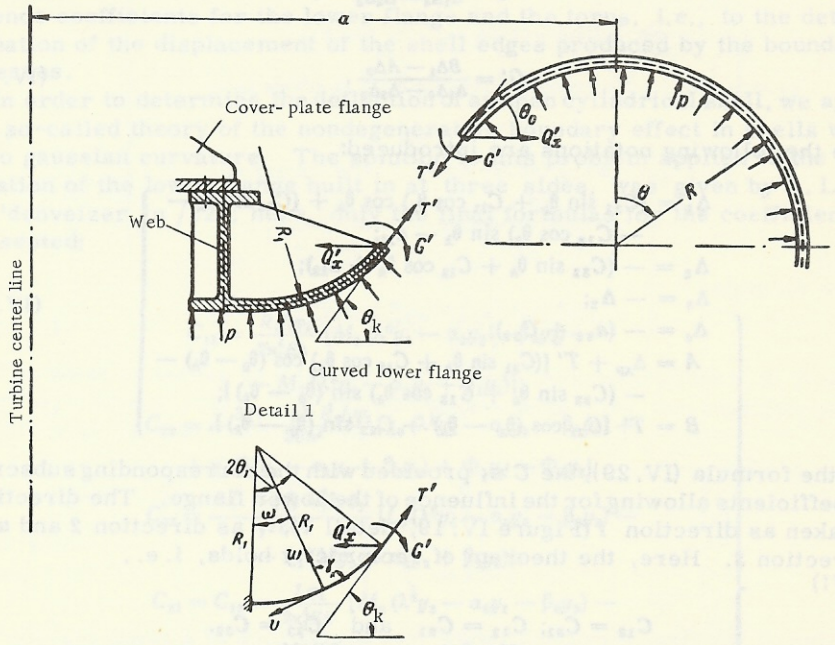


FIGURE IV.19. Refined calculation of the junction between the scroll and the speed ring

The upper band of the turbine speed ring is calculated as a complicated ribbed shell-plate construction (Figure IV.19), fixed by its upper web to the cover-plate flange, and by its lower web to the stay vanes. The least rigid element in this construction is the lower curved flange. Since the stay vanes are distributed closely along the speed-ring circumference, the lower flange between two vanes resembles a short cylindrical plate whose length is l (as measured on the outer flange perimeter), built in along the junction line between the web and the stay vanes.

The bending moment G', the thrust force Q'_x and the meridian force T' at the junction between the lower flange and the scroll must all be determined.

Since, in a toroidal symmetrical shell, the meridian force only slightly depends on Q'_x and G', the force T' is determined irrespective of Q'_x and G'.

The scheme assumes the existence of an inflexion point at the junction.

In order to determine the forces Q'_x and G' at the joint between the scroll and the lower flange, two conditions are stipulated under which the relative radial displacement and angles of twist are equal to zero.

These conditions are expressed by two equations:

$$\left.\begin{aligned} Q'_x\Delta_1 + G'\Delta_2 &= A; \\ Q'_x\Delta_3 + G'\Delta_4 &= B, \end{aligned}\right\} \qquad \text{(IV. 26)}$$

by solving them, we obtain

$$Q'_x = \frac{A\Delta_4 - B\Delta_2}{\Delta_1\Delta_4 - \Delta_2\Delta_3}. \qquad \text{(IV. 27)}$$

$$G' = \frac{B\Delta_1 - A\Delta_3}{\Delta_1\Delta_4 - \Delta_2\Delta_3}. \qquad \text{(IV. 28)}$$

where the following notations are introduced:

$$\left.\begin{aligned} \Delta_1 &= (C_{31}\sin\theta_k + C_{11}\cos\theta_k)\cos\theta_k + (C_{33}\sin\theta_k - \\ &\quad - C_{13}\cos\theta_k)\sin\theta_k - a_{11}; \\ \Delta_2 &= -(C_{32}\sin\theta_k + C_{12}\cos\theta_k + a_{12}); \\ \Delta_3 &= -\Delta_2; \\ \Delta_4 &= -(a_{22} + C_{22}); \\ A &= \Delta_{xp} + T'[(C_{31}\sin\theta_k + C_{11}\cos\theta_k)\cos(\theta_0 - \theta_k) - \\ &\quad - (C_{33}\sin\theta_k + C_{13}\cos\theta_k)\sin(\theta_0 - \theta_k)]; \\ B &= T'[C_{21}\cos(\theta_0 - \theta_k) - C_{23}\sin(\theta_0 - \theta_k)]. \end{aligned}\right\} \qquad \text{(IV. 29)}$$

In the formula (IV. 29), the C's, provided with the corresponding subscripts, are coefficients allowing for the influence of the lower flange. The direction v is taken as direction *1* (Figure IV. 19, detail 1), γ as direction *2* and w as direction *3*. Here, the theorem of reciprocity holds, i.e.,

$$C_{13} = C_{31};\ C_{12} = C_{21} \quad \text{and} \quad C_{23} = C_{32}.$$

The letter a denotes the influence coefficients on the periphery of the toroidal shell, where direction *1* coincides with that of Q'_x, and direction 2 is opposed to that of the force causing moment G'. For a torus we have

$$a_{12} = -a_{21},$$

Δ_{x_p} = the radial displacement for the moment-free condition due to the hydrostatic pressure is determined by the well-known formula of the theory of shells

$$\Delta_{x_p} = \frac{pRa}{E\delta}[1 - 2\mu - (1 - \mu)\bar{\alpha}\sin\theta_0], \qquad \text{(IV. 30)}$$

where R = radius of the shell cross section;
a = radius of the torus axis;
δ = shell thickness;
μ = Poisson's ratio;
$\bar{\alpha} = \frac{a}{R}$.

The total meridian stress is

$$\sigma_1 = \frac{\sigma G'}{\delta^2} + \frac{T'}{\delta}.^{*} \qquad \text{(IV. 31)}$$

T' here is found from the formula

$$T' = \frac{pR}{2} \cdot \frac{2 - \bar{\alpha} \sin \theta_0}{1 - \bar{\alpha} \sin \theta_0}. \qquad \text{(IV. 32)}$$

Thus, the solution of the problem reduces to the determination of the influence coefficients for the lower flange and the torus, i.e., to the determination of the displacement of the shell edges produced by the boundary stresses.

In order to determine the deflection of an open cylindrical shell, we apply the so-called theory of the nondegenerative boundary effect in shells with zero gaussian curvature. The solution to this problem applied to the computation of the lower flange built in at three sides, was given by A. L. Gol'denveizer in /22/; here, only the final formulas for the coefficients are presented:

$$\left.\begin{aligned}
C_{11} &= \frac{R_1 f_1 \varphi_1}{2\varkappa_1^4 Eh} [M_0 (\lambda^8 y_5 - \alpha_0 y_3 - \beta_0 y_4) - \\
&\quad - M_1 (\lambda^8 y_6 - \alpha_1 y_3 + \beta_1 y_4)]; \\
C_{22} &= -\frac{3(1-\mu^2) R_1 f_1 \varphi_1}{2Eh^3} [\chi_0 (\lambda^8 y_3 - \alpha_0 y_1 - \beta_0 y_2) + \\
&\quad + \chi_1 (\lambda^8 y_4 - \alpha_1 y_1 + \beta_1 y_2) + \Phi_1 y_1 - \Phi_2 y_2]; \\
C_{33} &= \frac{3(1-\mu^2) R_1^3 f_1 \varphi_1}{2Eh^3} [L_0 (\lambda^8 y_4 - \alpha_0 y_2 - \beta_0 y_3) - \\
&\quad - L_1 (\lambda^8 y_5 - \alpha_1 y_2 + \beta_1 y_3)]; \\
C_{21} = C_{12} &= \frac{f_1 \varphi_1}{2\varkappa_1^4 Eh} [M_0 (\lambda^8 y_3 - \alpha_0 y_1 - \beta_0 y_2) - \\
&\quad - M_1 (\lambda^8 y_4 - \alpha_1 y_1 + \beta_1 y_2)]; \\
C_{31} = C_{13} &= \frac{R_1 f_1 \varphi_1}{2Eh\varkappa_1^4} [M_0 (\lambda^8 y_4 - \alpha_0 y_2 - \beta_0 y_3) - \\
&\quad - M_1 (\lambda^8 y_5 - \alpha_1 y_2 + \beta_1 y_3)]; \\
C_{23} = C_{32} &= -\frac{3(1-\mu^2) R_1^2 f_1 \varphi_1}{2Eh^3} [L_0 (\lambda^8 y_3 - \alpha_0 y_1 - \beta_0 y_2) - \\
&\quad - L_1 (\lambda^8 y_4 - \alpha_1 y_1 + \beta_1 y_2)],
\end{aligned}\right\} \qquad \text{(IV. 33)}$$

where y_ν —the basic functions—are determined from the following formulas for $\omega = -2\theta_1$ (Figure IV. 19, detail 1)

$$\left.\begin{aligned}
y_0 &= \frac{1}{2} (\operatorname{ch} a\omega \cdot \cos b\omega + \operatorname{ch} b\omega \cdot \cos a\omega); \\
y_1 &= \frac{1}{2\lambda} \left[\cos \frac{\pi}{8} (\operatorname{sh} a\omega \cdot \cos b\omega + \operatorname{ch} b\omega \cdot \sin a\omega) + \right. \\
&\quad \left. + \sin \frac{\pi}{8} (\operatorname{ch} a\omega \cdot \sin b\omega + \operatorname{sh} b\omega \cdot \cos a\omega)\right];
\end{aligned}\right\} \qquad \text{(IV. 34)}$$

* [Meaning of σ in first term on right side unclear.]

$$
\left.
\begin{aligned}
y_2 &= \frac{1}{2\sqrt{2}\lambda^2}(\operatorname{ch} a\omega\cdot\cos b\omega - \operatorname{ch} b\omega\cdot\cos a\omega + \operatorname{sh} a\omega\cdot\sin b\omega + \\
&\qquad + \operatorname{sh} b\omega\cdot\sin a\omega);\\
y_3 &= \frac{1}{2\lambda^3}\left[\sin\frac{\pi}{8}(\operatorname{sh} a\omega\cdot\cos b\omega - \operatorname{ch} b\omega\cdot\sin a\omega) + \right.\\
&\qquad \left. + \cos\frac{\pi}{8}(\operatorname{ch} a\omega\cdot\sin b\omega - \operatorname{sh} b\omega\cdot\cos a\omega)\right];\\
y_4 &= \frac{1}{2\lambda^4}(\operatorname{sh} a\omega\cdot\sin b\omega - \operatorname{sh} b\omega\cdot\sin a\omega);\\
y_5 &= \frac{1}{2\lambda^5}\left[\cos\frac{\pi}{8}(\operatorname{ch} a\omega\cdot\sin b\omega + \operatorname{sh} b\omega\cdot\cos a\omega) - \right.\\
&\qquad \left. - \sin\frac{\pi}{8}(\operatorname{sh} a\omega\cdot\cos b\omega + \operatorname{ch} b\omega\cdot\sin a\omega)\right];\\
y_6 &= \frac{1}{2\sqrt{2}\lambda^6}(\operatorname{ch} b\omega\cdot\cos a\omega - \operatorname{ch} a\omega\cdot\cos b\omega + \operatorname{sh} a\omega\cdot\sin b\omega + \\
&\qquad + \operatorname{sh} b\omega\cdot\sin a\omega);\\
y_7 &= \frac{1}{2\lambda^7}\left[\sin\frac{\pi}{8}(\operatorname{ch} a\omega\cdot\sin b\omega - \operatorname{sh} b\omega\cdot\cos a\omega) - \right.\\
&\qquad \left. - \cos\frac{\pi}{8}\times(\operatorname{sh} a\omega\cdot\cos b\omega - \operatorname{ch} b\omega\cdot\sin a\omega)\right].
\end{aligned}
\right\} \qquad \text{(IV. 34)}
$$

In these formulas

$$\lambda = \sqrt{\varkappa_1}\cdot\sqrt[4]{\frac{R_1}{h}}\cdot\sqrt[8]{3(1-\mu^2)}; \qquad \text{(IV. 35)}$$

$$\varkappa_1 = 4{,}7300\,\frac{R_1}{l}; \qquad \text{(IV. 36)}$$

h = half the lower-flange thickness.

$$\left.
\begin{aligned}
a &= \lambda\cos\frac{\pi}{8};\\
b &= \lambda\sin\frac{\pi}{8};
\end{aligned}
\right\} \qquad \text{(IV. 37)}$$

φ_1 = value of the first eigenfunction of the oscillations of a beam rigidly fixed at both ends to an elastic foundation.

For $x_1 = \frac{l}{2}$

$$\varphi_1 = \sin k_1x_1 - \operatorname{sh} k_1x_1 - \frac{\sin k_1l - \operatorname{sh} k_1l}{\cos k_1l - \operatorname{ch} k_1l}\cdot(\cos k_1x_1 - \operatorname{ch} k_1x_1). \qquad \text{(IV. 38)}$$

Here, $k_1 = 4.7300\,\frac{1}{l}$;

f_1 = first term of the Fourier expansion according to the eigenfunction φ_1 for a single stress.

$$f_1 = \frac{1}{k_1l}\cdot\frac{2 - \cos k_1l - \operatorname{ch} k_1l - \frac{\sin k_1l - \operatorname{sh} k_1l}{\cos k_1l - \operatorname{ch} k_1l}(\sin k_1l - \operatorname{sh} k_1l)}{\left(\frac{\sin k_1l - \operatorname{sh} k_1l}{\cos k_1l - \operatorname{ch} k_1l}\right)^2}. \qquad \text{(IV. 39)}$$

The other coefficients in the relationship (IV. 33) are determined from the formulas

$$\left.\begin{aligned} \alpha_0 &= \lambda^8 \frac{y_2 \cdot y_6 - y_1 \cdot y_7}{y_0 y_6 - y_1 y_5}; & \beta_0 &= \lambda^8 \frac{y_0 y_7 - y_2 y_5}{y_0 y_6 - y_1 y_5}; \\ \alpha_1 &= \frac{\lambda^8 y_3 y_6 + y_0 y_1}{y_0 y_6 - y_1 y_5}; & \beta_1 &= \frac{y_0^2 + \lambda^8 y_3 y_5}{y_0 y_6 - y_1 y_5}; \\ M_0 &= \frac{F_3}{F_0 F_3 - F_1 F_2}; & M_1 &= \frac{F_2}{F_0 F_3 - F_1 F_2}; \\ L_0 &= \frac{F_1}{F_0 F_3 - F_1 F_2}; & L_1 &= \frac{F_0}{F_0 F_3 - F_1 F_2}, \end{aligned}\right\} \qquad \text{(IV. 40)}$$

where

$$\left.\begin{aligned} F_0 &= y_0 + \alpha_0 y_6 + \beta_0 y_7; & F_1 &= y_1 + \alpha_1 y_6 - \beta_1 y_7; \\ F_2 &= \lambda^8 (y_1 + \alpha_0 y_7) - \beta_0 y_0; & F_3 &= \lambda^3 (y_2 + \alpha_1 y_7) + \beta_1 y_0; \end{aligned}\right\} \qquad \text{(IV. 41)}$$

also

$$\left.\begin{aligned} \Phi_1 &= \frac{y_6}{y_0 y_6 - y_1 y_5}; & \Phi_2 &= \frac{y_5}{y_0 y_6 - y_1 y_5}; \\ \chi_0 &= -\frac{F_1 (\lambda^8 \Phi_1 y_7 + \Phi_2 y_0) - F_3 (\Phi_1 y_6 - \Phi_2 y_7)}{F_0 F_3 - F_1 F_2}; \\ \chi_1 &= \frac{F_0 (\lambda^8 \Phi_1 y_7 + \Phi_2 y_0) - F_2 (\Phi_1 y_6 - \Phi_2 y_7)}{F_0 F_3 - F_1 F_2}. \end{aligned}\right\} \qquad \text{(IV. 42)}$$

The state of stress in a toroidal shell was investigated by V.S. Postoev and V.I. Mikheev /72/. The following formulas give the coefficients of influence at the built-in shell edge:

$$a_{11} = (1 - \bar{\alpha} \sin \theta_0)^2 \frac{2\lambda_1 R}{E\delta\bar{\alpha}^2}; \quad a_{22} = -\frac{R}{D\lambda_1}; \quad a_{12} = -a_{21} = \frac{R^2}{2D\lambda_1^2} \sin \theta_0. \qquad \text{(IV. 43)}$$

where

$$\lambda_1 = k \sqrt{\frac{\sin \theta_0}{1 - \bar{\alpha} \sin \theta_0}}, \qquad \text{(IV. 44)}$$

$$k^2 = \sqrt{3(1 - \mu^2)} \cdot \frac{R^2}{a\delta}; \qquad D = \frac{E\delta^3}{12(1 - \mu^2)}.$$

An example of scroll casing computation is given below for the following parameters:

Radius of the lower-flange section	$R_1 = 42$ cm
Distance between the ribs on the outer circumference (assuming 24 ribs)	$l = 116$ cm
Half the lower-flange thickness	$h = 3$ cm
Poisson's ratio	$\mu = 0.3$
Radius of the entrance cross section of the scroll	$R = 297$ cm
Thickness of the scroll wall	$\delta = 3.2$ cm
Pressure inside the scroll casing	$p = 13$ kg/cm^2

$$\theta_0 = \theta_k = 55°.$$

1. $\varkappa_1$, λ_1, a and b are determined from the formulas (IV. 35 to IV. 37). They are

$$\varkappa_1 = 1.7126;\ \lambda_1 = 2.8700;\ a = 2.6516;\ b = 1.0983.$$

2. The basic functions y_ν are given by the formulas (IV. 34):

$$y_0 = 0.9176;\ y_1 = -0.9512;\ y_2 = 0.4599;\ y_3 = -0.1474;$$
$$y_4 = 3.5376 \times 10^{-2} y_5 = -6.7928 \cdot 10^{-3};$$
$$y_6 = 1.0869 \cdot 10^{-3};\ y_7 = 1.4348 \cdot 10^{-4}.$$

3. The auxiliary coefficients are computed from formulas (IV. 40 to IV. 42):

$$\alpha_0 = -306.1693;\ \beta_0 = -2.5210 \cdot 10^3;\ \alpha_1 = 294.686;$$
$$\beta_1 = -997.44;\ F_0 = 0.9466;\ F_1 = -0.7740;$$
$$F_2 = -1.8627 \cdot 10^3;\ F_3 = 1.0071 \cdot 10^3;\ M_0 = -2.0621;$$
$$M_1 = 3.8140;\ L_0 = 1.5847 \cdot 10^{-3};\ L_1 = -1.9381 \cdot 10^{-3};\ \Phi_1 = -0.1989;$$
$$\Phi_2 = 1.2432;\ \chi_0 = -1.9381 \cdot 10^{-3};\ \chi_1 = -2.3214 \cdot 10^{-3}.$$

4. The first eigenfunction and the first term of the Fourier expansion are determined from formulas IV. 38 and IV. 39:

$$\varphi_1 = 1.4659;\ f_1 = 0.8163.$$

5. The influence coefficients are determined from formulas (IV. 33 and IV. 43):

$$EC_{11} = 74.8;\ EC_{22} = -1.81;\ EC_{33} = -6.53 \cdot 10^2;$$
$$EC_{12} = 7.50;\ EC_{13} = 205.1;\ EC_{23} = 29.0;$$
$$Ea_{11} = 4093.6;\ Ea_{22} = -10.1;\ Ea_{12} = 143.79.$$

6. The moment-free displacement of the shell Δ_{xp} and the force T' per unit length according to formulas (IV. 30 and IV. 32), are

$$E\Delta_{xp} = 72110;\ T' = 5060 \text{ kg/cm}.$$

7. The displacements are determined from formulas (IV. 29) :

$$E\Delta_1 = -4364.6;\ E\Delta_2 = -125.48;\ E\Delta_3 = 125.48;$$
$$E\Delta_4 = 11.92;\ EA = 7072.1 \cdot 10^2;\ EB = 378.69 \cdot 10^2.$$

8. The moment per unit length of the joint between the scroll and the speed ring is given by formula (IV. 28):

$$G' = 70.5 \cdot 10^2 \text{ kg};$$

the resulting meridian stresses in the built-in edge, computed from formula (IV. 31), are

$$\sigma_1 = 5630 \text{ kg/cm}^2.$$

When using the method which ignores the effect of speed-ring deformation, the stress at the scroll joint is

$$\sigma_1 \approx 1900 \text{ kg/cm}^2.$$

The considerable effect of the deformation of the lower speed-ring flange on the stresses in the scroll was confirmed at the LMZ laboratory by model tests of the scroll casings for the turbines of the Bratsk HEP.

Analysis of this solution shows that the stresses at the joint depend mainly on the rigidity of the lower speed-ring flange. Thus, the bending stresses decrease if the flange rigidity is increased by means of additional ribs. The smoothness of junction between the lower speed-ring flange and the scroll wall plays an important part.

Even a small inflexion of 7 to 10° increases the stresses considerably. The shape of the lower flange also affects the state of stress. The most suitable shape of the junction is a conical ribbed surface.

It should be noted that the upper ring in modern high-power turbines is embedded in concrete for increased rigidity; since the foregoing calculations did not allow for the influence of the concrete, the bending stresses under field conditions are smaller than the calculated values.

20. THE SPEED RING

The function of the speed ring is to transmit the loads from the concrete pit of the turbine, the weight of the turbine unit and the axial load of water to the turbine foundation. For concrete scroll casings, the speed ring consists of separate stay vanes or of an annular construction consisting of an upper and a lower ring held together by ribs (also called stay vanes or stationary guide vanes). The speed ring is mounted inside the scroll between its upper and lower cones. The stay vanes are streamlined to suit the flow lines in the scroll. The stay vanes are fastened to the concrete by top and bottom flanges. The dimensions of these flanges are chosen according to the permissible pressure on the concrete. One of the vanes is the scroll nose itself. Usually, the stay vanes inside the scroll are of the same profile, while in the open part of the case, the profile varies with the flow direction. Figure IV. 20 shows the location of the stay vanes in a semi-scroll casing. Some speed-ring designs are shown in Figure IV. 21. In designs where the thrust bearing is located on the turbine cover-plate, it is more convenient, and safer, to transmit the load to the foundation by means of an annular speed ring, than through separate stay vanes. When designing the speed ring and selecting its construction, consideration must be given to the fact that the annular speed ring will be the largest part of the turbine determining its dimensions and the required equipment for machining. The speed ring with bolted stay vanes and without a lower ring is simpler in construction. But, since the lower ring and the link between it and the lower ring of the distributor are absent, the turbine has no independent casing. The distributor rings are assembled into a single structure by means of the concrete, but this is liable to cause misalignment of the distributor due to settling of the concrete. The material for the speed

ring should be selected according to the load acting. If the speed ring is subject only to compression, it may be made of cast iron. If, on the other hand, the speed ring is subject to both compressive and tensile loads — as is usually the case with medium and high heads — the speed ring is made of steel. For welded-cast constructions, the upper and lower rings and the ribs (stay vanes) are made of cast steel, welded together as a single segment. Figure IV. 22 shows a welded-cast speed ring. Formerly, speed rings were made of a single all-cast segment, but with the advent of new casting techniques, previous methods became obsolete. Today, the segments are divided into smaller elements, which makes their casting more convenient. In welded constructions, the upper and lower rings and the ribs are made of steel plates roll-bent or stamped to shape. The type of speed-ring design is selected according to the parameters and dimensions of the turbine and the technological possibilities of manufacturing. For this purpose, a detailed technical and economic analysis and a comparison of alternative designs should be made. The speed rings for the turbines of the Volga and the Votinsk HEPs, designed by LMZ, are of the welded-cast type, as shown in Figures IV. 21,b and IV. 22. Welded speed rings with bolted stay vanes were designed by the KhTZ, for the large Kaplan turbines of the Kremenchug and Dnieprodzerzhinsk HEPs. Speed rings of this type are shown in Figure IV. 21,c. The upper band of the speed ring is fastened to the upper ring of the distributor. No lower band is provided. In the design of speed rings, the selection of a suitable shape for the outer edges of the upper and lower bands must be carefully made to obtain a smooth rounded transition line in the scroll segment. The transition from cone to plane between the speed ring and the scroll, as used in certain designs, is not practical, since in this case, higher stresses occur in the embedded junctions. The number of stay vanes (ribs) is usually taken as half the number of the guide vanes. The stay vanes are arranged so as to leave adequate space between the trailing edge of the stay vane and the guide vanes.

For semi-scroll casings, additional stay vanes are usually provided in the open part of the scroll to ensure better conditions of flow toward the distributor.

Experiments carried out at the laboratories of the LMZ, LPI, MISI, and other plants showed that the power characteristics of turbines with semi-scroll casings can be improved by a proper arrangement of the stay vanes near the nose of the open part of the scroll casings.

The dimensions of the stay vanes in the horizontal plane, as well as their shape and location, depend on the geometry of the turbine, on the conditions of flow, and on the strength required. The camber line of each stay vane is plotted from the flow lines; the vane profile is selected from the existing tested profiles and checked for strength.

Figure IV. 20 shows the location of the stay vanes of a turbine with a semi-scroll casing. In LMZ practice, the stay vanes are located on the base (mean) circle D_m passing through the nose.

$$D_m = \frac{D_a + D_b}{2}.$$

From the nose to vane No. 10, the stay vanes are located at equal angles of 30°, and from vane No. 10 to No. 14 at angles of 15°.

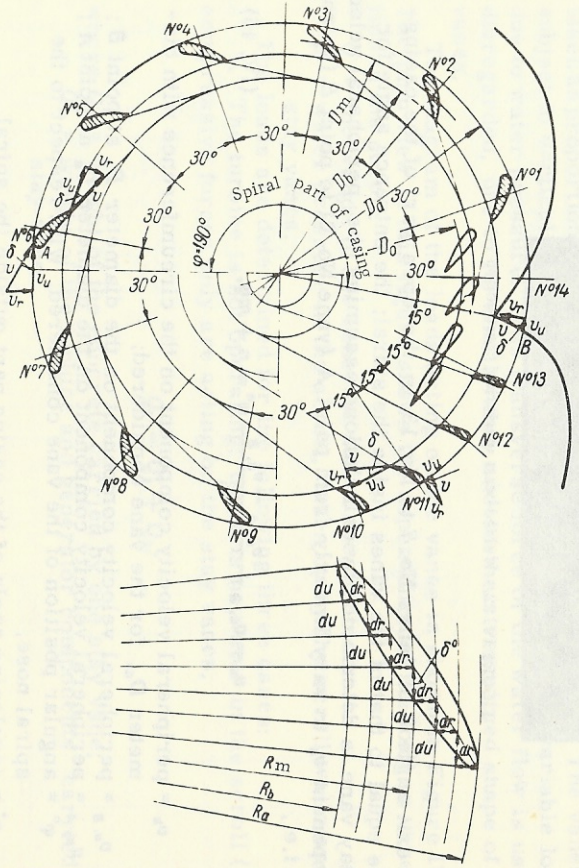


FIGURE IV. 20. Location of speed-ring stay vanes in the scroll casing

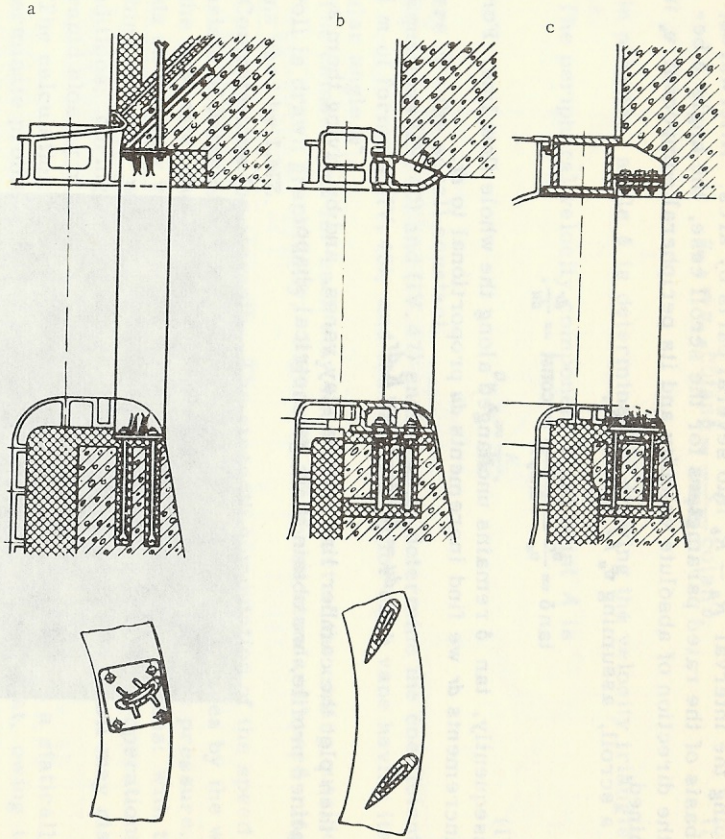


FIGURE IV. 21. Various types of speed- rings:

a—separate stay vanes; b—speed ring; c—speed ring with bolted stay vanes.

The camber line of the stay vanes is drawn as shown in the figure, i.e., by dividing the interval $R_a - R_b$ into several parts by arcs. Afterwards, on the basis of the rated parameters for the scroll case, the angle δ between the direction of absolute velocity and its peripheral component v_u is determined.

For a scroll, assuming $v_u r = \text{const} = K$,

$$\tan\delta = \frac{v_r}{v_u} = \frac{Qr}{2\pi b_0 r K} = \text{const} = \frac{dr}{du}.$$

Consequently, tan δ remains unchanged along the whole flow line. For given increments dr we find increments du proportional to dr.

$$du = dr\,\frac{v_u \cdot 2\pi b_0 r}{Q} = K_1 dr.$$

We then plot the camber line for the stay vanes, and by giving them a streamlined profile, we obtain their geometrical shape.

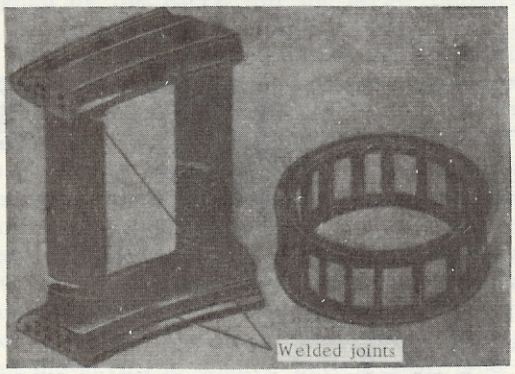


FIGURE IV. 22. Welded- cast speed ring construction

The exit angle δ of vanes No. 7 to No. 13 in the open part of the casing is made equal to that of the vanes inside the spiral; the entrance angle for each stay vane is determined by calculations assuming the peripheral velocity component v_u to vary linearly from point A (vane No. 6) to point B (spiral nose), i.e.,

$$v_u = v_{u,B} + \frac{v_{u,A} - v_{u,B}}{\varphi_1^\circ}\,\varphi^\circ = n + m\varphi, \qquad \text{(IV. 45)}$$

where v_u = peripheral velocity component on the circumference with diameter D_a, for the vane considered;
$v_{u,B}$ = peripheral velocity component on the diameter D_a at point B;
$v_{u,A}$ = peripheral velocity component on the diameter D_a at point A;
φ° = angular position of the vane considered, with respect to the spiral nose;
φ_1° = enveloping angle of the casing part outside the spiral.

The velocity $v_{u,B}$ depends on the nose shape, and is determined from equation

$$v_{u,B} = v_{r,B}\operatorname{cotan}\delta = \frac{Q}{2\pi b_0 R_a}\operatorname{cotan}\delta, \qquad \text{(IV. 46)}$$

In practice, angle δ is determined by drawing the velocity triangle at the nose.

The peripheral velocity component v_u at point A is

$$v_{u,A} = \frac{K}{R_a}, \qquad \text{(IV. 47)}$$

where K = the scroll constant.

Equations (IV. 40) and (IV. 47) enable us to determine the coefficients n and m of formula (IV. 45), and the value of v_u for each vane having its particular angle $\varphi°$.

The camber line for each stay vane in the part of the casing outside the scroll is drawn graphically. Figure IV. 23 shows standard speed-ring designs used by LMZ.

Computations for strength. The strength computation of the speed ring consists of determining the stresses caused in the stay vanes by the weight of the concrete, the weight of the turbine unit, and the water pressure. The loads on the stay vanes are determined for the following cases: with the turbine stopped; with no water in the scroll; under normal operational conditions; during load drop, when the pressure in the scroll may rise due to rapid closing of the distributor.

The calculation of the forces acting on each stay vane is a statically indeterminate problem; for simplification it is assumed that, owing to the reduced rigidity of the upper and lower rings (bands), each stay vane can be considered as an independent element. The load on the stay vanes is taken as proportional to the angular position $\varphi°$ of each vane. The vanes are subject to vertical loads, steady loads due to weight, and variable loads due to water pressure. The transverse force of the water flow is usually disregarded, due to its small value and to the streamlined shape of the vanes.

The diagram of the loads acting on the vanes is shown in Figure IV. 24. The plan view in this figure shows the dependence of the load on vane location in the scroll.

Q = the weight of the concrete and of the turbine unit.

p = water pressure in the scroll, taken up by the scroll walls and the stay vanes.

The loads are determined for the following three cases:

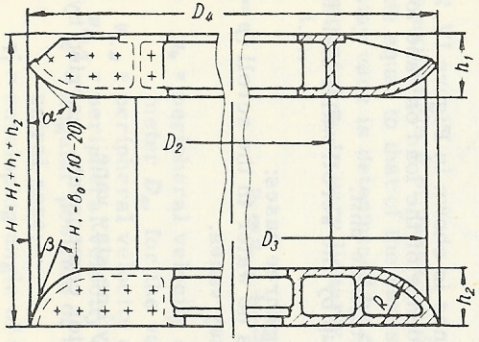
I. The turbine is not operating; there is no water in the scroll ($p = 0$); compressive forces only are acting on the stay vanes.

$$Q_I = Q_1 + Q_2,$$

where Q_1 = weight of the concrete carried by one stay vane;

Q_2 = weight of the turbine and generator components carried by one stay vane.

Variant No. 1 (for concrete scroll casings)



Variant No. 2 (for metal scroll casings)

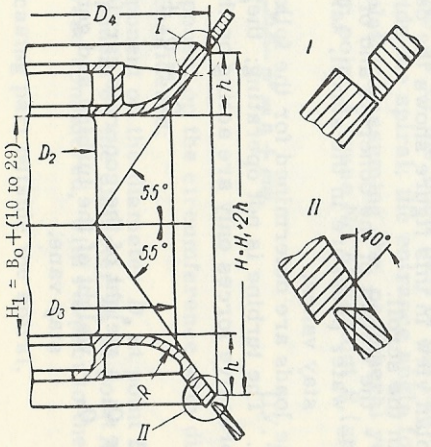


FIGURE IV. 23. Speed- ring designs for concrete and steel scroll casings

Variant No. 1

Runner diameter D_1	D_2	D_3	D_4	$\sim R$	h_1	h_2
2750	3 750	4 300	4 400	300	350	250
3000	4 100	4 700	4 800	300	350	250
3300	4 500	5 150	5 250	300	400	300
3700	5 000	5 750	5 850	350	400	300
4100	5 550	6 350	6 450	350	450	350
4500	6 100	7 000	7 100	400	450	350
5000	6 750	7 700	7 800	400	500	400
5500	7 450	8 550	8 650	500	500	400
6000	8 150	9 350	9 450	500	550	450
6600	8 950	10 250	10 350	600	550	450
7200	9 450	10 850	10 950	600	550	500
8000	10 450	11 950	12 050	600	550	500
9000	11 800	13 500	13 600	600		
9300	12 150	13 900	14 000	600		

The angles α and β are determined according to the scroll casing angles

Variant No. 2

Runner Diameter D_1	D_2	D_3	D_4	Number of stay vanes, including the nose	R	h
1800	2600	3 050	3300	8	200	210
2000	2850	3 350	3600		200	230
2250	3200	3 750	4000		200	230
2500	3300	3 900	4 150	12	250	250
2750	3650	4 300	4 550		250	250
3000	4000	4 700	5 050		300	320
3300	4400	5 150	5 500		300	320
3700	4900	5 700	6 050		350	350
4100	5450	6 300	6 650		350	350
4500	6000	6 950	7 350		400	410
5000	6600	7 650	8 050		400	410
5500	7300	8 450	8 850		500	460
6000	8000	9 250	9 650		500	460
6600	8800	10 150	10 550		600	500

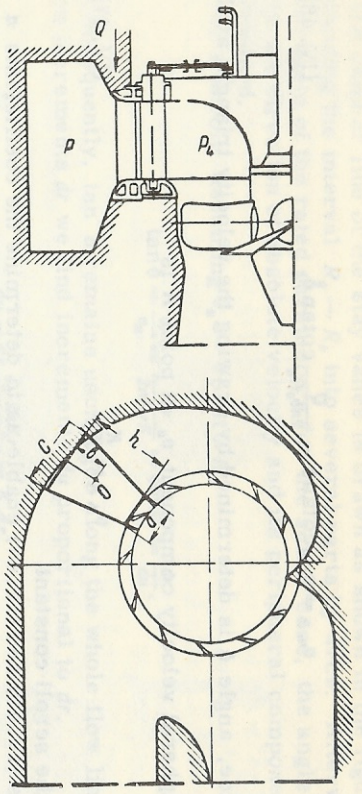


FIGURE IV. 24. Loads acting on the stay vanes

The weight of concrete Q_1 carried by one stay vane is usually determined by the power-plant designers in accordance with its location.

The weight of the turbine and generator parts carried by one stay vane is found from the formula

$$Q_2 = \frac{\Sigma G \cdot \varphi^\circ}{360^\circ}, \qquad \text{(IV. 48)}$$

where ΣG = total weight of the turbine and generator parts carried by the stay vanes (stator and rotor of the generator, turbine cover-plate, gate ring, thrust bearing, turbine shaft, runner, guide bearing, etc.);

φ° = angle between each stay vane.

II. The turbine is running under normal conditions ($p \neq 0$). In addition to the axial load due to the concrete and the unit weight, the stay vanes are also acted upon by the water pressure.

$$Q_{II} = Q_1 + Q_2 - P_1 - P_2 + P_3, \qquad \text{(IV. 49)}$$

where P_1 = load due to water pressure on the scroll-casing ceiling, transmitted to the stay vane;

P_2 = load due to water pressure on the speed ring and on the upper water passages of the turbine, transmitted to the stay vane;

P_3 = axial load acting on the runner and transmitted to the stay vane.

When determining the load P_1, it must be noted that the water-pressure load on the casing ceiling transmitted to the casing wall and to the stay vane is proportional to the angle φ° between the stay vanes.

Then a trapezoid is drawn between the contour of the spiral and the stay vanes; its centroid (Figure IV. 24) is determined, and the load P_1 is calculated from formula

$$P_1 = \frac{b}{h} p_1 f, \text{ where } b = \frac{1}{3} h \frac{2a + c}{a + c}, \quad f = \frac{(a + c) h}{2}.$$

Consequently,

$$P_1 = \frac{1}{3} h \frac{(2a + c)}{(a + c)} \cdot \frac{1}{h} \cdot \frac{(a + c) h}{2} p_1$$

or

$$P_1 = \frac{1}{6} (2a + c) h \cdot p_1, \qquad \text{(IV. 50)}$$

where a, c, and h = dimensions of the trapezoid (Figure IV. 24);

p_1 = pressure on the scroll-case ceiling, determined from the formula

$$p_1 = \gamma \left(H - \frac{v_{cn}^2}{2g} \right),$$

where H = level difference between headwater and scroll-casing ceiling.

v_{cn} = velocity of flow in scroll casing.

Consequently,

$$P_1 = \frac{\gamma}{6} h (2a + c) \left(H - \frac{v_{cn}^2}{2g} \right). \qquad \text{(IV. 51)}$$

The load due to water pressure on the speed ring and from the upper water passages of the turbine, taken up by one stay vane, is determined from the formula

$$P_2 = p_2 \frac{\pi}{4} (D_a^2 - D_s^2) \frac{\varphi^\circ}{360^\circ}, \qquad \text{(IV. 52)}$$

where D_a = diameter of the circle formed by the stay-vane leading edges;
D_s = diameter of the turbine shaft.

The pressure in the water passages is

$$p_2 = \gamma \left(H_1 - \frac{v_2^2}{2g} \right),$$

where H_1 = level difference between the headwater and the center of the distributor.

$$v_2 = \alpha \frac{Q}{F} = \alpha \frac{Q}{\pi D_0 b_0}.$$

The coefficient $\alpha \cong 1.5$ used in these formulas allows for the nonuniformity of velocities.

$$P_2 = \frac{\pi\gamma}{4} \left(H_1 - \alpha^2 \frac{Q^2}{\pi^2 D_0^2 b_0^2 2g} \right) (D_a^2 - D_s^2) \frac{\varphi^\circ}{360^\circ}. \qquad \text{(IV. 53)}$$

The axial load of the water column acting on the runner and transmitted to the stay vane is

$$P_3 = \frac{P_z \varphi^\circ}{360^\circ}, \qquad \text{(IV. 54)}$$

where P_z = axial load of the water column on the runner.

III. Load drop and rapid closing of the distributor. The loads due to the weight of concrete, the weight of the hydro-unit parts, and the water pressure over and above the hydrostatic pressure, acting on the stay vane are

$$Q_{III} = Q_1 + Q_2 - P_4 - P_5 + P_6, \qquad \text{(IV. 55)}$$

where P_4 = load due to water pressure on the scroll-case ceiling, transmitted to the stay vane;
P_5 = force caused by the water pressure on the ring surface between the leading edge of the vane (D_a) and the pitch circle of the guide vane axes (D_p) transmitted to the stay vane;
P_6 = force caused by water pressure inside the distributor, transmitted to the stay vane. It is positive, since after a rapid closing of the distributor, a pressure drop (vacuum) occurs in the latter, so that the force is directed downward.

The force P_4 due to water pressure on the scroll-casing ceiling during drop of generator load is transmitted to the stay vanes and is calculated exactly as for normal conditions (formula (IV. 50))

$$P_4 = \frac{1}{6}(2a + c)\, h \cdot p_3, \qquad \text{(IV. 56)}$$

where p_3 = pressure on the scroll-casing ceiling, determined from the formula

$$p_3 = \gamma H \left(1 + \frac{\Delta H}{H}\right),$$

where ΔH = increase of head in the scroll case due to water hammer occurring during rapid closing of the distributor.

Consequently,

$$P_4 = \frac{\gamma}{6}(2a + c)\left(1 + \frac{\Delta H}{H}\right) hH. \qquad \text{(IV. 57)}$$

The force P_5 on the ring-shaped space between the speed ring and the distributor, transmitted to the stay vane, is computed from the formula

$$P_5 = p_3 \frac{\pi}{4}\left(D_a^2 - D_0^2\right)\frac{\varphi^\circ}{360^\circ}$$

or

$$P_5 = \frac{\pi\gamma\varphi^\circ}{4 \cdot 360^\circ}\left(D_a^2 - D_0^2\right)\left(1 + \frac{\Delta H}{H}\right)H. \qquad \text{(IV. 58)}$$

The force P_6 due to pressure of water inside the distributor is transmitted to the stay vane and is determined from the formula

$$P_6 = p_4 \frac{\pi}{4} D_0^2 \frac{\varphi^\circ}{360^\circ}, \qquad \text{(IV. 59)}$$

where p_4 = negative pressure inside the distributor, after sudden closing, usually taken as $p_4 = 1\ \mathrm{kg/cm^2}$.

After calculating the loads Q_{I}, Q_{II} and Q_{III}, acting on the stay vanes for these three possible operating conditions, one may either select the material and the required cross-sectional area of the stay vanes, or determine the compressive and tensile stresses on the existing areas.

The stay vanes, subject to compressive stresses, should be checked for buckling.

At the LMZ, only the stay vanes subject to the highest compressive stresses and those with the smallest cross-sectional area, are checked for buckling.

For strength computations, the stress is determined with allowance for buckling

$$\sigma = \frac{Q}{\varphi F}, \qquad \text{(IV. 60)}$$

where Q = load on the stay vane;
F = cross-sectional area of the stay vane;
φ = safety coefficient.

The coefficient φ depends on the material and on the slenderness ratio

$$\lambda = \frac{\mu l}{i}. \qquad \text{(IV. 61)}$$

where μ = coefficient;
l = stay-vane length;
i = minimum radius of inertia of the stay vane.

$$i = \sqrt{\frac{J}{F}}.$$

where J = minimum moment of inertia of the cross section.

The values of the coefficients φ for steel as functions of the slenderness ratio λ are given in Table IV. 2. This table is reproduced from reference /5/.

TABLE IV.2

Dependence of coefficient φ on the slenderness ratio λ

Slenderness ratio λ	0	10	20	30	40	50	60	70	80	90
Coefficient φ for steel (St.5; 30L)	1.0	0.98	0.95	0.92	0.89	0.86	0.82	0.76	0.70	0.62
Slenderness ratio λ	100	110	120	130	140	150	160	170	180	190	200
Coefficient φ for steel (St.5; 30L)	0.51	0.43	0.37	0.33	0.29	0.26	0.23	0.21	0.19	0.17	0.16

For speed rings made of separate stay vanes, the upper and lower flanges of the vanes should be designed with allowance for the permissible pressure on the concrete, and the foundation bolts must be calculated for strength.

21. PARAMETERS OF REACTION-TURBINE RUNNERS

The basic geometrical parameters of the Kaplan and Francis runners (number, [maximum] opening angle of the blades, the thickness and shape of the blades, as well as the dimensions of the hub or of the upper and lower rings (bands), etc.), which are chosen according to the static and dynamic strength requirements, have a marked effect on the hydrodynamic characteristics of the runner, as well as on its power and cavitation parameters.

For details on the dependence of hydrodynamic characteristics upon geometrical parameters, the reader is referred to the study by A. Yu. Kolton and I. E. Etinberg /53/. The present work presents a brief examination of the relationship between the geometrical and hydrodynamic characteristics of the runner only in reference to strength problems.

Francis runners. The basic geometrical parameters of the Francis runner are: number and thickness of blades (z_1 and δ), distributor height b_0,

shape of crown (upper ring), radius of curvature of lower ring (for low-speed runners) or the cone angle of the lower ring (for high-speed runners), and ratio between discharge (exit) diameter and nominal runner diameter $\frac{D_{ex}}{D_1}$.

The blade number, which has a great effect on the static and dynamic strength of the runner, is one of the most important factors determining the power and cavitation characteristics of the Francis turbine. At a relatively small blade number, the blades are subject to a high specific load, so that the cavitation characteristics are rather poor. On the other hand, a smaller over-all blade surface wetted by the water stream makes it possible to increase the efficiency and the specific speed. With the increase in the blade number, the specific load on the blades is diminished and the cavitation characteristics are improved.

However, a water flow greatly impeded by the [larger number of] blades, causing considerable skin friction, may cause not only reduction in efficiency, but also in the specific speed, in terms of both rpm and discharge. An excessive increase in the blade number is liable to restrict the water flow to such an extent as to worsen the cavitation characteristics instead of improving them.

The blade number (z_1) usually depends on the specific speed, and varies between 9 and 21. On the basis of experience, LMZ correlates the blade number with the specific speed (see Table IV. 3). Strength and rigidity of the runner may be improved if the blade number is increased (the runner dimensions remaining unchanged). High-head turbines, therefore, have a higher blade number, which improves the cavitation characteristics, but lowers the specific-speed characteristics (in terms of both discharge capacity and optimum unit speed).

TABLE IV. 3

Number of blades in Francis runners.

n_s*	60-80	120-150	180-200	200-250	250-300	300-350
z_1	21-19	19-17	17-15	15-14	14	14-12

Since the cavitation characteristics improve with reduction of δ, the blade thickness δ should be kept at a minimum value consistent with strength and rigidity requirements.

If the blade number is changed, the aspect of the universal characteristic of the runner may, within certain limits, be altered. The increase in the blade number displaces the point of optimum efficiency and the power-limiting line toward the smaller discharges.

The meridian projection through the runner (i.e., the contour water passages) (Figure III. 13) is defined by: the distributor height b_0, the radius of curvature of the lower ring (band) of the distributor, the angle α of the lower ring (band), and the shape of the runner hub cross-section.

The distributor height b_0 decreases with the increase in head, the runner thus becoming more rigid. If, for increased head, the distributor

* [n_s = specific speed; z_1 = blade number.]

height were not reduced, a small opening of the distributor would be required for the given discharge, causing a throttling of the water stream during its passage through narrow slits. Appropriate heights b_0 of the distributor for various heads, as used in turbine engineering practice, are tabulated in Figure III. 13.

The radius of curvature of the runner band R_2 and the angle α determine, to a large extent, the runner discharge (exit) diameter D_2. An increase in ratio $\frac{D_2}{D_1}$ increases the outlet cross-sectional area and reduces the flow velocity (pressure drop) after the runner. However, in such cases, the flow conditions around the lower runner band should not deteriorate, since otherwise the efficiency is reduced. The relationship between α and H may be seen from the table below (according to LMZ).

Range of α	Range of head (H)
6-20°	40-100 m
3-6°	100-150 m

Although the shape of the hub cross-section affects the turbine characteristic only slightly, a curved shape nevertheless ensures higher efficiency than a straight shape. On the other hand, a runner with a straight hub shape is easier to build. This is of particular importance when welded constructions are used. Therefore, the hub shape should be selected according to the turbine parameters with due regard for manufacturing and economic requirements.

High turbine efficiency demands runner blades of a complicated shape, determined by hydrodynamical computations. On the other hand, complicated shapes of Francis runner blades and interblade channels render the manufacturing process more difficult. With narrow and highly curved blade channels, for an all-cast runner, it is quite impossible to maintain the theoretically computed shape and the smoothness required. The hydrodynamical design of the Francis runner should therefore comply — as much as possible — with the manufacturing conditions, and among different runners with equivalent hydrodynamical characteristics, ease of manufacture should be the criterion governing final selection.

Kaplan runners. The basic geometrical parameters of the Kaplan runner are: the blade number, the blade-opening angle (or the ratio of blade length (l) to blade pitch (t) (l/t*), the blade thickness δ, and the diameter and shape of the hub.

Apart from the above-mentioned geometrical parameters of the runner, the shape of the throat ring also affects the cavitation and power characteristics of the runner to a great extent.

One of the basic parameters of the Kaplan runner, determining its hydrodynamical characteristics, is the shape, and especially the diameter, of the hub.

The increase of the hub diameter, by decreasing the discharge area, lowers the discharge capacity, the efficiency, and markedly increases

* [For the Russian definition of l/t see in this text page 42.]

the critical cavitation coefficient. This is of great importance, especially for high-head Kaplan runners, where a considerable increase of the hub-tip diameter ratio $\bar{d}_{hub} = \frac{d_{hub}}{D_1}$ is required, in order to accommodate a large number of blades subject to large hydrodynamic forces and moments.

Figure IV. 25 shows dependence of the hub-tip diameter ratio on the maximum head for turbines of different specific speeds. As can be seen, the ratio increases markedly with the increase in head, changing from 0.35 for heads of about 10 m, to 0.60 in the range of heads from 60 to 70 m. Such an increase in this ratio leads to a rapid increase in the (critical) cavitation coefficient, and to a corresponding reduction in the discharge capacity. This is the main obstacle to the use of Kaplan turbines for higher heads and hence the necessity to improve Kaplan runners yet further by reducing the hub-tip diameter ratio in every possible way. Another way of reducing $\bar{d}_{hub}$, apart from improving the hub design, is to develop a blade design ensuring minimum effect of hydrodynamical forces and moments exerted on the blades over a wide range of operating conditions. By reducing the forces and moments acting on the blades, it is possible to reduce the rigidity and strength of the blade-adjusting mechanism, and thus to reduce the hub sizes.

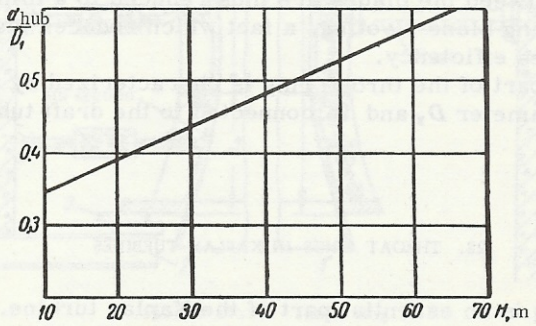


FIGURE IV. 25. Dependence of the hub-tip diameter ratio on head, for Kaplan turbines

The second important factor determining power and cavitation characteristics of Kaplan runners is the ratio of blade length l to blade pitch t (the l/t or pitch ratio), which determines the specific speed almost completely. If the ratio l/t is increased, and with it the over-all blade area, the specific speed decreases (due to the increased friction losses at the blades), and with it the critical cavitation coefficient. Since, with the increase in head, cavitation properties become very important, high-head plants use mainly low-speed runners with better cavitation characteristics and increased ratio l/t. The ratio l/t may be increased in two ways, either by increasing the blade-opening angle and maintaining the same number of blades, or simply by increasing the number of blades. Usually, the blade-opening angle does not exceed 70° to 80°. A further increase in the angle is not recommended, since it causes undesirable blade vibration.

The ratio l/t in a four-blade runner, with the above-mentioned opening angle is approximately l/t = 0.8 to 0.9; further increase of this ratio

may be obtained by increasing the number of blades. The maximum number of blades fitted in U. S. S. R. high-head Kaplan runners is eight. A further increase in the number of blades — as in Francis turbines — is liable to cause an excessive throttling of the stream flow and impair hydrodynamic characteristics.

It should be noted that, due to design considerations, the increase in the blade number involves a certain increase in the hub-tip diameter ratio; therefore, the gain [in efficiency] due to increase in the over-all blade area is not accompanied by a corresponding improvement in the cavitation characteristics. It is therefore advisable to avoid increasing the hub-tip diameter ratio when designing runners with an increased number of blades.

Power and cavitation characteristics require minimum blade thickness, but without impairing strength. The design of blades for minimum thickness requires precise computation of the static and dynamic blade strength and the accurate determination of the distribution of hydrodynamic loads on the blades under various operating conditions.

The throat-ring shape also affects the discharge capacity of the runner and its cavitation characteristics.

Usually, that part of the throat ring located above the runner center-line has a cylindrical shape, whereas the part below the runner is spherical. The clearances between the blades are thus reduced to a minimum and remain constant during blade pivoting, a fact which reduces leakages and consequently increases efficiency.

The spherical part of the throat ring is characterized by the throat (runner-discharge) diameter D_2 and is connected to the draft tube through a conical section.

22. THROAT RINGS IN KAPLAN TURBINES

The throat ring is an essential part of the Kaplan turbine. At its top, it is connected to the lower ring of the distributor, and at its bottom, to the draft-tube cone.

Figures III. 12 and III. 15 show the optimum profile of turbine water passages located near the throat ring (according to LMZ data).

The spherical part of the throat ring extends downward approximately a distance equal to the length of the blade at its maximum pivoting angle.

The cylindrical throat ring gives larger clearances between the blades and the ring and permits an easier access to the runner from above for installation or dismantling.

Throat rings are also provided with a spherical upper part manufactured outside the U. S S R. Openings with detachable covers are fitted in the upper part of the ring, through which the blades may be inserted or removed. For dismantling, the plates are removed, the blades brought with their peripheral sections into a vertical position, and the runner can thus be lifted upward.

Research was carried out at the LMZ laboratory to determine the influence of a completely spherical throat ring on turbine efficiency, but no gain in efficiency was observed. This may apparently be explained by a deterioration of the flow distribution around the lower ring of the distributor, due to the spherical throat ring.

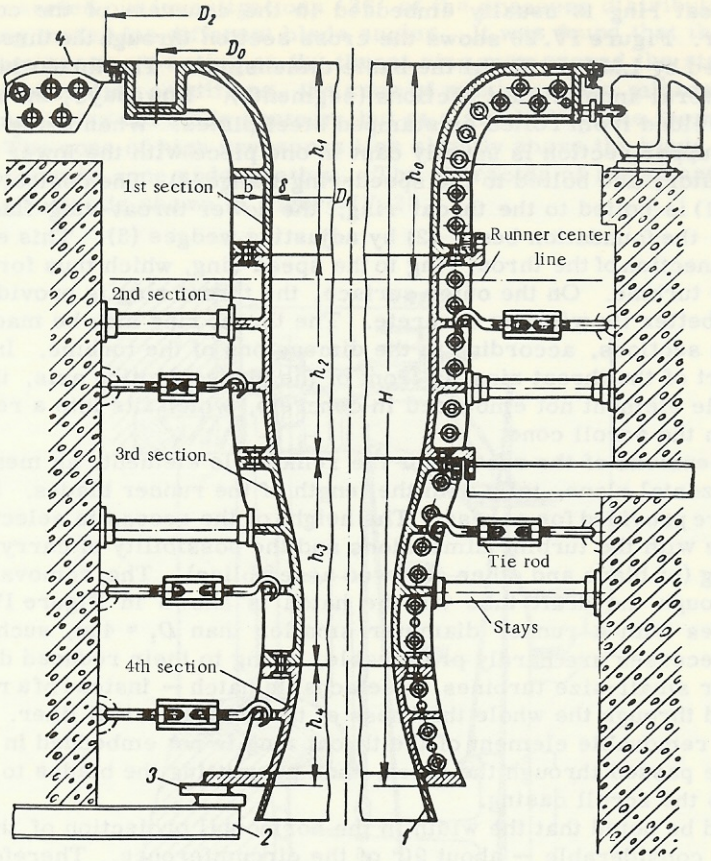


FIGURE IV.26. Throat ring

D_1	D_0	z_0	D_2	H	h_0	h_1	h_2	h_3	h_4	Number of parts per section				Number of horizontal ribs per section				δ	b	Number of	
										I	II	III	IV	I	II	III	IV			tie rods	stays
2750+1.5	3 200	24	3 650	1450	570	(320) 450	(520)	—	(610) 1000	1	(4)	—	1	—	(1)	—	2 (1)	25	110	24	12
3000+1.5	3 500	24	3 950	1600	625	(350) 500	(570)	—	(680) 1100	1	(4)	—	1	—	(1)	—	2 (1)	25	110	24	12
3300+1.5	3 850	24	4 310	1750	685	(380) 550	(620)	—	(750) 1200	2	(4)	—	1	—	(1)	—	2 (1)	30	130	24	12
3700+1.5	4 300	24	4 790	1950	770	(430) 600	(700)	—	(875) 1350	2	(4)	—	2	—	(1)	—	2 (1)	30	130	24	12
4100+2.0	4 750	24	5 240	2150	850	(480) 700	(770)	—	(900) 1450	2	(4)	—	2	—	(1)	—	2 (1)	30	130	24	12
4500+2.0	5 200	24	5 690	2400	935	520	850	—	1030	2	4	—	2	—	1	—	2	30	140	28	20
5000+2.0	5 800	24	6 360	2650	1040	600	900	—	1150	4	4	—	4	—	1	—	2	35	140	28	24
5500+2.0	6 350	24	6 910	2900	1140	680	950	—	1270	4	4	—	4	—	1	—	2	35	175	28	24
6000+3.0	7 000	24	7 565	3200	1240	760	1000	—	1440	4	4	—	4	—	2	—	2	35	175	48	32
6600+3.0	7 700	24	8 290	3500	1370	870	1050	—	1580	4	4	—	4	—	2	—	3	35	175	60	40
7200+3.0	8 400	32	9 020	3800	1500	1000	1100	—	1700	4	4	—	4	1	2	—	3	35	175	60	40
8000+3.0	9 300	32	9 940	4250	1660	1100	1200	1250	700	8	8	6	6	1	2	2	1	40	200	86	56
9000+3.5	10 500	32	11 190	4750	1870	1240	1350	1360	800	8	8	6	6	1	2	2	1	40	200	86	56
9300+3.5	10 800	32	11 490	4900	1930	1280	1400	1370	850	8	8	6	6	1	2	2	1	40	200	86	56

Note: the data in parentheses refer to design variants for runners of small diameters.

The throat ring is usually embedded in the concrete of the conical scroll liner. Figure IV. 26 shows the cross section through the throat ring standardized by LMZ, with all the basic dimensions. The throat ring consists of several annular cast sections (segments). Nowadays, the sections are welded from rolled or stamped steel plates. When using all-cast rings, the upper section is usually cast in one piece with the lower ring of the distributor, and bolted to the speed-ring flange (4). The conical draft-tube liner (1) is bolted to the throat ring; the lower throat-ring flange is secured to the foundation beam (2) by adjusting wedges (3). This ensures a rigid connection of the throat ring to the speed ring, which thus form the body of the turbine. On the outer surface, the throat ring is provided with ribs for a better tie with the concrete. The throat ring may be made in one piece or in sections, according to the dimensions of the turbine. In the central part of the throat ring, in front of the blade-pivoting axis, there is a removable element not embedded in concrete, which fits into a recess provided in the scroll cone.

The dimensions of the recess for the removable element, as measured in the horizontal plane, tally with the length of the runner blades. Special openings are provided for access. The height of the recess is selected in accordance with the turbine dimensions and the possibility of carrying out dismantling (of blade and other screwed assemblies). The removal of blades through the draft tube via the hatch is shown in Figure IV. 27. For turbines with a runner diameter smaller than D_1 = 4 m, such dismantling recesses are hardly practicable, owing to their reduced dimensions. For small-size turbines, a detachable hatch — instead of a recess— is provided through the whole thickness of the conical scroll liner. In this event, the removable element of the throat ring is not embedded in concrete, and may be passed through the hatch, thus permitting the blades to be removed into the scroll casing.

It should be noted that the width in the horizontal projection of this kind of hatch is considerable — about 90° of the circumference. Therefore, one fourth of the conical scroll liner has to be cut away, a fact which does not permit the scroll to be used for the location of the stay vanes; this renders the transmission of the loads to the foundation more difficult.

In certain designs, the throat ring is not embedded in concrete but bolted to the foundation. This facilitates throat-ring removal (e.g., for repairs), but increases the weight of the part considerably, due to the additional foundation elements required. Hence, this design (in the author's opinion) is not to be recommended. The cast-steel throat-ring is lined in the hatch area with stainless-steel plates which ensure a better protection against cavitation erosion.

During operation of the runner, the throat ring is subjected to fluctuating forces caused by increased and reduced pressure acting alternately.

The frequency of the periodical pressure fluctuations at points of the throat-ring walls is

$$K = \frac{nz_1}{60} \text{ c},$$

where n = turbine speed;
z_1 = runner-blade number.

VIGM carried out investigations /36/ of the pressure distribution in a throat-ring model for different blade angles. It was found that the value of the absolute pressure acting on the throat ring may exceed the static head. Under any operating conditions, the zone of maximum and minimum pressures is not along the blade contour, but at a small distance from the blade outline. The zone of high pressures lies slightly above the blade axis, and the low-pressure zone underneath it. The character of instantaneous pressure distribution is shown in Figure IV. 28.

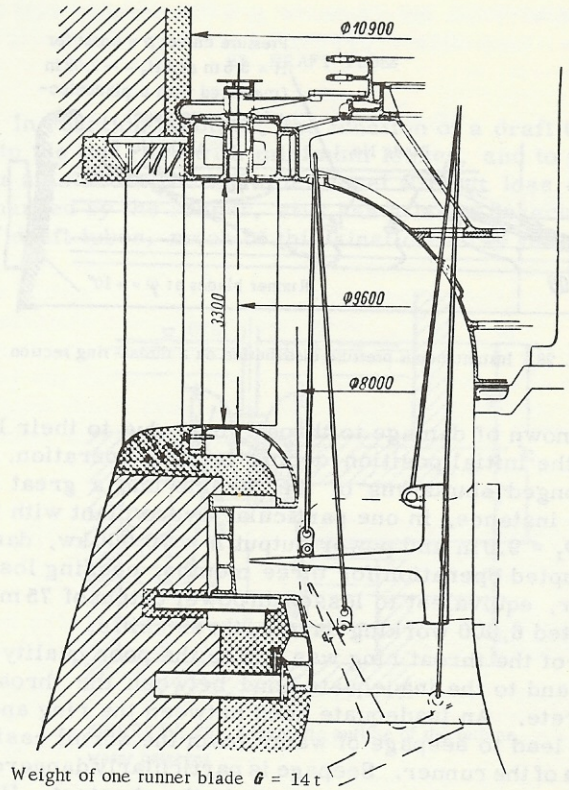


FIGURE IV. 27. Removal of the runner blade through the throat ring opening

Pressure fluctuations cause loosening of the throat-ring fastenings. The amplitude of the pressure fluctuation increases with head, a feature particularly dangerous in large turbines, where, for transportation reasons, the throat ring is made of separate sections, fastened together in vertical and horizontal plane by means of bolted flanges. The bolts in butt joints are subjected to fluctuating forces. In throat-ring design, close attention has therefore to be paid to the bolted joints of the sections.

Special attention must also be paid to the correct bond between ring and concrete. The secondary concrete around the throat ring is usually placed

after building the scroll cone, with space around the ring restricted, and the secondary concrete insufficiently hardened. Special elements — tie rods and jack screws — are used in embedding the throat ring in the secondary concrete (see Figure IV. 26).

The number of tie rods and jack bolts has to be chosen so as to provide sufficient space for the workers to place the secondary concrete between the throat ring and the primary concrete. Since the throat ring has a rather low rigidity, and is easily subject to radial deformations, the use of the above tightening elements ensures the correct shape of the throat ring during its installation.

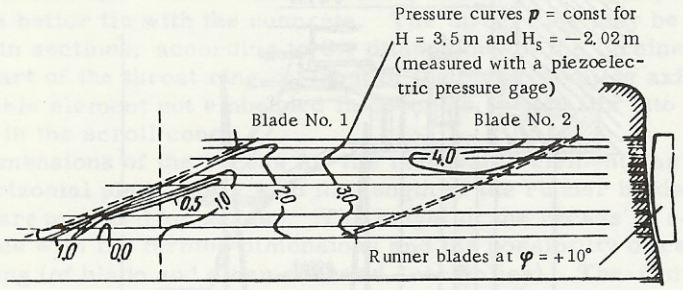


FIGURE IV. 28. Instantaneous pressure distribution on a throat-ring section

Instances are known of damage to throat rings due to their loosening and shifting from the initial position during turbine operation. Such damage involves prolonged shutdowns of the turbine and a great amount of repair work. For instance, in one particular hydro plant with turbines of runner diameter D_1 = 9.0 m and power output N = 70,000 kw, damage to the throat ring interrupted operation for three months, causing loss of 2.17 billion m3 of water, equivalent to losses in power output of 75 million kwhr. Repairs necessitated 6,000 working days in three shifts.

The movement of the throat ring was due to the poor quality of the secondary concrete, and to the inadequate bond between the throat ring and the primary concrete. An inadequate bond between the ring and the secondary concrete may lead to seepage of water from the scroll casing into the low-pressure area of the runner. Seepage is particularly dangerous in the area of the repair hatch, where the seepage path is the shortest. Here, the water may erode the concrete, washing out the alkali and the salts, and damaging the bond between the ring and the primary concrete. In such cases, a liner has to be provided to prevent seepage of water.

During concrete placing, special attention must be paid to preparation of the secondary concrete, its consistency, pouring conditions and quality, and the bond to the primary concrete.

The bond between the throat ring and the concrete should be checked periodically during operation if necessary; grout should be injected into the secondary concrete by means of pumps through special openings in the throat ring,

Experience in manufacturing welded throat rings for the Volga hydroelectric plant imeni Lenin, showed that welding permits the machining of the

inner surfaces of such rings to be dispensed with. The weight of welded throat rings — compared with cast rings — and the manufacturing time are thus reduced.

Some turbine builders use cast-iron throat rings, lined with steel plates assembled by bolts with conical heads.

These designs are not recommended, since the vibration of the steel plates caused by load fluctuations loosens the bolt fastenings, the plates are torn off, and the unlined inner surface of the throat ring is rapidly destroyed through cavitation.

23. DRAFT TUBES

General. In reaction turbines, the function of a draft tube is to discharge the water into the tail race with minimum losses, and to permit the setting of the runner axis above the tailwater level without loss of head. The water, discharged by the runner, still has a large reserve of kinetic energy. By means of draft tubes, much of this kinetic energy may be regained.

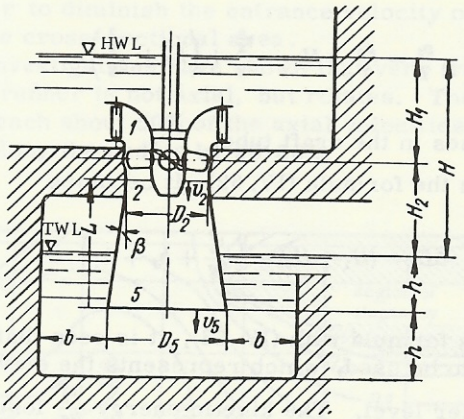


FIGURE IV. 29. Schematic outline of the turbine water passages

The draft tube is designed as a diverging discharge passageway, with a gradually increasing cross-sectional area (also called diffuser) and creates an additional suction head after the runner, thus permitting the kinetic energy to be efficiently regained. The discharge flow velocities, and consequently, the losses at the exit, both decrease.

The operational effectiveness of a draft tube may be ascertained by comparing the degree of use of the [available] head by a turbine with and without draft tube.

The specific energy before the runner is, according to Figure IV. 29,

$$E_1 = \frac{p_a}{\gamma} + H_1 + H_2 - h_1$$

where h_1 = head losses in the flow passages.

The energy at the runner exit is

$$E_2 = \frac{p_2}{\gamma} + H_2 + \frac{v_2^2}{2g};$$

consequently, the energy utilized by the runner is

$$\Delta E = E_1 - E_2 = \frac{p_a}{\gamma} + H_1 - \frac{p_2}{\gamma} - \frac{v_2^2}{2g} - h_1. \qquad \text{(IV. 62)}$$

When there is no draft tube, the pressure p_2 at the runner exit equals atmospheric pressure, formula (IV. 62) thus becoming

$$\Delta E_1 = H_1 - \left(\frac{v_2^2}{2g} + h_1\right). \qquad \text{(IV. 63)}$$

To the contrary, in the presence of a draft tube, the pressure $\frac{p_2}{\gamma}$ in the section after the runner is determined from Bernoulli's equation, written for sections (2) and (5) (Figure IV. 29),

$$\frac{p_2}{\gamma} = \frac{p_a}{\gamma} - H_2 - \frac{v_2^2}{2g} + \left(h_T + \frac{v_5^2}{2g}\right). \qquad \text{(IV. 64)}$$

where h_T = head losses in the draft tube.

By inserting $\frac{p_2}{\gamma}$ in the formula (IV. 62), it becomes

$$\Delta E_2 = (H_1 + H_2) - \left(\frac{v_5^2}{2g} + h_T + h_1\right). \qquad \text{(IV. 65)}$$

By comparing this formula with (IV. 63), it is seen that the draft tube permits the head H_2 to be used, which represents the elevation of the runner above the tailwater level. The kinetic energy $\frac{v_5^2}{2g}$ lost by the flow discharged through the draft tube is considerably smaller than $\frac{v_2^2}{2g}$ in the foregoing case, because of the divergent shape of the draft tube (diffuser).

The ratio of the entrance to the exit cross-sectional areas is usually taken as

$$n = \frac{F_2}{F_5} = 0.25 \text{ to } 0.35.$$

With ratios of this order, the energy losses at the draft tube exit are some 6 — 12% of the total kinetic energy of the flow discharged through the runner; a large part of this energy is recovered in the draft tube, which creates an additional suction head.

As shown by the formula (IV. 64), this dynamic suction head is

$$\frac{p_{dyn}}{\gamma} = \frac{v_2^2}{2g} - \left(\frac{v_5^2}{2g} + h_T\right). \qquad \text{(IV. 66)}$$

Draft-tube efficiency (also called divergence coefficient or coefficient of energy recovery) is the term used to denote the ratio of the dynamic suction head existing at the draft tube entrance to the dynamic suction head obtainable (in an ideal case) at the runner exit.

$$\eta_{dr} = \frac{\frac{p_{dyn}}{\gamma}}{\frac{v_2^2}{2g}} = \frac{\frac{v_2^2}{2g} - \left(\frac{v_5^2}{2g} + h_T\right)}{\frac{v_2^2}{2g}} \quad \text{(IV. 67)} \qquad \text{or} \qquad \eta_{dr} = 1 - \frac{v_5^2 + 2gh_T}{v_2^2}. \quad \text{(IV. 68)}$$

Since the flow velocity of the water in the draft tube is not uniform, η_{dr} is more accurately expressed by the formula

$$\eta_{dr} = \frac{\int_F \frac{p_{dyn}}{\gamma} v_{2z}\, dF}{\int_F \frac{v_2^2}{2g} v_{2z}\, dF}. \quad \text{(IV. 69)}$$

Consequently, the measures recommended for improving draft-tube efficiency are either to diminish the entrance velocity or to increase the draft-tube entrance cross-sectional area.

Experimental investigations have shown that very frequently the flow discharged by the runner is not axial, but rotates. The tangential velocities sometimes reach about 50% of the axial velocities, and, furthermore, they may change along the radius by 20-30%.

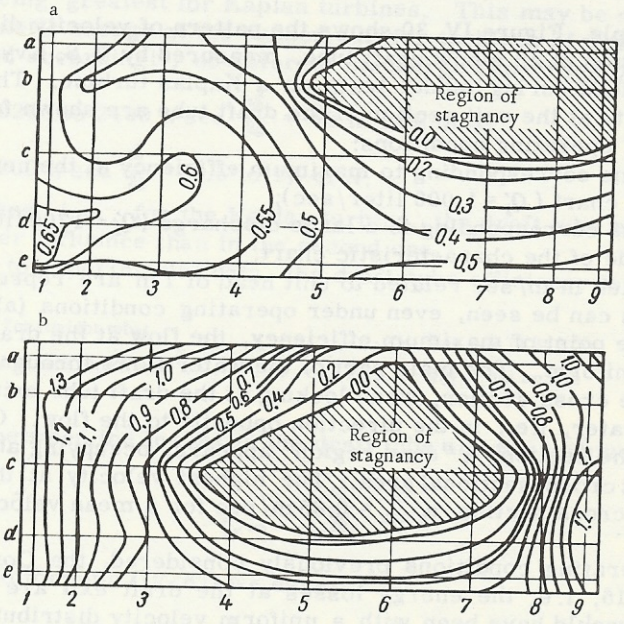


FIGURE IV. 30. Flow velocities for unit head of 1 m, at the exit section of an elbow draft tube (runner rotating counterclockwise as viewed from the tailwater)

It was also shown that this nonuniformity of flow may be observed not only at the entrance to the draft tube, but also at its exit. An exceptionally marked nonuniformity occurs at the entrance section of elbow draft tubes, since the elbow affects the flow considerably. The losses increase with the nonuniformity of flow velocities in the draft-tube cross-sections.

The degree of nonuniformity of velocity distribution is characterized by Coriolis coefficient K, which is the ratio of the actual specific kinetic energy at a given section to the specific energy calculated for the mean velocity at the same section, viz.

$$K = \frac{\int_F v^2 v_z dF}{v_m^2 Q}.$$

The Coriolis coefficient is always greater than unity and depends on the shape of the runner blades, the shape and dimensions of the draft tube, and the operational conditions of the turbine.

In bent draft tubes, owing to existence of an elbow, the value of K_5 is larger than for straight conical tubes. According to experimental data,

for straight conical draft tubes	K_5 = 1.2 to 1.5
for bent draft tubes with blade-control connections between distributor and runner in operation	K_5 = 1.5 to 2.5
for elbow draft tubes with blade-control connections out of operation	K_5 = 3.0 to 6.0

As an example, Figure IV. 30 shows the pattern of velocity distribution at the exit section of an elbow draft tube, measured by V. S. Kvyatkovskii /37/, at the VIGM during model tests on a Kaplan turbine. The curves of equal velocity at the exit section of the draft tube are shown for two different kinds of operating conditions:

a) conditions corresponding to maximum efficiency at the center of the characteristic chart (Q_I' = 1,000 liter/sec);

b) conditions corresponding to a large discharge (Q_I' = 1700 liter/sec), at the right side of the characteristic chart.

The velocities in m/sec related to unit head of 1 m are represented on the graph. As can be seen, even under operating conditions (a), corresponding to the point of maximum efficiency, the flow at the draft tube exit is highly nonuniform. The main part of the water flows through the lower left side of the cross section, when looking at the draft tube exit section from the tailwater, i.e., in the direction opposite to the flow. On the upper right side of the section, a "dead region" appears, occupying about a quarter of the total exit cross-sectional area. The highest velocity at the lower corner of the cross section $v_{5\,max}$ = 0.65 m/sec for a mean velocity of v_{5m} = 0.365 m/sec.

For the operating conditions previously considered, the Coriolis coefficient K_5 = 2.16, i.e. the energy losses at the draft exit are 2.16 as great as they would have been with a uniform velocity distribution over the cross section. Under different operating conditions, the flow was also

found to be nonuniform, but the character and intensity of the nonuniformity both change. When the discharge is small, the flow is more uniform and the stagnant regions are either very small, or nonexistent.

When the turbine operates at greater discharges (corresponding to the right side of the characteristic chart) the nonuniformity of the velocity increases and the Coriolis coefficient rises. This is illustrated in the same Figure IV. 30, by the curves b.

In this case, the stagnant region is shifted toward the center of the section. The water flows mainly through the right and left parts of the section. The maximum velocity at the left side is $v_{5\max} = 1.3$ m/sec, the Coriolis coefficient increases to $K_5 = 2.6$. According to data from the same study, the nonuniformity of flow increases, especially under conditions in which the blade-control connection between distributor and runner does not operate then, the Coriolis coefficient reaches $K_5 = 7.4$, and the stagnant region extends over half the draft tube exit section.

One suggestion made was to install guide vanes in the draft tube elbow to improve the flow conditions and make the flow velocity more uniform. Joint research carried out in wind tunnels by the LPI and LMZ laboratories in connection with the design of turbines for the Volga hydro plant imeni Lenin, showed that the flow pattern in the elbow draft tube and the power characteristics of the turbine may be improved in this way. However, such vanes should be adjustable to the correct position according to operating conditions. In view of the large over-all sizes of the draft tube, the construction of adjustable vanes presents a difficult engineering problem. Hence, economic considerations will decide whether such vanes should be used or not.

The importance of the draft tube varies with turbines of different specif-if speeds, being greatest for Kaplan turbines. This may be seen by comparing the kinetic energy at the runner exit for turbines of different specific speeds and accordingly, of different discharge capacities Q_1'.

For Q_1' = 2200 to 2400 l/sec $\frac{v_2^2}{2g}$ = 40 to 50% of H;

For Q_1' = 200 l/sec $\frac{v_2^2}{2g}$ = 0.5 to 1% of H.

In the first case, i. e., for the Kaplan turbine, the draft tube has evidently a much greater influence than in the second one.

According to experimental data, the draft-tube efficiency is:

For straight tubes . . . . . $\eta_{dr} = 0.75$ to 0.85

For bent draft tubes . . . . . $\eta_{dr} = 0.6$ to 0.75

The ratio between the losses in the draft tube and the turbine head is

$$\zeta_T = \frac{h_T + \frac{v_5^2}{2g}}{H}.$$

According to formula (IV. 67) we have

$$h_T + \frac{v_5^2}{2g} = (1 - \eta_{dr}) \frac{v_2^2}{2g},$$

$$\zeta_T = (1 - \eta_{dr}) \frac{v_2^2}{2gH}. \qquad \text{(IV. 70)}$$

Consequently, the losses in the draft tube are directly proportional to the kinetic energy of the flow.

According to I. E. Etinberg, for $\eta_{dr} = 75\%$, the losses in the draft tube are:

For Kaplan turbines . . . . . $\zeta_T = 10-12.5\%$

For Francis turbines . . . . . $\zeta_T = 0.12-0.25\%$

A reduction of η_{dr} by 10% may lead to an efficiency drop:

For Kaplan turbines . . . . . from 4 — 5%

For Francis turbines . . . . . from 0.05 — 0.1%

Therefore, in designing a Kaplan turbine, the shape of the draft tube has to be chosen very carefully. Its over-all sizes should be large enough to ensure as high a draft-tube efficiency as possible.

The draft tube is much less important for the efficiency of Francis turbines, especially with medium and high heads.

Since an accurate method for determining the stream lines in the draft tube does not yet exist, data provided by field or model tests are used to determine the dimensions and shape of the draft tube.

With the extensive use of Kaplan turbines, draft-tube model studies are finding increasing application, since turbine efficiency depends on the shape and dimensions of the draft tube, while its depth markedly affects the volume of excavations necessary to accomodate the powerhouse substructure, and consequently, the over-all cost.

Important design and constructional considerations such as these require the use of small draft tubes, but on the other hand, they lead to the reduction of turbine efficiency, especially for turbines operating at increasing load demands, with large unit discharges Q_1'.

The selection of optimum draft-tube dimensions suited to every type of power plant equipped with Kaplan turbines should be made on the basis of thorough economic calculations, by taking into account the operating conditions, the load curves, the output of the power system, etc.

For different draft-tube designs, A. V. Tananaev recommends the increase in the turbine output and in the average annual power output to be calculated from the increment in the turbine efficiency. The increase of the average annual output of the plant saves steam power and consequently lowers the generation costs of the thermal power plants serving the same power grid.

Such economic calculations are carried out by the designer of the power plant for various alternatives, and the selection of the final turbine parameters and draft-tube dimensions is made jointly with the turbine designer.

In order to ascertain the effect of the draft tube on turbine efficiency, V. C. Kviatkovskii studied the losses in the separate elements of a medium-speed Kaplan turbine (n_s = 550 to 600), and calculated the energy balance for different operating conditions. The analysis of the energy balance made it possible to establish the part played by each turbine component. It was thus found that at large discharges, the energy losses in the draft tube are much higher than in the runner.

The analysis of the energy balance for one Kaplan turbine, namely the distribution of losses among the runner, distributor, and draft tube for variations in unit discharge from $Q_1' = 500$ liter/sec to $Q_1' = 2{,}100$ liter/sec, is illustrated graphically in Figure IV. 31. At small discharges ($Q_1' = 500$ to 700 liter/sec), the greatest losses (14–18 %) occur in the runner and distributor. This may be explained by poor flow conditions about the distributor and runner vanes. The total losses in the draft tube are some 3%. At normal water discharges through the turbines ($Q_1' = 1{,}400$ to 1,600 liter/sec), corresponding to the point of maximum efficiency and normal operating conditions, the losses in the runner and distributor drop sharply to approximately 4%, whereas the losses in the draft tube increase. The losses at the draft-tube exit increase up to ~ 10%, while the hydraulic losses in the draft tube increase up to 3%. At maximum unit discharges ($Q_1' = 2{,}000$ to 2,100 liter/sec), corresponding to maximum power output, the losses in the runner and distributor are about the same, whereas the losses at the draft-tube exit increase markedly, reaching 14.5%; the hydraulic losses rise to ~ 7%, and consequently the total losses in the draft tube attain ~ 21.5%.

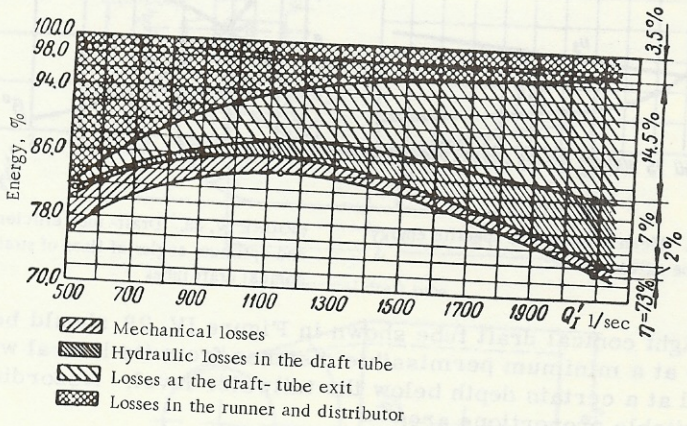


FIGURE IV. 31. Energy balance in a Kaplan- turbine model

Straight conical draft tubes. The simplest type is the straight conical draft tube shown in Figure IV. 29. At present, the use of this type is confined to small-size turbines, since considerable excavation is necessary for the required length $L = (3 - 5)D_1$, of the draft cone. This is not economical for large hydro plants.

Bent draft tubes (also called elbow tubes) with a depth of $h < 2.6D_1$ are used for large turbines.

The curves of mean velocity and specific energy at the exit section, as a function of head, are shown in Figure IV. 32. These curves are used in the selection of the draft-tube exit cross-section area F_5. With known exit cross-section area and entrance diameter D_2 of the tube, and given angle of flare $\beta°$, the length of the straight draft tube may be determined. The angle of flare should be taken in accordance with the length-to-diameter ratio L/D_1 (relative length) within certain limits established in practice.

For large angles $\beta°$, the increase in the losses due to the widening of the tube cross section is offset by the reduction in losses due to the greater exit cross-sectional area. We thus obtain an optimum value of $\beta°$ for each $\frac{L}{D_1}$, for which total losses in the draft tube are a minimum. The values of maximum draft-tube efficiency and optimum angle of flare for conical draft tubes of different length are given in Figure IV. 33, according to data by I. E. Etinberg. For one particular draft tube of length $L = 3D_1$, the optimum angle of flare $\beta° = 7°$ and the draft-tube efficiency $\eta_{dr} = 77\%$. For a shorter tube $L = 1.5D_1$, the optimum angle equals $\beta° = 9°$ and the tube efficiency is then reduced to $\eta_{dr} = 68\%$, i.e., by 9%. If the tube length is increased up to $L = 5D_1$, the draft-tube efficiency will increase up to $\eta_{dr} = 82\%$, i.e., by only 5%, compared with the tube of $L = 3D_1$.

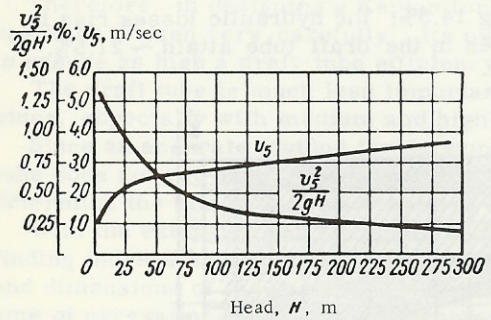


FIGURE IV. 32. Mean velocity and specific energy at the draft-tube exit-section

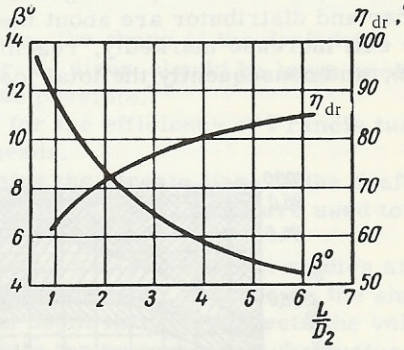


FIGURE IV. 33. Draft- tube efficiency and optimum angles of flare of straight conical draft tubes

The straight conical draft tube shown in Figure IV. 29 should be set in the tailrace at a minimum permissible distance from its lateral walls and bottom, and at a certain depth below the tailwater level. According to practice, the suitable proportions are:

$$b \geqslant (0.5\text{-}0.7)D_5,$$

$$h \geqslant (0.6\text{-}1.0)D_5.$$

Elbow draft tubes. Elbow draft tubes are of various shapes. A draft tube designed by LMZ is shown in Figure IV. 34. It consists of the conical flare (1), the draft-tube elbow (2), and the horizontal flare (3). The conical flare may have various heights h_3 for the same diameter of the tube D_3. The entrance diameter D_4 of the elbow changes accordingly. The elbows are geometrically similar for various draft-tube depths h.

A typical Kaplan-turbine draft-tube elbow, as designed by LMZ, is shown in Figure IV. 35. For minimum draft-tube heights, the elbow ensures the transition from the circular exit of the conical section to the rectangular entrance section of the horizontal flare. The elbow is built up of regular geometrical surfaces. From the circular entrance section of diameter D_4 the inner surface of the elbow bends in the direction of flow into torus (6) of

radius r, which then changes into a horizontal surface (7). A conical surface (1) extends from the entrance to the elbow, intersecting the horizontal-cylinder surface (2). The transition from the conical surface (1) to the toroidal surface of revolution (6) is accomplished by the inclined plane (5). The elbow surface on each side consists of the vertical plane (4) and the vertical cylindrical surface (3). This elbow design simplifies the lining and concreting. The height h_6 of the exit section is considerably smaller than the width B_5, thus ensuring a minimum elbow height h_4. In the horizontal plane, the elbow is usually asymmetrical with respect to the turbine center line. The excentricity m of the elbow depends on the scroll-casing dimensions, so that the draft tube can be accommodated within the scroll.

A dividing pier is sometimes provided in the horizontal diffuser of draft tubes for large turbines to reduce the draft tube width B_5. The pier thickness should be as small as possible without, however, impairing structural strength, since the presence of piers in the draft tube restricts the flow section.

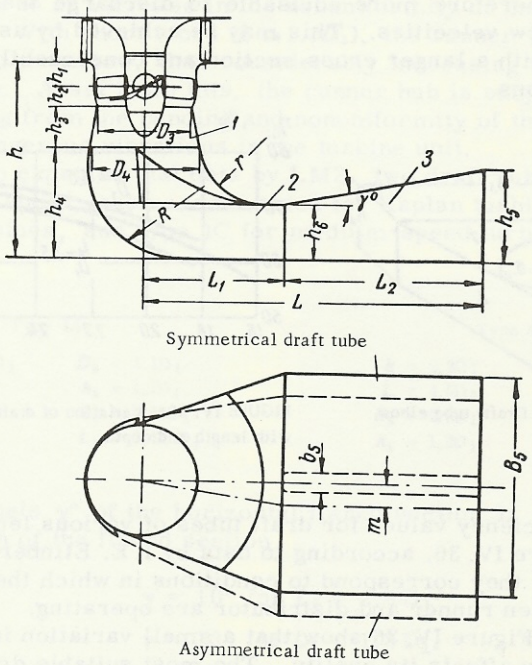


FIGURE IV. 34. Kaplan- turbine elbow draft tube

The elbow draft tube is actually a diffuser with a curved axis. A lengthening of the axis should therefore lead to an increase in the draft-tube efficiency. The axial length of the draft tube may be increased by increasing the depth h and the length L.

It was found experimentally that, with an increase in the depth and the length of the elbow draft tube, turbine efficiency increases with the specific speed. It is the increase of the draft-tube depth which proves to be

most effective for increasing turbine efficiency. The difference in the efficiencies of turbines with draft tubes having different exit cross sections may be calculated from the formula

$$\Delta\eta = \frac{K_5\left(v_5'^2 - v_5^2\right)}{2gH},$$

where v_5' and v_5 = mean exit velocities in the draft tubes compared,
and K_5 = Coriolis coefficient.

In determining the over-all sizes of draft tubes with the same exit cross section, a shorter and deeper draft tube is more suitable than a long and shallow one. This may be explained by the fact that the elbow has a greater hydraulic resistance than a straight pipe. Changes in direction in the draft tube are conducive to intensive eddies along the inner wall of the elbow. The pressure varies along the elbow, being lower at the inner wall, and increasing toward the straight section. This causes additional losses in the elbow. It is therefore more advisable to discharge the water into the draft tube at low velocities. This may be achieved by using a longer conical section, with a larger cross section and consequently, an elbow of larger dimensions.

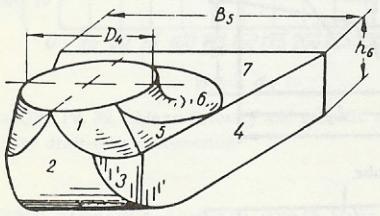


FIGURE IV. 35. Draft- tube elbow

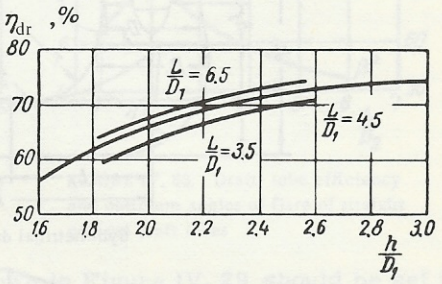


FIGURE IV. 36. Variation of draft tube efficiency with length and depth

Draft-tube efficiency values for draft tubes of various lengths and depths are given in Figure IV. 36, according to data by I. E. Etinberg on the basis of LMZ practice; they correspond to conditions in which the blade-control connections between runner and distributor are operating.

The curves in Figure IV. 36 show that a small variation in the draft-tube length only slightly affects its quality. The most suitable draft tube is that having $L = 4.5D_1$, since an increase in the tube length up to $L = 6.5D_1$, i.e., by $2D_1$ or by almost 50%, only slightly increases the tube efficiency, whereas a reduction in the draft-tube length to $L = 3.5D_1$, i.e., by approximately $1D_1$, reduces the value of η_{dr} to a larger degree.

The tube depth h affects the properties of the elbow draft tube to a larger extent. Reduction in depth from $h = 2.0D_1$ to $h = 1.6D_1$ i.e., by $0.4D_1$, lowers the draft-tube efficiency η_{dr} by 7.5%. The same reduction for a deeper draft tube from $h = 2.6D_1$ to $h = 2.2D_1$ lowers η_{dr} by only 3.5%.

For Kaplan turbines LMZ usually adopts two different draft-tube depths:

$$h = 1.915D_1;$$

$$h = 2.3D_1.$$

However, in one case, LMZ built an elbow draft tube with

$$h = 1.5D_1.$$

A series of economic calculations are usually required for the selection of the draft-tube depth: they refer to the power output for various draft-tube dimensions, the cost of additional excavation for a deeper tube, etc. Deep draft tubes ensure higher power output as a rule, but require a greater capital investment. The larger the required discharge capacity Q_1' of the turbine, the more suitable the use of a deeper draft tube, since otherwise the losses would increase excessively.

For Kaplan turbines, it is not advisable to use short (shallow) elbow draft tubes with a depth h less than $1.9D_1$, even if they prove to be economical, since this leads to an increase in the nonuniformity of the flow discharged by the runner. With short tubes ($L \cong 1.5D_1$), the runner-hub extension is located close to the elbow, thus considerably increasing the nonuniformity of flow velocity. Apart from this, the runner hub is subject to lateral forces resulting from the bending and nonuniformity of the flow in the elbow, and causing dangerous vibrations in the turbine unit.

According to experimental data by LMZ, two draft-tube types, depending on the specific speed, are recommended for Kaplan turbines: type 4A for low-speed turbines, and type 4C for medium-speed turbines (Figures IV. 34 and IV. 35).

Type 4A

$h = 1.915D_1$	$D_4 = 1.1D_1$
$L = 3.5D_1$	$h_4 = 1.1D_1$
$B_5 = 2.2D_1$	$h_6 = 0.55D_1$
$h_5 = 1.0D_1$	$L_1 = 1.417D_1$

Type 4C

$h = 2.3D_1$	$D_4 = 1.17D_1$
$L = 4.5D_1$	$h_4 = 1.17D_1$
$B_5 = 2.3D_1$	$h_6 = 0.584D_1$
$h_5 = 1.2D_1$	$L_1 = 1.5D_1$

The slope angle $\gamma°$ of the horizontal flared section is selected according to the length of the flared section

$$\gamma = 10° \text{ for } L_2 = 2.4D_1$$

$$\gamma = 13° \text{ for } L_2 = 1.8D_1.$$

The dimensions h_1, h_2, h_3, and D_3 are selected according to the runner type.

I. M. Shchapov studied the problem of the optimum length for elbow draft tubes; by analyzing the results of tests made by various designers and the available data on draft tubes in operation, Shchapov arrived at the conclusion that the correct selection of the draft-tube over-all sizes is of the utmost economic importance. He points out that the different draft-tube elements, such as cone, elbow, and horizontal flared section, recover energy differently. The conical part, which accounts for 11% of the total length of the draft tube, recovers about 50% of the energy recovered by the draft tube (the draft tube usually recovers 75% of the total energy), whereas the horizontal flared section, which represents 33% of the tube length regains

only about 20%. Some 5% of the kinetic energy is regained in the elbow. A study of existing hydroelectric plants showed that draft tubes of the following depths are mainly used:

in the U.S.S.R. . . . . $h = (1.9 \text{ to } 2.3) D_1$,

abroad . . . . . $h = (1.9 \text{ to } 2.5) D_1$.

The draft-tube lengths are:

in the U.S.S.R. . . . . $L = (4.2 \text{ to } 5.5) D_1$,

abroad . . . . . $L = (5.0 \text{ to } 5.7) D_1$.

Plants outside the U.S.S.R. are equipped with longer draft tubes, and recent data show that the latest hydroelectric plants are provided with still longer draft tubes, these being considered more economical. In the long run, reduction of draft-tube length to save capital investment is liable to cause greater losses.

Various investigations showed the importance of that region of the water passages where the throat ring joins the draft tube (Figure IV. 37).

Research on hemispherical throat rings was carried out at the LMZ and VIGM /55/, as well as in Czechoslovakia; it showed that a throat-diameter $D_2 = 0.97 D_1$ and a flare angle $\beta° = 7°$ should be recommended for high-speed turbines. In turbines for higher heads, the throat diameter D_2 should preferably be reduced to $0.943 D_1$. When D_2 is reduced, the turbine efficiency increases slightly, but the discharge capacity decreases and the critical cavitation coefficient (σ_{cr}) rises. The effect of throat cross section (profile) on cavitational and power characteristics of the turbine decreases with the increase in depth of the draft tube.

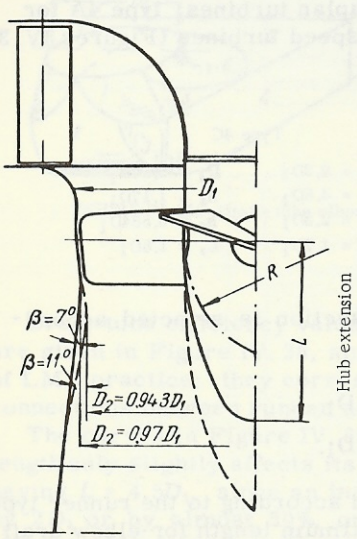


FIGURE IV.37. Shape of throat ring and runner-hub extension

Research carried out by F. F. Gubin and M. F. Gubin, at the MISI /25/, showed that the lengthening of the runner-hub extension (Figure IV. 37) improves turbine efficiency, which may be explained in this case by smoother changes in the cross-sectional discharge area at the draft-tube entrance.

The investigations carried out by I. N. Filatov at the LPI, showed, however, that the danger of the runner being damaged by hydraulic forces increases when the hub extension is made longer. Filatov studied conventional hub extensions ($l = 0.6 D_1$) and shorter ones ($l = 0.4 D_1$) under various operating conditions.

Shorter hub extensions were found to provide less favorable conditions for flow around the runner than conventional (longer) extensions, and to have

higher pressure fluctuations. On the other hand, transverse forces in conventional hub extensions are 1.5 times higher than in shorter hubs. Although these transverse forces (in absolute values), in a normal draft tube, are rather small (about 2% of the total axial forces) they may endanger the mounting of the runner, since they act periodically with high frequency. In shallower (shorter) draft tubes, the elbow is located nearer to the runner, and the transverse forces are considerably increased. Instances of hub-extension failures are not infrequent.

The elbow draft tubes used for Francis turbines are practically of the same shape as those for Kaplan turbines. Model tests and field investigations on Francis turbines showed that the flow after the runner is rotational under almost all operating conditions. The shape of the vortex, however, varies: it is almost vertical near the turbine center-line for high loads, and becomes spiral-shaped at part load.

The blades impart a certain rotation to the water flowing through the runner, and all these eddy lines leaving the blade edges converge toward the flow center in the low-pressure region.

Eddies cause periodical changes in the flow pressure below the runner at the flared entrance section of the draft tube. The perturbation forces induced by pressure fluctuations do not act only in the stream flow, but also on the draft-tube liner, loosening it and tearing off the plates.

These unsteady forces, acting together with the irregular, chaotic eddies on the draft-tube walls, cause mechanical vibrations, not only of the runner and the entire hydro unit, but also in the concrete foundations of the turbine bay and of the powerhouse.



FIGURE IV.38. Turbulent flow below the runner of a Francis turbine, under different operating conditions

Apart from the optimum-runner designs, it is therefore common laboratory practice to investigate the nature of the eddies, the causes of their increase, the amplitude of the pressure fluctuation in the water passages, and measures for reducing or eliminating the eddies. The most effective method known at present is to introduce air below the runner.

In these investigations, photographs and visual observations of the eddies are made, as are also oscillographic records of the pressure on the throat-ring walls both for different operating conditions of a single runner design and for different runner models.

The optimum design for runners should be selected by considering not only the maximum efficiency, the magnitude of the cavitation number σ and the shape of the characteristic curve corresponding to the field of the universal chart, but also the shape and distribution of the eddies, the amplitude of pressure fluctuations below the runner under various operating conditions, and the efficiency loss upon admission of air below the runner.

Some eddy shapes observed below the runner of a Francis turbine may be seen in Figure IV. 38. From reports on the Dnieper HEP, whose Francis turbines were supplied by the U. S. A. Newport-News Company before World War II, it is known that, due to poorly designed draft tubes (too narrow tube elbow), the rotational flow, under operating conditions differing slightly from the normal, caused vibrations of the draft-tube concrete to such an extent that turbine operation became impossible. Air had to be introduced below the runner in order to eliminate the vibrations. By changing the draft-tube shape and replacing the elbow, turbine operation was markedly improved.

It appears from the above that, in selecting over-all sizes for Francis-turbine draft tubes, due consideration should be given not only to efficiency, but also to operating performance of such turbines. Draft-tube dimensions, in particular depth, should not be too small, even if Francis turbines run at smaller unit discharges Q_1' and require a smaller discharge capacity, because, otherwise, a whirling flow would lead to dangerous transient phenomena.

For medium and high speed Francis turbines, LMZ recommends the draft tube of type 4H, having a depth not less than $L = 2.5D_1$. For low-speed turbines, the draft tube of type 20 is recommended; in this case, the depth may be reduced to $L = 2.3D_1$.

The following draft-tube dimensions, corresponding to the designations in Figure IV. 34, are recommended for Francis turbines:

Type 4H		Type 20	
h	$= 2.5D_1$	h	$= 2.3D_1$
L	$= 4.5D_1$	L	$= 3.5D_1$
B_5	$= 2.74D_1$	B_5	$= 2.17D_1$
h_5	$= 1.31D_1$	h_5	$= 9.937D_1$
D_4	$= 1.352D_1$	D_4	$= 1.04D_1$
h_4	$= 1.352D_1$	h_4	$= 1.04D_1$
h_6	$= 0.670D_1$	h_6	$= 0.510D_1$
L_1	$= 1.75D_1$	L_1	$= 1.410D_1$
$\gamma°$	$= 11°30'$	$\gamma°$	$= 11°30'$

Since draft-tube dimensions considerably affect the construction cost of powerhouse substructures, various new designs of draft tubes with smaller depth have been tested in laboratories. A shallow draft tube that would eliminate efficiency losses, has, however, not yet been designed.

Figure IV. 39 shows a small draft tube with a flared section, according to a design by I. V. Kotenev from the VIGM. Draft tube models of this shape have been tested.

The most suitable design had the following dimensions:

$h = 2.1D_1$ $\quad A_1 = 0.3D_1$
$D_2 = 1.42D_1$ $\quad A_2 = 0.445D_1$
$D_3 = 2.5D_1$ $\quad R = 0.58D_1$

Comparison with conventional draft tubes of depth $h = 2.24D_1$ showed that the turbine bay should be enlarged to give a tailrace width $B = (4.0 - 4.5)D_1$, instead of the usual $B = 3.5D_1$, and that the turbine efficiency is lowered by 1% for $Q_1' = 1500$ l/sec and by 2% for $Q_1' = 2000$ l/sec. Consequently, such draft tubes are not to be recommended.

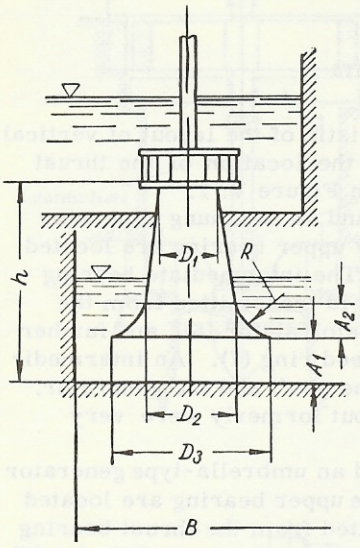


FIGURE IV. 39. Draft tube with flared section (diffuser)

Figure IV. 40 shows the schematic layout of a spreading draft tube ($h = (1.18-1.37)D_1$)with a concentric water discharge, suggested by V. G. Aivaz'yan (VNIIG).

Models of such draft tubes were also tested at the LMZ laboratory and compared with a customary elbow draft tube of $h = 1.915D_1$.

The tests showed that small spreading draft tubes have a low efficiency. The efficiency difference increases with the unit discharge Q_1'. Thus, whereas for $Q_1' = 1000$ liter/sec the efficiency loss caused by the best spreading draft tube was 1%, for $Q_1' = 2000$ liter/sec, the efficiency was reduced by 15%.

The low efficiency of small spreading draft tubes with a 90° flow rotation, may be explained by the shorter vertical diffuser and the steeper transitions in the discharge area, due to the reduced depth of the draft tube.

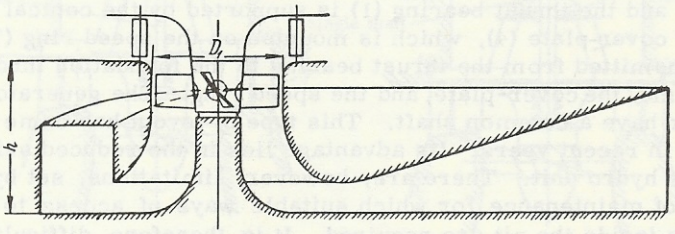


FIGURE IV. 40. Spreading [Moody] draft tube

Chapter V

TURBINE DESIGNS

24. LAYOUT OF TURBINE UNITS

Vertical turbine units. The main characteristic of the layout of vertical turbine units for large hydroelectric plants is the location of the thrust bearing. Four alternative layouts are shown in Figure V. 1.

1. A hydro unit with three guide bearings and an overhung generator (Figure V. 1, a). The thrust bearing (1) and the upper bearing are located above the generator on the upper bracket (2). The intermediate bearing is installed on the lower bracket (3). The load is transmitted from the thrust bearing through the bracket to the generator stator (6), and further to the foundation through the turbine pit and speed ring (7). An intermediate shaft is usually provided between the turbine shaft and the generator. Such layouts are only seldom used nowadays, but formerly were very common.

2. A hydro unit with two guide bearings and an umbrella-type generator (Figure V. 1, b). The thrust bearing (1) and the upper bearing are located on the lower bracket (3). The load is transmitted from the thrust bearing through the lower bracket and the concrete turbine pit to the speed ring (7) and then to the foundation. This design permits a smaller height of the unit than the former, as it dispenses with the loaded upper bracket. The lower bracket is smaller than the upper one shown in Figure V. 1, a. In this layout the intermediate shaft is usually omitted.

3. A hydro unit with two guide bearings and the thrust-collar frame on the turbine cover-plate (Figure V. 1,c). The upper bearing is located on the upper bracket (2) and the thrust bearing (1) is supported by the conical frame of the turbine cover-plate (4), which is mounted on the speed ring (7). The load is transmitted from the thrust bearing to the foundation through the conical frame, the cover-plate, and the speed ring. The generator and turbine runner have a common shaft. This type of layout has come increasingly into use in recent years. Its advantage lies in the reduced axial dimensions of the hydro unit. There are, however, limitations, set by the requirement of maintenance, for which suitable ways of access to the turbine components inside the pit are required. It is, therefore, difficult to use this design for small turbines ($D_1 < 4.0$ to 5.0 m).

4. The layout in Figure V. 1, d is similar to that in Figure V. 1, c. The thrust bearing (1) is supported by the turbine cover-plate (4). The only difference of this layout is the position of the oil-supply head (5). In the other three layouts, the oil-supply head for the runner servomotor is located above the generator in a special part of the powerhouse.

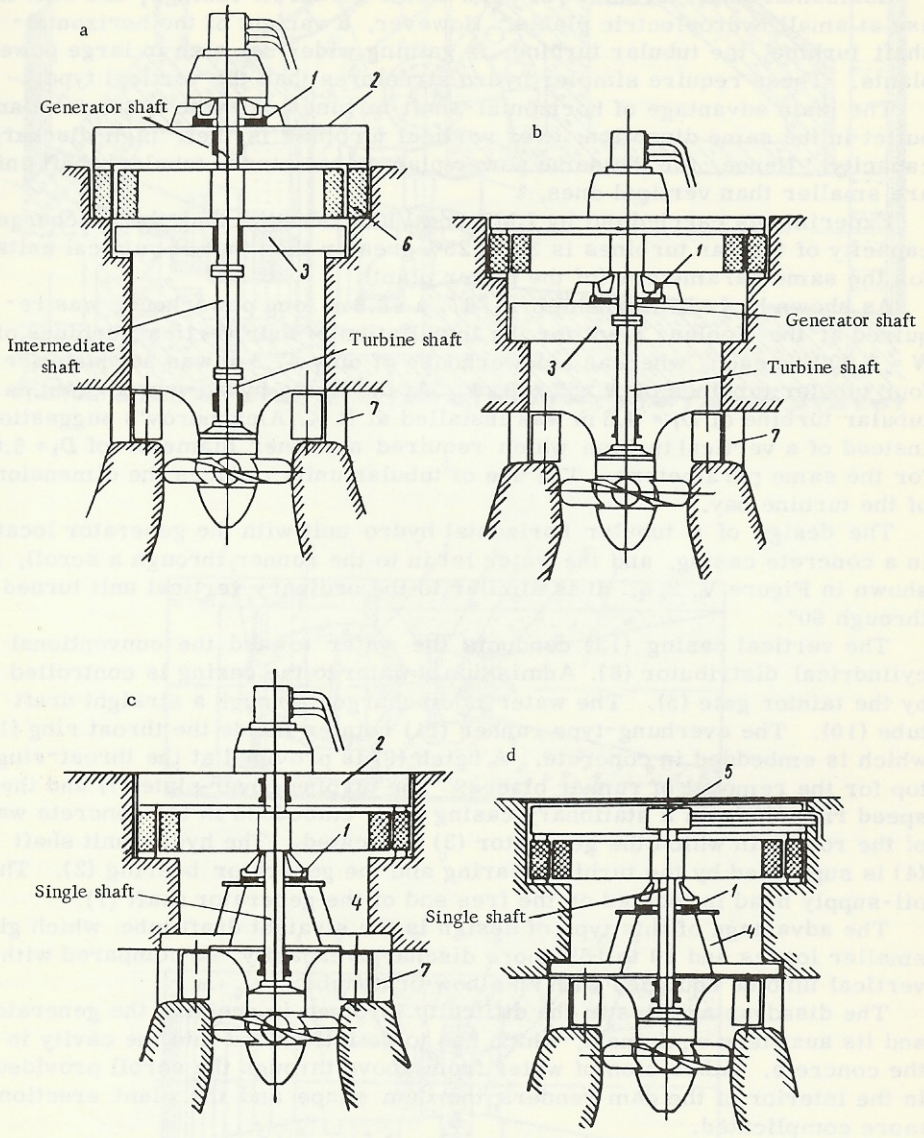


FIGURE V. 1. Various layouts of vertical turbine units

In Figure V. 1, d, the oil-supply head is mounted at the upper end of the turbine shaft inside the upper bracket, but not above the generator level. This design is used for open-air power plants where the powerhouse superstructure is dispensed with.

Horizontal-shaft turbines [in open flume or scroll casings] are still in use at small hydroelectric plants. However, a variant of the horizontal-shaft turbine, the tubular turbine, is gaining wider use also in large power plants. These require simpler hydro structures than the vertical type.

The main advantage of horizontal-shaft turbines, with the water inlet and outlet in the same direction, over vertical turbines is their high discharge capacity. Hence, for the same power-plant parameters, tubular-shaft units are smaller than vertical ones.

Experiments carried out by LMZ and VIGM showed that the discharge capacity of tubular turbines is 20 to 25% greater than that of vertical units for the same parameters (of the power plant).

As shown by L. B. Bernshtein in /6/, a 68.8 m long powerhouse was required at the Koblenz plant for the installation of four vertical turbines of N = 4,000 kw each, whereas a powerhouse of only 47.5 m was adequate for four tubular turbines of N = 5,200 kw. At the Kama hydro-power plant, a tubular turbine of D_1 = 4.5 m was installed at B.K. Alexandrov's suggestion, instead of a vertical turbine which required a runner diameter of D_1 = 5.0 m for the same parameters. The use of tubular units reduces the dimensions of the turbine bay.

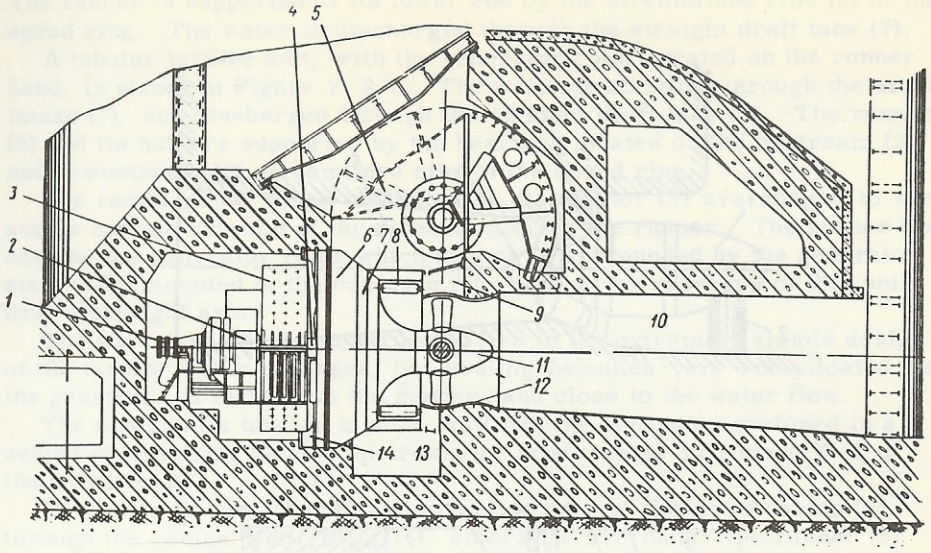
The design of a tubular horizontal hydro unit with the generator located in a concrete casing, and the water let in to the runner through a scroll, is shown in Figure V. 2, a. It is similar to the ordinary vertical unit turned through 90°.

The vertical casing (13) conducts the water toward the conventional cylindrical distributor (8). Admission of water to the casing is controlled by the taintor gate (5). The water is discharged through a straight draft tube (10). The overhung-type runner (11) rotates inside the throat ring (12), which is embedded in concrete. A hatch (9) is provided at the throat-ring top for the removal of runner blades. The turbine cover-plate (7) and the speed ring (6) form a stationary casing (14), embedded in the concrete wall of the room, in which the generator (3) is located. The hydro-unit shaft (4) is supported by the turbine bearing and the generator bearing (2). The oil-supply head is located on the free end of the generator shaft (1).

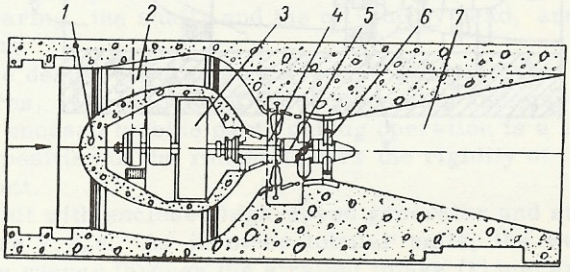
The advantage of this type of design is the straight draft tube, which gives smaller losses and 10 to 15% more discharge capacity, as compared with a vertical turbine equipped with an elbow draft tube.

The disadvantage lies in the difficulty involved in erecting the generator and its auxiliary equipment, which has to be introduced into the cavity in the concrete. Admission of water from above through the scroll provided in the interior of the dam renders the dam shape and the plant erection more complicated.

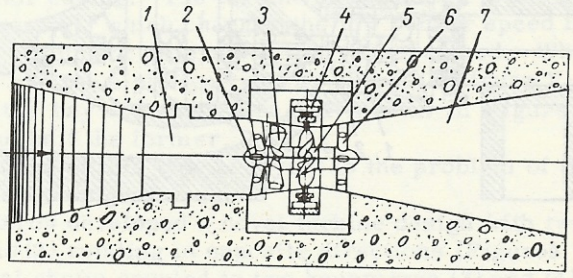
The plan view of a semi-tubular turbine unit with the generator located in a concrete pier is represented in Figure V. 2, b. The water stream admitted through the intake is divided into two branch channels (2), which surround the concrete casing (1) of the horizontal generator (3). The concrete casing is open at the top to facilitate servicing by a crane. Further on, the branch channels (2) converge into a conical flared section, which guides the water toward the axial distributor (4) and the adjustable-blade runner (5).



a

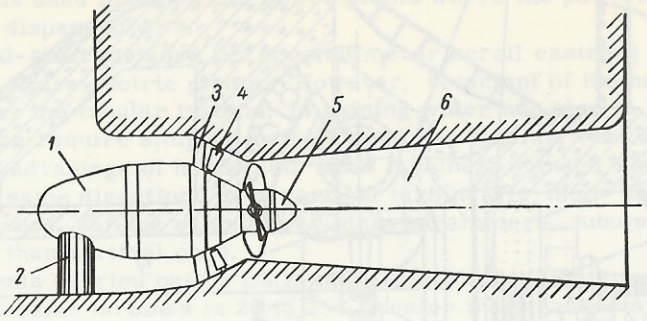


b

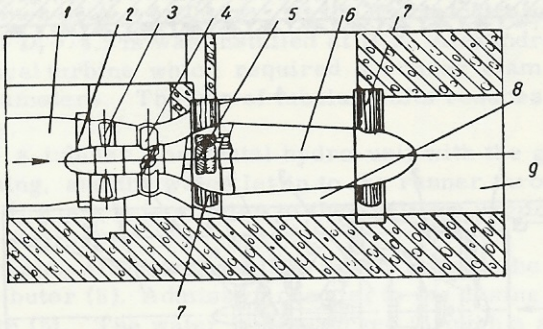


c

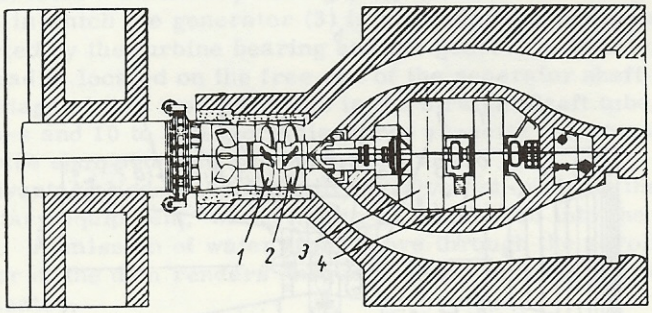
FIGURE V. 2. Designs of tubular-turbine units



d



e



f

FIGURE V. 2 (cont.). Designs of tubular hydro units

The runner is supported at its lower end by the streamlined ribs (6) of the speed ring. The water is discharged through the straight draft tube (7).

A tubular turbine unit, with the generator rotor located on the runner band, is shown in Figure V. 2, c. The water is admitted through the straight intake (1), and discharged through the straight draft tube (7). The runner (5) and its hub are supported by the bearings located on the upstream (2) and downstream (6) streamlined ribs of the speed ring.

The radial guide vanes of the axial distributor (3) are shaped to ensure a certain rotation of the stream entering the runner. The runner band carries the generator rotor which in turn is surrounded by the generator stator (4), mounted in the concrete pit. The water passages of this unit have a straight axis.

The advantage of this construction lies in the extremely simple design of the turbine water passages, but sealing becomes very complicated as the generator is located on the runner band close to the water flow.

The design of a tubular turbine unit with the generator enclosed in a sealed steel casing located upstream is represented in Figure V. 2, d (bulb-type unit).

The water flowing in the axial direction around the metal casing (1), through the conical distributor (4), enters the overhung-type runner (5) and is discharged through the straight draft tube (6). The steel casing is supported by the concrete structure and is connected to the foundation elements of the turbine with the aid of massive streamlined ribs (2) and stay vanes (3). A small generator, as well as several turbine components, such as the bearing, the shaft, and the oil-supply head, are located inside the steel casing.

This turbine design ensures an extremely simple layout of the auxiliary hydro structures. The impossibility of inspection and maintenance of the generator and encased turbine parts during operation is a serious drawback. The overhung position of the runner lowers the rigidity of the rotating parts of the hydro unit.

A tubular unit with enclosed high-speed generator and step-up gear is shown in Figure V. 2, e. As in other tubular units, the water is here admitted to the runner through the straight intake (1) and axial distributor (3). The runner (4) discharges the water through the annular channel (8) and the straight draft tube (9). The load is transmitted to the foundation through the ribs (2) located in front of the runner and by the ribs (7) mounted on the generator casing. The turbine is connected to the generator through the step-up gear (5), which changes the low runner speed into the high generator speed. Compact generators may thus be used. Whereas the width of the turbine bay for a pit-type unit as shown in Figure V. 2, b is $\approx 3.1 D_1$, the width of the bay for the hydro unit shown in Figure V. 2, e is $1.6 D_1$, i. e. it is about half the former.

A disadvantage of this type of layout is the problem of the complicated design of the step-up gear.

M. A. Kasparov developed a novel turbine design with two concentric runners (1) and (2) rotating in opposite directions (Figures V. 2, f). The unit has two coaxial shafts coupled to two generators (3) and (4). Theoretically, it is possible to connect both runners to the same generator, i. e., one runner to the rotor and the other to the stator, which thus also rotates, but in the opposite direction. In this type of unit with two runners rotating

in opposite directions, the total head is divided between the runners, the load on each blade being thus reduced. This fact permits the reduction of the hub-tip diameter ratio and, hence, of the cavitation coefficient; Kaplan turbines may thus be used at higher heads. It is, however, extremely difficult to design a unit of this type with two Kaplan runners rotating in opposite directions, and with two coaxial shafts.

25. DESIGN OF FRANCIS TURBINES

The Francis turbine is used for heads ranging from 30 to 450 m, its design depending on the head available.

Several vertical Francis turbines with runner diameters D_1 from 1.75 to 6.6 m, heads H from 36 to 300 m and power outputs N from 12,600 to 500,000 kw are shown in figures V.3 to V.10.

The figures show only the main turbine components: scroll casing, distributor with its actuating mechanism, runner with the shaft, guide bearing, foundation elements, etc. Auxiliary mechanisms—the oil, air, and water piping, devices for automatic control, transmissions to the switchgear, measuring equipment and the like, as well as the regulating equipment (governors)—are not shown.

From the constructional point of view, all vertical radial-axial turbines are identical: the water enters the steel scroll casing of circular cross section, passes through the distributor and the runner, and is discharged through a straight or elbow draft tube. The shaft is coupled to the runner through flanges, and is maintained in strictly vertical position by the guide bearing located on the turbine cover-plate. The distributor-actuating mechanism and its gate ring (spider) are also mounted on the cover plate.

The individual components of the Francis turbine may differ according to the general parameters, but in general, these turbines have not undergone substantial changes over the past 25 years. Developments have been mainly in the direction of improving the operating characteristics, simplifying the design, reducing the over-all weight, using cheaper materials, and improving production methods.

Some typical turbine designs are worthy of consideration. Sectional and plan views of a large Francis turbine with runner diameter $D_1 = 5.45$ m, designed by LMZ, are represented in figures V.3 and V.4. This turbine has a power output $N = 80,000$ kw under a head $H = 36$ m, a typical low-head Francis turbine design. The scroll casing (1) is welded of steel plates and assembled to the speed ring (2) which is embedded in concrete. The turbine cover-plate (3) is fastened to the top of the speed ring. Twenty-four holes for the location of guide vanes (4) are provided in the cover plate.

The lower guide-vane pivot is carried by the lower ring of the distributor (9), and the upper, by the bearings of the cover plate. The lever (5) fastened to the upper pivot is articulated by means of link (6) to the gate ring (7) located upon the cover plate.

The gate ring is connected to two servomotors (oil-pressure-operated pistons) (8), through cylindrical hinges and rods (10). Oil is supplied to the servomotors from the distributing valve of the governor through pipes. The rubber-lined guide bearing (11) is installed inside the cover-plate flange.

A water container (13) for bearing lubrication, connected with the water intake, is provided above the bearing. The water, leaving the bearing, is discharged into the throat ring and thence into the draft tube.

The turbine shaft (14) is connected to runner (18) by a flange and bolts (17). The cast runner consists of the upper conical disk with a flange, and the lower band held together by the runner blades. In order to obtain a well-streamlined shape, hub extension (16) is added to the runner hub.

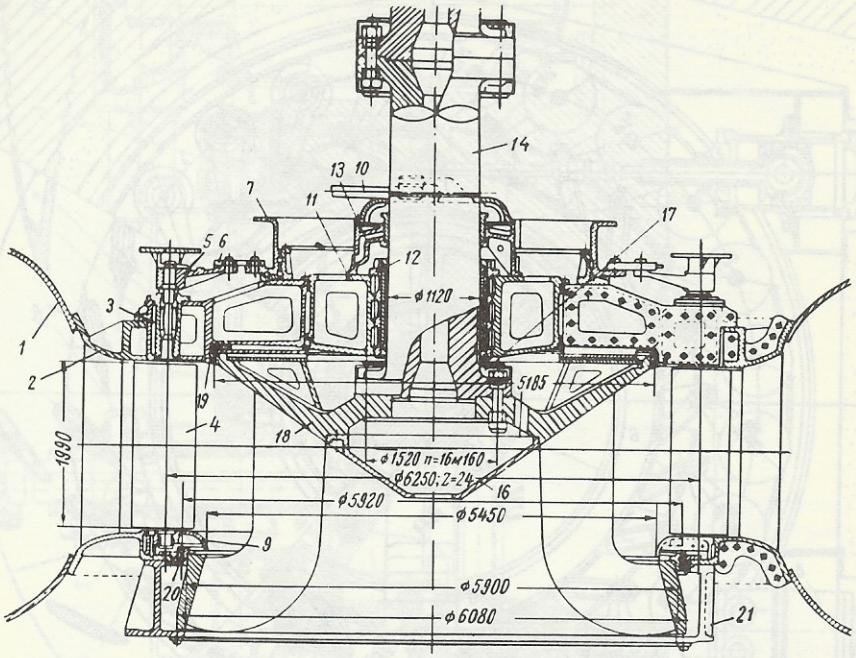


FIGURE V. 3. Sectional view of a Francis turbine (runner diameter D_1 = 5.45 m, power output N = 80,000 kw, head H = 36 m)

Rings (19) and (20) provided on the crown and the band for sealing the clearances, reduce the water leakage. The band rotates within the inner surface of foundation ring (21), which is connected to the turbine speed-ring and is embedded in concrete. Platform (15) and ladders are provided for access to the turbine pit, while a water pump is also provided to drain it. A special air valve located on the turbine cover-plate serves to prevent formation of vacuum (negative pressure) below the runner during sudden load drop resulting from regulation processes.

The sectional view of a vertical Francis turbine (designed by LMZ) for a higher head H = 60 m, is shown in Figure V. 5. The runner diameter is D_1 = 1.75 m and the power output N = 12,800 kw. The concrete pit is dispensed with, the generator being mounted on the concrete floor of the scroll casing (1). The lower part of the casing up to the horizontal axis is embedded in concrete. The scroll is connected to speed ring (2), which carries distributor (3). The servomotor (9) of the distributor is fastened to pedestal (10) near the scroll. In this design, babbitted guide bearing (4) is

lubricated by oil circulated in a closed cycle. From the upper receptacle (5), the oil flows through the special grooves provided in the guide-bearing lining into the lower receptacle (7). Pump (6) driven from the turbine shaft returns the oil into the upper receptacle. Stuffing box (8) located below the lower receptacle of the bearing prevents the water from penetrating into the space above the cover plate.

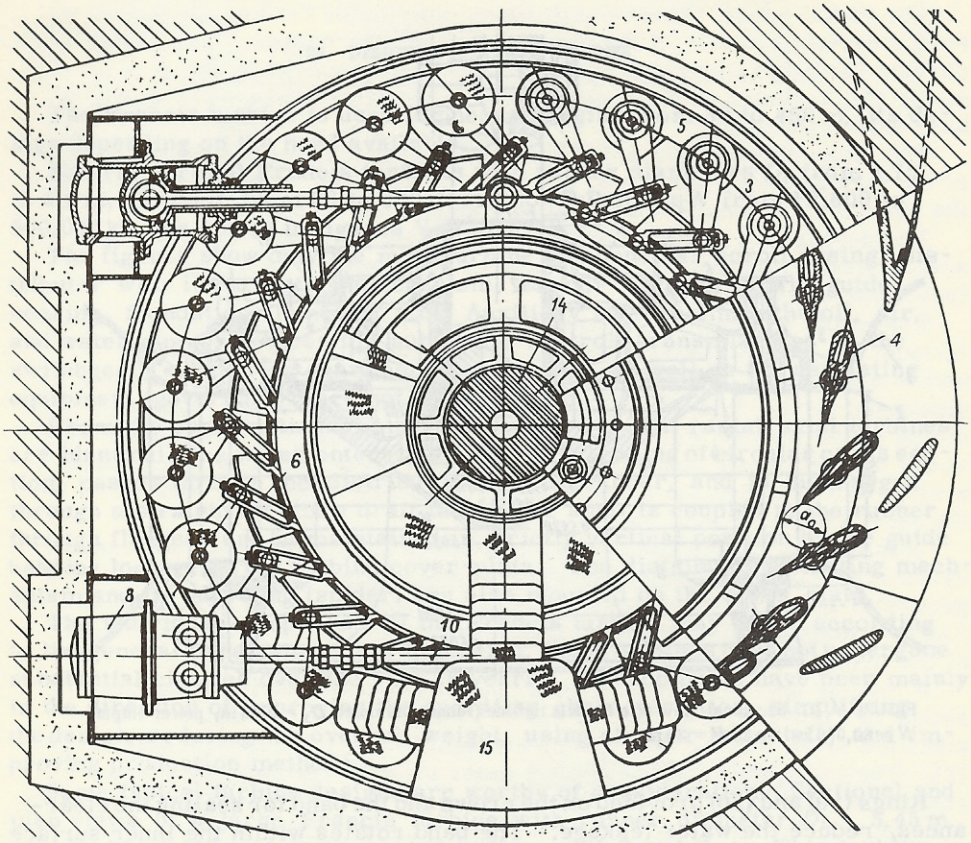


FIGURE V. 4. Plan view of a Francis turbine

Butterfly valve (12) actuated by a plunger-type sevomotor (11) mounted on the valve casing is installed in the water intake upstream from the scroll. The closed valve disk stops the water admission to the distributor. The turbine is equipped with idle discharge (13) and pressure regulator (14) which, upon closing of the distributor during regulation, moves upward and permits the water to bypass the runner (idle discharge), thus preventing increase in pressure in the pipeline ahead of the turbine.

Figures V. 6 and V. 7 show a high-power Francis turbine for $H = 285$ m. The turbine, designed by Ya. S. Degtyarev and L. G. Smolyarov and built by LMZ, has a runner diameter $D_1 = 2.85$ m and a power output of $N = 55{,}000$ kw.

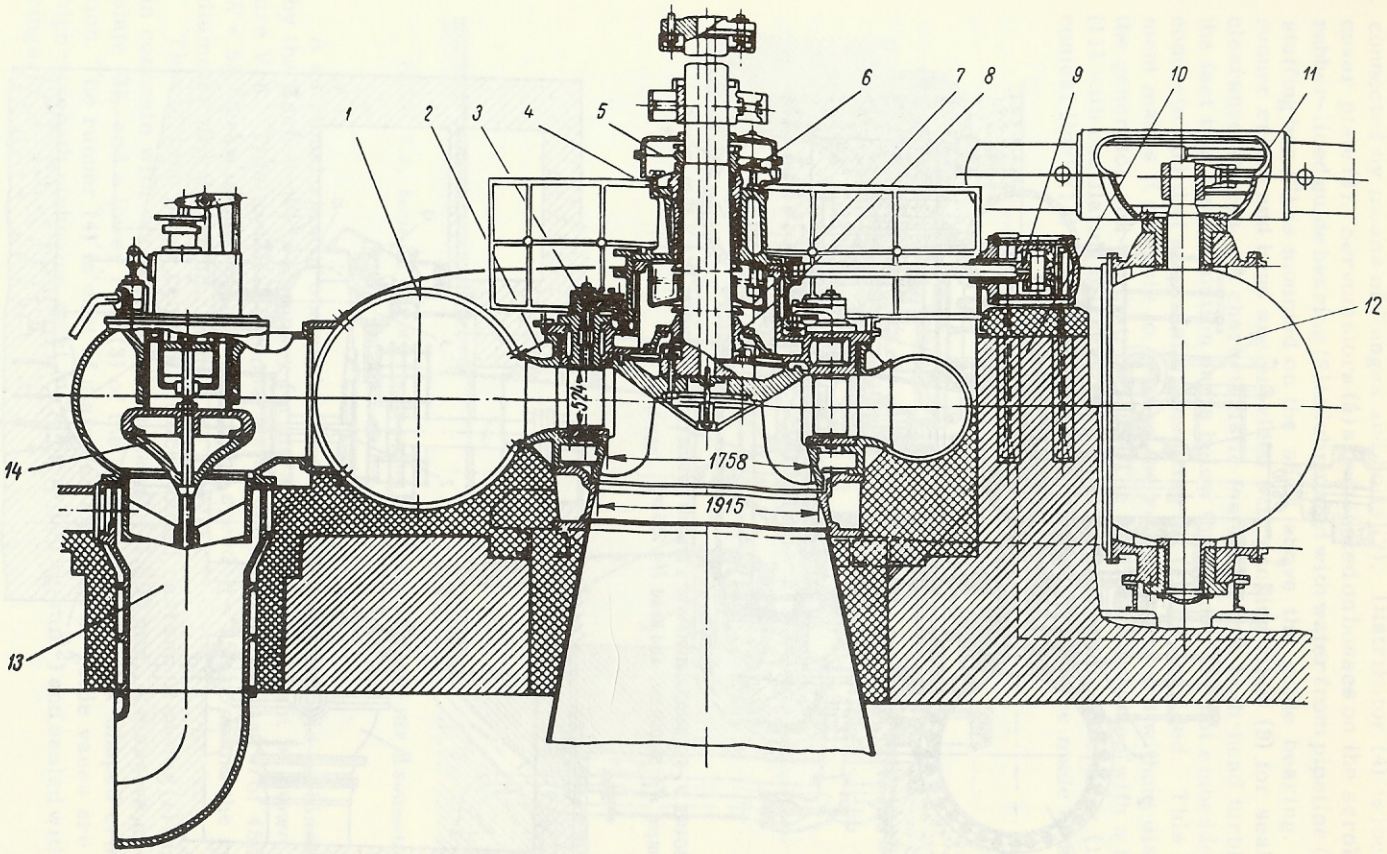


FIGURE V. 5. Sectional view of a Francis turbine (runner diameter D_1 = 1.75 m, power output N = 12,800 kw and head H = 60 m)

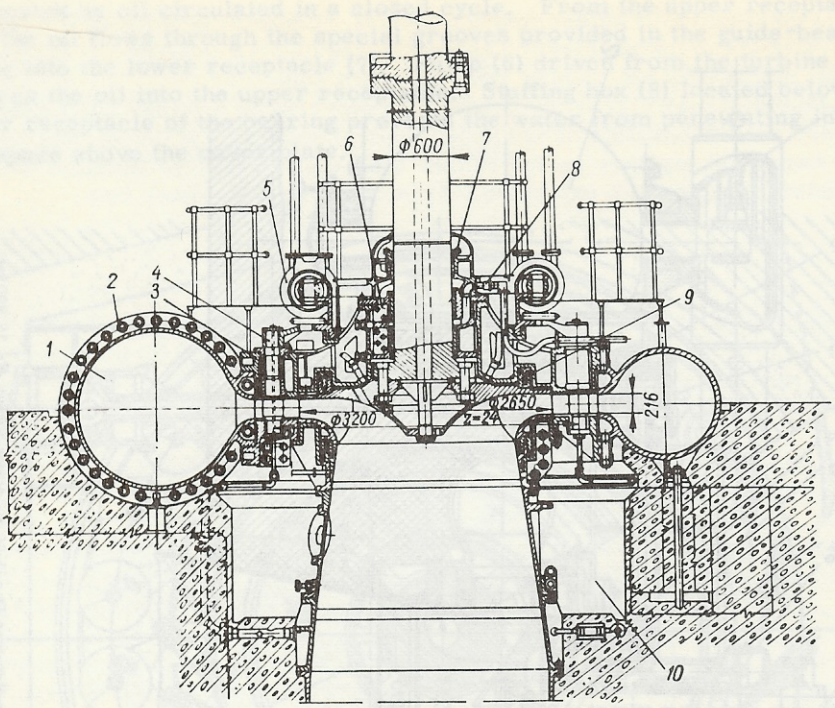


FIGURE V. 6. Sectional view of a Francis turbine (runner diameter D_1= 2.85 m, power output N= 55,000 kw, and head H= 285 m)

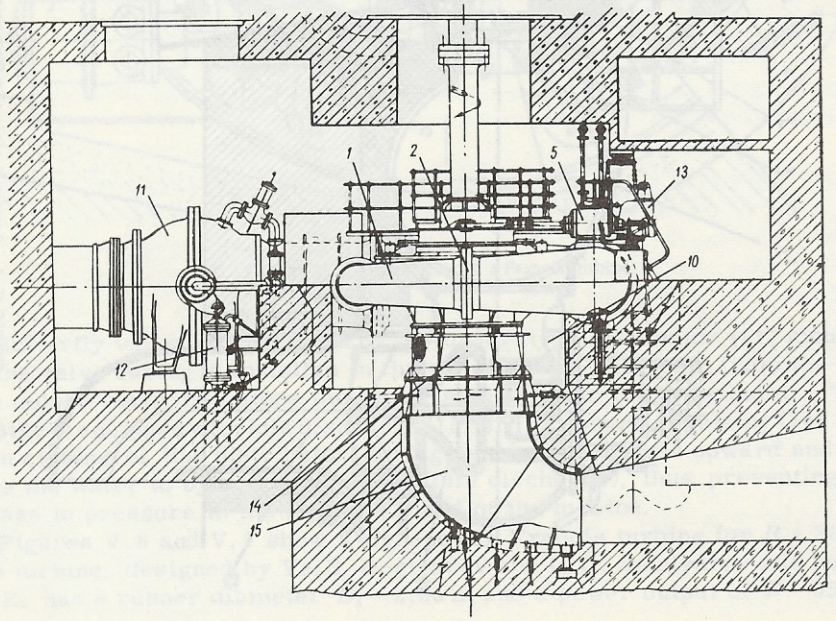


FIGURE V. 7. A 55,000 kw Francis turbine

The turbine has a cast-steel scroll casing (1) made of separate sections connected by means of flanges and bolts (2). Distributor (4) is located inside cover plate (3). Servomotors (5) are mounted on bosses on the scroll. The rubber-lined guide bearing (6) is lubricated with water from pipeline (8). The stuffing box (7) is mounted on the shaft above the guide bearing. The runner crown and band are provided with packing rings (9) for sealing the clearance spaces. A characteristic feature of this high-head turbine is the fact that the foundation parts below the runner are not embedded in concrete and that a special dismantling pit (10) is provided. This arrangement makes it possible to remove the runner downward without dismantling the generator and the distributor. The turbine is provided with a ball valve (11) with oscillating oil-servomotors (12), and an idle discharge (13). The conical liner (14) of the draft tube and the elbow (15) are made of steel.

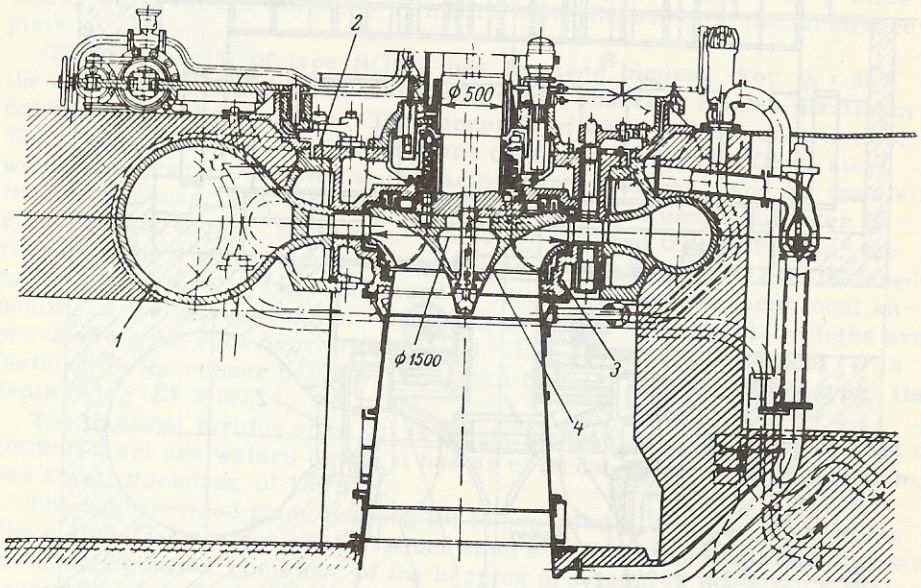


FIGURE V.8. Sectional view of a Francis turbine installed at the Fionnay HEP in Switzerland

A sectional view of one of the largest high-head Francis turbines built by the Escher–Wyss Company for the Fionnay hydro plant is shown in Figure V.8. This turbine develops $N = 46{,}400$ kw under a head H of 455 m, and $N = 53{,}000$ kw under $H_{max} = 471$ m; the speed $n = 750$ rpm and the runner diameter $D_1 = 1{,}500$ mm.

This turbine has a relatively thick-walled cast scroll casing (1) embedded in concrete with an entrance diameter $D_s = 1{,}200$ mm, a massive cast cover plate (2), and a lower ring (3) of the distributor of a box-shaped cross section. The runner (4) is cast of stainless steel. The guide vanes are cast of high-strength nichrome steel ($\sigma_u = 80$ to 100 kg/mm^2) and sealed with leather rings.

In field tests, the turbine had a maximum efficiency of $\eta = 92\%$.

Figure V. 9 shows the cross section through a Francis turbine unit (for particulars see caption of figure). LMZ has already built several turbines of this type which are now in process of installation.

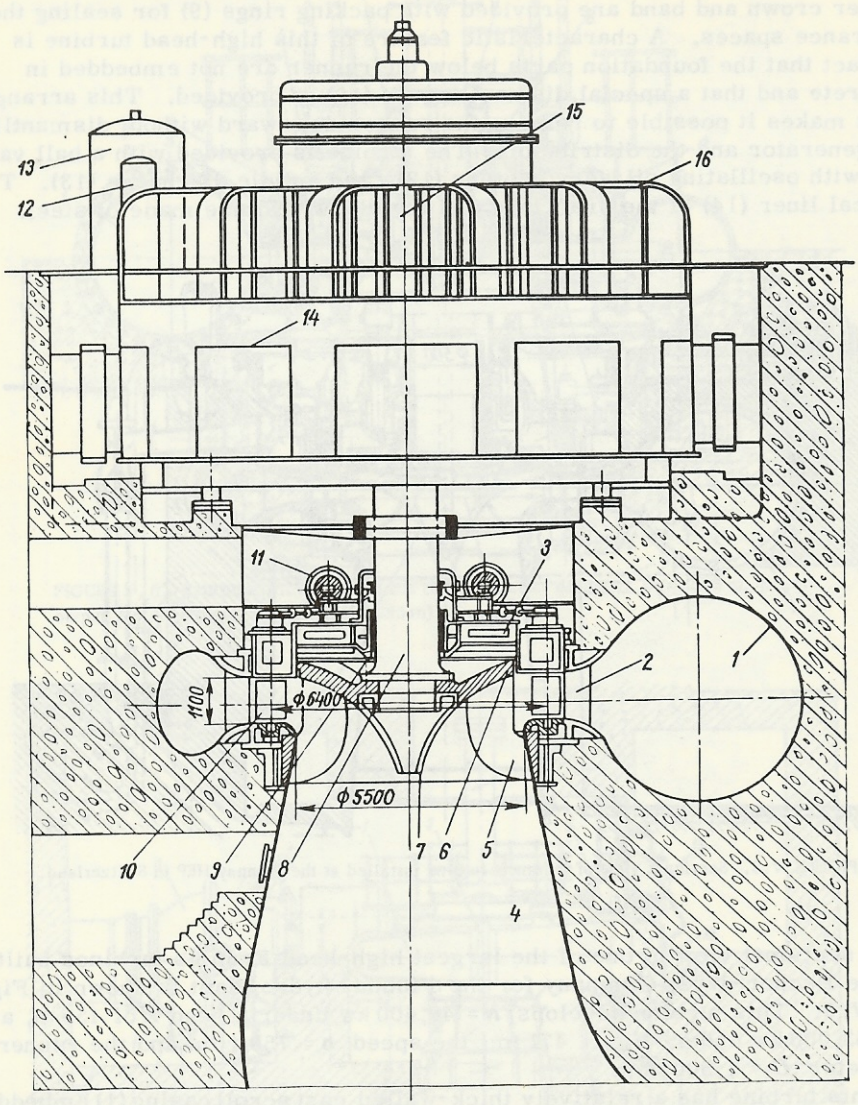


FIGURE V. 9. Sectional view of a Francis turbine (runner diameter $D_1 = 5.5$ m, power output $N = 230{,}000$ kw, $H = 100$ m, and $n = 125$ rpm)

The overhung-type generator (14) has the thrust bearing (15) located on the upper bracket (bridge) (16).

The scroll casing (1) with an extrance diameter $D = 7$ m is welded of grade SKhL 4 alloy steel plates, comprising thirty sections of varying

thickness. The maximum plate thickness is 30 mm, the minimum, 20mm. To permit easy railroad transportation, the largest sections are made of two parts. The cast speed ring (2), consisting of the upper and lower bands welded by the electroslag process to the streamlined stay vanes, is welded to the inside wall of the scroll. The speed ring is divided into four parts. The largest diameter of the assembled speed ring is 8,870 mm and its height 2,300 mm. Distributor (10) consists of 24 adjustable vanes, arranged along a circumference of diameter D_0 = 6,400 mm; the distributor height is b_0 = 1,100 mm ($0.2D_1$).

The gate ring is actuated by twin-type servomotors with a diameter of 500 mm. Each consists of two servomotors connected by a common rod; cast-iron pistons are provided on both sides of the rod, one for each cylinder.

The servomotor rod is articulated to the gate-ring pin by a slide block, while the servomotors themselves are installed on the turbine cover-plate.

The runner (5) of type RO662 has fourteen blades. For Q_1' = 860, the cavitation coefficient is σ = 0.083, which ensures, for the maximum output, a draft head H_s = 0. The runner is of welded-cast construction. The blades, the hub, and the band are cast separately of 20GS-L steel, welded together (while still at the factory) into a single piece by the electroslag process, and subsequently heat-treated. Runner diameter is 6,100 mm and height, 2,723 mm. For easy railroad transportation, the runner is made of two parts assembled in situ. The parts are fastened to the hub by 8 bolts and to the band by welding with subsequent local annealing of the welded seams. Seal rings (6) with machined labyrinths are provided on the runner crown and band. Hub extension (deflector) (7) is fastened to the runner bottom. The draft tube (4) is of the elbow type, its depth being $L = 2.6D_1$.

The [hollow] turbine shaft (8) is forged of 20GS steel and flanges cast of 20GS-L steel are welded to it. It has an external diameter d of 1,500mm, and a wall thickness of 150 mm.

The rubber-lined guide bearing (9) is provided with water lubrication. The cylindrical surface of the rubber liners has sixteen longitudinal grooves. In the upper water container of the bearing provision is made for a seal consisting of a ring mounted on the shaft and a rubber ring on the casing.

The EGP-150 hydraulic governor (12), and the MNU 12.5 oil-pressure unit (13), are located in the generator room of the powerhouse. A maximum turbine efficiency of η = 93.6% is predicted. The turbine is designed for a runaway speed n_r of 250 rpm. Figure V.10 shows the LMZ design of a turbine unit with a runner diameter D_1 = 7.5 m. The output N of this turbine will be 508,000 kw under a head H of 95 m.

A novel-type runner is used in this turbine; the unit discharge ($Q_1' \approx 1100$ l/sec) is notably high for its specific speed, thus enabling the runner to develop such a high power with the given diameter. A maximum efficiency of η = 94% is predicted.

According to the design, the scroll casing is to be of high-quality steel. The turbine is connected directly to the three-phase umbrella-type generator (4). The generator thrust bearing (3) is located on the turbine cover-plate (7). The fourteen-blade runner (1) is of welded construction. The crown, the band, and the blades are to be welded together in the shop

and transported by water to the power plant. The runner is secured to the shaft flange by means of fitted bolts; the one-piece shaft (2) for the whole hydro unit has cast flanges welded to the forged tubular shaft.

The upper flange of the shaft is bolted to the hub of the generator rotor (5). In this design, the distributor height is increased to $b_0 = 0.25D_1$; the distributor has twenty-four guide vanes (9) linked to the two pistons of the servomotors (6) installed on the turbine cover-plate.

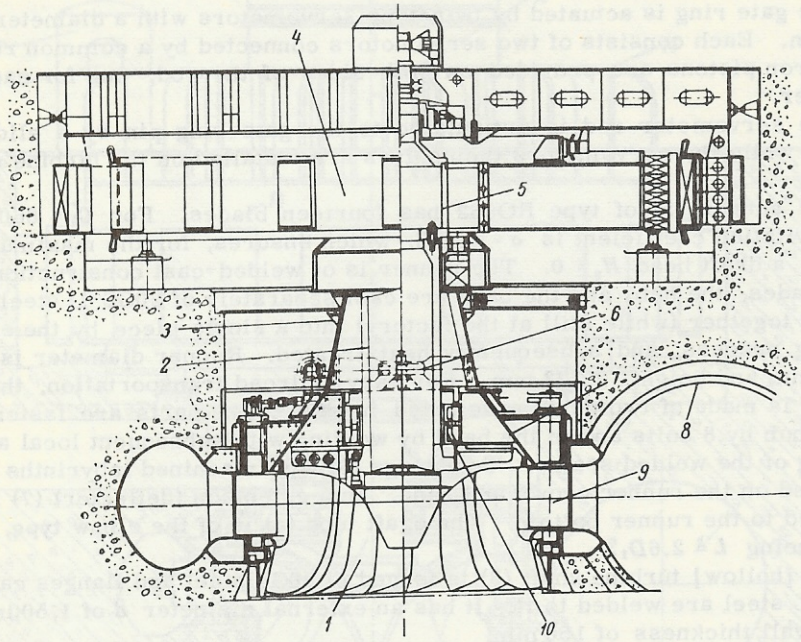


FIGURE V. 10. Sectional view of a Francis turbine (runner diameter D_1= 7.5 m, power output N = 508,000 kw, and head H = 95 m)

The box-shaped cover plate (7) has a conical frame which carries the load from the thrust bearing of the turbine unit. The turbine guide-bearing (10) is rubber-lined and water-lubricated. The designers succeeded in obtaining a low specific weight for the turbine: 2.5 kg/kw. The construction of the turbine was preceded by prolonged design-and experimental research work.

26. KAPLAN TURBINE DESIGNS

The design of the Kaplan turbine is more complicated than that of the Francis turbine, since it includes the blade-adjustment mechanism, which consists of a crank or slide-block arrangement located inside the runner hub. Usually, the piston of the servomotor which develops the force required to adjust the blades is also located inside the turbine shaft. Owing to the simultaneous adjustment of the runner blades and the distributor, regulation of the turbine is more complicated.

Compared with the Francis turbine, the Kaplan turbine has an additional distributing valve for the runner servomotor, and a blade-control valve for the simultaneous adjustment of the distributor and runner blades.

The more complicated design of these turbines, as compared with the Francis turbine, is more than offset by the gain in energy (kwhr) due to the simultaneous blade-and guide-vane control. Kaplan turbines have higher efficiencies at low heads and large water discharges; since the dismantling of the runner parts is always possible, runners of large diameters may be used. Hence, Kaplan turbines are extensively used in low-head power plants all over the world.

The U. S. S. R. has a great number of lowland rivers with low heads, a fact which favored the construction of hydroelectric power plants equipped with Kaplan turbines, and which resulted in its becoming the biggest supplier of large high-power Kaplan turbines in the world. Even before World War II, Kaplan turbines with a runner diameter $D_1 = 9$ m, built by LMZ for the Uglich and Rybinsk HEPs, were the largest in existence. After the war, even larger turbines were built at LMZ for the Volga HEPs imeni Lenin and imeni the XXII-nd Congress of the U. S. S. R. These turbines have runner diameters of $D_1 = 9.3$ m and a power output of $N = 126{,}000$ kw under a head $H = 22.5$ m.

Because of the high efficiencies of Kaplan turbines, engineers tend to employ them for still higher heads. Various designs of Kaplan turbines are given in Figures V. 11 to V. 20. A turbine of runner diameter $D_1 = 3.6$ m for a head $H = 20$ m, built by LMZ in the thirties, is represented in Figure V. 11. A large number of turbines built during that period by LMZ are of a similar design. The water enters the turbine through the scroll casing (6); the speed ring (5) consists of separate stay vanes whose flanges are embedded in the upper and lower concrete cones of the scroll. The lower ring (4) of the distributor is embedded in concrete and is connected to the throat ring (3); the lower part of throat ring (3) adjoins the foundation ring (1). These parts surround the turbine water-passages and together form a casing of the required shape for the runner. One of the throat ring segments is not embedded in concrete and is provided with an opening for blade removal. The upper ring (7) of the distributor and the cover plate (8) are located above the runner. The bearings of the guide-vane (18) are located in the upper ring of the distributor which is embedded in the concrete of the turbine pit. For the easy dismantling of the vanes the upper distributor ring is provided with openings covered by the bearing flanges. Lever (17), fastened to the upper guide-vane pivot is connected through link (16) to gate ring (15). The gate ring is connected by links and rods with two piston-type servomotors (14), installed inside the turbine pit. The oil-lubricated guide bearing (9) having babbitted shells (10) is located inside the turbine cover-plate. The lubricating oil flows in a closed cycle from upper receptacle (12), through the oil grooves into the rotating receptacle (13) located on the shaft below the bearing; from there, the oil is returned by means of Pitot tubes and a pump. A special cooling pipe is sometimes provided in the upper receptacle to cool the oil. Labyrinth seals (19) preventing the leakage of water into the bearing are mounted on turbine shaft (11) which is connected by flanges at its top end to the generator shaft, and at its bottom end to runner cover-plate (20). The servomotor cylinder, cast integral with runner hub (22), is located below the runner cover-plate. Piston (21) and rod (26) move inside the cylinder. This servomotor de-

sign — typical of LMZ and several foreign companies — is best suited for the transmission of the actuating force along the shortest route. The oil is supplied to the servomotor through a pipe inside the hollow turbine shaft. The oil-supply head, located on the top end of the shaft above the generator, is connected with the runner distributing-valve through a pipe. Cross-piece (25), fastened to the lower end of the servomotor piston rod, is connected through lugs and links (24) to the levers keyed to the blade pivots. Each blade pivot is guided in two bronze bearings located inside the runner hub. The streamlined hub extension (2) is fastened to the runner from below.

Figure V. 12 shows a cross section through an LMZ turbine of similar parameters, but of more recent design, (runner diameter D_1 = 3.6 m, H = 17.5 m and power output N = 11,000 kw).

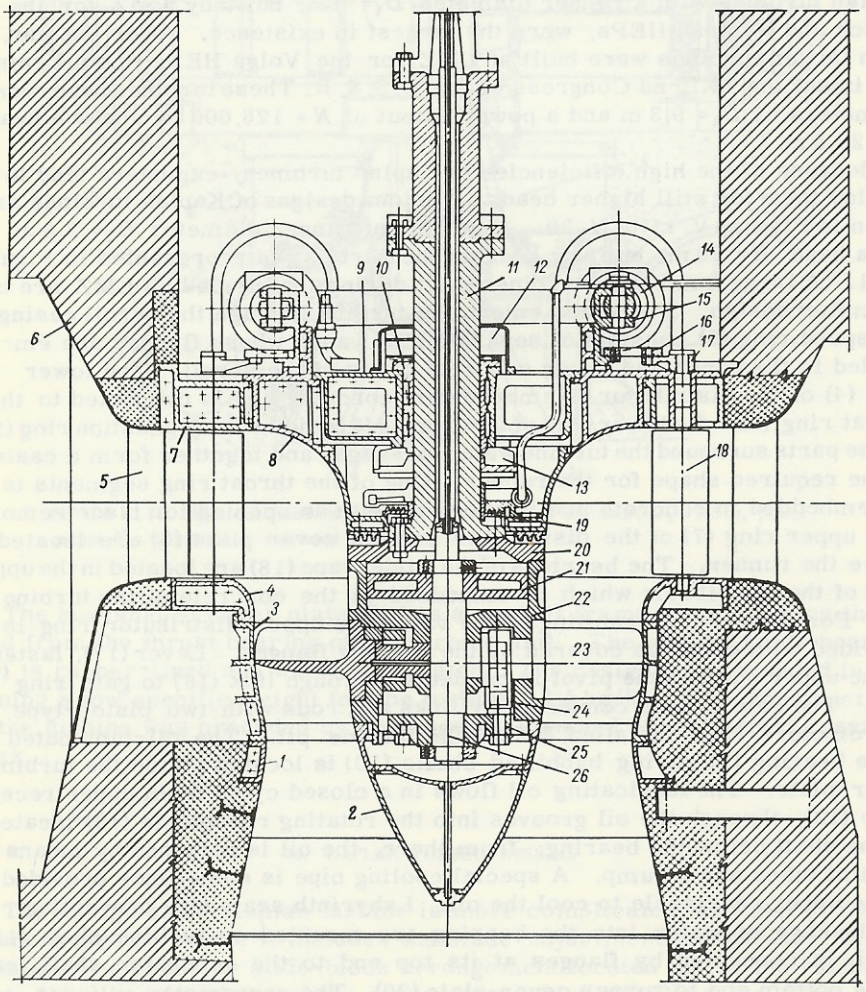


FIGURE V. 11. Sectional view of a Kaplan turbine (runner diameter D_1 = 3.6 m, power output N = 12,500 kw, and head H = 20 m)

In this design, the upper distributor ring is fastened to the turbine cover plate (2), but there is a special upper foundation ring (1) embedded in the concrete of the turbine pit. The housing (3) of the guide bearing is located closer to runner (10) than in the previous design. This was made possible by using water-lubricated rubber-lined shells (4), which permit the bearing seal to be dispensed with. The water for lubrication enters the upper container (5) through pipeline (6) either from the scroll casing or from the water mains of the power plant.

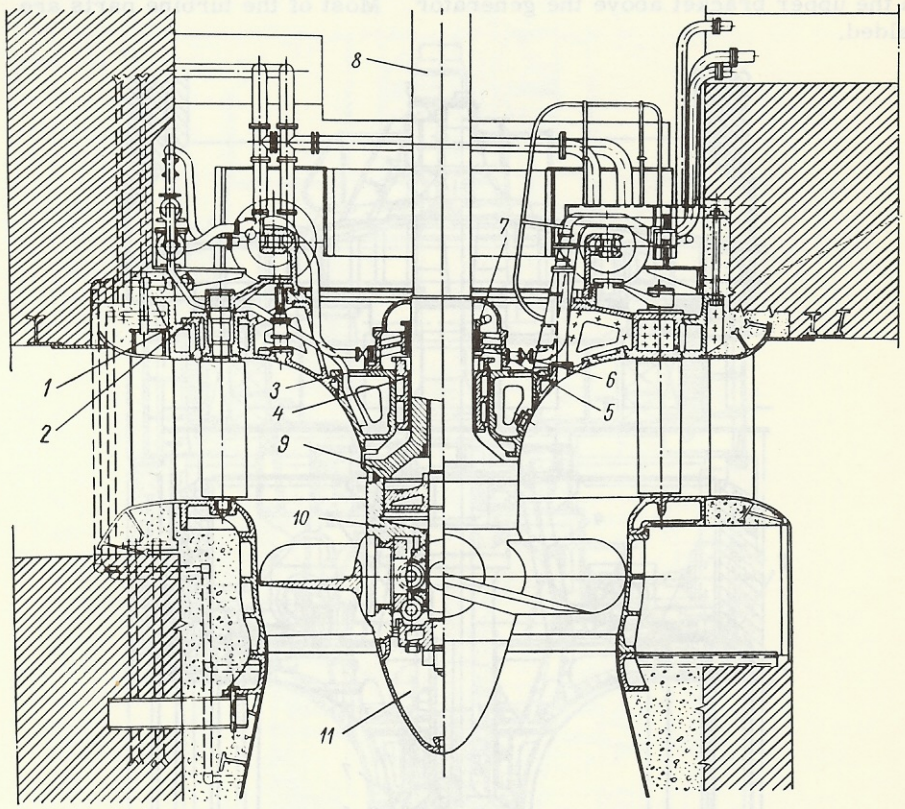


FIGURE V. 12. Sectional view of a Kaplan turbine (runner diameter D_1 = 3.6 m, power output N = 11,000 kw, and head H = 17.5 m)

The stuffing box (7) is provided on the shaft above the water container. The turbine shaft (8) has at its lower end a large flange (9), which serves as the cover of the servomotor cylinder (10). The runner is covered from below by one hub extension (11) only, and not by two, as in the previous design.

Figure V. 13 shows a turbine built by KhTZ, with a runner diameter D_1 = 8.0 m, power output N = 58,000 kw and head H = 14.2 m. A characteristic feature of this construction is the installation of the thrust bearing stays (4) on the cover plate (3). The over-all size of the hydro unit was thus reduced and the generator brought closer to the turbine. In the hydro

units shown in figures V. 11 and V. 12, the thrust bearing is not mounted on the turbine cover-plate, but on the generator bracket. As shown in Figure V. 13, the turbine speed ring consists of the stay vanes (1) bolted to the upper distributor ring (2); the ring is embedded into the concrete pit of the turbine. The cast flange (7) which also serves as a cover for the runner servomotor (9), is welded to the hollow shaft (6). The blade-adjustment mechanism has neither rods nor cross-pieces. Crank transmission (10) connects the servomotor piston (8) directly to each blade lever (11). The oil is supplied to the runner servomotor through the shaft from the oil-supply head (5), located on the upper bracket above the generator. Most of the turbine parts are welded.

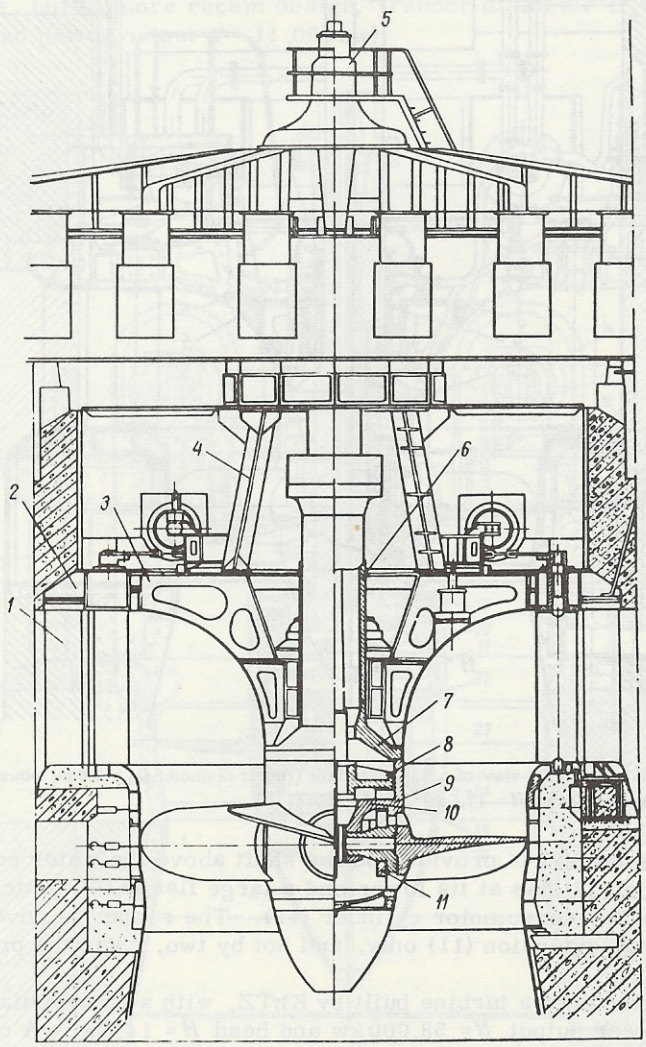


FIGURE V.13. Sectional view of a Kaplan turbine (runner diameter D_1 = 8.0 m, power output N = 58,000 kw, and head H = 14.2 m)

For the first time in the U. S. S. R., a turbine with the thrust bearing located on the cover plate was designed by V. M. Orgo of the LMZ, and built by the Syrzan' Heavy Machinery Plant. Units of this type, with a runner diameter D_1 = 5 m and a power output N = 21,800 kw, were installed at the Kama HEP. Figure V. 14 shows the cross section through the unit. Turbine and generator have a common shaft. The load from the generator rotor, which is supported by the turbine cover-plate, is transmitted to the turbine speed ring. A special foundation ring embedded in the concrete pit transmits the load from the generator stator to the turbine speed ring.

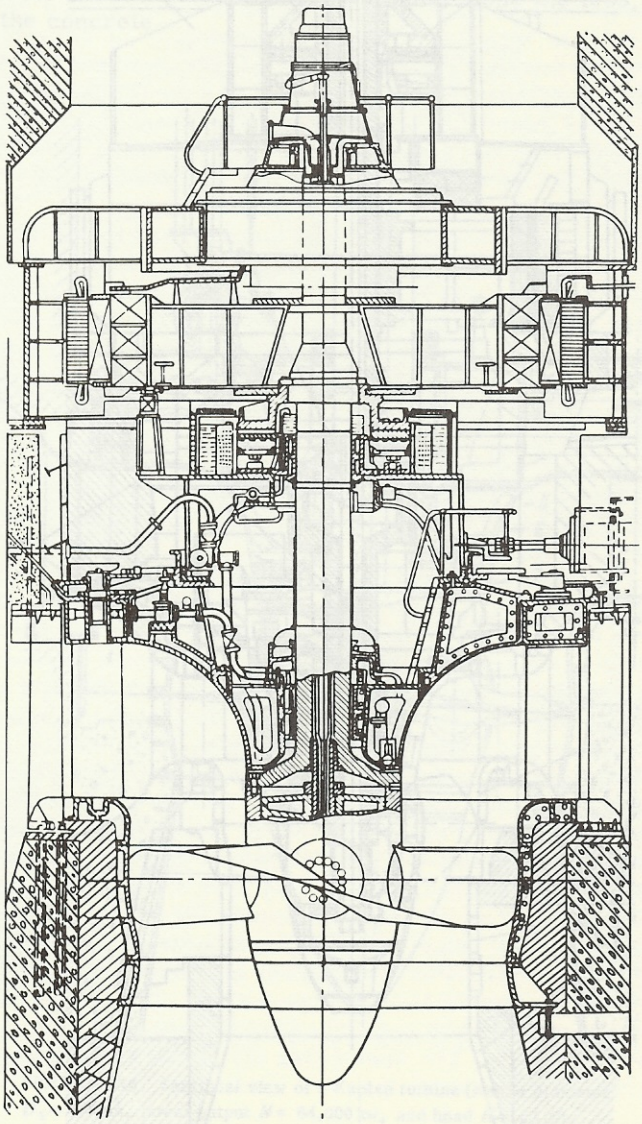


FIGURE V.14. Cross section through hydro unit of the Kama HEP

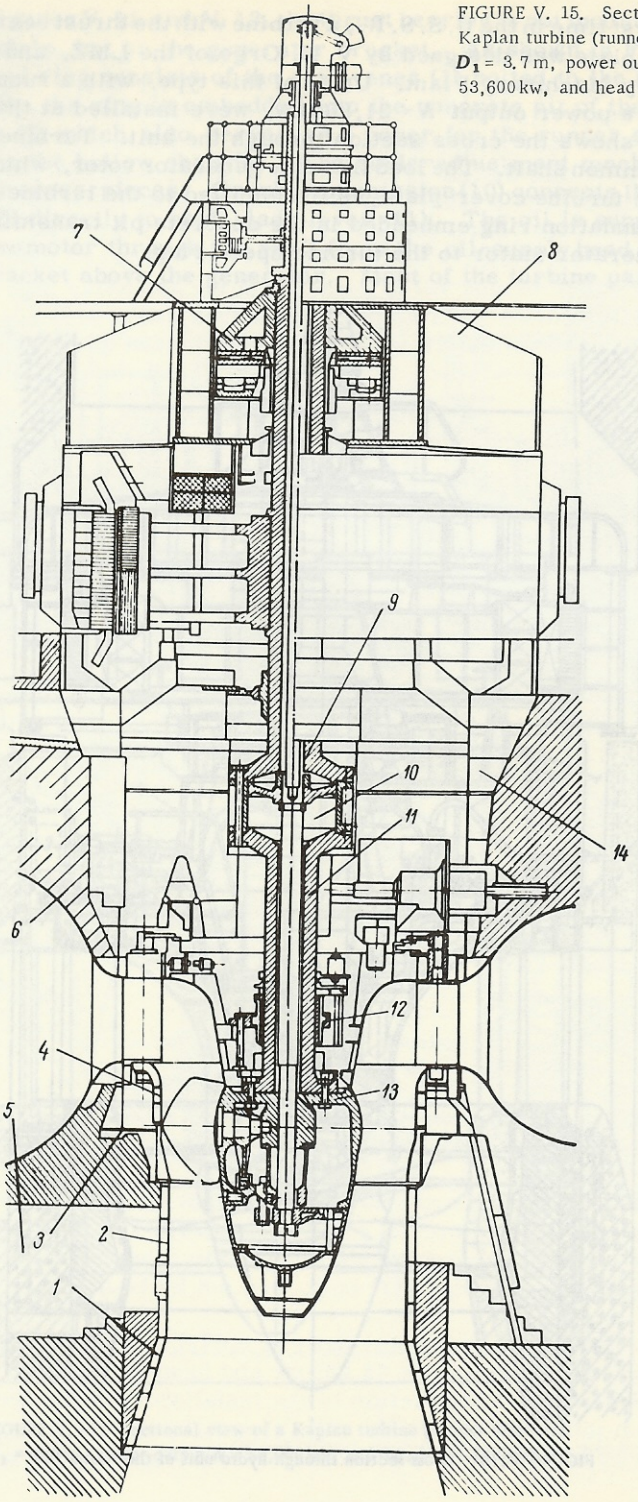


FIGURE V. 15. Sectional view of a Kaplan turbine (runner diameter D_1 = 3.7 m, power output N = 53,600 kw, and head H = 56 m)

Figure V. 15 shows a turbine unit with a runner diameter D_1 = 3.7 m, power output N = 53,600 kw, and head H = 56 m. The turbine was built by the ČKD Plant in Czechoslovakia, and installed at the Slapy hydroelectric plant [on the Vltava]. A circular steel scroll (6), welded to the speed ring (3), was provided because of the high head. There is a marked difference between the foundation parts of this unit and those described above. The conical and cylindrical draft-tube liners (1) and (2) extend the turbine water passages below the runner. The lower ring of the distributor and the throat ring (4) are not embedded in concrete and are accessible through manhole (5). It is thus possible to replace worn-out parts without demolishing the concrete foundation. These parts must, none the less, be securely attached to the concrete.

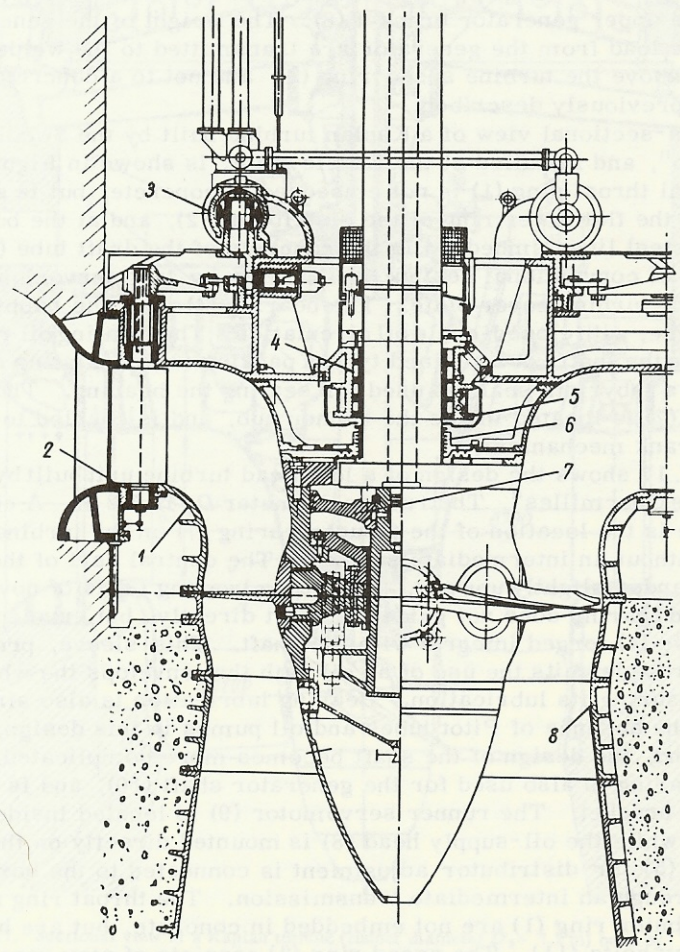


FIGURE V. 16. Sectional view of a Kaplan turbine (runner diameter D_1 = 4.75 m, power output N = 64,000 kw, and head H = 52 m)

Owing to the large hub diameter $d_h = 0.6D_1$, and the vertical position of the blade levers (instead of horizontal, as in the other designs), the hub extension of runner (13) is rather long; the cylindrical liner of the draft tube, thus, also becomes relatively long. The blade levers are coupled to the cross-piece) by means of intermediate bell-crank levers. A characteristic feature of this design is the location of the runner oil-pressure-operated servomotor (10) between the flanges of the turbine shaft (11) and the generator shaft (9), and not inside the runner hub. Although this design is employed by several firms outside the U.S.S R., it would seem to be disadvantageous, since it requires a long rod to transmit a large force from the servomotor piston to the runner-blade levers, and the total weight of the parts is thus increased. The distributor is of conventional design. The babbitted guide bearing is periodically grease-lubricated. The turbine is coupled to the overhung-type generator. The thrust bearing (7) is supported by the upper generator bracket (8). The weight of the generator parts and the load from the generator are transmitted to the welded-casing (14) located above the turbine speed-ring (3), and not to a concrete pit, as in the designs previously described.

The cross-sectional view of a Kaplan turbine built by the Swedish company "Nohab", and installed at the Lasele plant, is shown in Figure V. 16. The spherical throat ring (1) is not embedded in concrete, but is secured at the top to the flat lower ring of the distributor (2), and at the bottom to the conical steel liner embedded in the concrete of the draft tube (8). The distributor, of conventional design, is actuated by two servomotors (3) located on the turbine cover-plate. The bearing (4) is of the babbitted oil-lubricated type, with closed-cycle oil circulation. The rotating oil receptacle is mounted on the shaft. A combined type of packing (6), consisting of a stuffing-box and a labyrinth seal, is used for sealing the bearing. The runner servomotor (7) is located inside the runner hub, and is coupled to the blades through a crank mechanism.

Figure V. 17 shows the design of a low-head turbine unit built by the Swiss "Ateliers des Charmilles". The runner diameter D_1 is 7.2 m. A characteristic feature is the location of the thrust-bearing (7) on the turbine cover-plate (6), without an intermediate support. The central part of the cover plate is expanded slightly upward. The guide bearing (3) is of novel design. The babbitted bearing does not guide the shaft directly, but envelops a ring-shaped sleeve (4) forged integral with the shaft. This sleeve, projecting downward, permits the use of an oil bath that envelops the whole bearing, thus ensuring its lubrication. Bearing lubrication is also simplified because of the absence of Pitot tubes and oil pumps in this design, but on the other hand, the design of the shaft becomes more complicated. A similar guide bearing is also used for the generator shaft (10), and is supported by a special bracket. The runner servomotor (9) is located inside the generator hub, while the oil-supply head (8) is mounted directly on the rotor. Servomotor (5) for distributor adjustment is connected to the box-shaped gate ring through an intermediate transmission. The throat ring and the lower distributor ring (1) are not embedded in concrete, but are held by means of stay bolts (11). The speed ring (2) consists of stay vanes bolted to the upper ring of the distributor.

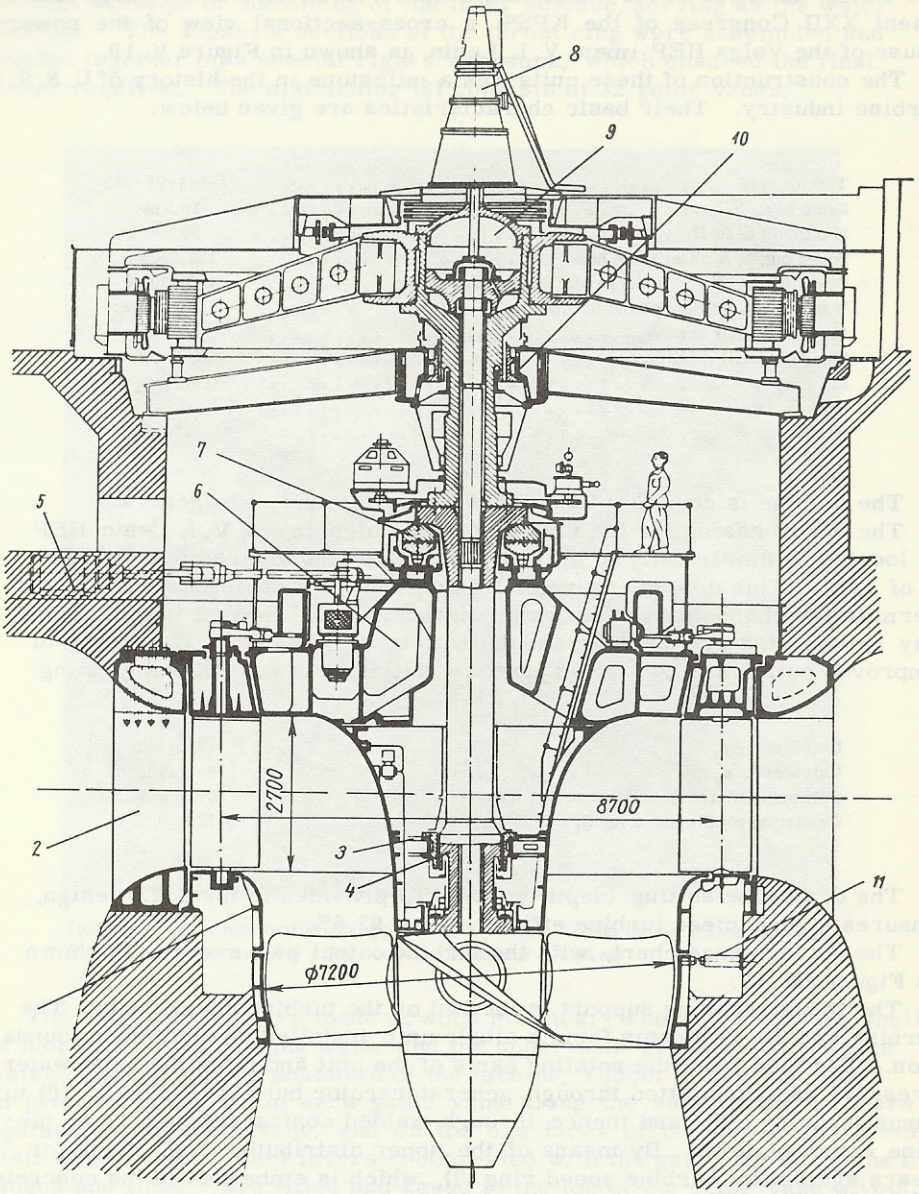


FIGURE V.17. Sectional view of a Kaplan turbine (runner diameter D_1 = 7.2 m) built by "Ateliers des Charmilles" (Switzerland)

Figure V.18 shows a cross section through one of the largest units in the world, installed at the Volga HEP imeni V.I. Lenin and the Volga HEP imeni XXII Congress of the KPSS; a cross-sectional view of the powerhouse of the Volga HEP imeni V.I. Lenin, is shown in Figure V.19.

The construction of these units was a milestone in the history of U.S.S.R. turbine industry. Their basic characteristics are given below:

Turbine type	PL-587-VB-930
Rated head H_r	19.5 m
Maximum head H_{max}	30 m
Power output N under rated head	108,500 kw
Power output N_{max} under heads from 22.5 to 30 mm	126,000 kw
Water discharge through the turbine Q_{max}	700 m^3/sec
Maximum draft head H_{smax}	4.5 m
Rated (normal) speed	68.2 rpm
Runaway speed	140 rpm
Runner diameter D_1	9.3 m
Axial load P	2350 t

The turbine is coupled to a 123,500 kw three-phase 50 c generator.

The scroll casing for the turbine of the Volga imeni V.I. Lenin HEP is located symmetrically to the turbine center-line and has a nose angle α of 130°. This design ensures minimum over-all casing dimensions and permits the channels for floodwater discharge to be located in the turbine bay between the scroll casing and the draft tube. The PL-587 runner, of improved output and cavitation characteristics, has the following rating:

Unit discharge, Q_1'	1850 l/sec
Unit speed, n_1'	118 to 170 rpm
Optimum efficiency η with a model runner (D_1= 460 m)*	87 to 88%
Cavitation coefficient σ for Q_1' = 1850 liter/sec	0.72 to 0.75%

The draft tube setting (depth $h = 2.38D_1$) provided in the LMZ design, ensures a guaranteed turbine efficiency η = 93.5%.

The performance chart, with the turbine output parameters, is shown in Figure III. 16.

The thrust-bearing support is located on the turbine cover-plate. The turbine and the generator form a single unit, installed on a common foundation. The load from the rotating parts of the unit and from the axial water pressure is transmitted through generator-rotor hub (9) (Figure V.18) to thrust bearing (10), and thence through welded conical frame (11) to turbine cover-plate(5). By means of the upper distributor ring, the latter bears against the turbine speed ring (3), which is embedded in the concrete cone (4) of the scroll (Figure V.18). From the speed ring, the load is transmitted to the foundation. The speed ring (3) consists of the upper and lower rings and streamlined stay vanes welded to them, and carries the

* [Obvious misprint. Should read 460 mm.]

distributor, whose lower ring (6), together with the throat ring (1), are fastened to the lower ring of the speed ring. For the first time in U.S.S.R. turbine construction, the throat ring was welded of steel plates, stamped without subsequent machining of the inner surface, serving as the water passage. The separate sections of the throat ring were assembled and welded together on a special rigid framework, which ensured the final shape required. The distributor (2) consists of 32 guide vanes.

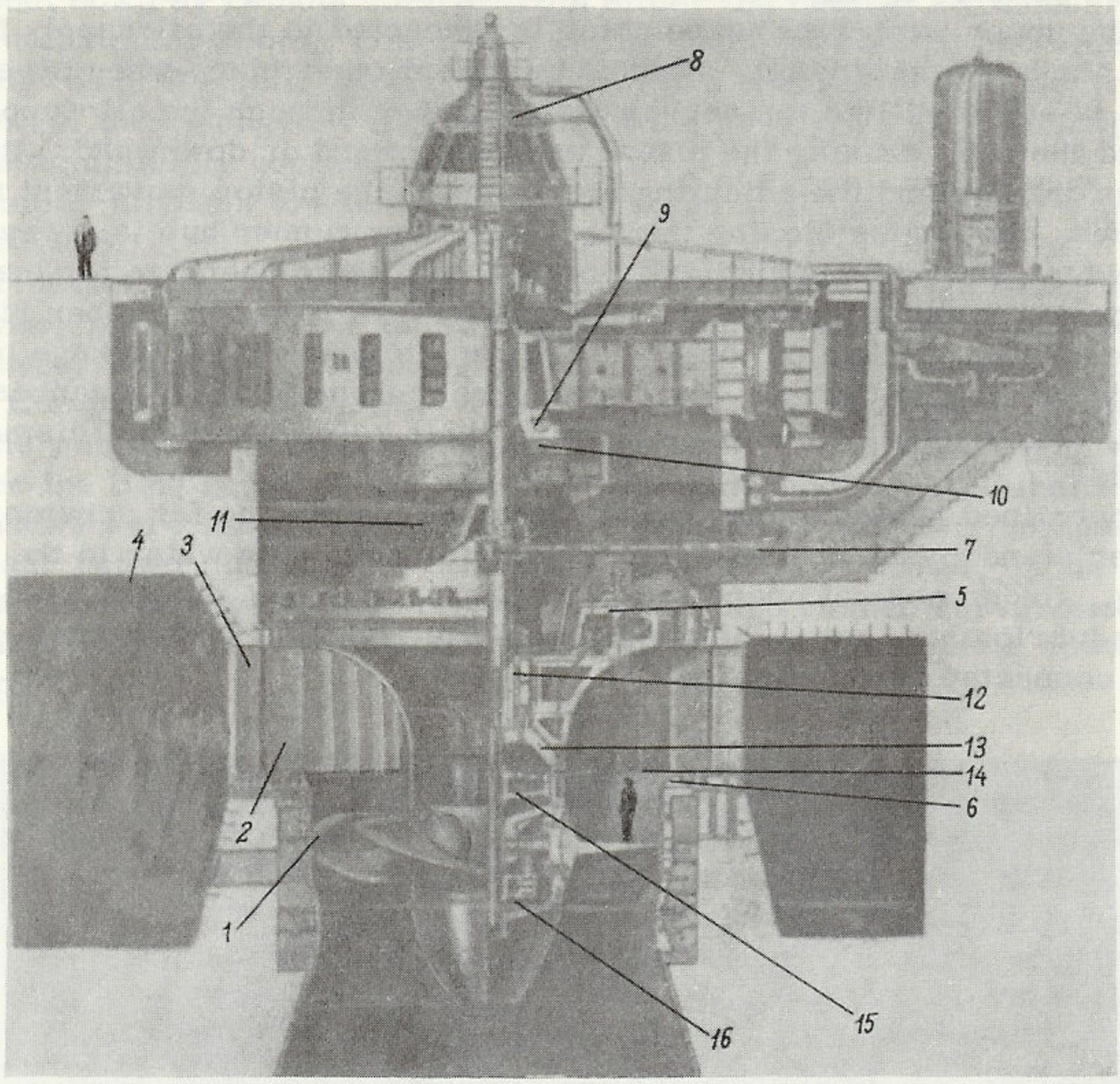


FIGURE V. 18. Cross section through the world's largest Kaplan turbine (runner diameter D_1 = 9.3 m, power output N = 126,000 kw, and head H = 22.5 m)

The vane bearings are made of wood plastics. The lower bearing shell is lubricated with running water and the upper with grease. To reduce water leakages during shutdown of the turbine, rubber rings are fitted in grooves provided on each guide vane along the edge where it bears against the adjacent vane, and on the end faces of the upper and lower distributor rings. Steel levers — connected with the gate ring by means of hinges and links — are fitted and keyed to the top of the guide-vane pivots. The gate ring is connected to two piston servomotors (7), each of 800 mm diameter. The total force of the servomotor is 227 t. One of the servomotors is provided with a locking device to keep the guide vanes in the closed position when there is no pressurized oil in the servomotors. Oil is supplied to the servomotors through pipes from the governor pressure oil system. The guide bearing (12) is water-lubricated.

The runner consists of the hub (15) — the largest turbine part ever manufactured in one piece, weighing 80 t — and the streamlined hub extension connected to it from below. At its top, the hub is connected to servomotor (14) with cover (13), which is bolted to the turbine-shaft flange. The pivots of the six adjustable blades and their adjusting mechanism are mounted in the hub. The blade-adjustment mechanism consists of a lever fitted to the pivot and a link articulated to the cross piece (16). The cross piece is mounted on a steel rod, which, at its top, is connected to the cast-iron piston. By means of rods passing through the hollow turbine shaft, the upper part of the servomotor is connected to the oil-supply head located above the generator. Blade adjustment takes place when pressurized oil is admitted into the servomotor cylinder through the oil-supply head and the rod, causing the piston to move upward or downward. By means of the rod and the adjusting mechanism, the piston movement turns the blades, opening or closing them. The hollow runner hub is always full of oil, which should be periodically replenished to compensate for leakages from the servomotor. Special seals consisting of elastic rubber rings are fitted inside the hub on the blade flanges, to prevent oil leakage between the blade pivots and the hub, and water penetration via the clearances into the hub. The design of the seals permits their removal without dismantling the blades.

Rubber-lined guide bearing. Two separate pipes, one for service, the other for stand-by purposes, are provided for supplying water to the guide bearing. Under normal operating conditions, only one pipe is used for bearing lubrication, but if the water supply is insufficient, the stand-by pipe is connected automatically.

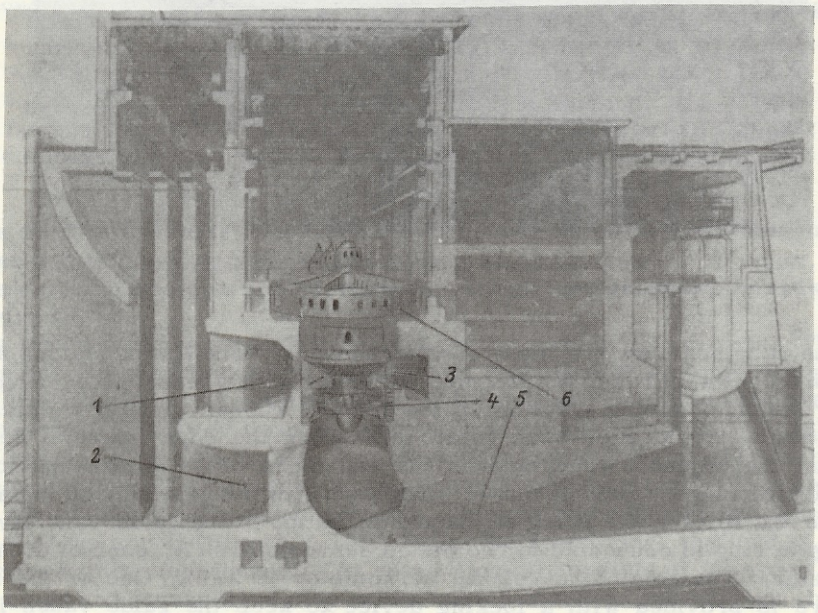


FIGURE V. 19. Sectional view of the powerhouse of the Volga HEP imeni V. I. Lenin:

1 — scroll casing; 2 — channel for floodwater discharge; 3 — distributor; 4 — runner; 5 — draft tube; 6 — generator.

Apart from the above-mentioned parts, the turbine is equipped with several auxiliary mechanisms, including two valves for preventing formation of vacuum. The water is supplied to the bearing and is removed from the cover plate through pipes by means of a pump and an ejector, both provided with automatic float control.

The turbine and its auxiliaries are designed for full automatic control: machine room personnel merely supervise the automatic-control system.

At the Volga HEP imeni V. I. Lenin, the turbine units may be started up and shut down by remote control from either the central switchboard or the load-dispatching room. Other operations, such as normal and emergency shut-downs of the unit, speed regulation when changes in load occur, connection of the emergency mechanisms of the governor, and lubrication are also automatically controlled.

Similar turbines are installed at the Volga HEP imeni XXII Congress of the KPSS.

On the basis of U. S. S. R. experience in manufacture and operation of Kaplan turbines, planning is now under way for a unit of improved design and performance, adapted to the power characteristics of the Volga HEP imeni XXII Congress of the KPSS. The objectives are to reduce the height and the weight of the turbine unit, to improve erection conditions, and to reduce the time required for building, which depends on the turbine design.

Studies were made of the layout of turbine units and their components, such as: runner, distributor, servomotor of the distributor, guide bearing, shafts, turbine cover-plate, oil-supply head, and runner servomotor.

The schematic layout of one of the alternative designs is shown in Figure V. 20.

Turbine rating:

Power output N	126,000 kw
Head H	22.5 m
Runner diameter D_1	9.3 m

As the unit is intended as an outdoor installation without a special generator room, the oil-supply head (6) is mounted inside the generator shaft. The governor equipment is located inside the dam at an intermediate elevation. The whole unit has a single hollow shaft (7), with cast flanges welded to its ends.

The distributor is of the standard type; the guide vanes are driven by two toroid piston servomotors (8), located on the turbine cover-plate (3).

The shaft is coupled to the generator hub (5) and is supported by the thrust bearing (4) located directly on the turbine cover-plate (3), whose central part bulges upward. The stay vanes (1) and the upper ring of the distributor (2) are bolted together and embedded in concrete. The shaft is guided by the water-lubricated babbitted bearing (9). The lower shaft flange, which also serves as a cover for the runner servomotor, is connected to the cylindrical part of the runner hub (13). The servomotor piston, of the differential type, is connected to the blade levers by means of a crank mechanism. The antifriction bearings for the blade pivots considerably reduce the friction moment. Each runner blade (11) is bolted to its pivot. The standard throat ring is of welded construction.

This design ensures maximum compactness of layout, as the height of the unit has been reduced to the minimum. Most of the parts are welded, the total turbine weight being thus reduced.

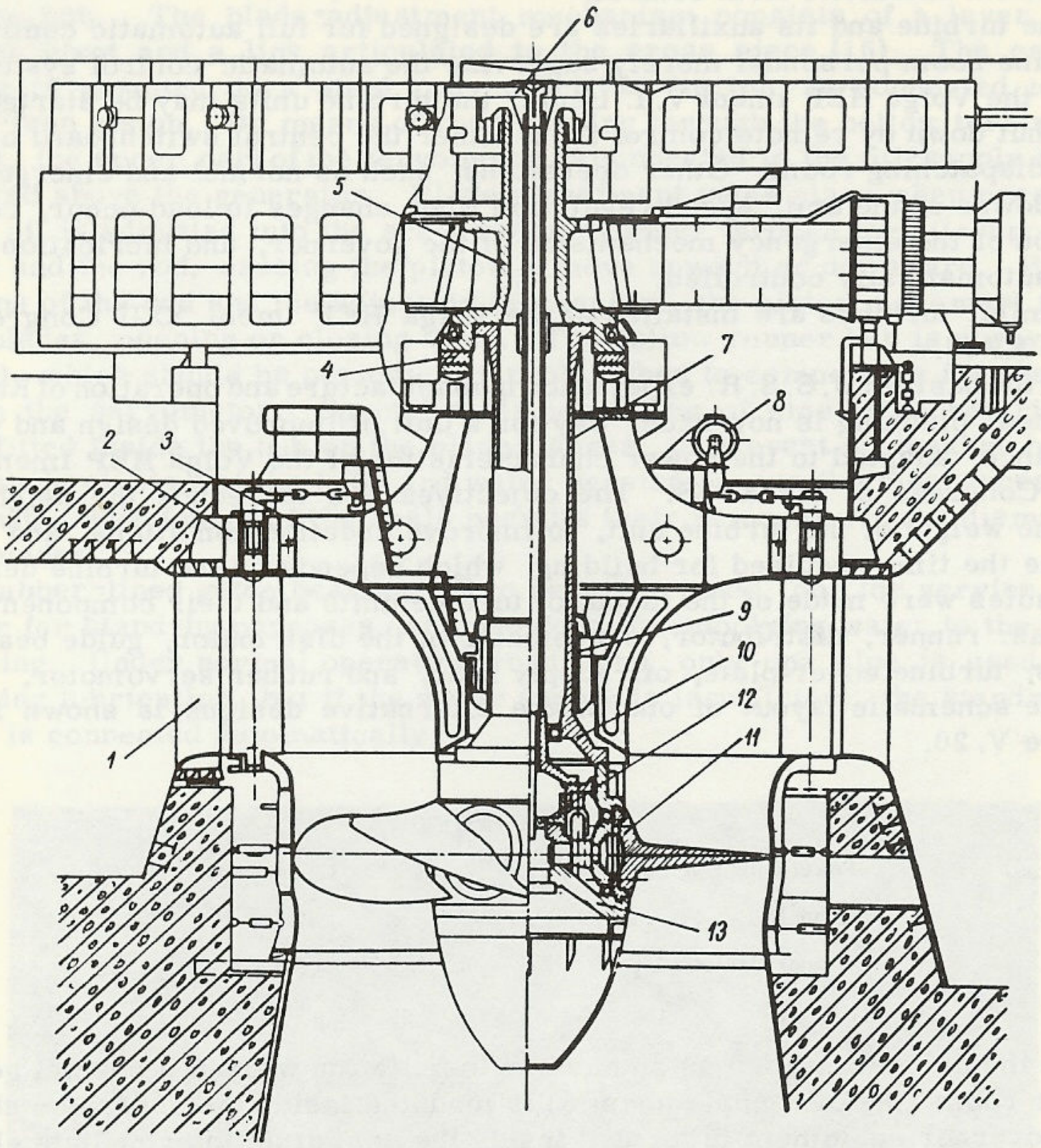


FIGURE V. 20. Sectional view of a Kaplan turbine of minimum height, with runner diameter D_1 = 9.3 m

28. DESIGNS OF HORIZONTAL-SHAFT TURBINES

Horizontal-shaft turbines were introduced in large hydroelectric plants only in recent years, so that their designs are not yet standardized. Individual designs will therefore be reviewed, together with several horizontal-shaft turbines already in operation.

A horizontal-shaft spiral-case Francis turbine, for N = 1700 kw and H = 52.4 m, manufactured by LMZ in the thirties, is shown in Figure V. 21. The water enters the turbine through a steel scroll casing (2) and is discharged through the elbow draft tube (4). The horizontal shaft is carried by three water-lubricated babbitted bearings (1 and 6). The frontal bearing (1) is of the radial-axial type. The turbine shaft is connected by a flexible coupling to the generator. A flywheel (7) mounted on the turbine shaft is provided to keep speed constant. The turbine and the supporting frame are mounted on steel and concrete beams. This construction is suited for low-power horizontal-shaft scroll-casing turbines. Since, in this design, the shaft passes through the draft tube elbow, it impairs the hydraulic characteristics of the turbine by restricting the water passage. Designs with the generator placed in a different position with regard to the scroll, in which the shaft does not pass through the draft tube, were more frequently used; however, the overhung-type runner increases the over-all sizes of the unit to some extent and reduces the rigidity.

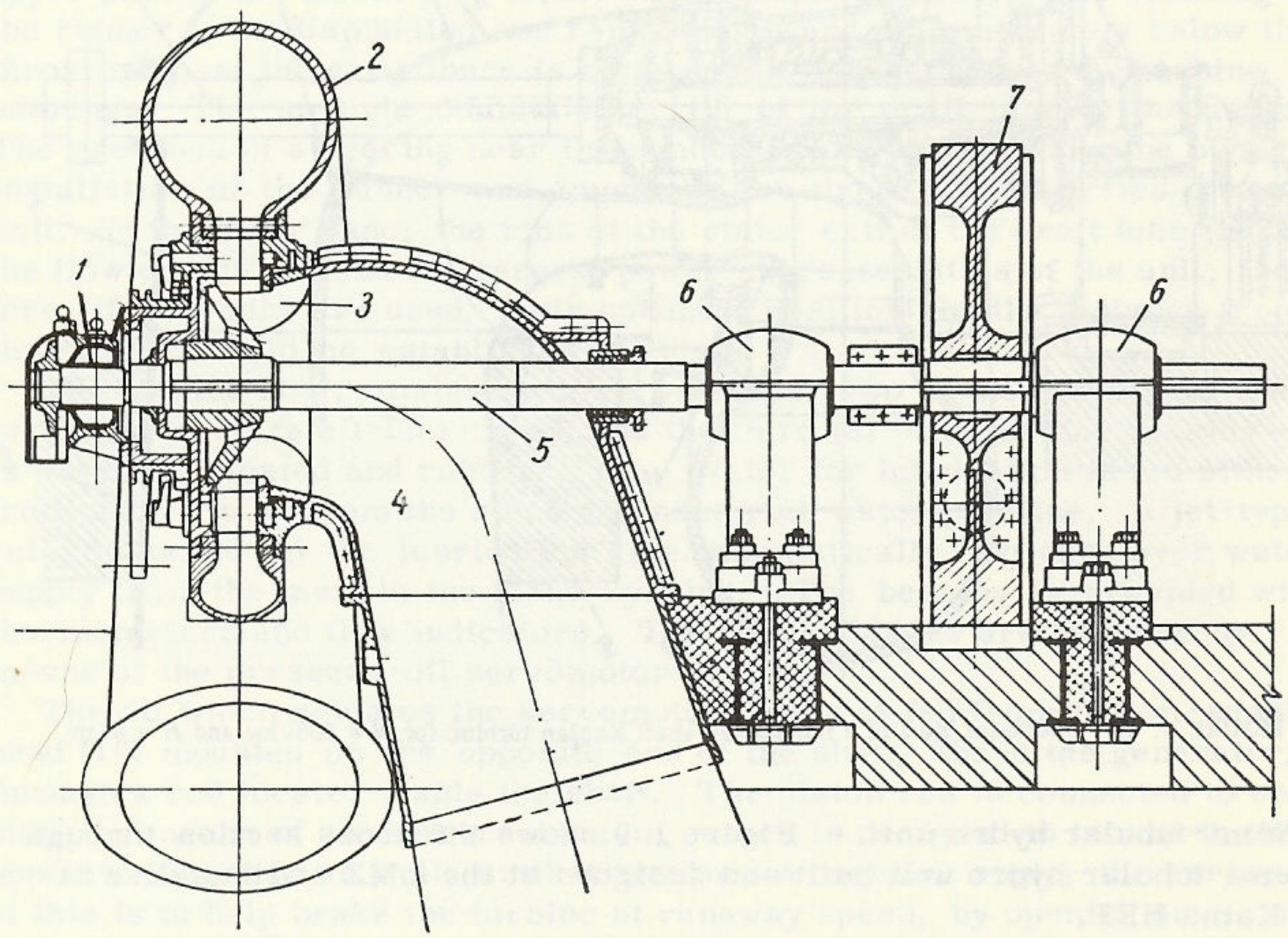


FIGURE V. 21. Horizontal-shaft turbine for N = 1700 kw and H = 52.4 m

A horizontal-shaft Kaplan turbine built in recent years by the Swiss firm "Ateliers des Charmilles" for the Rachet plant, (N = 3,680 kw, H = 56 m, n = 500 and 420 rpm) is shown in Figure V. 22. Despite the disadvantage referred to — shaft location in the draft-tube elbow — this type of Kaplan turbine is of marked interest for its novel design and use for high heads, although it has not gained wide acceptance so far. The water enters through a steel scroll casing (10), upon which the distributor (2) with the driving mechanism and the gate ring (1) are mounted. The eight blades (3) of

the runner rotate in a spherical throat ring (11). The water is discharged through the elbow draft tube (7) and the cone (8), which is embedded in the concrete of the foundation (9). A rather elongated hub extension (4) enclosing the turbine shaft (6) adjoins the runner hub; it is ribbed and provided with a baffle (5) which divides the draft tube elbow into two passages.

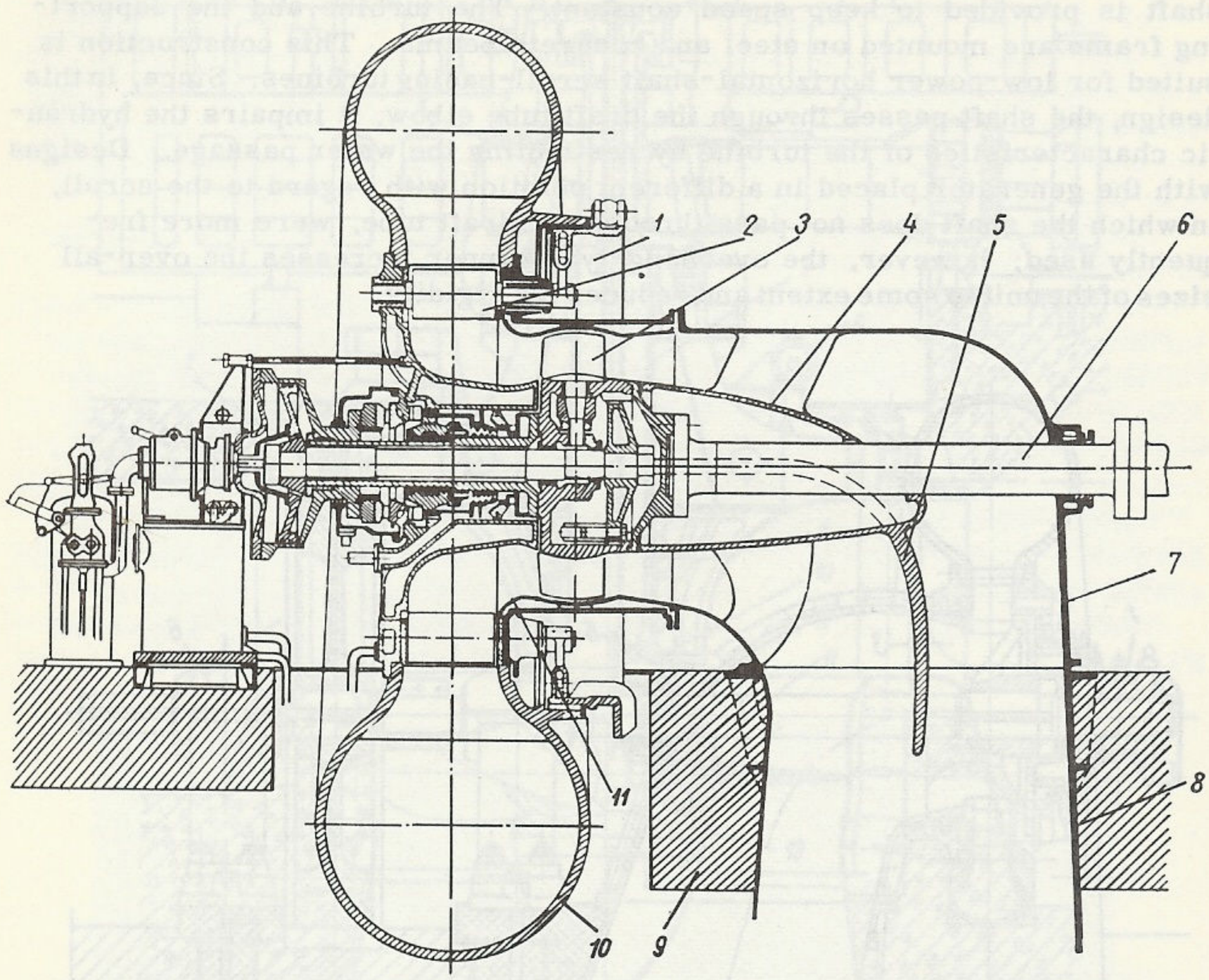


FIGURE V. 22. Sectional view of a horizontal-shaft Kaplan turbine for N = 3680 kw and H = 56 m

Semi-tubular hydro unit. * Figure 1. 9 shows the cross section through a semi-tubular hydro unit built and designed at the LMZ and installed at the Kama HEP.

Turbine rating:

Output N	20,800 kw
Head H	16 m
Speed n	125 rpm
Runner diameter D_1	4.5 m

---

* Designed by V. M. Orgo and S. K. Bugrin.

This turbine has been in operation for a long time. The design of the water passages is not the most appropriate for this type of unit, but had to be adapted to the sizes of the already existing dam and its turbine bay, which was initially designed for vertical-shaft units.

The channels (1) which envelop the concrete casing have a rectangular entrance cross section which gradually assumes a circular form toward the turbine speed ring. The channels are provided with steel liners which protect the walls and eliminate seepage, while special concrete ribs are provided in each channel in order to strengthen the generator casing.

The distributor has twelve radial guide vanes, which control the water discharge and, when closed, ensure complete shutdown of the turbine. They are actuated by the gate ring mounted on the casing which encloses the distributor. The connection between the gate ring and the vanes is ensured by universal links. The gate ring is actuated by two vertical servomotors, located in the turbine pit, each of which has a diameter of 350 mm, with its piston connected by rods to the gate ring. The distributor is located close to the speed ring which consists of two parts embedded in concrete. The upper part of the throat ring is not embedded in concrete, thus enabling the runner to be dismantled and removed upward. Immediately below the throat ring, at the exit, there is a stator (6), which carries the turbine bearings. The straight conical liner (7) of the draft tube is downstream. The presence of a bearing near the runner makes unnecessary the overhung installation of the runner and improves the dynamic properties of the unit; on the other hand, the ribs at the stator exit at the draft tube impair the flow conditions and the general power characteristics of the unit; therefore, if such ribs are used, their optimum position and the distance from the runner should be established by tests.

The turbine shaft rotates in three bearings: two of them are near the generator and are oil-lubricated, and the third (8)—the turbine bearing—is water-lubricated and rubber-lined. Water for lubrication is fed either from the main or from the stand-by industrial-water pipeline. A jet-type relay installed on the lubrication line automatically switches over water supply from the main to the stand-by pipe. The bearing is provided with thermometers and flow indicators. The runner blades are adjusted by means of the pressure-oil servomotor (11).

The oil which actuates the servomotor piston is fed from the oil-supply head (10) mounted on the opposite end of the shaft, above the generator, through a rod located inside the shaft. The piston rod is connected to each blade by means of a crank mechanism, which is designed to turn it in the opposite direction as well, until it assumes a negative angle; the purpose of this is to help brake the turbine at runaway speed, by opening or closing the blades. At runaway speed, the blades are turned to negative angles by a special high-pressure pump unit. The shaft flange is fastened to the generator flange with fitted bolts. A special jack is provided inside the stator for shaft alignment; it also serves to support the shaft during erection of the rotor. The turbine unit is designed for full automatic control and has all the required protection and signalling devices.

Tubular turbines. A sectional view of a tubular turbine built by LMZ for the Ortachalskaya HEP is shown in Figure V. 23.

Turbine rating:

Output N	6,300 kw
Head H	10.5 m
Speed n	125 rpm
Runner diameter D_1	3.3 m

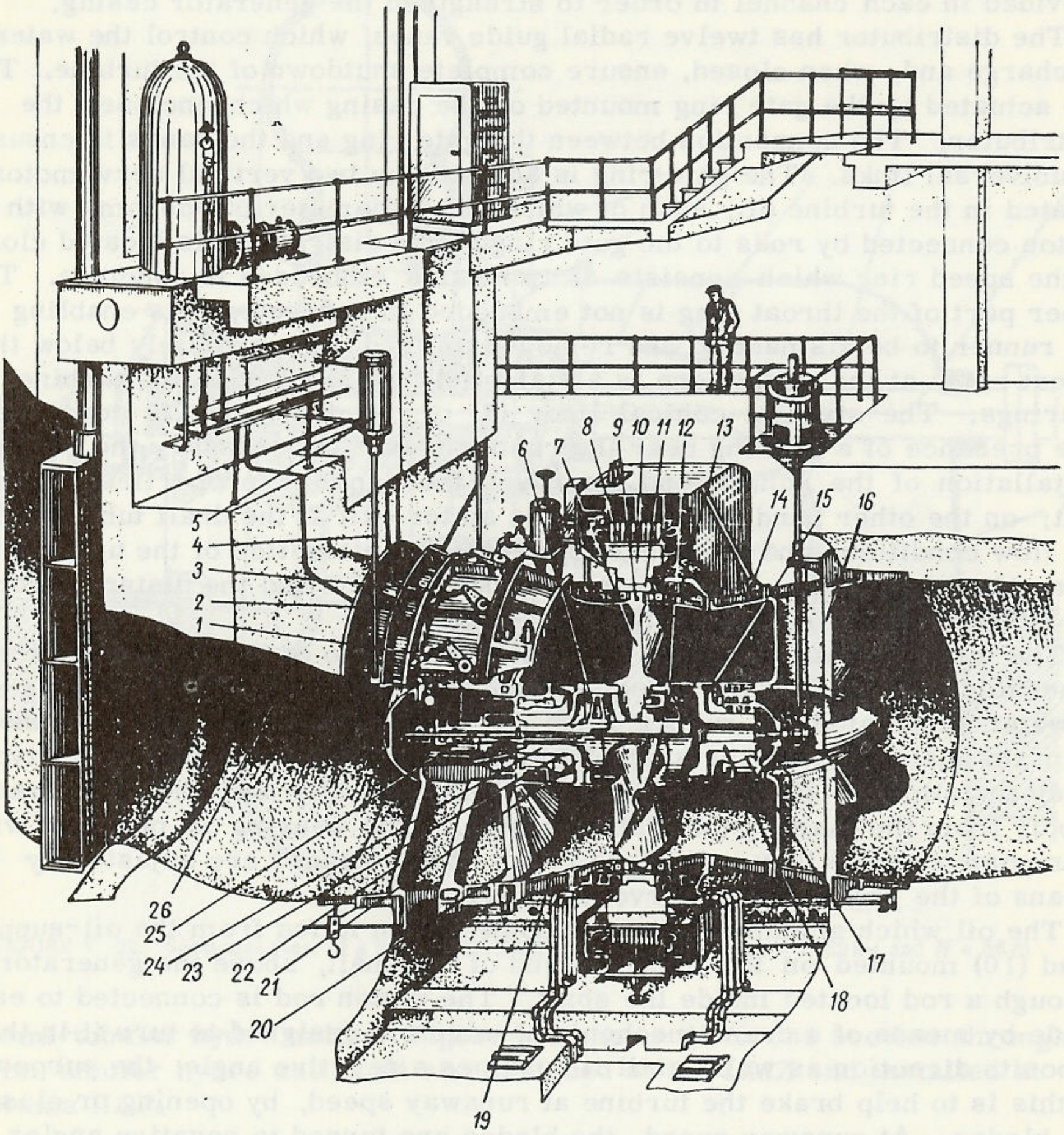


FIGURE V.23. Sectional view of tubular hydro unit (runner diameter D_1 = 3.3 m) for N = 6,600 kw

This unit is the largest of its kind in the world. The water enters from the straight intake (26), and passes by the ribs (22) of the stator front and the distributor (20). The actuating mechanism of the distributor consists of levers (1), links (3) and gate ring (2), which is connected to the piston-type servomotors (5) through the rod (4). From the distributor, the water enters the hemispherical throat ring (19), flows through the runner

and is discharged through the conical section of the draft tube (14), past the ribs of the stator exit (16). The runner blades (7) are adjustable; the blade-adjustment mechanism is located inside the runner. The adjustment force required is developed by the piston servomotor (6), connected to the blades through cross piece (12) by means of a crank mechanism. Oil is supplied to the servomotor (6) from the oil-supply head (25) through hollow rods.

The runner-hub journals (18 and 24) are supported by the water-lubricated bearings (17 and 23). The roller bearings are of the self-aligning type. Thrust pads (15 and 21) take up the axial load in two directions, and are also water-lubricated. The runner blades are fitted at their tips with special pins (9), to which the runner band (11) is secured. The generator stator (8) surrounding the rotor (10) is tightly fitted to the runner band. In this way, the generator rotor and the runner form a single part of the hydro unit. Labyrinth seals (13) and contact seals are provided on each side of the runner band to prevent water from leaking into the generator. Since there is no shaft and the water energy is transmitted directly from the runner blades to the generator, the unit is very compact, but its main disadvantage is that the generator is too close to the water flow. Experience in operation indicates that it is difficult to achieve watertight sealing; therefore, the generator must be operated, in practice, under high humidity or even dripping water, and thus a special insulation of the windings is required. Apart from this, experience has shown that the fastening of the band to the blade pins requires careful design. The design may be markedly simplified if a fixed-blade propeller-type runner is used. A hydro unit with large rotating masses that are concentrated at a great distance from the axis of rotation requires very careful design and workmanship since the slightest inaccuracies in manufacture, assembling, or alignment can lead to serious vibration. The unit components should be capable of functioning safely for an extended period, since dismantling and reassembly are difficult operations and should be avoided. It is advisable to use water-lubricated guide and thrust bearings as far as possible, because with oil-lubricated bearings, which require special seals to prevent the water from penetrating into them, the design becomes more complicated. The operation of tubular hydro units at the Ortachal'skaya HEP, where the water is heavily silt-laden, did in fact cause considerable difficulties.

Since U.S.S.R. turbine industry has little experience in the design of tubular units, foreign designs and experience in their manufacture and operation deserve close attention. Papers in technical periodicals report that the Escher-Wyss Company built and installed more than 75 tubular units with a total power output of some 110,000 kw between 1936 and 1957. According to company data, complicated constructional problems arose in connection with the sealing of the outer band of the runner, which has a tangential velocity of more than 20 m/sec.

The first unit of this kind was built by Escher-Wyss for the Iller River HEP, while later plants were built on the Lech, Saalach, and other rivers. They required a low-head turbine (H from 7 to 8 m), with a discharge capacity of $Q = 20\ m^3/sec$. The runner diameter varied from $D_1 \approx 1.5$ to 2.0 m. The schematic diagram of this turbine is shown in Figure V. 24.

The runner (7) has fixed blades surrounded by a band. The generator rotor (5) is hot-pressed to the runner band. The generator stator (4) rests on the feet embedded in the concrete bay. The turbine runner has two journals (8), supported by bearings mounted on the streamlined hollow ribs, (2 and 6). Oil pipes for bearing lubrication and pipes for the discharge of water seeping through the seals are installed inside the ribs. One of the journal bearings is provided with thrust pads. The axial distributor (3) with its movable guide vanes controls the water discharge; the guide vanes are pivoted by means of spherical hinges connected to the gate ring (9), actuated by two pressure-oil servomotors.

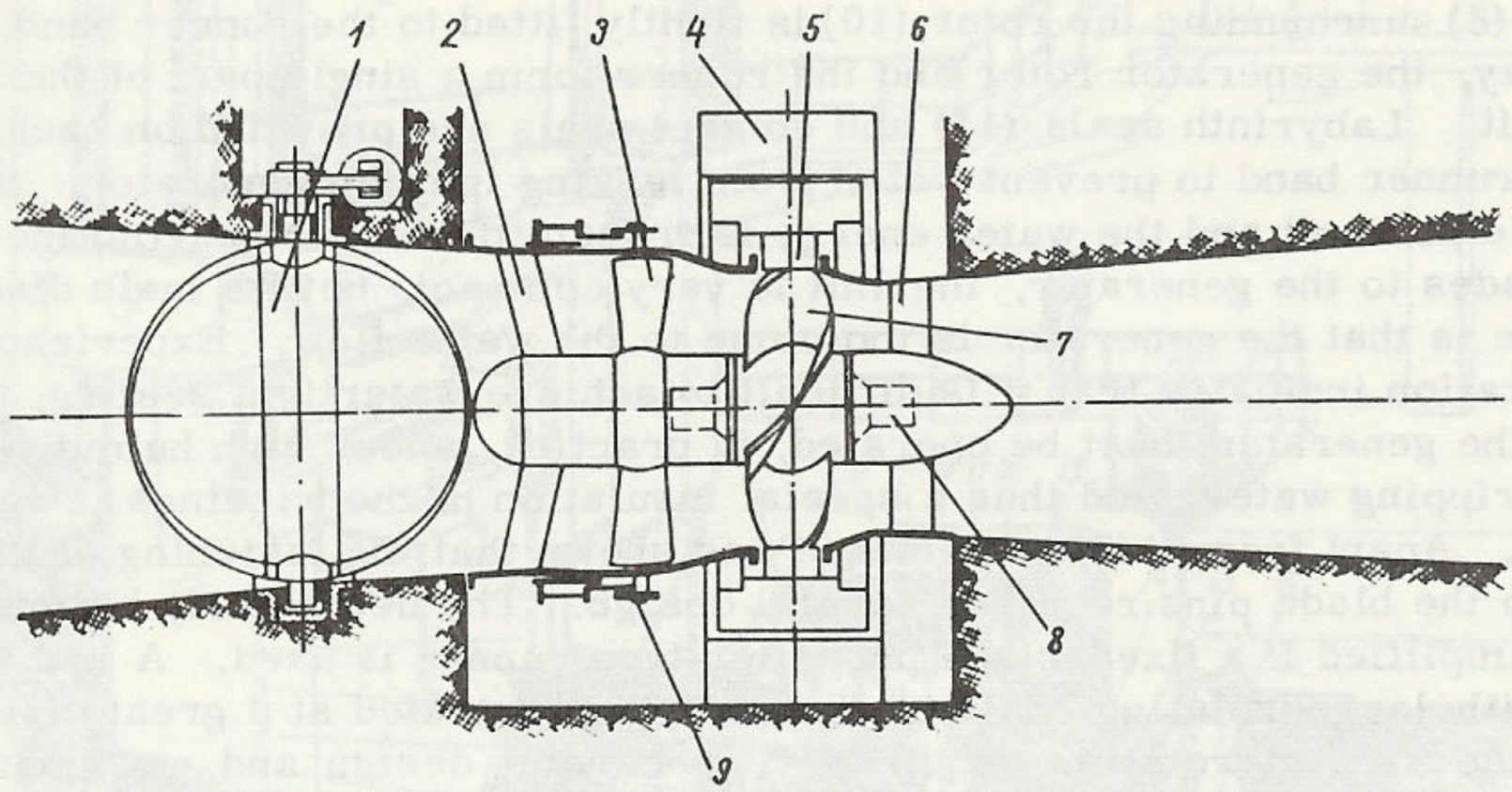


FIGURE V. 24. Tubular turbine unit of the Iller HEP (D_1= 1.5 m, H= 7.0 m)

The runner with its hub, blades, and band, is of the all-cast design. The turbine bearings are pressure-oil lubricated and sealed by means of stuffing boxes of special design. The clearances between the revolving band and the throat ring are also sealed with spongy rubber seals fastened with shroud rings. Rings of a special material line the runner band at the seals, in order to protect the band from wear. The bands are adequately watertight so that water leakages do not exceed 2.5 liter/sec. The leakage water is discharged into an annular chamber and thence into a collecting pit. Tubular turbines have straight or inclined shafts of slopes up to 1:2.5; no special difficulties arose during erection of the unit. A pressure-oil actuated butterfly valve (1) is installed upstream from the water intake of each turbine. Special electric pumps are provided for each turbine for the removal of seepage water from the machine room. An emergency engine-driven pump is provided for possible breakdown in current supply to the main electrical pumps.

Special high-capacity pits which take a few hours to fill up with leakage water whenever the pumps stop removing the water from the turbine are provided in the machine room.

Studies made at the Escher-Wyss laboratories on tubular-turbine models showed that the additional losses due to friction and water leakages at the outer band are offset by the reduction of hydraulic losses in the water passages of the turbine, which has a straight draft tube instead of the customary elbow type.

Field tests were carried out in 1948 on the turbine installed at the Lech River power plant. Measurements showed the capacity and efficiency to exceed the rated figures. Maximum efficiency reached 92.4%.

A tubular turbine with double regulation (with a Kaplan runner) was put into operation in 1951 at one of the Iller cascade-system plants. Experience in operation showed that all the problems connected with the use of Kaplan runners in tubular turbines could be successfully solved.

In the light of experience in operation of propeller and Kaplan turbines, Escher-Wyss draws the conclusion that tubular turbines are suited for spillway power plants with heads ranging from 6 to 15 m. At higher heads, difficulties arise due to increase in mechanical stresses in the runner. By using a solid runner band instead of composite bands, the design becomes more simple. For easy transportation, the band diameter should not exceed 4.5 m, which corresponds to a maximum runner diameter of D_1= 3.3 m.

Turbine runners for N = 17,000 hp and with a diameter D_1 = 4.9 m are known to have been built in a number of places.

Experience in operation of tubular turbines at the Lech River cascade system equipped with 9 similar units each consisting of six turbines, is most instructive. The cascade has 54 tubular units altogether, developing 64,000 kw, which were built between 1940 and 1950.

Most plant breakdowns were due to faults in the electrical equipment. With a runner diameter of 1.95 m, most trouble was caused by the sealing of the runner band whose velocity is 22 m/sec. At first, the water leakages amounted to 50 liter/sec and the seals had to be removed about every 4,500 hours. In the new design, the seals operate for 20,000 working hours without changing the rubber, and the leakages through the clearances amount to only 2 to 4 l/sec.

In the initial design, the replacement of seals involved partial dismantling of the generator, which required three to four men working for three weeks. In the new designs, for the replacement of seals, water supply to the turbine is simply shut off and all the work may be done by one or two men in one or two days.

The service life of the spongy rubber seals, estimated at about 17 to 20 thousand working hours, depends mainly on the resistance of rubber to wear and the effects of oil. Synthetic rubber of a special composition proved satisfactory.

Electrical breakdowns occurred at the transformers due to low-quality insulation of the generator-stator windings, wetting of insulation, etc. Submerged hydro units should preferably be fitted with an emergency diesel unit to pump out the seepage water, developing about 0.7 to 1% of the installed generator capacity.

From the available field data, the Escher-Wyss Company concludes that with due improvement in turbine and seal design, tubular turbines are the most reliable low-head prime movers and fully justify their use from the standpoint of both individual unit efficiency and plant output.

The bulb-type tubular unit of the Beaumont-Montais HEP. A novel construction, combining turbine, generator, and casing in a single unit, is shown in Figure V. 25.

This unit was designed and built by the French companies "Neyrpic" and "Alsthom", for the Beaumont-Montais plant.

Turbine rating:

Output N	8,800 kw
Head H	9.5 to 12.5 m
Speed n	150 rpm
Runner diameter D_1	3.8 m

The total weight of the hydro unit is 280 t. Sixteen front and four rear columns (stay vanes) carry the casing, which encloses the turbine and generator. The water enters the runner through the distributor (2). The twenty guide vanes are connected by means of levers and links to the gate ring (3), which is actuated by two servomotors.

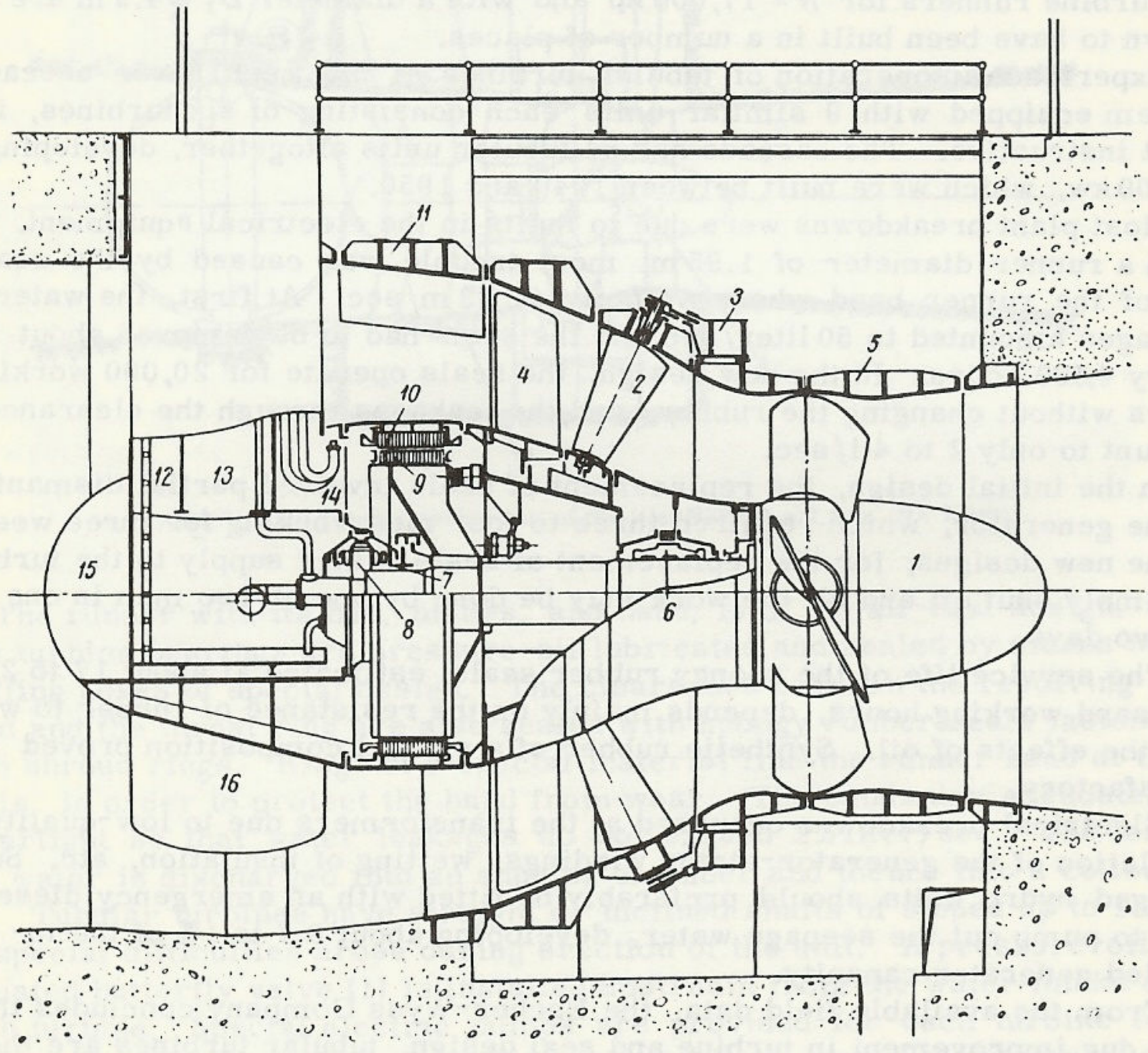


FIGURE V. 25. Sectional view of a tubular unit with the generator inside the casing, N = 8,800 kw and D_1 = 3.8 m

The vane length b_0 is 1,030 mm. The four adjustable blades of runner (1) revolving inside the hemispherical throat ring (5) are made of stainless steel. The hydro-unit shaft is supported by two self-aligning, ring-lubricated bearings (6 and 7). The disk thrust bearing (8) is located next to the guide bearing (7). The oil is circulated by a centrifugal pump. Both rotor (9)

and stator (10) of the generator are air-cooled. The upper part of the water intake (11) and the throat ring (5) are removable, and not embedded in concrete. The hub extension is supported by three hollow ribs. The upper rib is intended for control-communication lines; compartment (12) is used for locating the pipelines, compartment (13) is a manhole, and compartment (14) houses cable and bus-bar terminals.

The two lower ribs (16) are used for ventilation and the supply of cooling water. Access to runner bearing (6) and the hub extension is by inspection manholes in the generator rotor. The hub cap (15) is used as an oil tank. The bearings are equipped with graphite packings. The speed ring (4) is of the detachable type. The turbine is assembled on the erection bay in a vertical position and then lowered down horizontally. The unit is designed to work as a turbine only, but in France, models are also built at present as reversible pump-turbine units.

Tubular turbine units with step-up gears. A tubular unit with a step-up gear (designed by TsKTI) is shown in Figure V.26. The runner diameter is D_1 = 5.0 m, the power output N = 27,000 kw, and the head H = 15 m. The turbine is coupled to the generator through a step-up gear which increases the speed from 68.2 to 1000 rpm, thus permitting the use of a high-speed small-size generator which may be accommodated within the casing (bulb). The casing actually forms an extension of the runner hub [but at its upstream end]. The water flows in around the entrance stator, which is provided with massive ribs (1) and forms the first support of the hydro unit. Thence the water passes through distributor (3) and enters the runner (6). It finally flows around the casing (11), in the middle of which are located stay vanes (10) of the exit stator, which forms the second support of the hydro unit. The power developed by the runner is transmitted to generator rotor (12) through step-up gear (9). Both turbine and generator are supported by two bearings each (4 and 8) and (13 and 14). The axial bearing (7) is split in halves and placed close to the runner. The blades are turned by servomotor (5), which receives oil from the pressure-oil unit through oil pipe (2) passing inside the stator ribs, and through the oil-supply head located inside the runner shaft. The distributor (3) is adjusted by the gate ring enclosed in the turbine casing and actuated by two servomotors (15).

A similar tubular hydro unit design could have been attained by locating the generator upstream from the runner, but then the length of the water intake structures would have been considerably greater, as also would be the width of the powerhouse. The oil supply to the servomotor of the overhung runner also becomes more complicated, since it cannot be effected through the generator shaft because of the presence of the step-up gear. An exit stator lowers the turbine efficiency. The double step-up gear permits the use of a generator of very high speed and small dimensions. Had a single step-up gear been employed instead, the speed of the generator would have been only 750 rpm, while its over-all dimensions would have been considerably larger.

Figure V.27 shows the sectional view and the kinematic diagram of a step-up gear. The runner is coupled to the carrier arm (1) of the first gear train. The planet gears (2) with the spindles on the carrier arm engage the sun wheel (8) to which the generator is coupled. The planet wheels also engage the crown wheel (3), which is coupled to the sun wheel (4) of the second train. The carrier (7) of the second train is fixed to the gear

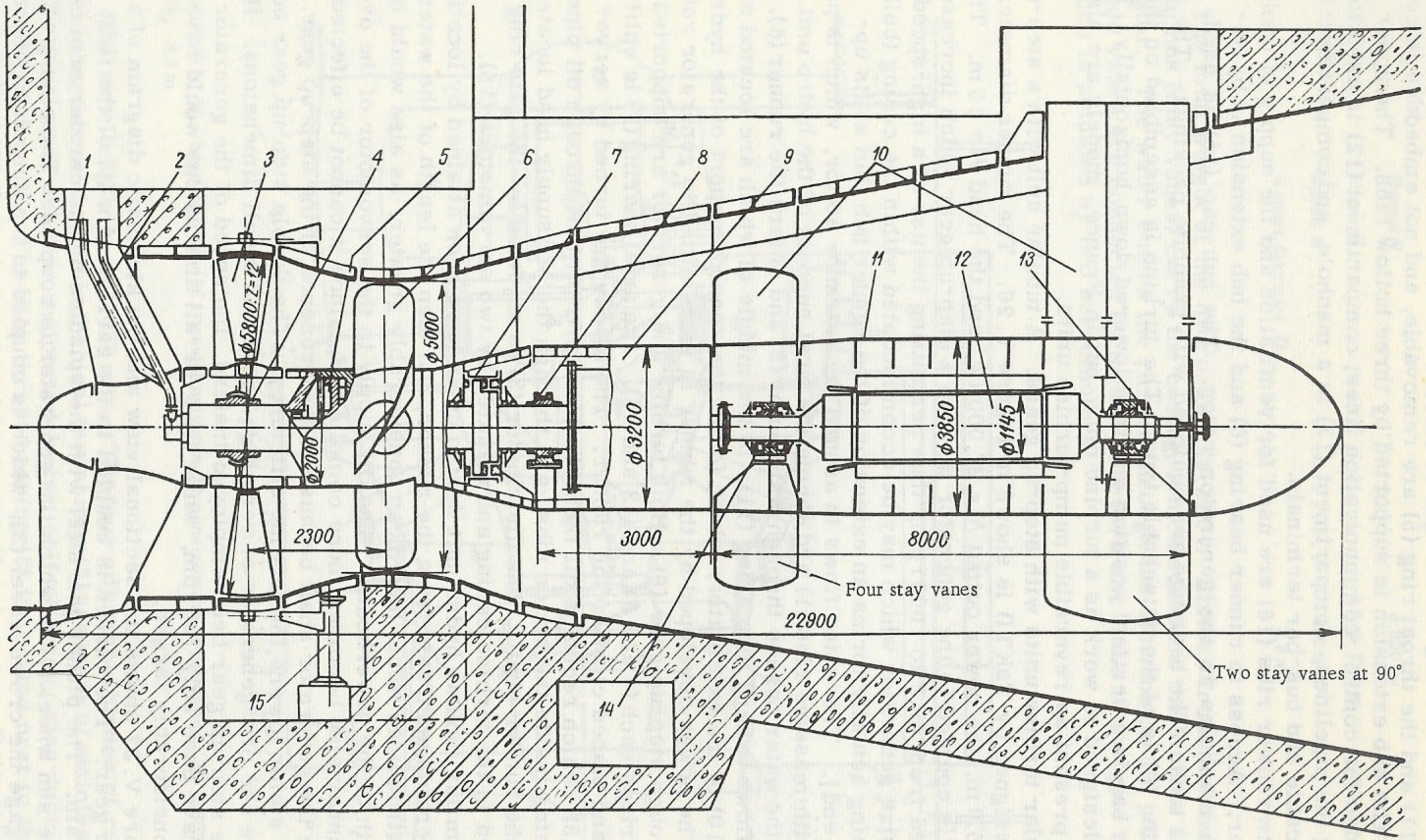


FIGURE V. 26. Sectional view of a tubular unit with multiplying gear (N= 27,000 kw and D_1 = 5.0 m)

casing. The crown wheel (5) of the second train is coupled to the carrier (1) of the first train. The design is of the closed differential drive type.

In the first (differential) train, the power supplied by the turbine is divided into two parts. The first part is transmitted directly by the carrier (1) to the driven sun wheel (8). The second part is received by the driven sun wheel (4) from the driving carrier through the second train. This arrangement permits large torques to be transmitted.

The efficiency of the planetary gear is η = 97.5 to 98%.

The speed ratio of the multiplying gear is

$$i = 1 + k_1 + k_1 k_2,$$

where k_1 and k_2 = the speed ratios of the gear trains with the carrier locked.

Some of the characteristics inherent in the design and manufacture of the planetary step-up gear devised by O. A. Pyzhe and Yu. A. Derzhavets are worthy of note.

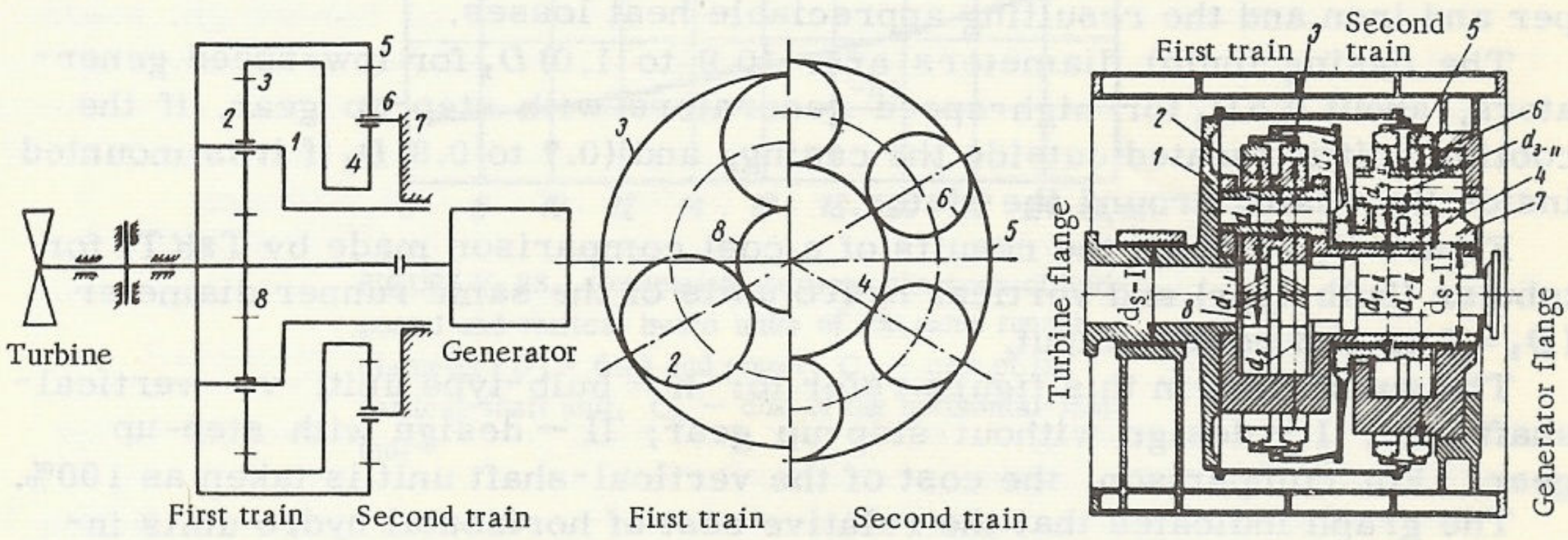


FIGURE V. 27. Kinematic diagram and cross section of the multiplying gear:

d_1—diameter of sun wheel; d_2—diameter of crown wheel; d_3—diameter of the planet wheel bearing; d_4—diameter of planet wheel; d_5—diameter of shaft bearing.

The gears are of the herringbone type; the plain bearings are babbitted.

The sun and crown wheels in both gear trains are of floating design without bearings, to compensate for inaccuracies due to manufacture. The crown wheels are resilient.

The crown wheels are split in halves to ensure a uniform distribution of the load. The two halves are joined to form a single wheel by means of a dog coupling.

Sun and crown wheels are coupled to their respective shafts by dog couplings which ensure self-alignment of the floating gears.

The planet wheels turn on babbitt-lined spindles. The center holes of the planet wheels have to be ground, nitrided, and honed, thus ensuring that the babbitt lining will not be overstrained.

Because of the high permissible contact load between the teeth, they require surface hardening. Sun and planet wheels are small in size, so

that they can be nitrided, and subsequent teeth grinding is not necessary. Crown wheels should be hardened only to a degree that would not preclude their subsequent milling.

New designs of step-up gears for hydro units clearly prove that they can be made for outputs of up to 70,000 kw.

However, notwithstanding its high efficiency, the planetary step-up gear is a complicated and expensive mechanism, requiring a special manufacturing technique.

The weight of the step-up gear depends upon the power transmitted, and varies from 3.2 to 5.5 kg per kw. In view of the high cost of the planetary gear (about 3 rubles per kg of weight), its use is economically justified only in special circumstances. The installation of a tubular unit without a step-up gear — with the turbine coupled directly to a low-speed generator — might prove more economical. Special small-size generators, with high specific loadings of copper and iron parts, provided with forced cooling, would then be required.

The rotor may be cooled by compressed air (p = 3.5 to 4 kg/cm^2), or distilled water flowing in a closed cycle. However, the efficiency of small-size generators drops owing to the high specific loading of the active copper and iron and the resulting appreciable heat losses.

The casing (bulb) diameters are: (0.9 to 1.0) D_1 for low-speed generators, about 0.5 D_1 for high-speed generators with step-up gear, if the cooling unit is located outside the casing, and (0.7 to 0.8) D_1 if it is mounted inside the casing around the stator.

Figure V. 28 gives the results of a cost comparison made by TsKTI for tubular (bulb-type) and vertical hydro units of the same runner diameter (D_1 = 6 m) and power output.

The subscripts in this figure refer to: h — bulb-type unit; v — vertical-shaft unit; I — design without step-up gear; II — design with step-up gear. For comparison, the cost of the vertical-shaft unit is taken as 100%.

The graph indicates that the relative cost of horizontal hydro units increases with the head, and that a bulb-type unit with step-up gear is more expensive than a unit without.

Performance ratings of horizontal bulb-type units are of interest to the designer. The maximum specific discharge of most existing turbines ranges between 2,300 and 2,400 liter/sec. The full-load efficiency of bulb-type turbine units is 4 to 4.5% higher than the efficiency of vertical turbines. However, this increase in the turbine efficiency cannot be fully exploited since a turbine coupled directly to the generator requires a small-size generator operating under overload conditions, a fact that introduces additional losses. Its efficiency, compared with that of standard generators, is therefore 1.5 to 2% lower.

The efficiency of a high-speed generator used in hydro units with multiplying gears is 0.8 to 1% greater than that of vertical units, but the losses in the gear amount to 2.5%, which means that in practice total losses will be about the same as in the former design. Consequently, in spite of the fact that the efficiency of bulb-type tubular turbines exceeds that of vertical turbines by 4 to 5%, the difference between the efficiencies of the complete unit is only 2.5 to 3%.

For optimum load, i.e., at the point of optimum efficiency of the turbine, the difference will be from 1 to 1.5%, and from 0.5 to 0.8% between the efficiencies of the complete unit.

The fact that the mechanisms located inside the casing (bulb) have a difficult access should be considered a constructional shortcoming of bulb-type units.

Mechanisms and seals that require inspection and maintenance, become accessible through the manholes provided in the casing walls only after the turbine is shut down and the water is drained out.

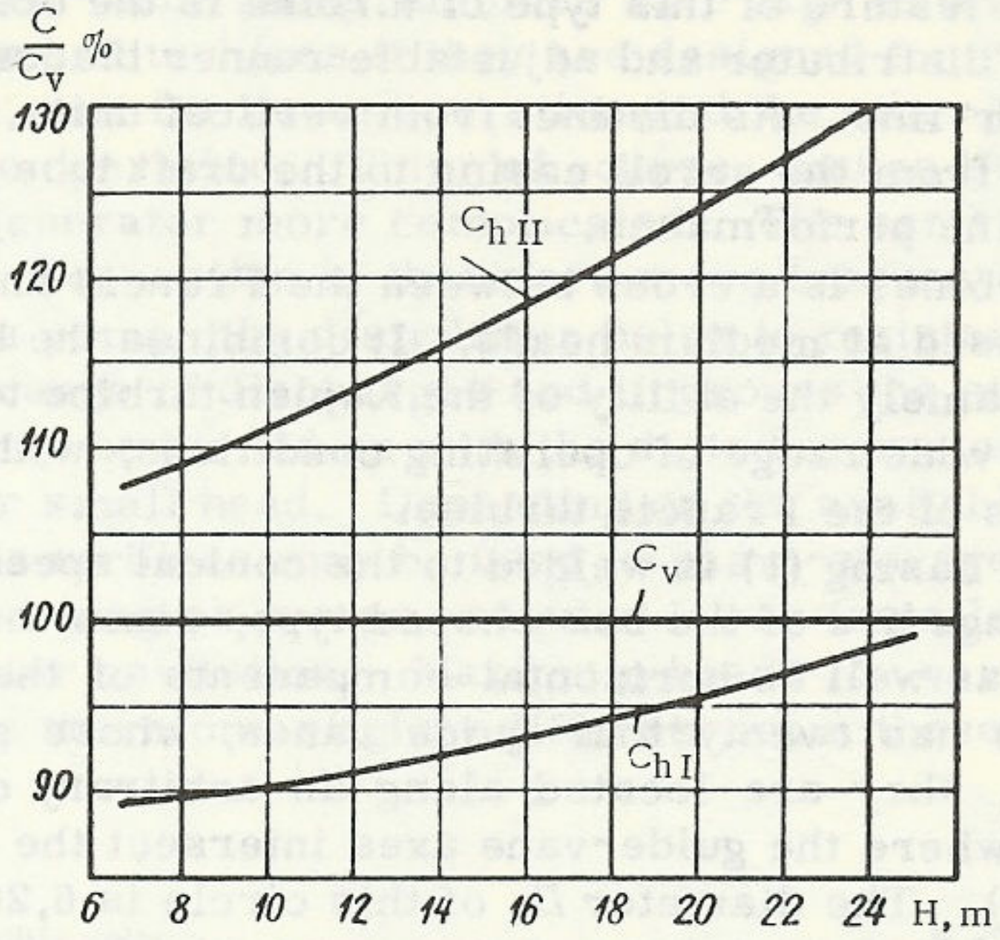


FIGURE V. 28. Comparison between the costs of horizontal and vertical hydro units of the same runner diameter (D_1 = 6 m) and power: C_v — cost of the vertical-shaft unit; C_h — cost of the horizontal-shaft unit

Difficulties also arise in erection and dismantling. The generator and the step-up gear can be installed only after their assembly, a fact which necessitates increased crane hoisting capacity and large-size access openings in the powerhouse. All these shortcomings make operation of the plant by no means an easy task. On the whole, the design of horizontal-shaft units is more complicated than that of vertical turbines.

Overhung-type runners used in such designs are subject to additional transverse forces, which are liable to cause vibration of the unit. Moreover, the supports of horizontal-shaft units bear a heavier load.

As the turbine bulb has to withstand the water flow, it must be carefully designed and proportioned, especially when operated at increased discharge.

Horizontal-shaft hydro units have smaller outputs and dimensions than vertical units. To obtain the same power output, as in plants with vertical units, the number of horizontal units must be increased. In deciding on the use of horizontal units, the designer should, therefore, carefully compare their disadvantages with the advantages resulting from reduced dimensions and shorter erection time.

Diagonal turbines. Figure V.29 shows a diagonal turbine design developed by V.S. Kviatkovskii /38/, and refined at LMZ by L.G. Smolyarov and V.M. Nemm. The turbine, intended for installation at the Bukhtarma HEP, has a power output of N = 77,000 kw, speed n = 150 rpm, at a head H = 61 m.

A characteristic feature of this type of turbine is the oblique location (slope angle 45°) of distributor and adjustable runner blades with respect to the turbine center-line. As distinct from vertical units, in this design the water passages from the scroll casing to the draft tube are straight, improving the turbine performance.

The diagonal turbine* is a cross between the Francis and the Kaplan turbines, and can be used at medium heads. It combines the best features of both these types, namely the ability of the Kaplan turbine to maintain high efficiencies over a wide range of operating conditions, with the good cavitation characteristics of the Francis turbine.

The steel scroll casing (1) is welded to the conical speed ring (2). The upper and lower rings are of the box-shaped type, since the speed ring is subject to vertical as well as horizontal components of the weight loads. The distributor (3) has twenty-four guide vanes, whose profile changes along their height; they are located along an arbitrary circle (drawn through the points where the guide-vane axes intersect the outer surface of the water passages). The diameter D_0 of this circle is 6,200 mm.

On account of the oblique setting of the vanes, the bearing supporting flanges are spherical, to ensure identical angular location and alignment of all the bearings.

The guide vanes are coupled with the gate ring (8) through levers and links with spherical hinges, while the gate ring itself is connected to the servomotor piston by means of the shaft (9).

The runner (4) has ten adjustable blades. The runner diameter (taken as that of a circle passing through the points where the blade axes intersect the throat-ring) is D_1 = 4,350 mm. The ratio of hub diameter to runner diameter $\frac{d_{hub}}{D_1}$ = 0.65. The largest diameter of the runner hub is 3,400 mm.

Studies made by the designers indicate that the rotary (vane-type) servomotor (7), the cross piece (6), and the radial blade levers (5), are the most suitable blade-adjustment mechanism for the runner blades of a diagonal turbine. In a rotary servomotor, the rods supplying the oil to the servomotor, located within the shaft, also rotate. The other turbine parts, such as shaft, bearing, governor and auxiliary equipment, do not differ from similar parts of a vertical turbine.

A comparison between the diagonal and Francis turbines of identical ratings, both intended for the Bukhtarma HEP, shows that the diagonal turbine is 20% heavier (370, as against 312 t), its manufacture involves 50% more labor (55,000 normal hours as against 36,000), while construction and assembly of distributor and runner are more complicated.

* [Termed "Deriaz turbine" after its inventor.]

Reversible pump-turbine units. Pumped-storage power plants. At present, it is common practice to mount the reversible pump-turbine unit and the motor-generator on the same shaft. If the water flows from the upper storage reservoir into the runner, the unit works as a turbine, driving the electric generator. Should the generator be required to function as an electric motor, it drives the runner, which pumps water from the lower to the upper storage reservoir.

Reversible fixed-blade pump-turbines have high efficiencies when working both as pumps and turbines if they are designed for running at different rotational speeds, one for pump operation and the other (usually 10 to 20% lower) for turbine operation. This, of course, makes the design of the reversible motor-generator more complicated. The same rotational speed for both manners of operation is therefore more frequently used. When the unit operates as a pump, the distributor helps to maintain high efficiencies within the whole range of discharges and improves the starting conditions, since the pump may be turned on with the distributor closed and the discharge pipe under small head. Depending on the available head, either Kaplan or Francis turbines may be used in pump-storage installations. Reversible units, working as pumps, require lower installation than ordinary turbines, to counter cavitation. Maximum heads for various types of reversible units are therefore slightly different from those for ordinary turbines.

Kaplan reversible units	$H < 20$ m
Diagonal reversible units	$H = 20$ to 60 m
Francis reversible units	$H = 20$ to 200 m or more

As yet no reversible units have been constructed or installed in the U.S.S.R.

One of the largest pump-storage plants outside of the U.S.S.R., is the Traquaio HEP in Brazil; it is equipped with reversible Kaplan units, which operate under a head $H = 6.7$ m. The power output as a turbine is $N = 2,540$ kw, with the speed $n = 150$ rpm. Horizontal-shaft units, with $D_1 = 5.8$ m, $H = 5.5$ m, $N = 9,000$ kw, and $n = 88$ rpm, are installed at Saint-Malo in France.

The largest reversible Francis-type units constructed so far are installed at the Hiwassee pump-storage plant (in the U.S.A.). As turbines, their parameters are $H = 58$ m, $N = 59,000$ kw, $n = 105$ rpm, $\eta = 89\%$. The outer runner diameter is $D_1 = 6.75$ m. As pumps, their parameters are $H = 62.5$ m, $N = 75,000$ kw, $n = 105$ rpm, $\eta = 90\%$.

D. P. Deriaz /104/ adapted [his] diagonal turbine (Figure V. 30) as a reversible unit pump-turbine at the Sir Adam Beck-Niagara HEP. The unit rating is: $H = 12.1$ to 27.4 m, turbine output $N = 33,500$ kw; pump-capacity $N = 47,800$ kw, discharge $Q = 1,386$ m^3/sec, speed $n = 92.3$ rpm, and maximum runner diameter (with the blades open) 6.3 m. The turbine has no distributor.

Owing to the adjustable runner blades, high efficiencies are attained within a wide range of heads, with a single rotational speed.

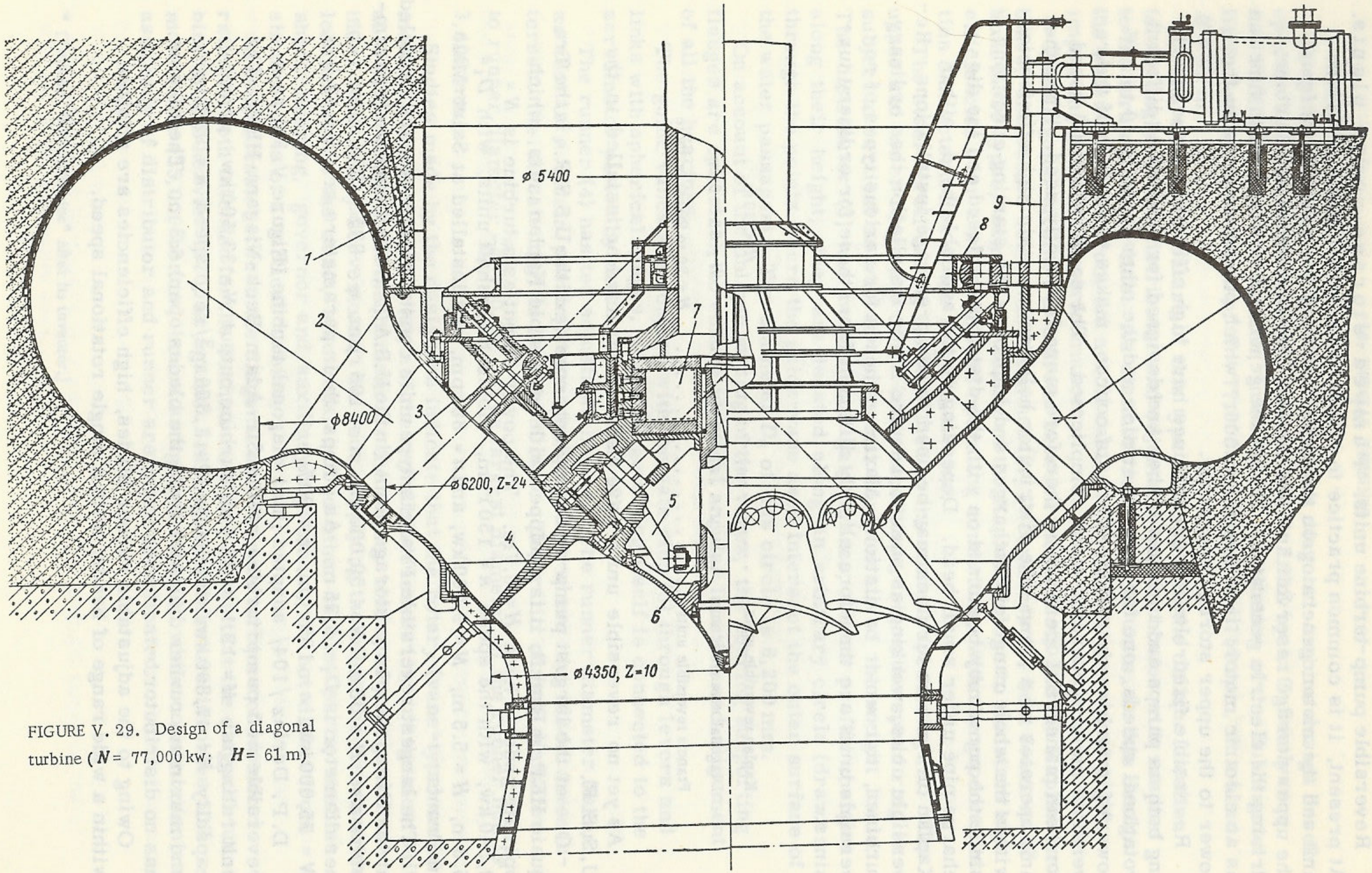


FIGURE V. 29. Design of a diagonal turbine (N = 77,000 kw; H = 61 m)

A ring-shaped rotary servomotor (4), with a turning angle of 52°, was provided to turn the blades (5), set at 45°. Oil is supplied to the servomotor through the turning rod (3).

When the unit works as a turbine, the stay vanes (1) guide the incoming water flow toward the runner; when the unit operates as a pump, the kinetic energy is converted into a pressure head in the diffuser provided with flaps (6) to minimize losses. Bearing (2) is oil-lubricated.

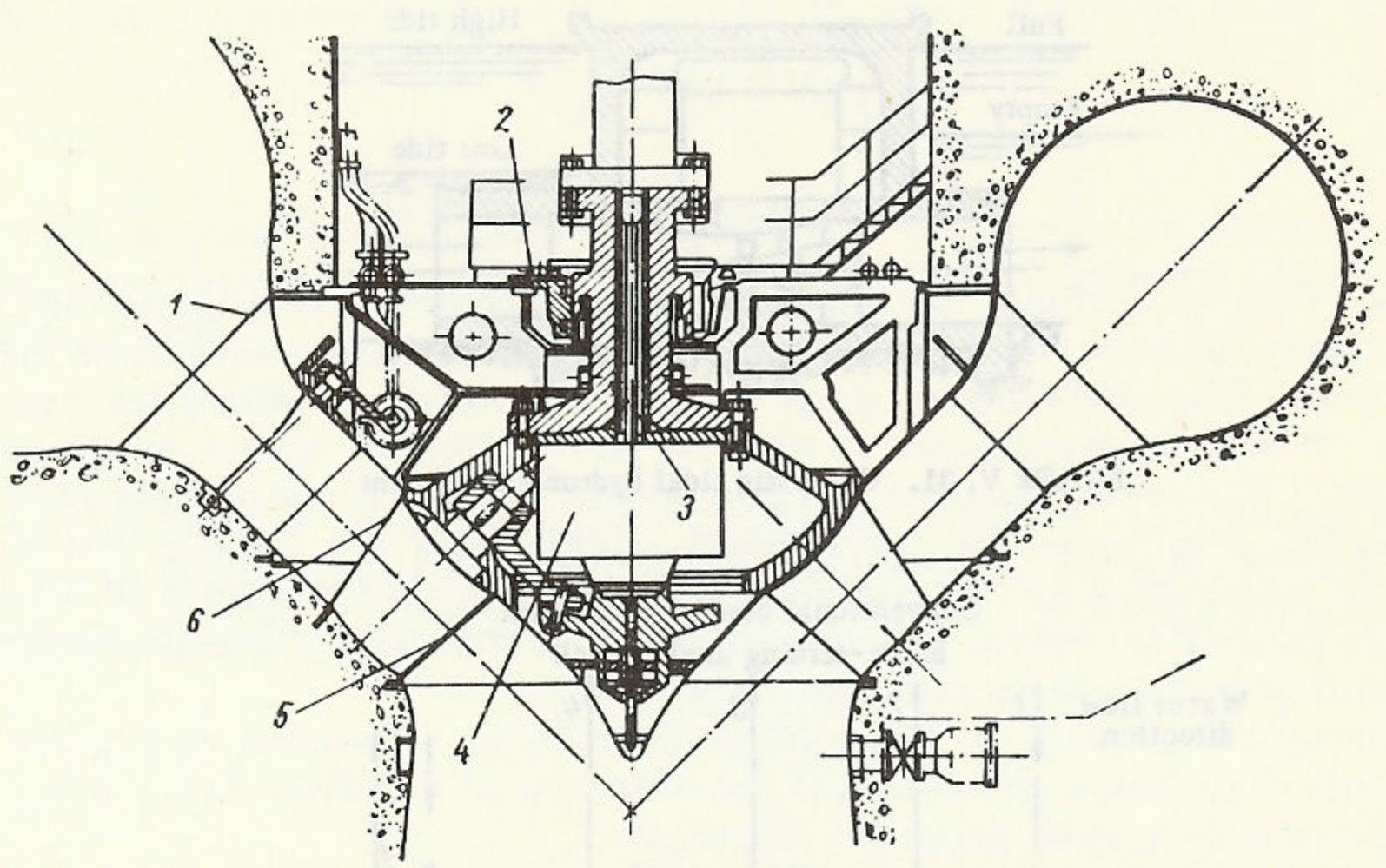


FIGURE V. 30. Reversible pump-turbine unit, installed at the Sir Adam Beck–Niagara Power Plant, N_{turb} = 33,500 kw

Tidal hydroelectric plants. The natural fluctuation of tidal energy is illustrated by a broken sine curve. This energy fluctuates over a period of fourteen days, reaching maximum values at full moon and new moon nine times greater than in the first and last quarter. These irregularities are not suitable for energy conversion; L. B. Bernshtein (7) proposed an effective method of eliminating them by using a horizontal bulb-type Kaplan unit which operates as a reversible pump-turbine.

If, at night, with excess energy in the system, the unit is set to work as a pump (Figure V. 31), it may either pump the water out of the basin into the sea (during low tide), or fill the basin (when the tide is flowing in).

The water level in the basin may thus be lowered with respect to the sea level at low tide, or raised with respect to the sea level at high tide.

The additional quantity of water obtained in this way may be used to generate power at any time (for instance, at peak hours), regardless of the state of the tide. The horizontal bulb-type unit may also be used as a water discharge opening, with the generator disconnected and the blades at a suitable angle, for a quick equalization of water level when the tide is changing and the unit is switched over to operate as a pump.

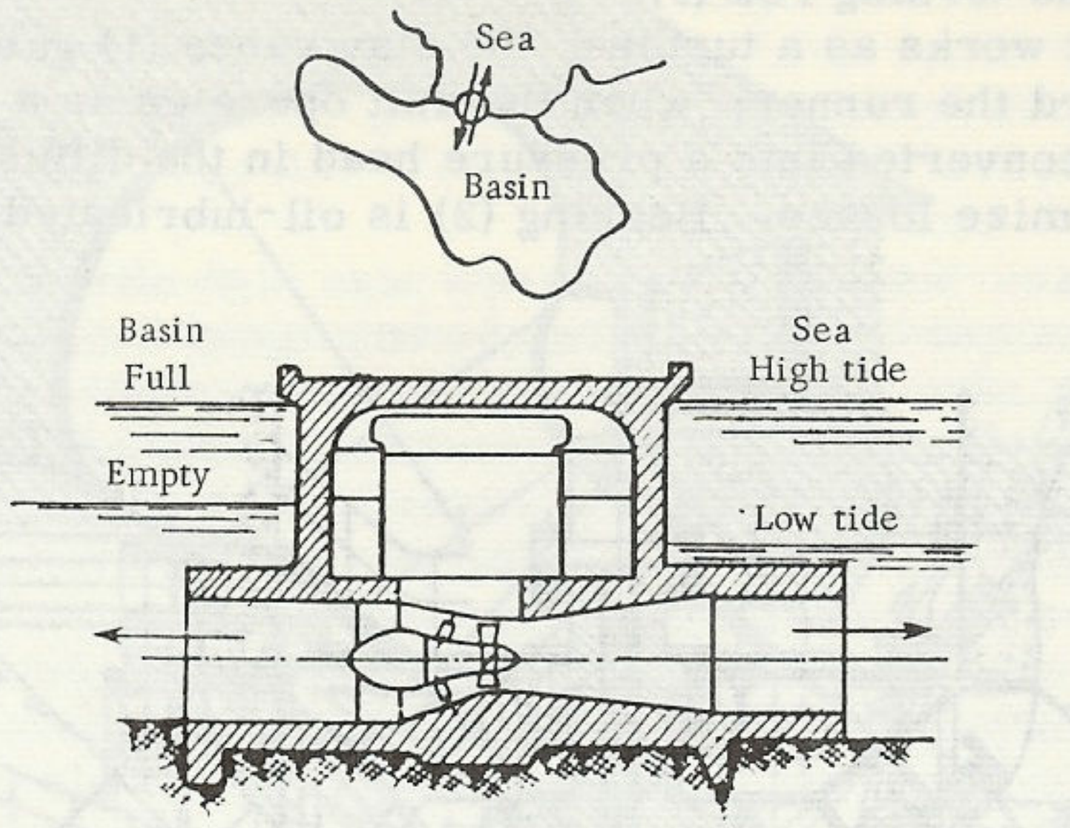


FIGURE V. 31. One-basin tidal hydroelectric plant

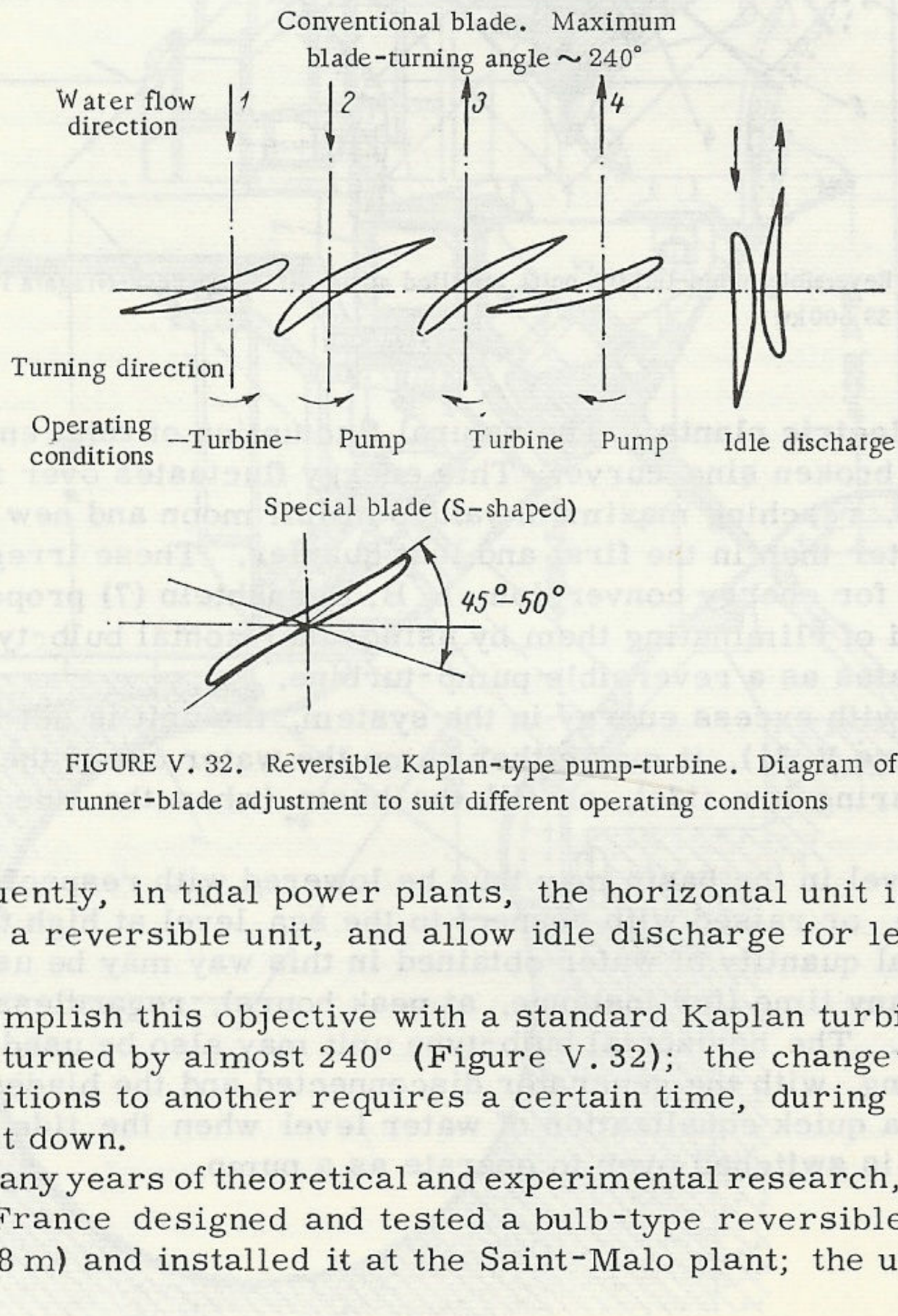


FIGURE V. 32. Reversible Kaplan-type pump-turbine. Diagram of runner-blade adjustment to suit different operating conditions

Consequently, in tidal power plants, the horizontal unit is required to operate as a reversible unit, and allow idle discharge for level equalization.

To accomplish this objective with a standard Kaplan turbine, the blades have to be turned by almost 240° (Figure V. 32); the change-over from one set of conditions to another requires a certain time, during which the turbine is shut down.

After many years of theoretical and experimental research, the "Neyrpic" Works in France designed and tested a bulb-type reversible unit (N = 9,000 kw, H = 5.8 m) and installed it at the Saint-Malo plant; the unit may be run

to suit different operating conditions: as a turbine, as a reversible pump-turbine and for idle discharge. A particular feature of the blade design is its S-shape, permitting flow along the curved blade tip and the convex blade side without impact losses under all conditions. The blades have to be turned by 50° only for adjustment to any operating conditions, and the transition from one type of operation to another (with the same direction of flow) is effected without stopping the unit.

Chapter VI

THE DISTRIBUTOR

30. TYPES AND DESIGNS OF DISTRIBUTORS

In the reaction turbine, the function of the distributor is to guide the incoming water stream toward the runner, and control the water flow through the turbine. The distributor guide vanes are arranged along its circumference. When the distributor is closed, admission of water to the runner is shut off. The water discharge through the turbine is also controlled by adjusting the position of the guide vanes. When they are turned, the direction of the water flow at the distributor exit changes (variation of $\alpha°$, Figure VI. 1). In Kaplan turbines, the discharge is controlled by simultaneous adjustment of guide vanes and runner blades.

The schematic layout of the radial distributor is shown in Figure VI.1 (plan view). The basic geometrical parameters of the distributor are:

1) distributor circle diameter D_0;

2) number of guide vanes z_0;

3) distributor height b_0 (not given in the figure);

4) guide vane (chord) length L, consisting of entrance length L_2 and exit length L_1; $(L = L_1 + L_2)$;

5) maximum vane thickness δ;

6) distance between the points where two neighboring vanes touch in their closed position L_0; the distances from the axis of vane-rotation to the points of contact are respectively L_{0_1} and L_{0_2}

$$L_0 \approx L_{0_1} + L_{0_2};$$

7) relative excentricity n_0, [is defined in equation (VI.23)]

$$n_0 = \frac{L_{0_1} - L_{0_2}}{2L_0};$$

8) shape of the vane profile (for the guide vane considered it is symmetrical);

9) ratio $\frac{L}{t}$ of the vane length to the vane pitch measured on the circle of diameter D_0;

10) diameter of the gate ring D_g [internal distributor diameter].

These parameters are constant for a given distributor design.

The variable parameter a_0 — the so-called distributor opening — represents the least distance between the trailing edge of one vane and the surface

of the neighboring vane and characterizes the position of the vanes during turbine regulation. The distributor opening a_0 depends on the turbine dimensions and on the number of guide vanes. During rotation of the guide vanes, usually carried out by a servomotor connected to the gate ring, the distributor opening a_0 changes and so does the cross-sectional area of the passages between the vanes.

However, the control of water discharge through the turbine is due not so much to variation of the discharge cross section of the distributor, but rather to the variation of the angle $\alpha°$.

In order to prove this, let us recall the basic equation of the turbine:

$$\eta g H = v_{u_1} u_1 - v_{u_2} u_2.$$

With an accuracy sufficient for practical purposes, we assume that the following relation is valid for the flow in the space between the distributor and the runner:

$$v_{u_0} r_0 = v_{u_1} r_1. \tag{VI. 1}$$

Let us further assume that the radial velocities v_{r_0} at the distributor exit, and the meridian velocities at the runner exit v_{m_2} have a uniform distribution over the cross section and may be calculated from the formulas

$$\left.\begin{aligned} v_{r_0} &= \frac{Q}{2\pi r_0 b_0}; \\ v_{m_2} &= \frac{Q}{F_2}, \end{aligned}\right\} \tag{VI. 2}$$

where F_2 is the entrance cross-sectional area of the runner. By inserting the values of the velocities in the turbine equation and considering the relations in the velocity triangles, we obtain

$$v_{u_1} = \frac{r_0}{r_1} v_{u_0} = \frac{r_0}{r_1} v_{r_0} \cot\alpha_0 = \frac{Q}{2\pi r_1 b_0} \cot\alpha_0; \tag{VI. 3}$$

$$v_{u_2} = u_2 - v_{m_2} \cot\beta_2 = u_2 - \frac{Q}{F_2} \cot\beta_2. \tag{VI. 4}$$

After transformation, we obtain

$$Q = \frac{\frac{\eta g H}{\omega} + u_2 r_2}{\frac{1}{2\pi b_0} \cot\alpha_0 + \frac{r_2}{F_2} \cot\beta_2}. \tag{VI. 5}$$

Consequently,

$$Q = f(b_0, \alpha_0, \beta_2).$$

In this way, any changes in the discharge at constant head and rotational speed may be carried out by modifying one of the following three

parameters:

1) the distributor height b_0;
2) the angle of water flow at the distributor exit α_0;
3) the angle of water flow at the runner exit β_2.

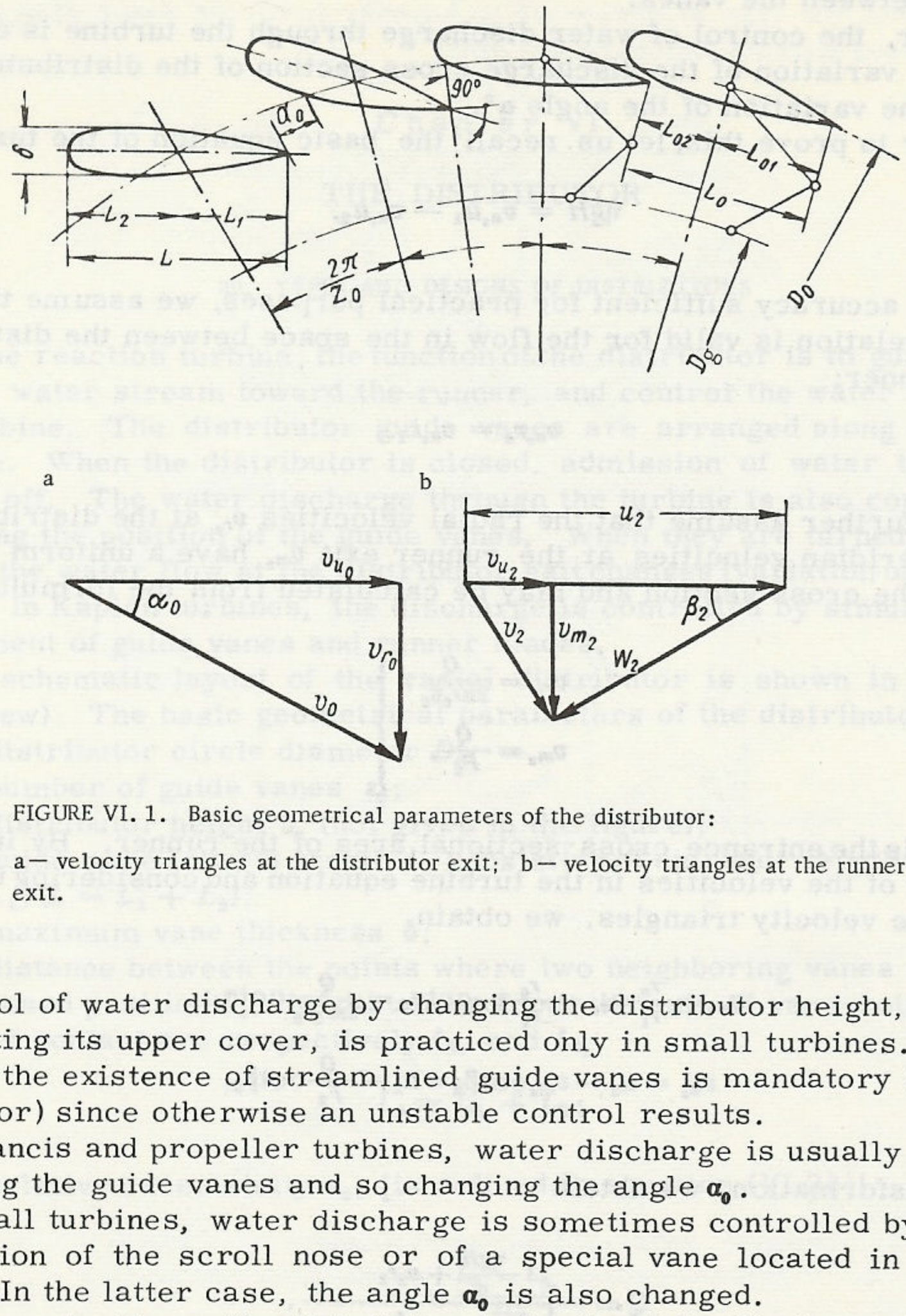


FIGURE VI. 1. Basic geometrical parameters of the distributor:

a — velocity triangles at the distributor exit; b — velocity triangles at the runner exit.

Control of water discharge by changing the distributor height, achieved by adjusting its upper cover, is practiced only in small turbines. In this method, the existence of streamlined guide vanes is mandatory (for a fixed distributor) since otherwise an unstable control results.

In Francis and propeller turbines, water discharge is usually controlled by turning the guide vanes and so changing the angle α_0.

In small turbines, water discharge is sometimes controlled by varying the position of the scroll nose or of a special vane located in the scroll casing. In the latter case, the angle α_0 is also changed.

In Thoma turbines, the distributor is fixed and the discharge is controlled by adjusting the runner blades, i.e., by changing the angle β_2. Such turbines are not common.

In Kaplan turbines, the water discharge is controlled by the simultaneous adjustment of the guide vanes and runner blades, i.e., by the variation of α_0 and β_2.

Frictional losses during the flow of water through the distributor are negligible compared with losses of head during the admission of water into the distributor. Such losses markedly affect distributor efficiency. To

reduce them the scroll casing and the distributor should be designed so that the angle of attack, i.e., the angle between the flow-velocity vector inside the scroll casing and the tangent to the vane profile at its leading edge is as small as possible within the most important range of operating conditions.

Guide vanes of different profiles are shown in Figure VI. 2:

1) "negative" curvature, convex toward the turbine axis (Figure VI, 2, a);

2) symmetrical profile (Figure VI. 2, b);

3) "positive" curvature, concave toward the turbine axis (Figure VI.2, c).

All these profiles are represented for the same distributor opening a_0 but with different angles $\alpha°$.

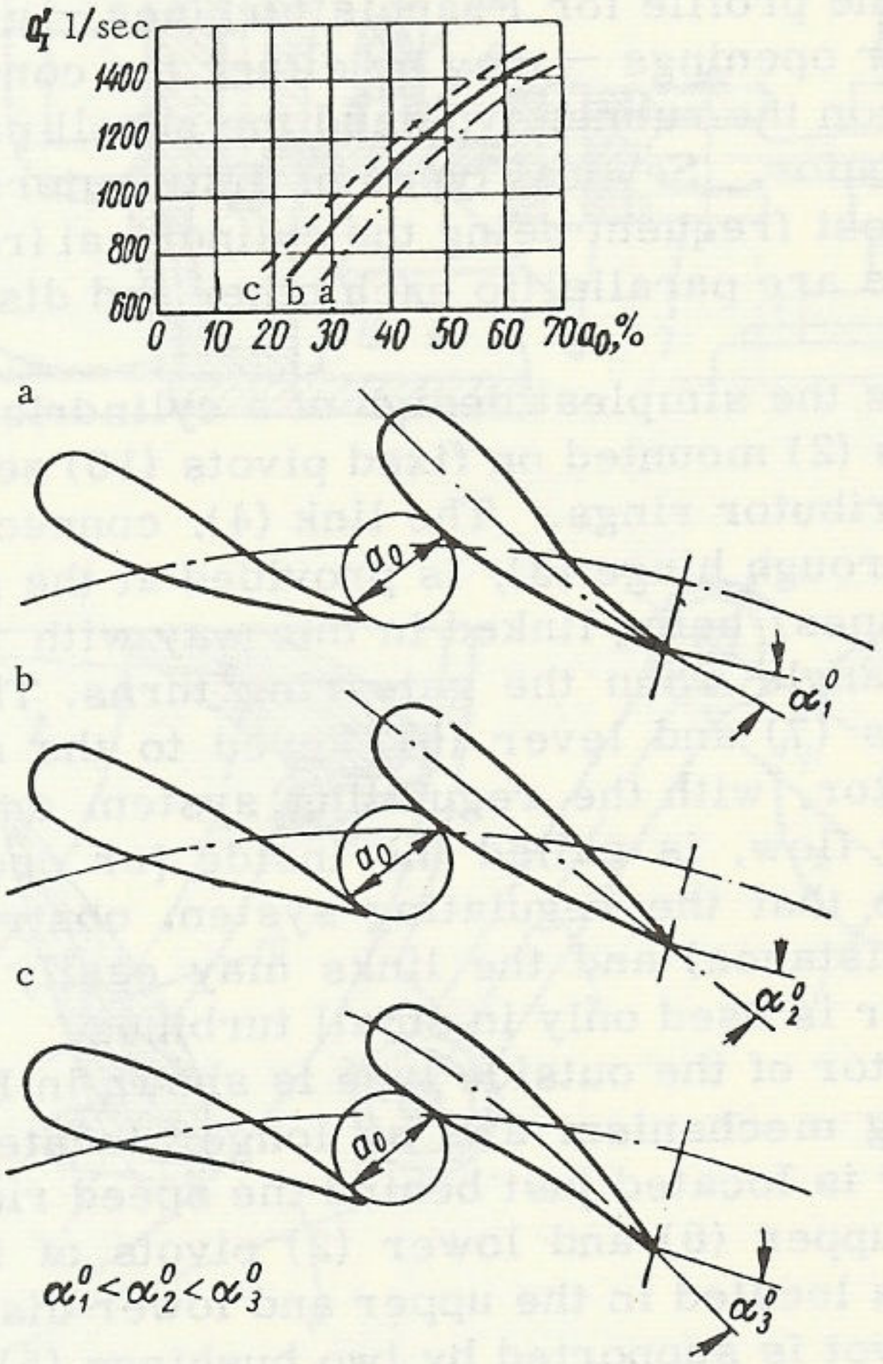


FIGURE VI.2. Change in unit discharge Q_I' for distributors with different vane profiles:
a—negative vane curvature; b—symmetrical vane profile; c—positive curvature.

The concave profile shows the greatest angle $\alpha°$. As shown in Figure VI. 2, guide vanes with the same opening a_0, but of different profile, have different discharge capacities. The distributor with concave-profile vanes and maximum angle $\alpha°$, also has the greatest discharge capacity. For instance, a 50 percent opening of the convex-profile distributor allows a unit discharge of 1200 liter/sec, the symmetrical profile of 1300 liter/sec, and the concave profile of 1380 liter/sec.

In most medium-speed turbines, the water flow undergoes excessive rotation at the scroll exit, so that the distributor has to straighten the flow. Guide vanes with positive curvature, having their concavity toward the turbine axis, are better suited in this case.

In open-flume turbine installation, where the water flow is almost radial, convex guide vanes (with "negative" curvature) are more advisable, since they impart an additional rotation to the flow.

The best solution for Kaplan turbines with semi-scroll casings would be to use guide vanes of two different profiles — convex for the open part and concave inside the scroll. Considerations of design, however, render this inadvisable. The intermediate profile is therefore usually employed in high-speed Kaplan turbines; the symmetrical guide-vane profile is also convenient from the design standpoint.

The best guide-vane profile for Francis turbines — usually operated with small distributor openings — may be either the convex or the concave profile, depending upon the runner type and the scroll parameters.

Cylindrical distributor. Several types of distributors are in common use nowadays, the most frequent being the cylindrical (radial) distributor, where the guide vanes are parallel to each other and distributed along a cylindrical surface.

Figure VI. 3 shows the simplest design of a cylindrical distributor, consisting of guide vanes (2) mounted on fixed pivots (10) secured to the upper (1) and lower (9) distributor rings. The link (4), connected to the vane and to the gate ring (8) through hinge (3), is provided at the guide-vane bottom end. All the guide vanes, being linked in this way with the gate ring, are adjusted to the same angle when the gate ring turns. The latter is turned by means of the rods (7) and lever (6), keyed to the actuating shaft (5). This kind of distributor, with the regulating system on the vanes placed directly in the water flow, is called the inside [or open-flume] type. Its disadvantages are that the regulating system obstructs the water flow (as an additional resistance) and the links may easily corrode. Hence, this kind of distributor is used only in small turbines.

A modern distributor of the outside type is shown in Figure VI. 4. The parts of the actuating mechanism are no longer located in the water flow. The distributor is located just behind the speed ring composed of stay vanes (3). The upper (8) and lower (2) pivots of the guide vane (4), are guided in bearings located in the upper and lower distributor rings (6) and (1). The upper pivot is supported by two bushings (5) made either of bronze or of wood plastics and mounted in the distributor socket (7). The lever (9) is fitted on the upper end of the upper pivot; through the link (10), the lever is articulated to the gate ring (11) mounted on top of the turbine cover-plate (12). Connection with the distributor servomotor is provided by a rod.

This design is widely used, although it is not applicable to every shape of the turbine water passages.

Conical distributor. A conical distributor with the guide-vane axes forming a conical surface is shown in Figure VI. 5. The lower ring (2) of the conical distributor must invariably be removable, to allow the mounting and removal of the inclined vanes (4). The foundation ring (1) is located below the lower ring. The dimensions of this ring depend on the stay vanes (3). The guide vane has upper and lower pivots, guided in bearings. The upper bearing (6) is mounted in the cover plate (5). Lever (9) is mounted on the

upper pivot (7) of the guide vane; it is connected by a system of links and hinges with the gate ring (8) driven by a servomotor.

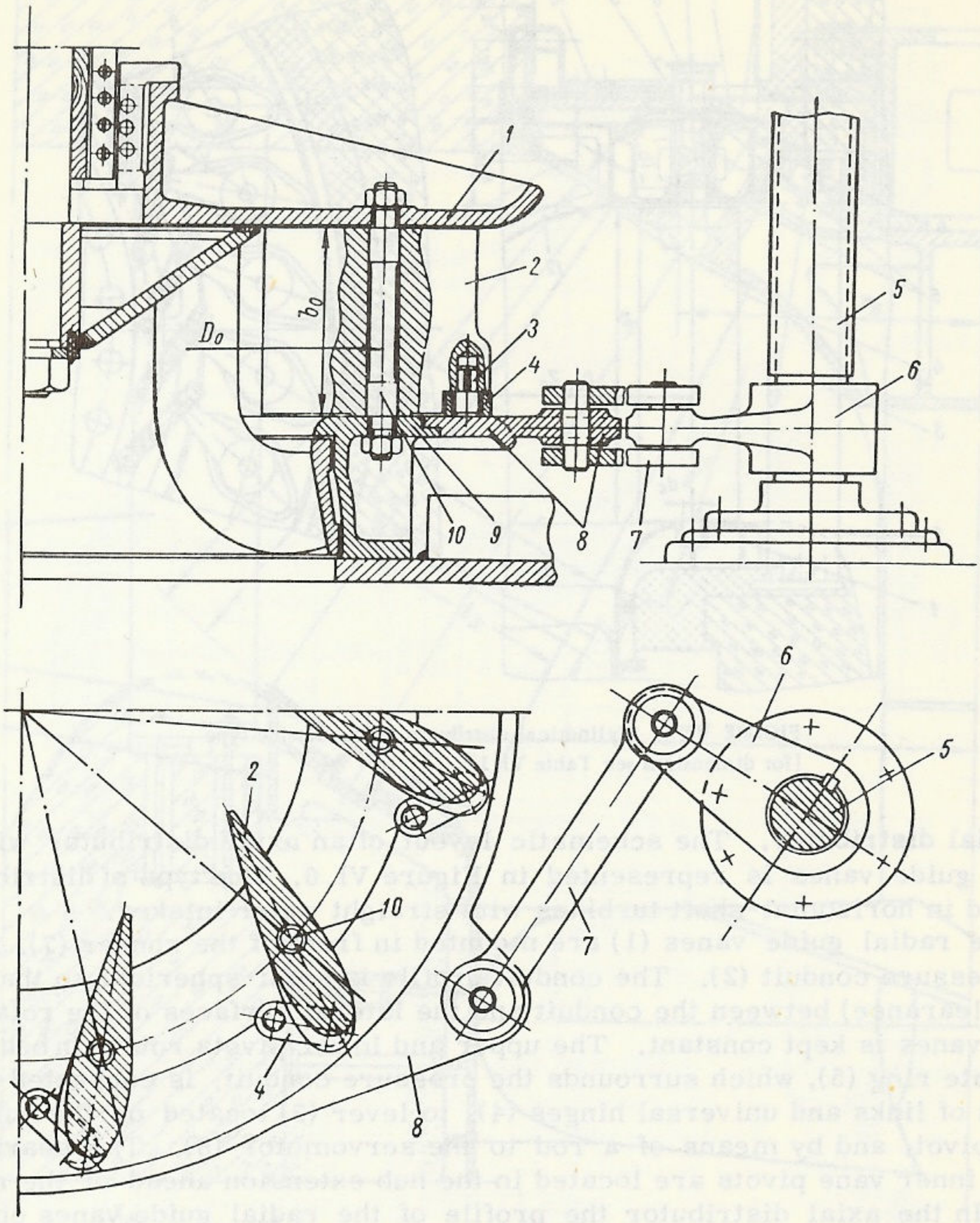
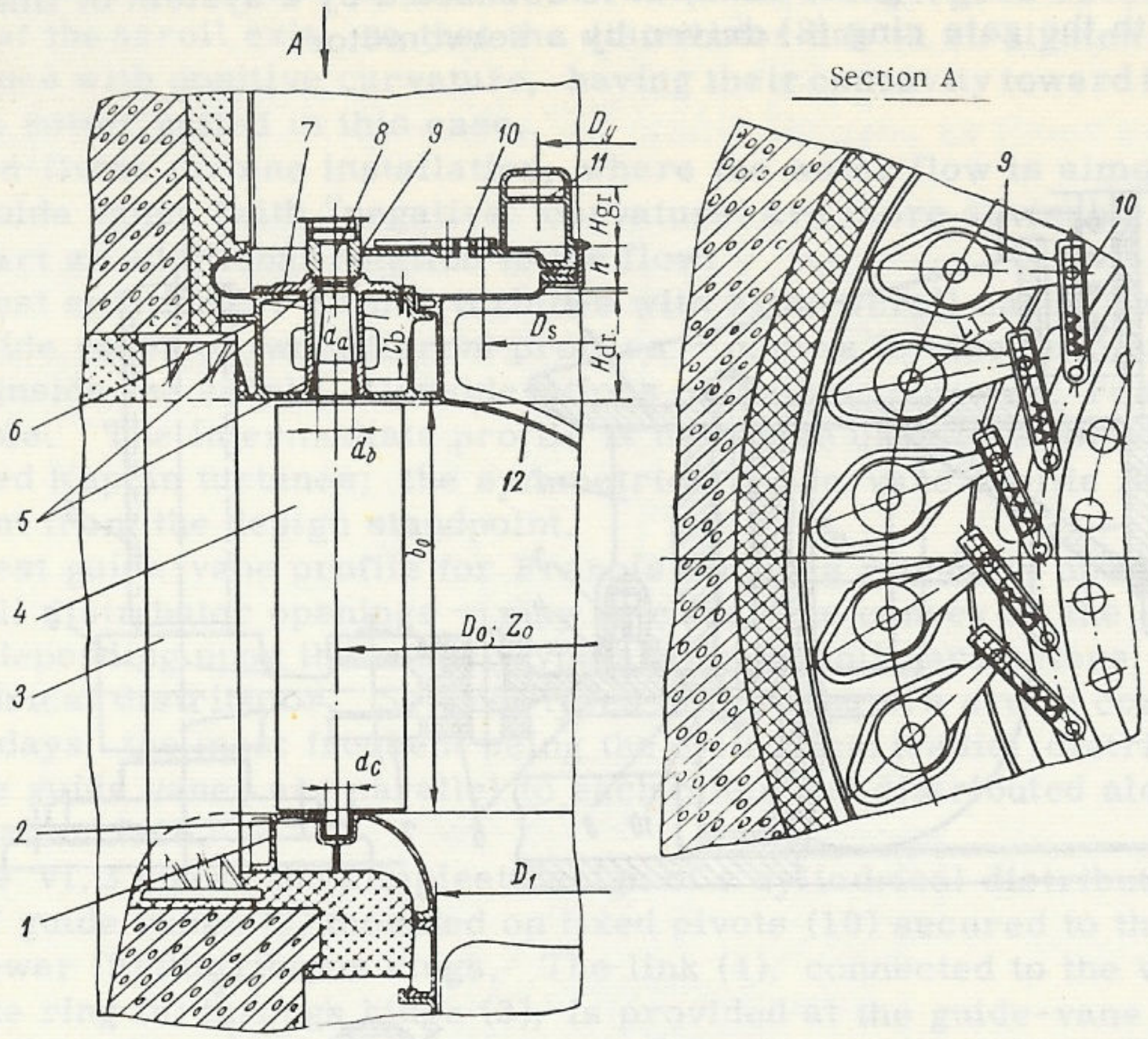


FIGURE VI.3. Cylindrical distributor of the inside type

Owing to the inclined position of the guide vanes, the conical distributor is smaller than the cyclindrical. However, since the profile of the inclined vane changes along its height, the inclined position of the vanes involves constructional difficulties, due to the need for universal hinges, for the vanes whose profile changes with length.

The lateral surfaces of the vanes and the mating surfaces on the distributor rings should be spherical. With the conical distributor, the assembly and dismantling of parts is quite complicated, but its weight is smaller than that of a cylindrical distributor.



Section A

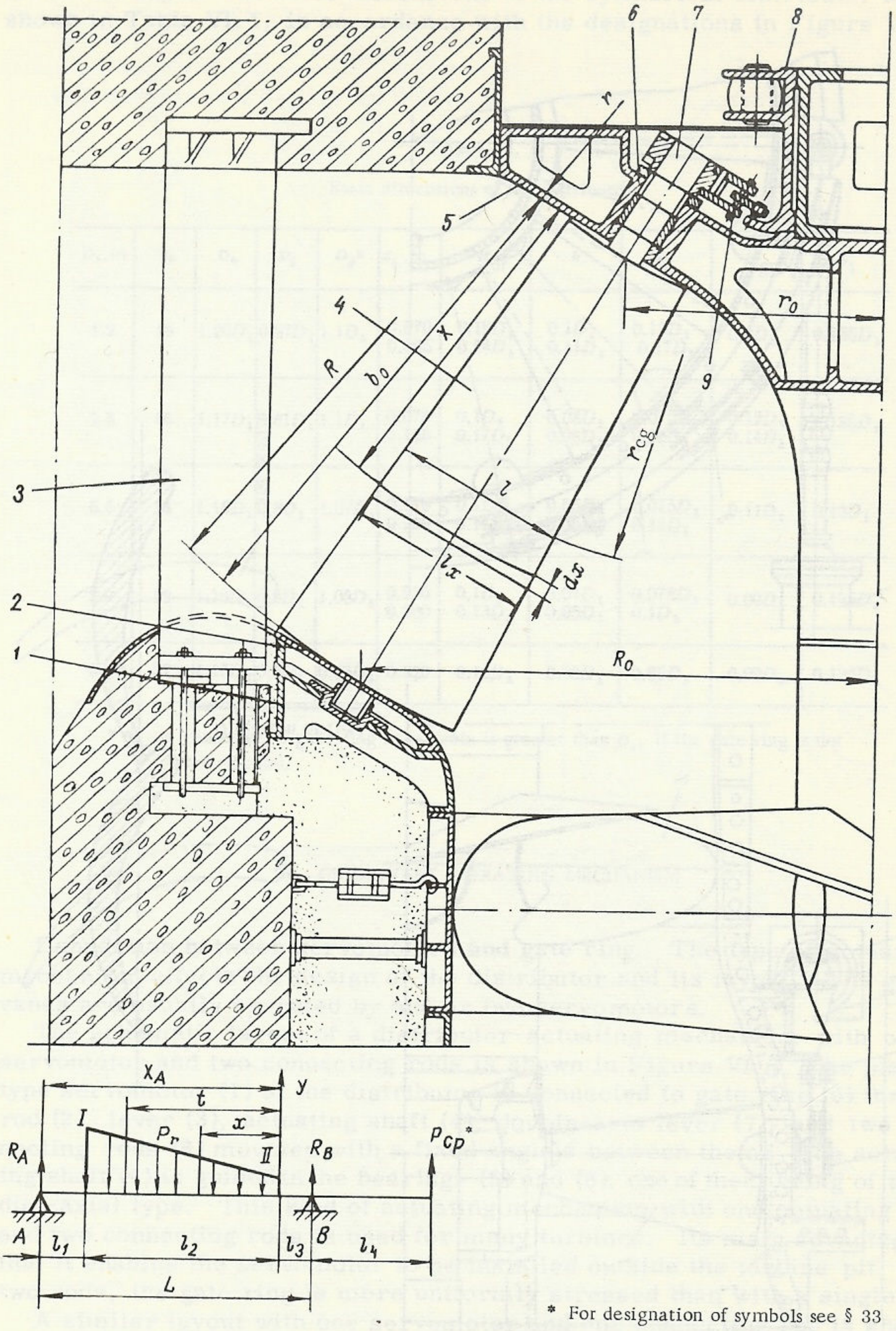
FIGURE VI.4. Cylindrical distributor of the outside type
[for dimensions see Table VI.1]

Axial distributor. The schematic layout of an axial distributor with radial guide vanes is represented in Figure VI.6. This type of distributor is used in horizontal-shaft turbines with straight water intakes.

The radial guide vanes (1) are mounted in front of the runner (7), inside the pressure conduit (2). The conduit profile is semi-spherical so that the gap (clearance) between the conduit and the lateral surfaces of the rotating guide vanes is kept constant. The upper and lower pivots rotate in bearings. The gate ring (5), which surrounds the pressure conduit, is connected by means of links and universal hinges (4), to lever (3) located on the outer vane pivot, and by means of a rod to the servomotor (6). The bearings of the inner vane pivots are located in the hub extension ahead of the runner. In the axial distributor the profile of the radial guide vanes changes along the radius. Flat vanes are most simple in design, but do not permit high turbine performance. Twisted vanes are the most effective, provided they also permit tight closing, i.e., the edges of two adjacent vanes should be able to make close contact with each other. The axial distributor has smaller dimensions and weight than cylindrical and conical distributors.

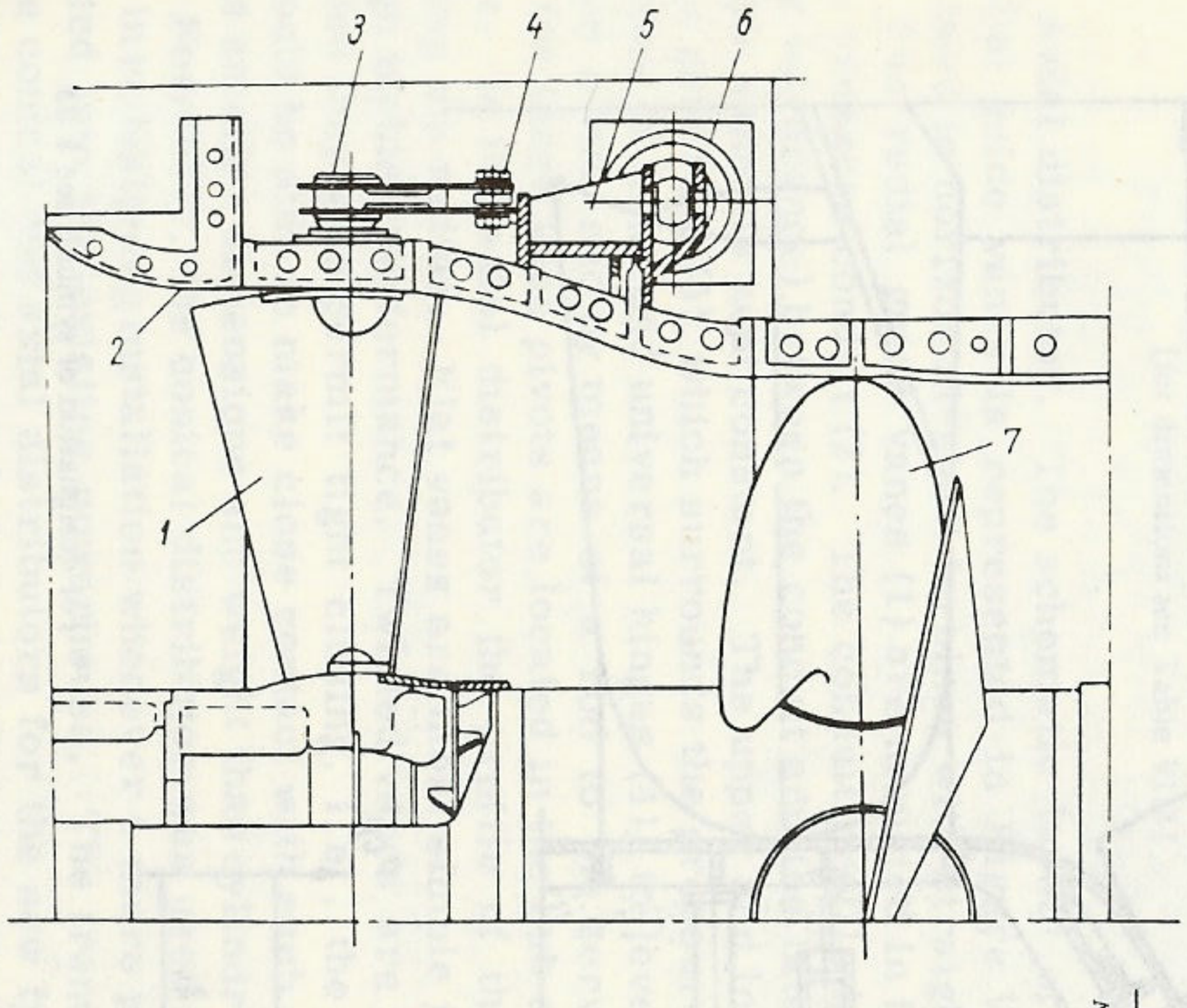
Formerly, the conical distributor was used only in special cases, such as in redesigning installation whenever a more powerful turbine had to be fitted into the existing powerhouse. The trend in modern practice is to use conical and axial distributors for the new types of diagonal and horizontal turbines, such as tubular, semitubular, bulb-type, and so on.

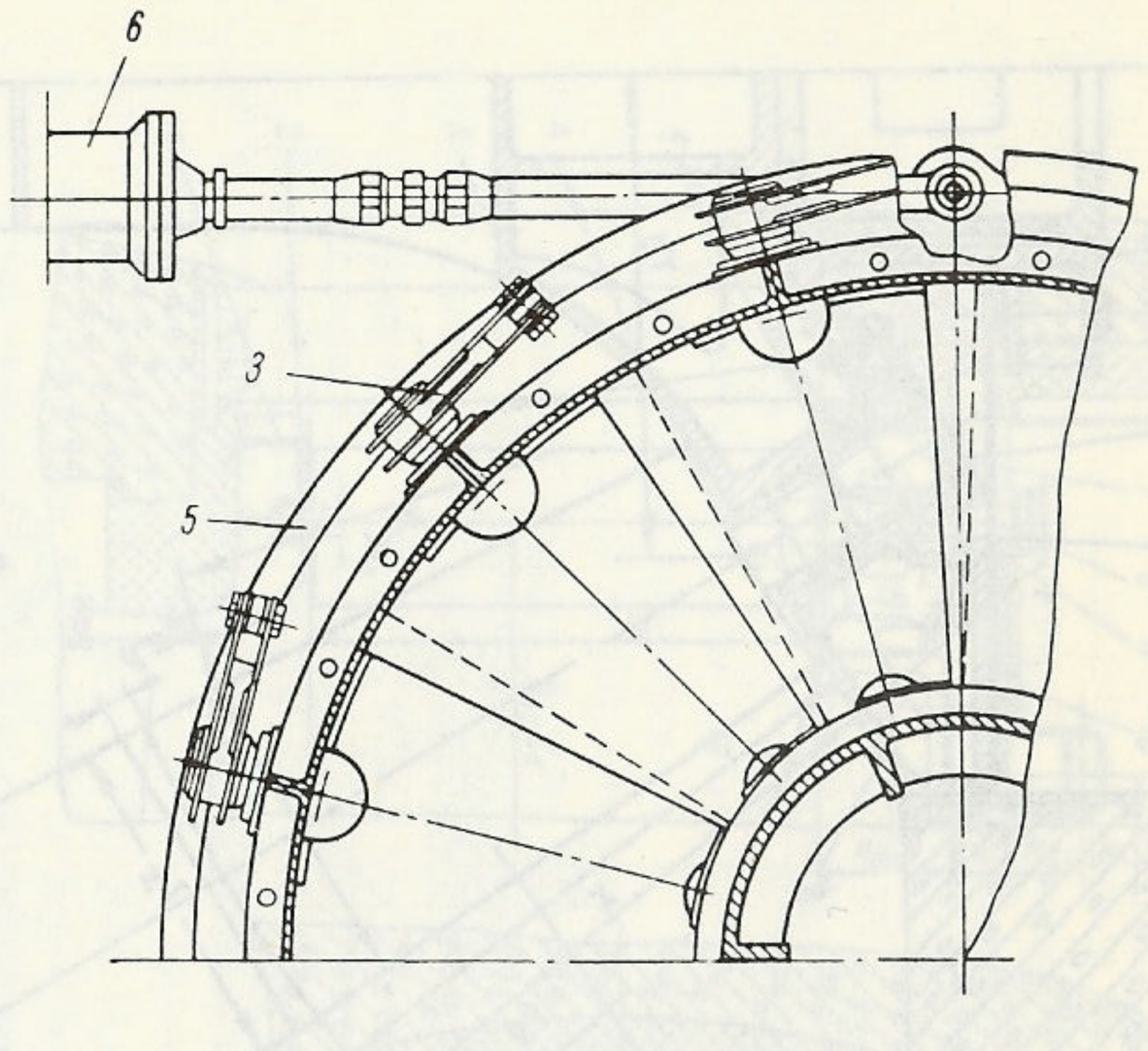
For the cylindrical distributor, the most commonly used layouts, designs, and methods of calculation are considered in detail below.



* For designation of symbols see § 33

FIGURE VI. 5. Conical distributor





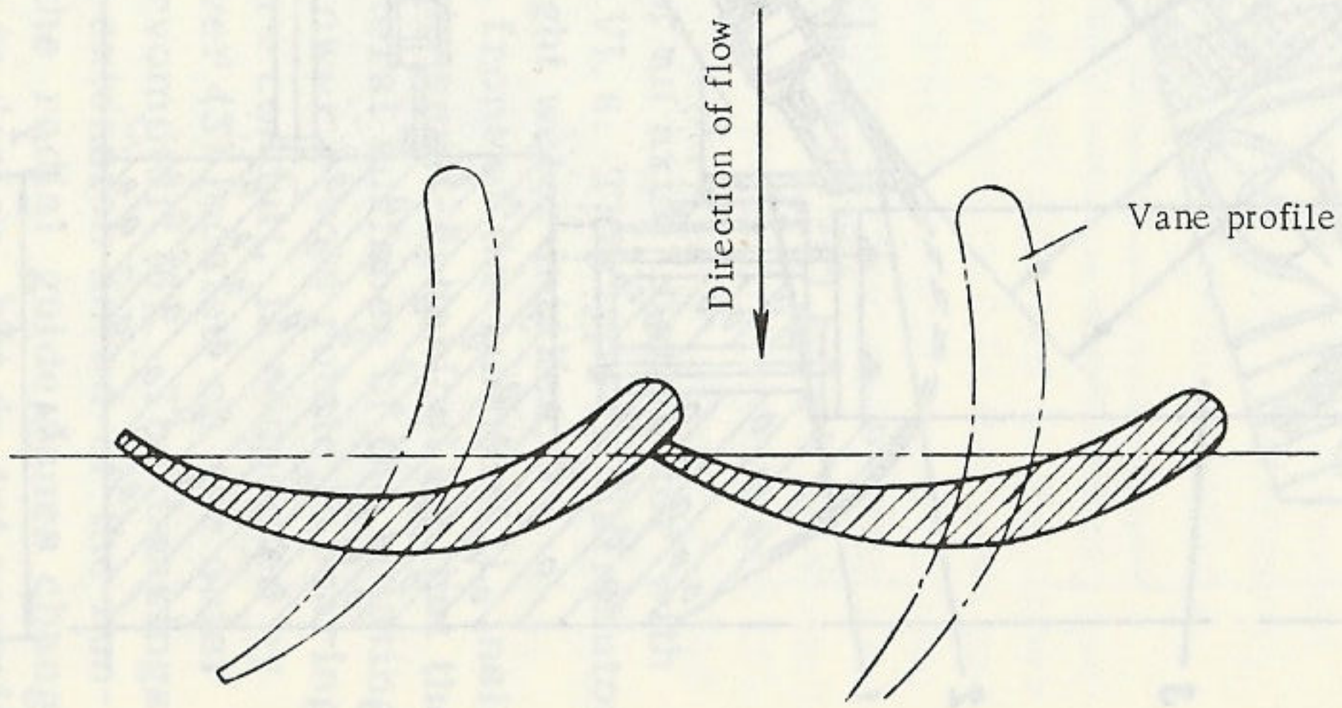


FIGURE VI. 6. Axial distributor

The distributor parts for various types of turbines have been standardized at the LMZ. The basic dimensions of the cylindrical distributor are shown in Table VI. 1, in accordance with the designations in Figure VI. 4.

TABLE VI. 1

Basic dimensions of the distributor

D_1, m	z_0	D_0	D_s	D_y*	d_b, m	H_{dr}	h	l_b	H_{gr}	L_1
1.2	16	$1.20D_1$	$0.87D_1$	$1.1D_1$	0.070 0.085	$0.19D_1$ $0.24D_1$	$0.1D_1$ $0.11D_1$	$0.13D_1$ $0.17D_1$	$0.2D_1$	$0.135D_1$
2.5	16	$1.17D_1$	$0.81D_1$	$1.1D_1$	0.078 0.125	$0.1D_1$ $0.17D_1$	$0.05D_1$ $0.08D_1$	$0.075D_1$ $0.12D_1$	$0.12D_1$ $0.14D_1$	$0.135D_1$
5.5	24	$1.16D_1$	$0.8D_1$	$1.07D_1$	0.170 0.250	$0.1D_1$ $0.16D_1$	$0.05D_1$ $0.06D_1$	$0.075D_1$ $0.12D_1$	$0.11D_1$	$0.13D_1$
8.0	32	$1.16D_1$	$0.8D_1$	$1.03D_1$	0.230 0.300	$0.1D_1$ $0.13D_1$	$0.04D_1$ $0.05D_1$	$0.075D_1$ $0.1D_1$	$0.09D_1$	$0.125D_1$
9.3	32	$1.15D_1$	$0.8D_1$	$0.83D_1$	0.320	$0.12D_1$	$0.03D_1$	$0.85D_1$	$0.09D_1$	$0.122D_1$

* D_y = diameter of gate-ring eye-circle is greater than D_s, if the gate ring is not box-shaped.

31. GUIDE-VANE OPERATING MECHANISM

Connection between servomotors and gate ring. The type of actuating mechanism affects the design of the distributor and its layout. The guide vanes are usually operated by one or two servomotors.

The schematic layout of a distributor-actuating mechanism with one servomotor and two connecting rods is shown in Figure VI. 7. The piston-type servomotor (1) of the distributor is connected to gate ring (9) through rod (2), lever (3), actuating shaft (4), double-arm lever (7), and two connecting rods (8) mounted with a fixed angle α between them. The actuating shaft (4) is guided in the bearings (5) and (6), one of them being of the radial-axial type. This kind of actuating mechanism with one actuating shaft and two connecting rods is used for many turbines. Its main advantage is that it enables the servomotor to be installed outside the turbine pit. With two rods, the gate ring is more uniformly stressed than with a single rod.

A similar layout with one servomotor and one connecting rod is shown in Figure VI. 8. The servomotor (2) is mounted on the foundation plate (1) comprising the bearing (5). The actuating shaft (6) guided in the bearing is connected through lever (4) and rod (3) with the piston-type servomotor.

The lever (7), keyed to the lower end of the shaft, is connected to the gate ring (9) through the rod (8). This mechanism is installed at the Svir-III power-plant turbines supplied by the Swedish WK company. The disadvantage of this type of mechanism is that the gate ring is loaded unilaterally by a single rod, thus requiring proper guiding elements on the turbine cover-plate. In this design, the gate ring is guided by cylindrical rollers (10).

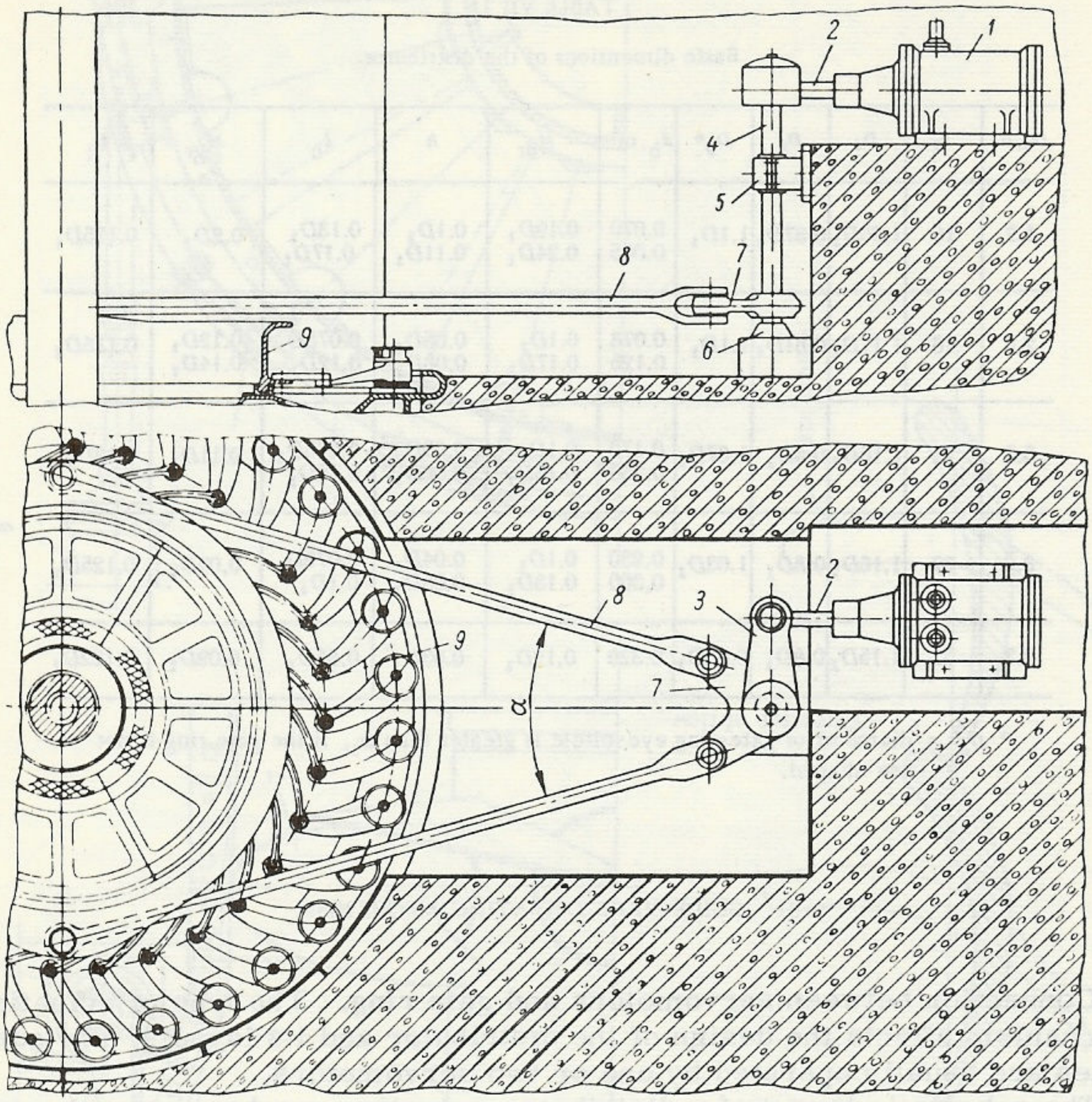


FIGURE VI.7. Schematic layout of distributor-actuating mechanism with one servomotor and two connecting rods

Figure VI.9 shows the schematic layout of an actuating mechanism with two servomotors connected directly to the gate ring. Both servomotors are arranged inside the steel casing (7) embedded in the turbine concrete pit. Each servomotor piston is connected through rod (2) and hinge (4) to gate ring (3). The gate ring is mounted on a special frame (8) on the turbine cover-plate (9). The gate ring is connected with the guide vanes through link (5) and lever (6). This actuating mechanism is extremely simple and is widely used in various countries; its main advantage is the existence of two connecting rods which operate on the principle of "couple of forces", permitting the gate ring to be made relatively small and to be easily guided on the cover plate.

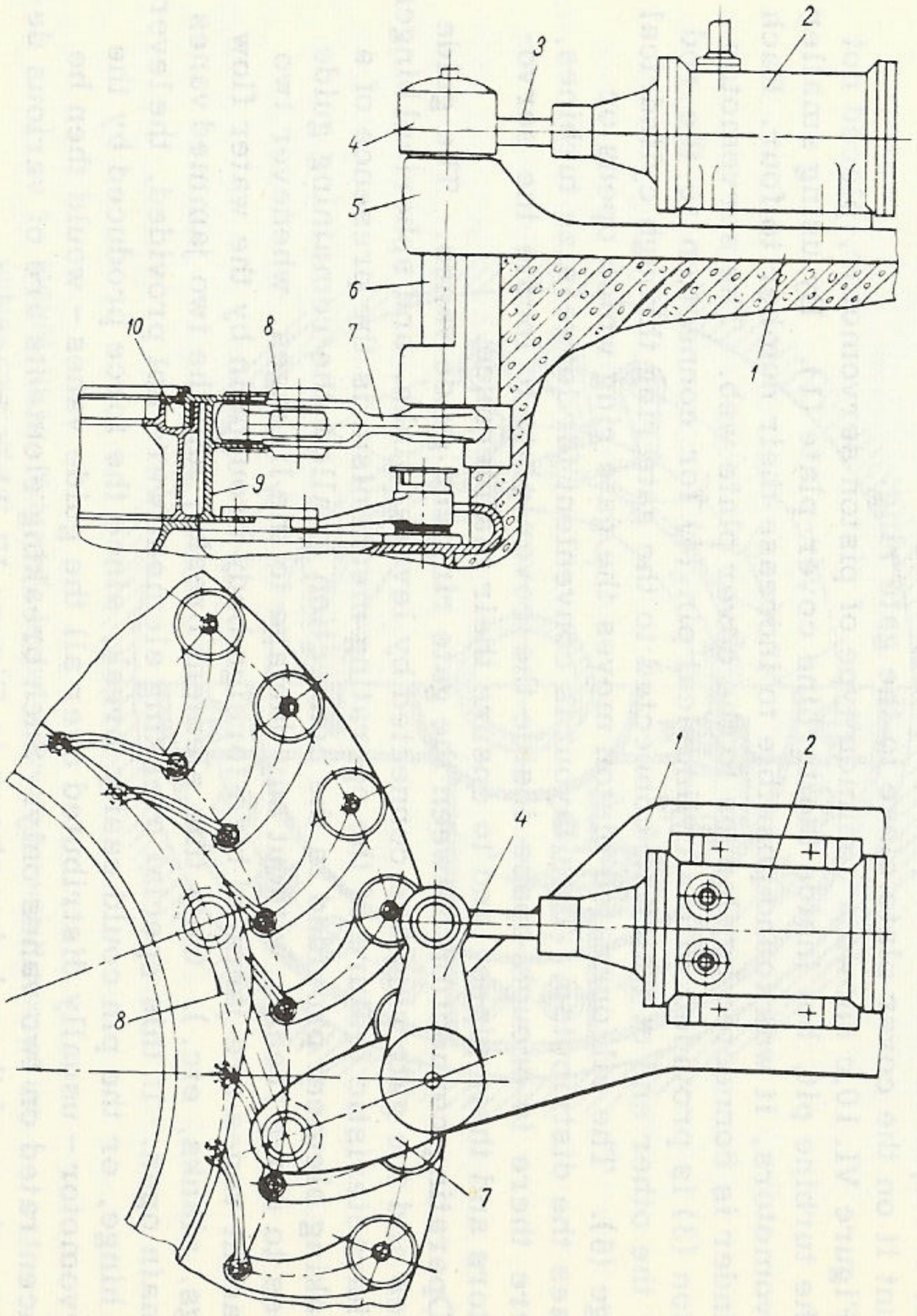


FIGURE VI.8. Distributor-actuating mechanism with one servomotor and one connecting rod

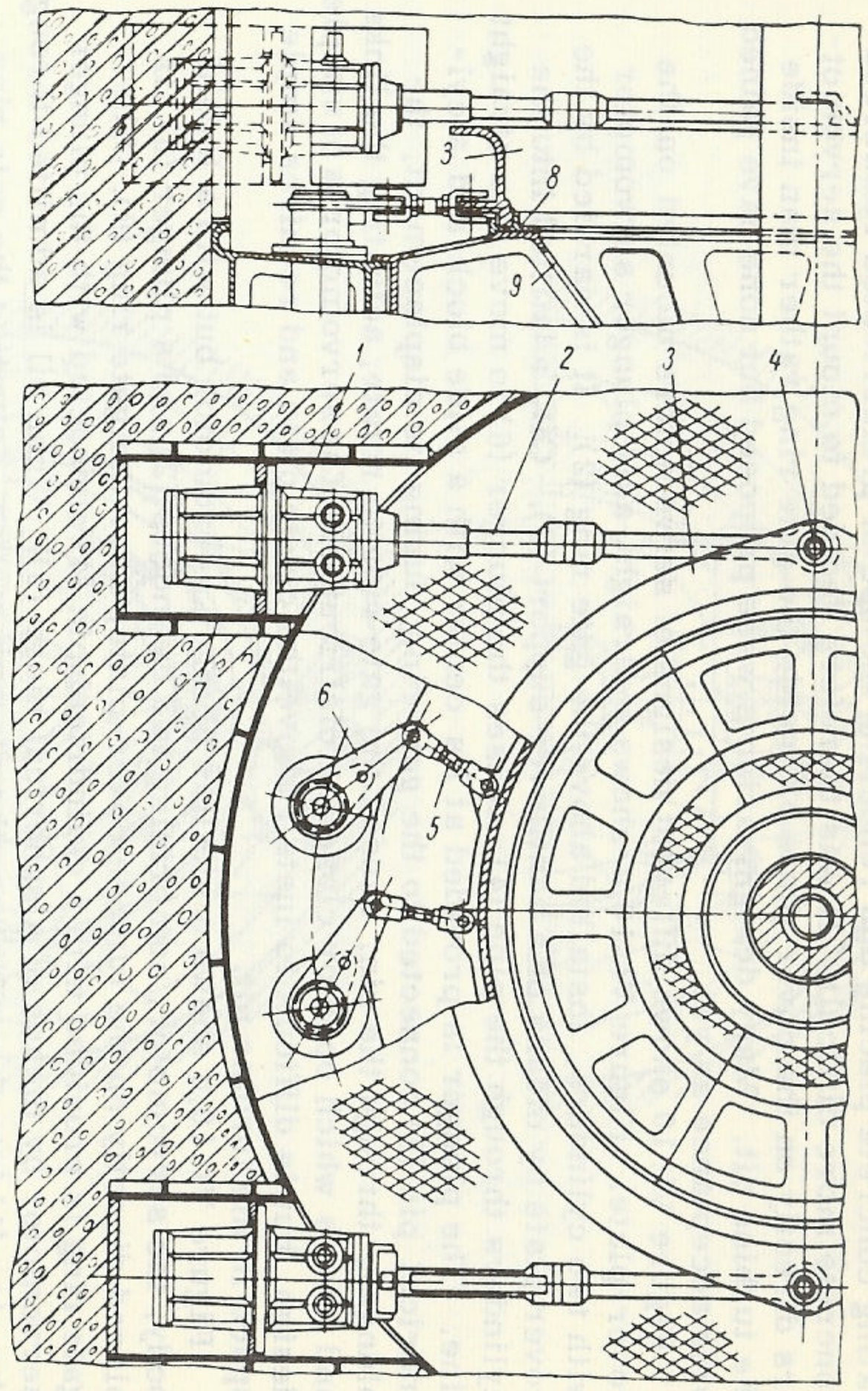


FIGURE VI.9. Distributor-actuating mechanism with two servomotors

Recently, this type of mechanism drew the criticism of powerhouse designers, since it requires special cavities in the concrete pit, thus complicating concrete placing and rendering the use of prefabricated reinforced concrete more difficult. It was therefore decided to mount the servomotors directly on the cover plate or inside the gate ring rather than inside the turbine pit. Many design variants were proposed but none have gained wide acceptance as yet.

Figure VI. 10 shows different designs of servomotors mounted on the cover-plate. Figure VI. 10,a shows a straight-axis plunger servomotor with two cylinders, installed above the gate ring (2). It is carried by the cover plate by means of a cantilever support (3). Oil, admitted into the cylinders through the pipe (4), causes the plunger (6) to move in a straight line. The plunger is provided at its center with a slide block and a cylindrical pin (5) connected to the gate ring; during its displacement, the plunger, through the pin, causes the gate ring to rotate, actuating the links and levers which open or close the distributor. The servomotor is of simple design, but is difficult to install above the cover plate and requires ample space in the turbine pit.

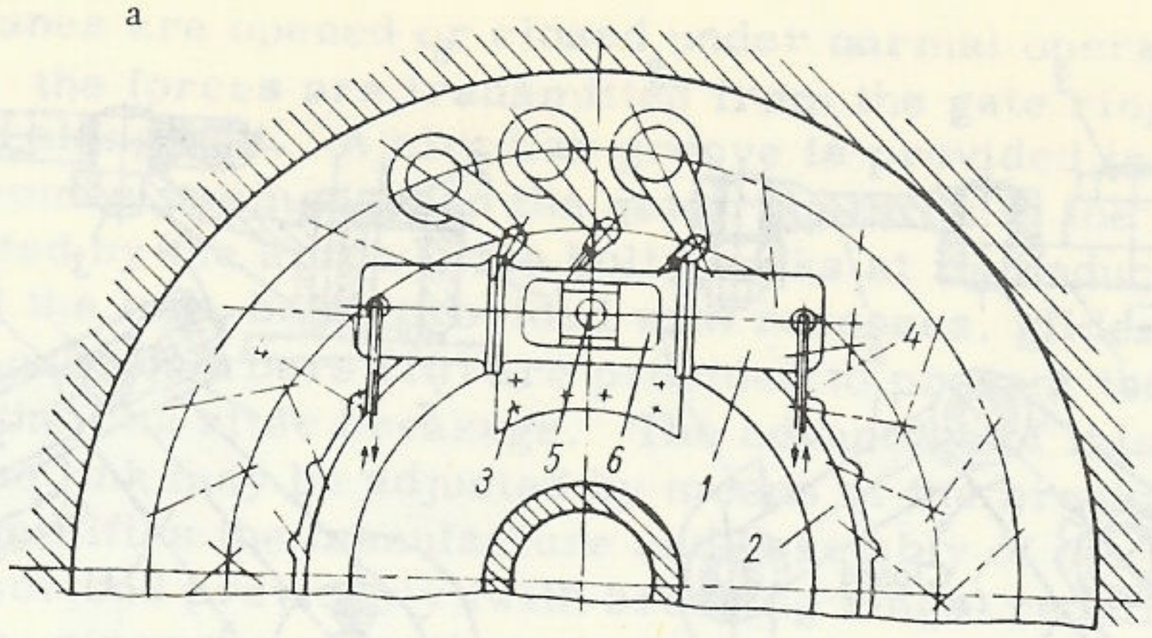
Figure VI. 10,b shows a similar plunger servomotor but with a toroid body; the servomotor, comprising two cylinders (2) and a plunger (3), is placed directly on the turbine cover-plate, near the gate ring (6). The gate ring is provided with a cylindrical pin (4) connected with the plunger servomotor by means of a spherical hinge (5). When oil is admitted through the pipe (1) into the cylinder, the plunger moves, actuating the gate ring which opens or closes the distributor.

It is more difficult to manufacture a toroid servomotor than a cylindrical, since it requires more complicated machining; it is, however, easier to mount it on the cover plate close to the gate ring.

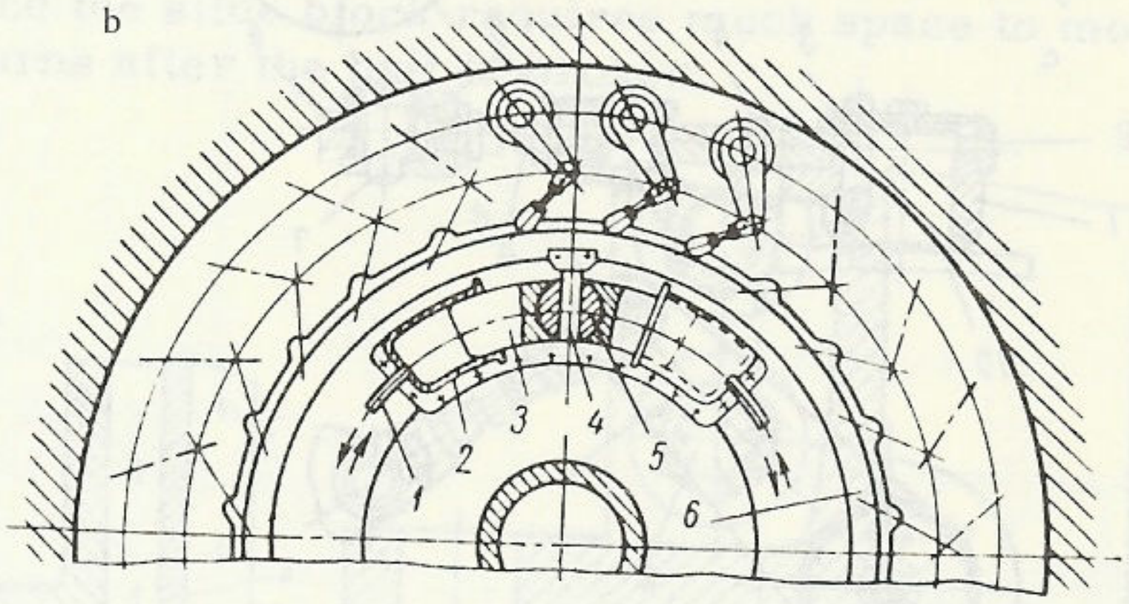
Figure VI. 10,c shows a common type of piston servomotor, placed not in the turbine pit, but inside the turbine cover-plate (1). By using smaller servomotors, it was found possible to increase their number to four. Each cylinder is connected by flanges to the cover plate web. The servomotor piston (3) is provided with a cylindrical pin (4) for connection to the rod (5), the other end of which is connected to the gate ring through cylindrical hinge (6). The oil-operated piston moves the gate ring which opens or closes the distributor. This layout is convenient for large-size turbines, where there is enough space inside the cover plate to locate the servomotors and their pipes, and to ensure their maintenance.

Operating connection between the gate ring and guide vanes. The guide vanes and the gate ring are connected by levers, links, and spherical hinges. A characteristic feature of the operating mechanism is the presence of a breaking element provided in the connection to allow the remaining guide vanes to close freely, without any damage to the linkages, whenever two adjacent vanes are jammed by a foreign body brought in by the water flow (logs, planks, etc.). Only this element breaks, and the two jammed vanes remain open. If this special breaking element were not provided, the lever, the hinge, or the pin could easily break, since the force produced by the servomotor – usually distributed over all the guide vanes – would then be concentrated on two vanes only. Such breaking elements are of various designs, three of them being shown in Figure VI. 11, a, b, and c.

a



b



c

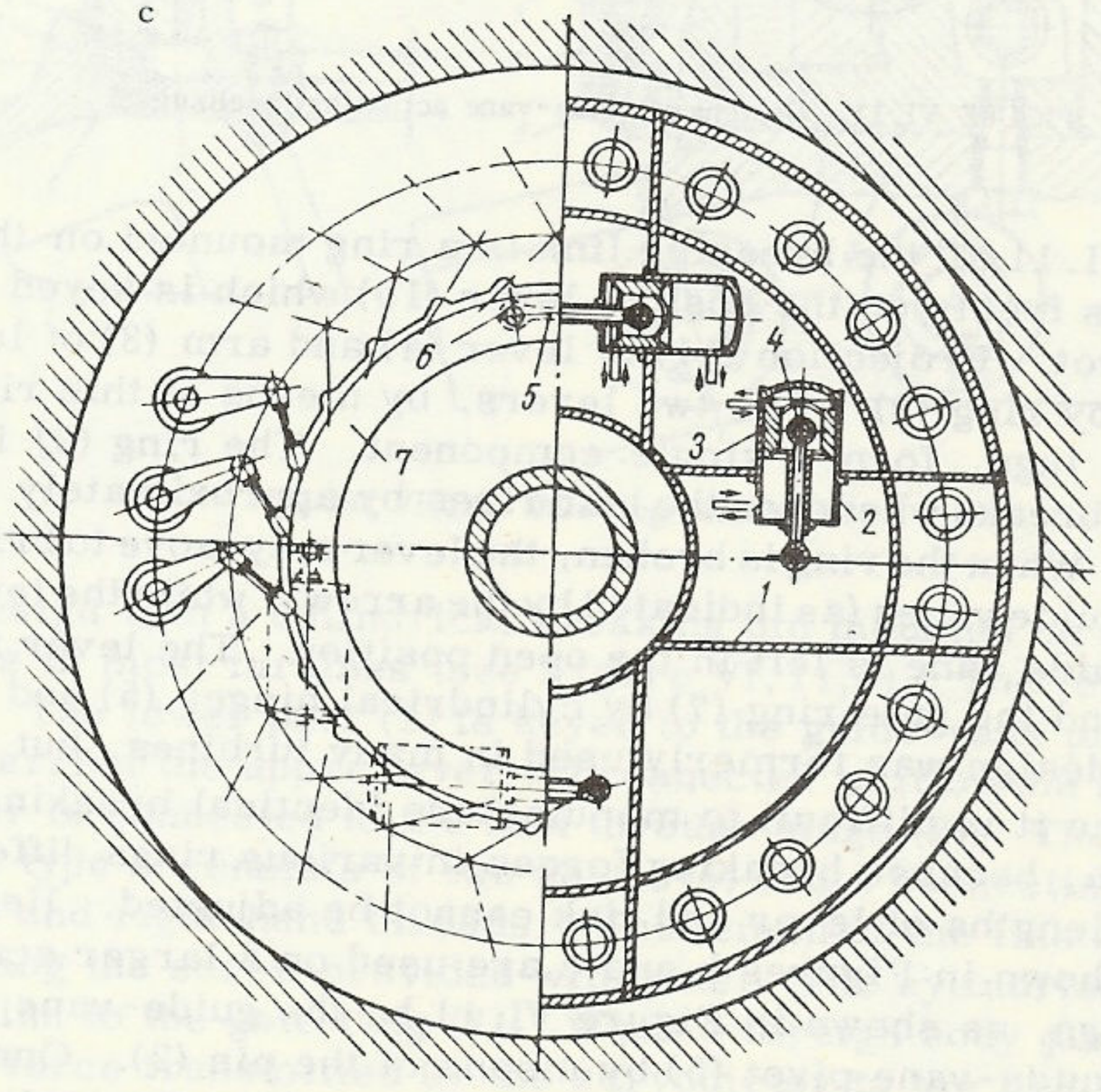


FIGURE VI.10. Schematic layout of servomotor installations on the turbine cover-plate:

a — straight-axis plunger servomotor; b — curved-plunger servomotor; c — piston servomotor, mounted inside the cover plate.

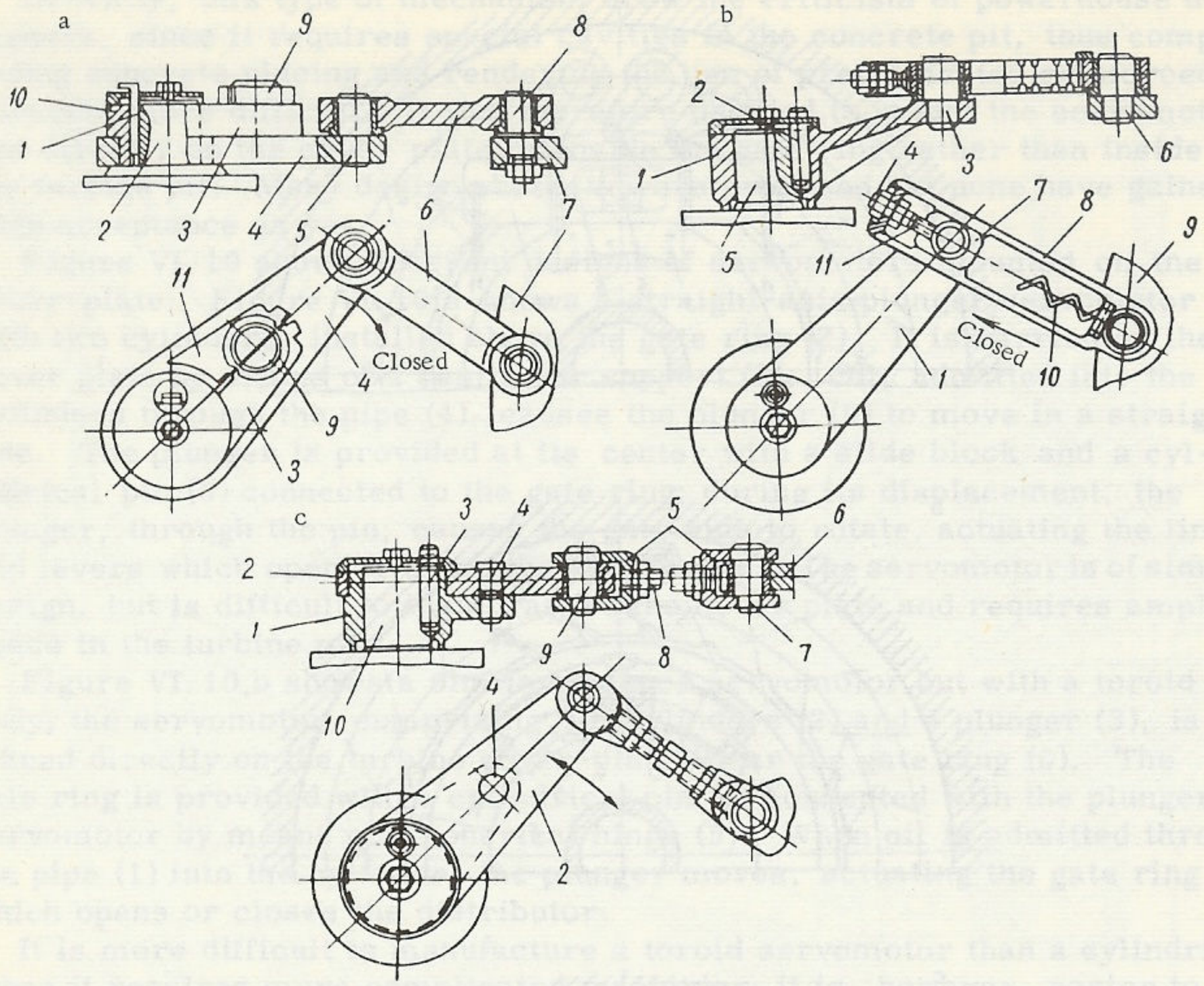


FIGURE VI.11. Designs of guide-vane actuating mechanisms

In Figure VI.11,a, the breaking link is a ring mounted on the lever. Lever (4) turns freely on the boss of lever (10) which is keyed to the upper guide-vane pivot. Projection (11) of lever (4) and arm (3) of lever (10) are held together by ring (9). The two levers, by means of this ring and the corresponding lugs, form a single component. The ring (9) is provided with cuts, and breaks whenever the load rises by approximately 50% above its normal value. When the ring is broken, the lever may move to bring about the closing of the guide vanes (as indicated by the arrow), while the lever (11) with the jammed guide vane is left in the open position. The lever is connected with link (6) and the gate ring (7) by cylindrical hinges (5) and (8), respectively. This design was formerly used in many turbines, but is no longer employed since it is difficult to manufacture identical breaking rings and seats for them, because breaking forces in various rings differ widely. Besides, the lengths of lever and link cannot be adjusted. Hence, the other two designs shown in Figures b and c are used on a larger scale.

In the design, as shown in Figure VI.11,b, the guide-vane lever (1) is keyed to the guide-vane pivot (5) by means of the pin (2). One lever end is connected to the slide block (7) through hinge (3); the slide block is connected by means of breaking bolt (11) and nuts (4) to the link (8), connected to the gate ring (9) by means of hinge (6).

When the vanes are opened or closed under normal operating conditions of the turbine, the forces are transmitted from the gate ring to the lever through the breaking bolt. A circular groove is provided in the bolt; if the guide vane becomes jammed when the gate ring turns in the closing direction (as indicated by the arrow), the bolt breaks at its reduced cross-sectional area and the link, being provided with recesses, glides along the slide block. The shock absorbers (10) are provided to prevent the slide blocks from striking the link after breakage. The advantage of this design is that the length of the link may be adjusted by means of the breaking bolt and its nuts, which simplifies the manufacture and assembly of the distributor. The design described previously (with breaking rings) requires more precise machining, since the actuating mechanism has no adjusting device. The disadvantage of the design with breaking bolts is that the link is rather cumbersome and the slide block requires much space to move freely when the gate ring turns after the bolt is broken.

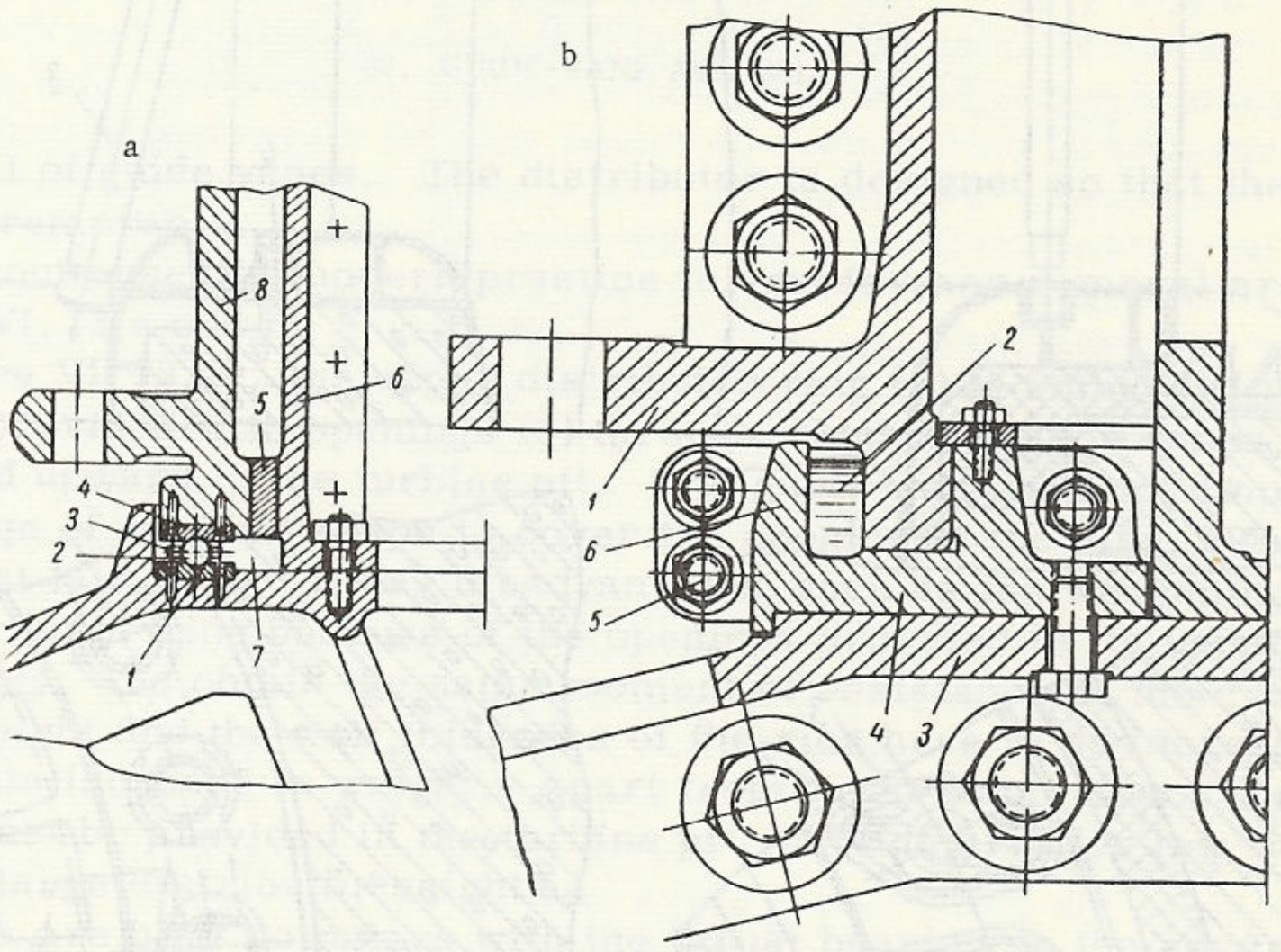


FIGURE VI.12. Gate ring bearings

Another design with a cylindrical breaking pin mounted on the lever is used nowadays in most turbines (see Figure VI.11,c). The lever consists of two parts. The lower part (1) is keyed to the guide-vane pivot (10) by pin (3), and carries the upper lever (2) connected to it by the breaking pin (4). The lever is connected to the link through hinge (9). The link – of the composite type – consists of two heads (5) and a connecting bolt (8) with left-hand and right-hand threads. The length of the link can be adjusted by turning the screw provided with nuts. The cylindrical hinge (7) connects the link to the gate ring (6). When a foreign body jams a guide vane, and the force transmitted by the servomotor to the link exceeds a predetermined limit, pin (4) breaks, freeing the upper lever. This design is independent of the closing direction of the gate ring, in contrast to designs (a) and (b) which depend on the closing direction, since their breaking elements function only for one direction.

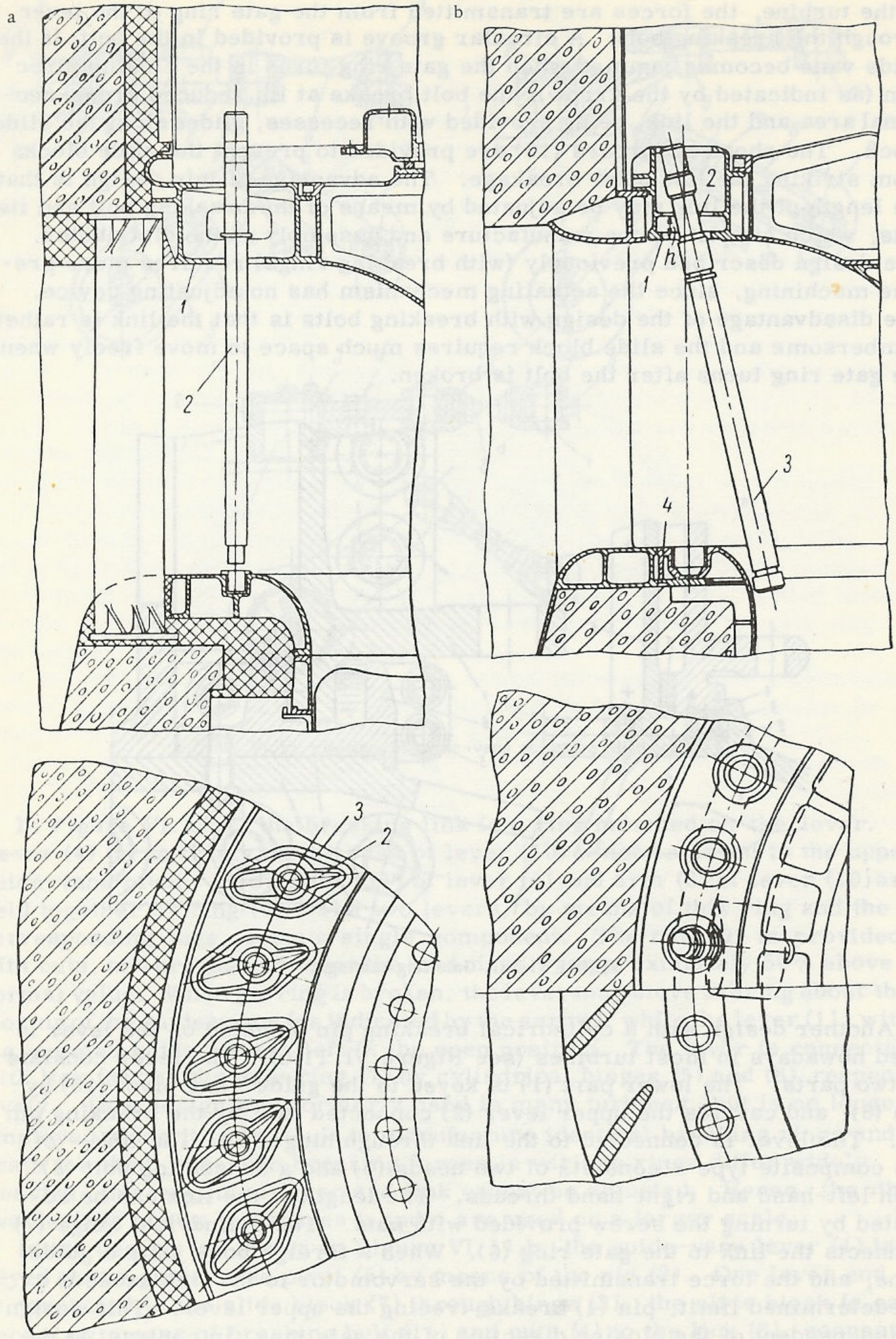


FIGURE VI. 13. Guide-vane removal

The gate-ring bearing. Designs of gate ring bearings are shown in Figure VI. 12. An axial ball bearing is shown in Figure VI. 12,a. The turbine cover-plate is provided with race (1) for the balls. The gate-ring weight is transmitted to the balls (2) guided by the cage (3), through the upper ball race (4). The gate ring (8) is guided in the radial direction by annular plates (5), fastened to the cylinder (6). Between the turbine cover-plate and the gate ring there is an oil-filled cavity (7). Although this arrangement ensures minimum friction, it is rather complicated because of the ball bearing. Since the gate ring does not weigh very much, and the frictional moment is not very great, the normal layout nowadays is simpler (shown in Figure VI. 12,b). The ball bearing is dispensed with. The gate ring (1) slides on an axial bearing (4) mounted on the turbine cover-plate (3). The bearing has a collar (6), which bounds the oil-filled cavity (2). The bearing is usually made of cast iron, and consists of several sections connected by bolts (5).

32. GUIDE-VANE ASSEMBLY

Removal of guide vanes. The distributor is designed so that the guide vanes are removable.

Two layouts used in modern practice for guide-vane removal are shown in Figure VI. 13,a and b.

In Figure VI. 13,a*, the upper distributor ring (1) is embedded in concrete and provided with openings (3) through which the guide vanes (2) can be removed upward to the turbine pit. The guide-vane bearing is provided with a flange of suitable shape to cover the opening in the ring. This is the simplest layout, but it has disadvantages, such as the weakening of the upper distributor ring because of the openings provided in its upper and lower flanges. To obtain the same moment of resistance of the cross section, the height and the wall thickness of the ring have to be increased, which entails increase in weight. Apart from this, ample space for runner removal must be provided in the turbine pit, particularly for low-head turbines with large distributor height b_0.

Turbines are built nowadays with the thrust bearing on the cover plate, so that the pit is not deep enough for vane removal, and the above layout may be impracticable. The layout shown in Figure VI. 13, b is more advantageous from this point of view, but guide vane removal is more complicated. The guide vane (3) is lifted upward until the lower vane pivot can be removed from its bearing, the vane is then tilted and lowered into the throat ring. From there it can be taken out through the scroll casing, the draft tube, or through special hatches in the cover plate. Holes should be provided in the lower flange (1) of the upper distributor ring so that the vanes may be raised up to flange (2). The distance h from the lower flange to the intermediate flange (2) should be large enough to enable the removal of the lower vane pivot from the bearing in the lower ring (4). In both layouts and under normal operating conditions, the holes of the lower ring are covered with bolted steel plates. In the second layout, the upper ring is more rigid, but the whole construction is more complicated because of the intermediate flange. Vane removal is rather difficult. Removal of the

* Inventor N. N. Kovalev, patent No. 50825.

guide vanes, without dismantling the upper ring and the cover-plate, is convenient only for relatively large turbines with the runner diameter $D_1 > 4$ m; in smaller turbines it is easier to dismantle the whole unit.

Guide vane bearing and its lubrication. Figure VI. 14 shows an oil-lubricated guide vane bearing designed by LMZ. The upper vane pivot is guided in the bronze bushings (1) and (2), and the lower one by the bronze bushing (3). Both upper bushings are pressed into guide-vane cast-iron bearing (4), which is mounted on the upper distributor ring (5) by a flange. The lower bushing is mounted on the lower distributor ring (6). A special seal is provided below the intermediate bushing (2) to prevent water from leaking through the bushing into the turbine pit. The seal consists of a leather or rubber cup (12), a rubber ring (13), and a lower ring (14). The lower ring is held by the bolt (15) screwed into the ring (16). This type of seal is used on a large scale. The grease for lubrication is supplied to the intermediate pivot through the pipe (7) and to the lower pivot through the pipe (8), by means of the lubricator (11). Pivot and vane should be provided with drilled holes to enable the installation of pipe (8) inside the vane body. The drilling of holes in guide vanes of large turbines is rather complicated. The pipe (8) is usually expanded at both ends. Bushings may be dispensed with for water-lubricated bearings. The pipe (9), which leads from the intermediate bushing into the turbine pit is provided for drainage of seepage water and maintenance of the seals. The lateral clearances of the guide vane are established and secured when mounting the lever (10) on the guide vane. The lever is keyed to the pivot in the required position and serves as the guide vane thrust-collar. The guide vane is suspended from the lever whose lower surface is supported by the collar of the upper bushing (1). The diameter of the upper pivot d_{up} is usually enlarged to provide a narrow clearance between the pivot and the bushing. Owing to the elastic deformation of the vane, the load is properly distributed along the guide vane. More details on this design will be given in the chapter on strength calculations. In recent designs, wood-plastic blocks are used instead of oil-lubricated bronze bushings for the guide vane bearings of many turbines. Wood-plastic linings may be either oil-lubricated or water-lubricated. If they are oil-lubricated, the guide vane design is as described above. When water lubrication is used, the seal must be arranged on the upper pivot instead of the intermediate.

Figure VI. 15 shows a variant of seal design. The guide bearing (9) is lined with wood-plastic bushes (1). The ring (4), the rubber ring (3), the sealing cup (2), and the oil ring (5) are mounted above the bush (1). The oil ring is provided on top with lubrication grooves for the lateral surface of the lever; oil is supplied to these grooves through pipe (7). The guide-vane lever (6) bears against the oil ring. The channel (8) is provided to check operation of the seal and absence of leakages. Since the guide vanes are used to shut down the turbine, they must close tightly. The surfaces of the contacting front and back of two neighbouring vanes, as well as the clearance between the lateral vane surfaces and both distributor rings, must be carefully sealed. Sealing may be effected either by tight fits between the vanes in contact and minimum clearances or by using rubber seals, which is more practical.

Figure VI. 14, section B–B, shows the manner in which a rubber seal is fitted. A special-profile rubber cord is placed in a recess provided in

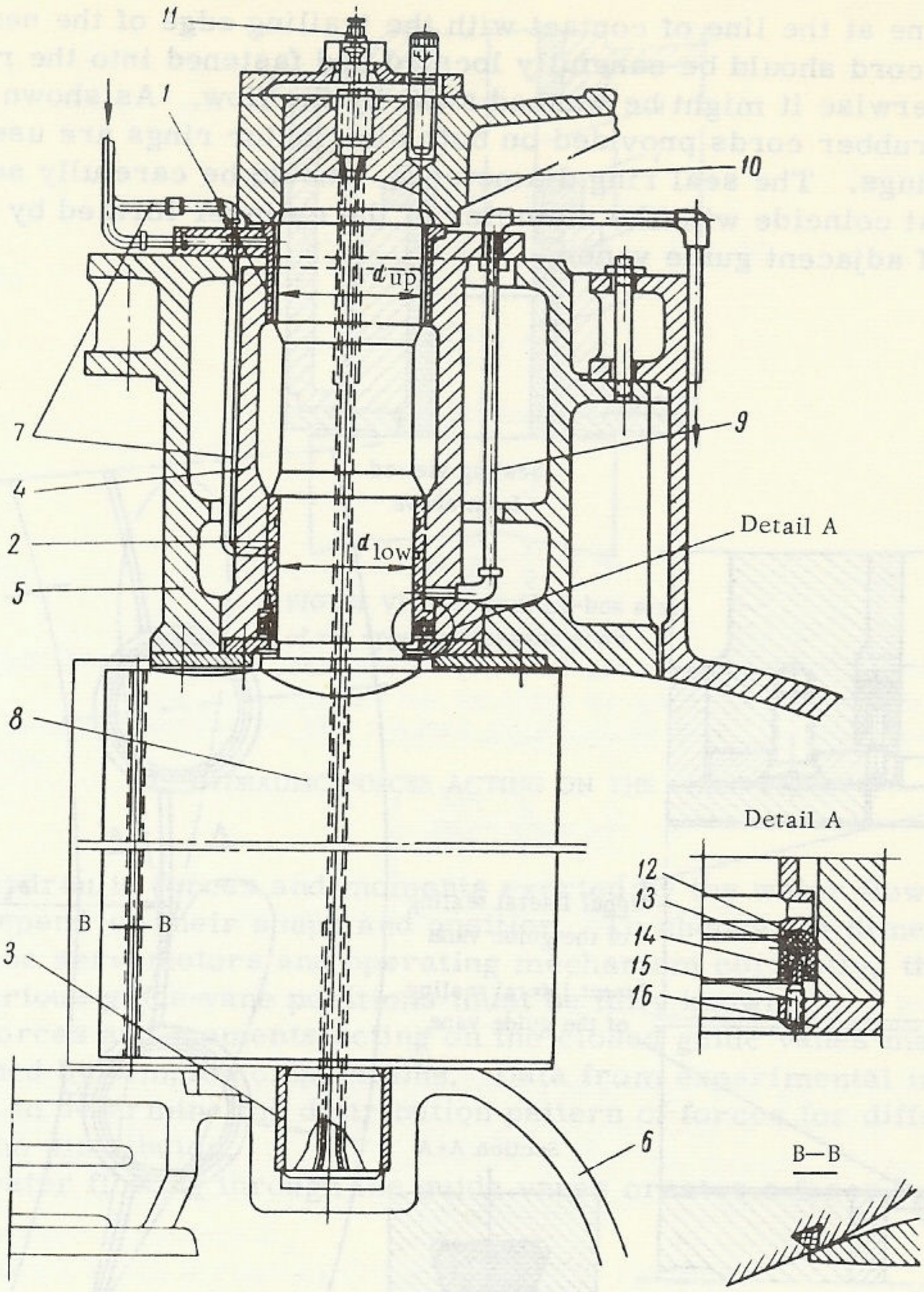


FIGURE VI.14. Oil-lubricated guide-vane bearing

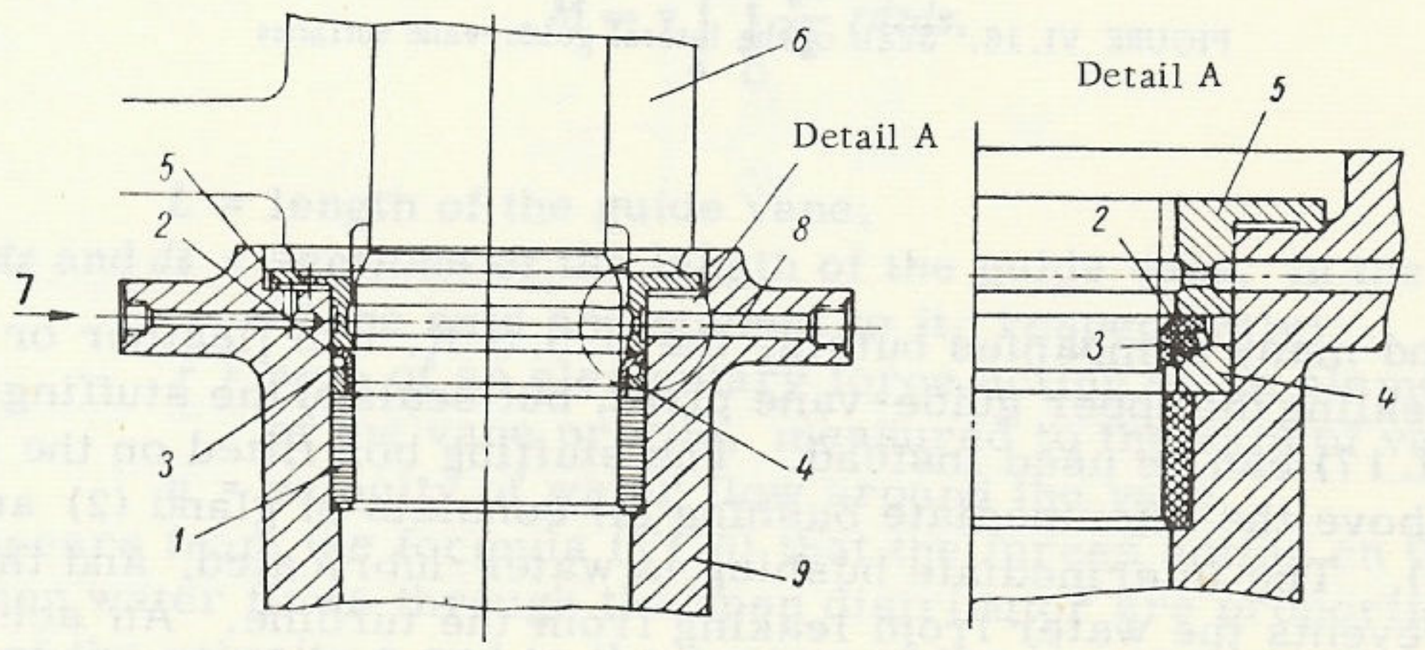


FIGURE VI.15. Seal design for the upper guide-vane bushing

the guide vane at the line of contact with the trailing edge of the next vane. The rubber cord should be carefully located and fastened into the recess, because otherwise it might be washed away by the flow. As shown in Figure VI. 16, rubber cords provided on both distributor rings are used for lateral sealings. The seal ring diameter D_s, should be carefully selected, since it must coincide with the diameter of the cylinder formed by the lines of contact of adjacent guide vanes.

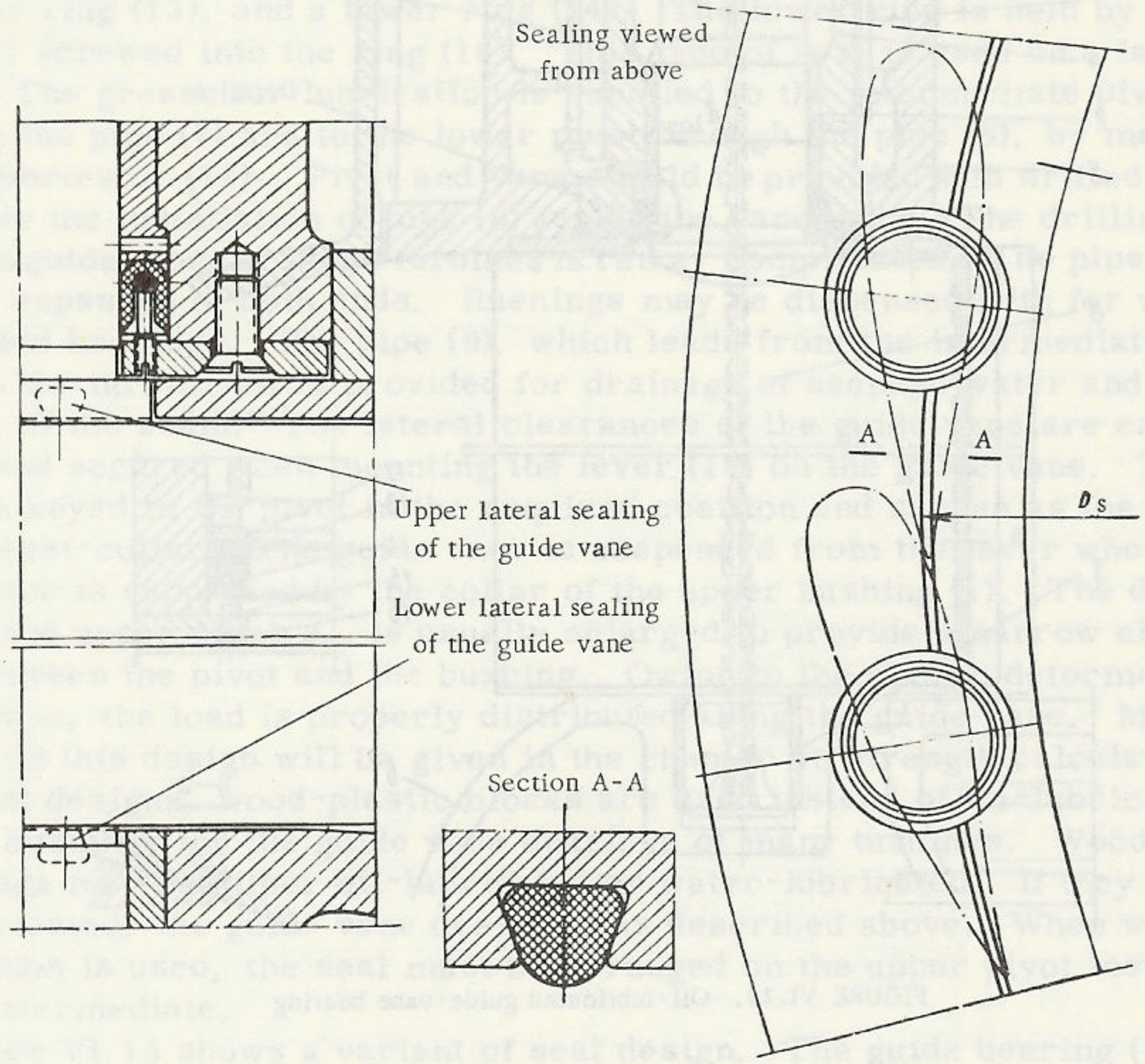


FIGURE VI.16. Seals of the lateral guide-vane surfaces

LMZ and many companies outside the U.S.S.R. use [leather or rubber] cups for sealing the upper guide-vane pivot, but seals of the stuffing-box type (Figure VI. 17) can be used instead. The stuffing box fitted on the guide-vane pivot (1) above the intermediate bushing (4) consists of gland (2) and the packing (3). The intermediate bushing is water-lubricated, and the stuffing box prevents the water from leaking from the turbine. An access hole (5) is provided in the upper distributor ring to tighten the gland (2) and seal the packing.

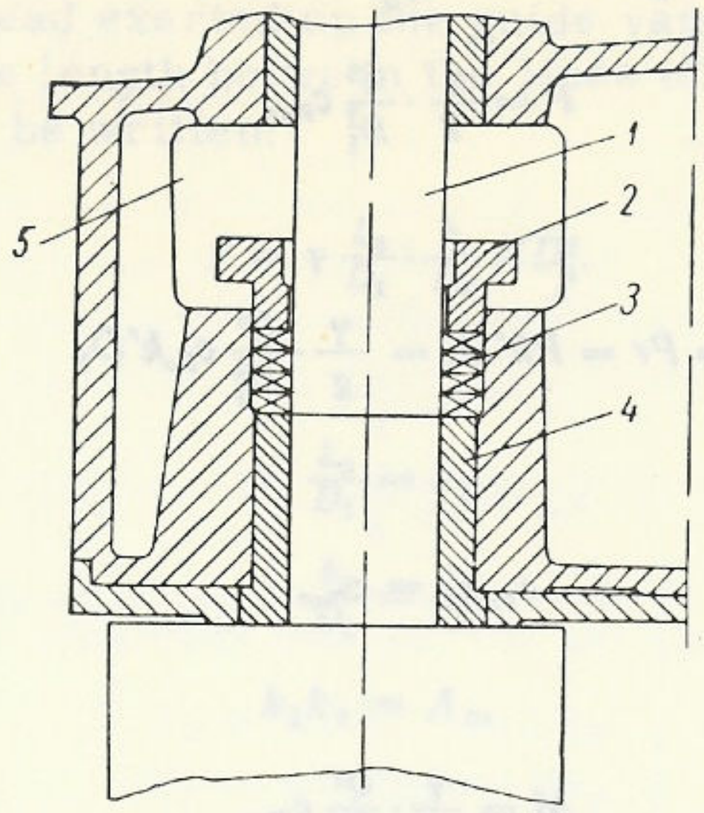


FIGURE VI. 17. Stuffing-box seal of the upper guide-vane pivot

33. HYDRAULIC FORCES ACTING ON THE GUIDE VANES

The hydraulic forces and moments exerted by the water flow on the guide vanes depend on their shape and position. To choose the dimensions of the guide-vane servomotors and operating mechanism correctly, the forces acting at various guide-vane positions must be fully known.

The forces and moments acting on the closed guide vanes may be easily determined by simple computations. Data from experimental investigations are used to determine the distribution pattern of forces for different openings of the distributor.

The water flowing through the guide vanes creates a force P, and a moment M:

$$P = \gamma \int_0^{b_0} \int_O^L \frac{v^2}{2g}\, dzds, \qquad \text{(VI. 6)}$$

$$M = \gamma \int_0^{b_0} \int_O^L \frac{v^2}{2g}\, rdzds, \qquad \text{(VI. 7)}$$

where L = length of the guide vane;

dz and ds = sections of the length of the guide vane, in the direction of the axis and normal to it, respectively;

r = arm of an elementary force, acting on an elementary area of the vane profile, measured to the axis of vane rotation;

v = velocity of water flow around the vane.

It appears from the formula (VI. 6) that the forces acting on the guide vane when water flows through the open distributor are proportional to the square of the velocity v and to the square of the linear dimensions. By substituting for the velocity the discharge Q which is proportional to it, and

inserting the proportionality factor c_{p_0}, we may write

$$P = \frac{\gamma}{g} \cdot \frac{Q^2}{D_1^2} c_{p_0}. \qquad \text{(VI. 8)}$$

Observing that

$$M = Pr = Pk'D_1 = \frac{\gamma}{g} \cdot \frac{Q^2}{D_1^2} c_{p_0} k' D_1$$

and denoting

$$c_{p_0} k' = c_{m_0},$$

we obtain

$$M = \frac{\gamma}{g} \cdot \frac{Q^2}{D_1} c_{m_0}. \qquad \text{(VI. 9)}$$

The dimensionless factors c_{p_0} and c_{m_0} depend on the shape of the distributor and of the scroll-casing as well as on the opening a_0.

Formulas (VI. 8) and (VI. 9) can be written

$$\left.\begin{aligned} c_{p_0} &= \frac{g}{\gamma} \cdot \frac{PD_1^2}{Q^2}, \\ c_{m_0} &= \frac{g}{\gamma} \cdot \frac{MD_1}{Q^2}, \end{aligned}\right\} \qquad \text{(VI. 10)}$$

and the values Q, P, and M expressed in terms of unit quantities

$$Q = D_1^2 \cdot \sqrt{H} Q_1';$$
$$P = D_1^2 H P_1';$$
$$M = D_1^3 H M_1'.$$

We then obtain for c_{p_0} and c_{m_0} the following expressions

$$\left.\begin{aligned} c_{p_0} &= \frac{P_1'}{\varrho Q_1'^2}; \\ c_{m_0} &= \frac{M_1'}{\varrho Q_1'^2}, \end{aligned}\right\} \qquad \text{(VI. 11)}$$

where $\varrho = \frac{\gamma}{g}$ = the density of the water.

Hence, c_{p_0} and c_{m_0} are respectively the force and the moment acting on the guide vane of a unit turbine (runner diameter D_1 = 1 m, head H = 1 m), and referred to the square of the corresponding velocity.

When the distributor is closed, the force acting on a guide vane is

$$P = \gamma H L_0 b_0. \qquad \text{(VI. 12)}$$

where H = average head exerted on the guide vane;
L_0 = guide-vane length between the lines of vane contact.
This formula may be written:

$$P = \gamma \frac{L_0}{D_1} \cdot \frac{b_0}{D_1} H D_1^2. \qquad \text{(VI. 13)}$$

Denoting

$$\frac{L_0}{D_1} = k_1;$$

$$\frac{b_0}{D_1} = k_2;$$

$$k_1 k_2 = A_0,$$

we obtain

$$P = A_0 \gamma H D_1^2. \qquad \text{(VI. 14)}$$

The moment acting on the closed guide vane with respect to the axis of rotation is

$$M = P r_0,$$

and, since $r_0 = k_3 D_1$, denoting $k_1 k_2 k_3 = B_0$, we obtain

$$M = B_0 \gamma H D_1^3. \qquad \text{(VI. 15)}$$

Coefficients A_0 and B_0 depend on the distributor design and not on the guide-vane shape. Consequently, for closed geometrically similar distributors, the forces are proportional to the head H and the square of the runner diameter D_1, while the moments are proportional to the head H and the cube of the runner diameter D_1.

It follows from formulas (VI. 14) and (VI. 15) that

$$A_0 = \frac{P}{\gamma H D_1^2}, \text{ and } B_0 = \frac{M}{\gamma H D_1^3},$$

but

$$\frac{P}{H D_1^2} = P'_1 \text{ and } \frac{M}{H D_1^3} = M'_1.$$

By simplifying, we obtain

$$\left.\begin{aligned} A_0 &= \frac{P'_1}{\gamma}, \\ B_0 &= \frac{M'_1}{\gamma}, \end{aligned}\right\} \qquad \text{(VI. 16)}$$

where γ = specific weight of water.
Coefficients A_0 and B_0 are referred to the unit turbine (see definition above).

The dimensionless coefficients A_0, B_0, c_{p_0} and c_{m_0} are of assistance in investigating the forces acting on the distributor. The following coefficients, A, B, c_p, and c_m, similar but having dimensions, were used by LMZ for the same purpose:

$$A = A_0\gamma,$$
$$B = B_0\gamma,$$
$$c_p = c_{p_0}\frac{\gamma}{g},$$
$$c_m = c_{m_0}\frac{\gamma}{g}.$$

The formulas determining the forces and moments become:
for the closed distributor

$$\left.\begin{aligned} P &= AHD_1^2, \\ M &= BHD_1^3, \end{aligned}\right\} \qquad \text{(VI. 17)}$$

for the open distributor

$$\left.\begin{aligned} P &= c_p\frac{Q^2}{D_1^2} = c_pD_1^2(Q_1')^2H, \\ M &= c_m\frac{Q^2}{D_1} = c_mD_1^3(Q_1')^2H. \end{aligned}\right\} \qquad \text{(VI. 18)}$$

Forces and moments were measured at LMZ laboratories and defined by means of c_p and c_m. Such tests consist of measuring the pressures on the guide-vane surface by means of piezometers. By integration, the force and the moment are then obtained. In practice, this is done by cutting grooves along the height and width of the vane; thin copper tubes are soldered into the grooves and connected to the piezometers.

Usually, in addition to the pressure, the hydraulic moment exerted on the blade is also measured directly, either with a dynamometer or with strain gages.

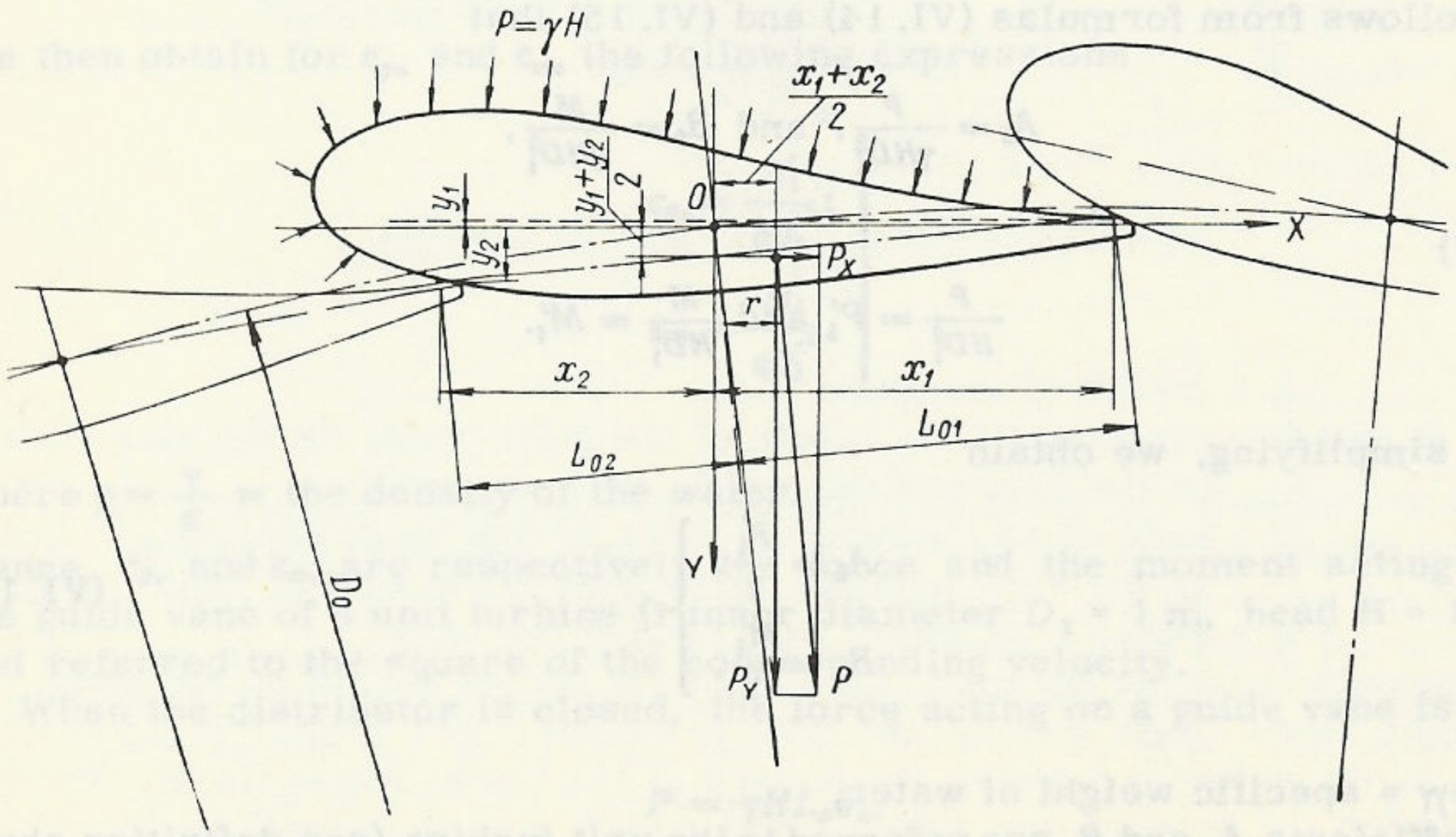


FIGURE VI. 18. Loads acting on the guide vane of a closed distributor

Investigations of the hydraulic forces acting on the guide vanes were carried out for the first time in 1940 by P. N. Nikol'skii at the LMZ /65/. He found that the water flow lines between the guide vanes do not depend on the operating parameters (Q_1' and n_1'), i. e., that within the distributor the direction of flow velocities does not change when the rotational speed or the water discharge through the runner is altered. Consequently, the distribution of pressure on the guide-vane surface may be measured for certain definite operating conditions and then extrapolated for any other conditions.

With a closed distributor, the guide vanes are subjected to pressure $P = \gamma H$ (Figure VI. 18).

The component forces along the axes X and Y are

$$\left.\begin{aligned} P_X &= \gamma H (y_2 - y_1) b_0; \\ P_Y &= \gamma H (x_1 - x_2) b_0, \end{aligned}\right\} \qquad \text{(VI. 19)}$$

where OX is drawn from the axis of rotation to the guide-vane trailing-edge;

OY is normal to OX;

x_1 and y_1 = coordinates of the contact point at the trailing edge;

x_2 and y_2 = coordinates of the contact point at the leading edge.

The resultant force is

$$P = \sqrt{P_X^2 + P_Y^2}. \qquad \text{(VI. 20)}$$

The angle α between the force (P) and the X axis is defined by

$$\tan \alpha = \frac{P_Y}{P_X}.$$

The coordinates of the application point of force P are

$$x = \frac{x_1 + x_2}{2};$$

$$y = \frac{y_1 + y_2}{2}.$$

The moments of the components P_X and P_Y are

$$M_{P_Y} = xP_Y;$$
$$M_{P_X} = -yP_X.$$

The resultant moment

$$M_P = rP = xP_Y - yP_X, \qquad \text{(VI. 21)}$$

where

$$r = \frac{L_{0_1} - L_{0_2}}{2} = \frac{M_P}{P} = \frac{xP_Y - yP_X}{\sqrt{P_X^2 + P_Y^2}},$$

is the arm of force P.

The moment tending to open the distributor is deemed positive (+) and the moment tending to close, negative (-).

Force P is applied practically at the middle of the height b_0.

The magnitude

$$r = \varepsilon_0 = \frac{L_{0_1} - L_{0_2}}{2} \qquad \text{(VI. 22)}$$

is called the absolute eccentricity for the closed distributor.

Ordinary guide vanes have a positive eccentricity ($L_{0_1} > L_{0_2}$). Thus, when they are closed, the hydraulic moment tends to open them; the danger of self-closing of the guide vanes and water hammer during closing is thus eliminated.

The magnitude

$$n_0 = \frac{\varepsilon_0}{L_0} = \frac{L_{0_1} - L_{0_2}}{2L_0}, \qquad \text{(VI. 23)}$$

called the relative excentricity, is usually taken in LMZ practice as $n_0 = 0.05$.

The hydraulic force P and moment M acting on the closed guide vanes are determined with satisfactory accuracy from the formulas

$$P = \frac{\pi D_0 b_0}{z_0} \gamma H, \qquad \text{(VI. 24)}$$

$$M = P\,\varepsilon_0 = \frac{\pi D_0 b_0}{z_0} \gamma H n_0 L_0,$$

but, $L_0 \cong \frac{\pi D_0}{z_0}$, hence

$$M = \frac{\pi^2 D_0^2}{z_0^2} b_0 n_0 \gamma H. \qquad \text{(VI. 25)}$$

The magnitude and the direction of the hydraulic force and moment change when the guide vanes turn and water flows around them.

The variation in the position of the application point and in the direction of the hydraulic force acting on the guide vane for different distributor openings a_0 is shown in Figure VI. 19. These data were obtained from laboratory tests by measuring the pressure distribution on the guide vanes.

Figure VI. 20 shows the variation of the coefficient c_m of the hydraulic moment as a function of the opening a_0 for symmetrical and asymmetrical guide-vane profiles. As shown in the figure, c_m is nearly equal to zero for a half-open distributor. The coefficient c_m of the asymmetrical profile with positive curvature varies the most, while the coefficient of the asymmetrical profile with negative curvature varies the least. The coefficient of the symmetrical profile is positive for small values of a_0, becoming almost equal to the coefficient of the asymmetrical profile for large openings.

The fact that the hydraulic-moment coefficient c_m depends on the vane profile, in particular for small vane openings, may be explained by the following:

The vane profile with the negative curvature turns the flow away from the runner; the reaction of the flow at the trailing edge of the vane is directed toward the runner and increases directly with the curvature.

The profile with the positive curvature turns the flow toward the runner, and consequently, the reaction of the flow at the trailing edge is in the opposite direction.

The variation of the hydraulic-pressure coefficient c_p acting on the symmetrical guide vane for different distributor openings, is represented on the same graph. The coefficient decreases with the increase in the distributor opening.

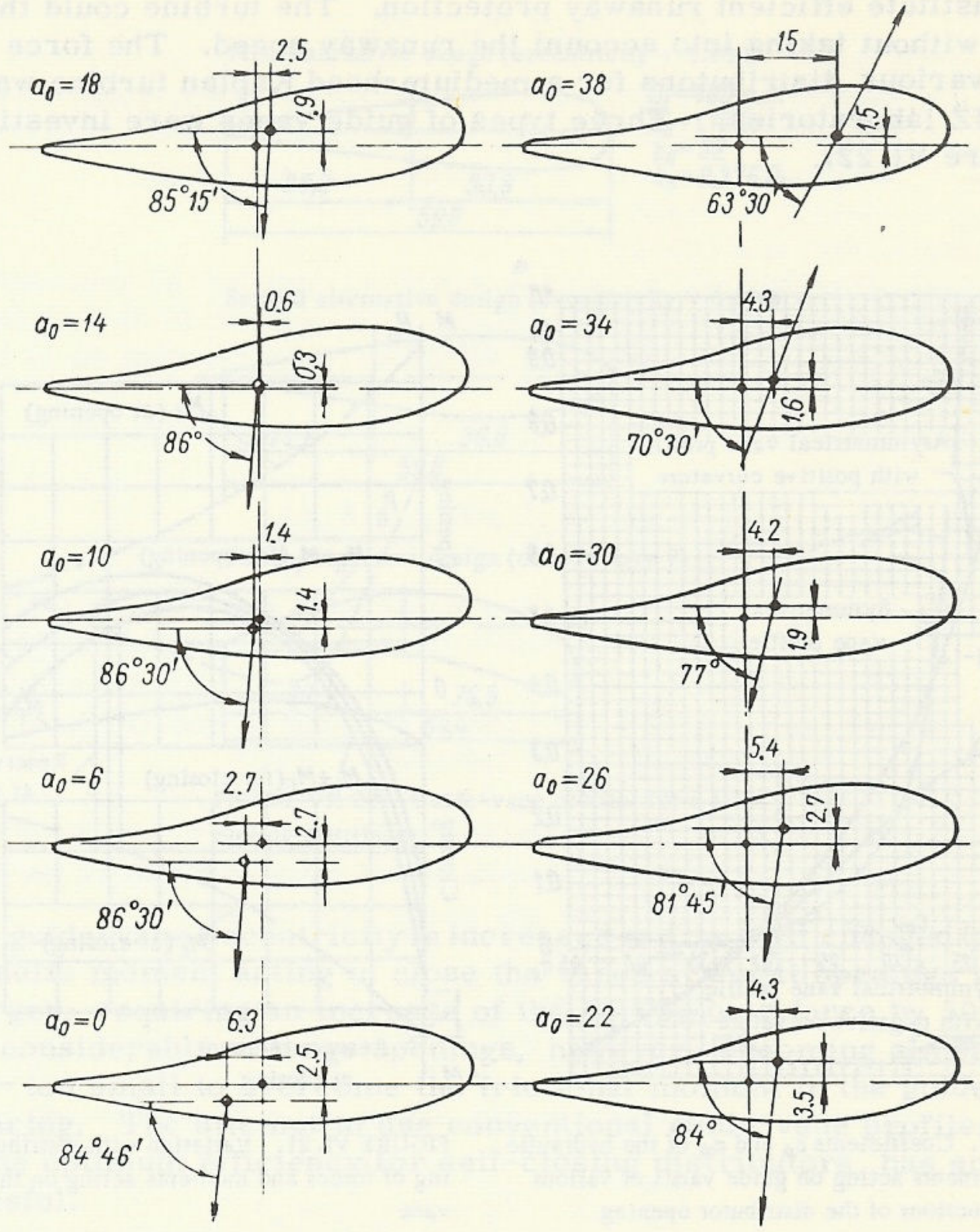


FIGURE VI. 19. Variation with distributor opening of application point and direction of the hydraulic force acting on a guide vane (dimensions given for a model runner D_1 = 460 mm)

For calculation of the hydraulic forces and moments of the prototype turbine for different distributor openings, formula (VI. 18) may be used. The coefficients c_p and c_m may be found from the appropriate model-test graphs.

The variation of the hydraulic moment acting on the guide vane is shown in Figure VI. 21. The moment reaches its maximum value when the distributor is closed, i.e., $a_0 = 0$; when the guide vanes open and water begins to flow in, the moment decreases to zero and then becomes negative, increasing at first and then once more approaching zero.

The nature of the variation of the moment is the same for different profile shapes; only the magnitude of the moment changes.

The self-closing distributor as a means of preventing turbine runaway was studied at the LMZ. If the guide vanes could be so shaped that the hydraulic moment would close them whatever their initial position, this would constitute efficient runaway protection. The turbine could then be designed without taking into account the runaway speed. The force distribution in various distributors for a medium-head Kaplan turbine was studied in the LMZ laboratories. Three types of guide vanes were investigated (see Figure VI. 22).

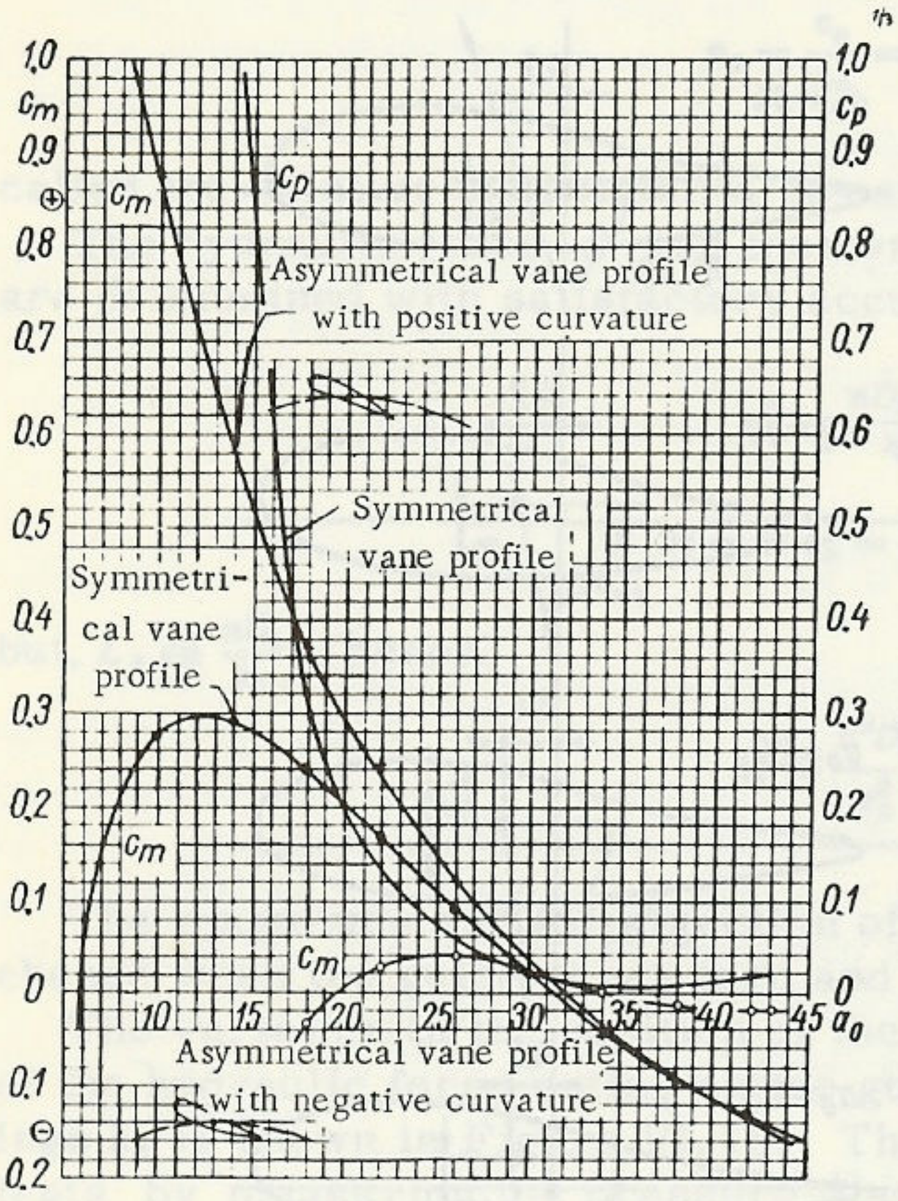


FIGURE VI. 20. Coefficients c_p and c_m of the hydraulic forces and moments acting on guide vanes of various profiles, as functions of the distributor opening

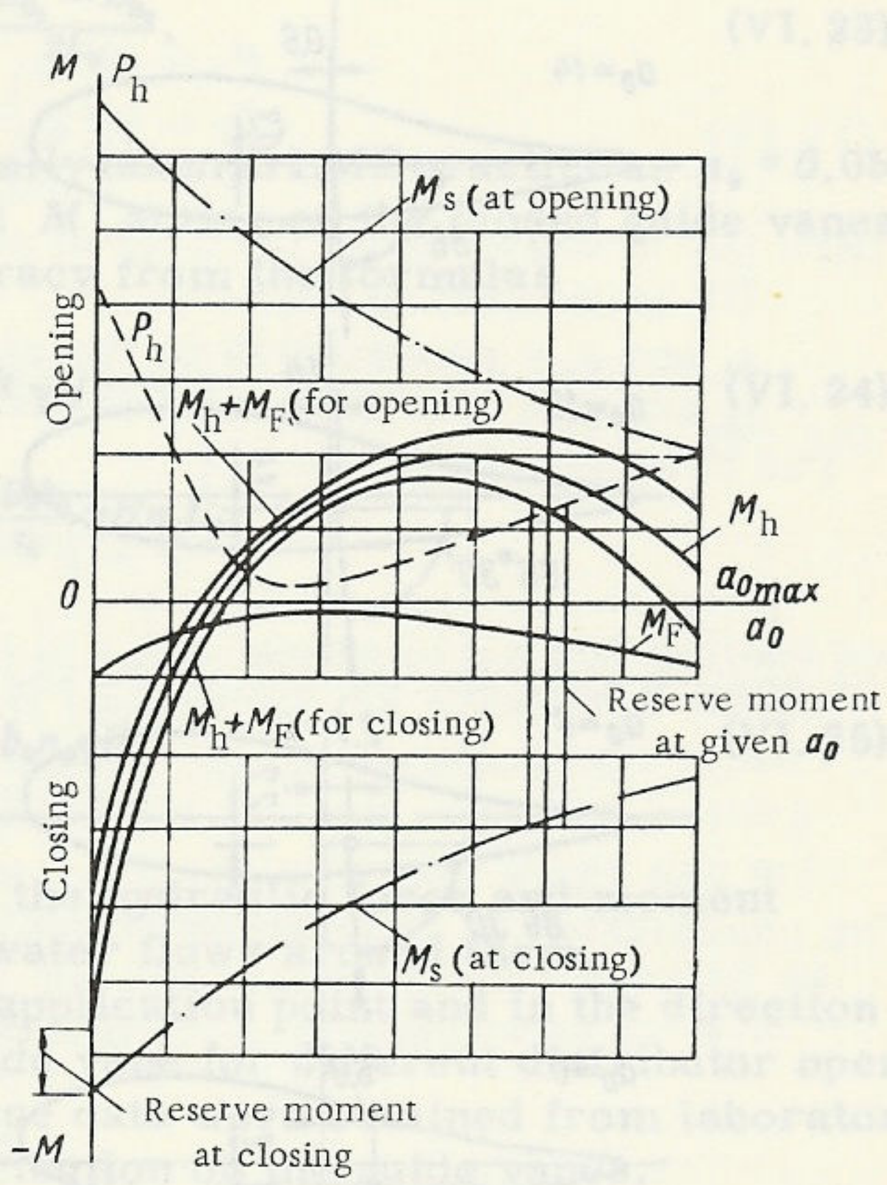


FIGURE VI. 21. Variation with distributor opening of forces and moments acting on the guide vane

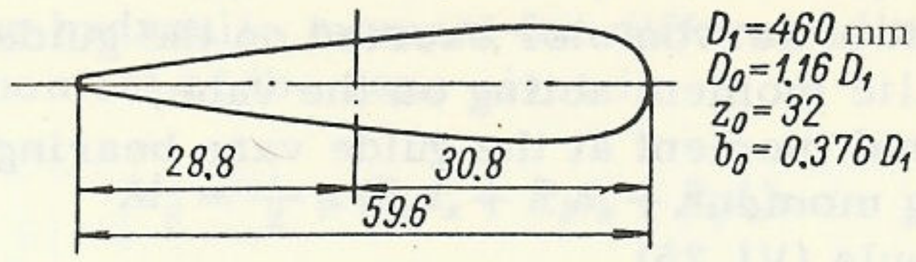
Power tests on models showed that turbine efficiency is the same with the first and second design variants, but that owing to the divergence from the vane shape of the flow direction at the scroll exit, the profile of the third type considerably lowers efficiency (by about 6 to 7%). This design was then discarded.

Investigation of the first and second designs showed that the magnitude and also the sign of the hydraulic moment depend on the setting of the guide vane with respect to the scroll casing.

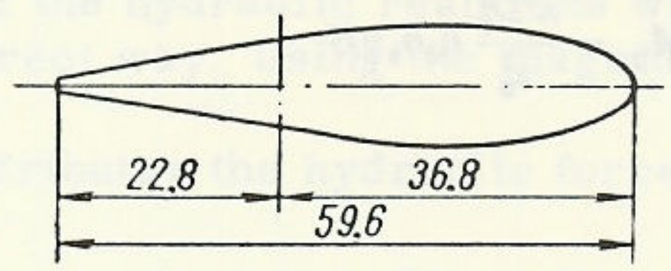
The resultant moment acting on all the guide vanes depends on the enveloping angle of the scroll. For small angles, which are typical of medium-head Kaplan turbines, the resultant moment exerted on the open guide vanes

having a symmetrical profile is almost equal to zero. Self-closing of the distributor is impossible in this case since the hydraulic moment is not sufficiently large to overcome the frictional forces in the guide-vane bearings.

First alternative design (excentricity + 0.039)



Second alternative design (excentricity — 0.067)



Third alternative design (excentricity 0)

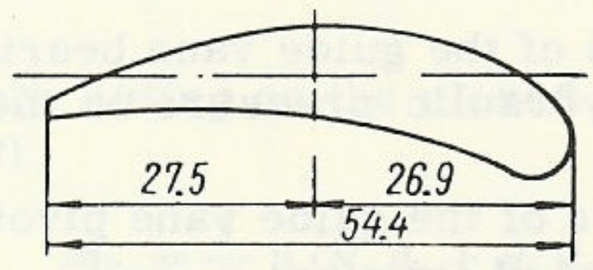


FIGURE VI. 22. Guide-vane profiles for a self-closing distributor

If the guide-vane eccentricity is increased and its sign changed (profile II) the hydraulic moment acting to close the vanes at small openings becomes much larger, requiring an increase of the servomotor force by 50%. It decreases considerably at large openings, however, becoming almost equal to zero — too small to overcome the frictional moment in the guide vane pivot bearing. The attempt to use conventional guide-vane profiles which ensure the optimum efficiency for self-closing distributors, has so far been unsuccessful.

34. DETERMINATION OF SERVOMOTOR PARAMETERS

In order to turn the guide vanes, not only the hydraulic moment, if acting against the direction of motion, but also the frictional moment occurring in the guide vane pivot bearings, has to be overcome.

Piston servomotors produce the force required to turn the guide vanes. The actuating force of the servomotor required for a certain distributor opening must overcome both the hydraulic and frictional moments, and must also ensure the necessary rotational speed of the guide vanes; the servomotor should also develop the force necessary to overcome friction in the actuating mechanism. To ensure tight contact of the vanes in the closed position,

the servomotor should impart adequate sealing force to all the connecting elements of the guide vanes. The additional moment exerted for this purpose on the guide vane pivot is called the sealing moment.

Consequently, the moment required to close the distributor is

$$M_{sc} \geqslant M_{hc} + M_{Fc} + M_{seal}, \tag{VI. 26}$$

where M_{sc} = moment of servomotor exerted on the guide vane;
M_{hc} = hydraulic moment acting on the vane;
M_{Fc} = frictional moment at the guide vane bearings;
M_{seal} = sealing moment.

According to formula (VI. 25)

$$M_{hc} = \frac{\pi^2 D_0^2}{z_0^2} n_0 b_0 \gamma H.$$

The frictional moment is

$$M_{Fc} = \frac{1}{2} \mu \left(R_{ac} d_a + R_{bc} d_b + R_{cc} d_c\right), \tag{VI. 27}$$

where R_{ac} R_{bc} and R_{cc} = reactions of the guide vane bearings, determined by the hydraulic pressure on the closed guide vane;
d_a, d_b and d_c = diameters of the guide vane pivots (Figure VI. 4);
μ = coefficient of friction;
for steel on bronze: μ = from 0.15 to 0.20;
for steel on wood plastics: μ = from 0.08 to 0.12.

When calculating the frictional moment, one usually neglects the effect of the servomotor force applied on the guide vane lever.

$$M_{seal} = P_{seal} L_0,$$

but,

$$L_0 = \frac{\pi D_0}{z_0}, \text{ and } P_{seal} = q b_0 h,$$

so that

$$M_{seal} = q b_0 h \frac{\pi D_0}{z_0}, \tag{VI. 28}$$

where q = pressure at the contact surface of the vanes;
h = width of the contact area.

Consequently, the required moment in the closed position of the guide vanes is

$$M_{sc} \geqslant \frac{\pi^2 D_0^2}{z_0^2} n_0 b_0 \gamma H + \frac{\mu}{2} (R_a d_a + R_b d_b + R_c d_c) + q b_0 h \frac{\pi D_0}{z_0}. \tag{VI. 29}$$

The moment required to turn the open guide vanes is

$$M_s = \pm M_h + M_F. \tag{VI. 30}$$

The sign of the hydraulic moment depends on the direction of movement: opening (+) and closing (−). The hydraulic moment computed from the formula (VI. 18) is

$$M_{\mathrm{h}} = c_m D_1^3 H\,(Q_1')^{\,2}.$$

Experimental values of c_m determined by laboratory tests should be used when calculating the hydraulic moment for different distributor openings.

The frictional moment at the vane pivot is

$$M_{\mathrm{F}} = \frac{1}{2}\,\mu\,(R_a d_a + R_b d_b + R_c d_c). \qquad \text{(VI. 31)}$$

The reactions in the vane bearings depend on the hydraulic force.

The magnitude of the hydraulic reactions with open distributor may be computed in an indirect way, using the magnitudes determined for the closed position.

For a closed distributor the hydraulic force is (VI. 24)

$$P_{\mathrm{hc}} = \frac{\pi D_0}{z_0}\, b_0 \gamma H.$$

The hydraulic force acting on the closed distributor is readily determined from formula (VI. 27)

$$M_{\mathrm{Fc}} = \frac{1}{2}\,\mu\,(R_{\mathrm{ac}} d_a + R_{\mathrm{bc}} d_b + R_{\mathrm{cc}} d_c).$$

It is convenient to express the bearing reactions in the closed distributor as a fraction of the hydraulic force, namely

$$R_{\mathrm{ac}} = k_a P_{\mathrm{hc}};$$
$$R_{\mathrm{bc}} = k_b P_{\mathrm{hc}};$$
$$R_{\mathrm{cc}} = k_c P_{\mathrm{hc}}.$$

Hence, the values of k_a, k_b, and k_c for the closed distributor are

$$k_a = \frac{R_{\mathrm{ac}}}{P_{\mathrm{hc}}};\quad k_b = \frac{R_{\mathrm{bc}}}{P_{\mathrm{hc}}};\quad k_c = \frac{R_{\mathrm{cc}}}{P_{\mathrm{hc}}}.$$

It may be assumed that the ratios of the reactions to the forces are the same for the open distributor, so that the frictional moment is

$$M_{\mathrm{Fc}} = \frac{1}{2}\,\mu\,(k_a d_a + k_b d_b + k_c d_c)\,P_{\mathrm{h}}. \qquad \text{(VI. 32)}$$

The value of P_{h} is determined from the formula (VI. 18)

$$P_{\mathrm{h}} = c_p D_1^2\,(Q_1')^2 H,$$

c_p is known from model test.

In calculations, one determines the hydraulic and resistance moments for different distributor openings, and tabulates the results (Table VI.2). The

determination should be made for 7 to 10 values of a_0. The required moment for rated as well as for maximum head must be determined.

The results are usually represented on a graph. Figure VI. 21 shows several values as a function of the distributor opening a_0: the hydraulic force P_h, the frictional moment M_F, the hydraulic moment M_h and the servomotor moment M_s during opening and closing of the guide vanes.

TABLE VI. 2

For head H = ..., n_1' = ...,

Number	a_{0m}, mm	a_0, mm	Q_1', l/sec	$(Q_1')^2$ m^4/sec^2	c_p	c_m	P_h, kg	M_h, kgm	M_F, kgm	M_h+M_F Distrib. openg.	$-M_h+M_F$ Distrib. closg.
1		0*									
2											
3											
—											
n	$a_{0m_{max}}$	$a_{0_{max}}$									

* Distributor closed.

Knowing the moment that has to be exerted on the guide vane, and selecting the proper kinematic linkages between the guide vane and the servomotor, one can determine the dimensions of the servomotor and the oil pressure required to ensure the force needed to turn the guide vanes.

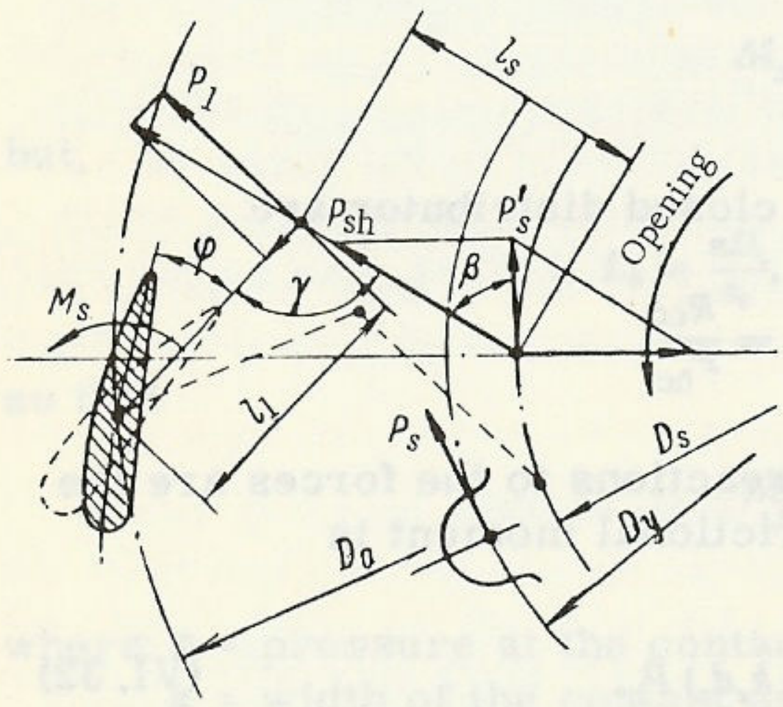


FIGURE VI. 23. Schematic diagram of the guide vane operating mechanism

The kinematic diagram of the guide-vane actuating mechanism adopted by LMZ is shown in Figure VI. 23. It ensures a certain correspondence between the required moment exerted by the servomotor on the guide-vane levers and the variation of the hydraulic moment on the vane. The required moment reaches its greatest value when the distributor is closed ($a_0 = 0$) or nearly closed. If the opening increases and the hydraulic moment decreases, the moment is also reduced. This may be easily verified by considering the following relations. From the kinematic diagram of the operating mechanism, it appears that the force of both servomotors P_s, applied at the lug of the gate ring at the diameter D_y will be transmitted to the hinge of the guide vane link as the force P_s' applied at the diameter D_s.

$$P_s' = \frac{P_s D_y}{z_0 D_s}. \tag{VI. 33}$$

The force acting along the link is

$$P_{sh} = P_s' \frac{1}{\cos\beta} = \frac{P_s D_y}{z_0 D_s \cos\beta}. \tag{VI. 34}$$

The force that produces the turning moment at the end of the vane lever is

$$P_l = P_{sh} \sin\gamma = \frac{P_s D_y \sin\gamma}{z_0 D_s \cos\beta}. \tag{VI. 35}$$

The moment of the servomotor is

$$M_s = P_l l_1 = \frac{P_s D_y}{z_0 D_s} l_1 \frac{\sin\gamma}{\cos\beta}. \tag{VI. 36}$$

Denoting all the constants by A,

$$\frac{P_s D_y}{z_0 D_s} l_1 = A, \tag{VI. 37}$$

$$M_s = A \frac{\sin\gamma}{\cos\beta}. \tag{VI. 38}$$

It appears from relation (VI. 38) that in order to obtain the greatest possible moment M_s, the angles β and γ should be taken as close as possible to 90°.

The diagram of the operating mechanism shown in Figure VI. 23 meets these requirements.

In the closed position of the distributor, when the maximum moment is required, the angle β is a maximum; it is usually between 70 and 80°. In the open position of the distributor, when the required moment may be smaller, the angle β is also less. The angle γ generally remains unchanged, i.e. nearly 90°.

For the design of the distributor, the exact values of these angles are determined in the following order:

The value of the maximum force P_s required from both servomotors, with the distributor closed, may be determined from formulas (VI. 29) and (VI. 36)

$$P_s \geqslant \frac{z_0 D_s}{D_y l_1} \cdot \frac{\cos\beta}{\sin\gamma} \left[\frac{\pi^2 D_0^2}{z_0^2} n_0 b_0 \gamma H + \frac{\mu}{2} (R_a d_a + R_b d_b + R_c d_c) + q b_0 h \frac{\pi D_0}{z_0} \right]. \tag{VI. 39}$$

Examination of this formula shows that to obtain the smallest forces required, and consequently, minimum servomotor dimensions, one should adopt the following dimensions for the guide-vane-actuating mechanism:

D — at a minimum;
l_1 — at a maximum;
β and γ — nearly 90°;
D_y — greater than D_s.

However, these requirements can be met only within certain limits. The diameter of the guide-vane pitch-circle is usually selected as small as permitted by the external dimensions of the runner, so that in the open position, the trailing edges of the guide vanes do not hinder rotation of the runner in the Francis turbine. In Kaplan turbines, the guide vanes should not extend too far into the throat ring, otherwise they will hinder the admission of water into the runner.

The length of the guide-vane lever l_1 is limited by the space actually available on the turbine cover-plate between the guide-vane circle (diameter = D_0) and the gate-ring (diameter = D_s), these diameters depending on the dimensions of shaft and bearing, and on the requirements for maintenance of the latter.

The fundamental relations for distributor proportions were established at the LMZ on the basis of practical turbine design.

The basic dimensions of a cylindrical distributor are given in Table VI. 1; the dimensions of the actuating mechanism in dependence on the runner diameter, as given in Figure VI. 24, are listed in Table VI. 3.

Usually, the distributor is built first and then the dimensions of the actuating mechanism are selected according to the servomotor stroke required to provide the required guide-vane opening.

The friction in the links of the operating mechanism is small enough to be neglected when calculating the servomotor force; this is usually done in order to simplify the calculations.

Once the actuating mechanism is selected and its position for different distributor openings known, the curves of the required servomotor moment M_s for different distributor openings a_0 may be plotted.

These curves are shown in Figure VI. 21 for the opening and closing of the distributor. The figure illustrates the relation between the moments exerted upon the guide vane, as well as the available reserve moment; as can be seen, the reserve moment is not the same for all distributor openings.

The moments M_h and M_F can be calculated for different heads. For the maximum head H_{max}, the largest moment required $M_{s\,max}$ is calculated.

Knowing the servomotor force P_s and the maximum moment $M_{s\,max}$, it is possible to determine the area of the servomotor piston and the minimum oil-pressure p_{min} in the regulating system which ensures the closing of the distributor:

$$F = \frac{P_{s\,max}}{p_{min}}. \qquad \text{(VI. 40)}$$

For one piston servomotor

$$F = \frac{\pi d_s^2}{4} - \frac{\pi d_r^2}{4}; \quad \frac{\pi}{4}(d_s^2 - d_r^2) = \frac{P_s}{p_{min}},$$

where d_s = servomotor cylinder diameter;
d_r = piston-rod diameter.

TABLE VI. 3

Basic dimensions of the parts of the distributor-actuating mechanism

D_1 — see remark 1	z_0	D_0	$\varphi°$	D_s	L_H	L_1	L_s for $\beta° = 70°$
1800	16	2150	22	1500	240	135	272
2000		2350		1600	270	150	317
2250		2650		1800	300	160	360
2500	24	2900	42	2000	330	170	266
2750		3200		2200	365	190	297
3000		3500		2400	400	210	327
3300		3850		2600	450	225	376
3700		4300		2950	500	250	397
4100		4750		3250	550	275	444
4500		5250		3600	600	300	491
5000		5800		4000	650	325	538
5500		6400		4400	700	350	610
6000		7000		4800	800	400	655
6600		7700		5300	900	450	700
7200	32	8400	42	5800	900	360	797
8000		9300		6400	1000	400	892
9000		10500		7300	1100	450	985

d_s — see remark 1 for $\beta° = 70°$	z_0	d	D	D_n	D_{br}	h
250	16	M36	52	44	36	34
300		M42	62	52	40	40
350		M48	70	60	50	46
200	24	M24	40	32	25	26
250		M30	46	38	30	34
300		M36	52	44	36	34
350		M42	62	52	40	40
400		M42	62	52	45	40
450		M48	70	60	50	46
500		M56	80	70	55	52
600		M64	92	80	60	60
700		M72	105	90	70	70
800		M80	115	100	80	80
500	32	M48	70	60	55	46
600		M56	80	70	60	52
700		M64	92	80	70	60
800		M72	105	90	80	70
900		M80	115	100	90	80

d_{ip} — see remark 1	d_p	D_κ	d_r	$d_0 \times l$
85	78	150	25	M20×60
95	85	170	30	
105	95	185	30	M24×70
115	105	195	35	
125	115	220	35	M30×80
135	125	235	40	
150	135	250	40	M36×100
170	150	275	50	M42×110
190	170	310	50	M48×120
210	190	330	50	
230	210	370	60	M56×130
250	230	400	60	
270	250	430	60	M64×140
300	270	460	70	
330	300	500	70	M72×160
360	330	550	80	

Remarks:

1. The basic dimensions of the parts of the distributor-actuating mechanism are selected according to: runner diameter D_1, servomotor diameter d_s, guide-vane number z_0, and diameter of guide vane intermediate pivot d_{ip}. The dimensions of the various parts depend on these parameters, and are given in the table.

2. The angle α between guide vane axis and lever axis is selected according to the guide vane profile.

3. Deviation from the standard design is allowed for Francis turbines with relatively large servomotors, where the link may be larger

4. Stops must be provided to limit guide-vane rotation.

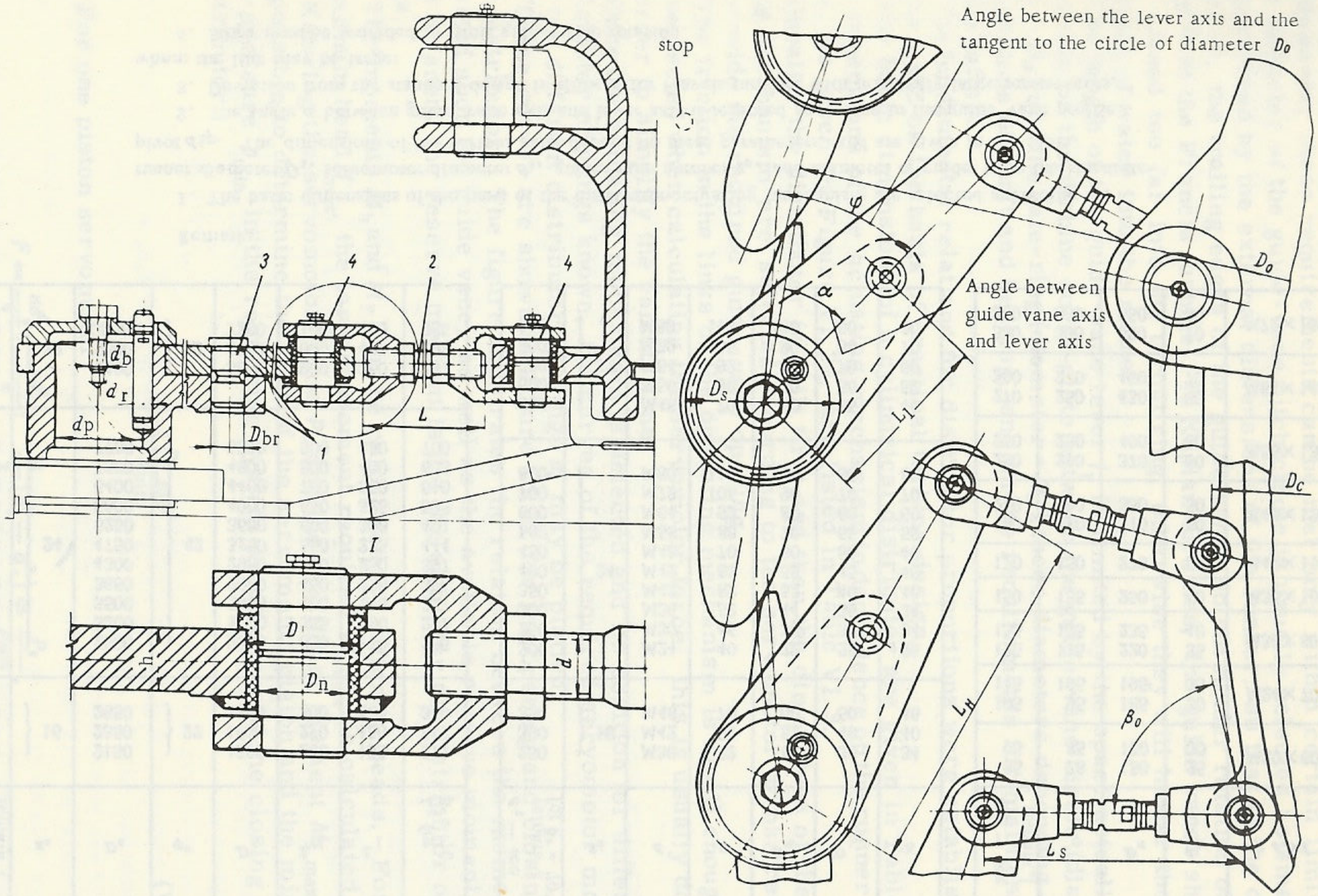


FIGURE VI. 24. Guide-vane-actuating mechanism

Consequently, the servomotor cylinder diameter is

$$d_s = \sqrt{\frac{4P_{s\,max}}{\pi p_{min}} + d_r^2}. \qquad \text{(VI. 41)}$$

For two servomotors

$$F = 2\left(\frac{\pi d_s^2}{4} - \frac{\pi d_r^2}{4}\right);$$

$$\frac{\pi}{2}\left(d_s^2 - d_r^2\right) = \frac{P_s}{p_{min}}. \qquad \text{(VI. 42)}$$

Hence, the diameter of one servomotor will be

$$d_s = \sqrt{\left(\frac{2P_{s\,max}}{\pi p_{min}} + d_r^2\right)}. \qquad \text{(VI. 43)}$$

Normally, the oil pressure p in the regulating system is 25 kg/cm^2; the minimum pressure under which emergency closing of the distributor occurs, p_{min} is 14 kg/cm^2.

In recent years, oil pressures in regulating systems have been increased to p = 40 at.

The servomotor stroke depends on the distributor design and is determined accordingly. The cylinder diameter may also be determined by approximate calculations from empirical formulas.

The following formula may be used for the preliminary selection of the cylinder diameter in accordance with LMZ standards:

$$d_s = \lambda D_1 \sqrt{k_0 H_{max}}, \qquad \text{(VI. 44)}$$

where λ = coefficient, depending on the blade number;
k_0 = distributor height related to runner diameter (relative height).

$$k_0 = \frac{b_0}{D_1}.$$

The value of λ is selected from Table VI. 4.

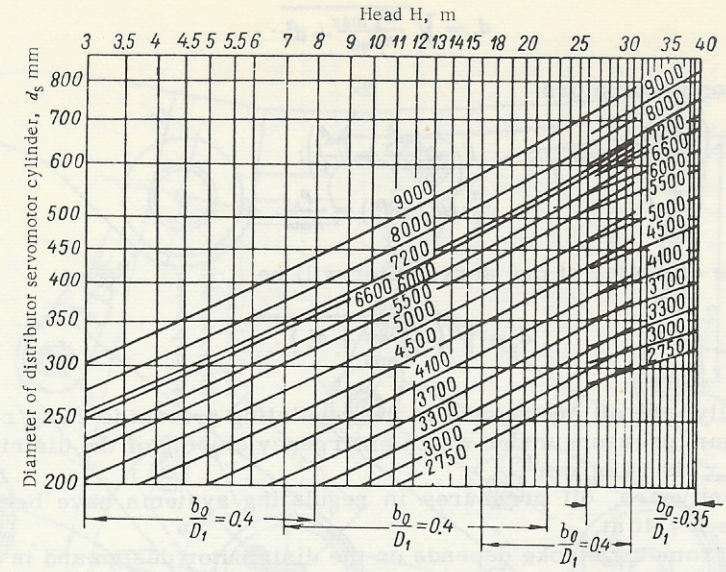
TABLE VI. 4

Values of coefficient λ

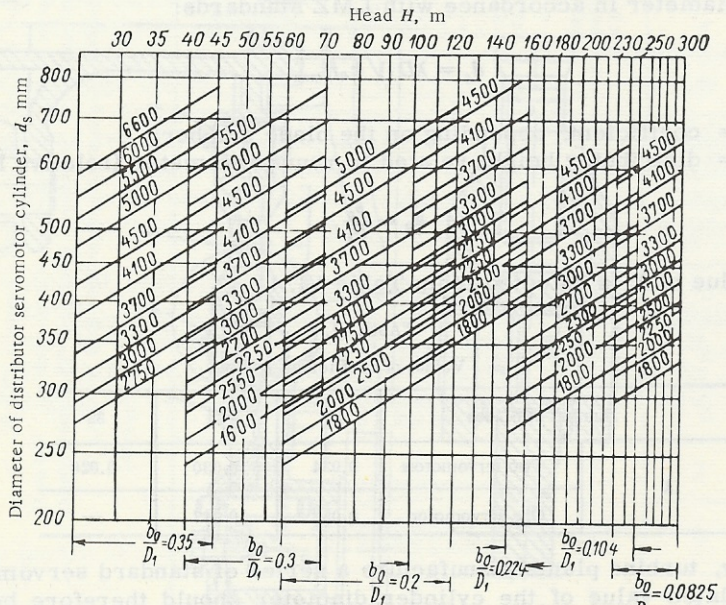
Number of blades		16	24	32
λ	Two servomotors	0.034	0.030	0.028
	One servomotor	0.053	0.047	—

Usually, turbine plants manufacture a series of standard servomotors. The calculated value of the cylinder diameter should therefore be adjusted to the nearest standard value of the series. At the LMZ, the standard diameters are:

$$d_s = 200,\ 250,\ 300,\ 350,\ 400,\ 450,\ 500,\ 600,\ 700,\ 800 \text{ mm}.$$



Kaplan turbine



Francis turbine

FIGURE VI. 25. Charts for the determination of the distributor-servomotor cylinder diameter

TABLE VI. 5

Coefficients for the determination of the distributor-servomotor cylinder diameter

D_1, m	Coefficient					
	A_1		A_2		A_3	
	Kaplan	Francis	Kaplan	Francis	Kaplan	Francis
1.8	—	0.0492	—	0.0217	—	0.00108
2.0	—	0.048	—	0.0214	—	0.00103
2.25	—	0.0492	—	0.0215	—	0.00106
2.5	0.0493	0.0492	0.0123	0.0139	0.064	0.00069
2.75	0.0493	0.0493	0.0123	0.014	0.0582	0.00069
3.0	0.0487	0.0487	0.0123	0.014	0.0533	0.00068
3.3	0.0479	0.0479	0.0123	0.014	0.0485	0.00067
3.7	0.0479	0.0479	0.0123	0.014	0.0435	0.00067
4.1	0.0485	0.0485	0.0123	0.0139	0.0393	0.00068
4.5	0.051	0.051	0.0123	0.0139	0.0356	0.00071
5.0	0.0527	0.0527	0.0123	0.0139	0.032	0.00074
5.5	0.0539	0.0539	0.0122	0.0139	0.0291	0.00075
6.0	0.0525	0.0525	0.0123	0.014	0.0267	0.00074
6.6	0.0516	0.0516	0.0123	0.014	0.0243	0.00072
7.2	0.0574	—	0.0088	—	0.0222	—
8.0	0.0564	—	0.0088	—	0.02	—
9.0	0.0564	—	0.0088	—	0.0178	

The servomotor stroke may be calculated approximately from the following empirical formula

$$S = (1.4 - 1.8)\, a_0. \qquad \text{(VI. 45)}$$

Smaller coefficients are adopted for turbines having a runner diameter up to 5 m.

According to LMZ standards, the guide-vane mechanism is actuated by two servomotors. The diameter of each servomotor cylinder is computed from the formula

$$d_s = D_1 \sqrt{A_1 \left[A_2 H_{max} + \left(\frac{H_{max}}{10} + 1 \right) A_3 \right] k_0}, \qquad \text{(VI. 46)}$$

where A_1 = coefficient allowing for the kinematic connection between guide vanes and gate ring;

A_2 = coefficient allowing for the guide-vane axis eccentricity and vane number;

A_3 = coefficient allowing for the moment necessary to ensure tightness between the guide vanes.

The values of the coefficients A_1, A_2 and A_3 are listed in Table VI. 5; they are calculated for a normal oil pressure in the regulating system of 25 kg/cm^2 and a minimum pressure of 14 kg/cm^2 in the servomotor for emergency closing [of the distributor]. The diameters of the distributor servomotor cylinders are given in charts (Figure VI. 25), plotted from formula VI. 46 for Kaplan and Francis turbines.

35. GRAPHICAL LAYOUT OF THE DISTRIBUTOR

The graphical layout of the distributor makes it possible to determine the servomotor stroke necessary to achieve full distributor opening, select the final kinematic diagram of the operating mechanism, and check that adjacent levers and links do not come into contact after the rupture of the breaking links when the actuating mechanism is in an extreme position.

In order to design the distributor, the opening a_0 should be known. The distributor opening a_0 depends on the turbine specific speed n_s. With higher specific speed, and consequently greater discharge capacity, the relative distributor opening should increase. High-speed turbines require a greater distributor height b_0.

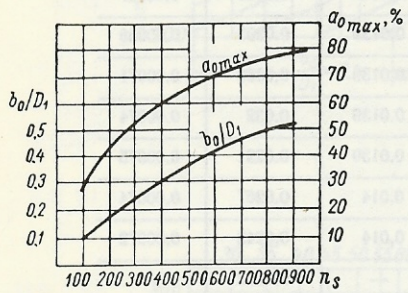


FIGURE VI. 26. Tentative values of the distributor opening a_0 and height b_0 as a function of specific speed n_s.

The tentative values of the maximum distributor openings a_0 and height b_0 are given in Figure VI. 26 as a function of the specific speed n_s. The curves are plotted from LMZ data.

In a low-speed turbine with n_s = 200, a_0 should be $\approx$ 43% of the maximum attainable opening (with the vanes in a radial position) and the distributor height $b_0 = 0.18D_1$; when n_s = .800, a_0 must be $\sim$ 77% and $b_0 = 0.5D_1$. At such high specific speeds, values of a_0 and b_0 smaller than those recommended are conducive to increased velocities in the distributor and thus to increased losses.

For practical design purposes, the opening of the distributor is determined from the universal chart of the given runner.

The discharge corresponding to a given guide vane profile, depending upon the opening a_0 and the runner type, may be determined by tests on the runner model. Curves of equal distributor opening a_0 are plotted on the universal chart.

When designing the full-scale turbine, experimental results from the universal chart, as well as data provided by turbine-model tests on profile, height, number, diameter, and setting of the guide vanes are used.

The guide vanes of the full-scale turbine are geometrically similar to those of the model.

The basic proportions of the guide-vane profile are standardized at the LMZ; they are represented in Figures VI. 27 and VI. 28 for symmetrical and asymmetrical concave profiles, respectively.

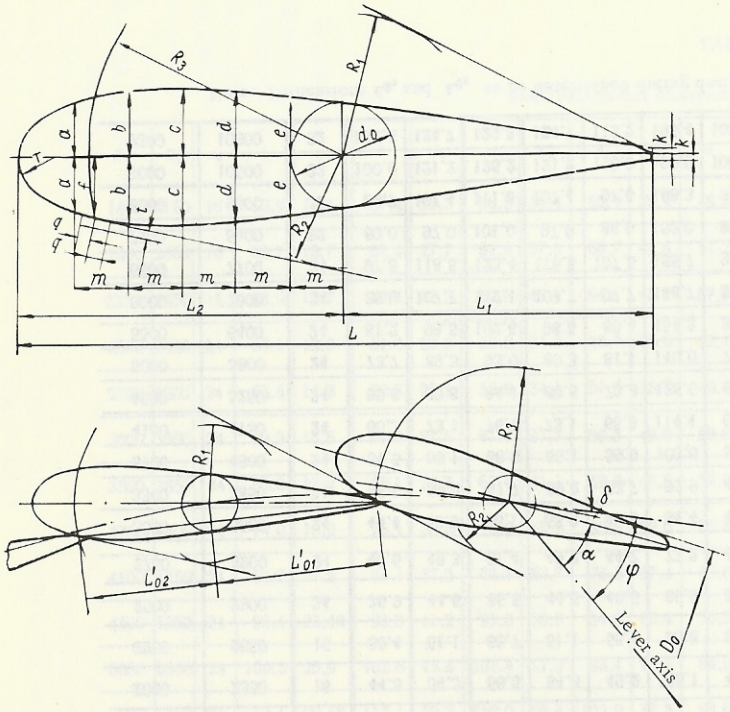


FIGURE VI. 27. Dimensions of the standard symmetrical guide- vane profile (LMZ): z_0 — number of guide vanes; n_0 eccentricity.

z_0	$\sim \varphi°$	tanδ	$\alpha°$	$\sim n_0$
16	22	0.1368	14	0.046
24	42	0.1305	35	0.040
32	42	0.1220	35	0.039

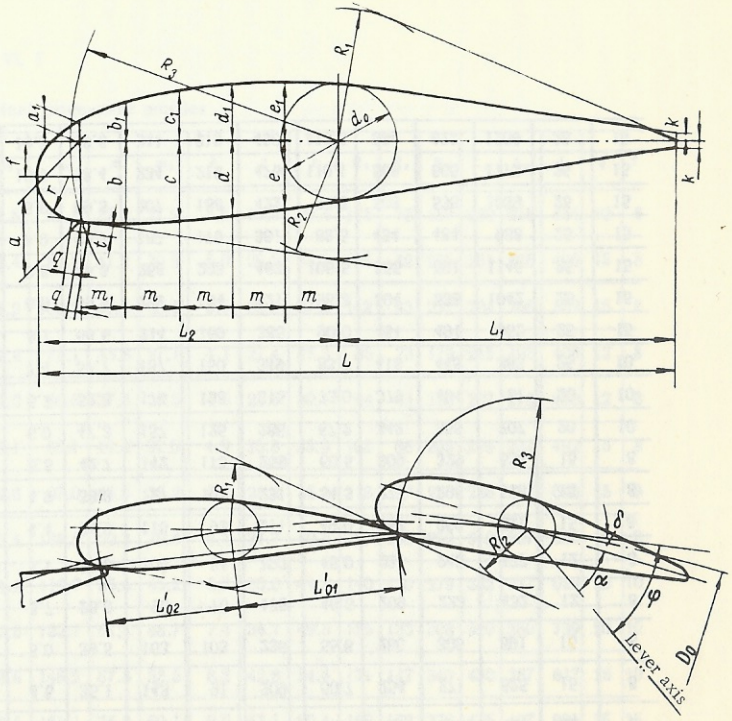


FIGURE VI. 28. Dimensions of the standardized asymmetrical guide-vane profile (LMZ)

z_0	$\sim \varphi°$	tanδ	$\alpha°$	$\sim n_0$
16	22	0.17	12	0.058
24	42	0.1523	33	0.051

TABLE VI. 6

Basic parameters of a symmetrical guide- vane profiles

D_1	D_0	z_0	a	b	c	d	e	d_0	m	k	r	R_1	R_2	R_3	f	L_1	L_2	L	q	t
1800	2150	16	41.0	49.7	51.7	49.7	45.1	77.9	41.2	4.1	32.1	130	82	192	46.0	233	248	481	12	8
2000	2350	16	44.8	54.3	56.5	54.3	49.2	85.1	45.1	4.5	35.1	143	91	209	50.7	254	271	525	15	8
2250	2650	16	50.4	61.1	63.7	61.1	55.4	95.8	50.7	5.0	39.5	163	103	236	55.6	286	305	591	15	8
2500	2900	24	36.9	44.6	46.5	44.6	40.5	69.9	37.1	3.7	28.9	96	76	175	40.5	209	223	432	12	8
2750	3200	24	40.6	49.3	51.4	49.3	44.7	77.2	40.9	4.1	31.9	106	84	193	45.0	231	246	477	12	8
3000	3500	24	44.4	53.9	56.1	53.9	48.8	84.4	44.7	4.4	34.9	116	92	211	49.0	252	269	521	15	8
3300	3850	24	48.9	59.2	61.7	59.2	53.7	92.9	49.2	4.9	38.3	127	101	231	54.5	277	296	573	15	8
3700	4300	24	54.5	66.1	68.8	66.1	59.9	103.6	54.9	5.5	42.7	142	113	259	60.5	309	329	638	15	8
4100	4750	24	60.3	73.1	76.1	73.1	66.3	114.4	60.6	6.0	47.3	157	125	286	67.2	342	365	707	20	10
4500	5250	24	66.6	80.8	84.1	80.8	73.3	126.6	67.0	6.7	52.3	176	138	315	73.0	379	404	781	20	10
5000	5800	24	73.7	89.3	93.0	89.3	81.1	140.0	74.1	7.4	57.7	187	150	349	83.7	418	445	863	25	10
5500	6400	24	81.2	98.5	102.6	98.5	89.4	154.2	81.8	8.1	63.6	214	169	385	90.0	461	491	952	25	15
6000	7000	24	88.9	107.7	112.1	107.7	97.7	168.7	89.4	8.9	69.6	232	184	421	98.3	504	538	1042	25	15
6600	7700	24	97.8	118.5	123.4	118.5	107.5	185.7	98.4	9.8	76.6	258	203	463	106.5	555	591	1146	25	15
7200	8400	32	80.0	97.0	101.0	97.0	88.0	152.0	80.5	8.0	62.7	187	170	381	88.5	454	484	938	25	15
8000	9300	32	88.7	107.4	111.8	107.4	97.6	168.3	89.2	8.9	69.5	207	188	422	97.8	503	536	1039	25	15
9000	10500	32	100.0	121.2	126.2	121.2	110.0	190.0	100.7	10.0	78.4	234	212	476	110.1	568	605	1173	25	15
9300	10800	32	102.8	124.7	129.8	124.7	113.2	195.4	103.5	10.3	80.6	241	219	490	113.8	584	622	1206	25	15

Note: Dimensions L_{0_1} and L_{0_2} to be determined during design

TABLE VI. 7

Basic parameters of asymmetrical guide-vane profiles

D_1	D_0	z_0	a	a_1	b	b_1	c	c_1	d	d_1	e	e_1	d_0	m	m_1	k	f	r	R_1	R_2	R_3	L_1	L_2	L	q	t
1800	2150	16	55.9	14.4	57.1	25.3	56.5	34.4	52.0	39.0	46.8	41.6	81.3	37.7	27.9	4.6	23.8	30.4	115	75	187	239	215	454	12	8
2000	2350	16	60.7	15.7	62.4	27.7	61.6	37.6	56.7	42.6	51.2	45.4	88.8	41.2	30.9	5.0	26.0	33.2	126	82	205	261	235	496	15	8
2250	2650	16	68.9	17.7	70.4	31.2	69.6	42.4	64.1	48.1	57.7	51.2	100.2	46.4	35.1	5.6	29.3	37.5	142	93	231	294	265	559	15	8
2500	2900	24	50.1	12.9	51.4	22.8	50.8	31.0	46.7	35.0	42.1	37.4	73.1	33.8	27.1	4.1	21.4	27.3	85	73	170	215	193	408	12	8
2750	3200	24	55.5	14.3	56.6	25.1	55.9	34.1	51.6	38.7	46.5	41.2	80.6	37.3	30.5	4.5	23.6	30.1	94	81	188	237	213	450	12	8
3000	3500	24	59.9	15.6	61.9	27.5	61.1	37.3	56.3	42.2	50.8	45.1	88.1	40.8	32.6	4.9	25.8	33.0	103	88	205	259	233	492	15	8
3300	3850	24	66.3	17.2	68.1	30.2	67.4	41.1	62.0	46.5	55.9	49.6	97.0	45.0	36.2	5.4	28.4	36.3	113	97	226	285	257	542	15	8
3700	4300	24	74.0	19.2	76.1	33.8	75.2	45.9	69.2	52.0	62.4	55.4	108.2	50.3	39.8	6.1	31.7	40.5	127	109	252	318	287	605	15	8
4100	4750	24	81.7	21.2	84.1	37.3	83.1	50.7	76.5	57.4	69.0	61.2	119.7	55.5	45.2	6.7	35.0	44.8	140	120	279	352	317	669	20	10
4500	5250	24	90.4	23.42	93.0	41.2	91.9	56.0	84.6	63.4	76.3	67.6	132.1	61.4	48.7	7.4	38.7	49.5	155	133	308	389	350	739	20	10
5000	5800	24	100.5	25.9	102.6	45.6	101.4	61.9	93.4	70.1	84.2	74.8	146.2	67.8	53.5	8.2	42.8	54.6	171	147	340	430	387	817	25	10
5500	6400	24	110.1	28.58	113.1	50.3	112.0	68.4	103.0	77.3	93.0	82.5	161.1	74.8	60.1	9.0	47.1	60.4	189	162	376	475	427	901	25	15
6000	7000	24	120.0	31.2	123.8	54.9	122.4	74.6	112.7	84.6	101.6	90.2	176.2	81.7	67.2	9.9	51.6	65.9	206	176	411	519	466	985	25	15
6600	7700	24	132.3	34.3	136.3	60.4	134.7	82.2	124.0	93.1	111.8	99.2	193.9	90.1	71.9	10.9	56.8	72.6	227	194	451	571	514	1085	25	15

Note: Dimensions L_{0_1} and L_{0_2} to be determined during design

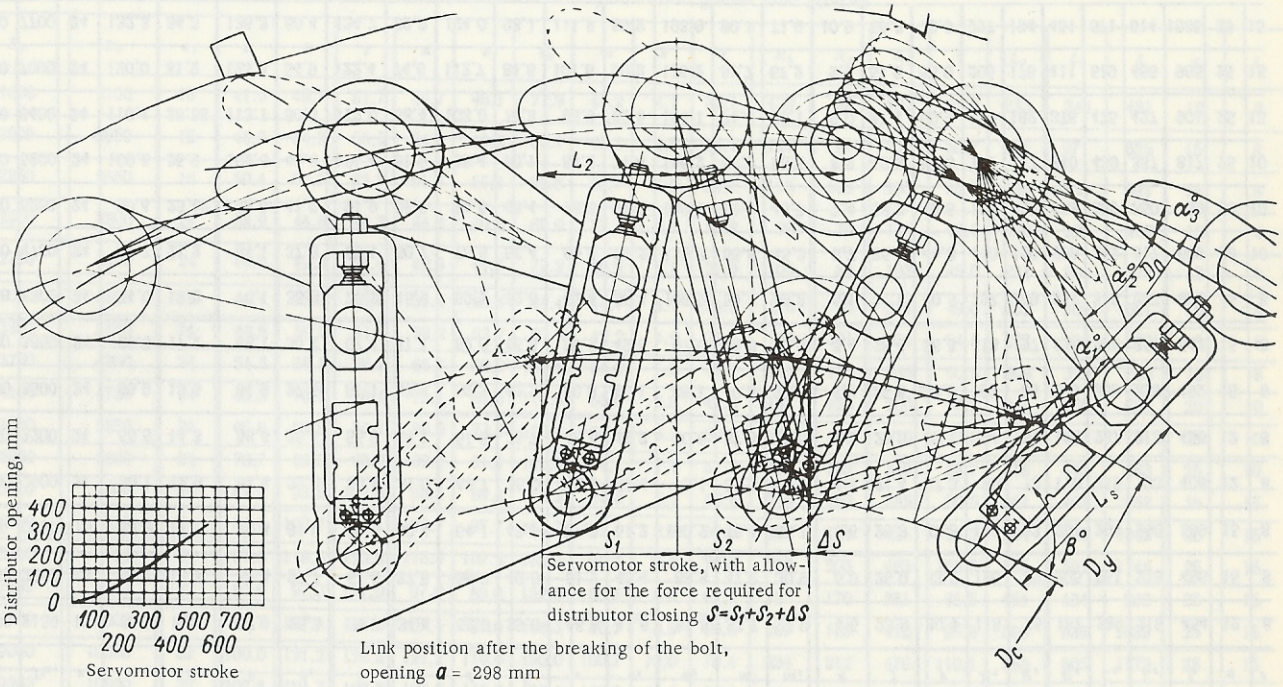


FIGURE VI. 29. Graphical layout of the distributor, including actuating mechanism with a breaking bolt in the link

After selecting the guide-vane profile according to the model tests, one determines the number of guide vanes and the pitch-circle diameter from the curve of the maximum distributor opening $a_{0\,m\,max}$, given on the universal chart, according to the rated turbine operating conditions.

Usually, the maximum distributor opening is determined for minimum head, so that the maximum discharge ensures the required power output in that condition. Under the rated or maximum head, it is not usually necessary to open the distributor completely.

The distributor opening a_{0max} for the full-scale turbine may be determined approximately from the formula

$$a_{0max} = a_{0\,m\,max} \frac{D_1 z_{0m}}{D_{1m} z_0}. \qquad \text{(VI. 47)}$$

After selecting the distributor proportions, with a_0 known, one proceeds to the graphical layout, as shown in Figure VI. 29. The adjacent guide vanes are drawn in to the largest possible scale, both for the closed position, and for several openings a_0. For each position of the guide vanes, one also draws the levers and links in the corresponding position, and determines the gate ring displacement along the diameters D_c and D_y. The displacement along the diameter D_y equals the servomotor-piston stroke s. The piston stroke s includes the stroke Δs to ensure the required force for the distributor closing, thus allowing for the elastic deformation of the actuacting mechanism.

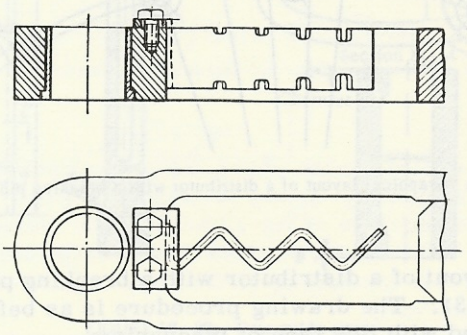


FIGURE VI. 30. Shock absorber in the guide-vane link

When plotting the layout of the distributor, templates cut from thick paper or cardboard to suitable scale are used for the guide vanes. These templates facilitate drawing. The positions which guide vanes, levers, and links assume after the rupture of the breaking link, when the kinematic linkage between the parts of the actuating mechanism is broken, should be exactly determined so as to prevent damage to these parts.

The position of the links with respect to the lever after the bolt breaks when the guide vane jams, with the lever in the open position, is represented by dotted lines in the figure. The link does not touch the link of the adjacent closed vane. The larger the distributor opening, the more difficult it becomes to prevent the links from touching when the connection between the parts of the mechanism is interrupted.

For this reason it is sometimes necessary to use curved levers.

The lower ring of the distributor or the speed ring should be provided with stops which limit the rotation of the guide vane around its axis and prevent dangerous vibrations or rotational movement of the guide vane after breaking-link rupture.

The links of the actuating mechanism represented in Figure VI. 29 are provided with shock absorbers (flexible stops) (see Figure VI. 30) which limit the movement of the slide block after breaking, thus preventing two adjacent links from touching. Apart from this, the guide-vane movement with the lever and the slide block is smoother after breaking.

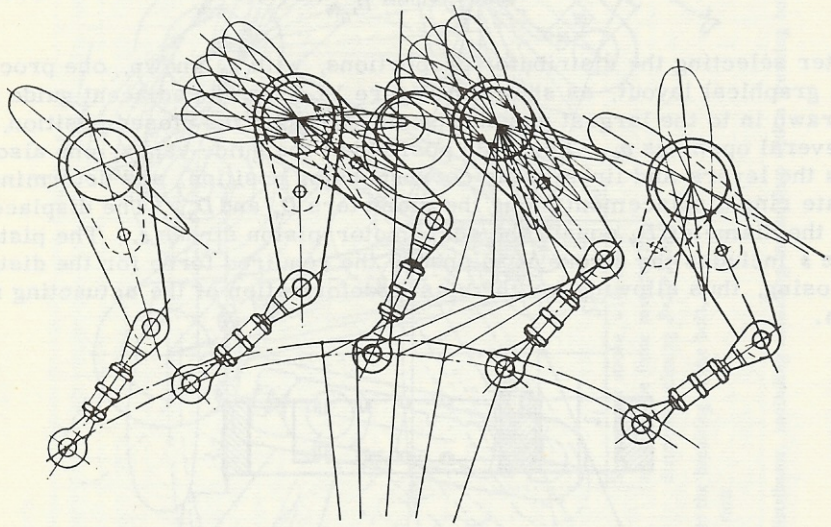


FIGURE VI. 31. Graphical layout of a distributor with a breaking pin in the lever

The graphical layout of a distributor with a breaking pin in the lever is shown in Figure VI. 31. The drawing procedure is as before. Latest Soviet turbines are provided with this type of mechanism.

36. THE GUIDE VANES

Design. A cast guide vane for a Kaplan turbine — of standard LMZ design — is shown in Figure VI. 32.

The guide vane consists of the streamlined vane body (2) and the upper (1) and lower (3) pivots. The upper pivot is longer than the lower one; its ground surfaces are guided in two bushings on the upper distributor ring. The lower pivot is guided in the bushing mounted on the lower distributor ring. The lever is fitted on the top end of the upper pivot — accurately machined for this purpose — and keyed by means of a pin.

The guide vane is usually hollow; the wall thickness is determined on the basis of strength considerations. The thickness of the guide-vane body at the joint with the upper pivot is often less than the pivot diameter: it is therefore necessary to ensure a smooth transition from the pivot to the vane body. Usually, the latter is not machined, but merely ground; hence, the guide-vane surface should be carefully cast.

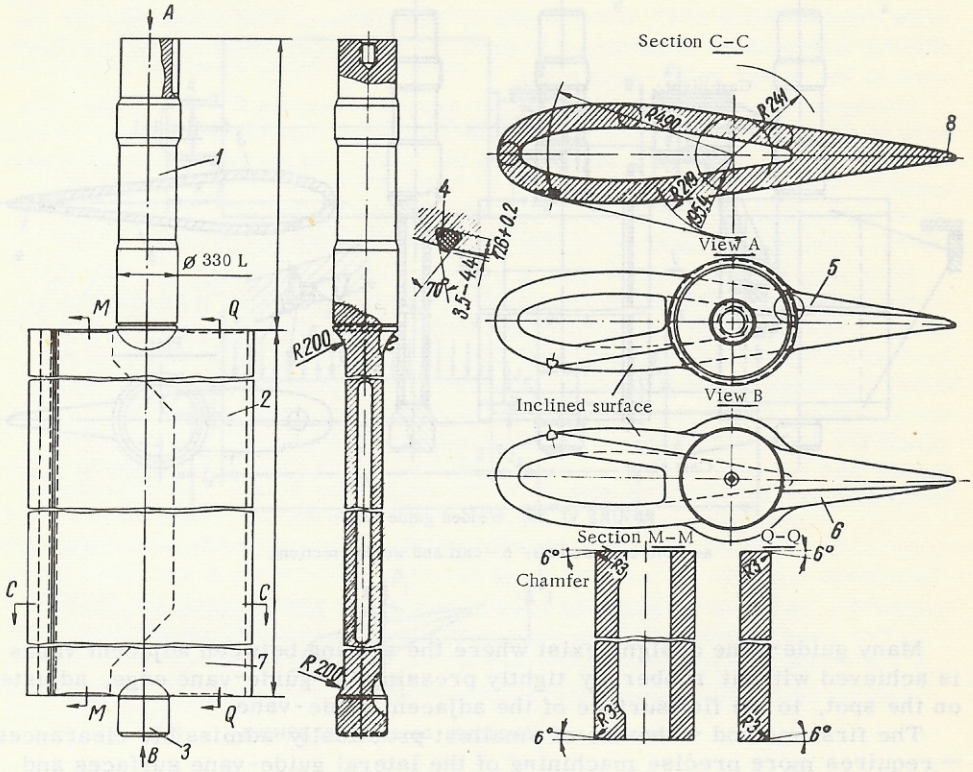


FIGURE VI. 32. Cast guide vane

Only trailing edge (8) and the contact line with the adjacent vane are machined. A dovetail-shaped groove is cut on the guide vane surface along this line for taking the rubber cord (4). Its position is defined by two radii (here R = 490 and R = 219) which may be determined from the graphical layout of the distributor. Experience in the operation of distributors with rubber seals between the guide vanes has shown that the shapes of rubber cord and groove must be carefully selected and matched. The rubber cord should be stretched tight in the groove, since otherwise it might be carried way by the water flow. The best procedure is to bond the rubber to metal plates and bolt them to the guide vanes, but this complicates guide-vane manufacture.

Alternative welded guide-vane designs are shown in Figure VI. 33. Another system of fastening the rubber seal to the guide vane is shown also.

The rubber cord (6) is pressed into metal plate (7) which is fastened by bolts (8) to the groove provided in the guide vane. In this way, the rubber is more securely fastened to the guide vane. When selecting the thickness of the sheet for the welded guide vane, the depth of the groove for the rubber seal should be taken into consideration.

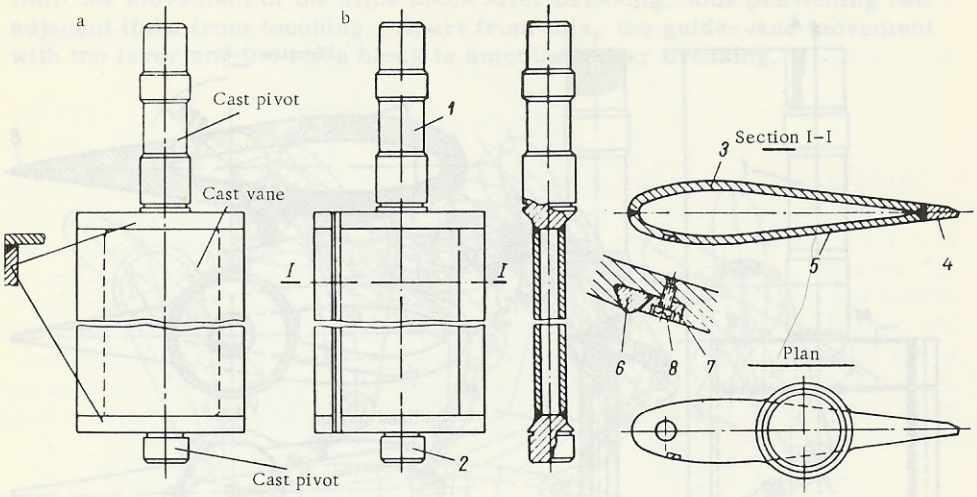


FIGURE VI. 33. Welded guide vane:

a—from cast sections; b—cast and welded sections.

Many guide-vane designs exist where the sealing between adjacent vanes is achieved without rubber by tightly pressing the guide-vane edge, adjusted on the spot, to the flat surface of the adjacent guide-vane.

The first method — the use of smallest practically-admissible clearances — requires more precise machining of the lateral guide-vane surfaces and more precise ring assembly.

When rubber cords are used to seal clearance spaces between the guide vanes and the upper and lower rings, the machining and assembly of the distributor parts may be done with larger tolerances. However, if the rubber seal is forced out of its groove, the leakages across the clearances may increase considerably.

Inclined surfaces (5 and 6) (see Figure VI. 32) are provided on the guide vane for better sealing of the clearances; when the guide vane closes, they are pressed against the rubber cord.

At large distributor openings in Kaplan turbines, the trailing edges of the guide vanes extend over the throat ring. It is therefore advisable to make the lower part (7) of the guide vane thinner, in order to avoid excessive rotation of the flow.

In welded guide vanes (Figure VI. 33), the pivot is welded to the guide-vane body all along its periphery; a reliable welded joint is thus obtained. It is not advisable to weld the pivot directly to the guide-vane body, because

the guide vane thickness is small compared with the pivot diameter. Alternative design *a* represents a guide vane made of cast parts, with pivot and guide-vane body welded together to form a single construction.

The fact that in this design the guide vanes are made up of separately cast parts considerably simplifies the casting process, permitting the use of mechanical molding. This design is recommended for steel guide-vanes.

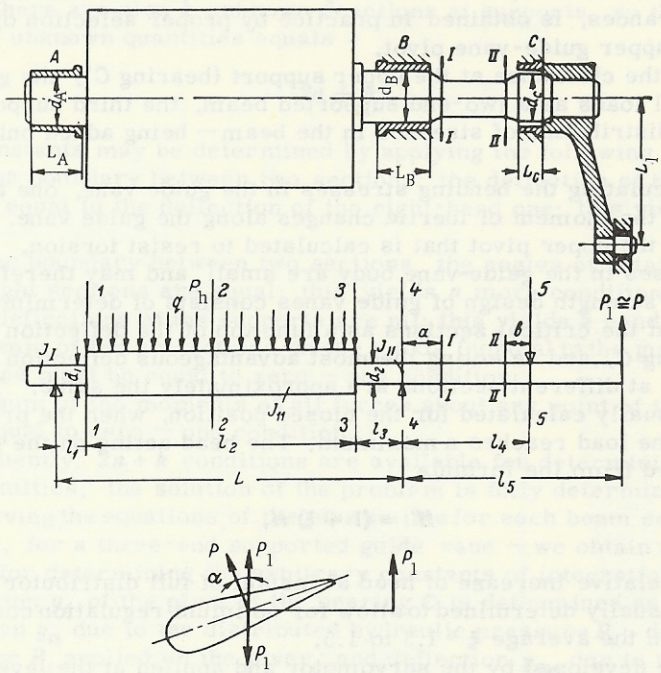


FIGURE VI. 34. Load distribution on a guide vane

The same figure shows a second design, a guide vane consisting of three plates (3), (4), and (5), welded together with vertical seams. Plate (4) is welded to the other two by electroslag welding. Plates (3) and (5) are stamped out according to the guide-vane profile.

Flat plates, cast together with the upper (1) and lower (2) guide-vane pivots, are welded both from above and below with horizontal seams to the guide-vane body. This design was developed at the LMZ, and the experiment proved quite satisfactory.

Welded guide vanes do not weigh less than cast vanes, but their cost is 40% lower; hence, their increased use in turbine construction nowadays.

Strength calculation. The guide vane is designed to resist both bending due to forces normal to its axis, and torsion due to moments applied to the lever.

In calculation for resistance to bending, the guide vane is assumed to be a beam resting on three supports, subjected to the load *q* due to water

pressure p_h distributed over the largest part of the beam span, and to the concentrated load P of the lever, exerted in the same plane, but at the overhung end (Figure VI. 34).

The support (bearing) C may be placed above the line which joins the bearings (A and B).

The stresses due to bending at the beam cross-sections vary with the displacement of C with respect to A and B; a position may always be found for which the bending and torsional stresses will be the smallest. The optimum displacement of C, determined by calculations with allowance for machining tolerances, is obtained in practice by proper selection of the clearance at the upper guide-vane pivot.

Owing to the clearance at the upper support (bearing C), the guide vane acts at small loads as a two-end supported beam, the third support — which effects a redistribution of stresses in the beam — being added only at large loads.

When calculating the bending stresses in the guide vane, one allows for the fact that the moment of inertia changes along the guide vane.

It is only the upper pivot that is calculated to resist torsion. The torsional stresses in the guide-vane body are small, and may therefore be ignored. The strength design of guide vanes consists of determining the stresses σ at the critical sections as a function of the deflection y at the upper bearing C, and selecting the most advantageous deflection at which the stresses at different sections are approximately the same. The guide vanes are usually calculated for the closed position, when the pressure is higher and the load reaches a maximum. The head acting on the guide vane is determined from the formula

$$H' = (1 + \xi) H, \tag{VI. 48}$$

where ξ = relative increase of head at instant of full distributor closing, usually determined to allow for optimum regulation conditions, on the average $\xi = 1.3$ to 1.5.

The force developed by the servomotor and applied at the lever is

$$P = P_1 \cos \alpha;$$

since $\cos \alpha \approx 1$, one usually takes

$$P = P_1.$$

The analytic method of calculating guide vanes by considering them as multiple-supported beams of variable rigidity was developed by A. E. Zhmud'. His technique is basically the following:

The differential equation of the elastic line for each section is written

$$EJy'' = M, \tag{VI. 49}$$

where E = modulus of elasticity;
J = moment of inertia;
y'' = second derivative of the deflection;
M = bending moment.

After the first integration we obtain

$$EJy' = \int M dx = A(x) + C. \tag{VI.50}$$

After the second integration we obtain from

$$EJy = \int dx \int M dx = B(x) + Cx + D \tag{VI.51}$$

two arbitrary constants. For n sections, $2n$ arbitrary constants are unknown. There are also k unknown reactions at supports, so that the total number of unknown quantities equals

$$2n + k.$$

The constants may be determined by applying the following conditions:

1) at the boundary between two sections, the deflection of the left-hand section is equal to the deflection of the right-hand one; this yields n conditions;

2) at the boundary between two sections, the angles of rotation of the left and right sections are equal; this yields n more conditions;

3) the deflections at the supports are nil; this yields k conditions;

4) the sum of the projections on the y axis (normal to the guide-vane axis) of all forces must be equal to zero — one condition;

5) the sum of the moments of all forces about any point of the beam must be equal to zero — one condition.

Consequently, $2n + k$ conditions are available for determining $2n + k$ unknown quantities; the solution of the problem is fully determined.

By deriving the equations of the elastic line for each beam section — in the given case, for a three-end supported guide vane — we obtain a system of equations for determining the arbitrary constants of integration. Here, the deflection y_c of the pivot at the bearing C is determined as the sum of deflection y_{c_I} due to the distributed hydraulic pressure P_h, deflection $y_{c_{II}}$ due to force P_1 applied on the lever, and deflection $y_{c_{III}}$ due to the reaction of support R_c.

$$y_c = y_{c_I} + y_{c_{II}} + y_{c_{III}}. \tag{VI.52}$$

Leaving aside the determination of the deflections, whose formulas the reader may find in S.A. Granovski's monograph /24/, we write their final expression.

The deflection at bearing C, due to hydraulic pressure:

$$y_{c_I} = kP_c a_3 \left[\frac{a_1^3 a_4}{3} \cdot \frac{J_{II}}{J_I} + \left(\frac{a_6 a_3^2}{3} - \frac{a_1^3 a_4}{3} - \frac{a_2^3}{8} - \frac{a_1 a_2^2}{6} \right) + \right.$$
$$\left. + \left(\frac{a_4}{3} - \frac{a_3^3 a_4}{3} - \frac{a_2^3}{48} + \frac{a_4^3}{6} - \frac{a_4^2}{6} - \frac{a_4^2}{2} + \frac{a_2^2 a_3}{8} \right) \frac{J_{II}}{J_{III}} \right]. \tag{VI.53}$$

The deflection at bearing C, due to the force P_1:

$$y_{c_{II}} = P_1 k \frac{a_5}{3} \left[\frac{a_1^3 a_6 J_{II}}{J_I} + a_6 (a_3^3 - a_1^3) + \right.$$
$$\left. + \left(a_6 + \frac{3}{2} a_5 a_6 - \frac{a_5^2}{2} - a_3^3 a_6 \right) \frac{J_{II}}{J_{III}} \right]. \tag{VI.54}$$

The deflection at bearing C, due to reaction R_c:

$$y_{c\,III} = R_c k \frac{\alpha_5^2}{2}\left[\alpha_1^3 \frac{J_{II}}{J_1} + (\alpha_3^3 - \alpha_1^3) + (1 - \alpha_3^3 + \alpha_6)\frac{J_{II}}{J_{III}}\right], \qquad \text{(VI. 55)}$$

where

$$k = \frac{L^3}{EJ_{II}};$$

$$\alpha_1 = \frac{l_1}{L}; \quad \alpha_2 = \frac{l_2}{L}; \quad \alpha_3 = \alpha_1 + \alpha_2;$$

$$\alpha_4 = \frac{l_3 + \frac{l_2}{2}}{L}; \quad \alpha_5 = \frac{l_4}{L}; \quad \alpha_6 = \frac{l_5}{L}.$$

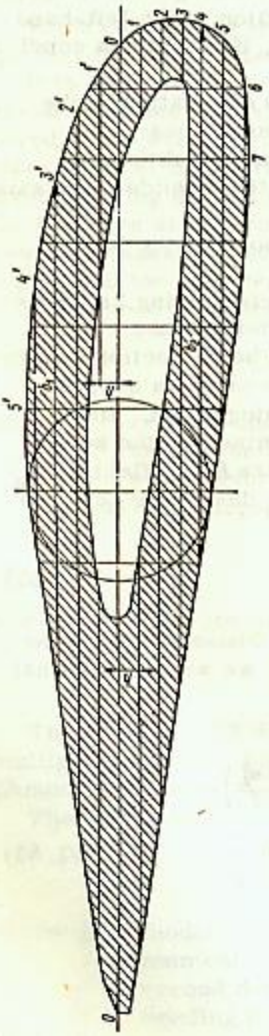


FIGURE VI. 35. Calculation diagram for determining the moment of inertia of the guide vane

and
- E = modulus of elasticity;
- J_1 = moment of inertia of the lower guide-vane pivot;
- J_{II} = moment of inertia of the guide-vane cross section;
- J_{III} = moment of inertia of the upper guide-vane pivot;
- $L, l_1, l_2, l_3, l_4, l_5$ = lengths as shown in Figure VI. 34.

The reactions at the supports A and B are

$$R_A = P_h a_4 + P_1 a_6 - R_c a_5 \qquad \text{(VI. 56)}$$

$$R_B = P_h\left(a_1 + \frac{a_2}{2}\right) - P_1(1 + a_6) + + R_c(1 + a_5). \qquad \text{(VI. 57)}$$

In calculating the guide vanes, the following procedure is adopted:

1. Determine the moment of inertia J and the section modulus W of the guide-vane pivots;

$$J_1 = \frac{\pi d_1^4}{64}\text{cm}^4; \quad W_1 = \frac{2J_1}{d_1} = \frac{\pi d_1^3}{32}\text{cm}^3;$$

$$J_{III} = \frac{\pi d_2^4}{64}\text{cm}^4; \quad W_{III} = \frac{2J_{III}}{d_2} = \frac{\pi d_2^3}{32}\text{cm}^3;$$

2. Determine the moment of inertia and section modulus of the guide-vane cross section by dividing the section into elementary areas, as shown in Figure VI. 35.

Let us denote by b_1 the width of the strips located above a given line $\overline{OO}$, and by b_2 the width of those located below. The distance between the strips is denoted by h. The guide vane cross-sectional area is

$$F = h(\Sigma b_1 + \Sigma b_2)\text{cm}^2. \qquad \text{(VI. 58)}$$

The static moment about $\overline{OO}$

$$S = h^2 \left[\Sigma b_1 \left(\frac{y}{h} \right) - \Sigma b_2 \left(\frac{y}{h} \right) \right]. \qquad \text{(VI. 59)}$$

The distance of the neutral axis from $\overline{OO}$

$$\Delta y = \frac{S}{F} \text{ cm}.$$

The moment of inertia with respect to the line $\overline{OO}$

$$J' = h^3 \left[\Sigma b_1 \left(\frac{y}{h} \right)^2 + \right.$$

$$\left. + \Sigma b_2 \left(\frac{y}{h} \right)^2 \right] \text{cm}^4. \qquad \text{(VI. 60)}$$

The correction for the distance of $\overline{OO}$ from the neutral axis

$$\Delta J = F \Delta y^2 \text{ cm}^4.$$

The moment of inertia with respect to the axis passing through the centroid of section

$$J = J' - \Delta J \text{ cm}^4. \qquad \text{(VI. 61)}$$

The minimum section modulus

$$W_{\min} = \frac{J}{y_{\max}} \text{cm}^3.$$

3. Determine the servomotor force P_1 applied at the lever

$$P_1 = \frac{P_S D_y}{z_0 D_S} \cdot \frac{\sin \gamma}{\cos \beta} \text{ kg},$$

where P_s is determined by the formula

$$P_s = \frac{\pi}{4} p \left(d_s^2 - d_r^2 \right). \qquad \text{(VI. 62)}$$

4. Determine the hydraulic pressure acting on the vane from the formula

$$P_h = \frac{\pi D_0 H' \gamma b_0}{z_0} \text{ kg}.$$

5. The load per unit length

$$q = \frac{P_h}{l_z} \text{ kg/cm}. \qquad \text{(VI. 63)}$$

6. Determine the coefficients α_i.
7. Determine the coefficient k.
8. Calculate the deflections at bearing C

$$y_{c_I},\ y_{c_{II}},\ y_{c_{III}}$$

from the formulas (VI. 53, VI. 54 and VI. 55).

9. Determine from the formula (VI. 52) the total deflection at bearing C.

10. Determine the maximum deflection, when $R_c = 0$

$$y_{max} = y_{c_I} + y_{c_{II}} \text{ cm}$$

11. Determine the reaction of the supports from the formulas (VI. 56 and VI. 57).

12. Determine the bending stresses at various vane sections.

At the joint (transition) between pivot A and guide-vane body, section 1-1

$$\sigma_{b_1} = \frac{R_A l_1}{W_1} \text{ kg/cm}^2 \qquad \text{(VI. 64)}$$

section 2-2 — in the guide-vane body

$$\sigma_{b_2} = \left[R_A\left(l_1 + \frac{l_2}{2}\right) - \frac{q l_2^2}{8}\right]\frac{1}{W_{II}} \text{ kg/cm}^2; \qquad \text{(VI. 65)}$$

section 3-3 — at the joint between guide-vane body and pivot B

$$\sigma_{b_3} = \left[R_A(l_1 + l_2) - \frac{q l_2^2}{2}\right]\frac{1}{W_{III}} \text{ kg/cm}^2; \qquad \text{(VI. 66)}$$

section 4-4 — in the pivot at bearing B

$$\sigma_{b_4} = \frac{P_1 l_5 - R_c l_4}{W_{III}} \text{ kg/cm}^2; \qquad \text{(VI. 67)}$$

section 5-5 — in the pivot below bearing C

$$\sigma_{b_5} = \frac{P_1(l_5 - l_4)}{W_{III}} \text{ kg/cm}^2. \qquad \text{(VI. 68)}$$

13. Determine the torsional stresses in pivots B and C

$$\tau = \frac{P_1 L_1}{2W_{III}} \text{ kg/cm}^2. \qquad \text{(VI. 69)}$$

14. Calculate the combined stress in pivots B and C

$$\sigma_c = \frac{\sigma_b}{2} + \frac{1}{2}\sqrt{\sigma_b^2 + 4\tau^2} \text{ kg/cm}^2. \qquad \text{(VI. 70)}$$

15. Determine the pressures in the pivots

$$\left.\begin{aligned} &\text{Pivot } A: \sigma_d = \frac{R_A}{d_A L_A} \text{kg/cm}^2 \\ &\text{Pivot } B: \sigma_d = \frac{R_B}{d_B L_B} \text{kg/cm}^2 \\ &\text{Pivot } C: \sigma_d = \frac{R_C}{d_C L_C} \text{kg/cm}^2 \end{aligned}\right\} \qquad \text{(VI. 71)}$$

16. By taking different predetermined values (in steps of 0.5 or 1 mm) for the deflections y_c within the range from $y_c = 0$ to $y_c = y_{max}$, find the stresses at the guide-vane sections, and the specific pressures, and determine the reaction of the supports. Enter the results in Table VI. 8.

TABLE VI.8

Form for entering the calculated stresses due to pressures and reaction of supports

y_c mm	Support reaction, kg			Bending stresses, kg/cm^2					Combined stresses			Pressure, kg/cm^2		
									Pivot B		Pivot C			
	R_C	R_A	R_B	σ_{b_1}	σ_{b_2}	σ_{b_3}	σ_{b_4}	σ_{b_5}	Section 3-3 σ_{c_3}	Section 4-4 σ_{c_4}	σ_{c_5}	Pivot A	Pivot B	Pivot C
0														
0.5														
1.0														
...														
...														
$y_{c\,max}$														

17. From the data obtained, plot the curves of the stress variation at various guide-vane sections as a function of the deflection at bearing C. Curves of this type are shown in Figure VI. 36.

Select on the graph the most advantageous deflection at bearing C, to which the most desirable stress distribution at the guide-vane sections corresponds. With the kinematic diagram of the guide-vane-actuating mechanism adopted by the LMZ, this occurs with deflections of about half the maximum value.

The reaction of the supports are usually as follows:

$$\left.\begin{aligned} R_a &= (0.4 - 0.5)\, P_h; \\ R_b &= (0.8 - 0.85)\, P_h; \\ R_c &= (0.4 - 0.5)\, P_h. \end{aligned}\right\} \qquad \text{(VI. 72)}$$

18. For the selected value of the clearance at bearing C, check the stresses at the sections between bearings B and C.

Section I—I:

bending moment

$$M_I = P_1 (l_5 - a) - R_c (l_4 - a), \qquad \text{(VI. 73)}$$

bending stress

$$\sigma_{b_I} = \frac{M_I}{W}. \tag{VI.74}$$

torsional stress

$$\tau = \frac{P_1 L_1}{2W}. \tag{VI.75}$$

combined stress

$$\sigma_{c_I} = \frac{1}{2}\sigma_{b_I} + \frac{1}{2}\sqrt{\sigma_{b_I}^2 + 4\tau^2}. \tag{VI.76}$$

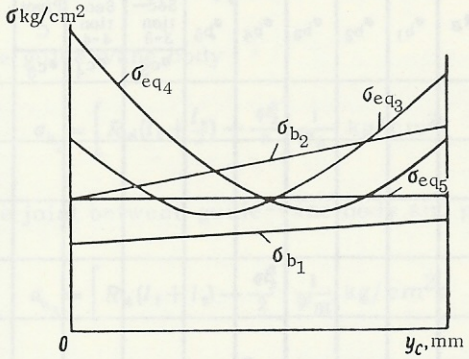


FIGURE VI.36. Stresses at guide-vane cross sections for various deflections

Section II—II:
bending moment

$$M_{II} = P_1 (l_5 - l_4 + b) - R_c b, \tag{VI.77}$$

bending stress

$$\sigma_{b_{II}} = \frac{M_{II}}{W}, \tag{VI.78}$$

combined stresses

$$\sigma_{c_{II}} = \frac{1}{2}\sigma_{b_{II}} + \frac{1}{2}\sqrt{\sigma_{b_{II}}^2 + 4\tau^2}. \tag{VI.79}$$

19. Determine the actual diameter of pivot C, allowing for a fit tolerance at pivot B usually taken as $\frac{A_3}{L_v}$.

The maximum clearance at pivot C

$$\Delta C_{max} = 2Y - \Delta B_{min} \tag{VI.80}$$

The minimum clearance at pivot C

$$\Delta C_{min} = 2Y - \Delta B_{max} - \delta_c, \quad \text{(VI. 81)}$$

where ΔB_{min} and ΔB_{max} = minimum and maximum diametrical clearances of pivot B;

δ_c = machining allowance for pivot C (taken according to third class (C_3) of allowances).

Actual maximum diameter of pivot C

$$d_{c\,max} = d_c - \Delta C_{min}. \quad \text{(VI. 82)}$$

Actual minimum diameter of pivot C

$$d_{c\,min} = d_c - \Delta C_{max}. \quad \text{(VI. 83)}$$

20. Check the strength calculation of the guide vane for the increase in force P_1 — namely P_1' — occurring on rupture of the breaking element provided at the lever or link.

Guide-vane bearing. The design of the guide-vane bearing may be seen in Figure VI. 14. The bearing is a cast-iron flanged cylinder. The flanges are provided for mounting the bearing on the upper ring of the distributor. Two antifriction-metal bushings inside the bearing serve to guide the upper pivot of the guide vane. Special grooves for the seals, and holes for lubrication, are provided in the bearing body. The bearing flange may be shaped so as to cover the holes in the ring provided for guide-vane removal. The bottom end of the bearing has a centering collar fitted — with small clearance — into its seat in the upper distributor ring.

The diagram of the forces acting on the bearing is shown in Figure VI. 37. The horizontal forces R_c and R_v are the reactions at the bearing-bushing centers; the vertical force due to water pressure acts upon the lower collar of the bearing and is of importance at high heads only.

Since reaction R_c is applied close to the supporting flange, in calculating the resistance of the bearing to bending, only reaction R_v is assumed to be acting. The fit of the lower bearing end into the upper distributor ring is usually adopted according to the second class of tolerances, $\frac{A}{C}$. This fit permits the clearance to be varied from zero to a certain value δ. According to this, the resistance of the bearing to bending is to be calculated for two cases: case one — a beam (a) rigidly fixed at one end, and freely supported at the other, and case two — a cantilever beam (b) with the deflection equal to the maximum fit clearance. The first case is shown in Figure VI. 37, a. The calculation is performed in the following order:

1. Determine reaction R_F at the support /73/

$$R_F = \frac{R_v}{2} \cdot \frac{3l_1^2 L - l_1^3}{L^3} = \frac{R_v}{2}\left(\frac{l_1}{L}\right)^2 \left(3 - \frac{l_1}{L}\right). \quad \text{(VI. 84)}$$

2. The moment at the fixed end A is

$$M_0 = -\frac{R_v}{2} \cdot \frac{l_1^3 + 2l_1 L^2 - 3l_1^2 L}{L^2} = -\frac{R_v l_1}{2}\left[\left(\frac{l_1}{L}\right)^2 + 2 - 3\frac{l_1}{L}\right]. \quad \text{(VI. 85)}$$

3. The moment at section I-I

$$M_I = -M_0 + R_a l_4, \tag{VI.86}$$

where

$$R_a = R_v - R_F.$$

4. The moment at section II-II

$$M_{II} = R_v \left(l_2 - l_3\right) \tag{VI.87}$$

5. The moment at section III-III

$$M_{III} = R_F l_3. \tag{VI.88}$$

6. Determine the corresponding section moduli

$$W_A;\quad W_I;\quad W_{II};\quad W_{III}.$$

7. Determine the stresses at the given sections

$$\sigma'_{b_A} = \frac{M_0}{W_A};\quad \sigma'_{b_I} = \frac{M_I}{W_I};\quad \sigma'_{b_{II}} = \frac{M_{II}}{W_{II}};\quad \sigma'_{b_{III}} = \frac{M_{III}}{W_{III}}. \tag{VI.89}$$

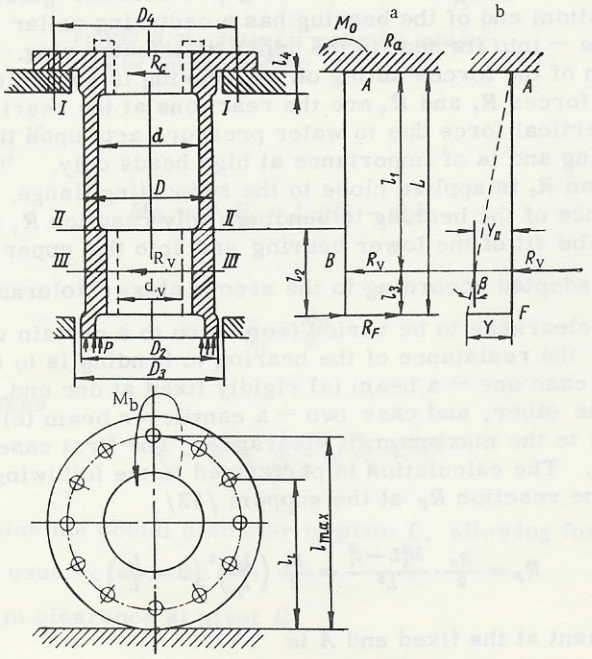


FIGURE VI.37. Stresses in guide-vane bearing

In order to find the stresses in the bearing when maximum clearance results in the assembly at an $\frac{A}{C}$ fit (alternative design b in Figure VI. 37), we first determine the maximum deflection at the bearing and the corresponding stresses, and later — since the stresses are proportional to the deformations — we calculate the stresses from the maximum possible deflection of the bearing within the limits of the maximum clearance.

The calculation procedure is as follows:

1. Determine the maximum deflection of the cantilever beam at section III, due to the force R_v

$$y_{III} = \frac{R_v l_1^3}{3EJ_1}, \tag{VI. 90}$$

where J_1 = moment of inertia of section I

$$J_1 = \frac{\pi (D^4 - d^4)}{64}.$$

2. Determine the deflection at point F. After the application of the force, the deflection y at point F is proportional to the length l_3

$$y = y_{III} + l_3 \tan \beta, \tag{VI. 91}$$

where

$$\tan \beta = \frac{3}{2} \cdot \frac{y_{III}}{l_1} = \frac{R_v l_1^2}{2EJ_1}.$$

3. Determine the stress corresponding to the maximum possible deflection.

At section A (the fixed end)

$$\sigma''_{b_A} = -\frac{R_v l_1}{W_A}. \tag{VI. 92}$$

At section I-I

$$\sigma'_{b_I} = \frac{-R_v (l_1 - l_4)}{W_I}. \tag{VI. 93}$$

At section II-II

$$\sigma''_{b_{II}} = \frac{-R_v (l_2 - l_3)}{W_{II}}. \tag{VI. 94}$$

At section III-III

$$M_b = 0; \quad \sigma_{b_{III}} = 0.$$

4. Determine the stress corresponding to the maximum possible deflection within the limits of the maximum clearance of an $\frac{A}{C}$ fit, by adding the stresses obtained for both cases.

At section A (the fixed end)

$$\sigma_{b_A} = \sigma'_{b_A} + \left(\sigma''_{b_A} - \sigma'_{b_A}\right)\frac{\delta}{y}. \tag{VI. 95}$$

At section I-I

$$\sigma_{b_I} = \sigma'_{b_I} + \left(\sigma''_{b_I} - \sigma'_{b_I}\right)\frac{\delta}{y}. \tag{VI. 96}$$

At section II-II

$$\sigma_{b_{II}} = \sigma'_{b_{II}} + \left(\sigma''_{b_{II}} - \sigma'_{I}\right)\frac{\delta}{y}. \tag{VI. 97}$$

At section III-III

$$\sigma_{b_{III}} = \sigma'_{I}\left(1 - \frac{\delta}{y}\right). \tag{VI. 98}$$

The bolts fastening the flange of the guide-vane bearing should be calculated for the force due to the water pressure on the bearing collar, and the force due to the guide-vane reactions R_v and R_c, which develop a moment tending to turn the bearing about the flange edge.

The force due to the water pressure

$$P_v = p\frac{\pi}{4}\left(D_4^2 - d_v^2\right), \tag{VI. 99}$$

where p = water pressure kg/cm^2.

The forces on the bolt due to the bending moment are calculated in the following way: assuming that the parts are absolutely rigid, we may consider that the bending moment on the bearing (M_b) produced by the support reactions R_v and R_c tends to turn the bearing about the flange edge, and is balanced by the sum of the forces acting on the bolts multiplied by their distances from the lower edge of the guide vane flange

$$M_b = \sum_{i=1}^{i=n} P_i\, l_i \tag{VI. 100}$$

where P_i = force acting on the i-th bolt;
l_i = distance from the i-th bolt to the lower flange;
n = number of bolts.

The force at any bolt may be expressed by the force P_{max} acting on the bolt farthest from the flange edge

$$P_i = P_{max}\frac{l_i}{l_{max}}.$$

so that

$$M_b = \sum_{i=1}^{i=n} \frac{P_{max}}{l_{max}} l_i^2 = \frac{P_{max}}{l_{max}} \sum_{i=1}^{i=n} l_i^2,$$

whence,

$$P_{max} = \frac{M_b l_{max}}{\sum_{i=1}^{i=n} l_i^2}. \qquad \text{(VI. 101)}$$

By adding this tensile force to the force due to water pressure, we obtain the total load acting on the bolt carrying the greatest load

$$P = P_{max} + \frac{P_v}{z},$$

where z = number of studs (bolts).

The stress in the bolt carrying the greatest load

$$\sigma_z = \frac{P}{f}, \qquad \text{(VI. 102)}$$

where f = minimum cross-sectional area of the threaded bolt, cm^2.

37. COMPONENTS OF THE GUIDE-VANE-ACTUATING MECHANISM

The components of the operating mechanism include (Figure VI. 24) the lever (1), link (2), breaking bolt or shear pin (3), and cylindrical hinge (4).

The parts of the guide-vane-actuating mechanism are designed to resist both the force transmitted from the servomotors to the closed distributor and the force causing rupture of the breaking link. Figure VI. 23 shows the diagram of the forces acting on the actuating mechanism.

Design of the guide-vane lever. The design of the guide-vane lever is shown in Figure VI. 38. It is advisable to select a box-shaped cross section for this part. To enable the link to move freely on the slide block when the bolt is broken, the lever head should be located higher then the hub. The lever itself is usually made of cast steel, and designed to resist bending and torsion.

The bending moment at sections I-I and II-II

$$M_I = P_1 l_1,$$
$$M_{II} = P_1 l_2.$$

The section modulus for a lever of box-shaped cross section

$$W = \frac{BH^3 - bh^3}{6H}.$$

Bending stress

$$\sigma_{b_I} = \frac{M_I}{W_I}; \quad \sigma_{b_{II}} = \frac{M_{II}}{W_{II}}. \qquad \text{(VI. 103)}$$

Torsional stress in section II-II

$$M_t = P_1 l.$$

Torsional stress in the box-shaped cross section II-II is

$$\tau_{II} = \frac{M_t \cdot 3 \cdot d_{max}}{\eta \Sigma (d^3 b)} \text{ kg/cm}^2. \qquad \text{(VI. 104)}$$

For the section shown in Figure VI. 38

$$\Sigma d^3 b = 2 d_1^3 B + d_{max}^3 h;$$

$\eta \approx 1.15$ – stress-concentration coefficient.

The combined stress in section II-II is

$$\sigma_c = \tfrac{1}{2} \sigma_{b_{II}} + \tfrac{1}{2} \sqrt{\sigma_{b_{II}}^2 + 4\tau_{II}^2} \text{ kg/cm}^2. \qquad \text{(VI. 105)}$$

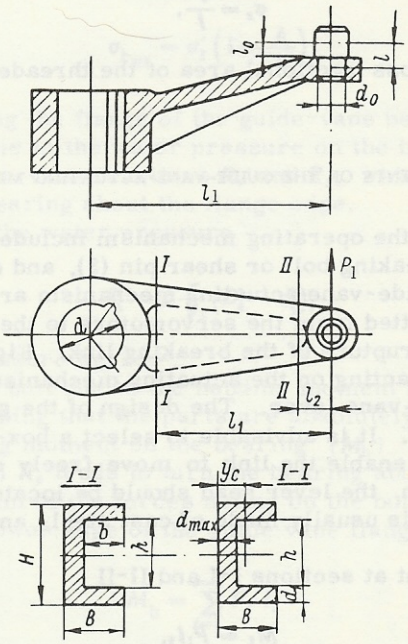


FIGURE VI. 38. Guide-vane lever

Design of the lever pin. The pin is made of steel 35 and designed to resist bending.

$$\sigma_b = \frac{M}{W} = \frac{P_1 l_0}{0.1 d_0^3} \text{ kg/cm}^2; \qquad \text{(VI. 106)}$$

where l_0 = arm of acting force, cm;

d_0 = pin diameter, cm.

Design of the lever keys. The key is made of steel 45 and designed to resist shear and crushing

$$\sigma_s = \frac{P_1 \frac{2l_1}{d}}{z_k l_k d_k} = \frac{2P_1 l_1}{z_k l_k d_k d} \text{ kg/cm}^2; \qquad \text{(VI. 107)}$$

where l_1 = lever length;
z_k = number of keys;
d_k = diameter of the round key;
l_k = key length;
d = diameter of key seat.

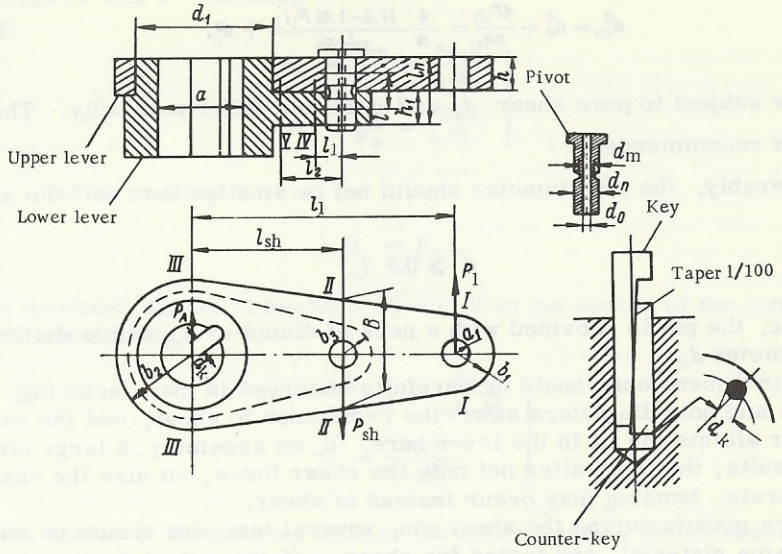


FIGURE VI. 39. Compound guide vane lever.

The crushing stresses in the key:

$$\sigma_{cr} = \frac{4P_1 l_1}{l_k d_k d} \text{ kg/cm}^2. \qquad \text{(VI. 108)}$$

A compound, cylindrical key, split lengthwise, is used to fasten the lever to the pivot (Figure VI. 39). The two parts, the actual key and the counter key, touch along an inclined plane of taper 1/100. The outer surface of the key parts is cylindrical in form, and of diameter d_k. Owing to the key taper, the assembly of the parts involves a tight fit. The surfaces must be in contact along a radial plane.

Design of the compound guide-vane lever. The compound lever (Figure VI. 39) consists of three parts: the upper and lower levers, and the grooved shear pin.

The shear pin. The force on the shear pin is

$$P_{sh} = \frac{P_1 l_1}{l_{sh}}. \qquad \text{(VI. 109)}$$

Shear pins are usually made of steel 45. The ultimate shear strength of this grade of steel σ_s = 4,900-5,600 kg/cm^2; thus, the area of the shear pin

$$F_{sh} = \frac{P_{sh}}{\sigma_s} = \frac{(1.3-1.4) P_1 l_1}{l_{sh} \sigma_s} \text{ cm}^2. \qquad \text{(VI. 110)}$$

The neck diameter d_m and the hole diameter d_o are determined by the relation

$$\frac{\pi\left(d_m^2-d_o^2\right)}{4}=F_{sh}=\frac{P_{sh}}{\sigma_s},$$

whence

$$d_m^2=d_o^2+\frac{4P_{sh}}{\pi\sigma_s}=\frac{4}{\pi}\frac{(1.3-1.4)P_1l_1}{l_{sh}\sigma_s}+d_o^2. \qquad \text{(VI. 111)}$$

To be subject to pure shear, d_n and d_o should differ markedly. The ratio $\frac{d_n}{d_o}$ = 3 is recommended.

Preferably, the pin diameter should not be smaller than half the pin length.

$$d \geqslant 0.5\ l_n.$$

Hence, the pin is provided with a neck of diameter d_m and is drilled out to a diameter d_o.

All pin dimensions should be carefully observed in manufacturing, since the neck and hole diameters affect the resistance to shear, and the outer diameter affects the fit in the lever bore. If, on assembly, a large clearance results, this may alter not only the shear force, but also the character of the strain: bending may occur instead of shear.

Before manufacturing the shear pin, several test pins should be made of the same material and tested for shear. If the actual force required to cause failure differs from that calculated, the neck diameter must be altered. The test pins should be cut from different parts of the same bar.

The upper lever. This is made of steel 3, and designed to resist tension and bending.

Section I-I (Figure VI. 39) — tension (calculated according to Lamé)

$$\sigma_{z_I}=\frac{P_1}{2a_1h}\cdot\frac{b_1^2+a_1^2}{b_1^2-a_1^2}. \qquad \text{(VI. 112)}$$

Section II-II — bending

$$\sigma_{b_{II}}=\frac{6P_1(l_1-l_{sh})}{h\left(B^3-d_n^3\right)}. \qquad \text{(VI. 113)}$$

Section III-III — tension (according to Lamé)

$$\sigma_{z_{III}}=\frac{P_{ul}}{2\frac{d_1}{2}h}\cdot\frac{b_2^2+\left(\frac{d_1}{2}\right)^2}{b_2^2-\left(\frac{d_1}{2}\right)^2}, \qquad \text{(VI. 114)}$$

where $P_{ul}=P_{sh}-P_1$.

The lower lever. This is made of steel 30L, and designed to resist tension, bending and torsion.

Section II-II — tension (according to Lamé)

$$\sigma_{b_{II}} = \frac{P_{sh}}{2\frac{d_n}{2}h_1} \cdot \frac{b_3^2 + \left(\frac{d_n}{2}\right)^2}{b_3^2 - \left(\frac{d_n}{2}\right)^2}. \tag{VI. 115}$$

Section IV and V — bending

$$\left.\begin{aligned} \sigma_{b_{IV}} &= \frac{M_{IV}}{W_{IV}} = \frac{P_{sh}\, l_1}{h_1 B_{IV}^2}, \\ \sigma_{b_V} &= \frac{M_V}{W_V} = \frac{P_{sh}\, l_2}{h_1 B_V^2}. \end{aligned}\right\} \tag{VI. 116}$$

The moment tending to twist the lever

$$M_t = P_{sh}\, l.$$

The torsional stress at sections IV and V in the center of the longer side of the cross section

$$\left.\begin{aligned} \tau_{IV_1} &= \frac{M_t}{\alpha_1 B_{IV} h_1^2} = \frac{P_{sh} l}{\alpha_1 B_{IV} h_1^2}, \\ \tau_{V_1} &= \frac{P_{sh}\, l}{\alpha_1 B_V h_1^2}. \end{aligned}\right\} \tag{VI. 117}$$

In the center of the shorter side of the cross section the stresses are

$$\tau_{IV_s} = \frac{P_{sh}\, l}{\alpha_2 B_{IV} h_1^2}; \qquad \tau_{V_s} = \frac{P_{sh}\, l}{\alpha_2 B_V h_1^2}.$$

The combined stresses

$$\left.\begin{aligned} \sigma_{c_{IV}} &= \tfrac{1}{2}\,\sigma_{b_{IV}} + \tfrac{1}{2}\sqrt{\sigma_{b_{IV}}^2 + 4\tau_{IV_s}^2}, \\ \sigma_{c_V} &= \tfrac{1}{2}\,\sigma_{b_V} + \tfrac{1}{2}\sqrt{\sigma_{b_V}^2 + 4\tau_{V_s}^2}. \end{aligned}\right\} \tag{VI. 118}$$

The coefficients α_1 and α_2 for the determination of the section moduli in torsion of a rectangular cross section are given in Table VI. 9 for different ratios $\frac{B}{h}$ (width B and height h).

TABLE VI. 9

Values of α_1 and α_2 for various ratios $\frac{B}{h}$

$\frac{B}{h}$	1.0	1.2	1.5	1.75	2.0	2.5	3.0	4.0	5.0	6.0	8.0	10.0	∞
α_1	0.208	0.219	0.231	0.239	0.246	0.258	0.267	0.282	0.291	0.299	0.307	0.312	0.333
α_2	1.0	0.93	0.86	0.82	0.79	0.77	0.75	0.74	0.74	0.74	0.74	0.74	—

Section III-III — tension (according to Lamé)

$$\sigma_{z_{III}} = \frac{P_1}{dH} \cdot \frac{b_2^2 + (0.5d)^2}{b_2^2 - (0.5d)^2}, \qquad \text{(VI. 119)}$$

where

$$P_t = P_{sh}\left(\frac{l_{sh}}{0.5d} - 1\right).$$

The lever key is designed to resist shear and crushing.

Distributor link. The material is steel grade L30.

The distributor link used in the actuating mechanism, with breaking bolt and slide block, is represented in Figure VI. 40. The link is designed to resist compression and buckling.

The compressive stresses at section A-A

$$\sigma_d = \frac{P_c}{(b_2 - b_1)c}. \qquad \text{(VI. 120)}$$

In order to determine the coefficient of reduction φ of the permissible stress it is necessary to determine the slenderness ratio λ of the link

$$\lambda = \frac{l}{i},$$

where l = length of link, cm;
i = radius of inertia, cm.

$$i = \sqrt{\frac{J}{F}},$$

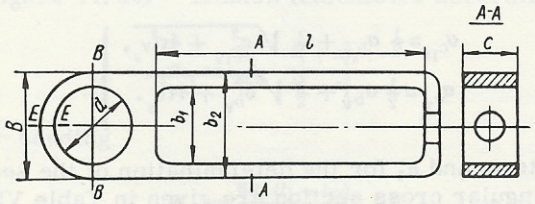


FIGURE VI. 40. Distributor link

where J = minimum moment of inertia, cm^4,

$$J = \frac{(b_2 - b_1)c^3}{12};$$

F = area of the stressed section,

$$F = (b_2 - b_1)c.$$

For the given link

$$i = 0.29c.$$

The slenderness ratio of the given link is then

$$\lambda = 3.45 \frac{l}{c}. \qquad \text{(VI. 121)}$$

For the value λ thus calculated, any handbook may be consulted to find the corresponding coefficient of stress reduction φ, whereupon one determines the admissible stress

$$R_к = \varphi R_z, \qquad \text{(VI. 122)}$$

where R_z = the admissible stress for the given steel grade.

The calculated value of σ_d obtained previously is compared for the compressive stress under normal operating conditions and under conditions of bolt breaking, and the safety factor, which usually varies between 6 and 8, is then determined.

Tensile stress at section B-B

$$\sigma_z = \frac{P_c}{(b-d)c}. \qquad \text{(VI. 123)}$$

Tensile stress at section E-E (according to Lamé)

$$\sigma_z = \frac{P_c}{cd} \cdot \frac{b^2+d^2}{b^2-d^2}. \qquad \text{(VI. 124)}$$

Breaking bolt. The bolt is provided with a groove whose diameter is selected so that the bolt will break under a force 40% greater than normal.

The design of the breaking bolt is shown in Figure VI. 41. Its short, threaded part is screwed into the link slide-block, while its long part is connected by two nuts with the distributor link. A square shoulder is provided to enable a spanner to be used.

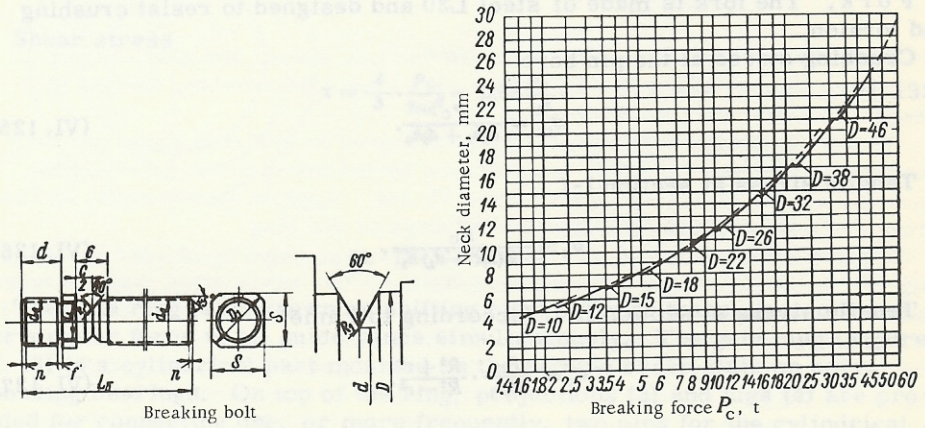


FIGURE VI. 41. Graph for selecting the neck dimensions of the breaking bolt

It is very difficult to calculate the dimensions of the bolt neck with precision, since the force required to break the bolt depends not only on the neck diameter d, but also on the ratio $\frac{D}{d}$, the radius R_1 of the neck fillet, the material of which the bolt is made, etc.

Figure VI. 41 shows the graph for determining the bolt-neck diameter according to data obtained at the LMZ as a result of experimental tests.

The bolt and neck diameters D and d, respectively, are selected on the graph according to the breaking force P_c; final selection is made, however, only after several tests with various bolts of identical diameter d, but of slightly different characteristics.

Compound link. Compound links are also used in actuating mechanisms, where the breaking link is a shear pin in the composite lever. The compound link consists of two forks, two pins, a tightening bolt with left-hand and right-hand threads, and two lock nuts.

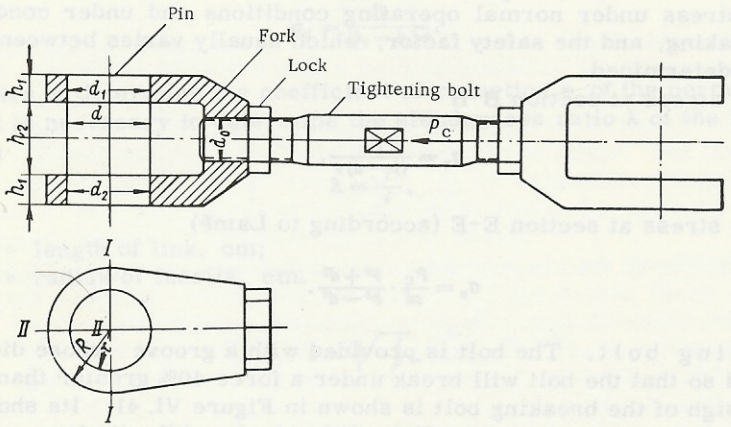


FIGURE VI. 42. Compound distributor link

Fork. The fork is made of steel L30 and designed to resist crushing and torsion.

Crushing stress at the pin bore

$$\sigma_{cr} = \frac{P_c}{d_1 h_1 + d_2 h_2}. \qquad \text{(VI. 125)}$$

Tensile stress at section I-I

$$\sigma_z = \frac{P_c}{2(2R - d_1)h_1}. \qquad \text{(VI. 126)}$$

Tensile stress at section II-II (according to Lamé)

$$\sigma_z = \frac{P_c}{2d_1 h_1} \cdot \frac{R^2 + r^2}{R^2 - r^2}. \qquad \text{(VI. 127)}$$

Thread of the fork (nut), and tightening bolt. The fork thread is designed to resist shear, bending, and crushing. The screw (tightening bolt) and nut are made of steel 25.

Shear stresses in the thread

$$\text{fork: } \tau = \frac{P_c}{\pi\beta H d_0}; \quad \text{nut: } \tau = \frac{P_c}{\pi\beta H d_b}. \tag{VI.128}$$

Bending in the thread

$$\text{fork: } \sigma_b = \frac{3P_c\,(d_0 - d_b)}{2\pi\beta^2 S d_0 H}; \quad \text{nut: } \sigma_b = \frac{3P_c\,(d_0 - d_b)}{2\pi\beta^2 S d_b H}. \tag{VI.129}$$

Crushing in the thread

$$\sigma_{cr} = \frac{P_c}{\frac{\pi}{4}\left(d_0^2 - d_b^2\right)\frac{H}{S}}, \tag{VI.130}$$

where d_0 = external thread diameter;
d_b = internal thread diameter;
S = thread pitch;
β = thread-profile coefficient; for metric thread $\beta = 0.875$;
H = nut height.

Stress at the threaded part of the tightening bolt

$$\sigma_z = \frac{P_c}{\frac{\pi d_b^2}{4}}. \tag{VI.131}$$

Fork pin. The pin is designed to resist bending and shear.

Bending stress

$$\sigma_b = \frac{M_b}{W} = \frac{\frac{P_c}{2}\left(\frac{h_2 + h_1}{2} - \frac{h_2}{4}\right)}{\frac{\pi d^3}{32}} = \frac{\frac{P_c}{8}(h_2 + 2h_1)}{\frac{\pi d^3}{32}};$$

$$\sigma_b = \frac{4P_c\,(h_2 + 2h_1)}{\pi d^3}. \tag{VI.132}$$

Shear stress

$$\tau = \frac{4}{3} \cdot \frac{P_c}{\frac{2\pi d^2}{4}} = 0.85\frac{P_c}{d^2}. \tag{VI.133}$$

38. THE GATE RING

The gate ring (also known as shifting ring) permits transmission of the servomotor force to all guide vanes simultaneously. The gate ring (Figure VI. 43) is a cylindrical part mounted on the turbine cover-plate on corresponding bearings. On top of the ring, projections (3) and lugs (4) are provided for connecting one, or more frequently, two pins for the cylindrical hinges of the servomotor rods.

Formerly, gate rings having two flanges on top were in common use. At present, a design of lesser weight is more frequently used, provided with one flange only. The vertical cylindrical web (1) of the ring is sometimes simple, but more often double; the resulting box-shaped cross section of the ring is more difficult to manufacture, but imparts greater rigidity to the ring.

The lower gate ring flange (2) provides the connection with the pins of the cylindrical links.

In the cast design variant, the gate ring is a massive part with web thickness of about 60 mm. The vertical web of the welded box-shaped ring is about 30 mm thick.

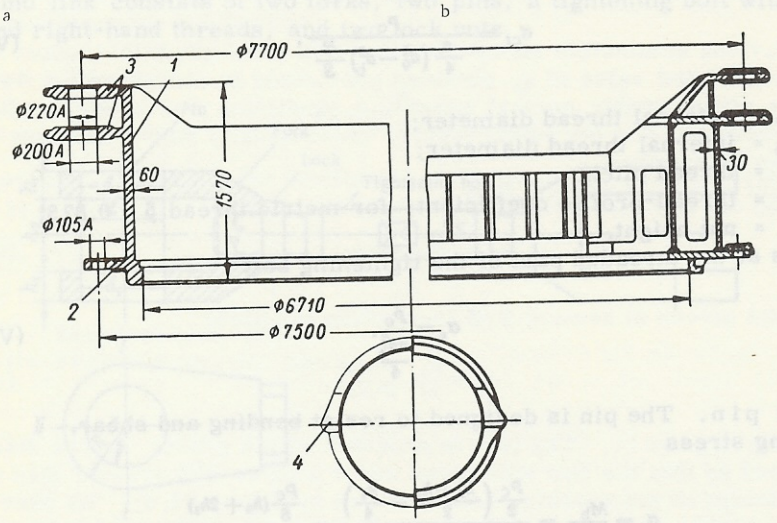


FIGURE VI. 43. Gate ring for the turbines of the Volga HEP imeni Lenin

a—cast design, weight 22 t; b—welded design, weight 15 t.

Notwithstanding the double walls and the box shape, the gate ring of welded design weighs 30% less than a cast ring. At present, welded gate rings are more frequently used.

Gate ring design. The gate ring is designed to resist bending and torsion due to the two forces *P*, transmitted by the servomotor rods to pins mounted in the gate ring lugs (Figure VI. 44). Approximately equal forces from the link pins act upon the lower flange of the ring.

Pfarr's method, based on the theory of curved beams, is used in designing the gate ring. This theory proceeds from the assumption that the external forces (servomotor forces, and forces applied to the distributor links) act in one plane, and all the ring cross sections are subject to bending. At the LMZ, A. E. Zhmud' developed a more accurate calculation method, based on the general theory of curved beams; in this method, the upper and lower gate ring flanges are designed to resist bending, and the cylindrical section between the upper and lower flange is assumed to transmit the torsional moment only.

For this purpose, the following gate ring loading scheme is considered. The lower flange is subject to the equal forces P_i, applied under a certain angle to the corresponding radius, and located on the circumference of diameter D_c at equal intervals. There are z_0 such forces. If each force were resolved into components along the radial and tangential directions,— i.e., P_{iQ} and P_{i_N} — the radial components P_{iQ} would balance each other, and the forces P_{i_N} would produce the moment

$$M_I = \frac{P_{i_N} D_s z_0}{2}. \qquad \text{(VI. 134)}$$

This moment is balanced by the moment of the stresses occurring in the region between the lower flange (I) and the annular section (II). Thus, the design involves calculating a closed ring subject to the above-mentioned forces. The stresses at the joints are considered to be uniformly distributed around the whole flange circumference and directed tangentially. The upper flange (III) is a single or double ring, according to the number of flanges composing it. With a gate ring having two lugs, the forces developed by two servomotors produce one moment only.

$$M_{III} = PD_y, \qquad \text{(VI. 135)}$$

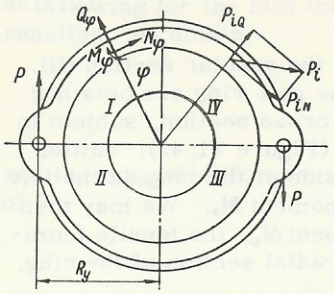
where the servomotor force is

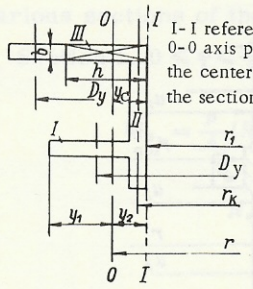
$$P = \frac{P_{s1} + P_{s2}}{2} \text{ kg};$$

where P_{s_1} = force of the first servomotor;
P_{s_2} = force of the second servomotor;
D_y = diameter of the circle on which the lugs are located.

This moment is balanced by the stresses at the joint between flange (III) and ring (II), the stresses being considered as uniformly distributed around the mean circle of the ring. Actually, the internal stresses will not be quite uniformly distributed; consequently, a safety factor must be introduced, and the transition from the flange to the annular section of the gate ring must be reinforced

Diagram of forces





I-I reference axis
0-0 axis passing through the center of gravity of the section

FIGURE VI. 44. Design of gate ring

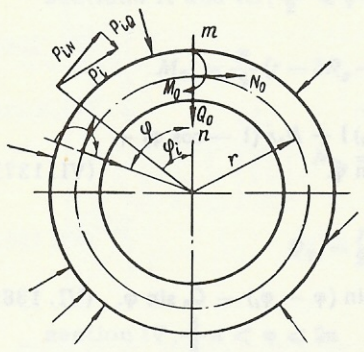


FIGURE VI. 45. Annular part of gate ring: diagram of forces

The annular section (II) is subject to torsional stresses only. By applying the condition for equilibrium of all external moments acting upon the gate ring:

$$M_{\text{I}} = M_{\text{III}}. \tag{VI.136}$$

This moment is also the torsional moment on the annular section (II).

The formulas for the strength calculation of the gate ring are obtained in the following way: consider a ring of constant cross section, subject to arbitrarily distributed forces P_i and moments M_i (Figure VI. 45); cutting the ring along a plane mn, the action of the right side of the ring on the left may be replaced by the forces N_0 and Q_0 and the moment M_0. We may then write the general expression for the bending moment M_φ, the tensile (compressive) force N_φ and the shear force Q_φ at any radial section of the ring. The angle φ is measured from section mn.

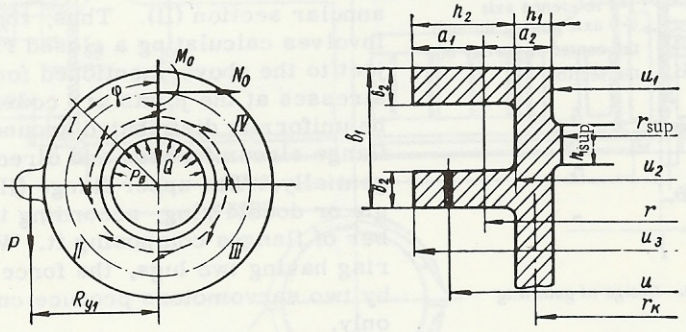


FIGURE VI. 46. Gate ring with one lug

The bending moment

$$M_\varphi = \sum M_i + M_0 + \sum P_{i_N} [r_i - r\cos(\varphi - \varphi_i)] + N_0 r(1 - \cos\varphi) + \\ + \sum P_{i_Q} r \sin(\varphi - \varphi_i) + Q_0 r \sin\varphi. \tag{VI.137}$$

The tensile force

$$N_\varphi = \sum P_{i_N} \cos(\varphi - \varphi_i) + N_0 \cos\varphi - \sum P_{i_Q} \sin(\varphi - \varphi_i) - Q_0 \sin\varphi. \tag{VI.138}$$

The shear force is

$$Q_\varphi = \sum P_{i_N} \sin(\varphi - \varphi_i) + N_0 \sin\varphi + \sum P_{i_Q} \cos(\varphi - \varphi_i) + \\ + Q_0 \cos\varphi. \tag{VI.139}$$

Omitting further transformations of these expressions, the final formulas for gate ring design may be given.

Gate ring with one lug. The gate ring with one lug is uniformly supported around a circumference of radius r_{sup}. We may consider that the support reaction acts as an internal pressure p_b exerted upon half the ring.

Allowing for the fact that the servomotor force is balanced by the support reaction, we obtain

$$P = 2\int_0^{\frac{\pi}{2}} p_b h_{sup} r_{sup} \cos\varphi \, d\varphi, \tag{VI.140}$$

and the tangential forces, applied at the radius r_κ are expressed in terms of P

$$\Delta T = \frac{P}{2\pi} \cdot \frac{R_y}{r_\kappa} d\varphi. \tag{VI.141}$$

The relations for the moments and forces as a function of angle φ, for various sections of the gate ring, are

Section I, $0 \leqslant \varphi \leqslant \frac{\pi}{2}$

$$M_{\varphi_1} = \frac{P}{4}(R_y - r - \gamma) + \frac{PR_y}{2\pi}\varphi - \frac{P}{4} r \sin\varphi - \frac{P(R_y - r)\cos\varphi}{\frac{\pi k' E\gamma}{G(r-\gamma)} + \pi}; \tag{VI.142}$$

$$N_{\varphi_1} = \frac{P}{2} + \frac{P}{4}\sin\varphi + \frac{P}{\pi^2} \cdot \frac{(R_y - r)\cos\varphi}{\frac{k' E\gamma}{G(r-\gamma)} + 1}; \tag{VI.143}$$

$$Q_{\varphi_1} = \frac{PR_y}{2\pi r_\kappa} + \frac{P}{2\pi} \cdot \frac{(R_y - r)\sin\varphi}{\frac{k' E\gamma}{G(r-\gamma)} + 1}; \tag{VI.144}$$

sections II and III, $\frac{\pi}{2} \leqslant \varphi \leqslant \frac{3}{2}\pi$

$$M_{\varphi_2} = \frac{P}{4}(r - 3R_y - \gamma) + \frac{PR_y}{2\pi}\varphi + \frac{Pr}{4}\sin\varphi - \frac{P(R_y - r)\cos\varphi}{\frac{\pi k' E\gamma}{G(r-\gamma)} + \pi}; \tag{VI.145}$$

$$N_{\varphi_2} = -\frac{P}{4}\sin\varphi + \frac{P}{\pi r} \cdot \frac{(R_y - r)\cos\varphi}{\frac{k' E\gamma}{G(r-\gamma)} + 1}; \tag{VI.146}$$

$$Q_{\varphi_2} = \frac{PR_y}{2\pi r_\kappa} + \frac{P}{\pi^2} \cdot \frac{(R_y - r)\sin\varphi}{\frac{k' E\gamma}{G(r-\gamma)} + 1} + \frac{P}{4}\cos\varphi; \tag{VI.147}$$

section IV, $\frac{3}{2}\pi \leqslant \varphi \leqslant 2\pi$

$$M_{\varphi_2} = \frac{P}{4}(3R_y + r + \gamma) + \frac{PR_y}{2\pi}\varphi + \frac{Pr}{4}\sin\varphi - \frac{P(R_y - r)\cos\varphi}{\frac{\pi k' E\gamma}{G(r-\gamma)} + \pi}; \tag{VI.148}$$

$$N_{\varphi_2} = \frac{P}{2} + \frac{P}{4}\sin\varphi + \frac{P}{\pi^2} \cdot \frac{(R_y - r)\cos\varphi}{\frac{k' E\gamma}{G(r-\gamma)} + 1}; \tag{VI.149}$$

$$Q_{\varphi_3} = \frac{PR_y}{2\pi r_\kappa} + \frac{P}{\pi^2} \cdot \frac{(R_y - r)\sin\varphi}{\frac{k' E\gamma}{G(r-\gamma)} + 1} - \frac{P}{4}\cos\varphi. \tag{VI.150}$$

where E = modulus of elasticity;
G = modulus of rigidity
k' = factor depending on the shape of the cross section: for a rectangular cross section $k' = 1.2$; for double tee cross section, $k' = 2.0$ to 2.4 /85/;
γ = distance of neutral axis from axis passing through the centroid of the section

$$\gamma = r_{c.g.} - r; \tag{VI. 151}$$

r = radius of neutral axis.

The position and radius r of the neutral axis are determined by the equation (Figure VI. 46)

$$\int (u - r)\, du = 0;$$

with the designations adopted in Figure VI. 46, we obtain

$$r = \frac{2b_2h_2 + b_1h_1}{2b_2 \ln \frac{u_3}{u_2} + b_1 \ln \frac{u_2}{u_1}}. \tag{VI. 152}$$

Gate ring with two lugs. The moments and forces are directly proportional to angle φ measured counterclockwise. Their values are different at sections I, II, III, and IV (Figure VI. 44).

The formulas for the various sections will be:

section I, $0 \leqslant \varphi \leqslant \frac{\pi}{2}$

$$M_{\varphi_1} = \frac{P}{\pi} R_y \varphi - \frac{P}{2} r \sin \varphi; \tag{VI. 153}$$

$$N_{\varphi_1} = \frac{P}{2} \sin \varphi; \tag{VI. 154}$$

$$Q_{\varphi_1} = \frac{P}{\pi} \cdot \frac{R_y}{r_\kappa} - \frac{P}{2} \cos \varphi; \tag{VI. 155}$$

sections II and III, $\frac{\pi}{2} \leqslant \varphi \frac{3}{2}\pi$

$$M_{\varphi_2} = -PR_y + \frac{P}{\pi} R_y \varphi + \frac{P}{2} r \sin \varphi; \tag{VI. 156}$$

$$N_{\varphi_2} = -\frac{P}{2} \sin \varphi; \tag{VI. 157}$$

$$Q_{\varphi_2} = \frac{P}{\pi} \cdot \frac{R_y}{r_\kappa} + \frac{P}{2} \cos \varphi; \tag{VI. 158}$$

section IV, $\frac{3}{2}\pi \leqslant \varphi \leqslant 2\pi$

$$M_{\varphi_3} = -2PR_y + \frac{P}{\pi} R_y \varphi - \frac{P}{2} r \sin \varphi; \tag{VI. 159}$$

$$N_{\varphi_3} = \frac{P}{2} \sin \varphi; \tag{VI. 160}$$

$$Q_{\varphi_3} = \frac{P}{\pi} \cdot \frac{R_y}{r_\kappa} - \frac{P}{2} \cos \varphi. \tag{VI. 161}$$

where P = force of one servomotor;
r = radius, passing through the centroid of the section;
$r_к$ = mean radius of the annular part (section II) of the gate ring;
R_y = distance of gate-ring lug from center of gate ring.

By means of these formulas, we can determine the bending moment and the tensile and shear forces for various angles φ, which are usually taken in intervals of $15° \left(\frac{\pi}{12}\right)$.

It is well to bear in mind that the values of φ at various sections are interrelated by:

$$\varphi_{2(3)} = \pi \mp \varphi_1; \quad \varphi_4 = 2\pi - \varphi_1.$$

Consequently, to determine the stress diagram for the whole ring, it is sufficient to make the calculation for section I only, since for $\varphi_2 = \pi - \varphi_1$

$$M_{\varphi_2} = -M_{\varphi_1}; \quad N_{\varphi_2} = N_{\varphi_1}; \quad Q_{\varphi_2} = Q_{\varphi_1}.$$

From considerations of symmetry, the stress diagram for sections III and IV will actually be a repetition of the curves plotted for sections I and II.

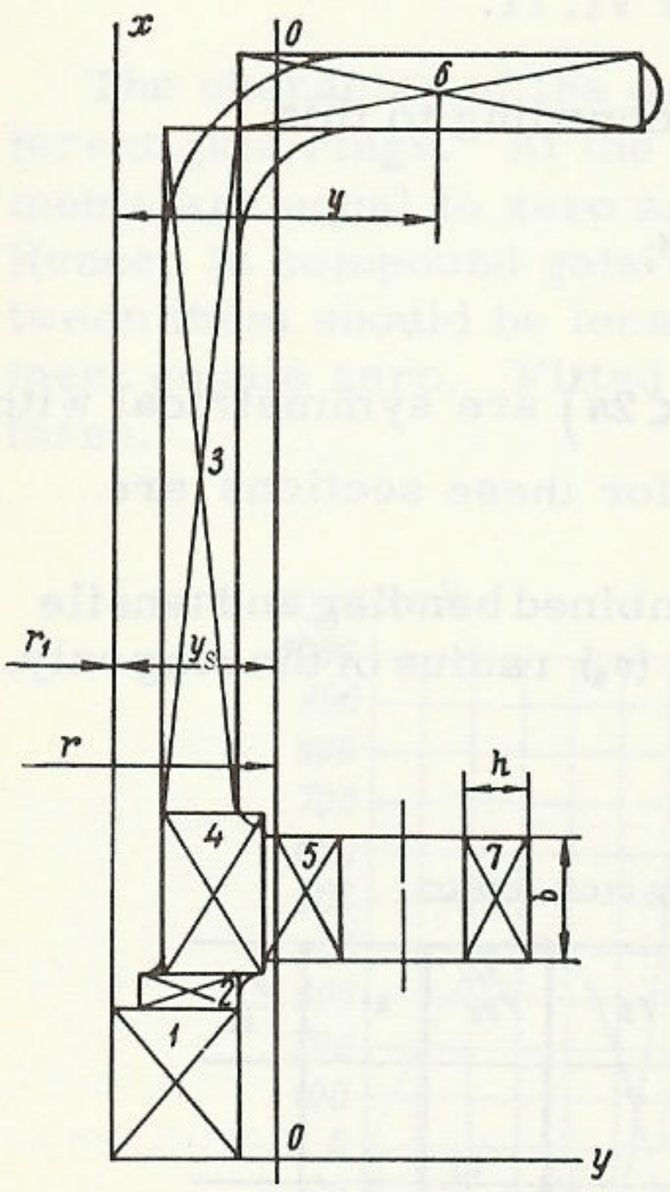


FIGURE VI. 47. Diagram for determining the section modulus of the gate ring

The stresses at the ring cross sections are calculated from the following formulas:

bending — on the outside radius

$$\sigma_{b_1} = \frac{M_\varphi}{W_1};$$

bending — on the inside

$$\sigma_{b_2} = -\frac{M_\varphi}{W_2}.$$

Section modulus of the outer flange

$$W_1 = \frac{J}{y_1}.$$

Section modulus of the inner flange

$$W_2 = \frac{J}{y_2}.$$

The moment of inertia of the section (Figure VI. 47) with respect to the x axis which is parallel to the axis that passes through the centroid (0-0) is:

$$J = \sum Fy^2 + \sum \frac{Fh^2}{12} - y_s^2 \sum F. \qquad \text{(VI. 162)}$$

Radius of the axis passing through the centroid of section

$$r = r_1 + y_s$$

Ordinate of the center of gravity of the section

$$y_s = \frac{\Sigma Fy}{\Sigma F}. \qquad \text{(VI. 163)}$$

To determine the moment of inertia, the cross section is divided into a series of rectangles, and the results are tabulated as in Table VI. 10.

Tensile stress

$$\sigma_z = \frac{N_\varphi}{F}. \qquad \text{(VI. 164)}$$

Shear stress

$$\tau = \frac{Q_\varphi}{F}. \qquad \text{(VI. 165)}$$

The stresses are calculated for different angles and the results tabulated, as in Table VI. 11.

The following relations between the stresses at section I and the other ring sections are used to determine the stress diagram for a gate ring with two lugs.

Section I, $0 \leqslant \varphi \leqslant \frac{\pi}{2}$; σ_1^I, σ_2^{II} and τ^I from Table VI. 11.

Section II, $\frac{\pi}{2} \leqslant \varphi_2 \leqslant \pi$ or $\varphi_2 = (\pi - \varphi_1)$, and according to this

$$\sigma_1^{II} = -\sigma_1^I; \quad \sigma_2^{II} = -\sigma_2^I \text{ и } \tau^{II} = \tau^I;$$

Section III $\left(\pi \leqslant \varphi_3 \leqslant \frac{\pi}{2}\right)$ and section IV $\left(\frac{3}{2}\pi \leqslant \varphi_4 \leqslant 2\pi\right)$ are symmetrical with respect to sections I and II; the stress diagrams for these sections are identical with those of sections I and II.

The stress diagram is usually plotted for the combined bending and tensile (compressive) stresses on the outer (σ_1) and inner (σ_2) radius of the ring only.

TABLE VI. 10

Determination of the moment of inertia of the ring cross section

Number	b	h	F	y	y^2	Fy	Fy_z	h^2	$\frac{Fh^2}{12}$
1									
2									
. . .									
. . .									
n									
Σ									

TABLE VI. 11

Determination of the stresses in the gate ring

	φ_0	M_φ	N_φ	Q_φ	σ_{θ_1}	σ_{θ_2}	σ_z	$\frac{\sigma_1}{\sigma_{b_1}+\sigma_z}$	$\frac{\sigma_2}{\sigma_{b_2}+\sigma_z}$	τ
0 ≤ φ ≤ π/2	0°									
	15°									
	30°									
	45°									
	60°									
	75°									
	90°									

The character of the curves shown in Figure VI. 48 is the same for different gate rings. At the cross sections $\varphi = 0$ and $\varphi \cong \pi$, the bending moments are equal to zero and only the shear forces have to be considered. Hence, in compound gate rings consisting of two halves, the junctions between them should be located at those cross sections where the bending moment equals zero. Fitted bolts are provided in order to take up the shear force.

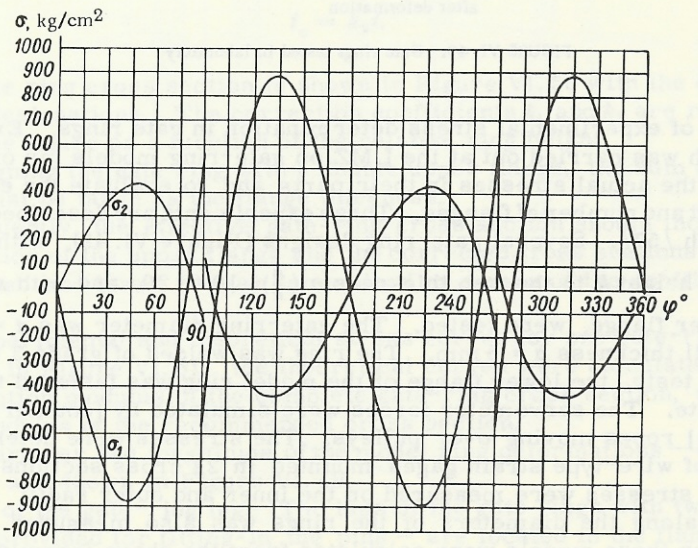


FIGURE VI. 48. Stress diagram in the gate ring

The shear stress in the bolt

$$\sigma_{\text{bolt}} = \frac{Q_\varphi}{zf}. \qquad \text{(VI. 166)}$$

where z = number of tight-fit bolts;
f = cross-sectional area of the fitted bolts.

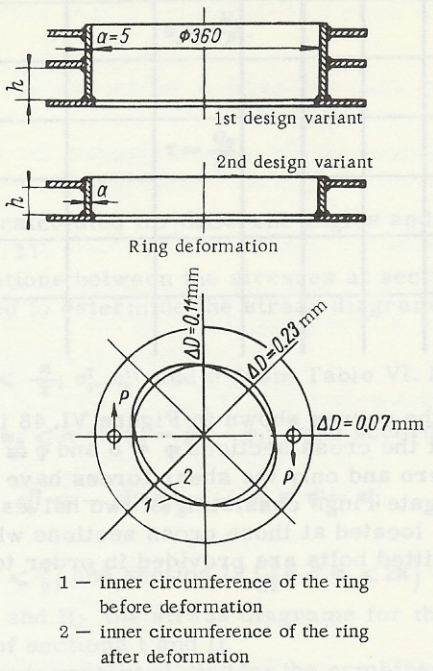


FIGURE VI. 49. Gate rings tested in laboratory

Results of experimental stress determination in gate rings. Experimental research was carried out at the LMZ on gate-ring models in order to determine the actual stresses in their parts and to evaluate the effect of their height and number of flanges. These experiments are described by M. S. Kustanovich /57/. Several gate-ring designs (Figure VI. 49), with the ratio of the ring height h to the web thickness a ($\frac{h}{a}$)= 10 to 20, and with single and double upper flange, were tested. The gate-ring diameter was d = 360 mm, and the wall thickness a = 5 mm. The ring was welded of grade 3 steel. During the tests, the lower flange of the model ring was fastened to a stationary plate. The servomotor forces were simulated by [counterweights attached to] ropes moving over pulleys. The stresses were determined by means of wire-type strain gages mounted in 24 cross sections of the ring. The stresses were measured on the inner and outer radii; the deformation along the diameters of the rings was also measured. The stresses for these models were calculated from the above formulas. The calculations were made for bending and tension caused by two horizontal forces applied at the lugs.

The model tests showed that the character of stress variation, as established by these tests, fully agrees with the theoretical results for all the design variants. However, the values of the analytical and experimental stresses are not equal; they depend on the relative dimensions of the ring cross section.

In order to make the calculated stresses equal to the actual stresses, they should be corrected by suitably selecting the section modulus of the ring cross section. The cross-section height considered in calculation is therefore to be corrected in accordance with the wall thickness.

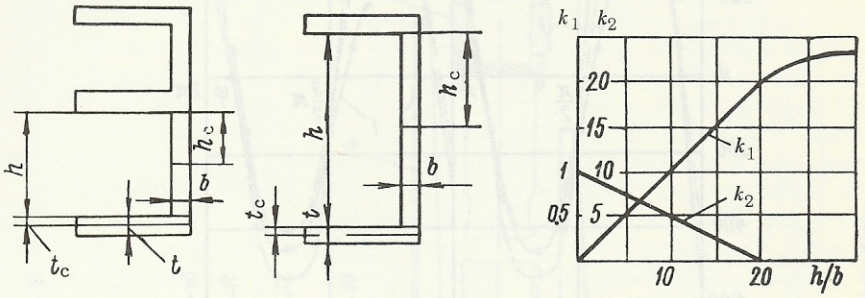


FIGURE VI. 50. Correction coefficients k_1, k_2.

The corrected height should be

$$h_c = k_1 b.$$

The thickness of the lower flange should also be corrected according to the formula

$$t_c = k_2 t. \qquad \text{(VI. 167)}$$

The gate ring cross section is shown in Figure VI. 50 with the corresponding designations. The correction coefficients k_1 and k_2 are represented in the same figure as a function of the relative ring height.

In designing the gate ring with a double upper flange, the sum of both flanges must be taken as the flange thickness.

Consequently, the effective gate-ring cross section should include the cross section of the upper flange and the corrected cross sections of the cylindrical web and lower flange, determined by means of the coefficients k_1 and k_2.

The experimental and theoretical stress curves for one gate-ring design are shown in Figure VI. 51; the theoretical curves were calculated considering the section modulus of the complete gate-ring cross section, and the section modulus of the recommended cross section.

The character and magnitude of the model ring deformations — determined by tests — are shown in Figure VI. 49.

Design of the gate-ring lug. The lugs of the gate rings with two upper flanges — provided for fitting-in the pins — are located in the flange itself; for this purpose the flanges are extended.

In gate rings with one flange currently used, one lug is located in the flange, and the second on a special projection.

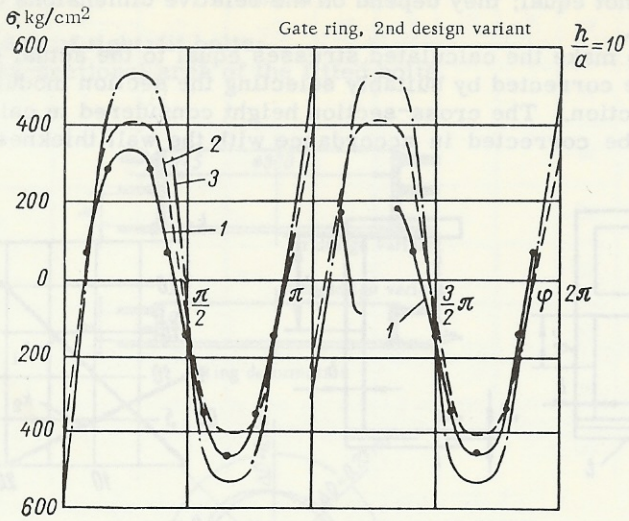


FIGURE VI. 51. Stresses at different gate-ring cross sections:

1 — experimental stresses; 2 — theoretical stresses, considering the section modulus of the complete cross section; 3 — corrected theoretical stresses.

Figure VI. 52 shows axonometrically a gate ring with a projection for mounting the lug. The stresses are determined at sections $A - B$ and $C - D$.

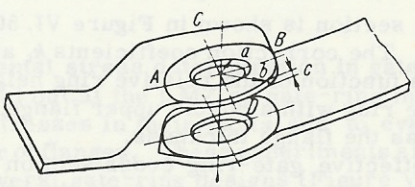


FIGURE VI. 52. Gate ring with projection

Stress at section $A - B$ (according to Lamé)

$$\sigma = \frac{P_1}{4ac} \cdot \frac{b^2 + a^2}{b^2 - a^2}. \qquad \text{(VI. 168)}$$

Stress at section $C - D$ (according to Lamé)

$$\sigma = \frac{P_1}{4(b - a)c}. \qquad \text{(VI. 169)}$$

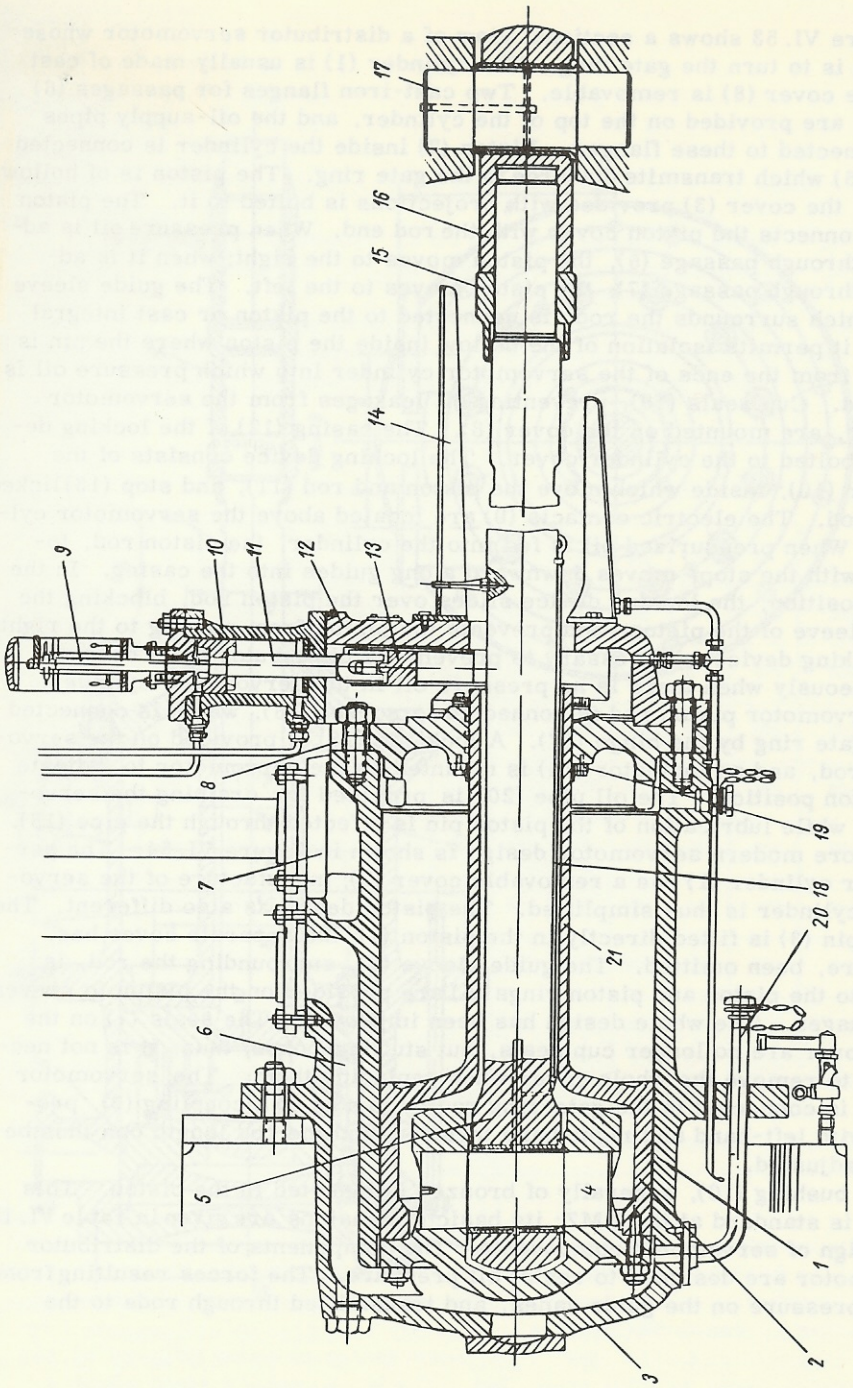


FIGURE VI. 53. Distributor servomotor with locking device

39. DISTRIBUTOR SERVOMOTOR

Figure VI. 53 shows a sectional view of a distributor servomotor whose function is to turn the gate ring. The cylinder (1) is usually made of cast iron; the cover (8) is removable. Two cast-iron flanges for passages (6) and (7), are provided on the top of the cylinder, and the oil-supply pipes are connected to these flanges. Piston (2) inside the cylinder is connected to rod (5) which transmits the force to the gate ring. The piston is of hollow design; the cover (3) provided with projections is bolted to it. The piston pin (4) connects the piston cover with the rod end. When pressure oil is admitted through passage (6), the piston moves to the right; when it is admitted through passage (7), the piston moves to the left. The guide sleeve (21), which surrounds the rod, is connected to the piston or cast integral with it; it permits isolation of the hollow inside the piston where the pin is located from the ends of the servomotor cylinder into which pressure oil is admitted. Cup seals (19), preventing oil leakages from the servomotor cylinder, are mounted on the cover (8). The casing (12) of the locking device is bolted to the cylinder cover. The locking device consists of the cylinder (10), inside which move the piston and rod (11), and stop (13) linked to the rod. The electric contacts (9) are located above the servomotor cylinder. When pressurized oil is fed into the cylinder, the piston rod, together with the stop, moves downward along guides into the casing. In the lower position, the locking device slides over the piston rod, blocking the guide sleeve of the piston, and prevents the piston from moving to the right. The locking device is necessary to prevent the distributor from opening spontaneously when there is no pressure oil in the servomotor cylinder. The servomotor piston rod is connected to socket (16), which is connected to the gate ring by the hinge (17). A lock-nut (15) is provided on the servomotor rod, and an indicator (14) is mounted on the servomotor to indicate the piston position. The oil pipe (20) is provided for draining the servomotor, while lubrication of the piston pin is effected through the pipe (18).

A more modern servomotor design is shown in Figure VI. 54. The servomotor cylinder (1) has a removable cover (2); manufacture of the servomotor cylinder is thus simplified. The piston design is also different. The piston pin (3) is fitted directly in the piston (4); the separate cover has, therefore, been omitted. The guide sleeve (5), surrounding the rod, is bolted to the piston and piston rings (6) are provided on the piston to prevent oil leakages. The whole design has been improved. The seals (7) on the front cover are no longer cup seals, but stuffing-boxes; thus, it is not necessary to remove the whole cover when replacing them. The servomotor rod (8) is connected to the gate-ring rod by means of a coupling (9), provided with left-hand and right-hand threads, and the rod length can thus be easily adjusted.

The bushing (10), generally of bronze, is inserted in the piston. This design is standard at the LMZ; its basic dimensions are given in Table VI. 12.

Design of servomotor components. The components of the distributor servomotor are designed to resist oil pressure. The forces resulting from water pressure on the guide vanes, and transmitted through rods to the

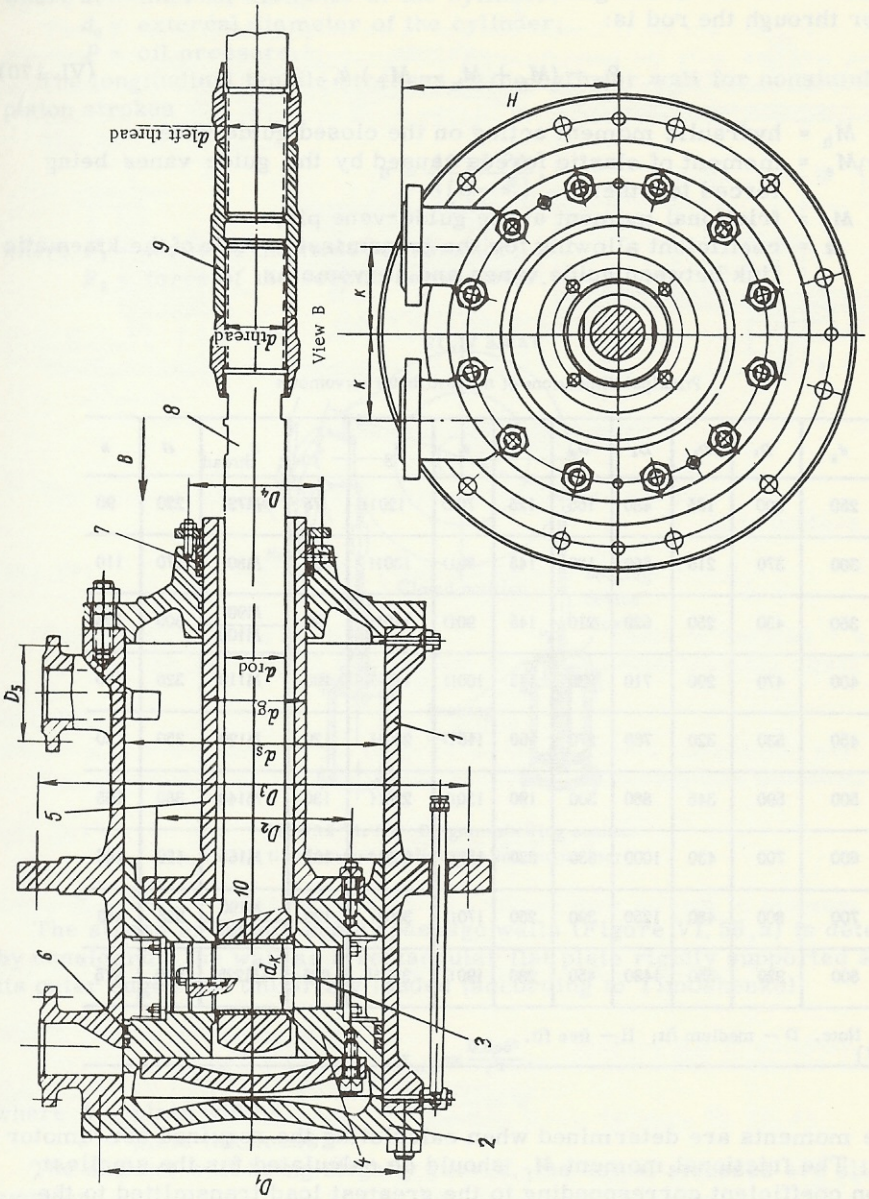


FIGURE VI, 54. Distributor servomotor

servomotor, should also be allowed for. Since the water pressure on the vanes exerts the greatest loads when the guide vanes are closed, the servomotor parts are designed for this condition.

Figure VI. 55 shows the kinematic diagram of the connection between the servomotor and the closed guide vanes. The force transmitted to the servomotor through the rod is:

$$P_{cl} = (M_h + M_e - M_f)\, k, \qquad \text{(VI. 170)}$$

where M_h = hydraulic moment acting on the closed guide vane;
M_e = moment of elastic forces caused by the guide vanes being forced together;
M_f = frictional moment at the guide-vane pin;
k = coefficient allowing for the transmission ratio of the kinematic link between guide vanes and servomotor.

TABLE VI. 12

Principal dimensions of the distributor servomotor

d_s	D_1	D_2	D_3	D_4	D_5	d_k	d_g	d_{rod}	d_{thread}	H	k
250	300	185	480	165	125	70D	120H	75	M72	220	90
300	370	215	560	180	145	80D	130H	80	M80	270	110
350	430	250	620	210	145	90D	140H	90	M90 / M100	300	125
400	470	290	710	230	145	100D	170H	100	M110	320	130
450	530	320	760	270	160	115D	200H	120	M120	350	150
500	590	345	880	300	190	130D	220H	130	M140	380	165
600	700	430	1000	330	220	150D	260H	165	M165	450	185
700	800	480	1250	390	250	170D	300H	190	M190 / M210	535	210
800	920	550	1430	450	280	190D	350H	225	1M225	620	275

Note. D — medium fit; H — free fit.

The moments are determined when calculating the required servomotor force. The frictional moment M_f should be calculated for the smallest friction coefficient corresponding to the greatest load transmitted to the servomotor by the guide vanes.

Servomotor cylinder. The servomotor cylinder (Figure VI. 56) is generally made of cast iron, but, of late, a welded steel-plate design has also been introduced. The stress in the cylinder wall due to

oil pressure may be determined from the formula used in boiler design

$$\sigma_z = \frac{Pd_i}{(d_e - d_i)}, \qquad \text{(VI. 171)}$$

where d_i = internal diameter of the cylinder;
d_e = external diameter of the cylinder;
P = oil pressure.

The longitudinal tensile stresses in the cylinder wall for nonsimultaneous piston strokes

$$\sigma = \frac{4(P_1 + P_2)}{\pi(d_e^2 - d_i^2)}, \qquad \text{(VI. 172)}$$

where P_1 = force of the first servomotor;
P_2 = force of the second servomotor.

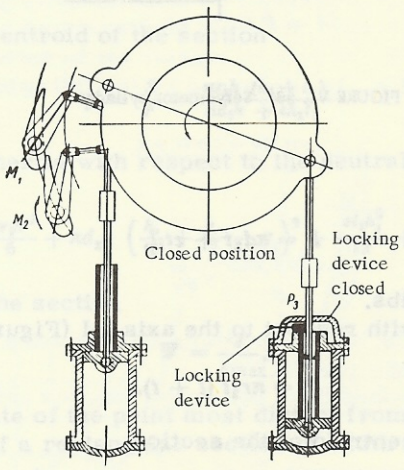


FIGURE VI. 55. Diagram showing connection between guide vanes and servomotor

The stress in the oil-supply passage walls (Figure VI. 56, a) is determined by considering the wall as a rectangular flat plate rigidly supported along its outer edges and uniformly loaded (according to Timoshenko)

$$\sigma_{max} = \frac{0{,}5pb^2}{t'^2}, \qquad \text{(VI. 173)}$$

where b = plate width;
t' = plate thickness.

The channel wall being slightly curved, the actual stresses are slightly smaller.

The stresses in the cylinder flange are determined approximately. In order to allow for the effect of the flange ribs, we may assume that the cylinder flange acts like a plain flange. The web thickness is found

from the condition that the modulus of the actual section together with the ribs is equal to the modulus of an equivalent rectangular section. Figure VI. 56, b shows a cross section of the flange, developed along the diameter d_2.

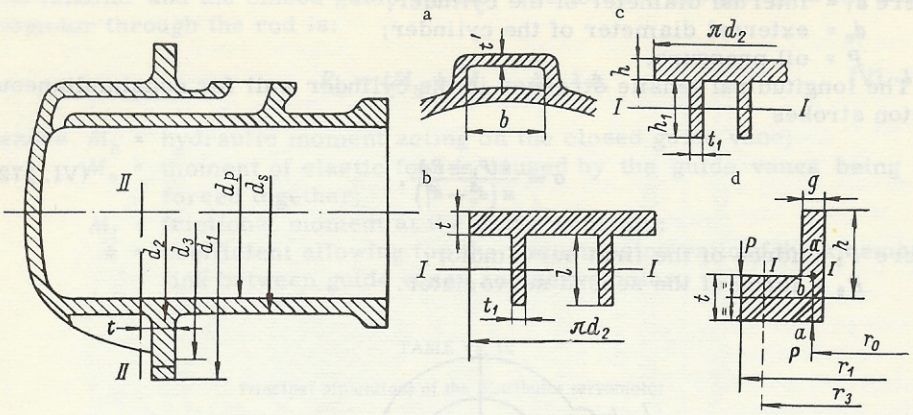


FIGURE VI. 56. Servomotor cylinder

The section area

$$F = \pi d_2 t + z t_1 l, \tag{VI. 174}$$

where z = number of ribs.

The static moment with respect to the axis I-I (Figure VI. 56, b)

$$S = \pi r_2 t (l + t). \tag{VI. 175}$$

The ordinate of the centroid of the section

$$y_s = \frac{S}{F} = \frac{\pi r_2 t (l + t)}{\pi d_2 t + z t_1 l}. \tag{VI. 176}$$

The moment of inertia with respect to the neutral axis

$$J = \frac{\pi r_2 t^3}{6} + \pi d_2 t \left(\frac{l}{2} + \frac{t}{2} - y_s\right)^2 + \frac{z t_1 l^3}{12} + z t_1 l y_s^2. \tag{VI. 177}$$

The modulus of the section

$$W = \frac{J}{y_{max}}, \tag{VI. 178}$$

where y_{max} = ordinate of the point most distant from the neutral axis.

The modulus W_1 of a rectangular section of width πd_2 and thickness t_2 is

$$W_1 = \frac{\pi d_2 t_2^2}{6}. \tag{VI. 179}$$

From the condition of equality of moduli, we obtain

$$t_2^2 = \frac{6W}{\pi d_2}, \tag{VI. 180}$$

which yields the value of t_2.

The cylinder-wall thickness h' is determined from the condition that the section modulus of a cylinder wall strengthened by ribs and the section modulus of a wall without ribs of thickness g, are equal.

For the developed cross section II-II (Figure VI. 56, c):

The section area

$$F = \pi d_2 h + z h_1 t_1. \tag{VI. 181}$$

The static moment with respect to axis I-I

$$S = \pi r_2 h\ (h_1 + h). \tag{VI. 182}$$

The ordinate of centroid of the section

$$y_S = \frac{S}{F} = \frac{\pi r_2 h\ (h_1 + h)}{\pi d_2 h + z h_1 t_1}. \tag{VI. 183}$$

The moment of inertia with respect to the neutral axis

$$J = \frac{\pi r_2 h^3}{6} + \pi d_2 h \left(\frac{h_1}{2} + \frac{h}{2} - y_S\right)^2 + \frac{z t_1 h_1^3}{12} + z t_1 h_1 y_S^2. \tag{VI. 184}$$

The modulus of the section

$$W = \frac{J}{y_{max}},$$

where y_{max} = ordinate of the point most distant from the neutral axis.

The modulus W_1 of a rectangular section of width πd_2 and thickness g is

$$W_1 = \pi d_2 \frac{g^2}{6},$$

consequently,

$$g^2 = \frac{6W}{\pi d_2},$$

which yields the value of g.

The stresses in the flange are determined at the LMZ from the formulas for thin-neck flanges. These formulas are:

The radial stress at point b of section $a - a$ (Figure VI. 56, d)

$$\sigma_{r_0} = \frac{2.86M}{(r_1 - r_0)\, t^2} \frac{3.33\left(\frac{r_1}{r_0}\right)^2 \log_{10}\left(\frac{r_1}{r_0}\right) + 0.389\left[\left(\frac{r_1}{r_0}\right)^2 - 1\right]}{4.33\left(\frac{r_1}{r_0}\right)^2 + 2.33 + 1.18 \frac{\left[\left(\frac{r_1}{r_0}\right)^2 - 1\right] t^3 Z}{V r_0 g^5}}; \tag{VI. 185}$$

The axial stress at the transition from web to flange (section $I - I$)

$$\sigma_{I-I} = \sigma_{r_0}\left(\frac{t}{g}\right)^2; \tag{VI. 186}$$

the tangential stress at point b (normal to the plane of the paper)

$$\sigma_{t_0} = \frac{2.86M}{(r_1 - r_0)\,t^2}\left\{\frac{\left(\frac{r_1}{r_0}\right)^2 \log_{10}\left(\frac{r_1}{r_0}\right)}{\left(\frac{r_1}{r_0}\right)^2 - 1} + 0.117 - \frac{\left(\frac{r_1}{r_0}\right)^2 + 1}{\left(\frac{r_1}{r_0}\right)^2 - 1} \times \right.$$

$$\left. \times \frac{3.33\left(\frac{r_1}{r_0}\right)^2 \log_{10}\left(\frac{r_1}{r_0}\right) + 0.389\left[\left(\frac{r_1}{r_0}\right)^2 - 1\right]}{4.33\left(\frac{r_1}{r_0}\right)^2 + 2.33 + 1.18\,\frac{\left[\left(\frac{r_1}{r_0}\right)^2 - 1\right] t^3 Z}{\sqrt{r_0 g^5}}}\right\}. \tag{VI. 187}$$

In these formulas

$$M = P\,(r_1 - r_0), \tag{VI. 188}$$

z, a function of h, g, and r_0, is expressed by the following formula

$$z = \frac{\cos h2c + \cos 2c + 2}{\sin h2c - \sin 2c}, \tag{VI. 189}$$

where

$$c = 1.285\,\frac{h}{\sqrt{g r_0}}. \tag{VI. 190}$$

The formulas for radial and tangential stresses were simplified at the LMZ by means of auxiliary charts.

The following designations have been used for this purpose:

In formula (VI. 185)

$$F_1 = 2.86\left[3.33\left(\frac{r_1}{r_0}\right)^2 \log_{10}\left(\frac{r_1}{r_0}\right) + 0.389\left(\frac{r_1}{r_0}\right)^2 - 1\right], \tag{VI. 191}$$

$$F_2 = 4.33\left(\frac{r_1}{r_0}\right)^2 + 2.33, \tag{VI. 192}$$

$$F_3 = 1.18\left[\left(\frac{r_1}{r_0}\right)^2 - 1\right]; \tag{VI. 193}$$

in formula (VI. 187)

$$F_4 = 2.86\left[\frac{\left(\frac{r_1}{r_0}\right)^2 \log_{10}\left(\frac{r_1}{r_0}\right) + 0.117}{\left(\frac{r_1}{r_0}\right)^2 - 1}\right], \tag{VI. 194}$$

$$F_5 = 2.86\,\frac{\left(\frac{r_1}{r_0}\right)^2 + 1}{\left(\frac{r_1}{r_0}\right)^2 - 1}\left\{3.33\left(\frac{r_1}{r_0}\right)^2 \log_{10}\left(\frac{r_1}{r_0}\right) + 0.389\left[\left(\frac{r_1}{r_0}\right)^2 - 1\right]\right\}. \tag{VI. 195}$$

We then obtain:
the radial stress at point *b* (Figure VI. 56, d)

$$\sigma_{r_0} = \frac{P}{t^2} \cdot \frac{F_1}{F_2 + \frac{t^3}{\sqrt{r_0 g^5}} ZF_3}; \qquad \text{(VI. 196)}$$

the tangential stress at point *b*

$$\sigma_{t_0} = \frac{P}{t^2}\left[F_4 - \frac{F_5}{F_2 + \frac{t^3}{\sqrt{r_0 g^5}} ZF_2}\right], \qquad \text{(VI. 197)}$$

the force P is

$$P = \frac{r_3 - r_0}{r_1 - r_0} Q, \qquad \text{(VI. 198)}$$

where Q = clamping force of bolts on flanges;
r_3 = radius of bolt location;
r_1 = outer radius of the flange;
r_0 = radius to point *b*.

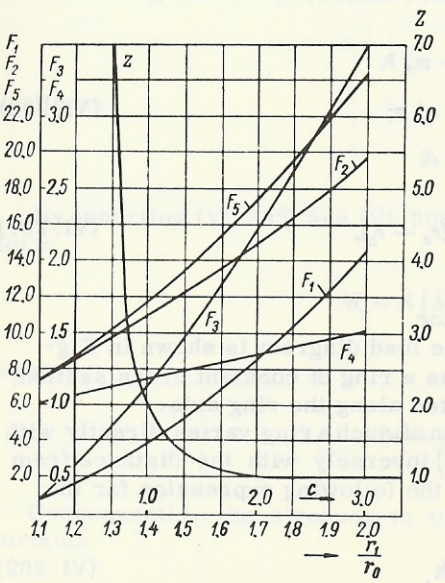


FIGURE VI. 57. Functions F_1, F_2, F_3, F_4, F_5, and Z used in the design of the flange

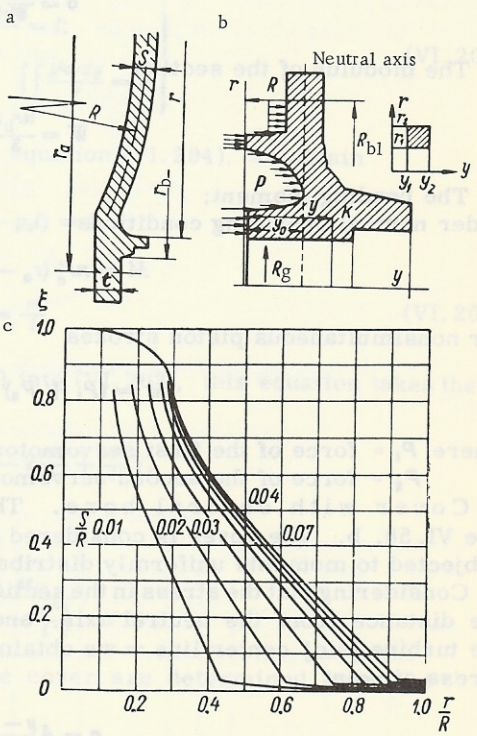


FIGURE VI. 58. Diagram for designing the servomotor cover:
a — blind cover; b — cover with a central bore;
c — curves $\xi = f\left(\frac{r}{R}; \frac{s}{R}\right)$.

The functions F_1, F_2, F_3, F_4, F_5 and Z are represented in Figure VI. 57.

Blind cover. A schematic diagram of the cover is shown in Figure VI. 58. The cover is designed like a plate with rigidly supported outer edges. The curvature is allowed for by a coefficient which depends on the ratios $\frac{r}{R}$ and $\frac{s}{R}$,

where R = radius of curvature of the cover-section center line;
s = thickness of the cover wall;
r = outer radius of the curved part of the cover.

The curves of the coefficient $\xi = f\left(\frac{r}{R};\ \frac{s}{R}\right)$ are given in Figure VI. 58, c.

The stress in the cover is determined by the formula

$$\sigma = 0.75\xi p \frac{r_a}{s^2}, \tag{VI. 199}$$

where r_a = radius of bolt location.

The cover flange is considered, with sufficient accuracy, as a beam of span r_b, and is designed either as loaded under normal operating conditions, or assuming that the piston strokes are not simultaneous.

The stress in the flange

$$\sigma = \frac{M}{W}.$$

The modulus of the section

$$W = \frac{\pi r_b t^2}{3}.$$

The bending moment:
under normal operating conditions

$$M = \pi r_a^2 (r_a - r_b) p; \tag{VI. 200}$$

for nonsimultaneous piston strokes

$$M = (P_1 + P_2)(r_a - r_b), \tag{VI. 201}$$

where P_1 = force of the first servomotor;
P_2 = force of the second servomotor.

Cover with central bore. The load diagram is shown in Figure VI. 58, b. The cover is considered as a ring of constant cross section, subjected to moments uniformly distributed along the ring axis.

Considering that the stress in the section of such a ring varies directly with the distance from the neutral axis, and inversely with the distance from the turbine [sic] center line — we obtain the following expression for the stress at point

$$\sigma = A \frac{y - y_0}{r}, \tag{VI. 202}$$

where A is a constant.

The bending moment at the cover section will be

$$M_b = \iint_s \sigma (y - y_0)\, dr dy.$$

Inserting the value of σ we obtain

$$M_b = A\left[\iint_s \frac{y^2 dr dy}{r} - 2y_0 \iint_s \frac{y dr dy}{r} + y_0^2 \iint_s \frac{dr dy}{r}\right]. \qquad \text{(VI. 203)}$$

Since the sum of the shear forces in the section is equal to zero, we have, therefore,

$$\iint \sigma dr dy = 0.$$

Inserting the value of σ, we obtain

$$A\left[\iint_s \frac{y dr dy}{r} - y_0 \iint_s \frac{dr dy}{r}\right] = 0. \qquad \text{(VI. 204)}$$

By denoting

$$\left.\begin{aligned} \iint_s \frac{dr dy}{r} &= l; \\ \iint_s \frac{y dr dy}{r} = m; \quad \iint_s \frac{y^2 dr dy}{r} &= n \end{aligned}\right\} \qquad \text{(VI. 205)}$$

and inserting these expressions into equation (VI. 204), we obtain

$$A\,(m - y_0 l) = 0.$$

Hence,

$$y_0 = \frac{m}{l}. \qquad \text{(VI. 206)}$$

By inserting (VI. 205) and (VI. 206) into (VI. 203), this equation takes the form

$$M_b = A\left(n - 2\frac{m^2}{l} + \frac{m^2}{l}\right),$$

whence,

$$A = \frac{M_b}{\left(n - \frac{m^2}{l}\right)}.$$

Consequently, the stresses in the cover are determined from the formula

$$\sigma = \frac{M_b\left(y - \frac{m}{l}\right)}{r\left(n - \frac{m^2}{l}\right)}. \qquad \text{(VI. 207)}$$

The bending moment acting at the cover sections is determined from formula

$$M_b = \frac{p}{3}\left[R_{bl}^3 - R_g^2\,(3R_{bl} - 2R_g)\right], \qquad \text{(VI. 208)}$$

where p = oil pressure;
R_{bl} = radius of bolt location;
R_g = radius of the boring (outer radius of guide sleeve).

The coefficients l, m and n are readily determined for a rectangle (Figure VI. 58,a)

$$\left.\begin{aligned} l &= 2\int_{y_1}^{y_2}\int_{r_1}^{r_2}\frac{dr\,dy}{r} = 2(y_2 - y_1)\ln\frac{r_2}{r_1};\\ m &= 2\int_{y_1}^{y_2}\int_{r_1}^{r_2}\frac{y\,dr\,dy}{r} = (y_2^2 - y_1^2)\ln\frac{r_2}{r_1};\\ n &= 2\int_{y_1}^{y_2}\int_{r_1}^{r_2}\frac{y^2\,dr\,dy}{r} = \frac{2}{3}(y_2^3 - y_1^3)\ln\frac{r_2}{r_1}. \end{aligned}\right\} \qquad \text{(VI. 209)}$$

In the cover cross section these coefficients may be determined by the graphoanalytic method, dividing the section into elementary rectangles.

The formulas (VI. 209) then become

$$\left.\begin{aligned} l &= \sum_{i=1}^{n} 2\,(y_{2i} - y_{1i})\ln\frac{r_{2i}}{r_{1i}};\\ m &= \sum_{i=1}^{n}(y_{2i}^2 - y_{1i}^2)\ln\frac{r_{2i}}{r_{1i}};\\ n &= \sum_{i=1}^{n}\frac{2}{3}(y_{2i}^3 - y_{1i}^3)\ln\frac{r_{2i}}{r_{1i}}. \end{aligned}\right\} \qquad \text{(VI. 210)}$$

When calculating, it is convenient to tabulate the numerical results (see Table VI. 13).

TABLE VI. 13

Numerical values of coefficients l, m, n

No. of the section element	y_2	y_1	$y_2 - y_1$	y_2^2	y_1^2	$y_2^2 - y_1^2$	y_2^3	y_1^3	$\frac{2}{3}(y_2^3 - y_1^3)$	$\frac{r_2}{r_1}$	$\ln\frac{r_2}{r_1}$	l_i	m_i	n_i
1														
2														
. . .														
. . .														
n														
												$\sum l_i$	$\sum m_i$	$\sum n_i$

The greatest stresses will be at the point whose coordinates are y_{max} and r_{min}.

Piston cover with guide sleeve. When calculating the bending strength of the servomotor piston, it is considered as separated from the guide sleeve, i.e., we assume that the cover section is able to turn about the pin.

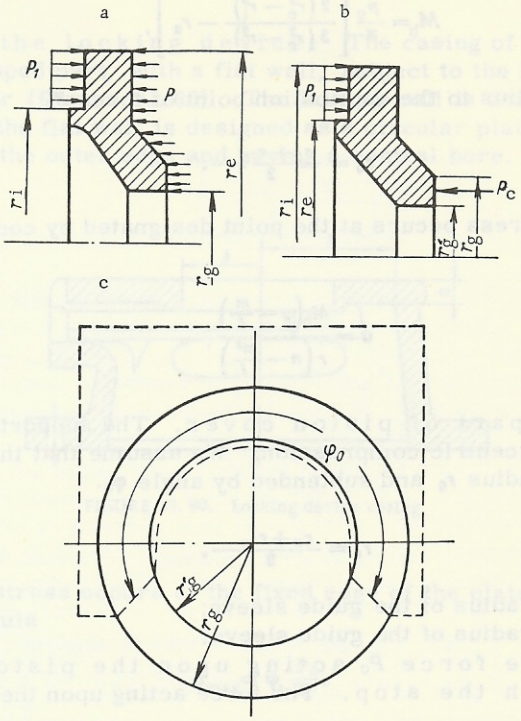


FIGURE VI. 59. Diagram for designing the piston cover and the guide sleeve:

a — normal operation; b — servomotor [piston] rests on the locking device (stop); c — front view of guide sleeve.

The cover is designed for normal operation when oil pressure is available, i.e., under action of the load from the guide vanes, and also when the servomotor is in the locked position.

The calculation method for the piston cover is the same as for the servomotor cover.

Under normal operation (Figure VI. 59, a), the bending moment exerted upon the cover is

$$M = \frac{2}{3} p_e \left(\frac{r_e^3 - r_i^3}{r_e^2 - r_i^2} - \frac{r_e^3 - r_g^3}{r_e^2 - r_g^2} \right), \qquad \text{(VI. 211)}$$

where

$$p_e = (r_e^2 - r_g^2)\, p.$$

When the servomotor is in the locked position (i.e., it rests on the stop), the force P_c acts on the piston cover (Figure VI. 59, b).

The bending moment exerted upon the cover

$$M_b = \frac{P_c}{\pi}\left[\frac{2(r_e^3 - r_i^3)}{3(r_e^2 - r_i^2)} - r_0\right], \qquad \text{(VI. 212)}$$

where r_0 is the radius to the application point of force P_c;

$$r_0 = \frac{r_g + r'_g}{2}.$$

The greatest stress occurs at the point designated by coordinates y and r, and equals

$$\sigma = \frac{M_b\left(y - \frac{m}{l}\right)}{r\left(n - \frac{m^2}{l}\right)}. \qquad \text{(VI. 213)}$$

Supporting part of piston cover. The supporting part is designed to resist excentric compression. We assume that the load is applied along the arc of radius r_0 and subtended by angle φ_0.

$$r_0 = \frac{r_g + r'_g}{2}, \qquad \text{(VI. 214)}$$

where r_g = outer radius of the guide sleeve;
r'_g = inner radius of the guide sleeve.

Compressive force P_c acting upon the piston surface in contact with the stop. The force acting upon the elementary area $r_0 d\varphi$

$$dP_c = \frac{P_c}{\varphi_0}\, d\varphi.$$

The arm l of the force

$$l = r_0 \sin \varphi.$$

The bending moment

$$M = \frac{P_c r_0}{\varphi_0}\int_0^{\varphi_0} \sin\varphi d\varphi = P_c r_0 \frac{1 - \cos\varphi_0}{\varphi_0}. \qquad \text{(VI. 215)}$$

Area of the frontal surface of the guide sleeve

$$F = \pi (r_g^2 - r_g'^2). \qquad \text{(VI. 216)}$$

Section modulus of the guide sleeve

$$W = \frac{\pi (r_g^4 - r_g^4)}{4r_g}. \qquad \text{(VI. 217)}$$

Compressive and bending stresses in the guiding cylinder

$$\sigma = \frac{P_c}{F} + \frac{M}{W}. \qquad \text{(VI. 218)}$$

Casing of the locking device. The casing of the locking device is a box-shaped part, with a flat wall, subject to the force due to the locked distributor (Figure VI. 60). The lateral wall is designed to resist breaking, while the flat wall is designed as a circular plate rigidly supported (fixed) at the outer edge and having a central bore.

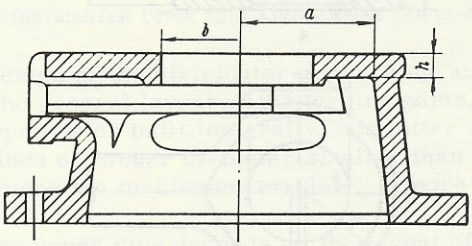


FIGURE VI. 60. Locking device casing

The greatest stress occurs at the fixed edge of the plate, and is determined from formula

$$\sigma_{max} = \varphi_b \frac{P_c}{h^2}. \qquad \text{(VI. 219)}$$

where φ_b = coefficient depending on the ratio $\frac{b}{a}$;

$$\frac{b}{a} = 0.1;\ 0.2;\ 0.3;\ 0.4;\ 0.5;$$

$$\varphi_c = 2.3;\ 1.3;\ 0.8;\ 0.4;\ 0.2;$$

h = plate thickness;

P_c = force exerted by the distributor [in the closed position].

Fork of the locking device. The fork of the locking device (Figure VI. 59, c) is designed to resist the pressure due to force P_c.

Area of contact between frontal part of guide sleeve and stop (locking device)

$$F_1 = \frac{\varphi_0}{2}(r_g^2 - r_g'^2). \qquad \text{(VI. 220)}$$

Pressure on area F_1 of the fork

$$\sigma_{d_1} = \frac{P_c}{F_1}. \qquad \text{(VI. 221)}$$

Area of contact surface between fork and cover of the locking device

$$F_2 = \frac{\varphi_0}{2}(r_{eo}^2 - r_{bo}^2), \qquad \text{(VI.222)}$$

where r_{eo} = external radius of the supporting part of the casing cover;
r_{bo} = radius of the hole in the casing cover.

Pressure on area F_2 of the fork

$$\sigma_{d_2} = \frac{P_c}{F_2}. \qquad \text{(VI.223)}$$

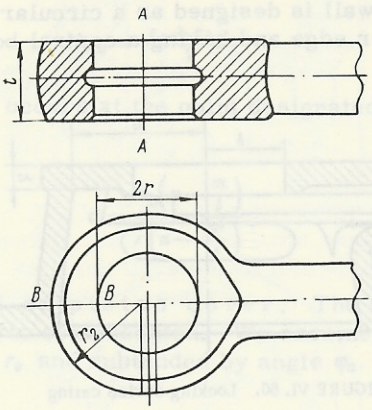


FIGURE VI. 61. Rod end (head)

Servomotor rod. The servomotor rod is designed to resist buckling. The magnitude of the critical force depends upon the slenderness ratio λ

$$\lambda = \frac{\mu L}{i}, \qquad \text{(VI.224)}$$

where μ = length coefficient; when the ends are hinged, $\mu = 1$;
L = rod length;
i = radius of inertia.

Usually, for servomotor rods $\lambda > 100$, the critical force being determined from Euler's formula

$$P_{cr} = \frac{EJ\pi^2}{\mu^2 L^2}, \qquad \text{(VI.225)}$$

where J = moment of inertia of the rod $\left(J = \frac{\pi d^4}{64}\right)$;
d = rod diameter.

The safety factor for the maximum force acting on the rod is

$$n = \frac{P_{cr}}{P} = \frac{EJ\pi^2}{\mu^2 L^2 P}. \qquad \text{(VI.226)}$$

Usually, $n \geqslant 5$.

Rod end (head). The end of the rod is shown in Figure VI. 61; it is designed to resist tension at two cross sections: A—A and B—B.

Section A—A

$$\sigma_z = \frac{P}{F_A} = \frac{P}{2(r_2 - r)t}. \qquad \text{(VI. 227)}$$

Section B—B (according to Lamé)

$$\sigma_z = \frac{P}{2rt} \cdot \frac{r_2^2 + r^2}{r_2^2 - r^2}, \qquad \text{(VI. 228)}$$

where r_2 and r = radii of rod end;
t = rod width.

40. DISTRIBUTOR UPPER RING AND TURBINE COVER-PLATE

Design. The design of the distributor upper ring and the turbine cover-plate depends on the general layout of the turbine parts. These two components may be separate or built integrally, the latter usually being the case with Francis turbines of runner diameter smaller than 7 m. If the thrust collar is mounted upon the turbine cover-plate, a more rigid plate construction is required.

The design of the upper ring depends on the layout of the embedded parts, If the turbine is provided with a foundation ring or a speed ring, the upper distributor ring is removable and is not embedded in concrete. If the embedded parts are separate columns, the foundation ring and the upper ring of the distributor are usually made integral and embedded in concrete.

A dimensioned drawing of the upper distributor ring of the turbines for the Volga plants imeni Lenin and imeni XXIInd Congress of the KPSS is shown in Figure VI. 62. The upper-ring cross section is box-shaped, with holes for inserting the guide-vane bearings. The ring is provided on the outside with a flange (1) for connecting to the turbine speed ring, and on the inside with another flange (2) for securing the turbine cover-plate. The inner diameter of the internal flange should be a little larger than the runner-blade diameter, so that the runner can be removed without dismantling the upper ring. The upper distributor ring is the largest part in the turbine (except for the speed ring). For large-size turbines, it usually has to be made of several parts. The upper distributor ring of the turbines for the Volga plant imeni Lenin is composed of eight flanged sections bolted together; the flanges (6) are provided with holes (3) for the bolts. The location of the holes is shown in section A of Figure VI. 62. The flanges are connected by fitted bolts (4) to ensure accurate assembly; conical pins are sometimes used instead. The shape of the distributor ring is clearly visible in sections A and B, while its inner ribs (5) are shown in section B. The outer flange is double and provided with ribs, a design which permits a considerable increase in the resistance moment of the flange, in accordance with the strength requirements. The upper ring, viewed both from above and below, is shown in Figure VI. 62,c and d. The dimensions of one ring section are shown in Figure VI. 63. The largest dimension — 4592 mm — determines the number of sections which form the ring.

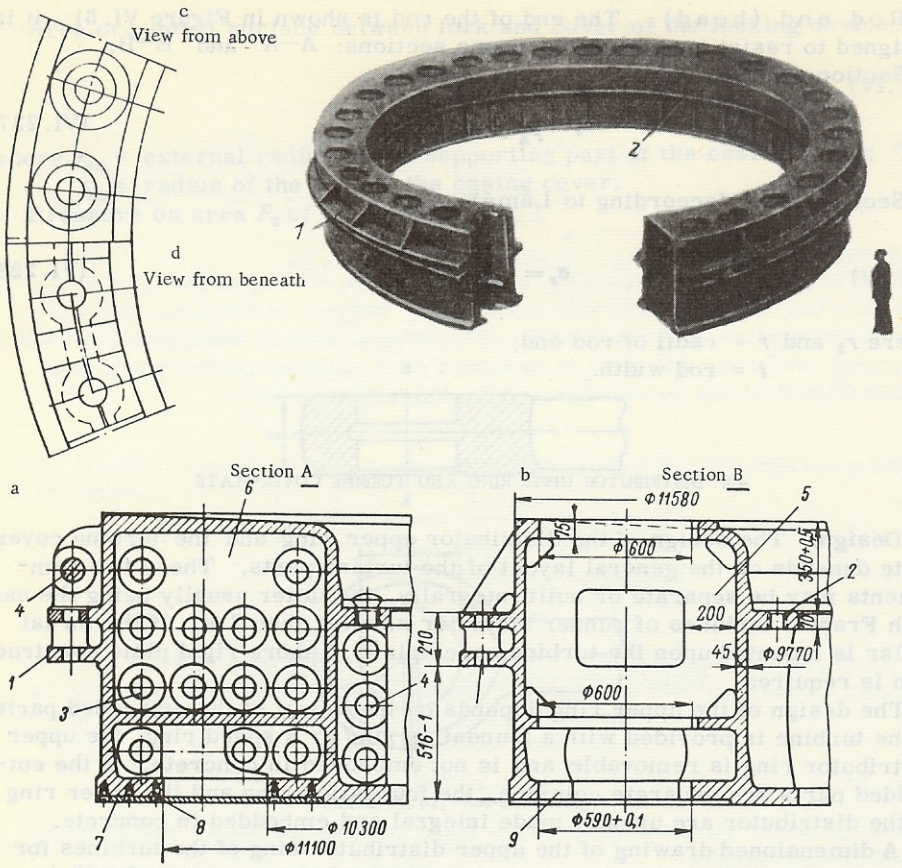


FIGURE VI. 62. Upper distributor ring of the turbines for the Volga plant im. Lenin

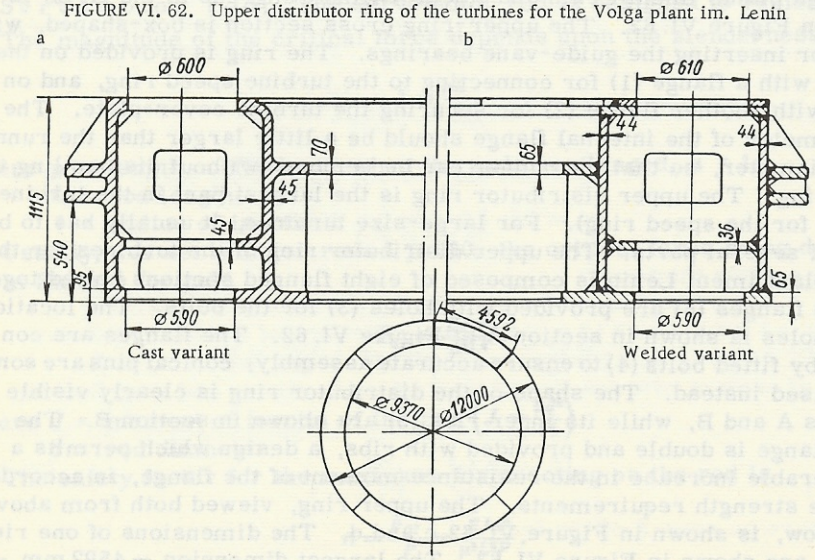


FIGURE VI. 63. Cast and welded designs for the upper distributor ring of the turbines for the Volga plant im. Lenin

The number of component sections in the upper ring and the other parts is determined in accordance with the dimensions of one section of the ring, its weight, and the available railroad and shop transportation facilities; the available hoisting tackle in the casting and machine shops should also be taken into consideration if the parts are cast.

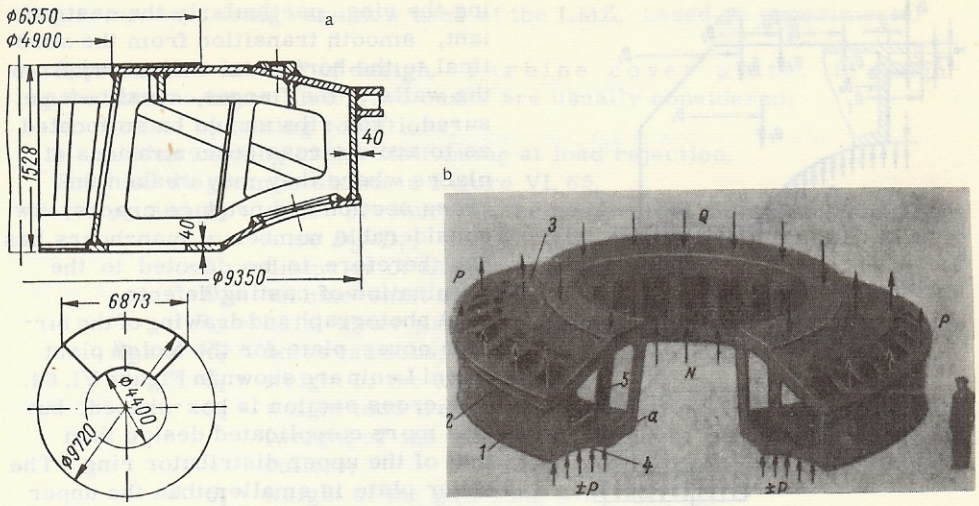


FIGURE VI. 64. Cover plate of the turbine for the Volga plant im. Lenin:

a — cast variant, weight 60 t; b — welded variant, weight 53.8 t.

The cast and welded designs are compared in Figure VI. 63, and, as can be seen, the shape of the ring is practically the same for both designs. With the welded design, the vertical and horizontal walls of the ring are joined together in a box-shaped construction. The blanks for the welded design are simple in shape, being stamped or rolled out from steel plate. The welded design permits the use of thinner walls compared with the cast variant, thus permitting a saving in weight. Both cast and welded variants of the upper distributor ring were tested for the turbines of the Volga plant imeni Lenin. The total weight of the cast ring is about 83.8 t, whereas the welded ring weighs 69.7, i. e., 14.1 t less. If the machining allowances necessary for the cast parts, particularly for such complicated shapes, are taken into account, the saving in weight of the welded design is even greater. For instance, the cast and welded blanks for the same upper distributor ring weighed 129.8 t and 79.6 t, respectively, the difference being 50.2 t. As a consequence of the smaller machining allowances, the amount of labor required for machining the welded part is also less; machining time was 4524 normal hours for the cast, as against 3483 hours for the welded variant.

There are no inner stresses in the welded design; rolled steel plates and sections have, moreover, higher strength.

All the problems connected with the manufacturing and machining of such a large part as the upper distributor ring should be carefully weighed beforehand.

Figure VI. 62 shows the lining (7), fastened from below to the ring by means of screws (8). This lining covers the openings (9) provided in the lower flange of the distributor ring for guide vane removal. In shaping the ring, particularly the cast variant, smooth transition from the vertical to the horizontal walls, and from the walls to the flanges, must be ensured. The ribs should be so located as to avoid stress concentrations at places where they may weaken the cross section and produce cracks; a considerable number of man-hours has has therefore to be devoted to the elimination of casting defects.

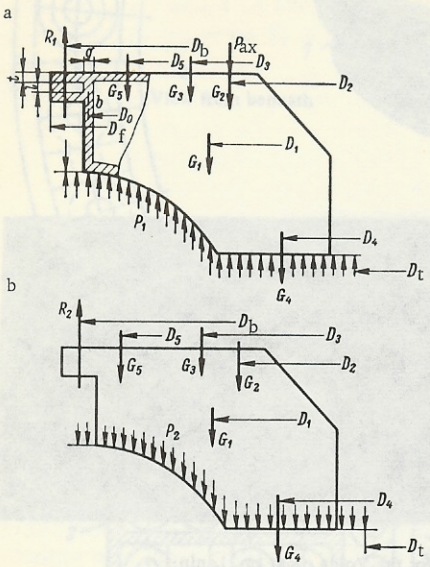


FIGURE VI. 65. Diagram of loads acting upon the cover plate of a Kaplan turbine:

a — normal operating conditions; b — sudden closing of the distributor.

A photograph and drawing of the turbine cover plate for the Volga plant imeni Lenin are shown in Figure VI. 64. The cross section is box-shaped, but of a more complicated design than that of the upper distributor ring. The cover plate is smaller than the upper ring, and is therefore made up of a smaller number of sections. The welded design of the cover plate is shown in Figure VI. 64. The cast cover plate weighs about 60 t, while the net weight of the welded cover plate is about 53.8 t; the blanks for the welded and cast cover plates weigh 60 and 78 t, respectively. The cover plate consists of the outer vertical wall (1), the outer flange (2), the upper cover (3), the lower flange (4) and the webs (5). The lower flange has a streamlined shape because it forms part of the water passages of the turbine. Owing to the double curvature of the lower flange (welded variant), its manufacture is difficult and it is usually pressed from steel plates. With the given turbine design, the cover plate is subject not only to water pressure from below, but also to the load from the thrust collar on the upper cover flange (3); consequently, it carries large compressive loads. In designing the turbine cover, it is very important to select the number and dimensions of the webs between its upper and lower flanges correctly.

Sectional views of turbines with various cover plate designs are shown in Figures V. 11 to V. 16. An intermediate support is sometimes used for mounting the thrust collar on the turbine cover plate (Figure V. 18). If the thrust collar is installed directly on the cover plate, the upper flange of the cover extends upward and the total height of the cover plate increases (Figure V. 17); this type of cover plate is larger and heavier, but, since there is no intermediate support, the design is more economical.

In strength computations, the annular parts of the distributor, the upper ring and the cover plate were considered until recently as rigid rings, subject to bending at the most critical section by hydraulic and weight loads. The stresses in the webs were thereby neglected. Experience in operation has shown, however, that the cover-plate webs are subject to considerable local stresses causing cracks at the corners at the transition from the vertical to the horizontal plates. Consequently, more accurate methods of ring component design are now used at the LMZ, based on experimental data.

Approximate method of design. Turbine cover plate. In designing the turbine cover plate, two cases are usually considered:

1) normal operating conditions;
2) sudden closing of the distributor at load rejection.

The load diagram is shown in Figure VI. 65,

where p_1 and p_2 = water pressure on the cover plate along the circumference D_b—D_t;
D_b = diameter of flange bolt-hole circle;
D_t = turbine-shaft diameter;
P_{ax} = axial water pressure upon the runner;
R_1 and R_2 = bolt reactions;
G_1 = weight of the cover plate;
G_2 = weight load transmitted by the thrust-collar frame (weight of the generator, runner, main shaft, and thrust collar);
G_3 = weight of the gate ring with bearing;
G_4 = weight of the guide bearing and cover-plate cone;
G_5 = weight of the servomotors (if mounted on the cover plate);
D_1, D_2, D_3, D_4, D_5 = diameters at which the weight loads are acting.

The pressure p_1 is determined according to the actual head as the difference between the maximum headwater level an the elevation at which the lower cover-plate flange is installed, with allowance for the pressure reduction due to water velocity.

The pressure p_2 is determined according to the vacuum under the cover plate, usually taken from 5 to 10 m. W. G.

$$p_1 = \left(H_1 - \frac{v^2}{2g}\right)\gamma \text{ kg/cm}^2, \qquad \text{(VI. 229)}$$

where H_1 = difference between the headwater level and elevation of distributor;
v = average velocity in the distributor region.

Consequently, the force due to water pressure acting upon the half ring is

$$P_1 = \frac{p_1\pi\left(D_b^2 - D_t^2\right)}{2 \cdot 4} \text{ t}. \qquad \text{(VI. 230)}$$

The diameters $D_1 \ldots . D_5$ are determined from the static moments of the weights of the respective part.

The total moment exerted upon half the cover plate under any operating conditions equals the sum of the moments of all forces and reactions.

First case. Bending moment due to weight loads

$$M_{G_1} = -\frac{G_1}{2} \cdot \frac{D_1}{\pi} \text{ t·m}$$

$$M_{G_2} = -\frac{G_2}{2} \cdot \frac{D_2}{\pi} \text{ t·m}$$

$$M_{G_3} = -\frac{G_3}{2} \cdot \frac{D_3}{\pi} \text{ t·m}$$

$$M_{G_4} = -\frac{G_4}{2} \cdot \frac{D_4}{\pi} \text{ t·m}$$

$$M_{G_5} = -\frac{G_5}{2} \cdot \frac{D_5}{\pi} \text{ t·m.}$$

Hence,

$$M_G = -\sum_{i=1}^{5} M_i \text{ t·m.} \qquad \text{(VI. 231)}$$

Bending moment due to axial water pressure on runner

$$M_{ax} = -\frac{P_{ax}}{2} \cdot \frac{D_2}{\pi} \text{ t·m.} \qquad \text{(VI. 232)}$$

Bending moment due to water pressure on the cover plate

$$M_{p_1} = \frac{P_1}{2} r_{p_1} = \frac{p_1 (D_b^2 - D_t^2)\,\pi}{2 \cdot 4} \cdot \frac{2 (D_b^3 - D_t^3)}{3\pi (D_b^2 - D_t^2)} = \frac{p_1}{12} (D_b^3 - D_t^3) \text{ t·m.} \qquad \text{(VI. 233)}$$

Bending moment due to bolt reactions

$$M_{R_1} = \frac{R_1}{2} \cdot \frac{D_b}{\pi} \text{ t·m,} \qquad \text{(VI. 234)}$$

where $R_1 = -(G + P_{ax} - P_1)$ t.

Total moment, tending to bend half of the turbine cover-plate,

$$M_1 = M_{R_1} + M_{p_1} + M_G + M p_{ax} \text{ t·m.} \qquad \text{(VI. 235)}$$

Second case. Forces due to water pressure p_2 (vacuum) upon the cover plate

$$P_2 = p_2 \frac{\pi}{4} (D_b^2 - D_t^2) \text{ t.} \qquad \text{(VI. 236)}$$

Bending moment due to force P_2

$$M_{P_2} = -\frac{p_2}{12} (D_b^3 - D_t^3) \text{ t·m.} \qquad \text{(VI. 237)}$$

Bending moment due to bolt reactions

$$M_{R_2} = \frac{R_2}{2} \cdot \frac{D_b}{\pi} \text{ t} \cdot \text{m}, \qquad \text{(VI. 238)}$$

where

$$R_2 = -(G + P_2) \text{ t}.$$

Total moment, tending to bend half of the turbine cover plate,

$$M_2 = M_{R_2} + M_G + M_{P_2} \text{ t} \cdot \text{m}. \qquad \text{(VI. 239)}$$

The maximum stress in the upper and lower flanges of the cover plate is determined from formula

$$\sigma = \frac{M_{1.2} y_{b.t}}{2J} \text{ kg/cm}^2 \qquad \text{(VI. 240)}$$

where $y_{b.t}$ = distance from neutral axis to most distant points of the upper and lower flanges;

J = moment of inertia of the critical section of the turbine cover plate.

$$J = \sum Fy^2 + \frac{\sum Fh^2}{12} - y_c^2 \sum F, \qquad \text{(VI. 241)}$$

where y_c = coordinate of the neutral axis of the critical section

$$y_c = \frac{\sum Fy}{\sum F}.$$

The computation is similar for the design with the upper ring made integral with the cover plate. The load diagram is shown in Figure VI. 66. The weight of the distributor parts, the force on the distributor, and the sudden pressure rise when the distributor is closed, must be added to G_2

The cover plate of the Francis turbine is designed for three cases: normal operating conditions, sudden load drop, and failure of the labyrinth seals. The diagram of the loads acting upon this type of cover plate is shown in Figure VI. 67, where G_1 = distributor weight; G_2 = weight of the guide bearing; q_1, q_2 = pressure below the labyrinth seal under different operating conditions.

Upper distributor ring. The upper distributor ring is designed for two cases: normal operating conditions, and sudden closing of the distributor. The diagram of the loads acting upon the upper ring is shown in Figure VI. 68, where G = total weight load on the upper ring.

$$G = G_1 + G_2 + G_3; \qquad \text{(VI. 242)}$$

G_1 = weight of the upper ring;
G_2 = weight of the guide vanes;
G_3 = weight of the levers, bearings, and other parts;
p_1 = water pressure, under normal operating conditions;
p_2 = water pressure, at sudden closing of the distributor;
q = vacuum acting on the distributor during sudden closing.

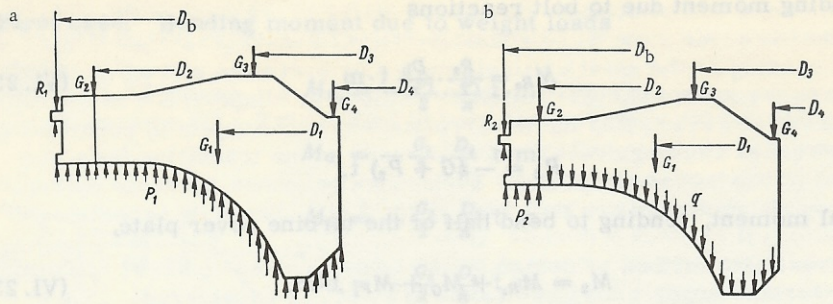


FIGURE VI. 66. Diagram of the loads acting upon the turbine cover plate combined with the upper distributor ring:

a — normal operating conditions; b — sudden closing of the distributor.

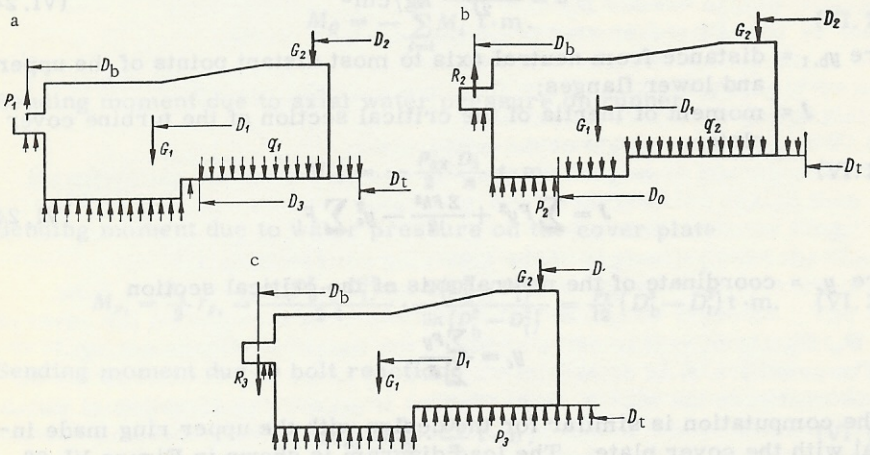


FIGURE VI. 67. Diagram of the loads acting upon the cover plate of a Francis turbine:

a — normal operating conditions; b — sudden closing of the distributor; c — failure of the labyrinth seal.

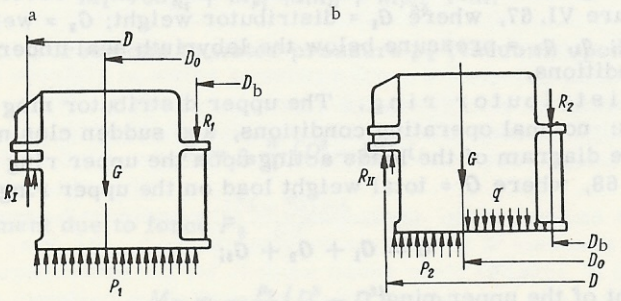


FIGURE VI. 68. Diagram of the loads acting upon the upper distributor ring:

a — normal operating conditions; b — sudden closing of the distributor.

First case: Bending moment

$$M_I = M_c + M_{RI} + M_{P1} + M_{R1}\ \text{t·m} \tag{VI.243}$$

$$M_c = -\frac{G D_0}{2\pi}\ \text{t·m}, \tag{VI.244}$$

$$M_{RI} = \frac{R_I D}{2\pi}\ \text{t·m}, \tag{VI.245}$$

$$R_I = R_1 + G + P_1, \tag{VI.246}$$

$$P_1 = -\frac{p_1}{\gamma}\cdot\frac{\pi}{4}(D^2 - D_b^2), \tag{VI.247}$$

$$M_{P_1} = \frac{p_1}{\gamma}\cdot\frac{D^3 - D_b^3}{12}. \tag{VI.248}$$

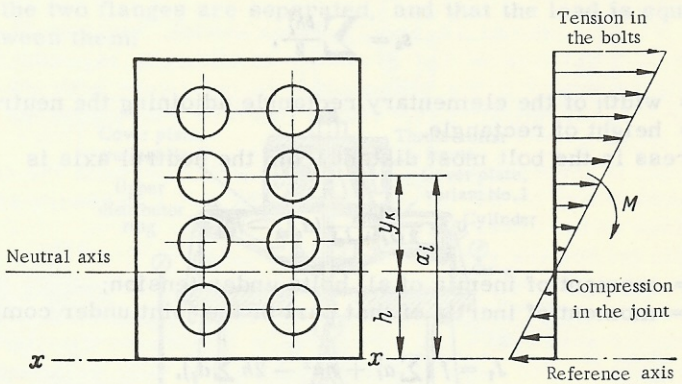


FIGURE VI.69. Diagram for computing the stress in the bolts of the flange joint

Second case: Bending moment

$$M_{II} = M_{R_{II}} + M_{P_2} + M_q + M_c + M_{R_2}\ \text{t·m}. \tag{VI.249}$$

The maximum stress in the upper and lower flanges, for both cases

$$\sigma_{1,2} = \frac{M_{I,\,II}\, y_{b.t}}{2J}\ \text{kg/cm}^2. \tag{VI.250}$$

When the turbine rings are designed in this manner, the permissible stresses are

for cast iron, up to 600 kg/cm^2,

for cast steel, up to 1000 kg/cm^2.

The bolts of the cover plate flange joint. In this design, the joint is considered as a fixed cantilever beam, subject to bending.

The bolts located on one side of the joint's neutral axis are subject to tension, while the part of the cover plate on the other side of the neutral axis is under compression.

The ordinate h of the neutral axis is determined from equation

$$\Phi(h) = s_1 + ks_2 = 0, \tag{VI.251}$$

whose solution may be tabulated by assuming several values for h;

s_1 = static moment of the bolts under tension;

s_2 = static moment of compressive force on the joint;

k = ratio of the moduli of elasticity of the cover plate and bolt materials.

The horizontal axis $x - x$ passing through the upper or lower cover-plate surface is taken as the reference axis.

$$s_1 = f(\Sigma a_i - nh),$$

where f = cross-sectional area of the bolt;

a_i = distance from the i-th bolt to the axis $x - x$;

n = number of bolts under tension.

Σa_i is calculated for the loaded bolts only

$$s_2 = \sum \frac{bh_i^2}{2}, \qquad \text{(VI.252)}$$

where b = width of the elementary rectangle adjoining the neutral axis;

h_i = height of rectangle.

The stress in the bolt most distant from the neutral axis is

$$\sigma = \frac{M_{max}}{2(J_1 + J_2)}(a_{max} - h), \qquad \text{(VI.253)}$$

where J_1 = moment of inertia of all bolts under tension;

J_2 = moment of inertia of that part of the joint under compression.

$$J_1 = f(\Sigma a_i^2 + nh^2 - 2h\Sigma d_i), \qquad \text{(VI.254)}$$

$$J_2 = \sum \frac{bh^3}{3}. \qquad \text{(VI.255)}$$

Cover-plate flange. The flange of the cover plate is designed to resist bending. The calculation is approximate, the assumption being that the flange is rigidly fixed to the vertical flat wall.

The bending moment is

$$M = Rl, \qquad \text{(VI.256)}$$

where R = maximum bolt reaction;

l = distance between bolt axis and cover-plate wall.

The modulus of section W of the flange cross section is determined in the usual way.

For the ribbed flange, the modulus is

$$W_1 = \frac{J}{y_c}; \quad W_2 = \frac{J}{h + k - y_c}. \qquad \text{(VI.257)}$$

The moment of inertia

$$J = \frac{\pi D_0 k^3}{12} + \pi D_0 k\left(y_c - \frac{k}{2}\right)^2 + \frac{zbh^3}{12} + zbh\left(k + \frac{h}{2} - y_c\right)^2. \qquad \text{(VI.258)}$$

Position of the neutral axis

$$y_c = \frac{\sum F_i y_i}{\sum F_i} = \frac{zbh\left(k + \frac{h}{2}\right) + \pi D_0 k \frac{k}{2}}{zbh + \pi D_0 k}, \qquad \text{(VI. 259)}$$

where z = number of ribs;
b = rib thickness;
h = rib height;
k = flange thickness;
D_0 = outer diameter of the developed cover plate wall.

The stress values are determined with greater accuracy from formulas (VI. 196) and (VI. 197).

In designing the double flange of the cover plate (Figure VI. 65), one assumes that the two flanges are separated, and that the load is equally distributed between them.

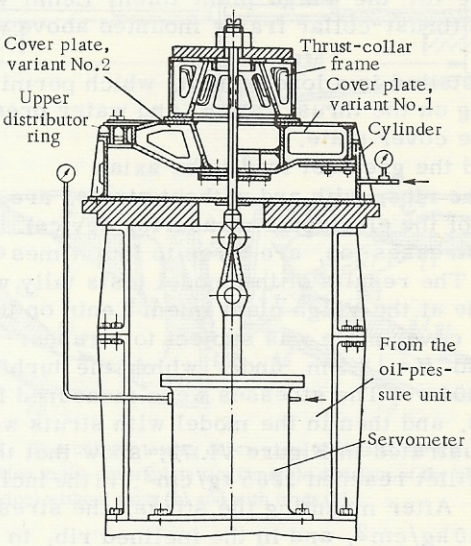


FIGURE VI. 70. LMZ unit for testing a metal cover-plate model

Experimental research data. A model, fabricated of steel plates, of the cover plate for the turbine of the Volga plant imeni Lenin, was tested at the LMZ in order to determine the actual stresses. The largest diameter of the model was 930 mm, equivalent to a scale of roughly 1/10. The tests were carried out with two kinds of loads, tending to reproduce the real operating conditions:

1) the axial load, transmitted by the thrust-collar frame;
2) the water pressure on the lower part of the cover plate.

Three design variants of the cover plate were tested, one of them being a cover plate made integral with the upper ring of the distributor.

The schematic layout of the test unit is shown in Figure VI. 70. Its principal element is a flanged cylinder, with the cover plate fixed on the flange. The water pressure upon the cover plate is simulated by oil pressure acting on a piston in the cylinder. The cover plate supports the model of the thrust-collar frame. The oil-pressure force, transmitted to it through a rigid plate, serves equally as a substitute for the rotor weight and force on the runner. The strains in the cover plate set up by this loading were measured by means of strain gages, and the stresses were computed from the average values of the strains. The tests showed the maximum stresses to occur at the inner edges of the ribs, with highest stresses found in the rib fillets. By providing struts (diagonals) between the ribs, the stresses may be considerably reduced.

The stresses in the sections between the ribs, the bottom, and the walls are negligible.

Figure VI. 71, a shows an experimental model, built by the Institute of Science of Machines of the Academy of Science, reproducing the cover plate of the turbine for the Volga plant imeni Lenin with the adjacent parts — the conical thrust-collar frame mounted above with the runner hub suspended from it.

The model is installed in a loading unit, which permits the simulation of axial loads acting on the thrust collar, and water pressure acting on the lower surface of the cover plate.

The tests proved the greatest load to be axial.

The strains in the ribs, with and without struts, are shown in Figure 71, b (in scale divisions of the electronic measuring device). The strains, and consequently, the stresses too, are three to four times smaller when struts are incorporated. The results of the model tests tally well with the field measurements made at the Volga plant imeni Lenin on the cover plate of turbine No. 2. The cover plate was subject to a runner-weight load P = 1370 t, and to a head H = 18.9 m, under which the turbine developed a power of N = 80,000 kw. The stresses were measured first in the cover plate without struts, and then in the model with struts welded to the ribs.

The results, illustrated in Figure VI. 72, show that the greatest stresses σ in the upper-rib fillet reached 2265 kg/cm^2; in the inclined rib the stresses were 2255 kg/cm^2. After mounting the struts, the stresses in the upper rib decreased to 820 kg/cm^2, and in the inclined rib, to 1355 kg/cm^2.

As part of this same research project, a series of cover plates of similar design, installed in several hydroelectric plants, were tested. The field strain-measurements made under different operating conditions on cover plates at several plants showed that in a number of cases large stresses occur in the ribs, especially at the fillets. Cracks, caused by high static stresses (σ = 1140 kg/cm^2) that exceed the normal strength of cast iron, were found in the ribs of cast-iron covers. These cracks are also caused by instantaneous build-up of vacuum below the cover plate during distributor closing at sudden load drops. These load drops change the direction of stresses: e. g., in the turbines of the Svir'II HEP, the stresses changed from σ = + 1140 kg/cm^2 to −910 kg/cm^2.

It was also found that at all normal operational conditions, dynamic stresses, whose intensity reaches 12% of the value of static stresses, are liable to appear.

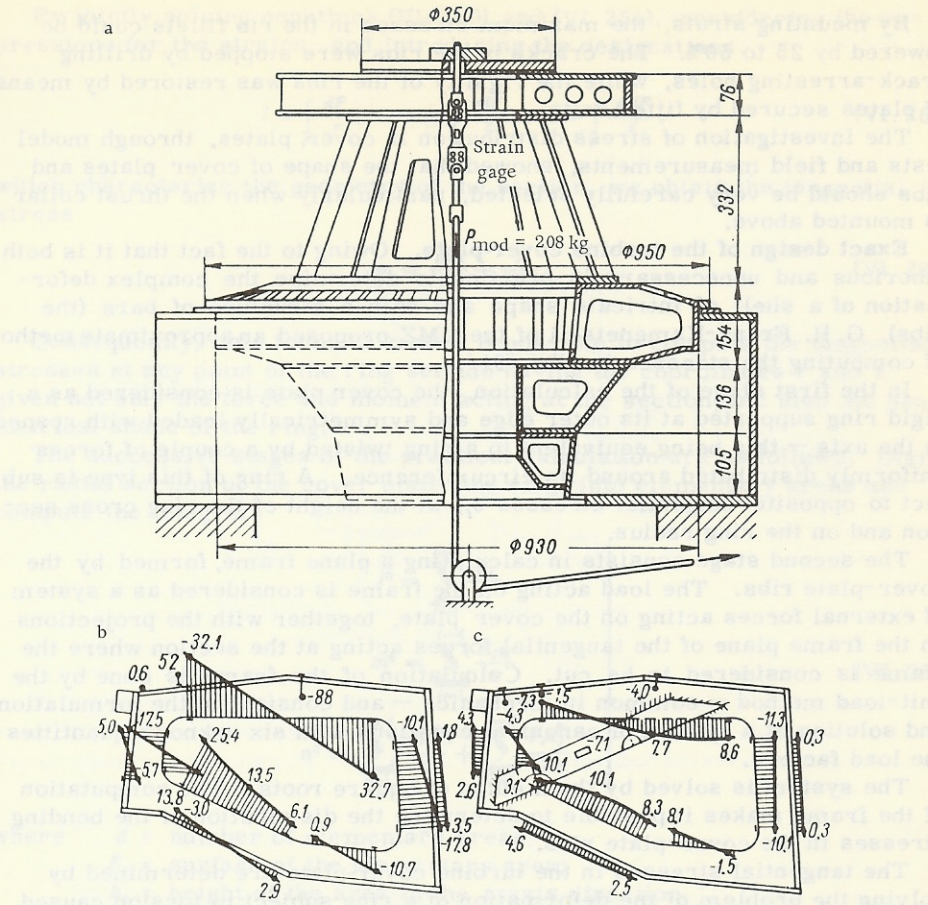


FIGURE VI. 71. Test unit for testing cover-plate models at the I.S.M. (a) and strain distribution in the cover-plate ribs (in scale divisions of the electronic measuring device) without struts (b) and with struts (c).

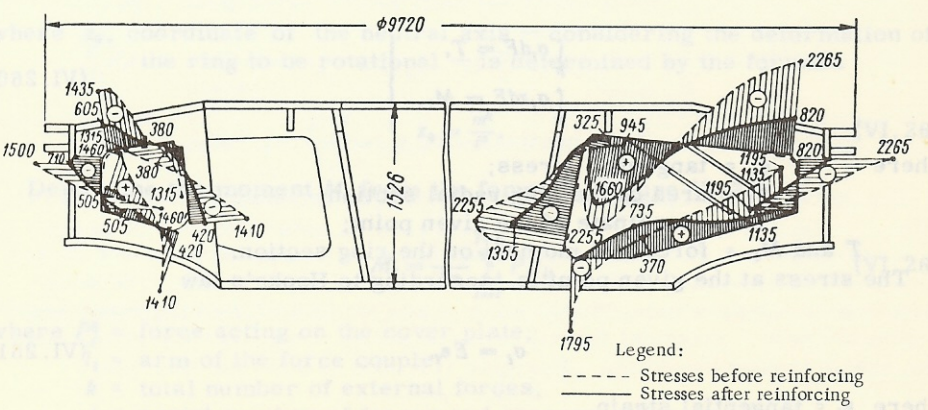


FIGURE VI. 72. Distribution of the total stresses in different ribs of the cover plate of the turbine for the Volga plant im. Lenin

By mounting struts, the maximum stresses in the rib fillets could be lowered by 25 to 50%. The cracks in the ribs were stopped by drilling crack-arresting holes, while the rigidity of the ribs was restored by means of plates secured by fitted bolts.

The investigation of stress distribution in cover plates, through model tests and field measurements, showed that the shape of cover plates and ribs should be very carefully selected, particularly when the thrust collar is mounted above.

Exact design of the turbine cover-plate. Owing to the fact that it is both laborious and unnecessary in practice to determine the complex deformation of a shell of intricate shape and with a structure of bars (the ribs), G. H. Frank-Kamenetskii of the LMZ proposed an approximate method of computing the stresses in ribs /91/.

In the first stage of the calculation, the cover plate is considered as a rigid ring supported at its outer edge and symmetrically loaded with respect to the axis — this being equivalent to a ring twisted by a couple of forces uniformly distributed around its circumference. A ring of this type is subject to opposite tangential stresses σ_t, at the height of the ring cross section and on the ring radius.

The second stage consists in calculating a plane frame, formed by the cover-plate ribs. The load acting on the frame is considered as a system of external forces acting on the cover plate, together with the projections on the frame plane of the tangential forces acting at the section where the frame is considered to be cut. Calculation of the frame is done by the unit-load method — common in mechanics — and consists in the formulation and solution of a system of canonical equations with six unknown quantities — the load factors.

The system is solved by the method of square roots. The computation of the frame makes it possible to determine the distribution of the bending stresses in the cover-plate ribs.

The tangential stresses in the turbine cover-plate are determined by solving the problem of the deformation of a ring subject to torsion caused by a couple of forces uniformly distributed around its circumference, and to compression induced by an axisymmetric radial load. For this purpose, the ring cross section is assumed to be constant.

The equations of equilibrium for the ring sections are:

$$\left.\begin{aligned} \int_F \sigma_t dF &= T, \\ \int_F \sigma_t z dF &= M_t, \end{aligned}\right\} \qquad \text{(VI.260)}$$

where σ_t = tangential stress;
F = area of the ring radial section;
z = coordinate of the given point;
T and M_t = force and moment on the ring section.

The stress at the given point is, according to Hooke's law

$$\sigma_t = E\varepsilon_t, \qquad \text{(VI.261)}$$

where ε_t = tangential strain.

By jointly solving equations (VI. 260) and (VI. 261), considering the expressions for the strains, and introducing the designations

$$l = \int_F \frac{dF}{r}; \quad m = \int_F \frac{zdF}{r}; \quad n = \int_F \frac{z^2 dF}{r}, \tag{VI. 262}$$

which characterize the geometry of the section, we obtain the tangential stress

$$\sigma_t = \frac{M_t z}{nr} + \frac{T}{lr}. \tag{VI. 263}$$

Consequently, this formula makes it possible to compute the tangential stresses at any point of the ring section having the coordinates r and z, given not only the force and moment acting at the section, but also the geometrical shape of the ring.

The successive stages of the practical calculation are as follows. Divide the radial section of the cover plate (the ring) into elementary areas and compute the integrals

$$\left.\begin{aligned} l^0 &= \sum_{i=1}^{i=d} \frac{F_i}{r_i} \\ m^0 &= \sum_{i=1}^{i=d} \frac{F_i z_i}{r_i} \\ n^0 &= \sum_{i=1}^{i=d} \frac{F_i z_i^2}{r_i} + \sum_{i=1}^{i=d} \frac{F_i h_i^2}{12 r_i}, \end{aligned}\right| \tag{VI. 264}$$

where d = number of elementary areas;
F_i = surface of the elementary area;
h_i = height of the area in the z-axis direction;
r_i, z_i = coordinates of the centroid of the elementary area.

Determine the value of the integral n from the relation

$$n = n^0 - z_0 m^0, \tag{VI. 265}$$

where z_0, coordinate of the neutral axis — considering the deformation of the ring to be rotational — is determined by the formula

$$z_0 = \frac{m^0}{l^0}. \tag{VI. 266}$$

Determine the moment M_t from the formula (Figure VI. 73)

$$M_t = \frac{1}{2\pi} \sum_{i=1}^{i=k} P_i l_i, \tag{VI. 267}$$

where P_i^0 = force acting on the cover plate;
l_i = arm of the force couple;
k = total number of external forces;
i = serial number of forces and corresponding arms.

Determine the tangential force T, as the product of water pressure and half the diametral projection of the ring subject to water pressure p

$$T = p\int_0^h r dz,$$

where h = height of the ring subject to water pressure (Figure VI. 73).

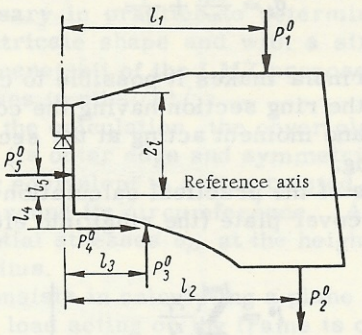


FIGURE VI. 73. Forces on the turbine cover-plate

The tangential force may be expressed as the sum of the horizontal projections of the external forces

$$T = -\sum_{i=1}^{i=k} P_{ir}^0, \qquad \text{(VI. 268)}$$

where P_{ir}^0 = horizontal projection of forces P_i^0.

The tangential stresses are determined in the light of two assumptions.

Assumption I. The distribution of the stresses in the cover-plate sections is considered as obeying the law of beam flexure, the stresses being independent of the radius of the fiber considered

$$\sigma_t = \frac{M_t}{J}(z - z_c),$$

where z_c = coordinate of the neutral axis; $z_c = \frac{\sum Fz}{\sum F}$.

The maximum stresses occur in the fibers farthest from the neutral axis.

Assumption II. The stresses in the cover-plate sections are determined with allowance for the rotational deformation of the ring. The assumption, in other words, is that each cross section of the ring turns under a certain angle — identical for all cross sections — and that the cross section shape remains constant. Formula (VI. 263) is used for this case.

$$\sigma_t = \frac{M_t}{n}\cdot\frac{z}{r} + \frac{T}{lr}.$$

Design of the cover-plate ribs. In designing the cover-plate ribs, an isolated radial sector of the cover plate containing one single rib is considered.

The sector is considered as a closed, plane frame (Figure VI. 74). In addition to part of the external load, each of the ribs is subjected to tangential stresses σ_t (previously determined) acting on each rib from the cut side of the cover plate.

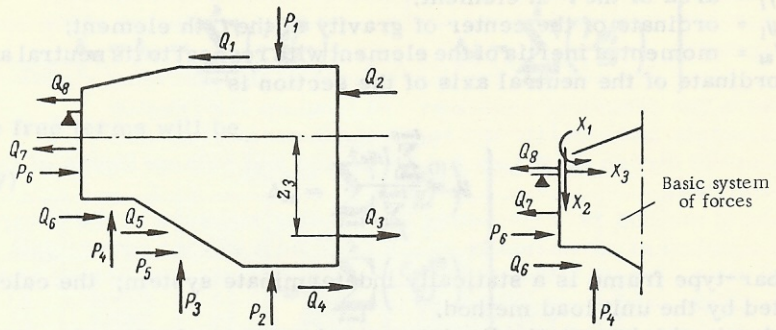


FIGURE VI. 74. Schematic diagram of the plane frame

The external forces are the loads P_t, and the forces Q_i, which are projections of the tangential forces acting in the section of the isolated sector. These external forces are determined from formulas

$$P_i = \frac{1}{k_0} P_i^0, \tag{VI. 269}$$

$$Q_i = \frac{1}{n} \cdot \frac{F_i z_i}{r_i} \sum_{i=1}^{i=k} P_i l_i - \frac{1}{l} \cdot \frac{F_i}{r_i} \sum_{i=1}^{i=k} P_{ir}, \tag{VI. 270}$$

where k_0 = number of radial cover-plate ribs;

P_i^0 = total force acting upon the cover plate;

$\sum_{i=1}^{i=k} P_i l_i$ = resultant moment of the external forces acting in the frame plane;

$\sum_{i=1}^{i=k} P_{ir}$ = resultant horizontal load;

n and l = geometrical parameters of the section;

z_i and r_i = coordinates of the centroid of the elementary area; z_i is measured from the neutral axis of the section;

F_i = surface of the elementary area.

The coordinates of the point of application of the force Q_i are determined from

$$z_c = z_i + \frac{h^2}{12 z_i}, \tag{VI. 271}$$

where h = height of the elementary rectangle.

The moments of inertia of the bar-type frame are determined in the normal way from the formula

$$J = \sum_{i=1}^{i=n} J_{0\,i} + \sum_{i=1}^{i=n} f_i y_i^2 - y_c^2 \sum_{i=1}^{i=n} f_i, \tag{VI.272}$$

where i = serial number of the elementary area;
n = number of elements;
f_i = area of the i-th element;
y_i = ordinate of the center of gravity of the i-th element;
J_{0i} = moment of inertia of the element with respect to its neutral axis.

The ordinate of the neutral axis of the section is

$$y_c = \frac{\sum_{i=1}^{i=n} f_i y_c}{\sum_{i=1}^{i=n} f_i}. \tag{VI.273}$$

The bar-type frame is a statically indeterminate system; the calculation is effected by the unit load method.

In order to obtain a statically determined system, the frames are cut at an arbitrary section and unknown moments x_1 and forces x_2 and x_3 applied (Figure VI. 74). A statically determinate system, called the basic system, then results for which the moment diagrams of the unit loads and of the actual applied load (Figure VI. 75) can be constructed.

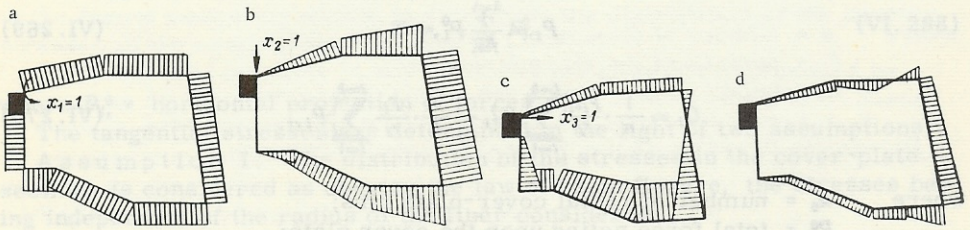


FIGURE VI. 75. Diagrams of the bending moments caused by unit forces x_1 (a); x_2 (b); x_3 (c) and by the external load (d)

The unknown loads and moments are determined from the canonical equations by the unit-load method.

$$\left.\begin{aligned} \delta_{11}x_1 + \delta_{12}x_2 + \delta_{13}x_3 + \Delta_{1p} &= 0 \\ \delta_{21}x_1 + \delta_{22}x_2 + \delta_{23}x_3 + \Delta_{2p} &= 0 \\ \delta_{31}x_1 + \delta_{32}x_2 + \delta_{33}x_3 + \Delta_{2p} &= 0 \end{aligned}\right|. \tag{VI.274}$$

The coefficients and free terms of the canonical equations (in the case of straight bars) may be determined from Vereshchagin's formula and are given in equations (VI. 275) and (VI. 276).

The coefficients of the canonical equations are

$$\left.\begin{aligned} \delta_{11} &= \sum_{i=1}^{k}\left(\frac{F_i y_c^{(1)}}{EJ}\right); \qquad \delta_{12} = \delta_{21} = \sum_{i=1}^{k}\left(\frac{F_2 y_c^{(1)}}{EJ}\right); \\ \delta_{22} &= \sum_{i=1}^{k}\left(\frac{F_2 y_c^{(2)}}{EJ}\right); \qquad \delta_{13} = \delta_{31} = \sum_{i=1}^{k}\left(\frac{F_3 y_c^{(1)}}{EJ}\right); \\ \delta_{23} &= \delta_{32} = \sum_{i=1}^{k}\left(\frac{F_3 y_c^{(2)}}{EJ}\right); \qquad \delta_{33} = \sum_{i=1}^{k}\left(\frac{F_3 y_c^{(3)}}{EJ}\right). \end{aligned}\right\} \quad \text{(VI. 275)}$$

The free terms will be

$$\left.\begin{aligned} \Delta_{1p} &= \sum_{i=1}^{k}\left(\frac{F_p y_c^{(1)}}{EJ}\right); \\ \Delta_{2p} &= \sum_{i=1}^{k}\left(\frac{F_p y_c^{(2)}}{EJ}\right); \\ \Delta_{3p} &= \sum_{i=1}^{k}\left(\frac{F_p y_c^{(3)}}{EJ}\right). \end{aligned}\right\} \quad \text{(VI. 276)}$$

In formulas (VI. 275) and (VI. 276) the designations are:

F_1, F_2, F_3, F_p = areas of the respective moment diagram;
$y_c^{(1)}$, $y_c^{(2)}$, $y_c^{(3)}$ = ordinates of the diagram of unit moments, the ordinates being measured above the centroid of the respective diagram;
EJ = rigidity of the bar;
k = number of frame bars.

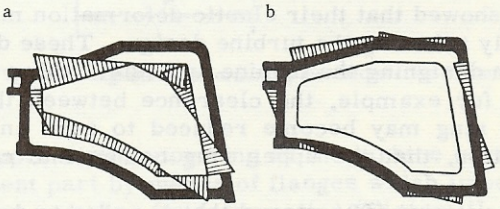


FIGURE VI. 76. Stress distribution in the cover-plate ribs:
a — inside fiber; b — outside fiber.

After determining the unknown quantities x_1, x_2, and x_3, it is possible to construct the moment diagram of the frame, and calculate the stresses on the inner and outer fibers of the rib. The stress pattern is shown in Figure VI. 76. To sum up, in designing the cover-plate ribs, the procedure is as follows:

1) calculate the moments of inertia and moduli of the frame bars;

2) design the frame according to the predetermined position of the centroid; determine the coordinates of the joints and the length of each bar;

3) determine the external loads acting upon the frame, and the coordinates of their points of application;

4) calculate and tabulate the reactions and the coordinates of their points of application;

5) select the basic system of plotting the unit diagrams;

6) calculate and tabulate the moments of the external forces;

7) calculate and tabulate the areas, and the coordinates of the centroids of the diagrams;

8) calculate and tabulate the coefficients of the canonical equations;

9) solve the canonical equations and tabulate the results;

10) calculate and tabulate the resultant moment diagram;

11) plot the stress diagrams for the inside and outside fibers of the cover-plate ribs.

The above method of calculating the bending stresses in the cover-plate ribs was checked experimentally at the LMZ on a welded cover-plate model. The tests were carried out with TPD-10 wire strain-gages having a gage length of 10 mm, and a resistance of 120 ohm.

The model was tested under three types of loadings: axial load, internal pressure, and joint action of an axial load and internal pressure.

For inside fibers, the experimental results agreed in general with those calculated. However, because of the number of assumptions made during the calculation, it should be understood that the method described above yields only approximate results, in particular for the outside fibers.

Experimental data gathered during field and model tests tend to indicate that a correction factor must be introduced into the calculation to obtain more accurate results.

Deformation of the annular distributor parts. In larger parts, such as the cover plate, etc., rigidity is not less important than mechanical strength. Experience in manufacture, erection, and operation of large-size annular parts showed that their elastic deformation may reach large values, considerably affecting the turbine design. These deformations must be allowed for when designing the turbine and establishing the clearances for moving parts; for example, the clearance between the guide-vane tips and the upper ring may become reduced to such an extent because of elastic deformation, that the upper ring comes into contact with the guide vanes.

G. H. Frank-Kamenetskii /90/ proved that in order to determine with satisfactory accuracy deformation of such parts as the upper distributor ring, they should be considered as rigid rings, for which the deflection ω_0 of the inner edge with respect to the outer edge may be determined by the formula

$$\omega_0 = c_0 \frac{Pb^2}{En} \text{ cm}.$$

If the outer edge of the ring is supported, the deflection of an arbitrary point of the ring is

$$\omega = \omega_0 \frac{b-r}{b-a} \text{ cm},$$

where a and b = inner and outer radii of the circles of the bolt holes on the upper-ring flanges;
P = nominal load on the ring;
r = radius to the point where bending is measured;
n = integral determined from formula (VI. 262);

$$c_0 = \frac{\left(\frac{b}{a} - 1\right)^2}{2\pi \left(\frac{b}{a}\right)^2}.$$

The values of c_0 for different $\frac{b}{a}$ are given in Table VI. 14.

TABLE VI. 14

Coefficient c_0 for different ratios $\frac{b}{a}$

$\frac{b}{a}$	c_0	$\frac{b}{a}$	c_0	$\frac{b}{a}$	c_0	$\frac{b}{a}$	c_0
1.0	0	1.6	0.0224	2.1	0.0437	2.7	0.0631
1.1	0.00132	1.7	0.0270	2.2	0.0474	2.8	0.0658
1.2	0.00442	1.8	0.0314	2.3	0.0508	2.9	0.0683
1.3	0.00848	1.9	0.0357	2.4	0.0541	3.0	0.0707
1.4	0.0130	2.0	0.0398	2.5	0.0573	4.0	0.0895
1.5	0.0170			2.6	0.0603		

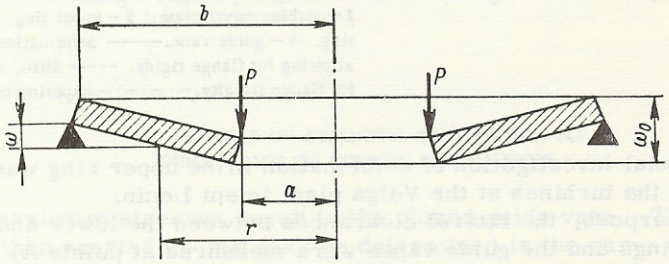


FIGURE VI. 77. Diagram for determining the deformation of annular parts

Usually, the upper distributor ring or the turbine cover plate are connected to the adjacent part by means of flanges which impart a greater rigidity to the ring, thus reducing its deformation (Figure VI. 78). The effect of the flanges may be approximately allowed for by introducing the coefficient k_1, the deflection of the ring then becoming

$$\omega_0 = c_0 k_1 \frac{Pb^2}{En}.$$

The coefficient k_1 is equal to

$$k_1 = \frac{1}{1 + \frac{z_b h_b^2 E_b F_b}{2\pi E n l_b}},$$

where z_b = number of bolts;
h_b = arm of bending moment;
F_b = cross-sectional area of bolt;
E_b = modulus of elasticity of bolt;
l_b = bolt length.

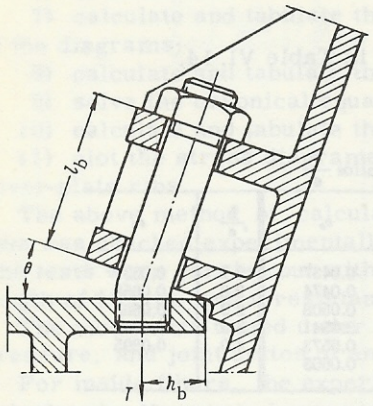


FIGURE VI. 78. Deformation of the flange joint

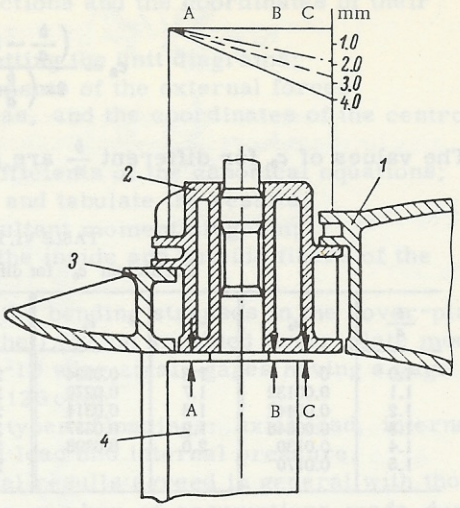


FIGURE VI. 79. Deformation of the upper ring:

1 — turbine cover plate; 2 — upper ring; 3 — speed ring; 4 — guide vane. ——— deformation, without allowing for flange rigidy. ----- ditto, allowing for flange rigidity. — · — · — · — experimental data.

Experimental investigation of deformation in the upper ring was carried out on one of the turbines at the Volga plant imeni Lenin.

For this purpose, the lateral clearances between the lower and upper distributor rings and the guide vanes were measured at points A,. B and C (Figure VI. 79).

The deformation of the upper ring was caused by the weight of distributor and rotor transmitted through the thrust-collar frame, mounted on the cover plate.

In order to obtain sufficiently accurate data on the nature of the phenomenon, the deformations due to different weight loads, such as distributor, generator rotor, or turbine runner, were measured during the actual erection of the hydro unit.

From the measurements made on one turbine, it was ascertained that even with a small initial loading, the upper ring is appreciably deformed, but on further loading the deformations increase at a slower rate.

When the load was removed, the upper ring did not return to its former position, and permanent deformation apparently occurred. It seems, therefore, that the deformations of the upper ring are of two kinds, elastic and plastic. Plastic deformation may be considered to be a consequence of the leveling of the irregularities on the machined surfaces, of the clearance reduction at the contact surface of the flange joint and of a certain deformation of the flanges.

A comparison between the elastic deformations of the upper ring, both calculated and experimentally determined, is set out in Table VI. 15, in accordance with Figure VI. 79.

Deformations were calculated both with (k_1 =0.79). and without (k_1 = 1) taking into account the rigidity of flange connections.

TABLE VI. 15

Comparison of the upper ring deformations, calculated and experimentally determined

Points	A, mm	B, mm	C, mm
Calculated deformations for k_1 = 1	0.74	2.29	3.25
Calculated deformations for k_1 = 0.79	0.58	1.81	2.56
Experimental deformations	0.61	1.59	1.80

As can be seen from table and diagram, the deformations calculated with allowance for flange rigidity agree satisfactorily with the experimental results.

41. REMARKS ON STRENGTH CALCULATION FOR GUIDE VANES OF CONICAL DISTRIBUTORS

The maximum stresses occur in the closed guide vane. The hydraulic moment then exerted upon it may be determined in the same way as for the cylindrical distributor.

$$M_h = n_0 l P_2,$$

where n_0 = relative eccentricity;

l = length of the guide-vane arc, on which the center of gravity of the vane is located (Figure VI. 5).

Considering that the guide vane is part of a conical surface, the radius to the center of gravity on the development may be determined from the following formula:

$$r_{c.g} = r_m + \frac{(R-r)^2}{12 r_m}, \qquad \text{(VI. 277)}$$

where $r_m = \frac{R+r}{2}$,

R and r = respective radii of curvature of the lower and upper guide-vane edges.

The hydraulic forces acting on the conical guide vane in the closed position

$$P_h = \gamma HF = \gamma H\pi (R^2 - r^2)\frac{\delta}{2\pi}, \qquad \text{(VI. 278)}$$

where $\delta = \frac{2\pi}{z_0} \cdot \frac{R_0}{R}$ = vane pitch angle on a developed cone base (Figure VI. 5).

When determining the pivot-bearing reactions and the stresses in the conical guide vane, it should be noted that the load varies along the vane length according to the diagram in Figure VI. 5.

The hydraulic force upon an element of the guide vane are

$$dP_h = \gamma Hl_x dx = \gamma H\delta (x + r)\, dx. \qquad \text{(VI. 279)}$$

The bearing reactions are determined from the equations of statics

$$\left.\begin{aligned} \Sigma y &= R_A - P_h + R_B + P_m = 0; \\ \Sigma M_A &= \int_0^{l_2} dP_h (x_A - x) - R_B L - P_m (L + l_4) = 0 \end{aligned}\right\} \qquad \text{(VI. 280)}$$

or

$$\int_0^{l_2} \gamma H\delta (x + r)(x_A - x)\, dx = R_B L + P_m (L + l_4).$$

The stresses in the guide-vane body are determined from the bending moment in the part subject to water pressure $(0 < x < l_2)$

$$M_b = R_A (x_A - x) - \int_x^{l_2} dP_h (t - x),$$

where t = integration variable

$$x < t < l_2;$$
$$dP_h = \gamma H\delta (t + r)\, dt,$$

consequently,

$$M_b = R_A (x_A - x) - \int_x^{l_2} \gamma H\delta (t + r)(t - x)\, dx. \qquad \text{(VI. 281)}$$

The coordinate x of the section subject to maximum bending moment, is determined from

$$\frac{dM_b}{dx} = 0.$$

The moment of inertia of the guide vane may be calculated in the normal way.

The design of the guide-vane actuating mechanism [for a conical distributor] is similar to the design of the actuating mechanism of the cylindrical distributor.

Chapter VII

FRANCIS TURBINE RUNNERS

42. RUNNER DESIGNS

The Francis runner is employed over a wide range of heads and specific speeds n_s.

Figure VII. 1 illustrates the change in the shape of the water passages of the Francis runner at various specific speeds ranging from $n_s = 60$ to $n_s = 400$.

At a low specific speed ($n_s = 60$), the leading edge (1) of the runner blade is usually located in a vertical plane, and on a larger diameter than trailing edge (3) ($D_2 < D_1$), which is almost horizontal. The profiles of the upper (2) and lower (4) bands of the runner are similar. The runner hub (5) is close to the upper band (2). The ratio of the runner entrance opening to the diameter b_0/D_1 is not large. The runner blade extends in length from the leading to the trailing edge.

For runners of higher specific speed ($n_s = 190$), the upper (2) and lower (4) bands differ markedly in shape and profile, and the leading (1) and trailing (3) edges are located close to each other on nearly conical surfaces. In this case, the ratio b_0/D_1 is greater, while the entrance (D_1) and exit (D_2) diameters are practically equal.

Runners of still higher specific speed ($n_s = 400$) have even shorter blades, and higher ratios b_0/D_1. The upper band (2) and the runner hub (5) form a single element. In this case, $D_2 > D_1$.

The design of the basic runner components — blades, upper and lower rings, and hub — has to be adapted to the specific speed used, because of the strict relationship between the size of these components and the speed.

Nowadays, turbine engineers employ Francis runners with stamped blades welded to the lower and upper bands, all-cast constructions with profiled blades, and welded-cast constructions. Depending on its sizes, the runner may be of one piece or of several pieces bolted or welded together.

Figure VII. 2 shows a runner with stamped blades.

The blades (2), stamped of steel plates, are welded to the cast-iron hub (1) and to the lower band (3). This type of runner is in common use for medium-size turbines.

For a runner diameter $D_1 = 1.0$ m, the blade is usually 10 mm thick ($s_1 = 10$ mm) and is inserted into the hub and band over a depth of $s_2 = 30$ to 40 mm.

The radius of curvature of the leading edge is equal to half the blade thickness $R = 0.5\, s_1$, while the radius of the trailing edge varies from 1 to 2 mm. The blade ends, cast into the band and hub, are dovetailed.

The blades are stamped in special stamping dies.

A core with stamped steel blades is introduced into the mold for casting the hub and band. Particular care should be taken when inserting the blade into the core, which should be made beforehand in a special box.

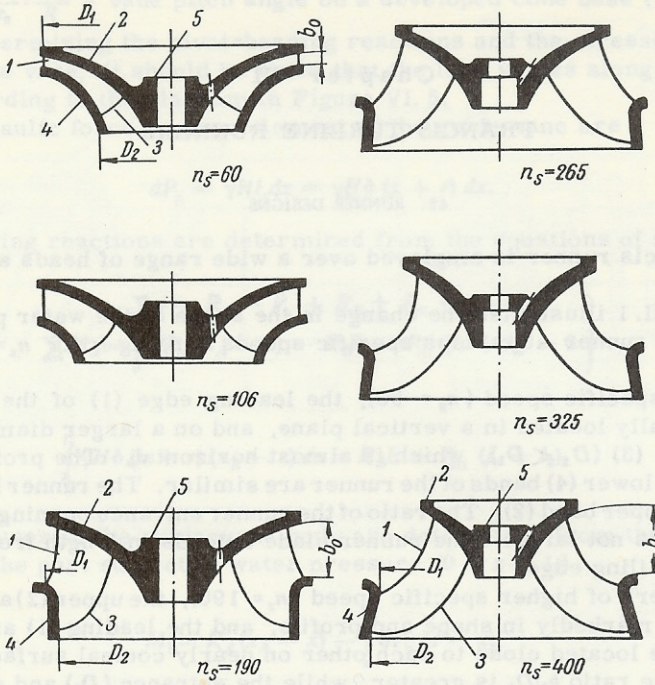


FIGURE VII. 1. Profiles of Francis runners for different specific speeds (n_s = 60 to 400)

Figure VII. 3 shows the design of an all-cast runner. The upper band (2), blades (3) and lower band (4) are cast together — usually of carbon or stainless steel. For large-size runners, the upper band (1) is made removable. Seal rings (5 and 6, 7 and 8) are provided at the upper and lower rings for reducing water leakages across the runner. The number of blades z_1 usually varies from 14 to 18.

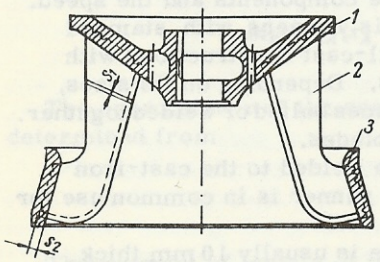


FIGURE VII. 2. Francis runner with stamped blades

Blade profile, and blade location in the space between the upper and lower rings, have a considerable effect upon runner efficiency; particular attention should therefore be paid to the casting and machining of the blades and to their proper location and configuration.

Two views are required to make the model for casting the runner: the plan view and the elevation, usually drawn to scale, on which sections perpendicular to the runner axis are represented — as shown in Figure VII. 4.

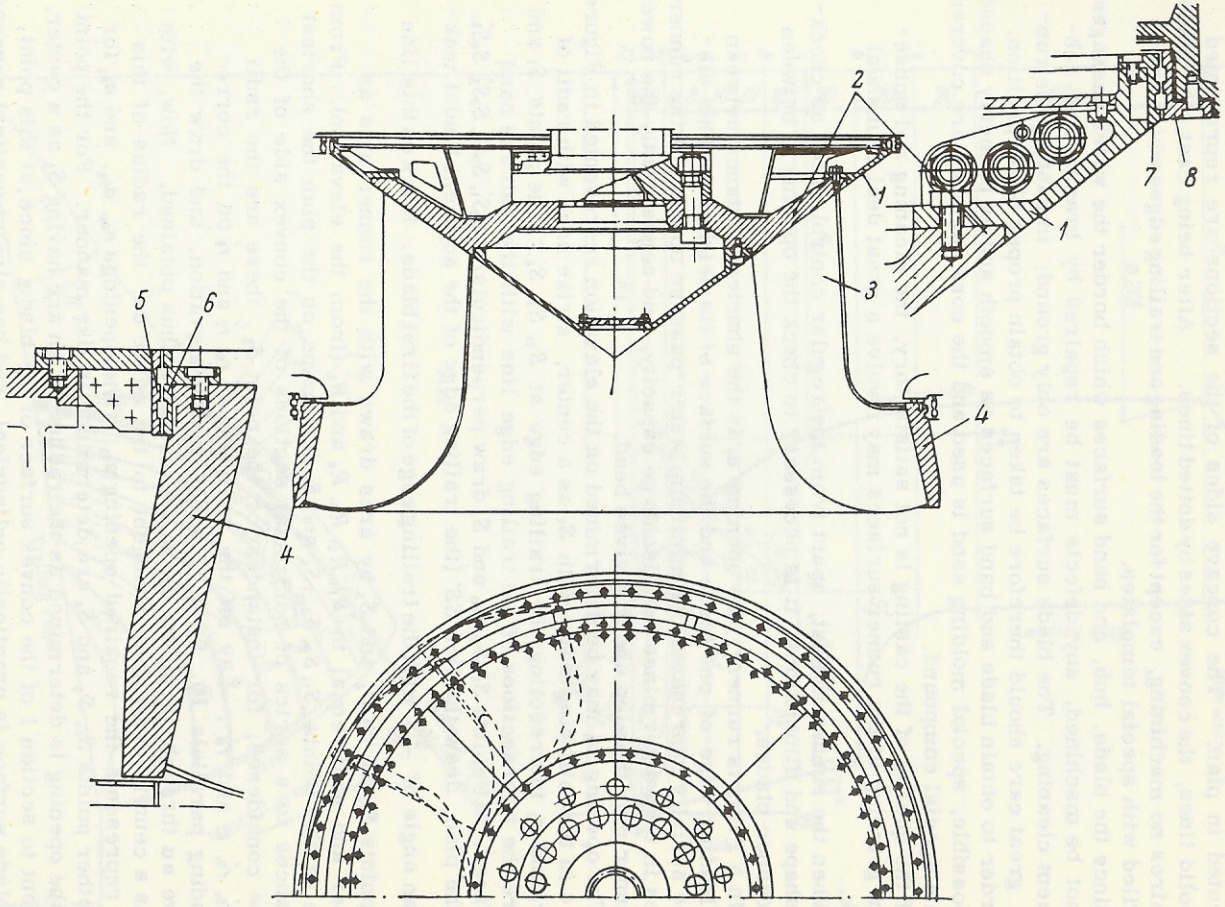


FIGURE VII. 3. All-cast Francis runner

To obtain the elevation, the points of the leading and trailing edges are rotated about the runner axis, superimposing the projections on a plane passing through the axis; thus, the distances between the blade points and the turbine axis remains undistorted (cylindrical projections).

The profiles of blade sections perpendicular to the turbine axis are represented in plan. The concave sides of the sections are represented by solid lines, the convex sides by dotted lines. After being cast, the blade requires no machining, except for the leading and trailing edges which are profiled with special templates.

Since the blade, hub, and band surfaces which border the water passages cannot be machined, any defects must be repaired by brazing and subsequent cleaning. The blade surfaces are only ground; in casting the runner, great care should therefore be taken to obtain proper blade position. In order to obtain blade and band surfaces as smooth and as properly shaped as possible, special molding sand is used and the core surfaces are covered with a special compound.

If the quality of the casting is not satisfactory, the cleaning and subsequent grinding of the runner surfaces may involve a great deal of manual work.

When the runner is cast, apart from the regular controls such as checking shape and dimensions, it is necessary to check the opening a_0 between the runner blades.

[In a Francis runner], the opening a_0 is the shortest distance between the leading edge of one blade and the surface of its neighbor. This distance actually represents the minimum water-passage opening of the runner, which in turn determines the discharge capacity, and consequently the power a runner may develop under a given head.

The opening a_0 may be determined on the elevation represented in Figure VII. 4 in the following way: with S_1 as a center, strike arcs with radii of r_2, r_3 and r_4 intersecting the trailing edge at S_2, S_3, S_4. The points S_1 and S_5 are the intersections of the trailing edge line with the hub and band surfaces. At points S_1, S_2, S_3 and S_4 draw perpendiculars S_1S_1', S_2S_2', S_3S_3', S_4S_4'. On the plan, draw the line SS' (the trailing edge of the adjacent blade) making an angle of $\frac{2\pi}{z_1}$ with the trailing edge of the first blade. Mark on this line the points S_1, S_2, S_3, S_4 and S_5 by arcs drawn with the runner axis as center and radii equal to R_1, R_2, R_3, R_4 and R_5 (from the elevation). From each of the points S_1, S_2, S_3, S_4 and S_5 determine on the plan the shortest distances to a series of horizontal sections of the convex side of the blade considered; for instance, for the point S_3, these are the radii r_{10}', r_9', r_8', r_7' and r_6'. Lay off the radii r_{10}', r_9', r_8', r_7' and r_6' on the corresponding parallels 10, 9, 8, 7 and 6 in the elevation, and draw the curve $\alpha\alpha$ through the points α_{10}', α_9', α_8', α_7' and α_6' thus obtained. Now, with S_3 as a center, draw an arc tangent to the curve $\alpha\alpha$; the radius of this arc represents the required opening a_{03}. The openings a_{01}, a_{02}, and a_{04} for the other points S_1, S_2 and S_4 are determined in like manner. For the point S_5, the opening is determined as the radius of an arc having S_5 as a center, tangent to section 1 of the convex surface of the blade, since, at this point, the blade surface is practically cylindrical, and has almost vertical generatrices.

On the basis of long experience in the construction of hydro turbines, LMZ established the tolerances for shape and dimensions of Francis-runner

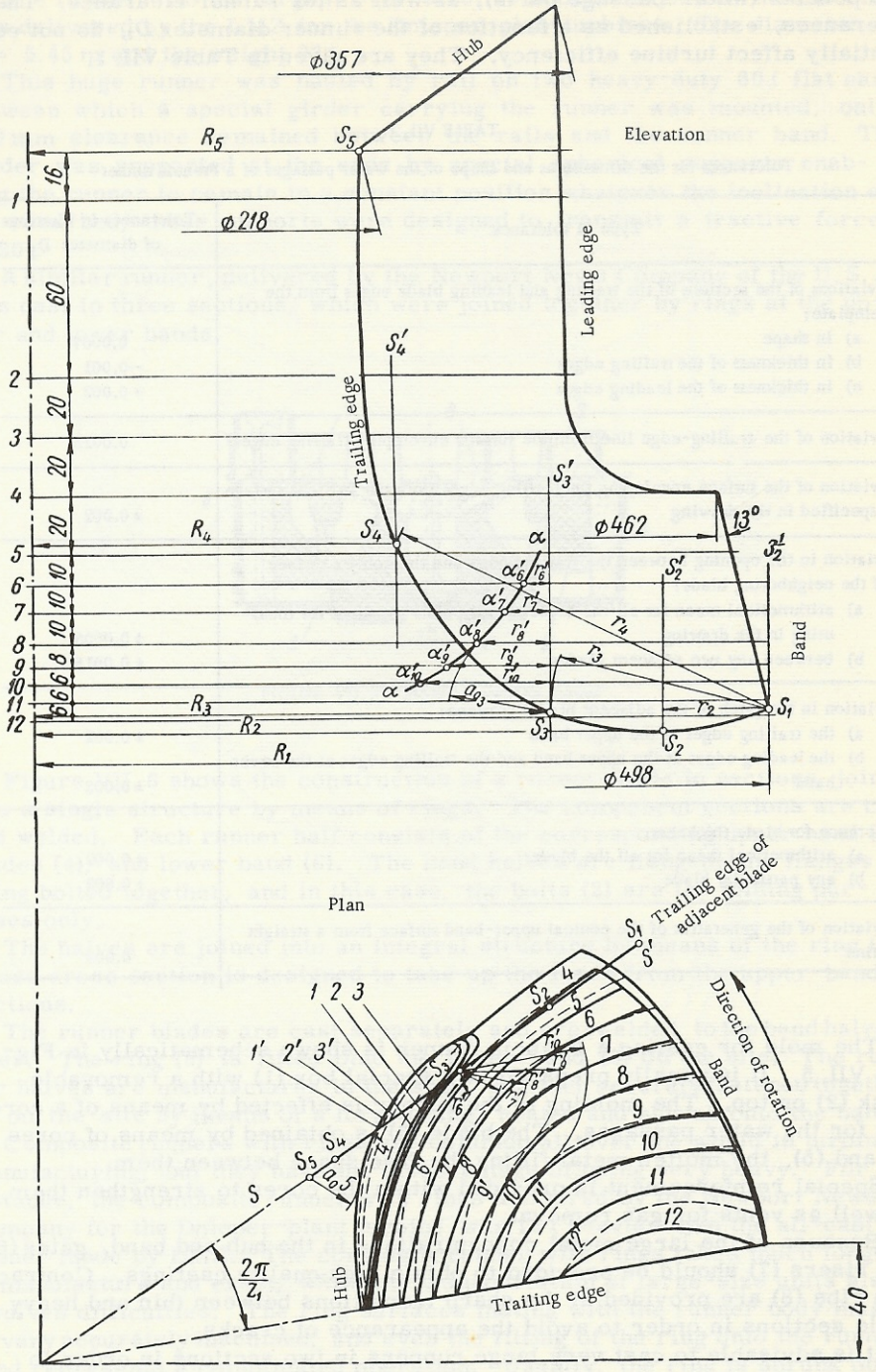


FIGURE VII. 4. Blade of a Francis runner

components (water-passage parts), as well as for runner clearance. These tolerances, established as a function of the runner diameter D_1, do not essentially affect turbine efficiency. They are given in Table VII. 1.

TABLE VII. 1

Tolerances for the dimensions and shape of the water passages of a Francis runner

Type of tolerance	Tolerances in fractions of diameter D_1
Deviations of the sections of the trailing and leading blade edges from the template:	
a) in shape	0.0007
b) in thickness of the trailing edges	—0.001
c) in thickness of the leading edges	+ 0.002
Deviation of the trailing-edge line from the surface enveloping trailing edges	0.0015
Deviation of the surface enveloping the trailing edges from the vertical surface specified in the drawing	± 0.002
Variation in the opening between the trailing edge and the convex surface of the neighboring blade:	
a) arithmetical mean for all the blades at all points specified for measuring in the drawing	± 0.0005
b) between any two adjacent blades	± 0.0015
Variation in the pitch of the adjacent blades between:	
a) the trailing edges at the upper band	± 0.002
b) the leading edges at the upper band and the trailing edges at the lower band	± 0.003
Tolerance for blade thickness:	
a) arithmetical mean for all the blades	± 0.002
b) any particular blade	± 0.003
Deviation of the generatrix of the conical upper-band surface from a straight line	0.003

The mold for casting a Francis runner is shown schematically in Figure VII. 5. It is usually prepared in a special box (1) with a removable flask (2) on top. The molding of the runner is effected by means of a core box for the water passages. The blade (3) is obtained by means of cores (4) and (5), the molten metal filling the free space between them.

Special reinforcement is provided within the cores to strengthen them, as well as vents for gas removal.

Because of the large metal concentrations in the hub and band, gates (6) and risers (7) should be provided to obtain high-quality castings. Contraction ribs (8) are provided at the sharp transitions between thin and heavy blade sections in order to avoid the appearance of cracks.

It is advisable to cast very large runners in two sections in order to make possible their transportation by rail.

The runner with the largest over-all dimensions ever built in the U.S.S.R. was delivered by the LMZ for the Dnieper-plant turbines. The diameter D_1 = 5.45 m and the weight 92 t.

This huge runner was hauled by rail on two heavy-duty 60 t flat cars, between which a special girder carrying the runner was mounted; only 250 mm clearance remained between the rails and the runner band. The girder was supported at the ends by special spherical supports enabling the runner to remain in a constant position whatever the inclination of the road-bed; these supports were designed to transmit a tractive force of 80 t.

A similar runner, delivered by the Newport News Company of the U. S. A., was cast in three sections, which were joined together by rings at the upper and lower bands.

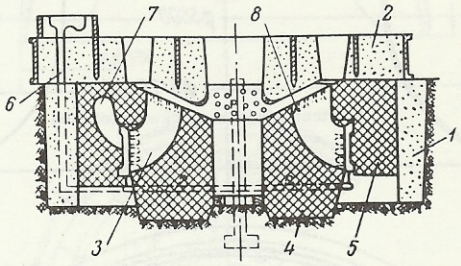


FIGURE VII.5. Mold for casting runner

Figure VII. 6 shows the construction of a runner made in sections, joined into a single structure by means of rings. The component sections are cast and welded. Each runner half consists of the corresponding upper band (1), blades (4), and lower band (6). The band halves are flanged, the flanges being bolted together, and in this case, the bolts (2) are for joining purposes only.

The halves are joined into an integral structure by means of the ring (3), whose cross section is designed to take up the loads from the upper-band sections.

The runner blades are cast separately and arc-welded to the band halves later. The ring (5) is fitted onto the lower band (6) on the site. The runner halves are manufactured in the shop, and then securely fastened together on the site by means of a forged ring, heated and shrunk onto the band.

Composite runners with rings are common all over the world in turbine manufacturing, but they have the disadvantage of being very heavy. For instance, the composite runner with rings delivered by the Newport News Company for the Dnieper-plant turbine was 12 t heavier than the all-cast runner made by LMZ. The composite runner with rings takes much longer to manufacture and erect, while the transportation of large-size units also involves difficulties. The ring surfaces mating with the runner body must be very accurately machined, and even the fitting of the ring onto the runner band represents a complicated operation. Usually, the ring is shrunk onto the band, requiring a special heating installation. If, for transport reasons,

the ring has to be made in halves and welded on the site, the design without rings — with the lower band welded on the site — is more convenient. The cross-sectional areas of the lower band and ring differ very little in size; the technical problems to be surmounted in welding the ring are the same as with the lower band.

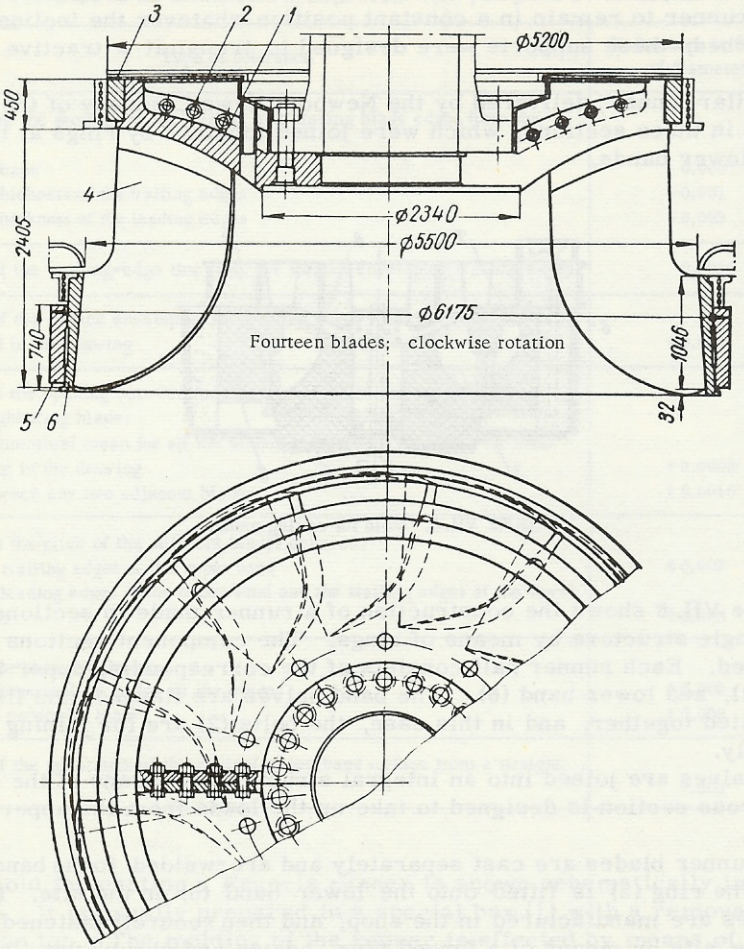


FIGURE VII. 6. Runner made of sections and assembled with rings

Owing to their design and dimensions, the upper-band sections may be fastened by means of bolted flanges. This type of runner design—in sections, with the lower band welded and the upper one bolted — is used at the LMZ for large-capacity turbines.

The schematic drawing of a Francis runner with nominal diameter D_1 = 7.5 m and power output of 500,000 kw (design) is shown in Figure VII. 7.

The runner, of external diameter D = 8260 mm and height h = 4200 mm, consists of four sections. According to the number of blades, the number

of sections may be identical (for sixteen blades) or slightly different (for fourteen to fifteen blades). Each section consists of a quarter of the upper band (1), three or four blades (2), and a quarter of the lower band (3). At the upper band, the sections are joined by means of four bolts (d = 190 mm); at the lower band, the sections are welded. The total runner weight is 250 t, the weight of one blade being 7 t.

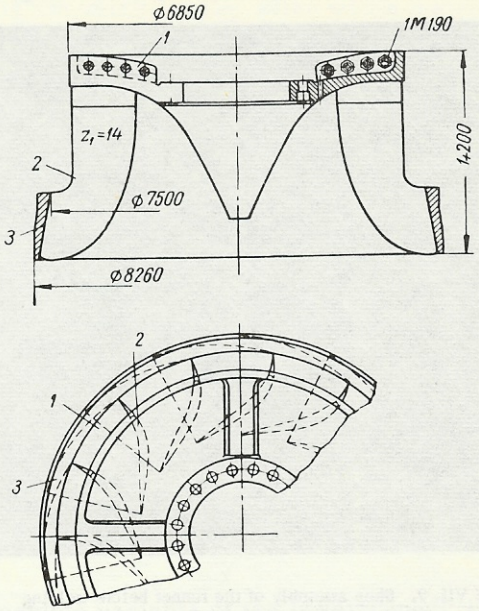


FIGURE VII. 7. Compound turbine runner

The runner is divided into four sections for railroad transportation. Figure VII. 8 shows schematically a special flat car provided with a girder for carrying one section. The runner section weighs 77 t, the girder 37 t, so that the capacity of the flat car should be about 120 t.

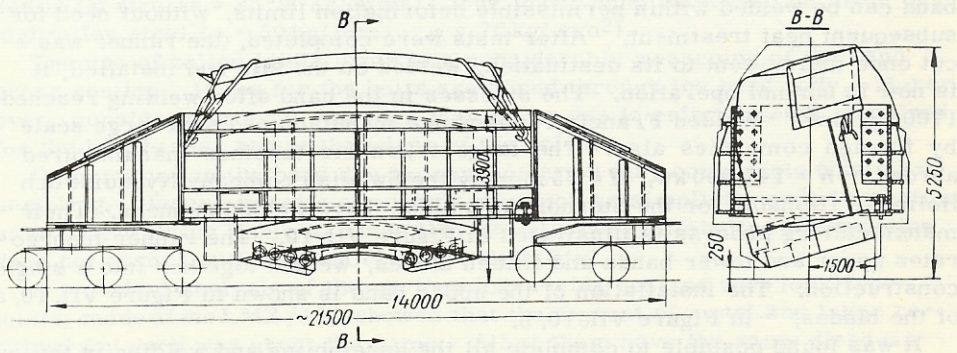


FIGURE VII.8. Schematic diagram of a section of a large turbine runner during its transportation

An examination of the figure clearly shows that even with a clearance of 250 mm between the rails and the lowest extremity of the runner, it is scarcely possible to remain within the fourth class of loading-gage tolerances. The huge runner must be securely fastened. Figure VII. 9 shows a runner of similar construction, with diameter D_1 = 5.5 m, and output N = 226,000 kw, during shop assembly before welding.

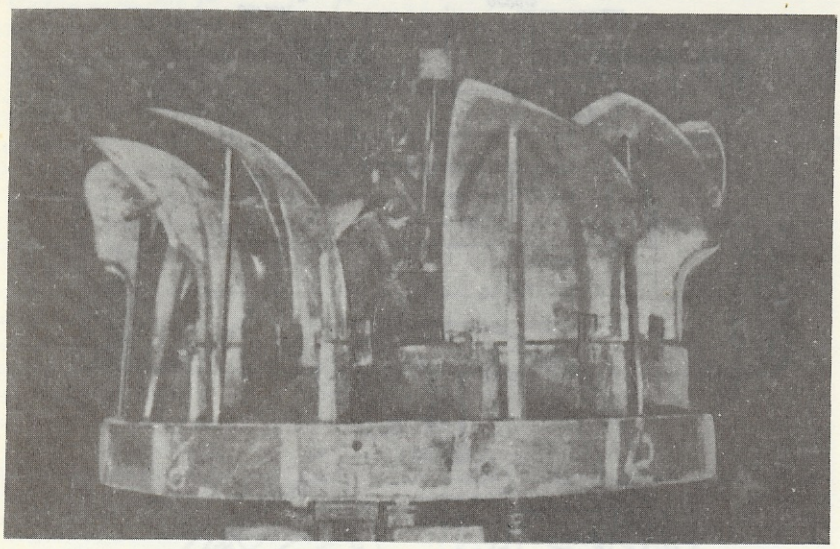


FIGURE VII. 9. Shop assembly of the runner before welding

The manufacture of this runner at the LMZ was preceded by engineering research into the various design variants for fastening the runner parts, and by special tests on a turbine runner of diameter D_1 = 5.45 m developing an output of N = 78,000 kw. The compound runner was made up of two sections, with the lower band welded. Research into the best method of welding the band was carried out under the guidance of Z. M. Gamze.

It was thus found, that with the appropriate manufacturing technique, the band can be welded within permissible deformation limits, without need for subsequent heat treatment. After tests were completed, the runner was cut once more, sent to its destination, welded on the site and installed; it is now in normal operation. The stresses in the band after welding reached 1700 kg/cm^2. Welded Francis runners are manufactured on a large scale by foreign companies also. The largest Francis turbines manufactured abroad — N = 147,000 kw, H = 75 m — by the Swedish company Nydquist och Holm AB (Nohab), for the Stornorrfors plant, have welded runners. Their manufacturing process is illustrated in Figure VII. 10. The runner incorporates upper and lower bands and fifteen blades, welded together into a single construction. The installation of the upper band is shown in Figure VII. 10, a, of the blades, —in Figure VII. 10, b.

It was found possible to complete all the assembling and welding in the shop because the runner was transported by water. The runner is made

of stainless steel, since water flowing at high velocity, especially under high heads, usually contains grit, mostly quartz particles.

Stainless steel withstands cavitation damage and mechanical wear better.

To avoid welding the lower band during installation, it can be fastened by mechanical means — bolts, cylindrical pins, or lock joints. These techniques have been developed by various plants, and their description is given below, although they have not yet been put into practical use.

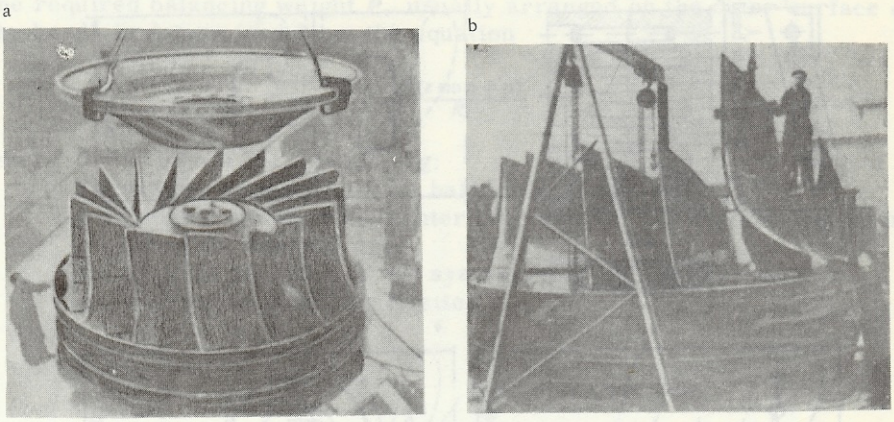


FIGURE VII. 10. Welded runner of the Stornorrfors-plant turbine, N = 130,000 kw, manufactured by the Swedish Nohab Company. Shown during construction.

A number of possible variants of the lower runner-band assembly are shown in Figure VII. 11 (1, 2, 3, and 4). The first version is a bolted band. It was devised for the first time at the KhTZ for a large-size runner of D_1 = 7.2 m and N = 500,000 kw. The height of the lower band H = 1,380 mm, and the thickness $s \cong$ 250 mm. Because the cross section is relatively small, as few as 7 bolts of diameter d = 110 mm suffice. In this case, the maximum stress in each bolt, considering the centrifugal force at runaway speed ($n_r = 1.65\, n_{normal}$) and the negative allowance of fitting, attains 4,000 kg/cm^2. Bolts of high-alloy steel are therefore used (for instance, of 34KhN3M steel (σ_y = 85-90 kg/mm^2). The lower band must also be made of high-alloy steel (σ_y = 50 kg/mm^2; σ_u = 70 kg/mm^2).

The use of bolted joints leads to a considerable weakening of the band cross section. Holes for the bolts are bored through the band body. Moreover, considerable local stresses may occur due to enlargements machined for the bolt heads, and at the edges of the holes.

Deformation in the band due to transportation may complicate final assembling. Hence, in spite of advantages such as simplicity and elimination of on-site welding liable to cause thermal stresses, the bolted construction does not ensure sufficient safety and reliability.

A technical analysis of the various lower-ring designs with lock-type joints, made at the LMZ /10/, showed that the amount of metal and labor required for each was about the same. All of them have the same disadvantages compared with the ring-assembly design. The ring envelops the

whole band around its outer circumference, and by compressing the surface of the joints tightly, gives a smooth shape to the band. The lock-type joint assembly ensures local fastening only. Should the band become deformed through aging, transportation, and storage, which quite often happens, then there is a risk that the lock will not fit in the joint. If the runner is aligned beforehand by means of spacers, additional stresses may occur when the lock is mounted that may cause fracture of the runner.

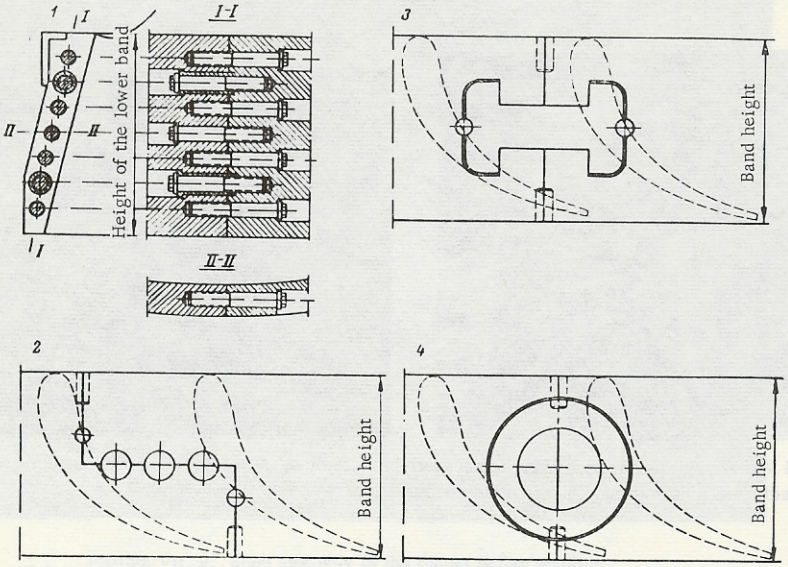


FIGURE VII.11. Mechanical assembling of the lower runner band:

1 — bolted; 2 — with cylindrical pins; 3 — with an I-shaped lock; 4 — with a ring-shaped lock.

A further disadvantage of lock-joint assembly is the difficulty in prestressing the band joints, which lowers the rigidity of the structure and may, as an after-effect, weaken the assembly itself. For all these reasons, lock-joint assembly is not advisable.

I-shaped or ring-shaped locks are mounted in a groove of adequate dimensions cut into the band by milling or turning. The joint should be prestressed by inserting the lock while hot, so that the forces acting in the runner do not cause its failure.

Francis runners should be provided with a location for the balancing weight. The balancing is done after the final machining. Since the runner is of complicated shape and large dimensions, dynamic balancing would seem indicated, but the large size and weight render this practically impossible under shop conditions. Hence, in turbine manufacture, static balancing only is employed. Experience shows that static balancing — if effected with care — proves sufficient for normal turbine operation. The static balancing of Francis and Kaplan runners is carried out on a spherical surface. The arrangement is shown schematically in Figure VII.12. The column

(1) of the balancing stand carries a support (2) with a spherical surface. The runner (3) to be balanced is mounted on the support in such a way that its center of gravity is located some 100 to 200 mm below the center of the sphere, thus achieving a stable equilibrium. Balancing is done in the following order: the runner is moved off-center with respect to the stand center-line. Two spirit levels (4) are set at an angle of 90° on the band surface. The angle of deviation of the system from the vertical is determined by means of the spirit levels, after which the system is brought into the horizontal position by means of the balancing weight P. The value of the required balancing weight P, usually arranged on the outer surface of the band, is determined from the equation

$$P = \frac{G(z \sin \alpha + \mu)}{R} \text{ kg},$$

where G = weight of the system, kg;
R = radius of location of the balancing weight, cm;
z = distance between the center of gravity of the system and the center of the sphere, cm;
α = angle of deviation of the system from the vertical axis;
μ = coefficient of rolling friction.

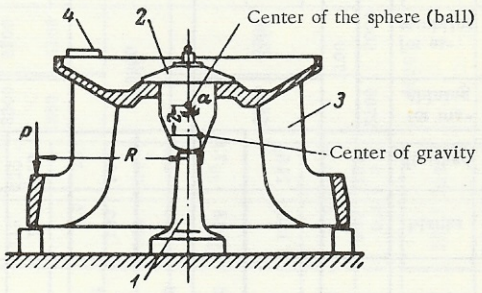


FIGURE VII. 12. Balancing of the Francis runner

The balancing weight is arc-welded to the band, and then covered with a lining. The balancing attains an accuracy such that a moment of 0.2 kgm throws the system off-balance.

The results of a cost-comparison analysis of various designs of Francis runners for a powerful turbine ($N \cong 260{,}000$ kw, $H = 100$ m) with the outer diameter $D = 6.6$ m and height $h = 3.05$ m, are set forth — as an example — in Table VII. 2.

In the table, the following six design variants are considered:

1) integral runner;
2) runner made of two halves with rings on the upper and lower bands;
3) runner made of two halves with ring on the lower band. The upper band is secured with bolts;
4) runner made of two halves with the lower band welded. The upper band is secured with bolts;

TABLE VII.2

Cost-comparison figures of various designs of Francis runners

Type of design	Type of blank	Number of blanks for one runner	Material	Type of blank	Weight, t		Man-hours		Cost, rubles					Other work
									Blanks		Machining (incl. overhead expenses)	Manual labor (incl. overhead expenses)	Total cost including overhead expenses	
					blanks	finished	for machining	for assembling	per ton	of the complete blank				
Integral runner	Integral casting	1	30 L steel	Cast	145	125	2700	5000	600.0	87,000.0	2700.0	5000.0	94,700.0	No other work required
							7700							
Runner made of two halves, with rings on the lower and upper bands	Half the runner	2	30 L steel	Cast	140	115	4300	5200	600.0	84,000.0	4300.0	5200.0	123,500.0	Welding and fitting of two rings on the spot
	Upper ring	1	Alloy steel	Forged	18	7.0			500.0	9,000.0				
	Lower ring	1	Alloy steel	Forged	35	17.0	9500		600.0	21,000.0				
				Total weight	193	139				114,000.0				
Runner made of two halves, with one ring on the lower band. The upper ring is secured with bolts.	Half the runner	2	30 L steel	Cast	142	116	3900	5100	600.0	85,200.0	3900.0	5100.0	116,200.0	Welding, fitting of one ring, and bolting of the upper band on the spot
	Lower ring	1	Alloy steel	Forged	35	17								
	Bolt	10	35 steel	Forged	3.0	2.0	9000		350.0	1,050.0				
				Total weight	180	135				107,250.0				

TABLE VII.2, continued

Type of design	Type of blank	Number of blanks for one runner	Material	Type of blank	Weight, t		Man-hours		Cost, rubles					Other work
					blanks	finished	for machining	for assembling	Blanks		Machining (incl. overhead expenses)	Manual labor (incl. overhead expenses)	Total cost including overhead expenses	
									Per ton	of the complete blank				
Runner made of two halves, with the lower band welded. The upper band is secured with bolts.	Half the runner	2	30 L steel	Cast	146	125	2960	5100	600.0	87,600.0	3000.0	5100.0	96,700.0	Welding of the lower band and bolting of the upper one, on the site
	Bolts	10	35 steel	Forged	3.0	2.0			350.0	1,050.0				
				Total weight	149	127	8060			88,650.0				
Runner made of two halves. The lower band is secured with an I-shaped lock, the upper band with bolts.	Half the runner	2	30 L steel	Cast	146	125	3460	5200	600.0	87,600.0	3500.0	5200.0	98,600.0	Assembling of both bands on the site.
	Lock	2	40 steel	Forged	3.0	2.0			400.0	1,200.0				
	Bolts	10	35 steel	Forged	3.0	2.0			350.0	1,050.0				
	Pins	8	35 steel	Forged	0.3	0.2			350.0	105.0				
				Total weight	152.3	129.2	8660			89,955.0				
Runner made of two halves. The lower band is secured with cylindrical pins, the upper band with bolts.	Half the runner	2	30 L steel	Cast	151	125	3300	5200	600.0	90,600.0	3300.0	5200.0	100,600.0	
	Pins	12	35 steel	Forged	1.5	1.0			350.0	525.0				
	Bolts	10	35 steel	Forged	3.0	2.0			350.0	1,050.0				
				Total weight	155.5	128	8500			92,175.0				

5) runner made of two halves. The lower band is secured with an I-shaped lock. The upper band is secured with bolts;

6) runner made of two halves. The lower band is fastened with cylindric keys. The upper band is assembled with bolts.

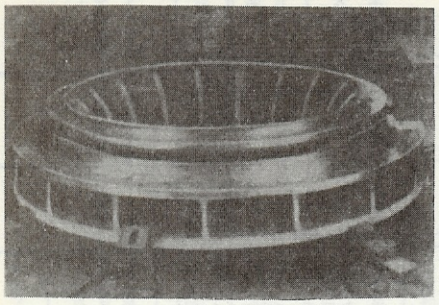


FIGURE VII. 13. Machining of runner for a high-head turbine on a vertical lathe

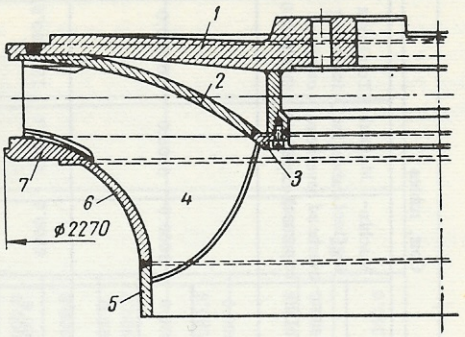


FIGURE VII. 14. Welded high-head runner

The basic material used for runners is ordinary carbon steel grade 30L.

As can be seen from the table, the first design variant — integral runner — is the best; it has the smallest weight, requires the smallest number of man-hours, and costs the least. It is followed by the fourth design, with the lower band welded and the upper one bolted. Compared with the integral runner, the net weight of this version is 2 ton more; it requires another 360 man-hours on machining, and is 2000 rubles more expensive. Runners (2) and (3), with bands, weigh more, require a longer production time and involve a higher cost. Examination of the table shows that the most advantageous solution from the view of cost is the integral runner, while the variant with the welded lower band is second best.

Figure VII. 13 shows a Francis runner, developing N = 50,000 kw under a head of H = 300 m, mounted on a vertical lathe for machining the lower-band outer surface. This runner is characterized by low and rather long blades. The clearance between the blades and runner bands is therefore relatively small, making it difficult to work inside. Recently, however, some manufacturers have started welding this kind of runner.

A runner of welded construction for the high-head turbines of the Loch Sloy [Great Britain] plant — N = 33,500 kw — is shown in Figure VII. 14. It was designed so that most of the welding could be done from the outside.

The carbon-steel upper runner band (1) is welded along the circumference by means of a cylindrical part to the turbine water passages. The two-ply steel blades (4) are welded together by means of the annular segments (3), (5), and (7). The segments (2) and (6), welded to the blades, make up the lower and upper surfaces of the runner water-passages.

43. AXIAL WATER PRESSURE

The water stream flowing through the runner and partially leaking through the clearances at the upper and lower bands exerts an axial pressure on the runner. The magnitude of the force depending on the head, runner dimensions and type, and on the design of the runner and its seals.

Specific speed	Runner type	Coefficient, k
280	RO-123	0.34-0.41
235	RO-211	0.28-0.34
200	RO-82	0.22-0.28
190	RO-638	0.20-0.26
100	RO-533	0.08-0.14
90	RO-246	0.07-0.12

When designing the hydro unit shaft and the thrust bearing, the magnitude of the axial force must be determined.

The approximate value of the axial water-pressure force on a Francis runner, of a standard series of the LMZ, may be determined from the empirical formula

$$P_{ax} = k\frac{\pi}{4} D_1^2 H_{max} \text{ t}, \qquad \text{(VII. 1)}$$

where k = coefficient, depending on the runner type.

The values shown in the above table are used by the LMZ for standard runners. The lower values of k should be taken for larger turbines.

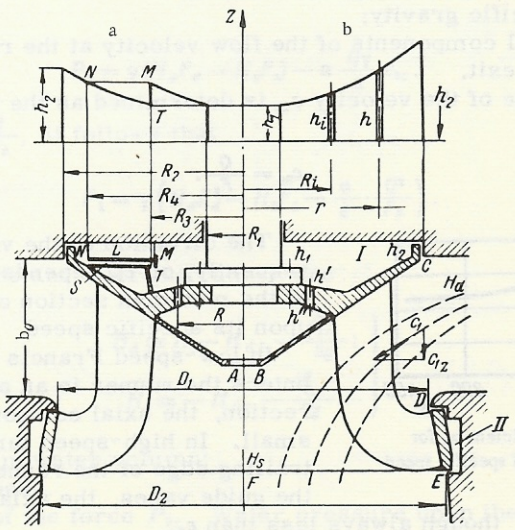


FIGURE VII. 15. Axial pressure distribution on the runner

When computing the axial pressure by empirical formulas, the design of the runner and its seals is ignored. Exact formulas for the axial pressure, however, take all the factors into consideration. The axial pressure acting on the Francis runner is determined at LMZ in the following way:

The total axial load is made up of the following components:

$$P_{ax} = P_1 + P_2 + P_3 - P_4, \qquad \text{(VII. 2)}$$

where P_1 = force due to the action of the water flow on the inner part of the runner;
P_2 = force due to water pressure on the upper band;
P_3 = force due to water pressure on the lower band;
P_4 = force due to the displacement of the runner (according to Archimedian principle).

Determination of the force P_1. To determine the force P_1, resulting from the action of the water flow upon the inner cavity of the runner, the equation of momentum is used (Figure VII. 15).

According to the theorem of momentum, the instantaneous variation of the momentum of the mass of liquid ABCDEF (for steady motion) in any direction equals the projection on the said direction of all the forces acting on the given mass of liquid.

The equation of the momentum for the projection on the z axis will be

$$\frac{Q\gamma}{g} c_{2z} - \frac{Q\gamma}{d} c_{1z} = -P_1 + P_d - P_s, \qquad \text{(VII. 3)}$$

where P_1 = axial component of the runner force acting upon the mass of liquid, of opposite sign to the force to be calculated;
P_d = axial component of the pressure force on the lateral surface having generatrix CD;
P_s = pressure force upon the surface of a circle of radius EF;
Q = discharge through the turbine;
γ = specific gravity;
c_{1z} and c_{2z} = axial components of the flow velocity at the runner entrance and exit.

The magnitude of the velocity c_{2z} is determined as the mean value over the section

$$c_{2z} = \frac{Q}{F_s}. \qquad \text{(VII. 4)}$$

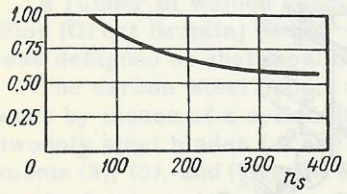


FIGURE VII. 16. Coefficient α, for runners, as a function of specific speed

The direction of the velocity c_1 and consequently, of c_{1z} depends upon the geometry of the meridian section of the runner, i.e., upon its specific speed.

In low-speed Francis turbines, the flow enters the runner in an almost radial direction, the axial component c_{1z} thus being small. In high-speed turbines, where the trailing edge of the runner blade is far from the guide vanes, the axial component c_{1z} will be considerable, though always less than c_{2z}.

Let us denote

$$c_{2z} - c_{1z} = \alpha c_{2z}, \qquad \text{(VII. 5)}$$

where α = a coefficient, less than unity, determined experimentally for each type of runner.

When $c_{1z} = 0$, $\alpha = 1$; for $c_{1z} \neq 0$, $\alpha < 1$. Then the equation (VII. 3) becomes

$$\frac{\alpha Q \gamma}{g} c_{2z} = -P_1 + P_d - P_s,$$

whence,

$$P_1 = P_d - P_s - \frac{\alpha Q \gamma}{g} c_{2z}. \qquad \text{(VII. 6)}$$

In laboratory tests, the axial load acting on the runner model is measured by weighing. H_d and H_s — the pressures before and after the runner (in m W. G.) — are also measured.

Then, the magnitudes of P_2, P_3 and P_4 are determined. With the values obtained, and P_{ax} measured, the coefficient α is found.

On the basis of LMZ experimental data, A. Yu. Kolton recommends for the coefficient α the approximate values given in Figure VII. 16 shown as a function of specific speed.

The values of P_d and P_s are

$$\left.\begin{aligned} P_d &= \gamma H_d F_d; \\ P_s &= \gamma H_s F_s, \end{aligned}\right\} \qquad \text{(VII. 7)}$$

where F_d = area of the projection of the lateral surface CD;

F_s = area of the circle of radius EF.

Consequently, the axial component of the stream flow acting on the runner is

$$P_1 = \gamma (H_d F_d - H_s F_s) - \alpha \frac{Q\gamma}{g} c_{2z}.$$

But, since $c_{2z} = \frac{Q}{F_s}$, it follows that

$$P_1 = \gamma \left(H_d F_d - H_s F_s - \frac{\alpha}{g} \cdot \frac{Q^2}{F_s} \right). \qquad \text{(VII. 8)}$$

The heads before and after the runner are

$$\left.\begin{aligned} H_d &\cong H - H_{dr} - \frac{c_{1m}^2}{2g}; \\ H_s &\cong - H_{dr} - \frac{c_{2m}^2}{2g}, \end{aligned}\right\} \qquad \text{(VII. 9)}$$

where H = head, m water column;

H_{dr} = draft head.

Determination of the force P_2. Water pressure upon the upper and lower bands depends upon the design of the seals and the pressure-relief arrangements provided on the bands. Because of the runner rotation, the water

where h_1 = head at the inner diameter of the runner band (at the shaft) m;
h_2 = pressure at the outer diameter, m.

The values h_1 and h_2 are determined allowing for the head losses in the band seals and pressure-relief openings provided in the upper-band flange at the radius R, (see Figure VII. 15).

The water leakages through the upper-band seal (at the radius R_2) and the pressure-relief openings, and further on, through the runner hub extension, are

$$q = \mu_1 F_{seal}\sqrt{2gh_{seal}} = \mu_2 F_{op}\sqrt{2gh_{op}} = \mu_3 F_{rc}\sqrt{2gh_{rc}}, \qquad \text{(VII. 17)}$$

where μ_1; μ_2; μ_3 = discharge coefficients;
F_{seal}; F_{op}; F_{rc} = respective cross-sectional areas which determine the discharge across the seals, pressure-relief openings and hub extension clearance;
h_{seal}; h_{op}; h_{rc} = respective head losses in the seal passage, relief openings, and hub-extension opening.

The head losses are

$$\left.\begin{aligned} h_{seal} &= H_d - h_2; \\ h_{op} &= h' - h''; \\ h_{rc} &= h'' - H_s, \end{aligned}\right\} \qquad \text{(VII. 18)}$$

where h_2 = pressure at the outer diameter of the runner band;
h' = pressure before the relief opening;
h'' = pressure after the relief opening.

By taking $\mu_1 = \mu_2 = \mu_3$, we obtain from equation (VII. 17)

$$F_{seal}^2 h_{seal} = F_{op}^2 h_{op} = F_{rc}^2 h_{rc},$$

hence,

$$\left.\begin{aligned} \frac{h_{seal}}{h_{op}} &= \left(\frac{F_{op}}{F_{seal}}\right)^2 = m_1; \\ \frac{h_{op}}{h_{rc}} &= \left(\frac{F_{rc}}{F_{op}}\right)^2 = m_2. \end{aligned}\right\} \qquad \text{(VII. 19)}$$

According to equation (VII. 11), we have

$$h_2 = h' + \frac{\omega_1^2}{2g}\left(R_2^2 - R^2\right) = h' + \Delta h_4. \qquad \text{(VII. 20)}$$

By combining equations (VII. 18), (VII. 19), and (VII. 20), we obtain

$$h' = \frac{m_1 m_2}{1 + m_2 + m_1 m_2} H_s + \frac{1 + m_2}{1 + m_2 + m_1 m_2} H_d - \frac{1 + m_2}{1 + m_2 + m_1 m_2} \Delta h_4;$$

denoting

$$\frac{m_1 m_2}{1 + m_2 + m_1 m_2} = k_1;$$

$$\frac{1 + m_2}{1 + m_2 + m_1 m_2} = k_2,$$

where h_1 = head at the inner diameter of the runner band (at the shaft) m;
h_2 = pressure at the outer diameter, m.

The values h_1 and h_2 are determined allowing for the head losses in the band seals and pressure-relief openings provided in the upper-band flange at the radius R, (see Figure VII. 15).

The water leakages through the upper-band seal (at the radius R_2) and the pressure-relief openings, and further on, through the runner hub extension, are

$$q = \mu_1 F_{seal}\sqrt{2gh_{seal}} = \mu_2 F_{op}\sqrt{2gh_{op}} = \mu_3 F_{rc}\sqrt{2gh_{rc}}, \qquad \text{(VII. 17)}$$

where μ_1; μ_2; μ_3 = discharge coefficients;
F_{seal}; F_{op}; F_{rc} = respective cross-sectional areas which determine the discharge across the seals, pressure-relief openings and hub extension clearance;
h_{seal}; h_{op}; h_{rc} = respective head losses in the seal passage, relief openings, and hub-extension opening.

The head losses are

$$\left.\begin{aligned} h_{seal} &= H_d - h_2; \\ h_{op} &= h' - h''; \\ h_{rc} &= h'' - H_s, \end{aligned}\right\} \qquad \text{(VII. 18)}$$

where h_2 = pressure at the outer diameter of the runner band;
h' = pressure before the relief opening;
h'' = pressure after the relief opening.

By taking $\mu_1 = \mu_2 = \mu_3$, we obtain from equation (VII. 17)

$$F_{seal}^2 h_{seal} = F_{op}^2 h_{op} = F_{rc}^2 h_{rc},$$

hence,

$$\left.\begin{aligned} \frac{h_{seal}}{h_{op}} &= \left(\frac{F_{op}}{F_{seal}}\right)^2 = m_1; \\ \frac{h_{op}}{h_{rc}} &= \left(\frac{F_{rc}}{F_{op}}\right)^2 = m_2. \end{aligned}\right\} \qquad \text{(VII. 19)}$$

According to equation (VII. 11), we have

$$h_2 = h' + \frac{\omega_1^2}{2g}\left(R_2^2 - R^2\right) = h' + \Delta h_4. \qquad \text{(VII. 20)}$$

By combining equations (VII. 18), (VII. 19), and (VII. 20), we obtain

$$h' = \frac{m_1 m_2}{1 + m_2 + m_1 m_2} H_s + \frac{1 + m_2}{1 + m_2 + m_1 m_2} H_d - \frac{1 + m_2}{1 + m_2 + m_1 m_2} \Delta h_4;$$

denoting

$$\frac{m_1 m_2}{1 + m_2 + m_1 m_2} = k_1;$$

$$\frac{1 + m_2}{1 + m_2 + m_1 m_2} = k_2,$$

we obtain the expression for determining the pressure before the relief opening.

$$h' = k_1 H_s + k_2 H_d - k_2 \Delta h_4. \qquad \text{(VII. 21)}$$

With h' known, h_1 may be determined from equation (VII. 11)

$$h_1 = h' + \frac{\omega_1^2}{2g}\left(R_1^2 - R^2\right)$$

and h_2 can be subsequently determined.

Determination of pressure P_3. The pressure P_3 upon the lower band is taken as the sum of three components: water pressure on the upper side, on the lower side, and on the lateral surface of the lower band.

The entire head H_d usually acts on the upper side.

The lateral surface and the lower side are subject to the head H_s, since the clearance at point E is usually large and not provided with a seal.

The shape of the lower runner band differs with the specific speed (Figure VII. 1); the pressure upon it may be directed downward or upward.

Determination of force P_4. The force due to the displacement of the runner is determined according to the Archimedian principle:

$$P_4 = -\gamma V, \qquad \text{(VII. 22)}$$

where V = volume of the runner.

A special part — the deflector — (Figure VII. 15, a) is sometimes provided on the upper band to lower the water pressure. It consists of a casing fastened to the upper band. Its upper part is a flat ring of large width upon which another flat disk L of the same dimensions is fixed to the cover-plate ribs. The space created between these rings has a free exit to the periphery. Owing to the collar M on the inner diameter, there is a narrow clearance T between the stationary and rotating rings.

When the runner rotates, the water present in the space between the rings is carried away by the rotating disk S and thrown by centrifugal force to the periphery at point N. It flows further between the fixed disk L and the turbine cover-plate into the central cavity above the runner, whence it falls through the relief opening into the runner hub extension.

An equal amount of water flows in through the inner clearance T, in place of the water expelled by centrifugal force. However, since the clearance is small and the water passes through it with difficulty, the pressure in the space between the disks is lowered.

As shown by the pressure diagram in Figure VII. 15, the pressure rise from M to N is equal to the clearance losses in the seal, this being the pressure drop between M and T. The diagram is stepped and has a smaller area than similar diagrams plotted for a runner without deflector (Figure VII. 15, b).

Consequently, the total force upon the upper band is lowered, this reduction being proportional to the difference between the water pressures and to the area of the rotating ring of the deflector. The larger the relative area of the disk, the smaller the clearance, and consequently the greater — for a given rotational speed — the effect.

The Francis runner is subject to the action of both centrifugal and hydraulic forces. In high-output turbines, these forces reach high values and induce considerable stresses in the runner parts.

In designing high-output Francis runners, an exact method of calculation is used nowadays. This method will be described later.

At the same time, an approximate method is used for preliminary studies..

According to this method, the stresses caused by the centrifugal forces at the radial sections of the outer and inner bands are determined; this calculation includes only the stresses produced in the bands by the centrifugal forces and that of the blades due to their own mass.

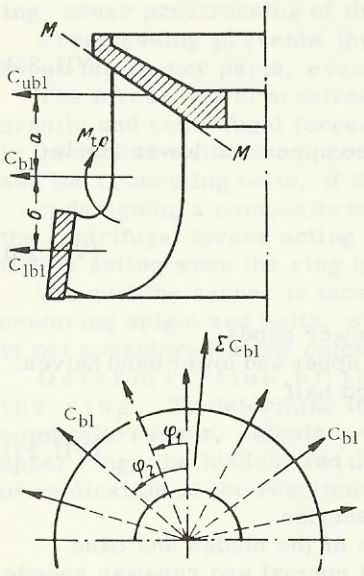


FIGURE VII.17. Centrifugal forces acting upon the runner

The centrifugal forces due to the mass of the blades, acting upon the bands, are considered as inversely proportional to the distance between the centers of gravity of the blades and of the bands. These centrifugal forces are calculated as for a beam supported at both ends, without considering the way the blades are fixed into the band.

The approximate calculation of one-piece and composite runners, with a detailed description of the calculation method and an illustrative example which also includes the determination of the centrifugal forces due to the other runner parts, is given by L. G. Smolyarov in /24/; only the general order of procedure is described below.

Integral runner. For calculation, we assume that the runner, consisting of upper and lower bands and blades, is subject to the action of a system of forces as shown in Figure VII. 17. The centrifugal forces of the blades c_{bl} are taken up by the lower and upper bands, and their moment by the upper band at the section M—M.

The order of calculation is as follows:

1. Determine the centrifugal forces of each blade

$$c_{bl} = \frac{G_{bl}}{g}\omega^2 R_{Cbl}$$

where G_{bl} = blade weight;
ω = angular velocity at normal and runaway speeds;
R_{Cbl} = radius of location of the blade center of gravity.

In calculating the centrifugal force, the blade should be divided into a series of sections, normal to the runner axis, at small height intervals Δh. The area F of each section is determined, and then the elementary volume $F\Delta h$, the center of gravity of this volume, and the elementary centrifugal

force $\Delta c = \frac{F\Delta h\gamma}{g} r\omega^2$. By integrating along the blade length, we find the total centrifugal force.

2. Determine the resultant centrifugal force of the blades acting upon half the runner at normal and runaway speeds

$$\Sigma c_{bl} = c_{bl} + 2c \cos \varphi_1 + 2c_{bl} \cos \varphi_2 + \ldots = c_{bl}(1 + 2\cos\varphi_1 + 2\cos\varphi_2 + \ldots). \quad \text{(VII. 24)}$$

3. Assume that the centrifugal force due to the blades Σc_{bl} is transmitted to the lower and upper bands in inverse proportion to the distances b, a between the application point of the force and the lower and upper bands, respectively.

$$\left.\begin{aligned} c_{ubl} &= \Sigma c_{bl} \frac{b}{a+b}; \\ c_{lbl} &= \Sigma c_{bl} \frac{a}{a+b}. \end{aligned}\right\} \quad \text{(VII. 25)}$$

4. Calculate the centrifugal forces of half the upper and lower bands

$$\left.\begin{aligned} c_{ub} &= \frac{1}{2} \cdot \frac{G_{ub}}{g} \omega^2 R_{ub}; \\ c_{lb} &= \frac{1}{2} \cdot \frac{G_{lb}}{g} \omega^2 R_{lb}, \end{aligned}\right\} \quad \text{(VII. 26)}$$

where G_{ub}, G_{lb} = weights of half the upper and lower bands;
R_{ub}, R_{lb} = radii of centers of gravity of the upper and lower band halves.

The radius of the center of gravity of the band half

$$R_{ub,\,lb} = \frac{2}{\pi} R_{u,\,l}, \quad \text{(VII. 27)}$$

where $R_{u,l}$ = radius of the centroid of the band section.

5. Determine the resultant centrifugal force of the blades and band halves acting upon the upper and lower bands at normal and runaway speeds

$$\left.\begin{aligned} c_u &= c_{ubl} + c_{ub}; \quad c_{ur} = c_{ublr} + c_{ubr}; \\ c_l &= c_{lbl} + c_{lb}; \quad c_{lr} = c_{lblr} + c_{lbr}. \end{aligned}\right\} \quad \text{(VII. 28)}$$

6. Determine the stresses in the upper and lower bands at normal and runaway speeds

$$\left.\begin{aligned} \sigma_u &= \frac{c_u}{2F_u}; \quad \sigma_{ur} = \frac{c_{ur}}{2F_{ur}}; \\ \sigma_l &= \frac{c_l}{2F_l}; \quad \sigma_{lr} = \frac{c_{lr}}{2F_{lr}}, \end{aligned}\right\} \quad \text{(VII. 29)}$$

where F_u and F_l = areas of the respective band sections.

7. Determine the stresses caused by the moment. These will be the greatest at the section M-M — at the transition between the blades and the upper band. The stresses should be calculated from a formula determined by laboratory tests, which were carried out on a similar runner model until failure by torsion was reached

$$\sigma = \sigma' \left(\frac{D_{lm}}{D_{lp}}\right)^3 \frac{N_{max}}{M_t \omega}, \quad \text{(VII. 30)}$$

where D_{lm} = diameter of the runner model;
D_{lp} = diameter of the full-scale runner;
M_t = torque causing the model failure;
σ' = breaking stress in the model corresponding to M_t;
N_{max} = maximum turbine output;
ω = angular turbine velocity.

The usual methods for determining the areas, static moments, and coordinates of the centroids of plane figures are to be employed in determining the center of gravity and weight of the blade. Data obtained by direct measurements on the runner model are sometimes used.

Compound runner. The manner in which the runner is assembled should be considered. The rings are hot-pressed onto the runner and, after cooling, cause prestressing of the runner parts.

Prestressing prevents the occurrence of clearances in the joints between the runner parts, even when the runner rotates at runaway speed.

The forces due to prestressing should therefore be added to the hydraulic and centrifugal forces acting on the runner. The centrifugal forces in the blades and in the upper and lower band parts tend to stretch the rings and the connecting bolts, if such are used.

In designing a composite runner, it is therefore necessary to determine the centrifugal forces acting upon the parts of the runner, as well as the forces acting when the ring is fitted on it.

The turbine runner is mounted on the flanges of the shaft by means of a centering spigot and bolts, which take over part of the load. This, however is not considered in the calculation.

Determination of the centrifugal forces acting upon the ring. To determine the resultant centrifugal force of one part of the composite runner, calculate the centrifugal forces of its components: the upper ring, the blades, and the lower ring. Then find the height z of the point of application of the resultant of all centrifugal forces

$$z = \frac{\sum c_i z_i}{\sum c_i}, \qquad \text{(VII. 31)}$$

where c_i = centrifugal forces;
z_i = distance between the plane of reference and the line of action of the i-th centrifugal force;
$\sum c_i$ = resultant centrifugal force inducing tension in the rings and bolts.

The distance between the plane of reference and the centroid of the band cross section is

$$y = \frac{\sum F_i y_i}{\sum F_i}, \qquad \text{(VII. 32)}$$

where F_i = cross-sectional area of the individual rings and bolted joints;
y_i = distance between the plane of reference and the centroid of the given partial area.

Usually, the point of application of the resultant centrifugal force and the centroid of the section do not coincide, i.e.,

$$z \neq y.$$

We have, therefore, a case of eccentric loading, where both tension and bending take place

$$\sigma = \sigma_z + \sigma_b. \tag{VII. 33}$$

The stresses are

$$\sigma_z = \frac{\Sigma c}{\Sigma F};$$

$$\sigma_b = \frac{M}{W} = \frac{\Sigma c\,(z - y_0)\,h}{J}, \tag{VII. 34}$$

where ΣF = total cross-sectional area of the rings and bolts;
J = moment of inertia of the rings and bolts;
h = maximum height of section above neutral axis.

With the stresses known, determine the forces acting upon the ring and bolted joint, if any.

The force on the upper ring is

$$P_{ur} = \frac{\Sigma c}{\Sigma F} 2F_{ur}, \tag{VII. 35}$$

where F_{ur} = cross-sectional area of the upper ring.

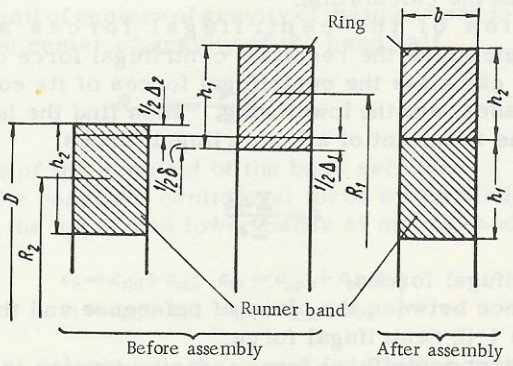


FIGURE VII. 18. Schematic diagram for designing the ring

The additional loading of the upper ring due to the eccentric application of the centrifugal force is

$$P_{ur_1} = \frac{\Sigma c\,(z - y)\,h}{J} 2F_{ur}. \tag{VII. 36}$$

The stresses in the upper ring may be compressive or tensile, according to the relative position of the application point of the resultant force and the center of gravity of the whole system. If the point of application of the resultant centrifugal force is located farther from the upper ring than the center of gravity, compressive stresses occur in the upper ring and tensile stresses in the lower.

For the lower ring, the loads are determined in a similar way. Knowing the forces acting upon the rings, and computing the centrifugal forces in the rings at normal and runaway speeds, one may then calculate their strength.

Design of the runner ring. For tight assembly, the inner diameter of the ring should be smaller than the corresponding outer diameter of the runner band by the value δ (see Figure VII. 18).

After assembly, tensile stresses occur in the ring, and compressive stresses in the runner band. When the runner is rotating, the centrifugal force augments the tensile stresses in the ring and reduces the compressive stresses in the band.

For the Francis runner considered here, the thickness h is small compared with the radius R; hence we may use the formula for the determination of stresses in thin vessels.

Tensile stresses in the ring are

$$\sigma_{z_I} = \frac{(p + c_r) R_1}{h_1}. \qquad \text{(VII. 37)}$$

Compressive stresses in the runner band

$$\sigma_{z_{II}} = \frac{(p - c_b) R_2}{h_2}. \qquad \text{(VII. 38)}$$

Ring deformation

$$\Delta_1 = \frac{2(p + c_r) R_1^2}{E_1 h_1}. \qquad \text{(VII. 39)}$$

Runner-band deformation

$$\Delta_2 = \frac{2(p - c_b) R_2^2}{E_2 h_2}, \qquad \text{(VII. 40)}$$

where p = pressure between ring and band caused by the prestressing;
c_r = centrifugal force per unit ring-surface;
c_b = centrifugal force per unit runner-band surface;
E_1 and E_2 = moduli of elasticity of the ring and runner band materials;
R_1 and R_2 = average radii of the ring and runner band sections;
h_1 and h_2 = thicknesses of the ring and band sections.

The total deformation is

$$\delta = \Delta_1 + \Delta_2 = \frac{2(p + c_r) R_1^2}{E_1 h_1} + \frac{2(p - c_b) R_2^2}{E_2 h_2} =$$

$$= 2p\left(\frac{R_1^2}{E_1 h_1} + \frac{R_2^2}{E_2 h_2}\right) + \frac{2c_r R_1^2}{E_1 h_1} - \frac{2c_b R_2^2}{E_2 h_2},$$

which becomes, after rearranging,

$$p = \frac{\frac{1}{2}\delta E_1 h_1 - c_r R_1^2}{R_1^2 + R_2^2 \frac{E_1 h_1}{E_2 h_2}} + \frac{c_b R_2^2}{R_2^2 + R_1^2 \frac{E_2 h_2}{E_1 h_1}}. \qquad \text{(VII. 41)}$$

By inserting the value (VII. 41) in equations (VII. 37) and (VII. 38), we obtain:

$$\sigma_{z1} = \frac{\delta E_1}{2R_1\left(1+\frac{R_2^2}{R_1^2}\cdot\frac{E_1h_1}{E_2h_2}\right)} + \frac{c_r R_1 \frac{R_2^2}{R_1^2}\cdot\frac{E_1h_1}{E_2h_2}}{h_1\left(1+\frac{R_2^2}{R_1^2}\cdot\frac{E_1h_1}{E_2h_2}\right)} + \frac{c_b R_1}{h_1\left(1+\frac{R_1^2}{R_2^2}\cdot\frac{E_2h_2}{E_1h_1}\right)}; \quad \text{(VII. 42)}$$

$$\sigma_{z2} = \frac{\delta E_1 h_1 R_2}{2h_2R_1^2\left(1+\frac{R_2^2}{R_1^2}\cdot\frac{E_1h_1}{E_2h_2}\right)} - \frac{c_r R_2}{h_2\left(1+\frac{R_2^2}{R_1^2}\cdot\frac{E_1h_1}{E_2h_2}\right)} - \frac{c_b R_2 \frac{R_1^2}{R_2^2}\cdot\frac{E_2h_2}{E_1h_1}}{h_2\left(1+\frac{R_1^2}{R_2^2}\cdot\frac{E_2h_2}{E_1h_1}\right)}. \quad \text{(VII. 43)}$$

Knowing the dimensions of the ring and band, we calculate the centrifugal force per unit of surface, and determine the stresses in ring and band for any prestressing.

In order to prevent changes in the assembly when the speed varies, prestressing must be maintained under all operating conditions, i.e., the band should always be under compressive stresses. It follows from the equation (VII. 43) that the band is always subject to compression, i.e., $\sigma_{z2} > 0$, if

$$\delta > \frac{2R_1^2}{E_1h_1}\left(c_r + c_b\frac{R_1^2}{R_2^2}\cdot\frac{E_2h_2}{E_1h_1}\right). \quad \text{(VII. 44)}$$

The centrifugal forces in the ring, considered as of constant section, are determined as follows:

The elementary centrifugal force

$$\Delta c_r = \Delta m R_1 \omega^2,$$

where $\Delta m = \frac{h_1 dF\gamma}{g}$ = element of the ring mass;

ω = angular velocity.

The centrifugal force acting per unit ring surface

$$c_r = \frac{\gamma}{g} h_1 R_1 \omega^2. \quad \text{(VII. 45)}$$

The centrifugal force acting per unit band surface is calculated by dividing the centrifugal force P_r by the projection of the band surface

$$c_b = \frac{P_r}{Db}, \quad \text{(VII. 46)}$$

where P_r = resultant centrifugal force acting on the band as given by expression (VII. 35);

D = outer band diameter;

b = band height.

Determination of the heating temperature of the ring. The ring must be heated so that it can be pressed onto the band.

It is usually heated to the temperature required for the inner diameter to become larger than the outer diameter of the band.

If R is the radius of the centroid of the ring section at ambient temperature, then $R + \frac{\delta_1}{2}$ is the radius of the centroid after a temperature rise of $\Delta t°$ C.

The developed length of the heated ring

$$L_1 = 2\pi\left(R + \frac{\delta_1}{2}\right). \qquad \text{(VII. 47)}$$

On the other hand, if α is the coefficient of linear expansion of steel,

$$L_1 = 2\pi R\,(1 + \alpha\Delta t). \qquad \text{(VII. 48)}$$

Consequently, by combining equations (VII. 47) and (VII. 48), we obtain

$$\Delta t = \frac{\delta_1}{2R\alpha}, \qquad \text{(VII. 49)}$$

but,

$$\Delta t = t_2 - t_1, \qquad \text{(VII. 50)}$$

where t_2 = temperature of the heated ring;
t_1 = ambient temperature;
δ_1 = value by which the ring diameter is to be increased, usually $\delta_1 \cong 1.5\delta$;
δ = value of the calculated prestressing.

From (VII. 49) and (VII. 50) we obtain

$$t_2 = \frac{\delta_1}{2R\alpha} + t_1 = \frac{0.75\delta}{R\alpha} + t_1. \qquad \text{(VII. 51)}$$

45. EXACT STRENGTH CALCULATION OF MEDIUM-HEAD RUNNERS

As shown in the foregoing paragraph, the approximate method has two significant disadvantages:

1. It does not enable us to determine the stresses in the runner blades.
2. It does not permit sufficient accuracy in the design of bands and rings, since the loads on the bands due to the blades are known only approximately.

Thus, the approximate method may be used only for preliminary calculation.

A. Ya. Aronson /2, 3/, at LMZ, developed an exact method for calculating the stresses in the runners of large turbines.

This method is based on the assumption that the runner is equivalent to a system of bars, the blades being considered as twisted curved bars of varying cross section. At one end the bars are assumed to be rigidly fixed to the inner band, at the other end they join the outer band. This schematic approach does not seem to be fully justified. Actually, the blades are complicated surfaces, so that it is not always permissible to simulate them by bars. It was established experimentally that, with the geometrical correlations characteristic of medium-head runners, the stress component

in the direction of the bar axis considerably exceeds the stress component in the direction perpendicular to the axis. Thus, the stresses in the bar are unidirectional, i,e., the bar may be considered as a thin tube. When a thin tube is twisted, the sections do not remain plane, but warp; because of the unequal warping, the torsion near the fixed end is impeded, and additional bending stresses occur. The calculations show, however, that these additional stresses are confined to a narrow region near the fixed end and vanish quickly further along the tube. It is thus possible to simplify the problem again, i.e., to use — with satisfactory accuracy — the theory of slender bars for the determination of the stresses in the runner.

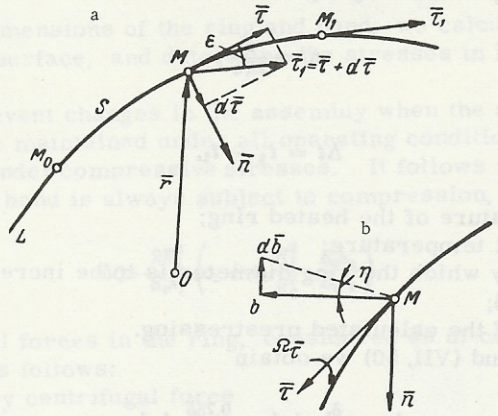


FIGURE VII. 19. Geometry of curved lines

This theory allows us to calculate the stresses in the bars and determine the stresses in the bands and rings with greater accuracy.

A comparison between the results of calculation and of model and field tests shows that the errors are small, i.e., the approximations are permissible.

For a better understanding of the methods for the design of runners, the basic principles of the theory of slender bars /2, 59/ are now given in brief.

Basic principles of the theory of slender bars. The position of a point M on the curve L (Figure VII. 19) may be determined either by the arc S with the point M_0 taken as a reference, or by the radius vector $\bar{r}$ with respect to any point O taken as a pole.

The expression of the unit vector $\bar{\tau}$, tangent to the curve at point M is

$$\bar{\tau} = \frac{d\bar{r}}{dS}. \qquad \text{(VII. 52)}$$

The vector $\bar{\tau}$ and that adjacent to it $\bar{\tau}_1 = \bar{\tau} + d\bar{\tau}$ determine a certain plane. The vector $d\bar{\tau}$ also lies in the same plane, and, being the increment of a unit vector, is perpendicular to the latter. Consequently,

the vector $d\bar{\tau}$ is parallel to, and oriented in the same direction as, the unit vector $\bar{n}$ of the principal normal to the curve. The unit vector of the binormal is determined as a vector product

$$\bar{b} = \bar{\tau}_1 \times \bar{n} . \qquad \text{(VII. 53)}$$

The three vectors $\bar{\tau}$, $\bar{n}$, $\bar{b}$ determine the natural trihedron of the curve at point M (a trihedron is a system of three unit vectors mutually perpendicular and drawn from the same point).

If the point M moves along the curve with unit velocity, i.e., $\frac{dS}{dt} = 1$, then $dS = dt$, and consequently, one may replace differentiation with respect to S by differentiation with respect to t. When the point M moves, the axes of the natural trihedron, though remaining mutually perpendicular, rotate.

Let us determine the vector Ω of the angular velocity of this rotation — the Darboux vector. Like any vector, it may be resolved into components along the unit vectors.

$$\bar{\Omega} = \Omega_\tau \bar{\tau} + \Omega_n \bar{n} + \Omega_b \bar{b}. \qquad \text{(VII. 54)}$$

The problem may be considered as solved if the projections Ω_τ, Ω_n and Ω_b upon the axes $\bar{\tau}$, $\bar{n}$ and $\bar{b}$ are known.

As is known from kinematics, $\frac{d\bar{\tau}}{dS}$ considered as velocity of the end of vector $\bar{\tau}$ may be represented in the form

$$\frac{d\bar{\tau}}{dS} = \bar{\Omega} \times \bar{\tau}$$

and similarly,

$$\left.\begin{aligned} \frac{d\bar{n}}{dS} &= \bar{\Omega} \times \bar{n} ; \\ \frac{d\bar{b}}{dS} &= \bar{\Omega} \times \bar{b} . \end{aligned}\right\} \qquad \text{(VII. 55)}$$

By inserting (VII. 54) in (VII. 55), we obtain

$$\left.\begin{aligned} \frac{d\bar{\tau}}{dS} &= -\Omega_n \bar{b} + \Omega_b \bar{n}; \\ \frac{d\bar{n}}{dS} &= -\Omega_b \bar{\tau} + \Omega_\tau \bar{b}; \\ \frac{d\bar{b}}{dS} &= -\Omega_\tau \bar{n} + \Omega_n \bar{\tau}. \end{aligned}\right\} \qquad \text{(VII. 56)}$$

In expression (VII. 56) Ω_n must be equated to zero, since the vectors $\bar{n}$ and $d\bar{\tau}$ and, consequently also $\frac{d\bar{\tau}}{dS}$, have the same direction.

$$\left.\begin{aligned} \frac{d\bar{\tau}}{dS} &= \Omega_b \bar{n}; \\ \frac{d\bar{n}}{dS} &= -\Omega_b \bar{\tau} + \Omega_\tau \bar{b}; \\ \frac{d\bar{b}}{dS} &= -\Omega_\tau \bar{n}. \end{aligned}\right\} \qquad \text{(VII. 57)}$$

Ω_b is determined from the first equation (VII. 57) by scalar multiplication with $\bar{n}$. (N. B. The scalar product of the two vectors is the product between the vector lengths and the cosine of the angle between them).

$$\left(\frac{d\bar{\tau}}{dS}\cdot\bar{n}\right)=\Omega_b\,[\bar{n}\cdot\bar{n}]=\left(\frac{d\bar{\tau}}{dS}\right)|\bar{n}|\cos\left(d\bar{\tau}_1\bar{n}\right)=\left(\frac{d\bar{\tau}}{dS}\right)$$

or

$$\Omega_b=\left(\frac{d\bar{\tau}}{dS}\right).$$

It follows from Figure VII. 19, that, with the error being an infinitesimal of a higher order than two,

$$(d\tau)=(\bar{\tau})\,\varepsilon=\varepsilon;$$

therefore,

$$\left(\frac{d\bar{\tau}}{dS}\right)=\frac{\varepsilon}{dS}=\frac{1}{\varrho},$$

or

$$\Omega_b=\frac{1}{\varrho}. \qquad \text{(VII. 58)}$$

By scalar multiplication of the third equation of (VII. 57) with $\bar{n}$, we obtain

$$\left(\frac{d\bar{b}}{dS}\cdot\bar{n}\right)=-\Omega_\tau.$$

It appears from Figure VII. 19, b, that for $\Omega_\tau>0$, the vectors $d\bar{b}$ and $\bar{n}$ are in opposite directions, i.e.,

$$(d\bar{b}\cdot\bar{n})=-(d\bar{b})=-2\sin\frac{\eta}{2}=-\eta,$$

and consequently,

$$\Omega_\tau=\frac{\eta}{dS}=\frac{1}{T}, \qquad \text{(VII. 59)}$$

where the scalar T represents the twist of the curve.

In a left-handed coordinate system $T>0$ ($T<0$) when $\Omega_\tau>0$ ($\Omega_\tau<0$), i. e., when moving along the curve, we see the axes $\bar{n}$ and $\bar{b}$ turning along a left-handed (right-handed) screw (the motion of the vector along the screw corresponds to a translational motion along the screw axis).

Consequently, the vector of angular velocity of the trihedron — the Darboux vector — is expressed by

$$\bar{\Omega}=\frac{\bar{\tau}}{T}+\frac{\bar{b}}{\varrho};$$

for the derivatives of the unit vectors of the natural trihedron, we obtain the Fronais formulas

$$\left.\begin{aligned} \frac{d\bar{\tau}}{dS} &= \frac{\bar{n}}{\varrho}; \\ \frac{d\bar{n}}{dS} &= \frac{\bar{b}}{T} - \frac{\bar{\tau}}{\varrho}; \\ \frac{d\bar{b}}{dS} &= -\frac{\bar{n}}{T}. \end{aligned}\right\} \qquad \text{(VII. 60)}$$

Let us consider a curved bar whose axis — the locus of the centroids of the bar cross sections — is a curve of double curvature (Figure VII. 20). The left-handed coordinate system xyz is selected so that the axis z coincides with the tangent to the bar axis at the point considered, i.e., with the direction of the $\bar{\tau}$ axis of the natural trihedron, and the axes x and y are directed along the principal axes of inertia of the bar cross section. In the plane normal to the axis, the axes x and y thus form with the axes $\bar{n}$ and $\bar{b}$, respectively, an angle f varying from section to section.

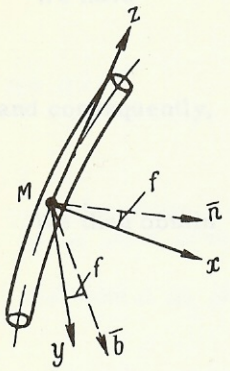


FIGURE VII. 20. Geometry of slender bars

Let us imagine that the area M of these trihedrons moves along the bar axes with unit velocity.

Then, the trihedron of axes x, y, z will rotate with the angular velocity $\bar{\omega}(p, q, r)$, where p, q, r are projections of vector $\bar{\omega}$ upon the axes x, y, z and the trihedron of axes τ, n, b with the angular velocity $\bar{\Omega}(\Omega_\tau, \Omega_n, \Omega_b)$, where Ω_τ, Ω_n, Ω_b are projections of Darboux's vector.

The angular velocities $\bar{\Omega}$ and $\bar{\omega}$ will differ from each other by the relative angular velocity of the axes x, y, z trihedron with respect to the trihedron $\bar{\tau}, \bar{n}, \bar{b}$. The vector of this relative angular velocity is directed along the τ axis, so that we may write

$$\bar{\omega} = \bar{\Omega} + \frac{df}{dS}\bar{\tau},$$

whence,

$$\begin{aligned} p &= \Omega_x, \\ q &= \Omega_y, \\ r &= \Omega_z + \frac{df}{dS}. \end{aligned}$$

On the other hand,

$$\Omega = \Omega_\tau \bar{\tau} + \Omega_b \bar{b},$$

therefore,

$$\left.\begin{aligned} p &= \Omega_x = \Omega_b \sin f = \frac{\sin f}{\varrho}; \\ q &= \Omega_y = \Omega_b \cos f = \frac{\cos f}{\varrho}; \\ r &= \Omega_z + \frac{df}{dS} = \frac{1}{T} + \frac{df}{dS}. \end{aligned}\right\} \qquad \text{(VII. 61)}$$

These results may be interpreted in the following way:

p = projection of the curvature of element dS upon the plane yz;

q = ditto upon the plane zx;

r = bar twist, composed of the geometrical twist and the twist caused by the variation of angle f.

Small deformations of slender bars. Clebsch equation. Let us take a point M on the bar axis before its deformation and construct the trihedron of axes x_0, y_0, z_0 in such a way that z_0 is tangential to the bar axes and x_0 and y_0 directed along the main axes of inertia of the cross section.

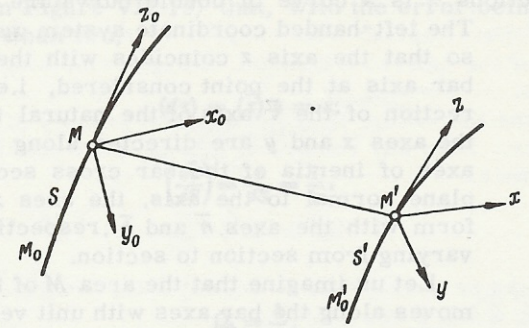


FIGURE VII. 21. Diagram for computing the deformation of bars

Let us denote by $\omega_0 (p_0, q_0, r_0)$ the angular velocity by which the trihedron of axes x_0, y_0, z_0 rotates when the point M moves along the bar axis with unit velocity, where p_0, q_0, r_0 are projections of the angular velocity ω_0 upon the axes x_0, y_0, z_0 determined by relation (VII. 61).

The coordinate system for the deformed bar is determined as follows (Figure VII. 21): the z axis is tangential to the axis of the deformed bar, the point M being located at M'; the points located upon the axis x_0 move along a certain curve tangential to this axis at point M'; the above points, together with the axis z, determine a certain plane; the perpendicular to the axis z lying in this plane is the axis x; axis y is obtained by erecting a perpendicular to axes x and y. The direction of the axes is selected to obtain a system of coordinates similar to x_0, y_0, z_0.

Furthermore, for $M_0M = M_0'M'$ (where point M' moves along the bar axis), the trihedron of axes x, y, z has the angular velocity $\overline{\omega} (p, q, r)$

To make the trihedrons x_0, y_0, z_0 and x, y, z coincide, it is first necessary:

1) to move point M over MM'; denote the projections of this vector on the axes x_0, y_0, z_0 by u, v and w;

2) to impart to the trihedron of axes x_0, y_0, z_0 a rotation about the point M', to make them coincide with the axes x, y, z. Let us denote the vector of this small rotation by $\overline{\theta}$ and its projections on the axes x_0, y_0, z_0, namely the rotations about these axes, by α, β, γ.

The values u, v, w and α, β, γ are variable. With u, v, w given, we determine the axis of the deformed bar.

The rotation about the axis z must be given in order to determine the axes x and y.

Considering that one more condition is imposed upon the six quantities mentioned by the fact that the bar length does not change, we then have three relations altogether.

Let us tabulate the cosines of the angles between the axes x_0, y_0, z_0 and x, y, z. We denote the unit vectors of x_0, y_0, z_0 by $\bar{i}, \bar{j}, \bar{k}$

Rotated through the angle θ, the axis x_0 assumes the position x, and the unit vector $\bar{i}_0$ becomes the unit vector $\bar{i}$, directed along the axis x. Then

$$\bar{i} = \bar{i}_0 + \bar{\theta} \times \bar{i}_0 ,$$

where the second term represents the displacement of the end of vector i_0.

We have

$$\bar{\theta} = \alpha \bar{i}_0 + \beta \bar{j}_0 + \gamma \bar{k}_0 ,$$

and consequently,

$$\bar{i} = \bar{i}_0 - \beta \bar{k}_0 + \gamma \bar{j}_0$$

We then obtain

$$\left.\begin{aligned} \cos(x, x_0) &= (\bar{i}, \bar{i}_0) = 1; \\ \cos(x, y_0) &= (\bar{i}, \bar{j}_0) = \gamma; \\ \cos(x, z_0) &= [\bar{i}, \bar{k}_0) = -\beta. \end{aligned}\right\} \qquad \text{(VII. 62)}$$

The table of cosines thus has the form

	x	y	z
x_0	1	$-\gamma$	β
y_0	γ	1	$-\alpha$
z_0	$-\beta$	α	1

The apexes of the trihedrons x_0, y_0, z_0 and x, y, z move with the unit velocities $\bar{v}_0 = \bar{\tau}_0$ and $\bar{v} = \bar{\tau}$. We may consider that the motion of apex M' of the second trihedron is composed of the motion relative to the first trihedron and the transportation motion of this latter

$$\bar{v} = \bar{v}_e + \bar{v}_r, \qquad \text{(VII. 63)}$$

where $\bar{v}_e = \bar{v}_0 + \bar{\omega}_0 \times M\bar{M}'$ = transportation velocity, i.e., velocity of point M' fixed to the trihedron.

$$M(x_0, y_0, z_0);$$

v_r = relative velocity, whose projections upon the axes x_0, y_0, z_0 are

$$\frac{du}{ds};\ \frac{dv}{ds};\ \frac{dw}{ds},$$

but, according to (VII. 63)

$$\bar{\tau} = \bar{\tau}_0 + (\bar{\omega}_0 \times \overline{MM'}) + v_r. \qquad \text{(VII. 64)}$$

By projecting this equation on the axes x_0, y_0, z_0 and taking into account that $\tau_{x0} = \beta$; $\tau_{y0} = -\alpha$; $\tau_{z0} = 1$ (see table of cosines), we obtain the first set of Clebsch's equations

$$\left.\begin{aligned} \beta &= q_0 w - r_0 v + \frac{du}{ds};\\ -\alpha &= r_0 u - p_0 w + \frac{dv}{ds};\\ 0 &= p_0 v - q_0 u + \frac{dw}{ds}. \end{aligned}\right\} \qquad \text{(VII. 65)}$$

The angular velocity $\bar{\omega}$ of the trihedron $M'(x, y, z)$ may be considered as the geometrical sum of the angular velocity $\bar{\omega}_0$ of the trihedron $M(x_0, y_0, z_0)$ and the angular velocity $\bar{\omega}_r$ of M' relative to M.

According to the above, the projections of $\bar{\omega}_r$ upon the x_0, y_0, z_0 axes are

$$\frac{d\alpha}{ds},\ \frac{d\beta}{ds},\ \frac{d\gamma}{ds}.$$

We may write

$$\bar{\omega} = \bar{\omega}_0 + \bar{\omega}_r,$$

and by projecting this equation upon the axes x, y, z we obtain

$$p = \omega_{0x} + \omega_{rx} = p_0 + q_0\gamma - \beta r_0 + \frac{d\alpha}{ds} + \gamma\frac{d\beta}{ds} - \beta\frac{d\gamma}{ds};$$

$$q = \omega_{0y} + \omega_{ry} = q_0 + r_0\alpha - \gamma p_0 + \frac{d\beta}{ds} + \alpha\frac{d\gamma}{ds} - \gamma\frac{d\alpha}{ds};$$

$$r = \omega_{0z} + \omega_{rz} = r_0 + p_0\beta - \alpha q_0 + \frac{d\gamma}{ds} + \beta\frac{d\alpha}{ds} - \alpha\frac{d\beta}{ds};$$

or, by denoting

$$\delta_p = p - p_0; \qquad \delta_q = q - q_0; \qquad \delta_r = r - r_0,$$

and by neglecting the infinitesimals of a higher order, we obtain the second set of Clebsch's equations, which determine the changes in curvature δ_p and δ_q and the twist δ_r

$$\left.\begin{aligned} \delta_p &= \gamma q_0 - \beta r_0 + \frac{d\alpha}{ds};\\ \delta_q &= \alpha r_0 - \gamma p_0 + \frac{d\beta}{ds};\\ \delta_r &= \beta p_0 - \alpha q_0 + \frac{d\gamma}{ds}. \end{aligned}\right\} \qquad \text{(VII. 66)}$$

Equilibrium of slender bars, Kirchhoff's equations. The equilibrium of an element of bar, taken between two sections whose distance ds is infinitely small, and subject to the action of forces mutually balanced, is determined by the equation of equilibrium (Figure VII. 22)

$$\bar{F}ds + \bar{v} + \frac{d\bar{v}}{ds}ds - \bar{v} = 0;$$

$$\bar{L} + \frac{d\bar{L}}{ds}ds - \bar{L} + \left[\bar{\tau}ds \times \left(\bar{v} + \frac{d\bar{v}}{ds}ds\right)\right] + \bar{k}ds = 0.$$

where $\bar{F}$ and $\bar{k}$ = vectors of forces and moments per unit bar length;
$\bar{v}$ and $\bar{L}$ = force and moment, equivalent to the load, exerted by the rest of the bar on the element considered.

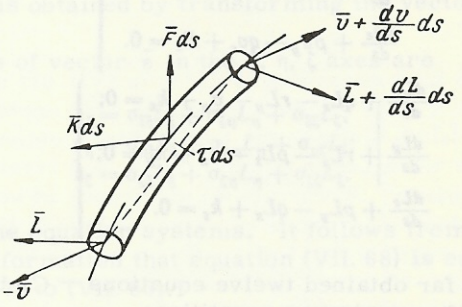


FIGURE VII. 22. Equilibrium of slender bars

By omitting the higher order terms, we obtain

$$\frac{d\bar{v}}{ds} + \bar{F} = 0;$$

$$\frac{d\bar{L}}{ds} + [\bar{\tau} \times \bar{v}] + \bar{k} = 0.$$

By resolving the vector v into components along the unit vectors of x, y, z, we obtain

$$\bar{v} = v_x\bar{i} + v_y\bar{j} + v_z\bar{k};$$

we may write

$$\frac{d\bar{v}}{ds} = \frac{dv_x}{ds}\bar{i} + \frac{dv_y}{ds}\bar{j} + \frac{dv_z}{ds}\bar{k} + v_x\frac{d\bar{i}}{ds} + v_y\frac{d\bar{j}}{ds} + v_z\frac{d\bar{k}}{ds}.$$

As is known from kinematics,

$$\frac{d\bar{i}}{ds} = \bar{\omega} \times \bar{i}\ ;\quad \frac{d\bar{j}}{ds} = \bar{\omega} \times \bar{j}\ ;\quad \frac{d\bar{k}}{ds} = \bar{\omega} \times \bar{k}\ ;$$

we then obtain

$$\frac{d\bar{v}}{ds} = \frac{dv_x}{ds}\bar{i} + \frac{dv_y}{ds}\bar{j} + \frac{dv_z}{ds}\bar{k} + \bar{\omega} \times \left(v_x\bar{i} + v_y\bar{j} + v_z\bar{k}\right).$$

By denoting

$$\frac{d\bar{v}}{ds} = \frac{dv_x}{ds}\bar{i} + \frac{dv_y}{ds}\bar{j} + \frac{dv_z}{ds}\bar{k}.$$

we obtain

$$\frac{d\bar{v}}{ds} = \frac{d'\bar{v}}{ds} + \bar{\omega}\times\bar{v},$$

$$\frac{d\bar{L}}{ds} = \frac{d'\bar{L}}{ds} + \bar{\omega}\times\bar{L},$$

or, projecting on the axes, we obtain the six Kirchhoff relations

$$\left.\begin{aligned} \frac{dv_x}{ds} + qv_z - rv_y + F_x = 0; \\ \frac{dv_y}{ds} + rv_x - pv_z + F_y = 0; \\ \frac{dv_z}{ds} + pv_y - qv_x + F_z = 0. \end{aligned}\right\} \qquad \text{(VII. 67)}$$

$$\left.\begin{aligned} \frac{dL_x}{ds} + qL_z - rL_y - v_y + k_x = 0; \\ \frac{dL_y}{ds} + rL_x - pL_z - v_x + k_y = 0; \\ \frac{dL_z}{ds} + pL_y - qL_x + k_z = 0. \end{aligned}\right\} \qquad \text{(VII. 68)}$$

In all, we have so far obtained twelve equations — Clebsch's and Kirchhoff's — containing fifteen unknown quantities:

$$p,\ q,\ r,\ u,\ v,\ w,\ \alpha,\ \beta,\ \gamma,\ v_x,\ v_y,\ v_z,\ L_x,\ L_y,\ L_z.$$

The three missing equations may be obtained from the relations between stress and strain,

$$\left.\begin{aligned} L_x = A\delta_p; \\ L_y = B\delta_q; \\ L_z = C\delta_r. \end{aligned}\right\} \qquad \text{(VII. 69)}$$

where

$$A = EJ_x; \quad B = EJ_y; \quad C = 2G\iint \Phi\, dr.$$

$\frac{1}{A}, \frac{1}{B}, \frac{1}{C}$ are often referred to as the yieldingness of the bar (in bending and torsion).

The formulas (VII. 69) may be expressed in an invariant form by introducing the tensor σ of the bar yieldingness. The principal axes of the tensor are the axes x, y, z, σ being represented by

$$\sigma = \begin{Vmatrix} \frac{1}{A}, & 0, & 0 \\ 0, & \frac{1}{B}, & 0 \\ 0, & 0, & \frac{1}{C} \end{Vmatrix} \qquad \text{(VII. 70)}$$

The components of the tensor σ in any coordinates may be determined by the well-known formulas for the transformation of tensor components.

The components of the yieldingness tensor in ξ, η, ζ coordinates are $\sigma_{\xi\xi}$, $\sigma_{\xi\eta}$; $\sigma_{\xi\zeta}$, etc. The yieldingness tensor referred to these axes has the form

$$\sigma = \left\{ \begin{matrix} \sigma_{\xi\xi}; & \sigma_{\xi\eta}; & \sigma_{\xi\zeta}; \\ \sigma_{\eta\xi}; & \sigma_{\eta\eta}; & \sigma_{\eta\zeta}; \\ \sigma_{\zeta\xi}; & \sigma_{\zeta\eta}; & \sigma_{\zeta\zeta}. \end{matrix} \right\} \qquad \text{(VII. 71)}$$

The relation (VII. 71) may now be written as

$$\bar{\varepsilon} = \sigma \bar{L}, \qquad \text{(VII. 72)}$$

i.e., the vector $\bar{\varepsilon}$ is obtained by transforming the vector $\bar{L}$ by means of tensor σ.

The components of vector $\bar{\varepsilon}$ in the ξ, η, ζ axes are

$$\left. \begin{aligned} \varepsilon_\xi &= \sigma_{\xi\xi} L_\xi + \sigma_{\xi\eta} L_\eta + \sigma_{\xi\zeta} L_\zeta; \\ \varepsilon_\eta &= \sigma_{\eta\xi} L_\xi + \sigma_{\eta\eta} L_\eta + \sigma_{\eta\zeta} L_\zeta; \\ \varepsilon_\zeta &= \sigma_{\zeta\xi} L_\xi + \sigma_{\zeta\eta} L_\eta + \sigma_{\zeta\zeta} L_\zeta. \end{aligned} \right| \qquad \text{(VII. 73)}$$

Integration of the equation systems. It follows from the equations of equilibrium and deformation that equation (VII. 68) is equivalent to system (VII. 65) and (VII. 67) to (VII. 66).

As noted above, equations (VII. 68) and (VII. 67) may be written in the vectorial form

$$\frac{d\bar{v}}{ds} = -\bar{F}; \qquad \text{(VII. 74)}$$

$$\frac{d\bar{L}}{ds} + [\bar{\tau} \times \bar{v}] = 0. \qquad \text{(VII. 75)}$$

Consequently, on the basis of the analogy between stresses and strains, we may write

$$\frac{d\bar{b}}{ds} + [\bar{\tau} \times \bar{\theta}] = 0; \qquad \text{(VII. 76)}$$

$$\frac{d\bar{\theta}}{ds} = \bar{\varepsilon}, \qquad \text{(VII. 77)}$$

where $\bar{b}$ = vector of displacement of point M of the bar axis due to its deformation;

$\bar{\theta}$ = vector of rotation of the tangent to the bar axis at point M, due to bar-axis deformation.

After integration, equation (VII. 74) takes the form

$$\bar{v} = \bar{v}_0 - \int_{s_0}^{s} \bar{F}(l)\, dl. \qquad \text{(VII. 78)}$$

By inserting the expression of v in equation (VII. 75), and integrating — after putting $\tau ds = dl$, we obtain

$$\bar{L} = \bar{L}_0 - (\bar{l} - \bar{l}_0) \times \bar{v}_0 + \int_{s_0}^{s} d\bar{l}(t) \times \int_{s_0}^{s} \bar{F}(t_1)\, dt,$$

whence, by changing the order of integration according to the Dirichlet formula, we obtain

$$\bar{L} = \bar{L}_0 - (\bar{l} - \bar{l}_0) \times \bar{v}_0 + \int_{s_0}^{s} [\bar{l}(s) - \bar{l}(t)] \times \bar{F}(t)\, dt \qquad \text{(VII. 79)}$$

and by analogy

$$\bar{\theta} = \bar{\theta}_0 + \int_{s_0}^{s} \bar{\varepsilon}\, dt, \qquad \text{(VII. 80)}$$

$$\bar{b} = b_0 + (\bar{l} - \bar{l}_0) \times \bar{\theta}_0 - \int_{s_0}^{s} [\bar{l}(s) - \bar{l}(t)]\, \bar{\varepsilon}(t)\, dt. \qquad \text{(VII. 81)}$$

The solution of the four equations (VII. 78) to (VII. 81) depends on twelve arbitrary constants, i.e., the projections of the four vectors $\bar{v}_0$, $\bar{L}_0$, $\bar{b}_0$, $\bar{\theta}_0$. The term $\bar{b} = b_0 + (\bar{l} - \bar{l}_0) \times \bar{\theta}_0$ defines the small displacement of the bar as a rigid body. With a bar whose ends are not fixed, this term may be dropped.

Calculation of the blade. According to the theory of slender bars, the stresses in a bar loaded by a system of external forces may be determined from the equations of equilibrium and from the equations which relate the displacement and angle of twist of the bar sections to its properties. In the vectorial form these equations are

1) equation of equilibrium

$$\frac{d\bar{v}}{ds} = -\bar{F}; \quad \frac{d\bar{L}}{ds} + [\bar{\tau} \times \bar{v}] = 0.$$

2) equation of deformations

$$\frac{d\bar{\theta}}{ds} = \sigma \bar{L}; \quad \frac{d\bar{\delta}}{ds} + [\bar{\tau} \times \bar{\theta}] = 0,$$

where $\bar{v}$ = vector of external load;
$\bar{F}$ = vector of internal forces;
$\bar{L}$ = vector of external moment;
$\bar{\tau}$ = unit vector tangent to bar axis;
$\bar{\theta}$ = vector of rotation of the tangent to the bar;
$\bar{\delta}$ = vector of displacement of a point on the bar axis;
s = coordinate of the section on the bar axis;
σ = yieldingness tensor referred to the principal axes of inertia of the section

$$\sigma = \begin{vmatrix} \frac{1}{A}, & 0, & 0 \\ 0, & \frac{1}{B}, & 0 \\ 0, & 0, & \frac{1}{C} \end{vmatrix},$$

where A, B, C = flexural and torsional rigidities

$$A = EJ_x;\ B = EJ_y,$$

$$C \approx \frac{G}{4\pi^2} \cdot \frac{F^4}{J_p},$$

where J_x and J_y = moments of inertia of the section with respect to the axes x and y;
E = modulus of elasticity;
G = shear modulus;
F = cross-sectional area of the section;
J_p = polar moment of inertia of the section.

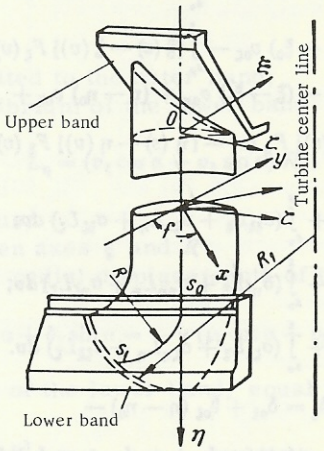


FIGURE VII. 23. Schematic diagram for the design of a Francis runner blade

After integration, the equations of equilibrium and deformation become

$$\bar{v} = \bar{v}_0 - \int_{s_0}^{s} \bar{F}(v)\,dv;$$

$$\bar{\theta} = \bar{\theta}_0 - \int_{s_0}^{s} \sigma \bar{L}(v)\,dv;$$

$$\bar{L} = \bar{L}_0 - (\bar{r} - \bar{r}_0) \times \bar{v}_0 + \int_{s_0}^{s} [\bar{r}(s) - \bar{r}(v)] \times \bar{F}(v)\,dv;$$

$$\bar{\sigma} = \bar{\sigma}_0 \bar{\theta}_0 \times (\bar{r} - \bar{r}_0) - \int_{s_0}^{s} [\bar{r}(s) - \bar{r}(v)] \times \sigma \bar{L}\,dv,$$

where $\bar{r} = \bar{r}(s)$ = equation of the bar axis*.

The solution of these equations depends on four arbitrary vectors $\bar{v}_0$, $\bar{L}_0$, $\bar{\theta}_0$, $\bar{\delta}_0$ — equivalent to twelve arbitrary constants, determined from boundary conditions.

* [Apparently two-dimensional, since $\xi - \xi_0 = 0$.]

When projected upon the axes ζ, ξ, η (Figure VII. 23), the equations of equilibrium and deformation take the form

$$\left.\begin{aligned} v_\xi &= v_{0\xi} - \int_{s_0}^{s} F_\xi(v)\,dv; \\ v_\eta &= v_{0\eta} - \int_{s_0}^{s} F_\eta(v)\,dv; \\ v_\zeta &= v_{0\zeta} - \int_{s_0}^{s} F_\zeta(v)\,dv. \end{aligned}\right\} \qquad \text{(VII. 82)}$$

$$\left.\begin{aligned} L_\xi &= L_{0\xi} - (\eta - \eta_0)\,v_{0\zeta} + \int_{s_0}^{s} [\eta(s) - \eta(v)]\,F_\zeta(v)\,dv; \\ L_\eta &= L_{0\eta} + (\xi - \xi_0)\,v_{0\zeta} - \int_{s_0}^{s} [\xi(s) - \xi(v)]\,F_\zeta(v)\,dv; \\ L_\zeta &= L_{0\zeta} - (\xi - \xi_0)\,v_{0\eta} + (\eta - \eta_0)\,v_{0\xi} + \\ &+ \int_{s_0}^{s} \{[\xi(s) - \xi(v)]\,F_\eta(v) - [\eta(s) - \eta(v)]\,F_\xi(v)\}\,dv. \end{aligned}\right\} \qquad \text{(VII. 83)}$$

$$\left.\begin{aligned} \theta_\xi &= \theta_{0\xi} + \int_{s_0}^{s} (\sigma_{\xi\xi}L_\xi + \sigma_{\xi\eta}L_\eta + \sigma_{\xi\zeta}L_\zeta)\,dv; \\ \theta_\eta &= \theta_{0\eta} + \int_{s_0}^{s} (\sigma_{\eta\xi}L_\xi + \sigma_{\eta\eta}L_\eta + \sigma_{\eta\zeta}L_\zeta)\,dv; \\ \theta_\zeta &= \theta_{0\zeta} + \int_{s_0}^{s} (\sigma_{\zeta\xi}L_\xi + \sigma_{\zeta\eta}L_\eta + \sigma_{\zeta\zeta}L_\zeta)\,dv. \end{aligned}\right\} \qquad \text{(VII. 84)}$$

$$\left.\begin{aligned} \delta_\xi &= \delta_{0\xi} + \theta_{0\zeta}(\eta - \eta_0) - \\ &- \int_{s_0}^{s} [\eta(s) - \eta(v)]\,[\sigma_{\zeta\xi}L_\xi + \sigma_{\zeta\eta}L_\eta + \sigma_{\zeta\zeta}L_\zeta]\,dv; \\ \delta_\eta &= \delta_{0\eta} + \theta_{0\zeta}(\xi - \xi_0) + \\ &+ \int_{s_0}^{s} [\xi(s) - \xi(v)]\,[\sigma_{\zeta\xi}L_\xi + \sigma_{\zeta\eta}L_\eta + \sigma_{\zeta\zeta}L_\zeta]\,dv; \\ \delta_\zeta &= \delta_{0\zeta} + \theta_{0\xi}(\eta - \eta_0) - \theta_{0\eta}(\xi - \xi_0) - \\ &- \int_{s_0}^{s} \{[\xi(s) - \xi(v)]\,[\sigma_{\eta\xi}L_\xi + \sigma_{\eta\eta}L_\eta + \sigma_{\eta\zeta}L_\zeta] - \\ &- [\eta(s) - \eta(v)]\,[\sigma_{\xi\xi}L_\xi + \sigma_{\xi\eta}L_\eta + \sigma_{\xi\zeta}L_\zeta]\}\,dv. \end{aligned}\right\} \qquad \text{(VII. 85)}$$

Calculation of the integrals included in the equations is generally very awkward; A. Ya. Aronson recommends evaluating them numerically in order to simplify the calculation procedure.

By considering the boundary conditions, we obtain the following.

1. Assuming that the upper blade end is rigidly fixed to the upper band, and selecting the origin of coordinates at the upper blade end (Figure VII. 23), we have for the case of $s = 0$

$$\left.\begin{aligned} \bar{\theta}_0 &= 0, \text{ i.e., } \theta_{0\xi} = \theta_{0\eta} = \theta_{0\zeta} = 0; \\ \delta_0 &= 0, \text{ i.e., } \delta_{0\xi} = \delta_{0\eta} = \delta_{0\zeta} = 0. \end{aligned}\right\} \qquad \text{(VII. 86)}$$

These conditions are fulfilled with satisfactory accuracy, since the upper band is provided with flanges bolted to the shaft and is of heavy construction.

2. The lower blade end is fastened to the lower band which is free to move with it. Then for $s = s_L$ we have:

a) condition of free movement of the blade end together with the band in the direction of the turbine axis.

$$v_\eta = G_{zb} + \Delta P, \tag{VII. 87}$$

where

$$G_{zb} = \frac{G_b}{z}$$

G_b = weight of band;
z = number of blades;
ΔP = pressure transmitted to the outer band;

b) condition of equilibrium of the lower band

$$L_\eta = (v_\zeta \cos\alpha - v_\xi \sin\alpha)\, R_1, \tag{VII. 88}$$

where R_1 = runner radius;
α = angle between axes ξ and R;

c) condition of equal radial displacements of the band and runner

$$\delta_\zeta \cos\alpha + \delta_\xi \sin\alpha = -\gamma\,(v_\xi \cos\alpha + v_\zeta \sin\alpha), \tag{VII. 89}$$

where γ = yieldingness of the lower band, equal to

$$\gamma = \frac{R_1^3}{2EJ}\left[\frac{1}{\sin^2 v}\left(\frac{v}{2} + \frac{\sin v \cos v}{2}\right) - \frac{1}{v}\right],$$

where $v = \frac{2\pi}{z}$;

J = minimum moment of inertia of the band section;

d) condition of lower blade end fixed to the runner band

$$\theta_\xi = 0; \tag{VII. 90}$$

$$\theta_\zeta = 0; \tag{VII. 91}$$

$$\delta_\zeta \cos\alpha - \delta_\xi \sin\alpha = R\theta_\eta; \tag{VII. 92}$$

$$\theta_T = -\beta L_T, \tag{VII. 93}$$

where T = direction of tangent to the band at the point of junction with the blade.

$$\beta = \frac{1}{En}\left(n = \int \frac{\eta^2 dF}{r}\right).$$

By replacing in equations (VII. 87) and (VII. 92) the values of the shearing forces, moments, angles of rotation and displacements for $s = s_L$ by their

values for $s = 0$, from equations (VII. 82) and (VII. 85), we obtain after transformations a system of equations for determining the constants $L_{0\xi}$, $L_{0\eta}$, $L_{0\zeta}$, $v_{0\xi}$, $v_{0\eta}$, $v_{0\zeta}$

$$\left.\begin{aligned}
a_{11}L_{0\zeta} + a_{12}L_{0\eta} + a_{13}L_{0\xi} + b_{11}v_{0\zeta} + b_{12}v_{0\eta} + b_{13}v_{0\xi} + \\
+ d_1 = 0; \\
a_{21}L_{0\zeta} + a_{22}L_{0\eta} + a_{23}L_{0\xi} + b_{21}v_{0\zeta} + b_{22}v_{0\eta} + \\
+ b_{23}v_{0\xi} + d_2 = 0; \\
a_{31}L_{0\zeta} + a_{32}L_{0\eta} + a_{33}L_{0\xi} + b_{31}v_{0\zeta} + b_{32}v_{0\eta} + \\
+ b_{33}v_{0\xi} + d_3 = 0; \\
a_{41}L_{0\zeta} + a_{42}L_{0\eta} + a_{43}L_{0\xi} + b_{41}v_{0\zeta} + b_{42}v_{0\eta} + \\
+ b_{43}v_{0\xi} + d_4 = 0; \\
L_{0\eta} + b_{51}v_{0\zeta} + b_{53}v_{0\xi} + d_5 = 0; \\
v_{0\eta} = C_5.
\end{aligned}\right\} \qquad \text{(VII. 94)}$$

The constant coefficients a_{ij}, b_{ij}, d_i are functions of the given load and the bar geometry.

By inserting the constants $v_{0\xi}$ ..... $L_{0\zeta}$ obtained by solving the system (VII. 94), into the formulas (VII. 82) and (VII. 83), all the components of external loads and moments acting on any blade section may be determined.

The components of the vectors of moments and forces with respect to the principal axes of inertia x, y of each section may be determined from the formulas for projections of vectors.

The resultant stress at a point having coordinates x, y is determined by the formula

$$\sigma = \frac{P_z}{F} + \frac{L_x y}{J_x} + \frac{L_y x}{J_y}. \qquad \text{(VII. 95)}$$

The following order of calculation is convenient for design. Construct the bar axis on the theoretical drawing of the blade; the axis is represented by a straight line tangent to a circular arc of radius R (Figure VII. 23). The bar axis passes through the centroid of the blade cross section bounded by the upper and lower bands. The strength characteristics in blade bending, torsion, and twist are to be determined at each cross section.

For greater accuracy of calculation, the bar axis should be divided into a large number of sections. The values of $A = A(s), B = B(s)$ and $C = C(s)$ required to calculate σ may be determined on the basis of the strength characteristics of the end sections.

Loads acting on the blade. The loads due to centrifugal forces $q = q(s)$ at various sections are calculated below.

$$q(s) = \frac{m\omega^2}{h_\kappa} R(s). \qquad \text{(VII. 96)}$$

The projections of the load $q(s)$ upon the axes ξ and ζ are:

$$\left.\begin{aligned}
q_\xi = \frac{m\omega^2}{h_\kappa} R(s) \cos\varphi; \\
q_\zeta = \frac{m\omega^2}{h_\kappa} R(s) \sin\varphi,
\end{aligned}\right\} \qquad \text{(VII. 97)}$$

where φ = angle between R and ξ.

A. Ya. Aronson recommends tabulation for calculating the integrals needed in the determination of the coefficients a_{ij}, b_{ij}, d_i. He advises calculating the coefficients themselves — as illustrated by the following example — by numerical integration according to the trapezoidal rule.

The blades for several runner variants were designed in this way at the LMZ, the calculated diagrams being then compared with the experimental results of field tests. These data are represented in Figure VII. 24, which shows that calculated and experimental stress values due to centrifugal forces agree satisfactorily.

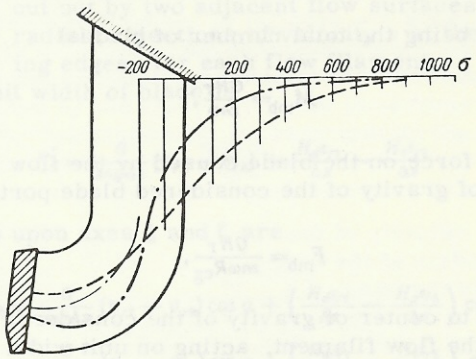


FIGURE VII. 24. Stress diagram of the runner blade:
—·—·—·— calculated; ———— experimental (field tests).

The results obtained in calculating the stresses caused by hydrodynamic loads do not agree so well with experimental data, probably owing to inaccurate knowledge of the loads acting on the blade. The value of the maximum stresses, however, is close to those measured. The stresses caused in the blade by the action of centrifugal forces occurring at runaway speed differ little from the stresses due to uniform hydrodynamical loading; the calculation may therefore be carried out for both cases. At normal speed the centrifugal forces cause small stresses.

The hydraulic loads acting on the blades may be determined as follows:

Suppose the flow in a Francis runner to be irrotational or of uniform velocity, for which cases the meridian distribution of the flow velocities is known. Then, according to the law of momentum, the moment of the mutual interaction between the Francis runner and the water flow is expressed by the formula

$$M_m = \frac{G}{g}(v_{u1}R_1 - v_{u2}R_2), \qquad \text{(VII. 98)}$$

where G = weight of the water flowing through the turbine;
v_{u1} and v_{u2} = peripheral projections of the absolute velocity at the runner entrance and exit;
R_1 and R_2 = radii of the runner entrance and exit.

The head is then

$$H_T = \frac{v_{u1}u_1 - v_{u2}u_2}{g}. \qquad \text{(VII. 99)}$$

If we consider that the stream flowing through the runner is composed of filaments of equal discharge $G' = \frac{G}{n}$, the moment exerted by the flow filament on the runner being

$$M_m = \frac{GH_T}{n\omega},$$

and on one blade (z being the total number of blades)

$$M_{mb} = \frac{GH_T}{zn\omega}, \qquad \text{(VII. 100)}$$

then the peripheral force on the blade caused by the flow filament and applied at the center of gravity of the considered blade portion

$$F_{mb} = \frac{GH_T}{zn\omega R_{cg}}, \qquad \text{(VII. 101)}$$

where R_{cg} = radius to center of gravity of the considered blade portion.

The load due to the flow filament, acting on unit width of the considered blade portion

$$F'_{mb} = \frac{GH_T}{zn\omega R_{cg}\Delta s} \qquad \text{(VII. 102)}$$

where Δs = flow-filament thickness.

The projections of the load vector on the axes ξ, ζ are

$$F'_{\xi mb} = \frac{GH_T \sin\alpha}{zn\omega R_{cg}\Delta s} \qquad \text{(VII. 103)}$$

$$F_{\zeta mb} = \frac{GH_T \cos\alpha}{zn\omega R_{cg}\Delta s} \qquad \text{(VII. 104)}$$

where α = angle between the direction of the radius to each point and the axis ξ.

Apart from the peripheral force, the blade is also subject to radial and axial forces.

We obtain for the axial force the expression

$$F_\eta = \frac{G}{zng}(v_{\eta 1} - v_{\eta 2}) + H_d s_d - H_s s_s, \qquad \text{(VII. 105)}$$

The load per unit width of blade is

$$F'_\eta = \frac{G}{zng\Delta s}(v_{\eta 1} - v_{\eta 2}) + H_d \frac{s_d}{\Delta s} - H_s \frac{s_s}{\Delta s}, \qquad \text{(VII. 106)}$$

where $v_{\eta 1}$ and $v_{\eta 2}$ = projections of velocity v on the axis η at the leading and trailing edges for each flow filament;

s_d and s_s = area of horizontal projections of truncated cones with the generatrices on the leading and trailing edges, cut out by two adjacent flow surfaces;

H_d and H_s = head at leading and trailing edges.

The radial force exerted by the flow filament on the blade is

$$F_r = \frac{G}{zng}(v_{r1} - v_{r2}) + H_d s_{r1} - H_s s_{r2}, \qquad \text{(VII. 107)}$$

where s_{r1} and s_{r2} = areas of cylindrical projections of truncated cones with the generatrices on the leading and trailing edges cut out by two adjacent flow surfaces;

v_{r1} and v_{r2} = radial projections of velocity v at the leading and trailing edges, for each flow filament.

The load per unit width of blade is

$$F_r' = \frac{G}{zng\Delta s}(v_{r1} - v_{r2}) + \frac{H_d s_{r1}}{\Delta s} - \frac{H_s s_{r2}}{\Delta s}. \qquad \text{(VII. 108)}$$

The projections upon axes ξ and ζ are

$$F_{r\xi}' = \frac{G}{zng\Delta s}(v_{r1} - v_{r2})\cos\alpha + \left(\frac{H_d s_{r1}}{\Delta s} - \frac{H_s s_{r2}}{\Delta s}\right)\cos\alpha; \qquad \text{(VII. 109)}$$

$$F_{r\zeta}' = \frac{G}{zng\Delta s}(v_{r1} - v_{r2})\sin\alpha + \left(\frac{H_d s_{r1}}{\Delta s} - \frac{H_s s_{r2}}{\Delta s}\right)\sin\alpha. \qquad \text{(VII. 110)}$$

The components of the hydrodynamic loads per unit blade width along the axes ξ, η, and ζ are thus:

$$F_\xi = \frac{G}{zn\Delta s}\left[\frac{H_T}{\omega R_{cg}}\sin\alpha + \frac{1}{g}(v_{r1} - v_{r2})\cos\alpha\right] + \left(\frac{H_d s_{r1}}{\Delta s} - \frac{H_s s_{r2}}{\Delta s}\right)\cos\alpha; \qquad \text{(VII. 111)}$$

$$F_\eta = \frac{G}{zng\Delta s}(v_{\eta 1} - v_{\eta 2}) + H_d\frac{s_d}{\Delta s} - H_s\frac{s_s}{\Delta s}; \qquad \text{(VII. 112)}$$

$$F_\zeta = \frac{G}{zn\Delta s}\left[\frac{-H_T}{\omega R_{cr}}\cos\alpha + \frac{1}{g}(v_{r1} - v_{r2})\sin\alpha\right] + \left(\frac{H_d s_{r1}}{\Delta s} - \frac{H_s s_{r2}}{\Delta s}\right)\sin\alpha. \qquad \text{(VII. 113)}$$

Loads and stresses were determined at the LMZ by the above formulas (VII. 111), (VII. 112), and (VII. 113), for the blades of the same runner, under the assumptions of irrotational or uniform-velocity flow in the runner. Although the resulting loads were different, the stresses were practically the same, thus proving that the stresses in the blades depend very little on the distribution of velocities.

Calculation of the runner band. In calculating the runner, the forces and moments exerted by the blades on the upper and lower bands must be

determined. Apart from these, the bands are subject to centrifugal forces and pressure drop.

The stresses in the bands may be determined separately for each loading pattern, and totalled afterwards. The order of calculation is as follows:

The blades exert upon the band a system of twisting moments whose vectors are directed along the tangent to the band axis, as well as forces that cause tension and bending

$$M = -L_T \text{ and } T = v_r.$$

Apart from these forces, the band is subject to a system of moments $M_1 = -L_\eta$, whose vectors are parallel to the turbine center line, and to centrifugal forces due to the rotation of the band.

The stresses in the band due to centrifugal forces are determined by the formula

$$\sigma = \frac{R_m G \omega^2}{2\pi g F}, \qquad \text{(VII. 114)}$$

where ω = angular velocity of the runner;
R_m = mean radius of the band;
G = weight of the band;
F = cross-sectional area of the band.

The stresses due to the twisting moment exerted upon the band are determined by the formula for the torsion of rings /90/

$$\sigma = \frac{Mnh}{4\pi J_{max}}, \qquad \text{(VII. 115)}$$

where h = height of the band;
J_{max} = maximum moment of inertia of the band cross section;
n = number of blades.

The stresses due to the action of radial forces upon the band may be obtained from the formula for closed curved beams.

The bending stresses at the blades

$$\sigma = \frac{TR_m b}{12 J_{min}} \theta, \qquad \text{(VII. 116)}$$

where b = mean thickness of the band;
J_{min} = minimum moment of inertia of the band section;
$\theta = \frac{\pi}{n}$.

At the sections between blades, the stresses are

$$\sigma = \frac{TR_m b}{24 J_{min}} \theta. \qquad \text{(VII. 117)}$$

The tensile stresses in the band, due to force T are

$$\sigma = \frac{1}{2} \cdot \frac{T}{F} \cdot \frac{1}{\sin\theta};$$

$$T = -(v_\xi \cos\alpha + v_\zeta \sin\alpha). \qquad \text{(VII. 118)}$$

The stresses due to the moments L_η may be calculated from the formula

$$\sigma = \frac{M_1 b}{2J_{\min}}\left[0.3183\cos\beta' \sum_{i=1}^{n} \sin i\theta - \sin\beta' \sum_{i=1}^{n} \cos i\theta + \right.$$
$$\left. + \frac{\theta}{2}\sum_{i=1}^{n}\left(1 - \frac{\beta'}{2}z\right) - \frac{h}{2}\right] \qquad \text{(VII. 119)}$$

(the formula is taken from the "Handbook for Strength Calculation of Aircraft" /80/),

where β' = central angle measured from the junction between blade and band: $0 < \beta' < \theta$.

The inner band is subject to the load exerted by blades, water pressure and centrifugal forces. The effect of the latter at normal speed is small.

The forces exerted by the blades upon the band form a system of forces and moments which, combined with the reactions in the bolts of the shaft flange, tend to twist the band.

The stresses caused by the twisting of the upper band are determined from the formula

$$\sigma = \frac{M\left(y - \frac{m}{l}\right)}{r\left[\left(n - \frac{m^2}{l}\right) + \frac{1}{2\pi}\cdot\frac{n_2 F_2 h_2^2}{l_2}\right]}, \qquad \text{(VII. 120)}$$

where y = coordinate of the calculation point with respect to the adopted axis;

r = radius of the calculation point with respect to the turbine axis;

$$l = 2\int_{r_1}^{r_2} \frac{y_2 - y_1}{r}\,dr;$$

$$m = \int_{r_1}^{r_2} \frac{y_2^2 - y_1^2}{r}\,dr;$$

$$n = \frac{2}{3}\int_{r_1}^{r_2} \frac{y_2^3 - y_1^3}{r}\,dr.$$

$\frac{1}{2\pi}\cdot\frac{n_2 F_2 h_2^2}{l_2}$ — allows for the effect of the connection of the inner band with the shaft flange on the rigidity;

n_2 = number of bolts;

F_2 = cross-sectional area of bolt;

h_2 = distance between the flange edge and the bolted joint between runner and shaft;

l_2 = total bolt length;

M = bending moment acting at the section considered.

Subscript 1 indicates the lower side of an elementary rectangle of the band cross section, subscript 2 — the upper one.

Several runners were calculated at the LMZ by the above method. The results showed that under normal operating conditions the stresses due to

centrifugal forces are small, and the calculation may be performed for the hydrodynamic load only. At runaway speed the stresses due to centrifugal forces increase considerably, but, since these are emergency conditions, higher stresses may be permitted.

The maximum stresses occur at the joints between the blades and the lower and upper bands.

The stress distribution at the most critical section depends on the geometry of the section.

The stresses in the lower band being rather small, the band may be relatively thin.

At the upper band, the increase in conicity of the streamlined surface causes a stress concentration in the blade trailing edge close to the band and a reduction of the load on the leading edge. Consequently, a reduction in the inner-band conicity strengthens the blade without appreciably lowering the strength of the band.

The results of runner-strength calculation, compared with experimental data obtained by model tests and field measurements, turned out to be satisfactory.

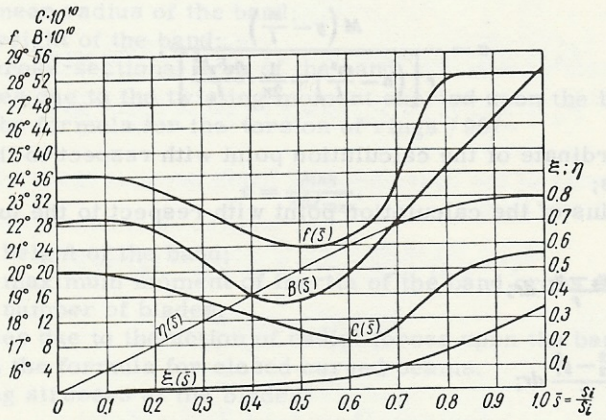


FIGURE VII. 25. Dependence of f, B, C, η and ξ on $\bar{s}$

Thus, for instance, with the RO-640 runner, the calculated maximum stresses in the blade-trailing edge caused by centrifugal forces were σ = = 1150 kg/cm^2 and the experimental stresses σ = 1200 kg/cm^2; at the leading edge, the calculated stresses were σ = 580 kg/cm^2, the experimental ones σ = 700 kg/cm^2. With the RO-662 runner, the calculated stresses were σ = 1600 kg/cm^2, the experimental, σ = 1360 kg/cm^2. With the RO-123 runner for the turbines of the Dnieper power plant, the calculated maximum stresses caused by hydrodynamic loads were σ = 580 kg/cm^2 and the measured stresses σ = 670 kg/cm^2. The following example illustrates the calculation made at the LMZ by the method described above.

Strength calculation of the blade of the medium-head RO-697 runner by the slender bar method:

Runner diameter D_1 = 750 cm

Number of blades z = 14

TABLE VII. 3

Variation of areas, moments of inertia, rotation angles and rigidities along the bar axis

Sections	s_l cm	$\frac{s_l}{s_L}$	f degrees	F cm^2	J_x cm^4	J_y cm^4	J_p cm^4	A kg cm^2	B kg cm^2	C kg cm^2
I	0	0	24	2960	$7.7 \cdot 10^6$	$13.5 \cdot 10^4$	$783.5 \cdot 10^4$	$1618 \cdot 10^{10}$	$28.4 \cdot 10^{10}$	$19.9 \cdot 10^{10}$
II	47.2	0.1275	24	2960	$7.7 \cdot 10^6$	$13.5 \cdot 10^4$	$783.5 \cdot 10^4$	$1618 \cdot 10^{10}$	$28.4 \cdot 10^{10}$	$19.9 \cdot 10^{10}$
III	183	0.494	21	2420	$6.25 \cdot 10^6$	$7.3 \cdot 10^4$	$632.3 \cdot 10^4$	$1312 \cdot 10^{10}$	$15.3 \cdot 10^{10}$	$11.0 \cdot 10^{10}$
IV	250	0.673	22.5	2510	$8.88 \cdot 10^6$	$11.69 \cdot 10^4$	$899.7 \cdot 10^4$	$1865 \cdot 10^{10}$	$24.5 \cdot 10^{10}$	$8.95 \cdot 10^{10}$
V	308	0.812	28	3270	$11.92 \cdot 10^6$	$17.9 \cdot 10^4$	$1209.9 \cdot 10^4$	$2508 \cdot 10^{10}$	$37.6 \cdot 10^{10}$	$19.2 \cdot 10^{10}$
VI	371	1.000	28	3680	$16.10 \cdot 10^6$	$25.45 \cdot 10^4$	$1635.45 \cdot 10^4$	$3380 \cdot 10^{10}$	$53.5 \cdot 10^{10}$	$22.8 \cdot 10^{10}$

$A = J_x E$ $\quad k_1 = 7.5$ $\quad E = 2.1 \cdot 10^6$

$B = J_y E$ $\quad k_2 = 56.25$ $\quad G = 0.8 \cdot 10^6$

$C = \frac{F^4 G}{4\pi^2 J_p}$ $\quad k_4 = 3164$

Maximum runner radius R_1 = 395 cm

Length of bar axis s_L = 371 cm

Angle between axes ξ and r for $s = s_L$ $\alpha = 12°30'$.

The variation of areas, moments of inertia, rotation angles, and rigidities along the bar axis for six blade cross sections are listed in Table VII. 3. The sections are numbered beginning from the upper band. The variation of f, B, C, η and ξ with respect to s is given in the chart in Figure VII. 25.

Calculation of stresses due to centrifugal forces. The centrifugal forces acting upon the blade are determined by formulas (VII. 96) and (VII. 97).

The determination of stresses due to centrifugal forces that occur at runaway speed is set forth in Tables VII. 4 to VII. 13.

TABLE VII. 4

Components along axes ξ and ζ of the centrifugal force acting on the blade

Section	φ	R_1	q	$\sin\varphi$	$\cos\varphi$	q_ξ	q_ζ	F cm^2
I	19°	268	$-6.35\omega^2$	0.3256	0.9455	$-6.00\omega^2$	$-2.07\omega^2$	2960
II	19°	268	$-6.35\omega^2$	0.3256	0.9455	$-6.00\omega^2$	$-2.07\omega^2$	2960
III	18°40′	275	$-5.33\omega^2$	0.3201	0.9474	$-5.05\omega^2$	$-1.70\omega^2$	2420
IV	17°50′	295	$-5.92\omega^2$	0.3062	0.9520	$-5.63\omega^2$	$-1.81\omega^2$	2510
V	16°	326	$-8.53\omega^2$	0.2756	0.9613	$-8.20\omega^2$	$-2.35\omega^2$	3270
VI	12°30′	395	$-11.65\omega^2$	0.2164	0.9763	$-11.40\omega^2$	$-2.52\omega^2$	3680

The intensities of loads q_ξ and q_ζ for different values of x, are given in Table VII. 5

TABLE VII. 5

Values of load intensities

x	$\frac{q_\xi}{\omega^2}$	$\frac{q_\zeta}{\omega^2}$	x	$\frac{q_\xi}{\omega^2}$	$\frac{q_\zeta}{\omega^2}$
1	2	3	0.55	—5.10	—1.60
0.05	—6.00	—2.00	0.65	—5.50	—1.75
0.15	—5.90	—1.90	0.75	—7.00	—2.10
0.25	—5.70	—1.85	0.85	—8.80	—2.50
0.35	—5.40	—1.80	0,95	—10.70	—2.50
0.45	—5.20	—1.75			

TABLE VII. 6

Computation of integrals C_1 to C_9, C_6 to C_{23} and their combinations occurring in equations (VII. 94), used for determining the coefficients a_{ij}; b_{ij}; d_i

x	$\frac{C_1}{s_L}$	$\frac{C_2}{s_L}$	$\frac{C_3}{s_L}$	$\frac{C_4}{s_L}$	$\bar{\eta}$ [3]	$\bar{\eta}F_\xi$	$\int$ [6]	$\frac{C_5}{s_L^2}$ [5] − [7]	$\frac{C_6}{s_L}$	ξ [3]	ξF_ξ	$\int$ [11]	$\frac{C_7}{s_L^2}$ [10] − [12]	ξ [2]	ξF_η	$\int$ [15]	η [1]	ηF_ξ	$\int$ [18]	$\frac{C_8}{s_L^2}$
	1	2	3	4	5	6	7	8	9	10	11	12	13	14	15	16	17	18	19	20
0.05	0	0	0	0.0500	0	−0.1000	0	0	0	0	0	0	0	0	0	0	0	−0.3000	0	0
0.15	−0.6000	0	−0.2000	0.1500	−0.0200	−0.2850	−0.0100	−0.0100	−0.0050	0.0005	0.0025	0	0.0005	0	0	0	−0.0600	−0.8850	−0.0300	0.0300
0.25	−1.1900	0	−0.3900	0.2500	−0.0780	−0.4625	−0.0385	−0.0395	−0.0100	0.0029	0.0185	0.0010	0.0019	0	0	0	−0.2380	−1.4250	−0.1185	0.1195
0.35	−1.7600	0	−0.5750	0.3500	−0.1725	−0.6300	−0.0848	−0.0877	−0.0150	0.0072	0.0270	0.0028	0.0044	0	0	0	−0.5280	−1.8900	−0.2610	0.2670
0.45	−2.300	0	−0.7550	0.4500	−0.3020	−0.7875	−0.1478	−0.1542	−0.0200	0.0132	0.0350	0.0055	0.0077	0	0	0	−0.9200	−2.3400	−0.4500	0.4700
0.55	−2.8200	0	−0.9300	0.5500	−0.4650	−0.8800	−0.2265	−0.0285	−0.0350	0.0256	0.0560	0.0090	0.0166	0	0	0	−1.4100	−2.8050	−0.6840	0.7260
0.65	−3.3300	0	−1.0900	0.6400	−0.6486	−1.1200	−0.3145	−0.3341	−0.0750	0.0600	0.1312	0.0146	0.0454	0	0	0	−1.9814	−3.5200	−0.9645	1.0169
0.75	−3.8800	0	−1.2650	0.7250	−0.8634	−1.5225	−0.4265	−0.4369	−0.1300	0.1297	0.2730	0.0277	0.1020	0	0	0	−2.6481	−5.0750	−1.3165	1.3316
0.85	−4.5800	0	−1.4750	0.7800	−1.1099	−1.9500	−0.5788	−0.5311	−0.200	0.2434	0.5000	0.0550	0.1884	0	0	0	−3.4464	−6.8640	−1.8240	1.6224
0.95	−5.4600	0	−1.7250	0.7950	−1.3584	−1.9875	−0.7738	−0.5846	−0.2900	0.4226	0.7250	0.1050	0.3176	0	0	0	−4.2998	−8.5065	−2.5104	1.7894
	−6.5300	0	−1.9750	0.7950	−1.5751	−1.9875	−0.9725	−0.6026	−0.2900	0.6320	0.7250	0.1775	0.4545		0	0	−5.2077		−3.3610	1.8467

Formulas:

$$\frac{C_1}{s_L} = 0.1 \sum F_\xi \qquad \frac{C_4}{s_L} = \bar{\eta} \qquad \frac{C_7}{s_L^2} = [10] - [12]$$

$$\frac{C_2}{s_L} = 0.1 \sum F_\eta \qquad \frac{C_5}{s_L^2} = [5] - [7] \qquad \frac{C_3}{s_L^2} = [14] - [16] - [17] + [19]$$

$$\frac{C_3}{s_L} = 0.1 \sum F_\zeta \qquad \frac{C_6}{s_L} = \bar{\xi} \qquad C_8 = C_6$$

TABLE VII. 7

Computation of integrals C_1 to C_8, C_9 to C_{23} and their combinations occurring in equations (VII. 94) used for determining the coefficients a_{ij}; b_{ij}; d_i

x	$\eta^2 \sin^2 f \times \frac{C}{B} \times \frac{8}{}$	$\boxed{11} + \bar{\xi}^2$	$10^{10} - C_9$	$1 - \sin^2 f \times \frac{C}{B} \times$	$\boxed{\eta^2 \cdot 14}$	$10^{10} C_{10}$	$\bar{\eta} \sin f \times \cos f \times \frac{C}{B} \times$	$10^{10} C_{11}$	$-\bar{\xi} \sin f \times \cos f \times \frac{C}{B} \times$	$10^{10} C_{13}$	$\cos^2 f \cdot \frac{C}{B}$	$10^{10} C_{14}$	$\bar{\xi}^2 \sin^2 f \times \frac{C}{B} \times$	$\boxed{13} + \bar{\eta}^2$	$10^{10} C_{12}$
	1	2	3	4	5	6	7	8	9	10	11	12	13	14	15
0.05	0.1161	0.1161	0.0058	0.8839	0	0	0.2608	0.0130	0	0	0.5857	0.0293	0	1.0000	0.0500
0.15	0.1100	0.1125	0.0059	0.8900	—0.0445	—0.0023	0.2501	0.0130	0.0125	0.0007	0.5684	0.0296	0.0003	1.0003	0.0521
0.25	0.1009	0.1034	0.0061	0.8991	—0.0450	—0.0026	0.2379	0.0140	0.0119	0.0077	0.5605	0.0330	0.0003	1.0003	0.0588
0.35	0.1034	0.1059	0.0076	0.8966	—0.0448	—0.0032	0.2559	0.0183	0.0128	0.0009	0.6334	0.0452	0.0003	1.0003	0.0714
0.45	0.1017	0.1042	0.0087	0.8983	—0.0449	—0.0037	0.2615	0.0218	0.0131	0.0011	0.6725	0.0560	0.0003	1.0003	0.0833
0.55	0.0767	0.1667	0.0167	0.9233	—0.2770	—0.0277	0.1980	0.0198	0.0594	0.0059	0.5115	0.0512	0.0069	1.0069	0.1007
0.65	0.0405	0.2905	0.0323	0.9439	—0.4012	—0.0446	0.1181	0.0131	0.0694	0.0077	0.3439	0.0382	0.0140	0.7365	0.0818
0.75	0.0426	0.4026	0.0287	0.9131	—0.3835	—0.0274	0.1234	0.0088	0.1058	0.0076	0.3575	0.0255	0.0313	0.5213	0.0372
0.85	0.0097	0.6497	0.0325	0.8925	—0.2142	—0.0107	0.0607	0.0030	0.1618	0.0081	0.3803	0.0190	0.0688	0.1588	0.0079
0.95	0.0022	1.4422	0.0656	0.9030	—0.1625	—0.0074	0.0274	0.0012	0.2189	0.0100	0.3431	0.0156	0.1397	0.1622	0.0074

x	$\frac{C_{13}}{s_L} \cdot 10^{10}$	$\frac{C_{14}}{s_L} \cdot 10^{10}$	$\frac{C_{15}}{s_L} \cdot 10^{10}$	$\frac{C_{16}}{s_L} \cdot 10^{10}$	$\frac{C_{17}}{s_L} \cdot 10^{10}$	$\frac{C_{18}}{s_L} \cdot 10^{10}$	$\frac{C_{19}}{s_L} \cdot 10^{10}$	$\frac{C_{20}}{s_L} \cdot 10^{10}$	$\frac{C_{21}}{s_L} \cdot 10^{10}$	$\frac{C_{22}}{s_L} \cdot 10^{10}$	$\frac{C_{23}}{s_L} \cdot 10^{10}$	$\frac{1}{s_L}(\cos\alpha \times C_{17} + \sin\alpha \times C_{23}) 10^{10}$	$\frac{1}{s_L}(\cos\alpha \times C_{18} + \sin\alpha \times C_{22}) 10^{10}$	$\frac{1}{s_L}(\cos\alpha \times C_{19} + \sin\alpha \times C_{24}) 10^{10}$	$(\cos\alpha C_{22} - \sin\alpha C_{16}) \times \frac{1}{s_L} 10^{10}$	$(\cos\alpha C_{23} - \sin\alpha C_{15}) \times \frac{1}{s_L} 10^{10}$	$(\cos\alpha C_{24} - \sin\alpha C_{17}) \times \frac{1}{s_L} \times$
	16	17	18	19	20	21	22	23	24	25	26	27	28	29	30		
0.05	0.0006	0	0.0015	—	—	—	—0.0003	0	—0.0006	0.0014	0	0.0005	0	—0.0004	—0.0009		
0.15	0.0020	0.0001	0.0044	—	—	—	—0.0009	0	—0.0020	0.0039	0.0001	0.0018	0	—0.0013	—0.0030		
0.25	0.0035	0.0002	0.0082	—	—	—	—0.0015	0	—0.0035	0.0072	0.0002	0.0031	0	—0.0023	—0.0052		
0.35	0.0064	0.0003	0.0158	—	—	—	—0.0027	0	—0.0064	0.0140	0.0003	0.0056	—0.0001	—0.0040	—0.0096		
0.45	0.0098	0.0005	0.0252	—	—	—	—0.0038	0	—0.0098	0.0225	0.0005	0.0088	—0.0001	—0.0058	—0.0151		
0.55	0.0109	0.0032	0.0282	—	—	—	—0.0082	0.0117	—0.0111	0.0251	0.0056	0.0088	—0.0107	—0.0104	—0.0169		
0.65	0.0084	0.0049	0.0244	—	—	—	—0.0174	0.0224	—0 0090	0.0219	0.0096	0.0044	0.0208	—0.0188	—0.0141		
0.75	0.0064	0.0055	0.0185	—	—	—	—0.0172	0.0151	—0.0074	0.0165	0.0087	0.0025	0.0135	—0.0182	—0.0112		
0.85	0.0023	0.0063	0.0148	—	—	—	—0.0233	0.0067	—0.0039	0.0136	0.0076	—0.0028	0.0051	—0.0232	—0.0070		
0.95	0.0010	0.0080	0.0124	—	—	—	—0.0501	0.0038	—0.0039	0.0113	0.0086	—0.0098	0.0020	—0.0491	—0.0065		

Note: there are no entries in columns 19, 20 and 21, since they are not used in the present calculation..

$$C_9 = \boxed{2}\frac{1}{C}$$

$$C_{10} = \boxed{5}\frac{1}{C}$$

$$C_{11} = \boxed{7}\frac{1}{C}$$

$$C_{12} = \boxed{14}\frac{1}{C}$$

$$C_{13} = \boxed{9}\frac{1}{C}$$

$$C_{14} = \boxed{11}\frac{1}{C}$$

$$\frac{C_{15}}{s_L} = C_{11}\bar{\eta}$$

$$\frac{C_{16}}{s_L} = C_{13}\bar{\eta}$$

$$\frac{C_{17}}{s_L} = C_{14}\bar{\eta}$$

$$\frac{C_{18}}{s_L} = C_{11}\bar{\xi}$$

$$\frac{C_{19}}{s_L} = C_{13}\bar{\xi}$$

$$\frac{C_{20}}{s_L} = C_{14}\bar{\xi}$$

$$\frac{C_{21}}{s_L} = (\xi C_{10} - \bar{\eta} C_9)$$

$$\frac{C_{22}}{s_L} = (\xi C_{13} - \bar{\eta} C_{10})$$

$$\frac{C_{23}}{s_L} = (\xi C_{13} - \bar{\eta} C_{11})$$

$\sin\alpha = 0.2164$

$\cos\alpha = 0.9763$

TABLE VII. 8

Computation of integrals C_1 to C_8, C_9 to C_{23} and their combinations occurring in equations (VII. 94), used for determining the coefficients a_{ij}; b_{ij}; d_i

1	$0.1 \sum \boxed{3,6}$	0.021	17	$0.1\, s_L^2 \sum \boxed{20,3};\ \boxed{12,6}$	3399.7327	33	$0.1\, s_L \sum \boxed{26,6};\ \boxed{9,5}$	—83.961
2	$0.1 \sum \boxed{6,6}$	—0.013	18	$0.1\, s_L^2 \sum \boxed{8,3};\ \boxed{8,6}$	—344.1025	34	$0.1\, s_L^2 \sum \boxed{27,6};\ \boxed{4,5}$	89.4666
3	$0.1 \sum \boxed{8,6}$	0.0126	19	$0.1\, s_L^2 \sum \boxed{10,6};\ \boxed{13,5}$	110.1128	35	$0.1\, s_L^2 \sum \boxed{28,6};\ \boxed{9,5}$	—72.9497
4	$0.1 \sum \boxed{15,6}$	0.0551	20	$0.1\, s_L \sum \boxed{15,6};\ \boxed{9,5}$	—0.8088	36	$0.1\, s_L^2 \sum \boxed{29,6};\ \boxed{4,5}$	—1278.6849
5	$0.1 \sum \boxed{10,6}$	0.00427	21	$0.1\, s_L \sum \boxed{6,6};\ \boxed{4,5}$	—3.0311	37	$0.1\, s_L^2 \sum \boxed{25,6};\ \boxed{9,5}$	—156.9107
6	$0.1 \sum \boxed{12,6}$	0.03426	22	$0.1\, s_L \sum \boxed{10,6};\ \boxed{9,5}$	—0.2337	38	$0.1\, s_L^2 \sum \boxed{30,6};\ \boxed{9,5}$	94.9723
7	$0.1\, s_L \sum \boxed{6,6};\ \boxed{9,5}$	0.4563	23	$0.1\, s_L \sum \boxed{10,6};\ \boxed{4,5}$	1.0759	39	$0.1\, s_L^2 \sum \boxed{25,6};\ \boxed{4,5}$	1058.4593
8	$0.1\, s_L \sum \boxed{8,6};\ \boxed{4,5}$	5.0975	24	$0.1\, s_L^2 \sum \boxed{6,6};\ \boxed{8,5}$	688.205	40	$0.1\, s_L^2 \sum \boxed{30,6};\ \boxed{4,5}$	—674.4409
9	$0.1\, s_L \sum \boxed{8,6};\ \boxed{9,5}$	—0.1744	25	$0.1\, s_L^2 \sum \boxed{15,6};\ \boxed{13,5}$	289.0461	41	$0.1\, s_L^3 \sum \boxed{27,6};\ \boxed{8,5}$	—3574.5368
10	$0.1\, s_L \sum \boxed{8,6};\ \boxed{4,5}$	1.9032	26	$0.1\, s_L^2 \sum \boxed{10,6};\ \boxed{20,5}$	812.0819	42	$0.1\, s_L^3 \sum \boxed{26,6};\ \boxed{13,5}$	37787.9601
11	$0.1\, s_L^2 \sum \boxed{3,6};\ \boxed{8,5}$	—1257.7635	27	$0.1\, s_L \sum \boxed{25,6}$	5.0975	43	$0.1\, s_L^3 \sum \boxed{25,6};\ \boxed{20,5}$	694481.4296
12	$0.1\, s_L^2 \sum \boxed{6,6};\ \boxed{13,5}$	—189.394	28	$0.1\, s_L \sum \boxed{30,6}$	—3.3204	44	$0.1\, s_L^3 \sum \boxed{29,6};\ \boxed{8,5}$	321708.3093
13	$0.1\, s_L^2 \sum \boxed{8,6};\ \boxed{20,5}$	1053.5042	29	$0.1\, s_L \sum \boxed{26,6}$	—1.5285	45	$0.1\, s_L^3 \sum \boxed{28,6};\ \boxed{13,5}$	30636.8866
14	$0.1\, s_L \sum \boxed{10,6};\ \boxed{9,5}$	—0.2337	30	$0.1\, s_L \sum \boxed{28,6}$	—1.9255	46	$0.1\, s_L^3 \sum \boxed{30,6};\ \boxed{20,5}$	—434050.8935
15	$0.1\, s_L \sum \boxed{12,6};\ \boxed{9,5}$	—0.6901	31	$0.1\, s_L \sum \boxed{27,6}$	—0.8496		—	—
16	$0.1\, s_L \sum \boxed{4,5};\ \boxed{12,6}$	5.6948	32	$0.1\, s_L \sum \boxed{29,6}$	—4.9528		—	—

$s_L = 371$ cm; $s_L^2 = 137\,641$; $s_L^3 = 51\,064\,811$

Note: The figures in boxes in Tables VII. 8 and VII. 9 indicate: before the comma, the number of the column; after the comma, the number of the table.

TABLE VII. 9

Computation of coefficients a_{ij}; b_{ij}; d_i

1	$a_{11} = \boxed{3,7}$	0.0126	17	$a_{33} = \boxed{31,7} - \bar{\xi} s_L \sin L \boxed{2,7}$	0.4843
2	$a_{12} = \boxed{2,7}$	−0.013	18	$b_{31} = \frac{\gamma}{s_L} \sin\alpha + \boxed{33,7} - \boxed{34,7} - \bar{\xi} s_L \left(\boxed{20,7} - \boxed{21,7}\right) \sin\alpha$	−110.4357
3	$a_{13} = \boxed{1,7}$	0.021	19	$b_{32} = -\boxed{37,7} + \bar{\xi} s_L \sin\alpha \boxed{14,7}$	163.4776
4	$b_{11} = \boxed{7,7} - \boxed{8,7}$	−4.4612	20	$b_{33} = \frac{\gamma}{s_L} \cos\alpha + \boxed{39,7} - \bar{\xi} s_L \sin\alpha \boxed{23,7}$	1091.1568
5	$b_{12} = -\boxed{9,7}$	0.1744	21	$d_3 = \frac{-\gamma}{s_L} (\cos\alpha C_1 + \sin\alpha C_3) + \boxed{41,7} - \boxed{42,7} + \boxed{43,7} - \bar{\xi} s_L \sin\alpha \left(\boxed{24,7} - \boxed{25,7} + \boxed{26,7}\right)$	693514
6	$b_{13} = \boxed{10,7}$	1.9032	22	$a_{31} = \boxed{28,7} - (R_1 + \bar{\xi} s_L \cos\alpha) \boxed{5,7}$	−4.4738
7	$d_1 = \boxed{11,7} - \boxed{12,7} + \boxed{13,7}$	−14.8653	23	$a_{32} = \boxed{30,7} - (R_1 + \bar{\xi} s_L \cos\alpha) \boxed{4,7}$	−12.8538
8	$a_{21} = \boxed{6,7}$	0.0343	24	$a_{33} = \boxed{32,7} - (R_1 + \bar{\xi} s_L \cos\alpha) \boxed{2,7}$	−1.4628
9	$a_{22} = \boxed{5,7}$	0.0043	25	$b_{41} = \boxed{35,7} - \boxed{36,7} - (R_1 + \bar{\xi} s_L \cos\alpha) \twoheadrightarrow\twoheadleftarrow \left(\boxed{20,7} - \boxed{21,7}\right)$	609.6534
10	$a_{23} = \boxed{3,7}$	0.0126	26	$b_{42} = -\boxed{38,7} + (R_1 + \bar{\xi} s_L \cos\alpha) \boxed{14,7}$	−157.657
11	$b_{21} = \boxed{14,7} - \boxed{10,7}$	−2.1369	27	$b_{43} = \boxed{40,7} - (R_1 + \bar{\xi} s_L \cos\alpha) \boxed{23,7}$	−963.0268
12	$b_{22} = -\boxed{15,7}$	0.6901	28	$d_4 = \boxed{44,7} - \boxed{45,7} + \boxed{46,7} - (R + \bar{\xi} s_L \cos\alpha) \twoheadrightarrow\twoheadleftarrow \left(\boxed{24,7} - \boxed{25,7} + \boxed{26,7}\right)$	−467869.4414
13	$b_{23} = \boxed{16,7}$	5.6948	29	$b_{51} = C_6 - R_1 \cos\alpha$	−515.4885
14	$d_2 = \boxed{17,7} + \boxed{18,7} - \boxed{19,7}$	2945.5174	30	$b_{53} = R_1 \sin\alpha$	85.478
15	$a_{31} = \boxed{27,7} - \bar{\xi} s_L \sin\alpha \boxed{5,7}$	5.2183	31	$d_5 = -C_7 + R_1 C_3 \cos\alpha - R_1 C_1 \sin\alpha$	−138043.2373
16	$a_{32} = \boxed{29,7} - \bar{\xi} s_L \sin\alpha \boxed{4,7}$	3.0768			

TABLE VII. 10

System of equations for determining the arbitrary constants

$\frac{a_{11}}{0.0126}$	$L_{0\zeta}+$	$\frac{a_{12}}{-0.0130}$	$L_{0\eta}+$	$\frac{a_{13}}{0.0210}$	$L_{0\xi}+$	$\frac{b_{11}}{-4.6412}$	$v_{0\zeta}+$	$\frac{b_{13}}{1.9032}$	$v_{0\xi}+$	$\frac{d_1}{-14.8653}$	$=0$
$\frac{a_{21}}{0.0343}$	$L_{0\zeta}+$	$\frac{a_{22}}{0.0043}$	$L_{0\eta}+$	$\frac{a_{23}}{0.0126}$	$L_{0\xi}+$	$\frac{b_{21}}{-2.1369}$	$v_{0\zeta}+$	$\frac{b_{23}}{5.6948}$	$v_{0\xi}+$	$\frac{d_2}{2945.5174}$	$=0$
$\frac{a_{31}}{5.2183}$	$L_{0\zeta}+$	$\frac{a_{32}}{3.0768}$	$L_{0\eta}+$	$\frac{a_{33}}{0.4843}$	$L_{0\xi}+$	$\frac{b_{31}}{-110.4357}$	$v_{0\zeta}+$	$\frac{b_{33}}{1091.1568}$	$v_{0\xi}+$	$\frac{d_3}{693514.6246}$	$=0$
$\frac{a_{41}}{-4.4738}$	$L_{0\zeta}+$	$\frac{a_{42}}{-12.8538}$	$L_{0\eta}+$	$\frac{a_{43}}{-1.4628}$	$L_{0\xi}+$	$\frac{b_{41}}{609.6534}$	$v_{0\zeta}+$	$\frac{b_{43}}{-963.0268}$	$v_{0\xi}+$	$\frac{d_4}{-467869.4414}$	$=0$
$\frac{0}{0}$	$L_{0\zeta}+$	$\frac{1}{1}$	$L_{0\eta}+$	$\frac{0}{0}$	$L_{0\xi}+$	$\frac{b_{51}}{-515.4885}$	$v_{0\zeta}+$	$\frac{b_{53}}{85.4780}$	$v_{0\xi}+$	$\frac{d_5}{-138043.2373}$	$=0$

TABLE VII. 11

Solution of the system, by the Gauss method for determining arbitrary constants

$L_{0\zeta}$	$L_{0\eta}$	$L_{0\xi}$	$v_{0\zeta}$	$v_{0\xi}$	Free term	Σ
0.0126	—0.0130	0.0210	—4.6412	1.9032	—0.1487	—2.8661
0.0126	0.0074	0.0012	—0.2666	2.6338	16.7400	19.1285
0.0343	0.0043	0.0126	—2.1369	5.6948	29.4552	33.0643
0.0343	0.0202	0.0032	—0.7257	7.1699	45.5700	52.0719
0.0522	0.0308	0.0048	—1.1044	10.9116	69.3515	79.2465
1.0000	0.5900	0.0920	—21.1571	209.0345	1328.5727	1518.1321
0.0447	0.1285	0.0146	—6.0965	9.6303	46.7869	50.5085
0.0447	0.0264	0.0041	—0.9457	9.3438	59.3872	67.8605
0	0.1	0	—51.5488	8.5478	—138.0432	—180.9442
	1.0000	0	—515.4880	85.4780	—1380.4320	—1809.4420
	0.0204	—0.0198	4.3746	0.7306	+16.8887	+21.9945
	0.0204	0	—10.5160	1.7438	—28.1608	—36.9126
	0.0159	—0.0094	1.4112	1.4751	+16.1148	+19.0076
	0.0159	0	—8.1963	1.3591	—21.9489	—28.7701
	0.1021	0.0105	—5.1508	0.2865	—12.6003	—17.3520
	0.1021	0	—52.6313	8.7273	—140.9421	—184.7440

Table VII.11 cont.

$L_{0\zeta}$	$L_{0\eta}$	$L_{0\xi}$	$v_{0\zeta}$	$v_{0\xi}$	Free term	Σ
		0.0198	—14.8906	1.0132	—45.0495	—58.9071
		1.0000	—752.0505	51.1717	—2275.2272	—2975.1060
		0.0094	—9.6075	—0.1160	—38.0637	—47.7778
		0.0094	—7.0693	0.4810	—21.3871	—27.9660
		0.0105	47.4805	—8.4408	128.3418	167.3920
		0.0105	—7.8965	0.5373	—23.8899	—31.2386
			2.5382	0.5970	16.6766	19.8118
			1.0000	0.2352	6.5702	7.8054
			55.3700	—8.9778	152.2317	198.6309
			55.3770	13.0247	363.8380	432.2396
				—22.0025	—211.6063	—233.6087
				1	9.6174	10.6174
			1		4.3082	5.3082
		1			472.6181	473.6181
	1				—18.3173	—17.3173
1					—644.9348	—643.9348

$v_{0\xi} = -961.74$ $v_{0\eta} = 0$ $v_{0\zeta} = -430.82$
$L_{0\xi} = -47261.81$ $L_{0\eta} = 1831.73$ $L_{0\zeta} = 64493.48$

TABLE VII. 12

Calculation of the bending moments along the blade length

x	$C_{4}v_{0\xi}$	$C_5 - \boxed{12}$	L_ξ	$C_6 v_{0\xi}$	$\boxed{18} - C_7$	L_η	$C_4 v_{0\eta}$	$\boxed{18} + C_8$	$C_8 v_{0\eta}$	$\boxed{19} - C_6 v_{0\eta}$	L_ζ
1	2	3	4	5	6	7	8	9	10	11	12
0.05	—7992	7304	—39958	0	—28	—1860	—17840	—15775	—	—	48718
0.15	—23975	20562	—26500	799	634	—1198	—53521	—43225	—	—	21268
0.25	—39959	31205	—16057	1598	1158	—674	—89202	—63023	—	—	1470
0.35	—55942	39287	—7975	2398	1572	—260	—124882	—74161	—	—	—9668
0.45	—71925	44892	—2370	3197	1532	—300	—160563	—78254	—	—	—13761
0.55	—87909	48502	1240	5594	1327	—505	—196243	—76303	—	—	—11810
0.65	—102294	49233	1971	11988	1844	0	—228356	—66738	—	—	—2245
0.75	—115880	49262	2000	20778	793	—1000	—258684	—55388	—	—	9105
0.85	—124671	47895	633	31967	—2856	—4688	—278309	—43506	—	—	20987
0.95	—127068	45364	—1898	46352	—6777	—8609	—283661	—33430	—	—	31063

$L_\xi = L_{0\xi} + \boxed{3}$ $\quad L_\eta = L_{0\eta} + \boxed{6}$ $\quad L_\zeta = L_{0\zeta} + \boxed{11}$

TABLE VII. 13

Calculation of the stresses in the leading and trailing edges

s	L_ξ	L_η	L_ζ	$\cos(\xi, x)$	$\cos(\eta, x)$	$\cos(\zeta, x)$	$\cos(\xi, y)$	$\cos(\eta, y)$	$\cos(\zeta, y)$	L_x	L_y
1	2	3	4	5	6	7	8	9	10	11	12
0	—47 262	—1 832	64 493	—0.9136	0	0.4067	0.4067	0	0.9136	69 408	39 700
0.1275	—26 000	—1 700	27 000	—0.9136	—0.0365	0.4067	0.4067	0.0163	0.9136	34 798	14 065
0.4940	0	—1 000	—13 200	—0.9336	—0.1214	0.3584	0.3584	0.0466	0.9336	—4 610	—12 371
0.6730	2 500	—1 200	0	—0.7484	—0.4804	0.3827	0.3100	0.1990	0.9239	—1 295	536
0.8120	1 200	—3 000	17 000	—0.3974	—0.6358	0.4695	0.2113	0.3380	0.8830	9 412	14 251
1.000	—3 000	—11 000	37 500	—0.0883	—1.2362	0.4695	0.0470	0.6573	0.8830	31 469	25 930

$$L_x = L_\xi \cos(x,\xi) + L_\eta \cos(x,\eta) + L_\zeta \cos(x,\zeta)$$
$$L_y = L_\xi \cos(y,\xi) + L_\eta \cos(y,\eta) + L_\zeta \cos(y,\zeta)$$

J_x	J_y	x_1	y_1	x_2	y_2	$\frac{\sigma_{y_1}}{\omega^2}$	$\frac{\sigma_{y_2}}{\omega^2}$	$\frac{\sigma_{x_1}}{\omega^2}$	$\frac{\sigma_{x_2}}{\omega^2}$	$\frac{\sigma_1}{\omega^2}$	$\frac{\sigma_2}{\omega^2}$	σ_1 kg/cm^2	σ_2, kg/cm^2
13	14	15	16	17	18	19	20	21	22	23	24	25	26
$7.7 \cdot 10^6$	$13.5 \cdot 10^4$	20.6	—75.7	—15	—28.5	—6.07	4.42	—0.683	—0.258	—6.753	4.1620	—2600	1602
$7.7 \cdot 10^6$	$13.5 \cdot 10^4$	20.6	—75.7	—15	—28.5	—2.15	1.56	—0.344	—0.130	—2.494	1.4300	—960	550
$6.25 \cdot 10^6$	$7.3 \cdot 10^4$	18.7	—77.5	—12.7	—39.4	3.30	—2.15	0.057	0.029	3.357	—2.1210	1292	—817
$8.88 \cdot 10^6$	$11.69 \cdot 10^4$	21.4	—92.0	—13.3	—43.5	—0.098	0.061	0.014	0.008	—0.084	0.0690	—32	27
$11.95 \cdot 10^6$	$17.9 \cdot 10^4$	22.5	—97.0	—15.8	—20	—1.790	1.26	0.052	0.012	—1.738	1.2720	—669.0	490
$16.10 \cdot 10^6$	$25.45 \cdot 10^4$	25.5	—103	25	162	—2.59	2.54	0.127	—0.200	—2.463	2.3400	—948	901

σ_1 — stress in the leading edge;
σ_2 — stress in the trailing edge;
$n = 93.6$ rpm;
$n_r = 187$ rpm;
$\omega_r = 19.6$ 1/sec;
$\omega_r^2 = 385$ 1/sec^2.

For medium-head runners (H up to 100 m) with relatively short, wide blades, the slender-bar method yields satisfactory results which agree with those found experimentally. The method does not apply to high-head runners with long, narrow blades.

The construction of low-speed high-head runners is similar to that of centrifugal pump runners (Figure VII. 26); the "double calculation" method /81/ may therefore be used in calculating their strength. According to this method, the lower runner band is calculated as a freely rotating disk; the upper band is calculated by allowing for the centrifugal forces due to the blades. To simplify, one considers the blade mass as uniformly distributed over the lateral surface. Consequently, the upper band carries a certain part of the mass, of varying thickness, sometimes referred to as "lateral load".

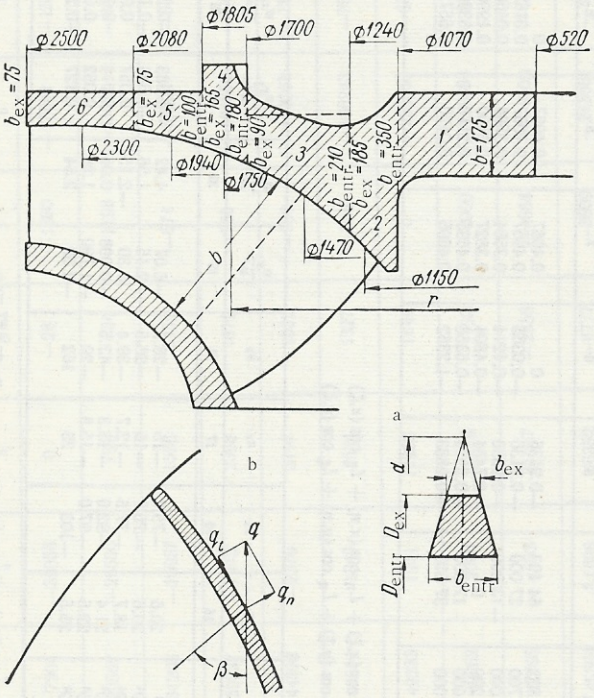


FIGURE VII. 26. Schematic diagram for the calculation of a high-head Francis runner

The runner blades are calculated as a beam supported at both ends, with loads uniformly distributed along the edges.

The order of calculation is shown below.

Runner band. For certain bands of conical shape and uniform thickness, with no lateral load acting, the stresses at any radius r are a linear function of the stresses σ_{r1} and σ_{t1} at a given radius r_1; i.e., if the radial

and tangential stresses — σ_{r1} and σ_{t1} — at a given radius r_1 are known, then σ_r and σ_t may be determined for any radius r.

$$\left.\begin{aligned}\sigma_r &= \alpha_r\sigma_{r1} + \alpha_t\sigma_{t1} + \alpha_c' T_d;\\ \sigma_t &= \beta_r\sigma_{r1} + \beta_t\sigma_{t1} + \beta_c' T_d.\end{aligned}\right\} \qquad \text{(VII. 121)}$$

With lateral load,

$$\left.\begin{aligned}\sigma_r &= \alpha_r\sigma_{ri} + \alpha_t\sigma_{ti} + \bar{\alpha}_c' T_d;\\ \sigma_t &= \beta_r\sigma_{ri} + \beta_t\sigma_{ti} + \bar{\beta}_c' T_d;\\ T &= \left(\frac{D}{1000}\cdot\frac{n}{1000}\right)^2,\end{aligned}\right\} \qquad \text{(VII. 122)}$$

where α_r, α_t, α_c', β_r, β_t, β_c' $\bar{\alpha}_c'$, $\bar{\beta}_c'$ = coefficients (see below);

D = diameter, mm;

n = rpm;

T_d — relates to diameter d (In Figure VII. 26,a).

According to this, the steps to be taken are as follows:

1. Divide the band into sections of the simplest conical shape and uniform thickness.

2. At first (i.e., for a rotating band), assume arbitrary tangential stresses at the inner diameter σ_{t0}' of the band, taking $\sigma_{r0}' = \sigma_{r0}$. Find the stresses at the beginning and end of each section, and in particular, several values for the radial stresses σ_{rd}' at the outer diameter of the band.

3. Secondly, for a stationary band (n = 0), assume a certain arbitrary tangential stress σ_{t0}'' and, supposing that σ_{r0}'' = 0, find the stresses σ_r'' and σ_t'' at the beginning and end of each section, and in particular at the outer diameter of the band $\sigma_r' = \sigma_{rd}''$.

4. Determine the maximum tangential stresses in the disk

$$\sigma_{t0} = \sigma_{t0}' - \varphi\sigma_{t0}'', \qquad \text{(VII. 123)}$$

where

$$\varphi = \frac{\sigma_{rd}'}{\sigma_{rd}''}.$$

5. Refined stress calculations. If the band thickness changes abruptly from b to b^*, the stresses at section b^* will be expressed in terms of stresses at section b by

$$\left.\begin{aligned}\sigma_r^* &= \frac{b}{b^*}\sigma_r;\\ \sigma_t^* &= \sigma_t + \mu(\sigma_r^* - \sigma_r),\end{aligned}\right\} \qquad \text{(VII. 124)}$$

where μ = Poisson's ratio.

6. Determine the coefficients α_r, α_t, β_r, β_t, α_c', β_c', $\bar{\alpha}_c'$, $\bar{\beta}_c'$:

a) for the band portion of uniform thickness

$$\alpha_r = \beta_t = 0.5\,(1 + x^2); \qquad \text{(VII. 125)}$$

$$\alpha_t = \beta_r = 0.5\,(1 - x^2); \qquad \text{(VII. 126)}$$

$$\alpha_c = -220\left(\frac{3+\mu}{8} - \frac{1+\mu}{4}x^2 - \frac{1-\mu}{8}x^4\right); \qquad \text{(VII. 127)}$$

$$\beta_c = -220\left(\frac{1+3\mu}{8} - \frac{1+\mu}{4}x^2 - \frac{1-\mu}{8}x^4\right), \qquad \text{(VII. 128)}$$

where $x = \frac{D_1}{D}$;

D_1 = nominal diameter;
D = current diameter;

The factor 220 represents the value of $\frac{\gamma}{g}\omega^2 r^2$ for $D = 1000$ mm, $n = 1000$ rpm and $\gamma = 7.85 \cdot 10^3$ kg/m^3;

b) for conical disks with lateral load

$$\bar{\alpha}_c' = \alpha_c' a' + \alpha_s' h'; \qquad \text{(VII. 129)}$$

$$\bar{\beta}_c' = \beta_c' a' + \beta_s' h', \qquad \text{(VII. 130)}$$

where

$$a' = 1 + \frac{D_{ex}\, s_{entr} - D_{entr}\, s_{ex}}{D_{ex} - D_{entr}};$$

$$h' = \frac{(s_{ex} - s_{entr})\,a}{D_{ex} - D_{entr}}; \quad s_{ex} = \frac{y}{b_{ex}}; \quad s_{entr} = \frac{y}{b_{entr}}.$$

The coefficients α_s', β_s', α_r, α_t, β_r, β_t are functions of $t = \frac{D_{ex}}{d}$ and $t_1 = \frac{D_{entr}}{d}$, and may be determined from the charts (Figure VII. 27), where

d = diameter of the complete cone of the conical portion,

$$d = D_{entr} + \frac{b_{entr}}{b_{entr} - b_{ex}}(D_{ex} - D_{entr}). \qquad \text{(VII. 131)}$$

The equivalent thickness of the lateral load is determined by the formula

$$y = \frac{b\delta z}{2\pi r \sin\beta}, \qquad \text{(VII. 132)}$$

where b = blade width at radius r;
δ = blade thickness at radius r;
z = number of blades;
β = angle between blade and runner circumference.

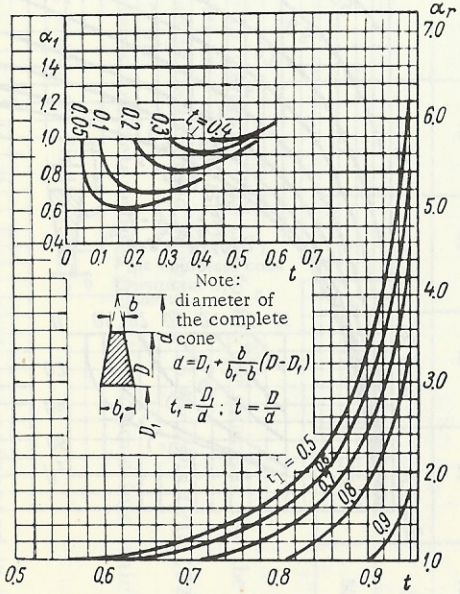
Runner blade. The load on the runner blade is the sum of the centrifugal force of the runner itself, plus the band reactions and the water pressure.

The blade and the inner band are calculated to resist runaway speed.

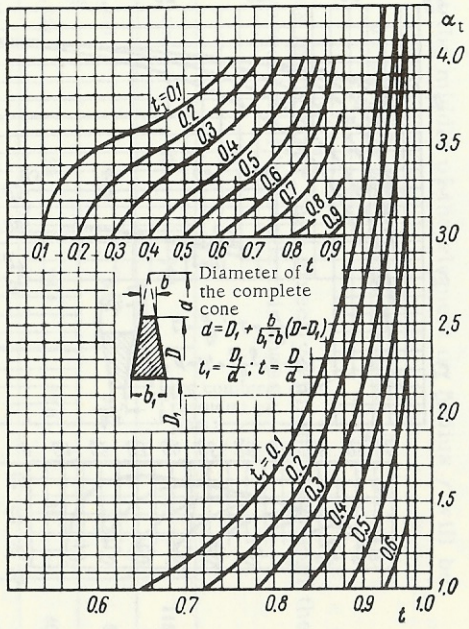
The order of calculation is as follows: cut out an element of the blade of width $l = 1$ cm, and assume it as built into the surfaces of disk and band. By neglecting the curvature and introducing the average length of element b, we obtain a rigidly fixed, uniformly loaded beam. The centrifugal force load per unit length of the element is

$$q = \frac{\gamma}{g}\delta r\omega^2, \qquad \text{(VII. 133)}$$

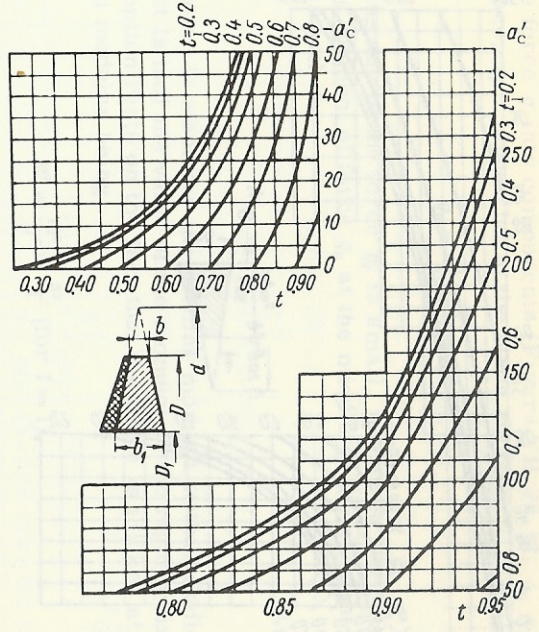
where δ = blade thickness, assumed as uniform along the element length;
r = radius to center of the element;
ω = angular velocity of the element.



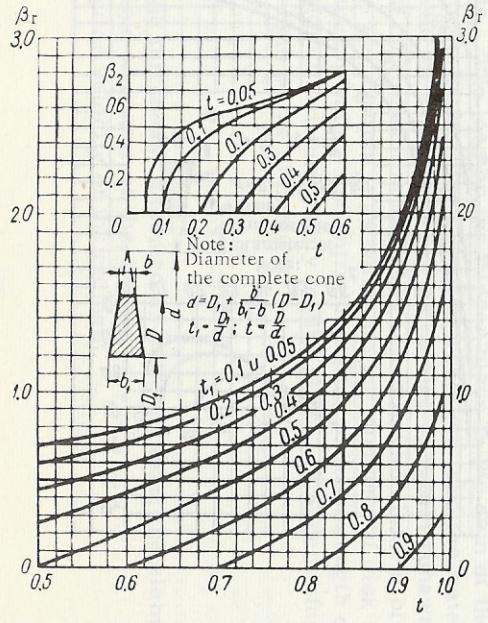
Coefficient α_r for conical disks



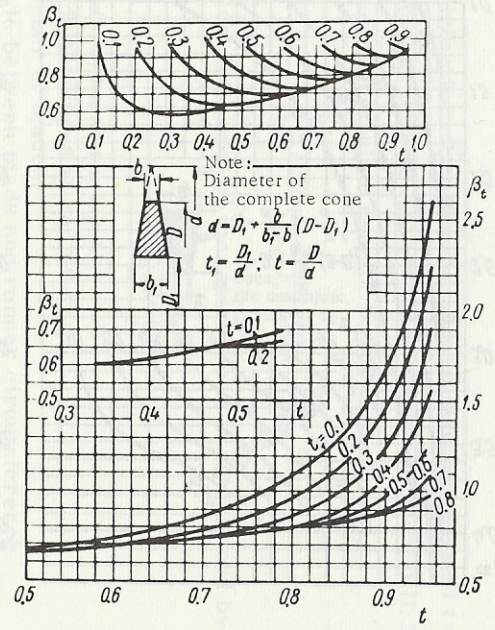
Coefficient α_t for conical disks



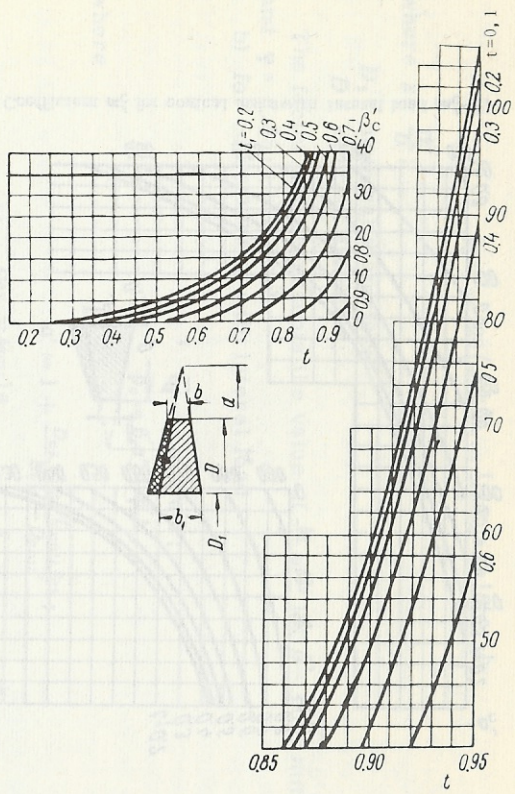
Coefficient α'_c for conical disks with lateral load ($\alpha'_c<0$)



Coefficient β_r for conical disks



Coefficient β_t for conical disks



Coefficient β'_c for conical disks with lateral load ($\beta'_c<0$)

FIGURE VII. 27. Graphs for determining the coefficients for formulas (VII. 121) and (VII. 122)

Resolve the force q into components (Figure VII. 26, b): q_n — normal to the blade surface; q_t — tangential to the blade surface

$$q_n = \frac{\gamma}{g} \delta \omega^2 r \cos \beta. \qquad \text{(VII. 134)}$$

Since bending due to the force q_t is small, it may be neglected.

The bending moment of force q_n at the middle of the element section (relative maximum) is

$$M_b = \frac{\gamma \delta \omega^2}{24g} b^2 r \cos \beta. \qquad \text{(VII. 135)}$$

The calculation is made for the bending moment at the middle of the blade, where it is half the value of the moment at the rigidly-fixed ends.

This assumption rests on the fact that the blade is thicker at the ends.

The section modulus being

$$W = \frac{l\delta^2}{6} = \frac{\delta^2}{6} \text{ (for } l = 1),$$

the stresses at the middle of the element on radius r will be

$$\sigma_b = \frac{M_b}{W} = \frac{\gamma \omega^2}{4g} \cdot \frac{b^2}{\delta} r \cos \beta = \frac{0.22}{\delta} \left(\frac{n}{1000} \right)^2 b^2 r \cos \beta. \qquad \text{(VII. 136)}$$

The stresses in the blade vary directly with the square of the rotational speed, and inversely with the blade thickness.

$2r$, cm	230	194	175	147	115
δ, cm	4.85	5.94	5.87	5.25	5.03
b, cm	25	28.4	32.8	35	40.5
β_0°	70	52	45	21	15
$\sin \beta$	0.94	0.788	0.707	0.358	0.259
y, cm	4.1	8.1	11.3	25.4	50

The procedure is illustrated in the following example for the calculation of the runner shown in Figure VII. 26.

The lateral load is determined according to formula (VII. 132) for different radii (diameters).

All the coefficients are determined for all sections into which the disk is divided.

For a rotating band, we find

1. $\sigma_{r0} = 0$

$\sigma_{t0} = 1000$ kg/cm^2 (further on σ is always expressed in kg/cm^2)

2. $\sigma_{r1} = \alpha_r \sigma_{r0} + \alpha_t \sigma_{t0} + \bar{\alpha}_c T_d = 365 - 47.6 = 317.4$

$$\sigma_{t1} = \beta_r \sigma_{r0} + \beta_t \sigma_{t0} + \beta_c T_d = 635 - 25 = 610$$

3. $\sigma^*_{r_1} = \frac{b_2}{v_1} \sigma_{r1} = 0.5 \cdot 317.4 = 158$

$$\sigma^*_t = \sigma_{t1} + \mu (\sigma^*_{r1} + \sigma_{r1}) = 562$$

4. $\sigma_{r2} = \alpha_r \sigma^*_{r1} + \alpha_t \sigma^*_{t1} + \bar{\alpha}_c T = 253$

$$\sigma_{t2} = \beta_r \sigma^*_{r1} + \beta_t \sigma^*_{t1} \bar{\beta}_c T = 1075$$

5. $\sigma^*_{r2} = 223$

$$\sigma^*_{t2} = 1075 + 0.3\,(223 - 253) = 1066$$

6. $\sigma_{r3} = \alpha_r \sigma^*_{r2} + \alpha_t \sigma^*_{t2} + \bar{\alpha}_c T = 1.8 \cdot 223 + 0.4 \cdot 1066 - 334 = 495$

$$\sigma_{t3} = \beta_r \sigma^*_{r2} + \beta_t \sigma^*_{t2} + \beta_c T = 0.66 \cdot 223 + 0.83 \cdot 1066 - 290 = 742$$

7. $\sigma^*_{r3} = \frac{90}{180} \sigma_{r3} = 246$

$$\sigma^*_{t3} = 742 + \mu (\sigma^*_{r3} - \sigma_{r3}) = 668$$

8. $\sigma_{r4} = 1.0 \cdot 246 + 0.09 \cdot 668 - 49 = 256$

$$\sigma_{t4} = 0.09 \cdot 246 + 0.95 \cdot 668 - 50 = 607$$

9. $\sigma^*_{r4} = \frac{165}{110} 256 = 384$

$$\sigma^*_{t4} = 607 + 0.3\,(384 - 256) = 645$$

10. $\sigma_{r5} = 1.3 \cdot 384 + 0.2 \cdot 645 - 106 = 523$

$$\sigma_{t5} = 2.8 \cdot 384 - 0.9 \cdot 645 - 40 = 2010$$

11. $\sigma_{r6} = 1.3 \cdot 523 + 0.2 \cdot 2010 - 233 = 847$.

Second calculation (for a stationary band)

1. $\sigma_{r0} = 0$; $\sigma_{t0} = 100$.
2. $\sigma_{r1} = 36.5$; $\sigma_{t1} = 63.5$.
3. $\sigma^*_{r1} = 18.3$; $\sigma^*_{t1} = 58$.
4. $\sigma_{r2} = 41.2$; $\sigma_{t2} = 125.2$.
5. $\sigma^*_{r2} = 36.4$; $\sigma^*_{t2} = 123.8$.
6. $\sigma_{r3} = 115$; $\sigma_{t3} = 127$.
7. $\sigma^*_{r3} = 57$; $\sigma^*_{t3} = 110$.
8. $\sigma_{r4} = 67$; $\sigma_{t4} = 110$.
9. $\sigma^*_{r4} = 100$; $\sigma^*_{t4} = 120$.
10. $\sigma_{r5} = 154$; $\sigma_{t5} = 388$.
11. $\sigma_{r6} = 278$.

According to formula (VII. 123), the coefficient

$$\varphi = \frac{847}{278} = 3.05.$$

Consequently, the maximum stresses in the inner band are

$$\sigma_{t0} = \sigma'_{t0} - \varphi \sigma_{t0} = 1000 - 305 = 695.$$

TABLE VII. 14

Determination of coefficient for calculating the stresses in the blade caused by centrifugal forces

No. of section	D_{entr}	D_{ex}	x	b_{entr}	b_{ex}	s_{entr}	s_{ex}	d	t_1	t	α_r	α_t	β_r	β_t	α_c'	β_c'	α_s'	β_s'	a'	h_1
1	52	107	0.485	—	—	—	—	—	—	—	0.635	0.365	0.365	0.635	—74.5	—38.5	—	—	—	—
2	107	124	—	35	18.5	1.43	2.7	143	0.75	0.87	1.62	0.2	4.0	0.9	—30	—10	—25	—10	—5.6	10.7
3	124	170	—	21	9	1.21	2.82	204	0.610	0.835	1.8	0.4	0.66	0.83	—58	—19	—37	—23	—2,12	7.15
4	170	180.5	—	18	16.5	0.628	0.685	296	0.575	0.612	1.0	0.09	0.09	0.95	—5	—2	—4	—5	0.714	1.6
5	180.5	208	—	11	7.5	0.735	1.08	267	0.676	0.780	1.3	0.2	2.8	0.9	—20	—6	—14	—5	—0.53	2.65
6	208	250	—	7.5	5	0.547	0.82	334	0.623	0.750	1.3	0.2	3.3	0.85	—22	—9	—15	—10	—0.19	2.18

The values required for calculating the formula (VII.124) are determined below.

No. of section	D_{ex} (d)	α_r	α_t	β_r	β_t	$\bar{\alpha}_c'$	$\bar{\beta}_c'$	T_d	$\bar{\alpha}_c' T_d$	$\bar{\beta}_c' T_d$
1	107	0.635	0.635	0.635	0.635	—74.5	—38.5	0.64	47.6	24.6
2	143	2.62	0.2	4.0	0.9	—100	—51	1.15	—115	58.6
3	204	2.8	0.40	0.66	0.83	—142	—123.6	2.35	—334	—290
4	296	1.0	0.09	0.09	0.95	—10	—10.1	4.94	—49.4	—50
5	267	1.3	0.2	2.8	0.4	—26.6	—10.1	4.0	—106.5	—40.4
6	334	1.3	0.2	3.3	0.85	—36.9	—23.5	6.3	—233	—148

The stresses in the blade are determined according to formula (VII. 136).

$\beta = 65°$; $\cos\beta = 0.423$;

$r = 80$ cm;

$b = 4$ cm;

$b' = 35$ cm;

$b'' = 18$ cm;

$$b = \sqrt{(b')^2 + (b'')^2} = \sqrt{(35)^2 + (18)^2} = 39.4 \text{ cm};$$

$n_r = 750$ rpm;

$$\sigma_b = \frac{0.022}{4} \cdot 0.423 \cdot 0.563 \cdot 80 \cdot 1550 = 163.$$

The lower band being less stressed than the upper band, there is no need to determine the stresses in the latter.

47. RUNNER-BAND SEALS

Labyrinth seals are commonly used to reduce water leakages past the runner blades, and thus increase turbine efficiency.

Their designs vary with the head applied.

At small and medium heads, the seals are made of a couple of rings, forming a smooth or grooved narrow channel. For production reasons, the channel width is selected as small as possible.

At high heads the seal rings are indented, with the protrusions and recesses fitting into each other. With one pair of seal rings, the seals are termed simple; with two, double.

The design of a channel seal for the lower and upper rings of a Francis runner is shown in Figure VII. 28. The seal rings (2) and (4), provided with annular grooves, are fitted in the band. They are opposite stationary rings (3) and (5), provided with similar grooves, and located in the turbine cover plate and on the lower runner foundation. Figure VI. 28, a shows the narrow channel, alternating with a wider space created by the grooves. For seals of 5000 mm diameter, the width of the channel is usually about 2.5 mm, while the enlarged section is 100 mm wide and 40mm high.

The alternation of narrow channels with annular grooves is actually an alternation of varying cross-sectional areas of the passage through which the water leaks, the resistance is thus increased and the amount of leakage reduced, owing to the sudden variations in the flow velocity /68/.

Pfleiderer recommends making the grooves narrow, since otherwise their effect might diminish. Figure VII. 28,c shows a diagram of the pressure drop across channels with and without groove. Line AB represents the pressure drop along a simple channel, line ABCD the pressure drop along a grooved one. The drawing clearly shows that by excessively enlarging the groove, results may be worse than with no groove at all; if the width exceeds CD_1, the pressure may even rise. Grooves on both sides, as shown in Figure VII. 28,a, are more effective than grooves on one side only (Figure VII. 28,c).

A deflector is located above the runner band. The water that passes through the band clearance leaks past the runner into the draft tube through the relief tube (1).

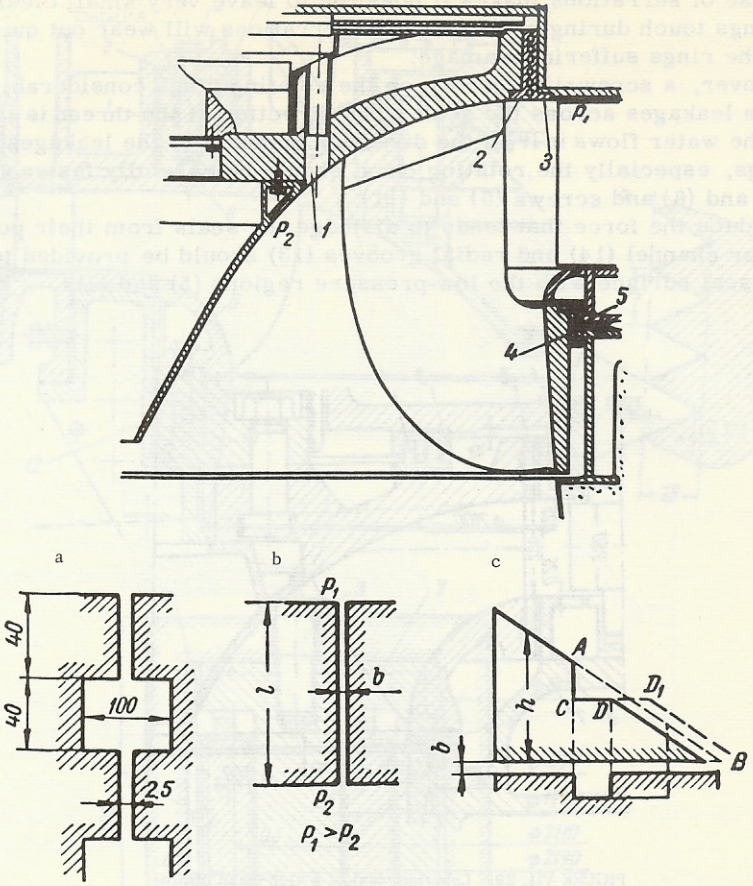


FIGURE VII. 28. Channel seal for the band of a medium-head Francis runner

Another seal design for higher heads ($H \cong 200$ m) is shown in Figure VII. 29. The outer diameters of the lower and upper bands are sealed with smooth seal rings (1), (2) and (7), (8), which form long, narrow channels. Additional indented seal rings (3), (4) and (5), (6) are mounted on the bands at a smaller radius. The outer ring provides a relatively long channel, while the indentations in the labyrinth seal are comparatively small.

An opening (9) is provided in the runner band for the drainage of seepage water into the draft tube.

Figure Vii. 30 shows in detail a serrated (threaded) labyrinth seal for a high-head runner ($H \sim 300$ m); the indentations in the seal are relatively high, but they are only two in number. For a runner diameter of 2000 mm, their height is about 200 mm, and the channel width only 0.5 mm. The stationary rings (2) and (10) have smooth indentations, while the rotating rings (4) and (9) have helical protrusions and recesses (serrations) (see Figure VII. 30, a). The pitch of the helix is 3 mm, with an angle of 55°. This design was successfully used by L. S. Smolyarov for high-head turbines.

The use of serrations makes it possible to leave very small clearances; if two rings touch during operation, the serrations will wear out quickly without the rings suffering damage.

Moreover, a screw-like groove on the rotating rings considerably reduces the leakages across the seal. The direction of the thread is selected so that the water flows in it in the direction opposite to the leakages. The seal rings, especially the rotating ones, should be carefully fastened with bolts (3) and (8) and screws (6) and (11).

To reduce the force that tends to dislodge the seals from their position, an annular channel (14) and radial grooves (13) should be provided to connect the seal surface with the low-pressure regions (5) and (7).

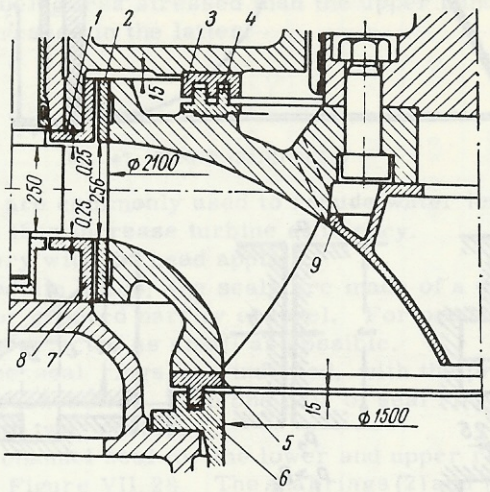


FIGURE VII. 29. Labyrinth seal of a high-head turbine (H = 200 m)

In the design described, protective steel rings (1 and 12) are provided to protect the turbine cover plate and the foundation ring from wear. The rings are made of carbon or alloy (stainless) steel.

The problem of correct clearance between seal rings is very important. A narrow clearance reduces water leakages, but allows the rings to rub against each other and undergo wear. The clearance in the turbine shaft bearing must also be taken into account to obviate any dangerous rubbing in the labyrinth when the shaft is rotating. The clearance between two adjacent labyrinth seals is a matter for the production engineer to decide.

The tolerances that can reasonably be obtained on the available machine tools must be taken into account. Machining of large sealing rings to tolerances individually should be avoided, and by employing a slightly more complex production process, a pair of matched rings should be machined according to standard specifications.

Apart from this, the losses in labyrinth seals are due to the friction between water and rotating parts. Hence, when designing labyrinth seals, the turbine designer must consider the gain in efficiency due to reduction in leakages, and the efficiency loss due to friction, and strive for maximum efficiency.

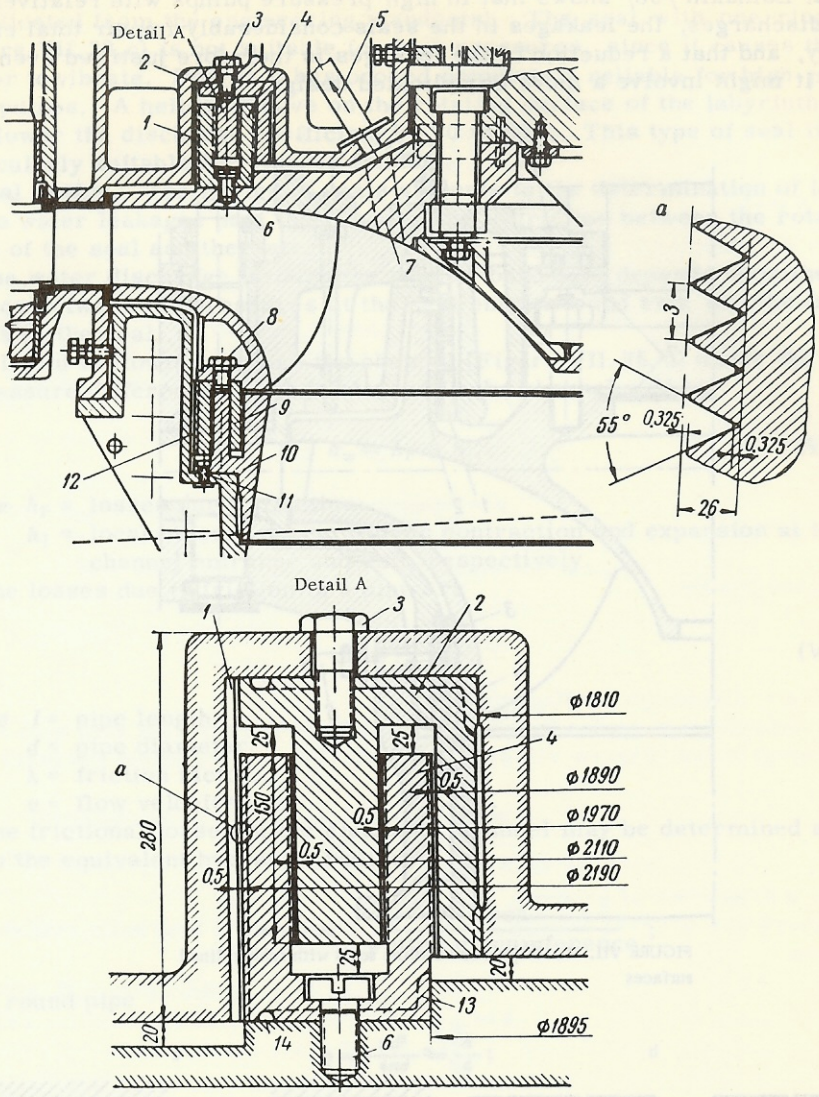


FIGURE VII. 30. Labyrinth seal for a high-head turbine (H = 300 m)

Figure VII. 31 shows another version of a high-head turbine seal, with rubber-lined surfaces (1) and (3) on the stationary cover plate and foundation ring. The smooth, matched seal rings (2) and (4) are mounted on a projection of the upper ring and the outer surface of the lower ring. By using rubber-lined sealing surfaces, the clearance channel may be reduced to the utmost, thus also reducing water leakages; in this case, it is absolutely necessary to provide for water-supply lines (5) and (6) to lubricate the rubber surfaces.

In this design, additional labyrinth seals (7) and (8) are provided to prevent water from leaking into the turbine-shaft bearing.

A. A. Lomakin /58/ shows that in high-pressure pumps with relatively small discharges, the leakages in the seals considerably impair total efficiency, and that a reduction of the leakages is therefore justified even though it might involve a more complicated design.

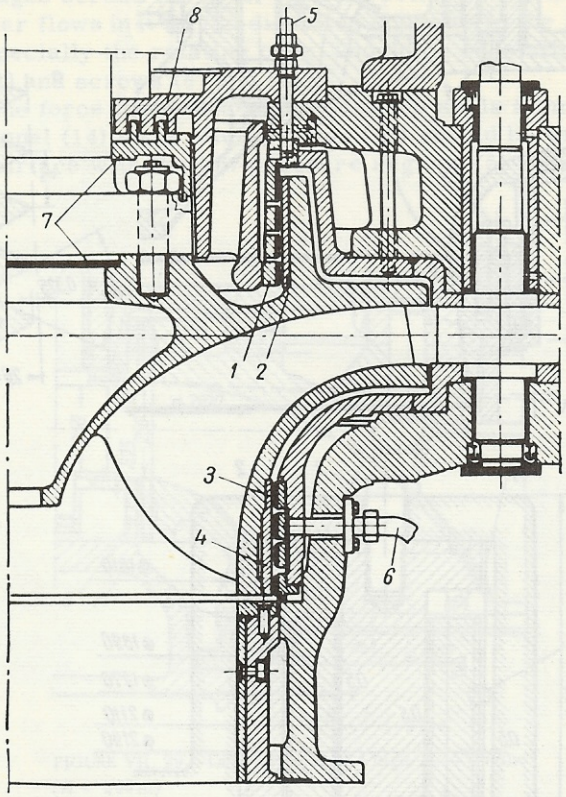


FIGURE VII. 31. High-head turbine seals with rubber-lined surfaces

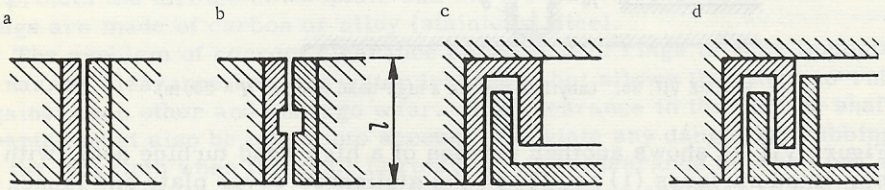


FIGURE VII. 32. Types of pump seals

Several designs of seals for pumps are shown in Figure VII. 32. Design b, with a discontinuous channel, lowers the leakages by 20 to 30% compared with the simple channel seal of design a. Labyrinth seals with several clearances at different diameters enable the discharge coefficient for the same seal height (l) to be lowered considerably; designs c and d are more

complicated from the engineering standpoint. The seal with one ring (Figure VII. 32,c) is not suitable for high pressures, since it causes the runner to vibrate. Design d has proved completely reliable for high-pressure pumps. A helical groove on the rotating surface of the labyrinth seal may lower the discharge coefficient by 30 to 50%. This type of seal is particularly suitable for viscous fluids.

Seal design. The design of seals amounts to the determination of losses due to water leakages past the runner, and to friction between the rotating parts of the seal and the water.

The water discharge through the runner-band seal depends upon the difference between the pressures at the seal entrance and exit, and the friction losses in the seal.

If liquid is flowing through the channel (Figure VII. 28, b) under the action of pressure difference, the head losses in the channel will be

$$h_\omega = h_F + h_l, \qquad \text{(VII. 137)}$$

where h_F = losses due to friction;
h_l = local losses, due to sudden contraction and expansion at the channel entrance and exit, respectively.

The losses due to friction in a pipe are

$$h_F = \frac{\lambda l}{d} \cdot \frac{v^2}{2g}, \qquad \text{(VII. 138)}$$

where l = pipe length;
d = pipe diameter;
λ = friction factor;
v = flow velocity.

The frictional losses in the clearance channel may be determined according to the equivalent hydraulic radius

$$\varrho = \frac{f}{P} = \frac{\text{area}}{\text{wetted circumference}};$$

for a round pipe

$$\varrho = \frac{\pi d^2}{4\pi d} = \frac{d}{4};$$

for a clearance channel

$$\varrho = \frac{\pi D b}{2\pi D} = \frac{b}{2},$$

where D = diameter at which the channel is located;
b = channel width.

Consequently, the frictional losses in the clearance channel are

$$h_F = \frac{\lambda l}{2b} \cdot \frac{v^2}{2g}. \qquad \text{(VII. 139)}$$

Local losses in the clearance channel at a constriction or widening of the section are

$$h_1 = \zeta \frac{v^2}{2g} = 1.5 \frac{v^2}{2g},$$

whence

$$h_w = \left(\frac{\lambda l}{2b} + 1.5\right) \frac{v^2}{2g};$$

Since $v = \frac{q}{f}$,

where q = discharge through the channel;

f = cross-sectional area of the channel,

we obtain

$$q = f \sqrt{\frac{2gh_w}{\frac{\lambda l}{2b} + 1.5}}. \qquad \text{(VII. 140)}$$

Denoting

$$\mu = \frac{1}{\sqrt{\frac{\lambda l}{2b} + 1.5}},$$

we obtain finally

$$q = \mu f \sqrt{2gh_w},$$

where μ = discharge coefficient.

By considering, instead of a simple channel, a labyrinth seal with rectangular grooves (Figure VII. 28, a), the discharge coefficient becomes

$$\mu = \frac{1}{\sqrt{\frac{\lambda l}{2b} + 1.5 + 1.1z}},$$

where z = number of grooves.

If there are several labyrinth seals or a system of hydraulic resistances, we have

$$q = \sqrt{\frac{2g\Sigma h_w}{\Sigma \frac{1}{F_i^2 \mu_i^2}}}. \qquad \text{(VII. 141)}$$

The head losses Σh_u may be determined from Bernoulli's equation, if the pressures before and after the seals p_1 and p_2 are known (Figure VII.28).

$$\Sigma h_w = \frac{p_1}{\gamma} - \frac{p_2}{\gamma} + z_{1-2} + \Delta h_u, \qquad \text{(VII. 142)}$$

where $\frac{p_1}{\gamma}$ = head at the seal entrance (before the band);

$\frac{p_2}{\gamma}$ = head at the seal exit (at the clearance of the runner cone);

z_{1-2} = difference between the elevations of the seal channel entrance and exit;

Δh_u = pressure due to water rotation in the seal clearances

$$\Delta h_u = \frac{\left(\frac{1}{2}u_1\right)^2 - \left(\frac{1}{2}u_2\right)^2}{2g}$$

but

$$u_1 = \frac{\pi D_1 n}{60}, \quad u_2 = \frac{\pi D_2 n}{60}.$$

Hence, after the substitution, we obtain

$$\Delta h_u = 3.49 \cdot 10^{-5} \cdot n^2 (D_1^2 - D_2^2),$$

where n = turbine speed, rpm;
D_1 and D_2 = diameters of seals, m.

The head at the band-seal entrance

$$\frac{p_1}{\gamma} = \nabla_{hw} - \nabla_{r1} - \frac{v_1^2}{2g} + \frac{p_a}{\gamma}, \qquad \text{(VII. 143)}$$

where ∇_{hw} = headwater level;
∇_{r1} = level of entrance to the band seal;
v_1 = absolute water velocity inside the seal

$$v_1^2 = v_{m1}^2 + v_{u1}^2,$$

but

$$v_{m1} = \frac{Q}{F_1}; \quad v_{u1} = \frac{60\eta g H}{\pi D n},$$

p_a = atmospherical pressure; $\frac{p_a}{\gamma} \cong 10$ m.

The head at the exit of the runner-cone clearance is

$$\frac{p_2}{\gamma} = \frac{p_a}{\gamma} - H_s - \frac{v_{m2}^2}{2g}, \qquad \text{(VII. 144)}$$

where H_s = draft head.

$$v_{m2} = \frac{Q}{F_2}.$$

The friction coefficient λ should be selected according to the character of the fluid flow — laminar or turbulent.

The Reynolds number Re is used to characterize the fluid flow

$$\mathrm{Re} = \frac{d v_{av}}{\nu}, \qquad \text{(VII. 145)}$$

where d = pipe diameter;
v_{av} = average flow velocity;
ν = coefficient of kinematic viscosity.

For a steady laminar flow — characterized by $\mathrm{Re} \leqslant 2320$ — the friction coefficient is determined by the formula

$$\lambda = \frac{64}{\mathrm{Re}}. \qquad \text{(VII. 146)}$$

If the flow is turbulent, a boundary layer is formed near the pipe walls. Two cases may occur: the thickness of the boundary layer δ is greater than the height k of the pipe surface roughness ($\delta > k$), i.e., the pipe walls are hydraulically smooth; or, the boundary-layer thickness is smaller than the roughness height ($\delta < k$), i.e., the walls are rough.

The thickness of the boundary layer is determined by the formula

$$\delta = d\frac{N}{\mathrm{Re}}\sqrt{\frac{8}{\lambda}} = 2b\frac{N}{\mathrm{Re}}\sqrt{\frac{8}{\lambda}}. \qquad \text{(VII. 147)}$$

where N = constant; for water $N = 11.6$;

λ = a given friction coefficient (0.03 to 0.07);

$$\mathrm{Re} = \frac{dv}{\nu} = \frac{2b\sqrt{v_{av}^2 + \left(\frac{u}{2}\right)^2}}{\nu},$$

where v_{av} = average radial flow velocity in the channel $v_{av} = \frac{q}{\pi D b}$;

u = peripheral velocity.

The coefficient of kinematic viscosity is 10^{-6} m^2/sec at 20°C.

For turbines where the peripheral velocity inside the seal exceeds 10^6 m/sec, Re may be determined approximately from the relation

$$\mathrm{Re} \cong \frac{bu}{\nu}.$$

The height k of the surface roughness depends on the surface finish of the seal ring.

By comparing the roughness height k with the thickness of the boundary layer, we may determine the type of the fluid flow.

If $\delta > k$, the friction coefficient is determined from the formula

$$\lambda = \frac{1}{[2\log(\mathrm{Re}\sqrt{\lambda} - 0.8)]^2}. \qquad \text{(VII. 148)}$$

The value of λ is assumed to be known; if, however, a large discrepancy is found between the given and the calculated values, a new and more accurate value should be assumed, and the calculation repeated.

If $\delta < k$, λ is determined by the formula

$$\lambda = \frac{1}{\left(1.74 + 2\log\frac{r}{k}\right)^2} = \frac{1}{\left(1.74 + 2\log\frac{b}{k}\right)^2}, \qquad \text{(VII. 149)}$$

where r = pipe radius;

b = clearance of the seal.

Power losses. The leakages through the seal should be evaluated by means of the power losses, which are

$$\Delta N_q = \frac{\gamma\eta}{102} qH \text{ kw}, \qquad \text{(VII. 150)}$$

for $\eta = 0.9$

$$\Delta N_q = 8.8qH \text{ kw}, \qquad \text{(VII. 151)}$$

where q = discharge through the seal, m^3/sec;
H = turbine head, m.

The power losses due to the friction of the water stream against the rotating part of the seal ring may be determined by means of data used in pump design /58/.

The moment exerted upon one disk side by friction of a fluid in a closed vessel may be expressed by

$$M = c_f \varrho R_2^5 \omega^2, \tag{VII. 152}$$

where c_f = coefficient of friction;
ϱ = density of fluid;
R_2 = outer radius of the disk;
ω = angular velocity.

The friction coefficient is a function of the Reynolds number. For a rotating disk $Re = \frac{R_2^2 \omega}{\nu}$.

Under laminar-flow conditions

$$c_f = \frac{\pi}{Re} \cdot \frac{R_2}{s} + Re\left(\frac{s}{R_2}\right)^3 \left[0.0146 + \left(\frac{s}{Re}\right)^2 0.1256\right], \tag{VII. 153}$$

where s = distance between the disk and the vessel wall.

At the point of transition from laminar to turbulent flow

$$c_f = \frac{1.334}{\sqrt{Re}}. \tag{VII. 154}$$

For turbulent flow

$$c_f = \frac{0.0465}{\sqrt{Re}}. \tag{VII. 155}$$

Power losses due to disk friction (for a constant disk velocity)

$$\Delta N_F = \frac{M\omega}{102} = 0.0098 c_f \varrho R_2^5 \omega^3 \text{ kw}. \tag{VII. 156}$$

For water at t = 20° C ($\nu = 10^{-6}$ m^2/sec), and for $Re = 7 \cdot 10^6$, values commonly used in pump design, we obtain c_f = 0.00232. Formula (VII.156) then becomes

$$\Delta N_F = 0.0006 u_2^3 D_2^2 \text{ hp}. \tag{VII. 157}$$

According to A. A. Lomakin, the frictional moment exerted upon rotating surfaces immersed in water should be determined from formula

$$M = \tau_0 l 2\pi r^2, \tag{VII. 158}$$

where τ_0 = tangential stress at the wall;
l and r = length and radius of the cylindrical surface.

The tangential stresses τ_0 at the wall, for turbulent flow, are determined by the equation

$$\tau_0 = \frac{\lambda}{8} \varrho v_0^2 = \frac{\lambda}{8} \varrho \left(\frac{\omega r}{2}\right)^2, \tag{VII. 159}$$

where v_0 = flow velocity in the clearance between the rotating surface and the container wall, assumed to be equal to half the peripheral velocity $u=\omega r$.

Consequently,

$$M = 0.196\lambda l\varrho\omega^2 r^4 \text{ kgm.} \quad \text{(VII. 160)}$$

for $\lambda=\frac{0.316}{\sqrt[4]{\text{Re}}}$ we obtain $M=\frac{0.062}{\sqrt[4]{\text{Re}}}\varrho_1 l\omega^2 r^4$ kgm,

whence the power loss of a smooth cylindrical surface is

$$\Delta N_F = \frac{\omega M}{102} = \frac{6.1\cdot 10^{-4}}{\sqrt[4]{\text{Re}}}\varrho l\omega^3 r^4 \text{ kw} \quad \text{(VII. 161)}$$

The total power loss is

$$\Delta N = \Delta N_q + \Delta N_F. \quad \text{(VII. 162)}$$

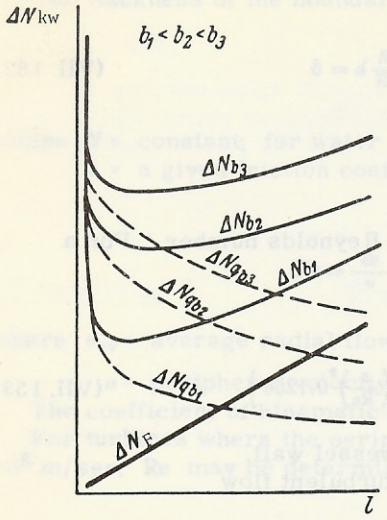


FIGURE VII. 33. Relationship between power losses and channel length l, for various clearance widths b

The seal designer usually considers several clearance widths (b) and seal lengths (l), and plots the corresponding curves of power losses as shown in Figure VII. 33.

These curves show that for a given labyrinth clearance, the volumetric losses drop rapidly at the beginning as the channel length increases, and then decrease slowly. The frictional loss ΔN_F varies directly with the channel length.

The total power loss ΔN drops abruptly at the beginning, and then slowly increases.

The final selection of the seal parameters (clearance and length) is made on the basis of these curves.

The seals are usually made of carbon steel for low-head turbines, and of chromium steel for medium and high-head turbines. For matched seal rings it is advisable to use metals of different hardnesses; these are less liable to wear when rubbing against each other.

Chapter VIII

KAPLAN RUNNERS

48. RUNNER DESIGNS

In a Kaplan runner, the diameter of the hub and the number of blades depend on the specific speed n_s. As a rule, higher head, and consequently, lower specific speed, entail greater hub diameter and a larger number of blades. The basic interrelations between the various dimensions of the Kaplan runner are shown in Figures III. 12 and III. 15.

The location of the blade-actuating mechanism (blade operator) inside the hub is a characteristic feature of Kaplan runners.

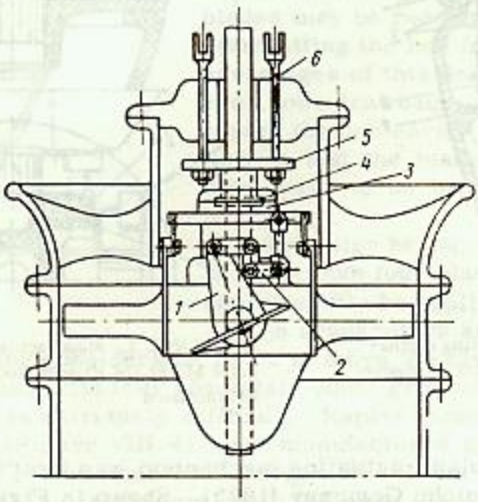


FIGURE VIII. 1. The blade-actuating mechanism proposed by Professor Kaplan

Development of the design of blade-actuating mechanisms. The design of the mechanism, as first proposed by Professor Kaplan, is shown in Figure VIII. 1. The runner blades are inserted by means of pivots into the runner hub. The blade lever (1) is connected to the sleeve (3) by means of links and the cranked lever (2). The sleeve (3), free to move in the axial direction, turns together with the runner. The axial movement of the sleeve is effected by means of the double collar (4), ring (5) and rods (6).

This particular blade-adjusting design never became popular in turbine construction, due to one major disadvantage — the main parts and links of the mechanism are immersed in water and impede the flow. The lever mechanism, for converting the translational movement of the sleeve along the shaft axis into the rotational movement of the blades, is still used, although eventually, different constructional solutions were adopted.

The design of the blade-actuating mechanism developed in two different ways: with the use of guide-blocks, or in the form of a pure crank-drive mechanism.

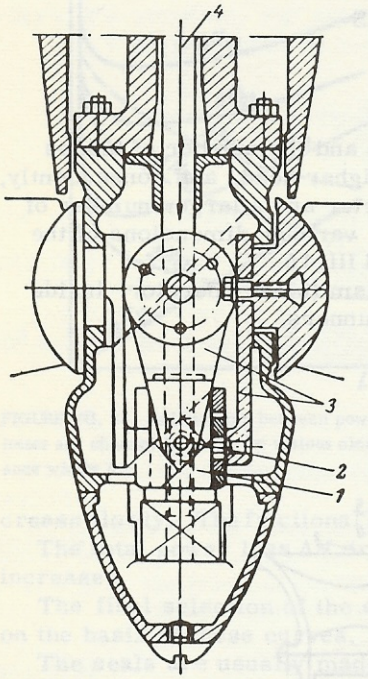


FIGURE VIII. 2. Blade-actuating mechanism with guide blocks and oblique grooves

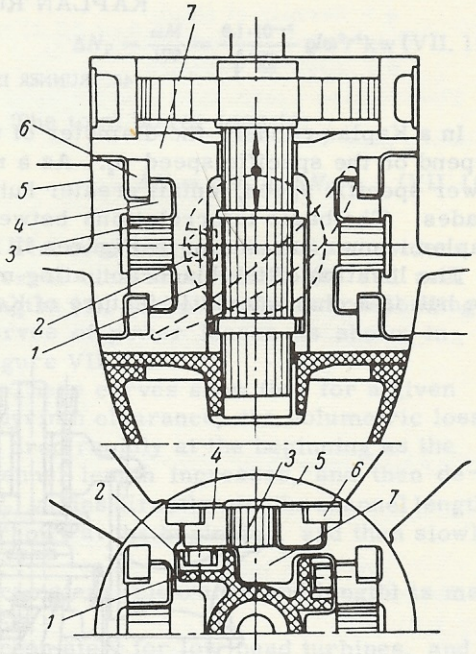


FIGURE VIII. 3. Blade-actuating mechanism with guide blocks and straight grooves made by "Verkstaden Kristinehamn

The guide-block blade-actuating mechanism was first used by "Fritz und Neumayer", Munich, Germany (1925). Shown in Figure VIII. 2, the actuating mechanism in this design is located inside the runner hub. The rod which transmits the force needed for blade adjustment moves axially along the turbine shaft inside the hub.

Blade adjustment is effected by the axial movement of a guide block (1) of rectangular cross section, connected to the rod (4). The guide block (1) is connected with the blade levers (3) by means of slide blocks (2), and links. The slide blocks are located in oblique grooves cut into the guide-block surfaces. This design was never widely used, since, due to the friction in the oblique grooves, great force was required for the adjustment, while the need to machine accurately equal oblique grooves into the four surfaces presented a difficult production problem. In the U.S.S.R., it was

incorporated in the small turbines at the Pervomaisk HEP and in the auxiliary turbines at the Svir' III HEP. The "Verkstaden Kristinehamn" plant in Sweden used another blade-actuating mechanism design featuring guide blocks (Figure VIII. 3). The blades are rotated by means of slide blocks (2) moving in horizontal grooves provided in the crosshead (1). These slide blocks are pivoted on the pin of the crank ring (4), which is bolted to the flange of the blade (5). The translational movement of the rod and crosshead is converted into the rotational movement of the blades by means of the slide blocks.

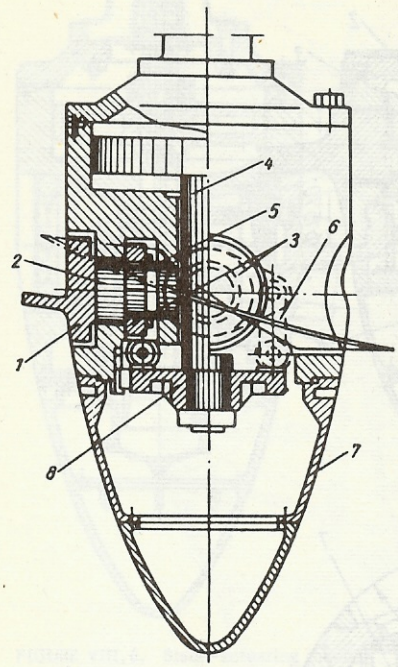


FIGURE VIII. 4. Blade-actuating mechanism with crank drive

The centrifugal forces, developed by the blade and crank drive, are taken up by a special ring (6), mounted to the hub.

The crank ring (4) is carried by the pivot (3) cast integral with the hub (7). This design is still used by the Swedish firm without substantial modification. In the U.S.S.R., a series of large turbines — at Svir' III, Zemo-Avchal'sk, and other plants — are equipped with mechanisms of this type. The fact that the blades may be readily removed without dismantling the hub is one of the main advantages of this design. It has, however, one drawback: the crosshead occupies the hub cavity, so that the blade flanges and the blade-actuating mechanism have to be located on the hub periphery.

Under high heads, and with runners of more than four blades, this design cannot easily be applied.

The crank-drive arm is relatively small, thus requiring considerable force to move the blades, while manufacture of a crosshead with four absolutely equal grooves and a profiled hub provided with pivot is extremely difficult. Kaplan runners with crank-drive mechanisms (Figure VIII. 4) were manufactured by "Stork", "Voith", and "Escher-Wyss", and later by "Morgan and Smith" in the U.S.A. The runner blade (1) is cast integral with the pivot (2), and is guided by two bearings. The crosshead (8) is located inside the lower part of the hub, and the lever (3) is much longer than that shown in Figure VIII. 3. The lever is mounted on the blade pivot, and secured by means of ring (5). Blade adjustment is effected by the axial movement of the rod (4) and crosshead (8), articulated via link (6) to lever (3), which is mounted on the blade pivot. The hub extension (7) is connected to the hub from below. This design exploits the inner cavity of the hub more efficiently, there being room for more than four blades; it has been used for a number of turbines of various sizes and power outputs. The design of the runner for the Ryburg-Schwörstadt plant (runner — D_1 = 7.0 m, turbine output — N = 30,000 kw) is shown in Figure VIII. 5. It has five blades (4), which are cast integral with

the pivots; the outer diameter of the hub (2) is 3000 mm. The force required to adjust the blades is transmitted through a 280 mm diameter connecting rod (1). The crosshead (5) of box-shaped cross section, is secured to the rod end. The guiding cylinder (6) is attached to the crosshead from below, and the lever (7) is keyed to the blade.

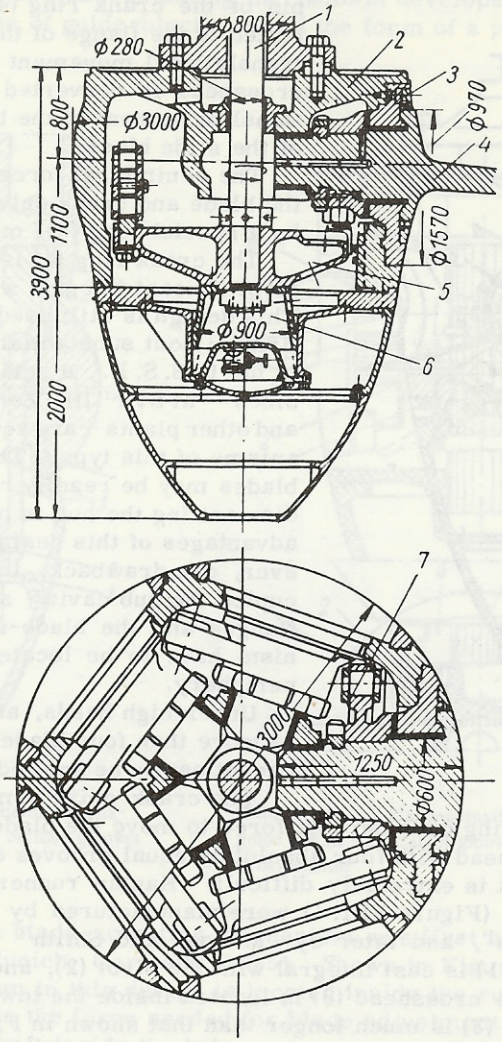


FIGURE VIII. 5. Kaplan runner of the Ryburg-Schwörstadt turbine

A detachable ring (3) which permits simultaneous removal of blades and lever – thus facilitating maintenance – is characteristic of this type of design. However, the fact that the blade is cast integral with the pivot is a disadvantage, since both manufacture and removal become more complicated: to remove the blade, the hub must also be removed, and the link and the lever dismantled.

LMZ started building Kaplan turbines as early as 1928, its first model being a 400 hp turbine for the Pervomaisk HEP. The blade-actuating mechanism was of the guide-block oblique groove type (Figure VIII. 2). Later, N. N. Kovalev used a crank-lever mechanism (Figure VIII. 4) for a large 12,500 kw turbine. During manufacture and assembly, a number of difficulties arose, due to the blades being cast integral with the pivots. Hence, a new type of crank-drive mechanism with removable blade pivots was later built at the LMZ.

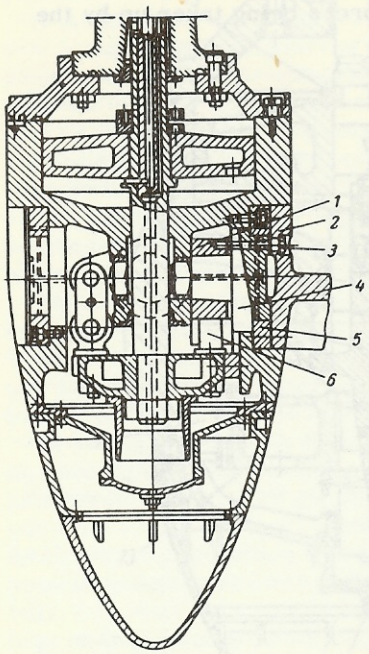


FIGURE VIII.6. Blade-actuating mechanism with crank drive and removable pivot

The runner design developed by A. P. Murzin for a turbine of N = 15,000 kw is shown in Figure VIII. 6. The blade (2) and the pivot (4) are separate elements. Flange (5) takes up the centrifugal forces from the blade. The lever (1) is connected to the collar of the pivot by means of bolts (3), so that blade, pivot, and lever form a single component. Assembly is thus facilitated, since the actuating mechanism may be fitted before the blades, these being mounted during the last stage of assembly. This LMZ design proved quite satisfactory during manufacture and assembly, as well as during operation.

A further refinement was introduced by S. A. Granovskii for the turbines of N = 70,000 kw for the Rybinsk HEP. The lever (1) and the holes in the crosshead (6) were omitted, and the link coupled by means of pins cast integral with the blade pivots and the crosshead. This design (Figure VIII. 7) involves slightly more complicated machining of the crosshead, but the hub weighs about 10 to 15 t less, while assembly time is reduced. The runner-hub diameter D is 3.7 m, the runner length, 7.5 m, and the runner weight, about 300 t. The hub body (3) is a heavy machined steel casting, weighing about 70 t. Four blades (6) each weighing 20 t are fixed to the hub body, together with their pivots (5) and blade-actuating mechanism. The centrifugal forces caused by the blades, reaching 1000 t at runaway speed, are taken up by special rings (4), forged of high quality nickel-chromium steel, each secured by twenty-five 90 mm-diameter bolts to the hub body. The blade flange is secured by eleven bolts (11), 150 mm in diameter, to the pivot (5), upon which pin (15) is eccentrically located. The crosshead (8), connected by links (7) to the blade pivots, is connected to the oil-servomotor rod (13), by means of a heavy detachable steel ring (10). The steel servomotor rod of 600 mm diameter is designed to resist a force of nearly 1200 t.

The oil servomotor, consisting of the cylinder (2), piston (14), and cover (1), is located above the hub. The oil pressure-driven piston develops the force required to turn the blades. A streamlined hub extension (9) is provided at the bottom of the hub.

Modern blade-actuating mechanism design for standard heads. Since Kaplan turbines are used on a very large scale, it is essential — especially at high heads — to increase the specific speed of the runners, and improve cavitation properties and reliability. Runners with small hub diameters and a large number of blades are suitable. Blade-actuating mechanisms devised in recent years are described below. Their salient feature is the absence of a supporting ring, the centrifugal forces being taken up by the runner hub.

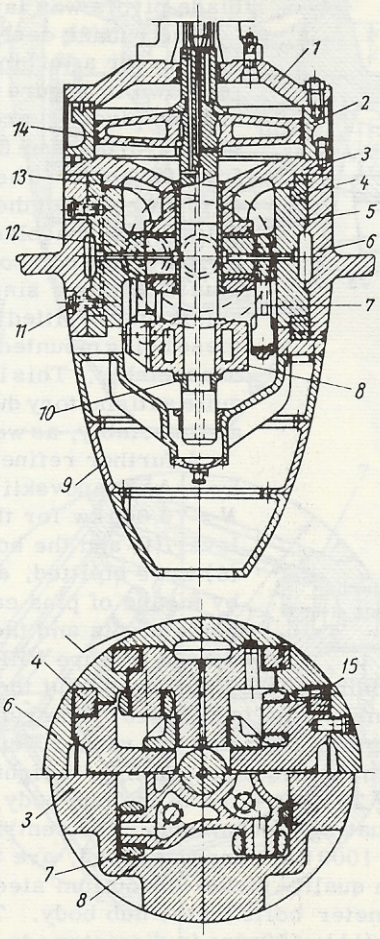


FIGURE VIII. 7. Kaplan runner D_1 = 9.0 m, N = 70,000 kw for the Rybinsk HEP

The runner designed at LMZ by Ya. S. Dehterev for turbines of the Volga plant imeni Lenin is shown in Figure VIII. 8. It is the largest Kaplan runner in the world (D_1 = 9.3 m). Its blade-actuating mechanism – typical of many of turbines manufactured at LMZ in recent years — will be described in detail.

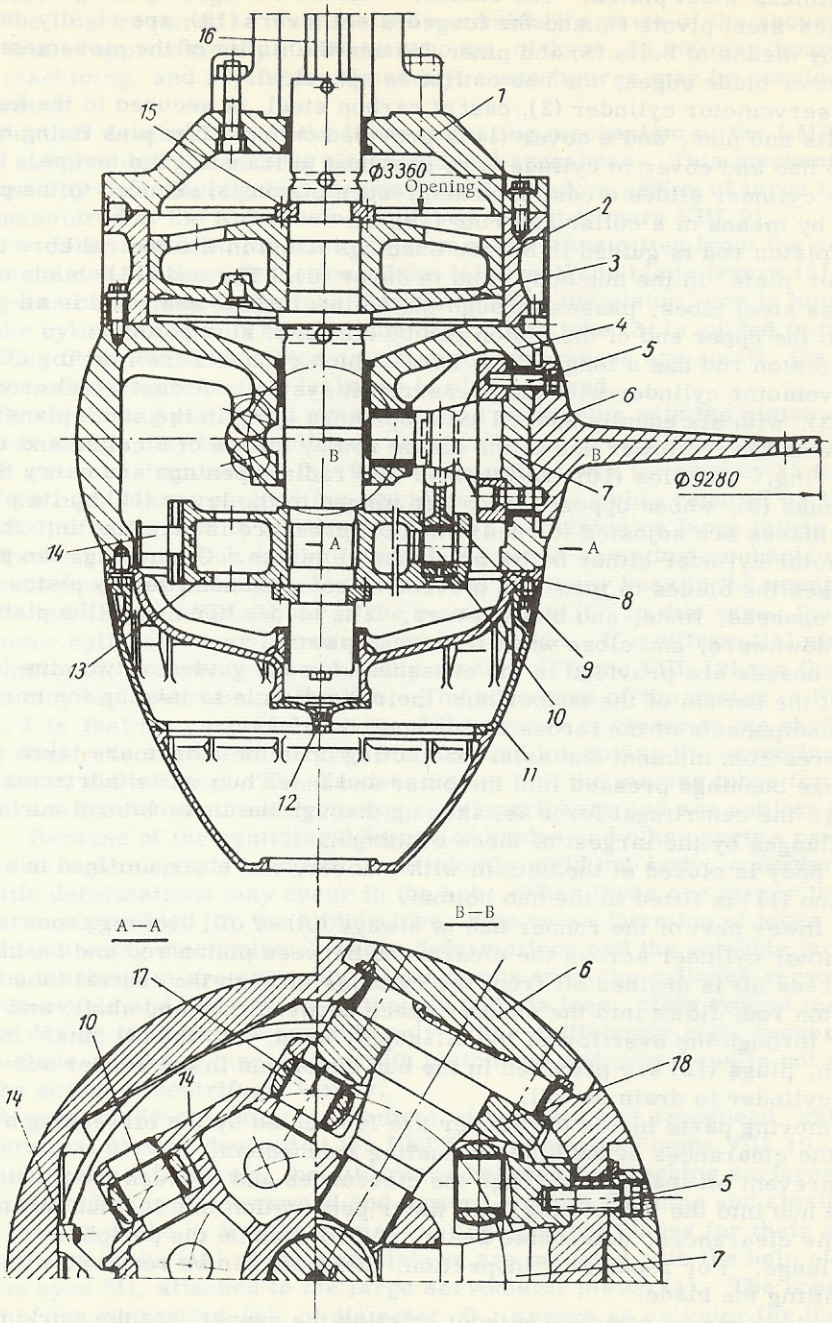


FIGURE VIII. 8. Turbine runner for the Volga HEP imeni Lenin: D = 9.3 m, N = 126,000 kw

The runner has six blades (6), cast of stainless or carbon steel lined with stainless-steel plates. The blades, fitted into the hub openings (4), the forged-steel pivots (7),and the forged-steel levers (18), are rigidly connected by means of bolts (5) and pins. Within the limits of the movement of the inner blade edges, the hub outline is spherical.

The servomotor cylinder (2), cast of carbon steel, is secured to the hub with bolts and pins, and a cover (1) is provided on top. The pins fixing cylinder to hub and cover to cylinder are designed to transmit the torque. Inside the cylinder slides a cast-iron semi-open piston (3) secured to the piston rod by means of a collar and ring (15).

The piston rod is guided in bronze bushings fitted in the central bore of the cover plate, in the hub body, and in cover (8). The rod (16), made of seamless steel tubes, passes through the hollow turbine shaft and is secured to the upper end of the piston rod by means of stud bolts.

The piston rod has a longitudinal bore, which connects the interior of the servomotor cylinder with the pressure oil system. A cast-steel crosshead (13), with six equally spaced axial openings lying in the same plane, is connected to the lower end of the piston rod by means of a collar and retaining ring. The pins (10) are inserted into radial openings and carry the blade links (9), whose opposite ends are hinged to the lever (17) by its pin.

The blades are adjusted (turned) when oil pressure is admitted into the servomotor cylinder either below or above the piston. On moving, the piston causes the blades to turn, the movement being transmitted by piston rod, crosshead, links, and blade levers. The blades open when the piston moves downward, and close when it moves upward.

Two bosses are provided in the crosshead for the guides of two pins (14) fitted at the bottom of the runner hub; their function is to take up the horizontal components of the forces acting upon the links.

The reaction moment and axial load acting upon the blades are taken up by bronze bushings pressed into the outer and inner hub walls (horizontal bearing); the centrifugal force is taken up through the inner lateral surface of the flanges by the largest of these bushings.

The body is closed at the bottom with a cover, and a streamlined hub extension (11) is fitted to the hub bottom.

The lower part of the runner hub is always full of oil, flowing from the servomotor cylinder across the clearances between piston rod and bushing. The excess oil is drained off from the cylinder through the central tube of the piston rod, flows into the annular space between tube and shaft, and further through the overflow of the oil-supply head, into the oil tank. In addition, plugs (12) are provided in the hub cover and in the runner servomotor cylinder to drain the oil.

All moving parts inside the runner are lubricated by the oil leaking across the clearances of the blade-actuating mechanism.

To prevent oil leakages through the clearances and between the pivots and the hub into the throat ring, and water penetration into the hub through the same clearances, detachable seals are provided on the periphery of the blade flange. For repairs or inspection, the seals can be removed without dismantling the blade.

Any blade can be removed without hoisting the runner into the working bay. Removal is effected by means of special equipment; the blade is lowered into the draft tube, and taken to the working bay, using the same

equipment, the blade is then refitted. Blade removal and refitting may also be carried out through the scroll.

The time required to machine and assemble the parts of the above runner totaled approximately 50,000 man-hours, of these, 30,000 man-hours were for machining, and 20,000 for assembly; these figures may be considered standard.

Further development of the blade-actuating mechanism at the LMZ led to a simpler design, without piston rod and crosshead. This mechanism, devised by G.S. Shchegolev, became widely used, a series of large turbines manufactured at the KhTZ being equipped with it (Figure VIII.9).

The force required for blade adjustment is transmitted from the servomotor piston (1) through the long links (4) directly to blade levers (5). Each long link moves inside the tube (3) connected to the piston, and is hinged on the cylindrical pin (2) in the tube head. The tube (3) is guided in the bushing (6) in the servomotor cover; since clearances are small, the necessary sealing to prevent oil leakages is also ensured.

By combining piston and crosshead and dispensing with the piston rod, runner design may be simplified, and weight and production time reduced. With a runner diameter of $D_1 = 9.3$ m, the weight was lowered by 25 to 30 t, and the man hours required for machining and assembly reduced by 1500 to 1800, of which 300 to 350 hours were for machining on large lathes.

Two variants of hub design in which the blade-actuating mechanism has no crosshead are possible: the cover with the inner boss in the upper part of the hub (Figure VIII.9), or in the cover below it. In this case, the servomotor cylinder cover increases the hub weight. If a differential piston is employed, the cover becomes unnecessary (Figure VIII.10) and the inner boss may be located below the hub. The advantage of the design in Figure VIII.9 is that the center of gravity of the runner is closer to the shaft bearing, thus reducing the cantilever moment and improving the operating conditions of the bearing. The disadvantage is that the moving tubes for the links are located on the servomotor cover periphery and are subject to loading. Because of the centrifugal forces of blades and other parts – particularly at higher speeds – and an insufficiently rigid hub body, considerable elastic deformations may occur in the hub. When these are larger than the clearance provided for the sliding tube, they cause jamming of tubes and blade-actuating mechanism. These deformations and the possible jamming of the mechanism are particularly dangerous when the cylinder servomotor is removable and the rigidity of the hub body is less. This type of mechanism design is therefore possible only with a sufficiently rigid runner hub. The blade-actuating mechanism with piston rod and crosshead is not subject to the action of centrifugal forces.

A novel blade-actuating mechanism without rod and crosshead, using a differential piston, devised at the KhTZ, is shown in Figure VIII.10. It has two salient features: the difference between the working surfaces of the piston during its downward and upward strokes (opening and closing), and the use of the hydraulic moment acting upon the blades for their adjustment. The links (12) of the blade levers are mounted with the help of hinges to the eyes (3), attached to the large servomotor piston (4). The upper part of the runner hub (5), of diameter D_c, serves as cylinder for the servomotor. The small (stationary) piston consists of sleeve (10) – an extension of the inner hub body – and its cylinder (of diameter D_1) is the

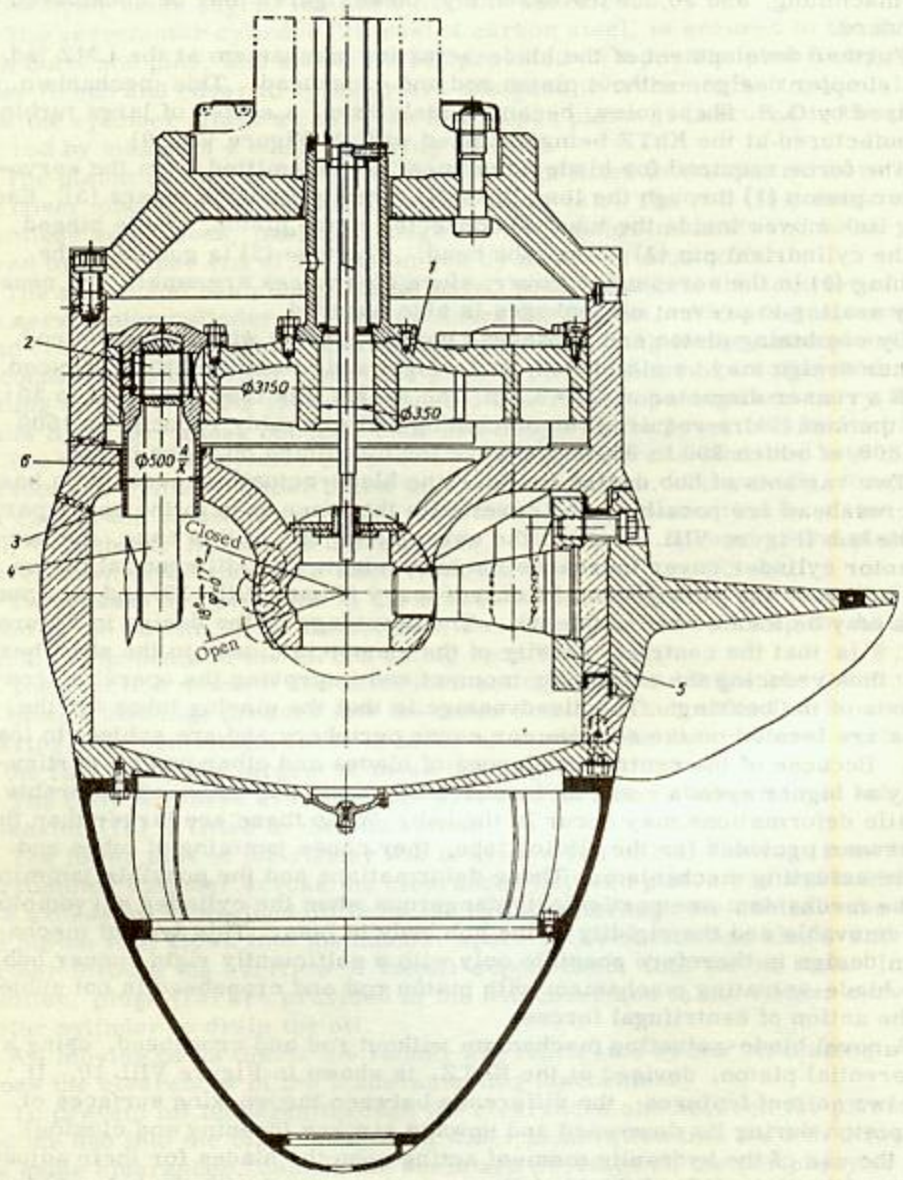


FIGURE VIII. 9. Blade-actuating mechanism with crank lever drive, without connecting rod or crosshead

inner cavity of the large piston (4). Two pressure spaces – A and B – are formed in this way. When pressure-oil is admitted into space A, the piston moves downward and the servomotor force for actuating the runner blades overcomes the hydraulic moment. When oil is admitted into space B, the whole piston moves upward, with the hydraulic moment assisting the servomotor force. In this design, the blade rotation axis is displaced toward the trailing edge, so as to make the hydraulic moment always tend to close the blades. The enlarged shaft flange (1) serves as a cover for the servomotor space A, and space B is closed at the top with cover (2), to which the oil-supply tubes are connected.

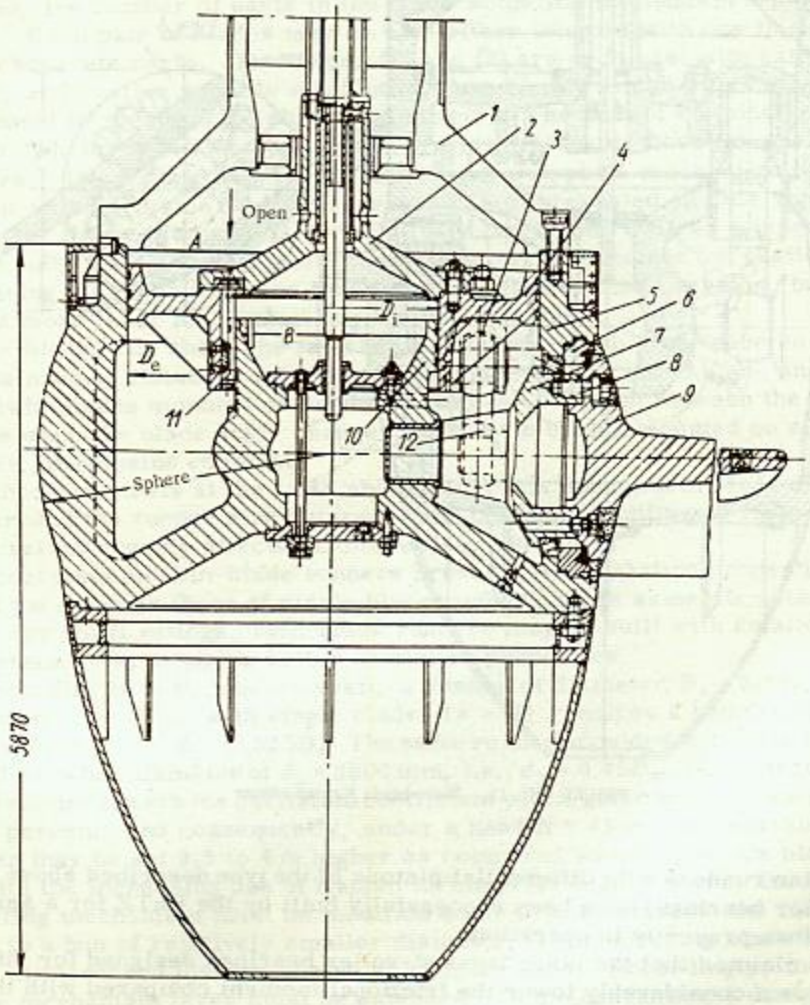


FIGURE VIII. 10. Blade-actuating mechanism with crank-drive and differential piston

The large blade pivot is guided by a tapered-roller bearing – the rollers being mounted between the ring (6) and the pivot collar (7) – unlike the plain bearings usually employed for this purpose. The blade flange (9) is secured to the pivot (7) by means of the bolts (8). In order to balance the torque exerted by the links due to their inclination, the piston (4) is guided in cylindrical pins (11).

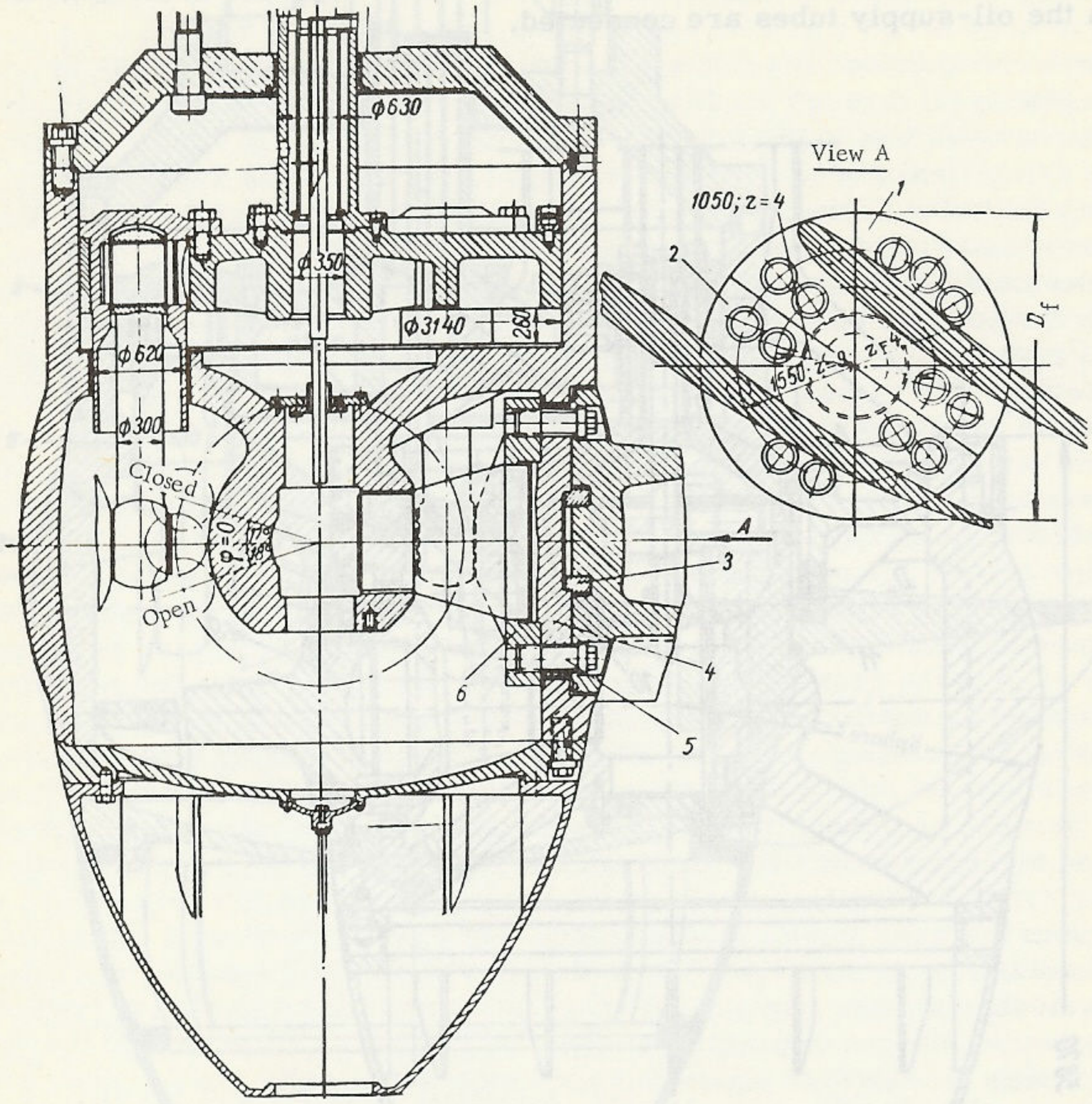


FIGURE VIII. 11. Twin-blade Kaplan runner

Kaplan runners with differential pistons of the type described above (without roller bearings) have been successfully built by the KhTZ for a series of turbines presently in operation.

It is claimed that the large tapered-roller bearings designed for this mechanism considerably lower the frictional moment compared with the normal plain bronze bearings. As yet, however, they have not been tried out in practice.

Design of actuating mechanisms for higher heads. To use Kaplan turbines for higher heads, their cavitation properties must first be improved,

thus permitting them to be set at a much lower elevation with respect to the tailwater level as compared with Francis turbines. The cavitation properties can be improved, in the first place, by increasing the over-all blade area, and in particular, the blade number. With a larger number of blades, on the other hand, it becomes difficult to locate the blade-actuating mechanism inside the runner hub, since this involves an increase in the number of parts which it must house. Apart from this, the loads become greater at higher heads, so that the dimensions of the parts must also be increased. All this causes an increase in hub diameter.

S. P. Mikhanovskii /62/ proposed a twin-blade Kaplan runner for high heads (Figure VIII. 11). As opposed to the ordinary runner, each flange is provided with two blades, but although the number of blades is thus doubled, the number of parts in the blade-actuating mechanism remains the same. Each pair of blades may be cast either integral with one flange, or in two separate parts. The blades (1) and (2) are each cast with half the flange, and — after suitable machining — are firmly joined into a single component by means of the shrunk-on ring (3). The rest of the blade parts – pivot (4), lever (6), and bolts (5) – are identical with those for ordinary runners. The blades may be actuated by any type of mechanism. The variant without piston rod or crosshead is represented in this figure. Here, the flange diameter D_f is relatively large and requires a large number of bolts (5). The composite design is more convenient for casting and machining the blade surfaces than the all-cast twin-blade version, but requires more labor for assembling the blade halves.

The blade body should be fastened to its flange with great care so as to maintain equal distances (pitch) between blades at the rated blade angle. With twin blades mounted on separate flanges, the pitch between the blades varies when the blade angle changes; with twin blades mounted on single flanges, it remains constant.

Laboratory tests at the LMZ showed that this nonuniform blade distribution around the runner circumference, at blade angle differing from the rated values, hardly affects turbine efficiency.

Model tests on twin-blade runners proved their cavitation properties to be about the same as those of single blade runners of the same diameter. However, for equal ratings, twin-blade runners may be built with smaller hub diameters, thus attaining better cavitation properties.

According to S. P. Mikhanovskii, a runner of diameter D_1 = 8.5 m, under a head H_{max} = 45 m, with single blades (z = 7) requires a hub diameter d_h = 4450 mm, i.e., $d_h = 0.525 D_1$. The same runner provided with twin blades (z = 8) has a hub diameter of d_h = 3800 mm, i.e., $d_h = 0.45 D_1$. The reduction in hub diameter lowers the cavitation coefficient σ at a given specific speed by 5 to 10 percent, and consequently, under a head H = 45 m, the twin-blade runner may be set 2.5 to 4 m higher as compared with single-row blades.

With the increasing use of Kaplan turbines for higher heads, the blade-actuating mechanism must be modified so as to accommodate the mechanism in a hub of relatively smaller diameter, while ensuring blade adjustment at increased load generated at a higher head. Accordingly, the arm of the mechanism lever must be extended. In the conventional design, the lever is located, in the horizontal cross section of the hub, in the same plane as the blade pivots, but in the new design, the lever is extended downward as in one of the early types shown in Figure VIII. 2. Figure VIII. 12 shows a modern design with slide blocks and oblique grooves for an eight-blade runner (D_1 = 6.6 m, H = 60 m).

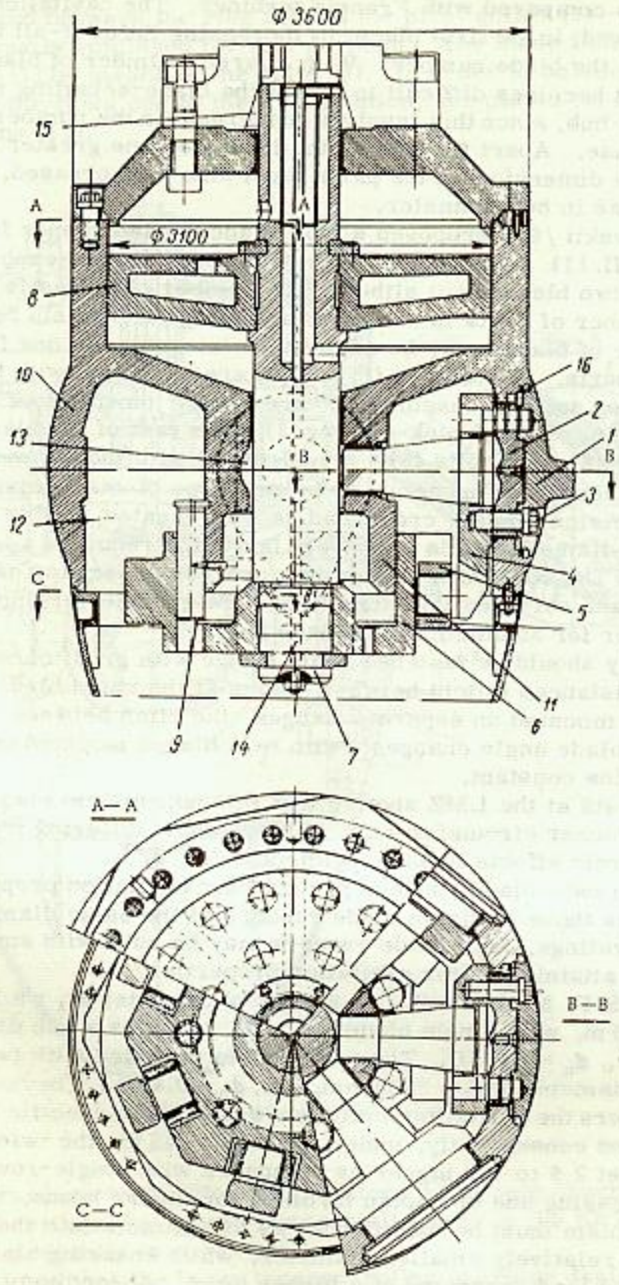


FIGURE VIII. 12. Kaplan runner of D_1 = 6.6 m, with guide-block mechanism and oblique grooves, for a head H = 60 m

Each blade (1) is secured to the pivot (2) and lever (4) by means of seven bolts (3) of 150 mm diameter. The lever extends downward and its pin is inserted in guide block 5, located in an oblique groove cut into one of the sides of the octahedral element (6). This element is connected to the piston rod (7) and is guided by the cylinder (11), which is part of the inner boss of the hub (10). Cylindrical pins (9) retain the octahedral element and take up the torque. The servomotor cylinder and piston (8) are located above.

The main disadvantage of this design, as stated before, is the friction between the guide block and the grooves, which increases the force required and complicates the manufacturing process. However, in modern workshops, the machining of surfaces and grooves of this type is not a major difficulty.

The hub cross section shows that in the blade-axis plane no space is available, so that levers of the necessary length must be arranged vertically.

Other designs of crank-drive blade-actuating mechanisms, with the long lever extending down the hub, are shown in Figure VIII. 13 (with inclined link) and Figure VIII. 14 (with double transmission). In the first variant (Figure VIII. 13), the lever (1) is connected to the crosshead (3) through the inclined link (2). The crosshead is guided by the inner boss of the runner body. In this design, the layout is simpler than in the foregoing, and levers of various lengths may be used, depending on the shape of the runner hub extension.

The blade-actuating mechanism with double transmission (Figure VIII. 14) is more complicated. By means of the link (2), lever (1) is connected with cranked lever (3) pivoted on hinge (6) mounted in the hub. By means of the link (4), the lower lever arm is connected to the crosshead (5), while the crosshead itself is guided in the central boss of the hub body. The layout, though more intricate, makes it possible to select various ratios between the lengths of the two arms and various relative positions of the parts, thus giving different variations of the torque as a function of the blade position, as well as increased servomotor efficiency. The advantage of this design, compared to other variants, is a smaller torque exerted upon the crosshead.

Basic types of blade-actuating mechanisms. All the blade-actuating mechanisms so far described may be grouped into five basic types: two with guide blocks and three with crank drive (shown in Figure VIII. 15):

1) with crank drive and vertical link (Figure VIII. 15, a);
2) with guide blocks and horizontal grooves (Figure VIII. 15,b);
3) with oblique grooves (Figure VIII. 15,c);
4) with crank drive and inclined link (Figure VIII. 15, d);
5) with crank drive and double transmission (Figure VIII. 15,e).

By examining this diagram and considering the relationship between the force P_s and the torque M_1, exerted upon the blades, characteristic of the mechanism, one may write the relationship for the force P_s — neglecting friction between the mechanism parts — for the types (Figure VIII. 15,a and b) with crank drive and with guide blocks.

$$P_s = \frac{M_1}{l_1 \sin \alpha}, \qquad \text{(VIII. 1)}$$

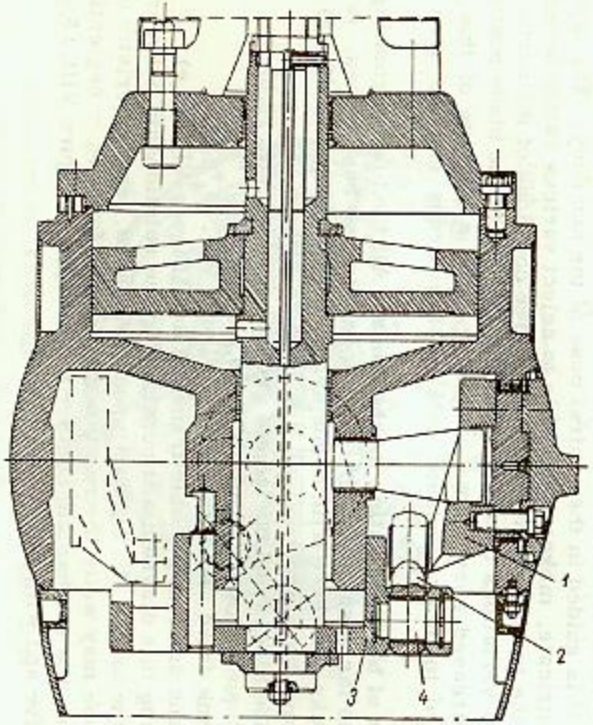


FIGURE VIII. 13. Blade-actuating mechanism with inclined link

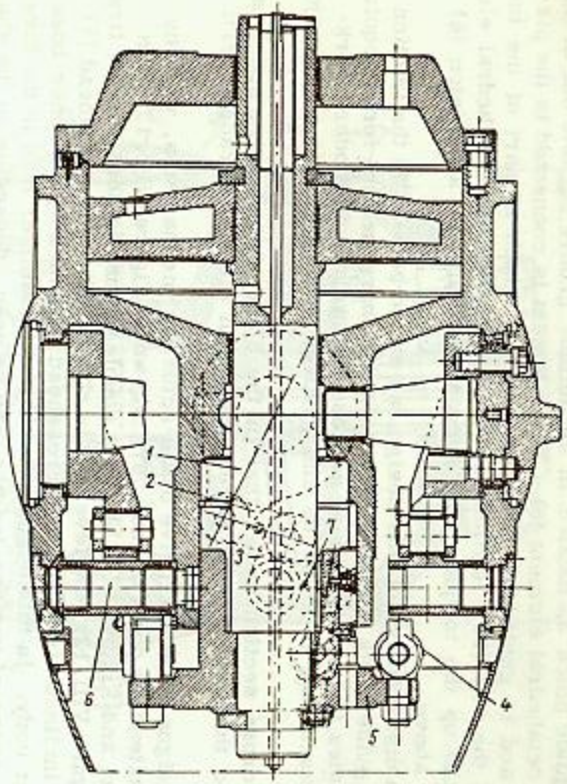


FIGURE VIII. 14. Blade-actuating mechanism with double transmission

where l_1 = length of the blade-lever arm;
α = angle between link and lever.

The angle α is usually selected close to 90°, and the force required therefore depends mainly on the length of the lever l_1.

The length of the lever is limited, since it is located in a horizontal plane, where the space is restricted by the hub wall.

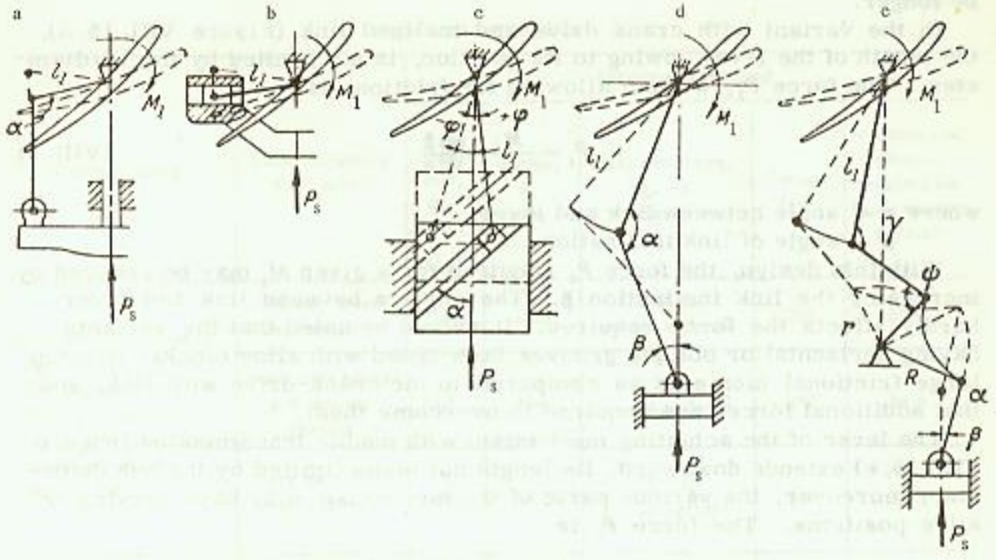


FIGURE VIII.15. Basic types of blade-actuating mechanism

In the mechanism with guide blocks and oblique grooves (Figure VIII.15,c), the lever extends downward and its length is not limited by the relatively small hub diameter. Neglecting friction, the force P_s is

$$P_s = \frac{M_1}{l_1} \cdot \frac{\sin \alpha}{\cos (\alpha + \varphi)}, \qquad \text{(VIII. 2)}$$

where α = angle of groove inclination;
φ = angle of lever inclination.

The angle φ of the lever inclination is not large: it varies between ±5° and ±10°.

The angle of the groove inclination is usually chosen between 30° and 60°.

According to the angle α selected, the relation $\frac{\sin \alpha}{\cos (\alpha + \varphi)}$ varies between the limits:

for α = 30°

$$\frac{\sin \alpha}{\cos (\alpha + \varphi)} = 0.6;$$

for $\alpha = 60°$

$$\frac{\sin\alpha}{\cos(\alpha+\varphi)} = 1.7.$$

If the groove-inclination angle is only $\alpha = 30°$, the force P_s required to produce the moment M_1 is a third of that required for $\alpha = 60°$. In the variant with guide blocks and oblique grooves, it is therefore easy to reduce the force P_s, in which case, however, the servomotor-piston stroke will be longer.

In the variant with crank drive and inclined link (Figure VIII. 15, d), the length of the lever, owing to its position, is not limited by the hub diameter. The force P_s, without allowing for friction, is

$$P_s = \frac{M_1}{l_1} \cdot \frac{\cos\beta}{\sin\alpha}, \qquad \text{(VIII. 3)}$$

where α = angle between link and lever;
β = angle of link inclination.

With this design, the force P_s required for a given M_1 may be reduced by increasing the link inclination β. The angle α between link and lever hardly affects the force required. It should be noted that the variants having horizontal or oblique grooves both fitted with slide blocks, develop large frictional moments as compared to the crank-drive with link, and that additional forces are required to overcome them.

The lever of the actuating mechanism with double transmission (Figure VIII. 15, e) extends downward, its length not being limited by the hub diameter; moreover, the various parts of the mechanism may have varying relative positions. The force P_s is

$$P_s = \frac{M_1}{l_1} \cdot \frac{r}{R} \cdot \frac{\cos\beta \sin\psi}{\sin\alpha \sin\gamma}, \qquad \text{(VIII. 4)}$$

where R and r = arms of the double lever;
$\alpha, \beta, \gamma, \psi$ = angles between the parts of the mechanism.

This design has two characteristic features: the value of the force may be varied within wide limits, while various laws of variation of required force with blade position may also be obtained.

A longer hub is required in this design, and, owing to the greater number of links, the frictional moment is also greater than in conventional mechanisms.

Hub dimensions for higher heads. With conventional Kaplan runners, the dimensions of the hub are determined mainly by the design of the blade-actuating mechanism located in it.

There are two mutually dependent stages in designing a blade-actuating mechanism: the arrangement of the blades inside the hub, and their rotation (adjustment).

At higher heads, the loads acting upon the runner increase, as do the hydraulic moments. Greater servomotor forces are therefore required to turn the blades; they may be obtained by increasing either servomotor diameter or oil pressure in the governor system. Greater forces involve larger dimensions of the blade-actuating mechanism, so that the hub diameter has to be increased.

The required forces, and consequently, the parts of the actuating mechanism and the hub diameter, may be reduced by using a mechanism with a higher transmission ratio between servomotor and blade.

At the LMZ, L. N. Petrov and L. D. Esin /70/ studied several blade-actuating mechanism designs. Runner servomotor ratings for various mechanisms are presented in Table VIII. 1.

TABLE VIII. 1

High-head turbine data

Turbine rating		Blade-actuating mechanism	Servomotor required				
			Diameter, D_s mm	Stroke, S, mm	Maximum force, kg, for pressure p	Torque t·m	Minimum oil pressure required for blade rotation, kg/cm^2
Head H = 43 m, runner diameter D_1 = 5.0 m, hub diameter d_h = 0.55D_1, number of blades z = 7, maximum blade-adjustment angle = 30°		Ordinary lever mechanism	2150	196	1044 for p = 30 kg/cm^2	205	20.8
		With slide blocks and oblique grooves	2100	345	827 for p = 25 kg/cm^2	285	18.6
		Lever mechanism with inclined link	1940	310	705 for p = 25 kg/cm^2	219	18.5
Runner diameter D_1 = 6.6 m, hub diameter d_h = 0.545D_1, number of blades z = 8,	H = 50 m	Ordinary lever mechanism	3100	225	1808 for p = 25 kg/cm^2	407	18.5
	H = 60 m	With slide blocks and oblique grooves	3100	404	1808 for p = 25 kg/cm^2	730	13.0

As can be seen from this table, for a turbine with runner diameter D_1 = 5.0 m, and head H = 43 m, it is the blade-actuating mechanism with inclined link that requires a servomotor of the smallest diameter and torque. The mechanism with slide blocks and oblique grooves requires a servomotor of larger diameter and a greater maximum force. The largest and most powerful servomotor is needed for the ordinary crank-drive mechanism; this may be explained by the short crank arm, characteristic of this type.

A turbine with runner diameter D_1 = 6.6 m, hub diameter d_h = 0.545D_1 and eight blades was successfully used at a head of H = 50 m. The same turbine, equipped with a slide-block mechanism and built for an even higher head — H = 60 m, requires for blade rotation a minimum oil pressure of only 13.0 kg/cm^2, instead of 18.5 kg/cm^2.

The importance of selecting the most appropriate type of blade-actuating mechanism — particularly at high heads — can be seen from the data in

Table VIII. 1. At higher heads it is also advisable that runner and blade-actuating mechanism parts be calculated more exactly.

The strength calculation is usually made for the most unfavorable loading conditions, considering not the force required to turn the blades, but the maximum force that may be developed by the servomotor piston.

Exact calculation makes it possible to reduce excess safety margins, and also to obtain blade-actuating mechanisms of smaller dimensions, and consequently smaller hub diameters, thus giving the runner better cavitation properties.

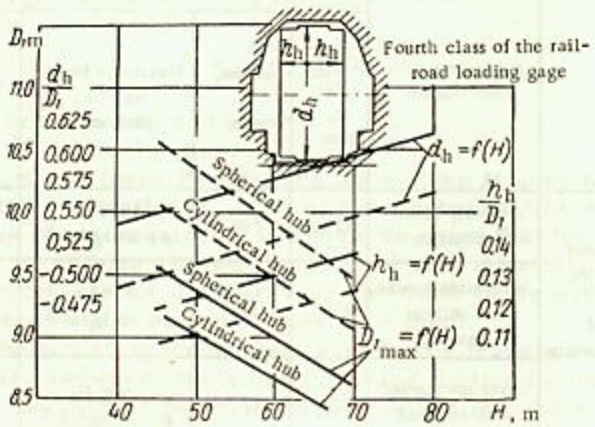


FIGURE VIII. 16. Chart for determining the hub dimensions of high-head runners:
——— blade removable from pivot
– – – – blade fixed to pivot.

The studies carried out at the LMZ made it possible to establish minimum dimensions for runner hubs housing high-head blade-actuating mechanisms, as well as limiting values for runner diameters which nevertheless permit transportation of the integral runner hub.

The chart shown in Figure VIII. 16 represents the runner diameter $D_1 = f(H)$, hub diameter $d_h = f(H)$, and hub height $h_h = f(H)$ as a function of head, for various blade designs with removable and fixed pivots. A blade-actuating mechanism with inclined link was considered in each case. It appears that in the case of removable pivots, since the pivot-blade assembly has to fit inside the hub, a large hub is required and the diameter of the runner has to be made smaller. For instance, at $H = 60$ m, with a spherical hub, the runner diameter equals only $D_1 = 9.0$ m if the blade pivots are removable, and $D_1 = 9.75$ m if they are not; in the first case, a hub diameter of $d_h = 0.575 D_1$ is required, while in the second case, $d_h = 0.525 D_1$, and correspondingly, $h = 0.118 D_1$ instead of $h = 0.13 D_1$.

According to the chart, the following hub dimensions are recommended in relation to the head.

Runners with removable blades:

Head H = 35—40 m	Hub diameter		$d_h = 0.54\,D_1$
" H = 40—50 m	"	"	$d_h = 0.56\,D_1$
" H = 50—60 m	"	"	$d_h = 0.58\,D_1$
" H = 60—70 m	"	"	$d_h = 0.6\,D_1$

Runners with fixed blades

Head H = 35—40 m	Hub diameter	$d_h = 0.49\,D_1$
" H = 40—50 m	" "	$d_h = 0.51\,D_1$
" H = 50—60 m	" "	$d_h = 0.53\,D_1$
" H = 60—70 m	" "	$d_h = 0.55\,D_1$

Sealing and lubrication of the blade-actuating mechanism. In all modern Kaplan turbines, the blade-actuating mechanism is lubricated with oil provided by the governor system. Several firms use pressure lubrication, effected by piston pumps connected to the crosshead, which provide periodic oil supply to the friction surfaces of the blade pivots.

In the LMZ and KhTZ designs, lubrication is effected periodically by oil flowing from the servomotor cylinder across the clearances in the rod bushing. The oil flows when pressure builds up in the lower part of the cylinder. For pressure relief, the servomotor communicates through a pipe with an overflow tank, located in the oil-supply head above the generator; the pressure inside the hub is therefore equal to the static pressure of the liquid column (1.5 to 2.0 atm). Special seals — usually located between the blade flanges and the runner hub — are provided to seal the hub against water and prevent the oil from leaking out. The lubrication of the blade-actuating mechanism is illustrated in Figure VIII. 12. From the servomotor cylinder the oil flows through the clearance between rod and bushing into the cavity (13), whence it enters the bushings of the inner and outer blade-pivot bearings and the working surfaces of the levers; from there it passes into hub cavity (12) which is connected with the annular space (15) inside the shaft by means of the pipe (14) passing through the rod. Space (15) is connected at its upper end with the overflow tank of the oil-supply head. The oil from the runner may flow through the clearances between the blade pivots and their bearings, and this leakage may be considerable, particularly around the edge of the blade flange located below the rotation axis, owing to the vacuum that usually exists below the runner blades. At high heads which exceed the pressure inside the runner, water may leak into the hub along the upper part of the flanges, above the blades, where the water is under high pressure. The seals of the blade flanges — usually located along their peripheries (16) — are therefore under increased pressure above the blades, and under vacuum below them /29/.

Blade-flange seals commonly used in hydropower engineering until recently are shown in Figure VIII. 17. Each blade seal consists of a set of rings — one leather or rubber ring (1) pressed against the surfaces A and B of the blade flange, two spring rings (2) made of phosphor bronze, two rubber rings (3) and one steel ring (4), fitted on the stud bolt (5) and pressed by the nut (6) against the hub. The spring ring (2) presses the seal ring (1) against the blade. In this manner, the surface (A) is sealed and oil is prevented

from leaking out of the hub, while at (B) water is prevented from entering the runner. Oil and water under pressure force the spring ring against rubber ring (1).

High-quality spring rings provide a reliable sealing of the blades; but, unforturnately, to change the seals, either the blades or the runner must be dismantled, causing extended turbine shutdown.

With large runners, the diameter of the flange increases and with it the dimensions of the spring ring, so that it becomes difficult to manufacture it of high quality.

A recent innovation is the use of blade seals with separate helical springs, which may be removed to change the seal ring without dismantling the blades.

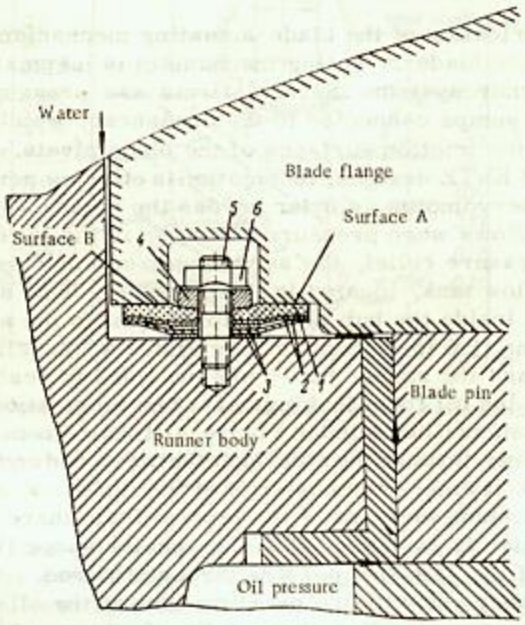


FIGURE VIII. 17. Blade-flange seals with spring rings

Figure VIII. 18 shows a removable blade seal used for the turbines of the Volga HEP imeni Lenin. It consists of a steel ring (2) secured with bolts (1) to the runner blade, and provided with thirty-six internal cylindrical bores in which helical springs (3) are fitted. A removable ring secured by means of screws (5) to the blade ring is pressed by the springs against the seal ring (6) and packing (14) – both made of either leather or rubber. The outer surface of the ring (4) (on the seal side) is plated with stainless steel. The seal ring (6) is pressed into the hub by the ring (7) – consisting of four sections – secured with bolts (8).

The springs (3) exert upon the ring (4) the force required to press the rubber ring (6) against the ring (7) in order to prevent oil from leaking out of the hub, and water from entering it.

In order to prevent oil leakages through the clearances between the blade ring (2) and pressure ring (4), the packing is provided; it is fastened with two rings — the inner one (11) and outer one (12), each of them made of six parts. These rings are secured to the rings (2) and (4) by screws (13). The seal (packing) is covered with a removable lid (9) consisting of 6 parts fastened by bolts (10).

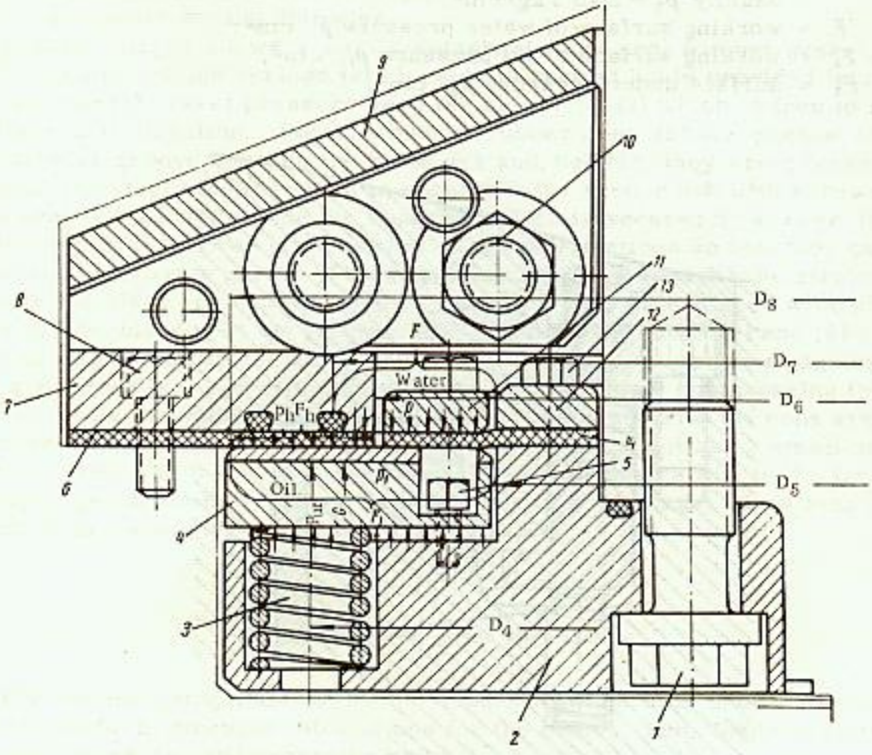


FIGURE VIII, 18. Detachable blade-flange seal with separate springs

If the seal ring (6) or packing (14), or even the springs, have to be renewed, the cover (9) and ring (7) may be detached and removed piece by piece, without removing the blade. The rubber ring (6) is cut and taken off first, then the sections of the inner and outer rings (11) and (12) are detached one by one; finally, the diaphragm is cut into parts and removed. It is not necessary to remove the ring (4), but only to displace it, in order to change the springs. Assembly is carried out in the reverse order. The rubber ring and the packing may be either stretched across the blade or glued together on the spot like the leather ring.

Operating experience with seals of this kind shows that the dimensions of the component parts must be checked very carefully, particularly the uniform thickness of the seal ring (6) and machining accuracy of the contact surface of ring (4). The concavity or convexity of the latter should not exceed 0.08 mm. The pressure ring (4) should not be very stiff; when deformed by the action of the springs, it comes into contact with ring (6).

The springs are designed to exert the force P

$$P = pF - p_1F_1 - p_2F_2, \qquad \text{(VIII, 5)}$$

where p = water pressure, kg/cm^2;
p_1 = oil pressure, kg/cm^2;
p_2 = pressure (predetermined) exerted between rings (4) and (6), usually p_2 = 2 to 3 kg/cm^2;
F = working surface of water pressure p, cm^2;
F_1 = working surface of oil pressure p_1, cm^2;
F_2 = surface under pressure p_2, cm^2.

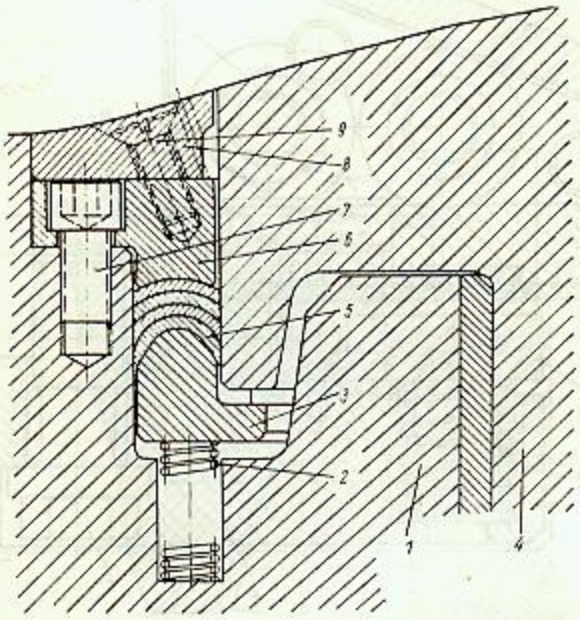


FIGURE VIII, 19. Blade seal of the cuff type — partly detachable

The pressures are

$$p = \left(H_1 - \frac{v^2}{2g}\right)\gamma,$$

where H_1 = static water head to the runner axis;
v = velocity of water flow through the runner;
γ = specific weight of water;

$$p_1 = H_2\gamma_1 + p_u + p_c,$$

where H_2 = static oil head inside the hub;
γ_1 = specific weight of oil;
p_u = oil pressure, acting when the runner is rotating;
p_c = pressure due to centrifugal force of ring (4) on the sealing surface.

The number of springs may be determined approximately from the formula

$$z = \frac{\pi D}{k + d}, \qquad \text{(VIII. 6)}$$

where D = diameter of spring pitch circle;
k = distance between springs, usually 5 to 7 cm;
d = outer spring diameter.

Figure VIII. 19 shows a partly-detachable cup seal without gasket. Helical compression springs (2), located in special seats provided into the runner hub (1), exert pressure upon the steel ring (3) which is free to move in the radial direction. Four leather or rubber cups (5) are packed into the annular groove between the blade (4) and hub (1); they are pressed against the steel ring (6) which is secured to the runner hub with screws (7). The seal is enclosed inside the cover (8) which is secured by screws (9). Both ring (6) and cover (8) are made of several sections so that they can be removed in separate parts. If the ring (5) is resilient enough to be stretched across the blade, or can be glued on in situ, it may be replaced without removing the blade. At the junction with blade (4) the rings (3) and (6) are shaped so as to allow the spreading of the cups by pressing them against the groove walls. For effective sealing, both adequate compressing force and accurate machining of the groove walls in contact with the cups are required. This type of seal is of simple construction; it has a small number of parts, and takes up little room. Its disadvantage lies in the fact that the springs cannot be replaced without removing the blade, since ring (3), is made in one piece.

49. FORCES ACTING UPON THE RUNNER

The forces acting upon the runner blades must be fully known before we can perform strength calculations for the blades, hub, blade-actuating mechanism parts, and generator drive.

The diagram of the forces acting upon the runner blade is presented in Figure VIII. 20, where P = lifting force, P_u = peripheral force, P_z = axial pressure, P_c = centrifugal force and G = blade weight.

The lifting force P, applied at the center of pressure at radius r, may be resolved into an axial force P_z and a peripheral force P_u. The lifting force P creates a hydraulic moment $M_h = Pe$, which tends to turn the blade about its axis of rotation. The axial forces P_z, together with the weights of the blades (Gz) and hub, produce an axial load carried by the thrust bearing.

The peripheral force P_u creates a torque transmitted to the generator rotor through the main shaft.

The centrifugal force P_c is taken up by the hub. It has a considerable influence — particularly at runaway speed — on the force required to adjust the blades. Consequently, the determination of these forces and moments under various operating conditions is necessary for correct design of the runner and blade-actuating mechanism, as well as for calculating the shaft and thrust bearing. With the characteristics of the flow and the geometry of the blade known, it is easy to determine the approximate analytical expression for the axial force P_z.

However, as a rule, the axial force and hydraulic moment exerted upon the blade are determined in laboratory tests.

The method applied at the LMZ for determining the forces acting upon the blade is set forth by M. V. Gushchin and V. G. Makarov in /27/.

The hydraulic moment M_h exerted upon the runner blade is determined by means of strain gages that measure the torsional strain of the pivot For this purpose, the blade is attached by an elongated pivot made of a material ensuring absence of residual deformation. By means of cables passing through the shaft, and a current collector, the strain gages are connected to the electrical strain-measuring installation. Experience has shown that in measuring the hydraulic moment the error does not exceed 10 to 15%.

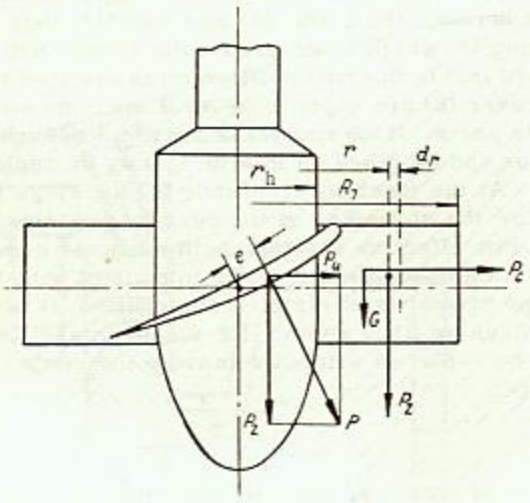


FIGURE VIII, 20. Diagram of the forces acting upon the runner blade

The axial pressure P_z acting upon the runner model is determined by measuring the strains induced in special beams, to which the thrust collar is secured. These strains are also determined by means of wire strain gages. In measuring axial pressure the error does not exceed 3 to 5%.

The measurements are usually carried out for seven or eight blade angles. For each of these, five or six distributor openings are studied, at various rotational speeds, in the operating region of the universal turbine chart. Consequently, the hydraulic forces are measured at two or three hundred points within a wide range of turbine operating conditions and for conditions in which the regulating connection between distributor and runner blades is either functioning or not.

The results of model tests are expressed as dimensionless values. The unit axial force equals

$$P'_{1z} = \frac{P_z}{D_1^2 H \gamma}. \qquad \text{(VIII. 7)}$$

Under isogonic conditions, the unit forces are the same for a given series of geometrically similar turbines. The magnitude of the axial force for various turbines of the series varies directly with the head and with the square of the runner diameter.

The results of laboratory tests are usually plotted as curves on Q_1' and n_1' coordinates, for various values of the unit force P_{1z}'.

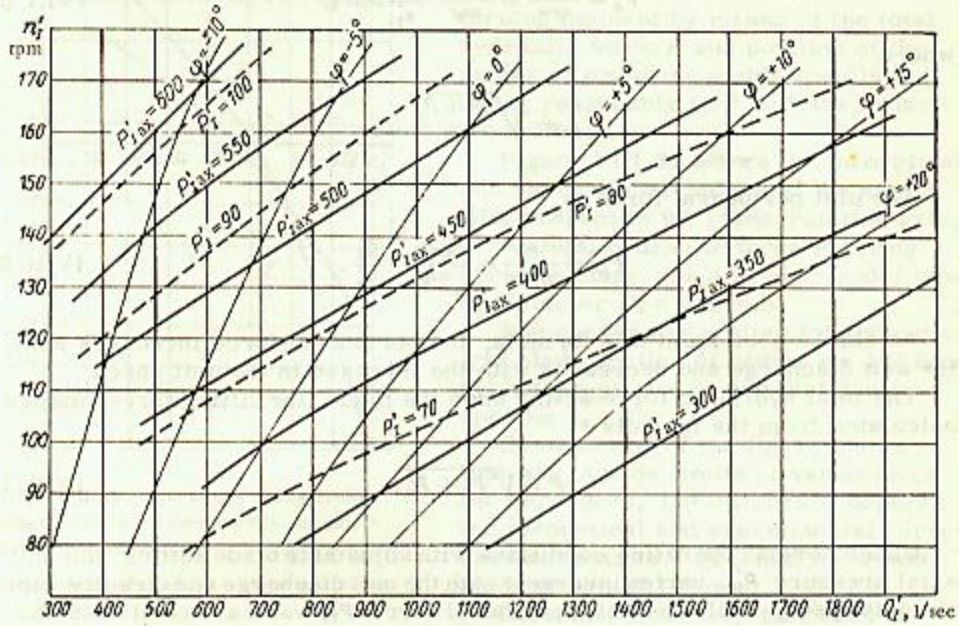


FIGURE VIII.21. Reduced axial force P_{1ax}', acting upon all the blades, and resultant unit force P_1' acting upon one blade of the PL-587 runner

The curves of the resultant unit force P_1' acting upon one blade and of its axial component P_{1ax}' acting upon all the blades of the PL-587 runner are shown in Figure VIII.21. The values of P_{1ax}' given are not dimensionless like those in Formula (VIII.7), but dimensional, according to the LMZ formula:

$$P_{1ax}' = \frac{P_z}{D_1^2 H}.$$

The character of the curves is similar for all runner categories. It appears from the graph, that with the normal regulating connection between distributor and blades operating, the unit axial force P_{1z}' varies inversely with the unit discharge Q_1' and hence with the blade angle $\varphi°$, and directly with the unit speed. The maximum value of the unit axial force corresponds to small blades angles. It should be noted that, according to experimental data, the axial force varies inversely with the unit speed for fixed blade setting when the turbine operates as a pump.

For a strength calculation of the blade-actuating mechanism, not only the axial water pressure, but also the total hydraulic force composed of the axial and the peripheral force must be known.

The peripheral force P_u may be determined if the rotational speed and the turbine output are known, and if this force is related to the mean cylindrical section which divides the annular area between the outer blade diameter and the hub diameter into two equal parts.

$$P_u = \frac{N}{z_1 r \omega} = \frac{30\eta}{\pi z_1 r} \cdot \frac{Q_1'}{n_1'} D_1^3 H\gamma. \qquad \text{(VIII. 8)}$$

where

$$r = \sqrt{\frac{R_1^2 + r_h^2}{2}}.$$

The unit peripheral force is

$$P_{1u}' = \frac{P_u}{D_1^2 H\gamma} = \frac{30\eta D_1}{\pi z_1 r} \cdot \frac{Q_1'}{n_1'}. \qquad \text{(VIII. 9)}$$

As can be seen from this formula, the peripheral force increases with the unit discharge and decreases with the increase in the unit speed.

The total hydraulic force acting upon the blade (the lifting force) may be calculated from the formula

$$P = \sqrt{P_z^2 + P_u^2}. \qquad \text{(VIII. 10)}$$

Under normal operating conditions with adjustable blade setting, the unit axial pressure P_{1z}' varies inversely with the unit discharge and directly with the unit speed, while the unit peripheral force P_{1u}' varies directly with the unit discharge and inversely with the unit speed, so that the resultant unit hydraulic force

$$P_1' = \sqrt{P_{1z}'^2 + P_{1u}'^2} \qquad \text{(VIII. 11)}$$

may have a different character depending on the unit speed and discharges: the force may either increase or decrease.

Figure VIII. 21 also shows the curves of variation of the resultant unit hydraulic force, acting upon one blade of the PL-587 runner, with the unit speed n_1 and unit discharge Q_1' for various blade-setting angles, with the turbine operating under adjustable blade conditions. In this case, the resultant unit force varies directly with the unit speed and inversely with the unit discharge.

In addition to the hydraulic forces acting upon the blade, the distance e from the point of application of the resultant force to the rotation axis of the blade should also be known. This permits us to determine the hydraulic moment exerted upon the blade

$$M_h = eP = M_1' D_1^3 H\gamma. \qquad \text{(VIII. 12)}$$

The value of the hydraulic moment depends on the arm e (Figure VIII. 20) that characterizes the distance from the center of pressure to the rotation axis of the blade, but the position of the center of pressure depends on the operating conditions, and varies for different n_1', Q_1' and $\varphi°$. The absolute value of the arm e is not great, so that, the axis of rotation being fixed, not only the value, but also the sign of the hydraulic moment may change under varying operating conditions.

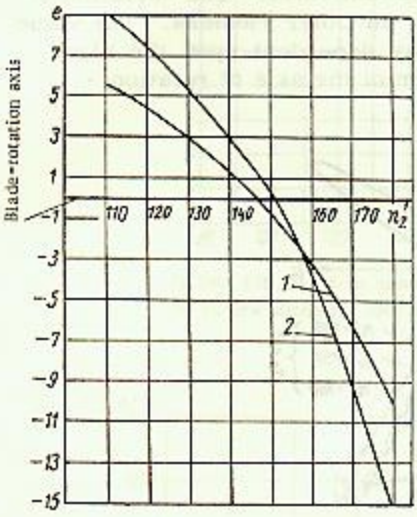


FIGURE VIII. 22. The arm of the hydraulic moment, calculated theoretically and determined experimentally:

1 — experimental curve; 2 — calculated curve.

The theoretical calculation of the turning moment by means of the total hydraulic force P and position of the center of pressure yields results that agree reasonably well with the experimental data.

Figure VIII. 22 shows the theoretical and experimental values of the arm e, with respect to the blade-rotation axis, of the total hydraulic force P acting upon the blade, for a runner model type of diameter D_1 = 460 mm.

The curves are plotted for the central blade section of radius r = 175 mm, at blade angle φ = 0° and distributor opening a_0 = 22.

Examination of the figure shows that within wide limits of variation of the unit speed, the difference between the theoretical and experimental curves does not exceed 3 or 4 mm for a total blade length of 196 mm.

It seems, however, that even so slight a difference is unsatisfactory for practical purposes, since the rotation axis of the blade is usually selected so close to the center of pressure that the smallest error in the determination of the center location may alter the value of the hydraulic moment considerably. In the given case, the error may reach 50 percent. Hence, in turbine design, the position of the center of pressure and the hydraulic moment are usually determinable by tests only.

Experimental data on the pressure center of the blade of a given runner type, for a blade angle φ = +10°, distributor openings a_0 = 26 and a_0 = 34, and various unit speeds (n_1' = 130, 150, and 180) are shown in Figure VIII. 23.

It appears from the figure that the position of the center of pressure depends on the operating conditions; when the unit speed and the distributor opening (discharge) increase, the center of pressure moves toward the trailing edge.

Figure VIII. 24 shows — for fixed blade-setting — the experimental curves of variation in the unit hydraulic moment exerted upon the same blade set at an angle φ = +10°, for various distributor openings, as a function of unit speed: $M_1' = f(n_1')$ (a_0 = const and $\varphi°$ = const). Figure VIII. 25 shows the curves of the unit moments and forces as a function of unit discharge and speed, for fixed-blade conditions φ = +5° for the PL-587 runner. It appears

from the graphs that the value of the unit hydraulic moment varies considerably when the speed of the turbine changes. At low speeds, the hydraulic moment tends to close the blades.

With increasing unit speed the center of pressure moves toward the trailing edge; the closing moment decreases, passes through zero, and becomes negative at high speeds, tending to open the blades. At runaway speed, the opening moment reaches its maximum value. The variation of the moment with the speed is also similar in other runners. The value and direction of the moment are essentially dependent upon the blade shape and dimensions, and upon the location of the axis of rotation.

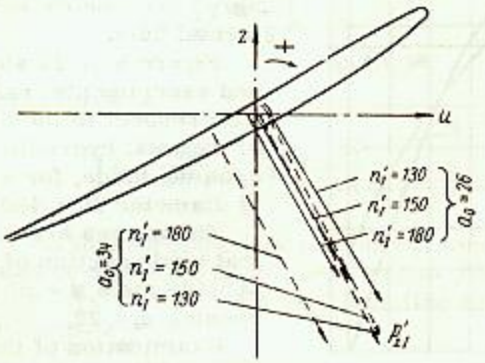


FIGURE VIII. 23. Position of the center of pressure at different operating conditions

The curves of variation of unit hydraulic moments acting upon the PL-587 runner blades in dependence on n_1' and a_1', for adjustable blade settings (with regulation connection operative), are represented in Figure VIII. 26.

Inspection of the curves shows that for adjustable blade settings, the unit hydraulic moment M_1' varies little in the working region of the chart, when the unit discharge increases.

The moment M_1' varies drastically with the increase in unit speed. At high unit speeds, the moment tends to open the blade, at low ones, to close it.

This variation in the unit hydraulic moment obtains if the axis of rotation of the blade is arranged near the center of pressure so that the moment is as small as possible, and its extremal values for closing and opening approximately equal. This permits the most efficient use of the servomotor force, which is approximately the same at opening and closing. It should be noted, however, that since the closing moment usually corresponds to low unit speeds, i.e. to high heads for full-scale turbines, and the opening moment to high unit speeds, it is advisable that the greatest value of the positive unit moment M_1' (in the working region of the turbine) be smaller than the absolute value of the negative moment, in a relation inversely proportional to the head ratio.

A more favorable relation between the extremal values of the unit moment may be obtained by displacing the axis of rotation toward or away from the trailing edge.

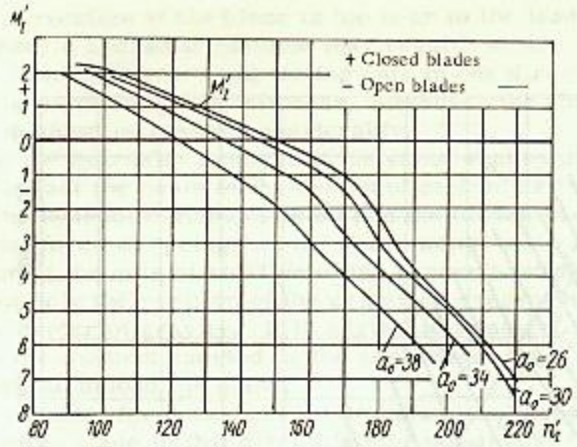


FIGURE VIII, 24. Unit hydraulic moments as a function of unit speed for various distributor openings under fixed-blade conditions

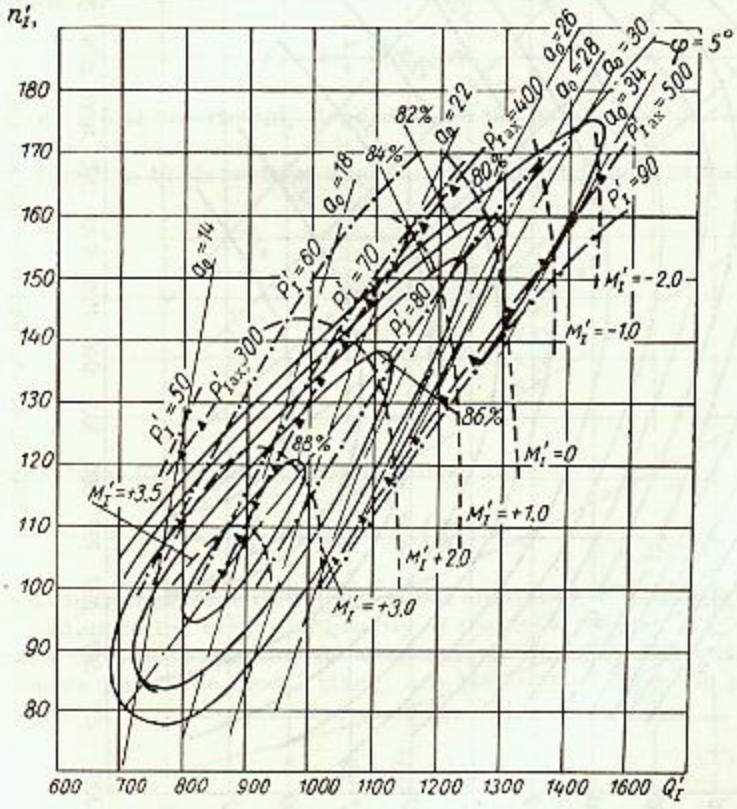


FIGURE VIII, 25. Unit moments and forces as functions of unit discharge and speed under fixed-blade conditions $\varphi = +5°$, for the PL-587 runner

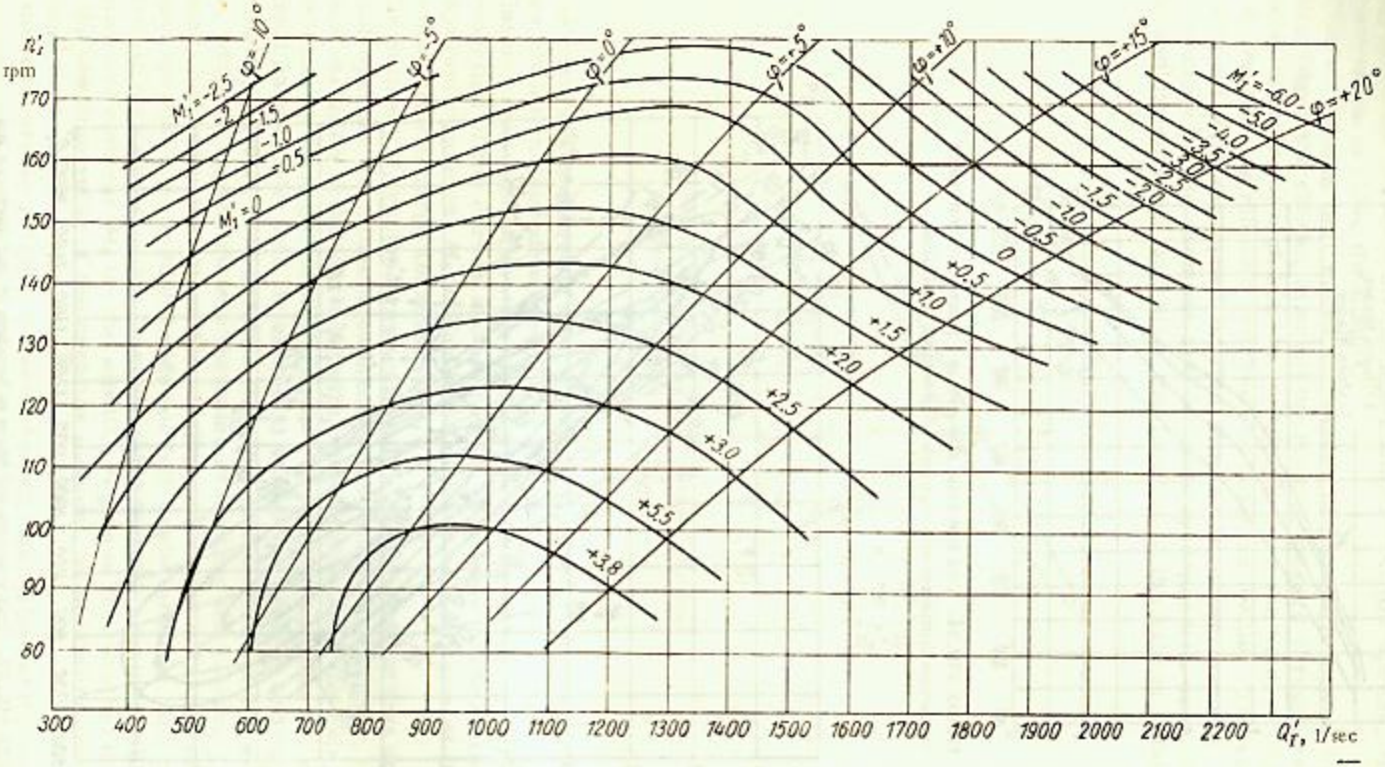


FIGURE VIII.26. Unit hydraulic moment acting upon the blade of the PL-587 runner, with adjustable-blade setting

If the axis of rotation of the blade is too near to the leading or trailing edge of the blade, a hydraulic moment may result, which, even at the extremal values, has the same sign, acting only in one direction under different operating conditions. In this case, however, the absolute value of the hydraulic moment increases considerably.

Maintaining the hydraulic moment at the same sign by displacing the axis of rotation is in fact the basis of the design of self-adjusting Kaplan runners, where the hydraulic moment acts upon the blades in one direction, and the external force of springs on the servomotor in the other.

The location of the axis of rotation of the runner blade should be selected considering not only the position of the center of pressure, but also the position of the center of gravity. It is advisable to select the axis in such a manner that the moment exerted by the centrifugal force about the axis of rotation tends to unload the blade.

Since the hydraulic force is directed downward and creates a moment tending to bend the blade in that direction, the position of the rotation axis with respect to the center of gravity should be selected so that the moment due to the centrifugal force is directed upward. The center of gravity should therefore be located below the axis of blade rotation.

For preliminary calculations, the axial pressure may be determined from the formula

$$P_z = k \frac{\pi}{4} D_1^2 H_{\max} m, \qquad \text{(VIII. 13)}$$

where k = empirical coefficient, depending on the number of blades and the blade angle.

For the smallest blade-setting angles, the largest values of the coefficient k are

Number of blades	Coefficient k
4	0.85
5	0.87
6	0.90
7	0.93

The centrifugal force acting upon the blade is

$$C = \frac{G}{g} \omega^2 R_{cg} = \frac{G}{g} \left(\frac{\pi n}{30}\right)^2 R_{cg},$$

where G = weight of blade with flange, pivot and lever, $G = G_f + G_b + G_p + G_l$;
R_{cg} = radius to the center of gravity of the blade system.

It is convenient to determine the weight of the blade by expressing it in terms of the weight of the model blade; the latter may obviously be weighed. The formula is

$$G_b = G_{mb} \frac{D^3}{D_m^3} \cdot \frac{\gamma}{\gamma_m},$$

where the subscript m denotes model data.

If no model data are available, the weight of the blade may be determined approximately by calculating the blade volume. For this purpose, the blade is divided into a series of truncated pyramids, whose volumes may be calculated from known formulas.

In determining the center of gravity of the blade system, one usually assumes that the centers of gravity of the blade, flange, pivot, and lever lie on the axis of rotation of the blade. The radius to the center of gravity may be either evaluated from model data or determined from the formula

$$R_{cgb} = \frac{\Sigma R_i \Delta V_i}{V},$$

where $R_i \Delta V_i$ = static moment of the elementary volume;
V = volume of blade;
R_i = radius to center of gravity of the elementary volume.

The position of the centers of gravity of the flange blade, pivot, and lever are determined by a graphical-analytic method.

The position of the center of gravity of the blade system may be determined from the equation of the static moments with respect to the turbine rotation axis

$$GR_{cg} = G_b R_{cgb} + G_f R_{cgf} + G_p R_{cgp} + G_l R_{cgl};$$

$$R_{cg} = \frac{G_b R_{cgb} + G_f R_{cgf} + G_p R_{cgp} + G_l R_{cgl}}{G}. \qquad \text{(VIII. 14)}$$

The position of the center of gravity of the blade depends on the blade thickness and geometrical shape in plane.

For turbines already built, equipped with runners of various types, the position of the center of gravity may be determined from the following formulas:

Radius to the center of gravity	(0.3 to 0.35) D_1
Distance from axis of rotation (in the direction of the trailing edge)	(0.01 to 0.02) D_1
Distance below axis of rotation	(0.05 to 0.02) D_1

50. DETERMINATION OF THE REQUIRED RUNNER SERVOMOTOR FORCE

Most conventional servomotors are located inside the runner hub and, therefore, their maximum diameter is limited by its size. If the servomotor is located outside the runner, between the shaft flanges or inside the generator hub, its diameter is not limited by the dimensions of the turbine water passages. However, the general layout of the turbine unit requires the use of a servomotor of minimum size. The servomotor-piston stroke depends on the design of the blade-actuating mechanism.

The servomotor force depends on the magnitude and application point of the forces acting upon the runner blade, on the frictional moments at the pivot bearings and in the links of the kinematic elements of the actuating mechanism, and on the kinematic layout itself.

The force developed by the servomotor is determined by its diameter and by the oil pressure. The diameter is largely predetermined by the size of the runner hub which in turn depends on the size of the water passages in the turbine. The calculation of the servomotor force essentially amounts to the determination of the required oil pressure for the selected blade-actuating mechanism design and servomotor diameter, for various turbine operating conditions.

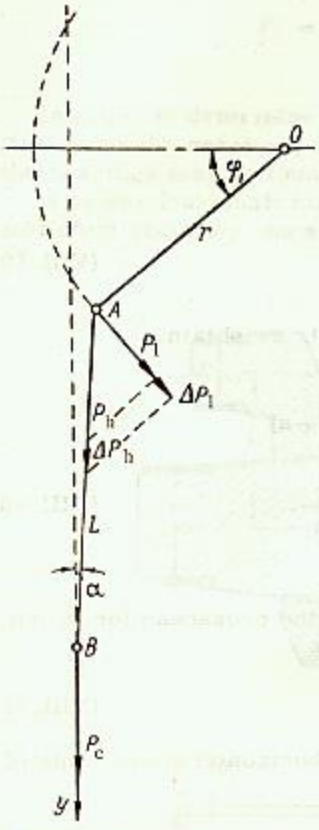


FIGURE VIII. 27. Diagram for determining the servomotor force

Calculation of the servomotor force for a mechanism with lever drive and pivots supported by two bearings. The force diagram is represented in Figure VIII. 27, where P_l = force on the lever, P_h = force on the link, r = lever radius, L = link length, P_c = = force on the crosshead pin, α = angle of link inclination, φ_1 = angle of lever rotation from the medium position.

In order to turn the blades by means of the lever, we must apply force P_l, which may be determined from the equation of equilibrium

$$P_l r = \pm M_h + M_f . \qquad \text{(VIII. 15)}$$

With the force P_l applied on the lever known, the frictional losses may be determined, and the required servomotor force calculated.

If at the lever pin a certain part, denoted by ΔP_h, of the force on the link is wasted in friction, then the force on the link is

$$P_h = \frac{P_l}{\cos(\varphi_1 + \alpha)} + \Delta P_h . \qquad \text{(VIII. 16)}$$

The frictional moment at the lever pin is overcome by the moment of the additional force ΔP_l, acting on the arm r

$$\Delta P_l r = f P_h \frac{d_p}{2},$$

where d_p = diameter of the lever pin;
f = coefficient of friction.

From the equation of frictional moments, it results that

$$\Delta P_h = \frac{f P_h \frac{d_p}{2}}{r \cos(\varphi_1 + \alpha)} . \qquad \text{(VIII. 17)}$$

From equations (VIII. 16) and (VIII. 17)

$$P_l = P_h \left[1 - \frac{f \frac{d_p}{2}}{r \cos(\varphi_1 + \alpha)} \right] \cos(\varphi_1 + \alpha). \qquad \text{(VIII. 18)}$$

The force on the crosshead pin, allowing for the frictional force ΔP_c

$$P_c = P_h \cos\alpha + \Delta P_c .$$

The force ΔP_c referred to arm r, becomes

$$\Delta P_c = \frac{f P_c \frac{d_p}{2} \cos\alpha}{r \cos(\varphi_1 + \alpha)}.$$

Consequently, [for $\cos\alpha \approx 1$]

$$P_h = \frac{P_c}{\cos\alpha}\left[1 - \frac{f\frac{d_p}{2}}{r\cos(\varphi_1+\alpha)}\right]. \qquad \text{(VIII. 19)}$$

By inserting the expression (VIII. 19) in (VIII. 18), we obtain

$$P_1 = \frac{P_c}{\cos\alpha}\left[1 - \frac{f d_p}{2r\cos(\varphi_1+\alpha)}\right]^2 \cos(\varphi_1+\alpha)$$

and hence,

$$P_c = \frac{P_1 \cos\alpha}{\left[1 - \frac{f d_p}{2r\cos(\varphi_1+\alpha)}\right]^2 \cos(\varphi_1+\alpha)}. \qquad \text{(VIII. 20)}$$

The servomotor force has not only to overcome the crosshead force, but also the friction at the crosshead guides ΔP_s

$$P_s = P_c + \Delta P_s . \qquad \text{(VIII. 21)}$$

The friction at the crosshead pins is due to the horizontal components of the forces applied on links and crosshead:

$$\Delta P_s = f P_c \tan\alpha \frac{r_h}{r_k}, \qquad \text{(VIII. 22)}$$

where r_h = radius of link location;
r_k = radius of guide location.

Consequently, from expressions (VIII. 21) and (VIII. 22), we obtain

$$P_s = P_c \left(1 + f\tan\alpha \frac{r_h}{r_k}\right).$$

Considering also the expression (VIII. 20), we have

$$P_s = \frac{P_1 \left(1 + f\tan\alpha \frac{r_h}{r_k}\right) \cos\alpha}{\left[1 - \frac{f d_p}{2r\cos(\varphi_1+\alpha)}\right]^2 \cos(\varphi_1+\alpha)}$$

whence,

$$P_1 = \frac{P_s \left[1 - \frac{f d_p}{2r\cos(\varphi_1+\alpha)}\right]^2 \cos(\varphi_1+\alpha)}{\left(1 + f\tan\alpha \frac{r_c}{r_k}\right)\cos\alpha}.$$

By inserting the value of P_1 in the initial equation (VIII. 15), we obtain the formula for the servomotor force

$$P_s = \frac{\left(1 \pm f\tan\alpha \frac{r_h}{r_k}\right)\cos\alpha(\pm M_h + M_f)}{\left[1 - \frac{fd_p}{2r\cos(\varphi_1+\alpha)}\right]^2 \cos(\varphi_2+\alpha)r}. \qquad \text{(VIII. 23)}$$

In order to determine the frictional moment at the blade pivot, we must first know the reactions in the pivot bearings. Generally, the reactions of the bearings may be found from the three-dimensional force diagram.

With vertical-shaft turbines, the axial force may be considered, with sufficient accuracy, as acting in the direction of the turbine rotation axis.

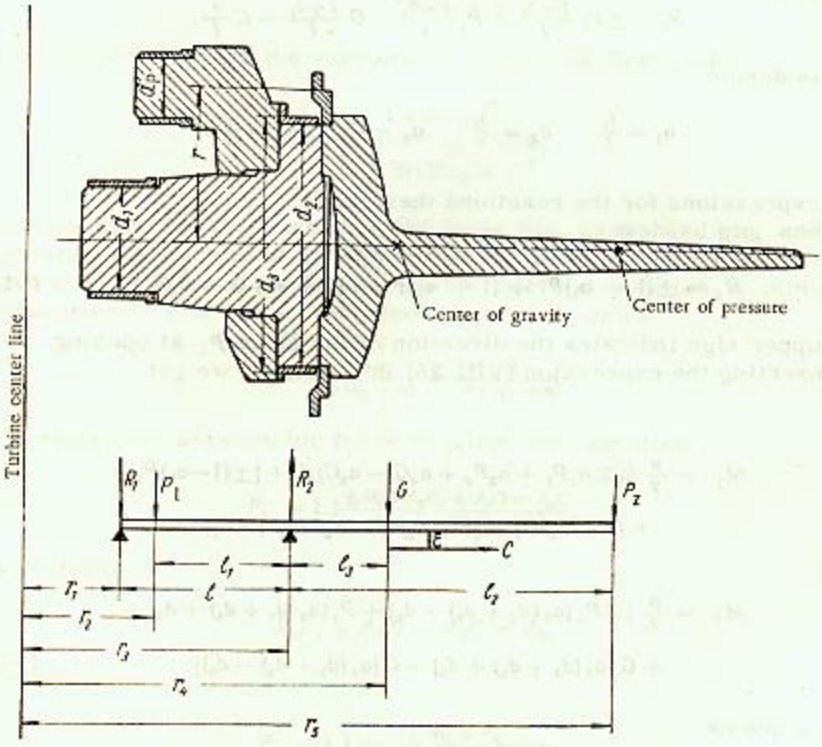


FIGURE VIII. 28. Diagram of loads on the blade pivot

In conformity with the blade-operating mechanism diagram (Figure VIII. 28), the frictional moment in the blade-pivot bearings is

$$M_f = \frac{\mu}{2}(R_1 d_1 + R_2 d_2 + C d_3). \qquad \text{(VIII. 24)}$$

The designations used in the figure are:

P_z = axial force upon one blade;

P_1 = force on the lever;

G = weight of blade assembly (blade, pivot, lever, and link);

C = centrifugal force;
R_1, R_2 = reactions of bearings;
l, l_1, l_2, l_3 = distances between bearings and applied forces;
r_1, r_2, r_3, r_4, r_5 = radii to points of application of the forces;
ε = arm of the centrifugal force;
d_1, d_2, d_p = pivot and pin diameters;
d_3 = diameter of bearing surface carrying the centrifugal force.

The reactions R_1 and R_2 may be determined from formulas of statics for two operating conditions (opening and closing)

$$R_1 = \mp P_1 \frac{l_1}{l} + P_2 \frac{l_2}{l} + G \frac{l_3}{l} - C \frac{\varepsilon}{l};$$

$$R_2 = \pm P_1 \frac{l - l_1}{l} + P_2 \frac{l + l_2}{l} + G \frac{l + l_3}{l} - C \frac{\varepsilon}{l}.$$

Let us denote

$$\alpha_1 = \frac{l_1}{l}; \quad \alpha_2 = \frac{l_2}{l}; \quad \alpha_3 = \frac{l_3}{l}; \quad \alpha_4 = \frac{\varepsilon}{l}.$$

The expressions for the reactions then become

$$\left.\begin{aligned} R_1 &= \mp \alpha_1 P_1 + \alpha_2 P_2 + \alpha_3 G - \alpha_4 C; \\ R_2 &= \pm (1 - \alpha_1) P_1 + (1 + \alpha_2) P_2 + (1 + \alpha_3) G - \alpha_4 C. \end{aligned}\right\} \qquad \text{(VIII. 25)}$$

The upper sign indicates the direction of the force P_1 at opening.
By inserting the expression (VIII. 25) in (VIII. 24), we get

$$M_f = \frac{\mu}{2} \{(\mp \alpha_1 P_1 + \alpha_2 P_2 + \alpha_3 G - \alpha_4 C) d_1 + [\pm (1 - \alpha_1) P_1 + (1 + \alpha_2) P_2 + (1 + \alpha_3) G - \alpha_4 C] d_2 + C d_3\}$$

whence

$$M_f = \frac{\mu}{2} \{\mp P_1 [\alpha_1 (d_1 + d_2) - d_2] + P_2 [\alpha_2 (d_1 + d_2) + d_2] + G [\alpha_3 (d_1 + d_2) + d_3] - C [\alpha_4 (d_1 + d_2) - d_3]\}. \qquad \text{(VIII. 26)}$$

Let us denote

$$\frac{\mu}{2} [\alpha_1 (d_1 + d_2) - d_2] = A_1;$$

$$\frac{\mu}{2} [\alpha_2 (d_1 + d_2) + d_2] = A_2;$$

$$\frac{\mu}{2} [\alpha_3 (d_1 + d_2) + d_3] = A_3;$$

$$\frac{\mu}{2} [\alpha_4 (d_1 + d_2) - d_3] = A_4.$$

We then get

$$M_f = \mp A_1 P_1 + A_2 P_2 + A_3 G - A_4 C. \qquad \text{(VIII. 27)}$$

By inserting the relation (VIII. 27) in (VIII. 23) we get

$$P_s = \frac{\left(1 + f\tan\alpha \frac{r_h}{r_k}\right)}{\left[1 - \frac{fd_p}{2r\cos(\varphi_1 + \alpha)}\right]^2} \cdot \frac{\cos\alpha}{\cos(\varphi_1 + \alpha)} \cdot \frac{\pm M_h \mp A_1 P_1 + A_2 P_z + A_3 G - A_4 C}{r}.$$

By inserting in this expression the value of P_1 and transforming, we obtain

$$P_s = \frac{\left(1 + f\tan\alpha \frac{r_h}{r_k}\right)}{\left[1 - \frac{fd_p}{2r\cos(\varphi_1 + \alpha)}\right]^2} \cdot \frac{\cos\alpha}{\cos(\varphi_1 + \alpha)} \times$$

$$\times \frac{\pm M_h + A_2 P_z + A_3 G - A_4 C}{r \pm A_1}. \qquad \text{(VIII. 28)}$$

In this expression for the servomotor force, the first factor

$$K_1 = \frac{1 + f\tan\alpha \frac{r_h}{r_k}}{\left[1 - \frac{fd_p}{2r\cos(\varphi_1 + \alpha)}\right]^2}$$

makes allowance for the friction at the lever pin, crosshead pin, and crosshead guides. For the type of mechanism considered, $K_1 \approx 1.1$.

Since the deviation of the link from the vertical position is minimal, and consequently $\cos\alpha \approx 1$, the second factor becomes

$$K_2 = \frac{\cos\alpha}{\cos(\varphi_1 + \alpha)} \approx \frac{1}{\cos(\varphi_1 + \alpha)}.$$

Therefore, the servomotor force required for one blade

$$P_s = 1.1 \frac{\pm M_h + A_2 P_z + A_3 G - A_4 C}{(r \pm A_1)\cos(\varphi_1 + \alpha)}.$$

By denoting

$$A_2 P_z + A_3 G - A_4 C = A_0,$$

we obtain

$$P_s = 1.1 \frac{\pm M_h + A_0}{(r \pm A_1)\cos(\varphi_1 + \alpha)}.$$

By replacing the coefficients in the last expression by their values, we obtain

$$P_s = 1.1 \frac{\pm M_h + \frac{\mu}{2}\left\{\left[\frac{l_2}{l}(d_1 + d_2) + d_3\right] P_z + \left[\frac{l_2}{l}(d_1 + d_2) + d_3\right] G - \left[\frac{e}{l}(d_1 + d_2) - d_3\right] C\right\}}{\left[r \pm \frac{\mu}{2}\left[\frac{l_2}{l}(d_1 + d_2) - d_3\right]\right]\cos(\varphi_1 + \alpha)}. \qquad \text{(VIII. 29)}$$

The upper signs correspond to the opening of the blades.

Formula (VIII. 29) gives the required servomotor force for one blade. It depends upon the magnitude of the hydraulic moment M_h, the value of the axial force P_z, the weights of blade, lever and pivot $G\gamma$, the centrifugal force C, and the geometrical characteristics of the blade-adjusting mechanism.

Since the hydraulic moment and axial force P_z depend on Q_1' and n_1', and the centrifugal force depends on the speed, the calculation of the servomotor force should be performed for various operating conditions.

In order to obtain smaller values for the servomotor force in the formula (VIII. 29), it is important to have as small diameters d_1, d_2 and d_3 as possible, and as large a distance l between bearings as possible. Yet, the pivot diameters are usually selected according to the load they are subjected to and the permissible specific pressure. The distance between bearings is limited by the hub diameter which is determined by the runner size. It is therefore obvious that in designing the blade-actuating mechanism, maximum exploitation of the space in the hub cavity must be aimed at.

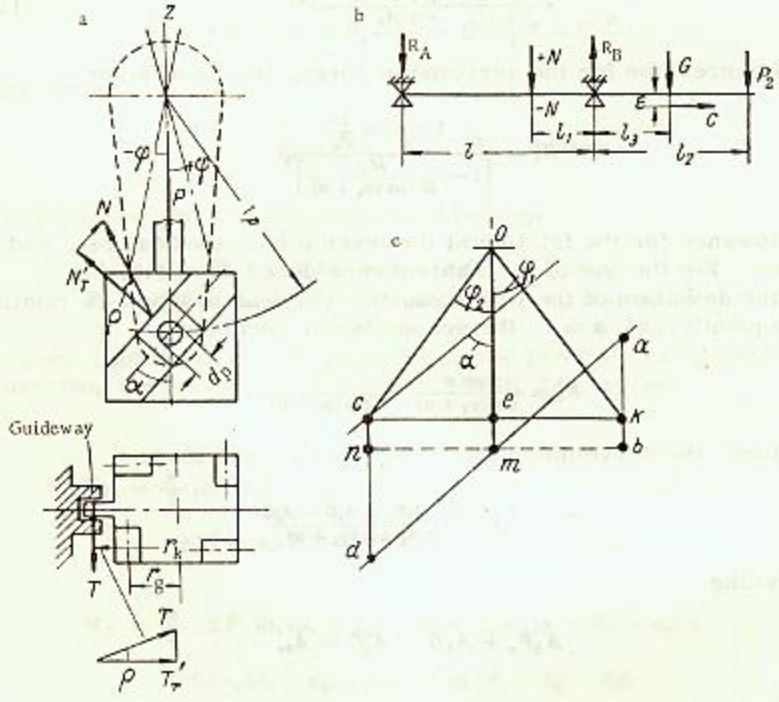


FIGURE VIII. 29. Diagram of the blade-actuating mechanism with slide-block drive

Several types of blade-actuating mechanisms were considered in the foregoing chapter; their advantages and limitations were also analyzed from the standpoint of the required servomotor force.

With an increase in speed, the centrifugal force increases proportionally with the square of the speed, and the frictional moment also increases considerably. Therefore, the servomotor force required to turn the blades at runaway speed is much greater than at normal speed.

Calculation of the servomotor force required for a mechanism with slide blocks and oblique grooves. The diagram of the mechanism with slide blocks and oblique grooves is represented in Figure VIII. 29, a. With this type of mechanism, the lever is inclined downward. Slide blocks are

fitted to the lever pins and move in the oblique grooves. The crosshead is connected to the piston rod and is kept from turning about the vertical axis by means of a guideway.

The following forces act upon the crosshead: P = servomotor force, N = reaction of the slide block, with allowance for friction, and T = reaction of guideway with allowance for friction.

The equilibrium conditions for the vertical forces and the moments about the z axis are:

$$\left.\begin{aligned} P - Tz_k \sin\varrho - Nz_1 \sin(\alpha+\varrho) &= 0; \\ Tr_k z_k \cos\varrho - Nr_g z_1 \cos(\alpha+\varrho) &= 0, \end{aligned}\right\} \qquad \text{(VIII. 30)}$$

where z_k = number of guideways;
z_1 = number of blades;
ϱ = angle of friction;
α = angle of inclination of the crosshead grooves;
r_k = radius at which guideway reaction is located;
r_g = radius at which the slide block is located.

From (VIII. 30), we obtain

$$T = N\frac{\cos(\alpha+\varrho)}{\cos\varrho}\cdot\frac{r_g z_1}{r_k z_k};$$

$$N = \frac{P}{z_1}\cdot\frac{1}{\cos(\alpha+\varrho)\frac{\sin\varrho}{\cos\varrho}\cdot\frac{r_g}{r_k}+\sin(\alpha+\varrho)}.$$

By substituting $\frac{\sin\varrho}{\cos\varrho} = \tan\varrho = \mu$, we obtain

$$\left.\begin{aligned} N &= \frac{P}{z_1}\cdot\frac{1}{\mu\frac{r_g}{r_k}\cos(\alpha+\varrho)+\sin(\alpha+\varrho)}; \\ T &= \frac{P}{z_1}\cdot\frac{r_g z_1\cos(\alpha+\varrho)}{r_k z_k\cos\varrho\left[\mu\frac{r_g}{r_k}\cos(\alpha+\varrho)+\sin(\alpha+\varrho)\right]}. \end{aligned}\right\} \qquad \text{(VIII. 31)}$$

The reactions on the slide block and guideway, neglecting the frictional forces, are:

$$N_T' = N\cos\varrho, \quad T_T' = T\cos\varrho.$$

The required servomotor force is determined from the equation

$$M_1 = P_1 l_1 = \pm M_h + M_f, \qquad \text{(VIII. 32)}$$

where M_h = hydraulic moment upon one blade;
M_f = frictional moment in the pivot and lever bearings.

The force on the lever, allowing for the friction is

$$P_1 = N\cos(\alpha+\varphi+\varrho) - \mu N\frac{d_p}{2l_1} = N\left[\cos(\alpha+\varphi+\varrho) - \mu\frac{d_p}{2l_1}\right].$$

By inserting the value of N we obtain

$$P_1 = \frac{P}{z_1} \cdot \frac{\cos(\alpha + \varphi + \varrho) - \mu \frac{d_p}{2l_1}}{\mu \frac{r_g}{r_k} \cos(\alpha + \varrho) + \sin(\alpha + \varrho)}, \qquad \text{(VIII. 33)}$$

where φ = angle of lever (blade) rotation, having either the sign (—) or (+);

d_p = diameter of the lever pin.

The frictional moment at the blade pivots is

$$M_f = \frac{\mu}{2}(R_A d_A + R_B d_B + C d_m),$$

d_A = diameter of bearing A;

d_B = diameter of bearing B;

d_m = mean diameter of the lever collar;

R_A, R_B = reactions of blade pivot;

C = centrifugal force.

The reactions of bearings R_A and R_B are determined from formulas of statics. For the sake of simplicity, the forces are considered to act in one plane.

$$R_A = -\left(\pm N \frac{l_1}{l}\right) + P_z \frac{l_2}{l} + G \frac{l_3}{l} - C \frac{\varepsilon}{l};$$

$$R_B = \pm N \frac{l - l_1}{l} + P_z \frac{l + l_2}{l} + G \frac{l + l_3}{l} - C \frac{\varepsilon}{l},$$

where l_1, l_2, l_3, l and ε = distances according to Figure VIII. 29,b;

G = weight of pivot, lever and blade;

P_z = axial force of water on the blade.

By denoting

$$\alpha_1 = \frac{l_1}{l}; \quad \alpha_2 = \frac{l_2}{l}; \quad \alpha_3 = \frac{l_3}{l}; \quad \alpha_4 = \frac{\varepsilon}{l},$$

we obtain

$$R_A = -(\pm N \alpha_1) + P_z \alpha_2 + G \alpha_3 - C \alpha_4;$$

$$R_B = \pm N (1 - \alpha_1) + P_z (1 + \alpha_2) + G (1 + \alpha_3) - C \alpha_4.$$

By inserting in the expression for M_f the values of R_A and R_B and denoting

$$\frac{\mu}{2}[\alpha_1 (d_A + d_B) - d_B] = A_1,$$

$$\frac{\mu}{2}[\alpha_2 (d_A + d_B) + d_B] = A_2,$$

$$\frac{\mu}{2}[\alpha_3 (d_A + d_B) + d_B] = A_3,$$

$$\frac{\mu}{2}[\alpha_4 (d_A + d_B) - d_m] = A_4,$$

we obtain

$$M_f = -(\pm N) A_1 + P_z A_2 + G A_3 - C A_4. \qquad \text{(VIII. 34)}$$

The force N is positive when the piston moves downward, and negative when the piston moves upward.

By inserting in expression (VIII. 32) the value of P_1 from (VIII. 33), and of M_f from (VIII. 34), we obtain the required servomotor force

$$P = \frac{z_1 (\pm M_h + P_2 A_2 + GA_3 - CA_4)\left[\mu \frac{r_S}{r_k} \cos(\alpha + \varrho) + \sin(\alpha + \varrho)\right]}{l_1 \cos(\alpha + \varphi + \varrho) - \mu \frac{d_p}{2} - A_1}. \qquad \text{(VIII. 35)}$$

The servomotor stroke is calculated in the following manner as a function of the blade rotation angle $\pm\varphi$ (Figure VIII. 29, b)

$$S = S_1 + S_2;$$

$S_1 = \overline{ak}$ = from mid-position downward;
$S_2 = \overline{cd}$ = from mid-position upward.

$$S_1 = \overline{ak} = \overline{ab} - \overline{kb},$$

since

$$\overline{ab} = \overline{mb} \cot\alpha = \overline{ok} \sin\varphi_1 \cot\alpha = l_1 \sin\varphi_1 \cot\alpha;$$

$$\overline{kb} = \overline{cm} = \overline{ok}(1 - \cos\varphi_1) = l_1 (1 - \cos\varphi_1).$$

then

$$S_1 = l_1 \sin\varphi_1 \cot\alpha - l_1 (1 - \cos\varphi_1)$$

or

$$S_1 = l_1 \left(\frac{\sin\varphi_1}{\tan\alpha} + \cos\varphi_1 - 1\right), \qquad \text{(VIII. 36)}$$

$$S_2 = \overline{nd} + \overline{cn},$$

but

$$\overline{nd} = \overline{nm}\tan\alpha = l_1 \sin\varphi_2 \tan\alpha; \quad \overline{cn} = l_1 (1 - \cos\varphi_2).$$

Consequently,

$$S_2 = l_1 \sin\varphi_2 \tan\alpha + l_1 (1 - \cos\varphi_2)$$

or

$$S_2 = l_1 \left(\frac{\sin\varphi_2}{\tan\alpha} - \cos\varphi_2 + 1\right). \qquad \text{(VIII. 37)}$$

Calculation of the servomotor force for a mechanism with lever drive. The schematic layout of the mechanism is shown in Figure VIII. 30.

The equilibrium conditions for the vertical forces and the moments about the z axis are:

$$\left.\begin{aligned} \frac{P}{z_1} z_1 - N z_1 \cos\beta - T z_k \sin\varrho = 0; \\ z_1 N r_h \sin\beta - T z_k r_k \cos\varrho = 0, \end{aligned}\right\} \qquad \text{(VIII. 38)}$$

where P = servomotor force;
N = force acting along the link, allowing for friction;
T = force exerted on the crosshead guideway, allowing for friction;
z_1 = number of blades;
z_k = number of guideways;
β = angle of link inclination;
ϱ = angle of friction;
r_h = radius of link location;
r_k = radius of guideway location.

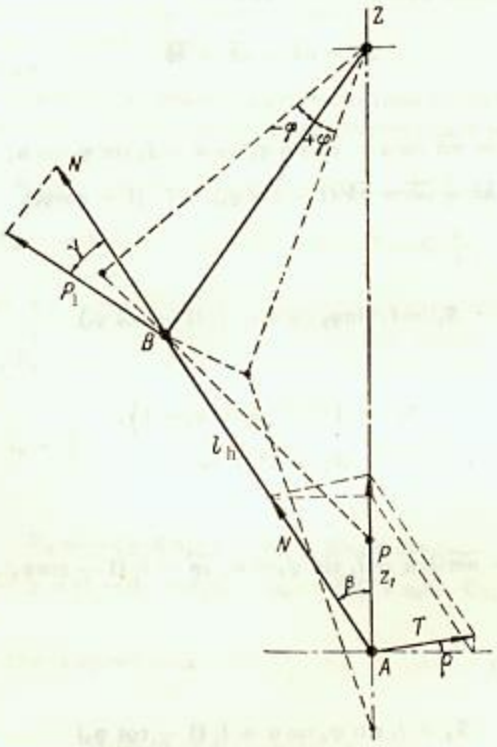


FIGURE VIII.30. Layout of the blade-actuating mechanism with inclined link

From (VIII. 38) we obtain

$$\left.\begin{aligned} T &= N \frac{r_h z_1}{r_k z_k} \cdot \frac{\sin\beta}{\cos\varrho}; \\ N &= \frac{P}{z_1} \cdot \frac{1}{\cos\beta + \mu \frac{r_h}{r_k} \sin\beta}. \end{aligned}\right\} \qquad \text{(VIII. 39)}$$

The moment exerted on the lever

$$M_1 = l_1 N \cos\gamma - \mu N (r_A + r_B) =$$
$$= N [l_1 \cos\gamma - \mu (r_A + r_B)];$$

$$M_1 = \frac{P}{z_1} \cdot \frac{l_1 \cos\gamma - \mu (r_A + r_B)}{\cos\beta + \mu \frac{r_h}{r_k} \sin\beta},$$

where r_A = radius of the link pin;
r_B = radius of the lever pin;
γ = angle between link and normal to lever.

Force on the guideway

$$T_k = T \cos\varrho = N \frac{\sin\beta}{\cos\varrho} \cos\varrho \frac{r_h z_1}{r_k z_k}.$$

By using the relations (VIII. 39), we obtain

$$T_k = \frac{P}{z_1} \cdot \frac{\sin\beta}{\cos\beta + \mu \frac{r_h}{r_k} \sin\beta} \cdot \frac{r_h z_1}{r_k z_k}. \qquad \text{(VIII. 40)}$$

The servomotor moment is determined by the relation

$$M = M_1 z_1 = (\pm M_h + M_f) z_1.$$

Since the blade pivots are mounted in the same manner as in the previous type of mechanism (Figure VIII. 29), the frictional moment may be expressed by (VIII. 34)

$$M_f = -(\pm N) A_1 + P_z A_2 + G A_3 - C A_4.$$

By inserting the values of M_1 and M_f we obtain

$$\frac{P}{z_1} \cdot \frac{l_1 \cos\gamma - \mu (r_A + r_B)}{\cos\beta + \mu \frac{r_h}{r_k} \sin\beta} = \pm M_h - (\pm A_1) N + P_z A_2 + G A_3 - C A_4.$$

By inserting the value for N from formula (VIII. 39)

$$P = \frac{z_1 (\pm M_h + P_z A_2 + G A_3 - C A_4) \left(\cos\beta + \mu \frac{r_h}{r_k} \sin\beta\right)}{l_1 \cos\gamma - \mu (r_A + r_B) \pm A_1}. \qquad \text{(VIII. 41)}$$

With the dimensions of the servomotor known, the oil pressure in the cylinder may be determined

$$p = \frac{z_1 P_s}{F}, \qquad \text{(VIII. 42)}$$

where F = the working area of the servomotor piston

The required servomotor force should be determined for various operating conditions, both for opening and closing of blades, and the curve illustrating the relationship between oil pressure and blade angle should be drawn.

The maximum oil pressure corresponds to the head under which the hydraulic moment reaches the greatest absolute value.

When the hydraulic moments under maximum and minimum heads are equal in absolute value but of different signs, the curves should be plotted for both heads.

Approximate calculations of the required runner-servomotor force (Figures VIII. 27, VIII. 28).

Starting data

Weight of blade G_b	14.36 t
Radius to center of gravity of the blade R_{cgb}	336 cm
Weight of blade flange G_f	4.1 t
Radius to center of gravity of the flange R_{cgf}	212 cm
Weight of blade pivot G_p	5.66 t
Radius to center of gravity of the pivot R_{cgp}	149.3 cm
Weight of lever G_l	4.14 t
Radius to center of gravity of the lever R_{cgl}	153.3 cm
Runner diameter D_1	930 cm
Runner hub diameter d_h	418 cm
Maximum head H_{max}	30 m
Number of blades z	6
Rotational speed:	
normal speed n_n	68.2 rpm
runaway speed n_r	140 rpm
Radius of the lever (distance from the lever pin to the blade-rotation axis) r	68 cm
Maximum blade angle φ	
at opening	21°30'
at closing	−12°
Maximum angle through which the lever turns from mid-position φ_1	
at opening	16°45'
at closing	16°45'
Maximum friction coefficient μ	0.12
Pivot diameters: d_1	48 cm
d_2	140 cm

Determination of calculational data.

1. Axial force

$$P_{ax} = \frac{k\pi\left(D_1^2 - d_h^2\right)}{4} H_{max} = \frac{1 \cdot 3.14\,(9.3^2 - 4.18^2)}{4} \cdot 30 = 1626 \text{ t.}$$

Axial force upon one blade

$$P_z = \frac{P_{ax}}{z} = \frac{1626}{6} = 271 \text{ t.}$$

Radius to center of pressure

$$R_{cp} = 345 \text{ cm.}$$

2. Total weight of the blade, including flange, pivot, lever, and other parts. The calculation is tabulated below.

TABLE VIII. 2

Weight and statical moments of the blade and other parts

Part	G, t	R_{cg}, m	GR_{cg}, tm
Blade	14.36	3.36	48
Blade flange	4.10	2.12	9
Blade pivot	5.66	1.493	8
Lever	4.14	1.533	6
Link and other parts	0.85	1.098	1
Total	29.11		72

Remark: the total weight may be rounded off to $G = 30$ t.

Radius to the center of gravity

$$R_{cg} = \frac{\sum G_i R_i}{\sum G_i} = \frac{720 \cdot 10^4}{29110} = 246 \text{ cm}.$$

3. The centrifugal force is determined from the formula

$$C = \frac{G}{g} R_{cg} \omega^2 = \frac{G}{g} R_{cg} \left(\frac{\pi n}{30}\right)^2.$$

Under normal turbine-operating conditions $n_n = 68.2$ rpm.

$$\omega = \frac{\pi n_n}{30} = \frac{3.14 \cdot 68.2}{30} = 7.15 \text{ sec}; \quad \omega^2 = 51 \text{ sec}^2.$$

At runaway speed $n_r = 140$ rpm.

$$\omega = \frac{\pi n_r}{30} = \frac{3.14 \cdot 140}{30} = 14.65 \text{ 1/sec};$$

$$\omega_r^2 = 215 \text{ 1/sec}^2.$$

The calculation of the centrifugal forces is set forth in Table VIII. 3.

TABLE VIII. 3

Centrifugal forces

Part	G, t	R_{cg}, m	Centrifugal force, t	
			$n_n = 68.2$ rpm	$n_r = 140$ rpm
Blade	14.36	3.36	251	1060
Blade with flange	18.46	3.09	297	1250
Blade with flange, pivot and other parts	30	2.46	384	1620

4. The hydraulic moment exerted upon the blade is determined by tests, and, for calculation purposes, is taken from charts.

5. Frictional moment at the blade pivots. For the given runner design, the diagram of the forces acting on the blade is presented in Figure VIII. 28.

Frictional moment

$$M_f = \frac{\mu}{2}(R_1 d_1 + R_2 d_2 + C d_3).$$

Reactions in bearings

$$R_1 = \mp \alpha_1 P_1 + \alpha_2 P_2 + \alpha_3 G - \alpha_4 C;$$

$$R_2 = \pm (1 - \alpha_1) P_1 + (1 + \alpha_2) P_2 + (1 + \alpha_3) G - \alpha_4 C.$$

The upper sign indicates the direction of the force P_1 during blade opening.

$$\alpha_1 = \frac{l_1}{l} = \frac{751}{1215} = 0.618; \quad \alpha_3 = \frac{l_3}{l} = \frac{611}{1215} = 0.503;$$

$$\alpha_2 = \frac{l_2}{l} = \frac{1531}{1215} = 1.26; \quad \alpha_4 = \frac{\varepsilon}{l} = \frac{8.22}{1215} = 0.00675.$$

By inserting the values of the reactions in the formula for the frictional moment, and again denoting

$$A_1 = \frac{\mu}{2}[\alpha_1 (d_1 + d_2) - d_2] = 0.06\,(0.618 \cdot 188 - 140) = -1.44 \text{ cm};$$

$$A_2 = \frac{\mu}{2}[\alpha_2 (d_1 + d_2) + d_2] = 0.06\,(1.25 \cdot 188 + 140) = 22.6 \text{ cm};$$

$$A_3 = \frac{\mu}{2}[\alpha_3 (d_1 + d_2) + d_3] = 0.06\,(0.503 \cdot 188 + 140) = 14.1 \text{ cm};$$

$$A_4 = \frac{\mu}{2}[\alpha_4 (d_1 + d_2) - d_3] = 0.06\,(0.00675 \cdot 188 - 151) = -8.95 \text{ cm},$$

we obtain

$$M_f = \mp A_1 P_1 + A_2 P_2 + A_3 G - A_4 C.$$

For $H = 30$ m, $P_2 = 271$ t,

$$A_2 P_2 + A_3 G - A_4 C = 22.6 \cdot 271 + 14.1 \cdot 30 + 8.95 \cdot 384 = 10000 \text{ tcm};$$

$$M_f = \pm 1.44 P_1 + 10000.$$

For $H = 14$ m, $P_2 = 126$ t,

$$A_2 P_2 + A_3 G - A_4 C = 22.6 \cdot 126 + 14.1 \cdot 30 + 8.95 \cdot 384 = 6720 \text{ tcm};$$

$$M_f = \pm 1.44 P_1 + 6720.$$

6. Determination of the angle of link inclination. According to Figure VIII. 31 where r = radius of the lever, L = link length, a = displacement of point of lever suspension, α = angle of link inclination, φ_1 = angle of the lever rotation, we have

$$\sin \alpha = \frac{EC}{L};$$

$$EC = KO - KE - CO;$$

$$EC = r - a - r \cos \varphi_1;$$

$$\sin \alpha = \frac{r}{L}(1 - \cos \varphi_1) - \frac{a}{L};$$

$$\sin \alpha = \frac{2r}{L} \sin^2 \frac{\varphi_1}{2} - \frac{a}{L}.$$

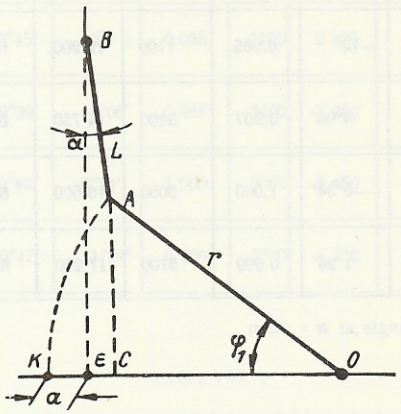


FIGURE VIII. 31. Determination of the angle of link inclination

The angle α is considered positive when the link is inclined to the right.

The calculation of angle α is set forth in Table VIII. 4.

TABLE VIII. 4

Determination of the angle of link inclination

Lever rotation angle φ_1	$\frac{\varphi_1}{2}$	$\sin \frac{\varphi_1}{2}$	$\sin^2 \frac{\varphi_1}{2}$	$\sin \alpha$	α
—16°45′	—8°23′	—0.1458	0.0212	0.0142	0°49′
—14°45′	—7°23′	—0.1285	0.0165	0.0079	0°26′
—9°45′	—4°53′	—0.0852	0.0073	—0.0044	—0°15′
—4°45′	—2°23′	—0.0357	0.00127	—0.0125	—0°39′
0°15′	0°8′	0.0023	0.000053	—0.000071	—0°49′
2°15′	1°8′	0.0198	0.000392	—0.0137	—0°47′
5°15′	2°38′	0.0459	0.0021	—0.0114	—0°39′
9°15′	4°38′	0.0808	0.00653	—0.0054	—0°18′

$$\frac{2r}{L} = \frac{2 \cdot 68}{103} = 1.34;$$

$$\frac{a}{L} = \frac{1.44}{103} = 0.0142.$$

TABLE VIII. 5

Determination of the servomotor force required at opening, for H = 30 m

φ	φ_1	α	$\varphi_1 + \alpha$	$\cos(\varphi_1 + \alpha)$	M_h, tcm	$1.1(M_h + A_0)$, tcm	$(r + A_1) \times \cos(\varphi_1 + \alpha)$, cm	P_s, t	p kg/cm^2
—12°	—16°45′	0°49′	—15°56′	0.962	—2800	7 900	64	123.5	8.7
—10°	—14°45′	0°26′	—14°19′	0.969	—1600	9 250	64.4	143.5	10.2
—5°	—9°45′	—0°15′	—10°	0.985	1100	12 200	65.5	186.5	13.15
0	4°45′	—0°59′	4°06′	0.997	3400	14 750	66.3	223	15.7
5°	0°15′	—0°49′	—0°34′	1.000	5050	16 500	66.5	249	17.55
7°*	2°15′	—0°47′	1°28′	0.999	5700	17 260	66.4	260	18.3

* 7° — maximum blade angle at H = 30 m

TABLE VIII. 6

Determination of the servomotor force required at opening, for H = 14 m

φ	φ_1	α	$\varphi_1 + \alpha$	$\cos(\varphi_1 + \alpha)$	M_h, tcm	$1.1(M_h + A_0)$, tcm	$(r + A_1) \times \cos(\varphi_1 + \alpha)$, cm	P_s, t	p kg/cm^2
—12°	—16°45′	0°49′	—15°56′	0.962	—6 000	790	64.0	12.35	0.88
—10°	—14°45′	0°26′	—14°19′	0.969	—5 600	1230	64.4	19.15	1.35
—5°	—9°45′	—0°15′	—10°	0.985	—4 800	2110	65.5	32.2	2.28
0	4°45′	—0°39′	4°06′	0.997	—4 000	2990	66.3	45.2	3.18
5°	0°15′	—0°49′	—0°34′	1.00	—3 300	3760	66.5	56.5	3.98
10°	5°15′	—0°39′	4°36′	0.997	—2 900	4200	66.4	63.4	4.46
14°	9°15′	—0°18′	8°57′	0.988	—27 000	4420	65.8	67.2	4.75

TABLE VIII. 7

Determination of the servomotor force required at closing, for H = 30 m

φ	φ_1	α	$\varphi_1 + \alpha$	$\cos(\varphi_1 + \alpha)$	M_h, tcm	$1.1(-M_h + A_0)$, tcm	$(r - A_1) \times \cos(\varphi_1 + \alpha)$, cm	P_s, t	p, kg/cm^2
—12°	—16°45′	0°49′	—15°56′	0.962	—2800	14 100	66.7	213	15.2
—10°	—14°45′	0°26′	—14°19′	0.969	—1600	13 750	67.1	189.5	13.55
—5°	—9°45′	—0°45′	—10°	0.085	1100	9 800	68.4	143.5	10.25
0	4°45′	—0°39′	4°06′	0.997*	3400	7 260	69.2	105	7.23
5°	0°15′	—0°49′	—0°34′	1.000	5050	5 450	69.4	78.5	5.61
7°	2°15′	—0°47′	1°28′	0.999	5700	4 730	69.4	68.3	4.88

TABLE VIII. 8

Determination of the servomotor force required at closing, for H = 14 m

φ	φ_1	α	$\varphi_1 + \alpha$	$\cos(\varphi_1 + \alpha)$	M_h, tcm	$1.1(-M_h + A_0)$, tcm	$(r - A_1) \times \cos(\varphi_1 + \alpha)$, cm	P_s, t	p, kg/cm^2
—12°	—16°45′	0°49′	—15°56′	0.962	—6000	14 000	66.7	210	14.96
—10°	—14°45′	0°26′	—14°19′	0.969	—5600	13 550	67.1	202	14.4
—5°	—9°45′	—0°15′	—10°	0.985	—4800	12 700	58.4	186	13.2
0	4°45′	—0°39′	4°06′	0.997	—4000	11 800	69.2	169	12.2
5°	0°15′	—0°49′	—0°34′	1.00	—3300	11 000	69.4	159	11.32
10°	5°15′	—0°39′	4°36′	0.997	—2900	10 600	69.2	153	10.9
14°*	9°15′	—0°18′	8°57′	0.988	—2700	10 380	68.5	151	10.8

* 14° — maximum blade angle at H = 14 m

For structural considerations, the displacement of the point of lever suspension is assumed to be $a = 14.4$ mm.

The relationship between the blade angle and the deviation of the lever from mid-position is expressed by the formula

$$\varphi = \varphi_1 - 4°45',$$

where φ = blade angle;

φ_1 = angle of lever deviation from mid-position.

7. Determination of the required servomotor force.

For $H = 30$ m

$$P_s = 1.1 \frac{\pm M_h + 10000}{(r \pm A_1)\cos(\varphi_1 + \alpha)}.$$

For $H = 14$ m

$$P_s = 1.1 \frac{\pm M_h + 6720}{(r \pm A_1)\cos(\varphi_1 + \alpha)}.$$

Knowing the required servomotor force, we may determine the oil pressure in the servomotor

$$p = \frac{zP_s}{F},$$

where F = working surface.

At opening

$$F_1 = 85\,000 \text{ cm}^2;$$

at closing

$$F_2 = 84\,000 \text{ cm}^2.$$

With these formulas, we determine the required servomotor force and oil pressure, at blade opening and closure, for $H_{max} = 30$ m and $H_{min} = 14$ m.

The calculation is given in Tables VIII. 5 through VIII. 8.

The values obtained are plotted on a chart (Figure VIII. 32) illustrating the relationship between oil pressure and blade angle at opening and closing for heads $H = 30$ m and $H = 14$ m.

Examination of the figure shows that the oil pressure is higher at opening than at closing, for a head $H = 30$ m, and, vice versa, for a head $H = 14$ m. This may be explained by the variation of the hydraulic moment with the blade angle.

8. Determination of the pivot reactions.

$$R_1 = \mp \alpha_1 P_1 + \alpha_2 P_2 + \alpha_3 G - \alpha_4 C;$$

$$R_2 = \pm (1 - \alpha_1) P_1 + (1 + \alpha_2) P_2 + (1 + \alpha_3) G - \alpha_4 C;$$

$$P_1 = \frac{P_s}{K} = \frac{P_s \cos(\varphi_1 + \alpha)}{1.1};$$

$$R_1 = \mp \frac{0.618}{1.1} \cos(\varphi_1 + \alpha) P_s + 12.6 \times 271 + 0.503 \cdot 30 - 0.00675 \cdot 384;$$

$$R_1 = \mp 0.566 \cos(\varphi_1 + \alpha) P_s + 355;$$

$$R_2 = \pm \frac{1 - 0.618}{1.1} \cos(\varphi_1 + \alpha) P_s + (1 + 1.26) \cdot 271 +$$

$$+ (1 + 0.503)\, 30 - 0.00675 \cdot 384;$$

$$R_2 = \pm 0.347 \cos(\varphi_1 + \alpha) P_s + 656.$$

The calculation is given in Table VIII. 9.

The values of the pivot reactions are required for the subsequent strength calculation of the pivots and other parts.

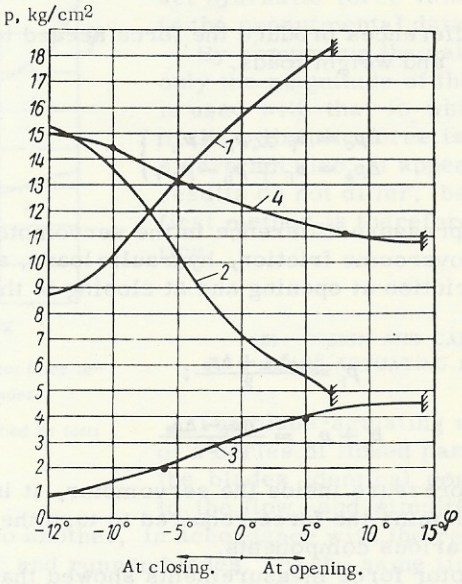


FIGURE VIII. 32. Required oil pressure in the runner servomotor:

1—opening; H = 30 m; 2—closing, H = 30 m;
3—opening; H = 14 m; 4—closing, H = 14 m.

TABLE VIII. 9

Determination of the pivot reactions

Conditions	Piston movement	P_s, t	R_1, t	R_2, t
Operating conditions	At opening	260	210	745
	At closing	213	471	585
Maximum servomotor pressure p = 27 kg/cm^2	At opening	384	148	784
	At closing	378	564	528

Experimental Data on the Measurement of the Force required for Actuating the Runner Servomotor

The actual forces required to adjust the runner blades are determined during operation by measuring the oil pressure inside the servomotor cylinder when the piston moves upward and downward.

If p_c is the measured pressure in the cylinder at closing (piston moving upward) and p_o is the measured pressure at opening (piston moving downward), the pressure difference in the servomotor at closing and at opening is

$$\left.\begin{aligned}\Delta p_c &= p_o - p_c;\\ \Delta p_o &= p_c - p_o.\end{aligned}\right\} \qquad \text{(VIII. 43)}$$

These pressure differences produce the force needed to overcome friction, hydraulic loads, and weight loads.

Consequently,

$$\left.\begin{aligned}\Delta p_c &= p_F \pm p_h + p_w;\\ \Delta p_o &= p_F \mp p_h - p_w,\end{aligned}\right\} \qquad \text{(VIII. 44)}$$

where p_F, p_h, and p_w = pressure difference in the servomotor required to overcome friction, hydraulic loads, and weight loads.

Considering that friction at opening and at closing is the same, it results from (VIII. 44)

$$p_F = \frac{\Delta p_c + \Delta p_o}{2}; \qquad \text{(VIII. 45)}$$

$$p_h + p_w = \frac{\Delta p_c - \Delta p_o}{2}. \qquad \text{(VIII. 46)}$$

By measuring the pressure inside the servomotor, it is therefore possible not only to determine the force required to turn the blades, but also to obtain data on its various components.

Results of servomotor force measurements showed that the calculated values (see example above) are too large.

Smaller forces are required to turn the blades than those obtained by calculation.

To illustrate this, the curves of the servomotor forces required to turn the blades of a turbine of $D_1 = 9.3$ m under $H = 20$ m are represented in Figure VIII. 33. The calculated, as well as the actually measured values, are plotted on the graph, for various blade angles, both at opening and closing. It is clear from the figure that the calculated values considerably exceed those measured.

By analysing the experimental results and the servomotor force values calculated by the method used at the LMZ, S. P. Mikhanovskii /63/ came to the conclusion that any discrepancy may be explained by the fact that the value of the hydraulic force P_h, corresponding to the closed position of the blades, used in calculating the servomotor force was excessive. Under operating conditions, the actual hydraulic force is smaller.

Figure VIII. 21 shows the values of the reduced axial hydraulic pressure. In the working region of the universal chart, with the blades

open, the axial pressure is considerably smaller than at small blade angles. In the calculation of the servomotor force, an increase in the axial pressure results in higher bearing reactions, and consequently in higher frictional moments. In addition, greater forces involve larger parts. The use of the correct pressure value, therefore, permits a reduction in the required servomotor force, as well as the use of smaller and less stressed parts.

The results obtained by S. P. Mikhanovskii in calculating the servomotor force with exact hydraulic-force values were quite close to the experimental data.

By comparing the calculation in which only the magnitude of the hydraulic force is used with that in which the direction of the hydraulic force is taken into consideration also, it appears that the final results do not differ; being simpler, the first method is therefore used in practice.

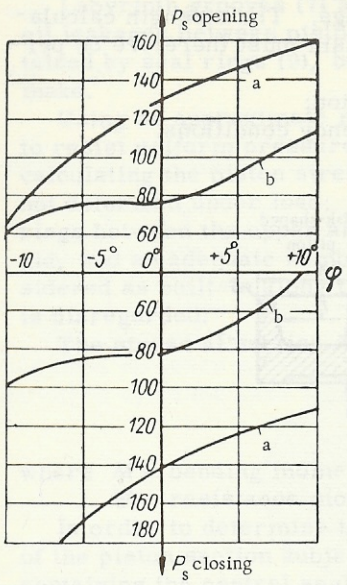


FIGURE VIII. 33. Servomotor force required to turn the runner blades:

a — calculated; b — obtained by tests on the actual turbine.

51. DESIGN AND CALCULATION OF THE BLADE-ACTUATING MECHANISM PARTS

The blade-actuating mechanism consists of a series of linked parts, which impart to the blades identical positions with respect to the flow, and simultaneous motions from one position to another, in accordance with the regulating connection between distributor and runner blades. At the same time, some of these parts also serve to secure the blades to the runner hub.

Diagrams of blade-actuating mechanisms, with cranks or slide-blocks to transform the linear movement of the servomotor piston into the angular movement of the blade and so adjust it to the required angle, were considered in detail in the first section of Chapter VIII.

The design of the blade-actuating mechanism with crank drive, being most common in turbine construction, will be examined in detail. In a mechanism of this type (see Figure VIII. 4), the piston is connected to a rod; a crosshead, connected by means of cylindrical pins to the links, is mounted at the opposite ends of the rod. Each link is connected at its other end, also through cylindrical pins, to the end of a lever connected with the blade pivot. The pivot is usually removable from the blade.

The design and calculation of the following parts of the blade-actuating mechanism, viz., servomotor, piston rod, crosshead, eyes, link, lever, and blade pivot, is given below.

When the turbine is operated under variable load conditions, these parts are subject to forces determined by the interaction of the blades and the water flow.

During blade adjustment, the loads on the parts depend on the force required to adjust the blades. Apart from this, the mechanism parts may have to sustain forces determined by the maximum servomotor force, either when the centrifugal forces increase at higher speeds, or when the pivot becomes misaligned and jams in its bearings. The strength calculation for the parts of the blade-actuating mechanism must therefore be performed for two conditions:

a) loading under conditions of normal operation;

b) maximum servomotor force under emergency conditions.

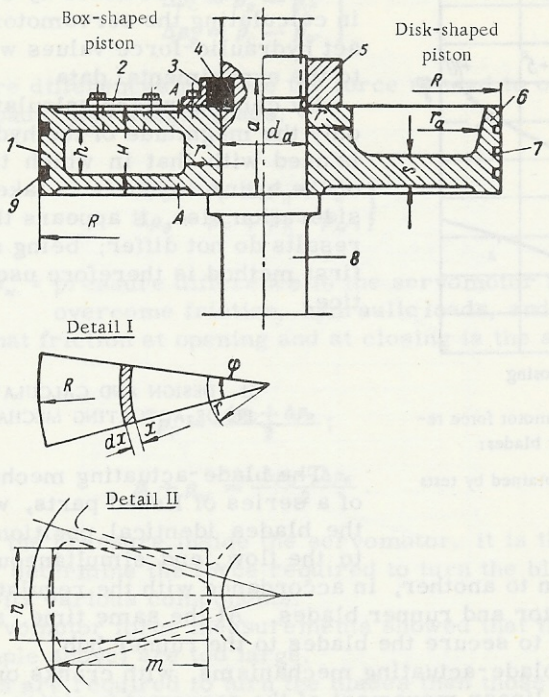


FIGURE VIII. 34. Schematic drawing of the servomotor piston

Servomotor piston. Two designs for the servomotor piston are in common use: the box-shaped section (1) (Figure VIII. 34) with radial web, or the simpler disk shape (6). The piston is made of cast iron.

The box-shaped section, with a higher resistance modulus, is used for servomotors on large turbines, and the disk-shaped piston for servomotors on smaller units.

For casting, the box-shaped piston should be provided at each of its compartments with two or three holes for the casting cores. These holes are covered afterwards with the bolted covers (2). A less convenient method is to close the holes with threaded plugs. The piston is fitted to the rod (8) provided with a collar, and secured with a nut (5) if the rod diameter is small, or with a retaining ring (4) if the diameter is large. If the piston is

secured by means of a locking ring, the piston rod groove should be carefully machined to ensure a tight fit between rod and retaining ring, so that the latter is subjected to shear. The retaining ring is made of two parts held together by ring (3).

Labyrinth grooves (7) are provided in the piston for sealing, reducing oil leakages between piston and cylinder. A more reliable sealing is obtained by seal rings (9), but in large-sized pistons these are difficult to make.

Using an approximate method, the box-shaped piston should be calculated to resist uniform pressure exerted either from below or from above. In calculating the piston strength, we assume that the piston cross section is not deformed under load; this assumption is sufficiently accurate if the rings between the upper and lower covers of the piston are sufficiently rigid, and an adequate number of radial webs is provided. The piston is considered as built-in along the inner surface; the effect of tangential stresses is disregarded.

The stress at section A—A (on the inner outline of radius r) is

$$\sigma = \frac{M}{W},$$

where M = bending moment;
W = resistance modulus.

In order to determine the bending moment and the resistance modulus of the piston section subject to uniformly distributed pressure p, a sector containing the central angle φ is cut out (Figure VIII. 34, detail I).

At the distance x, the force $px\varphi dx$ acts upon the elementary area. The moment exerted by it at the built-in end is

$$dM = px\varphi\, dx\, (x - r).$$

By integrating from r to R, and neglecting the infinitesimals of second order, we obtain

$$M = p\varphi \int_r^R (x^2 - rx)\, dx = p\varphi \frac{(R-r)^2(2R+r)}{6}.$$

The modulus of the built-in section

$$W = \varphi r \frac{H^3 - h^3}{6H}.$$

The radial stresses at the inner edge

$$\sigma = p \frac{H(R-r)^2(2R+r)}{r(H^3 - h^3)}. \qquad \text{(VIII. 47)}$$

If the piston is considered as a circular plate of constant thickness, built-in along the inner edge, the equivalent thickness t of the plate may be determined by equating the moduli W of the radial piston section with the radial section of a plate of constant thickness — i.e., a rectangle of width $R - r$ and height (thickness) t

$$W = \frac{(R-r)t^2}{6}.$$

Hence, the equivalent thickness of the plate

$$t = \sqrt{\frac{6W}{R-r}}. \qquad \text{(VIII. 48)}$$

The radial stresses at the inner edge of the plate

$$\sigma = k\frac{pR^2}{t^2}, \qquad \text{(VIII. 49)}$$

where k = coefficient depending on the ratio $\frac{R}{r}$.

R/r	4.0	4.2	4.4	4.6	4.8	5.0	5.2	5.4	5.6	5.8	6.0
k	3.01	3.15	3.29	3.43	3.56	3.68	3.80	3.92	4.03	4.13	4.24

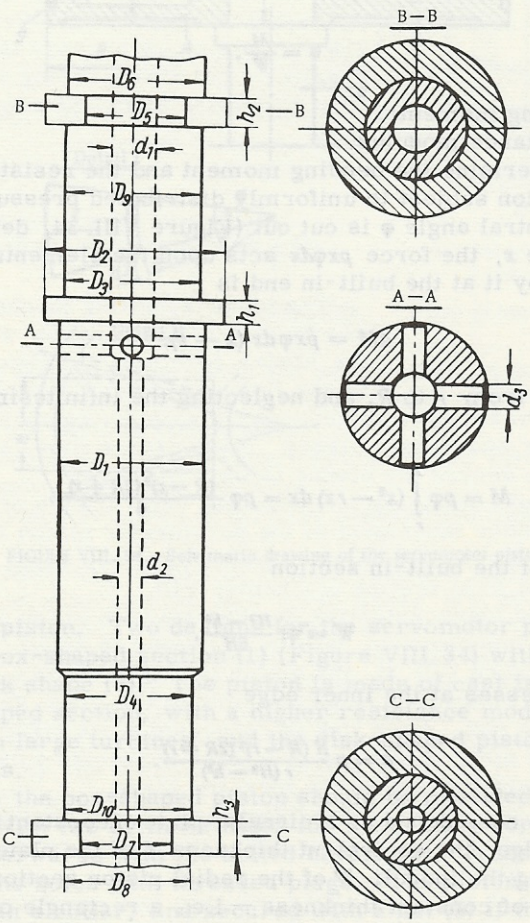


FIGURE VIII. 35. Schematic drawing of the piston rod

In addition, the local stresses in the piston bottom should be determined. The bottom consists of a number of sector plates, bounded by two circular arcs and two radial webs. The plate segment is calculated approximately as an equivalent rectangular plate, having the sides m and n, with the outer edge free (Figure VIII. 34, detail II).

The stresses in a plate of this kind may be determined from the formula

$$\sigma = \frac{0.75pn^2}{s^2(1+1.6\alpha^3)}, \qquad \text{(VIII. 50)}$$

where p = pressure, kg/cm^2;

$\alpha = \frac{n}{m}$;

m = long side of the rectangle;

n = short side of the rectangle;

s = piston-bottom thickness.

The calculation of the disk-shaped piston merely amounts to the calculation of radial stresses σ_1 due to the load on the disk between radii r_a and r, and stresses σ_2 in the band between R and r_a.

$$\left.\begin{aligned}\sigma_1 &= \pm k_1 p \frac{r_a^2}{s^2};\\ \sigma_2 &= \pm k_2 \frac{P}{s^2},\end{aligned}\right\} \qquad \text{(VIII. 51)}$$

where

$$P = \pi(R^2 - r_a^2)p;$$

k_1 and k_2 depend on the ratio $\frac{r}{r_a}$.

For pistons made of SCh 21-40 cast iron, the permissible stress should be taken σ_y = 700 kg/cm^2.

Piston rod. The piston rod of the servomotor, made of forged steel, is designed to resist tension and compression at critical sections, these being determined by the bores and channels required for oil supply. The critical sections are usually those adjoining the retaining ring or nut and the collar where the holes for oil discharge are located.

A tube to relieve the inner runner hub cavity of excess pressure oil is located inside the central rod bore. The annular space outside it is for supplying oil to the servomotor cylinder below the piston. The grooves are calculated according to the permissible oil velocity and discharge. The stresses in the rod are determined by the forces developed when the piston moves downward at opening and upward at closing [of the blades]. For this purpose we select the maximum force P_s produced by the piston. When the piston moves upward, the rod is under tension, and the upper and lower retaining rings have to resist shearing. When it moves downward, the rod is under compression, and the rod collar, under shear and crushing.

The calculation of the piston rod (Figure VIII. 35) takes place in the following order:

1. Piston moves downward (at opening).

Section A—A:
Compressive stress

$$\sigma = \frac{P_S}{F_1},$$

where

$$F_1 = \frac{\pi}{4}(D_1^2 - d_1^2) - 2(D_1 - d_1)d_3.$$

Collar:
Shear stress

$$\tau = \frac{P_S}{F_2},$$

where

$$F_2 = \pi D_1 h_1.$$

Crushing stress

$$\sigma = \frac{P_S}{F_3},$$

where

$$F_3 = \frac{\pi}{4}(D_2^2 - D_3^2).$$

Shoulder:
Crushing stress

$$\sigma = \frac{P_S}{F_4},$$

where

$$F_4 = \frac{\pi}{4}(D_1^2 - D_4^2).$$

2. Piston moves upward (at closing).

When the piston moves upward (at closing), the sections below the locking rings should also be checked against failure in tension.

Section B—B:
Tensile stress

$$\sigma = \frac{P_S}{F_5},$$

where

$$F_5 = \frac{\pi}{4}(D_5^2 - d_1^2).$$

Crushing stress

$$\sigma = \frac{P_S}{F_6},$$

where

$$F_6 = \frac{\pi}{4}(D_6^2 - D_5^2).$$

Section C—C:
Tensile stress

$$\sigma = \frac{P_S}{F_7},$$

where

$$F_7 = \frac{\pi}{4}(D_7^2 - d_2^2).$$

Crushing stress

$$\sigma = \frac{P_S}{F_8},$$

where

$$F_8 = \frac{\pi}{4}(D_8^2 - D_7^2).$$

The permissible stress for piston rods of grade 35 steel is σ_y = 1100—1200 kg/cm^2. The ultimate stress is σ_u = 1600 kg/cm^2.

Retaining ring. The retaining ring should be designed to resist shearing due to the servomotor force when the piston moves upward.

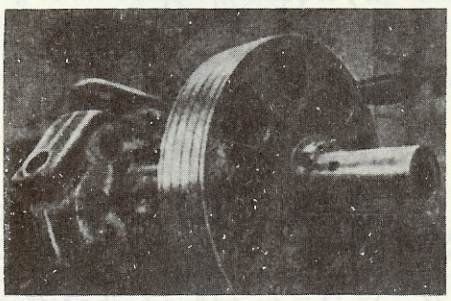


FIGURE VIII. 36. Crosshead with rod and piston on the balancing stand

Upper retaining ring:
Shear stress

$$\tau = \frac{P_S}{F_9},$$

where

$$F_9 = \pi D_9 h_2.$$

Lower retaining ring:

Shear stress

$$\tau = \frac{P_S}{F_{10}},$$

where

$$F_{10} = \pi D_{10} h_3.$$

A shear stress of τ = 600 to 700 kg/cm^2 is permissible for a retaining ring made of grade 35 steel.

Crosshead. The crosshead is made of steel and fitted to the rod.

A view of the piston rod crosshead during assembly is shown in Figure VIII. 36. The crank links are connected to the crosshead by means of cylindrical pins; the force produced by the servomotor piston is transmitted by means of the crosshead through the links to the blade levers. The shape of the crosshead, in plan, depends upon the number of links connected to it.

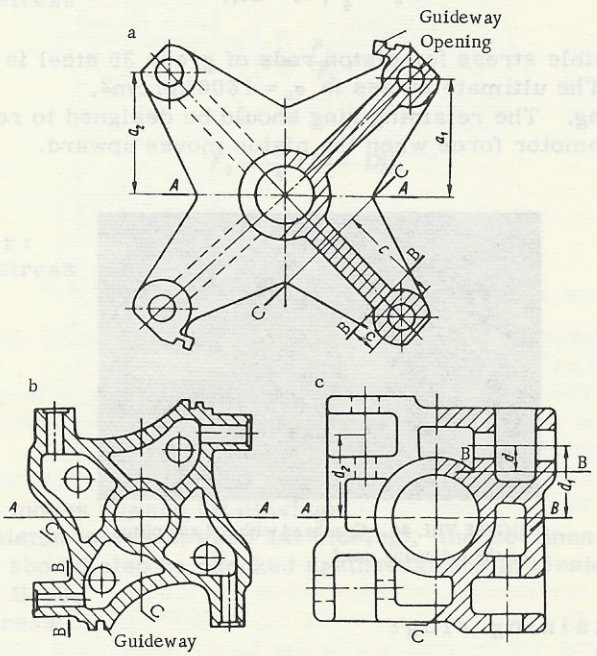


FIGURE VIII. 37. Various crosshead designs

The links may be connected to the crosshead through eyes, through pins cast with the crosshead, or through separate pins fixed into it. Various types of crosshead designs are shown in Figure VIII. 37 and in the relevant runner sections.

The design of crossheads with eyes (Figure VIII. 37,a) is now most commonly used. The eyes are inserted into the holes in the crosshead

where they are secured with nuts. A pin, connected to one or two links, is fitted into the eye. This type of crosshead, though incorporating additional parts, the eyes, is quite easy to manufacture since only fair precision is required. Furthermore, as regards machining, only the central bore and the four holes have to be drilled.

Slight errors in the hole position are compensated for when locating the eyes, while the proper location of the holes for the link pins is also determined on assembly. The design of the crosshead cast integral with the pins (Figure VIII. 37, b) is more complicated. The pins must be very precisely machined, and very accurately located in plan and in elevation, since no compensating devices are available and the links are fitted directly on the pins.

The advantage of this type of design lies in its smaller weight, due to the absence of eyes and the smaller number of parts. It is therefore suitable for large turbines, and was used at the LMZ for units with a runner diammeter D_1 = 9.3 m.

Crossheads with separately attached pins (Figure VIII. 37, c) were used at the LMZ for turbines with runner diameters D_1 = 9.3 m installed at the Volga HEP imeni Lenin. The pins are set into special openings provided in the crosshead walls. This design is simpler than the previous one, but still necessitates all openings being perfectly machined and precisely located with respect to one another. The crosshead is usually cast of carbon steel, though a welded crosshead was also manufactured at the LMZ. Although its shape becomes more intricate, in this case the design as a whole is more suitable than the cast steel variant.

Despite the great variety of designs, crossheads are all calculated similarly to resist bending at the central section A — A, and at the sections B — B and C — C. The approximate location of these sections is shown in the relevant schematic drawings.

The bending moment at the central section is determined by the formula:

$$M = \sum_{i=1}^{n} P'_s a_i = P'_s \sum_{i=1}^{n} a_i,$$

where P'_s = servomotor force, apportioned to one blade;
a_i = arm of the force;
n = number of pins located on one side of section A—A.

Section A — A is taken as the critical section — where the bending moment is the greatest — while sections B — B and C — C are selected according to the crosshead design.

Resistance modulus of the crosshead section

$$W = \frac{J_e}{y_{max}}.$$

Moment of inertia of the section

$$J = \sum \frac{Fh^2}{12} + \sum Fy^2 - y_c^2 \sum F.$$

Ordinate of the neutral axis

$$y_c = \frac{\sum Fy}{\sum F}.$$

Bending stress

$$\sigma = \frac{M}{W}.$$

The stresses are determined under normal operating conditions and maximum servomotor force. The adopted permissible stress for a crosshead made of grade 30L steel is σ_y = 1000 to 1100 kg/cm^2.

Crosshead guide. The crosshead is usually prevented from turning by two prismatic sliding guides. As a rule, these are welded to the runner hub and slide with their base along the guideways provided in the crosshead.

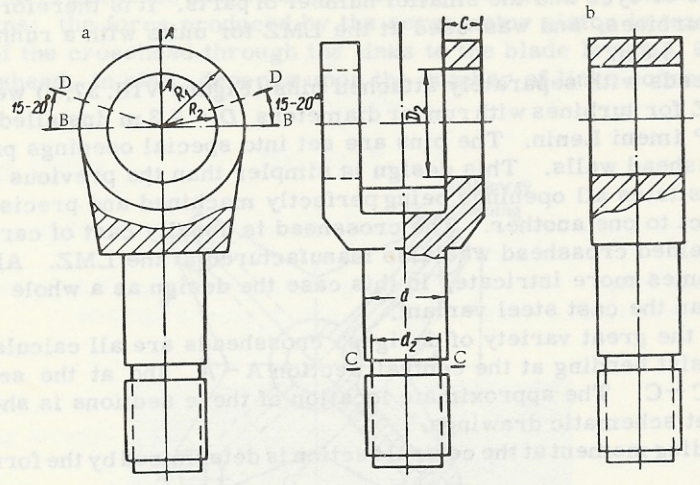


FIGURE VIII. 38. Eye designs

Owing to the inclined position of the links (slope angle α), a horizontal force component $P_s \tan \alpha$ tends to rotate the crosshead, where P_s is the servomotor force.

The force exerted upon the guideway is determined by the formula

$$P_k = \frac{P_s \tan \alpha}{z_k} \cdot \frac{r_h}{r_k}, \qquad \text{(VIII. 52)}$$

where r_h = radius to link pin;
r_k = radius to guideway;
z_k = number of guideways.

The guide is calculated to resist bending, shear, and crushing. The permissible shear stress for grade 3 steel is τ = 500 to 600 kg/cm^2.

Eye. The eye is a connecting element between crosshead and link. It comprises a cylindrical part inserted into a crosshead hole and secured with a nut, and a head.

Two alternative eye designs are shown in Figure VIII. 38.

Figure VIII. 38, a shows the more common design, where the eye head consists of two jaws bored out to take a cylindrical pin. The link fits into the eye head.

The design shown in Figure VIII. 38,b has a simple head; the pin is driven into the boring of the head, and twin links are fitted on the pin on both sides of the eye head. The eyes are usually made of forged steel.

At the LMZ, the strength of the eye is usually checked at three sections, A—A, B—B, and C—C.

The section A—A is calculated according to Lamé, for nominal and maximum servomotor forces.

In accordance with the designations on the figures, the stresses at section A—A are

$$\sigma = \frac{P_1}{2R_2 c} \cdot \frac{R_1^2 + R_2^2}{R_1^2 - R_2^2}. \qquad \text{(VIII. 53)}$$

where $P_1 = \frac{P_s}{2}$ is the servomotor force applied to one jaw of the eye.

Tensile stress at section B—B

$$\sigma = \frac{P_1}{F_2} = \frac{P_1}{2(R_1 - R_2)c}.$$

Tensile stress at section C—C

$$\sigma = \frac{P_S}{F_3} = \frac{P_S \cdot 4}{\pi d_2^2}.$$

Crushing stress at the boring

$$\sigma = \frac{P_1}{F} = \frac{P_1}{D_2 c}.$$

For eyes of grade 35 steel, the permissible stresses σ_y = 1100 to 1200 kg/cm^2.

For more accurate eye design, tests were carried out and the stress conditions measured with strain gages. Both design variants were tested under a large number of loads, up to failure.

The eyes were subjected to breaking stresses at section D—D located at an angle of 15 to 20° to section B—B (Figure VIII. 38). The stresses at D—D differed little from stresses at B—B. Higher stresses were found in the internal fibers.

The strength was calculated by several methods, and the results compared with the experimental data /52/.

The calculations were as follows (Figure VIII. 39):

*I*a = curved beam subjected to a concentrated load;
*I*b = curved beam subjected to a uniformly distributed load;
*I*c = curved beam subjected to a load with the distribution following a cosine curve;
II = ring subjected to distributed loads /10/;
III = thin-walled ring (according to Lamé).

Figure VIII. 39 shows the stress diagrams of the eye, loaded by P = 10 t, as obtained by tests and calculated as above.

Figure VIII. 40 shows the relationship between the stresses in the outer fiber at section D—D of the eye and the load, as obtained by tests and calculation.

Comparison of the experimental data with the stresses calculated by various methods, shows that Lamé's formula yields results 20 to 50%

lower than the measured stresses. The nearest results are obtained by the approximation to a curved beam subjected to a uniformly-distributed load. In addition, the character of the stress distribution is also close to the experimental results.

This approximation should therefore be employed. The load diagram is shown in Figure VIII. 41.

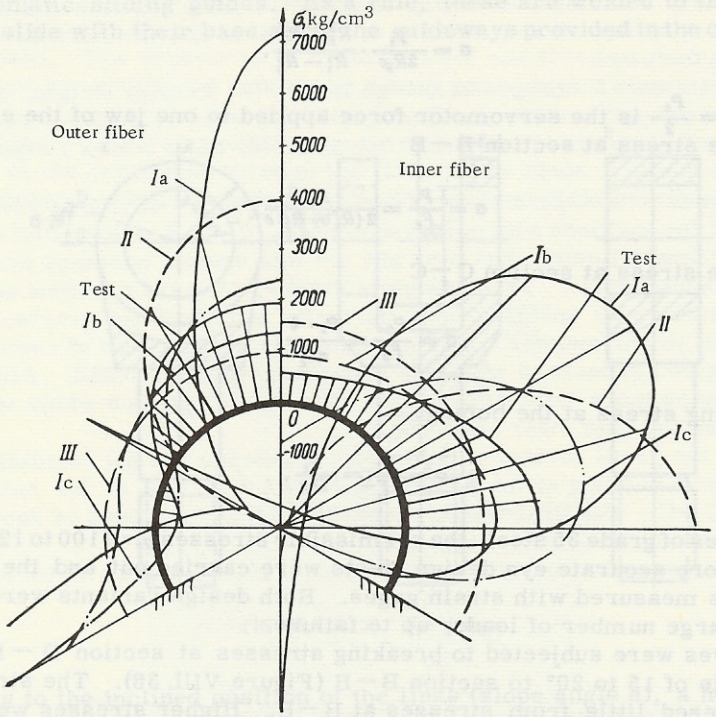


FIGURE VIII. 39. Diagram of stresses in the eye, according to experimental and calculated data

If P = applied force, q = uniform load per unit length, R_0 = mean radius of curvature, φ = variable angle, then

$$P = 2\int_0^{\frac{\pi}{2}} R_0 q \cos\varphi \, d\varphi = 2R_0 q.$$

whence

$$q = \frac{P}{2R_0}. \qquad \text{(VIII. 54)}$$

From Castigliano's theorem, we obtain the expressions for the horizontal displacement of a point and for the angle of rotation. From the condition

that the angle of rotation and the horizontal displacement are, because of symmetry, equal to zero, we obtain

$$f = \frac{\partial u}{\partial x_1} = \int_0^{\frac{\pi}{2}} \frac{M_I R_0 d\varphi}{EJ} \cdot \frac{\partial M_I}{\partial x_1} + \int_{\frac{\pi}{2}}^{\frac{2\pi}{3}} \frac{M_{II} R_0 d\varphi}{EJ} \cdot \frac{\partial M_{II}}{\partial x_1} = 0; \qquad \text{(VIII. 55)}$$

$$\theta = \frac{\partial u}{\partial x_2} = \int_0^{\frac{\pi}{2}} \frac{M_I R_0 d\varphi}{EJ} \frac{\partial M_I}{\partial x_2} + \int_{\frac{\pi}{2}}^{\frac{2\pi}{3}} \frac{M_{II} R_0 d\varphi}{EJ} \cdot \frac{\partial M_{II}}{\partial x_2} = 0. \qquad \text{(VIII. 56)}$$

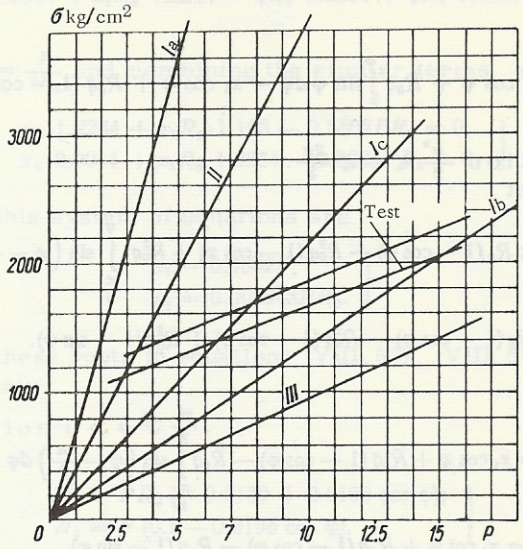


FIGURE VIII. 40. Stresses in the outer fiber at section D—D of the eye (Figure VIII. 38) as a function of load

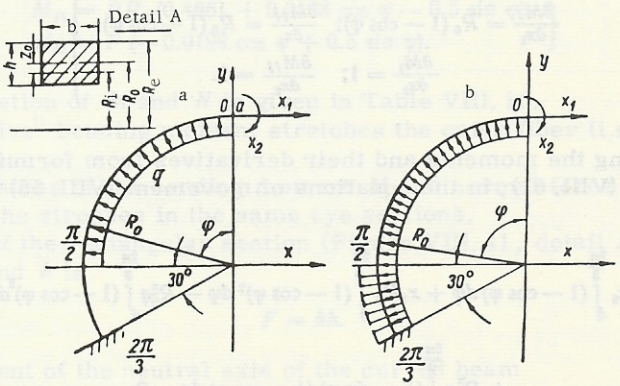


FIGURE VIII. 41. Load diagram of the eye considered as a curved beam

As the effect of the normal and shearing forces upon deformation is small, it may be neglected.

The bending moments and normal forces will be calculated for two sections.

First section $0 \leqslant \varphi \leqslant \frac{\pi}{2}$.

Bending moment

$$M_I = x_2 + x_1 R_0 (1 - \cos \varphi) - R_0^2 q \int_0^{\varphi} \sin \varphi \, d\varphi =$$

$$= x_2 + x_1 R_0 (1 - \cos \varphi) - R_0^2 q (1 - \cos \varphi). \qquad \text{(VIII. 57)}$$

Normal force

$$N_1 = x_1 \cos \varphi + R_0 q \int_0^{\varphi} \sin \varphi \, d\varphi = x_1 \cos \varphi + R_0 q (1 - \cos \varphi). \qquad \text{(VIII. 58)}$$

Second section $\frac{\pi}{2}^* \leqslant \varphi \leqslant \frac{2\pi}{3}$.

Bending moment

$$M_{II} = x_2 + x_1 R_0 (1 - \cos \varphi) - R_0^2 q (1 - \cos \varphi) + R_0^2 q \int_{\frac{\pi}{2}}^{\varphi} \sin \left(\varphi - \frac{\pi}{2} \right) d\varphi =$$

$$= x_2 + x_1 R_0 (1 - \cos \varphi) - R_0^2 q (1 - \cos \varphi) + R_0^2 q (1 - \sin \varphi). \qquad \text{(VIII. 59)}$$

Normal force

$$N_{II} = x_1 \cos \varphi + R_0 q (1 - \cos \varphi) - R_0 q \int_{\frac{\pi}{2}}^{\varphi} \sin \left(\varphi - \frac{\pi}{2} \right) d\varphi =$$

$$= x_1 \cos \varphi + R_0 q (1 - \cos \varphi) - R_0 q (1 - \sin \varphi). \qquad \text{(VIII. 60)}$$

Derivatives

$$\left.\begin{aligned} \frac{\partial M_I}{\partial x_1} = R_0 (1 - \cos \varphi); \quad \frac{\partial M_{II}}{\partial x_1} = R_0 (1 - \cos \varphi); \\ \frac{\partial M_1}{\partial x_2} = 1; \quad \frac{\partial M_{II}}{\partial x_2} = 1. \end{aligned}\right\} \qquad \text{(VIII. 61)}$$

By inserting the moments and their derivatives from formulas (VIII. 57), (VIII. 59) and (VIII. 61), in the equations of movement (VIII. 55) and (VIII. 56), we obtain,

$$\frac{EJ}{R_0^2} \cdot f = x_2 \int_0^{\frac{2\pi}{3}} (1 - \cos \varphi) \, d\varphi + x_1 R_0 \int_0^{\frac{2\pi}{3}} (1 - \cos \varphi)^2 \, d\varphi - R_0^2 q \int_0^{\frac{2\pi}{3}} (1 - \cos \varphi)^2 d\varphi +$$

$$+ R_0^2 q \int_{\frac{\pi}{2}}^{\frac{2\pi}{3}} (1 - \sin \varphi)(1 - \cos \varphi) \, d\varphi = 0; \qquad \text{(VIII. 62)}$$

*[The Russian original reads $0 \leqslant \varphi \leqslant \frac{2\pi}{3}$, obviously a misprint.]

$$\frac{EJ}{R_0}\theta = x_2\int_0^{\frac{2\pi}{3}} d\varphi + R_0 x_1\int_0^{\frac{2\pi}{3}}(1-\cos\varphi)\,d\varphi - R_0^2 q\int_0^{\frac{2\pi}{3}}(1-\cos\varphi)\,d\varphi +$$

$$+ R_0^2 q\int_{\frac{\pi}{2}}^{\frac{2\pi}{3}}(1-\sin\varphi)\,d\varphi = 0. \qquad \text{(VIII. 63)}$$

After calculating the integrals, equations (VIII. 62) and (VIII. 63) become

$$x_2\cdot 1.2284 + x_1 R_0\cdot 1.193 - qR_0^2\cdot 1.193 + qR_0^2\cdot 0.0326 = 0;$$

$$x_2\cdot 2.0944 + x_1 R_0\cdot 1.2284 - qR_0^2\cdot 1.2284 + qR_0^2\cdot 0.0236 = 0.$$

By putting $q = \frac{P}{2R_0}$ and combining the similar terms, we obtain

$$\left.\begin{aligned} x_2\cdot 1.2284 + x_1 R_0\cdot 1.193 - 0.5802 PR_0 &= 0;\\ x_2\cdot 2.0944 + x_1 R_0\cdot 1.2284 - 0.6024 PR_0 &= 0. \end{aligned}\right\} \qquad \text{(VIII. 64)}$$

The roots of this system of equations are

$$\left.\begin{aligned} x_1 &= 0.4802P;\\ x_2 &= 0.005943 PR_0. \end{aligned}\right\} \qquad \text{(VIII. 65)}$$

By inserting these roots in equations (VIII. 57), (VIII. 58), (VIII. 59) and (VIII. 60), we obtain

First section $0 \leqslant \varphi \leqslant \frac{\pi}{2}$.

$$\left.\begin{aligned} M_I &= PR_0(-0.0139 + 0.0198\cos\varphi);\\ N_I &= P(0.5 - 0.0198\cos\varphi). \end{aligned}\right\} \qquad \text{(VIII. 66)}$$

Second section $\frac{\pi}{2} < \varphi < \frac{2\pi}{3}$.

$$\left.\begin{aligned} M_{II} &= PR_0(0.4861 + 0.0198\cos\varphi - 0.5\sin\varphi);\\ N_{II} &= P(-0.0198\cos\varphi + 0.5\sin\varphi). \end{aligned}\right\} \qquad \text{(VIII. 67)}$$

The calculation of M and N is given in Table VIII. 10.

The "positive" bending moment stretches the outer fiber (i.e., increases the curvature).

Once the values of the bending moment M and normal force N are found, we calculate the stresses in the same eye sections.

The area of the rectangular section (Figure VIII. 41, detail A) with dimensions h and b is

$$F = bh.$$

Displacement of the neutral axis of the curved beam

$$z_0 = R_0 - \frac{h}{\ln\frac{R_e}{R_i}}.$$

Static moment of the section with respect to the neutral axis

$$S = Fz_0.$$

For the outside fiber

$$\frac{S_Q}{z} = \frac{SR_e}{\frac{h}{2} + z_0}.$$

For the inside fiber

$$\frac{S_Q}{z} = \frac{SR_i}{\frac{h}{2} - z_0}.$$

Stress

$$\sigma = \frac{Mz}{S_Q} + \frac{N}{F}. \qquad \text{(VIII. 68)}$$

The stress is calculated for the inside and outside fibers for the same values of $\varphi°$(0; 30; 60; 90 and 120), as $\frac{M}{PR_0}$ and $\frac{N}{P}$.

TABLE VIII. 10

Values of M and N

$\varphi°$	cos φ	0.0198 cos φ	sin φ	0.5 sin φ	$\frac{M}{PR_0}$	$\frac{N}{P}$
0	1.0	0.0198	0	0	0.0059	0.4802
30	0.866	0.0171	0.50	0.25	0.0032	0.4829
60	0.50	0.0099	0.866	0.433	—0.004	0.4901
90	0	0	1.0	0.5	—0.0139	0.5000
120	—0.50	—0.0099	0.866	0.433	0.0432	0.4429

Link. The link is usually made of cast steel, and its holes are fitted with liners of high-quality bronze to resist pressures of up to 300 kg/cm^2.

The shackle itself is designed to resist tension at three sections: A—A, B—B and C—C, at normal operating conditions and at maximum servomotor force.

Section A—A.

Stress according to Lamé

$$\sigma = \frac{P_h}{2rd} \cdot \frac{R^2 + r^2}{R^2 - r^2},$$

where r, R and d = dimensions of the link according to the drawing.

Section B—B.
Tensile stress

$$\sigma = \frac{P_h}{F_2},$$

where

$$F_2 = 2(R - r)d.$$

Section C—C.
Tensile stress

$$\sigma = \frac{P_h}{F_3},$$

where

$$F_3 = a(2b + c).$$

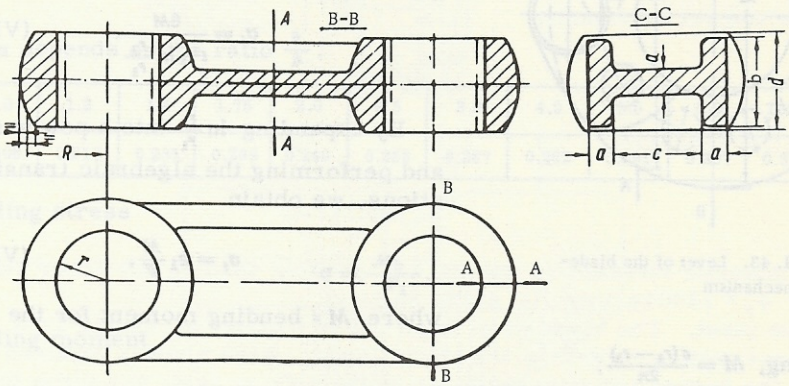


FIGURE VIII. 42. Link design

Permissible stresses σ_y = 900 to 1000 kg/cm^2 are adopted for links cast of 30 L steel.

Lever. In modern blade-actuating mechanisms, the lever is usually a steel ring provided with a pin and mounted on the blade pivot (Figure VIII. 43).

Because of the limited space inside the hub, the lever is sometimes chamfered. It is bolted to the blade flanges (see Figure VIII. 8), and cylindrical pins are also provided to transmit the torque from lever to blade.

Apart from torque, the lever hub also takes up the centrifugal forces of the blade and transmits them to the runner hub. Designs with the lever keyed to the blade pivot are also frequently used (see Figure VIII. 5). It is also possible to provide a pin on the pivot flange and to connect the lever directly to the pivot.

The design in Figure VIII. 43 was used by LMZ for many large turbines and proved successful in operation.

The lever is subject to the joint action of the force applied on its pin from the servomotor, and to the centrifugal force due to its mass, as well as that of the blade and pivot.

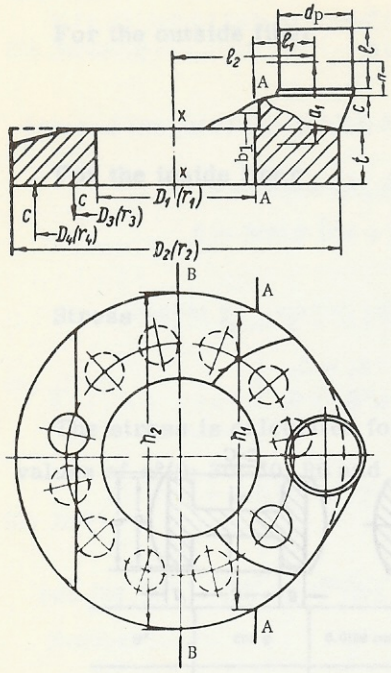


FIGURE VIII. 43. Lever of the blade-actuating mechanism

In LMZ practice, the lever is designed according to the following approximate method.

The body of the lever is considered as a ring of height t, without pin, loaded by the centrifugal force, with a central bore for the supporting collar. A ring of this type may be calculated either as a plate (flange), or as a rigid ring subjected only to tangential stresses.

With the ratios between the plate thickness and width currently used in levers, it is advisable to employ the second method.

The tangential stresses in the ring are /85/

$$\sigma_t = \frac{6M}{t^2 r_1 \ln \frac{r_2}{r_1}}. \qquad \text{(VIII. 69)}$$

By expanding $\ln \frac{r_2}{r_1}$ into a power series and performing the algebraic transformations, we obtain

$$\sigma_t = k_1 \frac{M}{W}, \qquad \text{(VIII. 70)}$$

where M = bending moment for the given ring, $M = \frac{c(r_4 - r_3)}{2\pi}$;

W = section modulus, $W = \frac{bt^2}{6}$;

k_1 = coefficient allowing for the nonuniform distribution of stresses along the ring radius,

$$k_1 = \frac{r_m}{r_1} \cdot \frac{1}{1 + \frac{1}{12}\left(\frac{b}{r_m}\right)^2},$$

where r_m = mean radius of the section, $r_m = \frac{r_1 + r_2}{2}$;

b = width of the section, $b = r_2 - r_1$.

If the ratio $\frac{b}{r_m} < 0.4$, one may put

$$k_1 = \frac{r_m}{r_1} = \frac{1}{2}\left(1 + \frac{r_2}{r_1}\right). \qquad \text{(VIII. 71)}$$

The weakening of the section due to the bolt holes may be approximately allowed for by assuming the section modulus to be

$$W = \frac{(b - d)\, t^2}{6},$$

where d = hole diameter.

The servomotor force transmitted through link and lever pin induces bending and torsion in the lever body. The stresses are determined at sections A—A and B—B.

Section A—A.

Section A—A is calculated as an equivalent rectangle of width b_1 designed to resist torsion and bending from the normal and maximum servomotor forces.

Torsional stress

$$\tau = \frac{M_t}{W_t}.$$

Twisting moment

$$M_t = P_1 a_1.$$

Section modulus in torsion

$$W_t = \alpha h_1 b_1^2,$$

where α depends on the ratio $\frac{h}{b}$.

$\frac{h}{b}$	1.0	1.2	1.5	1.75	2.0	2.5	3.0	4.0	5.0	8.0	10.0	∞
α	0.208	0.219	0.231	0.239	0.246	0.258	0.267	0.282	0.291	0.307	0.312	0.333

Bending stress

$$\sigma = \frac{M_b}{W_1}.$$

Bending moment

$$M_b = P_1 l_1.$$

Section modulus in bending

$$W = \frac{b_1 h_1^2}{6}.$$

Section B—B.

The diametral section B—B is calculated to resist bending from both normal and maximum servomotor forces.

Bending moment

$$M_b = P_t l_2.$$

Modulus

$$W_2 = \frac{J_x}{y_{max}}$$

Moment of inertia of section B—B with respect to the neutral axis x—x

$$J_x = \frac{t\left(D_2^3 - D_1^3\right)}{12}.$$

For levers made of grade 35 steel, the permissible stress in the lever body is $\sigma_y = 1000$ to $1200\,kg/cm^2$.

Lever pin. The lever pin (Figure VIII. 43) is calculated to resist bending, shearing, and specific pressure on the bushing, both during normal operation and at maximum servomotor force.

Bending moment

$$M_b = P_1 a = P_1 \left(\frac{l}{2} + c\right).$$

Section modulus in bending

$$W = \frac{\pi d_p^3}{32}.$$

Shear stress

$$\tau = \frac{4}{3} \cdot \frac{P_1}{F_h}.$$

Area subject to shearing

$$F_h = \frac{\pi d_p^2}{4}.$$

Specific pressure

$$p_{sp} = \frac{P_1}{d_p l}.$$

Permissible stresses in the pin are greater than in the lever body, namely $\sigma_y = 1300\,kg/cm^2$ for grade 35 steel.

Blade pivot. The blade pivot (also called journal or shank) is a massive steel casting bolted to the blade flange. Each pivot is mounted in a hole in the runner hub perpendicular to the turbine axis, and turns freely in bronze bushings fitted into the holes provided in the hub. By means of a stop collar, the pivot is prevented from moving in the radial direction.

Over twenty years of operational experience with Kaplan turbines has shown the use of bronze bushings in the blade-pivot bearing to be fully justified. Bearing wear is usually negligible, despite the fact that the rotational movement of the pivot is often oscillatory and the velocity too slow to form an oil film. Proper selection of diametrical clearances — with due allowance for the elastic deformation of the pivot — is of supreme importance.

A recent innovation is the use of roller bearings for the blade pivot which make it possible to reduce the force required for blade adjustment. These require a special anticorrosive lubricant and reliable seal to prevent oil from leaking out and water from seeping in.

A number of manufacturers in the U. S. A. have successfully incorporated roller bearings. The Terry adjustable-blade propeller turbine at the Austin Dam HEP, equipped with roller bearings /103/, has been in operation for thirteen years, with satisfactory results.

Other models incorporating a similar device have been just as successful elsewhere in the U. S. A.:

Pickwick HEP — units no. 5 and 6	$D_1 = 7.5$ m,	$H = 14.3$ m
Rock Island HEP — six units	$D_1 = 5.57$ m,	$H = 13.7$ m
Rochester HEP — one unit	$D_1 = 3.1$ m,	$H = 7.6$ m
Hallon-Forne HEP* — one unit	$D_1 = 2.0$ m,	$H = 10.3$ m

The pivot is calculated as a beam resting on two supports (Figure VIII.44) loaded by a system of forces which act upon the runner blade; the force transmitted through link and lever, the axial water pressure P_z and the blade weight G, are also considered as external forces.

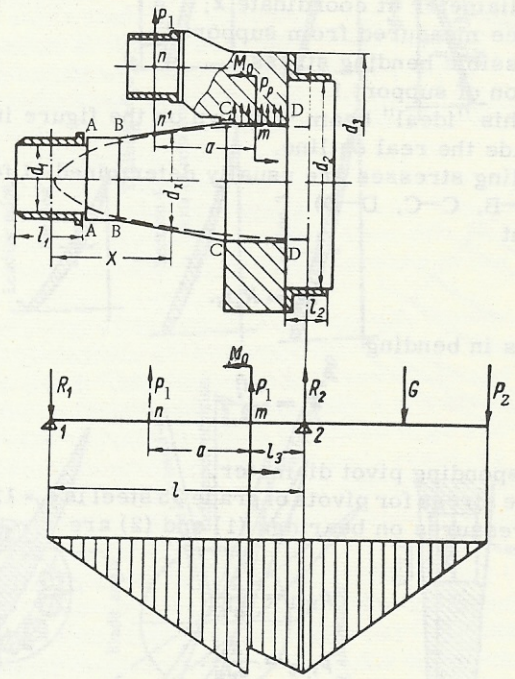


FIGURE VIII.44. Blade-pivot design

The values of the pivot reactions R_1 and R_2 are used in determining the specific pressures at the pivots, as well as the frictional moments that oppose the blade rotation and — together with the hydraulic moment — determine the required servomotor force. These reactions are determined by formulas of statics during the calculation of the servomotor force. The force from the servomotor P_1 is considered as applied at section n. Since, in actual fact, the force P_1 is applied to the pivot at section m, in order to make the statical relation hold true and maintain the reaction values, the additional moment $M_0 = P_1 a$ is applied at section m. The counterbalancing moment, acting upon the pivot from the supporting collar, is neglected.

The diagram of the bending moments is represented in Figure VIII.44. At each of the sections considered, the bending moment may be expressed as the product of the reaction R and the corresponding arm. In calculating

* [Transliterated from Russian.]

the bending moments at the pivot sections, there is thus no need to consider the system of external forces if the maximum value of the reaction R is known.

In designing the pivot, the aim should be to attain uniform stress distribution along its length. It is theoretically possible to design a beam of uniform bending strength by using the following formula:

$$d_x = \left(\frac{32}{\pi} \cdot \frac{R_1}{\sigma_a}\right)^{\frac{1}{3}} x^{\frac{1}{3}}, \qquad \text{(VIII. 72)}$$

where d_x = pivot diameter at coordinate x;
x = distance measured from support 1;
σ_a = permissible bending stress;
R_1 = reaction of support 1.

The outline of this "ideal" beam — drawn on the figure in dotted lines — may be traced inside the real outline.

The actual bending stresses are usually determined at four sections of the pivot (A—A, B—B, C—C, D—D).

Bending moment

$$M_b = R_1 x_i.$$

Section modulus in bending

$$W = \frac{\pi d_i^3}{32},$$

where d_i = corresponding pivot diameter.

The permissible stress for pivots of grade 35 steel is σ_y= 1200 to 1300 kg/cm^2.

The specific pressures on bearings (1) and (2) are

$$p_{sp1} = \frac{R_1}{d_1 l_1};$$

$$p_{sp2} = \frac{R_2}{d_2 l_2}.$$

The specific pressure on the collar should be calculated in terms of the centrifugal force at normal and runaway speed.

$$p_{sp3} = \frac{c}{F_3},$$

where the area is

$$F_3 = \frac{\pi}{4}\left(d_3^2 - d_2^2\right).$$

52. RUNNER BLADES

Blade shape. The shape of a Kaplan runner blade (Figure VIII. 45) consists of the blade itself (1), with flange (2) at its inner part. Sometimes the flange is cast integral with the pivot; blade construction is then simpler, but its main disadvantage is that machining, assembly, and dismantling become more complicated.

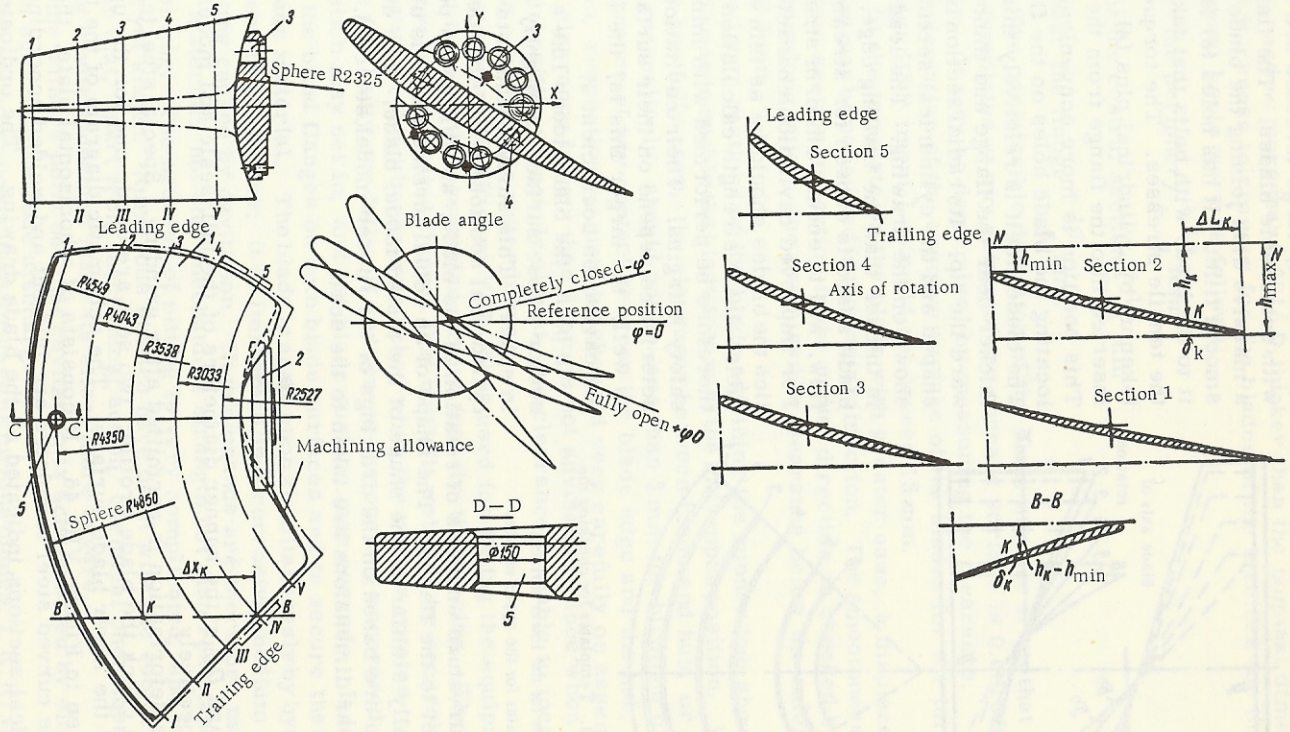


FIGURE VIII. 45. Runner blade

With large blades it is difficult to produce a good casting at the transition from pin to blade, since blowholes, porosities, and contraction stresses inevitably occur there. For this reason, large turbines are built with detachable blades. The flange is a massive disk joining the blade by a smooth fillet. It has holes (3) fastening it to the blade with bolts that take up the tensile stresses. The torque is taken up by cylindrical pins (4), usually inserted into the flange from the rear. This position is more convenient for locating the blade holes on the flange. The blade itself is relatively thin, being thicker near the flange and thinner toward the tip. Its radial section is wedge-shaped and the cylindrical sections are shown on the drawing. The leading edge is thicker than the trailing edge. This blade shape is chosen for streamlined flow, and to ensure uniform strength. For improved cavitation characteristics the blades should be as thin as possible; their strength calculation should therefore be performed with minimum safety margins. Their cavitation characteristics depend on their surface area as well; the larger this is, the lower the cavitation coefficient σ.

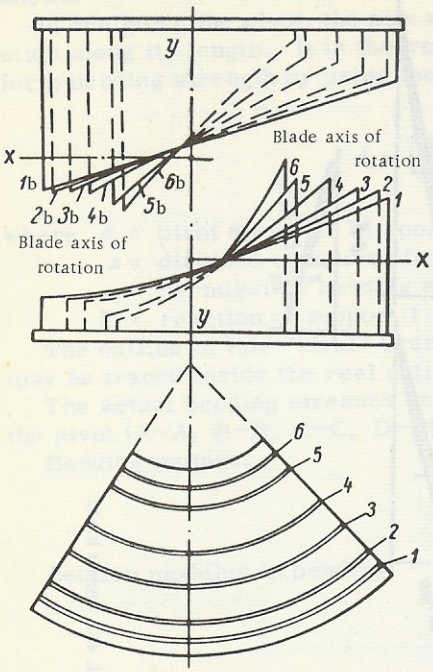


FIGURE VIII. 46. Templates for checking the blade profile:
1-6 — templates for the lower surface;
1b-6b — templates for the upper surface.

In plan, the blade looks like a ring sector whose surface is slightly curved in space. This surface consists of the cylindrical sections 1 — 5 that determine the curvature and axis of rotation of the blade, as well as its position with respect to the flange. The shape of an actual turbine blade is usually geometrically similar to the shape of the tested model blade. The drawings of the blade are based on the drawings of the runner model selected.

The linear dimensions are taken to the scale

$$\lambda = \frac{D_t}{D_{1m}},$$

where D_{1t} and D_{1m} — the runner diameters of the full-scale and model turbines, respectively.

No blade deformation is permitted after grinding. Special steel templates are used to check the blade profile; two sets are used, one for the upper, and one for the lower blade surface. The schematic diagram of the template is given in Figure VIII. 46. It consists of a horizontal plate, the base on which the curved steel templates are laid out and welded according to the cylindrical sections indicated on the blade drawing. The ordinates of each template determine the blade profile. Lines $x - x$ and $y - y$ are drawn upon the templates; their intersection lies on the axis of rotation.

The profiles at the leading and trailing edges are checked with flat templates. The following tolerances are allowed for the blade surface:

1. The blade thickness may, on the average, be no more than $0.0005 D_1$ thinner, and no more than $0.0015 D_1$ thicker than the nominal dimensions.

The thickness tolerances for the blades of the turbines for the Volga HEP imeni Lenin were as follows:

a) at the periphery $^{+10}_{-4}$ mm

b) at the central section $^{+15}_{-6}$ mm

c) near the flange $^{+17}_{-6}$ mm.

2. The permissible deviation of the blade surface from that indicated by the templates at any points of the concave surface is $0.0015 D_1$ on the average. It may be determined by measuring the clearance.

The deviation of the concave surface of the blades for the turbines at the Volga HEP imeni Lenin did not exceed 15 mm.

To fit the template on the blade with greater ease, a displacement of ± 15 mm may be permitted in the radial direction. The smoothness of the transition from section to section in the radial direction is checked by applying a 500 mm-long ruler; the permissible clearance below the ruler should not exceed 5 mm.

The inner sections of the blade adjoining the runner hub should be machined so as to enable the blade to turn to the fully-open position. When the blades are fully open, the clearance between blade and hub, or hub extension, respectively, should not be less than 5 mm for turbines of $D_1 = 9.3$ m. The absence of any contact between the blade edge and the hub, or hub extension, respectively, must be checked very carefully on assembling. However, clearance larger than 5 mm is not advisable, since when the blade is at mid-position or nearly closed, the clearance is liable to increase and lead to considerable water losses.

The opening (5) (Figure VIII. 45) is used for fitting the equipment required to hoist the assembled runner into the throat ring. These openings are covered with blind flanges that must fit well and be securely fastened, so that they cannot become detached when the runner rotates. If the blind flange fits badly, or falls off and leaves the opening uncovered, intensive cavitation may set in, and the blade surface may corrode. It is advisable to fit the blind flanges on both blade surfaces and to secure them with bolts.

Blade material. The blade is acted upon simultaneously by hydrodynamic and centrifugal forces; it is immersed in a corrosive medium and subjected to pitting caused by cavitation. High demands are therefore made on the blade material: not only mechanical strength but also resistance to cavitation pitting. The process of pitting is very complicated, and its real cause is not yet known. Numerous studies have dealt with the subject, and all concur that, apart from mechanical action, chemical phenomena also occur during cavitation which make its effect more severe.

Some authors point out that cavitation is accompanied by electrical phenomena such as electrode discharges.

In his study of metals used for casting turbine blades, I. R. Kryanin /56/ discussed the views of various authorities, his own laboratory research work, and field test results on the physical phenomena occurring during cavitation, and came to the conclusion that metal pitting results from the joint water

hammer and corrosion fatigue. The lower blade surface has to withstand considerable impacts, due to the very frequently occurring collapse of cavitation bubbles. The duration of each impact is several thousandths of a second, and its effect is therefore limited to the narrow surface layer of the blade, several hundredths of a millimeter deep. Since the material of the surface layer is absolutely inelastic and of a heterogenous structure, the stress distribution is nonuniform. Local stresses may occur, which exceed the yield strength. These may, if repeated, cause plastic deformations in the surface layer.

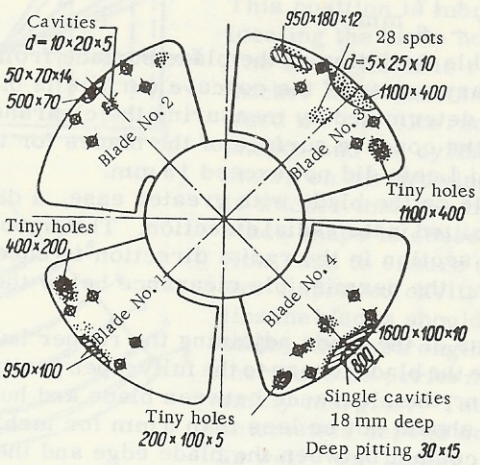


FIGURE VIII.47. Pitting of the lower blade surface after 34,000 hours of running (material — stainless steel)

Apart from plastic deformation, cavitation leads to work-hardening of the surface layer. The hardened layer cracks and crumbles under the fluctuating load of the water hammer forming pits. The water enters these pits and hastens the destructive process, since the oxides produced tend to enlarge the cracks. After the surface layer has been destroyed, the process continues: a new layer hardens, becomes brittle and eventually disintegrates. The pitting process intensifies, and local blisters unite to form continuous cavities.

The honeycombed surface does not sustain water-hammer stresses uniformly. Stress concentrations occur at many points. Under the continuous water action, this promotes the process of corrosion fatigue.

The joint action of water hammer and metal failure by corrosion fatigue eventually leads to the formation of deep wedge-shaped pitting which turns into typical corrosion-fatigue cracks.

Blades destroyed by cavitation pitting are shown in Figure VIII. 47. To withstand the destructive process they should be made of materials resistant to cavitation erosion.

In practice, the blades are made of 30L carbon steel, 20Kh 13NL high-alloy chromium steel, or 20 GSL low-alloy steel. Bimetallic (lined) blades are also used.

The cheapest material is ordinary 30L carbon steel, but its use is limited to small turbines, owing to its low resistance to cavitation erosion.

Apart from this, carbon steel has relatively poor mechanical properties and, if used, the blades are necessarily thicker, with poorer cavitation characteristics.

In large turbines the blades are usually made of high-chromium 20Kh14NL steel which has considerably higher resistance to cavitation erosion. The yield strength is 30 kg/mm^2, instead of 23 kg/mm^2 for 30L carbon steel. It is therefore used extensively in turbine construction.

However, this steel is not easy to cast, requiring a complicated casting technique. It has to be preheated to between 200 and 450° C for welding, which renders repairs more difficult under operating conditions.

A recent innovation is the manufacture of bimetallic blades, cast of carbon or low-alloy steel, and subsequently lined with welded stainless steel plates. Blades cast of 20 GSL manganese-silicon steel are lined with 3 to 4 mm thick plates made of EYa1T (1Kh18N9T) stainless austenitic steel. The yield strength of 20GSL steel is 30 kg/mm^2. The lining is made of 500×250 mm plates 3 mm thick, fastened to the blade by welding along the periphery as well as by electrowelded rivets.

To ensure high-quality welds, the distance between the plates must be 8 to 10 mm. Each plate should be drilled with 30 — 32 elliptical holes (dimensions 22×10 mm) for the rivets.

Rivets of 10 mm diameter were formerly used, but the plates usually became detached. The elliptical holes give a much larger welded area. The seam welded along the periphery is usually cleaned with an emery wheel. In this process, it is very important not to remove metal from the plate itself, since a reduction in thickness of as little as 1 mm may cause it to become detached when the turbine is running.

It is mainly the lower blade surfaces that are subject to cavitation pitting; the blade may therefore be lined on the lower side only, but then the fatigue strength of the blade material is liable to decrease.

It might be advantageous to manufacture bimetallic blades for large turbines by lining the blades with a cavitation-resistant metal. This technique has not yet been used in the U. S. S. R. for large turbines, but is successfully employed for the blades of small runners. Figure VIII. 48 shows the design of an experimental welded blade developed at the LMZ. It consists of a cast flange (2) to which the blade (1) is welded. The blade consists of 20GSL cast steel parts for the leading edge (6) and (7) and for trailing edge (5). The central part of the blade is welded of steel, and forms the frame of a box-shaped section provided with radial and circular ribs. The lower blade surface consists of 20 to 60 mm thick plates (8). The radial and circular ribs (3) and (4), respectively, are welded to these plates. The upper blade surface is made of plates (9) welded in between the radial and circular ribs.

After welding, the blade undergoes stress relieving by annealing. It is covered with a lining of stainless steel. No operating experience with such blades is yet available. The welded blade, manufactured for the Volga HEP imeni Lenin, weighs almost 7 t less than a cast blade. Thus, for a six-blade runner, the total weight is reduced by 42 t, and savings in metal being 60 t. Moreover, welded blades can be made in any machine construction plant, since no powerful electric furnaces are needed.

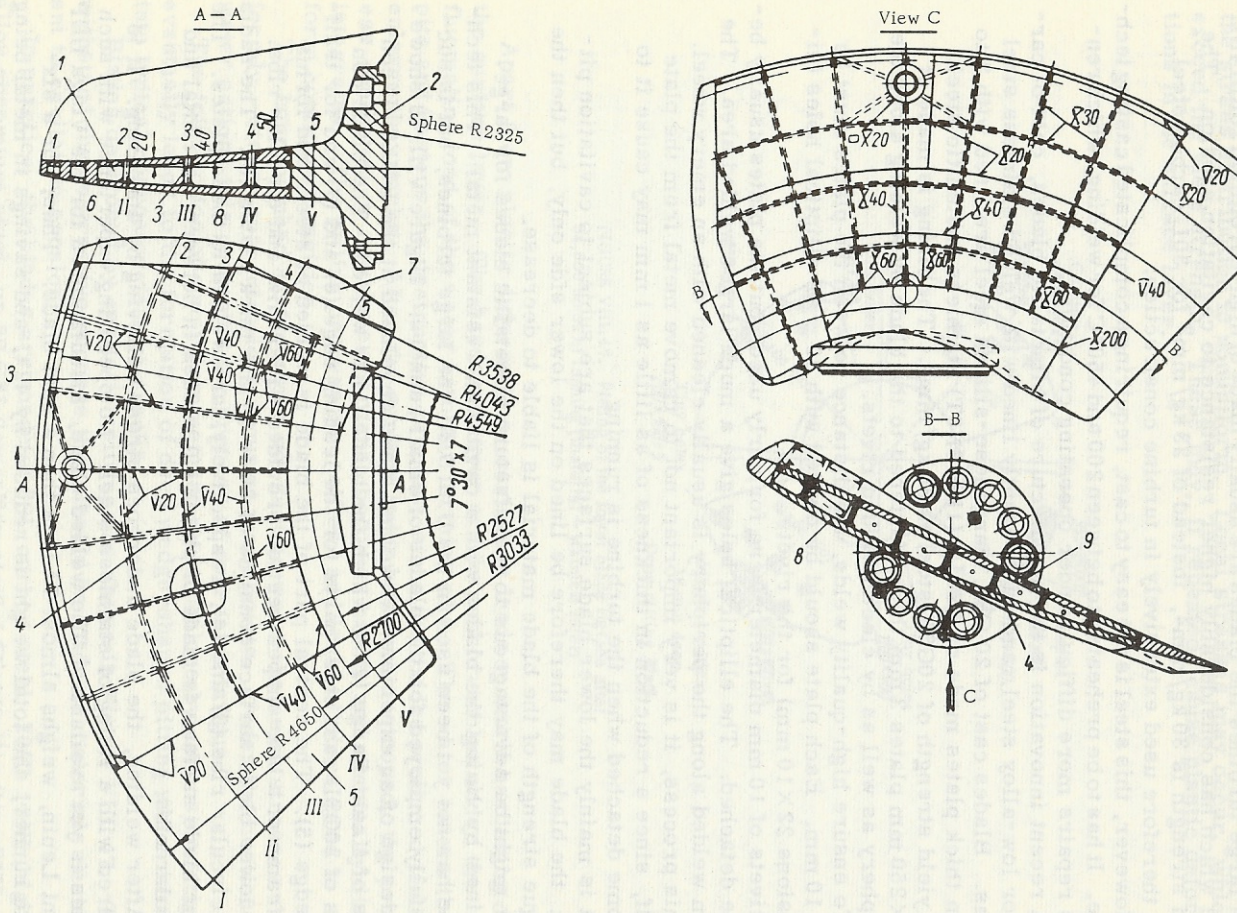


FIGURE VIII. 48. Welded blade

In order to protect carbon steel against cavitation, turbine builders outside the U. S. S. R. usually build up a layer of stainless steel at spots liable to pitting. It is advisable to build up at least two layers, since the chromium and nickel of the first layer dissolve during arc welding. The necessary composition of the built-up layer is obtained in the second layer. Building-up is done by means of automatic welding, and special devices are provided to maintain the proper distance between the electrodes and the blade surfaces. Lining is done at the factory much cheaper than during repairs at the hydroelectric plant itself.

The blade is usually cast with machining allowance. Special lathes are required to machine the curved blade surfaces.

It is advisable to employ precision blade casting which permits machining allowances to be dispensed with.

Strength calculation of the blade. The runner blade is a bent plate of nonuniform thickness restrained at one end; in plane, it has the shape of a ring sector loaded by a nonuniform pressure that depends on the operating conditions of the turbine. No precise and acceptable methods are as yet available for determining stress conditions in such rings, particularly since the pressure distribution on the blade under various operating conditions is unknown.

LMZ practice is to perform approximate blade calculations with the aid of experimental data obtained by model and field tests.

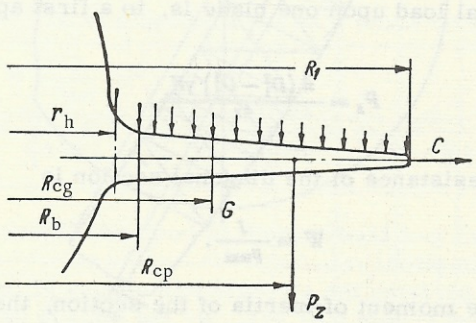


FIGURE VIII. 49. Radial section of the blade

The blade is calculated as a flat plate, subjected to a uniformly distributed pressure by a trial and error method. With blade dimensions that ensure maximum efficiency, the stresses under corresponding operating conditions can then be found.

This is done for the base and oblique sections near the trailing edge. The base section is checked for strength in bending and torsion, exactly like the built-in end of a cantilever beam.

The effect of centrifugal forces on the bending stresses at the base section is very slight, and is therefore usually neglected; hence the resulting bending stresses are assumed identical at normal and runaway speed.

Several oblique sections are selected for the calculation. Each is constructed either by direct measurements on the model blade, which is more expedient, or by using the drawing of the blade. The oblique section (for

instance B — B) is drawn on the plan view of the blade (see Figure VIII. 45). The point K — the intersection of this section with the cylindrical section II-2 — is determined by the coordinates Δx_κ and ΔL_κ. Along the cylindrical section II-2, this point is determined by the distance h_κ from the base plane NN. The thickness of the blade section is δ_κ. In order to construct the required profile of section B — B, the coordinates and thicknesses of other points of the oblique section are determined similarly.

The modulus of resistance of the oblique section is found, as usual, by approximation.

The bending moment at the base section (see Figure VIII. 49)

$$M_b = P_z (R_{cp} - R_b) + G (R_{cg} - R_b). \quad \text{(VIII. 73)}$$

The radius of the center of pressure is determined as the radius of the cylindrical section that divides the flow into two equal parts.

$$R_{cp} = \sqrt{\frac{R_1^2 + r_h^2}{2}}. \quad \text{(VIII. 74)}$$

where R_1 = outer radius of the runner;
R_b = radius of the cylindrical section at which the transition to the flange begins;
r_h = radius of the hub.

The hydraulic axial load upon one blade is, to a first approximation,

$$P_z = \frac{\pi (D_1^2 - D_f^2) \gamma H}{4z}. \quad \text{(VIII. 75)}$$

The modulus of resistance of the diagonal section is

$$W = \frac{J}{y_{max}}.$$

In determining the moment of inertia of the section, the direction of the neutral axis 0 — 0 should be taken parallel to the chord of the profile (Figure VIII. 50).

The moment of inertia with respect to the neutral axis is

$$J = \sum \frac{F_i h_i^2}{12} + \sum F_i y_i^2 - y_c^2 \sum F_i. \quad \text{(VIII. 76)}$$

The ordinate of the neutral axis is

$$y_c = \frac{\Sigma y_i F_i}{\Sigma F_i}.$$

The bending stress

$$\sigma_b = \frac{M_b}{W}.$$

The tensile stress

$$\sigma_t = \frac{C}{F}.$$

The centrifugal force should be calculated for normal and runaway speeds (C and C_t, respectively).

The total stress is

$$\sigma = \sigma_b + \sigma_t.$$

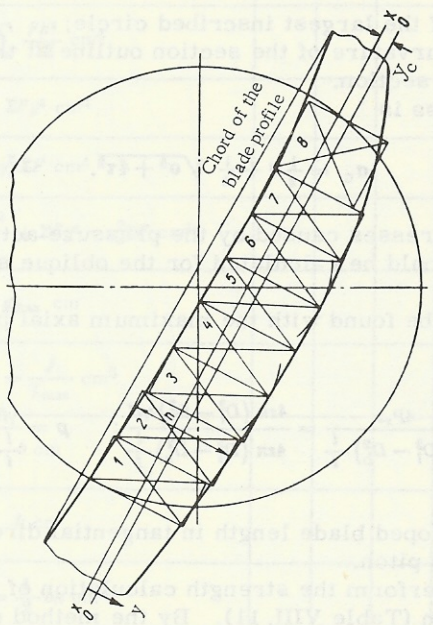


FIGURE VIII. 50. Determination of the moment of inertia of a cylindrical blade section

The torsional stresses at the blade-root section should be calculated for the maximum hydraulic moment. For this the polar moment of inertia of the root section must be known. Considering this section as plane and symmetrical, we obtain

$$J_\kappa = \frac{4J_x}{1 + 16\frac{J_x}{FS^2}}, \qquad \text{(VIII. 77)}$$

where J_x = moment of inertia about the neutral axis, taken as axis of symmetry;

F = area of the section;
S = length of the section.

The highest shear stresses are assumed at the points of tangency with the largest circle that can be inscribed in the outline of the section

$$\tau = \frac{M_t}{J_\pi} C_1,$$

where M_t = torsional moment, equal to the maximum hydraulic moment;

$$C_1 = \frac{D}{1 + \frac{\pi D^4}{16F^2}} \left[1 + 0.15 \left(\frac{\pi D^4}{16F^2} - \frac{D}{2r}\right)\right], \qquad \text{(VIII. 78)}$$

where D = diameter of the largest inscribed circle;
r = radius of curvature of the section outline at the point of tangency;
F = area of the section.

The combined stress is

$$\sigma_c = \tfrac{1}{2}\sigma + \tfrac{1}{2}\sqrt{\sigma^2 + 4\tau^2}.$$

Only the bending stresses caused by the pressure acting upon the part of the blade cut off should be calculated for the oblique sections at the trailing edge.

The pressure may be found with the maximum axial pressure from the formula

$$p = \frac{P_z}{F_b} = \frac{4P_z z}{\pi\left(D_1^2 - D_b^2\right)\frac{l}{t}} = \frac{4z\pi\left(D_1^2 - D_b^2\right)\gamma H}{4z\pi\left(D_1^2 - D_b^2\right)\frac{l}{t}}; \qquad p = \frac{\gamma H}{\frac{l}{t}} \text{ kg/cm}^2, \qquad \text{(VIII. 79)}$$

where l = mean developed blade length in tangential direction;
t = mean blade pitch.

It is advisable to perform the strength calculation of the obliquate sections in tabulated form (Table VIII. 11). By the method described, only the stresses at a few sections are found. The most highly stressed oblique sections should be determined empirically. The location of the critical sections was determined experimentally at the LMZ for standardized runners; in designing such turbines, therefore, the stresses at the critical sections can easily be calculated.

A precise design procedure for Kaplan runner blades was devised by L. M. Kachanov /34/. The blades are considered as flat slabs of nonuniform thickness, shaped like a circular ring sector and subjected to hydraulic pressure acting perpendicularly to the plate. This method also permits determination of the stresses due to the centrifugal forces at any point of the blade and of the natural frequency of the blades. The calculation is based on the Castigliano variational theorem and on the approximate integrals of the equation of equilibrium. Analysis by this method of a blade with a uniformly-distributed load has shown that the highest stresses occur at the trailing edge. Figure VIII. 51 shows the calculated stress distribution at the radial sections A — A, B — B, C — C, D — D, E — E, F — F,

TABLE VIII. 11

Calculation of oblique blade sections

Section	A—A	B—B	C—C	D—D	E—E	F—F
ΣFy cm^3						
ΣF cm^2						
$y_c = \frac{\Sigma Fy}{\Sigma F}$ cm						
$\sum \frac{Fh^2}{12}$ cm^4						
ΣFy^2 cm^4						
$y_c^2 \Sigma F$ cm^4						
$J = \sum \frac{Fh^2}{12} + \Sigma Fy^2 - y_c^2 \Sigma F$ cm^4						
y_{max} cm						
$W = \frac{J}{y_{max}}$ cm^3						
b cm						
h cm						
$F = \frac{1}{2} bh$ cm^2						
p kg/cm^2						
$P = pF$ kg						
$y = \frac{1}{3} h$ cm						
$M = Py$ kgcm						
$\sigma = \frac{M}{W}$ kg/cm^2						

and the mean values of stresses σ_r and $\tau_{r\varphi}$ in sectors I, II, III, IV, and V, extending over different angles. Along the blade the stresses σ_φ and σ_r vary according to a linear law, with different signs on opposite surfaces (detail N).

It was, however, found by tests carried out on actual blades under field conditions, that the greatest stresses occur at the base section of the blade near the flange (Figure VIII. 33).

The discrepancy between the actual and calculated stresses is apparently accounted for by the fact that a uniform pressure distribution was assumed in the calculation, blade curvature being neglected.

It should be noted, in addition, that the calculation method involves elaborate computations, and is therefore inconvenient in engineering practice.

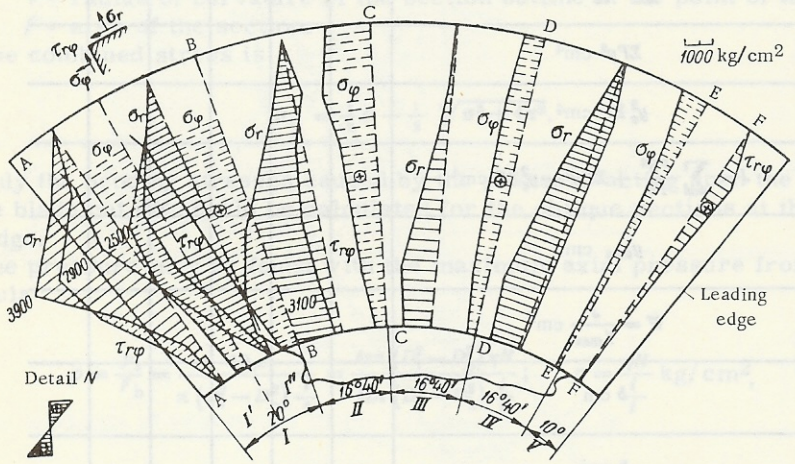


FIGURE VIII. 51. Calculation of stresses in the blade, by Kachanov's method

Experimental investigations of stress conditions in model runner blades subjected to static loads were carried out at the Machine Research Institute [IMASh] /12/.

Similar research was also conducted at the LMZ. Later, the IMASh, in conjunction with the LMZ, carried out measurements on several turbines in operation to establish the actual static and dynamic stresses in the blades under different operating conditions.

The following method was used at the LMZ in laboratory tests /66/: a metal model runner was subjected to a uniformly distributed load by means of a pneumatic device (Figure VIII. 52). The set-up consisted of model blade (1) fastened to support (2) welded to base (5). Rubber chamber (7) was located within box (3), mounted on support (4). Compressed air is led into the chamber through pipe (6). The clearance between blade and box was made as small as possible to prevent the chamber from getting jammed in. Cigarette paper dusted with talcum was laid between the rubber chamber and the blade surface to ensure minimum friction and uniform adherence of

the chamber to the blade surface. Brittle lacquer coatings were used initially to determine the direction of the principal stresses; later the stresses were measured with strain gages and electronic tensometers. Data obtained by measuring the stresses in the diagonal sections B — B, C — C, D — D, and at the flange A — A under a pressure of 5 atm, and by calculating them by the oblique section and Kachanov's methods, are given in Table VIII. 12 as an illustrative example.

It appears from the table that the highest stresses, reaching 1520 kg/cm^2 occur at the transition from blade to flange (section A — A), while the highest stresses in the body of the blade are only 1270 kg/cm^2.

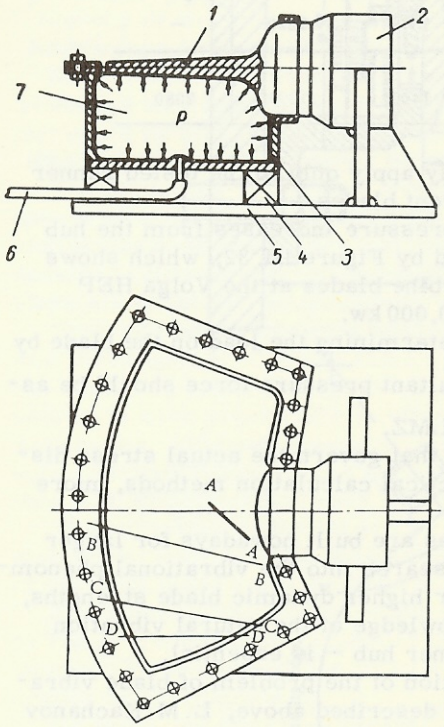


FIGURE VIII. 52. Blade model testing arrangement

The actual stresses are 20 to 30% lower than those calculated by the oblique section method, and 30 to 50% lower than those calculated by Kachanov's method. In reality, however, the pressure on the blade is not uniform, and the test results apply to static loading only; nevertheless the tests help define the data for calculating blade stresses more accurately.

A. A. Vasil'ev analyzed the test results for uniformly loaded models (tests were carried out by methods similar to the above and considered data obtained by investigating full-size turbines under field conditions of nonuniform pressure, with corrections for measured blade strain values. He came to the conclusion that with real loads applied to turbine blades, there is a linear relationship between the deflections and stresses and the loads at all blade points, and therefore the basic propositions of the theory of thin elastic plates are applicable to blades. When the blades are bent, their initial curvature induces membrane stresses; hence, during strain measurements, strain gages should be fixed to both blade sides.

The region of highest stresses is at the junction between blade and flange, and the principal stresses are radial (see Figure VIII. 33) showing the distribution of principal stresses on the upper side of the turbine blade for the Volga HEP imeni Lenin at an output of 25,000 kw. The calculation of the blade, therefore, consists of the strength calculation of its base section.

To allow for the nonuniformity of the bending-moment distribution, a multiplication factor of 1.3 is recommended.

The nonuniform thickness of the radial section considered in the calculation should be multiplied — for linear variation of the thickness along the

radius — by the ratio of the thickness of the base section to the thickness of the trailing edge. This ratio is approximately 5:1.

TABLE VIII.12

Comparison of blade stresses

Stresses in the model blade	Section			
	D—D	C—C	B—B	A—A
Highest experimental	1000	1100	1270	1520
Calculated by the method of oblique sections (maximum)	1260	1570	1590	—
Calculated by Kachanov's method	1500	1400	1770	2380

A. A. Vasil'ev's conclusions apparently apply only to the tested runner PL-587 and require correction for different blades.

According to experimental data, the pressure increases from the hub toward the periphery. This is illustrated by Figure III. 32, which shows the lines of equal specific load on the turbine blades at the Volga HEP imeni Lenin, measured at an output of 50,000 kw.

In calculating the base section, and determining the load on the blade by the formula $p = \frac{\gamma H}{l/t}$, the arm of the resultant pressure force should be assumed greater than is customary at the LMZ.

In order to establish the general laws that govern the actual stress distribution in blades, and improve the practical calculation methods, more experimental data are required.

Blade vibration. Since Kaplan turbines are built nowadays for larger heads and with larger blades, careful research into the vibrational phenomena, as well as fixing specifications for higher dynamic blade strengths, become necessary. To begin with, a knowledge of the natural vibration frequency of the blade — fitted to the runner hub — is essential.

There is as yet no mathematical solution of the problem of blade vibration. Apart from the calculation method described above, L. M. Kachanov suggested an approximate method of finding the frequency of natural vibrations, based on the thesis that the blade is a sectional plate with the outer edge fixed. This method makes it possible to determine two frequencies, corresponding to the first two modes of vibration.

The first frequency may be determined from the formula

$$f = KK_* \sqrt{\frac{E}{\gamma}} \cdot \frac{H}{(R_1 - r_h)^2 + (R_m\beta)^2} \text{ c}, \qquad \text{(VIII. 80)}$$

where K = coefficient determined by blade tests; E is in kg/mm^2; γ is in kg/mm^3; H = average blade thickness, mm; R_1 = outer blade radius, mm;

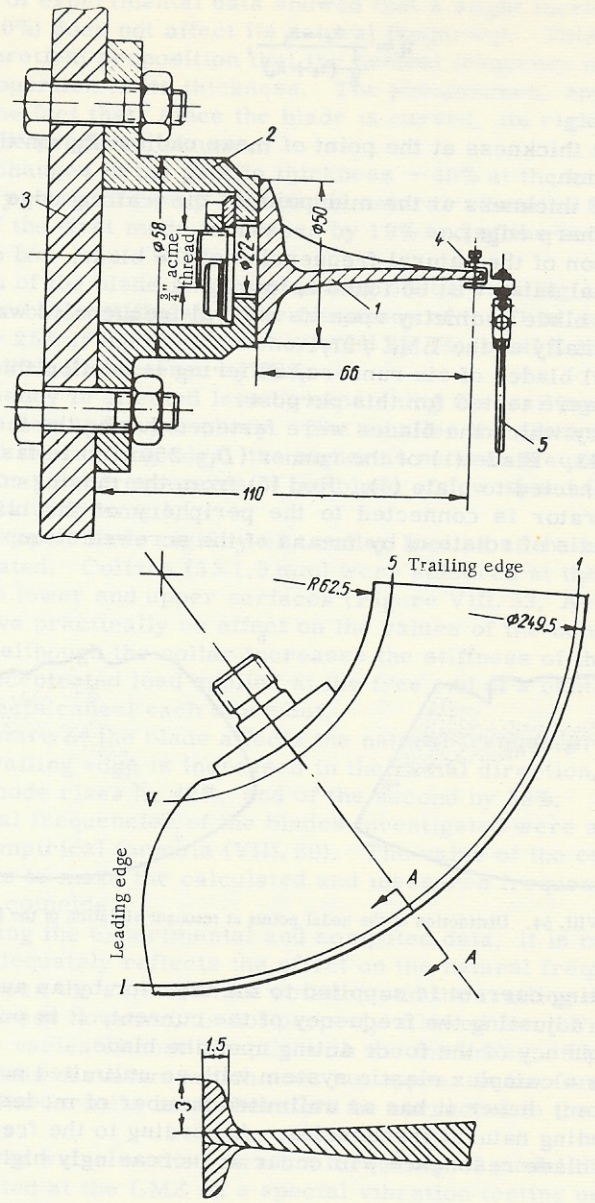


FIGURE VIII. 53. Fastening of the blade during vibration measurements

r_h = inner blade radius, mm; β = angle between axis of blade rotation and trailing edge, radians; $R_m = \frac{1}{2}(R_1 + r_h)$ = mean radius; K_* is selected from a special chart, according to the value of

$$\eta = \frac{h_2 - h_1}{\frac{1}{2}(h_2 + h_1)},$$

where h_2 = blade thickness at the point of mean radius R_m on the axis of rotation;

h_1 = blade thickness at the mid-point of the trailing edge (neglecting the sharp edge).

The calculation of the natural frequencies of the blade, and comparison with experimental data, will be found below.

The effect of blade geometry upon its natural frequencies was investigated experimentally at the LMZ /97/.

Bronze model blades of six runners, differing in section thickness and blade surface, were tested for this purpose.

The method by which the blades were fastened during the tests is shown in Figure VIII. 53. Blade (1) of the runner (D_1 = 250 mm) is fastened to hub (2) which is connected to plate (3). Rod (5) from the moving coil of an electrodynamic vibrator is connected to the periphery of the blade (in one plane with the axis of rotation) by means of the screwed clamp (4).

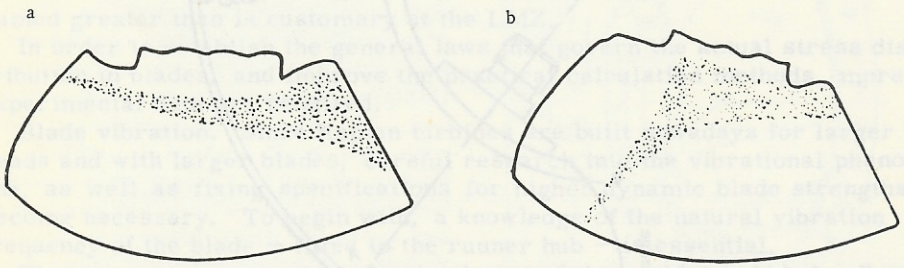


FIGURE VIII. 54. Distinction of the nodal points at resonant vibration of the blades

The alternating current is supplied to the vibrator by an audio-frequency oscillator. By adjusting the frequency of the current, it is possible to change the frequency of the force acting upon the blade.

The blade is a complex elastic system with an unlimited number of degrees of freedom; hence it has an unlimited number of modes of vibration with corresponding natural frequencies. According to the frequency of the applied force, blade resonance will occur at increasingly higher modes of vibration.

The first mode, peculiar to all the blades tested, is a flexural vibration with the node close to the clamped end; the second mode has a flexural-torsional character, with the node transverse to the blade.

Figure VIII. 54 shows the location of the nodes on the blade surface at resonance frequencies corresponding to the first and second modes:

a — flexural vibration (first mode);

b — flexural-torsional vibration (second mode).

Analysis of experimental data showed that a slight increase in the blade thickness (10%) does not affect its natural frequency. This seems to contradict the theoretical proposition that the natural frequency of a plate varies in direct proportion to its thickness. The phenomenon, apparently, is explained by the fact that, since the blade is curved, its rigidity depends only slightly on the profile thickness.

Greater changes in the profile thickness — 40% at the base and 20% at the periphery — significantly reduce the natural-vibration frequency. The frequency of the first mode increases by 19% and of the second mode by 17.5%.

Reduction of the blade length by cutting off the trailing edge considerably increases the blade stiffness. The frequency of the first mode of vibration increases by 25% if the blade is shortened by 8%, by 41% if shortened by 16%, and by 76% if shortened by 20%.

The frequency is affected less by shortening the trailing edge near the base section than at the periphery. The smaller the distance from the axis of rotation to the trailing edge, the higher is natural frequency. Consequently, the natural frequencies of the blade of low-speed (high-head) turbines are relatively small.

The effect upon blade rigidity of a collar located at the blade periphery was investigated. Collars (3×1.5 mm) were soldered at the periphery of one blade, to lower and upper surfaces (Figure VIII. 53, A — A). This appeared to have practically no effect on the values of the natural frequency. Apparently, although the collar increases the stiffness of the blade, it also acts as a concentrated load applied at the free end of a cantilever beam, thus both effects cancel each other out.

The curvature of the blade affects the natural frequency. If the curvature of the trailing edge is increased in the radial direction, the frequency of the first mode rises by 42%, and of the second by 36%.

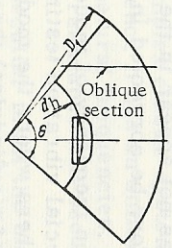
The natural frequencies of the blades investigated were also calculated by the semiempirical formula (VIII. 80). The value of the coefficient K was selected so as to make the calculated and measured frequencies of the reference blade coincide.

By analyzing the experimental and computed data, it is noted that the calculation adequately reflects the effect on the natural frequency of the distance between the axis of blade rotation and the trailing edge. The effect of blade thickness however, is not properly allowed for. From the formula, the frequency varies almost directly with the thickness. This is true for plates, but blade curvature which does not appear in the formula is also important. The formula must therefore be corrected in the light of experimental results.

The effect of water on the vibration frequency of model blades and plates was investigated at the LMZ on a special vibration testing unit /98/. This consisted of a tube with testing chambers where the models were fastened. The testing chamber simulated part of a cylindrical throat ring. The model blades were tested in air, stationary water, and water flowing with different velocities. Oscillations were set up by means of a vibrator through the boss used to fasten the model.

TABLE VIII.13

Calculated stresses in root and oblique blade sections



H_{max}, m	D_1, cm	$\frac{d_h}{D_1}$	$\frac{d_f}{D_1}$	δ_{max}, mm / $\frac{\delta_{max}}{D_1}$	θ	$R_{fillet,\ mean}$, m	$\frac{R_{fillet}}{D_1}$	$\frac{R_{fillet,\ mean}}{b_{max}}$	Stresses in root section	Stresses in oblique section
30	930	0.50	0.167	370/0.0395	79°	145	0.0156	0.390	1100	1000
32	720	0.55	0.194	295/0.0410	91°40'	115	0.0160	0.390	720	700
32	550	0.55	0.161	225/0.0410	91°40'	100	0.0182	0.445	880	700
32.5	370	0.567	0.213	150/0.0405	91°40'	70	0.0189	0.465	640	720
36	500	0.50	0.150	230/0.0460	91°40'	75	0.0150	0.325	950	790
44.8	370	0.52	0.162	175/0.0475	79°	60	0.0162	0.345	1080	1000
56	370	0.60	0.162	93/0.0250	90°	160	0.0435	1.630	1400	1400*

* Note: Blade failures occurred in this turbine.

The frequency of the excitation force was controlled by an audio-frequency oscillator, through an amplifier.

The wave pattern of the vibration was determined by means of sand during tests in air, and by means of a piezoelectric probe during tests in water. The probe consisted of a rod with a [piezoelectric] crystal of Seignette salt. The rod had a lead weight serving as inertial mass attached to one end, and touched the vibrating surface with the other end; the vibrations were transmitted to the crystal, whose electric signals were recorded on an oscillograph.

The tests showed that the vibration frequency of a bronze blade of the PL-495 runner (D_1 = 460 mm), is lowered by 40% for the first mode, by 31% for the second, and by 23% for the third, if the blade is immersed in water to a depth of not more than 20 mm. If the depth of immersion is less, the effect of the water upon the natural frequencies is also smaller. An increase in the flow velocity up to 3 m/sec (attainable on the testing unit) had practically no effect on the vibration frequency of the model. The vibration frequency of test models with high rigidity (very thick, or very curved) is less affected by water than the frequency of less rigid models.

The calculated stresses at the root and oblique sections of several turbines in operation are set forth in Table VIII. 13. Calculation was performed by the LMZ method, and the designations used are shown on the drawing. The stresses are calculated for normal speeds. It can be seen from the table that in turbines that are safe in operation, the stresses in the blades do not exceed 1100 kg/cm^2.

Instances of damaged blades, where the stresses reached 1400 kg/cm^2, are known. Although the actual causes of the damage are not precisely known, it may be safely assumed that the high stresses were a contributing factor.

Calculation of the bolts which fasten the blade flanges. The number of bolts which fasten the blade flange to the blade pivot should be determined according to the dimensions of the flange, the thickness of the root section, and design of the pivot fastening.

To obtain a large modulus of resistance, as few bolts as possible having larger individual sections should be used. The blade is usually located below its axis of rotation. The majority of bolts is therefore located on the upper part of the flange.

The loads carried by the bolts are generally calculated approximately, assuming the flange to be absolutely rigid. It is likewise assumed that, because of the bending moment, the flange tends to turn about the tangent to its contour at its lowest point (Figure VIII. 55). Since the bolts oppose this motion, the load is divided between the bolts in direct proportion to their distance from the tangent through 0. We may therefore write

$$P_z l_0 = \Sigma P_i l_i, \qquad \text{(VIII. 81)}$$

where P_z = hydraulic force which is assumed to act in the direction of the turbine axis corresponding to the pressure exerted upon the closed blade;

l_0 = distance between center of pressure and flange supports;

P_i = forces acting on the bolts;

l_i = height of bolt center line from tangent through 0.

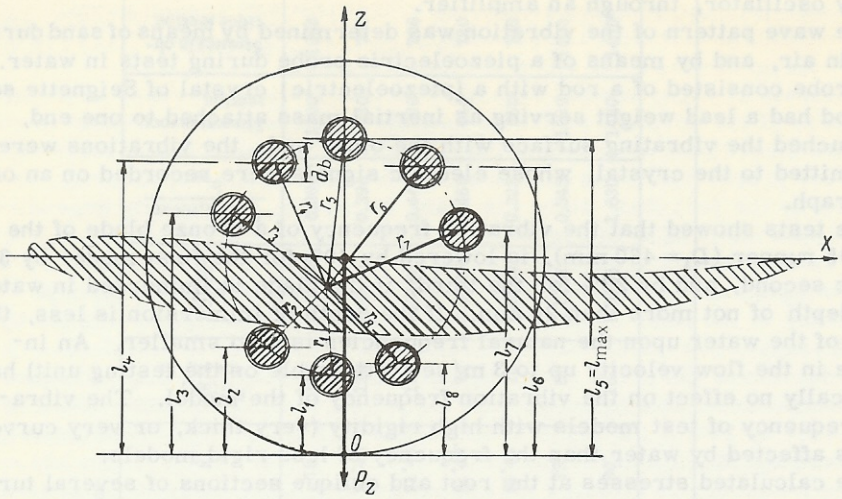


FIGURE VIII. 55. Schematic drawing of the blade flange

Expressing the force P_i by the maximum force P_{max} exerted upon the most distant bolt, we have

$$P_1 = P_{max}\frac{l_1}{l_{max}};\quad P_2 = P_{max}\frac{l_2}{l_{max}};\ \ldots;\ P_n = P_{max}\frac{l_n}{l_{max}}.$$

Consequently, according to (VIII. 81)

$$P_z l_0 = \frac{P_{max}}{l_{max}}\Sigma l_i^2,$$

whence the force acting upon the most distant bolt

$$P_{max} = \frac{P_z l_0 l_{max}}{\Sigma l_i^2}. \qquad \text{(VIII. 82)}$$

The stresses in the most distant bolt at the root section of the thread

$$\sigma_z' = \frac{P_{max}}{\frac{\pi}{4}d_1^2}. \qquad \text{(VIII. 83)}$$

The load exerted upon the bolts due to the centrifugal force C at normal and runaway speeds is inversely proportional to the distance (r_i) between the center of the bolt and the center of gravity of the blade (blade with flange), as shown in Figure VIII. 56.

$$C = \sum_{i=1}^{n} C_i, \qquad \text{(VIII. 84)}$$

where C_i = load on i-th bolt.

If C_2 is the load on the bolt located at the least distance from the center of gravity then

$$\frac{C_1}{C_2} = \frac{r_2}{r_1}; \quad \frac{C_3}{C_2} = \frac{r_3}{r_3}; \quad \cdots; \quad \frac{C_n}{C_2} = \frac{r_2}{r_n};$$

$$C_1 = C_2 \frac{r_2}{r_1}; \quad C_3 = C_2 \frac{r_2}{r_3}; \quad \cdots; \quad C_n = C_2 \frac{r_2}{r_n},$$

whence

$$C = \sum_{i=1}^{n} \frac{C_2 r_2}{r_i}.$$

Consequently,

$$C_2 = \frac{C}{r_2 \sum_{i=1}^{n} \frac{1}{r_i}}. \qquad \text{(VIII. 85)}$$

The stress due to the centrifugal force will be different in each bolt, being highest in the bolt nearest the center of gravity.

$$\sigma_z'' = \frac{C_2}{\frac{\pi}{4} d_1^2}. \qquad \text{(VIII. 86)}$$

The total stress in the bolt will be

$$\sigma_{tot} = \sigma_z' + \sigma_z''. \qquad \text{(VIII. 87)}$$

The most highly-loaded bolt can be determined if the total stress is known.

In another method for calculating the bolts of the blade flange, the flange is not considered as a separate part, and the bolts are considered as a beam subjected to bending and centrifugal forces. In this case, the maximum stresses occur in the bolts farthest away from the centroid of the bolt system.

Starting from the same assumption — namely that the flanges are rigid and that their deformation may be disregarded since they are small in comparison with the bolt deformation — B. A. Berkman proposed a more accurate method of calculation which allows for bolt prestressing.

Three different relative positions of the blade and pivot flanges are possible according to the loads exerted upon the blade:

1. The joint between the flanges does not open, and contact is maintained along the whole surface.
2. The joint opens, and contact is maintained only at a single point (Figure VIII. 56).
3. The joint opens, there being no contact whatsoever between the flange surfaces.

The second of these three positions may be considered as basic, the other two being particular cases derived from it.

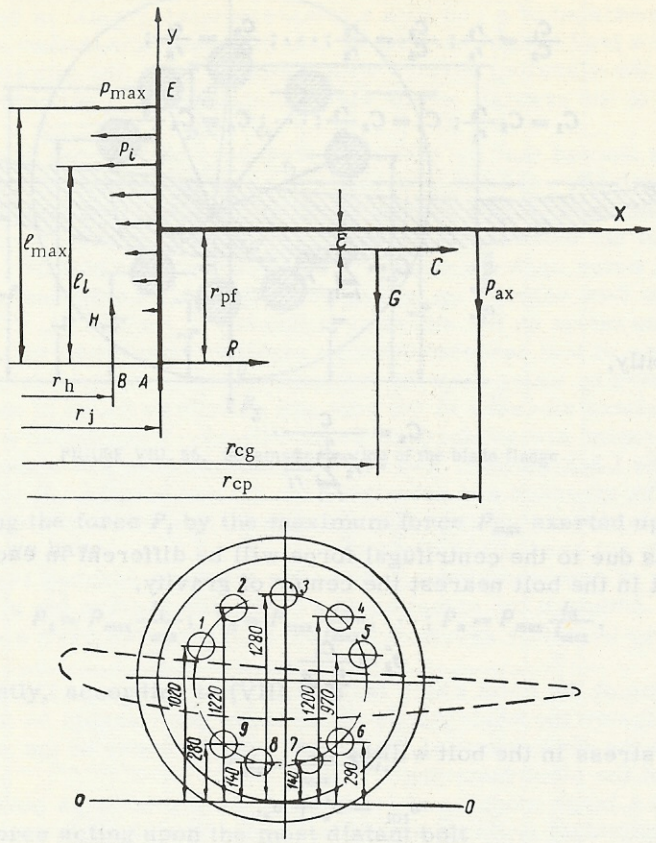


FIGURE VIII. 56. Location of bolts on the blade flange

Figure VIII. 56 shows the forces acting on the blade and blade flange when there is contact between blade and pivot flanges at point A, and the blade flange turns about this point. The following notations were adopted:

P_{ax} = axial force acting on one blade;
G = weight of blade and blade flange;
C = centrifugal force due to mass of blade and blade flange;
R = reaction at point A;
H = reaction at the projection provided for blade centering;
P_i = force on the blade flange due to the i-th bolt;
r_{cp} = radius to blade center of pressure;
r_{cg} = radius to blade center of gravity;
r_j = radius to joint;
r_h = mean radius of the support surface of the collar, i.e., to point of action B of force H;

r_{pf} = radius of pivot flange;
ε = distance between the flange axis and the center of gravity of the blade with flange;
l_i = distance from point A to i-th bolt;
l_{max} = distance from point A to the most distant bolt.

The sum of the moments of all the forces about point B, and the sum of the projections of all the forces on the X axis, are

$$\left.\begin{aligned} \sum_{i=1}^{n} P_i l_i - M = 0; \\ -\sum_{i=1}^{n} P_i + C + R = 0, \end{aligned}\right\} \qquad \text{(VIII. 88)}$$

where

$$M = P_{ax}(r_{cp} - r_h) + G(r_{cg} - r_h) + C(r_{pf} - \varepsilon);$$

n = number of bolts.

The force acting on the i-th bolt is

$$P_i = P_{i0} + P'_i, \qquad \text{(VIII. 89)}$$

where P_{i0} = prestressing force;
P'_i = additional force acting as a result of the external load.

Considering all the bolts to have been prestressed with equal force P_0, and inserting the value of P_i in equation (VIII. 88) we obtain

$$\left.\begin{aligned} P_0 \sum_{i=1}^{n} l_i + \sum_{i=1}^{n} P'_i l_i = M; \\ -nP_0 - \sum_{i=1}^{n} P'_i + C + R = 0. \end{aligned}\right\} \qquad \text{(VIII. 90)}$$

These two equations contain $(n + 1)$ unknown quantities P'_i and R. The problem is $(n - 1)$ times statically indeterminate. In order to solve it, $(n - 1)$ equations expressing the compatibility of deformations must be added.

These equations may be obtained by assuming the condition of absolute rigidity of the flanges, and are written

$$P'_i = \frac{P'_{max}}{l_{max}} \cdot l_i; \qquad \text{(VIII. 91)}$$

$$i = 1, 2, 3, \ldots, (n - 1).$$

Since

$$\frac{\sum_{i=1}^{n} l_i}{n} = l_{cg}, \qquad \text{(VIII. 92)}$$

where l_{cg} = height above A of the centroid of the bolt system, we have

$$\frac{P'_{max}}{l_{max}} \sum_{i=1}^{n} l_i^2 = M - nP_0 l_{cg}\ ; \qquad \text{(VIII. 93)}$$

$$R = nP_0 + \frac{P'_{max}}{l_{max}} \cdot nl_{cg} - C. \qquad \text{(VIII. 94)}$$

Examination of equation (VIII. 93) shows that, depending on the load acting and the prestressing, the right-hand side may be either positive or negative. If negative, the flange turns about point A in a counterclockwise sense; that is, however, impossible. The additional force acting on the most highly stressed bolt must therefore be found from formula

$$P'_{max} = \begin{cases} \dfrac{(M - nP_0 l_{cg})}{\sum_{i=1}^{n} l_i^2} \cdot l_{max} & \text{when } M > nP_0 l_{cg}\ ; \\ 0 & \text{when } M < nP_0 l_{cg}\ . \end{cases} \qquad \text{(VIII. 95)}$$

With P'_{max} known, all the other forces may be determined from formula (VIII. 91).

The case where the flange turns about the uppermost point E is of interest. This may happen either under conditions of reversed water hammer, when the axial force is directed upward, or if the center of gravity of the blade is below the blade axis of rotation. The magnitude of the moment about A is then

$$M^* = -P_{ax}(r_{cp} - r_h) - G(r_{cg} - r_h) + C(r_{pf} + \bar{\varepsilon}).$$

The other formulas do not change, but l_i should be replaced by the distance between the i-th bolt and point E_i.

Depending upon the prestressing force and the external load, the reaction R in formula (VIII. 94) may be either positive or negative. A negative value signifies that reaction R acts in the opposite direction to that shown in Figure VIII. 56.

If $R < 0$, contact between the flanges at point A ceases, i.e., the flanges tend to separate. In this event, the entire load on the blade and blade flange is carried by the bolts, which are to be calculated as a composite team formed by all the bolt sections. The highest stress occurs at the bolt farthest from the [imaginary] neutral axis, and is determined by the formula

$$\sigma_{max} = \frac{M_y (l_{max} - l_{cg})}{J_y} + \frac{C}{nf}, \qquad \text{(VIII. 96)}$$

where M_y = bending moment in the plane of the (imaginary) neutral axis for pure bending;

J_y = moment of inertia of all the bolt sections with respect to the same axis;

f = cross-sectional area of one bolt.

Since in pure bending the neutral axis passes through the centroid of the [combined] section, and the position of the centroid of all the bolt sections is determined by (VIII. 92), M_y and J_y may be expressed by

$$M_y = P_{ax}(r_{cp} - r_h) + G(r_{cg} - r_h) - C(l_{cg} - r_{pf} + \varepsilon); \qquad \text{(VIII. 97)}$$

$$J_y = f\left(\sum_{i=1}^{n} l_i^2 - nl_{cg}^2\right). \qquad \text{(VIII. 98)}$$

Thus, depending upon load and prestressing, the following cases may occur:

Case 1: $M < nP_0 l_{cg}$, $M^* < nP_0 l_{cg}$.

With the turbine in operation, the joint does not open, the prestressed bolts being under tension.

Case 2: $M > nP_0 l_{cg}$, $M > M^*$.

The joint opens when the turbine is running; the load on the bolt farthest from point A is determined by the formula

$$P_{max} = P_0 + P'_{max},$$

where P'_{max} is found from

$$P'_{max} = \frac{(M - nP_0 l_{cg}) l_{max}}{\sum_{i=1}^{n} l_i^2}.$$

Case 3: $M^* > nP_0 l_{cg}$, $M^* > M$.

The flange turns about the uppermost point E and the joint opens. The stress in the most highly loaded bolt may be found similarly as in case 2, with l_i replaced by l_i^* and M by M^*.

Case 4: the foregoing three cases may occur when the reaction R, determined by (VIII. 94), is positive.

$$R = nP_0 + \frac{P'_{max}}{l_{max}} nl_{cg} - C > 0.$$

If the reaction R is found to be negative, then the fourth case occurs, when the flanges separate and contact between them at point A ceases. In this case, the largest stress occurs at the bolts farthest from the [imaginary] neutral axis, and is determined by the formula

$$\sigma_{max} = \frac{M_y (l_{max} - l_{cg})}{J_{y_1}} + \frac{C}{nf}.$$

As an example, the calculation of the blade-flange bolts of the turbine for the Volga HEP imeni Lenin is given below.

Example. Initial data:

P_{ax} = 271 t;
G = 18.45 t;
C = 338 t under normal operating conditions, 1420 t at runaway speed;
r_{cp} = 338 cm;
r_{cg} = 309 cm;
r_j = 198 cm;
r_{pf} = 70 cm;
ε = 0.96 cm.

TABLE VIII.14

Location of blade-flange bolts

Number of bolts	l_i, cm	l_i^2, cm^2
1	102	10,404
2	122	14,884
3	128	16,400
4	120	14,400
5	97	9,409
6	29	841
7	14	196
8	14	196
9	28	784
Σ	654	67,514

To determine the effect of prestressing the bolts, the calculation will be performed for different values of P_0.

1. $P_0 = 0$.

From Figure VIII. 56, which shows the location of the bolts, we obtain Table VIII. 14.

Formula (VIII. 92) gives

$$l_{cg} = \frac{\sum_{i=1}^{n} l_i}{n} = \frac{654}{9} = 72.7 \text{ cm}.$$

Let us find the moment M.

At normal speed

$$M = 271\ (338—198) + 18.45\ (309—198) + 338\ (70—1) = 63\,350 \text{ tcm}.$$

At runaway speed

$$M = 271\ (338—198) + 18.45\ (309—198) + 1420\ (70—1) = 138\,050 \text{ tcm}.$$

According to (VIII. 95) we find at normal speed:

$$P'_{max} = \frac{63350 \cdot 10^3 \cdot 128}{67500} = 120\,000 \text{ kg};$$

at runaway speed

$$P'_{max} = \frac{138000 \cdot 10^3 \cdot 128}{67500} = 262\,000 \text{ kg}.$$

The reaction R is found from (VIII. 94): at normal speed

$$R = \frac{120000}{128} \cdot 9 \cdot 72.7 - 338\,000 = 275\,000 \text{ kg} > 0;$$

at runaway speed

$$R = \frac{262000}{128} \cdot 9 \cdot 72.7 - 1\,420\,000 = -80\,000 \text{ kg} < 0.$$

Consequently, at normal speed case 2 occurs, and the stress in the most highly-loaded bolt is

$$\sigma_{max} = \frac{P'_{max}}{f} = \frac{120000}{188} = 638 \text{ kg/cm}^2.$$

At runaway speed, case 4 occurs, and the stress in the most highly-loaded bolt should be found from (VIII. 96). The values M_y and J_y required for this purpose are:

$$M_y = 271\,(338-198) + 18.45\,(309-198) - 1420\,(72.7-70+1) =$$

$$= 34\,800 \text{ tcm};$$

$$J_y = 188\,(67\,500 - 9 \cdot 72.7^2) = 37.2 \cdot 10^5 \text{ cm}^4.$$

The largest stress is

$$\sigma_{max} = \frac{34800 \cdot 10^3\,(128 - 72.7)}{37.2 \cdot 10^5} + \frac{1420 \cdot 10^3}{9 \cdot 188} = 1357 \text{ kg/cm}^2.$$

2. If the bolts are prestressed to $\sigma_0 = 200 \text{ kg/cm}^2$, the prestressing force is

$$P_0 = \sigma_0 f = 37\,600 \text{ kg};$$

$$nP_0 l_{cg} = 9 \cdot 37\,600 \cdot 72.7 = 24.6 \cdot 10^6 \text{ kgcm}.$$

From (VIII. 95) we obtain:
at normal speed

$$P'_{max} = \frac{(63.3 - 24.6) \cdot 10^6 \cdot 128}{67500} = 73\,300 \text{ kg};$$

at runaway speed

$$P'_{max} = \frac{(138 - 24.6) \cdot 10^6 \cdot 128}{67500} = 215\,000 \text{ kg}.$$

The reaction R is:
at normal speed

$$R = 9 \cdot 37\,600 + \frac{73300}{128} \cdot 9 \cdot 727 - 338\,000 = 374\,000 \text{ kg} > 0;$$

at runaway speed

$$R = 9 \cdot 37\,600 + \frac{215000}{128} \cdot 9 \cdot 72.7 - 1\,420\,000 = 13\,000 \text{ kg} > 0.$$

Thus, with the bolts prestressed to only $\sigma_0 = 200 \text{ kg/cm}^2$, the flanges will no longer separate — as happens with no prestressing.

The stress in the most highly loaded bolt is, at normal speed

$$\sigma_{max} = \sigma_0 + \frac{P'_{max}}{f} = 200 + \frac{73300}{188} = 590 \text{ kg/cm}^2;$$

at runaway speed

$$\sigma_{max} = 200 + \frac{215000}{188} = 1340 \text{ kg/cm}^2.$$

3. We now assume $\sigma_0 = 800 \text{ kg/cm}^2$. In this case the prestressing force is $P_0 = \sigma_0 f = 150{,}000 \text{ kg}$.

From (VIII. 95) we obtain, at normal speed

$$P'_{max} = 0, \quad \text{since} \quad M < nP_0 l_{cg};$$

at runaway speed

$$P'_{max} = \frac{(138 - 98) \cdot 10^6 \cdot 128}{67500} = 75\,800 \text{ kg}.$$

It may readily be seen that the condition $R > 0$ is fulfilled under both assumptions. The stress in the most highly loaded bolt is, at normal speed

$$\sigma_{max} = \sigma_0 = 800 \text{ kg/cm}^2;$$

at runaway speed

$$\sigma_{max} = \sigma_0 + \frac{P'_{max}}{f} = 800 + \frac{75800}{188} = 1200 \text{ kg/cm}^2.$$

4. Let us now determine the prestressing required to prevent the flange-joint from opening under the most dangerous operating conditions, i. e. at runaway. From (VIII. 95) it results that the bolts must be prestressed to the point where the inequality

$$P_0 > \frac{M}{nl_{cg}}$$

holds true.

By inserting in this formula the value of M for runaway conditions, we obtain

$$P_0 > \frac{138 \cdot 10^6}{9 \cdot 72.7} = 211\,000 \text{ kg}.$$

To this corresponds

$$\sigma_0 = \frac{P_0}{f} > \frac{211000}{188} > 1120 \text{ kg/cm}^2.$$

If the bolts are prestressed to this point, the stresses do not increase above σ_0 under the action of the external loads on the blade.

TABLE VIII. 15

Calculated stresses for various amounts of prestressing

σ_0	Normal speed		Runaway speed	
	σ_{max}	k_n	σ_{max}	k_r
0	638	0	1360	0
200	590	0.34	1340	0.15
800	800	1	1200	0.667
1120	1120	1	1120	1

The results of the calculation performed for different prestressings are listed in Table VIII. 15.

In addition to the calculated values of σ_{max} at normal and runaway speed, the table includes the bolt-stress ratios k_n and k_r for normal and runaway speeds, respectively. The stress ratio is the algebraic ratio of minimum and maximum stresses $K = \frac{\sigma_{min}}{\sigma_{max}}$ in one cycle of load variation.

It is obvious that when the load on the blade varies from zero (turbine starting) to maximum (normal operation and runaway) the stress ratio is $K = \frac{\sigma_0}{\sigma_{max}}$.

As is well known from the theory of strength of materials, for fluctuating loads, the endurance limit of a material decreases with decreasing stress ratio.

It appears from the table that, with increasing prestressing of the bolts, the maximum stress at runaway decreases by up to 18%. However, the stress ratio markedly increases with increased prestressing, reaching unity at a prestress of $\sigma_0 = 1120\,kg/cm^2$. This proves the advantages of prestressing the bolts.

53. RUNNER-HUB BODY

The body of the runner hub is a part of intricate shape, large dimensions, and heavy weight, and forms the largest all-cast component of a turbine. Usually made of L30 steel, it is a hollow cylindrical thick-walled casting.

A cover with a boss for the inner pivots is provided on top of the body. Openings for fastening the runner blade pivots are provided in the hub body and the boss; their number depends on the number of blades. In small- and medium-size turbines, the hub is cast together with the servomotor cylinder, while in big turbines the cylinder is separate. Figure VIII. 57 shows two alternative types of hub-body designs: a — cast integral with the servomotor cylinder; b — with separate cylinder.

The design selected depends on the hub dimensions (d_h and L), which determine the transportability of the parts.

Dividing the hub into two parts simplifies casting but necessitates an additional bolted joint between hub body and cylinder which requires machining of the adjoining surfaces. Hence this design is, on the whole, more expensive.

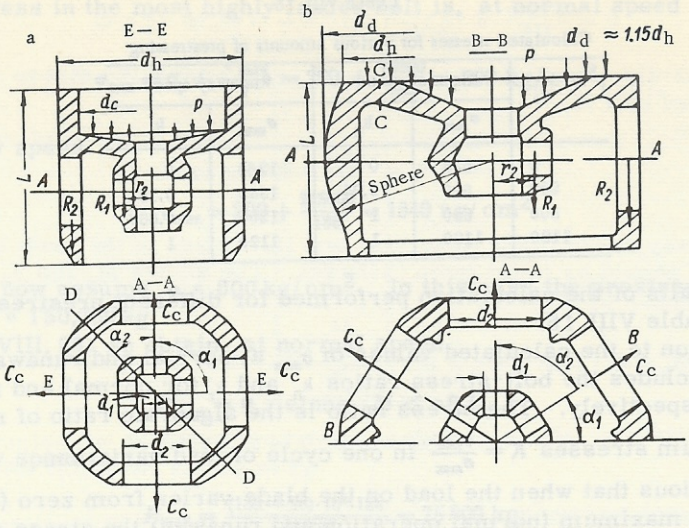


FIGURE VIII. 57. Runner-hub body:

a—with cast-in servomotor cylinder; b—with separate servomotor cylinder.

It is advisable to combine into a single part hub body and servomotor cylinder if this is practicable for casting and transport. For a runner of D_1 = 9.3 m, machining is reduced by 250 to 300 man hours for design "a" as compared with design "b"; this includes 100 to 120 hours turning on large lathes.

The contours of the hub body depend on the design of the runner hub, which may be made either cylindrical or spherical to locate the blades. A spherical hub offers better contact between the hub body and the blades with a maximum clearance of 2 to 5 mm that remains constant at all blade angles. With a cylindrical hub the clearance between the blades and the hub body should be determined with the blades fully open. As the blades rotate in the closing direction, the clearance increases appreciably, reaching a maximum when the blades are closed.

Because of the large clearances (up to several centimeters), water leakages increase considerably when the blades are near mid-position, lowering efficiency by up to 1%.

Consequently, the efficiency of a runner with cylindrical hub is lower than the efficiency of a runner with a spherical hub. However, since a spherical hub has, for equal values of d_h, a smaller discharge section, in the blade region the cavitation characteristics of the runner spherical hub are poorer than those of a runner with a cylindrical hub. The cavitation coefficient σ decreases by 3 to 6%.

The advantage of the spherical hub is an increased diameter at section A — A (Figure VIII. 57), which makes it easier to locate the blade-actuating mechanism and the removable seals.

The hub body being a complicated casting, care must be taken to provide adequate fillets, to maintain uniform section thicknesses as far as possible, and to avoid metal concentrations between the openings and the periphery.

For the latter purpose, hollow pockets are provided in the hub-body surface; these are closed later by welding on plates in order not to impair the streamlining of the hub. The pockets may also be used for attaching balancing weights.

Figure VIII. 58 shows the runner-hub body during machining.

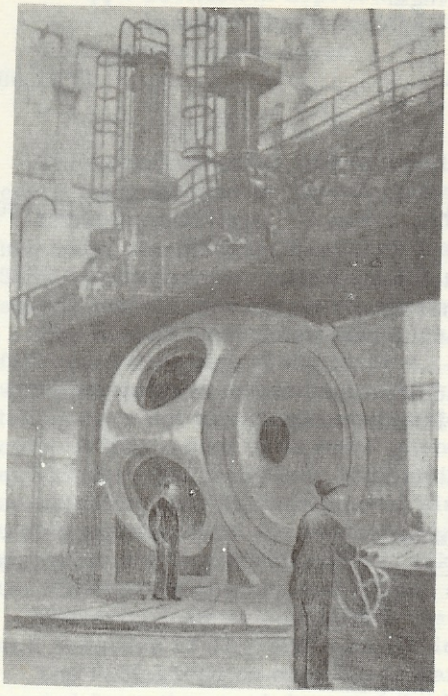


FIGURE VIII. 58. Machining the hub body on the lathe

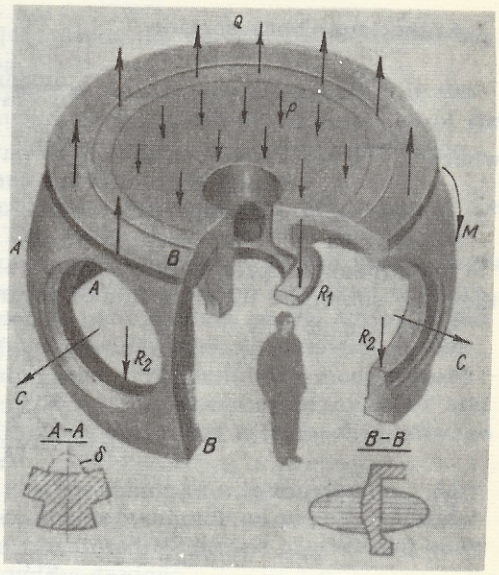


FIGURE VIII. 59. Forces acting on the hub body:

Q — load due to axial pressure and servomotor force; p — oil pressure in the servomotor; R_1, R_2 — loads from the blade pivots; C — centrifugal force; M — twisting moment.

Other hub-body forms are possible, depending upon the design of the blade-actuating mechanism.

Thus, in Figure V. 16, the runner-hub body is provided with a removable inner boss for the pivots, screwed to the hub.

Figure VIII. 10 shows a runner with a differential piston for blade adjustment. The cover of the hub body is located at the bottom.

Approximate calculation of the hub body. Calculation of the hub body is laborious because of its intricate shape and the complicated system of forces acting upon it (Figure VIII. 59). Loads caused by the axial water pressure and by the oil pressure in the servomotor cylinder, acting upon the hub body, are applied at its upper side, stressing the cover and the walls. The forces due to the pivot reactions are taken by the walls and the inner boss. In addition, centrifugal forces applied at the outer openings of the hub body act on it. Consequently, these forces also act on the walls between the openings of the body's outer surface.

The hub-body dimensions may be calculated approximately to resist tearing apart by the action of centrifugal forces, bearing reactions, and oil pressure, in the following manner:

Section A – A (Figure VIII. 57).

The stress at section A — A is determined by the action of the forces R_2, i.e., the pivot reactions on the bearings.

At the outer section

$$\sigma_1 = \frac{zR_2}{F_1}. \qquad \text{(VIII. 99)}$$

At the inner boss section

$$\sigma_2 = \frac{zR_1}{F_2}, \qquad \text{(VIII. 100)}$$

where F_1 = cross section of the outer body walls;

F_2 = cross section of the inner boss;

R_1 and R_2 = corresponding values of the reaction.

Sections E — E and D — D.

The stress at these sections may be determined on the assumption that they are subjected to the action of centrifugal forces.

Section E — E

$$\sigma_3 = \frac{\sum_{i=1}^{i=n} \frac{C}{2} \sin \alpha_1}{F_3}. \qquad \text{(VIII. 101)}$$

Section D — D

$$\sigma_4 = \frac{\sum_{i=1}^{i=n} \frac{C_\Gamma}{2} \cdot \sin \alpha_2}{F_4}. \qquad \text{(VIII. 102)}$$

where C = centrifugal force of the blade assembly at runaway speed;

F_3 = corresponding section at the plane E — E;

F_4 = corresponding section at the plane D — D.

Section C — C.

The stress at section C — C of the hub frame cover may be determined approximately as for a plate with the outer edge rigidly fixed, and subjected to uniform pressure and to a concentrated load at the center.

The stress due to uniform pressure is

$$\sigma_5' = \varphi_1 p \frac{R_c^2}{s^2}. \qquad \text{(VIII. 103)}$$

The stress due to the concentrated load is

$$\sigma_5'' = \varphi_2 \frac{zR_1}{s^2}, \qquad \text{(VIII. 104)}$$

where s = plate thickness;

R_c = radius to the built-in edge;

R_1 = reaction at the inner support;

z = number of blades;

p = oil pressure within the servomotor;

φ_1 = coefficient depending on the ratio $\frac{r_1}{R_c}$ (r_1 = radius of the central opening);

φ_2 = coefficient depending on the ratio $\frac{r_2}{R_1}$; (r_2 = radius of the circle to which the concentrated load is applied).

Total stress in the cover

$$\sigma_5 = \sigma_5' + \sigma_5''. \qquad \text{(VIII. 105)}$$

The actual stresses will be smaller, since the taper and the ribs of the cover were ignored in the calculation.

Experimental data. In order to find the real stress distribution in the hub body, the Machine Research Institute of the Academy of Sciences of the SSSR, in conjunction with the LMZ, carried out strain measurements on elastic models of a series of runner-hub bodies /75/.

The models were made of neoleucorite* and plexiglass, according to the full-scale drawings of the turbine. The scale of geometrical similarity was chosen so as to ensure ample space on the model to locate strain gages, taking care not to exceed practicable dimensions, of the blocks of neoleucorite. The model tests were intended to provide data on the action of the axial and radial loads (due to centrifugal forces), the oil pressure in the servomotor, and the servomotor piston load. The hub-body models were tested together with the adjacent parts, viz., the servomotor cylinder and the upper and lower hub covers, taking account of the relationship between the elasticities of parts and joints.

The axial load was applied to the hub by means of a lever device. Air at a pressure of 2 kg/cm^2 was led into the servomotor as pressure fluid.

The radial load on each blade was simulated by means of a weight suspended from the crank lever of the loading device.

An example of a loading device for producing the axial load is shown in Figure VIII. 60. The model to be tested (1) is mounted in reverse position and fastened to a shaft. The loading device is provided with a disk (7) fastened by means of a screw arrangement (6) to the cross beam (5). Rigid rods (4) (equal in number to the blades) serving as supports for the levers (3) (ratio 1:10) are fastened to disk (7). The shorter lever arm is connected by means of the shackles (8) and (10) and the dynamometric rod (9) to the profiled lever (12); this carries a pin (11) whose position corresponds to the blade center of pressure. The suspension (2) for the weights is attached to the longer arm of the lever (3). The dynamometric rod (9) made of 30KhGSA steel, having an elastic limit of about 80 kg/mm^2, to which a strain gage is glued, prevents misalignment and friction. The piston load on the inner side of the levers (12) is produced by a screw device (not shown in the figure) and acts in the same direction as the axial load. This load corresponds to a downward movement of the piston.

The stresses in the hub structure were measured at: the walls between the lateral hub openings (section A — A and section normal to it — Figure VIII. 59), the inner and outer sides of the opening contours, the bottom cover of the hub, the section of the central opening below the servomotor

* [A special plastic.]

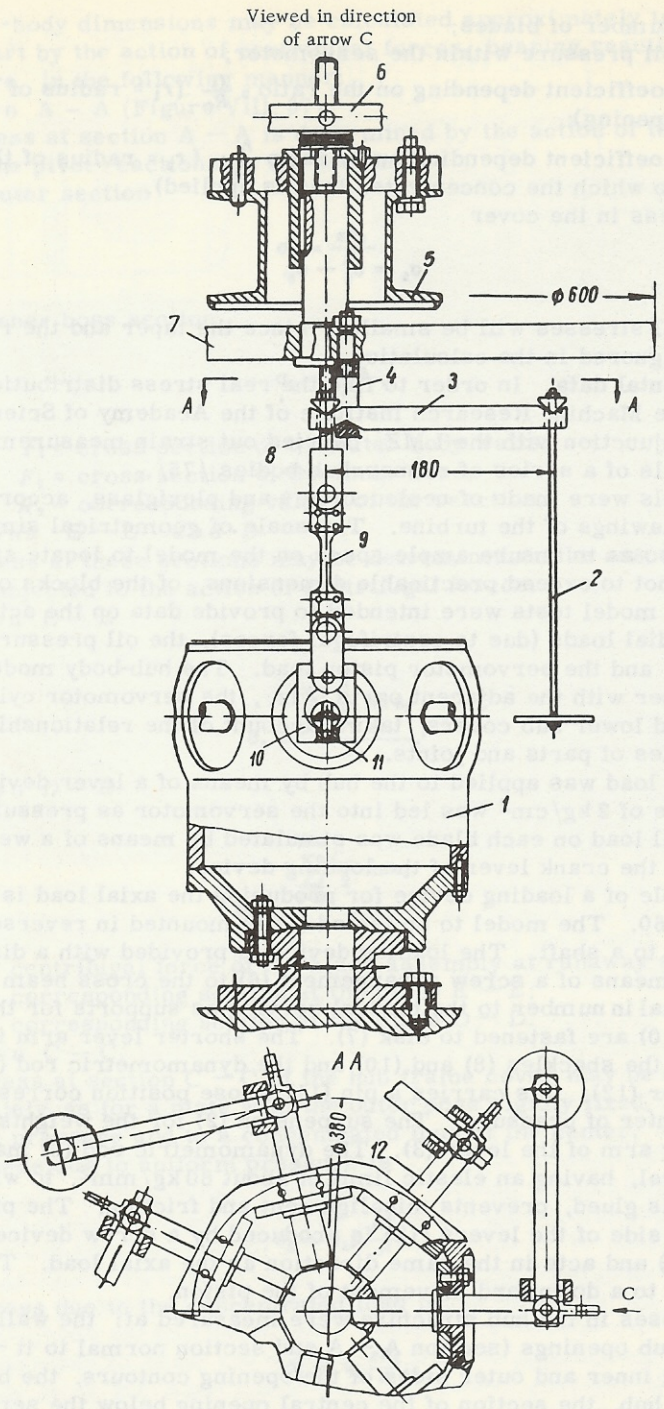


FIGURE VIII. 60. Loading device for testing the model of the runner-hub body under axial load

piston, and the servomotor cylinder cast integral with the hub body. It was found that, under axial and piston loads, the walls between the lateral openings are subjected to eccentrical tension, while the radial load causes mainly bending.

The most highly stressed wall region is located at mid-height.

At runaway speed the highest total stresses in the narrow wall section attain 800 to 1300 kg/cm^2 in various hub designs. At normal speed, the stresses are much lower (only one third to one fourth). The main component of the maximum total stresses is the stress due to the radial load of the runner. A typical diagram of the stresses in a longitudinal section through the walls between openings (section B — B) is shown in Figure VIII. 59. The inner rib of the wall (δ, section A — A) contributes to the leveling out of the highest stresses on the inside and outside surfaces of the wall by lowering the highest tensile stresses and increasing the compressive stresses. Maximum stresses occur on the edges of the openings at the extremities of the horizontal diameter, attaining 400 to 700 kg/cm^2. The stresses on the outside of the hub body are smaller than those on the inside.

At runaway speed, when the radial forces increase, the stresses at the lower points of the outline increase considerably, reaching 1000 to 1300 kg/cm^2. To reduce these stresses it is advisable to strengthen the lower hub band on the inside (Figure VIII. 59, section B — B).

The lower cover of the hub body was tested under the following loads: axial, radial, piston load (with piston in motion), and pressure inside the servomotor.

The stresses in the hub covers are smaller than those in the walls, and their distribution is like that in an annular plate with the inner edge fixed rigidly and the outer elastically. High stresses occur when the piston moves upward. The maximum stresses attain 600 to 850 kg/cm^2. Since ribs on the lower cover side lend considerable strength to the cover, they should always be provided. The stresses in the region of the central opening below the piston are small, not exceeding 300 kg/cm^2 at runaway speed.

The stresses on the lower side of the hub body along the contour adjoining the hub extension attain 400 to 700 kg/cm^2.

Stresses were also measured in hub bodies cast integral with the servomotor cylinder. The stresses in the cylinder depend on the direction of the piston stroke. When the piston moves upward, and oil pressure does not act on the cylinder, the stresses are considerably lower. The maximum stresses in the cylinder attain 500 to 800 kg/cm^2.

Tests were also carried out on hubs provided with blade-actuating mechanisms (actuators) without crossheads, where the drive from the piston is transmitted directly to the blade levers through openings in the bottom cover.

Cover deformations were measured, i.e., the displacement under the action of various loads of points on the edges of the cover openings for bushings. Hub bodies cast integral with the survomotor cylinder, as well as hubs without cylinders, were tested. It was found that under axial loads the displacements were almost the same in both cases, but under radial loads, with centrifugal forces acting, the deformations were markedly smaller in hubs cast integral with the survomotors. The deformations increase with speed and the highest overall deformations occur at runaway speeds, on the piston up-stroke. These tests determine the stiffness of the hub cover, and ensure that with the clearances chosen for the blade-operating

mechanism there is no metallic contact between the hub cover and the bushing for the servomotor piston rod. Clearances are usually chosen as small as possible to avoid excessive oil leakages into the runner hub. If there is danger of rod-bushing jamming, either the clearance or the stiffness of the hub body should be increased, for instance, at the expense of the cylinder-wall thickness. If the hub body is cast integral with a thick-walled servomotor cylinder, its rigidity increases considerably, and the elastic deformations of the hub cover are reduced.

These tests carried out on hub-body models in conjunction with the design of prototype turbines enables the most highly-stressed element of the assembly — the walls between the lateral openings — to be determined and the stresses in the other parts of the hub body to be found. Since the tests showed that stresses in many parts of the hub are very small, its cross-sectional area and weight could be reduced.

Exact calculation. On the basis of data provided by these tests, V. M. Malyshev and G. I. Kochnev (LMZ) devised an exact method of calculating the most highly stressed parts of the hub body, i. e., the walls between the lateral openings (section A — A, Figure VIII. 59) under the following loads:

1) oil pressure in servomotor cylinder;
2) axial load due to servomotor;
3) axial load due to water pressure on blades;
4) centrifugal forces.

The load diagram is shown in Figure VIII. 61. The method described below is more exact, since the transverse forces and the variation of the wall cross section were also taken into account.

In establishing the stress formulas, each load will be examined separately.

1. Oil pressure within servomotor cylinder. The walls between the lateral openings of the hub are considered as beams of nonuniform section, fastened with a ring at the bottom and a plate and a cylinder at the top. The bending moment M exerted upon the plate equals the sum of the bending moments exerted on the cylinder M_x and wall M_w.

Assuming that the plate is rigidly fixed at its inner and outer contours, the lower end being free to move but not to rotate (Figure VIII. 61, a), the bending moment M may be taken as being approximately equal to the moment at the built-in point of radius R.

The bending moment may be determined from the formula found by N. I. Prigorovskii /73/, for the stresses on the inner contour of a plate of this form.

$$\sigma_R = \frac{3p}{4s^2}\left[(R^2 - 3a^2) + \frac{4a^4}{R^2 - a^2}\ln\frac{R}{a}\right].$$

But since

$$\sigma = \frac{6M}{s^2},^*$$

the bending moment will be

$$M = \frac{P}{8}\left[(R^2 - 3a^2) + \frac{4a^4}{R^2 - a^2}\ln\frac{R}{a}\right], \qquad \text{(VIII. 106)}$$

* [This formula, as well as several of the following, is questionable from the point of view of dimensional analysis.]

where p = oil pressure in the cylinder;
R = mean radius of the cylinder wall;
a = radius to the inner edge of the cover.

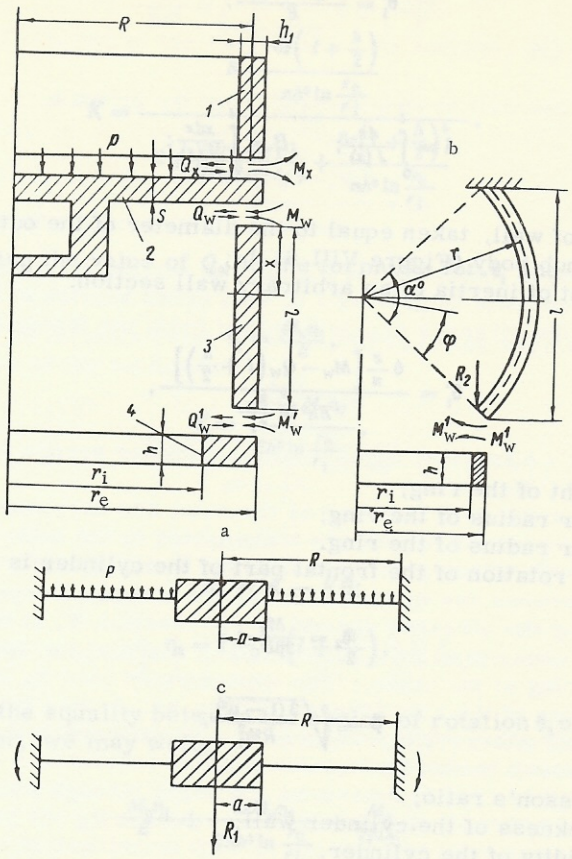


FIGURE VIII. 61. Schematic diagram for exact calculation of the hub-body stresses:

1 — cylinder wall; 2 — cylinder bottom; 3 — wall between openings; 4 — lower ring.

But

$$M = M_x + \frac{M_w z}{2\pi R}, \qquad \text{(VIII. 107)}$$

where z = number of blades.

M_x may be expressed in terms of M_w, because of the equality of the angles of rotation θ_1 of the wall and of the cylinder θ_2 ($\theta_1 = \theta_2$).

$$\theta_1 = \theta_1' + \theta_1'',$$

where θ_1 = total angle of rotation of the upper end of the wall;
θ_1' = angle of rotation of the wall;
θ_1'' = angle of rotation of the lower ring.

$$\theta_1' = \frac{M_w A - Q_w B}{E},$$

where

$$A = \int_0^l \frac{dx}{J(x)}; \qquad B = \int_0^l \frac{x dx}{J(x)};$$

l = length of wall, taken equal to the diameter of the outer openings of the hub body (Figure VIII. 61, b);
$J(x)$ = moment of inertia of an arbitrary wall section.

$$\theta_1'' = \frac{6\frac{z}{\pi}\left[M_w - Q_w\left(l + \frac{h}{2}\right)\right]}{Eh^3 \ln \frac{r_e}{r_i}},$$

where h = height of the ring;
r_e = outer radius of the ring;
r_i = inner radius of the ring.

The angle of rotation of the frontal part of the cylinder is /84/

$$\theta_2 = \frac{M_x}{2\beta D_c};$$

$$\beta = \sqrt[4]{\frac{3(1-\mu^2)}{R^2 h_1^2}},$$

where μ = Poisson's ratio;
h_1 = thickness of the cylinder wall;
D_c = rigidity of the cylinder.

$$D_c = \frac{Eh_1^3}{12(1-\mu^2)}.$$

The relationship between the moment M_w and the force Q_w may be found from the condition that the axial displacement of the point where the wall joins the plate must be equal to zero.

The resulting equation is

$$\frac{Q_w z (r_e + r_i)}{4\pi E h (r_e - r_i)} - \frac{6\frac{z}{\pi}\left[M_w - Q_w\left(l + \frac{h}{2}\right)\right]\left(l + \frac{h}{2}\right)}{Eh^3 \ln \frac{r_e}{r_i}} - \frac{M_w B}{E} + \frac{Q_w C}{E} = 0.$$

By determining Q_w from this equation, we obtain

$$Q_w = KM_w,$$

where

$$K = \frac{B + \dfrac{6z\left(l + \dfrac{h}{2}\right)}{\pi h^3 \ln \dfrac{r_e}{r_i}}}{C + \dfrac{z(r_e + r_i)}{4\pi h (r_e - r_i)} + \dfrac{6z\left(l + \dfrac{h}{2}\right)^2}{\pi h^3 \ln \dfrac{r_e}{r_i}}}.$$

By substituting the value of Q_w in the formulas for θ_1' and θ_1'', we obtain

$$\theta_1' = \frac{M_w \eta_1}{E},$$

$$\theta_1'' = \frac{6\dfrac{z}{\pi} M_w \eta_2}{Eh^3 \ln \dfrac{r_e}{r_i}}.$$

where

$$\eta_1 = A - KB;$$

$$\eta_2 = 1 - K\left(l + \frac{h}{2}\right).$$

Considering the equality between the angles of rotation θ_1 of the wall and θ_2 of the cylinder, we may write

$$\frac{M_w \eta_1}{E} + \frac{6z M_w \eta_2}{E\pi h^3 \ln \dfrac{r_e}{r_i}} = \frac{M_x}{2\beta D_c}. \qquad \text{(VIII. 108)}$$

M_x may be expressed in terms of M_w by using equation (VIII. 108)

$$M_x = M_w \frac{2\beta D_c}{E}\left(\eta_1 + \frac{6z\eta_2}{\pi h^3 \ln \dfrac{r_e}{r_i}}\right). \qquad \text{(VIII. 109)}$$

By jointly solving equations (VIII. 107) and (VIII. 109) we can find the bending moment acting on the wall

$$M_w = \frac{M}{\dfrac{2\beta D_c}{E}\left(\eta_1 + \dfrac{6z\eta_2}{\pi h^3 \ln \dfrac{r_e}{r_i}}\right) + \dfrac{z}{2\pi R}}. \qquad \text{(VIII. 110)}$$

By inserting the value of M from equation (VIII. 106) in equation (VIII. 110), we get

$$M_w = \frac{\frac{p}{8}\left[(R^2-3a^2)+\frac{4a^4}{R^2-a^2}\ln\frac{R}{a}\right]}{\frac{2\beta D_c}{E}\left(\eta_1+\frac{6z\eta_2}{\pi h^3 \ln\frac{r_e}{r_i}}\right)+\frac{z}{2\pi R}}. \qquad \text{(VIII. 111)}$$

The stress in the wall at $x=\frac{l}{2}$ is found from the formula

$$\sigma_1 = \frac{\left(M_w - Q_w\frac{l}{2}\right)y}{J}, \qquad \text{(VIII. 112)}$$

where J = moment of inertia of the wall cross section at $x=\frac{l}{2}$;
[y = distance from neutral axis of wall cross section at $x=\frac{l}{2}$].

At the LMZ, the stresses are determined from the formula

$$\sigma_1 = \frac{M_n y}{JK},$$

where K = 2 to 3 = empirical coefficient allowing for errors in the load diagram.

2. Stresses in the wall, induced by the axial and servomotor forces. The axial and servomotor forces are transmitted to the outer and inner hub bearings through the blade pivots. Reactions R_1 and R_2 occur at the bearings, and the stresses due to each of them are computed separately.

In determining the stresses caused by the reaction R_2 at the outer bearing, the wall is considered as a curved beam, fixed at the upper end and supported by a ring at the other. The concentrated load R_2 is applied at the mean diameter of the ring (Figure VIII. 61, b). In this figure r is the radius of wall curvature, which determines the distance from the centroid of the wall section to the turbine center line.

Mohr's method is used to determine the angle through which the end of the curved beam rotates under the force of reaction R_2.

$$\theta_1 = \frac{R_2 r^2}{E} D(\alpha), \qquad \text{(VIII. 113)}$$

where

$$D(\alpha) = \int_0^{\alpha} \frac{\left[\cos\frac{\alpha}{2}(\cos\varphi - 1) + \sin\frac{\alpha}{2}\sin\varphi\right] d\varphi}{J(\varphi)}.$$

The angle of rotation of the curved-beam end due to the moment M_w' is

$$\theta_2 = \frac{M_w' r}{E} F(\alpha), \qquad \text{(VIII. 114)}$$

where

$$F(\alpha) = \int_0^{\alpha} \frac{d\varphi}{J(\varphi)}.$$

The angle of rotation of the ring, due to the moment M_w'

$$\theta_3 = \frac{6M_w'z}{\pi E h^3 \ln \frac{r_e}{r_i}}. \qquad \text{(VIII. 115)}$$

The equation of combined deformations

$$\theta_1 - \theta_2 = \theta_3. \qquad \text{(VIII. 116)}$$

By inserting in formula (VIII. 116) the values of the angles θ_1, θ_2, and θ_3, we find the value of the moment M_w'

$$M_w' = \frac{R_2 r^2 D(\alpha)}{\frac{6z}{\pi h^3 \ln \frac{r_e}{r_i}} + rF(\alpha)}. \qquad \text{(VIII. 117)}$$

The stress in the section of the wall is determined by the formula

$$\sigma_2 = \frac{R_2}{F} + \frac{\left[M_w' - R_2 r\left(1 - \cos\frac{\alpha}{2}\right)\right] y}{J}, \qquad \text{(VIII. 118)}$$

where F and J are area and moment of inertia of the main wall section, respectively, [and y is measured from the neutral axis of the wall cross section].

In determining the stresses caused by reaction R_1 at the inner bearing, the load diagram is similar to that for the stresses due to pressure p (Figure VIII. 62, a), but the bending moment acts on the outer edge of the built-in plate encastré at both sides, and loaded by a concentrated force $R_1 z$ at the center (Figure VIII. 61, c).

The bending moment will be

$$M = \frac{R_1 z}{4\pi}\left[\ln\alpha\,(1+\mu) - \frac{\alpha^2 \ln\alpha}{\alpha^2 - 1}(1+\mu) + \frac{1-\mu}{\alpha^2} + 1\right],$$

where $\alpha = \frac{R}{a}$;

μ = Poisson's ratio.

This formula is obtained for the given problem from the general differential equation of thin circular plates /60/.

After transformations, the formula becomes

$$M = \frac{R_1 z}{4\pi}\left(1 - \frac{2\ln\alpha}{\alpha^2 - 1}\right). \qquad \text{(VIII. 119)}$$

The bending moment M_w is determined in a similar way as for pressure loads. The coefficient $K = 2$ to 3, as before.

The bending stress is determined by the formula

$$\sigma_3 = \frac{\left(M_w - Q_w \frac{l}{2}\right) y}{J}.$$

3. Determination of the stresses in the wall, due to the centrifugal forces. The wall is considered as a beam encastré at its ends with a uniformly distributed load

$$q = \frac{C}{l}.$$

where C = centrifugal force, due to the blade assembly (blade, pivot, etc.);
l = length of the wall (equal to the diameter of the outside opening).

Bending moment at the beam section

$$M_b = \frac{ql^2}{24}.$$

Bending stress

$$\sigma_4 = \frac{M_b y}{J}. \qquad \text{(VIII. 120)}$$

4. Total stress in the wall.

During downward motion of the piston

$$\sigma'_{tot} = \sigma_2 + \sigma_3 + \sigma_4. \qquad \text{(VIII. 121)}$$

During downward motion of the piston

$$\sigma''_{tot} = \sigma_1 + \sigma_2 + \sigma_3 + \sigma_4. \qquad \text{(VIII. 122)}$$

The stresses should be determined for the inside and outside of the wall.

5. Determination of the stresses in the bottom of the servomotor cylinder. The bottom of the cylinder is considered as an annular plate with the inner and outer edges rigidly fixed, the inner edge being capable of translatory motion but unable to rotate. The plate is subjected to uniform oil pressure, and to a load uniformly distributed along the inner contour (pivot reaction R_1).

The stress on the inner contour due to the pressure is given by /73/

$$\sigma_{1i} = -\frac{3p}{4s^2}\left[(R^2 + a^2) - \frac{4R^2a^2}{R^2 - a^2}\left(\ln \frac{R}{a}\right)\right]. \qquad \text{(VIII. 123)}$$

where s = bottom thickness.

On the outer contour

$$\sigma_{1e} = \frac{3p}{4s^2}\left[(R^2 - 3a^2) + \frac{4a^4}{R^2 - a^2}\left(\ln \frac{R}{a}\right)\right]. \qquad \text{(VIII. 124)}$$

The stress on the inner contour due to the reaction R_1 is given by

$$\sigma_{2i} = \frac{3zR_1}{2\pi s^2}\left[1 - \frac{2R^2}{R^2 - a^2}\left(\ln\frac{R}{a}\right)\right]. \qquad \text{(VIII. 125)}$$

where z = number of blades.

On the outer contour

$$\sigma_{2e} = \frac{3zR_1}{2\pi s^2}\left[1 - \frac{2a^2}{R^2 - a^2}\left(\ln\frac{R}{a}\right)\right]. \qquad \text{(VIII. 126)}$$

The total stress on the inner contour

$$\sigma_{tot,i} = \sigma_{1i} + \sigma_{2i}. \qquad \text{(VIII. 127)}$$

On the outer contour

$$\sigma_{tot,e} = \sigma_{1e} + \sigma_{2e}. \qquad \text{(VIII. 128)}$$

The stresses in the hubs of several actual turbines were calculated by this method, experimentally checked on models, and then recalculated according to actual conditions. The corresponding stresses are given in Table VIII. 16.

TABLE VIII. 16

Calculated and experimental stresses in the runner-hub bodies of several turbines in operation

Type of load	Stress notation	D_1 = 9.3		D_1 = 7.2		D_1 = 6.6	
		Calculated	Experimental	Calculated	Experimental	Calculated	Experimental
Axial	σ_e	−134	−177	− 31	− 41	−295	−277
	σ_i	759	520	600	573	+743	635
Servomotor force	σ_e	103	108	28	66	14	35
	σ_i	28	− 16	223	223	95	99
Pressure on cover	σ_e	100	125	35	56	63	79
	σ_i	− 85	−125	− 29	− 37	− 47	− 50
Centrifugal forces	σ_e	182	201	225	203	180	134
	σ_i	−154	−108	−194	−205	−133	−128

54. SERVOMOTOR CYLINDER AND COVER

Servomotor cylinder. A separate servomotor cylinder is used only in large turbines with runner diameters of 6 to 7 m or more.

The servomotor cylinder is usually cast of 30L steel, with two flanges (Figure VIII. 62). The lower flange is bolted to the hub; the cover of the servomotor cylinder is fastened with stud bolts to the upper flange.

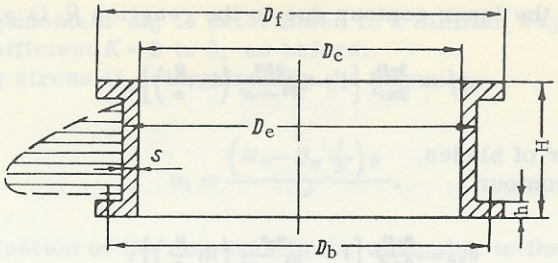


FIGURE VIII. 62. Cylinder of the runner servomotor

In designing the cylinder, its inner diameter D_c is calculated on the basis of the assumed servomotor performance. The wall thickness and flange dimensions D_f and h are then determined. The diameter of the stud bolts correspond to the thickness of the flange; the bolts should be located on as small a diameter as possible. The flange width $\left(\frac{D_f - D_e}{2}\right)$ is then small. Cylindrical radial pins are fitted between the flanges of the cylinder and of the adjoining parts in order to take up the tangential forces. The flange stud bolts are therefore under tension only. The pins are fixed in position by special shoulders. Special seals are provided between the cylinder flanges in order to prevent oil leakages out of the servomotor, and water penetration into it. Sealing is usually effected by a rubber ring laid into a groove in the flange joint; to ensure a reliable seal, groove and ring diameters must be exactly equal. Shapes and dimensions of the rubber ring are shown in Figure VIII. 63.

Calculation of the servomotor cylinder. The following forces and moments act on the servomotor cylinder:

1) axial water pressure;
2) axial force due to oil pressure in the cylinder;
3) axial load of the runner weight;
4) tangential force due to oil pressure in the cylinder;
5) twisting moment.

The axial loads induce tensile stresses in the cylinder wall

$$\sigma_{z1} = \frac{\left[P_{ax} + \frac{\pi}{4}\left(D_c^2 - d_{pr}^2\right) p + G_r\right]}{\frac{\pi}{4}\left(D_e^2 - D_c^2\right)} \qquad \text{(VIII. 129)}$$

where G_r = weight of the runner without servomotor-cylinder cover;
d_{pr} = diameter of piston rod;
p = oil pressure inside the cylinder.

The tangential stress in the cylinder walls due to the oil pressure is

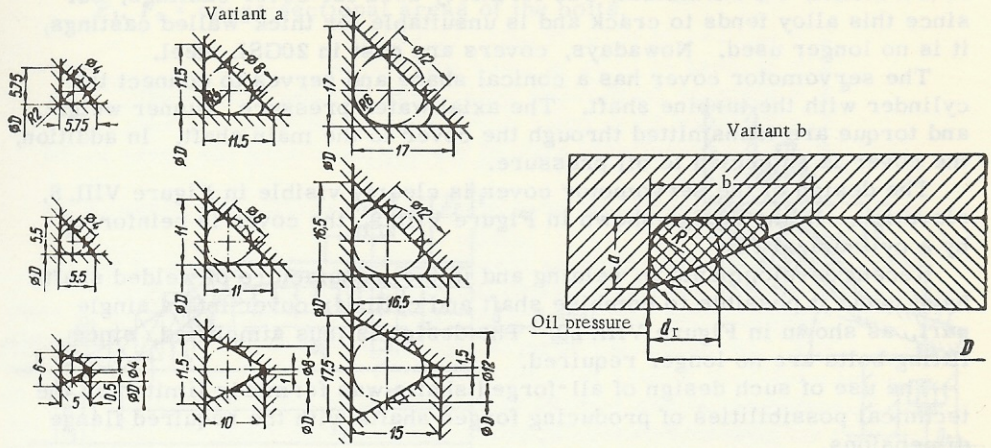
$$\sigma_{z2} = \frac{pD_c}{2s}. \qquad \text{(VIII. 130)}$$

This stress acts perpendicularly to σ_{z1}.

The total stress is

$$\sigma = \sqrt{\sigma_{z1}^2 + \sigma_{z2}^2} \qquad \text{(VIII. 131)}$$

The permissible breaking stress for 30L steel is up to 1000 kg/cm^2.



Diameter of ring	4	8	12
Diameter of groove circumference	Up to 200	From 200 to 500	From 500 to 1000

d_r	a	b	R	D
4	4	9	2	Up to 200
8	8	18	4	From 200 to 3000
12	12	27	6	Above 3000

FIGURE VIII. 63. Rubber-ring seal

The cylinder flanges sustain bending stresses, due to the bolts fastening them to the hub and to the servomotor cover.

The approximate value of the bending stresses in the flange may be determined by the formula

$$\sigma_b = \frac{\left[P_{ax} + \frac{\pi}{4}\left(D_c - d_{pr}^2\right) p + G_r\right]\left(D_b - D_e\right)}{\frac{\pi D_e h^2}{6}} \qquad \text{(VIII. 132)}$$

The maximum permissible bending stress is 1200 kg/cm^2. The radial, axial, and tangential stresses for thin web flanges can be found more accurately from (VI. 196), (VI. 197), and (VI. 198) /106/, since the thickness of the servomotor cylinders is usually less than the flange thickness.

Experimental investigations at the IMASh showed that in detachable servomotor cylinders, the maximum stresses occur at the lower cylinder flange. The stress diagram is shown in Figure VIII. 62. The highest total stresses were measured on the outside cylinder wall at the lower flange under normal operating conditions and with the piston moving downward, when axial forces due to the oil pressure in the servomotor are acting.

The values of these stresses were: axial 800 kg/cm^2, tangential kg/cm^2. At runaway speed, the stresses in the cylinder were slightly lower.

Cover of the servomotor cylinder. The cover of the servomotor cylinder is usually cast in high-strength carbon steel. A low-alloy chromium-nickel (2% nickel, 1% chromium) was formerly used for cover castings, but since this alloy tends to crack and is unsuitable for thick-walled castings, it is no longer used. Nowadays, covers are cast in 20GSL steel.

The servomotor cover has a conical shape and serves to connect the cylinder with the turbine shaft. The axial water pressure, runner weight, and torque are transmitted through the cover to the main shaft. In addition, the cover is subjected to oil pressure.

The design of the servomotor cover is clearly visible in Figure VIII. 8, elevation. In the design shown in Figure VIII. 9, the cover is reinforced by a cylindrical rib.

Recent developments in welding and in the manufacture of welded shafts have made it possible to combine shaft and cylinder cover into a single part, as shown in Figure VIII. 10. The design is thus simplified, since fitting bolts are no longer required.

The use of such design of all-forged shafts was formerly limited by the technical possibilities of producing forged shafts with the required flange dimensions.

The servomotor cylinder cover is secured to the cylinder with bolts and shear pins in a similar manner as the cylinder itself is secured to the hub body.

Stress calculation of the cover. The runner-cover* is considered as a circular ring of uniform cross section, subjected to a torque uniformly distributed along the ring.

The stresses in the cover may be found from formula (VI. 207)

$$\sigma = M_b \frac{y - \frac{m}{l}}{\left(n - \frac{m^2}{l}\right) r}. \qquad \text{(VIII. 133)}$$

The effect of the flange joints is ignored in this expression.

The flange joints securing the servomotor cover to the turbine shaft and cylinder strenghten the cover and lower the stresses in it. Exact calculation of the stresses in the flange joint is difficult. L. M. Kachanov /34/ suggested accounting for the effect of the flange joints on the basis of the following considerations:

After assembly, a pressure due to bolt prestressing acts between the contact surfaces of the flanges, ensuring a tight joint. When the load is applied to the cover, the conditions of contact between the flange surfaces alter. The pressure between them drops, but does not become zero. Since both the cover and the flange are massive parts, deformations at the joint mainly occur in the bolts.

If the cover is assumed to be a rigid body, each section of which rotates through the same angle, pressure increases temporarily. This is due to the additional tension exerted upon the bolt when the flange turns through the angle θ (Figure VIII. 64, b).

The additional strains $h_1\theta$ and $h_2\theta$, respectively, induce additional forces in the bolts:

* [Obvious misprint, should read servomotor cylinder cover.]

$$E\frac{h_1\theta F_1}{l_1}, \quad E\frac{h_2\theta F_2}{l_2},$$

where h_1, h_2 = shown in Figure 64, b;
l_1, l_2 = lengths of the bolts subjected to tensile stresses;
F_1, F_2 = cross-sectional areas of the bolts.

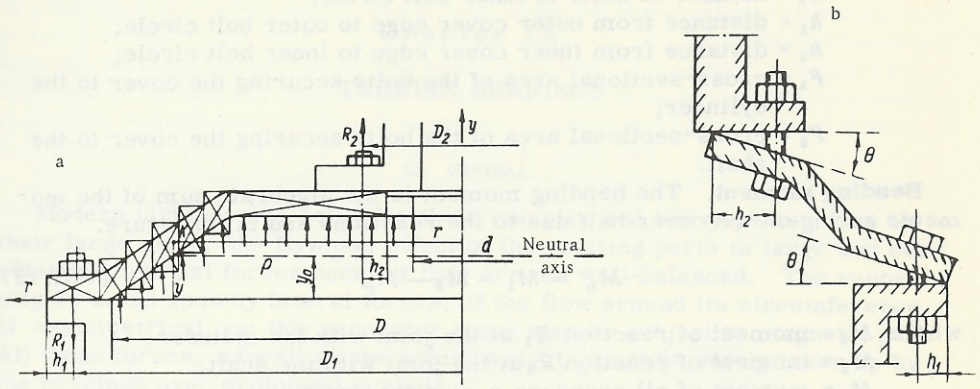


FIGURE VIII. 64. Forces acting upon the servomotor cover

The moments exerted on the cover by these forces are

$$\left.\begin{aligned}\frac{1}{2\pi}E\frac{h_1^2\theta F_1}{l_1}n_1,\\ \frac{1}{2\pi}E\frac{h_2^2\theta F_2}{l_2}n_2.\end{aligned}\right\} \qquad \text{(VIII. 134)}$$

These moments act in opposite directions to the bending moments exerted by the external loads. Consequently, the effect of the flange joints is to reduce the bending moment and the stresses in the cover.

By Hooke's law

$$\sigma = \frac{E\theta y}{r},$$

whence

$$E\theta = \sigma\frac{r}{y}. \qquad \text{(VIII. 135)}$$

By taking into account the approximate effect of the flange joints according to formulas (VIII. 134) and (VIII. 135), formula (VIII. 133) then becomes:

$$\sigma = \frac{M_b\left(y-\frac{m}{l}\right)}{r\left[\left(n-\frac{m^2}{l}\right)+\frac{1}{2\pi}\left(\frac{n_1F_1h_1^2}{l_1}+\frac{n_2F_2h_2^2}{l_2}\right)\right]}, \qquad \text{(VIII. 136)}$$

where y = coordinate of a point on the cover with respect to the adopted reference axis;

r = coordinate of the same point with respect to the axis of symmetry of the cover;

l, m, n = coefficients, functions of r and y, determined by formulas (VI. 209);

n_1 = number of bolts in outer bolt circle;

n_2 = number of bolts in inner bolt circle;

h_1 = distance from outer cover edge to outer bolt circle;

h_2 = distance from inner cover edge to inner bolt circle;

F_1 = cross-sectional area of the bolts securing the cover to the cylinder;

F_2 = cross-sectional area of the bolts securing the cover to the shaft.

Bending moment. The bending moment is the algebraic sum of the moments acting on the cover half due to the reactions and oil pressure.

$$M_b = M_1 - M_2 - M_p, \qquad \text{(VIII. 137)}$$

where M_1 = moment of reaction R_1 at the joint with the cylinder;

M_2 = moment of reaction R_2 at the joint with the shaft;

M_p = moment of oil pressure p upon the cover.

$$M_1 = \frac{R_1}{2} \cdot \frac{D_1}{\pi};$$

$$M_2 = \frac{R_2}{2} \cdot \frac{D_2}{\pi};$$

$$M_p = \frac{\pi (D^2 - d^2) p}{8} \cdot \frac{4}{3\pi} \cdot \frac{(R^3 - r^3)}{(R^2 - r^2)} = \frac{p}{12} (D^3 - d^3).$$

Consequently

$$M_b = \frac{1}{2\pi} (R_1 D_1 - R_2 D_2) - \frac{p}{12} (D^3 - d^3), \qquad \text{(VIII. 138)}$$

where

$$R_1 = G + P_{ax} + Q;$$

$$R_2 = R_1 - Q;$$

G = weight of runner without cover;

P_{ax} = axial water pressure;

Q = force due to oil pressure

$$Q = \frac{\pi}{4} (D^2 - d^2) p.$$

In LMZ practice, permissible stresses in the cover may attain 1000 to 1200 kg/cm^2.

Chapter IX

TURBINE BEARINGS

55. GENERAL

Modern turbines are noted for their massive and heavy parts. Due to their large mass, the flywheel effect of the rotating parts is large and considerable inertial forces occur if they are not well-balanced. The runner may be acted upon by lateral forces, if the flow around its circumference is asymmetrical, or the generator rotor may be subject to magnetic pull. All these forces, as well as the actual weight, must be safely taken up by the bearings over prolonged periods.

Since the turbine and generator essentially form one unit, sometimes even having a single common shaft, the supports of the shaft — guide and thrust bearings — must be designed and mounted with due consideration for the general layout of the power-house, hydro-unit design, and loads acting upon the generator rotor.

The main loads on the bearings in horizontal hydro units are the weight of the components acting perpendicularly to the shaft axis. The loads that act along the shaft are smaller in horizontal than in vertical units.

Axial loads are carried by the thrust bearing. The radial bearings of vertical units (mainly guide bearings) are subject only to accidental loads caused by the dynamical imbalance of the rotor, and by asymmetrical water flow.

The number of thrust bearings in horizontal hydro units, and of guide bearings in vertical units, depends on the design of the turbine and generator, and on the length of the shaft. Both guide and thrust bearings may be either plain or antifriction (ball or roller) bearings.

Oil- or water-lubricated plain bearings are mostly used in large turbines.

Oil-lubricated bearings are more generally in use, especially for horizontal hydro units. Water-lubricated bearings are used only as guide bearings in vertical turbines.

The guide bearings in large vertical turbines are of special design, which will be examined in detail further on.

In horizontal turbines, which are mostly of small size, axial bearings are similar to those used in general machine construction.

56. JOURNAL BEARINGS — A BRIEF SUMMARY

Oil-lubricated plain journal bearings for horizontal turbines differ mainly in their shells and lubrication systems. According to the mounting of

the shell, bearings may be classified into two basic types: rigid and self-aligning (spherical).

Rigid bearings are used when no appreciable deformation of the shaft or bearing housing is likely to occur.

Spherical self-aligning bearings permit their shell to assume various positions with respect to the housing, and to adjust themselves to variations in the shaft alignment.

Figure IX. 1 shows various types of oil-lubricated plain bearings for horizontal shafts.

Figure IX. 1, a shows a rigid bearing with ring lubricating. The oil ring is located in a groove in the upper shell and is supported freely on the shaft by which it is rotated, carrying oil from a receptacle beneath the shaft to the bearing surfaces. The ring is immersed in oil to a depth of about $\frac{1}{4}$ of its diameter. The volume of oil in the receptacle should be 1.0 to 1.5 times the volume of the journal. The following data are available on the required rate of oil supply /1/.

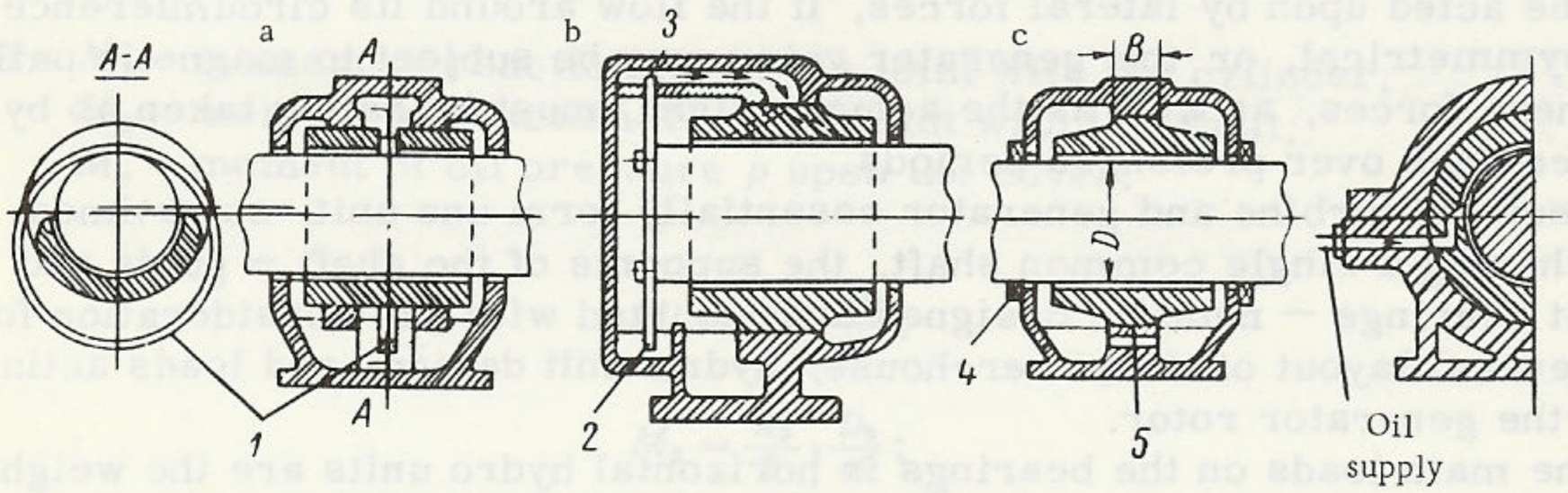


FIGURE IX. 1. Plain bearings for horizontal shafts

1 — oil ring; 2 — oil disk; 3 — scraper; 4 — seal; 5 — spherical seat.

An oil ring of 370 mm diameter, fitted to a journal of 225 mm diameter, and immersed to a depth of 50 mm, supplies oil at a temperature of 60°C at the rate of 1.2 liter/min at a speed of 500 rpm and 1.7 liter/min at 800 rpm; if the ring is immersed to a depth of only 25 mm, it supplies 1.0 liter min at 500 rpm, and 1.2 liter/min at 800 rpm.

The bearing shells are usually made from high-grade babbitt.

Tin-base B83 babbitt is usually used for lining radial thrust and axial bearings, and was formerly used also for turbine guide bearings.

Since tin is expensive and scarce, the B16 tin-lead-antimony alloy is used nowadays for turbine guide bearings.

The babbitts mentioned have the following composition and properties:

1) B83 babbitt: 83% Sn, 11% Sb, 6% Cu, specific weight 7.38, Brinell hardness at 17°C, $30H_B$, at 100°C, $13H_B$;

2) B16 babbitt: 16% Sn, 66.25% Pb, 16% Sb, 1.75% Cu, specific weight 9.29; Brinell hardness at 17°C, $30H_B$, at 100°C $13H_B$.

Figure IX. 1, b shows a bearing with disk lubrication. Oil is fed to the bearing by means of a ring or disk fastened to the shaft. The lower disk edge dips into the oil receptacle and rotation of the shaft causes the disk to carry some of the oil with it. A scraper is provided at the upper shell,

which causes the oil to flow by gravity to the surfaces. The amount of oil supplied is fixed experimentally; it increases markedly if the disk is immersed more deeply, or the rotational speed increased. The oil disk shown in Figure IX. 1,b is located on the journal end, but it may also be located in the middle of the bearing.

Figure IX. 1,c shows a bearing with pressure lubrication. A pump delivers oil to the bearing through a pipe. The oil is fed to the bearing surfaces either through a horizontal groove between the shells or through grooves in the lower shell. It is then collected in an oil receptacle in the bearing housing flowing from there into a cooler (if necessary) and back to the pump. Large turbines are provided with a filter between bearing and cooler to clean the oil. The oil pressure usually varies between 0.5 and 1.2 atm.

The shells of large bearings are provided with special grooves for water cooling. A spherical self-aligning bearing shell (5) is shown in Figure IX. 1,c. To avoid shattering of the load-carrying surface under repeated shocks, it is advisable to provide a spherical land of adequate width.

$$\left(\frac{B}{D} \geqslant 0{,}9\right).$$

The lubrication system for horizontal bearings is selected according to the circumferential velocity u and the specific bearing pressure.

$$p_0 = \frac{p}{dl}.$$

If $\sqrt{p_0 u^3} < 6$, grease lubrication may be used; no cooling is required.
If $\sqrt{p_0 u^3} = 6$ to 50, ring or disk lubrication is used, without cooling.
If $\sqrt{p_0 u^3} = 50$ to 100, ring or disk lubrication, with the oil cooled by water, or pressure lubrication may be used.
If $\sqrt{p_0 u^3} > 100$, pressure lubrication is used.

It should be kept in mind that for $u < 2.5$ m/sec and $u > 13$ m/sec, ring lubrication is not reliable.

The particular operating conditions must also be taken into account. If, for instance, there is no free access to the bearing for inspection of the lubricating system, it is advisable to use pressure lubrication, even if not required by the bearing load.

Journal bearings are designed for fluid friction which ensures minimum losses. To achieve minimum friction between two surfaces in relative motion, it is always necessary to interpose a lubricant layer between them.

The problem of fluid friction has been the subject of numerous researches since the basic propositions of the hydrodynamic theory of lubrication were first formulated by I. N. Petrov in 1883.

The basic equation of the theory of hydrodynamic lubrication is:

$$\frac{dp}{dh} = \frac{6\lambda u}{\theta} \cdot \frac{h - h_m}{h^3}, \qquad \text{(IX. 1)}$$

where λ = viscosity coefficient of oil, sec·kg/m^2.

The remaining notations are shown in Figure IX. 2,a. The equation defines the value of the load p_1, carried by a surface of length L and unit width:

$$p_1 = \frac{6\lambda u L^2}{h_1^2} T, \qquad \text{(IX. 2)}$$

where T = coefficient of lift.

Three basic cases may occur when two lubricated surfaces are in relative motion:

a) the moving surfaces are parallel to each other, and no pressure develops between them;

b) the surfaces are inclined to each other, and oil flows from the wide end of the clearance toward the narrow end: (the film is wedge-shaped). In this case, the surfaces may carry loads acting perpendicularly to the direction of motion;

c) the surfaces are inclined to each other, but the oil flows toward the wide end of the clearance. In this case the pressure in the lubricant film is negative.

In order to obtain fluid friction, the clearance between two sliding surfaces must be wedge-shaped. Oil of adequate viscosity, supplied continuously in the required amount, must fill the clearance.

For a given load and lubricant, fluid friction is only possible at relative velocities exceeding a certain minimum — the float-up velocity — of relative motion.

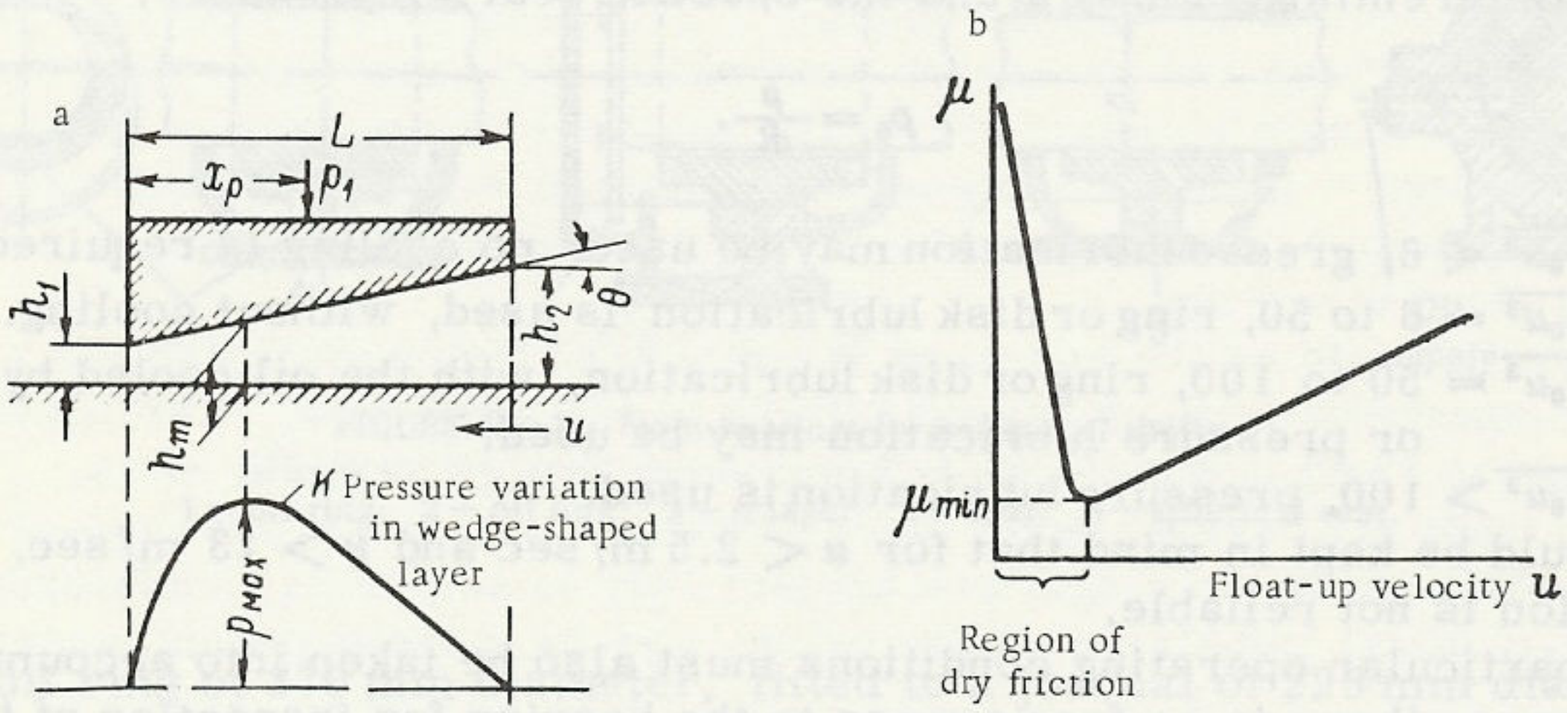


FIGURE IX. 2. Schematic hydrodynamic representation of lubrication:

a — pressure developed in wedge-shaped lubricant layer; b — friction coefficient for various velocities.

Figure IX. 2,b shows the variation of the friction coefficient with velocity for a given pressure. The friction coefficient passes through a minimum at a certain velocity which tests proved to be quite close to the float-up velocity. In practice, however, the bearings operate over long periods at velocities 2 to 3 times higher than the float-up velocity, although in this case the friction coefficient is higher.

In order to ensure fluid friction in horizontal journal bearings, a certain diametrical clearance δ between the journal and the bearing is required, depending upon rotational speed and oil viscosity. The proper selection of the smallest possible working clearance between journal and bearing is important for safe bearing operation. Figure IX. 3 shows the position of the journal both at rest and in motion.

At rest ($n = 0$), a wedge-shaped clearance is formed between the journal and the bearing (Figure IX. 3,a). On starting, when the journal speed is low, semidry or semiliquid friction develops. When the speed increases, the oil film develops oil pressure in the clearance, causing the journal to float up and become displaced in the direction of rotation (Figure IX. 3,b).

The pressure in the oil film varies directly with journal speed and oil viscosity. The greater their product, the larger must be the minimum clearance h_0.

In bearing design, the aim is to determine the conditions under which a load-carrying oil film may exist between journal and bearing. The relationship between the load-carrying capacity of the bearing and the clearances δ and h_0 is then found.

Without giving in detail the derivation of the formulas for determining these values, we merely state the formulas in final form as used in designing the bearings of electric machines.

The specific load on the bearing (acting on the unit area of the supporting surface of the shell is

$$p_m = \frac{p}{dl} = \frac{\lambda\omega}{2\psi^2 C_j}\Phi \text{ kg/m}^2, \qquad \text{(IX. 3)}$$

where $\psi = \frac{\delta}{d}$ = relative diametrical clearance;
Φ = load constant of the bearing;
$C_j = \frac{d+l}{2}$ = correction factor for oil side leakages.

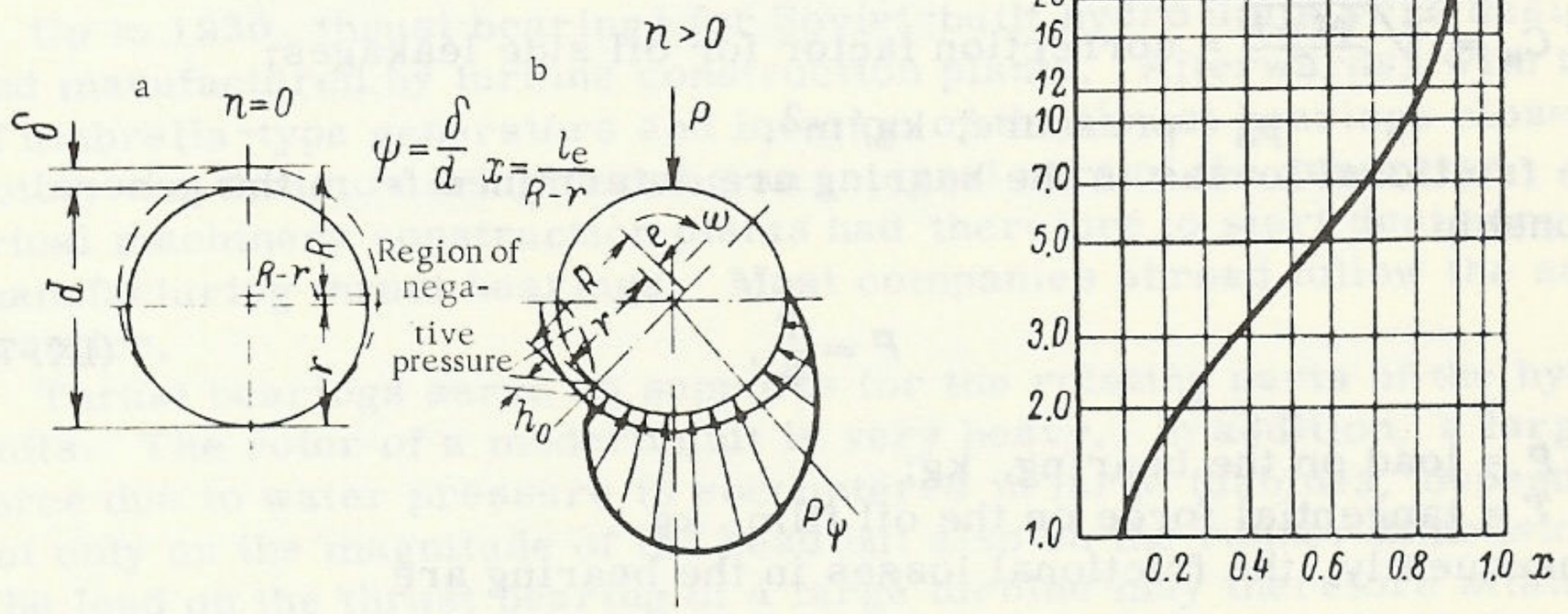


FIGURE IX. 3. Diagram for designing radial bearings

When designing a bearing, the journal diameter d and length l, pressure p, angular velocity ω, and oil viscosity λ are usually known. Consequently, the relative clearance may be determined from the formula (IX. 3)

$$\psi = \sqrt{\frac{\Phi\lambda\omega}{2C_j p_m}}.$$

The load constant of the bearing should be selected according to the relative eccentricity $x = \frac{e}{R-r}$ so as to ensure minimum frictional losses. It was found that optimum operating conditions may be expected for a relative eccentricity of x = 0.3 to 0.7. An eccentricity of about x = 0.5 should thus be adopted for split bearings to ensure a minimum friction coefficient.

The load constant is plotted in Figure IX. 3,c as a function of the relative eccentricity. With the relative clearance known, the diametrical clearance

$$\delta = \psi d \qquad \text{(IX. 4)}$$

and the minimum thickness of the oil film may be determined.

$$h_0 = R - r - e = (R-r)\left(1 - \frac{e}{R-r}\right) = \frac{\delta}{2}(1-x). \qquad \text{(IX. 5)}$$

The following minimum oil-film thickness is usual for bearings in large machines

Type of bearing	Operating characteristics	h_0, mm
Rigid	Long periods	0.2
Self-aligning	"	0.02
"	Short periods	0.002

Knowing h_0, we may select the type of bearing seat. The friction coefficient of the bearing may be calculated from the formula

$$\mu = \sqrt{2}\sqrt{\frac{\lambda\omega}{p_m}} \cdot C_\mu, \qquad \text{(IX. 6)}$$

where $C_\mu = \sqrt{\frac{\varphi d - l}{C}}$ = correction factor for oil side leakages;

p_m = pressure, kg/m^2.

The frictional losses in the bearing are determined from the general relationship

$$P = \frac{T}{\mu}, \qquad \text{(IX. 7)}$$

where P = load on the bearing, kg;

T = tangential force on the oil film, kg.

Consequently, the frictional losses in the bearing are

$$W = 9.81 P u \mu \text{ w}, \qquad \text{(IX. 8)}$$

where u = peripheral velocity of the journal, m/sec.

The oil flow through the bearing is determined from the condition that the outlet temperature of the oil should not exceed the permissible limit. The heat generated per second and removed by the oil is

$$W = Q\gamma C\theta, \qquad \text{(IX. 9)}$$

where γC = heat-absorption capacity of oil: on the average 1700 joule/liter;
θ = oil-temperature increase.

Consequently, the oil flow through the bearing is

$$Q = \frac{W}{1700\theta} \text{ l/sec.} \qquad \text{(IX. 10)}$$

For instance, with heat losses equivalent to 1 kw, and a temperature increase of 15° C, the required oil flow is about 2 — 5 liter/min.

The amount of oil that enters the wedge-shaped gap in the bearing is determined from formula

$$Q_i \approx 0.015\left(1 - \frac{x}{1.4}\right) nld^2\psi \text{ cm/sec,} \qquad \text{(IX. 11)}$$

where x and ψ = relative eccentricity and diametrical clearance, respectively;
n = speed, rpm;
l and d = journal length and diameter, respectively, cm.

The oil supply should be arranged so as to ensure oil flow to the inlet of the wedge-shaped gap in the quantity calculated by formula (IX. 11). It is not advisable to cut oil grooves in the loaded zone of the bearing, since openings or channels located in this region, where the pressure is highest, reduce the load-carrying capacity of the bearing.

57. THRUST BEARINGS FOR VERTICAL HYDRO UNITS — A BRIEF SUMMARY

Thrust bearings for vertical hydro units are usually located close to the generator rotor.

Up to 1930, thrust bearings for Soviet-built hydro units were designed and manufactured by turbine construction plants. Afterwards, with the use of umbrella-type generators and location of the thrust bearings close to the rotor, the thrust bearing became an integral part of the generator. Electrical machinery construction plants had therefore to start designing and manufacturing thrust bearings. Most companies abroad follow the same practice.

Thrust bearings serve as supports for the rotating parts of the hydro units. The rotor of a modern unit is very heavy. In addition, a large axial force due to water pressure is encountered in large turbines, depending not only on the magnitude of the head but also on the runner dimensions. The load on the thrust bearing of a large turbine may therefore attain large values. Thus, for instance, the axial load upon the record-size thrust bearings on the turbines manufactured by the "Elektrosila" plant imeni Kirov for the Volga imeni Lenin HEP attains 3000 t.

The thrust bearing in this type of machine is the most important stressed part involving complicated technical problems in design and manufacture. Three different thrust-bearing designs are shown in Figure IX. 4.

Figure IX. 4,a shows a thrust bearing used on low-power machines of small dimensions. The thrust bearing with its supporting disk is integral with the guide bearing (2). The disk supports the steel thrust collar (4)

fitted to the shaft (6) and secured to it by means of a key and nut (5). The thrust collar is also the journal of the guide bearing. The supporting ring is babbitted and fastened within the housing (3) which serves also as an oil bath. The oil receptacle (1) is attached to the housing from beneath. The oil to form the film between the supporting disk and the thrust collar is supplied through radial grooves cut into the babbitted supporting disk and chamfered at the edges. Oil circulation is ensured by the suction due to the centrifugal force acting when the thrust collar (4) rotates.

Designs of thrust bearings for large hydro units are shown in Figure IX. 4,b and c. The wedge-shaped load-carrying oil film is formed by means of self-aligning shoes. In variant (b), the self-aligning shoes (8) rotate, while in variant (c), the shoes (7) are stationary.

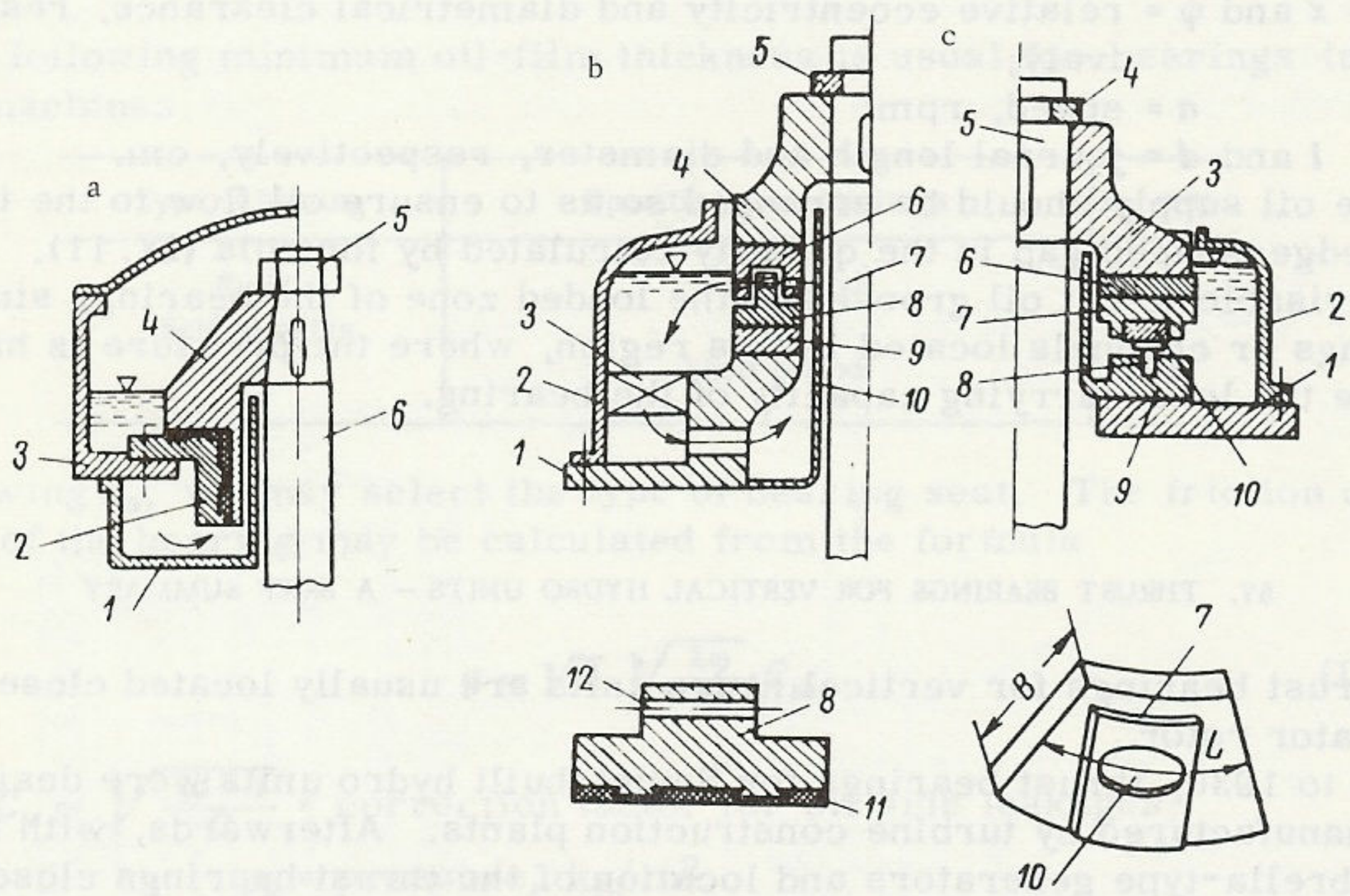


FIGURE IX. 4. Designs of thrust bearings for vertical hydro units

In self-aligning thrust bearings the proper selection of the support point of the shoe with respect to the center of load application is of great importance. The center of load application should be displaced in a direction opposite to the movement of the shoe about its supporting point (the center of gravity). The shoes can thus tilt, permitting the formation of an oil film.

The thrust bearing with a ring of moving shoes (Figure IX. 4,b) consists of the thrust collar (4), attached to the shaft (7) and secured to it by means of the locking ring (5). A steel ring (6) is fastened to the thrust collar from below; the ring is provided with seats and pivots (12) for fitting cast-iron shoes (8). The annular springs arranged between the ring (6) and the shoes, impart to the shoes inclinations varying with the load. The shoe surfaces are lined with babbitt (11). The shoes slide on a base ring (9) made of pearlitic malleable cast iron and fixed to the housing (1). The casings (2) and (10), fastened to the housing (1) form the oil receptacle of the thrust bearing. Lubricating oil is circulated by the pumping action of the rotating

shoes; oil cooler (3) may also be provided. Thrust bearings of this type, but with two rows of shoes (inner and outer), are used on the large hydro units of the Uglich and Rybinsk HEPs.

Thrust bearings with rotating shoes are convenient for turbines operating at very low speeds, since even at low speeds the suction of the rotating shoes provides enough oil for lubrication.

Figure IX. 4,c shows a thrust-bearing design with stationary cast-iron babbitted shoes (7). The steel ring (10) supported by the head of bolt (8) is located in a circular groove machined into the stationary shoe. The bolts are fixed in ring (9) mounted on frame (1). Steel ring (6), attached to thrust collar (3) which is secured to shaft (5) by means of lock ring (4), slides on the shoes. Casing (2) is fastened to the housing. A forced-feed oil circulating system may be used if the receptacle comprises an oil-cooling arrangement. Usually, six to twelve shoes are fitted in the thrust bearing, the shoe length-to-width ratio $\frac{L}{B} \approx 1$.

Thrust bearings with self-aligning stationary shoes are simpler in design, more easily manufactured and more readily aligned than those with rotating shoes. Sometimes, the thrust bearing is made integral with the guide bearing, the thrust collar serving as journal.

The design of a thrust bearing, when load P and speed n are given, is carried out in the following steps:

1) selection of the bearing pressure within the limits $p = 20$ to 40 kg/cm^2.

The bearing pressure adopted nowadays for large hydro units with very high axial loads, $p = 60$ kg/cm^2;

2) selection of the number of shoes z, the diameter of their inner circle of location D_i, the shoe-length-to-width ratio $\frac{L}{B} \approx 1$ and the clearance between the shoes (between 10 and 15% of the circumference);

3) computation of the diameter D_e of the circle of location of the outer shoes from the formula

$$D_i = \sqrt{D_e^2 + \frac{4P}{\pi p k}}, \qquad \text{(IX. 12)}$$

where k = 0.85 to 0.9 = coefficient depending on the clearance between the shoes;

4) determination of the mean peripheral velocity

$$u = \pi \frac{D_e + D_i}{2} \cdot \frac{n}{60}; \qquad \text{(IX. 13)}$$

5) determination of the load acting on unit width of the shoe

$$p_1 = \frac{P}{zB} \text{ kg/cm}; \qquad \text{(IX. 14)}$$

6) determination of the coefficient of friction by the formula known from the theory of two-dimensional oil flow

$$\mu = \left(\frac{\lambda u}{100 p_1}\right)^{1/2} H, \qquad \text{(IX. 15)}$$

where λ = oil viscosity;

H = coefficient of tangential force, depending on the ratios $\frac{L}{B}$ and $\frac{h_2}{h_1}$ and characterizing the inclination of the shoe; (h_1 = oil-film thickness at the trailing edge; h_2 = oil-film thickness at the leading edge);

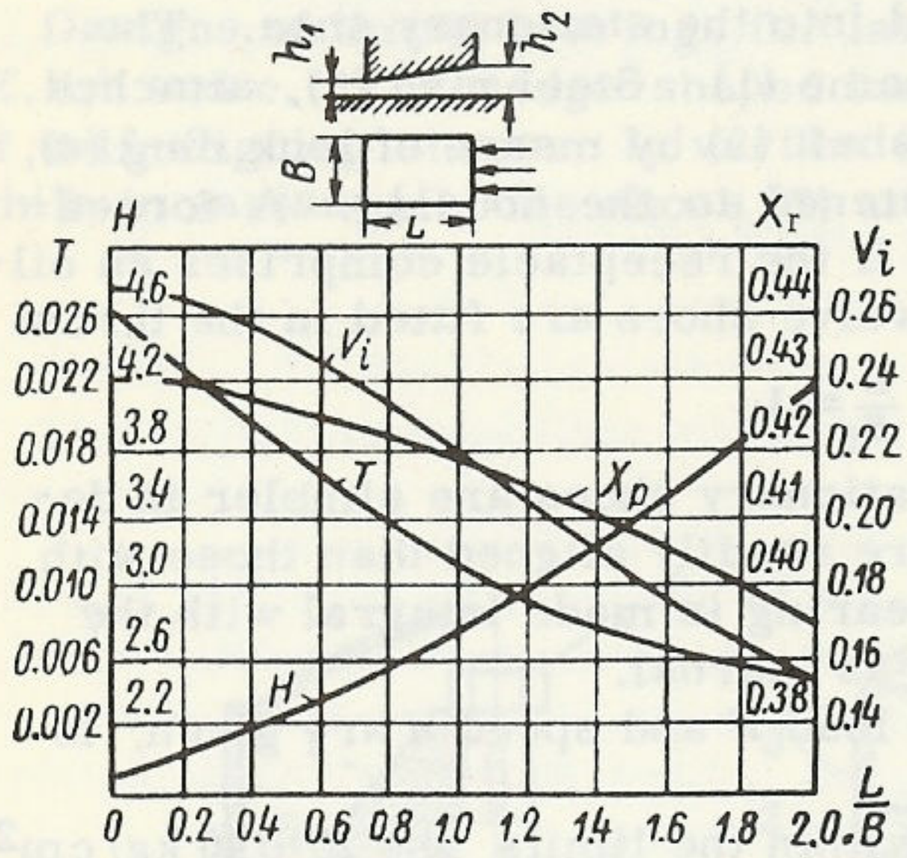


FIGURE IX. 5. Computation parameters for thrust bearings with $\frac{h_2}{h_1} = 2$

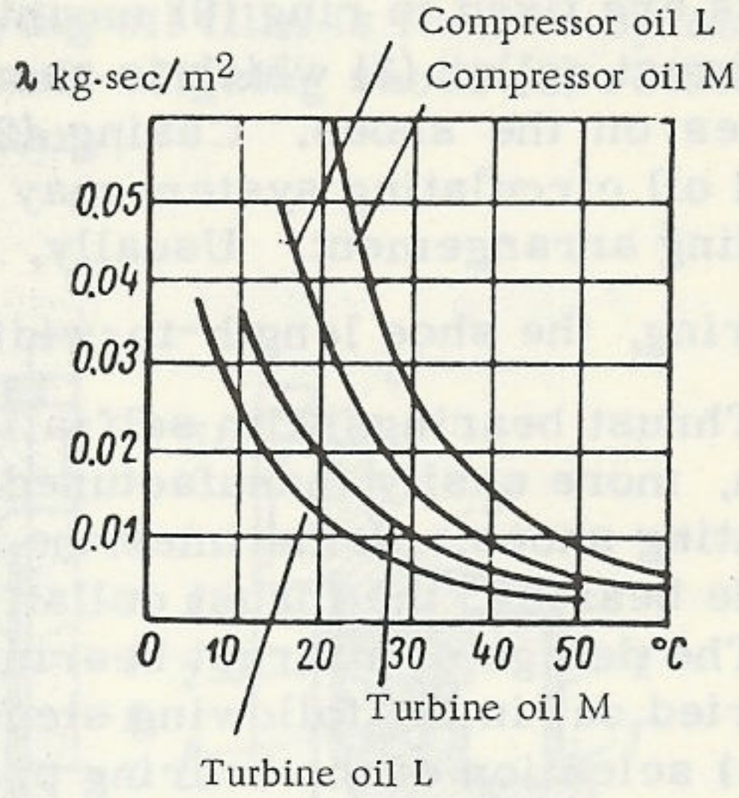


FIGURE IX. 6. Temperature dependence of oil viscosity

7) calculation, by formula (IX.8), of power losses due to friction for all shoes

$$W = 9.81\,Pu\mu \text{ w};$$

8) determination (for all shoes) of lubricant flow at the leading edge by the formula

$$Q = z \cdot 100 \cdot uLBV_i \left(\frac{\lambda u}{100 p_1}\right)^{1/2} \text{ cm}^3/\text{sec}, \qquad \text{(IX. 16)}$$

where V_i = coefficient of lubricant discharge;

9) determination of the temperature increase in the lubricant by formula (IX. 9)

$$\theta = \frac{W}{\gamma C Q};$$

10) determination of the oil-film thickness at the trailing edge of the shoe by formula (IX. 2)

$$h_1 = L\sqrt{6T\frac{\lambda u}{100 p_1}} \text{ mm},$$

where T = coefficient of lift h_1 should be greater than h_{min}.

The following safe values are permissible for thrust bearings with self-aligning shoes:

cast-iron shoes, $h_{min} = 0.05$ mm;

babbitted shoes, $h_{min} = 0.03$ mm;

11) computation of the distance on the mean circumference from the point of application of the resultant pressure to the trailing edge, by the formula

$$x_p = X_r L \text{ mm} \qquad \text{(IX. 17)}$$

[the mean circumference is defined as the circle whose diameter is $\frac{D_e + D_i}{2}$].

Figure IX. 5 shows the computation parameters for a thrust bearing $\frac{h_2}{h_1} = 2$ as a function of $\frac{L}{B}$ where H = coefficient of tangential force; X_r = coefficient of relative distance from the point of application of the resultant pressure to the trailing edge (data from the Elektrosila plant).

Figure IX. 6 shows the temperature dependence of the viscosity of various lubricants.

58. OIL-LUBRICATED TURBINE GUIDE BEARINGS

The guide bearings of vertical turbines have to carry the main shaft in a perfectly vertical position and take up the radial forces liable to arise during operation.

Figure IX. 7 shows two alternatives of oil-lubricated bearings, formerly in common use.

Figure IX. 7,a shows schematically an oil-lubricated bearing.

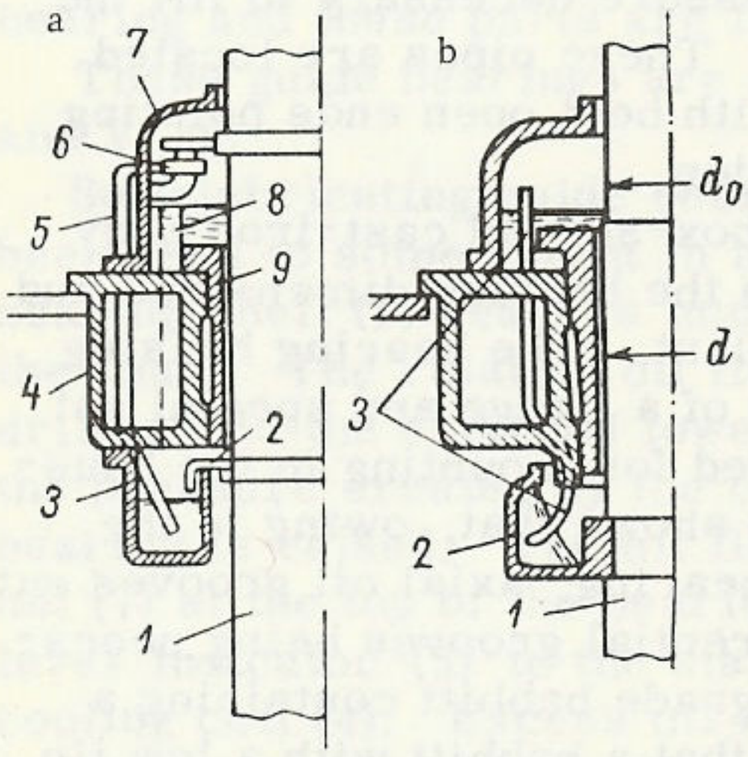


FIGURE IX. 7. Oil-lubricated turbine guide bearings

The removable babbitted shell (9) is fastened to housing (4). The upper oil receptacle (7) is mounted on the housing; the lower receptacle (3) is fastened to it from below. In the upper receptacle, the oil is kept at a predetermined level by means of the overflow pipe (8) and a float (not shown in the figure). The oil flows through the bearing grooves into the lower receptacle. To ensure better drainage, an oil-deflector ring (2) is provided on the shaft. The oil is returned from the lower receptacle through pipe (5) by pump (6), usually driven from the main shaft (1) through a gear or friction drive. A friction drive is preferable, since it enables switching the pump on or off while the turbine is running. The actuating force required for the frictional drive is provided by a spring, in which case the gear pump is mounted on a bracket attached to the upper receptacle. The guide bearings of large turbines are usually provided with an electrically driven stand-by pump, which is started when the normal oil

circulation is interrupted, and the oil level in the upper receptacle drops below the permissible limit. The pump motor is started by a floating device provided with electrical contacts in the upper receptacle. This standby pump is also switched on immediately before the turbine is started to pump the oil from the lower into the upper receptacle, filling the latter to normal level. During turbine shut-down the oil leaks through the bearing back into the lower receptacle.

For bearing lubrication, oil of the same grade as for the governor system (*L* turbine oil) is used.

For cleaning the oil when the turbine is running, a filter is usually employed, formed by the bearing housing and shell with a filtering screen which is periodically cleaned. The filter should be cleaned more frequently during the early stages of turbine operation than is necessary later, since the oil is more likely to contain impurities when the turbine is restarted after repairs or inspection than during normal operation.

For guide bearings operating at elevated temperatures (e.g., in hot climates), cooling coils are provided in the upper receptacle, cooling water being supplied from the industrial water main.

The lubricating oil should be cooled only in exceptional cases, since cooling introduces complications and sometimes leads to emergency shutdowns due to the presence of water in the lubricating oil.

To check bearing operation, the temperature of the babbitt lining is measured by means of a resistance thermometer; a thermal relay gives a signal when the temperature reaches a predetermined value. Bearings with lower stationary receptacle are used in high-speed turbines. For low- and medium-speed turbines it is preferable to attach the lower receptacle to the main shaft, as shown in Figure IX. 7,b, in which case the receptacle rotates together with shaft (1). A rotating receptacle (2) is more advantageous because the rotary motion gives rise to the pressure necessary to lift the oil through pipes (3) into the upper receptacle. These pipes are located within the lower receptacle and are provided with bent open ends pointing in a direction opposite to that of the shaft rotation.

Bearing housing. The housing is usually a box-shaped cast-iron body made from segments whose number depends on the bearing dimensions and the production facilities of the manufacturing plant. The bearing housing is fastened to the turbine cover-plate by means of a flange and special set screws. The babbitted cast-iron shell is flanged for mounting in the housing. Operating experience with guide bearings shows that, owing to the eccentricity of the journal with respect to the bearing, axial oil grooves cut into the shell are quite sufficient, no circumferential grooves being necessary. Formerly, shells were lined with high-grade babbitt containing a high percentage of tin (B83), but it was found that a babbitt with a low tin content (B16) may be used instead.

Special dovetail indentations should be cut into the cast-iron shell to secure the babbitt lining. The seats provided in the housing for the shell may be either conical or cylindrical, both alternatives having advantages as well as drawbacks. The advantages of the conical seat consist in the ease of assembly and dismantling, in the fact that no special care is needed in machining to obtain precise diametral dimensions, and in the relatively simple manner of adjusting the bearing diameter by raising or lowering the bearing with the aid of shims. These shims are usually 0.5 to 1.5 mm thick.

The disadvantages of this type of mounting are the complicated manufacture, the need for manual polishing (lapping) of large surfaces, and the inadmissibility of clearances in the joint.

Cylindrical shells are usually mounted on two to four cylindrical collars, the number depending on the bearing dimensions. The shell collars should preferably be machined according to the dimensions of the housing; tolerances may be less strict if machining is done in this way.

In modern practice the length of the babbitt lining does not exceed the shaft diameter.

$$l = (1.0 - 0.8)\, d.$$

The clearances between shaft and babbitt lining according to the shaft diameter are shown in Table IX. 1, which gives the current practice for operating turbines.

TABLE IX.1

Clearances for babbitted bearings according to the shaft diameter

Shaft diameter, mm	Clearance, mm	Shaft diameter, mm	Clearance, mm
80—120	0.08—0.19	500— 630	0.2 —0.31
120—180	0.1 —0.16	630— 800	0.23—0.35
180—260	0.12—0.18	800—1000	0.26—0.41
260—360	0.14—0.21	1000—1250	0.29—0.45
360—500	0.17—0.25	1250—1600	0.32—0.52

The upper and lower receptacles are made, depending on the bearing dimensions, of two or four parts bolted together. The joints between the bearing and these parts are fitted with gaskets to prevent oil leakages.

These guide bearings are shown schematically in Figures V. 5, V. 11, and V. 16.

Self-lubricating guide bearings. Self-lubricating guide bearings have been used to some extent in turbines (Figure IX. 8). The lower edge of the bearing shell (1) reaches into the oil receptacle (2) rotating together with the shaft. The rotating oil flows through a number of straight channels (3), drilled into the enlarged lower part of the bearing to the shaft, impelled by the pressure created by the centrifugal forces. Thus, the oil level in the bearing is raised. The oil flows along helical grooves to the annular channel (7) at the top of the bearing shell; from there it flows through the oil-level indicator (5) to the stationary oil receptacle (6), which contains a cooling coil (4). Excess oil flows through a pipe (not shown in the figure) back into the receptacle (2).

Figure IX. 9 shows a self-lubricating guide bearing of the oil-bath type used in hydroelectric generators. The shell (2) is immersed in the oil bath down to one third or one fourth of its height. The rotation of the shaft causes oil to flow into special grooves cut into the babbitt lining and spread over the bearing faces. The intermediate sleeve mounted on the shaft is a disadvantage of this design. To prevent the oil losses, a cylindrical shield forming the inner wall of the receptacle should be provided. This complicates the design of the intermediate sleeve.

Grease-lubricated guide bearings. Owing to their simple design, guide bearings with grease lubrication have been extensively used of late in turbines constructed abroad (Figure IX. 10).

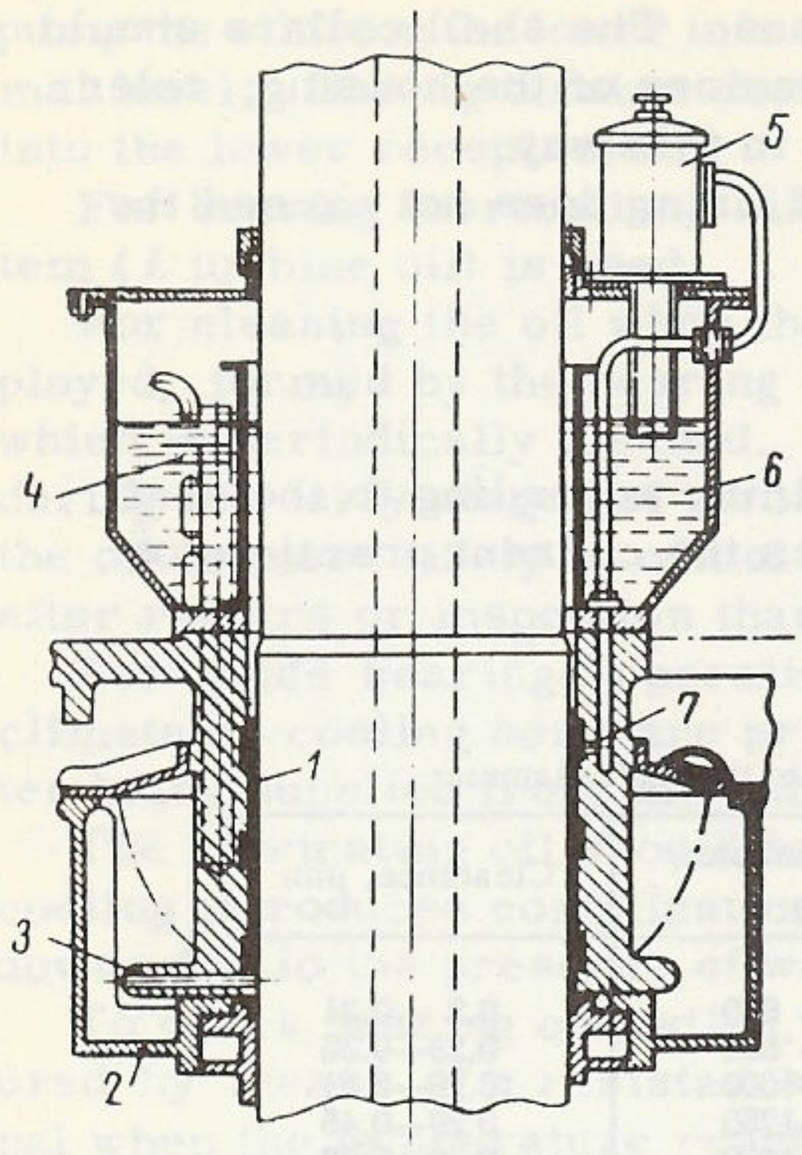


FIGURE IX.8. Self-lubricating guide bearing (built by "Nohab")

The babbitted shell (2) is sealed at top and bottom by labyrinth-type seals(3). The water container (4) and seal (5) are mounted on top of the shell. The container is supplied with water for lubricating and cooling the seal.

The oil is supplied to the bearing surface through pipe (1) to eight points on the circumference at mid-height.

The oil flows toward the lower and upper parts of the bearing. The oil supply system includes a pump, usually of the piston type, valves, and pipes. Used oil is carried off by the water and a continuous oil supply is therefore required. This causes some oil contamination by water. Oil consumption depends on the bearing dimensions; it may attain several kilograms per day. If grease is used as lubricant, separate cooling of the bearing must be provided, since grease does not carry away the heat generated fast enough. The cooling medium is usually water, supplied through the pipe (6) from the turbine scroll case and flowing across the bearing housing.

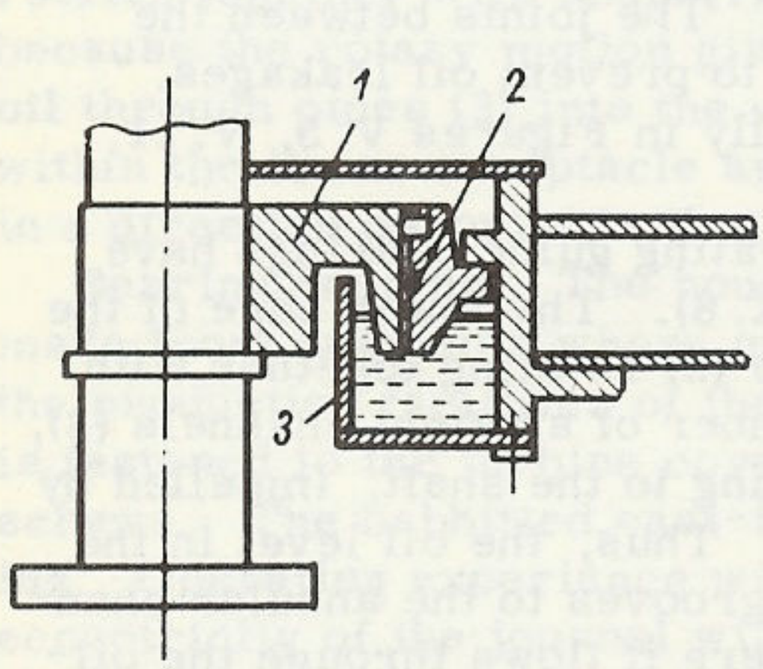


FIGURE IX.9. Self-lubricating guide bearing

The drawback of oil-lubricated bearings is that they require special seals. The guide bearing is located on the shaft close to the turbine water passages through which a large amount of water, often under high pressure, flows continuously. Special seals must be provided to prevent water from penetrating into the lubricating system, both when the turbine is running and when it is at rest. Apart from this, the seals prevent water from entering the turbine. The plant operators must constantly check the seals and the lubricating system; if water penetrates into the lubricating system, the oil must be changed. Water may leak into the bearing and into the turbine while at rest if the tailwater level is at a higher elevation than the bearing. Modern runners, having increasingly high specific speeds, involve the use of negative draft heads, in which case the bearing is practically always immersed. The seal between the runner and the bearing requires adequate space; runner overhang is thus increased, lowering the rigidity of the whole unit, and impairing its operational characteristics. Grease-lubricated bearings are

more convenient in this respect; they require no lower receptacle and have a grease container with smaller axial dimensions, and permit a shorter unsupported shaft length.

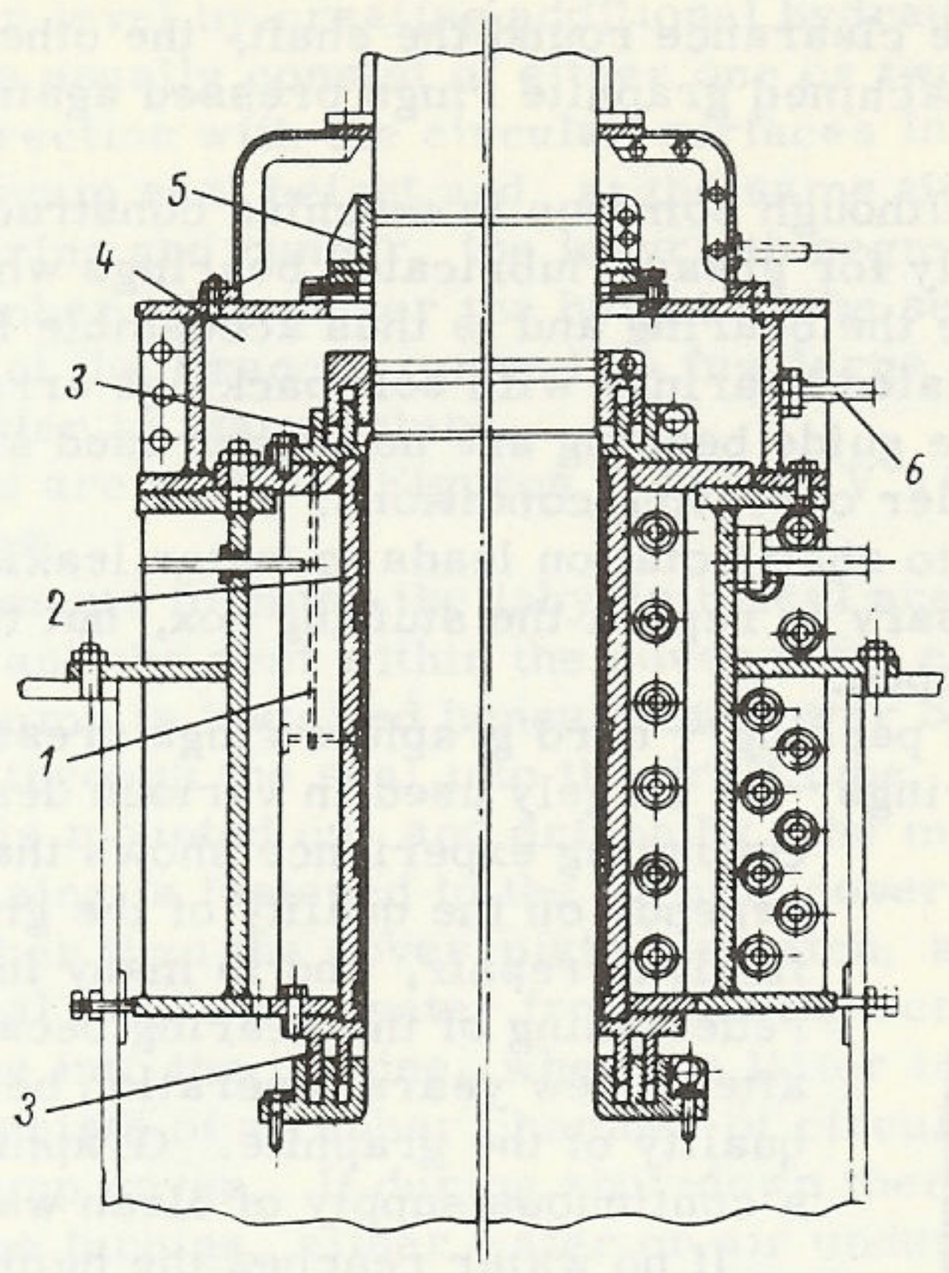


FIGURE IX.10. Grease-lubricated bearing

Most existing turbines with babbitted bearings have oil lubrication; grease lubrication has only recently been introduced (Figure V.15).

Babbitted guide bearings may last for from 5 to 8 years without relining. Some bearings have been in operation for twenty years without the linings being renewed, and without showing significant alteration in the clearances. The performance of bearings lined with B83 babbitt is higher than that of bearings with B16. On one particular turbine operating under unstable conditions with runner vibration, the bearings were relined with B16 babbitt — thereupon shaft play increased from 0.3 to 2 mm in two months. A fresh relining with B83 babbitt practically stopped play increase (in one year it increased from 0.3 to 0.4 mm only).

Oil contamination by water leads to accelerated shaft corrosion and rapid wear of babbitt and shaft. Oil-lubricated bearings should therefore have reliable seals and means for water drainage from the turbine cover-plate.

Grease-lubricated bearings have operated satisfactorily for three years in a hydroelectric plant without significant alterations in the linings. Oil consumption in a 700 mm-diameter bearing may reach 3 liters per 24 hours.

Stuffing box. Stuffing boxes are used between the stationary turbine cover-plate and the rotating shaft. They are of two designs: one with a manually-adjustable gland that may be pressed down as the soft packing wears out, sealing the clearance round the shaft, the other where the clearance is sealed with machined graphite rings pressed against the shaft by circular springs.

The first design, although common in machine construction, is used in hydraulic turbines only for grease-lubricated bearings where the stuffing box is arranged above the bearing and is thus accessible for maintenance purposes. Oil-lubricated bearings with soft packings arranged between the runner and the turbine guide bearing are no longer used since they have proved inadequate under operating conditions.

Packing wear due to shaft rotation leads to water leaking into the bearing. It is then necessary to repack the stuffing box, but this is possible only if the unit is stopped.

The second type of packing — hard graphite rings pressed against the shaft by means of springs — is largely used in various designs abroad. Operating experience shows that its reliability depends on the quality of the graphite. It is difficult to repair, and in many instances, radical redesigning of the bearing became necessary after a few years' operation because of the low quality of the graphite. Graphite packing requires a continuous supply of clean water.

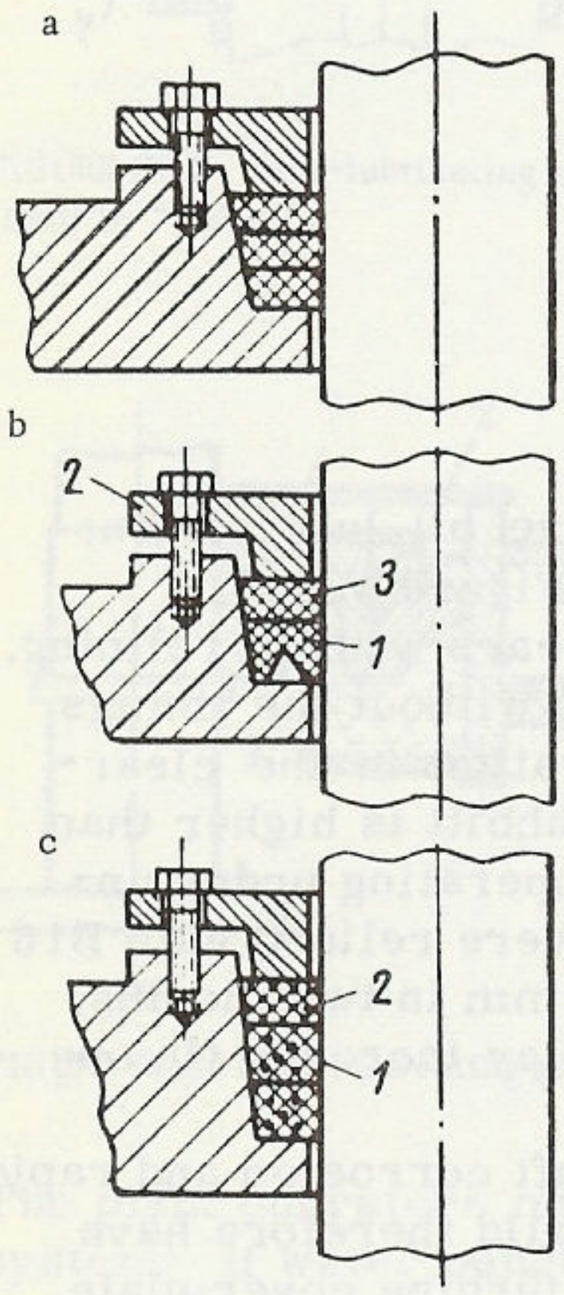


FIGURE IX. 11. Packing boxes

If no water reaches the hemp of which the packing consists, e. g., in case of low pressure in the water reservoir and tight packing at the bottom, the upper hemp layers may dry out. The tendency nowadays is to replace hemp by other materials.

Figure IX. 11 illustrates three different types of packing: a) ordinary hemp packing; b) rubber ring (1) and hemp layer (3) pressed down by gland (2). The ring is rubber cord of square section with V-shaped lips forced by the water pressure against both housing and shaft; c) rubber cords (1) with a braid of cotton fibers (2).

The packings represented in Figure IX, b and c have proved more reliable in operation than hemp packing. They ensure a better seal and require less frequent turbine stoppages to change the packing.

Experience has shown stuffing boxes on turbines coupled to pumps to be unreliable. Sand particles in the seepage water erode the shaft surface and fill up the pores in the packing, causing leakages. If the gland is pressed in further, shaft damage and seepage will increase. Damage to the shaft in the stuffing box zone cannot be repaired in situ; the shaft has to be dismantled and sent to the workshop for repair.

Labyrinth seals. Labyrinth seals are frequently used in turbine construction to prevent water from leaking into the turbine across the clearances between the stationary and rotating parts. Unlike stuffing boxes, which seal the clearances completely, labyrinth seals permit a certain clearance between the stationary and rotating turbine parts, but they reduce leakages to a safer level by creating additional hydraulic resistances.

Labyrinth seals usually consist of either one or two pairs of disks arranged in axial direction with the circular surfaces in mating recesses.

To obtain minimum seal height and, at the same time, reduce the distance between bearing and runner, the labyrinth segments should be shallow and several in number. Whenever the height of the seal is not restricted (e.g., by the band of the Francis runner), a few large segments are used, since they are easier to manufacture.

Labyrinth seals are shown in Figures V.11 and V.16 beneath the oil-lubricated bearings.

Two of the segments forming the labyrinth seal are mounted on the turbine cover-plate, and the rest within the cover-plate cone.

A centrifugal pump is installed beneath the lower oil receptacle to pump the water leaking through the seal into the draft tube. The impeller of the centrifugal pump is mounted on, and driven by, the main turbine shaft while the pump casing is fastened to the turbine cover-plate. If the tail-water level is higher than the cover-plate elevation, a sealing device is provided in the seal to prevent water from leaking across the clearances from the draft tube into the turbine, when the latter is at rest.

This device consists of a rubber chamber of circular section located in a recess of the pump cover. If during shut-down there is danger of water penetrating into the turbine, either water or air under a pressure of 1.5 to 2 kg/cm^2 is led into the rubber chamber. The latter then expands and seals the clearance. The seal should preferably be connected to electric contacts, which emit a signal whenever the sealing device is operative. The seal may be put into operation only when the turbine is completely at rest. The rubber chamber must be deflated and the steel rings pulled down by their own weight or by springs to provide the necessary clearance when the turbine is in operation. These devices are not very reliable.

Clean water, usually taken from the scroll case, and strained, is frequently led into the labyrinth seal. It enters at the center of the seal, so that one part flows toward the turbine runner, the other part flowing through the pump into the draft tube.

This is done, firstly, in order to lengthen the service life of the labyrinth seal by protecting the segments from wear caused by the silt-laden water always encountered in hydroelectric plants; secondly, by introducing water into the labyrinth, the possibility of air penetration into the turbine under certain operating conditions is excluded. Finally, if the clearances are small, a continuous water flow lubricates the seal and prevents possible damage.

The design of a labyrinth seal for turbine bearing is governed by the same considerations as that of the seal of the Francis runner. The value of a seal design is judged, on the one hand by the amount of water leaking through the seal, and, on the other hand, by the ease in manufacturing.

The need to minimize leakages makes it essential to reduce the clearances, or to increase the number or height of the segments. This involves either closer machining tolerances or increased axial seal dimensions.

These factors must be considered in labyrinth seal design. Owing to their complicated construction, labyrinth seals for bearings are seldom used nowadays.

60. WATER-LUBRICATED GUIDE BEARINGS

Water-lubricated guide bearings are widely used nowadays in turbine construction, particularly in the Soviet Union. In design, they are simpler than oil-lubricated bearings.

Water-lubricated bearings do not require seals, since the water that flows through the turbine has no damaging effect and is used as a lubricant on most installations. No auxiliary equipment for lubrication, such as tanks, pumps, etc., is needed. Since there are no seals the bearing may be located close to the runner. Operation and maintenance is thus simplified, too. The shells of water-lubricated bearings are usually of rubber (Figure IX.12), sometimes, also, of wood plastics.

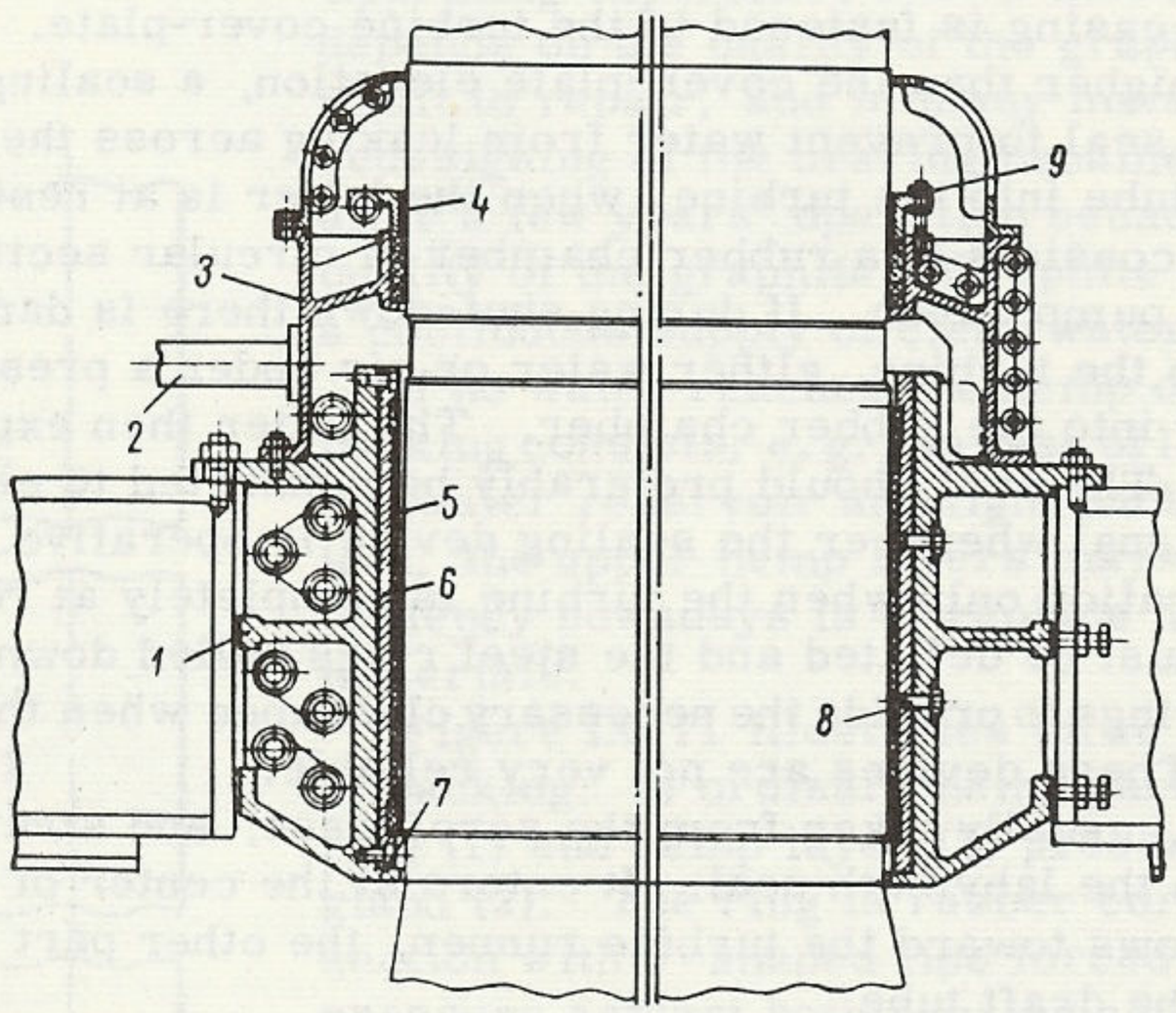


FIGURE IX.12. Rubber-lined water-lubricated bearing

The guide bearing consists of a cast-iron housing (1) made in sections fastened to the turbine cover plate; the housing encloses the rubber-lined shoes (6) fastened to it by bolts (7) and (8). The shoes (6) are part of a steel cylinder with rubber-lined inner surface (5). The water for cooling and lubricating the bearing flows through longitudinal grooves cut into the rubber. It is supplied through pipe (2) to reservoir (3). The clearance between reservoir and shaft is sealed by means of a stuffing box whose tightness may be adjusted by the gland (4) pressed down by studs (9). The sulfur content of the rubber increases shaft corrosion, which must therefore

be protected by a liner, preferably of stainless steel. Water is usually supplied to the bearing from two independent sources through separate pipes (Figure IX.13). A steady stream is led to the bearing from the water intake (1) provided on the scroll case. The water runs through a pipe provided with a strainer (2) and either a flow or a pressure relay (4), which makes it possible to control the flow through the pipe. If the flow drops below a minimum permissible value, the relay emits an electric impulse acting on solenoid valve (3), through which industrial water supply is connected. A similar solenoid valve is also fitted in the principal main.

If the water supply from the industrial main is insufficient, the hydro unit is shut down by relay action. The stand-by lubrication system ensures safe operation, and enables the plant to be automatically controlled. After passing through the bearing, the lubrication water is discharged into the water passage above the runner.

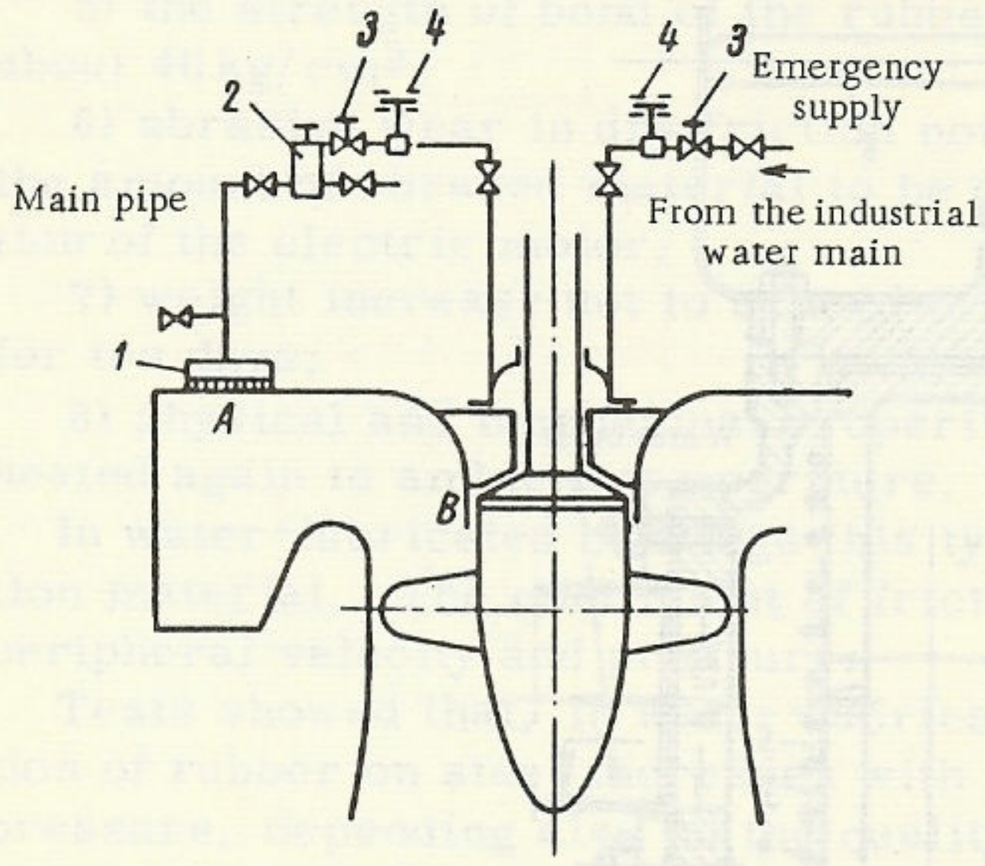


FIGURE IX.13. Schematic diagram of the water supply for bearing lubrication

If the turbine is operated under a low head, so that the pressure in the scroll case is insufficient to supply water to the bearing, a pump is installed to lift the water into a tank located from 15 to 17 m above the bearing. From the tank, the water runs by gravity to the bearing. Operating experience shows that pressure of 0.5 to 1.0 kg/cm^2 gage in the bearing reservoir is sufficient for lubrication.

Most important is a continuous water supply; if the bearing is allowed to run dry, the rubber lining may burn out because of lack of heat dissipation.

An adjustable strainer, as shown in Figure IX.14, is used to clean the water. It consists of a cast or welded body (1) and a drum (2) covered by two brass screens (3) and (4). One screen has 100 openings per square centimeter. The screen is made from a 2 mm-diameter brass-wire net (5). The drum can be rotated manually by wheel (6) one quarter-revolution of which cleans the strainer; the dirt retained by the strainer is carried away by the water into the drainage system. This type of strainer is only suitable for removing gross impurities from the water roughly. Water-lubricated bearings have proved highly satisfactory in Soviet power plants, being extremely reliable and easy to operate. One of the advantages of rubber-lined bearings is that they damp the vibrations of the shaft. Because of the elasticity of rubber, the shaft may rotate even if its center of gravity does not lie exactly on its geometrical center line.

Experience has shown that these bearings operate reliably if clean water is available; if there is silt in the water, the surface of the shaft lining becomes worn, in particular near the stuffing box. Hence, in the latest designs, stuffing boxes are replaced by radial seals consisting of two rings: a rubber ring fastened to the bearing housing, and a stainless steel ring pressed on the shaft. The water is prevented from penetrating into the

bearing by the rubber ring and drained through a pipe into the water passage above the runner; water pressure upon the rubber ring may be adjusted by means of a butterfly valve. A seal of this type is shown in Figure IX. 10, detail 5. The advantages of the radial seal compared with the stuffing box are: less wear of the shaft liner, longer service life of the seal, and less sensitivity to shaft play. In the latest hydro units a rubber sleeve is provided round the shaft, and the bearing shell is lined with metal. In this manner, even if the water is silt-laden, no wear is likely to occur on the shaft, and the bearing lining may be readily replaced when worn. This construction is likely to become standard design. Formerly the bearing was rather long (l = 1.5 d), but nowadays a length of 0.6 to 0.8 d is considered adequate.

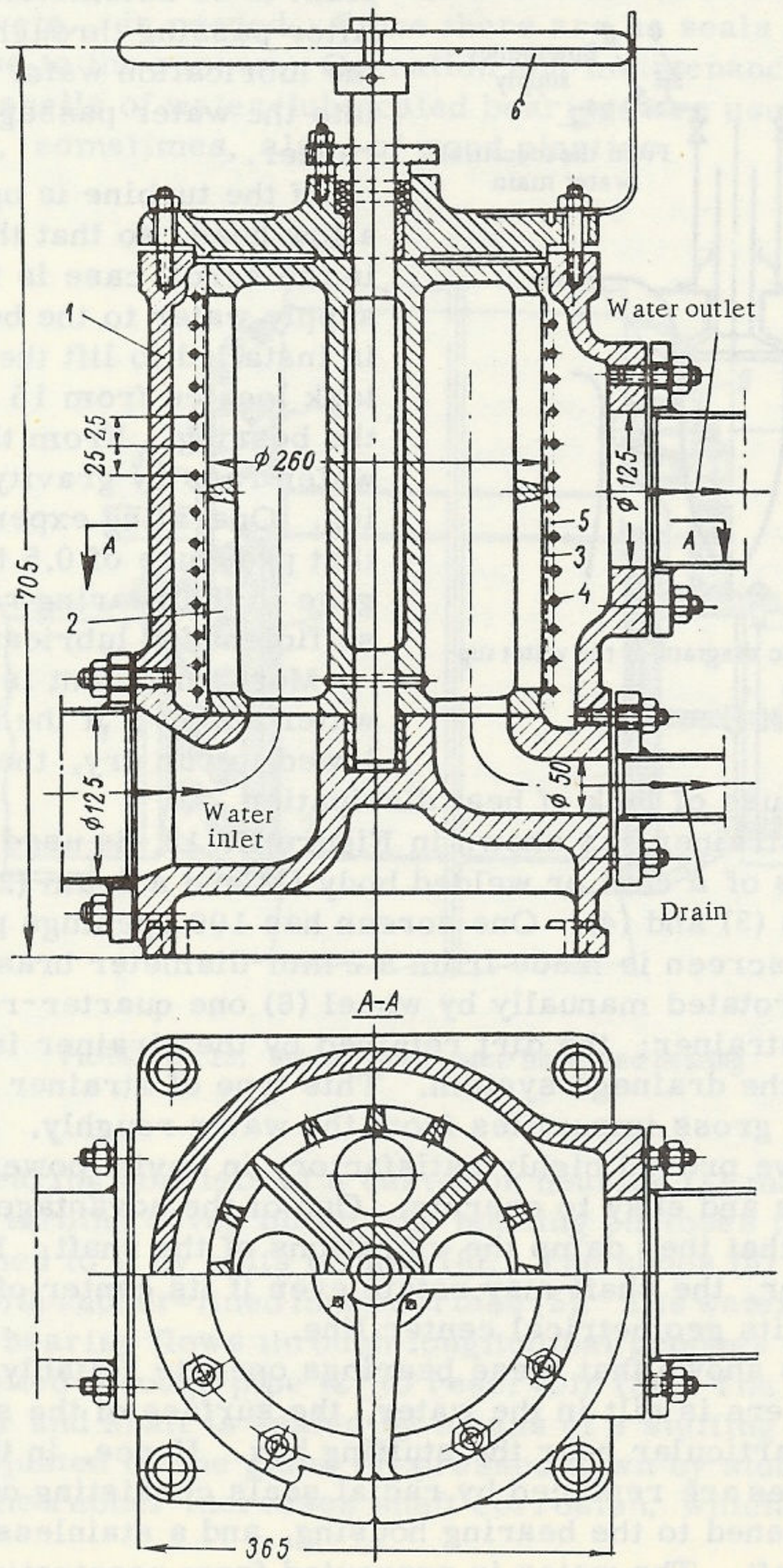


FIGURE IX. 14. Water strainer

Rubber-lined water-lubricated bearings in Francis and Kaplan turbines are shown in figures V.3, V.6, V.10, V.12, and V.18. In high-head turbines better lubrication may be obtained by introducing the water into the bearing (for H = 285 m, see Figure V.6) at mid-height.

Properties of rubber as a bearing material. A special type of rubber, No. 1626, is used for turbine guide-bearing liners. Its main physical and mechanical properties are as follows:

1) tensile strength not less than 200 kg/cm^2;

2) elongation at rupture no less than 400%;

3) deformation of a rubber specimen not to exceed 2% of its thickness when tested under a compressive stress of 5 kg/cm^2;

4) hardness between 8.3 and 12.6 kg/cm^2 (determined with the sclerometer according to GOST 263-53);

5) the strength of bond of the rubber to properly machined metal to be about 40 kg/cm^2;

6) abrasive wear in dry friction not to exceed 700 cm^3/kwhr (GOST 426-57); the amount of abraded material to be determined per unit energy consumption of the electric motor;

7) weight increase not to exceed 0.15% when immersed in river water for ten days;

8) physical and mechanical properties not to alter if cooled to -50°C and heated again to ambient temperature.

In water-lubricated bearings this type of rubber is an excellent antifriction material. The coefficient of friction of rubber on steel varies with peripheral velocity and pressure.

Tests showed that, in water-lubricated bearings, the coefficient of friction of rubber on steel increases with increasing peripheral velocity and pressure, depending also on the quality of the surface finish. The lowest value of the coefficient of friction lies between 0.005 and 0.01 at velocities of 1.5 to 3.5 m/sec. The coefficient of friction increases with temperature. Rubber is highly elastic, and endures much larger deformations than other materials.

In designing rubber-lined bearings, clearances should be selected according to the deformations expected. It is important that they should not exceed the clearances of the labyrinth seals. It is advisable to use a thin rubber layer to reduce the bearing deflections.

Figure IX.15 shows the properties of rubber as bearing material as obtained by experiment.

Figure IX.15,a gives the friction coefficient μ as a function of peripheral velocity u for pressures ranging from 1.0 to 3.5 kg/cm^2 with a cooling-water temperature of 43°C. It can be seen that the coefficient of friction decreases with increasing pressure. For all pressures the coefficient of friction decreases abruptly with increasing peripheral velocity at the beginning, remaining almost constant thereafter /102/.

Figure IX.15,b shows the variation of the coefficient of friction with temperature. Since the coefficient of friction increases with temperature, it is desirable to provide a large amount of cooling water to keep the temperature low.

Figure IX.15,c shows the deformation under compression of rubber test specimens of various thicknesses as a function of pressures.

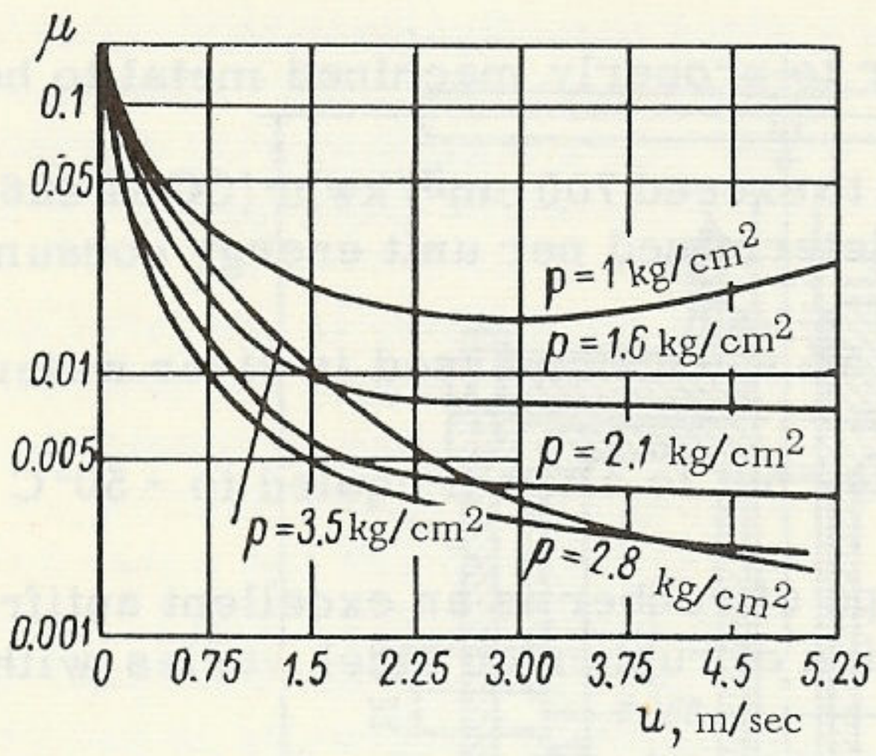
L. G. Smolyarov suggested the following empirical formula for the approximate determination of the coefficient of friction:

$$\mu = C\frac{\sqrt{u}}{p},$$

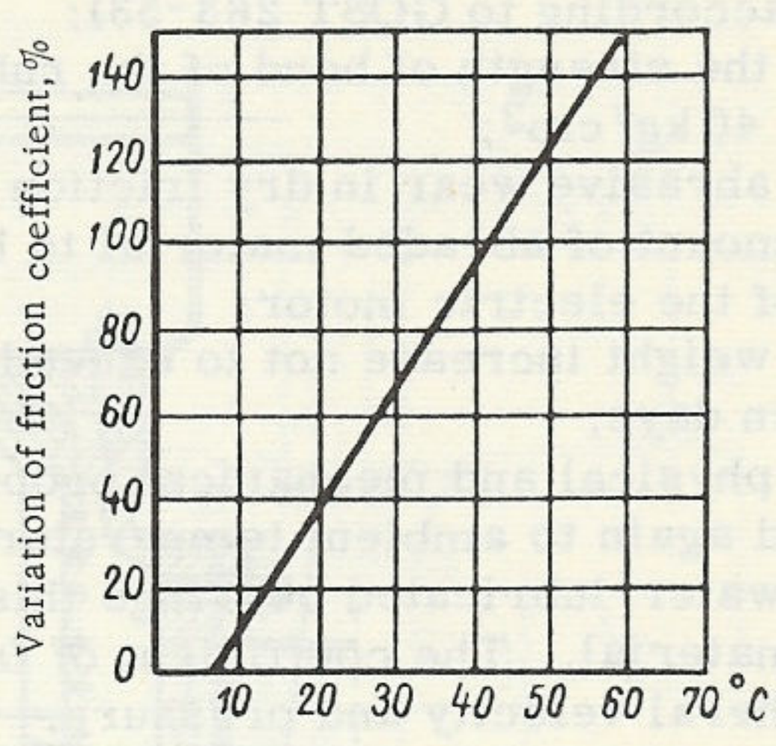
where u = peripheral velocity, m/sec;
p = pressure kg/cm^2;
C = coefficient depending on the peripheral velocity.

Peripheral velocity u, m/sec . . .	1.0	2.0	4.0	6.0	8.0	10.0
Coefficient C	0.25	0.2	0.16	0.15	0.13	0.125

a



b



c

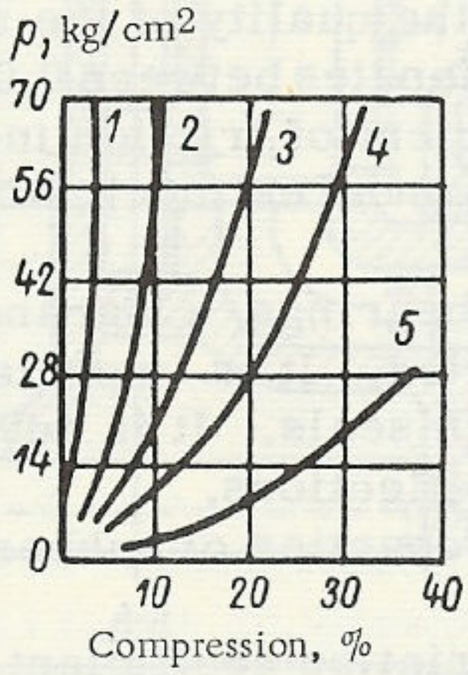


FIGURE IX.15. Properties of rubber as a bearing material:

1 — 6.3 mm; 2 — 12.7 mm; 3 — 19.0 mm; 4 — 25.4 mm; 5 — 25.4 mm (perforated).

The major advantage of rubber is its reduced wear. If sand gets into the bearing, the particles are pressed into the elastic surface of the rubber lining; by rolling upon it, they reach the nearest groove from where the water washes them out. Thus there is no bearing wear, even if the water contains sand. A drawback of rubber is its poor resistance to petroleum-base liquids and mineral oils. If the water reaching the bearing contains oil or kerosene even in small quantities, the rubber is dissolved, becoming

soft, sticky, and unserviceable. Rubber may be kept for a long time in damp sawdust at a temperature between 0° and + 20°C if shaded from sunlight. Under the action of sunlight and heat, it hardens and loses its elasticity. The friction in rubber bearings is fluid friction. To a certain extent, this is proved by the fact that the coefficient of friction decreases with increasing of peripheral velocity. The pressure distribution in the lubricant layer of the rubber bearing /96/ with the shaft rotating in either direction, was measured. It proved to be similar to the typical pressure distribution in an ordinary metal bearing. However, owing to the elasticity of rubber, the maximum pressure was lower. In the space bounded by the oil grooves, a wedge-shaped lubricant film carrying the shaft is formed between the latter and the rubber lining.

Rubber-lined bearings. Rubber-lined bearings are used in shipbuilding as tailshafts and were first used on hydroelectric turbines in the U. S. A. The LMZ started to fit rubber-lined bearings in medium and large turbines in 1935 /28/.

The first such bearing was installed by the LMZ on the Karamyshev turbine (N = 1350 kw, shaft diameter 380 mm); later, bearings of this type were fitted in the Uglich turbines (N = 65,000 kw, shaft diameter 1340 mm). The first bearings designed for these turbines were babbitt-lined and oil-lubricated; the design was later considerably simplified by the use of water-lubricated rubber bearings. The lower rotating receptacle, the oil pump, and the complicated labyrinth seals between the bearing and the shaft flanges were dispensed with. The weight of the bearing and seals was reduced from 66 to 41 t.

Table IX. 2 gives a comparison between babbitted oil-lubricated and rubber-lined water-lubricated bearings for the Uglich HEP.

TABLE IX.2

Comparative data for oil- and water-lubricated bearings

Type of bearing	Number of parts of bearing and seal	Weight, kg					
		Cast iron	Babbitt	Rolled sections	Standardized parts	Stainless steel	Total weight
Babbitt-lined	430	61,000	2,700	900	1,400	-	66,000
Rubber-lined	110	34,100	-	3,800	1,100	2,000	41,000

Thus, the use of rubber-lined bearings permitted 25,000 kg of metal to be saved in each turbine; in addition, machining hours per turbine were reduced by 2000.

In small turbines with shaft diameters between 100 and 200 mm, the rubber bearing usually consists of a metal bushing lined with rubber, with eight to fourteen longitudinal grooves cut into it for water lubrication and cooling.

The rubber shell for medium-size turbines with shaft diameters between 300 and 500 mm is usually made in two parts, bolted to the turbine-bearing housing.

In large turbines with shaft diameters exceeding 500 mm, the bearings usually have eight to twelve shoes. Figure IX.16,b shows such a shoe consisting of a curved steel plate (1), to which a rubber layer (2) is vulcanized. The shoes are fastened with bolts (3) to the bearing housing. To obtain a better bond between rubber and metal it is advisable to cut a fine thread on the bushing. Brass provides the best bond with rubber; hence large steel-shoe bearings, designed to take a rubber lining, have brass surfaces to which the rubber is vulcanized. A special copper-compound adhesive may also be used.

Experience has shown that the bond between vulcanized rubber and the brass surface of a steel shoe has a resistance to shearing of 25 kg/cm^2, while the resistance to shearing of rubber is 61 kg/cm^2. The thickness of the brass coating varies between 0.00125 and 0.0015 mm. First, the surface is rinsed and pickled; the brass coating is then applied by electroplating, using a direct current of 500 to 1000 amp at 6 to 12 v. The anode is a brass plate containing 70% copper and 30% zinc. The plating process lasts for about 20 minutes. On contact with air the brass-coated surface oxidizes; hence, if the rubber is not to be vulcanized immediately, the brass coating should be covered with liquid latex glue. The shoe is vulcanized in a special press mold whose dimensions and weight usually depend on the available load-hoisting facilities of the vulcanizing plant. This is a determining factor in selecting the number of shoes for the bearings of large turbines.

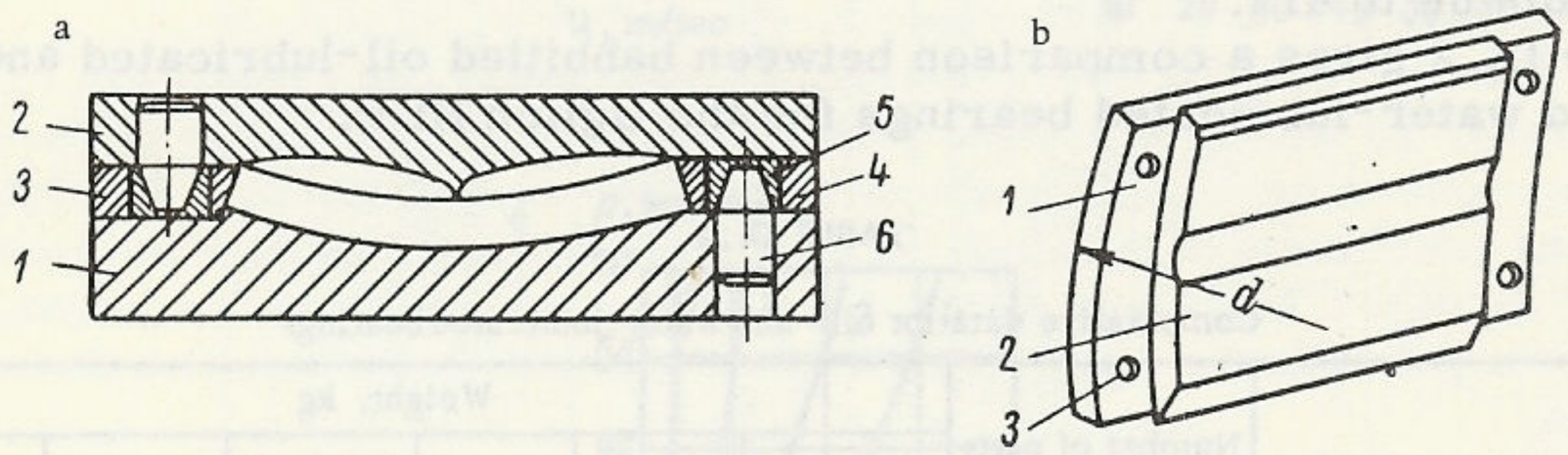


FIGURE IX.16. Rubber-lined bearing

Figure IX.16,a shows a cross section through a press mold for shoe vulcanizing. It consists of two parts: the lower part (1) and the upper part (2); in between are the distance plates — the left-hand plate (3) and the right-hand plate (4) — fastened with dowel sleeve (5) and conical pin (6). When assembled, the press mold encloses a space into which the shoe clad with sheets of raw rubber is inserted; vulcanization is then carried out under pressure. The shoe, after being lined in this manner, has a machining allowance. In the turbine plant the shoes are assembled into one single ring whose inner surface is then machined on a vertical lathe with special cutting tools of high-speed steel.

The KhTZ recently began using rubber shoe bearings without machining after vulcanization. Such bearings will undoubtedly become universal, since the rubber surface is smoother than that obtained by machining, and has better antifriction qualities. Longitudinal water grooves are usually cut into the bearing, the shape of the groove section being shown in Figure IX.17. The grooves serve for the passage of lubricating and cooling water,

as well as for removal of the sand and silt carried in. The shape and dimensions of the groove are determined empirically, and depend on the bearing size. Its depth varies between the limits

$$h_1 = (0.4 \text{ to } 0.5)\, h_2.$$

Rubber-lined bearings with helical instead of straight lubrication grooves have also been used in turbines. Single or double helical grooves of semicircular or trapezoid cross section are cut into the bearing surface along its length. Since the lubrication groove is rather long in this design, the hydraulic resistance increases and therefore lubricating water at an appreciable pressure is required; moreover, this type of groove is more liable to become clogged. Bearings with helical grooves are not widely used.

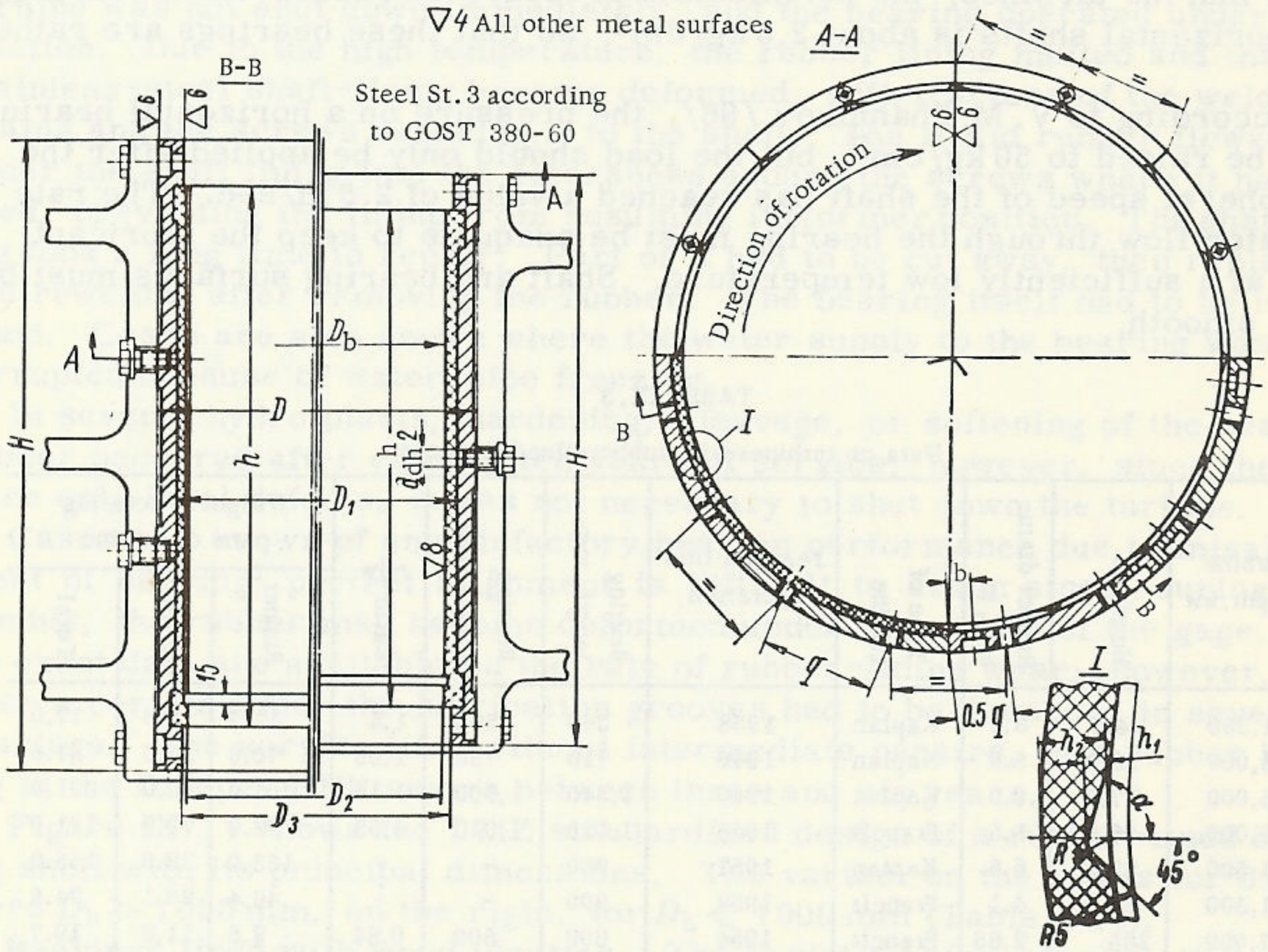


FIGURE IX.17. LMZ standardized rubber-lined bearing shell

Clearances in rubber-lined bearings are similar to, or slightly smaller than, those in metal-lined bearings, since rubber deforms easily. With large clearances shaft play increases. The lubricant film may be thinner in rubber-lined bearings than in metal bearings, since rubber can conform to any unevenness in the shaft. Bearings have even been used successfully in which the inner diameter was less than the shaft diameter. Bearings of this type reduce shaft vibration. In the event of excessive pressure, however, dry friction might occur between metal and rubber, causing the latter to overheat. It is therefore better to provide a small clearance in the bearing, ensuring the formation of an extremely thin water film.

Permissible loads on rubber-lined guide bearings depend on the shaft speed and the force applied. The latter is difficult to determine since, with uniform flow distribution, the turbine runner is theoretically balanced. There always exists, however, a certain imbalance of the rotor mass, as well as nonuniformity of the water flow; hence, forces always act on the bearing. These forces may be determined indirectly by setting up the heat balance for the bearing, as shown below. With the forces known, the pressure on unit bearing-area may be determined; it may then be compared with values adopted in previous designs, or in marine engineering. Determination of the permissible pressure is based upon the possible bearing deformation and rotational speed. The minimum peripheral velocity at which the lubricant film is capable of carrying a load is 0.5 m/sec. At this velocity, the load on the rubber-lined bearing should not exceed 3.5 kg/cm^2. Rubber-lined bearings in turbines usually operate at peripheral velocities from 1.5 to 12.0 m/sec, with bearing pressures up to 5 kg/cm^2.

In marine turbines, the permissible pressure on rubber-lined bearings for horizontal shafts is about 2.5 kg/cm^2, so that these bearings are rather long.

According to V. M. Shannikov /96/, the pressure on a horizontal bearing may be raised to 50 kg/cm^2, but the load should only be applied after the peripheral speed of the shaft has reached a value of 2.5 m/sec. The rate of water flow through the bearing must be adequate to keep the lubricant film at a sufficiently low temperature. Shaft and bearing surfaces must be very smooth.

TABLE IX.3

Data on turbines with rubber-lined bearings

Turbine output, kw	Head, m	Runner diameter, m	Type of turbine	Year put into operation	Bearing length, mm	Bearing length, mm	Ratio $\frac{l}{d}$	Weight of rotating parts of turbine		
								Runner	Shaft	Total
1,350	4.5	3.0	Kaplan	1938	380	565	1.5	12.7	4.3	17.0
15,000	13.0	5.0	Kaplan	1940	710	750	1.05	70.0	17.0	87.0
65,000	17.5	9.0	Kaplan	1940	1,340	1,600	1.18	304.0	87.0	391.0
75,000	36.5	5.5	Francis	1946	1,120	1,040	0.93	92.0	79.0	171.0
41,500	23.5	6.6	Kaplan	1951	900	-	-	133.0	22.0	155.0
61,500	60.0	4.1	Francis	1952	900	-	-	46.4	28.1	74.5
57,000	285	2.65	Francis	1954	600	500	0.84	8.5	11.2	19.7
85,000	40.0	5.5	Francis	1953	1,100	1,000	0.91	112.0	35.0	147.0
65,000	70.0	4.3	Francis	1955	1,000	-	-	47.0	30.0	77.0
90,000	31.5	7.2	Kaplan	1956	1,200	1,000	0.83	3,000.0	44.0	344
126,000	22.5	9.3	Kaplan	1956	1,420	1,150	0.82	426	60.0	486
200,000	98.0	5.5	Francis	Under construction	1,500	1,000	0.65	-	-	-
500,000	98.0	7.5	Francis	Projected	2,300	1,300	0.57	-	-	-

Rubber-lined bearings have been in service for a long time in many hydroelectric plants in the Soviet Union. Table IX. 3 gives data on several turbines equipped with these bearings.

Rubber-lined bearings with diameter D_b = 1340 mm have been in successful operation since 1940 in the large Kaplan turbines at the Uglich and Rybinsk hydro plants. All the turbines at the Volga HEPs imeni Lenin and imeni XXII Congress of the KPSS are equipped with rubber-lined bearings, with diameter D_b = 1400 mm. At the Volga plant they have been in successful operation since 1955. Bearings of this type are also giving reliable service on Francis turbines. The large Dnieper-plant turbines have been in operation since 1949, having rubber-lined bearings with diameter D_b = = 1120 mm. The high-head Gyumush turbines, in operation since 1954, with a head H = 285 m, have rubber-lined bearings with D_b = 600 mm. Powerful turbines are now being built at the LMZ for the Bratsk plant (N = 225,000 kw) having rubber-lined bearings with D_b = 1500 mm. The giant turbine (N = = 500,000 kw), designed for the Krasnoyarsk plant, will have a rubber-lined bearing with D_b = 2300 mm.

Cases are reported of rubber-lined bearings burning out when the lubricating water supply failed because of a drop in the headwater level. The turbine was not shut down immediately, and the bearing operated under dry friction. Due to the high temperature, the rubber lining melted and the stainless-steel shaft-lining became deformed, with fracture of the welded seams and the screws securing it to the shaft. The liquid rubber flowed under the shaft lining into the clearances around the screws where it hardened, preventing the lining from resuming its former position. The shaft lining took a long time to repair. Part of it had to be cut away, then replaced and rewelded after removing the rubber. The bearing itself had to be relined. Cases are also known where the water supply to the bearing was interrupted because of water-pipe freezing.

In several hydro plants, hardening, cleavage, or softening of the bearing rubber occurred after eight to ten years of service; however, since these were only local defects, it was not necessary to shut down the turbine.

Cases are known of unsatisfactory bearing performance due to misalignment of bearing; perfect alignment is difficult to attain since, during assembly, the rubber may become deformed under the weight of the gage. No exact data are available on the rate of rubber-lining wear; however, after a certain time, the lubrication grooves had to be deepened in several bearings. The service life, without intermediate repairs, of a rubber bearing in the Dnieper HEP varies between three and six years.

Figure IX.17 shows the LMZ standardized design of a rubber-lined bearing shell with its principal dimensions. The variant on the left is for diameters $D_b > 1000$ mm, on the right, for $D_b < 1000$ mm (Table IX.4).

Bearings lined with wood plastics. The Soviet turbine-construction industry also uses guide bearings with wood-plastic linings. They were introduced at the LMZ by I. M. Filipova /88/. Sheets of laminated wood plastics of type DSP-B10 or DSP-B20 (also known as lignofol) are used for this purpose. They are made 0.5 mm-thick layers of birch veneer, impregnated with either phenol- or cresol-formaldehyde (18 — 20%). The grade and the physical and mechanical properties of wood plastic depend on the direction of the fibers in the veneer layers. In DSP-B10 and DSP-B20 plastics one layer out of every ten or twenty is laid at a right angle to the rest. In this case, 90 to 95% of all the wood fibers end on face (3) (Figure IX.18,b). The antifrictional properties are higher in this direction, and swelling in water is practically eliminated. Bearings lined with wood-plastic may be either water- or oil-lubricated. Since water is a better

TABLE IX.4

Dimensions of LMZ standard rubber-lined bearings

D_b	D		D'	D_1	D_2	D_3	Number of		d	H	h	b	$\sim q$	R	$\alpha°$
	Bearing housing	Bearing lining					shoes z	bolts z_1							
$265^{+0.15}$	335A	$335^{\pm 0.027}$	340C	$295A_5$	$265^{+0.5}_{+1}$	280A	4	16	M16×2	280	200	20	128.2	7.5	70
$315^{+0.15}$	385A	$385^{\pm 0.031}$	390C	$345A_5$	$315^{+0.5}_{+1}$	330A	4	16	M16×2	319	230	20	147.3	7.5	70
$365^{+0.18}$	435A	$435^{\pm 0.031}$	440C	$395A_5$	$365^{+0.5}_{+1}$	380A	4	16	M16×2	350	270	20	166.4	7.5	70
$415^{+0.18}$	490A	$490^{\pm 0.031}$	495C	$445A_5$	$415^{+0.5}_{+1}$	430A	4	16	M16×2	380	300	20	187.5	7.5	70
$465^{+0.18}$	$540^{+0.07}$	$540^{\pm 0.035}$	$545_{-0.07}$	$495A_5$	$465^{+0.5}_{+1}$	480A	4	16	M16×2	410	330	20	206.6	7.5	70
$515^{+0.20}$	$590^{+0.07}$	$590^{\pm 0.035}$	$595_{-0.07}$	$545^{+0.9}$	$515^{+0.5}_{-1}$	$530^{+0.07}$	4	16	M16×2	440	360	20	225.8	7.5	70
$565^{+0.20}$	$640^{+0.08}$	$640^{\pm 0.040}$	$645_{-0.08}$	$595^{+0.9}$	$565^{+0.5}_{+1}$	$580^{+0.07}$	4	16	M16×2	470	390	20	245	7.5	70
$620^{+0.20}$	$695^{+0.08}$	$695^{\pm 0.040}$	$700_{-0.08}$	650^{+1}	$620^{+0.5}_{+1}$	$635^{+0.07}$	4	16	M16×2	500	420	20	264	7.5	70
$670^{+0.22}$	$755^{+0.08}$	$755^{\pm 0.040}$	$760_{-0.08}$	705^{+1}	$670^{+0.5}_{+1.5}$	$685^{+0.08}$	6	36	M20×2.5	560	460	30	194.1	7.5	70
$720^{+0.22}$	$805^{+0.08}$	$805^{\pm 0.045}$	$810_{-0.09}$	755^{+1}	$720^{+0.5}_{+1.5}$	$735^{+0.08}$	6	36	M20×2.5	590	490	30	207	7.5	70
$770^{+0.22}$	$860^{+0.09}$	$860^{\pm 0.045}$	$865_{-0.09}$	$810^{+1.1}$	$770^{+0.5}_{+1.5}$	$790^{+0.08}$	6	36	M20×2.5	620	520	30	222.6	10	75
$820^{+0.25}$	$910^{+0.09}$	$910^{\pm 0.045}$	$915_{-0.09}$	$860^{+1.1}$	$820^{+0.5}_{+1.5}$	$840^{+0.09}$	6	36	M20×2.5	640	540	30	235.5	10	75
$870^{+0.25}$	$960^{+0.09}$	$960^{\pm 0.045}$	$965_{-0.09}$	$910^{+1.1}$	$870^{+0.5}_{+1.5}$	$890^{+0.09}$	6	36	M20×2.5	660	560	30	248.5	10	75

Table IX. 4 cont.

D_b	D		D'	D_1	D_2	D_3	Number of		d	H	h	b	$\sim q$	R	$\alpha°$
	Bearing housing	Bearing lining					shoes z	bolts z_1							
$920^{+0.25}$	$1010^{+0.10}$	$1010^{\pm0.050}$	$1015_{-0.10}$	$960^{+1.1}$	$920^{+0.5}_{+1.5}$	$940^{+0.09}$	6	36	M20×2.5	680	580	30	261.4	10	75
$970^{+0.25}$	$1060^{+0.10}$	$1060^{\pm0.050}$	$1065_{-0.10}$	$1010^{+1.2}$	$970^{+0.5}_{+1.5}$	$990^{+0.09}$	6	36	M20×2.5	700	600	30	274.3	10	75
$1020^{+0.25}$	$1110^{+0.10}$	$1110^{\pm0.050}$	$1115_{-0.10}$	$1060^{+1.2}$	$1020^{+0.5}_{+1.5}$	$1040^{+0.10}$	6	36	M20×2.5	720	620	30	287.3	10	75
$1120^{+0.28}$	$1220^{+0.10}$	$1220^{\pm0.050}$	$1225_{-0.10}$	$1160^{+1.2}$	$1120^{+0.6}_{+1.6}$	$1140^{+0.10}$	8	64	M24×3	770	650	40	238	10	75
$1220^{+0.28}$	$1320^{+0.11}$	$1320^{\pm0.055}$	$1325_{-0.11}$	$1260^{+1.3}$	$1220^{+0.6}_{+1.6}$	$1240^{+0.10}$	8	64	M24×3	820	700	40	257.5	10	75
$1320^{+0.30}$	$1420^{+0.11}$	$1420^{\pm0.055}$	$1425_{-0.11}$	$1360^{+1.3}$	$1320^{+0.6}_{+1.6}$	$1340^{+0.11}$	8	64	M24×3	870	750	40	277	10	75
$1420^{+0.30}$	$1520^{+0.11}$	$1520^{\pm0.055}$	$1525_{-0.11}$	$1460^{+1.3}$	$1420^{+0.6}_{+1.6}$	$1440^{+0.11}$	8	64	M24×3	920	800	40	296.5	10	75
$1520^{+0.30}$	$1620^{+0.12}$	$1620^{\pm0.060}$	$1625_{-0.12}$	$1560^{+1.3}$	$1520^{+0.6}_{+1.6}$	$1540^{+0.11}$	8	64	M24×3	960	840	40	316	10	75
$1620^{+0.30}$	$1720^{+0.12}$	$1720^{\pm0.060}$	$1725_{-0.12}$	$1660^{+1.5}$	$1620^{+0.6}_{+1.6}$	$1640^{+0.12}$	8	64	M24×3	1000	880	40	335.5	10	75
$1720^{+0.35}$	$1830^{+0.12}$	$1830^{\pm0.065}$	$1835_{-0.12}$	$1760^{+1.5}$	$1720^{+0.7}_{+1.7}$	$1740^{+0.12}$	12	96	M30×3.5	1050	910	50	238.8	10	75
$1820^{+0.35}$	$1930^{+0.12}$	$1930^{\pm0.065}$	$1935_{-0.12}$	$1860^{+1.5}$	$1820^{+0.7}_{+1.7}$	$1840^{+0.12}$	12	96	M30×3.5	1080	940	50	252	10	75
$1920^{+0.40}$	$2030^{+0.13}$	$2030^{\pm0.070}$	$2035_{-0.13}$	$1960^{+1.5}$	$1920^{+0.7}_{+1.7}$	$1940^{+0.12}$	12	96	M30×3.5	1120	980	50	265	10	75
$2020^{+0.40}$	$2130^{+0.13}$	$2130^{\pm0.070}$	$2135_{-0.13}$	$2060^{+1.8}$	$2020^{+0.7}_{+1.7}$	$2040^{+0.13}$	12	96	M30×3.5	1140	1000	50	278	10	75

Remarks: 1. D'—the outer diameter of the metal shoe is provided with a machining allowance of 2.5 mm on the side of the press-mold (missing in Figure IX.17). 2. The rubber-lined surface of the metal shoe has an undercoat of brass. 3. The rubber is vulcanized with a machining allowance of 10 mm on the diameter D_b.

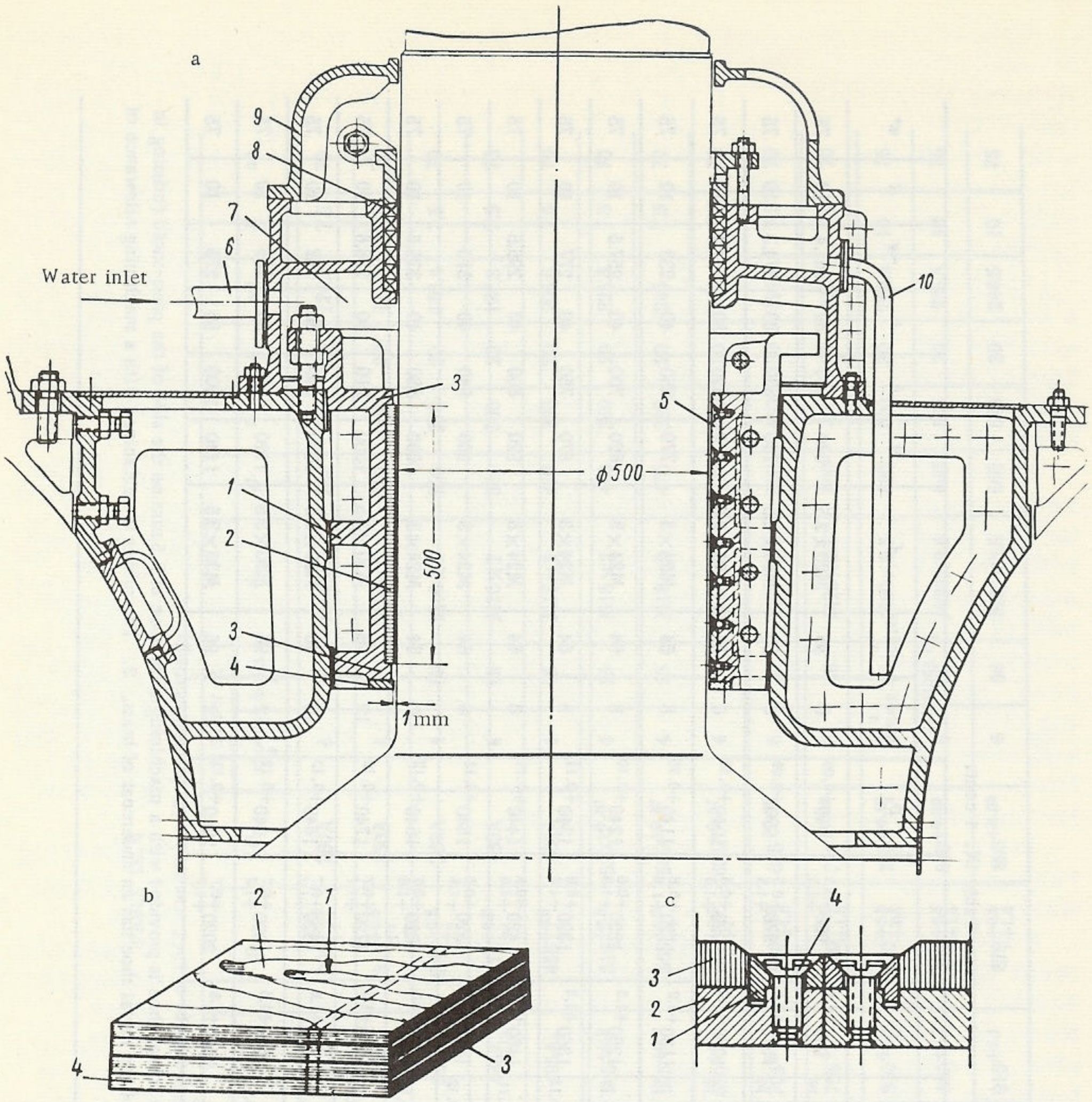


FIGURE IX.18. Bearing lined with wood plastics

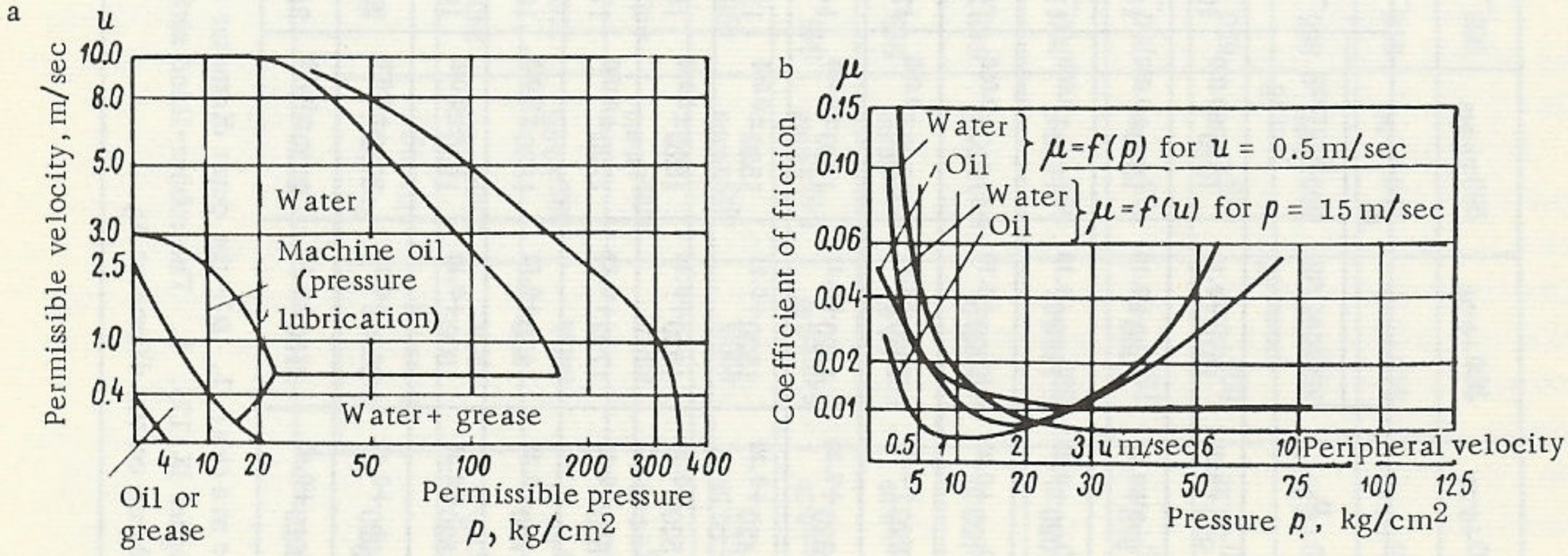


FIGURE IX.19. Characteristics of DSP wood plastics

a — lubrication recommended in dependence on pressure and velocity; b — coefficient of friction as function of pressure and velocity.

cooling medium than oil, higher pressures and speeds are permissible when water is the lubricant. Ya. S. Gallai /14/ recommends selecting the type of lubrication according to pressure and velocity from the diagram in Figure IX. 19,a.

DSP wood plastics have high antifriction qualities. The coefficient of friction μ depends on velocity and pressure, varying between 0.005 and 0.013 for velocities between 1.0 and 10 m/sec and pressures from 10 to 100 kg/cm^2. With water lubrication, the coefficient of friction decreases with increasing velocity and pressure (Figure IX. 19,b). The specific weight of the wood plastics used varies between 1.3 and 1.4 kg/cm^3; the heat conductivity is 1/160 that of bronze. Wood plastics become highly plastic under pressures of 100 to 200 kg/cm^2. This favors running-in the bearing but, on the other hand, the clearance increases considerably when the bearing is subjected to large pressures. Wood plastics tend to absorb water, mainly along the fibers; this causes swelling and changes in the bearing dimensions. The plastic material swells mainly in the direction opposed to that of the pressure. Special measures are required to restrict water absorption, e. g., enclosing the plastic in a metal frame. This limits water absorption to 2 or 3%. The mechanical and physical properties of DSP-B wood plastics differ basically from those of nonferrous metals and rubber. Owing to its fibrous structure, DSP plastics exhibit different properties in different directions: at the face (3), (Figure IX. 18,b) along the fibers, on the "edge" (4) across the fibers, and "on the flat" (1) in the direction of the pressure. Material characteristics are best at the face. The strength of DSP-B plastics is 600 kg/cm^2 in compression and 2600 kg/cm^2 in tension; the Brinell hardness is 30H_B. The modulus of elasticity is $0.3 \cdot 10^6$ kg/cm^2, and the maximum operating temperature 80° C.

In designing plastic-lined bearings, plates of the following dimensions are used:

Thickness	40, 45, 55, 60 mm
Length	700 to 1500 mm, in multiples of 100
Width	900 to 1200 mm, in multiples of 100
Tolerance of plate thickness . .	± 3 mm

In order to avoid shaft seizure through swelling, the bearing shoes should be located so that the face (3) of the material comes into contact with the turbine shaft and the sides of the shoe coincide with surface (2). Because of the low heat conductivity of wood plastics, the thickness of the bearing lining should be kept to a minimum; elastic deformations are also reduced in this way.

In LMZ practice, the standardized thickness is 12 to 25 mm, according to the bearing diameter. Cracks may occur if the thickness is inadequate. If the material swells, stresses of 150 to 200 kg/cm^2 may arise; it is therefore necessary to fix the shoes securely to the bearing.

Figure IX. 18,c shows the shoes (3) fastened by means of locking plates (1). The plates are provided with projections engaging in corresponding grooves in the cast-iron shell (2). The plate is fastened to the bearing by means of screws (4). The force arising when the wood-plastic lining (3) swells is taken up by projection (1).

In manufacturing the shoes, the wood-plastic plates are first cut into separate pieces (shown by dotted lines in Figure IX. 18,b).

The first machining operation is milling the shoe face with a special cutter to a radius equal to the inner radius of the metal shell.

The second operation is chamfering the shoe sides. When assembling, the last shoe must be provided with a special clearance for adjusting the locking plate and the shoes. The last operation is boring the shaft hole.

Figure IX. 18,a shows a cross section through a bearing lined with DSP wood plastic. The bearing consists of a cast-iron shell (1) divided into four segments. A wood-plastic lining (2) is fastened to each segment, as shown in Figure IX. 18,c by means of the locking plate (5). At the top and bottom of the shell, projections (3) prevent the wood plastics from swelling and sliding along the shaft.

To reduce water discharge through the bearing, ring (4) is inserted at its base. The clearance between the ring and the shaft is about 1 mm. The bearing clearances for wood-plastic lining are the same as for babbitt lining. A water chamber (7) with cover (9) and stuffing box (8) is arranged on top of the bearing. Water for lubrication is supplied through pipe (6) either from the scroll case or from the industrial water main. Water leaking across the packing is drained through pipe (10). The turbine shaft is lined with Kh18N9T stainless-steel plates. Adjustment of the clearance between the shaft and the bearing to take up wear is effected by means of brass shims inserted between the bearing-shell joints. The shims are of various thicknesses (0.5; 1.0; 1.5 mm). By removing shims, the shell may be lowered on the conical seat and the inner diameter of the bearing reduced.

Experience with wood-plastic-lined bearings shows that, under proper operating conditions, and with clean water used for lubrication, the bearing gives full satisfaction. The service life of a bearing lined with wood plastics is from five to six years. These bearings can operate even if the lubricating water supply fails for a short time.

However, if the turbine is running under unstable operating conditions characterized by increased rotor vibrations, e. g., cavitation, imbalance of the rotating parts, or misalignment, these bearings fail after a short time, the clearances exceeding permissible values.

Wood-plastic-lined bearings have been known to swell due to water absorption and inadequate fastening of the locking plates.

Heat balance of a water-lubricated guide bearing. Owing to the low heat conductivity of rubber linings, it may be safely assumed that all friction heat is carried away by the water. Water is usually supplied to the bearing at a pressure of 0.5 to 2.0 kg/cm^2 from two independent sources. When setting up the heat balance, the source with the lowest head should be taken into account. At the LMZ, computation is carried out in the following order:

If P is the load on the bearing, the following amount of heat is dissipated per second in the bearing:

$$A = \frac{Pu\mu}{427} \text{ kcal/sec}, \qquad \text{(IX. 18)}$$

where u = peripheral velocity of the shaft, m/sec;
μ = coefficient of friction;
427 = mechanical equivalent of heat.

The amount of heat raises the temperature of q liters of water per second flowing through the guide bearing by Δt degrees centigrade.

Consequently

$$q = \frac{A}{C\gamma\Delta t} = \frac{Pu\mu}{427C\gamma\Delta t} \text{ l/sec},$$

where C = specific heat of water, kcal/kg° C;

γ = specific weight of water;

whence the permissible radial load is

$$P = \frac{427qC\gamma\Delta t}{u\mu} \text{ kg}. \qquad \text{(IX. 19)}$$

The pressure on a bearing having diameter d and length l is

$$p = \frac{P}{dl} = \frac{427 \cdot qC\gamma\Delta t}{dlu\mu} \text{ kg/cm}^2. \qquad \text{(IX. 20)}$$

The maximum temperature rise of the water flowing through the bearing is

$$\Delta t = t_1 - t_2, \qquad \text{(IX. 21)}$$

where t_1 = 50° C = maximum permissible temperature of the rubber bearing;

t_2 = 25° C = maximum water temperature in summer.

The flow q (1/sec) for a given bearing should be calculated from the hydraulic losses in the water pipe and the bearing itself, and from the existing pressure-drop between water inlet A and outlet B into the throat ring (Figure IX. 13).

By analogy with the calculation described in Section VII (seal of the runner band), we may write the general formula for water flow through the bearing

$$q = \sqrt{\frac{2gh_w}{\Sigma\left(\lambda_i \frac{l_i}{d_i} \cdot \frac{1}{f_i^2} + \zeta_i \frac{1}{f_i^2}\right)}}, \qquad \text{(IX. 22)}$$

where h_w = head losses in the pipe between A and B;

λ_i = coefficient of friction in the pipe;

l_i, d_i = length and diameter of the i-th pipe section;

f_i = flow area of the i-th pipe section;

ζ_i = coefficient of local resistance.

In LMZ practice the following values are assumed for ζ_i /68/:

Pipe inlet	$\zeta_1 = 0.75$
90° bend	$\zeta_2 = 0.29$
45° bend	$\zeta_3 = 0.29$
Valve	$\zeta_4 = 0.2$
Strainer	$\zeta_5 = 3.0$
Solenoid valve	$\zeta_6 = 5.0$
Flow relay	$\zeta_7 = 5.0$
Outlet to bearing container	$\zeta_8 = 1.0$

A detailed sample calculation of water flow through a bearing is given by L. G. Smolyarov in /24/.

Figure IX.20 shows the relationship between the water flow for cooling and lubrication of rubber bearings and the shaft diameter obtained after prolonged operation of a series of turbines. The flow should not be less than the value shown in Figure IX. 20.

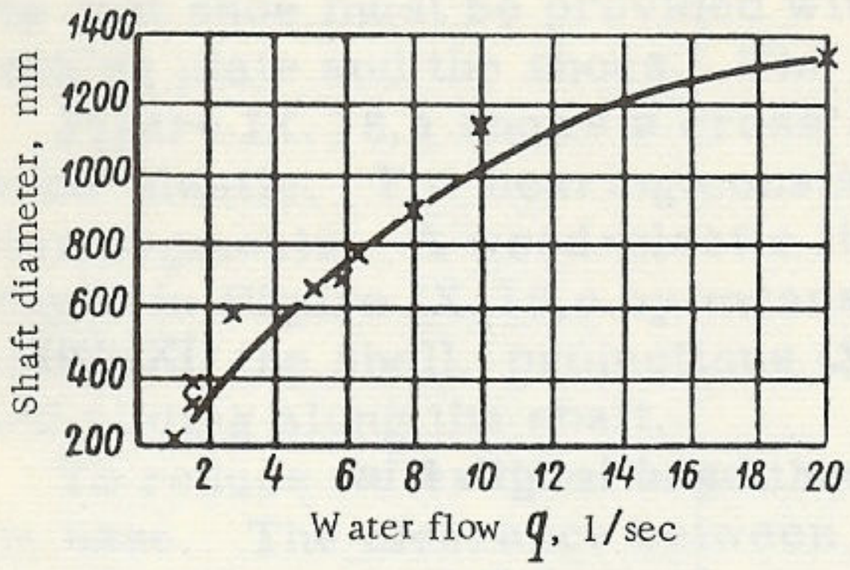


FIGURE IX.20. Statistical relationship between water flow for rubber-bearing lubrication and shaft diameter

With the flow q known, the pressure p may be calculated for normal and runaway speeds, and the results compared with values determined in practice, which usually do not exceed 5 kg/cm^2. This may serve as a check to the accuracy of the heat-balance computation.

The radial load on the guide bearing due to flow assymmetry may be determined approximately by assuming a given value for the hydraulic imbalance ΔM. For a hydraulic imbalance of two per cent of the shaft torque,

$$\Delta M = 0.02M,$$

where

$$M = 716.2\,\frac{1.36N}{n}\ \text{kgm and}\ \Delta M = 19.48\,\frac{N}{n}\ \text{kgm.}$$

The force due to the moment is

$$P = \frac{\Delta M}{r},$$

whence

$$P = 19.48\,\frac{N}{nr}\ \text{kg.} \qquad \text{(IX. 23)}$$

The radius r may be taken as approximately equal to the radius of the mean circumference that divides the runner area into equal parts.

Chapter X

TURBINE SHAFTS

61. GENERAL NOTES

Small and medium-size turbines may be built with vertical or with horizontal shafts. The shaft of small horizontal turbines is connected to the generator shaft by an elastic coupling. It is either connected to the runner hub by a flange or is keyed to it directly. In large horizontal turbines, the shaft lengths are interconnected by flanges.

Horizontal shafts are subjected to the weight of the rotating parts causing bending, and to the torque transmitted from the turbine to the generator; in addition, the water flow causes an axial tensile load. The horizontal shaft is usually mounted on two bearings.

Vertical shafts are subjected to axial tensile forces and transmit torque to the generator. The axial load consists of the weight of the rotating parts and of the axial water-pressure force. The shaft of a vertical turbine may also be subjected to lateral loads, due either to imbalance of the rotating parts or to nonuniform water flow. Torsional shaft vibrations may occur during regulation. According to the particular hydro-unit layout, the shaft may consist either of two parts (turbine and generator shafts) or of three (turbine, intermediate, and generator shafts).

Latest vertical-shaft units are fitted with a one-piece shaft for minimum length.

The layouts of several hydroelectric units with varying numbers of shaft sections are shown in Figure X.1.

The use of a one-piece shaft cuts construction costs, since intermediate flanges are eliminated. Moreover, the reduced stiffness of composite shafts which affects the operation of turbines is eliminated when using one-piece shafts. However, with a one-piece shaft of great length, the crane track level must be raised so that the shaft can be taken out of the turbine pit. It is therefore more convenient for assembly and dismantling to use a composite shaft consisting of two flanged sections instead of a one-piece shaft.

Shafts are usually forged of high-carbon steel; however, welded shafts are now being introduced.

Large turbine shafts are always provided with a central bore to permit inspection of the material. In Kaplan turbines, oil for the runner servomotor is supplied through the bore.

Stable and reliable turbine operation depends not only on the workmanship of the connections between the shaft lengths and between the shaft and adjacent parts, but also on the congruence of the center line of the shaft with its geometrical axis, and of the center lines of shaft and runner, as

well as on the clearance between shaft and bearing. In composite shafts the center line should be straight, a condition which depends mainly on the workmanship of the flange connections. Special attention should be paid to this in designing and manufacturing the shaft.

62. SHAFT DESIGNS

As a rule, high-power turbines operate at low speeds; hence the torque attains high values, requiring large shaft dimensions. In a number of turbines shaft diameter attains 1.5 m, the flange diameter being more than 2 m, and the shaft length over 6 m. Some large shafts weigh up to 70 t after machining. Forged shafts of still greater weight and size require large forging presses and corresponding metallurgical equipment.

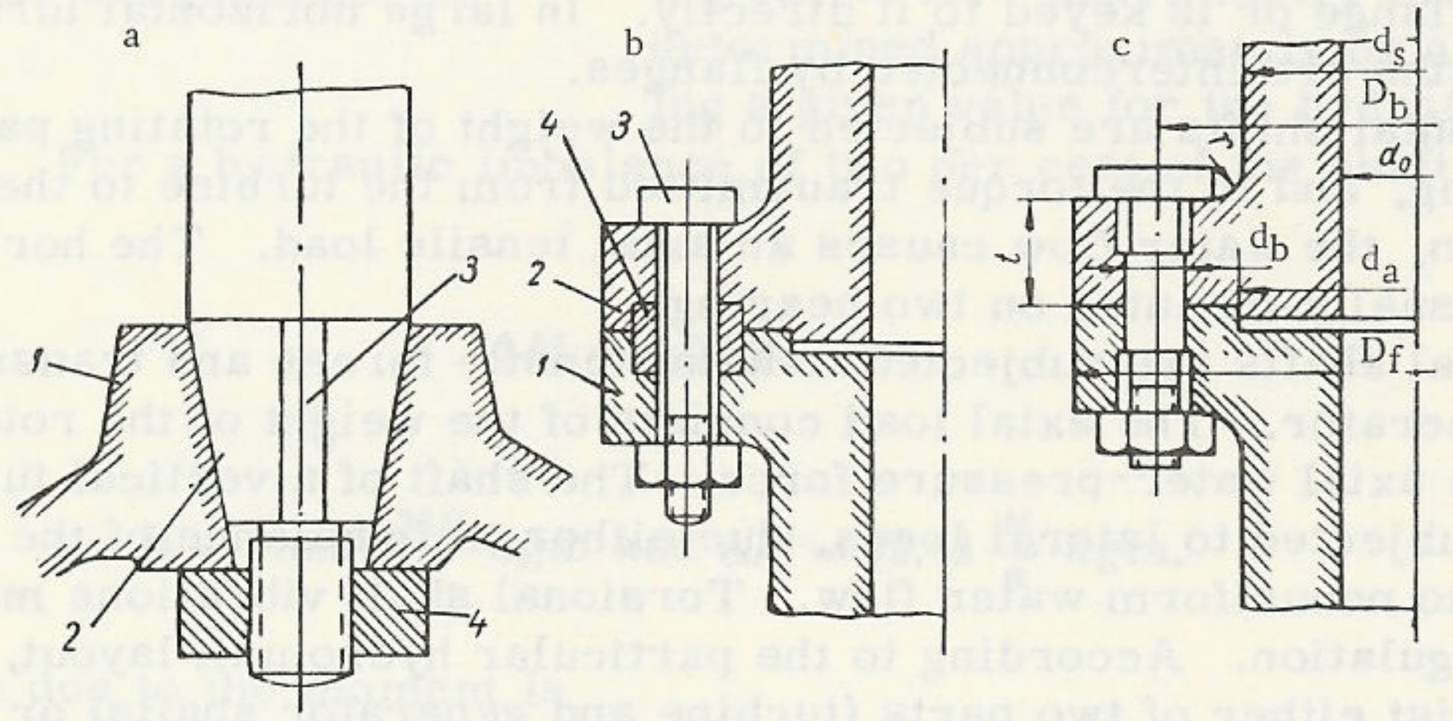


FIGURE X.1. Various shaft connections

a — tapered end with keys; b — with bolts and shear rings; c — with fitted bolts.

The shaft of vertical turbines is usually a cylindrical forged part, flanged at both ends for connecting to the runner and to generator-shaft flanges. It may also be connected to the runner by means of keys and a nut, a method formerly used also in large hydro units.

Figure X.1 shows various methods of connecting the shaft to the runner and to the generator shaft.

Tapered shaft ends of Francis turbines are sometimes connected to the runner (Figure X.1,a) without flanges. The runner hub (1) is fitted to the tapered end of shaft (2) and secured to it by means of key (3) and nut (4). The axial loads are taken up by the nut and the torque by the key. Thread cutting on such large diameters and precise machining of the conical contact surfaces are highly complicated operations, while proper adjusting of runner and shaft is laborious.

Connection with bolts and shear rings (Figure X.1,b). The flanges of the turbine shaft (1) and generator shaft (2) are connected by means of loosely-fitting bolts (3). These take up only axial loads, the torque being transmitted by the shear rings (4), fitted tightly into the flange grooves.

This design was formerly employed in some turbines; manufacture is more complicated, since more parts are required.

Flange connections between the shaft and runner by means of fitted bolts subjected to tension and shear (Figure X.1,c). This is the most common design. The central portions of the bolts, accurately machined and ground, are fitted into the holes with minimum clearance (0.02 to 0.04 mm), corresponding to an $\frac{A}{D}$ fit [Soviet classification]. Soviet experience shows this design ensures reliable flange connection provided the flanges of the adjoining parts are properly aligned by means of the spigot and recess of diameter d_a. The spigot is usually machined to a tolerance corresponding to fit P with respect to the actual diameter of the recess. The recess is machined to a second-class precision. To ensure accurate assembly of bolts and flanges, the holes should be machined simultaneously in both parts by means of reamers.

The convexity of adjoining flange faces, determined with a thickness gage and a straight rule, must be within the following limits:

Flange diameter < 1 m	. . . .	not more than 0.03 mm
Flange diameter > 1 m	. . . .	not more than 0.03 mm per 1 m of diameter

Diametrical play between spigot and recess of the flange should not exceed 0.02 mm for shaft diameters up to 1500 mm.

The flange diameter should be as small as possible to avoid large bending moments. Although large flanges involve difficulties in forging the shaft, the flange diameter should be large enough to locate the bolts and to ensure a smooth transition to the shaft without undue stress concentration. The following (empirically established) basic relations between flange dimensions of all-forged vertical-turbine shafts (see Figure X.1,c), are used in practice:

Flange diameter	$D_f = (1.5 \text{ to } 1.85)\,d_s$
Diameter of bolt circle	$D_b = (1.3 \text{ to } 1.45)\,d_s$
Flange thickness	$t = (0.20 \text{ to } 0.27)\,d_s$
Diameter of aligning spigot	$d_a = (0.9 \text{ to } 1.0)\,d_s$
Diameter of shaft bore for Kaplan turbines	$d_o = 0.5\,d_s$
Diameter of Francis turbine shaft bore	$d_o = 0.3\,d_s$
Fillet radius	$d_o = (0.07 \text{ to } 0.10)\,d_s$
Bolt diameter	$r = (0.10 \text{ to } 0.17)\,d_s$
Number of bolts	
for d_s = 250 to 800	z_b = 10 to 14
for d_s = 750 to 1600	z_b = 16 to 22

The dimensions of the flange and of the bolted joint should be selected according to these relations, and the stresses should be checked. For large welded shafts with thin walls, the recommended relations between the main dimensions of the flange are given in Table X.1 (according to LMZ data).

Figure X.2 shows the shaft of a high-power vertical turbine connected to the generator shaft and the runner cover.

The 5,195 mm long turbine shaft (3) is 1400 mm in diameter. The lower shaft flange is connected to the runner cover by means of eighteen fitted bolts (1) of 165 m diameter with IM160 thread. The nuts (2) are octagonal.

For safety reasons, bolt and nut heads are covered with removable caps (4) fastened to the bolts by means of screws (11). The shaft is guided in a rubber-lined bearing. The diametrical clearance between shaft and bearing, when new, varies from 0.25 to 0.4 mm.

TABLE X.1

Dimensions of thin-wall welded shaft flanges (LMZ data)

d_s	D_f	t	D_b	z	d_b	Bolt	d_s	D_f	t	D_b	z	d_b	Bolt
600	1000	150	820	12	85	1M80	1200	1830	240	1575	20	125	1M120
650	1050	150	870	16	85	1M80	1300	1940	250	1675	20	135	1M130
700	1100	160	920	16	85	1M80	1400	2070	260	1800	20	145	1M140
750	1150	160	970	18	85	1M80	1500	2160	270	1900	20	150	1M140
800	1230	170	1045	20	85	1M80	1600	2330	280	2030	20	170	1M160
850	1300	170	1110	20	90	1M85	1700	2450	290	2140	20	175	1M170
900	1360	180	1165	20	95	1M90	1800	2600	300	2280	20	180	1M175
950	1490	195	1280	20	100	1M95	1900	2710	310	2390	20	185	1M175
1000	1570	210	1350	20	105	1M100	2000	2860	320	2515	20	195	1M190
1100	1650	225	1425	20	115	1M110							

The spigot in the flange joint is provided with a rubber ring (5) for sealing, since oil under pressure flows through the shaft to the runner.

The generator-shaft flange (6) is connected to the turbine shaft flange by means of similar bolts. The shaft attachment (10) fastened to the end of the generator shaft serves also as oil outlet from the turbine oil-supply head.

Cast-iron guide bearings (7) with bronze linings (8) are fitted in the central bore of the turbine and generator shaft. The cast-iron bearings are secured to the shaft by means of locking screws (9). The bearing guides the pipe through which oil is fed to the runner servomotor. The turbine shaft is lined with stainless-steel plates (12) at the bearing and the stuffing box. In this example the lining is continuous over the bearing and the packing, but it is preferable to make the lining in sections that can be replaced separately when necessary. This is important since the lining wears more quickly at the packing than at the bearing.

Figure X.3 shows a forged turbine shaft with all dimensions for a 200,000 kw turbine. The shaft is relatively thin-walled, thus facilitating production of a one-piece forging. The transition from the relatively thick flange to the actual shaft is conical. The flange, its shape and the dimensions of the bolt holes, and of the machined surfaces are shown in Figure X.3A. Almost all shaft surfaces are machined to surface finish $\nabla 7$, with the exception of the surface in contact with the bearing and the packing which are machined to surface finish $\nabla 8$. Blanks for large two-flange shafts are not suitable for forging since they require much superfluous metal at both ends. The larger the flange diameter, the more difficult it is to forge the flange. A large machining allowance should be provided if the shaft is forged integral with the flanges.

Size and weight of the shaft usually increase considerably with increasing turbine output; this increases the difficulty of manufacturing it as a one-piece forging.

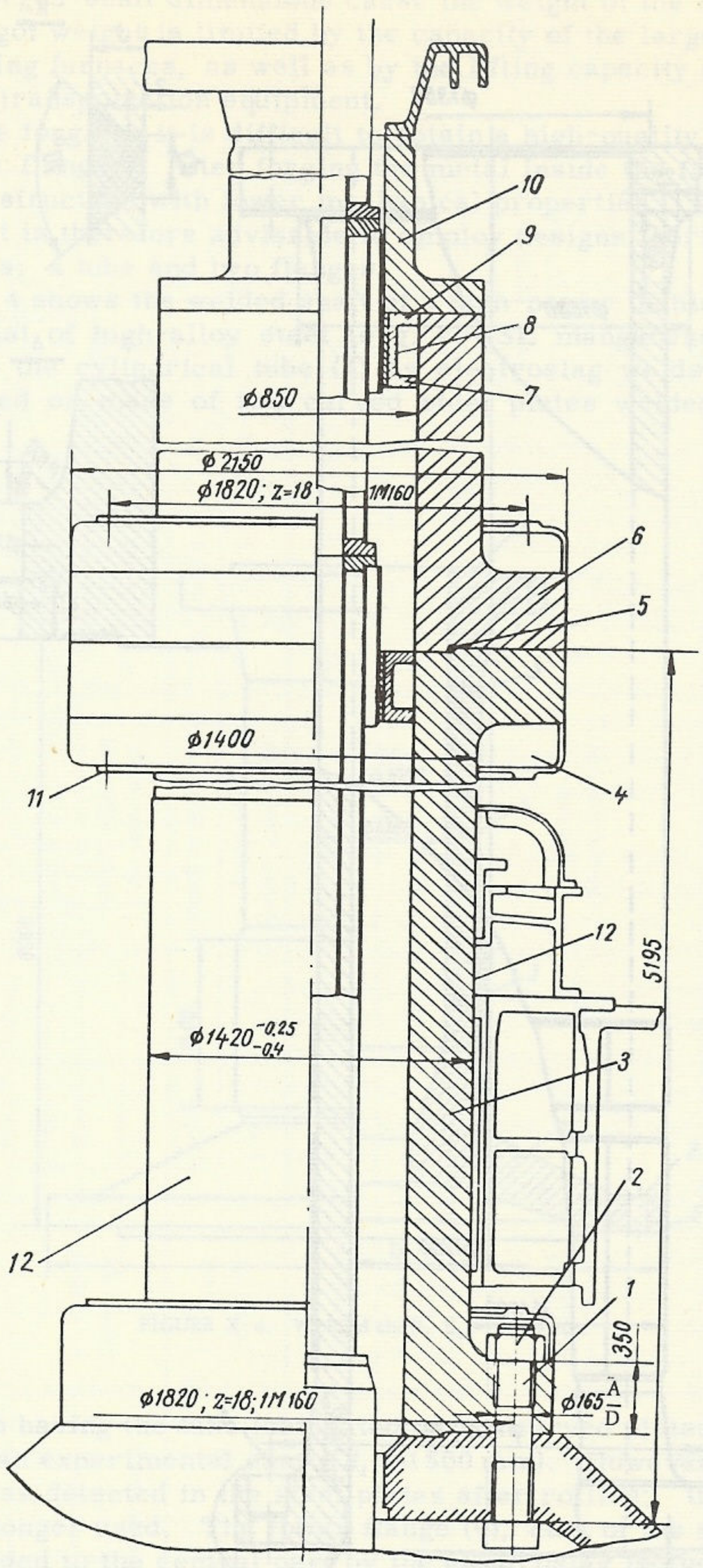


FIGURE X.2. Turbine shaft connected to generator shaft and runner cover

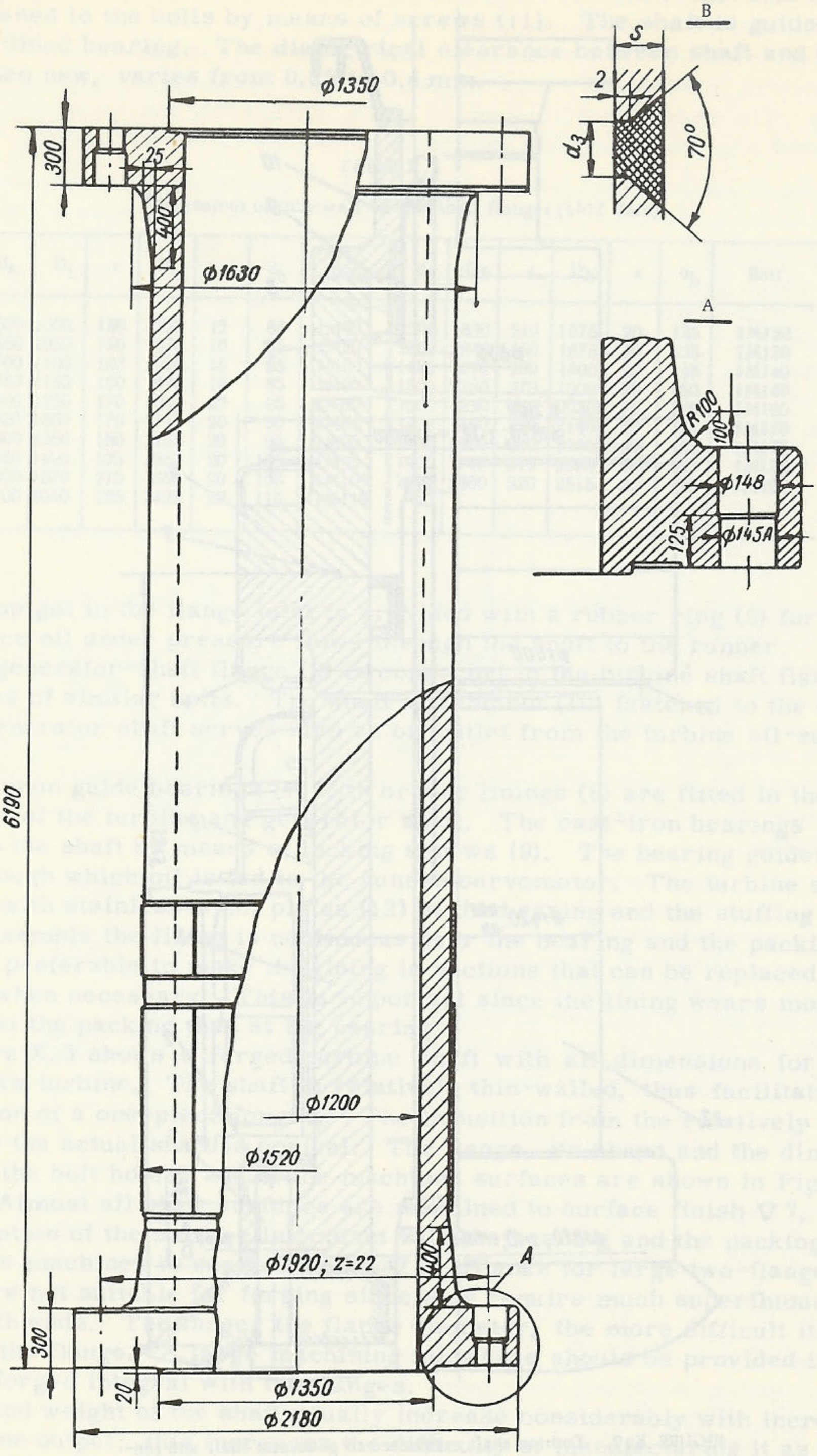


FIGURE X.3. Forged shaft, d_s = 1500 mm

Larger forged-shaft dimensions cause the weight of the ingot to increase. However, ingot weight is limited by the capacity of the large forging presses and the melting furnaces, as well as by the lifting capacity of the cranes and internal transportation equipment.

With large forgings it is difficult to obtain a high-quality forging, particularly at the flanges. After forging the metal inside the flange may have a cast-steel structure with lower mechanical properties. For large shaft dimensions it is therefore advisable to employ designs fabricated from simple blanks: a tube and two flanges.

Figure X.4 shows the welded shaft of a high-power turbine. The upper flange (1) cast of high-alloy steel (e.g. 20GSL manganese silicon steel) is welded to the cylindrical tube (4) by electroslag welds (3). The tube may be forged or made of two curved steel plates welded together longitudinally.

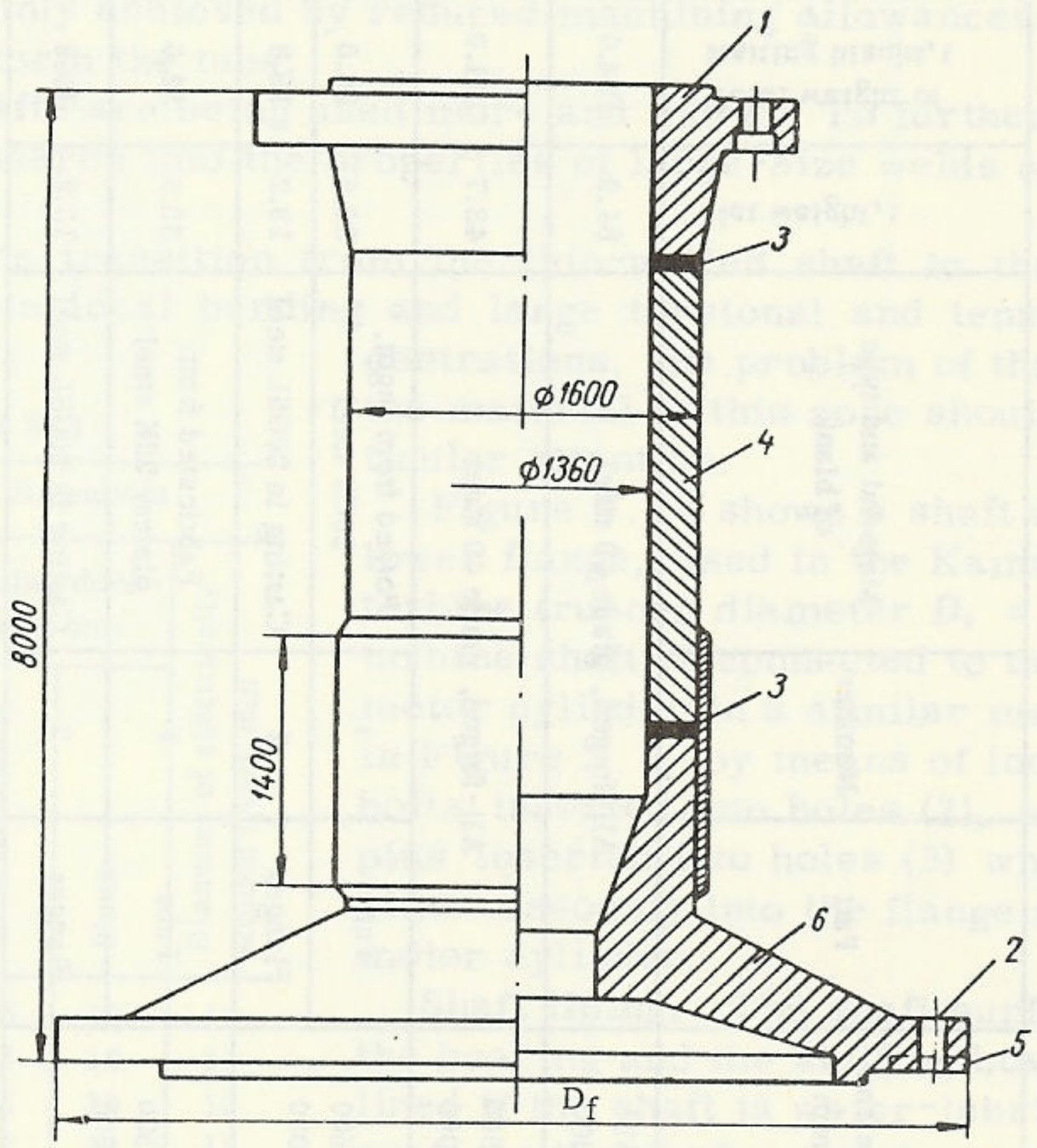


FIGURE X.4. Welded shaft, d_s = 1600 mm

The design having the tube fabricated of two curved plates was used at the LMZ for an experimental shaft (d_s = 1500 mm). However, a tendency to cleavage was detected in the steel plates after rolling; therefore, this design is no longer used. The lower flange (6), cast of the same steel grade, is welded to the central part by the electroslag method. In this design, the lower flange is larger than the upper flange, and is fastened directly to the runner servomotor-cylinder instead of the cover. The outer flange diameter D_f is equal to the outer diameter of the servomotor cylinder. In this design there is no joint between shaft flange and servomotor

TABLE X.2

Engineering-efficiency figures for various designs of shafts for the Bratsk HEP turbine

Type of shaft design	Shaft bore and length, mm	Part	Number	Material and type of blank	Net weight, t	Total weight of starting blanks, t	Total weight of metal used, t	Total time on machine tools, in machine hours		Scrap waste, t	Fraction of metal utilized
								Total	Turning between centers		
Forged shaft	1500/850 L = 6000	All-forged, grade 40 steel			64.0	124.0	223.0	1250	950	160.0	0.29
Forged shaft with thin walls	1800/1500 L = 6000	All-forged, grade 40 steel			43.7	111.0	200.0	1400	1100	156.0	0.22
Shaft from forged tube with flanges welded at both ends	1800/1500 L = 6000	Tube	1	Forged from ingot, 20GS steel	30.5	66.0	105.0	1330	850	90.0	0.33
		Flanges	2	Casting in 20GSL steel	13.2	19.8	27.0				
Shaft fabricated from two curved plates with flanges welded at both ends	1800/1500 L = 6000	Tube	1	Fabricated from plates; 22K steel	30.5	53.0	75.0	1000	480	58.0	0,43
		Flanges	2	Casting in 20GSL steel	13.2	19.8	27.0				

cover. This affords a substantial saving in metal and simplifies manufacture. The use of a similar design for forged shafts has so far been limited by the difficulties in obtaining a forged shaft with flanges of large dimensions; such shafts have therefore been used only in medium-size turbines.

With welded shafts no such limitations exist.

The use of welded shafts is advantageous also from the economic standpoint. This may be seen from Table X.2, where data are given for various shaft designs used for the Bratsk HEP turbines.

Two variants of forged shafts (ordinary and thin-walled), and one welded design are included.

For an ordinary forged shaft of 1500 mm diameter, a 223 t ingot is required; a thin-walled shaft requires 200 t; a forged tube for a welded shaft requires an ingot of only 105 t; this design reduces metal consumption by 35% compared with an all-forged shaft of equal dimensions; manufacturing costs are also less.

With a welded tube, the labor required for machining is reduced by 25%, this being mainly achieved by reduced machining allowances on the welded plates which form the tube.

Welded shafts are being used more and more. To further development, additional research into the properties of large-size welds and their strength is required.

Since at the transition from the thin-walled shaft to the flange there is considerable local bending and large torsional and tensile stress concentrations, the problem of the strength of the material in this zone should be given particular attention.

TABLE X.3

Shaft-lining dimensions

Shaft diameter, mm	Lining thickness, mm		Diameter of electrically welded rivets, mm
	After machining	Blanks	
250 — 400	5.5	10	10
450 — 700	6.5	10	10
750 — 1100	7.5	10	12
1100 — 1600	9.0	12	15

Figure V.14 shows a shaft with a large lower flange, used in the Kamsk HEP Kaplan turbine (runner diameter D_1 = 5.0 m). The turbine shaft is connected to the runner-servomotor cylinder in a similar manner, as shown in Figure X.4, by means of loosely fitting bolts inserted into holes (2), and cylindrical pins inserted into holes (5) which are drilled simultaneously into the flange and the servomotor cylinder.

Shaft lining. The shaft surfaces adjoining the bearing and the stuffing box are usually lined if the shaft is water-lubricated. Lining protects the shaft against corrosion, which is intensive when rubber bearings are used. because of the organic sulfur compounds contained in the rubber. The lining may be made of either bronze or stainless steel. If bronze is used, chemical reaction is liable to occur between metal and rubber, particularly if bearing and lining are both immersed in water.

In general, Soviet designers use linings of 1Kh18N9T stainless austenitic steel (ultimate strength = 58 kg/mm^2, yield strength = 20 kg/mm^2, elongation = 40%), which may be welded without preheating, which usually causes internal stresses.

Shaft linings made of stainless steel plates are shown in Figures X.2 and X.3. Depending on the diameter, the shaft lining consists of two or three parts, connected by welded seams. In longitudinal direction it may consist

of a single plate or of several plates welded together, depending on bearing length and available plate sizes.

The lining plates are usually provided with a machining allowance for subsequent turning of the shaft to the required dimensions. The lining parts, made of the same steel grade, are fixed on the shaft by special clamps and welded together. For better adhesion to the shaft the lining plates are secured by welded rivets (Figure X. 3,b) spaced at about 200 mm.

The thickness of the lining for various shaft diameters is shown in Table X. 3.

The disadvantage of this design is that the worn lining must be replaced in the workshop.

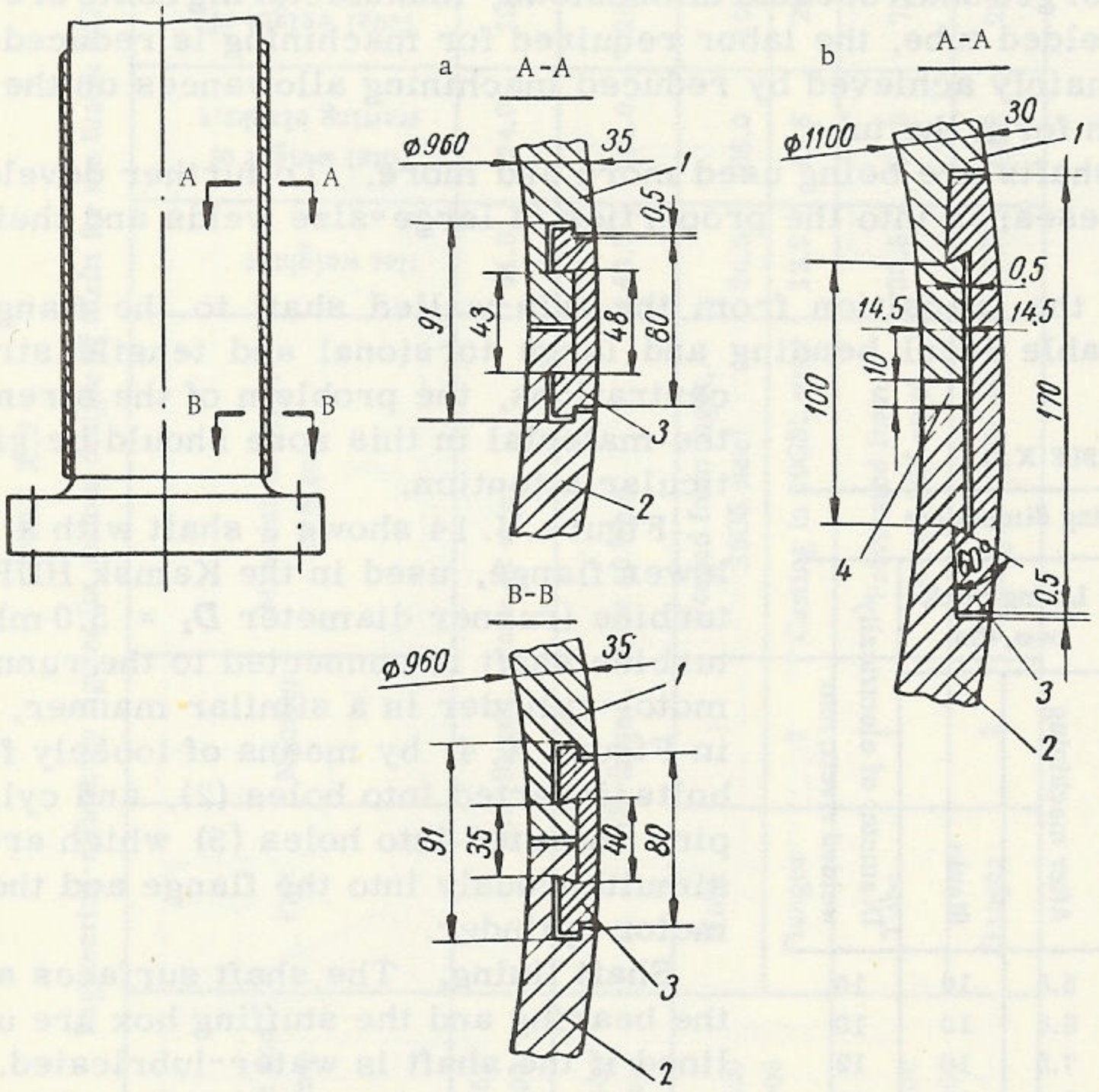


FIGURE X.5. Detachable shaft linings

a — Escher-Wyss design; b — LMZ design.

In one instance, however, a 600 mm-diameter shaft lining was replaced in situ. The new lining was made beforehand in the workshop, and fixed to a special drum simulating the turbine shaft. The lining was then machined on the drum according to the "as new" dimensions of the old lining, and was then welded to the shaft at the hydroelectric plant. The surfaces of the seams and welded rivets were manually ground away and the lining surface was checked by means of templates and a straight rule. The play of the shaft in the bearing did not exceed 0.1 mm after repairs had been effected.

Other methods of lining the shaft are also in use.

Figure X. 5,a shows a detachable lining used by Escher Wyss for a 960 mm diameter turbine shaft. It consists of two halves (1) and (2), connected by means of a wedge-shaped lock (3) which permits the assembly, dismantling, and replacement of the lining halves.

The lining in this design is 35 mm thick.

Figure X. 5,b shows another design of a detachable lining for a 1100 mm diameter shaft. The two halves (1) and (2) are joined by means of dovetailed lock (3) having a slight longitudinal taper. Oak pieces (4) are inserted into the joints between the two halves to facilitate assembly. This is done by first tightening the lining by means of bands, whereupon lock (3) is slipped cold over one of the joints, while another lock preheated to between 300 and 400°C is slipped over the other joint. After cooling, this causes prestressing that forces the lining tightly against the shaft. After the jackets are mounted, all the vertical joints (0.5 mm wide) must be carefully smoothed out, because any protruding edges may damage the bearing and cause accelerated wear. The detachable linings described were never widely used because of the large amount of labor required to make the lock joint, and because of the longitudinal seams on the shaft lining that cause bearing wear irrespective of surface finish.

Flame-spraying of small and medium turbine shafts with stainless steel has been successfully carried out at the Ural' Plant for Hydraulic Machine and Equipment /19/. The process consists of fusing by electric arc a grade OKh18N9 stainless-steel wire and spraying the particles on the shaft surface by a jet of compressed air. An EM-6 spray gun was used, the shaft being mounted on an ordinary lathe.

63. DESIGN OF VERTICAL TURBINE SHAFTS

The shaft of a vertical turbine is simultaneously subjected to tension and torsion.

At the LMZ, the shaft diameter is selected from a chart according to the torsional stress. The permissible torsional stresses τ_{max} may attain 400 to 450 kg/cm^2, which, including the tensile stresses, amounts to a combined stress of about 850 to 900kg/cm^2. The tensile stresses in the shaft during transverse and torsional oscillations, are later checked.

The strength of the shaft is calculated for the maximum shear stresses.

The torque is

$$M_t = 97\,400 \frac{N}{n} \text{ kgcm},$$

where N = power transmitted by the shaft, kw;

n = rpm.

The torsional stress in the shaft is

$$\tau = \frac{M_t}{W_p},$$

where

$$W_p = \frac{\pi}{16 d_e} (d_e^4 - d_o^4).$$

Thus

$$\tau = \frac{97400 N d_e 16}{\pi n (d_e^4 - d_o^4)} \text{ kg/cm}^2, \qquad \text{(X. 1)}$$

where d_e = outer shaft diameter;
d_0 = diameter of central shaft bore.

The tensile stress in the shaft is

$$\sigma_z = \frac{P}{F} = \frac{4P}{\pi\left(d_e^2 - d_0^2\right)}; \qquad (X.2)$$

$$P = p_z + G_0,$$

where p_z = axial water pressure;
G_0 = weight of runner and shaft.

The combined stress

$$\sigma = \sqrt{\sigma_z^2 + 4\tau^2}\ \text{kg/cm}^2. \qquad (X.3)$$

When the turbine operates under generator short-circuit conditions, the torque may increase four- or fivefold for a short period.

A. E. Zhmud' investigated these emergency operating conditions, and found that the additional shaft stresses depend on the ratio $\mu = \frac{J_1}{J_2}$, where J_1 = moment of inertia of the turbine runner, and J_2 = moment of inertia of the generator rotor.

In vertical-shaft units, the moment of inertia of the generator rotor considerably exceeds the moment of inertia of the turbine runner.

The value of μ varies between 0.02 and 0.15. Large values of μ correspond to low-speed units with large-size runners. The large moment of inertia of the generator rotor acting as flywheel damps the torsional oscillations occurring during short circuits, and reduces rotor acceleration; the relatively small moment of inertia of the turbine runner does not lead to any significant twisting of the turbine shaft; thus, the additional stresses in the shaft caused by the short-circuit are insignificant, and may be disregarded in strength calculations.

Shaft flanges. At LMZ the shaft flange is usually calculated by formulas (VI. 196, VI. 197, VI. 198).

The shaft flange is thus considered as an elastic plate joined to a shell at its inner edge, with the free outer edge subjected to a uniformly distributed load along it. For shafts in which the wall thickness exceeds the flange thickness, $(g \geqslant t)$ (Figure X. 6), the effect of shell deformation may be neglected. In this type of flange only the radial stresses need be calculated. The formulas of Waters and Taylor apply as follows:

Radial stresses

$$\sigma_r = \frac{p_p}{t^2} \cdot \frac{F_1}{F_2 A F_3}. \qquad (X.4)$$

Tangential stresses

$$\sigma_t = 0.3\sigma_r \left(1 + \frac{7}{3} A\right), \qquad (X.5)$$

where the rated force p_p is

$$p_p = \frac{r_3 - r_m}{r_1 - r_m}(p_z + G_0), \qquad (X.6)$$

F_1, F_2, F_3 = coefficients found from the chart (Figure X. 6);

$$A = 0.506 \left(\frac{t}{g}\right)^3 \sqrt{\frac{g}{r_m}}\, z,$$

where z = coefficient depending on shaft length and diameter (Figure VI. 57);
for turbine shafts $z = 1$;

r_1, r_3, r_m, t, g = flange dimensions according to Figure X. 6.

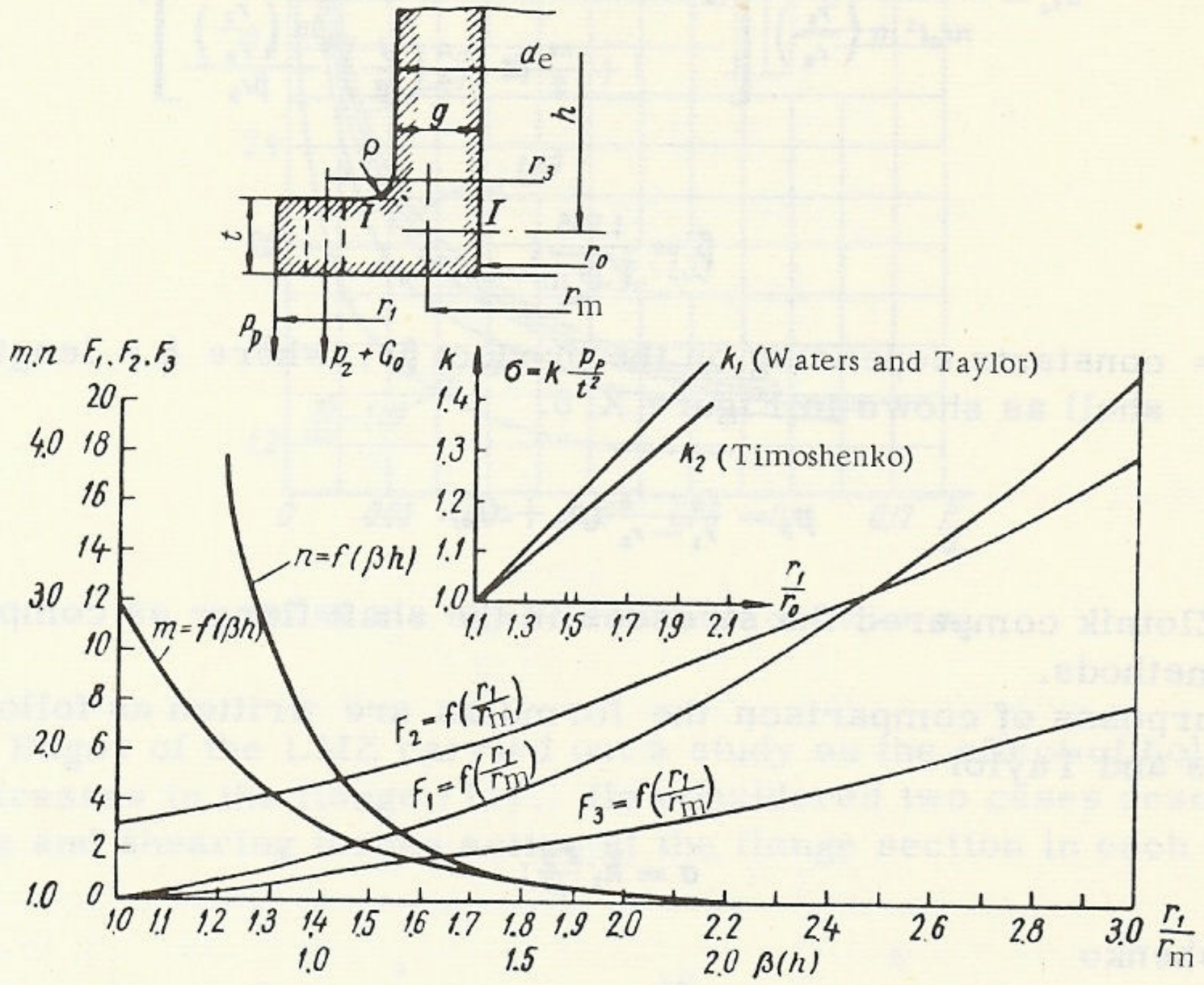


FIGURE X.6. Diagram for calculating the shaft-flange stresses

In a thin-walled shaft, where $g \leqslant t$, the axial stresses are highest:

$$\sigma_a = \sigma_r \left(\frac{t}{g}\right)^2. \qquad \text{(X. 7)}$$

The axial stresses should be added to the tensile stresses σ_z. Consequently, in this case, the combined stress in the shaft is

$$\sigma_{np} = \sqrt{(\sigma_z + \sigma_a)^2 + 4\tau^2}\ \text{kg/cm}^2. \qquad \text{(X. 8)}$$

The stress in the flange may also be calculated by S. P. Timoshenko's formulas, which assume that the flange is deformed like a rigid ring, with no distortion of the cross section. The outer edge of the ring is considered to be free, and the inner edge connected to the thin shell.

The bending stress at section I-I (Figure X. 6) is

$$\sigma_{I-I} = \frac{3P_p (r_1 - r_0)}{\pi r_0 g^2} \cdot \frac{1}{1 + \frac{m}{2}\beta t + \frac{n}{2}\left(\frac{t}{g}\right)^3 \frac{\ln\left(\frac{r_1}{r_0}\right)}{\beta r_0}}. \qquad \text{(X. 9)}$$

The shear stress at section I-I is

$$\tau_{I-I} = \frac{\beta P_p (r_1 - r_0)}{2\pi r_0 g} \cdot \frac{1}{1 + \frac{m}{2}\beta t + \frac{n}{2}\left(\frac{t}{g}\right)^3 \frac{\ln\left(\frac{r_1}{r_0}\right)}{\beta r_0}}. \qquad \text{(X. 10)}$$

The tangential bending stress at the inner flange edge is

$$\sigma_{t_0} = \frac{3P_p (r_1 - r_0)}{\pi r_0 t^2 \ln\left(\frac{r_1}{r_0}\right)} \left[1 - \frac{1 + \frac{\beta t}{2}}{1 + \frac{m}{2}\beta t + \frac{n}{2}\left(\frac{t}{g}\right)^3 \frac{\ln\left(\frac{r_1}{r_0}\right)}{\beta r_0}} \right], \qquad \text{(X. 11)}$$

where

$$\beta = \frac{1.285}{\sqrt{g r_m}};$$

m and n = constants depending on the product βh, where h = length of the shell as shown in Figure X. 6.

$$p_p = \frac{r_3 - r_0}{r_1 - r_0}(p_z + G_0).$$

L. S. Zlotnik compared the stresses in the shaft flange as computed by various methods.

For purposes of comparison the formulas are written as follows:

Waters and Taylor

$$\sigma = k_1 \frac{P_p}{t^2};$$

Timoshenko

$$\sigma = k_2 \frac{P_p}{t^2}.$$

The values of k_1 and k_2 for different ratios $\frac{r_1}{r_0}$ are given in Figure X. 6.

The chart shows that the differences in results of calculations by either formula do not exceed 7 to 8%; Timoshenko's formula yields smaller stress values. In both methods, the pattern of the stress distribution along the tubular part of the shaft is almost the same. The stress concentration at the fillet, of radius ϱ, between flange and shaft raises the torsional stresses.

The maximum shear stress is

$$\tau_1 = \alpha_\tau \tau, \qquad \text{(X. 12)}$$

where α_τ = coefficient of stress concentration, depending on the ratio of flange diameter to fillet radius ϱ.

The value of the stress coefficient should be selected from the graph in Figure X. 7.

In calculating the stresses in the shaft flange by these formulas, the effect of the bolts was not taken into account. The bolted flange joints play an important role by reinforcing the flanges and reducing the bending stresses

at the transition from the flange to the shaft, since by pressing the flanges tightly against each other, the bolts prevent flange twisting. This is particularly important in the design of thin-walled shafts, where the combined stress approaches the yield strength due to the high bending stresses.

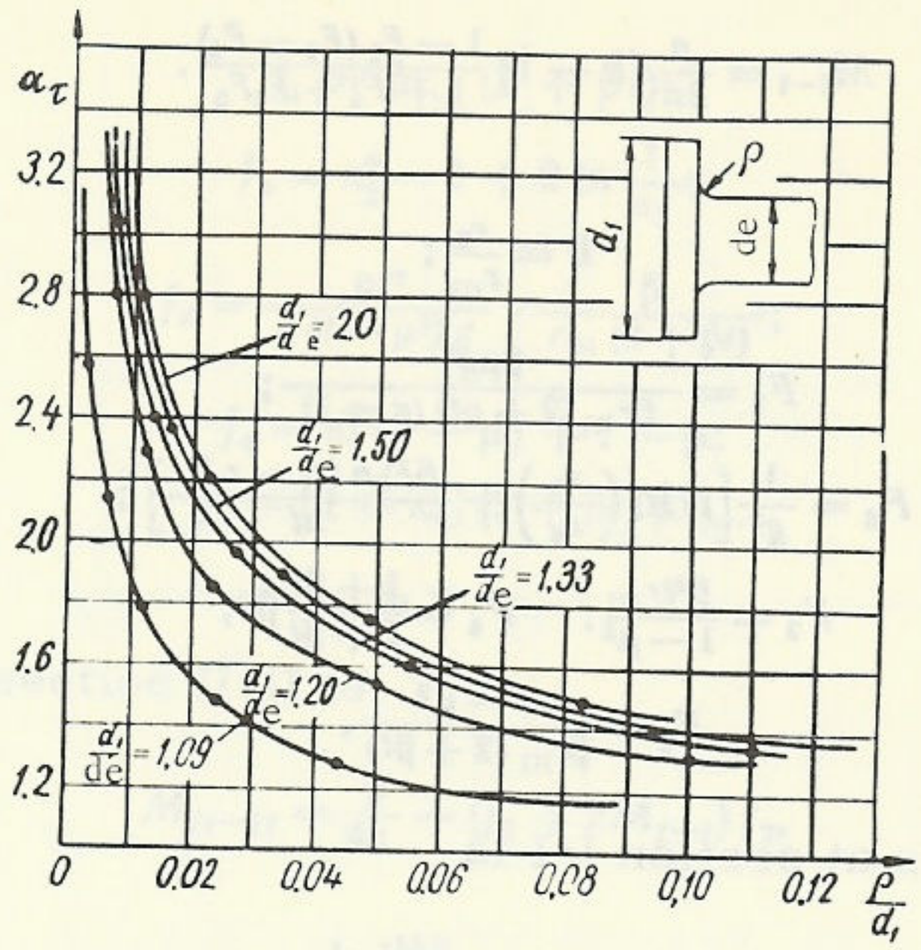


FIGURE X.7. Stress-concentration coefficient α_τ.

A. U. Bugov of the LMZ carried out a study on the effect of bolted joints on the stresses in the flange /11/. He considered two cases describing the moments and shearing forces acting at the flange section in each case.

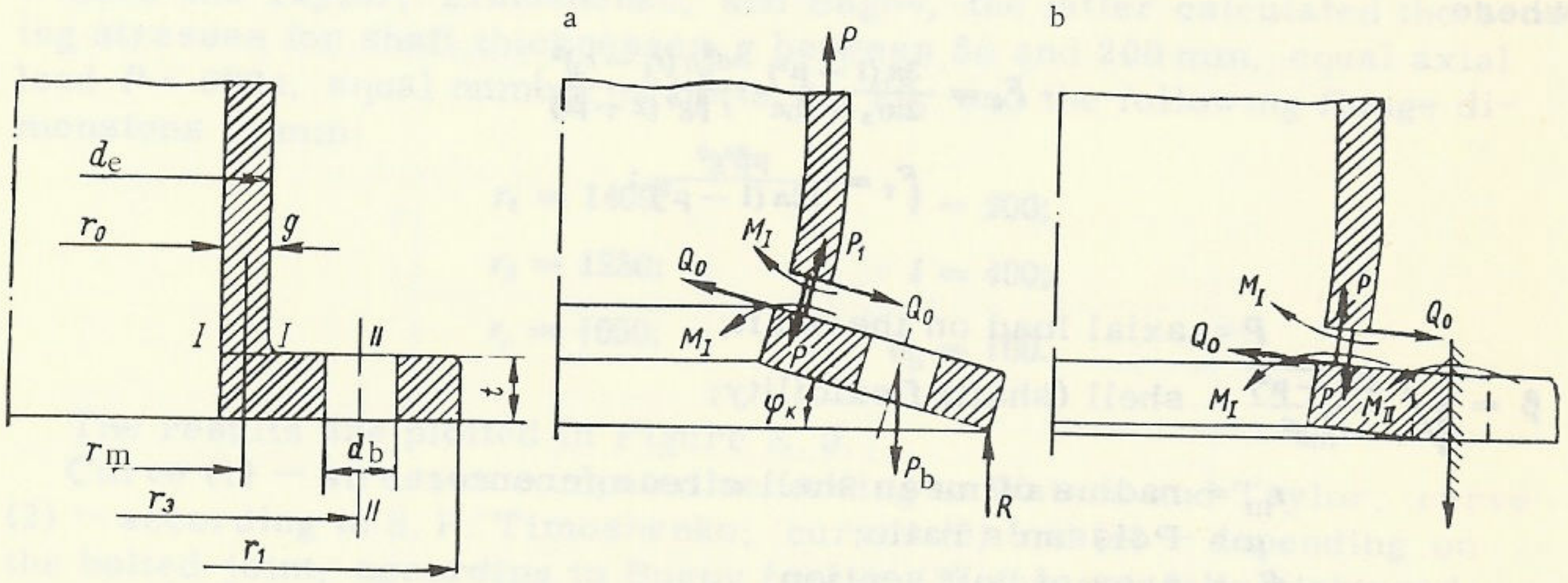


FIGURE X.8. Effect of bolted joints on stresses in the flange

a — bolts not fully tightened, flange may turn freely; b — bolts fully tightened, flange warps.

In the first case the bolts are not fully tightened. The axial load causes the section of the flange to turn through an angle φ without warping (Figure X. 8,a).

In the second case, the bolts are assumed to be fully tightened, causing considerable prestressing. The axial load on the shaft will therefore cause

deformation of the flange sections, and the stresses in the flange should be calculated for bending as an annular plate with the outer edge rigidly fixed by bolts and the inner edge connected to a shell (Figure X. 8,b).

In the first case, the bending moment at section I-I acting on unit length of the shaft mean circumference is

$$M_{I-I} = \frac{p}{2\pi}(k-1)\frac{1-F_1(F_2-F_3)}{1+F_4+F_2F_5}, \qquad (X.13)$$

where

$$k = \frac{r_2}{r_m};$$

$$F_1 = \frac{\beta\mu g^2}{6r_m(2+\varrho t)(\kappa-1)};$$

$$F_2 = \frac{1}{g^3}\left[t^3 \ln\left(\frac{r_1}{r_0}\right) + \frac{6F_b n (r_1-r_3)^2}{\pi l}\right];$$

$$F_3 = \frac{\beta^2 t r_m}{1-\mu^2}; \quad F_4 = \frac{1+\beta t}{2+\beta t}\beta t;$$

$$F_5 = \frac{1-\mu^2}{\beta r_m(2+\beta t)}.$$

The bending stress at section I-I is

$$\sigma_{I-I} = \frac{6M_{I-I}}{g^2}.$$

The bending moment at the cylindrical section II-II of the flange, which is weakened by the bolt holes, is

$$M_{II-II} = F_6(M_{I-I} + F_7 P), \qquad (X.14)$$

where

$$F_6 = \frac{3\pi(1-\mu^2)}{2\pi r_3 - d_b n}\cdot\frac{d_b^2 n (r_1-r_3)^2}{l\,\beta g^3(2+\beta t)};$$

$$F_7 = \frac{\mu\beta^2 g^2}{12\pi(1-\mu^2)};$$

P = axial load on the shaft;

$\beta = \sqrt{\frac{3(1-\mu^2)}{r_m^2 g^2}}$ = shell (shaft) flexibility;

r_m = radius of mean shell circumference;

μ = Poisson's ratio;

F_b = area of bolt section;

n = number of bolts;

l = effective length of bolts;

d_b = bolt diameter.

The remaining symbols, i.e., the flange dimensions, are as in Figure X.8.

The bending stress at section II-II is

$$\sigma_{II-II} = \frac{6M_{II-II}\kappa_2}{t^2} \qquad (X.15)$$

where

$$\kappa_2 = \frac{2\pi r_3}{2\pi r_3 - d_b n}.$$

In the second case, the bending moment at section I-I is

$$M_{I-I} = \frac{P}{4\pi} f_1 \frac{f_2 - f_3 f_4}{\left(\frac{t}{g}\right)^3 f_4 + f_5},$$

where

$$f_1 = \beta r_m (2 + \beta t);$$

$$f_2 = \kappa_2^2 - 1 + 2 \ln \frac{1}{\kappa_1};$$

$$f_3 = \frac{\mu t^3}{3(1-\mu^2) g} \cdot \frac{\beta}{r_m (2 + \beta t)};$$

$$f_4 = \kappa_1^2 (1 + \mu) + 1 - \mu;$$

$$f_5 = (1 - \kappa_1^2)(2 + \beta t) \beta r_m;$$

$$\kappa_1 = r_m.$$

The moment at section II-II is

$$M_{II-II} = \frac{P}{4\pi} + (f_6 + 2M_{I-I}) f_7,$$

where

$$f_6 = \frac{P}{2\pi} [\ln \kappa_1 (1 + \mu) + 1];$$

$$f_7 = \frac{\kappa_1^2}{\kappa^2 (1 + \mu) + 1 - \mu}.$$

To provide a basis for comparing results obtained by the methods of Waters and Taylor, Timoshenko, and Bugov, the latter calculated the bending stresses for shaft thicknesses g between 50 and 200 mm, equal axial load P = 900 t, equal number of bolts n = 20, and the following flange dimensions in mm:

$r_1 = 1400$; $t = 200$;

$r_3 = 1250$; $l = 400$;

$r_e = 1050$; $d_b = 160$.

The results are plotted in Figure X. 9.

Curve (1) — stresses computed according to Waters and Taylor; curve (2) — according to S. P. Timoshenko; curves (3) and (4) — depending on the bolted joint, according to Bugov (curve (3) for not fully tightened bolts, curve (4) for prestressed bolts). The chart shows that the stress according to curves (1) and (2) depends mainly on the shaft-wall thickness: the smaller this is, the higher is the stress.

For the bending stress, curves (3) and (4) give values which are nearly independent of the shaft-wall thickness. Curves (1) and (2) are markedly different from curves (3) and (4). The thinner the shaft wall, the greater is this difference. If the bolted joint is also taken into account in calculating the flange strength, the resulting bending stresses are smaller, particularly for thin-walled shafts. It must be noted, however, that these deductions have not yet been checked experimentally.

Permissible radial and tangential stresses in the shaft flange may attain 700 to 800 kg/cm^2.

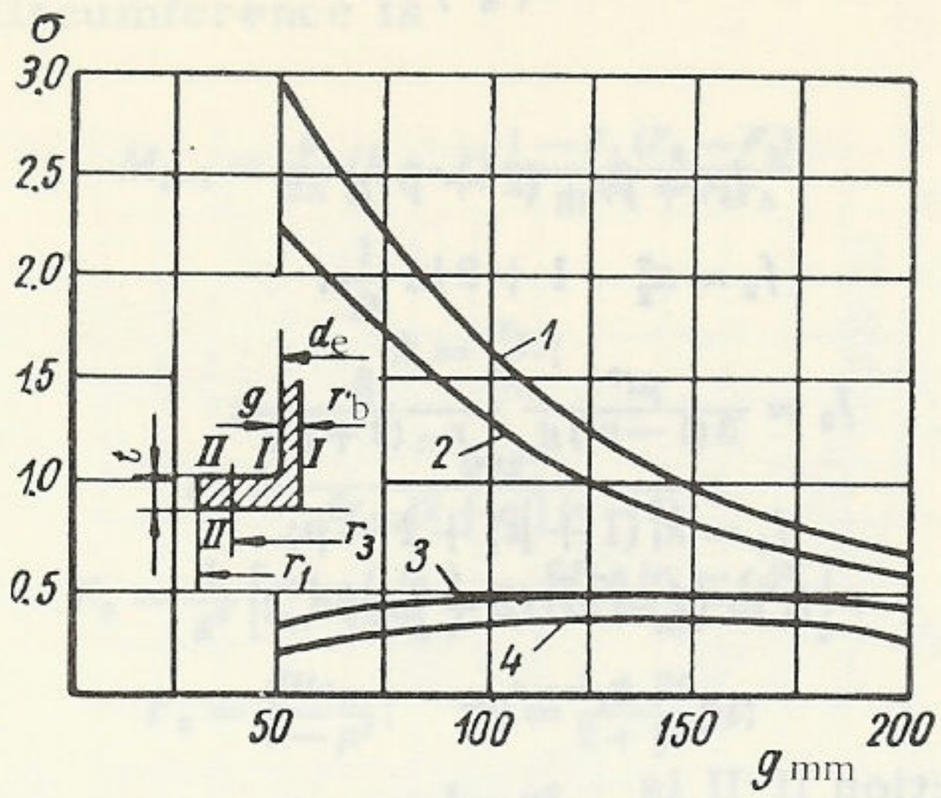


FIGURE X.9. Bending stresses in section I-I of the shaft, calculated by various methods

64. SHAFT VIBRATIONS

Transverse shaft vibrations. At certain critical speeds, when the number of revolutions per second coincides exactly with one of the natural shaft frequencies, strong vibrations may set in. Transverse vibrations may occur due to an asymmetry of the magnetic field in the generator, an imbalance of the rotating parts of the turbine, or a nonsymmetrical water flow.

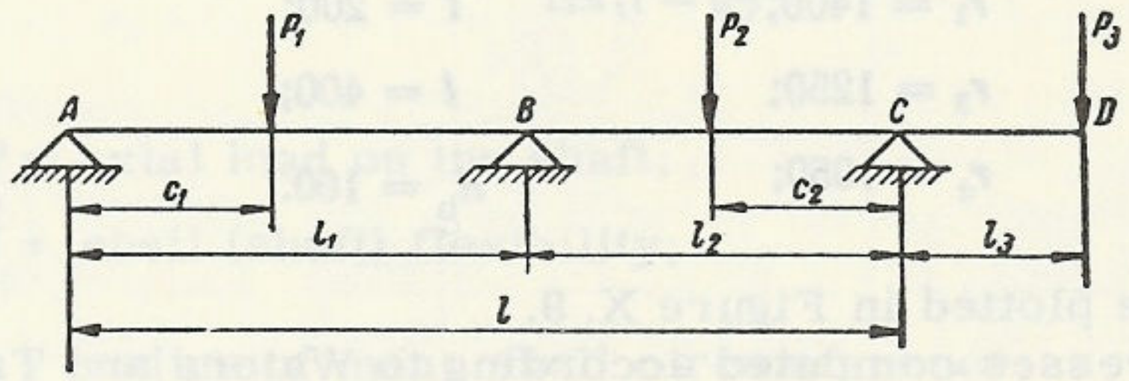


FIGURE X.10. Loads acting on horizontal shaft

Using Lagrange's equations, S. P. Timoshenko proposed a method for determining the natural frequency of a shaft of uniform cross section, with three bearings and two concentrated loads.

For a hydro unit with three bearings and three acting forces (Figure X. 10), the shaft vibrations may be determined similarly.

Figure X.10 shows the load diagram of the shaft, with the following notations:

P_1 = weight of generator rotor and shaft portion AB;

P_2 = weight of shaft portion BC;

P_3 = weight of turbine runner and shaft portion CD.

The statical deflections due to these forces are

$$\left.\begin{aligned} y_1 &= aP_1 + bP_2 + cP_3; \\ y_2 &= bP_1 + dP_2 + lP_3; \\ y_3 &= cP_1 + lP_2 + fP_3, \end{aligned}\right\} \qquad (X.18)$$

where a, b, c, d, l and f = deflection coefficients.

The kinetic energy of the system, when the weights P_1, P_2 and P_3 oscillate in the vertical plane through the shaft (Figure X.10) about their equilibrium positions, is

$$T = \frac{P_1}{2g}(y_1')^2 + \frac{P_2}{2g}(y_2')^2 + \frac{P_3}{2g}(y_3')^2. \qquad (X.19)$$

The forces that balance the deflections given by equations (X.18) may be found by Cramer's rule

$$\left.\begin{aligned} Q_1 &= \frac{y_1(df - l^2) + y_2(lc - bf) + y_3(bl - cd)}{c(bl - cd) + l(bc - dl) + f(ad - b^2)}; \\ Q_2 &= \frac{y_1(cl - bf) + y_2(af - c^2) + y_3(bc - al)}{c(bl - cd) + l(bc - dl) + f(ad - b^2)}; \\ Q_3 &= \frac{y_1(bc - cd) + y_2(bc - al) + y_3(ad - b^2)}{c(bl - cd) + l(bc - dl) + f(ad - b^2)}. \end{aligned}\right\} \qquad (X.20)$$

The change in potential energy is

$$V = \frac{Q_1 y_1}{2} + \frac{Q_2 y_2}{2} + \frac{Q_3 y_3}{2}.$$

Substituting from (X.20), we obtain

$$V = \frac{1}{2}\,\frac{y_1^2(df - l^2) + 2y_1y_2(cl - bf) + 2y_1y_3(bc - cd) + y_2^2(af - c^2) + 2y_2y_3(bc - al) + y_3^2(ad - b^2)}{c(bl - cd) + l(bc - al) + f(ad - b^2)}. \qquad (X.21)$$

Lagrange's equation is

$$\frac{d}{dt}\left(\frac{\partial T}{\partial g_i'}\right) - \frac{\partial T}{\partial g_i} + \frac{\partial V}{\partial g_i} = 0.$$

By considering (X.19) and (X.21) as well, we obtain the following differential equations:

$$\left.\begin{aligned} \frac{Q_1 y_1''}{g} + \frac{y_1(df - l^2) + y_2(cl - bf) + y_3(bl - cd)}{c(bl - cd) + l(bc - al) + f(ad - b^2)} &= 0; \\ \frac{Q_2 y_2''}{g} + \frac{y_1(cl - bf) + y_2(af - c^2) + y_3(bc - al)}{c(bl - cd) + l(bc - al) + f(ad - b^2)} &= 0; \\ \frac{Q_3 y_3''}{g} + \frac{y_1(bl - cd) + y_2(bc - al) + y_3(ad - b^2)}{c(bl - cd) + l(bc - al) + f(ad - b^2)} &= 0. \end{aligned}\right\} \qquad (X.22)$$

If the shaft vibrates at one of its natural frequencies,

$$y_1 = \lambda_1 \cos(pt - \alpha); \qquad y_2 = \lambda_2 \cos(pt - \alpha); \qquad y_3 = \lambda_3 \cos(pt - \alpha). \qquad (X.23)$$

By inserting the values of y_1, y_2 and y_3 from equation (X. 23) into equation (X. 22), and denoting the denominator $c(bl - cd) + l(bc - al) + f(ad - b^2)$ by A, we obtain

$$\left.\begin{aligned}
&\lambda_1\left(\frac{df - l^2}{A} - \frac{Q_1}{g}p^2\right) + \lambda_2\frac{cl - bf}{A} + \lambda_3\frac{bl - cd}{A} = 0;\\
&\lambda_1\left(\frac{cl - bf}{A}\right) + \lambda_2\left(\frac{af - c^2}{A} - \frac{Q_2}{g}p^2\right) + \lambda_3\frac{bc - al}{A} = 0;\\
&\lambda_1\frac{bl - cd}{A} + \lambda_2\frac{bc - al}{A} + \lambda_3\left(\frac{ad - b^2}{A} - \frac{Q_3}{g}p^2\right) = 0.
\end{aligned}\right\} \qquad (X.24)$$

To obtain the frequency, the determinant of these equations has to be equated to zero:

$$\left\{\begin{aligned}
&\frac{df - l^2}{A} - \frac{Q_1p^2}{g}; \quad \frac{cl - bf}{A}; \quad \frac{bl - cd}{A}\\
&\frac{cl - bf}{A}; \quad \frac{af - c^2}{A} - \frac{Q_2}{g}p^2; \quad \frac{bc - al}{A}\\
&\frac{bl - cd}{A}; \quad \frac{bc - al}{A}; \quad \frac{ad - b^2}{A} - \frac{Q_3}{g}p^2
\end{aligned}\right\} = 0.$$

After expanding the determinant, transforming, and denoting p^2 by κ, we obtain the equation of the frequency of the natural transverse shaft vibrations

$$\kappa^3 - \frac{g^2}{AQ_1Q_2Q_3}[(ad - b^2)Q_1Q_2 + (af - c^2)Q_1Q_3 + (df - l^2)Q_2Q_3]\kappa^2 + \qquad (X.25)$$
$$+ \frac{g^2}{AQ_1Q_2Q_3}(QQ_1 + dQ_2 + fQ_3)\kappa - \frac{g^3}{AQ_1Q_2Q_3} = 0.$$

The roots of the resulting cubic equation in p^2 give the frequencies of the three main modes of vibration of the system. To each value of p a particular critical speed corresponds

$$n_{cr} = \frac{30p}{\pi} \text{ rpm.}$$

A cubic equation of the type $y^3 - a_1y^2 + a_2y + a_3 = 0$ may be solved by Cardano's method. According to this method, a new unknown quantity x is introduced instead of y

$$y = x + \delta,$$

so that the equation becomes

$$x^3 + px - q = 0.$$

The roots of this equation (when there are three real roots) are determined by the formula

$$x = 2\sqrt[3]{r}\cos\frac{\varphi + 2\pi\gamma}{3},$$

where

$$r = \sqrt{-\frac{p^3}{27}}; \quad \cos\varphi = -\frac{q}{2r}; \quad \gamma = 0, 1, 2.$$

The deflection coefficients a_1, b, c, d, l and f may be found by considering the shaft to be a statically indeterminate beam resting on three supports. With the notations in Figure X. 10 we have

$$\left.\begin{aligned}
a &= \frac{1}{12ll_1^2EJ}\{4l_1^2(l-c_1)^2c_1^2 - c_1(-c_1^3 + l^2c_1 - l_2^2c_1)(l^2 - l_2^2 - c_1^2)\};\\
b &= \frac{1}{12ll_1l_2EJ}\{2l_1l_2c_1c_2(l^2 - c_1^2 - c_2^2) - c_1c_2(l^2 - l_2^2 - c_1^2)(l^2 - l_1^2 - c_2^2)\};\\
c &= \frac{1}{12ll_1EJ}\{2l_1l_2l_3c_1(l^2 - c_1^2) - l_3c_1(l^2 - l_1^2)(-c_1^2 + l^2 - l_2^2)\};\\
d &= \frac{1}{12ll_2^2EJ}\{4l_2^2(l-c_2)^2c_2^2 - c_2(-c_2^3 + l^2l_2 - l_1^2c_2)(l^2 - l_1^2 - c_2^2)\};\\
l &= \frac{1}{12ll_2^2EJ}\{2l_2^2l_3c_2(c_2^2 - 3lc_2 + 2l^2) - l_3c_2(l^2 - l_1^2)(l^2 - l_1^2 - c_2^2)\};\\
f &= \frac{1}{12ll_2^2EJ}\{4ll_2^2l_3^2(l + l_3) - l_3^2(l^2 - l_1^2)^2\}.
\end{aligned}\right\} \qquad (X.26)$$

LMZ designers generally determine the frequency of the first-mode transverse vibrations of a shaft of uniform rigidity by Rayleigh's approximate method. By this method, the complex system of the rotating parts is transformed into a system with one degree of freedom. This increases the rigidity of the system, the resulting vibration frequencies thus being slightly higher than the exact values.

By Rayleigh's method, the vibration frequency is

$$p = \sqrt{\frac{g\Sigma P_i y_i}{\Sigma P_i y_i^2}} \qquad (X.27)$$

and the critical speed

$$n_{cr} = \frac{30}{\pi}\sqrt{\frac{g\Sigma P_i y_i}{\Sigma P_i y_i^2}}, \qquad (X.28)$$

where P_i = force at i-th point;

y_i = deflection at i-th point due to the forces.

The values of the deflections, for various conditions of shaft loading common in turbine design, may be found from a chart drawn by L. S. Zlotnik (Figure X. 11) for a shaft supported at two points.

When there are several supports, the effect of the intermediate supports may be found from the reactions at these points.

The chart contains equal-deflection curves plotted for a beam supported at two points, the beam being loaded by unit force (P = 1) at any point between the supports or at the overhang. The abscissa gives the point of application of the force along the beam and the ordinate gives the points at which the deflections are to be found. The point of intersection of the coordinates gives the value of the deflection, according to the scale.

Considering the beam resting on four supports, and loaded as in Figure X. 12, the deflections due to the four forces are

$$\left.\begin{aligned}
y_1 &= a_{1-1}P_1 + a_{1-2}P_2 + a_{1-3}P_3 + a_{1-4}P_4;\\
y_2 &= a_{2-1}P_1 + a_{2-2}P_2 + a_{2-3}P_3 + a_{2-4}P_4;\\
y_3 &= a_{3-1}P_1 + a_{3-2}P_2 + a_{3-3}P_3 + a_{3-4}P_4;\\
y_4 &= a_{4-1}P_1 + a_{4-2}P_2 + a_{4-3}P_3 + a_{4-4}P_4.
\end{aligned}\right\} \qquad (X.29)$$

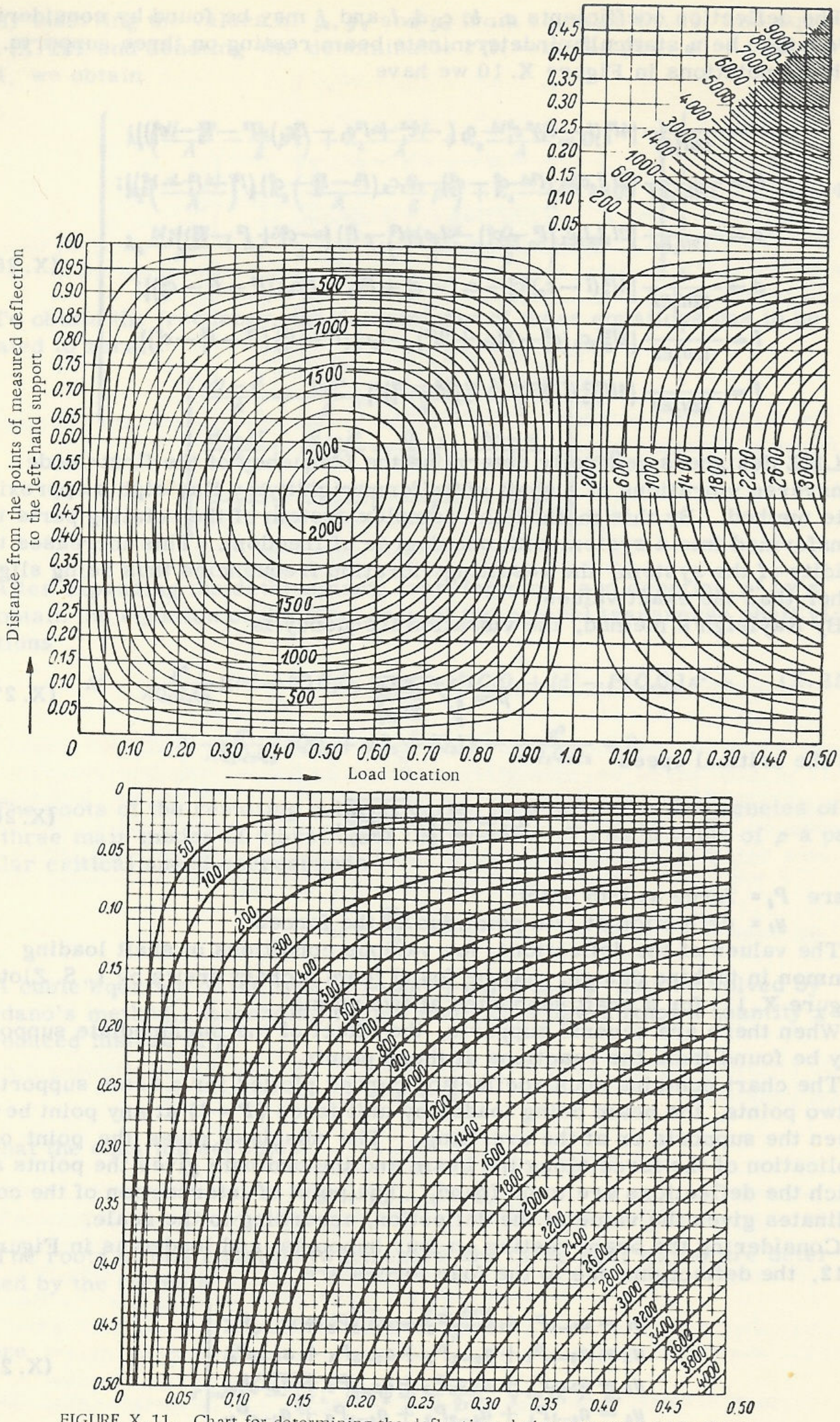


FIGURE X.11. Chart for determining the deflections during transverse shaft vibrations

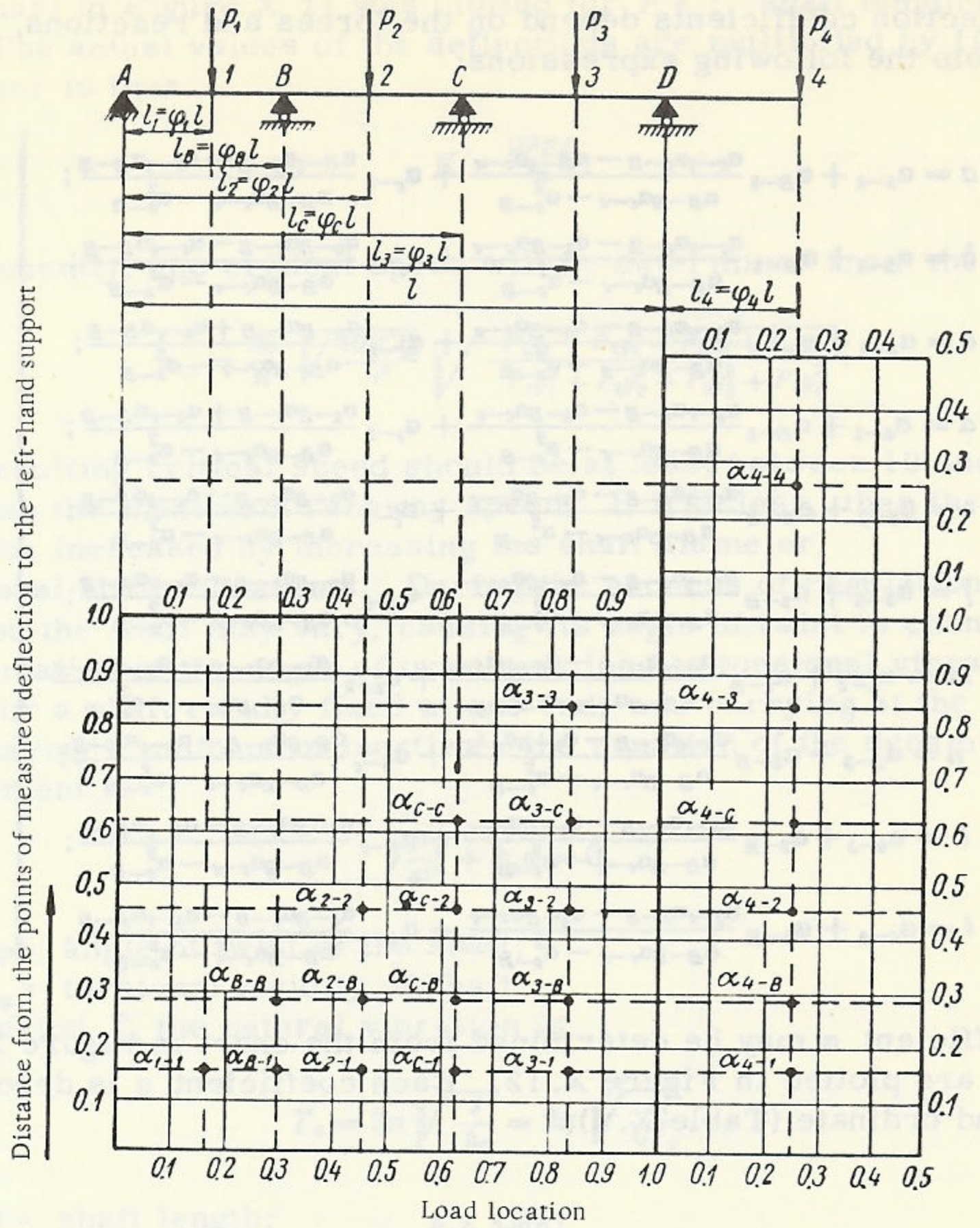


FIGURE X.12. Diagram for calculating the transverse vibrations of a four-support beam

The first subscripts of a indicate the point at which the deflection is to be determined; the second, the force causing the deflection.

According to the theorem of reciprocity we may write

$$\left.\begin{aligned} &a_{1-1} = a; && a_{2-3} = a_{3-2} = f;\\ &a_{1-2} = a_{2-1} = b; && a_{2-4} = a_{4-2} = m;\\ &a_{1-3} = a_{3-1} = c; && a_{3-3} = n;\\ &a_{1-4} = a_{4-1} = d; && a_{3-4} = a_{4-3} = k;\\ &a_{2-2} = e && a_{4-4} = l. \end{aligned}\right\}$$

The deflections are then

$$\left.\begin{aligned} y_1 &= aP_1 + bP_2 + cP_3 + dP_4; \quad y_2 = bP_1 + eP_2 + fP_3 + mP_4;\\ y_3 &= cP_1 + fP_2 + nP_3 + kP_4; \quad y_4 = dP_1 + mP_2 + kP_3 + lP_4. \end{aligned}\right\} \qquad (X.30)$$

The deflection coefficients depend on the forces and reactions, and can be found from the following expressions:

$$\left.\begin{aligned}
a &= \alpha_{1-1} + \alpha_{B-1}\frac{\alpha_{c-1}\alpha_{c-B} - \alpha_{B-1}\alpha_{c-c}}{\alpha_{B-B}\alpha_{c-c} - \alpha_{c-B}^2} + \alpha_{c-1}\frac{\alpha_{B-1}\alpha_{c-B} - \alpha_{c-1}\alpha_{B-B}}{\alpha_{B-B}\alpha_{c-c} - \alpha_{c-B}^2};\\
b &= \alpha_{2-1} + \alpha_{B-1}\frac{\alpha_{c-2}\alpha_{c-B} - \alpha_{2-B}\alpha_{c-c}}{\alpha_{B-B}\alpha_{c-c} - \alpha_{c-B}^2} + \alpha_{c-2}\frac{\alpha_{2-B}\alpha_{c-B} - \alpha_{c-2}\alpha_{B-B}}{\alpha_{B-B}\alpha_{c-c} - \alpha_{c-B}^2};\\
c &= \alpha_{3-1} + \alpha_{B-1}\frac{\alpha_{3-c}\alpha_{c-B} - \alpha_{3-B}\alpha_{c-c}}{\alpha_{B-B}\alpha_{c-c} - \alpha_{c-B}^2} + \alpha_{c-1}\frac{\alpha_{3-B}\alpha_{c-B} + \alpha_{3-c}\alpha_{B-B}}{\alpha_{B-B}\alpha_{c-c} - \alpha_{c-B}^2};\\
d &= \alpha_{4-1} + \alpha_{B-1}\frac{\alpha_{4-c}\alpha_{c-B} - \alpha_{4-B}\alpha_{c-c}}{\alpha_{B-B}\alpha_{c-c} - \alpha_{c-B}^2} + \alpha_{c-1}\frac{\alpha_{4-B}\alpha_{c-B} + \alpha_{4-c}\alpha_{B-B}}{\alpha_{B-B}\alpha_{c-c} - \alpha_{c-B}^2};\\
e &= \alpha_{2-2} + \alpha_{2-B}\frac{\alpha_{c-2}\alpha_{c-B} - \alpha_{2-B}\alpha_{c-c}}{\alpha_{B-B}\alpha_{c-c} - \alpha_{c-B}^2} + \alpha_{c-2}\frac{\alpha_{2-B}\alpha_{c-B} - \alpha_{c-2}\alpha_{B-B}}{\alpha_{B-B}\alpha_{c-c} - \alpha_{c-B}^2};\\
f &= \alpha_{3-2} + \alpha_{2-B}\frac{\alpha_{3-1}\alpha_{c-B} - \alpha_{3-B}\alpha_{c-c}}{\alpha_{B-B}\alpha_{c-c} - \alpha_{c-B}^2} + \alpha_{c-2}\frac{\alpha_{3-B}\alpha_{c-B} - \alpha_{3-c}\alpha_{B-B}}{\alpha_{B-B}\alpha_{c-c} - \alpha_{c-B}^2};\\
m &= \alpha_{4-2} + \alpha_{2-B}\frac{\alpha_{4-c}\alpha_{c-B} - \alpha_{4-B}\alpha_{c-c}}{\alpha_{B-B}\alpha_{c-c} - \alpha_{c-B}^2} + \alpha_{c-2}\frac{\alpha_{4-B}\alpha_{c-B} - \alpha_{4-c}\alpha_{B-B}}{\alpha_{B-B}\alpha_{c-c} - \alpha_{c-B}^2};\\
n &= \alpha_{3-3} + \alpha_{3-B}\frac{\alpha_{3-c}\alpha_{c-B} - \alpha_{3-B}\alpha_{c-c}}{\alpha_{B-B}\alpha_{c-c} - \alpha_{c-B}^2} + \alpha_{3-c}\frac{\alpha_{3-B}\alpha_{c-B} - \alpha_{3-c}\alpha_{B-B}}{\alpha_{B-B}\alpha_{c-c} - \alpha_{c-B}^2};\\
k &= \alpha_{4-3} + \alpha_{3-B}\frac{\alpha_{4-c}\alpha_{c-B} - \alpha_{4-B}\alpha_{c-c}}{\alpha_{B-B}\alpha_{c-c} - \alpha_{c-B}^2} + \alpha_{3-c}\frac{\alpha_{4-B}\alpha_{c-B} - \alpha_{4-c}\alpha_{B-B}}{\alpha_{B-B}\alpha_{c-c} - \alpha_{c-B}^2};\\
l &= \alpha_{4-4} + \alpha_{4-B}\frac{\alpha_{4-c}\alpha_{c-B} - \alpha_{4-B}\alpha_{c-c}}{\alpha_{B-B}\alpha_{c-c} - \alpha_{c-B}^2} + \alpha_{4-c}\frac{\alpha_{4-B}\alpha_{c-B} - \alpha_{4-c}\alpha_{B-B}}{\alpha_{B-B}\alpha_{c-c} - \alpha_{c-B}^2}.
\end{aligned}\right\} \quad (X.31)$$

The coefficient α may be determined from the chart in Figure X.11. The grid points are plotted in Figure X.12. Each coefficient α is denoted by its abscissa and ordinate (Table X.4).

TABLE X.4

Abscissae and ordinates of coefficients α

Coefficient	Abscissa	Ordinate	Coefficient	Abscissa	Ordinate
α_{1-1}	φ_1	φ_1	α_{2-2}	φ_2	φ_2
α_{B-1}	φ_B	φ_1	α_{c-2}	φ_c	φ_2
α_{2-1}	φ_2	φ_1	α_{3-2}	φ_3	φ_2
α_{c-1}	φ_c	φ_1	α_{4-4}	$1+\varphi_4$	φ_2
α_{3-1}	φ_3	φ_1	α_{c-c}	φ_c	φ_c
α_{4-1}	$1+\varphi_4$	φ_1	α_{3-c}	φ_3	φ_c
α_{B-B}	φ_B	φ_B	α_{4-c}	$1+\varphi_4$	φ_c
α_{2-B}	φ_2	φ_B	α_{3-3}	φ_3	φ_3
α_{c-B}	φ_c	φ_B	α_{4-3}	$1+\varphi_4$	φ_3
α_{3-3}	φ_3	φ_B	α_{4-4}	$1+\varphi_4$	$1+\varphi_4$
α_{4-B}	$1+\varphi_4$	φ_B			

According to the notations in Figure X.12,

$$\varphi_1 = \frac{l_1}{l};\quad \varphi_2 = \frac{l_2}{l};\quad \varphi_3 = \frac{l_3}{l};\quad \varphi_4 = \frac{l_4}{l};$$

$$\varphi_B = \frac{l_B}{l};\quad \varphi_c = \frac{l_c}{l}.$$

The chart in Figure X.11 was plotted for $P = 1$, shaft length $l = 1$, and $EJ = 1$. The actual values of the deflections are multiplied by 10^5. The scale factor is thus

$$K = \frac{10^5 EJ}{l^3}.$$

Consequently, the critical speed will be determined from the formula

$$n_{cr} = \frac{30}{\pi} \sqrt{\frac{10^5 EJg}{l^3}} \sqrt{\frac{P_1 y_1 + P_2 y_2 + P_3 y_3 + P_4 y_4}{P_1 y_1^2 + P_1 y_2^2 + P_3 y_3^2 + P_4 y_4^2}}. \quad (X.32)$$

The resulting critical speed should be at least between 10 and 15 percent higher than the maximum runaway speed. If it is less, then the shaft rigidity must be increased by increasing the shaft diameter.

Torsional shaft vibrations. During the process of regulation, the torque exerted on the shaft may vary, causing its angle of twist to change. A periodical variation of the angle of twist may lead to torsional vibration in the shaft. For a shaft rigidly fixed at one end, and carrying at the other end a mass having a moment of inertia J, the equation of the dynamic equilibrium movement is

$$J \frac{d^2\varphi}{dt^2} + k_\varphi \varphi = 0, \quad (X.33)$$

where φ = angle of twist of the shaft;
k_φ = torsional rigidity of shaft.

The period T_0 the natural vibration is

$$T_0 = 2\pi \sqrt{\frac{J}{k_\varphi}} = 2\pi \sqrt{\frac{Jl}{GJ_p}}, \quad (X.34)$$

where l = shaft length;
G = shaft modulus of elasticity in shear;
J_p = polar moment of inertia of the shaft cross section.

The frequency (in cps) is

$$f_0 = \frac{1}{T_0} = \frac{1}{2\pi} \sqrt{\frac{GJ_p}{Jl}}. \quad (X.35)$$

On a shaft with disks at both ends — as in a hydro-unit shaft, with the turbine runner at one end and the generator rotor at the other — the ends will be twisted in opposite directions under torsional vibrations. A certain section of the shaft (the node of the vibration) will remain stationary (Figure X.13). Considering the node as the point at which the shaft is fixed, and assuming that the two disks pass simultaneously through either equilibrium position, viz., the position of the untwisted shaft, and the position of maximum shaft deformation, we obtain the equality

$$2\pi \sqrt{\frac{J_1 l_1}{GJ_p}} = 2\pi \sqrt{\frac{J_2 l_2}{GJ_p}},$$

whence

$$l_2 = \frac{J_1}{J_1 + J_2} l.$$

Thus, the period of the first-mode vibration of a shaft carrying disks at both ends is

$$T = 2\pi \sqrt{\frac{J_1 J_2 l}{(J_1 + J_2) GJ_p}}.$$

The frequency (in cps) is

$$f = \frac{1}{T} = \frac{1}{2\pi} \sqrt{\frac{(J_1 + J_2) GJ_p}{J_1 J_2 l}}. \qquad \text{(X. 36)}$$

The critical speed of the shaft is

$$n_{cr} = 60f = \frac{30}{\pi} \sqrt{\frac{GJ_p (J_1 + J_2)}{J_1 J_2 l}} \text{ rpm}, \qquad \text{(X. 37)}$$

where J_1 = moment of inertia of the turbine runner;
J_2 = moment of inertia of the generator rotor;
l = equivalent shaft length.

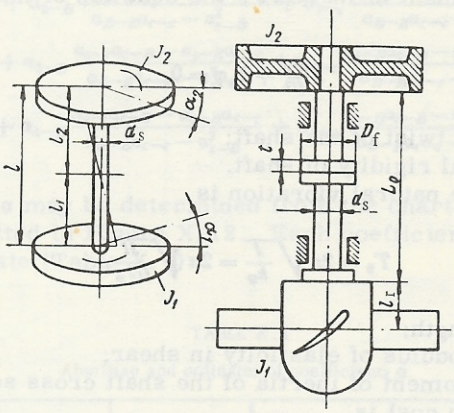


FIGURE X. 13. Torsional vibration of the shaft

When determining the critical shaft speed in torsional vibration (Figure X. 13), the equivalent length of the shaft is

$$l = L_0 - zt\left(1 - \frac{d_s^4}{D_f^4}\right) + l_r\left(\frac{d_s}{2\varrho}\right)^4, \qquad \text{(X. 38)}$$

where z = number of flanges;
L_0 = shaft length;
t = flange thickness;
d_s = shaft diameter;
D_f = flange diameter;
l_r = distance from runner flange to runner cg;
ϱ = radius of gyration of the runner

$$\varrho = \sqrt{\frac{J_1 g}{Q_r}}. \qquad \text{(X. 39)}$$

where Q_r is the runner weight.

The moment of inertia of the Kaplan runner may be approximated by the sum of the moments of inertia of the cylinder (runner hub) and the disk ring (blades)

$$J_{\Sigma 1} = J_h + J_b = \frac{Q_h}{g} \cdot \frac{r_h^2}{2} + \frac{zQ_b}{g} r^2_{cg.b} \text{ tmsec}^2, \qquad \text{(X. 40)}$$

where Q_h = hub weight;
Q_b = blade weight;
r_h = radius of runner hub;
z = number of blades;
$r_{cg.b}$ = radius of blade center of gravity.

The moment of inertia of the generator rotor is

$$J_2 = \frac{GD^2}{4g} \text{tmsec}^2, \qquad \text{(X. 41)}$$

where GD^2 is the flywheel effect of the generator rotor, mt^2.

The polar moment of inertia of the shaft is

$$J_p = \frac{\pi}{16}(d_s^4 - d_0^4).$$

The critical speed of the shaft should exceed the maximum possible runaway speed by at least 10-15 percent.

Excessive shaft vibrations may cause transverse vibrations in the bearings.

Permissible vibration amplitudes of the bearings operating under normal conditions, for various speeds and designs of the hydro unit are given in Table X. 5.

TABLE X. 5

Permissible amplitudes of transverse vibrations of hydro-unit bearings

Rpm	Double amplitude of transverse vibration, mm			
	Vertical hydro units			Horizontal hydro units
	Turbine	Generator		
		Umbrella type	Overhung type	
62.5	0.090	0.090	0.125	—
83.3	0.075	0.075	0.115	—
100.0	0.070	0.070	0.110	—
150.0	0.060	0.060	0.095	—
187.5	0.050	0.050	0.090	—
214.0	0.045	0.045	0.085	0.085
300.0	0.040	0.040	0.075	0.075
375.0	0.035	0.035	0.070	0.070
500.0	0.030	0.030	0.065	0.065
600.0	—	—	—	0.060
750.0	—	—	—	0.055
1000.0	—	—	—	0.050

When shaft vibrations exceed the normal values, the causes must be ascertained and eliminated. The hydro-unit bearings can ensure normal runner operation only if the unit is balanced, with no significant electric or hydraulic perturbation forces acting. Determination of the causes of excessive vibration is sometimes difficult, involving special tests of the unit in actual operation: under no-load conditions with and without water flow, with the generator working as a synchronous motor, and, finally, with the generator as a synchronous motor and the runner out of the water. The generator rotor must be balanced and matched to the generator shaft flanges with maximum precision. After assembly, the shaft alignment is usually checked with a steel wire or with a plumb line, the rotor being turned through 180° and the corresponding distances measured with a dial indicator. This method is more accurate. Methods of checking the shaft alignment are described in detail by Ya. F. Fiterman in /89/.

With relatively low-speed turbines, static balancing usually proves satisfactory under normal operating conditions. If the vibration of the hydro-unit bearings are caused by mechanical imbalance, dynamic balancing must be carried out. The following method is recommended: a trial weight P_0 is successively placed on the rotor at three points 120° apart, and the double amplitude of the vibration is measured in each case. The method is based on the fact that the vibration amplitude varies in direct proportion to the magnitude of the exciting forces

$$Q_1,\ R_1,\ R_2,\ R_3,\ \mu,\ \mu_1,\ \mu_2,\ \mu_3,$$

where Q_1 = exciting force due to rotor imbalance, causing vibrations of amplitude $\frac{1}{2}\mu$;

R_1, R_2, R_3 = exciting forces due to the trial weight when placed successively at three points 120° apart, causing — in combination with force Q — vibrations of amplitude $\frac{1}{2}\mu_1, \frac{1}{2}\mu_2, \frac{1}{2}\mu_3$.

With the value of P_0 known, we determine the imbalance vector by measuring μ_1, μ_2, and μ_3. This gives the magnitude and position of the required balancing weight.

65. CALCULATION OF THE FLANGE-JOINT BOLTS

In turbine construction, fitted bolts are usually prestressed to 1200 kg/cm^2, the prestressing load being two or three times the external load. Under these conditions, the axial load on the shaft cannot open the joint between the flanges. To check the prestressing of the bolts, a special measuring device (Figure X. 14) is used, which measures bolt elongation by means of a dial indicator. Rod (1) is introduced into the central opening of bolt (2) and fastened to the bolt head. The indicator dial is fastened to the other bolt end. The magnitude δ of the bolt elongation is determined by the indication on the dial. The required value of δ is found from the formula

$$\delta = \frac{l\sigma}{E} \text{ mm},$$

where l = length of the bolt;

σ = stress;

E = modulus of elasticity.

To avoid oil leakages from the servomotor cylinder, the bolts on the flange connection between the shaft and the cover of the Kaplan runner should not be bored through. A small undrilled portion should be left at the bottom, to which the measuring rod is attached.

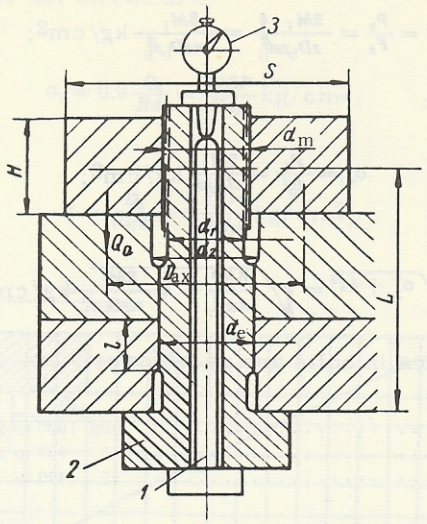


FIGURE X.14. Device for measuring the prestressing of the bolt

If an axial load P acts on the shaft, the axial force including prestressing acting on each bolt, is

$$Q_0 = \frac{1.7P}{z},$$

where z = number of bolts;
1.7 = prestressing coefficient.

The shearing force acting on the bolt is

$$P_0 = \frac{2M_t}{zD_b},$$

where D_b = diameter of bolt circle.

The tensile stress at the critical bolt section is

$$\sigma_{z_1} = \frac{Q_0}{F_1} = \frac{1.7P \cdot 4}{z\pi d_1^2} = \frac{6.8P}{\pi z d_1^2} \text{ kg/cm}^2, \qquad \text{(X. 42)}$$

where d_1 = diameter of the critical bolt section.

The stresses in the fitted part of the bolt are

a) tensile stress:

$$\sigma_{z_2} = \frac{Q_0}{F_2} = \frac{1.7P \cdot 4}{z\pi d_b^2} = \frac{6.8P}{\pi z d_b^2} \text{ kg/cm}^2,$$

where F_2 = cross-sectional area of the fitted part of the bolt

$$F_2 = \frac{\pi d_b^2}{4} \text{ cm}^2;$$

b) shear stress:

$$\tau = \frac{P_0}{F_2} = \frac{2M_t \cdot 4}{zD_b \pi d_b^2} = \frac{8M_t}{\pi z D_b d_b^2} \text{ kg/cm}^2; \qquad \text{(X. 43)}$$

c) crushing stress:

$$\sigma_{cr} = \frac{P_0}{d_b l} = \frac{2M_t}{zD_b l d_b} \text{ kg/cm}^2; \qquad \text{(X. 44)}$$

d) combined:

$$\sigma = \sqrt{\sigma_{z_z}^2 + 4\tau^2} = \sqrt{\frac{6{,}8P}{\pi z d_b^2} + 4\frac{8M_t}{\pi z D_b d_b^2}} \text{ kg/cm}^2. \qquad \text{(X. 45)}$$

Permissible stresses in bolts are as follows:

Combined stress	from 1000 to 1200 kg/cm^2
Tensile stress	" 900 to 1000 "
Shear stress	" 400 to 450 "

Calculation of the flange-joint nuts. The load including prestressing acting on the nut is

$$Q_0 = \frac{1.7P}{z}.$$

The actual force on the nut is

$$P_r = \frac{D_{ax} - d_m}{S - d_m} Q_0 = 1.7 \frac{D_{ax} - d_m}{(S - d_m) z},$$

where D_{ax} = diameter of the circle at whose periphery the axial force is applied;

d_m = mean diameter across thread;

S = width across flats.

$$D_{ax} = \sqrt{\frac{S^2 + d_2^2}{2}},$$

where d_2 = diameter of hole in the flange.

The tangential stress is

$$\sigma_{t_0} = k_1 \frac{P_r}{H^2} = 1.7 \frac{k_1 (D_{ax} - d_m) P}{H^2 (S - d_m) z}, \qquad \text{(X. 46)}$$

where H = thickness of nut;

k_1 = coefficient depending on the ratio $\frac{S}{d_m}$ (Figure X. 15).

The crushing stress of the nut (Figure X. 14) is

$$\sigma_{cr} = \frac{Q_0}{\frac{\pi}{4}\left(S^2 - d_2^2\right)} = \frac{6.8P}{\pi\left(S^2 - d_2^2\right)z}. \qquad (X.\ 47)$$

The stresses in the nut thread are:

a) bending stress:

$$\sigma_b = 0.9\frac{Q_0}{Hd_1} = \frac{1.53P}{Hd_1 z}\ \text{kg/cm}^2; \qquad (X.\ 48)$$

b) shear stress:

$$\tau = \frac{Q_0}{\pi H d_1} = \frac{1.7P}{\pi H d_1 z}\ \text{kg/cm}^2, \qquad (X.\ 49)$$

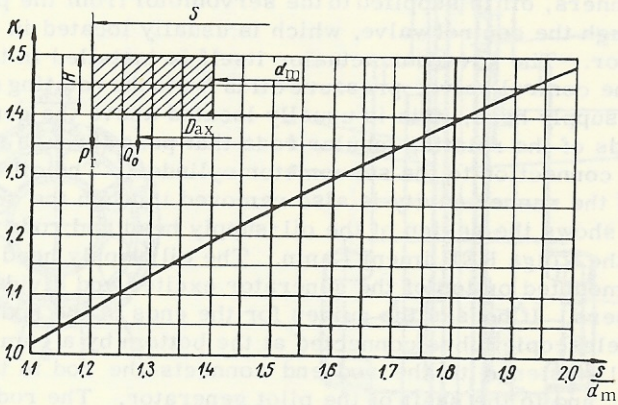


FIGURE X.15. Relationship between coefficient k_1 and ratio $\frac{s}{d_m}$

c) crushing stress

$$\sigma_{cr} = \frac{Q_0}{\pi d_m t a} = \frac{1.7P}{\pi d_m t a z}\ \text{kg/cm}^2, \qquad (X.\ 50)$$

where t = depth of thread;

$a = \frac{H}{s_1}$ = number of threads;

s_1 = thread pitch;

d_m = diameter at bottom of thread.

Maximum permissible bending and crushing stresses are 700 kg/cm^2.

Chapter XI

AUXILIARY EQUIPMENT

66. OIL SUPPLY HEAD AND RODS

In Kaplan runners, oil is supplied to the servomotor from the pressure-oil system through the control valve, which is usually located in or near the governor actuator. The governor actuator itself is installed in the machine room. From the control valve, pressure oil is fed to the rotating servomotor through the oil-supply head; this is usually located above the generator and encloses the ends of the rotating tubular rods that pass through the shaft and provide the connection to the servomotor cylinder. The oil from the servomotor and the runner cavity is also removed through the supply head.

Figure XI. 1 shows the design of the oil-supply head and rods for the turbine-runner of the Volga HEP imeni Lenin. The oil-supply head is a conical casing (2), mounted on top of the generator exciter and divided into separate oil chambers. It houses the guides for the ends of the rods (3) which consist of two telescopic tubes connected at the bottom by a common flange. A cross piece (1) fastened to the rod end connects the rod to the switch through a cable, and to the shaft of the pilot generator. The rod is not made of one piece but consists of three sections (5), (7), and (13) connected by flanges, because the shaft itself also consists of three sections: two shafts (turbine and generator) and the extension shaft. If the shaft is in one piece, the rod may also be made in one piece. Each section consists of an external steel tube (11) 426 mm in diameter and 14 mm thick, and an inner tube (12), 245 mm in diameter and 10 mm thick, welded to the flanges (8). Apart from these, the position of the tubes in relation to each other is fixed by screws (10). Cylindrical guide sleeves (9), welded to the outer tube, slide in bronze bushings (6) fitted in the shaft near the flange. Each flange is provided with one central hole and four peripheral holes (4) for the oil. When the rod is fitted inside the shaft, the three cavities (a), (b), and (c) are thus formed. Cavity (a), between the shaft and the outer tube, is connected to the discharge chamber of the oil supply head. Cavities (b) and (c), formed by the outer and inner tubes, are used to supply oil to the servomotor. They are connected at the top with the pressure chambers of the oil-supply head.

Figure XI. 2 shows an earlier design of an oil-supply head for large turbines. The supply head consists of the base (1) forming a cylindrical tank — the conical casing (2) having one discharge and two pressure chambers — and the end casing (3).

Bushings are provided in the chambers and the end casing to guide the end of tubular rod (6), connected at the top to lever (5) of the blade-control mechanism. The pilot generator (4) of the governor drive is mounted on

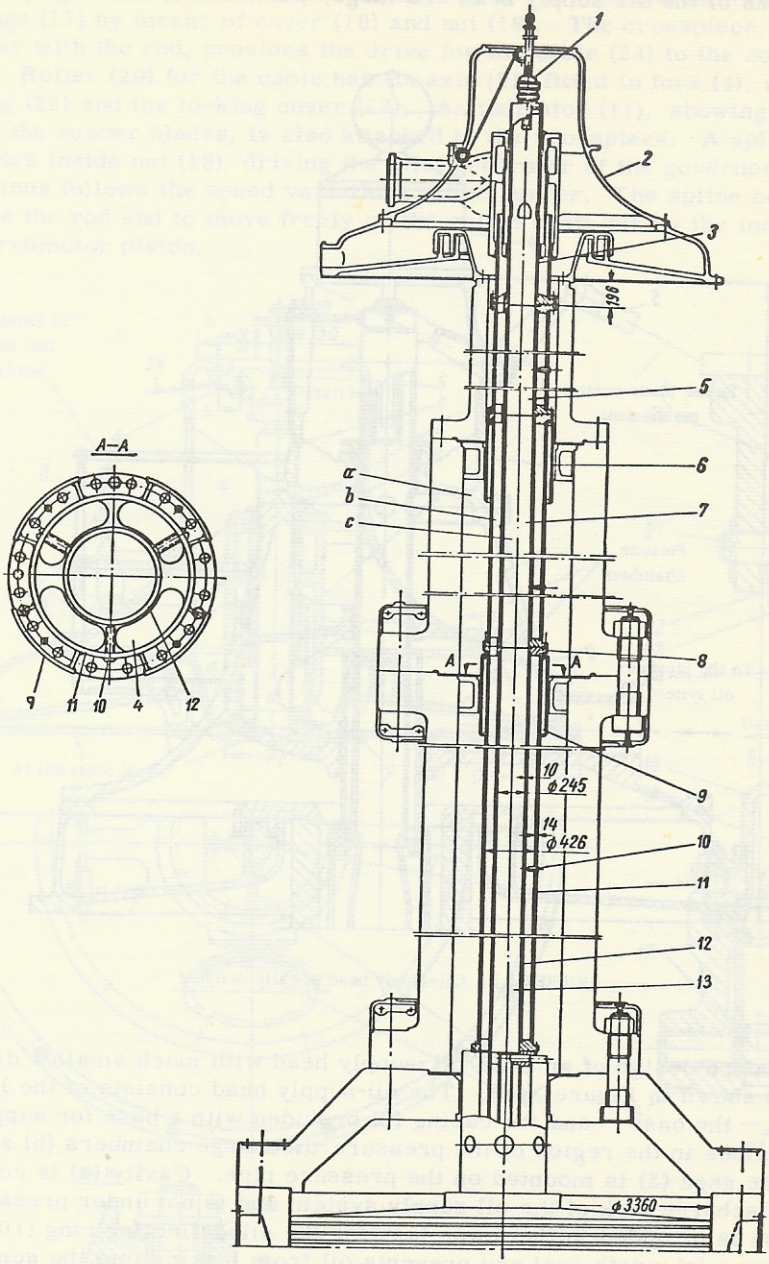


FIGURE XI.1. Oil-supply head and rods

top of the end casing. Because the oil inlet and outlet chambers are located one on top of the other, and the servomotor piston has a large stroke, the dimensions of the oil-supply head are large, particularly its height *H*.

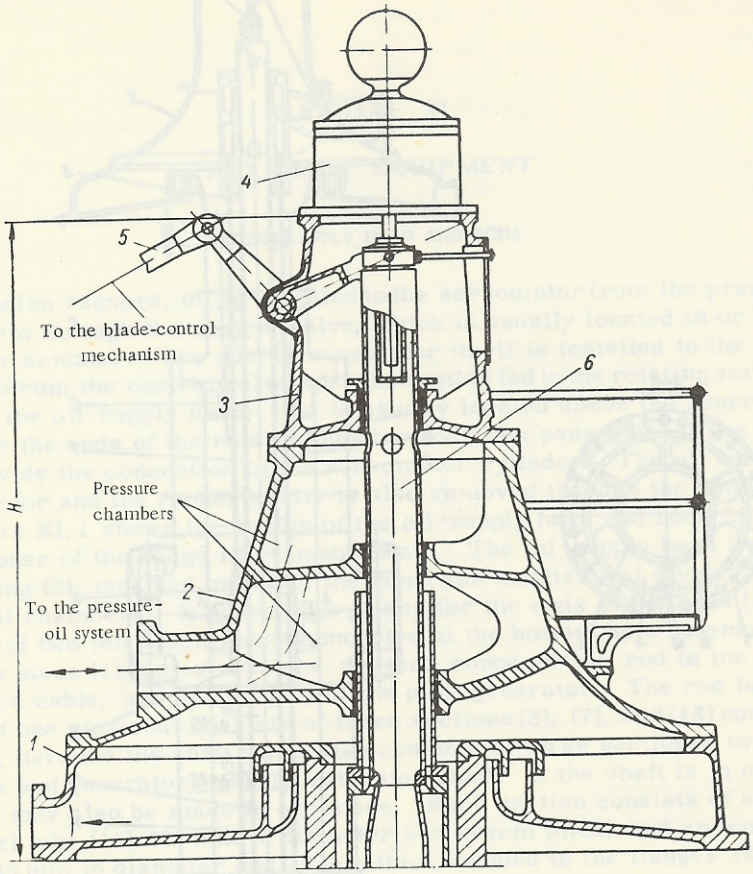


FIGURE XI.2. Oil-supply head of early design

A modern design of an LMZ oil-supply head with much smaller dimensions is shown in Figure XI. 3. The oil-supply head consists of the lower tank (1) — the base — and the casing (2) provided with a boss for supporting the pipes in the region of the pressure-discharge chambers (b) and (c). Pressure gage (3) is mounted on the pressure pipe. Cavity (a) is connected to the discharge tank of the oil-supply system and is not under pressure. A recess is provided in the lower tank for the oil-deflecting ring (10), which serves as a labyrinth seal and prevents oil from leaking into the generator. Bushings (7) guide the end of the rod which consists of two tubes (6) and (9). In order to make the supply head as small as possible with an adequate piston stroke, sleeve (8) with a collar at its end is fitted in the casing of the oil-supply head; the collar surrounds tube (6) and separates chamber (b)

from chamber (c), which would otherwise have been in communication through the radial openings in the rod end. The crosspiece (16) (detail N) fastened to the top of the rod is connected to the end of rod (25) and the two ball bearings (17) by means of cover (19) and nut (18). The crosspiece, moving together with the rod, provides the drive for the cable (24) to the control valve. Roller (20) for the cable has its axis (21) fitted in fork (4), with ball bearing (22) and the locking cover (23). An indicator (11), showing the position of the runner blades, is also attached to the crosspiece. A spline shaft (5) slides inside nut (18), driving the pilot generator of the governor motor, which thus follows the speed variations of the runner. The spline connection enables the rod end to move freely on the spline shaft during the motion of the servomotor piston.

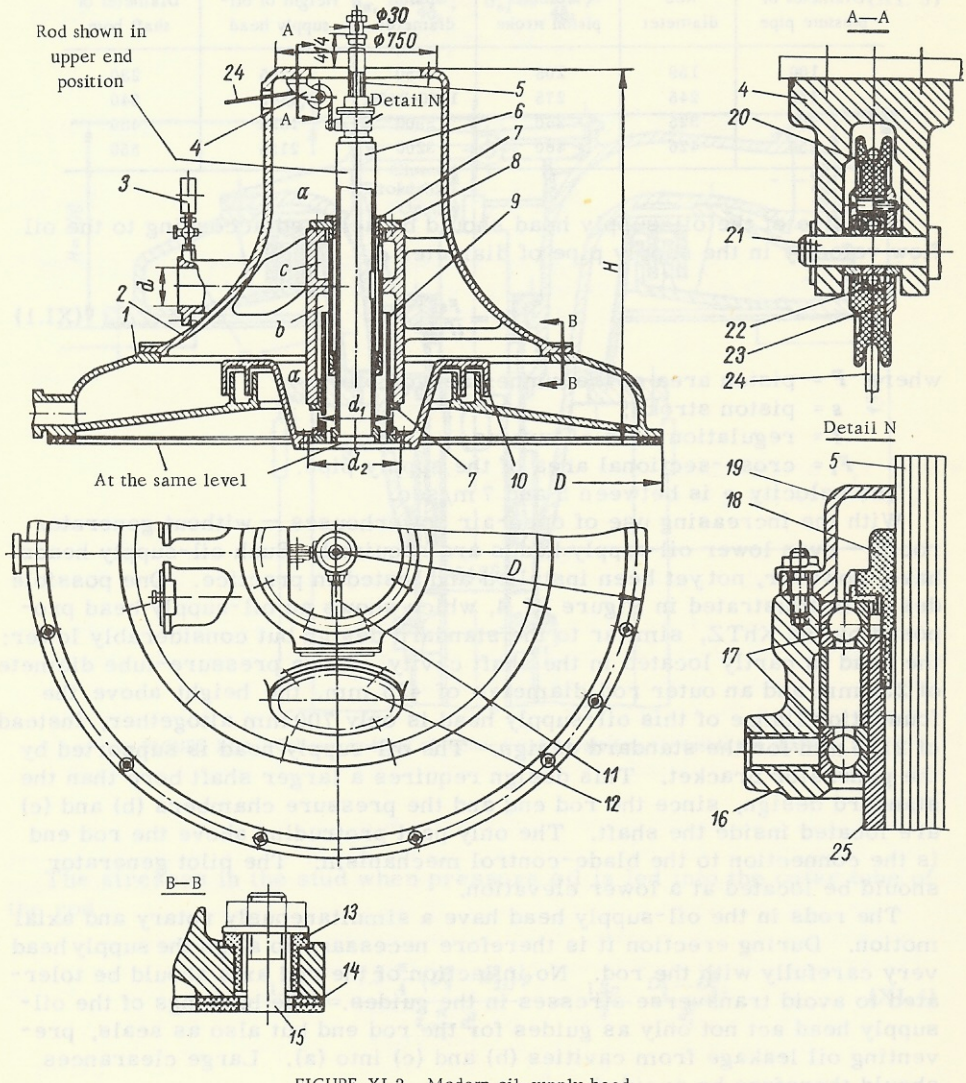


FIGURE XI.3. Modern oil-supply head

The oil-supply head, rods, and oil pipes form a closed electric circuit across the generator stator. Stray currents liable to cause corrosion are thus induced in these parts. Insulating gaskets must therefore be provided to protect the rods and the connections.

The gaskets (14) and bushings (13) made of textolite and the studs (15) of the oil-supply head are shown in section B—B. An inspection hole is provided in the oil-supply head, covered by lid (12).

This is the standard design at the LMZ, with the following dimensions (Table XI. 1).

TABLE XI.1

Principal dimensions of standard oil-supply head, mm

Diameter of pressure pipe	Rod diameter	Servomotor-piston stroke	Base diameter	Height of oil-supply head	Diameter of shaft bore
100	159	205	1450	1205	230
150	245	275	1750-2400	1445	340
200	325	360	2900	1825	430
250	426	460	3200	2155	550

The size of the oil-supply head should be selected according to the oil flow velocity in the supply pipe of diameter d,

$$v = \frac{Fs}{tF_1}, \qquad \text{(XI.1)}$$

where F = piston area of the runner servomotor;
s = piston stroke;
t = regulation time of turbine;
F_1 = cross-sectional area of the supply pipe.

The velocity v is between 5 and 7 m/sec.

With the increasing use of open-air powerhouses — without generator room — even lower oil-supply heads are required. Such oil-supply heads have, however, not yet been installed and tested in practice. One possible design is illustrated in Figure XI. 4, which shows an oil-supply head proposed by the KhTZ, similar to the standard design but considerably lower: the head is partly located in the shaft cavity. For a pressure-tube diameter of 250 mm and an outer rod diameter of 426 mm, the height above the foundation flange of this oil-supply head is only 700 mm altogether, instead of 2155 mm for the standard design. The oil-supply head is supported by the generator bracket. This design requires a larger shaft bore than the standard design, since the rod end and the pressure chambers (b) and (c) are located inside the shaft. The only part protruding above the rod end is the connection to the blade-control mechanism. The pilot generator should be located at a lower elevation.

The rods in the oil-supply head have a simultaneously rotary and axial motion. During erection it is therefore necessary to align the supply head very carefully with the rod. No inflection of the rod axis should be tolerated to avoid transverse stresses in the guides. The bushings of the oil-supply head act not only as guides for the rod end but also as seals, preventing oil leakage from cavities (b) and (c) into (a). Large clearances should therefore be avoided.

Design of the rods. The runner rods must be designed to withstand stresses, buckling, and transverse vibrations.

Stress calculations. The tangential stresses in the inner and outer tubes are:

$$\sigma_{t_1} = \frac{pD_1}{2\delta_1}; \quad \sigma_{t_2} = \frac{pD_2}{2\delta_2}, \tag{XI.2}$$

where D_1 and D_2 = outer diameters of inner and outer tubes;
δ_1 and δ_2 = thicknesses of inner and outer tubes;
[p = oil pressure].

The axial stresses are:

$$\sigma_{a_1} = \frac{pD_1}{4\delta_1}; \quad \sigma_{a_2} = \frac{pD_2}{4\delta_2}. \tag{XI. 3}$$

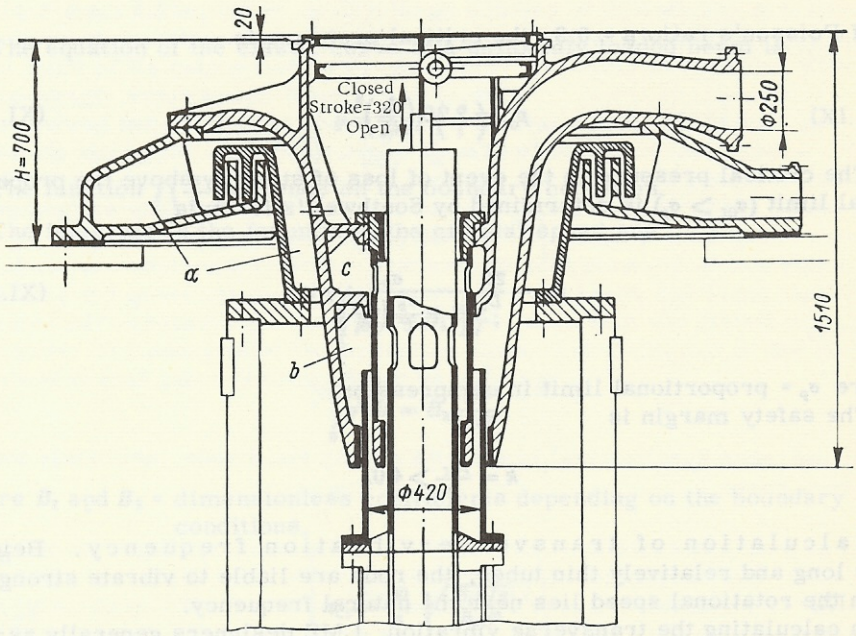


FIGURE XI.4. Oil-supply head of reduced size located partly inside the shaft

The stresses in the stud when pressure oil is led into the outer tube of the rod

$$\sigma = \frac{1.3Q}{f} = \frac{1.3\,\frac{\pi}{4}\left(D_2^2 - D_{2i}^2\right)p}{z\,\frac{\pi}{4}d_1^2} = \frac{1.3p}{z} \cdot \frac{D_2^2 - D_{2i}^2}{d_1^2}, \tag{XI.4}$$

where D_{2i} = inner diameter of the outer tube;

d_1 = root diameter of stud thread.

Resistance to buckling. The inner tube, subjected to external pressure, must be designed to resist buckling.

If the length of the rod tubes is

$$l > 1.73 D_1 \sqrt{\frac{D_1}{\delta_1}}, \tag{XI.5}$$

the critical pressure within the proportional limits ($\sigma_{cr} < \sigma_p$) that may cause buckling is determined by the formula

$$p_{cr} = \frac{E\delta_1^3}{4(1-\mu^2)\left(\frac{D_1}{2}\right)^3}. \tag{XI.6}$$

If Poisson's ratio $\mu = 0.3$, the critical pressure is

$$p_{cr} = 2.2E\left(\frac{\delta_1}{D_1}\right)^3. \tag{XI.7}$$

The critical pressure in the event of loss of stability above the proportional limit ($\sigma_{cr} > \sigma_p$) is determined by Southwell's formula

$$p_{cr} = \frac{2\delta_1}{D_1} \cdot \frac{\sigma_p}{1 + \frac{\sigma_p}{E}\left(\frac{D_1}{\delta_1}\right)^2}, \tag{XI.8}$$

where σ_p = proportional limit in compression.

The safety margin is

$$k = \frac{p_{cr}}{p} > 4.0.$$

Calculation of transverse-vibration frequency. Being very long and relatively thin tubes, the rods are liable to vibrate strongly when the rotational speed lies near the natural frequency.

In calculating the transverse vibration, LMZ designers generally assume the inner and outer tubes to be independent and vibrating separately. This lowers the calculated critical speed and thus increases the safety margin.

The rod is considered as an equal-span beam, with either freely supported or rigidly fixed ends, uniformly loaded all along its length by its own weight and the weight of the oil within. The weight and rigidity of the flange and connecting elements are neglected. If the spans are unequal, the largest is used for the calculation, thus increasing the safety margin.

The critical speed is determined by the formula

$$n_{cr} = \frac{30}{\pi} \sqrt{\frac{\int_0^l q(x)\, y(x)\, dx}{\int_0^l \varrho(x)\, y^2(x)\, dx}}, \tag{XI.9}$$

where $q(x)$ = distributed load;
$\varrho(x)$ = mass of rod per unit length;
$y(x)$ = deflection under the action of the distributed static load $q(x)$.

For tubes of uniform section:

$$q(x) = q = \text{const};$$

$$\varrho(x) = \varrho = \frac{q}{g} = \text{const}.$$

The critical speed is therefore

$$n_{cr} = \frac{30}{\pi} \sqrt{\frac{g \int_0^l y\,dx}{\int_0^l y^2\,dx}}. \tag{XI.10}$$

The equation of the elastic curve of a uniformly loaded beam is

$$y = \frac{ql^4}{EJ} f\left(\frac{x}{l}\right). \tag{XI.11}$$

The function $f\left(\frac{x}{l}\right)$ depends on the boundary condition.

The integrals in the formula of the critical speed are

$$\int_0^l y dx = B_1 \frac{ql^5}{EJ};$$

$$\int_0^l y^2 dx = B_2 \frac{q^2 l^9}{(EJ)^2},$$

where B_1 and B_2 = dimensionless coefficients depending on the boundary conditions.

Then

$$n_{cr} = \frac{30}{\pi} \sqrt{\frac{B_1 EJg}{B_2 q l^4}}. \tag{XI.12}$$

The load per unit length of the inner tube is

$$q_1 = f_1 \gamma_1 + f_{o1} \gamma_2. \tag{XI.13}$$

The weight load per unit length of the outer tube

$$q_2 = (f_1 + f_2)\,\gamma_1 + (f_{o1} + f_{o2})\,\gamma_2, \tag{XI.14}$$

where f_1 and f_2 = wall cross sections of inner and outer tubes;
f_{o1} and f_{o2} = effective cross section of inner and outer tubes;
γ_1 and γ_2 = specific weights of steel and oil, respectively.

By considering the tubes as uniformly loaded beams, the values of the dimensionless coefficients B_1 and B_2 may be determined for the following cases:

1) uniformly loaded beam with freely supported ends:

$$\left.\begin{aligned} \int_0^l y\,dx &= \frac{1}{5}\cdot\frac{ql^5}{24EJ};\\ \int_0^l y^2\,dx &= \frac{31}{630}\cdot\frac{q^2l^9}{(24EJ)^2}. \end{aligned}\right\} \qquad \text{(XI.15)}$$

Thus,

$$B_1 = \frac{1}{120}; \quad B_2 = \frac{31}{362880};$$

2) uniformly loaded beam with rigidly fixed ends:

$$\left.\begin{aligned} \int_0^l y\,dx &= \frac{1}{30}\cdot\frac{ql^5}{24EJ};\\ \int_0^l y^2\,dx &= \frac{1}{630}\cdot\frac{q^2l^9}{(24EJ)^2}. \end{aligned}\right\} \qquad \text{(XI.16)}$$

Thus,

$$B_1 = \frac{1}{720}; \quad B_2 = \frac{1}{362880};$$

3) two-span symmetrical beam with rigidly fixed ends, uniformly loaded, for each span:

$$\left.\begin{aligned} \int_0^l y\,dx &= \frac{3}{40}\cdot\frac{ql^5}{24EJ};\\ \int_0^l y^2\,dx &= \frac{754}{1000}\cdot\frac{q^2l^9}{(24EJ)^2}. \end{aligned}\right\} \qquad \text{(XI.17)}$$

Thus,

$$B_1 = \frac{3}{960}; \quad B_2 = \frac{754}{576000}.$$

67. TRANSMISSIONS AND PIPING

The mechanisms of the turbine-governing system are located at various points of the powerhouse, and interconnected by oil pipes and mechanical transmissions. The layout should be as simple as possible. The distributor servomotors are usually located in the turbine pit and, if possible, directly above it, in the machine room, the governor with the oil-supply head. In earlier designs, the mechanism usually consisted of rods and levers coupled through cylindrical pins in bushings. The large number of pins, with their inevitable clearances, caused considerable lost motion in the transmission system, interfering with the operation of the governor and causing hunting and instability. Hence, the bushings of the cylindrical pins are now replaced by ball bearings.

To reduce the elastic deformations of the rods, they are nowadays made of thin-walled steel tubes of relatively large diameter.

Cable transmissions have become very common of late. A 5 or 6 mm diameter steel cable, made up of a large number of thin wires, leads from the servomotor piston over rollers to the appropriate lever of the governor. At the point of its connection to the governor, the cable is provided with a counterweight which keeps it tightly stretched.

To protect the cable it is enclosed in a tubular casing filled with grease.

The oil piping for a Kaplan turbine usually consists of three parts. The part from the oil-supply head to the governor includes two pressure pipes connecting the pressure chambers of the oil-supply head with the control valve of the runner and a discharge pipe from the supply head to the sump tank of the pressure-oil system. The second part consists of two pipes connecting the governor control valve with the pressure and sump tanks. The third part connects the governor control valve with the distributor servomotor and consists of two pressure pipes, branching out in the turbine pit into four pipes leading to two servomotors.

68. PRESSURE REGULATOR

Pressure-regulator construction. Pressure regulators are used to prevent sudden pressure rise in the turbine penstock, mainly on high-head turbines (H = 100 to 150 m) with long penstocks. They are installed at the scroll-case inlet. When the guide vanes close rapidly, the pressure-regulator opens rapidly, closing slowly afterwards. Thus, while the discharge through the guide vanes is abruptly reduced, the combined discharge through the turbine and the pressure regulator, i.e., through the penstock, changes only slowly, and the pressure rise is insignificant. Pressure regulators usually permit the pressure rise in the penstock to be limited to between 15 and 20% of the static head. They are provided with an oil dashpot that causes them to open only if the guide vanes turn rapidly and a considerable pressure rise is likely. If the guide vanes turn slowly, the dashpot piston remains stationary, and the pressure regulator does not open.

The oil cylinder (1) of the dashpot (see Figure XI. 5) is connected to the pressure-regulator drive at point (B). Rod (4) is connected at point (A) with the transmission (not shown in the figure) to the distributor servomotor.

The spaces on both sides of piston (7) are connected with each other through orifice (8). When the piston moves downward rapidly (corresponding to distributor closure) the oil beneath the piston has not enough time to flow through the throttle valve upward. The; pressure below the piston rises and cylinder (1) moves downward together with point (B), causing the pressure regulator to open and to compress spring (2). The force of the spring causes the oil to flow through the orifice, and the cylinder to return to its former pisition, closing the pressure-regulator valve. The pressure regulator may be operated manually by means of handwheel (5). Check valve (6) opens during the upward motion of the piston. The oil dashpot is mounted on top of the pressure regulator.

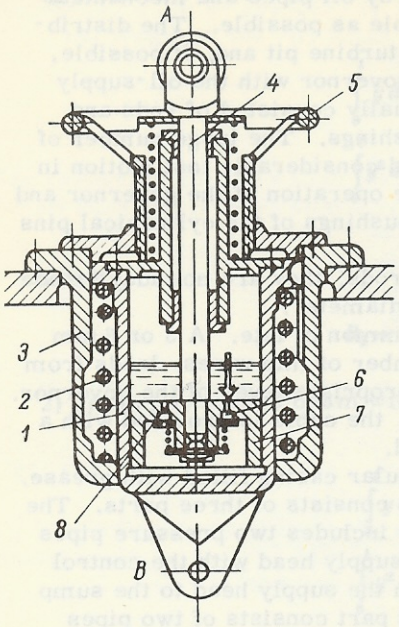


FIGURE XI. 5. Dashpot

The main parts of the pressure regulator are the water passage, determining its discharge capacity, and the valve drive.

Pressure-regulator water-passages of various designs are shown in Figure XI. 6 with their discharge-capacity curves.

A needle-valve pressure-regulator is shown in Figure XI. 6,a.

Needle valve (4) is mounted in the spherical casing (1). Valve movement is controlled by the large piston rod (2) guided in sleeve (3) and bushing (5) mounted in the outlet pipe (6), in which the needle point moves. Pressure regulators of this type are used by several European companies; LMZ also used them in early designs of small turbines.

Figure V. 5 shows a pressure regulator of this kind mounted on a 12,800 kw turbine.

The disadvantage of this design is that the valve closes downward. In the event of a fault in the actuating system, the valve is pressed against the seat by the water, causing the pressure to rise abruptly in the penstock. The water passages shown in Figure XI. 6,b and c do not have this drawback, since they open downward. If the actuating system fails, the valve opens under the water pressure, so that dangerous pressure rises in the penstock are averted.

The mushroom-disk valve (Figure XI. 6,b) (4) and conical valve (Figure XI. 6,c) (4) are secured to the bottom end of rod (1) whose movement is guided in boss (2); the bend (3) is mounted on top of outlet pipe (6), guide (5) in its interior.

The shape of the valve affects the discharge capacity of the pressure regulator.

B. P. Gur'ev determined experimentally /26/ the discharge capacity of valves of various shapes (Figure XI. 6,d). The discharge capacity of the

conical valve pressure-regulator is about 10% greater than that of the mushroom-disk type. At full opening of the mushroom-disk valve the discharge Q'_{1x} = 2300 liter/sec, of the conical valve, Q'_{1x} = 2500 liter/sec. In the closed position, the valve is pressed against the seat by the force P_s of the servomotor. Pressure may be applied either by oil from the oil-pressure system, or by water from the penstock.

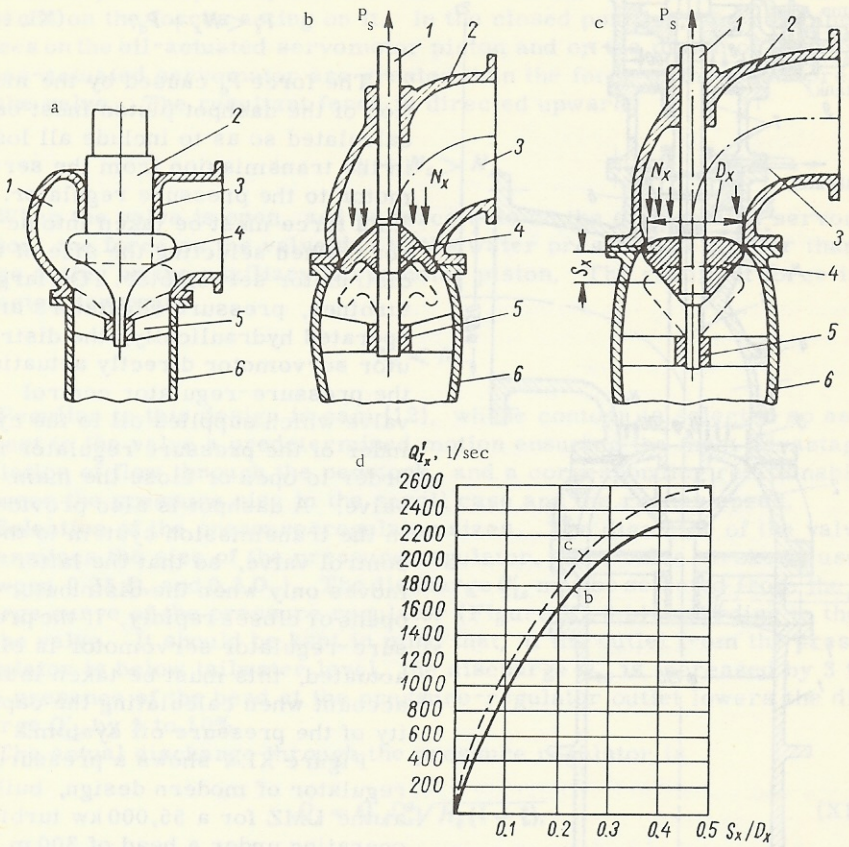


FIGURE XI.6. Pressure-regulator designs, and discharge-capacity curves

Small pressure regulators may be actuated by the distributor servomotor. The servomotor piston is connected by means of levers and rods to the piston of the dashpot mounted on the pressure regulator. Rapid movement of the distributor servomotor piston causes the dashpot piston also to move rapidly. The oil has not enough time to flow through the orifice, so that a force P_d acts upon the dashpot cylinder which is connected to the valve rod. The force P_d, together with the force of the water pressure N_x, causes the valve to open. Consequently, in the closed position of the valve, the force on the pressure-regulator servomotor piston should exceed the force of the water pressure on the valve:

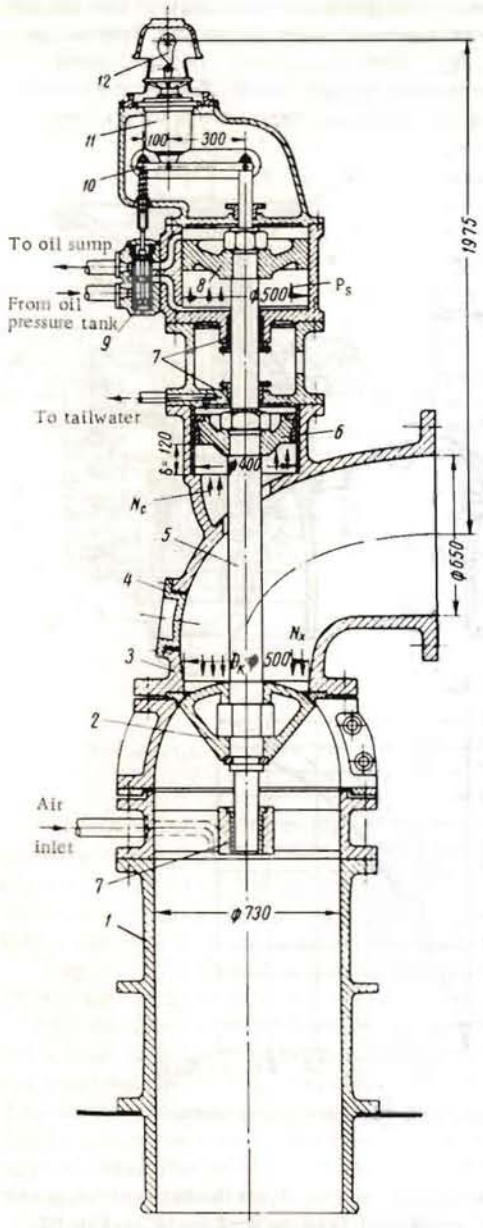


FIGURE XI.7. Pressure regulator (d = 500 mm)

$$P_s > N_x. \qquad \text{(XI. 18)}$$

So that the valve may open, the servomotor force must be less than the total resultant force of the water pressure on the valve and of the oil pressure on the dashpot cylinder.

$$P_s < N_x + P_d. \qquad \text{(XI. 19)}$$

The force P_d caused by the motion of the dashpot piston must be calculated so as to include all losses in the transmission from the servomotor to the pressure regulator. This force must be taken into account when selecting the size of the distributor servomotor. On large turbines, pressure regulators are operated hydraulically, the distributor servomotor directly actuating the pressure-regulator control valve which supplies oil to the cylinder of the pressure regulator in order to open or close the main valve. A dashpot is also provided in the transmission system to the control valve, so that the latter moves only when the distributor opens or closes rapidly. If the pressure-regulator servomotor is oil-actuated, this must be taken into account when calculating the capacity of the pressure oil system.

Figure XI.7 shows a pressure regulator of modern design, built at the LMZ for a 55,000 kw turbine, operating under a head of 300 m. Bend (3) of the pressure regulator with inspection hole (4) is fastened to the scroll casing by means of the 650 mm flange on the inlet. An auxiliary 400 mm-diameter water-actuated piston (6) moves in a cylinder on top of the bend. The piston is fastened to rod (5). Above this there is the 500 mm-diameter piston (8) with the oil-actuated servomotor. The control valve (9) of the oil servomotor is connected to dashpot (11) by means of transmission (10). The conical 500 mm-diameter valve (2) is secured to the bottom end of the rod, above guide bushing (7). The

cylindrical outlet has a diameter of 720 mm. The pressure regulator is hydraulically actuated. If the distributor is closed rapidly, the dashpot transmits the motion to the control-valve. This moves downward, the space beneath the piston of the oil-actuated servomotor is connected with the oil sump, and the water opens the valve — whose diameter is larger than that of the auxiliary piston. The control valve, actuated by the dashpot and the restoring link from the servomotor piston, moves upward and connects the space beneath the piston with the oil pressure tank. The pressure oil forces the piston upward, and the valve is closed. The position of the valve depends on the forces acting on it. In the closed position, the combined forces on the oil-actuated servomotor piston and on the piston of the auxiliary water-actuated servomotor are greater than the force of the water pressure on the valve. The resultant force is directed upward

$$P_s + N_s > N_x.$$

When the valve is open, and no force acts on the oil-actuated servomotor piston, the force on the valve due to the water pressure is greater than the force acting on the auxiliary servomotor piston. The resultant force is directed downward.

$$N_s < N_x.$$

Peculiar to this design is cam (12), whose contour is selected so as to impart to the valve a predetermined motion ensuring the most advantageous variation of flow through the penstock, and a corresponding relationship between the pressure rise in the scroll case and the runner speed.

Selection of the pressure-regulator sizes. The diameter of the valve D_v determines the size of the pressure regulator. The valve stroke is usually between 0.25 D_v and 0.3 D_v). The discharge Q'_{1x} may be selected from the discharge curve of the pressure regulator (Figure XI. 6,b) according to the type of the valve. It should be kept in mind that, if the outlet from the pressure regulator is below tailwater level, the discharge Q'_{1x} is increased by 3 to 5%. The presence of the bend at the pressure-regulator outlet lowers the discharge Q'_{1x} by 5 to 10%.

The actual discharge through the pressure regulator is

$$Q_x = Q'_{1x} D_x^2 \sqrt{H_0 (1 + \xi)}, \qquad \text{(XI. 20)}$$

where ξ = relative pressure rise in the penstock; usually ξ = 0.15 to 0.20;
H_0 = rated head.

The maximum discharge Q_x that can pass through the pressure regulator is

$$Q_x = Q_0 \left(1 - \frac{T_s}{T}\right), \qquad \text{(XI. 21)}$$

where Q_0 = maximum flow through the turbine;
T_s = time taken for guide-vanes to close with the pressure regulator operative, the increase in pressure and rpm being limited to permissible values;
T = ditto, but with the pressure regulator inoperative.

The interval T is

$$T = \frac{\sum Lv}{gH_0\sigma}, \qquad \text{(XI. 22)}$$

where $\sum Lv$ = sum of products of penstock-section lengths and velocities of water flowing through them;

σ = penstock pressure characteristic

$$\sigma = \frac{\xi}{\sqrt{1+\xi}}.$$

The diameter of the pressure regulator is

$$D_x = \sqrt{\frac{Q_x}{Q'_{1x}\sqrt{H_0(1+\xi)}}}. \qquad \text{(XI. 23)}$$

After determining the diameter of the pressure regulator, the required speed regulation is calculated on the basis of the discharge curves of pressure regulator and turbine.

With program control of the pressure-regulator valve, as proposed by A. E. Zhmud', the size of the pressure regulator can be reduced. In program-control operation, the pressure regulator opens more when the guide vanes start closing from fully-open position. Thus, the turbine-closing time is reduced so that the turbine-speed increase for a given pressure rise in the penstock is also reduced.

In designing pressure regulators, provision should be made for introducing under the valve, and for using energy dissipators for the outflowing water.

69. GATES AND VALVES

Gates and valves are commonly used for controlling the water flow through the penstock.

Long penstocks of high-head hydro power plants are, in general, equipped with two gates: one at the penstock inlet and the other immediately upstream from the turbine. The first is required for inspections and repairs of the penstock, the second (usually referred to as the turbine gate) performs the same function for the turbine, so that emptying the penstock in the event of an emergency turbine inspection is unnecessary. If the turbine is shut down for a long time, the closed gate reduces water leakages.

The penstock inlet of low- and medium-head turbines is usually provided with one gate only.

The gates on the steel penstocks in front of the turbine are part of the auxiliary equipment and are supplied by the turbine builders.

Gates and valves. Either butterfly or spherical valves, as shown in Figure XI. 8, are used on large turbines. The simplest type of butterfly valve consists of disk (1) and housing (2). The disk is pivoted in the housing

by two pins. When open, the plane of symmetry of the disk lies in the penstock axis, and the water flowing past it can enter the turbine.

To reduce water-flow fluctuations in the valve, the outlet diameter is smaller than the inlet diameter. The velocity of the water flowing through the valve is slightly raised by the reduction in pipe cross section due to the disk. Since the reduction of the valve-outlet cross section equals the reduction of the effective cross section due to the disk, the velocity remains approximately constant. The disk usually turns through an angle of 90°C, but designs exist with a smaller angle of rotation (75 to 80°). In this case the valve is sealed tightly when the disk, whose periphery fits the housing closely, is forced against the latter. Steel seal rings are sometimes used for this purpose. The disadvantage of this seal is that only part of the disk periphery is forced against the housing. The housing may also become deformed; furthermore, it is difficult to seal the clearances at the disk pivot. Angles of rotation of 90° are therefore more widely employed; a thick rubber tube of special shape arranged in the valve housing or in the disk is used as seal. The tube is inflated with air under a pressure of 5 to 6 atm above the water pressure in the penstock. This type of seal is shown in Figure XI. 9.

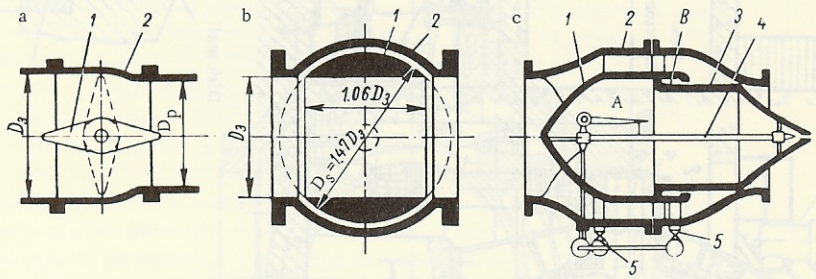


FIGURE XI.8. Schematic drawings of

a—butterfly valve; b—spherical valve; c—needle valve.

Butterfly valves, though cheap and simple in design, have the following drawbacks: the disk increases the resistance to water flow and promotes cavitation; the losses increase with the head, since the relative disk thickness and the flow velocity increase. Hence, butterfly valves as a rule are not used under heads higher than 200 m. Butterfly valves may have diameters up to 8.5 m.

Spherical valves do not have this drawback. When open, they do not throttle the water flow, and are therefore widely used on high-head turbines.

The valve (1) (Figure XI. 8) is turned by a servomotor through 90° about its pivots mounted in housing (2). The sealing is effected by seal rings, shown in Figure XI. 10.

The spherical valve is more complicated in construction than the butterfly valve. It is used only on relatively small high-head turbines, and is thus heavy and expensive. Such valves are made with diameters up to 3 m.

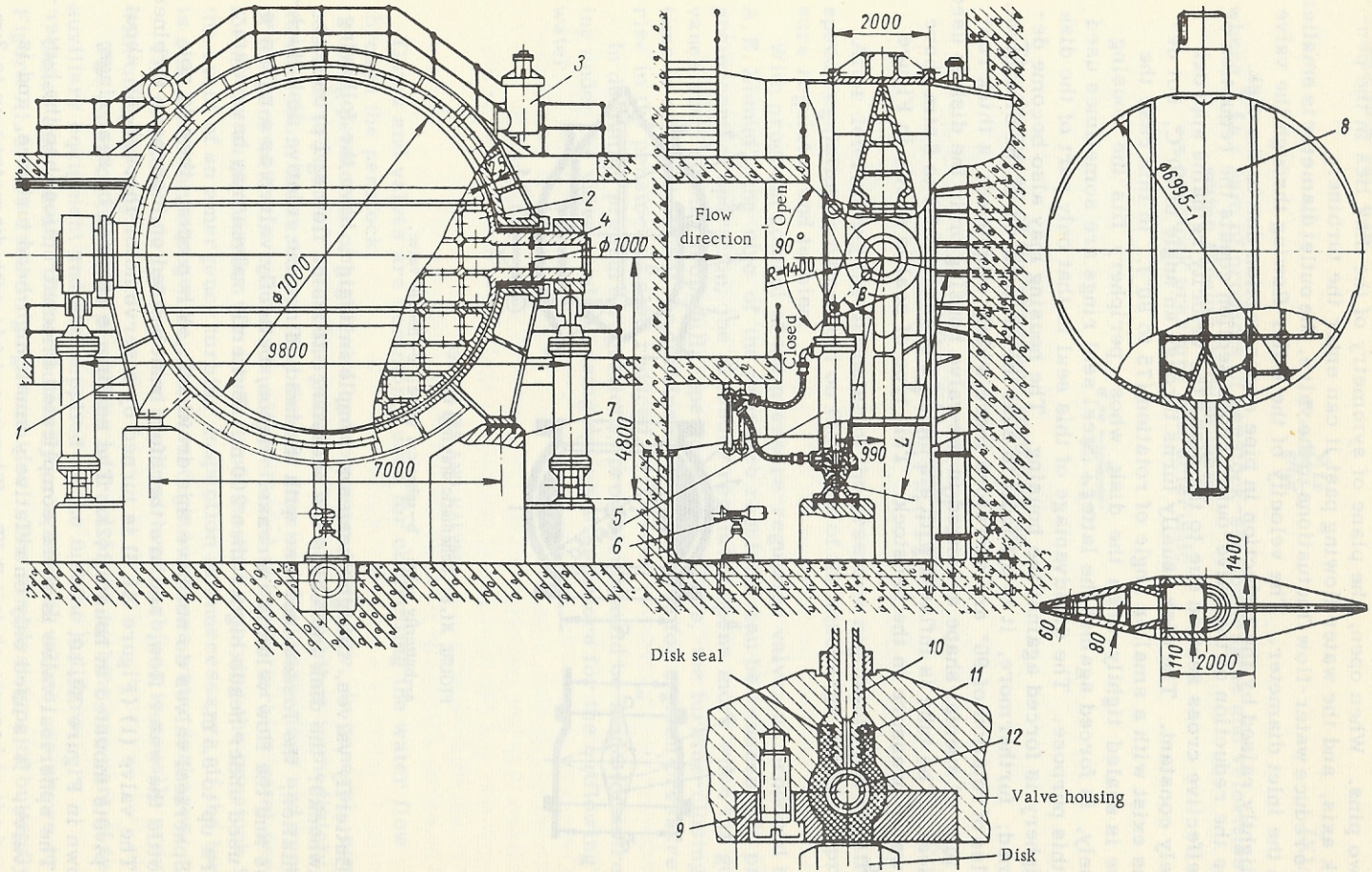


FIGURE XI.9. Butterfly valve, H = 100 m

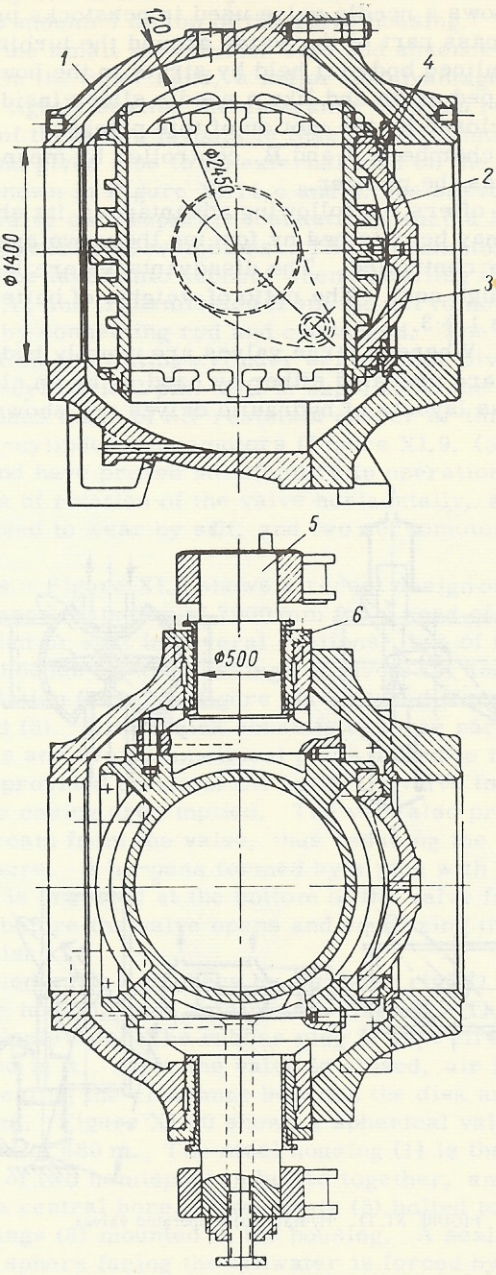


FIGURE XI.10. Spherical valve, $H = 680$ m

In butterfly and spherical valves the disk or sphere should be in fully-closed or fully-open position. Considerable flow disturbance is caused in intermediate positions.

Figure XI. 8,c shows a needle valve used in penstocks provided with branch pipes to by-pass part of the water around the turbine. The valve consists of a streamlined body (1) held by struts in the housing (2). A movable plunger (3) shaped at its end like a needle slides inside body (1). The valve is opened or closed by the motion of this plunger.

The pressure in chambers A and B, controlled by means of valves (5) pilot valve (4), moves the plunger.

The needle valve offers the following advantages: its shape is streamlined, a tight seal may be obtained by forcing the valve against its seat, and it can be readily controlled. The disadvantages are large size and weight, as well as high cost. The ratio of weights of butterfly, spherical, and needle valves is 1:2:3.

Valve operation. Whereas large valves are usually hydraulically operated, smaller ones are operated either by hand or by an electric motor and worm gear. Various layouts of hydraulic drives are shown in Figure XI.11.

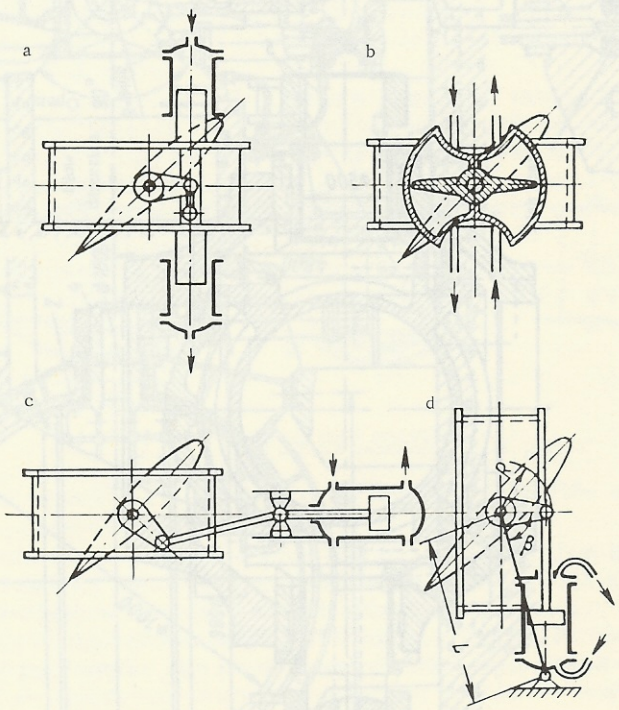


FIGURE XI.11. Hydraulically operated valves

In Figure XI. 11,a, the valve is operated by means of a plunger servomotor mounted on the valve housing. This layout is used with medium-size valves for small- and medium-size turbines. The plunger is sometimes

connected to the lever through a rack-and-pinion drive instead of a shackle. A radial force due to the servomotor causes bending of the valve pivot. The butterfly-valve drive by means of a rotary servomotor is shown in Figure XI. 11,b. The servomotor is mounted on top of the valve housing. The advantage of this layout lies in the small servomotor size and absence of radial loads on the upper pivot. On the other hand, a major disadvantage of this layout is the difficulty of tightly sealing the clearance between rotor and cylinder.

The advantage of these two layouts is that the servomotor force is balanced internally and gives rise to no external load on the valve housing.

In the layouts shown in Figure XI.11,c and d, the servomotors are located outside the valve on a separate foundation; such a layout is used for large valves with powerful servomotors. The servomotor forces act on the valve; this should be taken into account when installing the servomotor.

In Figure XI.11,c, the transmission from the servomotor piston rod to the valve lever is by connecting rod and crosshead. The layout in Figure XI.11,d consists of an oscillating-cylinder servomotor pivoted to the foundation by means of a cylindrical pin. Oil is supplied to the servomotor either through flexible hoses made of oil-resistant rubber or through the stationary pivot. Oscillating-cylinder servomotors (Figure XI.9, (5)) are common in Soviet practice, and have proved satisfactory in operation. It is advisable to arrange the axis of rotation of the valve horizontally, since the pivots are thus less exposed to wear by silt, and two servomotors may be more easily installed.

Butterfly valves. Figure XI.9 shows a recent design of a large butterfly valve with an entrance diameter of 7000 mm for a head of 100 m. The steel housing (1) is welded or cast in several sections; two of them at the sides are provided with bosses for the bearings of pivots (4) and with feet for securing to the foundation (7). The figure shows two different types of disks: cast (2) and welded (8). Either disk consists of three parts: the central part with the pivots and two symmetrical parts bolted to it. An air-inlet valve (vent) (3) is provided on top of the butterfly valve to admit air when the penstock or the casing are emptied. The vent also prevents formation of vacuum downstream from the valve, thus reducing the force on the disk due to water pressure. A by-pass formed by a pipe with an electrically-operated valve (6) is provided at the bottom of the valve for supplying water to the scroll case before the valve opens and equalizing the pressure on both sides of the disk.

The disk is sealed at its periphery by a rubber ring (11) inserted in a recess of the valve housing, and retained by ring (9). The connection to the air pipe is by nipple (10). The rubber ring is kept circular by a helical spring (12) inserted in it. After the valve is closed, air is admitted into the rubber ring, sealing the clearance between the disk and the ring.

Cylindrical gates. Figure XI.10 shows a spherical valve of 1400 mm diameter for a head of 680 m. The steel housing (1) is the main part of the valve; it consists of two hemispheres bolted together, and contains the steel sphere (2) having a central bore. Two pivots (5),bolted to the sphere, are guided in the bushings (6) mounted in the housing. A sealing disk (3), fitted so that part of the sphere facing the tailwater is forced by the water against a stainless-steel seal ring (4) fitted in the housing. To open the seal, a hole provided in the space between disk and sphere is opened to the atmosphere. The radial shift of the sealing disk is usually from 12 to 15 mm. A double-seal design (upstream and downstream from the sphere) which permits

repairs of the downstream seal has come into use recently. The connecting flanges of the valve housing shown in Figure XI.10 are not located on the axis of symmetry, in order to provide place for the pivots. All parts of the valve should be so dimensioned as to be able to withstand high water pressure.

The spherical valve may be rotated by means of a servomotor as shown in Figure XI.11.

Figure XI.12 shows a toroidal plunger servomotor for valves. The toroidal plunger (1) connected to the valve pivot (2) moves inside the annular casing (3) through which oil is supplied and discharged alternatively. It is very difficult to machine the circular surfaces of the toroidal plunger. For servomotors of this type, Allis-Chalmers employs square cross sections with rounded edges instead of circular cross sections.

Valve control. The control system of the valve depends on the servomotor layout and on function and design. The valve may have to be closed only when the turbine is at rest, or also in water flowing with normal velocity, or under emergency conditions if the penstock is damaged. As an illustrative example, Figure XI.13 shows the control system of a spherical valve of 1700 mm diameter, designed and built at the LMZ for a turbine operated under a head of 290 m. The mechanisms are shown with the valve in closed position. Two oscillating-cylinder servomotors (16), each of 400 mm diameter, connected to valve levers (15) and actuated by the oil supplied from oil pump (1) under a pressure of 25 kg/cm^2, provide the force required to turn the valve under emergency conditions when the guide vanes and pressure regulator fail to operate. A pipe with a nonreturn valve (2) is connected to the pressure-oil system. The total discharge through the pipeline is 33 m^3/sec, and the water velocity ~15 m/sec. The highest head, H_{max}, taking into account the pressure surge, is 374 m. The oil is fed by the pump into the main distributing valve (3), which supplies it to the closing side of the servomotor and to the locking valve (13) actuated by combined oil and water pressure. The water from chamber (A) of the housing (10) flows through the annular clearance into cavity (B) and forces the seal disk (7) against the housing. To open the valve, the distributing valve is moved upward by means of an electromagnet provided with a ratchet. Oil under pressure enters the locking valve (13) and flows from there to the hydraulically actuated bypass valve (12). Valves (12) and (13) open, and water starts flowing into the scroll case and pipe (6), the guide vanes being closed. Cavity (B) between the sphere and the sealing disk is connected by means of discharge pipe (11) with space (C) after water valve (9) is opened. The pressure within cavity (B) is suddenly lowered, and the water pressure in

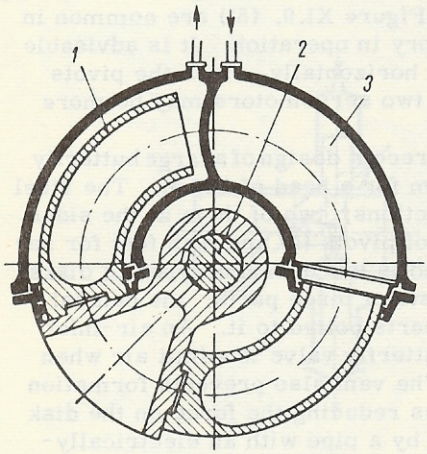


FIGURE XI.12. Toroidal-plunger servomotor

chamber (A) acting upon the outside of the sealing disk forces it away from the housing. The water then flows across the clearance space into space (C) and the turbine casing.

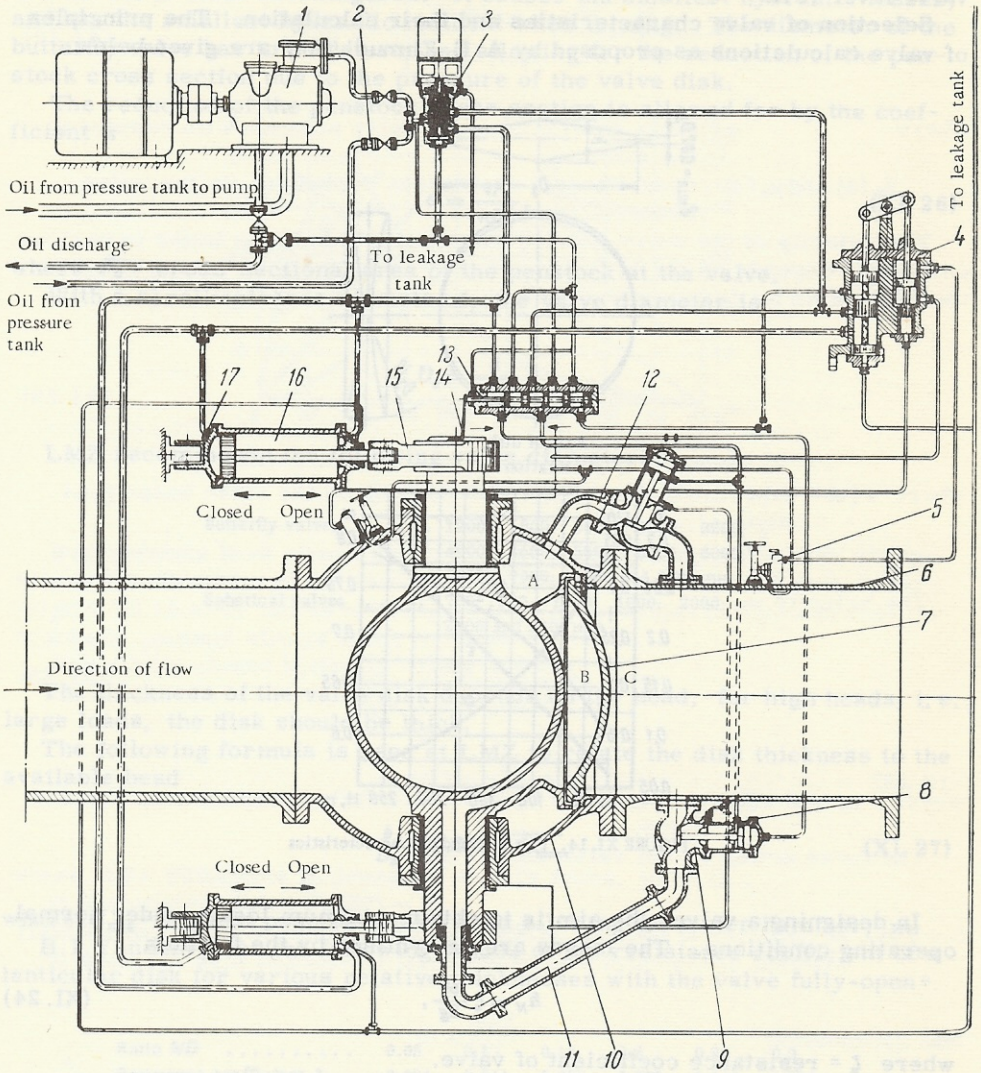


FIGURE XI.13. Control system of a spherical valve

If the pressure in the scroll casing rises, the control valve (4) actuated by combined oil and water-pressure supplies oil to the opening side of the servomotor (16) and the valve opens.

To close the valve, the electromagnet moves the distributing valve (3) into its lower position. Oil flows into the servomotor and the valve closes.

A moment is thus created tending to close the valve. To prevent the water cylinder of valve (4) from clogging, a strainer (5) is provided in the water pipe. The locking and throttling devices ensure the required operational sequence of the control mechanisms. The locking valve is connected to valve lever (14).

Selection of valve characteristics and their calculation. The principles of valve calculations as proposed by A. E. Zhmud' /64/ are given below.

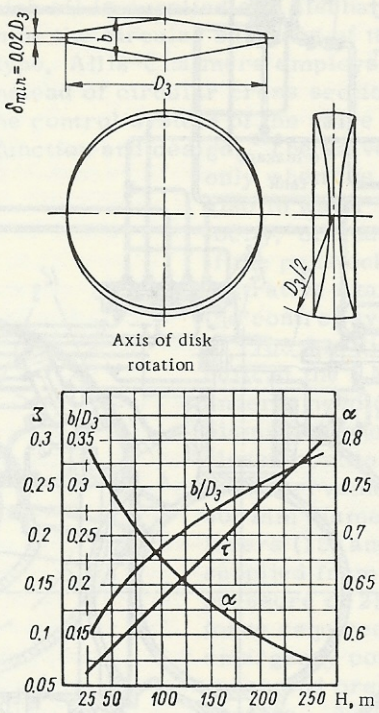


FIGURE XI.14. Flat disk and its characteristics

In designing a valve, the aim is to obtain minimum losses under normal operating conditions. The losses are determined by the formula

$$h_N = \zeta \frac{v^2}{2g}, \qquad \text{(XI. 24)}$$

where ζ = resistance coefficient of valve.

But, since

$$v = \frac{Q}{\frac{\pi D^2}{4}},$$

$$h_N = 0.0827\,\zeta \frac{Q^2}{D^4}. \qquad \text{(XI. 25)}$$

For fully-open spherical valves, $\zeta = 0$.

The principal dimensions of spherical valves are shown in Figure XI. 8, b. With butterfly valves, the value of ζ depends upon the relative disk thickness b/D and the disk shape.

B.I. Yanshin /100, 101/ found that a disk of lenticular shape (see Figure XI. 14) is most advantageous. It causes the smallest hydraulic losses, and has the smallest hydraulic moment when turning. The diameter of the butterfly valve has to be determined allowing for the reduction of the penstock cross section due to the pressure of the valve disk.

The reduction of the penstock cross section is allowed for by the coefficient α

$$\alpha = \frac{4F_0}{\pi D_3^2}, \qquad \text{(XI. 26)}$$

where F_0 = cross-sectional area of the penstock at the valve.

With a scroll-entrance diameter d, the valve diameter is

$$D_3 = \frac{d}{\sqrt{\alpha}}.$$

LMZ recommends the following valve diameters:

Butterfly valves	1200; 1600; 2000; 2500; 3200; 4000; 4500; 5000; 5600; 6000; 6500; 7000; 7500 and 8000 mm
Spherical valves	700; 800; 1200; 1600; 2000; 2500 and 3200 mm

The thickness of the valve disk depends on the head; for high heads, i.e., large loads, the disk should be thick.

The following formula is used at LMZ to relate the disk thickness to the available head

$$\frac{b}{D_3} \approx 0.054 \sqrt[3]{H_{max}}, \qquad \text{(XI. 27)}$$

where H_{max} = highest possible static head allowing for water hammer, m.

B.I. Yanshin gives the following values of the resistance coefficient of a lenticular disk for various relative thicknesses with the valve fully-open*.

Ratio b/D	0.05	0.1	0.15	0.2	0.25	0.3
Resistance coefficient ζ ..	0.031	0.044	0.065	0.096	0.147	0.222

The dependence of the relative disk thickness ζ and of the coefficients α on the head is shown in Figure XI. 14.

* [Russian original reads "fully closed".]

In designing a valve and determining the forces and moments acting on it, it is customary to use experimental data from model tests. The forces and moment due to the water flow vary in direct proportion to the square of its velocity

$$\left.\begin{aligned} P_i &= \lambda_i(\alpha) D_3^2 v^2; \\ M_i &= \mu_i(\alpha) D_3^3 v^2, \end{aligned}\right\} \qquad \text{(XI. 28)}$$

where α = angle determining the valve position with respect to the flow;

$\lambda_i(\alpha)$ and $\mu_i(\alpha)$ = experimental coefficient depending on the valve shape.

The velocity of the water flowing through the valve, the latter in various positions, depends on the hydraulic resistance. The head losses should therefore also be determined during the model tests

$$\Delta H = \varepsilon(\alpha) \frac{v^2}{2g}, \qquad \text{(XI. 29)}$$

where $\varepsilon(\alpha)$ = experimental coefficient depending on the valve shape [and angle α].

The velocity is:

$$v = \sqrt{\frac{2gH_0}{[\varepsilon(\alpha) - \varepsilon(0)] + \frac{2gH_0}{v_0^2}}}, \qquad \text{(XI. 30)}$$

where v_0 and $\varepsilon(0)$ = velocity and losses in the fully opened valve, respectively.

The force acting on the valve disk is thus

$$P_i = \frac{2g\lambda_i(\alpha)}{[\varepsilon(\alpha) - \varepsilon(0)] + \frac{2gH_0}{v_0^2}} \cdot H_0 D_3^2, \qquad \text{(XI. 31)}$$

and the moment

$$M_i = \frac{2g\mu_i(\alpha)}{[\varepsilon(\alpha) - \varepsilon(0)] + \frac{2gH_0}{v_0^2}} \cdot H_0 D_3^3. \qquad \text{(XI. 32)}$$

Figure XI.15 shows the forces and moments due to the water flow acting on the valve disk for two cases:

a) when the lower disk edge moves in the direction of flow during opening;
b) when the lower disk edge moves against the flow during opening.

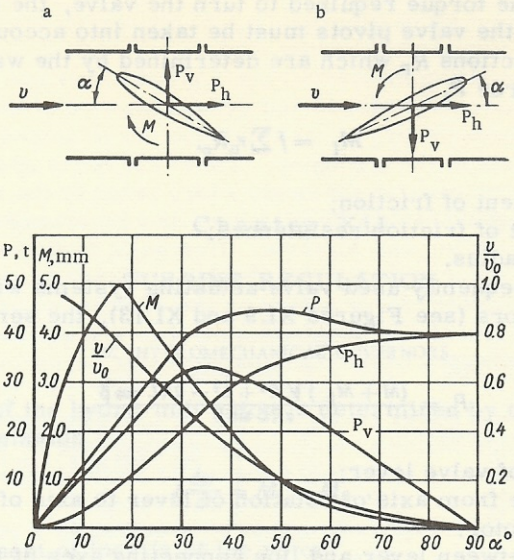


FIGURE XI.15. Forces and moments acting upon the valve disk

Experiments have shown that the horizontal force P_h on the disk always acts in the direction of the velocity, that the vertical force P_v acts upward (Figure XI.15,a) or downward (Figure XI.15,b), respectively, and that the hydraulic moment always tends to close the valve.

For a fully closed butterfly valve, $\alpha = 90°$:

1) the horizontal force is

$$P_h(90°) = \gamma \frac{\pi D^2}{4} \Delta H, \qquad \text{(XI.33)}$$

where ΔH = difference in pressure on disk faces, m W.G.;

2) the vertical force $P_v(90°) = 0$;

3) the hydraulic moment when the axis of rotation is vertical: $M\ (90°) = 0$;

4) when the axis of rotation is horizontal, a hydrostatic moment

$$M = \frac{\pi \gamma D_3^4}{64} \qquad \text{(XI.34)}$$

acts on the disk.

The curves in Figure XI.15, plotted from the experimental data obtained by B.I. Yanshin, illustrate the laws of variation of the velocity, hydraulic moment, and force acting on the disk when in various positions. The values are given for an equivalent hydraulic resistance $\varepsilon_e = 1$. If the resistance varies, the character of the velocity and moment curves changes. The character of the curve $\frac{v}{v_0} = f(\alpha)$ plays an important role in the calculation of water hammer.

Chapter XII

TURBINE REGULATION

70. HYDROMECHANICAL GOVERNORS

The motion of the hydro-unit rotor is determined by the basic equation of power transmission

$$J\frac{d\omega}{dt} = M_r - M_m ,$$

where J = moment of inertia of the rotor;
ω = angular speed;
M_r = moment of resistance forces (external load on the generator);
M_m = moment of driving force developed by the turbine.

The frequency of the electric current generated should be practically constant. Since it varies in direct proportion to the speed of the hydro unit, it is essential that $\frac{d\omega}{dt} \approx 0$. This is true if the moment of the driving force equals that of the resistance forces.

$$M_m = M_r .$$

To maintain a constant frequency, the moment of the driving force must conform with the varying load

$$M_m = \frac{\gamma Q H \eta}{\omega} ,$$

and the most convenient way of altering the moment of the driving force is to vary the flow through the turbine.

In Francis turbines, the flow is controlled by the guide vanes, in Kaplan turbines, by the guide vanes and runner blades jointly.

Hydraulic turbines are mostly designed for speed regulation, the governor responding to variations in the rotational speed.

The general theory of machine control and regulation has been examined in detail by many authors. Regulation problems specific to hydraulic turbines have been studied by I. N. Boznesenskii /13/.

Further research into regulation problems has been done at the LMZ in connection with the design of governors for high-power turbines.

The theory and design of modern hydraulic-turbine governors are treated in detail by Yu. I. Garkavi and M. O. Smirnov /16/.

The governor maintains constant the speed of the hydro unit by altering the driving moment M_m in accordance with the resistance moment M_r of the generator operating under varying loads.

To rotate the regulating elements, i.e., guide vanes and runner blades, large forces amounting to hundreds and even thousands of tons are required. These forces are produced by the main turbine servomotors which are the final-control elements of the governor. These elements are connected to the governor speed-responsive elements which react to the slightest change in speed. These speed-responsive elements may be classified as centrifugal (flyballs), hydraulic, and electric. Hydraulic turbines are generally provided with centrifugal governors, in which a change in speed causes a variation of the centrifugal force acting on the rotating weights, and therefore of their displacement. This displacement is transmitted to a control element directly connected to the distributing valve supplying pressure oil to the servomotors.

The weights of centrifugal governors are attached to the shaft by elastic suspensions of various designs, such as helical springs or leaf springs. The latter are widely used nowadays because of their simple design and high sensitivity.

The hydraulic speed-responsive element is driven by a pump that supplies oil to a cylinder at a pressure proportional to the turbine speed. The spring-loaded piston is displaced by the pressure oil actuating the regulating mechanisms.

The electric speed-responsive element is described in this book together with the electrohydraulic governor.

A number of intermediate oil-hydraulic amplifiers, distributing valves, and piston servomotors are inserted between the governor and the main servomotor to amplify the small impulses of the governor to the forces required to operate the guide vanes and runner blades. The distributing valves are usually piston valves, the piston being a cylindrical body with several lands. According to the position of the piston, some of the valve ports are covered by the lands. Pressure oil supplied either directly by the pump if the governor is of the direct-action type, or from the pressure tank if the governor is of the pressure-tank type, is fed to either end of the servomotor cylinder.

On governors of the direct-flow type /79/, the lands of the piston do not cover the ports completely, clearances being left between the edges of the lands and the ports. In mid-position, the valve piston has a slight reciprocating motion, thus creating the necessary pressure difference between the oil supplied continuously by the pump and the servomotor. Part of the oil compensates for the leakages in the servomotor, the rest returning to the sump.

Figure XII.1 shows schematically a direct-action governor. Pump (2) is driven continuously by electric motor (1) or through belts from the turbine shaft. The oil, drawn from sump (8), is supplied to distributing valve (4) through pipe (3). From the distributing valve the oil is fed to servomotor (6) through pipes (7). When the valve piston is in mid-position, the oil flows through the clearances between the piston lands and the ports into the sump. When the flyballs (5) cause the valve piston to move from mid-position, oil is admitted into the corresponding servomotor-cylinder port, producing the force required.

The direct-action governor is usually housed in a cylindrical casing which also contains the sump. The gear pump, horizontally located servomotor, the distributing valve, and the flyballs, are mounted on top of the casing.

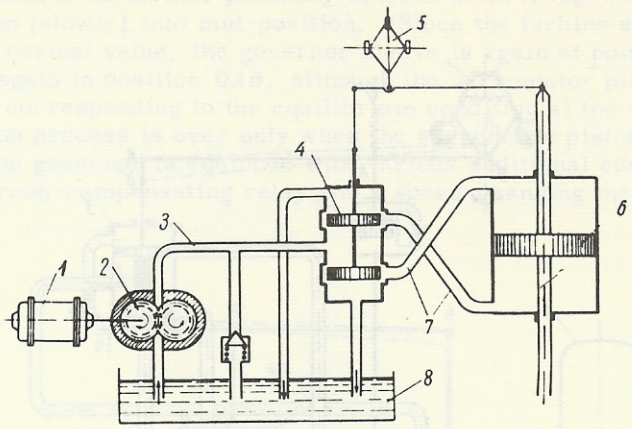


FIGURE XII.1. Direct-action governor

The force developed by the servomotor, and the time required for a full stroke, depend on the pump capacity. If the pump or the pump drive fail to operate properly, the governor cannot regulate the turbine. With this type of governor, automatic control of the turbine is difficult to arrange. Direct-action governors are therefore used only on small turbines.

In the pressure-tank governor (Figure XII.2) oil is supplied to distributing valve (3) from pressure tank (9). Oil level and pressure in the tank are controlled by pump (6), equipped with safety valve (5), relief valve (8) and check valve (7). Air supplied to the tank from a compressor builds up a sufficient pressure reserve to regulate the turbine for a short period, should oil-pump failure occur.

In the distributing valve (3) of this type of governor, the piston lands completely cover the ports when the piston valve is in mid-position, only a small amount of oil passing through to compensate for leakages in the governor system.

During regulation, when the distributing-valve piston changes its position, oil is fed from the pressure tank through the open ports into servomotor cylinder (4), developing the force required to turn the guide vanes. In Kaplan turbines, oil is fed simultaneously to the runner servomotor through its distributing valve, which is actuated by a special feedback mechanism that ensures the required synchronism between runner-blade and guide-vane rotation.

Hydro-turbine regulation differs from the regulation of other prime movers. Alteration of flow velocity through the turbine causes the appearance of water hammer, and a corresponding change in the head under which the turbine operates. For the generator to produce current of a given frequency, the turbine governor should ensure that, at the end of the regulation

process, the rotational speed is the same as at the beginning, i.e., its characteristic should be such as to ensure speed-droop compensation. By speed-droop (nonuniformity) is understood the ratio of the difference between no-load and full-load speeds to the normal speed. This condition is fulfilled by using a pilot-operated (indirect) governor provided with proportional-plus-floating control-elements [(isodrome control)] (Figure XII.2).

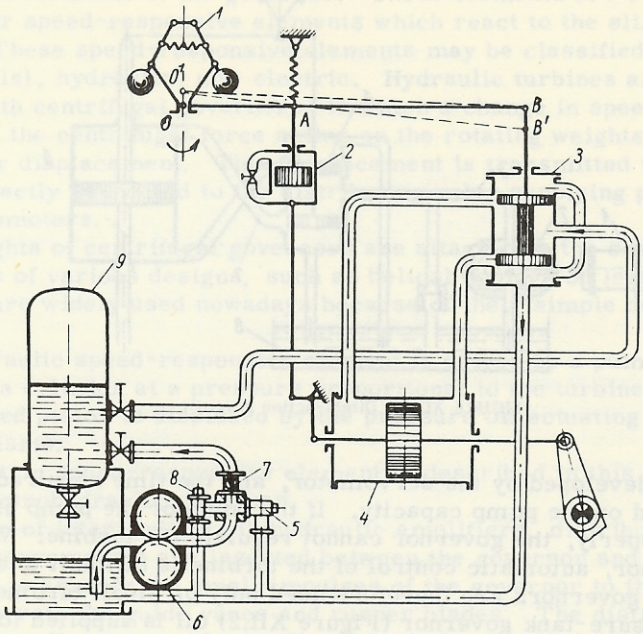


FIGURE XII.2. Pressure-tank governor

Speed is maintained constant by inserting a feedback (2) mechanism consisting of an oil dashpot and a cylinder with an oil-actuated piston. The two cylinder-ends are connected by a pipe with constriction. The dashpot cylinder is rigidly linked to the servomotor piston by a lever transmission, the dashpot piston being linked to the lever connecting the governor (1) with the regulating valve (3). Regulation is as follows: Under steady-operating conditions, the speed of the hydro unit is constant. The governor (1), the floating lever (*OAB*), and the distributing-valve piston (3) are in mid-position. The servomotor piston is maintained by the oil pressure and the resistance of the regulating mechanism in a position corresponding to equilibrium.

When the load on the generator drops, the speed increases, the angular velocity of the flyballs increasing with it, causing the governor sleeve to move upward. The floating lever turns about the fulcrum *A*, assuming the new position *O'AB'* and forcing the distributing valve downward. Oil is admitted into the right-hand servomotor cylinder end, and the piston moves to the left, acting upon the regulating mechanism which closes the gates and reduces water admission.

Simultaneously, through the oil dashpot which initially acts as a rigid connection since the oil cannot flow fast enough through the by-pass constriction, the servomotor piston forces point *A* upward. The lever, turning about fulcrum *O'*, compresses the spring and moves the distributing valve upward back to mid-position. The lever is now in position *O'B*. The spring, striving to assume its former position, returns point *A* together with the dashpot piston [slowly] into mid-position. [Since the turbine speed has returned to its normal value, the governor sleeve is again at point *O*. Thus, the lever is again in position *OAB*, although the servomotor piston is in a new position corresponding to the equilibrium condition at the reduced load.] The regulation process is over only when the servomotor piston stops moving.

The turbine governor is equipped with various additional control mechanisms: a droop-compensating relay and a speed-changing mechanism.

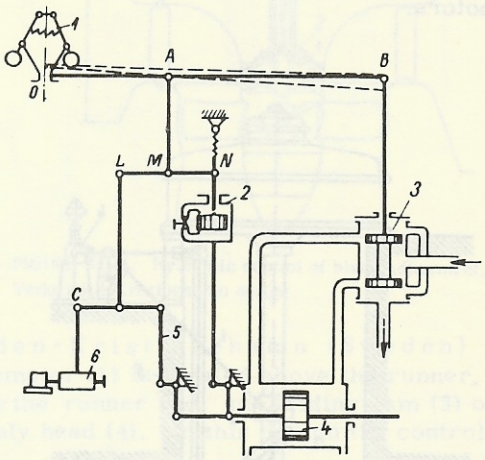


FIGURE XII.3. Governor with droop-compensating relay

The floating lever connecting governor (1) to the distributing valve (3) (Figure XII. 3) is provided at point *A* with, apart from the ordinary isodrome control, an additional linkage to the servomotor (4) through the droop-compensating mechanism and rod (5).

Toward the end of the regulation process, when point *B* is nearly at mid-position, fulcrum *A* at the end of lever *LMN* is not in mid-position because of the feedback by the droop-compensating mechanism. The governor sleeve connected to the floating lever is also not in mid-position corresponding to the normal speed. The unit thus operates at a steady speed different from the former.

The speed-adjustment mechanism permits synchronization of several hydro units in a system, with individual loads varying from no-load to maximum at normal frequency. The governor is adjusted by means of mechanism (6) linked to point *C*. Thus, steady operation is possible at various flyball positions corresponding to different speeds. An upward displacement of point *C* results in a higher speed, and vice versa.

Apart from the devices enumerated, the governor also includes a device for automatic turbine starting and stopping, a mechanism for limiting the guide-vane opening, and other miscellaneous equipment.

In Kaplan turbines a runner-blade control valve is also provided.

The simplest mechanical control of the blade-operating mechanism (formerly used by many works building Kaplan turbines) is shown in Figure XII.4. The force required to turn the blades is transmitted from the governor servomotor (4) to the guide vanes through the regulating shaft (5) and to the runner blades through rod (1) and mechanism (3). A double thrust-collar (2) is mounted on the shaft.

This method is appropriate for small turbines, but is inconvenient for medium and high-power turbines, since the considerable regulating forces require a corresponding increase in size of the rods, levers, and links. This type of control has therefore been superseded by hydraulic control with rotating servomotors.

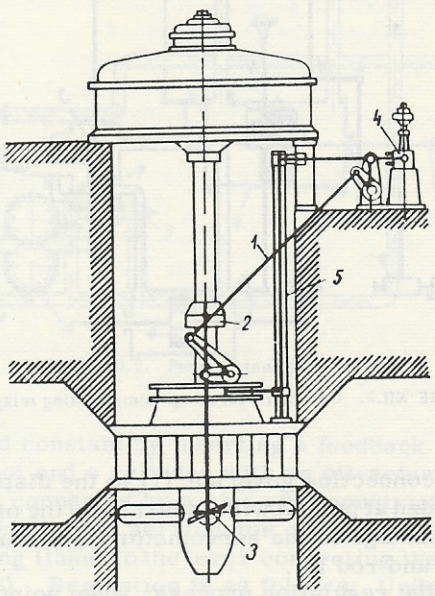


FIGURE XII.4. Mechanical blade control

Double regulation of Kaplan turbines with hydraulic control is shown schematically in Figure I.6.

The guide vanes are adjusted to the required opening by means of oil servomotor (4).

Oil is supplied to the distributor servomotor through the distributing valve (1), displaced by the governor (7), driven electrically from the main turbine shaft.

Runner blades (6) are adjusted simultaneously with the guide vanes. The force required to turn them is produced by the oil servomotor (3), controlled by the distributing valve (1), connected to the driving mechanism of the distributor by means of a rod system and the sliding cam (2).

Various layouts have been adopted for the main parts of the runner-blade adjusting mechanism. The most important are given below.

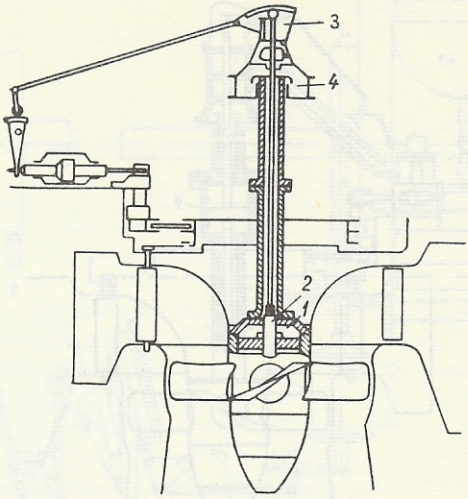


FIGURE XII.5. Hydraulic control of blade adjustment, Verkstaden-Kristinehamn design

1. Verkstaden-Kristinehamn (Sweden) design (see Figure XII.5). Servomotor (1) is located above the runner, distributing valve (2) in the hub inside the runner rod, and sliding cam (3) on top of the shaft above the oil-supply head (4). In this design the control valve is hydraulically operated.

The positive feature of this layout is the small distances of the servomotor and the distributing valve from the blade-operating mechanism, which permits minimum rod length. The large dimensions of the control valve, due to its long stroke which equals the servomotor piston stroke, are a drawback. If the control valve jams, the runner must be dismantled, which requires a good deal of work.

With this layout it is difficult to install a blade-position indicator.

2. Voith (West Germany) design (see Figure XII.6). The runner servomotor (1) is located outside the hub between the shaft flanges, while the distributing valve and the sliding cam are located inside the governor casing (2) in the machine room. A linkage (3) connects the distributing valve to the runner servomotor. The disadvantage of this layout is the great distance between the servomotor and the blade-operating mechanism. The distributing valve is readily accessible and its stroke is independent of the servomotor piston stroke, which is an advantage.

3. The layout employed by the LMZ for small and medium turbines is shown in Figure XII.7. The servomotor (1) is located inside the runner hub, thus requiring only a minimum rod length; the distributing valve (4) is mounted on the upper extension of the shaft inside the oil-supply head. The servomotor is hydraulically actuated through rod (2) rigidly connected to the servomotor piston. A cam wedge (6) is located inside

casing (5) which also encloses the auxiliary servomotor with the pilot valve. The linkage from the distributor servomotor is only slightly loaded, since the cam wedge actuates only the pilot valve.

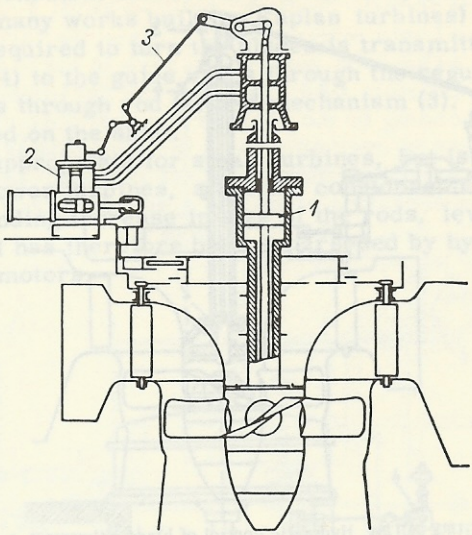


FIGURE XII.6. Hydraulic control of blade adjustment, Voith (Heidenheim) design

A series of LMZ turbines were equipped with this control and proved highly satisfactory in operation.

The location of the tubular distributing valve (4) in a special housing (3) above the generator is characteristic of this layout; the valve encloses the end of the control rod which is also used to feed oil to the servomotor. The arrangement also includes a runner-blade position indicator. This layout was first proposed by V. A. Time /82, 83/. Casing (5) is located in the machine room and contains, beside cam wedge (6) and pilot valve (7), also manual controls for the runner distributing valve and the cam wedge.

For large high-power turbines, these arrangements proved impractical, since the runner distributing valve mounted on the servomotor piston has the same stroke as the servomotor piston; its dimensions become very large, necessitating two, or even three, control stages, thus complicating the layout. The layout shown in Figure XII.8 was therefore specially devised at the LMZ by N. N. Kovalev and S. A. Branovskii for the high-power Rybinsk and Uglich hydro turbines. Distributing valve (1) is enclosed in the casing of the blade-control mechanism located in the machine room. Oil is supplied from the distributing valve to the runner servomotor (2) through the oil-supply head (3), mounted above the generator. Displacement of the distributing-valve piston is effected by cam wedge (4), connected by linkage (5) to the distributor servomotor (6). This layout is similar to that shown in Figure XII.6, the only difference being in the location of the runner servomotor (inside the runner hub) and of the distributing valve.

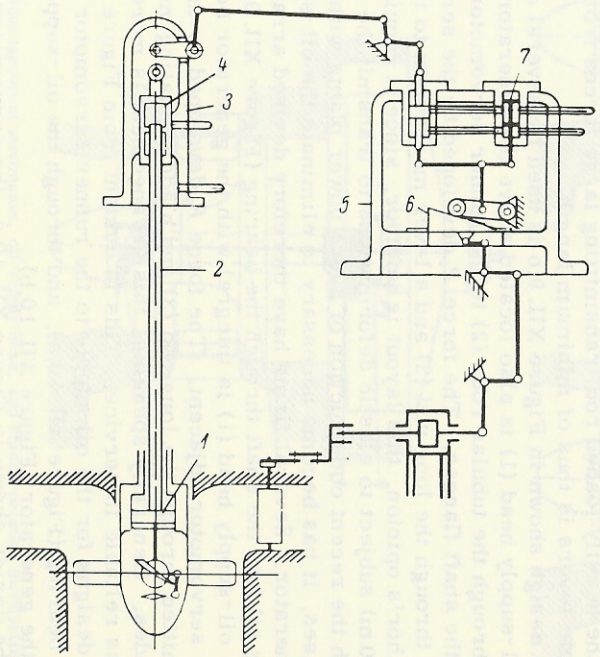


FIGURE XII.7. Hydraulic control of the runner blades used by the LMZ for medium turbines

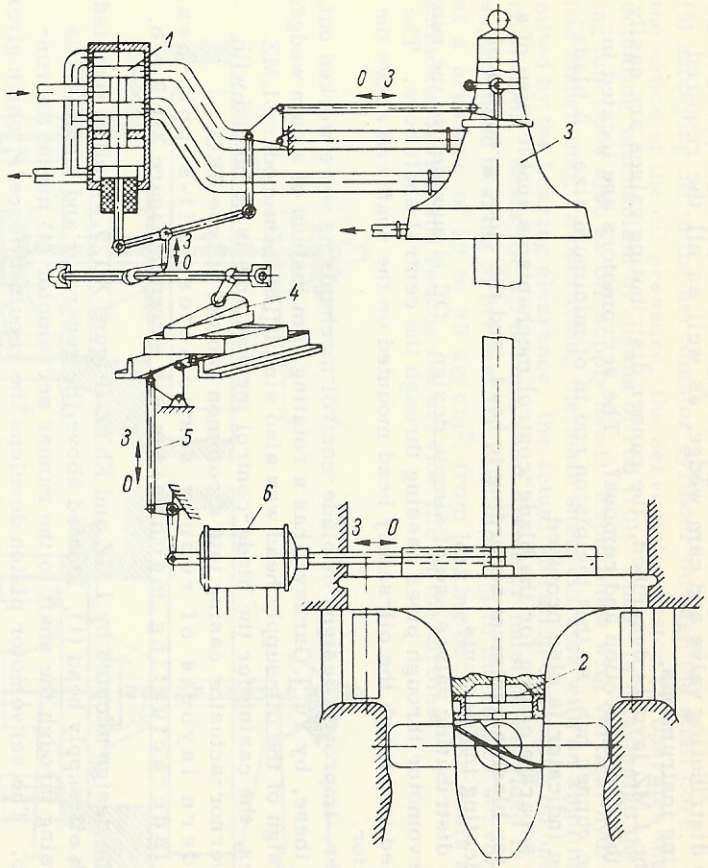


FIGURE XII.8. Hydraulic control of the Rybinsk turbines

The casing of the blade-control mechanism for the Rybinsk and Uglich turbines contains also the manual- and remote-control mechanism for the runner distributing valve and cam wedge, as well as all the required indicating instruments.

In the LMZ layouts described, the runner distributing valves are easily accessible for inspection and removal. The servomotors are located inside the runner hub, so that the piston rod is of minimum size. A blade-position indicator is also provided.

The separate casing for the blade-control mechanisms enables use of a wedge for blade adjustment according to head, and the close grouping of all indicating instruments.

The distributing valves are of simple design. Oil is supplied to the runner servomotor through pipes passing through the central shaft bore. The oil is led in through the oil-supply head mounted on the shaft end above the generator.

Later, improved designs of blade-control mechanisms were worked out. One of these, by Yu. I. Garkavi, has a rotating cam instead of a cam wedge. The design of the oil-supply head was also simplified. On modern LMZ turbines, the casing for the blade-control mechanisms is combined with the governor-actuator casing into a common cabinet of type RKO.

Modern layouts of runner servomotor, oil-supply head, and blade-actuating mechanism are shown in Figure XII. 9, a, b, and c.

In the design adopted by LMZ and KhTZ (Figure XII. 9, a), oil is supplied through oil-supply head (1), located above the generator and tubular rods (2) passing through the shaft to the runner servomotor (4) inside the runner hub. The servomotor piston develops the required force P_s which gives rise to a moment M_r acting on the blades by means of rod (3) and blade-actuating mechanism (5). This is the best location for the servomotor, since the heavily-loaded rod transmitting large forces from the piston to the blade levers is thus of minimum length.

The design shown in Figure XII. 9,b is used by several companies abroad. The oil-supply head (1) is also located above the generator and oil is supplied through the tubular rods (2) to the runner servomotor (4) located between the shaft flanges. The force P_s developed by the servomotor is transmitted through the long rod (3) and a lever mechanism to the blades. In the author's opinion, this layout is inferior, since it requires a longer rod (7 to 10 m) subject to elastic deformations to transmit the force.

With the recent construction of hydro power plants without separate power houses, it has become necessary to eliminate the oil-supply head above the generator. Several firms have therefore devised arrangements for admitting oil into the shaft through the bearing (Figure XII. 9,c).

The oil-supply head (1) is integral with the generator bearing, with the runner servomotor adjacent. The force P_s developed by the servomotor is transmitted through the long rod (3) and blade-actuating mechanism (5) to the blades. Generally speaking, this arrangement is more complicated and less reliable in service. This is evident from Figure XII. 10, which shows designs for the oil supply to the runner servomotor through the generator bearing (Figure XII. 10,a), and through the oil-supply head located above the generator (Figure XII. 10,b).

In the design shown in Figure XII. 10,a, the servomotor is located inside the generator, the servomotor cylinder (2) forming, at the same time,

the base of thrust collar (4) and the hub of the generator rotor (1); the generator bearing is mounted in the conical frame (6). Six channels are provided in the bearing, with corresponding borings in the shaft, for the pipes (8) and (9) supplying oil to the servomotor cylinder through the shaft bore. Under the action of the oil pressure, the servomotor piston (3) operates the blade-actuating mechanism by means of rod (10). Thus, in this design the bearing functions also as oil-supply head. Experience with vertical hydro units has shown that, in operation, the main shaft vibrates with an amplitude limited by the bearing clearance, the actual vibration depending on operating conditions. Seals for a 1400 mm shaft diameter must be provided in the oil-supply head bearing to prevent the oil, supplied to the runner servomotor at a pressure of 20 to 30 kg/cm^2, from leaking out. These seals are of intricate design and reduce the service life of the turbine.

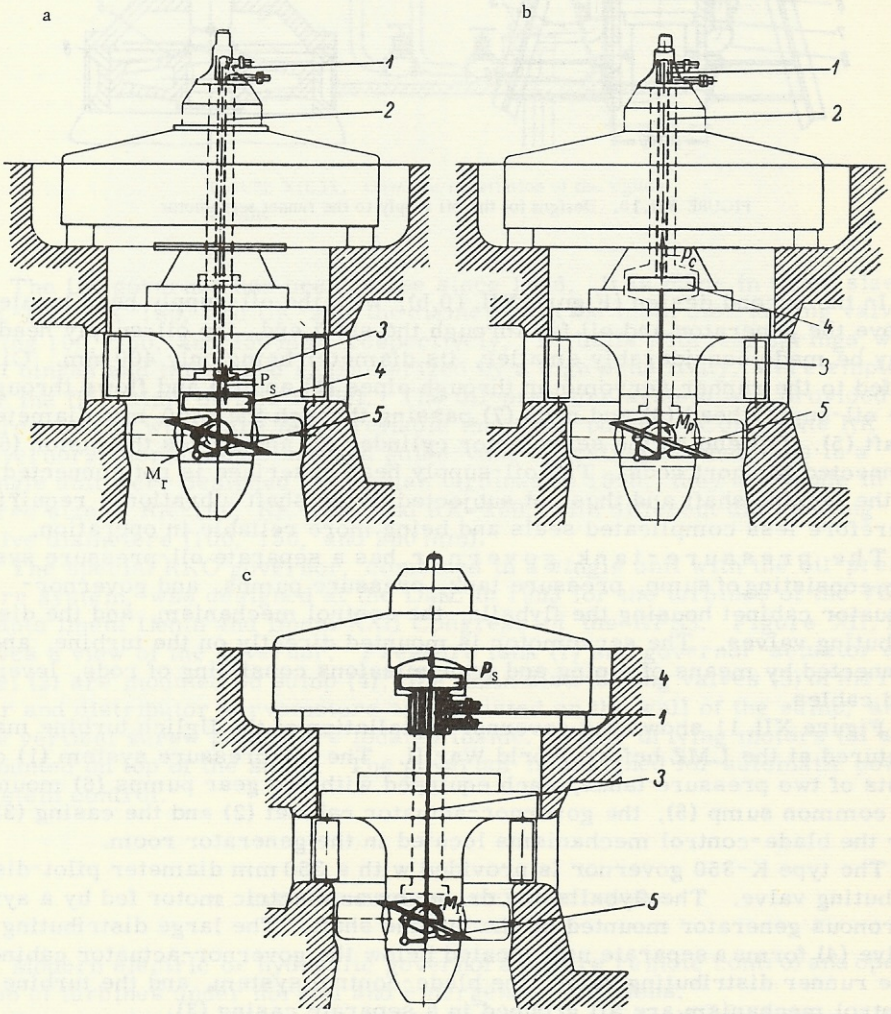


FIGURE XII.9. Various layouts of servomotor, oil-supply head, and blade-operating mechanism

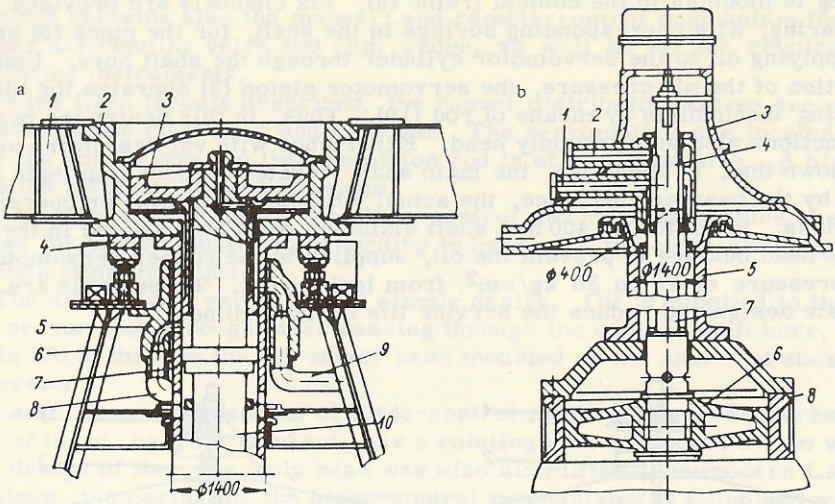


FIGURE XII.10. Designs for the oil supply to the runner servomotor

In the second design (Figure XII. 10,b), with the oil-supply head located above the generator and oil fed through the shaft end, the oil-supply head may be made considerably smaller, its diameter being only 400 mm. Oil is fed to the runner servomotor through pipes (1) and (2) and flows through the oil-supply head (4) and rods (7) passing through the 1400 mm diameter shaft (5). Oil enters the servomotor cylinder (8) and moves the piston (6) connected to short rods. The oil-supply head described is not connected to the turbine shaft and thus not subjected to the shaft vibrations, requiring therefore less complicated seals and being more reliable in operation.

The pressure-tank governor has a separate oil-pressure system consisting of sump, pressure tank, pressure pumps, and governor-actuator cabinet housing the flyballs, the control mechanism, and the distributing valves. The servomotor is mounted directly on the turbine, and connected by means of piping and transmissions consisting of rods, levers, and cables.

Figure XII. 11 shows the governor installation of the Uglich turbine manufactured at the LMZ before World War II. The oil-pressure system (1) consists of two pressure tanks, each equipped with two gear pumps (6) mounted on common sump (5), the governor-actuator cabinet (2) and the casing (3) for the blade-control mechanisms located in the generator room.

The type K-350 governor is provided with a 350 mm diameter pilot-distributing valve. The flyballs are driven by an electric motor fed by a synchronous generator mounted on the turbine shaft. The large distributing valve (4) forms a separate unit located below the governor-actuator cabinet. The runner distributing valve, the blade-control system, and the turbine control mechanism are all grouped in a separate casing (3).

Improved turbine governors of types UK, RK, RKO, and RO were built at the LMZ after World War II.

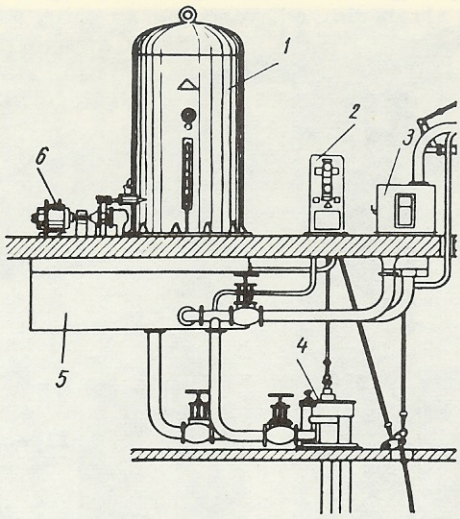


FIGURE XII.11. Governor installation of the Uglich turbine

The UK governor has been in use since 1946. It is made in three sizes: UK-100, UK-150, and UK-250, the diameters of the main distributing valves being 100, 150, and 250 mm, respectively. Flyballs with leaf springs, without hinges and links, and characterized by a high sensitivity, were employed for the first time on this model. The oil-pressure system was provided with screw pumps which are more reliable than gear pumps. Composite RK governors, combining blade and guide-vane operating mechanisms in a single unit were designed for Kaplan turbines in 1950; they are made in three sizes: RK-100, RK-150, and RK—250, with different distributing-valve diameters (100, 150, and 250 mm).

The special RKO governor, combined in a single unit with the oil-pressure system, was designed at the LMZ in 1953 for the turbines of the Volga plants imeni Lenin and imeni XXII Congress of the KPSS. Figure XII.12 gives a view of the governor. Pressure tank (1) and governor-actuator cabinet (2) are mounted on sump (4); the main distributing valves (3) of the runner and distributor servomotors are mounted on the wall of the sump, and the vertical screw pumps are located inside. Their driving motors (5) are mounted on top of the sump. The governor is designed for automatic power-system control.

71. BASIC PRINCIPLES OF AUTOMATIC CONTROL

Modern electric or hydraulic governors ensure remote control and operation of turbines under normal and emergency conditions.

The automatic control system of a hydro unit is usually devised with the following principles in mind:

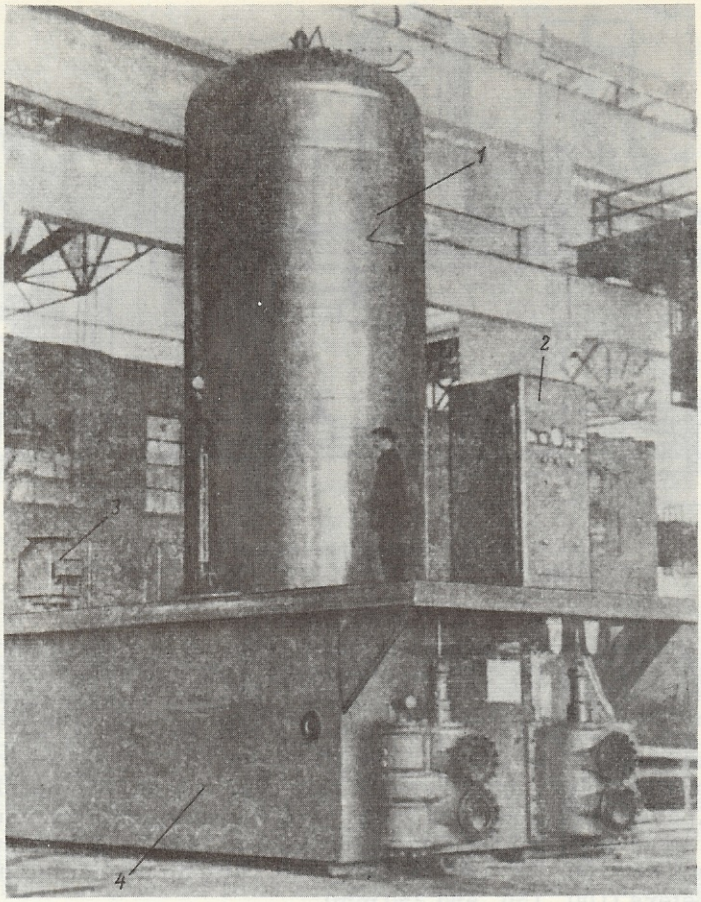


FIGURE XII.12. Type RKO-250 governor

1. The staff has to supervise automatically operated units only.
2. The unit is automatically started and stopped by a single control impulse, after which the mechanisms act in the required sequence.
3. Correct operation of the unit and its components is controlled by mechanical and electrical relays (pressure relays, level relays, speed relays, etc.). When one of the mechanisms fails to operate normally, a warning signal is given to indicate whether operation may continue for a certain time; if not, the unit is automatically shut down.
4. Emergency shutdown is effected automatically.
5. Provision is made for manual control of the turbine and its mechanisms for purposes of testing and adjustment.
6. The most important elements of the hydro-unit control system, such as oil pumps of the pressure-oil system are duplicated by stand-by units fitted with automatic-starting devices.

In line with the above, hydraulic equipment is designed to meet the following turbine-operating conditions:

1) automatic starting, operating in the following sequence after reception of the command: the guide vanes open, the unit starts running, the generator is synchronized, and switched into the net;

2) automatic control of rotational speed under varying loads;

3) automatic refilling of the pressure-oil tank (starting the main oil pump);

4) automatic starting of the stand-by oil pump when the pressure in the pressure-oil tank drops below a predetermined minimum;

5) automatic pumping of air into the pressure-oil tank when the oil level rises above normal;

6) automatic starting of the pump when the oil level rises in the sump;

7) automatic starting of the ejector (if provided) when the water level rises above the turbine cover-plate, with simultaneous indication on the control desk;

8) automatic stand-by lubrication of the turbine guide-bearing from the industrial water main (when water lubrication of bearings is employed);

9) automatic control of the air-admission valve feeding air through the turbine bore into the cavity below the runner when the unit is operating under unstable conditions;

10) automatic admission of compressed air into the water passages adjoining the runner when the unit operates as a synchronous motor for power-factor correction;

11) normal automatic shutdown which — after reception of the command — removes the load from the generator and disconnects it from the line, closes the turbine distributor, and brakes the hydro unit from low speed to a complete stoppage. After this, the unit is ready to be restarted;

12) emergency automatic shutdown;

a) by actuating the start-stop control system of the turbine;

b) by means of an emergency control valve supplying pressure oil from the oil pressure-system directly to the distributor servomotor when the overspeed relay acts;

c) by means of the quick-action intake gates;

13) automatic changing over of the hydro unit from operating as generator to operating as synchronous motor for power-factor correction: after reception of the command the distributor is closed, and the water removed from the throat ring down to a predetermined level.

To carry out automatic operation as described, the hydraulic equipment has to be provided with various automatic devices, such as:

1) a pressure relay controlling the fluid pressure and operating at predetermined pressures;

2) a time relay making the connections after a predetermined interval;

3) a temperature relay operating when a predetermined temperature is attained;

4) a flow relay operating at a predetermined flow velocity;

5) a speed relay operating at predetermined rotational speed of the hydro unit.

Automatic devices also include solenoid valves, hydraulically operated valves, float devices with electric switches, etc.

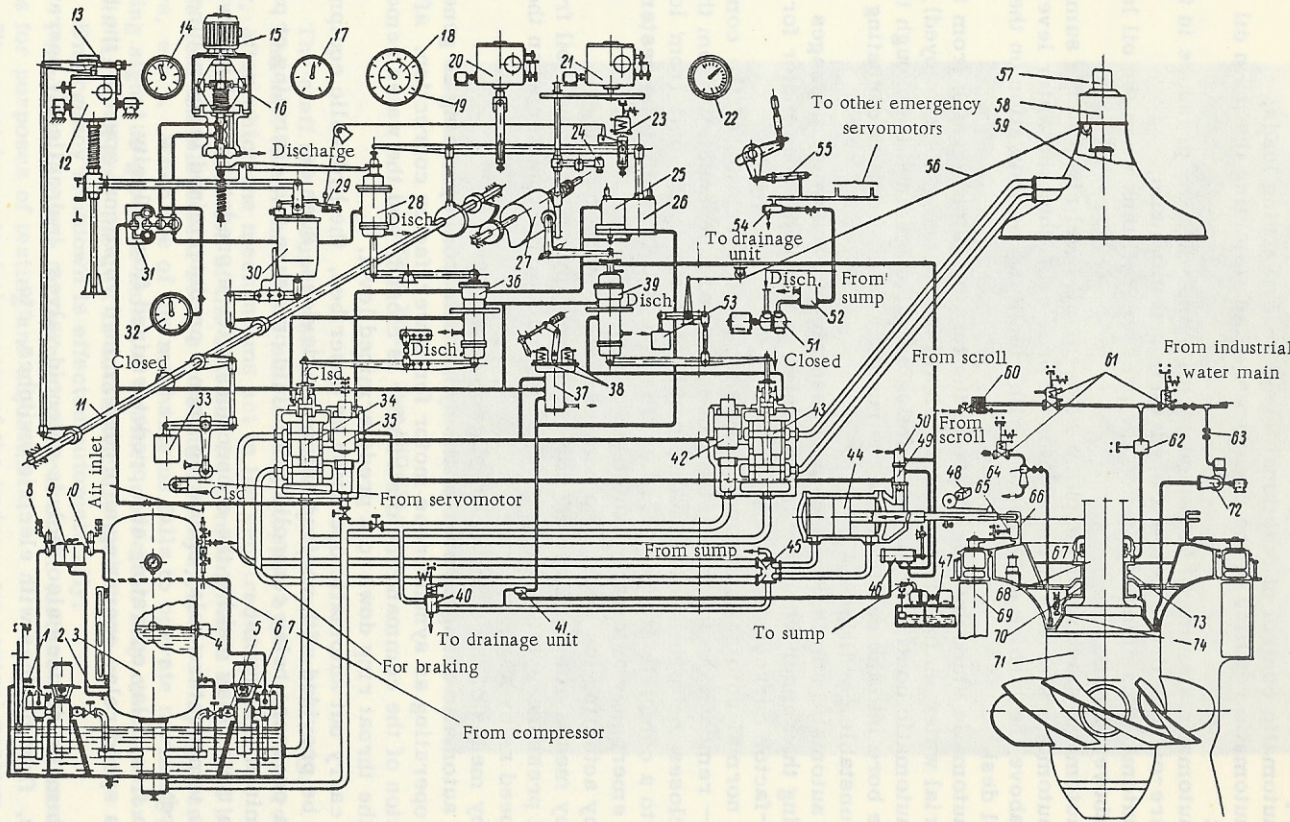

Discharge
Disch.
Closed
Clsd.
Air inlet
From servomotor
For braking
From compressor
To drainage unit
To other emergency servomotors
To drainage unit
From sump
Disch.
From sump
Closed
From scroll
From scroll
From industrial-water main
From sump
To sump

FIGURE XII.13. Schematic diagram of the RKO-250 governor

1—sump level indicator; 2—sump; 3—pressure tank; 4—level relay in pressure tank; 5—check valve; 6—electrically-driven oil pump; 7—relief valve; 8—pressure relay to switch-on the stand-by pump; 9—oil strainer; 10—minimum-pressure relay; 11—actuating shaft; 12—speed-adjustment mechanism; 13—droop-compensating mechanism; 14—speed-droop indicator; 15—synchronous motor; 16—flyballs; 17—electrotachometer; 18—runner-blade position indicator; 19—distributor-position indicator; 20—mechanism to limit opening; 21—planetary gear for adjusment to head; 22—adjustment indicator; 23—quick-action stop; 24—head-sensitive stop; 25—regulation starting-device; 26—governor starting device; 27—regulation cam; 28—auxiliary servomotor; 29—mechanism for cutting-out the dashpot; 30—dashpot; 31—oil strainer; 32—pressure gage; 33—counterweight; 34—main distributing valve of the distributor servomotor; 35—distributor hydraulic valve; 36—amplifier valve; 37—starting valve; 38—start and stop electromagnets; 39—amplifier-runner distributing-valve; 40—special valve; 41—emergency valve of the blocking device; 42—runner hydraulic valve; 43—main runner distributing valve; 44—distributor servomotor; 45—emergency distributing valve; 46—servomotor-blocking valve; 47—drainage unit; 48—push-button control; 49—servomotor stop; 50—stop-blocking valve; 51—high-pressure pumps; 52—safety valve; 53—counterweight; 54—special valve; 55—separate servomotor for emergency shutdown; 56—cable; 57—speed relay; 58—pilot generator; 59—oil-supply head; 60—strainer; 61—hydraulic valve; 62—lubrication flow relay; 63—pump-priming valve; 64—ejector; 65—contacts; 66—gate ring; 67—turbine stuffing-box; 68—turbine shaft; 69—distributor; 70—turbine bearing; 71—runner; 72—drain pump; 73—electrotachometer; 74—float relay.

72. INTERACTION OF GOVERNOR ELEMENTS IN THE KAPLAN TURBINE

Figure XII. 13 shows schematically the type RKO-250 governor used for high-power Kaplan turbines. Numbers 1 to 10 indicate the mechanisms and devices of the pressure-oil system; numbers 11 to 43, the mechanisms and devices grouped in the governor-actuator cabinet and the most important servomotor distributing-valves, numbers 44 to 74, the parts and mechanisms of the servomotor, the oil-supply head and the turbine itself. It is assumed that initially normal operating conditions obtain. When load is rejected, turbine output and consequently water flow are greater than the generator requires, resulting in increased generator speed. The speed of the pilot generator (58) also increases and, with it, the speed of the synchronous motor (15) driving the flyballs. The increased centrifugal forces cause the rotating weights to move outward, actuating the piston of the pilot distributing valve which moves upward, admitting oil to the auxiliary servomotor (28). The piston of the auxiliary servomotor moves downward, displacing the slide of amplifier valve (36), which actuates the main distribution valve (34) of the distributor servomotor.

Oil under pressure is fed from pressure tank (3) through distributor hydraulic valve (35) and main distributing valve (34) to the pressure end of the cylinder of distributor servomotor (44), whose opposite end is connected through main distributing valve (34) with sump (2). Oil pressure acting on the servomotor piston develops the force required to actuate distributor (69), reducing the water flow and thus also the power developed by the turbine. By means of a cable (not shown in the figure) the servomotor piston rotates the actuating shaft (11) which moves the blade-control cam (27). The lever, whose roller is pressed against the cam, actuates the amplifier runner-distributing valve (39). This valve forces down the piston of the main runner distributing valve (43); pressure oil is fed through runner hydraulic valve (42), oil-supply head (59), and the rod to the runner servomotor.

From the discharge end of the servomotor cylinder, the oil flows through the second rod, the discharge chamber of the oil-supply head, and a distributing valve into the sump. The oil pressure moves the servomotor piston with its rod. The axial rod movement is transmitted by means of a crosspiece, lever, and cable (56) to the main runner-distributing valve (43), causing it to return to its mid-position. The runner blades turn to an angle corresponding to the new distributor position.

In turning, the actuating shaft (11) pushes the cylinder of dashpot (30) upward. By its rapid motion, the dashpot cylinder carries the dashpot piston with it, which latter moves the piston of the auxiliary servomotor (28) toward its mid-position, thus causing also the main distributing valve (34) to move toward mid-position. The dashpot piston also moves the needle of the flyball control valve toward mid-position corresponding to normal speed. By means of a spring, the dashpot piston returns to its mid-position.

Regulation is a damped-oscillation process which comes to an end when the guide vanes and runner blades reach their new position. The new rotational speed of the unit depends on the permissible speed droop.

When the load on the unit is increased, the regulation process is similar but reversed.

In practice, the action of the various mechanisms of the governor system is much more complex because of the many auxiliary devices and mechanisms employed in the system.

A change of the equilibrium rotational speed maintained by the governor is effected by speed-adjustment mechanism (12) consisting of an electric motor and a reduction gear which moves the left end of the lever linked to dashpot (30). If, for instance, this end moves downward, the lever turns about its right end which is connected to the dashpot rod; a second lever, connected to the auxiliary servomotor (28), is moved simultaneously, so that finally the piston of servomotor (44) causes the distributor to open: turbine speed increases. By moving the speed adjustment mechanism in the opposite direction, equilibrium conditions at a lower speed are obtained.

The speed droop may be varied from 0 to 6% by means of the droop-compensating mechanism (13), connected to the actuating shaft and acting, as shown in Figure XII. 13, on the same lever to which the speed-adjustment mechanism (12) is connected. The blade-control mechanism operates as follows: regulation cam (27) is driven by gears from actuating shaft (11). A roller is pressed against the cam by oil pressure in the amplifier runner-distributing valve (39) acting on its lever. If, for instance, the distributor closes, the cam turns so that the amplifier runner-distributing valve (39) and, with it, the main runner-distributing valve (43) are actuated, and the runner servomotor closes the blades.

To permit adjustment of the blade-control mechanism connection to the head variations, the cam surface has a double curvature. Adjustment to head is effected by means of the planetary gear (21), provided with both manual and remote control.

The mechanism to limit opening (20) is actuated either manually or by remote control. It acts on the lever whose left end limits the upward (opening) motion of the valve of auxiliary servomotor (28).

Pressure oil system. The electrically driven vertical oil pump (6) transfers oil from the sump through non-check valve (5) and the isolating valve into the pressure tank (3). Oil under pressure is fed to the governor through the pressure pipe and flows back through the return pipe to

sump (2). When the pressure in the tank attains the required value, relief valve (7) opens, and oil is discharged from the pump directly into the sump; check valve (5) is then closed by the pressure, preventing reverse flow. If the relief valve fails to open, pressure may continue to rise. A safety valve must therefore be provided to prevent undue pressure rise in the tank.

Two pressure relays, operated by clean oil, are mounted on the duplex oil strainer (9). Pressure relay (8) switches on the stand-by pump if the oil pressure in the tank drops approximately 20% below normal.

Minimum-pressure relay (10) causes turbine emergency shut-down when the pressure in the tank drops below a predetermined minimum at which the distributor can still be closed.

A sump-level indicator (1), which signals whenever minimum or maximum oil level is reached, is provided in the sump. A level indicator and a level relay (4) are provided in the pressure tank.

Full automatic control of turbine operation involves additional equipment, and requires a strict sequence of operation in a modern unit designed for full automatic control, normal starting and shutdown procedure is as follows, provided the oil pressure system operates normally:

Turbine starting

1. The switchboard operator turns the main control key of the hydro unit into the "start" position.
2. The electromagnet moves the valve of the hydraulic valve (61) for water lubrication of the main turbine bearing. The electromagnet actuates the valve and is then de-energized. The hydraulic valve opens, water is fed to the turbine bearing (70) and the lubrication flow relay (62) closes the switches for the following operations.
3. The starting valve (37) is actuated. The distributor and runner hydraulic valves (35) and (42) open. The turbine blades are adjusted to the starting position, the distributor is closed, the servomotor-blocking valve (46) is actuated, and the servomotor stop (49) is disconnected.
4. The distributor opens until the starting position is reached. The unit starts to run. The governor-starting device (26) gradually opens the distributor, and the speed increases accordingly. The runner blades assume a corresponding position.
5. When normal speed is approached, the flyballs (16) take over the regulation of the turbine. The distributor opening is reduced to no-load value.
6. When normal speed is reached, the unit is ready for synchronization and connection to the line.

Unit shutdown

1. The unit is unloaded, the generator disconnected from the line, and the distributor closed to no-load position. The control key is turned to the "stop" position. Several relays, interacting to shut down the turbine, are put into operation.
2. The shutdown electromagnet, which actuates the remote-control valve, is switched on. The distributor is closed and the locking device is switched on.

3. When the speed drops to 35% of normal, the speed relay is actuated and energizes the generator-rotor brakes.

4. After the generator rotor has been braked, water to the bearing is shut off. The hydraulic valve on the industrial-water main closes. The runner blades assume their starting position. The hydraulic valves of the governor close.

Emergency shutdown

Automatic emergency shutdown of the turbine occurs in the event of equipment failure, storm damage, etc. The shutdown is connected by the contact switches of one of the following protective devices:

a) key for manual emergency shutdown;

b) relay protecting against failure of water supply to bearing;

c) relay protecting against pressure-drop in the oil tank;

d) overspeed relay.

The operating sequence during emergency shutdown is similar to that during normal shutdown.

Modern hydromechanical speed-regulation governors are extremely reliable and sensitive, and ensure stable regulating conditions.

However, the isodrome-control elements of the governor have a high inertia and therefore do not respond quickly to small speed variations or when the speed-adjustment mechanism is switched on. This drawback can be eliminated by reducing the inertia of the isodrome elements, or by completely cutting them out when the turbine supplies current to a large system.

The main limitation of existing hydromechanical governors in the light of modern requirements is that they do not ensure over-all speed regulation of a whole group of turbines, and require the use of additional frequency regulators or other devices.

As a recent development, governors are being provided with special electromagnetic corrective devices which permit group regulation. These devices, however, have many disadvantages. In order to solve the problem of group regulation, hydromechanical governors must be replaced by electrohydraulic governors (EHG).

73. ELECTROHYDRAULIC GOVERNORS

Increase in system power, extension and ramification of transmission lines, and automation of individual generating plants and entire power systems, have posed new problems and put forward new requirements concerning hydro-turbine governors.

It was once considered sufficient to ensure stable speed regulation to compensate for changes in the individual load on the unit and to permit adjustment of speed droop from 0 to 6 or 8%; these arrangements made possible operation in parallel of generating units, the load being apportioned to each according to the static characteristics of the hydromechanical governors, for which they were quite adequate.

Large hydroelectric units are nowadays practically always operated in parallel, and load distribution according to the static characteristics of their hydromechanical governor becomes inadequate for the following reasons:

1. The load is not distributed according to economic requirements, but according to the static characteristics of the governors which may be altered only by hand.

2. Under fluctuating-load conditions it becomes necessary, in order to maintain frequency constant, to employ secondary frequency control. This complicates the regulation system.

3. Even a high-power hydro unit is inadequate for the regulation of power-system frequency according to floating-control characteristics (with zero speed droop or close to it). Plants with a large number of high-power units can only maintain a constant frequency of the whole power system if stable parallel operation of these units is effected with floating-control characteristics.

4. In multi-unit plants, individual control of each unit becomes inconvenient. When the number of units in operation is changed, load redistribution among the units has to be carried out by adjusting the governor settings of each unit. This must also be done when the load carried by the entire plant varies, the frequency remaining constant.

All this creates a need for group regulation, which is to ensure:

a) control of any number of units at a given plant, as one single entity;

b) equal load distribution among individual units, or maintenance of uniform distributor openings;

c) automatic program-controlled variation of plant load;

d) operation of the whole plant with speed droop adjusted from the main switch panel;

e) adjustment, in accordance with the loading program, of the settings of the various governors, taking into account economic factors, power transmission, fluctuations, etc.

Obviously, with group regulation, the whole problem of turbine regulation changes.

Various electrohydraulic governors have been designed according to the above requirements.

The electrohydraulic governor designed at the LMZ consists of the hydromechanical actuator and the electrical equipment cabinets, both mounted in the machine room. The electrical equipment cabinet contains the electrical part of the governor only, while the actuator cabinet contains the hydromechanical devices. The governor ensures automatic control of the unit under the following conditions: no-load operation, individual operation, group operation of units and regulation of power supply to an entire power system.

A special tachogenerator of about 100va output — connected to the main shaft — transmits current at a frequency of 50 cycles to the electric measuring circuits of the governor. When the speed of the unit changes, the frequency of the tachogenerator supplies changes also, whereupon a discriminator responding to frequency variations emits an electric signal. After being amplified, this signal is transmitted to the electromechanical final-control element, where it is transformed into a mechanical displacement transmitted through the lever system of the amplifier valve to the

main governor valve. Being moved from its mid-position in direct proportion to the strength of the electric signal, the main governor valve feeds oil under pressure to the servomotor of the turbine distributor. The guide vanes turn in the direction corresponding to the sign of the electric signal.

The mechanical restoring link transmits the motion of the servomotor piston to the shaft located inside the governor. From there the motion is transmitted further to electric transducers (potentiometers) which actuate the following electrical elements of the governor system:

1) isodrome controls for varying the response characteristics within wide limits, and for automatic readjustment when the load changes from full to idling, or vice versa;

2) droop-compensating mechanism, which may be adjusted for speed droops from 0 to 10%;

3) speed-adjustment mechanism, permitting load control and synchronization of the unit for connection to the grid;

4) output or distributor-opening control for group regulation.

The distributor-opening limiting-mechanism is connected to the actuating shaft.

The governor electric relays provide for rapid readjustment of the governor when the operating conditions change. The energizing current for the relays is 220 v d. c. or a. c.

Starting, shutdown, manual control, and the limiting of the distributor opening are effected by the distributor-opening limiting-mechanism, which may be remote or manually controlled.

The governor electrical-equipment cabinet contains the following electrical devices: the frequency discriminator, the speed-adjustment mechanism, the blocking relays, the protective relays, the transformers, and the power control or device for group regulation. The electrical-equipment cabinet is connected to the governor-actuator cabinet and to the main switchboard of the plant by means of electric cables.

The frequency discriminator includes the device for measuring the rotational speed of the unit, the electrical isodrome controls, the phase-sensitive discriminator, the electronic amplifier, the relay for speed-droop compensation, the device for group regulation, etc. The frequency-discriminator generates an electric regulating signal of equal sign to, and directly proportional in strength to the magnitude, and to the required displacement of the governor distributing valve.

The contact system and protective relays are of the magnetic-switch type; they control all the automatic operations of hydro-unit control under starting, shutdown, and varying-load conditions, and protect the unit in the event of failure under normal operation.

Transformers are provided for the power supply to the electrical equipment. In contrast to the ordinary centrifugal governor with flyballs, the operations performed by electrohydraulic governors — measurement — act by means of electrical devices.

The resultant electrical signal (composed of two pulses) actuates the electromechanical devices which transform it into the proportional displacement of a rod. This displacement is then amplified hydraulically in several stages to the magnitude required to actuate the turbine distributor.

The main advantage of the electrohydraulic governor is that the regulating signals (from the speed-measuring instrument, isodrome controls, compensating mechanism, speed-adjustment mechanism, etc.) obtained in

the form of electric-voltage pulses may easily be combined in any desired proportion. Similarly, they can be combined with other electrical signals: from the device for group regulation, devices for water-flow and overcurrent measuring on the transmission lines, or from other governors.

Figure XII. 14 shows the wiring diagram of the frequency discriminator, tachogenerator, and operator.

Speed-measuring device. The device for measuring the rotational speed of the unit is based upon the variation with frequency of the impedance of an LC circuit (parallel-connected capacitor C_6 and choke coil L_1).

Since the tachogenerator for the LC circuit is connected to the main shaft, its frequency varies in direct proportion to the rotational speed. The values of C_6 and L_1 are selected so that resonance of the circuit occurs at a frequency of 50 c, corresponding to normal speed. At resonance, the circuit impedance rises abruptly (becoming infinite for an ideal circuit) and practically no current flows through it.

When the rotational speed rises or drops, a capacitive or inductive current, respectively, proportional to the speed deviation, flows in the circuit. This current is then combined with other regulating signals, rectified by a phase-sensitive rectifier, amplified, and fed to the actuator.

The extension rod of the actuator is moved in the corresponding direction, and the distributor opening is varied by means of the hydromechanical part of the EHR governor.

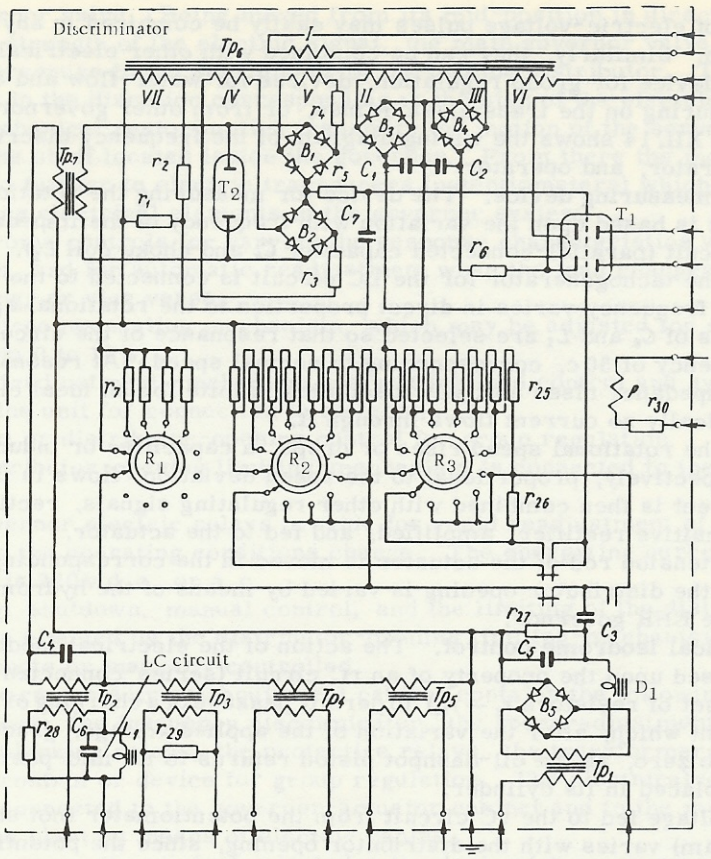
Electrical isodrome control. The action of the electrical isodrome control is based upon the property of an rC circuit (series-connected capacitor C_3 and a set of resistors $r_7 - r_{26}$) to permit passage of a charging or discharging current which, after the variation of the applied voltage, gradually decreases to zero, as the oil-dashpot piston returns to its mid-position after being displaced in its cylinder.

The voltage fed to the rC circuit from the potentiometer (not shown in the diagram) varies with the distributor opening, since the potentiometer is connected to the governor shaft.

Phase-sensitive rectifier. The phase-sensitive rectifier is a device which converts the a. c. signals from the speed-measuring device (the LC circuit), the compensating potentiometers, the speed-adjustment mechanisms, etc., into d. c. signals of corresponding magnitude and sign. These d. c. signals are then amplified by an electronic amplifier. The phase-sensitive rectifier consists of rectifying B_1 and B_2 bridges composed of crystal diodes of type DG-Ts27 (D7J), and the input transformer Tp_7. The control voltage is supplied by special windings of the power transformer Tp_6. The resistors r_3 and r_4, inserted in the circuits of these windings, limit the current flowing through the diodes. An a. c. signal fed to the primary winding of the transformer Tp_7 develops a corresponding d. c. voltage (the rectified signal) between the mid-point of the secondary winding and the common point of both rectifying bridges. The rectified signal is fed to the input of an electronic amplifier (one of the electronic valve grids).

Electronic amplifier. The purpose of the amplifier is to provide an electric signal of adequate strength at the discriminator output. It is a direct-coupled differential amplifier incorporating the double-triode T_1.

Droop-compensating device. A device, consisting of three potentiometers, is provided on the EHR governor to enable the unit to be operated on a static characteristic. The slide of one of the potentiometers is connected to the piston of the main servomotor. The voltage difference between the



Tachogenerator Operator

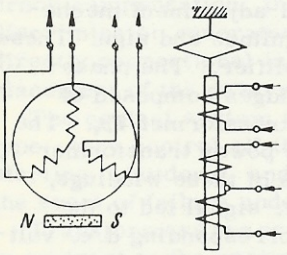


FIGURE XII. 14. Wiring diagram of discriminator, tachogenerator and operator of the electrohydraulic governor

T_1—electronic amplifier; T_2—gas-filled kenotron; R_1—controller for adjusting the isodrome-control time for no-load operation; R_2—controller for adjusting the isodrome-control strength for no-load operation; R_3—controller for adjusting the isodrome-control at full-load; T_{p_1}—input transformer of the isodrome-control circuit; T_{p_2}—input transformer of the frequency-regulation signal; T_{p_3}—input transformer of the distributor-opening adjusting signal; T_{p_4}—input transformer of the droop-compensating signal; T_{p_5}—input transformer for LC circuit tuning; T_{p_6}—power transformer; T_{p_7}—input transformer of the phase-sensitive device; B_1 and B_2—rectifying bridge of the phase-sensitive system; B_3 and B_4—rectifying bridges for the electronic-tube voltage supply; B_5—rectifying bridges for the isodrome-control circuit; D_1—choke coil of the isodrome-control circuit; L_1—choke coil of the LC circuit; P—contact switch relay for the isodrome-control link; r_1 and r_2—resistors in the oscillator circuit of the operator; r_3 to r_5—resistors in phase-sensitive circuit; r_6—cathode resistor of the tube V_1; r_7 to r_{10}—resistors in the isodrome-control circuit adjustment to no-load; r_{11} to r_{18}—resistors in the isodrome-control circuit for adjustment of isodrome control to no-load; r_{19} to r_{26}—resistances in the circuit for adjustment of isodrome-control to full-load; r_{27}—resistor in the filter circuit of the isodrome control; r_{28}—resistor for compensating the current fluctuations in the LC circuit; r_{29}—shunt resistor across the input winding of transformer T_{p_3}; r_{30}—resistor in the circuit of relay P; C_1 and C_2—filter capacitors in the electron-tube feeding circuit; C_3—capacitor of the isodrome-control circuit (in the differentiating circuit rC); C_4—phase-shifting capacitor; C_5—capacitor in the filter circuit of the isodrome-control; C_6—capacitor of the LC circuit; C_7—capacitor in the oscillator circuit of the operator coils.

outputs of another potentiometer varies in direct proportion to the servomotor stroke; the same potentiometer serves as voltage divider, by means of which the speed droop may be adjusted from zero to maximum.

The voltage divider supplies a voltage proportional to the speed droop; this voltage is combined with other regulating signals, amplified, and finally actuates the EHG governor.

Speed-adjustment mechanism. The mechanism for speed adjustment alters the distributor opening by means of a special potentiometer equipped with an electric motor, selsyn drive, and an electromagnetic clutch for their connection.

When the hydro unit is operated under individual-regulation conditions, the potentiometer is connected to the electric motor controlled by push-button contacts from the plant switchboard.

When the unit is operated under group-regulation conditions, the clutch automatically disconnects the electromotor and connects the selsyn drive (the selsyn receiver); the potentiometer slide follows the distributor opening, since the selsyn transmitter is connected to the actuating shaft.

Operator. The operator is the connecting element between the electrical and hydromechanical parts of the EHG governor. The electrical part of the operator consists of a moving-coil system whose action is based upon the motion of a solenoid in the magnetic field created by a permanent magnet. The solenoid actuates both a small hydraulic valve and the operator rod.

The hydromechanical part of this governor is shown schematically in Figure XII. 15.

All the elements are shown in the positions corresponding to normal operating conditions, with automatic control of the unit effected by the actuator (33 and 41). When the lever of the operator connecting switch is turned to the "automatic" position, pressure oil, admitted from the pressure pipe of the main distributing-valve cylinder (9) through valve (27) and strainer (28) into the space below piston (34), passes through the orifice into the space above piston (34).

The pressure in the space above piston (34) depends upon the position of cap (42) with respect to the rod end of piston (34), since the cap covers a radial opening in the rod through which the oil from the space above the piston drains into the sump. Piston (34) is a differential piston, so that the forces acting upon the piston balance each other when the pressures above and below the piston are inversely proportional to its areas.

When cap (42) is raised or lowered, piston (34) moves upward or downward, respectively. Cap (42) is rigidly connected to solenoid (37) held by lead spring (38). Solenoid (37) is placed in a constant magnetic field. When energized by the electric current from the discriminator, the solenoid moves together with the cap, followed by piston (34) with its rod, which moves slide (30) of the pilot valve by means of the lever and rod (31). Oil is admitted through pilot valve (29) into the auxiliary servomotor (11) whose piston is connected with the main distributing valve piston (10) and causes the latter to move.

The travel time of the distributor servomotor at distributor opening and closing, and the stroke of the main distributing-valve piston (10) are adjusted downward (closing) by means of nut (12) and upward (opening) by means of screw (14).

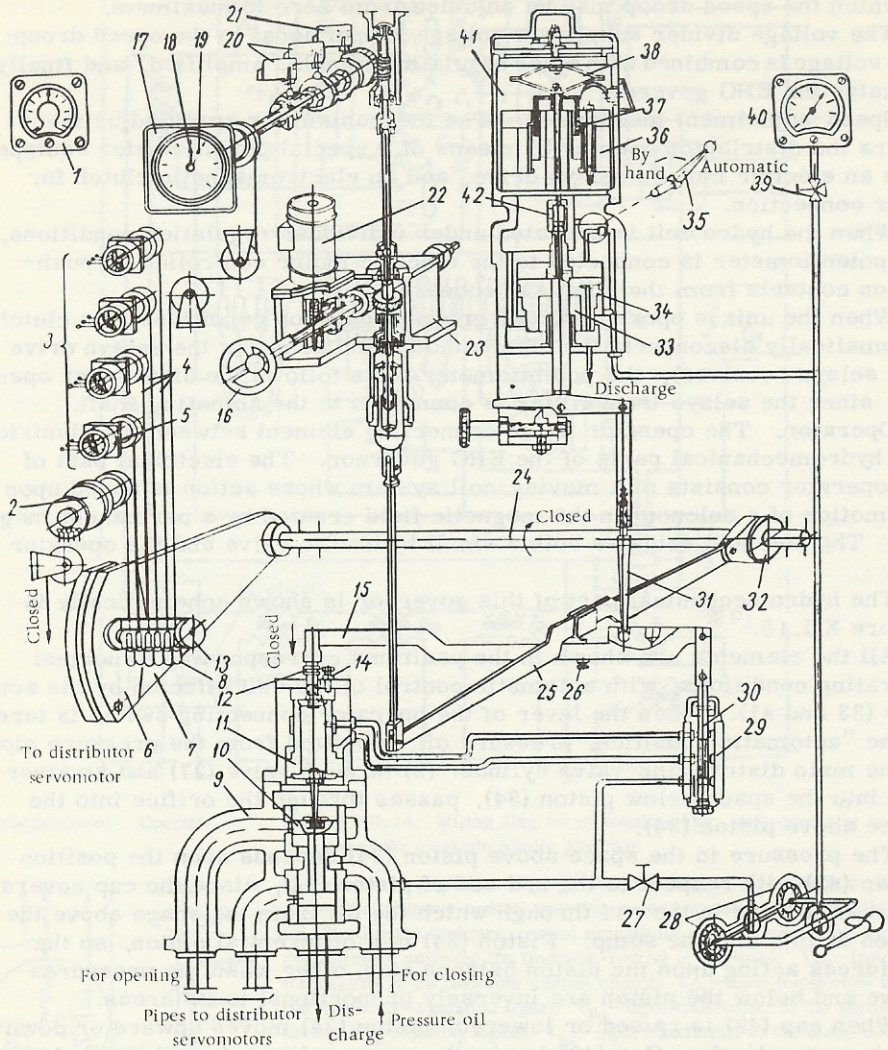


FIGURE XII. 15. Hydromechanical diagram of the electrohydraulic governor

1—electrical tachometer; 2—transducer of isodrome control; 3—restoring-link mechanism; 4—cable; 5—potentiometer; 6—weight; 7—lever; 8—cable ends; 9—main distributing-valve cylinder; 10—main distributing-valve piston; 11—auxiliary servomotor; 12—nut; 13—support; 14—screw; 15—lever; 16—handwheel; 17—main indicator; 18 and 19—pointers; 20—limit switches; 21—limiting switch; 22—electric motor; 23—reduction gear; 24—actuating shaft; 25—lever; 26—opening-control screw; 27—valve; 28—oil strainer; 29—pilot valve; 30—slide of the pilot valve; 31—rod; 32—lever; 33—hydromechanical part of the actuator; 34—piston of the operator auxiliary servomotor; 35—lever disconnecting the operator; 36—magnet; 37—solenoid; 38—leaf spring; 39—three-way cock; 40—pressure gage; 41—electrical part of the actuator; 42—cap.

Governor operating-sequence. If, for instance, load is rejected, so that the moment of the driving forces is greater than the moment of the resistance forces of the generator, the speed begins to rise. The frequency of the current supplied by the tachogenerator, rigidly connected to the hydro unit shaft, also increases. The electrical part of the governor causes the current intensity in the actuator solenoid to alter, so that the solenoid moves downward. The piston of the auxiliary servomotor is thus also forced downward. The right-hand end of the lever is lowered, pivoting lever (15) about the left hinge by means of rod (31).

The slide (30) of the pilot valve also moves downward, and oil is admitted into the space above the piston of servomotor (11), forcing main distributing-valve piston (10) downward. Simultaneously, the left-hand end of lever (15) moves downward, pivoting about the lower end of rod (31) and returns slide (30) to its mid-position, cutting of the pressure-oil supply to the auxiliary servomotor (11). The main distributing valve piston ceases moving downward. Through the port of main distributing-valve cylinder (9) oil is admitted into the distributor servomotor causing it to close the distributor. Through the feedback lever (7) is turned through a certain angle with the closing distributor, moving support (13) and with it, by means of the permanently stretched cables (4), the slides of potentiometers (5) from which electric signals are sent to the discriminator. After being combined and amplified, the signals cause solenoid (37) to move upward. This makes the slide of the pilot valve move upward too. Thus, the space above the piston of the auxiliary servomotor (11) is connected to the sump, and the main distributing-valve piston (10) moves upward, allowing pressure oil to enter the distributor servomotor: the distributor movement is stopped. The turbine governor is brought to a position that corresponds to the new load.

Operation of the distributor-opening limiting-mechanism. This mechanism is used to limit turbine output. For this purpose, the mechanism is set in the required position either manually, by means of handwheel (16), or by remote control through the electric motor (22).

Shaft rotation is transmitted through a helical gear to a screw; this turns and moves the nut, guided by a key, upward. The movement of the nut changes the position of the left-hand end of lever (25). If the mechanism is operated, for instance, so as to reduce the distributor opening, the left-hand end of lever (25) is lowered, thus pressing with its mid-point on the opening-control screw (26), which limits the upward travel of the pilot-valve slide (30). The distributor-opening limiting-mechanism may be used to close the distributor completely; for this, the left-hand end of lever (25) should be pulled downward to the maximum, its mid-point forcing down the right-hand end of lever (15) by means of screw (26) and, with it, the pilot valve slide (30).

This causes the distributor to close, after which the actuating shaft and lever (32) make slide (30) move upward and return main distributing-valve piston (10) to its mid-position.

The limit switches (20) and (21) connect and disconnect the electric motor (22) when the turbine is started and shut down.

The distributor-opening limiting-mechanism is provided with pointer (19) on the main indicator to indicate the permissible distributor opening. The main indicator (17) is connected with the actuating shaft by one of cables (4). Pointer (18) indicates the actual opening of the distributor.

Selection of governor. The dimensions of the governor are determined by the diameter of the main distributing valve. This diameter is usually taken as equal to the diameter of the pipe supplying oil to the servomotor of the regulating element. It is therefore necessary to obtain the required speed of the regulating element during the regulating process.

Oil flow through the main distributing valve is

$$Q_v = \frac{V_s}{T_c}. \qquad \text{(XII.1)}$$

where $V_s = V_{s_1} + V_{s_2}$ = total volume of both distributor servomotors;
T_c = time required for full servomotor piston travel determined by plant-regulation conditions*.

The diameter of the pipe connecting the main distributing valve with the servomotor is

$$d_p = \sqrt{\frac{4Q_v}{\pi v_o}}, \qquad \text{(XII.2)}$$

where v_o = oil flow velocity through the pipe.

The oil flow velocity v_o usually varies between 4 and 8 m/sec.

The velocity of the servomotor piston is

$$v_s = \sqrt{\frac{\Delta p 2g}{A_n \gamma}}, \qquad \text{(XII.3)}$$

where Δp = total oil pressure losses in the line from the pressure tank to the servomotor;
A_n = equivalent resistance coefficient referred to the servomotor-piston areas.
[γ = specific gravity of oil.]

The oil-pressure losses are

$$\Delta p = (0.3 \text{ to } 0.5)\, p_0,$$

where p_0 = oil pressure, 2 atm less than the pressure in the pressure tank.

The equivalent resistance coefficient of the system is

$$A_n = A_{no} + A_{nv} + A_{np} \qquad \text{(XII.4)}$$

where A_{no} = equivalent resistance coefficient of the oil pipe;
A_{nv} = equivalent resistance coefficient of the main distributing valve passages;
A_{np} = equivalent resistance coefficient of the main distributing-valve piston lands

$$A_{no} = \Sigma \zeta_i \left(\frac{F_n}{F_i}\right)^2. \qquad \text{(XII.5)}$$

* [Time required by distributor to close.]

where ζ_i = resistance coefficients of the oil pipe sections;
F_n = servomotor piston area;
F_i = cross section of the oil pipe.

With the distributing valves employed on turbine governor systems, the coefficient A_{nv} usually is

$$A_{nv} \approx 20 \left(\frac{F_n}{F_v}\right)^2,$$

where

$$F_v = \frac{\pi d_v^2}{4}; \qquad \text{(XII.6)}$$

d_v = valve diameter.

The coefficient A_{np} is

$$A_{np} \approx 0.9 \left(\frac{F_n}{d_v s}\right)^3, \qquad \text{(XII.7)}$$

where s = maximum effective distributing-valve stroke.

In hydraulic-turbine design practice:

for distributing valves of distributors

$$s_d = 0.1 d_v;$$

for distributing valves of runner servomotors

$$s_r = 0.15 d_v.$$

Calculation of rated power-plant regulation conditions makes it possible to determine the time required for the distributor servomotor to close the distributor after full load rejection. This time affects the speed rise of the hydro unit, the magnitude of the water-hammer in the penstock, and the pressure drop in the draft tube. A short closing time leads to small speed rise after load is rejected, but causes a considerable pressure rise in the scroll case. If the rated closing time is slightly longer, the pressure rise in the scroll case is less, but the speed may attain inadmissible values.

By calculating the rated plant-regulation conditions, the closing time and the magnitude of the flywheel effect of the hydro-unit rotor may be found, which give the permissible values of speed- and pressure rise during the regulation process after sudden load rejection. In practice, speed rise should not exceed 35 to 45%.

The permissible pressure rise $\xi = \frac{H_{max} - H_0}{H_0}$ is:

for high-head turbines ($H > 100$ m)

$$\xi = 0.15 \text{ to } 0.3;$$

for medium-head turbines ($H = 100$ to 40 m)

$$\xi = 0.3 \text{ to } 0.5;$$

for low-head turbines ($H < 40$m)

$$\xi = 0.5 \text{ to } 0.7.$$

The relationship between the rise in speed after sudden full load rejection and the flywheel effect is given with sufficient accuracy by the formula

$$\beta = \sqrt{1 + \frac{364 N T_{cl} f}{GD^2 n_0^2}} - 1, \qquad \text{(XII.8)}$$

where N = turbine shaft output;
T_{cl} = time required to close the distributor from full opening (usually a few seconds);
f = coefficient allowing for the effect of head variation under water-hammer conditions; it depends on the penstock characteristics and varies from 1.0 to 1.7;
n_0 = speed, rpm, before load rejection.

For full load rejection

$$T_{cl} = 0.9 T_c \quad \text{for Francis turbines;}$$

$$T_{cl} \approx 0.7 T_c \quad \text{for Kaplan turbines.}$$

The precise calculation of rated power-plant regulation-conditions makes it possible to determine the influence of the servomotor motion, the variation in turbine efficiency, the kinematic connections between distributor and servomotor, and the turbine characteristics. This calculation is usually performed during the final design of the hydro unit.

The magnitude of the flywheel effect is of great importance for steady operation, particularly during the regulation process.

The flywheel effect of the unit depends mainly on that of the generator, since the flywheel effect of the turbine is only about 10% of that of the generator. The flywheel effect of the generator is usually determined by the generator supplier, who establishes also the required distributor-closing time.

The magnitude of the flywheel effect required by regulation conditions depends on the hydro-unit output and speed, closing time of the distributor, and increase in head. These values are interdependent, and are determined during calculation of regulation conditions.

The flywheel effect of the generator is approximately

$$GD^2 = 3 (D_{ge}^4 - D_{gr}^4) l_g \text{ mt}^2, \qquad \text{(XII.9)}$$

where D_{ge} = outer diameter of the rotor;
l_g = length of the active iron [of the rotor];
D_{go} = inner diameter of the generator rim.

The inner diameter of the rim is

$$D_{go} = D_{ge} - 2h_p - 2h_0.$$

where h_p = height of the poles;
h_o = width of the rim.

The calculated value of the flywheel effect has to be increased by 10% to allow for the flywheel effect of the turbine runner and the armature of the exciter.

Determination of the sizes of the pressure-oil system. The pressure-oil system is characterized by the capacity of the oil-pressure tank.

Standard series of pressure-oil system are given in Table XII. 1.

TABLE XII. 1

Pressure-oil systems

Type of pressure oil system	Pressure tank			Sump				Pump		
	Volume, m^3	Inner diameter, mm	Height, mm	Volume, m^3	Height, mm	Length, mm	Breadth, mm	Pump delivery, l/sec	Capacity of electric motor	Number
MNU-0.6	0.6	700	1700	1.8	700	1600	1600	1.4	7	
MNU-1	1.0	900	1730	2.5	850	1600	1800	3.1	14	
MNU-1.6	1.6	1000	2210							
MNU-2.5	2.5	1100	2830	4.0	1150	1700	2100	5.8	28	
MNU-4	4.0	1300	3250							
MNU-5.6	5.6	1500	3430	8.0	1400	2400	2400	9.0	40	2
MNU-8	8.0	1800	3460							
MNU-10	10.0	2000	3520	12.5	1600	2800	2800	13.0	55	
MNU-12.5	12.5	2200	3660							
MNU-16	16.0	2x1800	3460	20.0	2200	3000	3000	18.0	75	
MNU-20	20.0	2x2000	3520							
MNU-25	25.0	2x2200	3660	26.0	2500	3200	3200	24.8	100	
MNU-30	30.0	2x2400	3740	30.0	2500	3700	3200			
MNU-36	36.0	2x2600	3840	35.0	2500	4000	3200	35	135	

To select the tank volume, the amount of oil required for the regulation process should be known. This is determined for the most unfavorable operating conditions of the servomotor to which the oil is supplied, allowing for leakages. When oil flows out, the pressure in the tank drops since the pump delivery is not equal to the maximum possible oil outflow from the tank.

After oil has been used for regulation, the air contained in the tank must maintain the minimum pressure required to close the distributor. The pressure drop in the system will (for the same volume of oil used) increase inversely with the amount of air and the pressure obtaining in the tank initially.

The total volume of the oil-pressure tank is

$$V_t = V_i + \Delta V + V_{res}, \tag{XII.10}$$

where V_i = volume of air required initially in the tank;
ΔV = maximum volume of oil supplied from the tank;
V_{res} = volume of the air reserve in the tank based on structural considerations.

Experience showed the expansion inside the tank is adiabatic. At any moment, the relationship between the volume of air V and the pressure in the tank is

$$pV^k = \text{const}, \tag{XII.11}$$

where $k = 1.41$ = adiabatic exponent.

The following relationship obtains between the air volume (V_0, p_0) initially, and after oil-discharge from the tank (V_1, p_1)

$$p_0 V_0^k = p_1 V_1^k. \tag{XII.12}$$

After an emergency shutdown of the turbine, the volume of air and the pressure in the tank are

$$\left.\begin{aligned} V_1 &= V_0 + \Delta V; \\ p_1 &= p_{min}, \end{aligned}\right\} \tag{XII.13}$$

where p_{min} = minimum permissible pressure in the tank required for closing the distributor.

Consequently, by (XII. 12) and (XII. 13) the required air volume in the tank is

$$V_0 = \frac{\Delta V}{\sqrt[k]{\frac{p_0}{p_{min}} - 1}}. \tag{XII.14}$$

The largest volume of oil taken from the tank is the sum of two volumes

$$\Delta V = \Delta V_p + \Delta V_{em} \tag{XII.15}$$

where ΔV_p = maximum oil volume used for regulation purposes;
ΔV_{em} = oil volume used for emergency shutdown.

Consequently, by (XII. 10), (XII. 14), and (XII. 15)

$$V_t = (\Delta V_p + \Delta V_{em})\left(\frac{1}{\sqrt[k]{\frac{p_0}{p_{min}} - 1}} + 1\right) + V_{res}. \tag{XII.16}$$

The values of ΔV_p and ΔV_{em} are calculated according to the following considerations:

The value of ΔV_p is usually determined for the most unfavorable regulation conditions which, in the Kaplan turbine, occur after complete closing of the runner blades and several oscillations of the distributor. After this, the hydro unit is again put on line and takes on the full load, which causes full opening of runner blades and distributor (this usually takes place smoothly). As a result, the pressure in the tank drops until the minimum-pressure relay operates, causing emergency closing of the distributor.

In a Kaplan turbine, the maximum volume of oil used during the regulation process is

$$\Delta V_p = (\alpha + 1)\, V_d + 2V_r - (T_{rc} + T_{ro})\,(\Sigma Q_p - q), \qquad \text{(XII.17)}$$

where V_d = volume of the distributor servomotor-cylinder;
V_r = volume of the runner servomotor-cylinder;
$\alpha = 1.5$ to 2 = number of distributor-servomotor piston-strokes effected during runner-blade closing;
T_{rc} and T_{ro} = closing and opening times of the runner blades;
q = oil leakages per unit time in the governor system;
ΣQ_p = total pump delivery per unit time regulation.

The volume of oil used under emergency conditions is

$$\Delta V_{em} = V_d + \frac{T_d}{T_{rc}} V_r + T_d q, \qquad \text{(XII.18)}$$

where T_d = closing time of the distributor.

In Francis turbines, maximum volumes of oil used for regulation and emergency shutdown are respectively

$$\Delta V_p = (\alpha + 1)\,[V_d - T_d\,(\Sigma Q_p - q)];^* \qquad \text{(XII.19)}$$

$$\Delta V_{em} = V_d + T_d q. \qquad \text{(XII.20)}$$

Consequently, the total volume of the pressure tank is, by (XII.16) to (XII.20).

for Kaplan turbines

$$V_t = \left[(\alpha + 2)\, V_d + \left(2 + \frac{T_d}{T_{rc}}\right) V_r - (T_{rc} + T_{ro})\,(\Sigma Q_p - q)\right] \times \left(\frac{1}{\sqrt[k]{\frac{p_o}{p_{min}} - 1}} + 1\right) + V_{res}; \qquad \text{(XII.21)}$$

for Francis turbines

$$V_t = [(\alpha + 2)\, V_d + T_d\,(\Sigma Q_p - q)(\alpha + 1) + T_d q] \times \left(\frac{1}{\sqrt[k]{\frac{p_o}{p_{min}} - 1}} + 1\right) + V_{res}. \qquad \text{(XII.22)}$$

* [The meaning of α is not clear in this formula, since Francis turbines have no adjustable blades.]

The relationship between the times required for full strokes of the distributor and runner servomotor-pistons is:

closing

$$T_{rc} = 6T_d ;$$

opening

$$T_{ro} = 3T_d .$$

The initial pressure in the tank is

$$p_o = p_u - \Delta p_i ,$$

where p_u = upper limit of the normal pressure in the tank;

$\Delta P_i = 1.5$ to $2.0\ kg/cm^2$ = pressure reduction caused by the action of the relief valve of the pump.

The minimum pressure in the tank is

$$p_{min} = p_r + \Delta p ,$$

where p_r = minimum pressure required in the servomotor, determined by the forces acting upon the distributor;

$\Delta p = 0.5$ to $1.0\ kg/cm^2$.

The pump delivery Q_p is determined by the time T_0 during which the oil for the regulation process flows from the tank. By (XII. 17) and (XII. 19) [$\Delta V_p = T_0 \Sigma Q_p$]

for Kaplan turbines

$$Q_p = \frac{(\alpha + 1) V_d + 2V_r}{\beta (T_0 + T_{rc} + T_{ro})} + \frac{q}{\beta} ; \qquad \text{(XII.23)}$$

for Francis turbines

$$Q_p = \frac{(\alpha + 1) V_d}{\beta (T_0 + T_d)} ; \qquad \text{(XII.24)}$$

for medium turbines

$$T_0 = 80 \text{ to } 140 \text{ sec} ;$$

for large turbines

$$T_0 = 140 \text{ to } 200 \text{ sec}.$$

For determining total pump delivery, it has been assumed that one pump discharges oil into the tank continuously, while the other works only part of the time:

$$\Sigma Q_t = \beta Q_t ,$$

where $\beta = 1.8$ — pump operation coefficient.

For various turbine types, the following approximate relationships exist between the pressure-tank volume and the servomotor-cylinder volumes:

for Kaplan turbines

$$V_t \approx (18 \text{ to } 20)\, V_d + (3 \text{ to } 4)\, V_r ; \qquad \text{(XII.25)}$$

for Francis turbines with pressure regulator and valve, if the latter is controlled by oil pressure from the pressure-oil system

$$V_t = (18 \text{ to } 20)\, V_d + 3V_v + (9 \text{ to } 10)\, V_{pr}, \qquad \text{(XII.26)}$$

where V_v and V_{pr} = volumes of the valve and pressure-regulator servomotor-cylinders, respectively.

The relationship under normal operating duties between the air and oil volumes V_a and V_o is usually

$$V_a = (0.6 \text{ to } 0.7)\, V_t ; \qquad \text{(XII.27)}$$

$$V_o = (0.3 \text{ to } 0.4)\, V_t . \qquad \text{(XII.28)}$$

The basic dimensions of the oil-pressure tank are determined by the total volume required, with the following relationship between the tank height and diameter

$$H = (2 \text{ to } 3)\, D. \qquad \text{(XII.29)}$$

The thickness of the pressure-tank walls is determined according to boiler-inspection standards by the formulas:

for the tank walls

$$s_w = \frac{pD_i}{\left(230 \frac{\sigma_a}{n} - p\right)\varphi} + C_w ; \qquad \text{(XII.30)}$$

for the cover

$$s_c = \frac{pD_e}{200 \frac{\sigma_a}{n}} + C_c , \qquad \text{(XII.31)}$$

where p = rated pressure, kg/cm^2;

D_i = inner diameter of the tank, mm;

D_e = outer diameter of the cover;

σ_u = ultimate strength, kg/mm^2;

n = safety factor;

φ = strength factor for welded seams;

y = coefficient allowing for the cover shape;

C_w and C_c = allowances (mm) for variation in the thickness of the rolled sheets, and for corrosion.

In designing the pressure tank, the following values are assumed: σ_u = = 41 kg/mm^2 for 20K steel; n = 4.35; φ = 0.95; C_w = 1 to 2 mm; C_c = 2 to 3 mm.

Chapter XIII

HYDRAULIC-TURBINE DESIGN AND MANUFACTURE

75. DESIGN PROCEDURE

The designing of a hydraulic turbine is usually performed in three stages: preliminary study, over-all design, and preparation of working drawings.

Preliminary study. The preliminary study of a new turbine design is carried out when the total plant capacity ΣN, the rated head H_r, and the head variation (between H_{min} and H_{max}) are known.

On the basis of these data, preliminary design entails selecting the main turbine parameters, such as: type of turbine, runner type and diameter, and speed, and determining the general layout of the hydro unit.

The particular turbine type (Kaplan, axial fixed-blade, Francis, or Pelton) is selected according to the [available] head. Each type has its advantages and limitations. Thus, for instance, Kaplan turbines are more suited to low heads. With simultaneous regulation of distributor and runner blades, they provide higher outputs and efficiencies under varying operating conditions than other turbines. Kaplan turbines are, however, more complicated in design and more expensive, and their water passages are larger.

The construction of the submerged parts of plants for Kaplan turbines is expensive, particularly the deep draft tubes. Special calculations are required to decide whether Kaplan or simpler Francis turbines should be used for high heads. In selecting the turbine characteristics, the number of hydro units to be installed in a plant must also be decided. Present trend is to prefer a small number of large units to a large number of small units.

The selection of the runner diameter D_1 and speed n depends largely upon the draft head. Higher turbine speed leads to smaller turbine and generator dimensions, requiring, however, a larger discharge capacity Q_1' and greater speed n_s. Turbines with high specific speeds are usually more prone to cavitation and therefore require higher draft heads, i.e., deeper draft tube settings. Several alternatives should be considered in this event, and compared from the economic standpoint.

In selecting the turbine type, special designs should also be considered; thus, for instance, a pumped-storage hydro plant should, in principle, be equipped with both turbines and pumps. A single hydro unit may also be used, however, designed to work either as turbine or as pump (reversible pump-turbine).

In tidal power plants the turbines planned are such reversible pump-turbine units. In selecting the basic characteristics of a hydraulic turbine, series-production of turbines of the same type should also be envisaged. For a large series of turbines of the same type, production costs can be

considerably reduced. Thus, e.g., the cost of the last turbines of a series of 20 identical units for the Volga HEP imeni Lenin was 40% lower than the cost of the first.

Economic analysis is usually performed jointly by the turbine and hydroplant designers.

In preparing the technical design of an HEP for given turbine types and sizes, it is important first to study the turbine water passages, from scroll casing to draft tube, and to solve the technically and economically important task of designing turbines of high-efficiency η with low cavitation coefficients σ for minimum over-all sizes (width B and depth L) of the turbine-block structure. These requirements, however, are conflicting. Thus, for high efficiency, free water passages of large dimensions (i.e. large sizes of the turbine block), are required, but this markedly increases construction costs. On the other hand, smaller water passages increase the flow velocity and reduce efficiency.

Over-all design. To reduce the depth of the submerged structures of the plant, a low draft tube is required, but this necessarily impairs flow conditions, since the proximity of the elbow to the runner increases flow nonuniformity in the outlet diffuser of the draft tube, and thus the losses in the draft tube. Therefore, to obtain high efficiencies, high draft tubes with large elbows are required.

A careful comparative study of various designs of water passages is necessary in order to ensure the required efficiency and low cavitation coefficients. Analytic computations and elaborate laboratory research (aerodynamic and hydrodynamic tests) are undertaken for this purpose.

Various designs for runners, scroll cases, draft tubes, etc., are investigated on special test rigs.

For the turbines of the Volga plant imeni Lenin, ten alternative runners were designed and tested, as well as draft tubes of various shapes and depths, such as: $L = 2.3D_1$, $L = 1.9D_1$, and $L = 1.5D_1$, conventional elbow type, hydrocone-type tubes, and draft tubes with guiding ribs in the elbow.

All the main turbine parts are first designed in several variants. After careful comparison the final design of each part and component is selected, and the turbine layout as a whole decided.

For this, the weights of the parts, the manufacturing process, the man-hours required, and the total cost for the different designs are compared.

For the Volga HEP imeni Lenin the following turbine parts were designed in several variants:

1) six runner variants with various blade-adjustment mechanisms;

2) the main turbine shaft in normal design, either with forged flanges or without flanges. A single shaft for both turbine and generator was also considered;

3) four distributor variants: conventional design, with the servomotor mounted on the turbine cover-plate, and with separate servomotors;

4) three variants for the foundation parts;

5) three variants for bearings, with oil or water lubrication, of conventional design, mounted above the turbine runner, or below it in a special bracket in the draft-tube cone.

The following alternatives were compared for the speed ring of the largest turbine, having a diameter of 14 m and weight of 166 t, installed at the Volga plant imeni Lenin:

1) speed ring (stator) cast in eight sections;

2) speed ring without the lower ring and with a welded lining;

3) speed ring with welded streamlined columns;

4) speed ring welded and cast with ribs welded to the lower lining.

Apart from the design itself, the following data were calculated for each alternative: a) weight of the finished part and of the blank; b) man hours required for machining, such as turning on vertical lathes, boring, and other operations; c) man hours required for manual operations in the shop and on erection; d) electrode consumption [for welding]; e) total cost; f) time required for manufacture and erection.

All these data were analyzed and compared, taking into account the novelty of the design and its reliability in operation, and the design was then finalized. Since the elements of the water passages were the same for all speed-ring variants, output and efficiency were not considered in this comparison.

The Francis runner for the Bratsk HEP turbine (D_1 = 5.5 m, N = 225,000 kw, H = 100 m, over-all runner dimensions 6×2.7 m, weight over 100 t) may serve as another illustrative example.

The following runner designs were compared before deciding upon the final solution:

1) all-cast integral runner;

2) runner in two halves, with the upper and lower band welded on erection;

3) runner in two halves, bolted at the upper band, and welded (on erection at the lower band;

4) runner in two halves, bolted at the upper band and secured by a fastening ring at the lower band;

5) runner in two halves, secured by fastening rings at the upper and lower bands.

The variant providing for final machining on site was finally selected, since otherwise the assembled runner could not have been transported.

A mechanical assembly-shop was therefore installed on the site of the Bratsk HEP, provided with the necessary equipment for the final machining of the runner, and with an electric furnace for final heat treatment after welding.

The following data were determined for each variant: a) weight of finished part and blank; b) cost of the half-runner blank; c) weight and cost of the connecting pieces of the runner (fasteners, rings, welds, etc.); d) cost of runner machining; e) nonrecoverable expenses for the equipment used in machining the runner on site and for heat treatment; f) total cost of the runner, including nonreceivable expenses. Manufacturing schedules were drawn up for each variant.

In comparing the alternatives, the reliability of the design and the accuracy with which the required water-passage shapes might be obtained for each design were also taken into account.

Working drawings. After the shape of all component parts of the water passages has been decided, the design of the actual turbine parts begins.

Experience gained in turbine operation should be used. The following aspects must also be considered: availability of plant to reduce production time to a minimum, simplicity of machining techniques, facilities for transportation to the erection site, means of obtaining blanks with minimum machining allowances.

Experience at the LMZ and KhTZ has shown that, besides all-cast parts, combined welded-cast, welded-forged, and fully fabricated parts can be used.

The type of blank to be used is decided upon on the basis of technical and economic analysis. The available machine tools and hoisting equipment are a decisive factor in the selection of a particular production technique. It is sometimes necessary to equip the shop with new machine tools. Thus, for instance, when the turbines for the Volga plant imeni Lenin were built, cost analysis showed it advisable to purchase special machine tools for parts whose machining on existing equipment would have been too expensive.

New machinery was installed in the turbine construction shops for machining the guide vanes, blade pivots, runner hubs, and other parts.

When preparing working drawings, the strength of each part must be either precisely calculated, or tested on a model. Since many turbine parts have a very intricate shape and do not lend themselves to precise analytical design, the stress pattern has to be determined experimentally in model tests. These tests lower the total cost of the turbine because an accurate determination of the stresses in the part under actual operating conditions makes it possible to adopt a lower safety margin, thus reducing the weight of the part. The 85 t rubber hub of the Volga plant imeni Lenin turbine can serve as an illustrative example. It is an intricate part as regards both shape and machining operations required, and is loaded by a complex system of forces. Model tests helped to determine not only the stress and strain distribution but also the effects of adjoining parts, and to decide upon the correct runner-hub design.

In studying the different designs for a specific part, the facilities of allied manufacturing branches have also to be taken into account.

The production methods for blanks of turbine shafts, runner blades, etc., also affects equipment requirements. Thus, for instance, a 75 t all-forged turbine shaft requires large forgings and special forging equipment; a composite welded shaft requires simpler blanks that can be produced with simpler machinery.

Production of stainless-steel all-cast runner blades of 20 to 25 t net weight is more complicated than manufacture of conventional low-alloy steel blades lined with stainless-steel plates. The new electrohydraulic governor entails use of new electrical equipment and instruments. Thus, the designing of new turbines exerts a direct effect upon allied industries.

In conclusion, in designing a large turbine the following problems must be solved:

1) design of water passages ensuring high efficiency and output;
2) reliable detailed design of the turbine parts;
3) design of the governor and the auxiliary equipment;
4) producing the turbine with minimum machining.

76. RUNAWAY PROTECTION IN HYDRO UNITS

In designing a turbine, operation under runaway conditions has also to be considered.

Turbine and generator must withstand the effects of full runaway speed for a short time, as stipulated in the delivery specifications of the order. According to the experience of Soviet hydro plants, actual runaway occurs only very seldom.

In all known instances of runaway, no serious damage was found when the unit was stopped. In plants with automatic regulation, out of twelve instances of runaway, four occurred during the governor-adjustment period, and eight during normal operation; the unit was shut down by the governor itself in five instances.

By statistical analysis, Gidroproekt found the probability of runaway occurring to be once every 24 years. The analysis covered 450 hydro units for a period of five years (1954 — 1958).

Instances of runaway in European hydroelectric plants are very rare; they occurred mainly during turbine starting and were due to distributing-valve jamming. Except for one instance in Finland, no damage whatsoever occurred and the turbines were shut down by closing the distributor.

Several instances of runaway in the U. S. A. which caused considerable damage are known; details are not available, however.

Because of this, large low-head turbines, irrespective of location or make, are always equipped with runaway-protection devices.

Experience shows that all existing protective devices receive the control impulse only after a significant time lag, starting to act only when the runner rotates already at 160% to 170% of its normal speed. Devices such as plain sliding gates are only lowered when the runner has reached full runaway speed.

The problem may be formulated thus:

1. Proceeding from the assumption that runaway is likely, the distributor may be used in conjunction with additional protective devices; the runner should be designed to withstand short-time runaway. In this case design is necessarily more complicated and a larger amount of material is needed.

It might also be advisable to provide an individual servomotor for each guide vane. This servomotor would be the final-control element of the governor under normal conditions, and would shut down the unit at runaway if connected to the emergency control-valve.

2. Proceeding from the contrary assumption, that runaway is unlikely, special protective devices could be omitted so as not to complicate the turbine, only the normal governor equipment with a stand-by pressure source being installed. The rotor can thus be designed to withstand smaller runaway speeds. Possible damage due to runaway will be considered accidental, and will be compensated for by the savings obtained through the more economical design.

The second alternative is undoubtedly economically sounder, since the probability of runaway occurrence is so small that the eventual costs of damage repair would be far less than the savings obtained by eliminating the heavy and costly runaway protective devices.

A quantitative analysis can be made only by means of specific calculations in each case.

According to the above, in Kaplan turbines having a runner diameter of 6 to 10 m it is advisable to use the distributor as a protective device, assuming that an emergency pressure-oil system is provided, and that the

control impulse is given immediately after load is rejected should the distributor fail to close.

The unit should therefore be designed so as to be able to withstand for a short time full runaway speed, and head gates should be provided together with means for changing the shear pins while the turbine is running.

In Kaplan turbines with runner diameters from 3 to 5 m it is possible to adjust the blades to mid-position for runaway protection in addition to the emergency shutdown control-valve.

77. MANUFACTURING TECHNIQUE

Extremely diversified metal-cutting equipment is required to manufacture a large turbine, and the inspection of the machining quality and accuracy is often difficult owing to the large dimensions and weight of the handled parts.

Apart from this, by the very nature of its design, the turbine cannot be completely assembled and tested in the shop. This circumstance stresses the necessity of high-quality manufacturing of the parts and complicates the production technique.

The machining of such large parts for the turbine of the Volga HEP imeni Lenin as, for instance, the 175 ton speed ring, the 53 t turbine cover-plate, the 85 t runner hub, the 70 t upper ring of the distributor, and others poses complicated problems as regards the manufacturing technique and the required equipment.

Handling such parts makes great demands on labor and floor space, and frequently requires special equipment and highly skilled workers.

Marking off, setting up on the machine, and similar operations are laborious when very large parts, liable to become deformed under their own weight, are machined.

The following may serve as an example: the roughly machined blank for the shaft of a large turbine weighs 58 t. After marking off, the part is to be machined on the lathe. One of the first operations is the correct mounting and centering of the shaft to the faceplate, the other end being mounted on a steady rest. The worker then cuts a control strip close to the faceplate after which he turns the shaft over with the strip toward the steady rest; the strip is checked for throw by a dial gage. If the throw exceeds 0.02 mm, another strip is cut, the shaft is set again in the reverse position, and the throw is checked once more.

This operation is repeated until the throw at both ends does not exceed from 0.01 to 0.02 mm. For very heavy shafts this operation takes up two weeks or more, even with highly-skilled workers. Actual machining only begins afterwards.

Complicated problems to be solved also arise in connection with the measuring of large-size parts, which has to be done during machining; temperature and weight of the measuring instrument, and the skill of the worker have a great influence on the high accuracy required.

The inspection of the material is also difficult since castings and forgings for the large parts met with in turbine construction have frequently an inhomogeneous internal structure. The place where the test specimen

has to be cut out must be properly selected so as to provide correct information on the properties of the part itself. It is not less difficult to discover hidden defects in the metal, such as cracks, cavities, etc.

If a complicated part is made from several sections it may easily be brought to the final shape with little machining, if the shape of the blank is close to that of the finished product.

The use of welded instead of cast parts for the turbine for the Volga plant imeni Lenin considerably reduced the weight of the turbine and the number of man hours for manufacturing. This is also valid for Francis turbines. Welding has therefore been widely employed for turbines in recent years. Such parts as scroll casings, speed rings, distributor rings, shafts, guide vanes, Francis runners, valve disks, and cylinders are nowadays made by welding.

Welding of Kaplan runner blades enables the shape of the blank to be closer to the shape of the finished part, with reduced weight of the blank, and less labor, production time, and cost. Other factors affect machining and assembly of the part and should be taken into account in the design. The following recommendations are tentative:

1. Make the shape of turbine parts as simple as possible to facilitate machining on high-productivity equipment; reduce to a minimum the time spent on auxiliary operations such as setting, centering, and clamping the parts in the fixtures.
2. Provide for optimum requirements regarding machining accuracy and surface finish.
3. In turbine design avoid interdependent parts that have to be machined together.
4. Introduce interchangeability on a large scale.
5. Promote extensive standardization of parts and components so as to reduce to a minimum the machine tools required.

The problems of economical design were solved for the first time at the LMZ by Z. M. Gamze; these are essential for the production of large series of turbines. One or a few units of different type may be manufactured by any method: complications in production due to an intricate design would not be as serious as when a large number of units have to be made to an uneconomical design. In this respect the experience in the manufacturing of a large series of [similar] turbines for the Volga HEP imeni V. I. Lenin and for the plant imeni XXII Congress of the KPSS is typical. These power plants were equipped with identical turbines, each having a runner diameter of 9.3 m and an output of 126,000 kw. Forty-two turbines had to be manufactured in a relatively short time for these two plants only.

When designing the turbines for the Volga HEP and considering the problems of construction and manufacture, it was deemed necessary to rebuild the shop and to equip it with new special machine tools. Lack of time made necessary the adoption of new methods characteristic of series production.

After analyzing the designs of the new turbines and the condition of the existing equipment, it was deemed advisable to order new, special-purpose lathes for the labor-consuming machining processes.

The new lathes were designed for high-speed cutting with rotating tools and stationary work-holding devices for the large blanks. These lathes made it possible to raise the productivity and to improve the machining quality.

A special purpose lathe for maching guide-vane pivots is shown in Figure XIII. 1

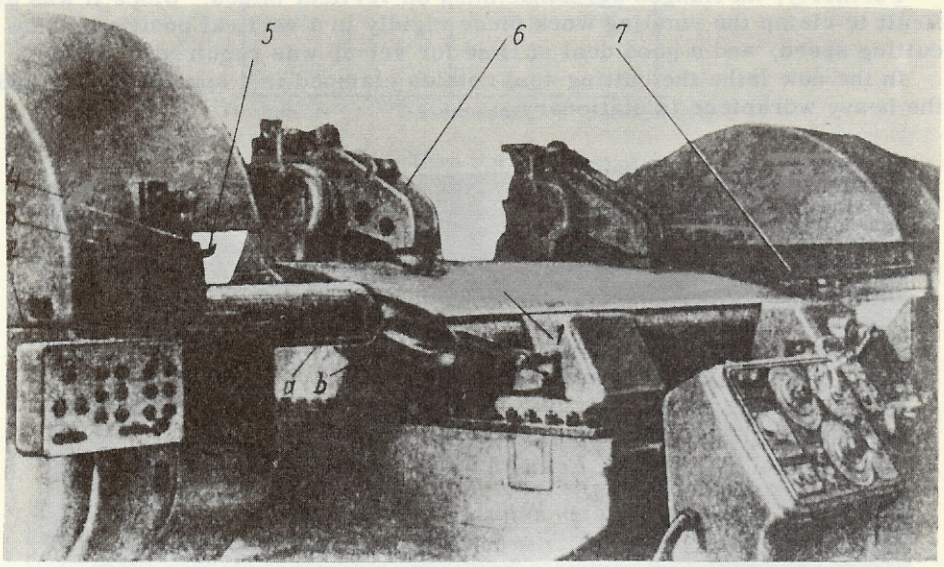


FIGURE XIII.1. Lathe for machining guide-vane pivots:

1— guide vane; 2— headstock; 3— slide rest; 4, 7— faceplates; 5— tools; 6— work-clamping device; a— pivot; b— guide-vane end-surface.

Formerly the guide-vane pivots were machined on center lathes. Because of the intricate shape of these pivots it was impossible to balance the guide vane perfectly, so that the pivots became oval. To obviate this, a very low cutting-speed was employed, but even so, oval-shape of the pivot could not be avoided.

During machining the guide-vane pivot is stationary in the lathe and rests upon its still unmachined surfaces. The correct mounting of the pivot between the centers (both pivots are usually machined simultaneously) is performed by a quick-acting device.

The machining of the guide vanes themselves provides another example. Formerly the guide vanes were roughly shaped by means of pneumatic presses and finished by means of flexible-spindle hand grinders.

This process was laborious without leading to high surface finish. Figure XIII. 2. shows a new special-purpose copying-milling machine designed to machine guide-vane surfaces; the copying devices are mounted at both ends of the machine table which has a longitudinal motion; the flange of the guide vane is clamped in the table and moves together with it.

The vane surface is machined simultaneously from both sides by two conical end-mills. Copying is performed by means of an electromagnetic follow-up device, connected through a complicated kinematic linkage, the models being the two guide-vane surfaces made to the scale of 1:5.

These milling machines made it possible to raise the productivity considerably and to improve the maching quality.

A special lathe for guide-vane flange machining also proved useful.

Formerly, the flanges were machined on vertical lathes. Since it was difficult to clamp the rotating work piece rigidly in a vertical position, a low cutting speed, and a good deal of time for set-up was required.

In the new lathe the cutting tool rotates clamped in a special chuck, and the heavy workpiece is stationary.

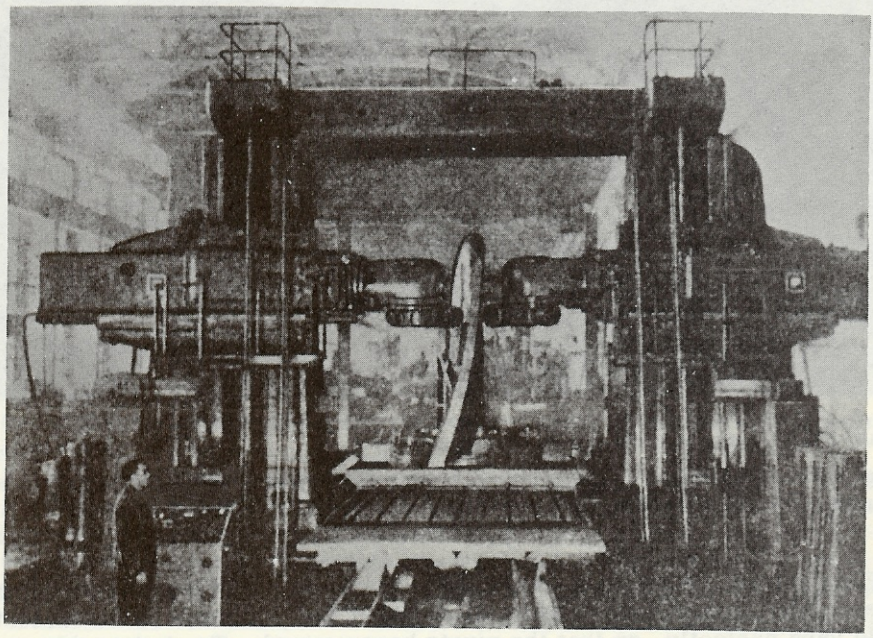


FIGURE XIII.2. Special-purpose copying-milling machine for guide-vane surface-finishing

During flange machining, the guide vane is set with its axis of rotation coinciding with the axis of the spindle, so that the machined frontal flange surface is normal to the axis of rotation of the guide vane.

Apart from these machines, other special-purpose machine tools were provided for machining the openings in the rubber hub below the blade pivots, the openings in the turbine-shaft flanges, the blade flanges, etc.

With the introduction of specialized equipment, production methods of the main turbine parts were radically changed, to the great benefit of Soviet turbine construction.

Series production is important for lowering costs and shortening production time. This is illustrated in Figure XIII. 3 which shows the reduction in cost and man hours in the manufacture of the twenty turbines for the Volga plant imeni V. I. Lenin. The curves prove that it is advisable to use turbines of the same type in several plants.

The chart in Figure XIII. 4 shows the man hours required for machining and assembling as a function of weight for Kaplan and Francis turbines.

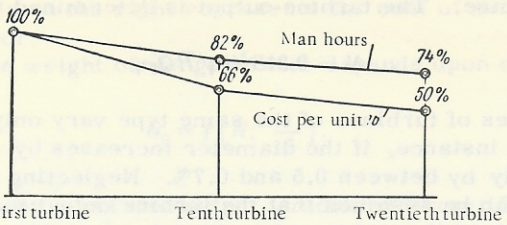


FIGURE XIII.3. Effect of series-production of hydro turbines on production costs and time

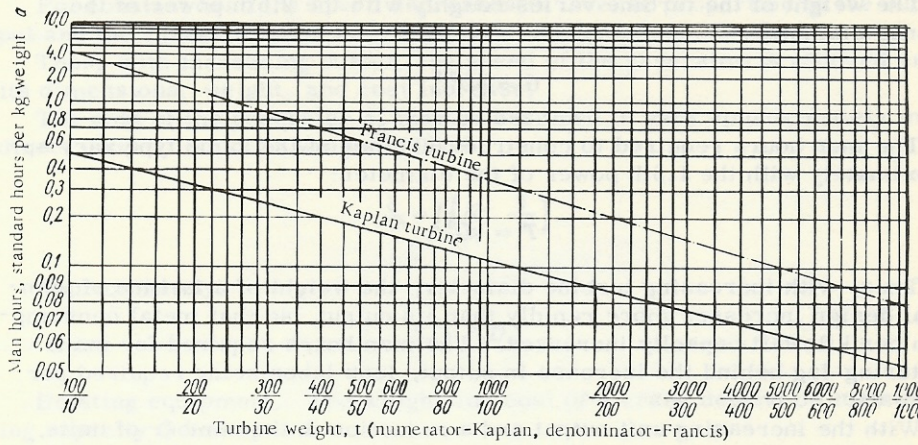


FIGURE XIII.4. Man hours required for assembling

Correct selection of the machining allowances is of particular importance for economical design. Frequently, the surfaces to be machines are of large dimensions, their machining and inspection being difficult. Machining allowances for large parts cannot be specified independently but must accord with the blueprint dimensions of mating parts. The optimum allowances for large diameters should be according to the type of fit, as recommended in GOST. It is advisable to carry out a technical analysis for each part in tabulated form, as done in Table VII. 2 for a Francis runner.

78. SELECTION OF TURBINE SIZE

Selection of the appropriate turbine size and output in large power plants should be coordinated with the selection of the remaining generators, gates, hoisting equipment, transformers, and miscellaneous electric equipment.

The optimum turbine may not match with the best available other equipment. The cost of the powerhouse structure, which largely depends on the turbine size, must also be taken into account.

An analysis of these factors is outlined below:

Hydraulic turbine. The turbine output is determined by the relation

$$N = 9.81 D_1^2 H \sqrt{H} Q_1' \eta.$$

The efficiencies of turbines of the same type vary only slightly for the same head. For instance, if the diameter increases by 100%, the efficiency increases only by between 0.5 and 0.7%. Neglecting the difference in efficiencies, it can be assumed that the turbine output increases as the square of the runner diameter:

$$N = \alpha D_1^2.$$

The weight of the turbine varies roughly with the 2.5th power of the runner diameter:

$$G = \beta D_1^{2.5}.$$

The man hours required to construct turbines of the same type vary approximately with the 1.5th power of the diameter:

$$T = \gamma D_1^{1.5}.$$

Thus, with increasing turbine diameter, the weight of a turbine of identical design increases more rapidly than its output, so that metal consumption per kilowatt capacity increases. The man hours required for manufacturing lag behind the increase in output, less labor being required per kilowatt.

With the increasing unit output and a reduction in the number of units, manufacturing time decreases.

All this is valid for turbines of the same design, and for runner diameters permitting transportation by ordinary means.

With high-power turbines, the large runner and the ring-shaped parts must be divided into separate transportable sections, to be assembled on the erection site by means of bolted joints, welding, securing rings, etc., with subsequent machining so that the man hours required and the costs increase.

As an example, consider a Francis runner (D_1 = 7.5 m) designed for a head of 100 m.

To comply with railroad transportation regulations the runner has to be divided into four sections, which are welded on site to form a single part.

Annealing and machining are required after welding, raising the costs.

When turbine dimensions become so large that the main parts have to be made in sections, costs increase rapidly because of the additional machining operations performed in the shop and on site. Transportation costs also increase.

The cost of a turbine consists mainly of the cost of the materials which depends on the turbine weight, and the cost of labor (including overhead), which varies directly with the difficulties involved in manufacture.

The cost of an hydraulic turbine may thus be given as the sum of two components

$$S_T \cong \kappa_{T1} D_1^{2.5} + \kappa_{T2} D_1^{1.5}.$$

The first member on the right represents the cost of materials, the second, the cost of labor.

Generators. The weight of the generator depends upon output and speed:

$$G_g = f\left(N;\ \frac{1}{n}\right).$$

For instance, if the generator output is doubled (from 175,000 kw to 350,000 kw), the specific weight is reduced by a factor of 1.5 or 1.6. For a speed reduction from 125 to 75 rpm at constant generator output, the specific weight increases by about 80%.

The dimensions of the generator vary inversely with its rotational speed.

For constant head the speed decreases in inverse proportion to the output and the runner diameter.

Thus, with increasing output, the speed of the generator is reduced and its dimensions, weight, and cost increase.

The cost of the generator S_g may be assumed to vary approximately in direct proportion to its weight. Thus

$$S_g = f\left(N;\ \frac{1}{n}\right).$$

Approximately,

$$S_g = K_g D_1.$$

Hoisting equipment. The weight and cost of a crane depend on its hoisting capacity Q and span L:

$$G_c = f(Q;\ L);\quad S_c = f_1(Q;\ L).$$

As shown above, with increasing output the speed decreases, and the dimensions and weight of the generator rotor, which is the heaviest part of the unit and determines the hoisting capacity of the crane, increase. Thus span and hoisting capacity of the crane increase with generator output.

The hoisting capacity Q of the crane is determined by the weight of the generator rotor, which may be considered to vary as the cube of the runner diameter, i.e.,

$$G_{rot} = \alpha_g D_1^3.$$

The span of the crane may be considered to vary in direct proportion to the runner diameter, i.e.,

$$L = \kappa_l D_1.$$

Consequently, the cost of the crane may be assumed to be

$$S_c = \kappa_c D_1^4.$$

Gates. The width of the gate at the intake is directly proportional to the runner diameter. The weight G_s of the plain sliding gates and their cost S_s

are approximately proportional to the third power of the width L, i.e., the third power of the runner diameter D_1:

$$S_s = \kappa_s D_1^3.$$

Penstocks. Penstocks for medium-head turbines are usually inside the dam, completely embedded in concrete. Their weight and cost therefore depend mainly on their diameter and wall thickness.

Since the wall thickness of the penstock is directly proportional to its diameter D, the penstock weight is

$$G_p = \kappa_p D_p^2.$$

If instead of one penstock, there are 2, 3, . . . n penstocks, the diameter of each, for the same total cross-sectional area, is

$$d = \frac{D_p}{\sqrt{n}},$$

and their total weight

$$\sum G_p = \kappa_p n \left(\frac{D_p}{\sqrt{n}}\right)^2 = \kappa_p D_p^2.$$

Thus, the total weight of the penstocks, and consequently their cost, will depend only slightly on the speed and output of the hydro unit.

Electrical equipment. With increasing unit output and the reduction in the number of units, the number of oil-circuit breakers, disconnecting switches, current transformers, as well as protective, control, and measuring devices, decreases. The number of power transformers also decreases.

On the other hand, the current and the power ratings of all the above-mentioned equipment increase, except for the protective, control, and measuring devices.

It may be assumed, on the whole, that a variation of 50 to 100% in the hydro-unit power does not sensibly affect the cost of the electrical equipment.

Powerhouse structures. The basic dimensions of the powerhouse concrete section depend on the dimensions in plan of the scroll case, and on the depth of the draft tube, i.e., the distance from the level of the lower slab beneath the draft tubes to the crane beams. The volume of rock excavated, if a powerhouse is required, depends on the surface of the concrete section and the draft head. The depth of the rock to be excavated depends on the distance from the distributor axis to the lower slab surface.

The cost of the powerhouse structure may be considered to be approximately

$$S_H = \kappa_H D_1^3.$$

The optimum values of the turbine output and runner diameter may be determined from the minimum expenditures ΣS_{min}

$$\Sigma S_{min} = S_t + S_g + S_c + S_s + S_p + S_e + S_H, + S_{a.e.}$$

The cost of the gates S_s, auxiliary equipment $S_{a.e.}$, penstock S_p, and electrical equipment S_e depend only slightly on turbine output and dimensions. They may therefore be denoted by the constant C.

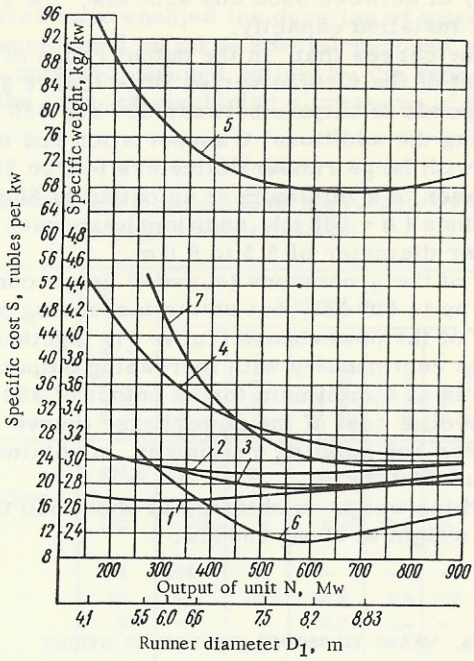


FIGURE XIII.5. Variation of specific cost and weight of the unit with unit output (head H = 100 m):

1 — cost of powerhouse structures (including cranes); 2 — cost of turbines; 3 — cost of turbines without additional transportation and special manufacturing expenses; 4 — cost of generator; 5 — total cost of powerhouse, including auxiliary-power and hoisting equipment; 6 — turbine weight; 7 — generator weight.

$$C = S_s + S_p + S_e + S_{a.e.}$$

The minimum cost of the powerhouse and equipment is then

$$\sum S_{min} = \kappa_{T1} D_1^2 + \kappa_{T2} D_1^{1,5} + \kappa_g D_1 + \kappa_c D_1^4 + \kappa_p D_1^3 + C,$$

where D_1 = runner diameter.

Several of the coefficients in the above formula are not constant even for a constant head, and depend upon output and number of units. Therefore, the relationship between the total cost of the powerhouse (including equipment) and the output of the unit, is very complex and cannot be solved analytically.

The comparison of costs for various design variants should therefore be made by direct calculations for each particular case.

Figure XIII. 5 shows results of actual calculations for several turbines with outputs varying between 200 Mw and 900 Mw, for a head of 100 m and installed plant capacity of between 5900 and 6300 Mw; the curves show the costs per kilowatt of installed capacity.

It appears from the curves that, in the output range of 300 to 500 Mw per unit, the specific cost of the turbine varies little (curve 2), but the lowest specific cost corresponds to outputs between 500 and 550 Mw.

Without considering the additional transportation and manufacturing expenses concomitant with large runner diameters (curve 3), the specific cost of the turbine decreases to a minimum at an output of 600 Mw.

For Francis turbines (H = 100 m), additional expenses are incurred commencing with a runner diameter of 5.5 to 6.0 m.

The specific cost of the generators (curve 4) drops continuously with increasing unit output up to 600 Mw, but starts increasing beyond 800 Mw.

The specific cost of the powerhouse (curve 1), together with the hoisting equipment, increases continuously with increasing output.

The specific cost is at a minimum for an output of 250 to 300 Mw.

The least total specific cost of the powerhouse (curve 5), including the cost of auxiliary-power and hoisting equipment, is obtained for a unit output of between 600 and 700 Mw.

The minimum turbine weight is obtained at about 550 to 600 Mw, and the minimum generator weight at about 700 Mw.

79. MEANS TO REDUCE THE TURBINE WEIGHT

The manufacture of large turbines involves great expense. The largest Kaplan turbine (N = 126,000 kw, H = 22.5 m, see Figure V. 15) for the Volga HEP imeni Lenin, has more than 50,000 parts. Many of these are large and heavy. The speed ring has an outer diameter of 14 m and weighs 166 t; the six runner blades each weigh 18.5 t; the turbine cover-plate has an outer diameter 1.5 m, a length 9.4 m, and weighs 60 t; the turbine-shaft diameter is 1.5 m, its length 12.5 m, and its weight 60 t.

Besides the many large and heavy parts forged, welded, or made of intricate castings, the turbine also has a number of comparatively small parts.

The weights of some parts for the turbines of the Volga plant imeni Lenin are given in Table XIII. 1. The table also shows the weight of the metal used for steel castings, forgings, and products of roll mills.

It appears from the table that most of the metal is used for the runner and the distributor, their combined weight being 877 t, or about two-thirds of the total weight of the turbine. A good deal of attention should therefore be paid in the design to reducing weight to a minimum.

The linings of the water passages and concrete pits, the foundation frames, the penstocks, etc., are usually fabricated from steel sheets and rolled sections. The amount of metal used for turbine parts made from castings is 75 to 85% of the total metal consumption.

With the considerable advances in welding techniques during recent years, welding is being employed more and more in turbine construction.

Foundation parts, distributor rings, turbine cover-plates, gate rings, runner hubs, bearing brackets, etc., are nowadays generally welded.

Welded structures are fabricated from various types of blanks. Flat parts are cut out from sheets; parts of cylindrical or annular shape are rolled; intricately-shaped parts are stamped.

Welded structures have enabled the duration of machining to be reduced, particularly that performed on large special-purpose machines. Important savings were thus obtained, caused mainly by the reduced surface area to be machined and the reduced machining allowances of the welded parts.

TABLE XIII.1

Weight of parts, and manhours required to manufacture the type PL-587-VB-930 turbine, N = 126,000 kw, H_{max} = 30 m, n = 68.8 rpm

No.	Type	Weight for each turbine, t	Material, t					Standard man-hours per turbine	Man hours	
			steel castings	cast iron	steel forgings	rolled sheets	other materials		for machining	for manual work and assembly
1	Runner	426.5	294	26	92	9	5	32,400	17,400	15,000
2	Foundation parts (without speed ring)	103	2.8	—	0.43	99.8	—	40,400 together with No. 13,14,15	14,500	25,900
3	Speed ring	174	174	—	—	—	—			
4	Turbine shaft	60	—	2.4	56.5	0.9	0.2	2,600	1,820	780
5	Runner rods	3.6	—	—	0.2	3.4	—	720 together with No. 11	420	300
6	Distributor	451	328.3*	35.4	11.3	74.1	2.0	45,200	17,300	27,900
7	Guide bearing	57	12	32	2	10	1	3,300	2,500	800
8	Distributor servomotor	21.3	3.1	12.8	2.1	3.1	0.2	2,200	1,800	400
9	Governor type RKO-250	5.5	—	0.8	0.7	4.0	—	6,300	6,000	300
10	Pressure-oil installation type MNU-32	38	—	—	—	38	—	8,600	8,000	600
11	Oil-supply head	8.2	—	7.6	—	—	0.6	—	—	—
12	Platforms and ladders	3.3	—	—	—	3.3	—	970	270	700
13	Turbine and servomotor pits	28.1	—	—	—	28.1	—	—	—	—
14	Lining of draft tube cone	26.3	—	—	—	26.3	—	—	—	—
15	Lining of scroll case	18.2	—	—	—	18.2	—	—	—	—
16	Other parts	22.3	—	10	—	12.3	—	11,310	9,990	7,320
	Total for each turbine	1446	814.2	127.0	165.23	330.6	9.0	160,000	80,000	80,000
		100%	56%	9%	11.5%	23%	0.5%			

* By using welded constructions the weight of steel castings was reduced to 170t, while the weight of rolled sheets increased to 200 t.

Welded structures made of simple blanks may have thin walls, thus avoiding internal structural defects frequently occurring in heavy intricate steel castings.

In the subsequent series of turbines for the Volga HEP imeni Lenin, a number of cast parts were for this reason replaced by welded parts.

Table XIII. 2 shows weights of two turbine variants for the Volga plant imeni Lenin and the man hours required for manufacturing. The table shows that the total weight of the parts of the cast variant is 376 t, and that of the welded only 303.2 t; thus, a weight reduction of 72.8 t was obtained. 16,218 standard man hours were required for machining the cast parts, and 10,754 standard man hours for the welded parts; thus a reduction of 5,464 standard man hours was obtained. These data confirm the advantages of employing welding. However, in the lower distributor ring and the turbine cover-plate the weight of rolled sheet steel used exceeds the weight of the cast blanks. This is explained by the fact that the surface areas of these parts which are to be machined are comparatively small, even for the castings; the small machining allowances for welded parts is explained by the fact that the blanks can be cut from rolled sheets to the exact shape. Because of the significant reduction in machining man hours, it is nevertheless advisable to substitute fabricated parts for castings even in these instances.

TABLE XIII.2

Comparison of welded and cast parts of turbines for the Volga plant imeni Lenin

Part	Cast				Welded					Savings		Labor saved, standard man hours	
	Weight, t		Standard man hours		Weight, t		Total material consumption	Standard man hours		Weight, t			
	finished product	blanks	machining and assembly	machining	finished product	blanks		machining and assembly	machining	finished product	metal	machining and assembly	machining
Foundation parts	111.7	169.9	5,500	4,870	89.3	96.0	132.1	3,030	2,670	22.4	37.8	2,480	2,200
Lower distributor ring	24.5	31.0	2,630	1,870	21.9	27.7	36.6	1,856	1,500	2.6	-5.6*	775	370
Upper distributor ring	83.8	129.8	7,000	4,524	69.8	79.6	118.5	5,512	3,483	14.0	11.3	1,480	1,041
Turbine cover-plate	60.0	78.0	3,207	2,440	54.4	60.0	90.9	2,384	1,696	5.6	-12.9*	823	744
Runner cone . . .	14.0	16.6	594	314	10.9	11.1	13.0	502	255	3.1	3.6	92	59
Gate ring	22.0	27.0	1,100	900	15.0	16.1	21.8	700	570	7.0	5.2	400	330
Thrust bearing .	60	75	1,500	1,300	41.9	47.6	66.9	680	580	18.1	8.1	820	720
Total . .	376.0	527.3	21,531	16,218	303.2	338.1	479.8	14,664	10,754	72.8	47.5	6,870	5,464

* Metal dissaving

In the construction of large turbines, welded-cast parts obtained by welding cast blanks together are also used, e. g., speed rings, guide vanes, etc.

To reduce the weight of parts and man hours required, combined blanks obtained by casting together two or more parts are sometimes used for parts formerly joined together by means of bolts, studs, and nuts. Although complicating blank design, this is advantageous whenever welding is impractical and mechanical fastening requires much work. By using, for the Dnieper HEP, an all-cast Francis runner (D_1= 5.5 m) instead of a runner made in three sections, its weight was reduced by 12 t and 1100 man hours were saved on assembly.

Combining the turbine and generator shafts of a large turbine into a single part reduced the shaft weight by 8 t, and assembly time by 800 man hours.

The component weights of the type RO-211-VM-410 Francis turbine (N= = 75,000 kw, H = 66.5 m, D_1 = 4.1 m) installed at the Bukhtarma HEP, are given in Table XIII. 3. For turbines in which only the scroll casing is welded, this latter, together with the speed ring and the distributor with its servomotor are the heaviest parts; their combined weight is 184 t, or more than 60% of the total weight of the turbine.

TABLE XIII. 3

Component weights and man-hours required for production of the type RO-211-VM-410 turbine

Type	Weight for each turbine, t	Material, t					Standard man-hours per turbine	Man-hours	
		steel castings	cast iron	steel forgings	rolled sheets and tubes	other materials		for machining	for manual labor and assembly
Runner with seals	48.5	42.0	—	—	6.0	0.5	6,300	2,600	3,700
Foundation parts	14.2	—	7.9	—	4.5	1.8	19,250	3,600	15,000
Speed ring	37.0	36.0	—	—	—	0.2	together with No. 11 and 12		
Turbine shaft	30.0	—	0.5	29.2	—	0.3	1,650	1,250	450
Guide bearing	4.4	—	3.6	—	0.6	0.2	1,050	650	400
Distributor	63.0	43.7	6.7	0.9	10.6	1.1	14,350	10,250	4,100
Distributor servomotor	7.3	0.4	5.4	1.2	0.1	0.2	1,500	900	600
Governor	1.9	—	0.6	—	1.1	0.2	3,700	2,700	1,000
Pressure-oil installation	2.6	—	0.3	—	1.6	0.7	4,000	1,800	2,200
Platforms and ladders	1.1	—	—	—	1.0	0.1	600	150	450
Turbine and servomotor pits, lining of draft tube cone	15.2	—	—	—	14.7	0.5	—	—	—
Scroll case	77.5	—	—	—	76.0	1.5	—	—	—
Other parts	9.7	—	0.80	2.3	4.8	1.8	2,250	1,000	1,250
	312.4	122.9	25.8	33.6	121.0	9.1	54,550	24,800	29,700
	100%	39%	8%	11%	39%	3%			

Figure XIII. 6 shows how the specific weight (kg/kw) of various types of turbines has been reduced since 1900. These curves show that, over a period of 30 years, the specific weight of Kaplan turbines for $H \cong 20$ m was

reduced from 27.5 kg/kw to 15 kg/kw; over a period of 50 years the specific weight of medium-head ($H \cong 60$ m) Francis turbines was reduced from 33 kg/kw to 7.5 kg/kw, or to less than one fourth. In high-head Francis turbines ($H \cong 200$ m), the specific weight was reduced from 12.5 kg/kw to 4 kg/kw. These figures show how turbine designs improved so that a considerable weight reduction could be obtained. They also show that the specific weight of the turbine varies considerably with the head.

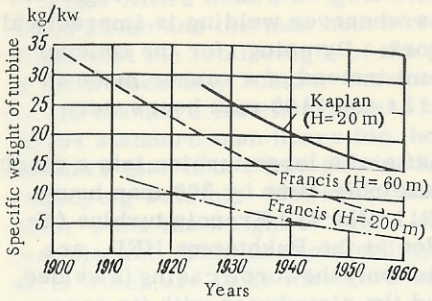


FIGURE XIII.6. Reduction of specific turbine weight over the last 60 years

Figure XIII.7 shows the specific metal consumptions [kg/kw] for several modern vertical turbines for various heads. These curves were plotted from actual turbine data. Low-head Kaplan turbines show the greatest specific metal consumption, high-head Francis turbines the lowest. With increasing head the specific metal consumption drops rapidly, particularly in the range H = 30 m to H = 100 m.

In the range H = 400 m to H = 100 m, the design of the scroll casing exerts a strong influence on specific metal consumption. On the basis of an analysis of the weight figures for various existing turbines built during the last 15 — 20 years, I. N. Umikov /86/ of the LMZ staff established charts to determine the theoretical weight of the turbine and its main parts. For this purpose Kaplan turbines were classified according to the number of blades (four-blade and six-blade), and Francis turbines according to the type of scroll casing (welded or cast), i.e., the turbines were in fact grouped according to the ranges of head under which they operate. The weights of these turbines are given in Figure XIII.8 for various runner diameters.

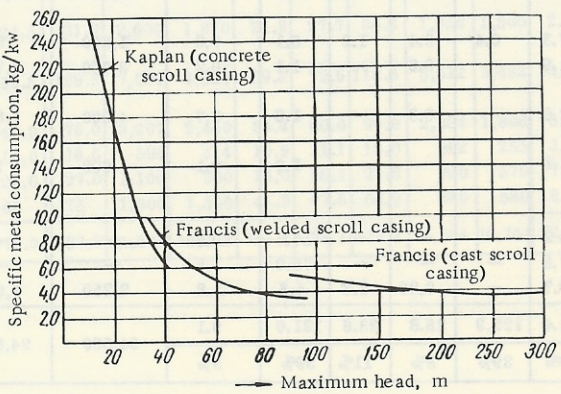


FIGURE XIII.7. Specific metal consumption of turbines

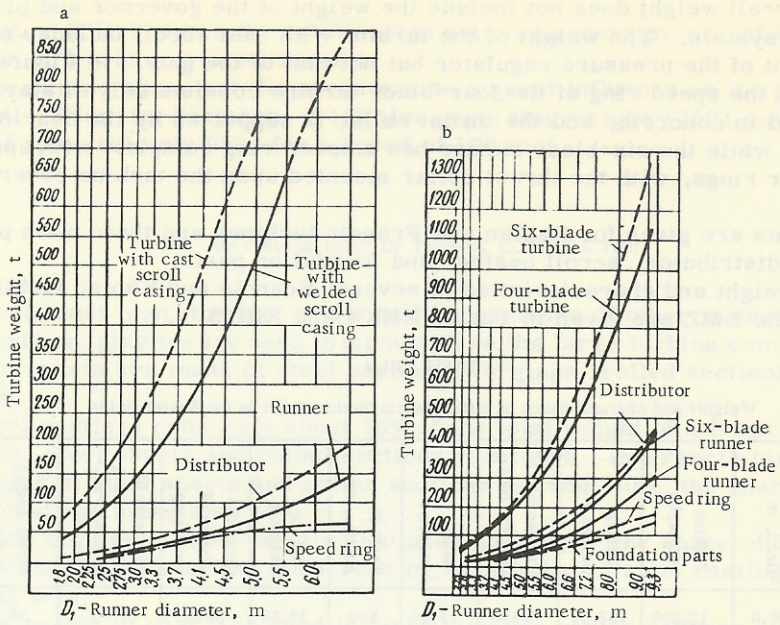


FIGURE XIII.8. Turbine weights (according to LMZ data):

a — Francis; b — Kaplan.

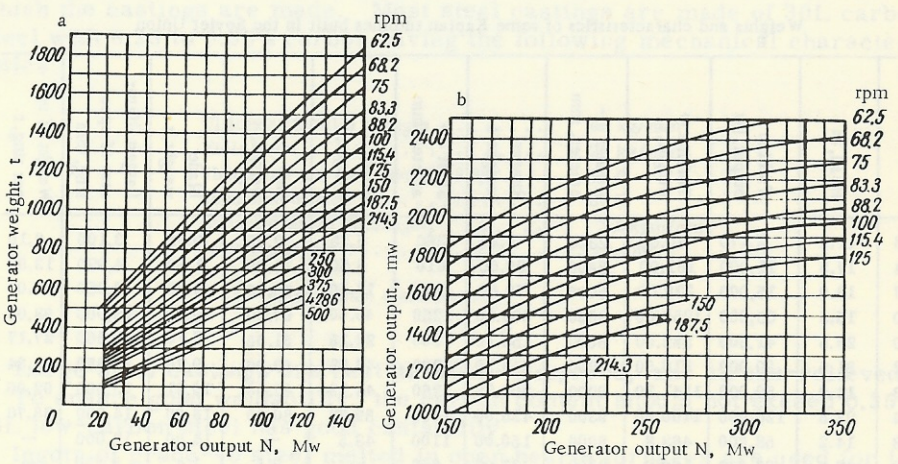


FIGURE XIII.9. Generator weights as function of outputs for different rotational speeds:

a — generators from 15 to 150 Mva; b — generators from 150 to 350 Mva (by courtesy of the "Elektrosila" plant).

The over-all weight does not include the weight of the governor and pressure-oil system. The weight of the turbine with cast scroll includes only the weight of the pressure regulator but not that of the gate. In Figure XIII. 8,b, the speed ring of the four-blade turbine consists only of stay ribs embedded in concrete, and the thrust collar is supported by the bearing bracket, while the six-blade runner has a speed ring complete with upper and lower rings, with the thrust collar mounted upon the turbine cover-plate.

Weights are given for Kaplan and Francis turbines and their main parts: runner, distributor, scroll casing, and foundation parts.

The weight and characteristics of several Francis and Kaplan turbines built at the LMZ are given in Tables XIII. 4 and XIII. 5

TABLE XIII. 4

Weights and characteristics of some Francis turbines built in the Soviet Union

Year built	Head, m	Turbine output, kw	Turbine weight, t	Runner diameter, mm	Runner weight, t	Shaft diameter, mm	Shaft weight, t	Outer diameter of speed ring	Diameter of scroll-casing entrance-section	Scroll casing weight, t
1933	36.0	15,300	126.50	2500	11.40	600	13.50	3865	3700	38.00
1939	35.5	21,000	229.00	3000	22.50	750	16.50	5780	4500	44.50
1946	36.3	75,000	660.00	5450	92.00	1100	46.00	8550	7620	160.00
1950	62.0	61,500	314.14	4100	46.43	900	28.13	6973	4964	84.33
1951	39.8	85,000	631.95	5450	112.75	1100	35.10	8495	7620	150.00
1953	285.0	55,200	165.54	2650	8.56	600	11.24	—	1700	40.00
1954	69.0	85,000	—	4300	47.00	970	29.50	—	—	—
1960	63.0	147,000	658.00	5500	99.00	1400	37.00	8430	7500	—
1960	96.0	215,000	807	5500	93.20	1500	37.10	8500	7000	—

TABLE XIII. 5

Weights and characteristics of some Kaplan turbines built in the Soviet Union

Year built	Head, m	Turbine output, kw	Turbine weight, t	Runner diameter, mm	Runner weight, t	Shaft diameter, mm	Shaft weight, t	Hub weight, t	Blade weight, t	Largest diameter of upper ring, mm	Weight of upper ring, t
1933	11.0	2,470	40.50	2300	6.24	360	5.25	2.20	0.65	3,100	3.10
1934	17.5	11,000	161.00	3600	30.00	610	6.50	11.00	1.60	4,920	13.00
1937	13.0	15,000	330.00	5000	70.00	750	17.50	29.00	4.00	7,280	30.00
1940	15.5	65,000	1256.00	9000	306.00	1250	43.60	67.00	20.00	13,000	98.00
1950	23.5	41,500	582.00	6600	153.10	900	22.15	51.05	6.10	9,660	27.17
1952	31.5	90,000	816.00	7200	248.10	1200	48.88	63.00	9.70	11,350	45.34
1953	14.0	59,000	1141.30	9000	300.20	1250	44.194	67.00	19.51	13,000	92.00
1954	22.5	126,000	1460.00	9300	426.00	1420	59.73	80.00	18.00	14,000	83.76
1958	14.2	58,000	463.8	8000	150.00	1100	43.5	—	14.00	12,000	—
1959	42.5	36,000	169.0	3700	31.03	650	—	9.5	1.4	5,850	—
1960	9.85	45,400	930.0	9300	184.00	1320	34	—	—	13,850	—
1960	25.75	41,750	321.0	5000	81.6	900	29.4	—	—	7,780	—

Figure XIII. 9 shows the relationship between generator weight and output for different rotational speeds.

The curves show that the speed exerts a great influence on the generator weight. Thus, for instance, a 100 Mva generator weighs 1350 t for a speed of 62.5 rpm, but only 950 t for a speed of 100 rpm.

80. MATERIALS USED IN TURBINE CONSTRUCTION

Steel, cast iron, bronze, and smaller quantities of other materials (babbitt, rubber, plastics are used to manufacture the large turbine components.

Most parts are made of steel castings, forgings, rolled sections, and sheets.

Steel castings constitute about 55% of the total weight of a large Kaplan turbine, steel sheets and rolled sections about 25%. In Francis turbines the share of steel sheets and rolled sections is about 40%, the share of steel castings being also 40%.

Since welding is more widely employed nowadays, the share of steel sheets and rolled sections is increasing, while that of steel castings is becoming less.

The weight of cast iron used in large turbines varies between 8 and 10% of the total weight of the turbine.

Forgings constitute about 10 to 12% of the total weight.

Steel castings are used for the largest parts such as the runner hub of Kaplan turbines, the runner of Francis turbines, the blades, guide vanes, turbine cover-plates, etc.

By reason of their complicated structure and large dimensions, the parts must often be cast with thick walls, and casting defects may therefore occur on the surfaces to be machined and at the transitions between sections.

Hence, good castability and weldability are essential for the steel from which the castings are made. Most steel castings are made of 30L carbon steel with 0.25 to 0.35% carbon having the following mechanical characteristics:

Ultimate (tensile) strength	45 kg/mm^2
Yield point	23 kg/mm^2
Elongation test specimen (l = 5 d)* ...	16 %
Reduction of area	30 %
Impact strength (Mesnager)	3.0 kgm/cm^2
Brinell hardness	128-180

* [l = 5, specimen diameters d.]

Large steel castings are heat-treated, tempered, and stress-relieved.

To ensure good weldability, the carbon content should not exceed 0.35%, 25L low-carbon steel has good castability.

Ingots of grade-40 steel melted in open hearth furnaces are used for important forgings such as turbine shafts. The carbon content varies from 0.35 to 0.45%. The approximate mechanical properties of the forging are as follows:

Ultimate (tensile) strength	48 kg/mm^2
Yield point	26 kg/mm^2
Elongation of the test specimen (l = 5 d)	16 %
Reduction of area	30 %
Impact strength (Mesnager)	4 kgm/cm^2

Steel sheets and rolled section shapes are usually made of hot-rolled carbon steel according to GOST 380-60 (carbon steel, standard quality) and GOST 1051-59 (structural high-quality steel).

Parts of the turbine water-passages, particularly the runner of the Francis turbine and the blades of the Kaplan turbine, operate under cavitation conditions. Since cavitation cannot be completely eliminated by proper selection of the turbine characteristics and blade profile, cavitation erosion should be localized by using cavitation-resistant materials. This applies in particular to the blade of the Kaplan runner.

High-chromium steel, grade 25Kh14NL, extensively used for large turbine blades, has the following chemical composition: carbon — 0.18 to 0.25%, chromium — 12.5 to 14.5%, nickel — 0.5 to 0.8%, silicon — 0.4 to 0.7%, manganese — 0.3 to 0.6%, sulfur — not more than 0.03%, phosphorus — not more than 0.03%. Yu. A. Nekhendzi was the first to use this steel for runner blades. Its mechanical properties are as follows:

Ultimate strength	55 kg/mm^2
Yield strength	30 kg/mm^2
Elongation of test specimen (l = 5 d)	14 %
Reduction of area	30 %
Impact strength (Mesnager)	30 kgm/cm^2
Brinell hardness	190-235

The service records of carbon and high-chromium steels are of interest.

A 40,000 kw Kaplan turbine, operating under a head 25 m, was provided with blades made of 30L carbon steel and 20Kh13NL chromium steel. After 13,000 hours of operation, no cavitation damage was discovered on the chromium-steel blades, whereas the lower surface of the carbon-steel blades was pitted on an area of 9 dm^2 to a depth of 4 to 5 mm after 4000 hours of operation and on an area of 30 dm^2 to a depth of 5 to 88 mm after 13,000 hours of operation.

However, on another, larger turbine (N = 65,000 kw) operating under a head of 17 m, also provided with 20Kh13NL high-chromium steel blades, cavitation damage was discovered on all blades on an area of 16 dm^2 to a depth of 10 mm after 34,000 hours of operation.

Other turbines showed similar damage after prolonged operation.

High-chromium steel has a considerable cavitation resistance and better mechanical properties than carbon steel. It is therefore extensively used in turbines.

However, this steel has poor castability, is prone to cracking, and can be smelted only in electrical furnaces. Casting blades of this steel is very difficult. Facing by welding is only possible after preheating the blades to a temperature of between 350° and 400°C, so that repairs in situ of corroded blades is very difficult.

When a large order for blades for the large turbines of the Volga HEP imeni Lenin was received, efforts were made to find steels of higher mechanical properties.

Systematic research carried out at the TsNIITMASh and at the LMZ on metals for large turbine blades has proved the difficulty of making large blades (20 t net weight) with the required ductility and impact strength from 25Kh14NL stainless steel. The properties of the material differ in the thin and thick sections of the blade and the blade castings show a considerable chemical inhomogeneity.

Data on the properties of steel are usually obtained from tests on comparatively thin cast test specimens, and only give an approximate idea of the true properties of the casting. An improved stainless steel—20Kh13NL—was found suitable for the blades. Its composition is: carbon — 0.17 to 0.22%, chromium — 11.5 to 13.5%, nickel — 0.6 to 1%, silicon — not more than 0.7%, manganese — 0.3 to 0.6%, sulfur — not more than 0.03%, phosphorus — not more than 0.03%, titanium — not more than 0.15%. The addition of titanium increases the impact resistance and improves the internal structure of the steel. This composition makes it possible to obtain a more uniform structure, higher mechanical strength, and ductility of the alloy.

For blade manufacture, I. R. Kryanin suggested 18DGSL copper steel of following composition: carbon — 0.14 to 0.20%, silicon — 0.6 to 0.8%, manganese — 1.0 to 1.3%, copper — 1.2 to 1.5%, sulfur — not more than 0.03%, and phosphorus — not more than 0.04%.

The mechanical properties of this steel are as follows:

Ultimate strength	60 kg/mm^2
Yield strength	42 kg/mm^2
Elongation of test specimen (l= 5 d)	14%
Reduction of area	30%
Impact strength	6 kgm/cm^2

Steel tested at the TsNIITMASh on the magnetostrictive vibrator showed satisfactory cavitation resistance. A nickel bar immersed in water and subjected to the action of a magnetic field undergoes changes in its length due to magnetic forces. Because of the high frequency of the mechanical vibrations, the water separates from the specimen surface in the first half of the cycle, impinging on it again in the second half. Strong perturbations of the water flow are thus caused, the bubbles collapsing against the specimen surface and damaging it. The test bars exhibited a high cavitation-resistance, and this steel grade was therefore used in manufacturing many types of blades for various turbines. Experience showed, however, that results of cavitation tests at the TsNIITMASh were not confirmed in operating practice. Blades made of 18DGSL steel suffered, not less than blades made of common 30L carbon steel, severe cavitation damage in operation. Apart from this, 18DGSL steel shows a tendency to crack and has a poor weldability. It is, therefore, no longer used for casting turbine blades.

A recent innovation is the manufacture of turbine blades from laminated metals. Castings of carbon or low-alloy steel are faced with welded stainless steel plates. This construction combines the high cavitation-resistant properties of stainless steel with the machinability and low cost of carbon steel. For this purpose TsNIITMASh created the 20GSL steel, having the following chemical composition: carbon — 0.16 to 0.22%, manganese — 1.0 to

1.3%, silicon — 0.6 to 0.8%, sulfur and phosphorus — each not more than 0.03%.

The mechanical properties of this steel are:

Ultimate strength	52 kg/mm^2
Yield strength	30 kg/mm^2
Elongation	14%
Reduction of area	30%
Impact strength	5 kgm/cm^2
Brinell hardness	156-197

After heat treatment this steel exhibits better mechanical properties than common carbon-steel. Casting defects may be repaired by welding with standard electrodes without preheating. No quenching structure or cracks appear in the welds, so that no subsequent heat treatment is required.

By reason of its mechanical properties, 20GSL silicon-manganese steel is far more extensively used in turbine construction than low carbon steels of grade 30L and 25L; it may be welded without preheating. It is therefore used not only for Kaplan runner blades, but also for Francis runners and other large parts which, apart from high mechanical properties, require good weldability. This steel is not cavitation-resistant and thus regions liable to erosion damage should be faced by welding, or lined with 1Kh18N9T steel. The fatigue limit of 20GSL steel in water is considerably lower than that of stainless steel (12 kg/mm^2 as against 19 kg/mm^2); this must be taken into consideration when selecting steel for blades or other parts subjected to vibrations.

Austenitic stainless steel (grade 1Kh18N9T) used to line the blades has the following chemical composition: carbon — 0.14%, chromium — 17 to 19%, nickel — 8 to 11%, silicon — 0.9%, manganese — 0.8%, titanium — not more than 0.8%. It is ductile and shows high chemical stability and good weldability.

The similar 20GS silicon-manganese steel is used for large forgings such as forged shells for turbine shafts.

A steel with austenitic-ferrite structure (10Kh18N3G3D2-L) is used at present in turbine construction for parts immersed in flowing water and subject to erosion.

The chemical composition of this steel is: carbon — not more than 0.1%, silicon — 0.3 to 0.5%, manganese — 2.5 to 3%, chromium — 17.5 to 19.5%, nickel — 3.0 to 3.5%, copper — 1.8 to 2.2%, sulfur and phosphorus — each not more than 0.03%. The mechanical properties of this steel are as follows:

Fatigue limit	55 kg/mm^2
Yield strength	30 kg/mm^2
Impact strength	2.0 kgm/cm^2
Brinell harndess	250-320

The erosion resistance of this steel is approximately 50 to 100% higher than that of carbon steel (according to TsNIITMASh data). However, it is very expensive and requires a complicated manufacturing process, particularly for casting pieces of nonuniform thickness. The castings show

nonuniform ductility, especially when their carbon content is high. The steel may be comparatively easily welded without preheating, especially after austempering. The parts of a welded structure should therefore undergo suitable heat treatment before welding. After welding they should undergo tempering to increase their hardness (260 to 320 H_B), and only afterwards should final machining be performed. If some parts (e.g., the runner body) require rough machining, this operation should be done before tempering.

High chromium and nickel content confers a high cavitation resistance to 10Kh18N3G3D2L steel.

I. N. Bogachev and R. I. Mints /9/ showed that cavitation resistance is conferred by a homogeneous solid-solution (austenitic or martensitic) structure. They suggest chromium-manganese-base medium-carbon steel (of grade 30G10Kh10) as most suitable.

These steels are self-hardening. Due to the shocks caused by cavitation on the metal layer, the austenite turns into martensite which hardens and becomes cavitation-resistant. This steel has not yet been used, however, in the construction of large turbine parts. Its technological operational properties are still unknown.

At the LMZ, components of comparatively small dimensions (guide vanes of small turbines, protective linings, seal rings, etc.) made of carbon steel, are surface-hardened through chemical and heat treatment (carburizing followed by quenching) to provide protection against erosion damage. Various compositions of cavitation-resistant alloys are also being considered for facings.

Rolled sheets of laminated materials (steel 3 + 1Kh18N9T and steel 3 + EI496) are frequently used for welded throat rings and for cavitation-resistant linings.

For scroll casings of large turbines, sheets at grade SKhL-4 (10KhSND) steel are now increasingly used. This steel has the following composition: carbon — 0.12%, manganese — 0.5 to 0.8%, silicon — 0.8 to 1.1% chromium — 0.6 to 0.9%, nickel — 0.5 to 0.8%, copper — 0.4 to 0.65%, sulfur and phosphorus — each not more than 0.04%.

The mechanical properties of this steel are as follows:
fatigue limit — 54 kg/mm^2, elongation of test specimen (1 = 5d) — 18%.

It can be welded without preheating but its use is restricted to sheets up to 32 mm thick.

BIBLIOGRAPHY

Publications in Russian.

1. Alekseev, A.E. Konstruktsii elektricheskikh mashin (Designs of Electrical Machines).— Gosenergoizdat. 1949.
2. Aronson, A.Ya. Primenenie teorii tonkikh sterzhnei k raschetu rabochego kolesa radial'no-osevoi turbiny (Application of the Theory of Thin Bars to the Design of Francis Runners).—In: Sbornik "Gidroturbostroenie", No.4, Mashgiz. 1947.
3. Aronson, A.Ya.—Energomashinostroenie, No.2. 1959.
4. Barkov, N.K. Avtomaticheskie regulyatory skorosti gidroturbin (Automatic Governors for Hydraulic Turbines).—Gosenergoizdat. 1947.
5. Belyaev, N.M. Soprotivlenie materialov (Strength of Materials).—GITL. 1950.
6. Bernshtein, L.B. Povyshenie effektivnosti nizkonapornykh GES (Increase in Efficiency of Low-head Hydro Plants).—Gidrotekhnicheskoe Stroitel'stvo, No.1. 1959.
7. Bernshtein, L.B. Prilivnye elektrostantsii v perspektivnoi energetike (Trends in the Development of Tidal Power Plants).—Gosenergoizdat. 1961.
8. Bleikh, F. Teoriya i raschet zheleznykh mostov (Theory and Design of Steel Bridges).—Gostransizdat. 1931.
9. Bogachev, I.N. and R.I. Mints. Kavitatsionnye razrusheniya zhelezouglerodistykh splavov (Cavitation Damage in Iron-carbon Alloys).—Mashgiz. 1959.
10. Bronovskii, G.A., Z.M. Gamze, and A.Ya. Gold'sher. Tekhnologicheskii analiz razlichnykh variantov konstruktsii rabochikh koles i valov gidroturbin Bratskoi GES (Technological Analysis of Various Designs for Runners and Shafts of the Turbines for the Bratsk Hydro Plant).—In: Sbornik "Gidroturbostroenie", No.4, Mashgiz. 1957.
11. Bugov, A.U. K raschetu prochnosti flantsev valov krupnykh gidroturbin (Calculation of Mechanical Strength of Large-turbine Shaft Flanges).—In: Sbornik "Gidroturbostroenie", No.4, Mashgiz. 1957.
12. Vasil'ev, A.A. Napryazheniya v lopasti provorotnolopastnoi turbiny. Problemy prochnosti v mashinostroenii (Stresses in the Kaplan Turbine Blades. Strength Problems in Machine Construction).—Izdatel'stvo AN SSSR. 1959.
13. Voznesenskii, I.N. Zhizn', deyatel'nost' (His Life and Work).—Selected Works, Mashigz. 1952.

14. Gallai, Ya.S. Primenenie drevplastikov v mashinostroenii (Application of Wood Plastics in the Construction of Machines).—Informatsionno-Tekhnicheskii Listok, No. 71, DNTP. 1956.
15. Gamze, Z.M. and A.Ya. Gold'sher. Tekhnologiya proizvodstva gidroturbin (The Manufacture of Hydraulic Turbines).—Mashgiz. 1950.
16. Garkavi, Yu.E. and M.I. Smirnov. Regulirovanie gidroturbin (Regulation of Hydraulic Turbines).—Mashigz. 1952.
17. Gvozdev, V.S., B.A. Vakhrameev, et al. Oborudovanie sel'skikh gidrostantsii (Equipment of Rural Hydro Stations).—Mashgiz. 1957.
18. German, A.N. Avtomatizatsiya gidroturbin (Automatic Control of Hydraulic Turbines).—Avtomatika i Telemekhanika. 1950.
19. German, A.L., et al. Tekhnologiya proizvodstva malykh gidroturbin (The Manufacture of Small Hydraulic Turbines).—Mashgiz. 1954.
20. Gidroturbostroenie (Construction of Hydraulic Turbines). Collection of Articles, Nos I, IV, and VIII.-Mashgiz. 1955, 1957, 1961.
21. Gidroturbostroenie (Syzranskii zavod) (Construction of Hydraulic Turbines (Syzran' Plant)). Collection of Articles.-Mashgiz. 1956.
22. Gol'denveizer, A.A. Teoriya tonkikh uprugikh obolochek (Theory of Thin Elastic Shells).—Gostekhizdat. 1953.
23. Gol'din, V.E. Tipizatsiya gidroturbin (Standardization of Hydraulic Turbines).—VNITOE. 1946.
24. Granovskii, S.A., V.M. Orgo, and L.G. Smolyarov. Konstruktsii gidroturbin i raschet ikh detalei (Designs of Hydraulic Turbines and Turbine Parts).—Mashgiz. 1957.
25. Gubin, F.F. Gidroelektricheskie stantsii (Hydroelectric Power Stations).—Gosenergoizdat. 1949.
26. Gur'ev, V.P. Ispytaniya gidravlicheskikh mashin (Testing of Hydraulic Machines).—Gosenergoizdat. 1953.
27. Gushchin, M.V. and V.G. Makarov. Metod opredeleniya silovykh kharakteristik rabochikh koles povorotnolopastnykh gidroturbin (Method for Determining the Forces Acting upon Kaplan Runners).—In: Sbornik "Gidroturbostroenie", No.1, Mashgiz. 1955.
28. Davydov, A.P. Rezinovye podshipniki dlya gidroturbin (Rubber-lined Bearings for Hydraulic Turbines).—Gosenergoizdat. 1958.
29. Degtyarev, Ya.S. Novye uplotneniya rabochikh koles povorotnolopastnykh gidroturbin (New Types of Seals for Kaplan Turbine Runners).—In: Sbornik "Gidroturbostroenie", No.1, Mashgiz. 1955.
30. Evdokimov, A.A. Maslonapornye ustanovki (Oil-pressure Installations).—Gosenergoizdat. 1950.
31. Zhmud', A.E. Vintovye nasosy (Screw Pumps).—Mashgiz. 1948.
32. Zhmud', A.E. Gidravlicheskii udar v gidroturbinnykh ustanovkakh (Water Hammer in Hydraulic Turbine Units).—Gosenergoizdat. 1953.
33. Zolotarev, T.L. Gidrosilovye ustanovki (Hydro-power Units).—Gosenergoizdat. 1944.

34. Kachanov, L.M. Voprosy prochnosti lopasti vodyanoi turbiny (Strength of the Hydraulic Turbine Blades).—Sbornik LGU im. Zhdanova. 1954.
35. Kvyatkovskii, V.S. et al. Malye gidroturbiny (Small Hydraulic Turbines). —Mashgiz. 1950.
36. Kvyatkovskii, V.S. Vozdeistvie potoka na kameru rabochego kolesa (Action of Water Flow on Runner Throat Ring).—Gidrotekhnicheskoe Stroitel'stvo, No.6. 1954.
37. Kvyatkovskii, V.S. Rabochii protsess osevoi turbiny (Working Process of Francis Turbines), Parts I and II.—Trudy VIGM. 1951-1952.
38. Kvyatkovskii, V.S. Dve novye sistemy reaktivnykh povorotnolopastnykh turbin (Two New Types of Adjustable-blade Reaction Turbines).—Gidrotekhnicheskoe Stroitel'stvo, No.11. 1957.
39. Kovalev, N.N. Gidroturbostroenie na LMZ (Construction of Hydraulic Turbines at the LMZ).—Sovetskoe Kotloturbostroenie, No.2. 1945.
40. Kovalev, N.N. Sovremennoe sostoyanie i puti razvitiya gidroturbin (Hydraulic Turbines — Present-day State and Development Trends).—Kotloturbostroenie, No.4. 1954.
41. Kovalev, N.N. Konstruktsii gidroturbin LMZ (Designs of LMZ Hydraulic Turbines).—In: Sbornik "Razvitie tekhniki na LMZ", Mashgiz. 1957.
42. Kovalev, N.N. Nekotorye voprosy razvitiya gidroturbostroeniya v nashei strane (Development of Hydraulic-turbine Construction in the U.S.S.R.).— Gidrotekhnicheskoe Stroitel'stvo, No.11. 1958.
43. Kovalev, N.N. Svarnye konstruktsii gidroturbin (Welded Hydraulic Turbines).— Svarochnoe Proizvodstvo, No.2. 1956.
44. Kovalev, N.N. Gidroturbina Kuibyshevskoi GES (The Hydraulic Turbine of the Kuibyshev Hydro Plant).—Energomashinostroenie, No.4. 1956.
45. Kovalev, N.N., S.A. Granovskii, et al. Novye turbiny Dneproges (The New Turbines of the Dnieper Hydro Plant).—Mashgiz. 1951.
46. Kovalev, N.N. and V.S. Kvyatkovskii. Gidroturbostroenie v SSSR (Construction of Hydraulic Turbines in the U.S.S.R.).—Gosenergoizdat. 1957.
47. Kovalev, N.N. Kompleksnoe reshenie voprosov tekhnologii i konstruirovaniya gidroturbin (Solving Complex Problems of Design and Manufacture of Hydraulic Turbines).—In: Sbornik "Peredovaya tekhnologiya mashinostroeniya", Izdatel'stvo AN SSSR. 1956.
48. Kovalev, N.N. and Z.M. Gamze. Uluchshenie tekhnologichnosti konstruktsii gidroturbin (Improved Economic Designs of Hydraulic Turbines). —Vestnik Mashinostroeniya, No.7. 1955.
49. Kovalev, N.N., N.I. Prigorovskii, G.E. Rudashevskii, and Yu.U. Edel'. Issledovanie davlenii i napryazhenii na lopasti rabochego kolesa gidroturbiny Narvskoi GES (Investigations on the Pressure and Stress Pattern in the Runner Blades of Turbines of the Narva Hydro Plant).—Energomashinostroenie, No.1. 1959.

50. Kovalev, N.N. Rabota LMZ po obratimym gidroagregatam (LMZ Develops Reversible Pump-turbine Units).—In: Sbornik "Vysokomanevrennye elektrostantsii i nasosnoe akumulirovanie", Izdatel'stvo AN SSSR. 1959.
51. Kovalev, N.N. Puti snizheniya stoimosti gidroturbin (Ways of Reducing the Cost of Hydraulic Turbines).—Trudy LPI, No.215. 1961.
52. Kovalenko, V.A. and G.Yu. Pupko. Issledovanie napryazhennogo sostoyaniya proushin (Analysis of Stress Pattern in Eye Bolts).—In: Sbornik "Gidroturbostroenie", No.4, Mashgiz. 1957.
53. Kolton, A.Yu. and I.E. Etinberg. Osnovy teorii i gidrodinamicheskogo rascheta vodyanykh gidroturbin (Theory and Hydrodynamical Calculation of Hydraulic Turbines).—Mashgiz. 1958.
54. Kolton, A.Yu. and I.E. Etinberg. Opredelenie osevykh usilii, deistvuyushchikh na rabochee koleso radial'no-osevoi turbiny (Determination of the Axial Forces Acting on the Francis-turbine Runner).—Kotloturbostroenie, No.1. 1950.
55. Kotenev, I.V. Vliyanie formy kamery rabochego kolesa turbiny na ee kharakteristiki (Influence of the Throat-ring Shape on the Turbine Characteristics).—Vestnik Mashinostroeniya, No.8. 1954.
56. Kryanin, I.R. Lopasti gidroturbin (Hydraulic-turbine Blades).—Mashgiz. 1958.
57. Kustanovich, M.S. Issledovanie metodiki rascheta reguliruyushchikh kolets (Analysis of the Methods for Calculating Gate Rings).—In: Sbornik "Gidroturbostroenie", No.1, Mashgiz. 1955.
58. Lomakin, A.A. Tsentrobezhnye i propellernye nasosy (Centrifugal and Axial Pumps).—Mashgiz. 1950.
59. Lur'e, A.I. and A.M. Kats. Teoriya uprugosti (Theory of Plasticity).—LPI. 1938.
60. Malyshev, M.V. Turbina Nizhne-Svirskoi GES (Turbine of the Lower Svir' Hydro Plant).—Byulleten' Svirstroya, Nos 17-18. 1939.
61. Malyshev, V.M. Razvorot rabochikh lopastei povorotnolopastnykh turbin v usloviyakh razgona (Changes in the Position of the Kaplan Runner Blades during Runaway).—Gidroturbostroenie, No.1. 1955.
62. Mikhanovskii, S.P. Dvukhperovaya gidroturbina (Twin-blade Hydraulic Turbine).—Energomashinostroenie, No.8. 1957.
63. Mikhanovskii, S.P. Raschet silovoi chasti, regulirovaniya rabochego kolesa povorotnolopastnoi gidroturbiny (Design of Runner Regulation of a Kaplan-type Turbine).—Energomashinostroenie, No.11. 1959.
64. Morozov, A.A. et al. Turbinnoe oborudovanie gidroelektrostantsii (Turbines for Hydro Plants).—Gosenergoizdat. 1958.
65. Nikol'skii, P.N. Izmerenie usilii, deistvuyushchikh na lopatki napravlyayushchego apparata (Measurement of Forces Acting on the Distributor).—In: Sbornik "Gidroturbostroenie", No.1, Mashgiz. 1955.
66. Nemm, V.A. Eksperimental'nye issledovaniya prochnosti detalei gidroturbin (Experimental Investigation of the Strength of Turbine Parts).—In: Sbornik "Gidroturbostroenie", No.1, Mashgiz. 1955.

67. Orakhelashvili, M.M. Samotormozhenie povorotnolopastnykh turbin umen'sheniem razvorota lopastei (Self-braking of Kaplan Turbines by Reducing of Opening Angle of the Blade).—Gidrotekhnicheskoe Stroitel'stvo, No.2. 1952.
68. Pavlovskii, N.N. Gidravlicheskii spravochnik (Hydraulic Handbook).—ONTI. 1937.
69. Perekhodtseva, A.M. Raschet na izgib kruglykh kol'tsevykh plastin (Calculation of Circular Ring Plates for Bending Strength).—TsAGI. 1939.
70. Petrov, L.N. and L.D. Esin. O konstruktivnykh osobennostyakh povorotnolopastnykh turbin na vysokie napory (Design Features of High-head Kaplan Turbines).—Energomashinostroenie, No.5. 1957.
71. Povkh, I.L. Modelirovanie gidravlicheskikh turbin v vozdushnom potoke (Aerodynamic Model Tests of Hydraulic Turbines).—Gosenergoizdat. 1955.
72. Postoev, V.S. and V.I. Mikheev. Napryazhennoe sostoyanie v toroobraznoi obolochke pri deistvii gidrostaticheskogo davleniya (Stress Pattern in a Toroidal Shell Subjected to Static Pressure).—Trudy Vsesoyuznogo Zaochnogo Lesotekhnicheskogo Instituta, No.7. 1961.
73. Prigorovskii, N.I. Plastinki i sosudy (Plates and Vessels).—ESM, Vol.1, Mashgiz. 1947.
74. Prigorovskii, N.I. Soprotivlenie materialov (Strength of Materials).—ESM, Vol.3, Mashgiz. 1955.
75. Prigorovskii, N.I. et al. Opredelenie napryazhenii i peremeshcheniya v detalyakh vtulok rabochikh koles gidroturbin na modelyakh (Determination of Stresses and Displacements in Hydro-turbine Runner Hubs with the Aid of Models).—In: Sbornik "Gidroturbostroenie", No.4, Mashgiz. 1957.
76. Prigorovskii, N.I. and A.N. Preiss. Issledovaniya napryazhenii i zhestkosti detalei mashin na tenzometricheskikh modelyakh (Experimental Determination of Stress Pattern and Rigidity of Machine Components on Tensometric Models).—Izdatel'stvo AN SSSR. 1958.
77. Rudashevskii, G.E. Voprosy mnogotochechnykh izmerenii deformatsii, davlenii i vibratsii na gidroturbinakh v ekspluatatsionnykh uslovyakh (Problems of Multiple-point Measurements of Strains, Pressure, and Vibrations in Hydraulic Turbines under Operating Conditions).—Institut Mashinovedeniya AN SSSR. 1959.
78. Smirnov, I.N. Gidravlicheskie turbiny (Hydraulic Turbines).—Gosenergoizdat. 1956.
79. Smirnov, M.I. Avtomaticheskie regulyatory protochnogo tipa (Flow Governors).—Katalogoizdat. 1939.
80. Spravochnik po raschetu samoletov na prochnost' (Handbook for Aircraft-strength Calculations).—Oborongiz. 1954.
81. Strakhovich, K.I. Tsentrifugal'nye i kompressornye mashiny (Centrifugal Machines and Compressors).—Mashgiz. 1940.
82. Time, V.A. Gidroturbiny konstruktsii LMZ (Hydraulic Turbines).—VKTO, Nos 5-6. 1932.

83. Time, V.A. Mekhanizmy povorota lopastei konstruktsii LMZ (LMZ Mechanisms for Turbine-blade Adjustment).—Kotloturbinnoe oborudovanie, No.2. 1933.
84. Timoshenko, S.P. Plastinki i obolochki (Plates and Shells)[Russian translation].—Gostekhizdat. 1948.
85. Timoshenko, S.P. Soprotivlenie materialov (Strength of Materials)[Russian translation].—Fizmatgiz. 1960.
86. Umikov, I.N. Vesovye pokazateli gidroturbin (Weight Parameters of Hydraulic Turbines).—In: Sbornik "Gidroturbostroenie", No.1, Mashgiz. 1955.
87. Usovershenstvovanie konstruktsii mashin i tekhnologii v krupnom paro-gidroturbostroenii (Improving the Design and Manufacture of Powerful Steam and Hydraulic Turbines).—Collection of articles, Trudy LMZ, No.3, Mashgiz. 1956.
88. Fillippova, N.M. Primenenie drevplastikov v uzlakh treniya gidroturbin (The Use of Wood Plastics in Friction Elements of Hydraulic Turbines).—In: Sbornik "Gidroturbostroenie", No.1, Mashgiz. 1955.
89. Fiterman, Ya.F. Montazh gidroturbin (Setting-up Hydraulic Turbines).—Gosenergoizdat. 1952.
90. Frank-Kamenetskii, G.Kh. Raschet deformatsii kol'tsevykh detalei (Calculation of Deformations in Annular Parts).—In: Sbornik "Gidroturbostroenie", No.4, Mashgiz. 1957.
91. Frank-Kamenetskii, G.Kh. K raschetu na prochnost' kryshki gidroturbiny (Strength Calculation of Hydro-turbine Covers).—In: Sbornik "Gidroturbostroenie", No.1, Mashgiz. 1955.
92. Tovetoles, F.P., N.N. Kovalev, I.N. Smirnov, et al. Ekspluatatsiya gidroturbin (Operation of Hydraulic Turbine).—Gosenergoizdat. 1941.
93. Chistyakov, A.M. K voprosu izucheniya masshtabnogo effekta v gidroturbinakh (Size Effect in Hydraulic Turbines).—Izvestiya VNIIG. 1954.
94. Shchapov, N.M. Turbinnoe oborudovanie gidrostantsii (Turbine Equipment for Hydroelectric Power Stations).—Gosenergoizdat. 1955.
95. Shchegolev, G.S. and Yu.E. Garkavi.—Gidroturbiny i ikh regulirovanie (Hydraulic Turbines and Their Regulation).—Mashgiz.
96. Shannikov, V.M. Rezinovye podshipniki v sudostroenii (Rubber-lined Bearings in Shipbuilding).—Sudostroenie, No.1. 1940.
97. Edel', Yu.U. and A.P. Stepanov. O vliyanii geometricheskikh parametrov lopasti gidroturbin na chastotu ee sobstvennykh kolebanii (Effect of the Geometric Parameters of the Runner Blades on Their Natural-vibration Frequency).—In: Sbornik "Gidroturbostroenie", No.1, Mashgiz. 1955.
98. Edel', Yu.U. and A.P. Stepanov. O vliyanii vody na chastotu kolebanii lopastei i plastin (Influence of the Water Flow on the Vibration Frequency of Blades and Plates).—In: Sbornik "Gidroturbostroenie", No.4, Mashgiz. 1957.
99. Entsiklopedicheskii spravochnik "Mashinostroenie" (Encyclopedic Handbook "Machine Construction"), Vol.12.—Mashgiz. 1949.

100. Yanshin, B.I. Obobshchenie kharakteristiki diskovykh zatvorov s ploskoskoshennym diskom (Systematization of Characterics of Butterfly Valves with Flat (Straight)-Beveled Disks).—Energomashinostroenie, No. 9. 1957.
101. Yanshin, B.I. Diskovye zatvory s ploskoskoshennymi diskami (Butterfly Valves with Flat-beveled Disks).—Kotloturbostroenie, No. 2. 1952.

Publications in Other Languages:

102. Blatly, I.R. and D.H. Cornell. Laboratory Testing Rubber Bearings.—India Rubber World, Vol. 14, No. 3. 1949.
103. Fisch, D. The Kaplan Turbine — Design and Trends.—Transactions of ASME, 76, No. 5. 1954.
104. Deriaz, P. and G. Warnock. Reversible Pump Turbines for the Sir Adam Beck-Niagara Pumping-generating Station, XII, No. 4. 1959.
105. K. Kardinal von Widdern. Hydraulische Anlagen.—Escher-Wyss Mitteilungen. 1954; Nechleba, M. Vodní turbiny, jejich konstrukce a příslusentsvi, Praha. 1954.
106. Waters, Taylor. The Strength of Pipe Flanges.—Mechanical Engineering. May 1927.